

Using iron to catch a ride - synthetic siderophores as molecular 'Trojan Horses' to visualize and treat MDR bacterial pathogens

Von der Naturwissenschaftlichen Fakultät
der Gottfried Wilhelm Leibniz Universität Hannover

zur Erlangung des Grades
Doktor der Naturwissenschaften
(Dr. rer. nat.)

genehmigte Dissertation von

Carsten Peukert, M. Sc.

2022

Referent: Prof. Dr. rer. nat. Mark Brönstrup

Korreferent: Prof. Dr. Russell Cox

Weiterer Korreferent: Prof. Dr. Wolfgang Maison

Tag der Promotion: 10.11.2022

Abstract

The rise in multidrug-resistant, bacterial infections, together with a shallow industrial discovery pipeline, urgently calls for novel diagnostic and therapeutic strategies. Bacterial cells, particularly Gram-negative pathogens with their double-layered cell wall, closely resemble a fortress that restricts the accumulation of small molecules. However, microbial transporters ensure a sufficient nutrient supply during infection of a host organism and act as gateways into the pathogen, e.g. for ferric iron, which plays a crucial role in microbial metabolism and growth. Siderophores, small bacterial molecule chelators, sequester Fe^{3+} from host proteins and are transported by bacterial, TonB-dependent transporters (TBDTs). Like a molecular “Trojan Horse”, synthetic siderophore mimics can hijack the siderophore transport system and actively translocate diagnostic or therapeutic payloads over the impervious bacterial membrane and accumulate at their site of action. This thesis expanded and evaluated the potential of synthetic and natural siderophores for the visualization and antibiotic therapy of MDR bacteria *in cellular* and *in vivo*. The structure of the DOTAM triscatecholate siderophore was adapted for an application as a bacteria-specific, gallium-68 labeled PET tracer for the detection of bacterial infections *in vivo*. Two tracers showed good *in vitro*, radiochemical and pharmacokinetic properties *in vivo* and selectively accumulated at the site of infection vs. a site of sterile inflammation. Similarly, chemiluminescent dioxetanes were attached to siderophores to yield a panel of siderophore dioxetane probes that detected Gram-positive and Gram-negative bacterial pathogens. The best compound exhibited superior stability in bacterial supernatant, detected low bacterial counts and even intracellular bacteria in infected lung epithelial cells. In an attempt to enhance the accumulation in Gram-negative bacteria and thus restore the activity of antibiotics used only against Gram-positive bacteria (e.g. lipopeptides, ansamycins, macrolides), chelators were conjugated via covalent and cleavable linker systems, to yield potent drug conjugates. Studies on siderophore receptor mutants of *E. coli* and *P. aeruginosa*, including transcriptomic and proteomic investigations, contributed information on the involved siderophore transporters as well as on the mechanistic response upon siderophore and conjugate addition. Peptide siderophore conjugates that target the TonB-dependent transport of ferric chelates in *Pseudomonas* successfully inhibited bacterial growth. This proof-of-concept established TonB as a novel target in antimicrobial therapy. The design, synthesis and biological evaluation of novel diagnostic and therapeutic siderophore conjugates represents an important milestone towards a clinical usage of this approach against MDR ESKAPE bacteria.

Keywords: drug conjugates; siderophores; diagnostics

Zusammenfassung

Die Zunahme multiresistenter bakterieller Infektionen und die geringe Zahl neuer Antibiotika machen neue Strategien dringend erforderlich. Bakterienzellen, insbesondere gramnegative Krankheitserreger, ähneln mit ihrer doppelschichtigen Zellwand einer Festung, welche die Anreicherung von Molekülen limitiert. Mikrobielle Transporter, welche die Nährstoffversorgung im Wirtsorganismus sicherstellen, fungieren als Schleusen wie z. B. für den Mikronährstoff Eisen, mit zentralen Rollen im bakteriellen Stoffwechsel und Wachstum. Dafür entreißen Siderophore, niedermolekulare Eisenchelatoren, Wirtsproteinen ihr Eisen und werden dann von bakteriellen, TonB-abhängigen Transportern aufgenommen. Wie ein "Trojanisches Pferd" können synthetische Siderophoranaloge dieses Transportsystem kapern und diagnostische oder therapeutische Nutzlasten über die Bakterienmembran transportieren. In dieser Arbeit wurden synthetische und natürliche Siderophore für die Visualisierung und antibakterielle Therapie von multiresistenten Keimen für die *in vitro* und *in vivo* Anwendung derivatisiert und biologisch evaluiert. Beispielsweise wurde die Struktur des DOTAM Siderophors für die Anwendung als bakterien-spezifischer, Gallium-68-markierter PET-Tracer zum Nachweis von Infektionen *in vivo* angepasst. Zwei Tracer zeigten gute *in vitro* Aktivitäten, hervorragende radiochemische und pharmakokinetische Eigenschaften *in vivo* sowie eine deutlich höhere Anreicherung an einem bakteriellen Infektionsherd als am Ort einer sterilen Entzündung. Ferner wurden chemilumineszente Dioxetane an Siderophore gekoppelt, um diagnostische Sonden zu erhalten, welche grampositive und gramnegative Krankheitserreger nachweisen. Eine Verbindung zeigte eine hohe Stabilität in bakteriellem Überstand und wies niedrige Keimzahlen sowie Bakterien in infizierten Lungenepithelzellen nach. Die Konjugation von Antibiotika, welche bisher nur gegen grampositive Bakterien aktiv waren (z.B. Lipopeptide, Ansamycine und Makrolide), an Eisenchelatoren verbesserte deren Anreicherung und antibiotische Potenz gegen gramnegative Keime. Dazu wurden die Naturstoffe über kovalente und spaltbare Linkersysteme an die Siderophore gekoppelt. Weitere Untersuchungen auf Transkriptom- und Proteomebene mit *E. coli* und *P. aeruginosa* Siderophorrezeptormutanten lieferten Daten zu den involvierten Transportern sowie über die bakterielle Adaption nach Zugabe von Siderophoren oder Konjugaten. Peptid-Siderophorkonjugate, welche direkt auf den TonB-abhängigen Transport von Eisen in *Pseudomonas* abzielten, hemmten das bakterielle Wachstum. Dieser erste Wirknachweis etablierte TonB als neues Ziel für die antimikrobielle Therapie. Das Design, die Synthese und die biologische Evaluation neuartiger diagnostischer und therapeutischer Siderophorkonjugate ist ein Meilenstein auf dem Weg zu einem klinischen Einsatz dieses Prinzips gegen multiresistente Keime.

Schlagwörter: Wirkstoffkonjugate, Siderophore, Diagnostik

Preamble

This doctoral thesis is a cumulative dissertation according to §8 (1) and (3) of the Common Regulations for the Doctorate in Natural Sciences (Dr. rer. nat.) at the Gottfried Wilhelm Leibniz Universität Hannover (PromO).

The publications and manuscripts in this thesis are listed sequentially below.^{FN1, FN2}

1. **Carsten Peukert**, Laura N. B. Langer, Sophie M. Wegener, Anna Tutov, Jens P. Bankstahl, Bianka Karge, Frank M. Bengel, Tobias L. Ross, and Mark Brönstrup. "Optimization of artificial siderophores as ⁶⁸Ga-complexed PET Tracers for *in vivo* imaging of bacterial infections". In: *Journal of Medicinal Chemistry* **2021** 64 (16), 12359-12378. DOI: 10.1021/acs.jmedchem.1c01054.
2. Lukas Pinkert, Yi-Hui Lai, **Carsten Peukert**, Sven-Kevin Hotop, Bianka Karge, Lara Marie Schulze, Jörg Grunenberg, and Mark Brönstrup. "Antibiotic conjugates with an artificial MECAM-based siderophore are potent agents against Gram-positive and Gram-negative bacterial pathogens". In: *Journal of Medicinal Chemistry* **2021** 64 (20), 15440-15460. DOI: 10.1021/acs.jmedchem.1c01482.
3. **Carsten Peukert**, Sachin Popat Gholap, Ori Green, Lukas Pinkert, Joop van den Heuvel, Marco van Ham, Doron Shabat und Mark Brönstrup. "Enzyme-activated, chemiluminescent siderophore-dioxetane probes enable the selective and highly sensitive detection of bacterial pathogens". In: *Angewandte Chemie International Edition* **2022** e202201423. DOI: 10.1002/anie.202201423.
Carsten Peukert, Sachin Popat Gholap, Ori Green, Lukas Pinkert, Joop van den Heuvel, Marco van Ham, Doron Shabat und Mark Brönstrup. "Enzymaktivierte, chemilumineszente Siderophor-Dioxetan-Sonden ermöglichen den selektiven und hochempfindlichen Nachweis von bakteriellen Krankheitserregern". In: *Angewandte Chemie* **2022** e202201423. DOI: 10.1002/ange.202201423.
4. Sarah Fritsch, Véronique Gasser, **Carsten Peukert**, Lukas Pinkert, Lauriane Kuhn, Quentin Perraud, Vincent Normant, Mark Brönstrup and Isabelle J. Schalk. "Uptake mechanisms and regulatory responses to MECAM- and DOTAM-based artificial siderophores and their antibiotic conjugates in *Pseudomonas aeruginosa*". In: *ACS Infectious Diseases* **2022** 8, 6 1134-1146. DOI: 10.1021/acsinfecdis.2c00049.

^{FN1} The compounds are numbered with roman numerals consecutively in the general introduction, the aims and the general discussion and outlook. The numbering within the manuscripts was left unchanged.

^{FN2} The compound spectra have been transferred to a separate file and can be found on a CD, together with electronic version this thesis, in the back.

5. **Carsten Peukert**, Véronique Gasser, Till Orth, Sarah Fritsch, Vincent Normant, Olivier Cunrath, Isabelle Schalk, Mark Brönstrup. "Trojan Horse siderophore conjugates induce *P. aeruginosa* suicide and qualify the TonB protein as a novel antibiotic target". *ChemRxiv*, **2022**. DOI: 10.26434/chemrxiv-2022-9zvfx
6. **Carsten Peukert**, Katharina Rox, Sven-Kevin Hotop, Bianka Karge, Mark Brönstrup. "Bridging diagnostics and therapy: Towards theranostic DOTAM-based sideromycins as potent and selective effectors for bacterial imaging and antimicrobial therapy". Added as a soon-to-be-submitted manuscript.
7. **Carsten Peukert**, Bianka Karge, Mark Brönstrup. "Cleavable RNA polymerase inhibitor siderophore conjugates as potent antimicrobial agents against multidrug-resistant bacteria." Added as a soon-to-be-submitted manuscript.

The individual author contributions of the above-listed publications are outlined in the following paragraphs in accordance with PromO §8 (3).

Ad 1.:

The article was published in a peer-reviewed, scientific journal, C.P. and L.N.B.L. contributed equally to this publication. In particular, the nine authors contributed as follows:

Carsten Peukert Conception of the study and supervision of the master thesis of A. Tutov, design of the DOTAM-based PET tracers, synthesis of compound **10**, **11**, **15**, [^{nat}Ga]**15**, re-synthesis of compounds **7** and **8**, growth recovery experiment for compound **15**, evaluation and curation of the organic chemistry and non-radioactive, biological data for publication, preparation of figures and tables, writing of the article and processing of the revision.

Laura N. B. Langer Conception of the study, establishment and optimization of the radiochemical tracer synthesis, their physicochemical characterization and the *in vivo* experiments, writing of the article and processing of the revision.

Sophie M. Wegener Support in the conception of the study, support with radiochemical synthesis and *in vivo* experiments, discussion of the results and revision of the article.

Anna Tutov Organic synthesis and characterization of the tracers **7**, [^{nat}Ga]**7**, **8**, [^{nat}Ga]**11**, **24**, **25/26**, **34/35**, **37** regarding their 'cold' gallium complexation properties and stability in buffer.

Jens P. Bankstahl Support in the conception of the study and with the PET/CT imaging in healthy and infected mice.

Bianka Karge Implementation of the growth recovery experiment for all compounds except **15** and of the cytotoxicity assay for all compounds.

Frank M. Bengel Support in the planning and execution of the study.

Tobias L. Ross Support in conception of the study, discussion of the results, writing of the article and processing of all revisions.

Mark Brönstrup Support in conception of the study, discussion of the results, writing of the article and processing of all revisions.

Reprinted (adapted) with permission from "Optimization of artificial siderophores as ⁶⁸Ga-complexed PET tracers for *in vivo* imaging of bacterial infections", Carsten Peukert, Laura N. B. Langer, Sophie M. Wegener, et al, *Journal of Medicinal Chemistry*, American Chemical Society, Aug 1, **2021**, copyright © 2021, American Chemical Society.

A one-time permission was granted by a request through Rightslink® according to ACS requirements (<https://pubs.acs.org/page/copyright/permissions.html>). A screenshot of this permission is included in the supplementary data section of this thesis.

Ad 2.:

The article was published in a peer-reviewed, scientific journal. L.P. and Y.H.L. contributed equally to this publication. In particular, the eight authors contributed to the work as follows:

Lukas Pinkert Conception of the study, organic synthesis and characterization of all MECAM-based siderophores and siderophore conjugates, preparation of figures and tables, writing of the article and processing of all revisions.

Yi-Hui Lai Conception of the study, generation of *E. coli* siderophore receptor and TonB, ExbB/D mutants, planning, execution and evaluation of growth recovery, antimicrobial susceptibility assays, generation and genomic characterization of resistant *E. coli* mutants, preparation of figures and tables, writing of the article and processing of all revisions.

Carsten Peukert Contribution to conception of the study. Execution and evaluation of the iron Chrome Azurol S assay, support in writing of the article and processing of revisions.

Sven-Kevin Hotop Implementation and evaluation of the LC/MS/MS uptake assay and discussion of the results.

Bianka Karge Implementation and evaluation of antimicrobial susceptibility assays.

Lara Marie Schulze Implementation and evaluation of DFT calculations of MECAM-based siderophores, preparation of figures.

Jörg Grunenberg Support in conception of the study, discussion of the results,

Mark Brönstrup Support in conception of the study, discussion of the results, writing of the article and processing of all revisions.

Reprinted (adapted) with permission from “Antibiotic Conjugates with an Artificial MECAM-based siderophore are potent agents against Gram-positive and Gram-negative bacterial pathogens”, Lukas Pinkert, Yi-Hui Lai, Carsten Peukert, et al, *Journal of Medicinal Chemistry*, American Chemical Society, Oct 1, 2021, copyright ©2021, American Chemical Society.

A one-time permission was granted by a request through Rightslink® according to ACS requirements (<https://pubs.acs.org/page/copyright/permissions.html>). A screenshot of this permission is included in the supplementary data section of this thesis.

Ad 3.:

The article was published in a peer-reviewed, scientific journal in an English and German version of the same manuscript. In particular, the eight authors contributed to the work as follows:

Carsten Peukert Conceived the study, performed siderophore, dioxetane and conjugate synthesis, conducted protein purification and biological assays. He analyzed and curated the experimental data for publication, wrote the manuscript, led the revision and corrected the proofs.

Sachin Popat Gholap Conducted dioxetane synthesis and wrote the manuscript.

Ori Green Conducted dioxetane synthesis and wrote the manuscript.

Lukas Pinkert Conducted siderophore synthesis.

Joop van den Heuvel Conducted protein purification and optimization.

Marco van Ham Conducted timsTOF MS/MS data acquisition and evaluation.

Doron Shabat Conceptualized the study and wrote the manuscript.

Mark Brönstrup Conceptualized the study, coordinated the research, wrote the manuscript, participated in the revision and correction of the proofs.

This work was published as an open access article under the terms of the Creative Commons Attribution License (CC BY-NC 4.0), which permits its use, distribution and reproduction in any medium, provided the original work is properly cited.

Ad 4.:

The article was published in a peer-reviewed, scientific journal. In particular, the seven authors contributed to the work as follows:

Sarah Fritsch Performed bacterial cultures, ^{55}Fe uptake assays, and iron competition experiments with PVD.

Véronique Gasser Conceived the idea and performed the RT-qPCR assays.

Carsten Peukert Synthesized the DOTAM siderophores as well as their conjugates, curated the chemical data for publication, wrote the manuscript, participated in the revision and in the proof editing.

Lukas Pinkert Synthesized all MECAM compounds and conjugates.

Lauriane Kuhn performed proteomic assays and data analysis.

Quentin Perraud Performed proteome data analyses.

Isabelle J. Schalk Conceived the idea, designed the experiments and wrote the manuscript.

Mark Brönstrup Conceived the idea, designed the experiments and wrote the manuscript.

Reprinted with permission from “Uptake mechanisms and regulatory responses to MECAM- and DOTAM-based artificial siderophores and their antibiotic conjugates in *Pseudomonas aeruginosa*”, Sarah Fritsch, Véronique Gasser, Carsten Peukert, et al, *ACS Infectious Diseases*, American Chemical Society, April **2022**, copyright ©2022, American Chemical Society.

A one-time permission was granted by a request through Rightslink® according to ACS requirements (<https://pubs.acs.org/page/copyright/permissions.html>). A screenshot of this permission is included in the supplementary data section of this thesis.

Ad. 5:

This publication was uploaded as a preprint on ChemRxiv and will soon be submitted to a peer-reviewed, scientific journal, C.P, V.G. and T.O. contributed equally. In particular, the 8 authors contributed to the work as follows:

Carsten Peukert Conceived the idea, conceptualized the study, performed conjugate design, synthesized DOTAM siderophore intermediates and siderophores, supervised the master thesis of T. Orth, curated the chemical data for publication, prepared figures and wrote the manuscript.

Véronique Gasser Conceived the idea, conceptualized the study, conducted/planned minimal inhibitory concentration, q-RT-PCR and growth kinetic experiments, curated the biological data for publication, prepared figures and wrote the manuscript.

Till Orth Designed covalent and cleavable TonB box siderophore conjugates, performed all peptide and siderophore peptide conjugate synthesis, characterization of intermediates and curation of analytical chemical data, participated in manuscript correction.

Sarah Fritsch Conducted antimicrobial activity profiling and growth kinetics of the siderophores TonB box peptides and TonB box peptide siderophore conjugates in *P. aeruginosa* mutants.

Vincent Normant Support with biological conjugate characterization.

Olivier Cunrath Support with western blotting and biochemical evaluation.

Isabelle Schalk Conceptualized the study and wrote the manuscript.

Mark Brönstrup Conceptualized the study, coordinated the research and wrote the manuscript.

This work was published as an open preprint under the terms of the Creative Commons Attribution License (CC BY-NC 4.0), which permits its use, distribution and reproduction in any medium, provided the original work is properly cited.

Ad. 6:

This publication manuscript was included as a separate chapter in this cumulative thesis and will soon be submitted to a peer-reviewed, scientific journal. In particular, the 5 authors contributed to the work as follows:

Carsten Peukert Conceived the idea, conceptualized the study, synthesized and characterized all intermediates and conjugates, conducted cellular labelling and antimicrobial activity experiments, curated the biological and chemical data for publication, wrote the manuscript.

Katharina Rox Conducted stability and plasma protein binding experiments, corrected and wrote the manuscript.

Sven-Kevin Hotop Conducted and evaluated the subcellular quantification of compounds in bacteria by LC-MS/MS.

Bianka Karge Conducted minimal inhibitory concentration and cytotoxicity assays.

Mark Brönstrup Conceptualized the study, coordinated the research and wrote the manuscript.

Ad. 7:

This publication manuscript was included as a separate chapter in this cumulative thesis and will soon be submitted to a peer-reviewed, scientific journal. In particular, the 3 authors contributed to the work as follows:

Carsten Peukert Conceived the idea, conceptualized the study, synthesized and characterized all intermediates and conjugates, conducted antimicrobial activity experiments, curated the biological and chemical data for publication, wrote the manuscript.

Bianka Karge Conducted minimal inhibitory concentration experiments.

Mark Brönstrup Conceptualized the study, coordinated the research and wrote the manuscript.

Table of Contents

Abstract.....	1
Zusammenfassung.....	3
Preamble.....	4
Table of Contents.....	13
List of Figures.....	17
List of Tables.....	20
List of Abbreviations.....	21
1. General Introduction.....	26
1.1 Antibiotics, the antimicrobial resistance crisis and potential solutions.....	26
1.1.1 A brief overview over novel antimicrobial strategies.....	31
1.2 The Trojan horse strategy.....	33
1.3 Siderophores in prokaryotes and their role in infections.....	33
1.4 Chemical structure, function and biosynthesis of siderophores.....	34
1.5 Bacterial iron acquisition systems.....	38
1.6 Siderophores as bacterial targeting vectors.....	40
2. Aims of the Thesis.....	58
3. Publication 1.....	60
Table of content graphic.....	61
Abstract.....	61
3.1 Introduction.....	62
3.2 Results and discussion.....	63
3.2.1 Gallium complexation.....	67
3.2.2 Growth recovery capabilities of cyclen-based siderophore analogues.....	69
3.2.3 Chemical stability and cytotoxicity.....	70
3.2.4 Radiochemical synthesis.....	71
3.2.5 Biodistribution studies in mice.....	74
3.2.6 PET/CT imaging of <i>E. coli</i> infected muscle vs. sterile-inflamed muscle in mice.....	75
3.3 Conclusion.....	79
3.4 Experimental section.....	81

3.4.1 Chemical Synthesis	81
3.4.2 Animal Experiments	103
Funding.....	103
Acknowledgements.....	103
Abbreviations	103
References	104
Supplementary material	111
4. Publication 2.....	139
Table of content graphic	140
Abstract	140
4.1 Introduction	141
4.2 Results.....	142
4.3 Discussion and conclusion.....	155
4.4 Experimental section.....	158
Abbreviations	190
Funding.....	190
Acknowledgments.....	190
References	191
Supplementary Information	197
5. Publication 3.....	230
Table of content graphic	231
Abstract	231
5.1 Introduction	232
5.2 Results and Discussion.....	234
5.3 Conclusion	248
Acknowledgement	249
Funding information	249
Conflict of interest	249
Keywords.....	249
References	250

Supporting Information.....	256
6. Publication 4.....	338
Table of content graphic	339
Abstract	339
6.1 Introduction.....	340
6.2 Results and Discussion.....	342
6.3 Discussion	351
Keywords.....	354
Materials and Methods.....	354
Author Contributions	355
Abbreviations used	356
Acknowledgements.....	356
References	357
Supporting information.....	365
7. Publication 5.....	384
Table of Content graphic.....	385
Abstract	385
7.1 Introduction.....	386
7.2 Results and discussion	388
7.3 Conclusion.....	397
Funding information	399
Conflict of interest	399
Acknowledgements.....	399
Abbreviations	399
References	400
Supporting information.....	406
8. Publication 6.....	498
Abstract	499
Table of content graphic	499
8.1 Introduction.....	500

8.2 Results and discussion	502
8.3 Conclusion.....	511
Acknowledgements.....	512
Funding information	512
References	513
Supporting information.....	518
9. Publication 7.....	562
Abstract	563
Table of content graphic	563
9.1 Introduction.....	564
9.2 Results and Discussion.....	566
9.3 Conclusion.....	577
Acknowledgements.....	577
Funding information	577
References	578
Supporting information.....	583
10. General Discussion and Outlook.....	696
10.1 Outlook on synthetic siderophores as bacteria-specific PET tracers	696
10.2 MECAM-based sideromycins and their resistance mechanisms	700
10.3 Bacteria-specific, optical diagnostics for the point-of-care detection of infections	701
10.4 From TonB targeting sideromycins towards small molecule drugs	703
10.5 A database for effective, streamlined sideromycin development	706
A. Supplementary Data.....	709
A.1 Publication 1	709
A.2 Publication 2.....	710
A.5 Publication 5.....	711
Acknowledgements	712
Curriculum vitae and List of Publications	713
General References	716

List of Figures^{FN3}

Figure 1.1. First modern antibiotic molecules.	26
Figure 1.2 Timeline of antibiotics market introduction and resistance occurrence.....	27
Figure 1.3. Antimicrobial strategies and microbial resistance.....	29
Figure 1.4. Schematic structure of the Gram-positive (a) and Gram-negative (b) cell wall. ...	30
Figure 1.5. Exemplary, novel strategies to combat AMR development.	32
Figure 1.6. The iron tug-of-war.	34
Figure 1.7. Overview on siderophore structures.	36
Figure 1.8. Spatial orientation of Fe-complexes.....	37
Figure 1.9. Biosynthesis of enterobactin XIX in <i>E. coli</i>	38
Figure 1.10. Schematic bacterial siderophore-mediated ferric iron uptake by Gram-negative and Gram-positive bacteria.....	39
Figure 1.11. Naturally occurring sideromycins.	41
Figure 1.12. Synthetic siderophore drug conjugates.	42
Figure 1.13. Chemical structure of antimicrobial sideromycins in clinical development.	43
Figure 1.14 Targets for bacterial infection-specific PET/SPECT tracers.	45
Figure 1.15. Jablonski diagram comparing fluorescence and chemiluminescence light emissive processes.....	47
Figure 1.16. Development of brightly emissive dioxetanes in aqueous environments.	48
Figure 1.17. Proposed mechanism of 1,2-dioxetane LIV decomposition and light emission.	49
Figure 1.18. Structures of (A) enterobactin XIX (B) triscatecholate DOTAM LVII and (C) MECAM LVIII siderophores.....	50
Figure 1.19. DOTAM siderophore mimetics LIX-LXIX and conjugates LXX-LXXI structures from K. Ferreira et al.....	51
Figure 1.20. Strain-promoted [3+2] cycloadditions.....	53
Figure 1.21. The necessity of cleavable linkers.	54
Figure 1.22. Thiol-disulfide exchange reaction.....	55
Figure 1.23. Principle of trimethyl lock linker systems.	57
Figure 2.1. Overview of siderophores as molecular ‘Trojan Horses’ for the diagnosis and treatment of bacterial infections in the scope of this thesis.	58
Figure 3.1 Structures of artificial siderophores investigated in this study.	64
Figure 3.2 Synthesis of siderophore-based PET imaging agents.....	66

^{FN 3} This lists the figures from the general introduction, the aim and the publications’ main texts. The supporting information figures are not included.

Figure 3.3 Formation of the 'cold' Ga-complex ^[natGa] 7	68
Figure 3.4 Growth recovery assay in siderophore-deficient <i>E. coli</i> mutants.	70
Figure 3.5. Radiochemical and physicochemical parameters and stability of gallium-68 complexes.	73
Figure 3.6. Biodistribution of [⁶⁸ Ga] 7 (left side, A-C) and [⁶⁸ Ga] 15 (right side, D-E) in male C57Bl/6N mice over 60 min of dynamic PET imaging.	74
Figure 3.7. <i>In vivo</i> PET imaging in mice infected with <i>E. coli</i> with [⁶⁸ Ga] 7	76
Figure 3.8. <i>In vivo</i> PET imaging in mice infected with <i>E. coli</i> with [⁶⁸ Ga] 15	78
Figure 4.1. Chemical structures of enterobactin (1), and artificial siderophores with DOTAM- (2), and MECAM-based (3) cores.	142
Figure 4.2. Syntheses of MECAM siderophores 8 – 11 , and structures of the final products 12 – 20	143
Figure 4.3. Characterization of 10	145
Figure 4.4. FepA is required for uptake of 8 in <i>E. coli</i>	147
Figure 4.5. Syntheses of intermediates 21 – 23 , MECAM-amino-penicillin conjugates 27 – 30 and chemical structures of 24, 31 , and the MECAM-daptomycin conjugate 32	149
Figure 4.6. Mechanism of resistance against 27 in <i>E. coli</i>	154
Figure 5.1. Design concept for bacteria-targeting chemiluminescent dioxetanes.	233
Figure 5.2. Synthesis of dioxetanes 1-2 and siderophore dioxetane probes 3-9	235
Figure 5.3. <i>In vitro</i> chemiluminescence induction.	237
Figure 5.4. Quenching of dioxetane chemiluminescence by catechols.	238
Figure 5.5. Probe-induced growth recovery in siderophore-deficient. <i>E. coli</i> and <i>P. aeruginosa</i> mutants.	239
Figure 5.6. Chemiluminescence kinetics in bacterial pathogens.	241
Figure 5.7. Characterization of turn-on fluorescent TML-coumarin DFO conjugate 10	242
Figure 5.8. Detection of intracellular bacteria in A549 lung epithelial cells.	244
Figure 5.9. LOD determination of siderophores probes.	246
Figure 6.1. Structures of MECAM (1/2), DOTAM (4/5) and the conjugates 3, 6 and 7	342
Figure 6.2. Iron scavenging from PVD-Fe by MECAM- and DOTAM-based siderophores.	343
Figure 6.3. Modulation of protein expression in <i>P. aeruginosa</i> in the presence of MECAMs 1 and 3	345
Figure 6.4. ⁵⁵ Fe uptake in <i>P. aeruginosa</i> strains mediated by the siderophores enterobactin, 1 and 3	346
Figure 6.5. Growth of TBDT-deficient <i>P. aeruginosa</i> mutants in the presence of 1 or 3	347
Figure 6.6. Modulation of protein expression in <i>P. aeruginosa</i> in the presence of DOTAM-based siderophore 4 and the associated conjugates 6 and 7	349

Figure 6.7. Growth of TBBDT-deficient <i>P. aeruginosa</i> mutants in the presence of DOTAM-based siderophores 4, 6 and 7.....	350
Figure 7.1 Iron delivery by enterobactin (ENT) and envisioned suicide TonB siderophore strategy.	388
Figure 7.2. Growth of <i>P. aeruginosa</i> PAO1 transformed with pMMB190-araC-pbad- <i>hasR</i> -His ₆ plasmid.....	389
Figure 7.3. Structures of the DOTAM and MECAM siderophores 2 and 4 , TonB box peptides 5-10 , and siderophore-peptide conjugates 11-34	391
Figure 7.4. Modulation of TBBDT gene expression by conjugates.	396
Figure 7.5. Growth kinetics of <i>P. aeruginosa pfeA</i> and <i>pirA</i> mutants in the presence of the conjugates.....	397
Figure 8.1. Conjugation of siderophores to natural products with exclusive activity in Gram-positive bacteria.	501
Figure 8.2. Structures of synthetic vancomycin, daptomycin and sorangicin A conjugates.	503
Figure 8.3. Intracellular accumulation of 3 , 9 and 10 in <i>E. coli</i>	506
Figure 8.4. Synthesis of the DOTAM-based theranostic 13 and the imaging conjugate 14	507
Figure 8.5. Labeling of bacterial pathogens with fluorescent DOTAM conjugates 13 and 14	508
Figure 8.6 Cellular antimicrobial activity of daptomycin 1 and theranostic 13	509
Figure 9.1. “Trojan Horse” strategy to increase the activity of antibiotics in Gram-negative pathogens.	565
Figure 9.2. Synthesis of mono and dicatechol rifamycin SV derivatives 3-6	567
Figure 9.3. Enzymatically cleavable ciprofloxacin siderophore conjugates.	569
Figure 9.4. Structural overview of covalent and cleavable RNAP-I siderophore conjugates.	572
Figure 10.1. Effective radiochelators and future development regarding monocatechol, bacteria-specific PET tracers.....	697
Figure 10.2. Outlook for triscatecholate, bacteria-specific PET tracers.	698
Figure 10.3. Bright outlook for siderophore dioxetane probes.....	701
Figure 10.4. Complementary strategies to convert TonB box peptide sideromycins to small molecule drugs.	704
Figure 10.5. Publications on siderophores and siderophore conjugates <i>per annum</i>	706
Figure 10.6. Vision for a siderophore repository to build conjugate activity relationships. ...	707
Figure A.1. Screenshot of the CCC RightsLink® request for Publication 1.	709
Figure A.2. Screenshot of the CCC RightsLink® request for Publication 2.	710
Figure A.3. Screenshot of the CCC RightsLink® request for publication 5.....	711

List of Tables^{FN4}

Table 1.1. Redox potential of iron bound to selected siderophores.....	35
Table 4.1. Minimal inhibitory concentrations (MICs) of 27 – 32 against bacterial pathogens ^a	151
Table 4.2. Minimal inhibitory concentrations (MICs) of 27 against <i>E. coli</i> wild type and knockout strains. ^a	153
Table 7.1. MIC values in <i>P. aeruginosa</i> $\Delta pvdF\Delta pchA$ strain for siderophores 2 and 4 , peptides 5-10 and peptide-siderophore conjugates 11-34	393
Table 8.1. Antimicrobial activity of daptomycin 1 , vancomycin 2 and their conjugates 1-8 . ^a	504
Table 8.2. Antimicrobial activity of sorangicin A (3) and its siderophore conjugates 9-12 . ^a	505
Table 8.3. Plasma stability, plasma protein binding (compound 14 , 26 and 26a) and cytotoxicity in four eukaryotic cells of the conjugates 13 , 14 and daptomycin 1	510
Table 9.1. MIC values ^a for compounds 8 to 17	570
Table 9.2. MIC values ^a for 18 to 37 in MDR <i>E. coli</i> , <i>S. aureus</i> , <i>P. aeruginosa</i> strains.	575

^{FN4} This lists the tables from the general introduction, the aim and the publications' main texts. The supporting information tables are not included.

List of Abbreviations

2,3-DHBA	- 2- ¹⁸ F-fluorodeoxyglucose (¹⁸ F-FDG)
AAC	- antibody antibiotic conjugates
ACN	- acetonitrile
AMP	- antimicrobial penetrating peptides (AMP)
BCN	- (1R,8S)-9-(13-methyl)bicyclo[6.1.0]non-4-yne
BCN-DOTA	- 2,2',2''-(10-(4-((2-(((1R,8S,9s)-bicyclo[6.1.0]non-4-yn-9ylmethoxy)carbonyl)amino)ethyl)amino)-1-carboxy-4-oxobutyl)-1,4,7,10-tetraazacyclododecane-1,4,7-triyl)triacetic acid
BET	- back electron transfer
BHL	- <i>N</i> -butanoyl-L-homoserine lactone
BLI	- β-lactamase inhibitors
Boc	- <i>tert</i> -butyloxycarbonyl
C/E-IEEL	- chemical/enzymatic initiated electron exchange luminescence
CAA	- casamino acid
CAR	- conjugate-based activity relationships
CAS	chrome azurol S
CCCP	- <i>m</i> -chlorophenylhydrazone
CER	- conjugate-based entry relationships (CER)
CFU	colony forming unit
corA	- coralloyronin A
CPP	- cell penetrating peptides
CT	- computed tomography
CuAAC	- copper-catalyzed azide alkyne cycloaddition
DBCO	- dibenzylcyclooctyne
DCM	- dichloromethane

List of Abbreviations

DFO	- desferrioxamine
DFT	- density functional theory
DHBS	- dihydroxybenzoylserine
DHP	- dihydrofolic acid
DHPS	- dihydropteroate synthetase
DIPEA	- diisopropyl ethyl amine
DMA	- dimethylacetamide
DMF	- dimethylformamide
DMSO	- dimethylsulfoxide
DOTA	- 1,4,7,10-tetraazacyclododecane-1,4,7,10-tetraacetic acid
DOTAM	- 1,4,7,10-tetraazacyclododecane-1,4,7,10-tetraacetamide
EA	- ethylacetate
EDCI	- 1-Ethyl-3-(3-dimethylaminopropyl)carbodiimid
ENT	- enterobactin
ESKAPE	- <i>E. coli</i> , <i>S. aureus</i> , <i>K. pneumoniae</i> , <i>A. baumannii</i> , <i>P. aeruginosa</i> , <i>E. faecium</i>
EWG	- electron-withdrawing group
FACS	- fluorescence-activated cell sorting
FERRI	- ferrichrome
Fmoc	- fluorenylmethoxycarbonyl
FRET	- Förster resonance energy transfer
Hb	- hemoglobin
HPLC	- high pressure liquid chromatography
HRMS	- high resolution mass spectrometry
IBX	- iboxamycin
IDCAM	- iron-depleted, cation-adjusted medium
IM	- inner membrane

LC	- liquid chromatography
LC/MS/MS	- liquid chromatography coupled to mass spectrometry
Lcn2	- lipocalin 2
LE	- labelling efficiency
LECs	- A549 human lung epithelial cells
LOD	- limit of detection
LPS	- lipopolysaccharides
MBLs	- metallo- β -lactamases
MDR	- multidrug-resistant
MECAM	- 1,3,5- <i>N,N,N'</i> -tris-(2,3-dihydroxybenzoyl)-triaminomethylbenzene
MIC assay	- minimal inhibitory concentration assay
MRI	- magnetic resonance imaging
MRSA	- methicillin-resistant <i>S. aureus</i>
NHE	- normal hydrogen electrode
NMM	- <i>N</i> -methyl morpholine
NMR	- nuclear magnetic resonance
NOTA	- 2,2',2''-(1,4,7-triazacyclononane-1,4,7-triyl)triacetic acid
NRPS	- non-ribosomal peptide synthetase
OM	- outer membrane
OMR	- outer membrane receptor
ONPG	- 2-nitrophenyl β -D-galactopyranoside
PAC	- peptide antibiotic conjugates
PBP	- periplasmic binding protein
PBS	- phospho-buffered saline
PCH	- pyochelin
PCR	- polymerase chain reaction
PE	- petrolether

List of Abbreviations

PEG	- polyethylene glycol
PET	- positron emission tomography
PG	- protecting group
PMF	- proton motive force
PPB	- plasma protein binding
PPI	- protein-protein interaction
PTS	- phosphotransferase system
PVD / PYO	- pyoverdine
QOR2	- quinone oxidoreductase 2
QS	- quorum sensing
RCP	- radiochemical purity
RCY	- radiochemical yield
RNAP	- RNA polymerase
RNAP-I	- RNA polymerase inhibitor
ROI	- regions of interest
RT-qPCR	- quantitative reverse transcription polymerase chain reaction
S/B ratio	- signal to background ratio
SAR	- structure activity relationship
SBP	- siderophore binding protein
SD	- standard deviation
SEM	- standard error of mean
SET	- single electron transfer
sorA	- sorangicin A
SPAAC	- strain-promoted azide-alkyne cycloaddition
SPECT	-single-photon emission tomography
TAC	- time-activity curves

TBDT	- TonB-dependent transporter
TBTA	- tris[(1-benzyl-1H-1,2,3-triazol-4-yl)methyl]amine
TCEP	- (tris(2-carboxyethyl)phosphine
TEA	- triethylamine
TEMPO	- 2,2,6,6-tetramethylpiperidinyloxy
TFA	- trifluoroacetic acid
THF	- tetrahydrofuran
THPTA	- tris(3-hydroxypropyltriazolylmethyl)amine
TLR	- toll-like receptor
TML	- trimethyl lock
TREN-CAM	- tripodal enterobactin analogue-catecholate coordinating moieties
UPEC	- uropathogenic <i>E. coli</i>
WBC	- white blood cells
WHO	- World Health Organization

1. General Introduction

1.1 Antibiotics, the antimicrobial resistance crisis and potential solutions

Among the manifold challenges to human health, infectious diseases protrude for their capability to impact the course of human history throughout the ages.¹ Of significant importance is their suddenness and their ability for extensive global repercussions, as illustrated by the recurring outbreaks of the bubonic plague in the Roman Empire (AD 542) and in the late middle ages (14th century).² The course of infectious disease is commonly of unequivocal and severe nature. Their progression, in contrast to other disease states, may be prompt and irreversible. Without an effective, available therapy, an acute infection frequently constitutes an ‘all-or-nothing’ scenario like a lottery game, with the host organism either rapidly perishing or recovering spontaneously.³

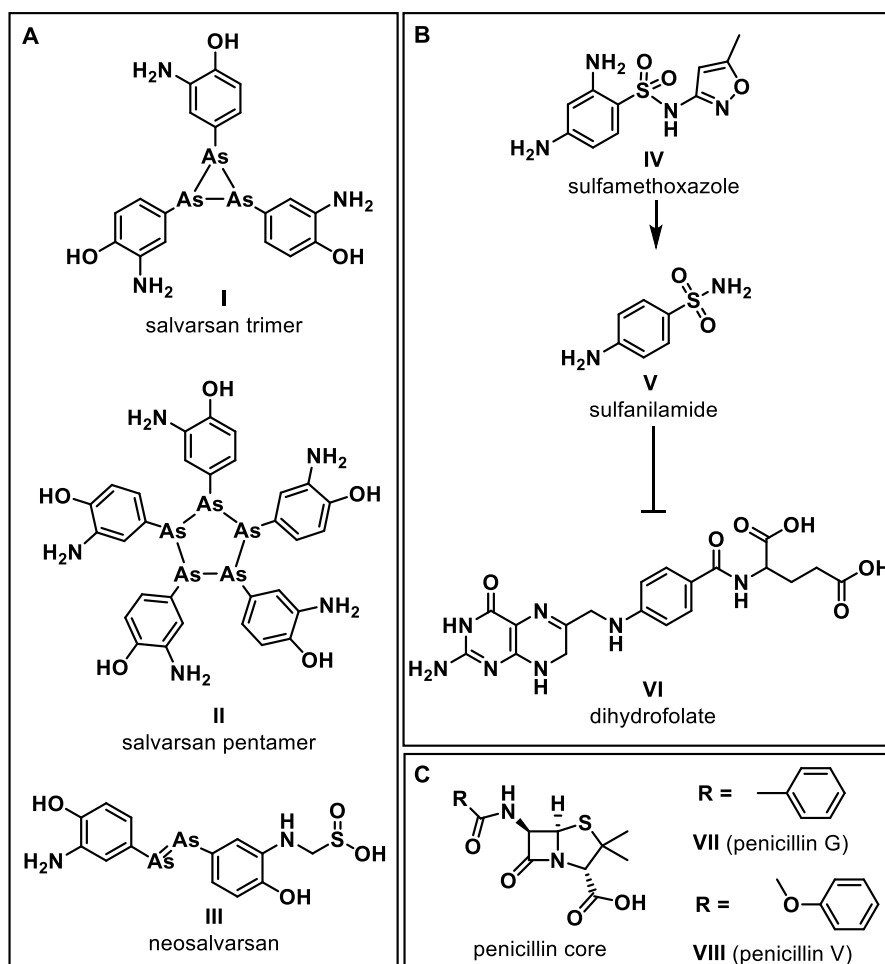


Figure 1.1. First modern antibiotic molecules. (A) Structures for the first, modern organoarsenics by the Ehrlich lab, depicted as a trimeric or pentameric structure as resolved in 2005 by mass spectral studies.⁴ The more tolerable and soluble neosalvarsan **III** was introduced in 1912.⁵ (B) The sulfonamide **IV** developed by G. Domagk, which is metabolized to its active form sulfanilamide **V** to inhibit the bacterial dihydropteroate synthase. (C) Structures of penicillin G (**VII**) and V (**VIII**) as the first β -lactam antibiotics.⁶

The synthesis of arsphenamine **I/II** (marketed name 'salvarsan'), by Paul Ehrlich's lab at Hoechst in 1907, was the first example how a molecule was optimized for a specific, biological activity by chemical synthesis. The study formed the basis for modern antimicrobial and pharmaceutical research.⁷ In 1912, the optimized 'neosalvarsan' (**III**), with its lower toxicity and higher water solubility, was introduced into the market (see Figure 1.1A).⁵ A team at the IG Farben, led by Gerhard Domagk, developed the first sulfonamide 'prontosil' in the 1930s, a dihydropteroate synthase inhibitor (Figure 1.1B). The compound was found to be metabolized (prodrug) to its active form, the sulfanilamide, by a team from the Pasteur institute later on.⁸ In 1928, the discovery of a fungal contamination by Alexander Fleming that inhibited bacterial growth, permitted the isolation and characterization of the penicillins' as the first clinically used members of the β -lactam family (Figure 1.1C).⁶ Mass production by Merck & Co allowed the first treatment in 1942. Further academic-industrial collaborations optimized the production and thus saved many wounded soldiers and civilians at the end of World War II (Figure 1.2). Simultaneously, this heralded the era of antibiotic chemotherapy.⁹ The discovery of specific antibiotics over the last 100 years is indicated by the colored arrows above the timeline in Figure 1.2. Arrows of the same color at the bottom indicate the occurrence of resistance for the same antibiotic class. The next 20 years marked the successive development of several of antibiotic classes (e.g. tetracycline, phenicols, aminoglycosides, macrolides), therefore termed the 'Golden Age' of antimicrobial chemotherapy. In consequence, the overall infectious disease mortality rate dropped about 20-fold to 36/100.000 citizens in the 1980s.

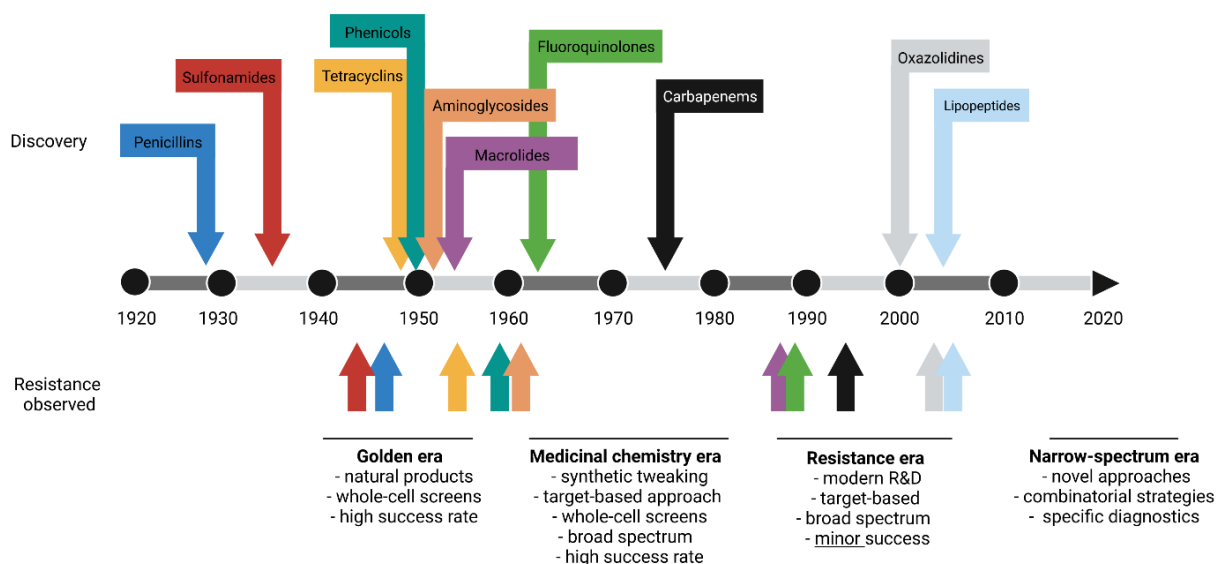
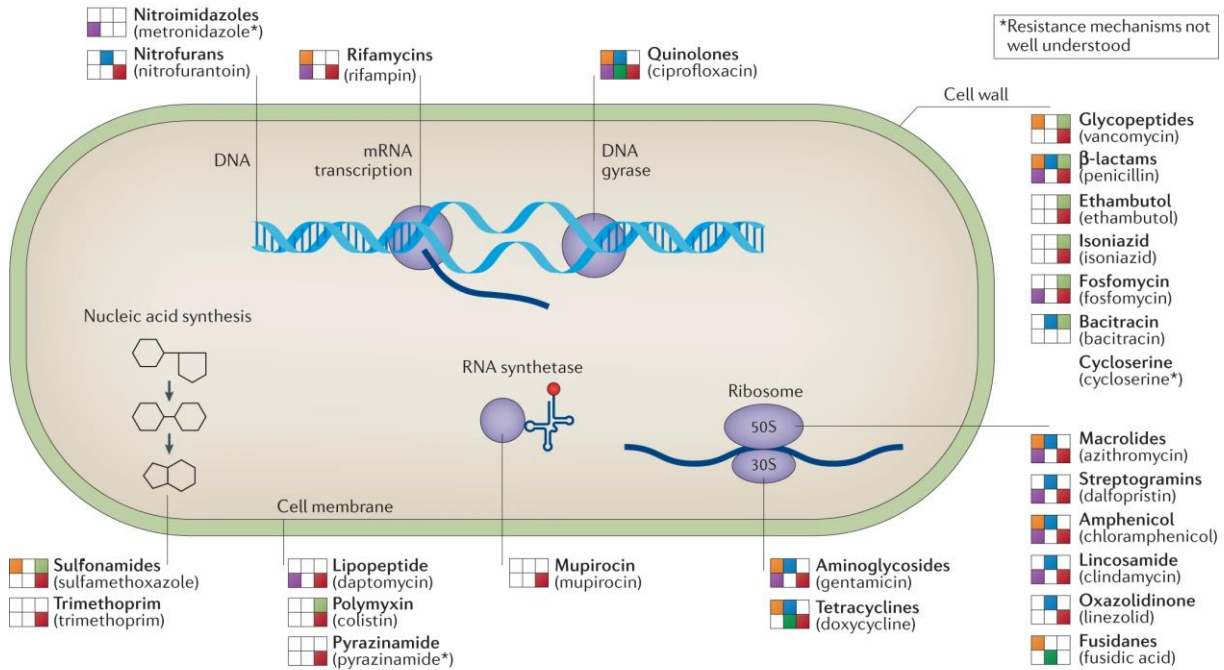


Figure 1.2 Timeline of antibiotics market introduction and resistance occurrence. Modified from literature, created with biorender.¹⁰

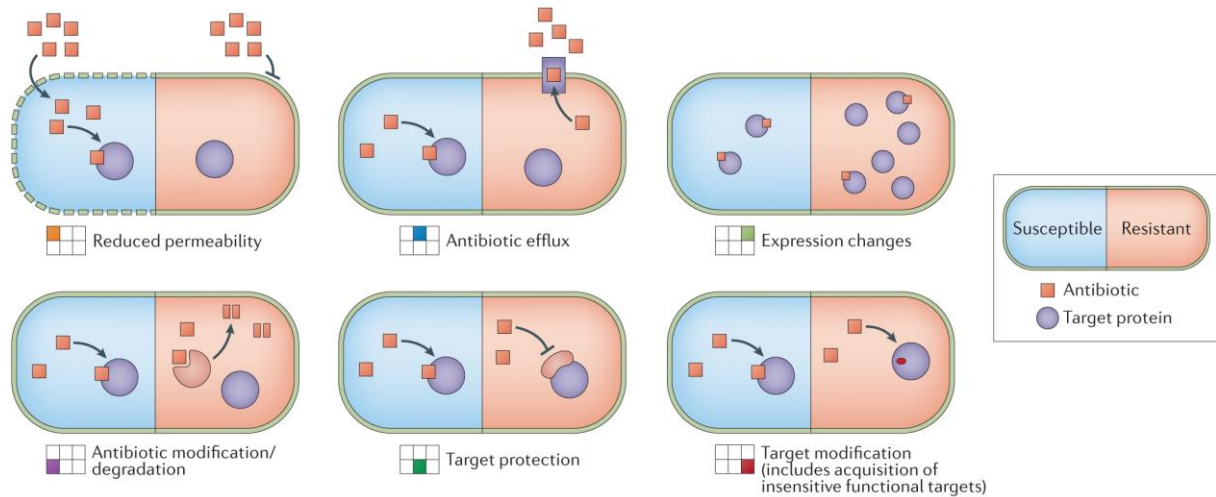
However, antibiotic discovery remained static at the end of 1980s, while the clinically observed microbial resistance increased substantially (discovery void).¹⁰ Amongst other things, the extensive, preventive antibiotics usage in the livestock industry (>50% of all antibiotics made) to foster animal growth and prevent disease spread as well as the supply without prescription in developing countries, together with a narrowing discovery pipeline has fueled this trend.¹¹ As most approved antibiotics before 2002 originated from natural products, it became more challenging and costly to identify new, active molecules, as the more prevalent structures were discovered already.¹² Taken together, this yielded the current resistance crisis, which threatens both our living standard as well as our societal wealth, with a menacing post-antibiotic era. Resistance was observed for all marketed antibiotics to date.¹⁰ Moreover, the majority of newly developed candidates in clinical trials, are structurally variations or combinations of established classes rather than compounds with inventive modes-of-action or impervious to circulating resistance mechanisms.¹³

The occurrence of resistance among bacteria to natural products is a superb example for natural selection through a better adaptation to environmental conditions and thus a more proficient reproduction of the species, as proposed by Darwin in the 19th century.¹⁴ Recently, results confirmed the emergence of methicillin-resistance in a pre-antibiotic era, as a part of a co-evolutionary adaption of *S. aureus*.¹⁵ The antiqueness of antibiotic resistance dates back 30.000 years for β -lactam, tetracycline and glycopeptide antibiotics, as confirmed in permafrost sediments.¹⁶ To the present day, most antibiotics address a few, well-characterized targets in prokaryotes, as shown in Figure 1.3A. In particular, they target structures or processes involved in DNA replication, transcription, RNA translation, cell wall or folate synthesis and the (outer) bacterial membrane.¹⁷ Prokaryotes employ a plethora of mechanisms to resist the bacteriostatic or bactericidal effects, e.g. by degradation, target modification or protection (Figure 1.3B).¹⁸ Resistance mechanisms can be intrinsic to the respective strain (efflux pumps or permeability) or rooted in distinct, genotypic variations (Figure 1.3C). Resistance genes can be shared among bacterial species, which occurs via horizontal gene transfer, defined as the conveyance of genetic information from one bacterium to another, which do not directly descend from each other, commonly by transduction, conjugation or transformation.¹⁹ Other resistance strategies by prokaryotic pathogens include (i) the formation of protective biofilms,²⁰ (ii) the formation of transiently, antibiotic tolerant persister cells,²¹ (iii) a joint gene regulation in response to population density (quorum sensing)²² and (iv) the secretion of virulence factors.²³ In addition, evidence accumulates that the composition and interplay within microbial communities impacts their response and evolution upon anti-infective treatment and thus their antibiotic susceptibility.²⁴

a Antibiotic targets in bacterial cells



b Mechanisms of antibiotic resistance



c Genetic determinants of resistance

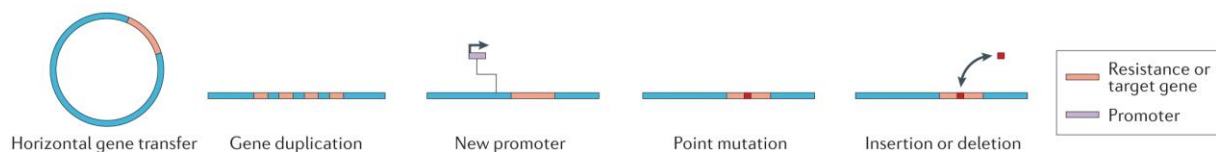


Figure 1.3. Antimicrobial strategies and microbial resistance. (A) Antibiotic agents clustered by target. The compound classes are shown in bold and examples are stated in the brackets below. (B) Resistance mechanisms are displayed with susceptible (left) and resistance (right) scenarios. The legend and color scheme is employed to summarize the found resistance mechanisms of the drugs above. (C) Genetic mechanisms that allow the acquirement of resistance to an antimicrobial are shown. Included from literature.¹⁷

The mortality and morbidity of hospital-acquired, so-called nosocomial, infections caused by multidrug-resistant (MDR) bacteria of the so-called ESKAPE panel (*Escherichia coli*, *Staphylococcus aureus*, *Klebsiella pneumoniae*, *Acinetobacter baumannii*, *Pseudomonas aeruginosa*, *Enterobacter faecium*), become an increasing obstacle for routine healthcare.²⁵ For this reason, the WHO released a list of 12 bacterial species that pose an imminent threat to human health in terms of clinical treatability and ongoing antibiotic development. Among the microbes that belong to the priority group 1 (critical) are *A. baumannii*, *Enterobacteriaceae* (e.g. *E. coli*) and *P. aeruginosa*.²⁶ These pathogens are all Gram-negative bacteria.

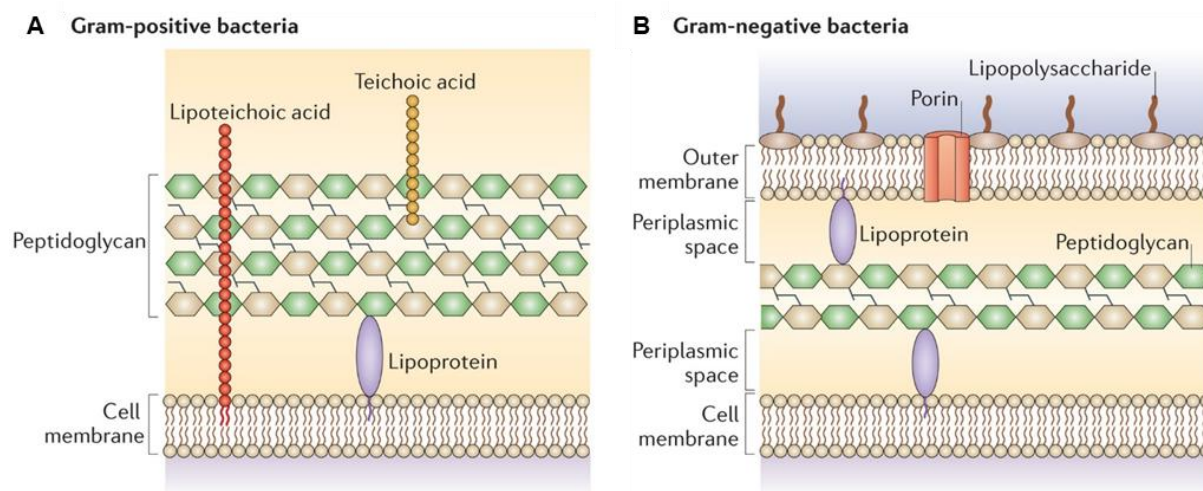


Figure 1.4. Schematic structure of the Gram-positive (a) and Gram-negative (b) cell wall. Included from literature.²⁷

Gram-positive and -negative bacteria are distinguished by their different cell wall composition (Figure 1.4). The Gram-positive cytosol is surrounded by a lipid bilayer membrane with embedded (trans-) membrane proteins (e.g. receptors, porins, channels). The membrane is covered by a thick peptidoglycan layer, also termed 'murein', which is anchored in the membrane by lipoteichoic acids. This mesh-like, teichoic acid-covered layer provides structural stability against osmotic pressure and can be stained purple with a crystal violet and iodine mixture (Gram staining).²⁸ In contrast, the Gram-negative counterpart has two phospholipid bilayers with a thinner murein layer in between, anchored in the outer membrane *via* Braun's lipoprotein and the outer membrane, which is composed of lipopolysaccharides (LPS). These limit the passage of large and hydrophobic compounds, much like a fortress with multiple ramparts.²⁹ Especially the outer bacterial membrane effectively decreases the diffusion-mediated penetration of many chemical frameworks, which otherwise exhibit a potent effect in Gram-positive species.³⁰

1.1.1 A brief overview over novel antimicrobial strategies

Numerous research programs are underway to investigate strategies to combat, reduce or eliminate the occurrence of microbial resistance. A selection of promising advancements is mentioned below without aspiring a comprehensive review of all strategies in the field.

For example, many studies explored the fusion of two antibiotic drugs, so-called 'hybrid antimicrobials', which often exceeded the potency of each single component or a simple mixture, due to synergistic effects upon conjugation.^{31,32} The hybrid antibiotic, CBR-2092 (**XI**), a DNA topoisomerase and DNA-targeted RNA polymerase (RNAP) inhibitor fusion exhibited rifampin-like potency against RNAP and a balanced activity against DNA gyrase and topoisomerase IV, while retaining activity against a quinolone-resistant strain (Figure 1.5A).³³ Intercellular communication or quorum sensing (QS) is used by many bacteria to facilitate concerted action between the single cells comprising a population. As these processes have significance in agriculture, environment and healthcare, molecules with the ability to manipulate these processes in a favorable fashion have been developed. For example, *N*-butanoyl-L-homoserine lactone (BHL, **XI**) plays an important role as an autoinducer, with RhIR as the cognate receptor in *P. aeruginosa*. Thus synthetic antagonists (**X**), as shown in Figure 1.5B, have been developed and belong to the class of so-called pathoblockers or quorum sensing inhibitors (QSI).³⁴ A third strategy employs structure-guided design and component-based total synthesis of natural products to explore novel chemical space and gain scaffolds with broad-spectrum, resistance-breaking properties. This was shown in the case of Iboxamycin (IBX, **XII**) by the separate optimization of the aminooctose and amino sugar fragments, which allowed complete exploration of the acylaminopyranoside scaffold.³⁵ Even last resort antibiotics like colistin, generally avoided due to their nephron- and neurotoxicity, are revisited. Recently researchers managed to reduce the hydrophobicity, lung surfactant binding and nephric accumulation of derivative **XIII** by distinct structural changes while its retaining antimicrobial activity (Figure 1.5C).³⁶ The inactivation of antibiotics by resistance enzymes, e.g. the increased prevalence of metallo- β -lactamases (MBLs), threatens the efficacy of e.g. the carbapenems' as broad-spectrum β -lactam antibiotics in everyday clinical practice. To permit the continued use of these first-line antimicrobials, high-throughput screens and subsequent structure activity relationship (SAR) studies were conducted and yielded e.g. **XIV** (QPX7728, xeruborbactam) as stable β -lactamase inhibitors (BLI), which restored the effect of meropenem at nanomolar concentrations (Figure 1.5D).^{37, 38} Other strategies include peptide/antibody antibiotic conjugates (P/AAC), antimicrobial or cell penetrating peptides (AMP/ CPP) and phage therapy (Figure 1.5E) to combat bacterial infections. More information on these approaches is cumulated in these references.^{39, 40, 41}

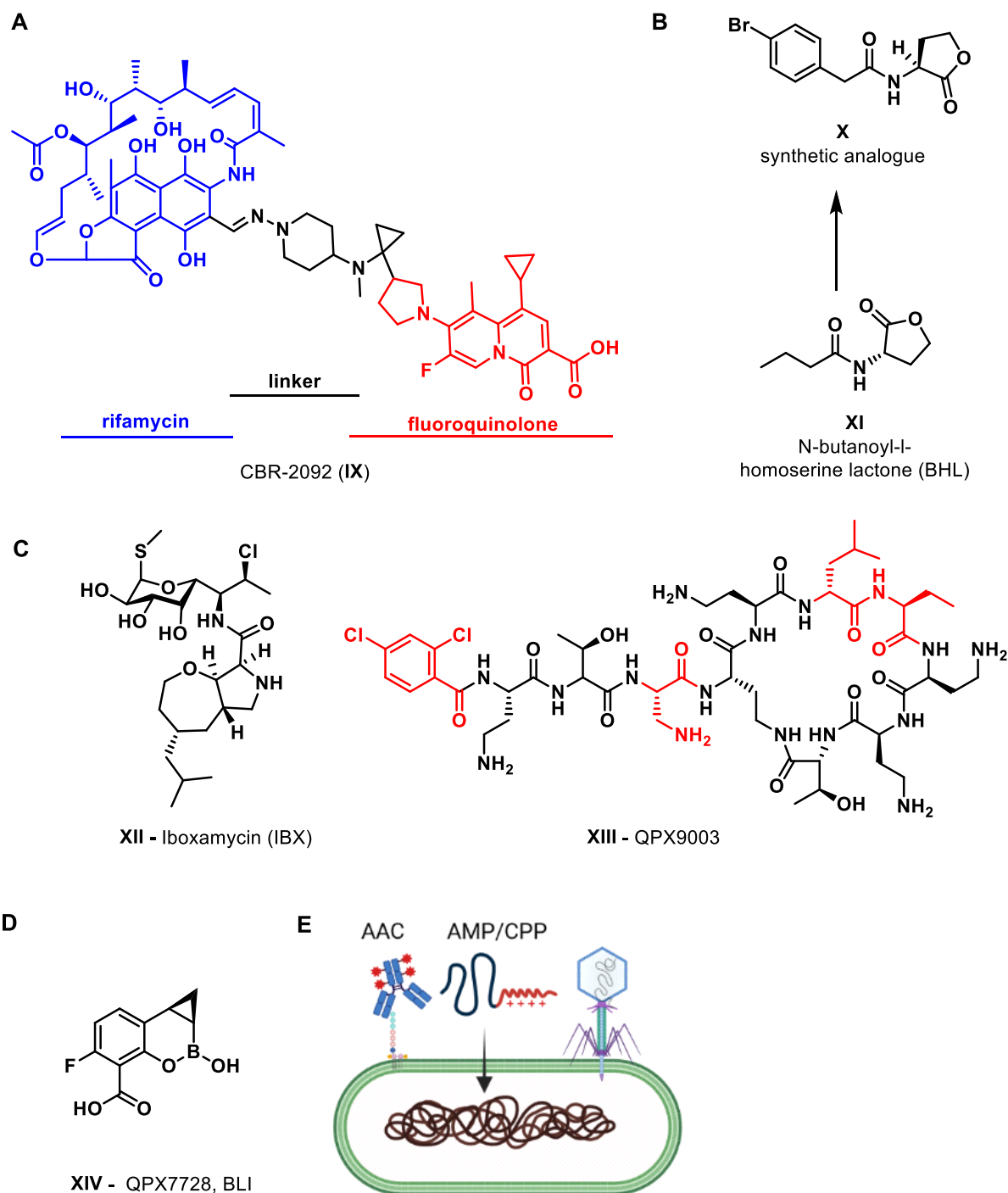


Figure 1.5. Exemplary, novel strategies to combat AMR development. (A) Hybrid antimicrobial **IX**,³³ (B) BHL-analogue **X** as a QS inhibitor (QSI) in *P. aeruginosa*,³⁴ (C) structure of 'Iboxamycin' (IBX, **XII**), a novel broad-spectrum lincosamide antibiotic,³⁵ an optimized colistin derivative **XIII** (QPX9003) with improved toxicity and retained potency *in vivo*, positions changed compared to colistin indicated in red.³⁶ (D) broad-spectrum, stable β -lactamase inhibitor **XIV** (BLIs, QPX7728), with nanomolar activities.^{37, 38} (E) Other innovative strategies use antibody antibiotic conjugate (AAC), antimicrobial peptides (AMP), cell penetrating peptides (CPP) or phage therapy to combat infections and antimicrobial resistance.^{39, 40}

1.2 The Trojan horse strategy

The impermeability of the Gram-negative cell envelope conflicts with basic cellular needs, e.g. nutrient uptake, molecule secretion for communication or defense as well as the elimination of waste products. Therefore, such functions are often performed by phospholipid bilayer-engulfed translocation systems, which can be roughly divided into (i) porins (passive diffusion), (ii) efflux pumps operating on proton motive force (PMF) and (iii) energy-dependent transport systems in the outer membrane, such as the TonB-dependent transporters (TBDT).^{42, 43, 44}

In reminiscence of the famous 'Trojan Horse', the related molecular concept exploits bacteria-specific (nutrient) acquisition transport systems that allow for an increased accumulation in the pathogens to visualize and medicate microbial infections. Among the multitude of identified transport systems, the best-studied systems include the maltose and the siderophore transport machineries. The so-called 'Trojan Horse' conjugates connect the natural substrate for a porin or TBDT to a labelling entity or an antibiotic payload. These conjugates profit from the active, energy-dependent internalization into bacteria and can enhance the activity and spectrum against Gram-negative species.^{45, 46}

1.3 Siderophores in prokaryotes and their role in infections

Ferric iron (Fe^{3+}) is a crucial micronutrient for most living organisms.⁴⁷ Elemental iron exists in the electronic configuration $[\text{Ar}]3d^64s^2$, upon oxidation to ferric iron this changes to $[\text{Ar}]3d^5$ and upon reduction to ferrous iron $[\text{Ar}]3d^6$. The ions' broad redox potential $E^\circ(\text{Fe}^{2+}/\text{Fe}^{3+}) = -0.3$ to $+0.7$ V, justifies its central role in manifold enzymatic reactions which involve an alteration of the redox state. Under physiological conditions, ferrous iron tends to oxidize to ferric iron while forming reactive oxygen species (ROS, OH^\cdot) in the presence of H_2O_2 according to the Fenton mechanism.⁴⁸ As these radicals, due to their reactivity, elicit severe tissue and cellular damage, iron remains mostly bound to proteins or co-factors to prevent oxidative harm to the organism.⁴⁹ Mammalian hosts use iron for the transport of oxygen through heme in red blood cells, generation of energy and major roles in the respiratory chain, amino acid catabolism and DNA biosynthesis.⁵⁰

Bacteria require iron for metabolic processes as an enzymatic mediator in redox reactions, to deal with oxidative stress, quorum sensing and biofilm development. The metal cation is key for the microbes to grow and exert their pathogenicity.^{51, 52} For this reason, a mammalian host ordinarily restricts iron access as low as 10^{-18} M, in order to prevent bacterial growth in the course of a microbial infection.⁵³ The pathogen has several options to sequester iron from host cells or proteins. Like a tug-of-war, the two opponents constantly attempt to prevail in this fight for iron (see Figure 1.6). First, iron is bound to transport proteins like lactoferrin or transferrin

(stage 1). Bacteria synthesize and secrete small molecule iron chelators, termed siderophores (Greek: iron carrier, <2 kDa) that strip host proteins from their bound ferric iron. The subsequent reuptake of the ferric complexes occurs *via* TBDT (stage 2).⁵⁴

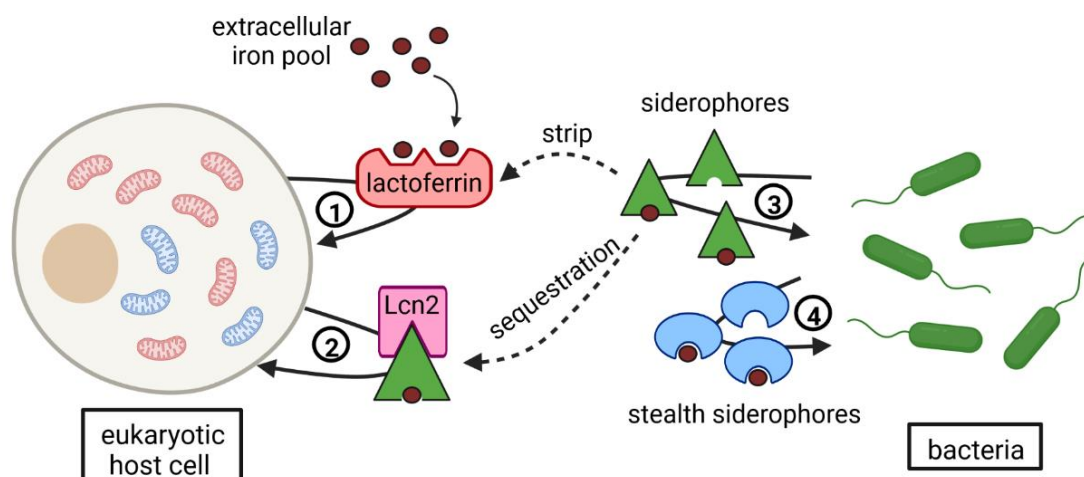


Figure 1.6. The iron tug-of-war. Competition of a eukaryotic host cell with bacteria for ferric iron. Host protein bound iron is sequestered by siderophores or high affinity siderophores. Siderophore binding proteins like lipocalin (Lcn2), prevent bacterial uptake and growth. Microbes can also produce ‘invisible siderophores’ (also called stealth siderophores) that cannot be bound by siderophore binding proteins. Adapted from literature, created with biorender.⁵⁵

In response, the host cells secrete lipocalin 2, which is stored in granules of neutrophils, as a first-line response to prevent the bacterial access to iron. Lipocalins are further upregulated through toll-like receptor (TLR) antigen binding (stage 3). The possible loss of access to ferric iron is so serious, that some pathogens have evolved stealth siderophores, which cannot be bound effectively by the siderophore binding proteins.⁵⁵ In the recent years, these ferric chelators were increasingly acknowledged for their role in bacterial virulence and as inducers for a host response by the induction of hypoxia, cytokine production and mitophagy.^{56, 57, 58}

1.4 Chemical structure, function and biosynthesis of siderophores

As bacteria require access to considerably higher iron concentrations, small molecule iron chelators are secreted to provide sufficient iron supply.⁵⁹ More than 500 siderophores, spanning a vast chemical space, have been characterized and unanimously employ a certain set of functional groups for iron complex formation e.g. α -hydroxy carboxylates, hydroxamates, phenols, catechols or combinations thereof (Figure 1.7A).⁶⁰ Most of the listed ligands are bidentate, but also combinations are known, connected through a suitable backbone, to build a hexadentate chelator. For example, the triscatecholate siderophore enterobactin (ENT, **XIX**)

of *E. coli* or its C-glycosylated analogue salmochelin S4 (**XX**) from *Salmonella*. Three major ligands found together in mixed-ligand siderophores are hydroxamates, α -hydroxy carboxylates and catecholate/phenolates as e.g. in pyoverdine (PYO, **XXI**) and pyochelin (PCH, **XXII**) from *P. aeruginosa* as well acinetobactin (**XXIII**) from *A. baumannii*.³⁹ Among these chelating moieties, the catechol has the highest affinity for Fe^{3+} due to its two adjacent *ortho*-phenolate atoms with high charge densities, which are also reflected by their pK_a values.⁶¹ Consistently, siderophores exhibit a higher affinity for ferric over ferrous iron. In nature, there are manifold, divalent cations (e.g. Cu^{2+} , Ni^{2+} , Mn^{2+} , Zn^{2+}) with crucial biological functions and thus a selective chelator for Fe^{2+} would be hard to afford.⁶² In the case of trivalent cations, the kinetically inert Co^{3+} as well as Al^{3+} and Fe^{3+} play important biological roles.⁶³ Al^{3+} can be found in soil and natural water and could compete with ferric iron for bacterial uptake through siderophore transport systems. However, due to the larger cation radius of Fe^{3+} (0.65 Å) compared to Al^{3+} (0.54 Å), most hexadentate siderophores exhibit a higher affinity for iron.⁶⁴ Moreover, the redox-mediated release of iron from its siderophore remains impossible for aluminum.⁶⁵ In sum, their chemical nature and physicochemical properties render siderophores selective for ferric iron.

Table 1.1. Redox potential of iron bound to selected siderophores. NHE = normal hydrogen electrode.

Siderophore	Chelator	$E_{1/2}$ vs. NHE redox potential [mV]
enterobactin	catechol	-750
desferrioxamine B	hydroxamate	-468
dihydroxybenzyl serine (DHBS)	catechol unstrained	-350
oxalate	acid	0
water	-	+770
bipyridyl	pyridine	+1120

The higher the affinity for Fe^{3+} , the more negative redox potential $E_{1/2}$ of the respective functionality (Table 1.1). A negative redox potential (e.g. < -450 mV) minimizes the occurrence of a redox reaction and thus the generation of tissue damaging hydroxyl radicals under physiological conditions in an aerobic environment. Catechol-based siderophores have the lowest redox potentials and hexadentate ligands have a more negative value than their bidentate counterparts (ENT vs. DHBS, Table 1). A decreased pH (an $\uparrow c(\text{H}^+)$), results in an increased $E_{1/2}$ and catechol moieties can undergo an internal redox reaction with ferric iron in an acidic milieu.⁶⁶

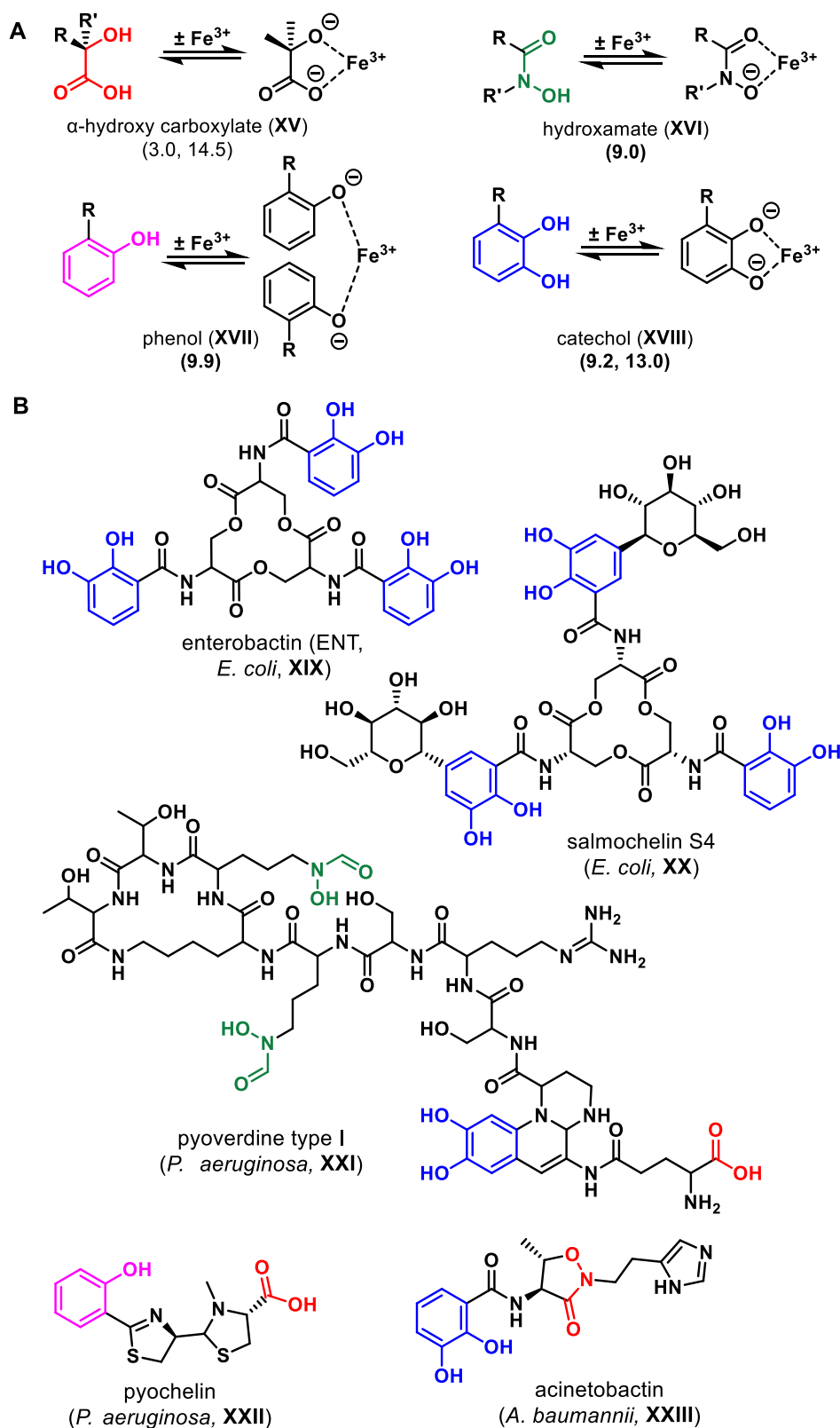


Figure 1.7. Overview on siderophore structures. (A) Widespread iron chelating functional groups, with their corresponding pK_a values in parenthesis. (B) Examples for siderophores from relevant microbial pathogens. Iron-binding groups are highlighted according to colors in (A), and their backbone is shown in black. Modified from literature.³⁹

For hexa- as well as for bidentate chelators, iron complexation is usually mononuclear, while tri- and tetradentate ligands may require multinuclear complex formation.^{67, 68} The chelators can be distinguished by their symmetry, e.g. the symmetrical catechols are found as enantiomeric pairs, while for the asymmetrical hydroxamates, geometric (same connectivity, variation in spatial arrangement) and optical isomers (enantiomers) exist. For octahedral iron complexes either a “left or right hand propeller” can be imagined, mostly restricted to the *cis* isomers due to stereochemistry (see Figure 1.8).⁶⁹

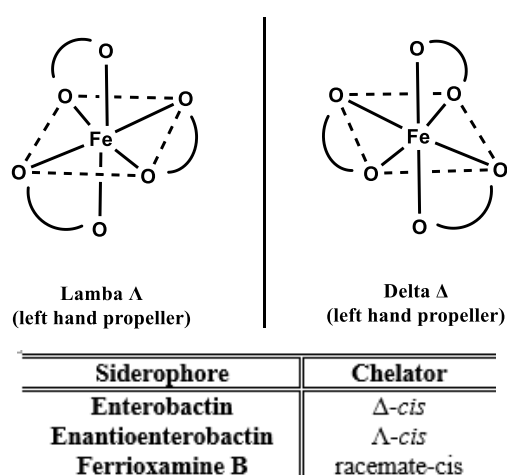


Figure 1.8. Spatial orientation of Fe-complexes. Modified from literature.⁶⁵

Bacteria, fungi and plants achieve a breathtaking siderophore structural diversity. Normally one species biosynthesizes just a fraction of siderophores, but the majority of microbes can hijack chelators secreted by other species, termed xenosiderophores, for their own iron supply.⁷⁰ The majority of siderophore classes is synthesized by non-ribosomal peptide synthetases (NRPSs), which resemble assembly lines with specialized domains that link amino acids. The synthetases structure into three domains for peptide bond formation, (i) adenylation, (ii) attachment to the peptide carrier protein and (iii) condensation. The growing polypeptide chain is passed on from one enzymatic domain to the next. Subdomains for amino acid cyclization, epimerization, methylation, reduction or oxidation exist and permit the structural diversity found in siderophore space, e.g. for the *Pseudomonas* siderophore PYO.^{71, 72} The primary siderophore ENT from *E. coli* is composed of the general building blocks serine and 2,3-dihydroxybenzoic acid (2,3-DHBA). The DHBA is afforded, similar as salicylate, by the chorismate pathway. First, chorismate is isomerized by EntC to *isochorismate* **XXV**, followed by removal of the acrylate (**XXVI**) and final aromatization by EntA, which affords the 2,3-DHBA (**XXVII**) (Figure 1.9). The assembly of the siderophore commences with the addition of serine (thioester formation) to the PCP domain of the NRPS. This is followed by a transfer of DHBA

to the amino function of serine (*N*-capping) to form DHBS units. Subsequent ester formation between several DHBS units and final ring closure yields the trilactone siderophore **XIX**, with the NRPS EntE/F, EntD and EntB.^{73, 65}

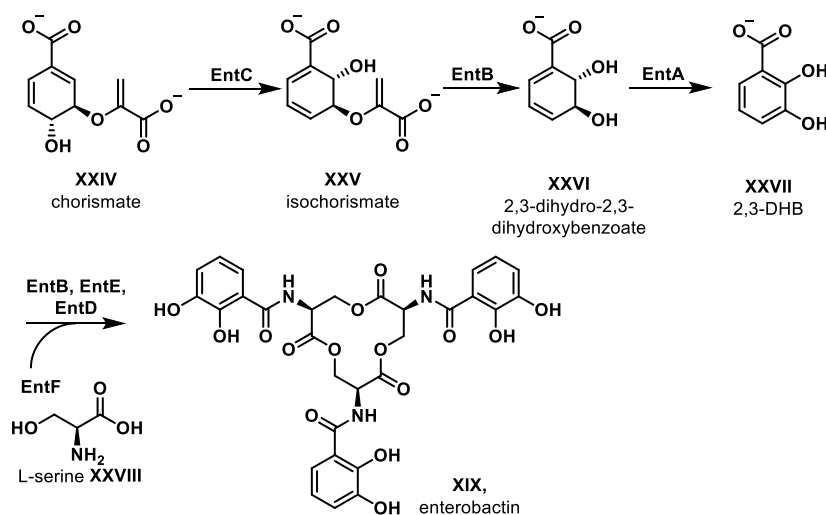


Figure 1.9. Biosynthesis of enterobactin **XIX** in *E. coli*. Modified from literature.⁶⁵

1.5 Bacterial iron acquisition systems

As siderophores, due to their charge and molecular weight, cannot be taken up by passive diffusion through porins, bacteria possess several iron transport systems. The transporter composition for the internalization of ferric chelates differs between Gram-positive and Gram-negative bacteria (Figure 1.10).⁷⁴ In Gram-negative bacteria, the interaction of ferric siderophores with chelator-specific outer membrane receptors (OMRs) induces internalization over the outer membrane into the bacterial periplasm. The energy for this uptake is provided by a transmembrane complex in the inner bacterial membrane composed of TonB and ExbB/D (*TonB* complex) in the form of proton motive force (PMF).⁷⁵ Together with the OMR these proteins form the TBDT, spanning the bacterial periplasm.^{76, 77} Exemplarily, the uptake of ferric ENT in *E. coli* is outlined: The ferric siderophore is recognized by its OMR FepA, whose structure is similar to those of porins and composed of 22 β -sheets, which are connected to an *N*-terminal plug domain that prohibits uncontrolled entry.^{74, 78} Simultaneously, the *C*-terminus of TonB, which protrudes into the periplasmic space, interacts with the TonB box, a conserved protein motif at the *N*-terminus of the OMR to promote the translocation.^{79, 80} A conformational change of the receptor and plug allows for the translocation across the outer membrane. After the transport into the periplasm, the complex is bound by a periplasmic binding protein (PBP, FepB for ENT).⁸¹

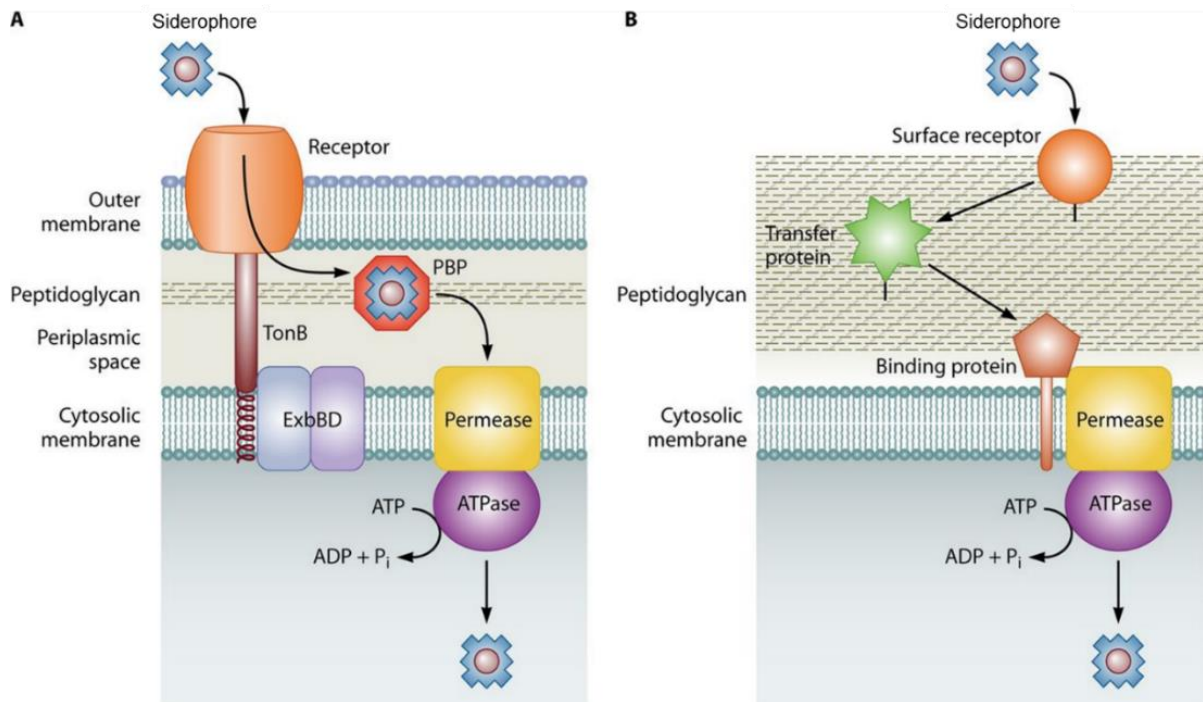


Figure 1.10. Schematic bacterial siderophore-mediated ferric iron uptake by Gram-negative and Gram-positive bacteria. PBP = periplasmic binding protein. Modified from literature.⁸²

The complex translocates into the cytosol through an ATP-dependent ABC transporter (FepC/D FepG). The ferric iron is released from the chelator via two different mechanisms below.^{83, 84, 85}

- (i) A reduction of Fe^{3+} reduces the stability of the complex, as Fe^{2+} is a softer Lewis acid than Fe^{3+} (HSAB concept) and thus leads to the dissociation of the metal.
- (ii) An enzymatic cleavage of the siderophore, e.g. the trilactone core of enterobactin, leads to a decreased affinity and denticity of the siderophore complex.

The liberated apo-siderophore is either degraded or recycled and secreted again by efflux pumps for another round of iron sequestration.⁸⁶ The efficient regulation of these uptake pathways, required for competitiveness in their respective ecological niche, is controlled at the genetic level. Sensor proteins tightly regulate OMR expression, for example through forfeit of their inhibitory effect on OMR transcription when ferric iron is absent (bacterial iron homeostasis).^{87, 88}

Gram-positive bacteria lack an additional outer membrane, but possess a cell wall composed of teichoic acid, murein and proteins that separates the cytoplasm from the extracellular space (Figure 1.10). Generally a siderophore-binding protein (SBP) interacts with the ferric siderophore and subsequently enables the active internalization by an ATP-dependent ABC transporter, permease.⁸⁹ Moreover, microbial pathogens can also accumulate ferrous iron

(Fe²⁺), the most prevalent iron oxidation state under anaerobic conditions and/or at low pH. This is complemented by the extracellular reduction of Fe³⁺ to Fe²⁺ by reductases.⁵¹ Aside ferric chelates as cargo for TBDTs, also heme, nickel complexes, carbohydrates or vitamin B₁₂ were found to be transported by TBDTs.⁹⁰ These machineries have also been parasitized by colicins and bacteriophages to enter bacteria.⁹¹ These transporters accept modifications and structural variations to an astounding degree. Generally, a successful binding to the TBDT's active site seems to promote transport. This even extends to extreme cases such as the rifamycin derivative CGP 4832, which was shown to bind the *E. coli* transporter FhuA, although its binding mode and chemical structure differ remarkably from that of the natural substrate ferrichrome or hydroxamates more generally.⁹²

1.6 Siderophores as bacterial targeting vectors

Similar to the famous 'Trojan Horse' from Homer's in his epic poem '*The Odyssey*' a properly linked payload can be efficiently translocated together with the siderophore.^{46, 59} The broad substrate tolerance of TBDTs renders siderophores attractive vehicles to enhance penetration especially into Gram-negative pathogens.

1.6.1 Natural sideromycins

Along those lines, several natural occurring siderophore antibiotic conjugates, also termed sideromycins, were discovered and characterized (Figure 1.11).⁹³ First representatives were discovered in the 1950s, namely the albomycins **XXXIII-XXXV**, which consist of a hydroxamate siderophore, a peptidase cleavable linker (blue) and a seryl-tRNA synthetase inhibitor as antibiotic (red).⁹⁴ Other well-known representatives of this family are the salmycins **XXIX-XXXII**, ferrimycin A₁ (**XXXVII**) and the microcins (**XXXVII**, MccE492(m)).³⁹ Commonly, the salmycins, but also the albomycins, exhibit their antimicrobial activity only following a payload release.⁹⁵ Both the albomycins and the salmycins, target protein biosynthesis with their antibiotic payloads.^{94, 95}

A class of structurally distinct sideromycins are produced by *Klebsiella*, *E. coli* and *Salmonella* bacteria – termed microcins.⁹⁶ These are composed of a linear peptide payload and a C-terminal salmochelin siderophore vector.⁹⁷ The uptake of this conjugate with its polypeptide payload (84 amino acids) was shown to be promoted by catechol siderophore TBDTs, for example by FepA, Fiu, CirA in *E. coli*. This illustrates that the formed pore after ferric ligand recognition must be relatively large and flexible for a broad range of substrates, and that the efficient uptake of a payload is not primarily depending on its size.⁹⁸ These conjugates impressively illustrate the potential of siderophore conjugates to enhance accumulation and

served as guidance for the development and synthesis of numerous artificial siderophore-antibiotic conjugates.

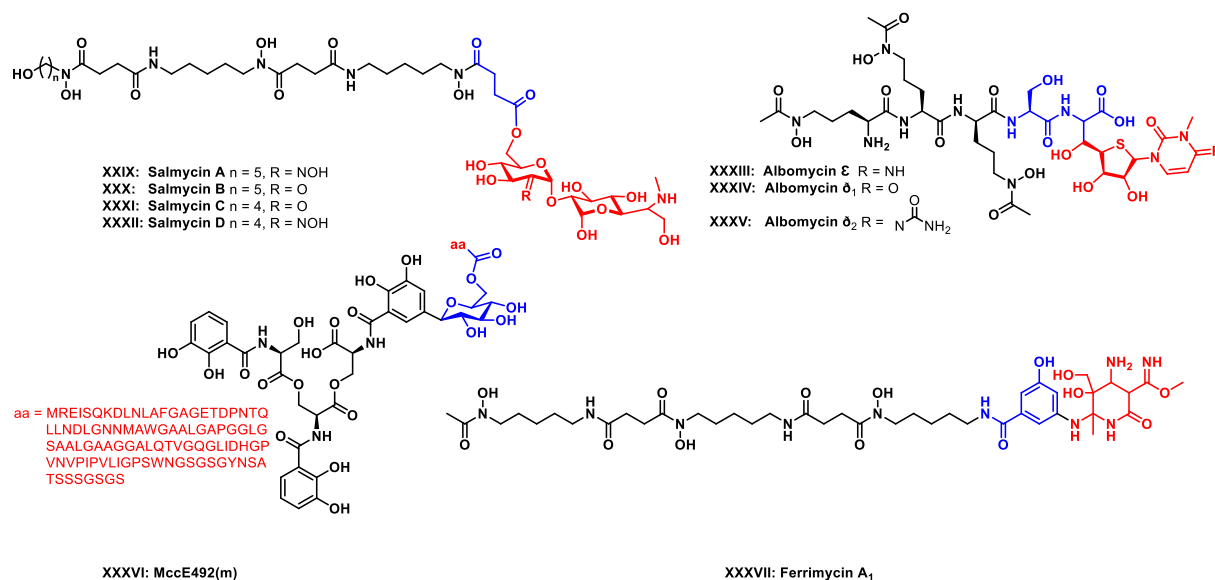


Figure 1.11. Naturally occurring sideromycins. The siderophore is shown in black, the (cleavable) linker in blue and the antibiotic payload in red. Reproduced from literature with modifications.³⁹ aa = amino acid

1.6.2 Synthetic sideromycins in pre-clinical development

Researcher used natural chelators as blueprint to design novel sideromycins with facilitated, scalable synthetic routes and improved stability while tuning their cellular and *in vivo* efficacy to extend their bacterial spectrum (Figure 1.12).⁴⁶ As the double membrane of Gram-negative bacteria restricts molecule accumulation and thus renders a big portion of antibiotics inactive, numerous research programs attempted to restore accumulation over this complex biological barrier.⁹⁹⁻¹⁰¹

The group of Marvin J. Miller pioneered a variety of approaches, e.g. with their ampicillin or daptomycin siderophore conjugates, that exhibited improved or restored activity in gammoproteobacteria (Figure 1.12A-B).^{102,103} The conjugation of the antibiotic daptomycin with lactivicin to fimsbactin yielded a mixed-ligand siderophore **XXXVIII** which had potent activity against MDR *A. baumannii* strains (Figure 1.12A).¹⁰² The same group combined a catechol siderophore with a cephalosporin linker that released the antibiotic oxazolidinone, whose activity was restored for the first time in Gram-negative bacteria (**XL**, Figure 1.12C).¹⁰⁴ The released antimicrobial could presumably penetrate the inner membrane and accumulate at the target site.^{105,106} This was also elegantly demonstrated for the conjugation of a fluoroquinolone

payload to a trimethyllock desferrioxamine combination that displayed potent activity against ESKAPE pathogens (**XLI**, Figure 1.12D).¹⁰⁷ An innovative enterobactin ciprofloxacin conjugate **XLII** by Nolan and coworkers relied on the IroD-mediated hydrolysis of the trilactone siderophore in the bacterial cytoplasm with potent activity against uropathogenic *E. coli* (UPEC). This work also highlighted the potential of leveraging pathogen-specific enzymes to develop a narrow-spectrum antibiotic strategy (Figure 1.12E).^{108, 109}

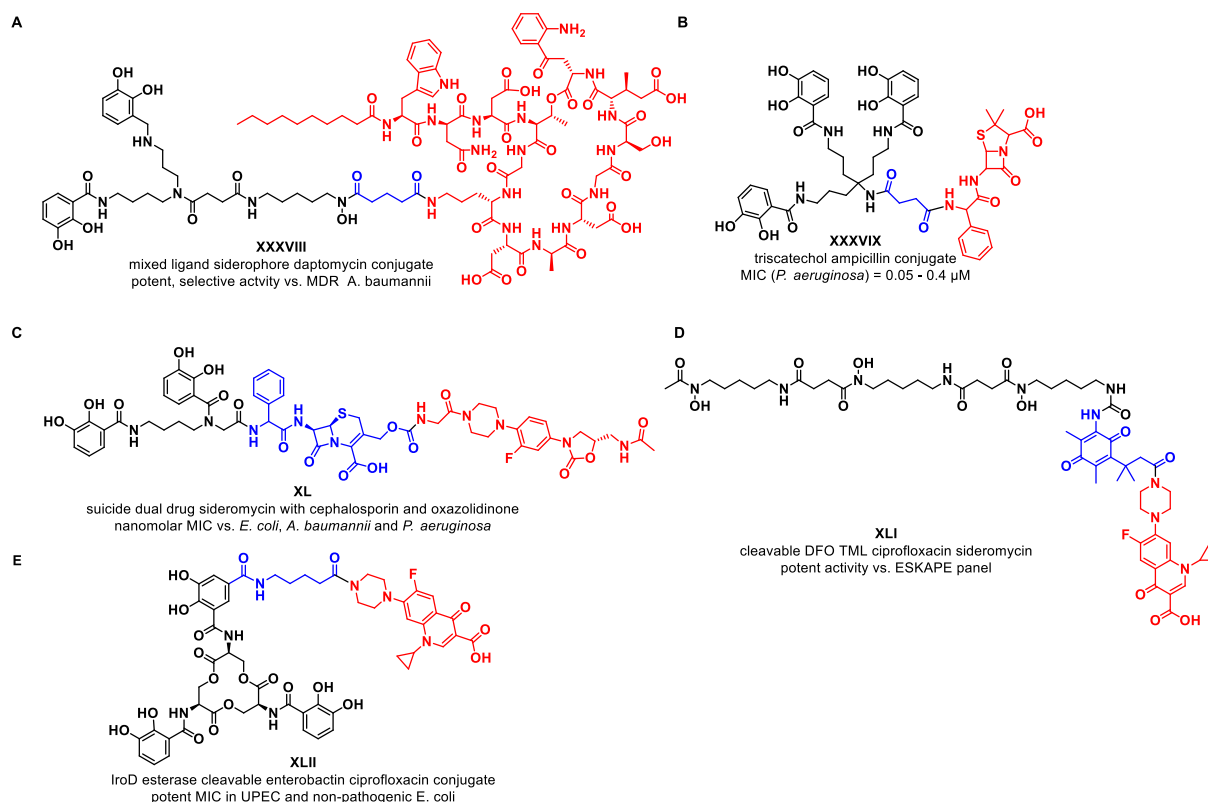


Figure 1.12. Synthetic siderophore drug conjugates. (Molecules from Miller and coworkers include mixed ligand daptomycin conjugate (A),¹⁰³ triscatechol β -lactam conjugate (B)^{102, 110} dual suicide cephalosporin oxazolidinone conjugate (C)¹⁰⁴ and desferrioxamine (DFO) trimethyllock (TML) ciprofloxacin conjugate (D).^{107, 111} (E) Salmochelins-inspired, IroD-cleavable enterobactin ciprofloxacin conjugate from Nolan and coworkers.^{108, 109} Siderophores in black, linker (if applicable) in blue and antibacterial drug in red.

1.6.3 Synthetic sideromycins in clinical utilization

The pharmaceutical industry was also interested in exploiting siderophores as molecular Trojan Horses mainly to enhance the activity of existing drugs. Pfizer explored monocyclic β -lactams coupled via heterocyclic linkers to hydroxypyridones, such as **XLIII** (Figure 1.17A).¹¹² However, disadvantageous pharmacodynamics and clinical results showed a rapidly attenuated efficacy through resistance development by loss of the siderophore receptors CirA/Fiu (*E. coli*) and PiuA/PirA (*P. aeruginosa*).^{113, 114} The monosulfactam **XLIV**, by Basilea,

originates from tigemonam and is fused to dihydroxypyridone, a bioisoster of a catechol unit, which was also shown to complex ferric iron (see Figure 1.17B).^{115, 116} While the compound was shown to be imported actively into bacteria, its efficacy remained relatively unaffected by efflux.¹¹⁷

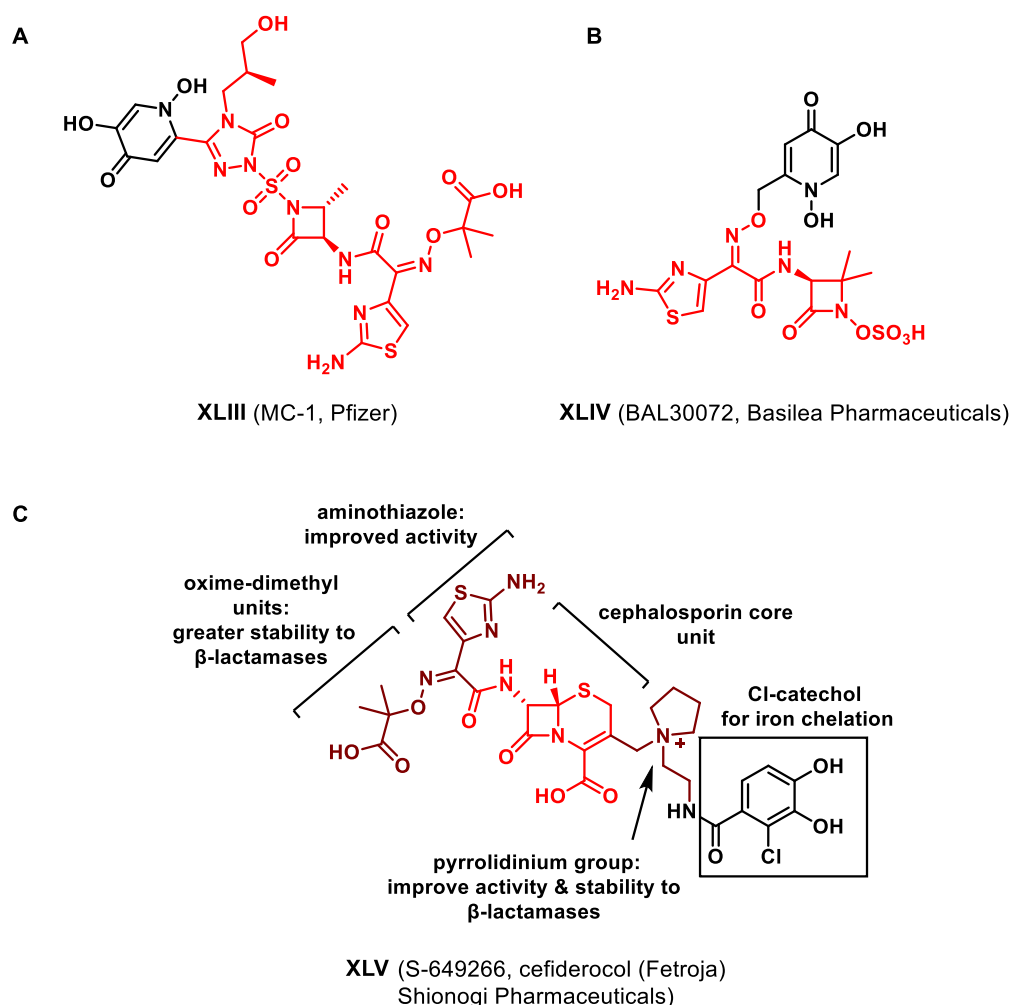


Figure 1.13. Chemical structure of antimicrobial sideromycins in clinical development. (A) Structure of **XLIII** from Pfizer.¹¹² (B) Structure of **XLIV** from Basilea.^{115, 116} (C) Structure of **XLV** (S-649266, cefiderocol, trade name Fetroja®) by Shionogi™. Depicted are the siderophore unit (black), the central cephalosporin nucleus antibiotic (red), residues and modifications enhancing antibiotic activity and/or stability to β -lactamases (brown). Information from literature.¹¹⁸

The synthetic sideromycin successfully passed a phase one trial and exhibited higher efficacy than well-established antibiotic competitors as aztreonam and rifampicin against *Acinetobacter spp.* and MDR *P. aeruginosa* strains (4-8 $\mu\text{g/ml}$ vs >32 $\mu\text{g/ml}$ for meropenem).^{116, 119} Cefiderocol **XLV** (S-649266, trade name: Fetroja®, Figure 1.17C), represents the only newly approved antibiotic with a novel mode of action and embodies the biggest success in the area

of siderophore antibiotic conjugates.^{120, 121, 122} It consists of a cephalosporin core (red, residues of ceftazidime and cefepime) with a pyrrolidinium group, connected to a chloro catechol for uptake via bacterial siderophore receptors.^{123, 124} After active transport into bacteria, the cephalosporin payload acts against the bacterial cell wall synthesis.¹²⁵ Fetroja® showed potent activity versus Gram-negative bacteria, improved stability against β -lactamase hydrolysis, including carbapenemases, and received approval in 2019 in the US and in Europe in 2020 for the treatment of uncomplicated urinary tract infections, for severe pneumonia and other indications.¹²⁶

1.6.4 Bacterial imaging and infection monitoring

With regard to bacterial imaging, several groups have developed siderophore fluorophore conjugates for the labelling of bacteria, e.g. the salmochelin conjugates by Lee et al.¹²⁷ A synthetically challenging linker attachment to the trilactone backbone of enterobactin was developed recently by the group of Klahn and co-workers.¹¹⁰ This linkage reduced interference with ferric iron complexation, as their payload was pointed away from the catechols. Their fluorophore conjugates restored bacterial growth and labelled siderophore-deficient, Gram-negative bacterial mutants. In contrast to Miller's enterobactin analogue (Figure 1.12B), their compounds did not exhibit any cytotoxic effects on human HepG2 cells.¹¹⁰ Despite their specificity, fluorophores typically lead to unspecific binding to membranes, require an external excitation light source and thus show a higher background signal compared to a chemiluminescent detection mode.¹²⁸ For the clinical diagnosis and detection of bacterial infections, traditionally approaches like microscopy, microbiology, but also PCR and mass spectrometry are employed. However, these methods require clinical samples (e.g. blood, urine or cerebrospinal fluid). This material needs to be obtained by repeated, invasive sampling procedures, may not reflect the biological dynamics of infections at deep body sites and if so, only provide a single time point.¹²⁹ In consequence, for a definite diagnosis tissue samples are required that can only be obtained by surgical procedures or biopsies, which additionally increase patient suffering. These methods are prone to sampling errors and contamination, not mentioning the difficulties to culture (anaerobic) unknown pathogens from this material *ex vivo*.¹³⁰ For these reasons, sophisticated imaging techniques such as ultrasonography, computed tomography (CT) or magnetic resonance imaging (MRI) are applied additionally. These all rely on unspecific, anatomic changes that occur in progressed stages of the infection and additionally are observed for several, unrelated diseases (e.g. inflammation, infection, cancer).¹³¹ More sensitive, nuclear imaging techniques e.g. with 2-¹⁸F-fluorodeoxyglucose (¹⁸F-FDG) for positron emission tomography (PET), are minimally invasive but enrich non-specifically at sites in the organism with high metabolic activity.¹³²

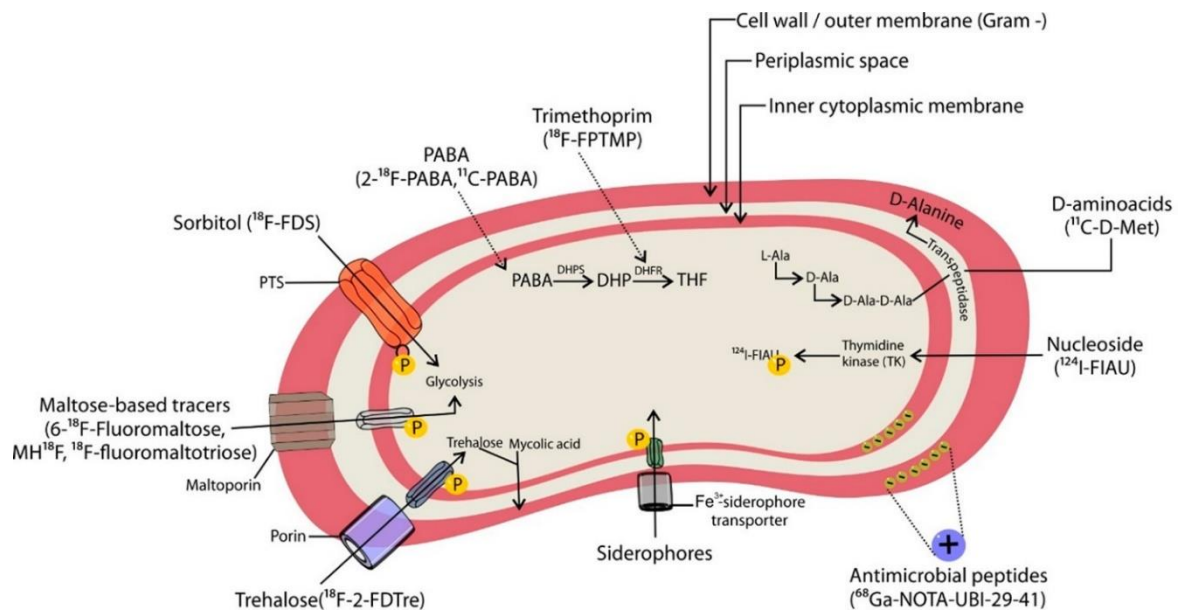


Figure 1.14 Targets for bacterial infection-specific PET/SPECT tracers. PTS = phosphotransferase system; DHPS = dihydropteroate synthetase; DHP = dihydrofolic acid; THF= tetrahydrofolic acid. Taken from Mota et al.¹³³

Multiple studies have centered on the development and evaluation of whole-body, non-invasive molecular imaging tracers that can specifically localize infection sites, and give a measure of the disease extent simultaneously.¹³³ PET and single-photon emission tomography (SPECT) have been used extensively in neurology and oncology, and harbor a comparable potential for infections. Together with CT or MRI as an anatomical reference method, these technologies allow for the dynamic monitoring and detection of the tracer accumulation at the site of infection.¹³³ First, the tracer selection was focused more on antibiotics as obvious molecular entities that are highly specific, well characterized *in vivo* but also disable or kill bacteria at high concentrations. The majority of radioactively labelled antimicrobials thus are not ideal tracer candidates, except their accumulation in microbes is much higher than in the eukaryotic cells of the host organism.¹³⁴ As a consequence, research turned towards unique pathogen processes like unique bacterial uptake and metabolic pathways, e.g. carbohydrate, folate and iron transport systems.^{135, 136} Some of these approaches are summarized in Figure 1.13.

Ferric iron sequestration by siderophores has been exploited by for bacteria-specific imaging. However, many siderophores like pyoverdine were found to be specific to particular species or subcategories of microbes, which limits their applicability for the detection of an infection with an unknown pathogen in everyday clinical practice.¹³⁷ Like ferric iron, Ga³⁺ is also triply

charged, possesses a comparable ion radius as high-spin Fe^{3+} , has similar coordinating preferences and thus forms stable complexes with many siderophores.¹³³ Siderophore transporters also cannot distinguish Fe^{3+} from Ga^{3+} complexes, and thus siderophores have been labelled with the PET isotope gallium-68 (^{68}Ga , half-life = 67.7 min, β^+ 88.9%, $E_{\text{max}} = 1899$ keV).¹³⁸ The γ -emitting ^{67}Ga (half-life = 78 h) is a SPECT isotope and also has found application in infection imaging.¹³⁹ Among recent examples [^{68}Ga]-pyoverdine tracer for the *in vivo* imaging of *P. aeruginosa* infections and a [^{68}Ga]-DFO tracer that accumulated in cellular assays and *in vivo* in a broad spectrum of prokaryotes.^{137, 140}

1.6.3.1 Dioxetanes as chemiluminescent reporters for biological applications

Advances in fluorescent technologies permitted the imaging of processes inside bacteria, animals and plants.¹⁴¹ However, fluorophore-based concepts rely on an external excitation light source that causes problems such as fluorophore-bleaching, photo-induced toxicity and unspecific physiological reactions due to the probe, which make the long-term live imaging in whole organisms challenging.^{128, 142} In contrast, chemi- and bioluminescent strategies, like the luciferin-luciferase system, essentially couple the transformation of a chemical entity (i.e. oxidation of luciferin) with the emission of light and thus do not require an external light source. In the context of biological systems, this prevents photo-induced damage or autofluorescence due to biomacromolecules.¹⁴³ The electronic processes leading to fluorescence and luminescence emission are summarized in Figure 1.15.¹⁴⁴

Despite these advantages, luminescence imaging has not been widely employed for biological applications due to compatibility issues with biological environments (toxicity) or due to quenching under aqueous conditions. Moreover, a luminescence signal can be absorbed by a fluorophore with a complementary excitation wavelength in a process termed 'Förster resonance energy transfer' (FRET), which has been employed to increase the quantum yield (Φ_{CL}) and intensity of luminescent systems.¹⁴³

In the 1960s, 1,2-dioxetanes were found to be the unstable intermediates in fireflies on the route to light emission. In 1968, the first stable dioxetane derivative was synthesized by Canadian scientists at the University of Alberta, as a solution in benzene whose decomposition after gentle heating led to the emission of blue light.¹⁴⁵ Nearly 20 years later, in 1987, Paul A. Schaap managed to afford the first stable, synthetic dioxetanes. These had an analyte-responsive protecting group (PG - e.g. phosphate, ester), which masked the phenol moiety of the probe.

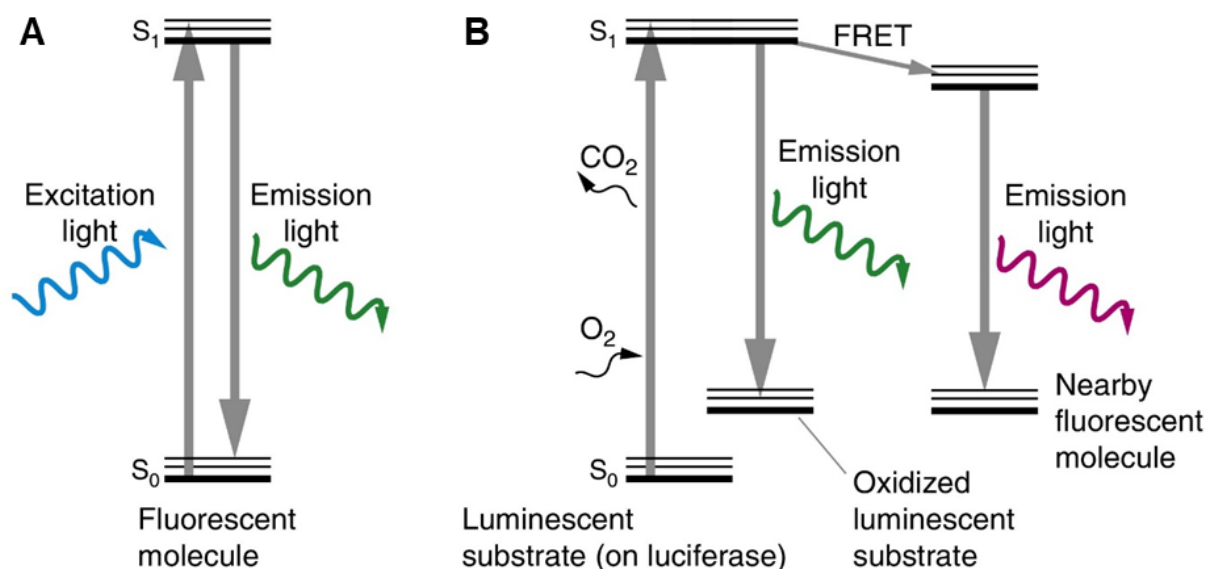
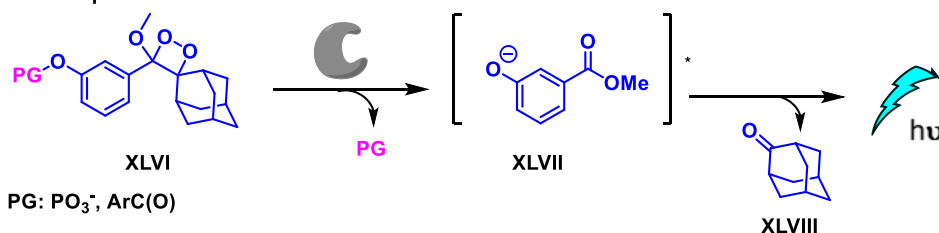


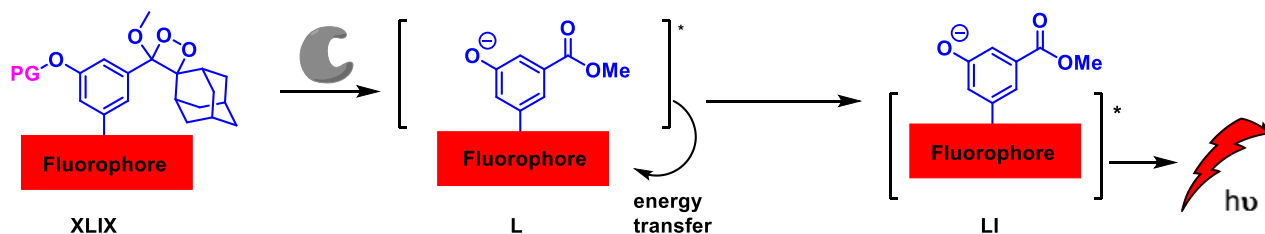
Figure 1.15. Jablonski diagram comparing fluorescence and chemiluminescence light emissive processes. **(A)** The fluorophore is excited from the ground state (S_0) with an appropriate excitation light source and reaches its excited state S_1 . The spontaneous decay back to the ground state under the emission of light is termed fluorescence. **(B)** The S_0 - S_1 transition of a luminescent substrate (e.g. luciferin - luciferase system) occurs during the enzymatic oxidation (also: a chemical reaction) to an unstable, cyclic intermediate which, following decomposition, yields an excited intermediate (S_1). This excited derivative decays back to its ground state under the emission of light. A nearby fluorescent molecule, with an excitation wavelength in the emitted light spectrum, can be excited by this emission in a process termed 'Förster resonance energy transfer' (FRET). This principle was used to amplify the signal of luminophores. Modified from Saito et al.¹⁴⁴

Chemical or enzymatic removal of this PG leads to the formation of an unstable, structurally distinct phenolate species, which decomposes through a chemiexcitation process (S_1 state) back to its ground state. This happens under the emission of a blue photon (chemical/enzymatic initiated electron exchange luminescence, C/E-IEEL) yielding the corresponding benzoate ester and adamantanone (Figure 1.16A).^{146, 147} Advantageously, no additional oxidation step is required in order to initiate light emission, which means that the probe can be applied to a wide range of chemical and biological problems.¹⁴⁸ In 2017, Shabat and coworkers adapted the dioxetane structure and either attached a fluorophore (FRET based enhancement) or an electron withdrawing group (EWG). Both alterations dramatically increased Φ_{CL} and enabled the development of remarkably efficient emitters under physiological conditions (Figure 1.16B and C).¹⁴⁹ This novel class of luminophores has been derivatised and subsequently applied for the visualization of manifold disease-associated processes *in vitro* and *in vivo*.^{150, 149, 151, 152}

A: Schaap's dioxetanes



B: FRET to enhance quantum yield



C: EWG to enhance quantum yield

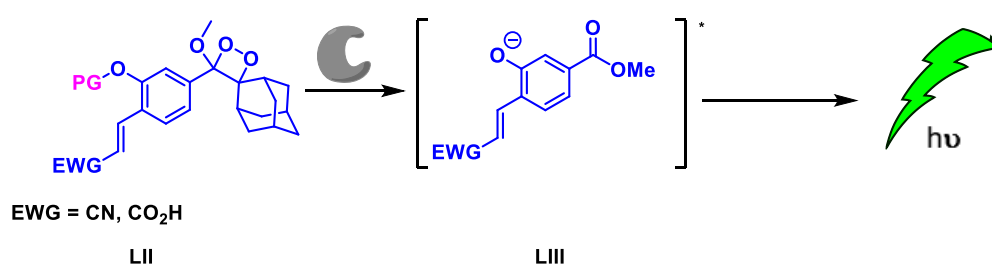


Figure 1.16. Development of brightly emissive dioxetanes in aqueous environments. (A) Schaap's dioxetanes. (B) Fluorophore conjugated dioxetanes to enhance chemiluminescence through FRET. (C) Electron-withdrawing group (EWG) modified dioxetanes with enhanced chemiluminescence. PG = protecting group, $h\nu$ = photon emission. Protecting group in pink, phenoxy dioxetane in blue. Modified from literature.^{153, 149}

A scheme depicting the mechanism for the light emission associated decomposition of excited phenoxy dioxetanes is depicted in Figure 1.17.¹⁵⁴ After a single electron transfer (SET) from the excited phenolate to the 1,2-dioxetane, heterologous bond cleavage of the O-O bond occurs, leading to **LVa** or **LVb**. After an intra- or intermolecular back electron transfer (BET), this yields the above mentioned benzoate ester **XLVII**. A more rapid chemiexcitation (\uparrow photons / period of time) reduces quenching, increases Φ_{CL} and thus improves the probe's signal to background (S/B) ratio and sensitivity.¹⁵² These advances also resulted in bright probes for the detection of *Mycobacterium tuberculosis*, *Listeria*, *Salmonella* and for the bacterial resistance enzymes carbapenemases and β -lactamases.^{155, 156, 157, 158} The development of broad spectrum dioxetane probes for Gram-negative and Gram-positive bacteria, which are not based on the presence of (secreted) resistance enzymes, was prohibited by the double-layered bacterial cell wall, acting as a tight biological barrier.¹⁵⁸

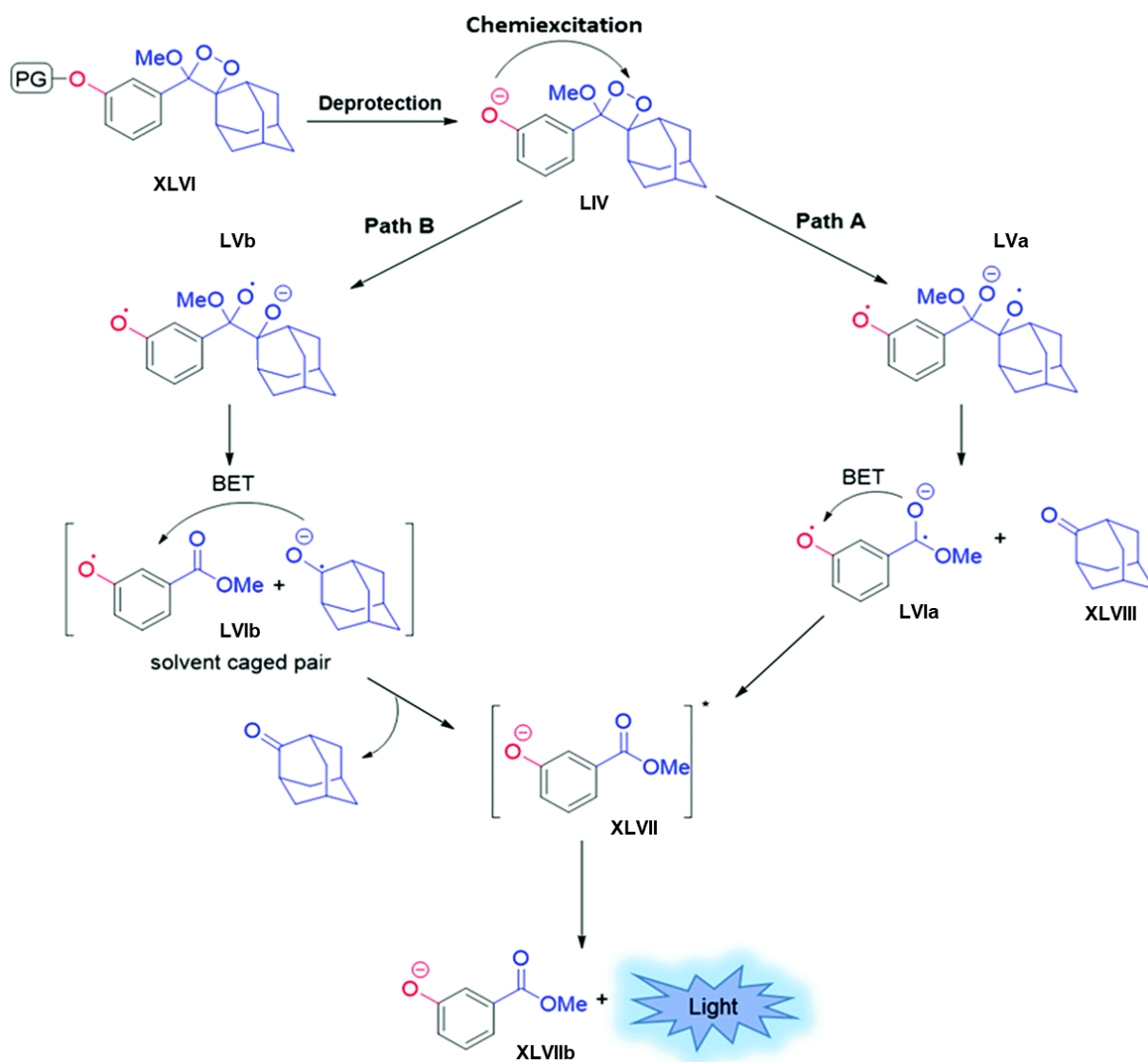


Figure 1.17. Proposed mechanism of 1,2-dioxetane **LIV** decomposition and light emission. Modified from literature.¹⁵⁴ PG = protecting group, BET = back electron transfer.

1.6.5 The DOTAM and MECAM siderophores

The usage of natural siderophores as targeting vectors for bacterial imaging and therapy is partially impeded due to the complicated synthetic access (scalability), the chemical lability of the vectors themselves and for some by the limited spectrum of targeted microorganisms.^{159, 160, 161, 137} Serendipitously, microbes also rely on so-called 'xenosiderophores', which are siderophores from other organisms and synthetic mimics, to satisfy their demand for ferric iron.¹⁶² A novel, bacteria-specific vector should either possess a narrow spectrum accumulation into previously untargeted, important pathogens or into as many bacterial species as possible. Moreover, the synthetic disconnections and procedures should be easily executable and scalable. In order to compete with their natural counterparts for ferric iron (e.g. enterobactin $K_a = 10^{52} \text{ M}^{-1}$)¹⁶³ the synthetic mimics as well as their conjugates should bind the metal cation with similar affinity.¹⁰⁶ In 2017, K. Ferreira et al. developed a stable and scalable enterobactin analogue, termed DOTAM siderophore (1,4,7,10-tetraazacyclododecane-1,4,7,10-tetraacetamide) for bacterial imaging and antibacterial therapy.¹⁶⁴ The chemical structures of ENT **XIX** and the DOTAM siderophore **LVII** are shown in Figure 1.18.

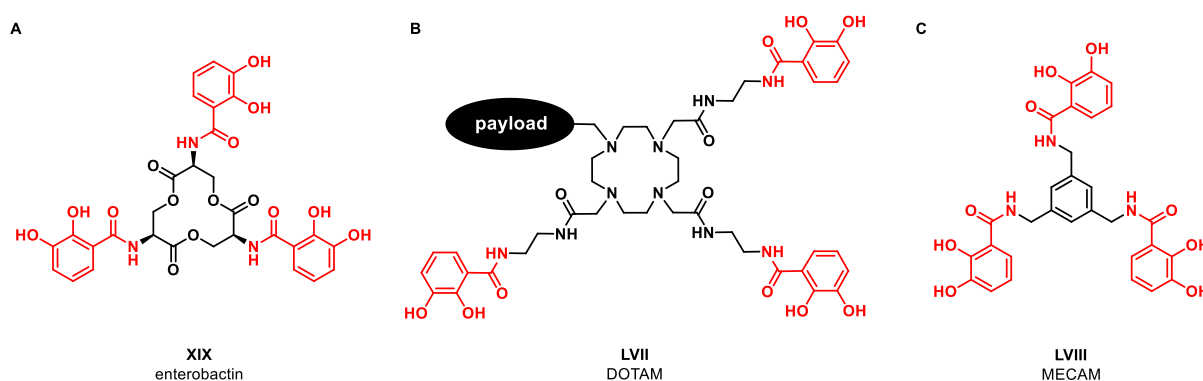


Figure 1.18. Structures of (A) enterobactin **XIX** (B) triscatecholate DOTAM **LVII** and (C) MECAM **LVIII** siderophores. Backbone of the respective chelator in black and chelator moieties in red.^{73, 164, 165}

Enterobactin consists of a serine trilactone core, which is equipped with three catechol chelators.⁷³ For the DOTAM siderophore analogue **LVII** the backbone is replaced by a tetradentate cyclen unit, which itself can host di- and trivalent cations. The cyclen gives rise to three arms, connected through ethylene diamine spacers, to terminal catechol functionalities, and a fourth arm for payload conjugation.^{166, 167} A summary of relevant DOTAM siderophores and conjugates by K. Ferreira et al is shown in Figure 1.19. A growth recovery assay in siderophore-deficient *E. coli* ΔentA and *P. aeruginosa* $\Delta\text{pvd}/\Delta\text{pch}$ mutants confirmed acceptance of the synthetic DOTAM siderophores as a xenosiderophore, which restored

bacterial growth under iron-limited conditions. A fluorescent bodipy DOTAM conjugate **LXIII** successfully illuminated bacteria from the ESKAPE panel in fluorescence-activated cell sorting (FACS) and fluorescence microscopy experiments. The cyanin 5.5 DOTAM conjugate **LXX** even detected a subcutaneous *P. aeruginosa* infection in a mouse model under iron-depleted conditions, while a DOTA-based control without catechols failed to accumulate at the site of infection. In sum, these results qualify DOTAM-based siderophores as effective, broad-spectrum targeting vectors for the delivery of diagnostic or antibiotic payloads into pathogenic bacteria.

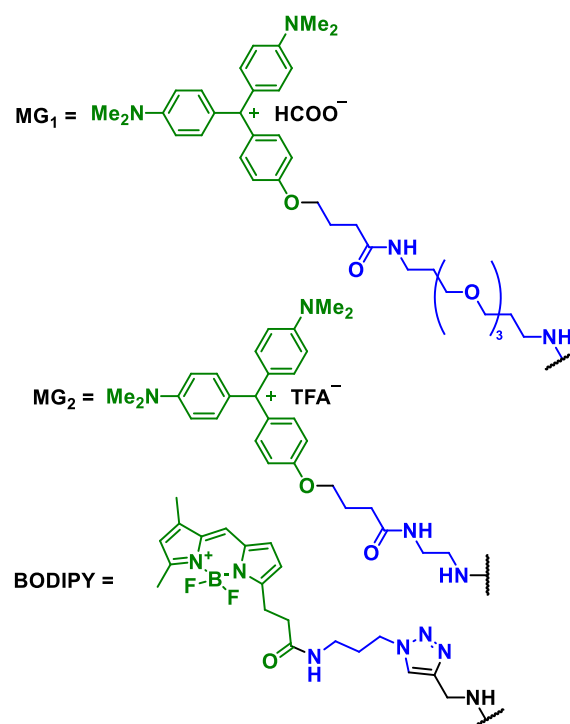
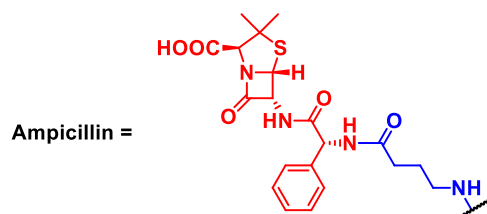
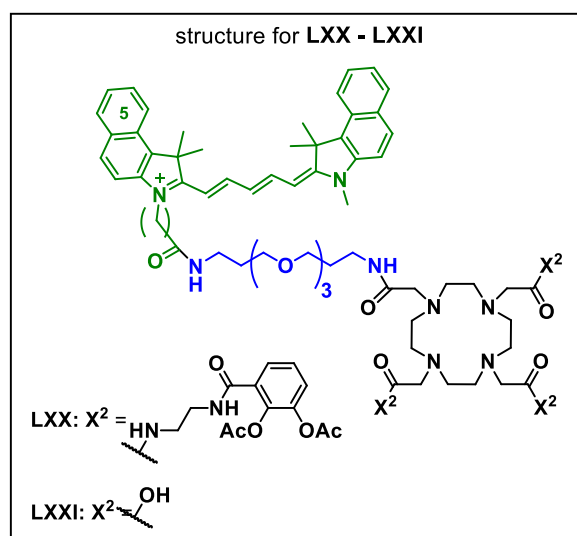
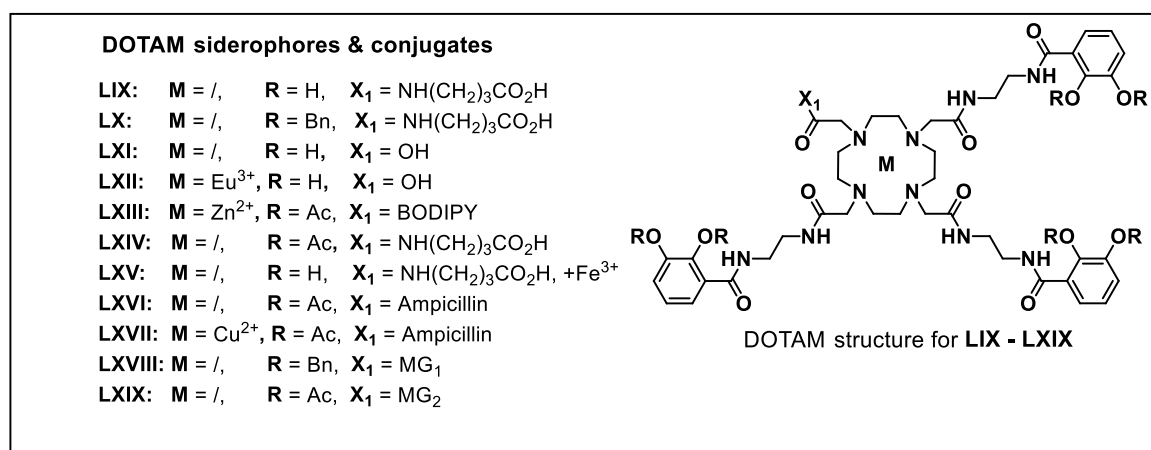


Figure 1.19. DOTAM siderophore mimetics **LIX-LXIX** and conjugates **LXX-LXXI** structures from K. Ferreira et al. Siderophore displayed in black, linkers in blue, fluorophores in green and antibiotics are highlighted in red. Adapted from literature.¹⁶⁴

Another noteworthy enterobactin analogue is the MECAM siderophore **LVII** (1,3,5-*N,N,N'*-tris-(2,3-dihydroxybenzoyl)-triaminomethylbenzene, Figure 1.18C), which forms very tight ferric complexes ($K_a = 10^{46} \text{ M}^{-1}$).^{65, 168, 105} The slightly decreased affinity is due to the parallel orientation of the catechols to the central benzene ring, in contrast to an orthogonal pre-orientation in the case of enterobactin due to the chirality of the α -amino groups.^{65,165}

1.6.6 Bioorthogonal labeling methods

The advances in bioorthogonal chemistry in the recent years have expanded the chemical toolbox to allow for efficient, controllable chemistry in aqueous, biological environments without affecting biomacromolecules or major interference with cellular processes.^{169, 170} These reactions have been applied, due to their high efficacy and specificity, widely for the synthesis of highly functionalized conjugates in the area of medicinal chemistry and life sciences.¹⁷¹ Two conjugation principles, relevant to this thesis, will be mentioned briefly below.

A team around the chemist Huisgen introduced the “1,3-dipolar cycloaddition reaction”, however this novel chemical transformation suffered from long reaction times, required high temperatures ($\geq 100 \text{ }^\circ\text{C}$) and isomer formation.¹⁷² This was resolved by the discovery of Meldal, Fokin and Sharpless in 2001, who used catalytic amounts of Cu(I) to chemoselectively react alkyne and azide moieties (copper-catalyzed azide alkyne cycloaddition – CuAAC). This yielded a drastically increased reaction rate and regioselectivity towards 1,4-substituted 1,2,3-triazoles, working for most substrates at ambient temperature in the presence of a variety of other functional groups in high yields.^{173 174} In 2004, a team around Carolyn Bertozzi realized that the strain-promoted azide-alkyne cycloaddition (SPAAC) can serve as a highly adaptable replacement for CuAAC, as no cytotoxic copper salts are needed (see Figure 1.20A).¹⁷⁵ Underlying reason for SPAAC is the decreasing stability of cycloalkynes with decreasing ring size. Actually their stability directly correlates with the C–C \equiv C–C angle, which, due to the cyclic structure, is unable to reach the optimal 180° for sp-hybridized carbon atoms.¹⁷⁶ Cyclooctyne was shown to be the smallest isolatable cycloalkyne, still with a significant deviation of its angle from linear (163°).¹⁷⁷ The resulting ring strain is responsible for the unique reactivity profile of medium-sized cycloalkynes, which can be exploited for strain-promoted reactions.¹⁷⁸ The logic behind the rapid and uncatalysed [3+2] addition of cycloalkynes with azides is based on the highly favorable enthalpic release of ring-strain. DFT calculations suggest that the transition from the highly strained single ring to a double ring system with better bond angles for the sp² carbon atoms of the formed triazole seems to be the driving force of SPAAC.^{178, 179}

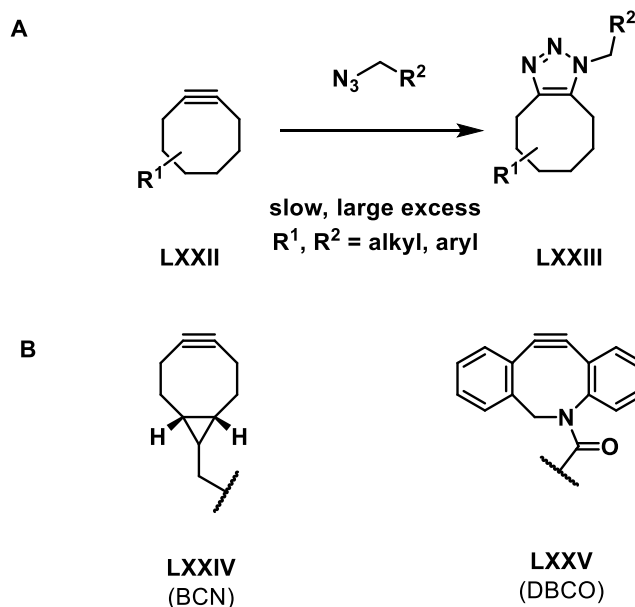


Figure 1.20. Strain-promoted [3+2] cycloadditions. (A) Original reaction by Bertozzi et al. (B) Improved, strained cyclooctynes with broad usage for biological and chemical challenges, namely BCN = (1R,8S)-9-(13-methyl)bicyclo[6.1.0]non-4-yne **LXXIV** and dibenzylcyclooctyne **LXXV**.¹⁷⁶

However, the rather slow reaction kinetics required immense excesses of reagents, long reaction times and still lead to comparably low yields, even less efficient than the traceless Staudinger-Bertozzi ligation.^{176, 180} This was resolved by the development of substituted cyclooctynes with increased ring strain and thus an increased reaction rate. Generally, two classes of cyclooctynes that are widely applied for a range of problems, can be distinguished: the aliphatic cyclooctynes (e.g. BCN) and the (di) benzyl cyclooctynes (e.g. DBCO -see Figure 1.20B). For **LXXIV**, the increased reactivity is induced by a fusion of cyclooctyne to an even more strained cyclopropane. In the case of **LXXV** and related building blocks, the enhanced reactivity is caused due to the increased ring strain conferred by the sp^2 -hybridized carbons.¹⁸¹ These inventions have made SPAAC one of the most reliable and often employed tools of chemical biologists.¹⁷¹

1.6.7 Cleavable linker systems

Conjugates for the diagnosis or therapy of bacterial infections generally consist of three parts: a targeting entity (carrier) connected via a suitable linker system (covalent or cleavable) to an effector (antibiotic or label). Numerous targeting entities, including peptides,⁴¹ carbohydrates,¹⁸² antibodies¹⁸³ and also siderophores,⁸¹ have been employed for the selective enrichment at the infection herd and/or within the bacterial pathogens. It has been observed that the steric hindrance of a substantially larger carrier unit can interfere with target binding

and thus with probe activation or antibiotic efficacy (Figure 1.21). Many carriers were shown to mainly accumulate in the bacterial periplasm without significant further transport into the cytosol of bacteria. Especially for payloads with cytoplasmic targets, the translocation over the second bacterial membrane, needs to be considered to restore activity. Thus a periplasmic, enzymatic release of the bound effector by a cleavable linker system may enable the autonomous translocation of the released payload over this membrane into the cytosol.

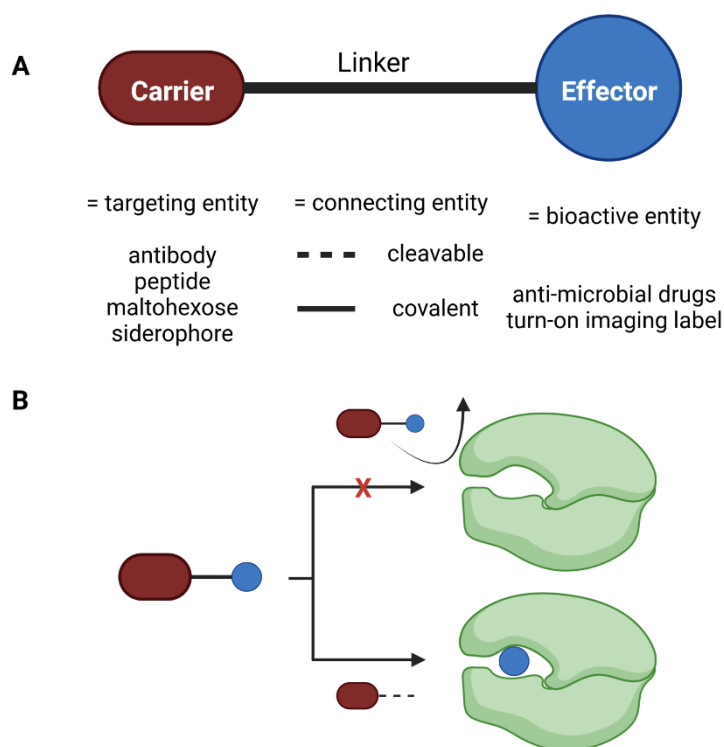


Figure 1.21. The necessity of cleavable linkers. (A) Employment of covalent or cleavable linkers for targeted conjugates. (B) Steric hindrance of high molecular weight carriers can impede target binding and decrease efficacy. A controlled release of a bound payload can restore the ability to bind the respective target. Therefore, a controlled release or activation of payload, after a specific 'environmental stimulus' based on a specific trigger/inducer combination is central to the area of targeted conjugates to allow for a selective activity solely at the target site, created with biorender.^{184, 185}

But daptomycin and β -lactam siderophore conjugates, with periplasmic sites of action, were not shown to require a controlled release.^{103, 186} On the contrary, sideromycins with much smaller effectors such as ciprofloxacin acting on gyrase, a cytoplasmic target, require cleavable linkers for a retained activity.^{109,107} For the successful employment of these prodrug strategies it is important to minimize adverse systemic effects (e.g. through linker instability) and attempt to enhance the pharmacokinetic properties of the respective compounds.¹⁸⁷

Broadly used, chemically accessible and highly versatile molecular release systems include disulfide linkers and the “trimethyl lock” (TML) system.

Disulfides can be afforded by the so-called thiol-disulfide exchange reaction, basically a reaction of a thiol with another thiol. A nucleophilic thiol attacks the disulfide bond, resulting in the formation of a new disulfide bond, which can occur reversibly, as long as both reaction partners are not hindered by steric or electronic effects (Figure 1.22A).¹⁸⁸ The introduction of a leaving group (e.g. pyridyl disulfide, **LXXVII**) can shift this equilibrium to the side of the product. This unit reacts with free thiols under basic conditions under the formation of a stable disulfide bond and stable pyridine-2-thiol as the driver of the reaction (see Figure 1.22B).

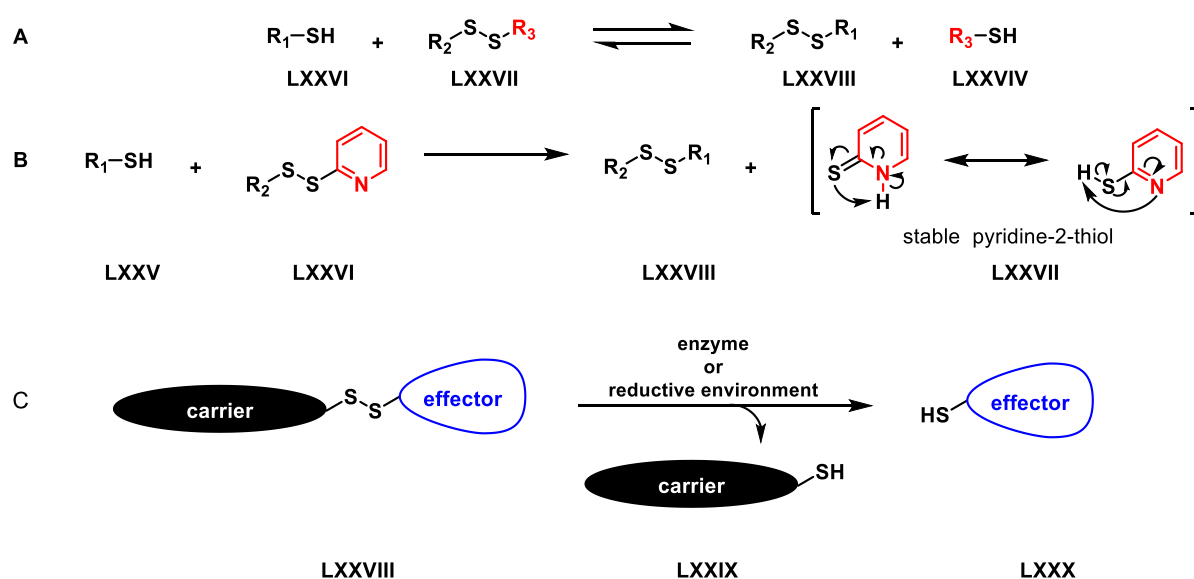


Figure 1.22. Thiol-disulfide exchange reaction. The ordinary thiol-disulfide exchange reaction is an equilibrium. (B) Thiol-pyridyl-disulfide permits the formation of stable pyridine-2-thiol as a good leaving group and driver of the reaction to the product side.¹⁸⁸ (C) Release of disulfide conjugated payload from carrier either by reducing enzymes or reducing agents (e.g. tris(2-carboxyethyl)phosphine - TCEP).

This reaction is also termed “pyridyl disulfide reaction” and characteristically has good yields as well as bioorthogonal reactivity under mild reaction conditions (pH 7.4, ambient temperature).^{189, 190} Disulfides are relatively stable, but reducing agents and reductive cellular environments can lead to their cleavage. In prokaryotes, but also in higher organisms, enzymatic processes can catalyze their cleavage, e.g. by thioredoxin or glutaredoxin-like enzymes.^{190, 191} This enzymatic release permits the usage of disulfides for the controlled release of the payloads from targeted conjugates. In particular, a carrier bound to its payload via a disulfide ensures accumulation at the site of action. Then the disulfide is cleaved, the payload released and able to interact with its cellular target with a reduced steric repulsion than for a non-cleavable linkage (Figure 1.22C).

In contrast, the TML is based on the sterically-driven lactonization of the trimethyl-substituted *o*-hydroxy dihydrocinnamic acid derivatives (Figure 1.23) to release ester, amide and thioester bound payloads.¹⁹² This linker has been modified regarding its chemical and enzymatically inducible triggers for diverse applications in cellular imaging, drug design and smart material development.¹⁹³ The term ‘trimethyl lock’ originates from the three interfering methyl groups that drive the fast cyclization to the corresponding lactone. Accordingly, the lactonization kinetics increase, with an increasing number of methyl substituents in the linker structure and can even surpass the reaction velocity of enzymes.¹⁹⁴ This swift reaction rate is ascribed to two effects working hand in hand:

- (i) the ‘stereo population control’ (steric locking through the three methyl moieties into a specific conformer)^{194, 195}
- (ii) the imminent release of ground state strain upon lactonization caused by a so-called ‘Thorpe-Ingold effect’ (e.g. between the geminal methyl and the aromatic methyl group)¹⁹⁶

Energy calculations with a force field model,¹⁹⁷ as well as crystal structure-based examinations support the above stated hypothesis.¹⁹⁸ Entropic and enthalpic contributions also have been suggested to impact the rate of lactone formation.¹⁹⁹ The immediate cyclization can be prevented by the protection of the phenolic moiety of **LXXXIV** with esters or ethers (alkyl, phosphate, *p*-nitro benzyl, as shown in Figure 1.23 (bottom left). Or by oxidation of the dihydroquinone **LXXXV** moiety to the corresponding benzoquinone **LXXXV**. Typically the synthesis of phenolic TML linkers commences from 3,5-dimethylphenol or 2,6-dimethylbenzene-1,4-diol and has originally been developed by Cohen, Borchardt and Carpino.^{194, 200, 201} Respective phenolic trigger moieties or benzoquinones have been designed to be responsive to certain chemical, enzymatic or photochemical stimuli and allow the controlled release of a coupled payload. Corresponding phosphate or alkyl ester modified TML systems conjugated to a DFO siderophore with ciprofloxacin as an antimicrobial payload have been synthesized by Miller and colleagues. These conjugates exhibited comparable growth inhibition zones to the unconjugated drug in Gram-negative and Gram-positive bacteria.²⁰² Recently, Otaka and co-workers developed a stimuli responsive amino acid version of the phenol trimethyl lock **LXXXIII** that cleaved peptides and proteins with UV and reduction triggerable groups (e.g. *o/p*-nitrobenzyl, Z (left) = *NH-R*).^{203, 204, 205} Similarly, Miller et al developed an amino benzoquinone TML (Z (right) = *NH-R*) and designed a ciprofloxacin TML DFO sideromycin, that was presumably cleaved by bacterial quinone oxidoreductases to exhibit comparable antibacterial activity.^{107, 206}

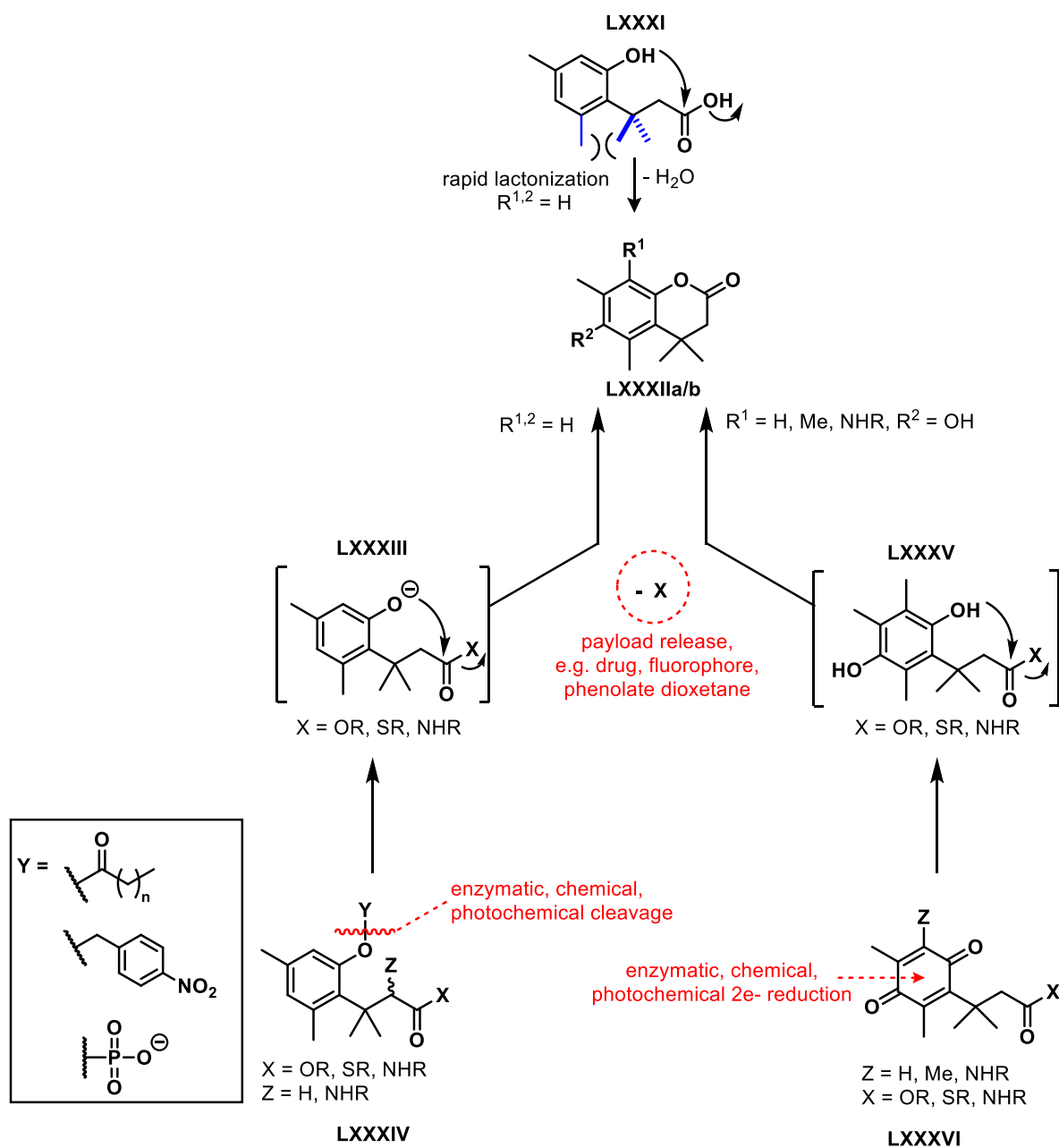


Figure 1.23. Principle of trimethyl lock linker systems. X = payload (e.g. drug, fluorophore, dioxetane), Y = trigger group (e.g. alkyl ester, p-nitro benzyl, phosphate), Z = NH-R (left side) furnishes amino acid like TML for the incorporation into peptides or conjugates, developed by Otaka et al. Z = NH (right side) yields amino TML by Miller et al.²⁰² Modified from literature.¹⁹³

2. Aims of the Thesis

The principal aim of this thesis was to explore the potential of artificial siderophores as molecular Trojan Horses for the cellular and *in vivo* visualization and treatment of MDR bacterial pathogens (Figure 2.1).

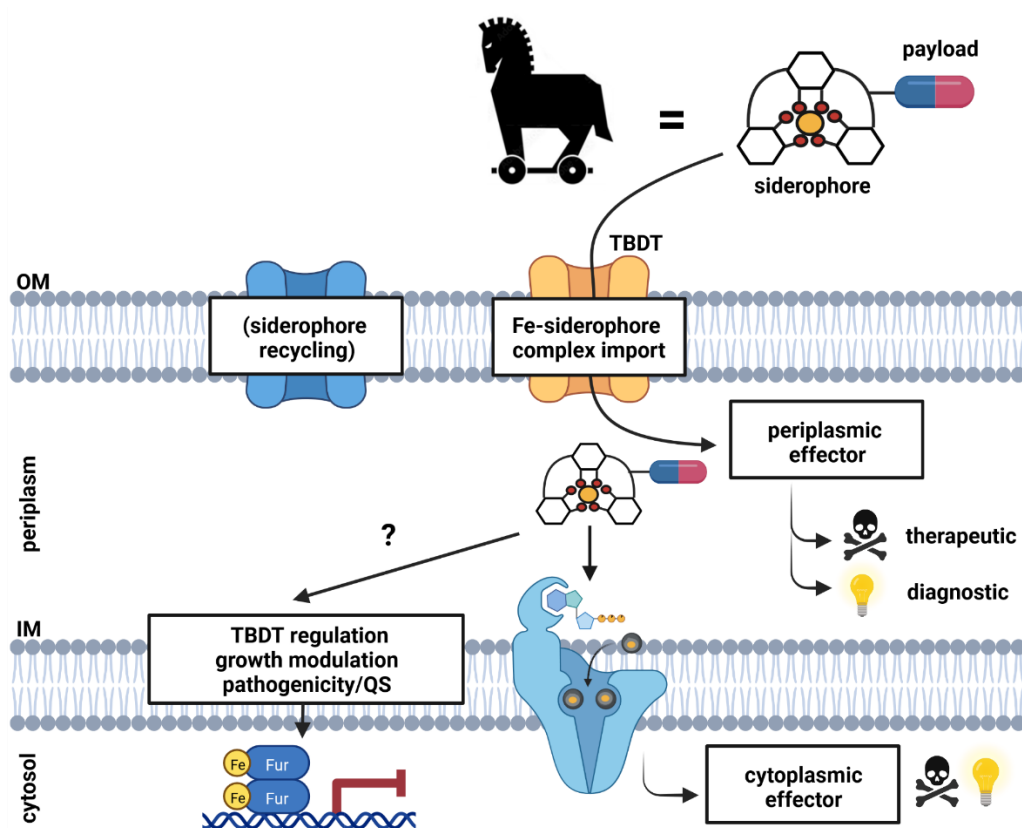


Figure 2.1. Overview of siderophores as molecular ‘Trojan Horses’ for the diagnosis and treatment of bacterial infections in the scope of this thesis. Created with biorender.

As outlined in the introduction, there are several highly innovative siderophore-based diagnostics and therapeutics. However, unanswered mechanistic questions regarding linker activation, subcellular accumulation in the bacteria and phenotypic adaptation of the bacteria following conjugate treatment leave a lot of room for the improvement of synthetic sideromycins. In this thesis, known siderophore scaffolds shall be modified with covalent or cleavable linker systems attached to imaging labels or potent natural product effectors to yield sideromycins for the visualization and treatment of infections with MDR bacterial pathogens. *In vitro*, *in cellular* and *in vivo* experiments shall examine the conjugates iron delivery capability, bacterial specificity, accumulation properties but also assess their antimicrobial properties and molecular mechanism in Gram-positive and Gram-negative bacterial pathogens.

In particular, the following aspects will be addressed:

- a) There is limited evidence on the uptake mechanism(s) of natural siderophores, and even less for artificial ones. The Thesis should contribute to the elucidation of uptake mechanisms, and also the bacterial response towards exposure with siderophores and sideromycins.
- b) The ability to image bacteria with fluorescent siderophore conjugates has been demonstrated before. A goal of this work will be to extend the applicability of such conjugates for diagnostic purposes by enhancing their sensitivity; chemiluminescence was proposed as a potential technical solution for this.
- c) In order to translate imaging probes to applications in larger animals (including humans), a catecholate-based PET probe will be developed.
- d) For therapeutic purposes, the well-established arsenal of β -lactam effectors will be expanded to potent antibiotics that have not been used in antibacterial conjugates so far. This includes RNAP inhibitors, for example.
- e) In order to obtain potent effectors as outlined in d) it might be necessary to develop cleavable linker chemistry for siderophore conjugation.

3. Publication 1: Optimization of artificial siderophores as ^{68}Ga -complexed PET tracers for *in vivo* imaging of bacterial infections

This chapter has been published as a peer-reviewed article in a scientific journal:

Carsten Peukert*, Laura N. B. Langer*, Sophie M. Wegener, Anna Tutov, Jens P. Bankstahl, Bianka Karge, Frank M. Bengel, Tobias L. Ross*, and Mark Brönstrup.

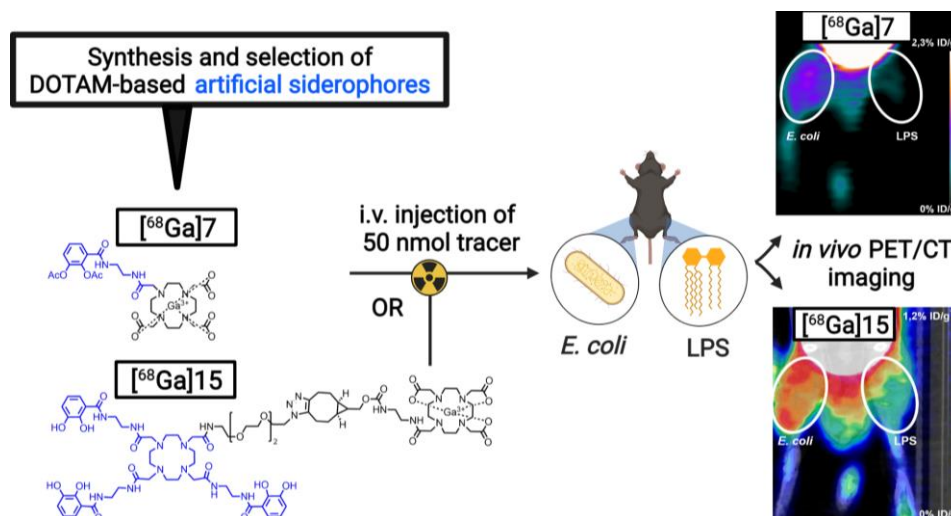
„Optimization of artificial siderophores as ^{68}Ga -Complexed PET tracers for *in vivo* imaging of bacterial infections”.

Journal of Medicinal Chemistry, **2021**, 64, 16, 12359-12378.

DOI: 10.1021/acs.jmedchem.1c01054

* these authors contributed equally

Table of content graphic



Abstract

The diagnosis of bacterial infections at deep body sites benefits from noninvasive imaging of molecular probes that can be traced by positron emission tomography (PET). We specifically labeled bacteria by targeting their iron transport system with artificial siderophores. The cyclen-based probes contain different binding sites for iron and the PET nuclide gallium-68. A panel of 11 siderophores with different binding sites for iron and the PET nuclide gallium-68 was synthesized in up to 8 steps, and candidates with the best siderophore potential were selected by a growth recovery assay. The probes $[^{68}\text{Ga}]7$ and $[^{68}\text{Ga}]15$ were found to be suitable for PET imaging based on their radiochemical yield, radiochemical purity, and complex stability *in vitro* and *in vivo*. Both showed significant uptake in mice infected with *Escherichia coli* and were able to discern infection from lipopolysaccharide-triggered, sterile inflammation. The study qualifies cyclen-based artificial siderophores as readily accessible scaffolds for the *in vivo* imaging of bacteria.

3.1 Introduction

Infections with pathogenic bacteria are a cause of high morbidity and mortality and therefore constitute a major threat for human health.¹ This situation is exacerbated by the rise of antimicrobial resistance, rendering established treatments ineffective, while the pipeline of novel, resistance-breaking antibiotics remains thin.^{2,3} Today's diagnosis of bacterial infections is based on clinical symptoms and the analysis of biofluids, typically blood or urine, using microbiological, genetic and mass spectrometric techniques. However, the analysis of biofluids struggles to detect early-stage infections at deep body sites (e.g. heart, brain, or medical implants) that are hardly accessible for sampling. For such cases, non-invasive imaging techniques with molecular probes that localize bacterial infections bear the potential to improve diagnostic capabilities significantly, as outlined by recent reviews in this and other journals.^{4,5} ⁶ In fact, infection imaging of vulnerable patient populations (e.g. following cancer chemotherapy or organ transplantation) has already become clinical practice, and it is mostly based on the detection of [¹⁸F]fluorodeoxyglucose (FDG) by positron emission tomography (PET). Because FDG is taken up by all metabolically active cells, the tracer has low specificity and cannot distinguish between sterile inflammation and infection.^{7,8} Therefore, some alternative approaches to identify bacteria-specific PET tracers have been pursued recently. For example, white blood cells (WBC) or antibodies could be labelled with ⁶⁷Ga, ^{99m}Tc or ¹¹¹In and have been successfully applied in the imaging of osteomyelitis or prosthetic joint infections.⁹ One strategy is to employ ¹⁸F-labeled carbohydrates that are internalized by transporters not expressed in eukaryotes.¹⁰⁻¹⁹ Also, essential bacterial metabolites have been converted to radioactive imaging probes.²⁰ In a different approach, antibiotic drugs or human antimicrobial defense peptides served as the scaffold for PET-probes.²¹⁻²⁴ Recently, D-[5-¹¹C]Glutamine could specifically discriminate live *E. coli* and MRSA in dual-infection murine myositis model versus sterile inflammation caused by heat-killed bacteria.²⁵

A third strategy, pursued in this study, is to utilize the active iron transport systems of bacteria for a selective and pronounced uptake of the probe. To cover their continued demand for iron ions, bacteria synthesize small molecular weight iron-chelators, so-called siderophores (*greek: sidero = iron, phoros = carrier*), that are secreted to the environment and actively internalized by bacterial outer membrane receptors, once loaded with iron.^{26,27, 28} Because Ga³⁺ ions exhibit similar coordination properties as Fe³⁺ ions, siderophore-based imaging probes have been proposed, which are loaded with the positron emitter gallium-68 instead of iron.⁴ First *in vivo* studies have been conducted to image the fungus *Aspergillus fumigatus* with [⁶⁸Ga]triacetyl fusarine and ferrioxamine derivatives,^{29, 30} or *Pseudomonas aeruginosa* with gallium-68 complexed pyoverdine.³¹ Lately, a ⁶⁸Ga-labelled version of the clinically used antidote desferrioxamine Desferal ®, DFO-B) has been repurposed in an acute murine myositis model to image Gram-positive and Gram-negative bacteria *in vivo*.³² Of note, siderophores have been

widely employed as Trojan Horses, transporting a broad range of payloads efficiently into bacterial cells.³³ The success of this concept has been underlined by the approval of the first siderophore-coupled antibiotic cefiderocol (Fetroja®) in 2019.^{34, 35} While the above mentioned studies use the iron binding site of a natural siderophore to incorporate the PET-tracer, we envisaged to (i) design bifunctional compounds with two separate binding sites for iron and the radionuclide and to (ii) employ a non-natural siderophore analog that is potentially accepted by a broad range of bacteria. This decoupling of tracer binding and uptake allows to optimize both functions independently. In a previous study, we have qualified artificial siderophores based on the cyclen scaffold as suited to accommodate two metals, label a broad range of bacteria, and detect infections in mice using optical imaging with tagged fluorophores.³⁶ While our previous probes were confined to cellular and small animal imaging, the current study reports a crucial step towards translation of the probes, i.e. their optimization to PET tracers for the imaging of large species including humans.

3.2 Results and discussion

We aimed to use the versatile cyclen scaffold to attach catecholate units for Fe³⁺ chelation and at the same time complex a Ga³⁺ ion via the cyclen core itself as a PET imaging tracer. In our original design,³⁶ cyclen was functionalized to a tetrapodal 1,4,7,10-tetraazacyclododecane-1,4,7,10-tetraacetic amide (DOTAM) to accommodate the metal for imaging.³⁷ However, the reaction times for Ga³⁺ incorporation were in the range of hours, which is incompatible with radiochemical synthesis and positron emitter half-lives. Because the rates of metal incorporation are much higher for 1,4,7,10-tetraazacyclododecane-1,4,7,10-tetraacetic acid (DOTA)-based cores with free carboxylic acid moieties,³⁸ we systematically varied the number of amide-linked catechols (for Fe-complexation) vs. number of carboxylates (for Ga-complexation) from 1:3 to 2:2 to 3:1 (Figure 3.1). In addition, the use of one DOTA and one DOTAM core that are conjugated to each other would enable an optimal 3:3 constellation (gallium-68 complexing acid to iron-complexing catechol units). In order to facilitate Ga-complex formation from DOTAM moieties, α -methyl substituents, which should exert a Thorpe-Ingold effect and reduce the bite angle at the cyclen core, were introduced as well.³⁹ The catechol units, representing bidentate iron binders, were partly masked as acetylated prodrugs, which are activated in the cellular environment, in order to prevent permanent inactivation of the catechol by enzymatic alkylation and to facilitate ⁶⁸Ga-complex formation.⁴⁰ ⁴¹ Starting from cyclen, we made use of optimized reaction conditions, which can yield each a specific substitution pattern, from a mono- to a tri-substituted core respectively (Figure 3.2).

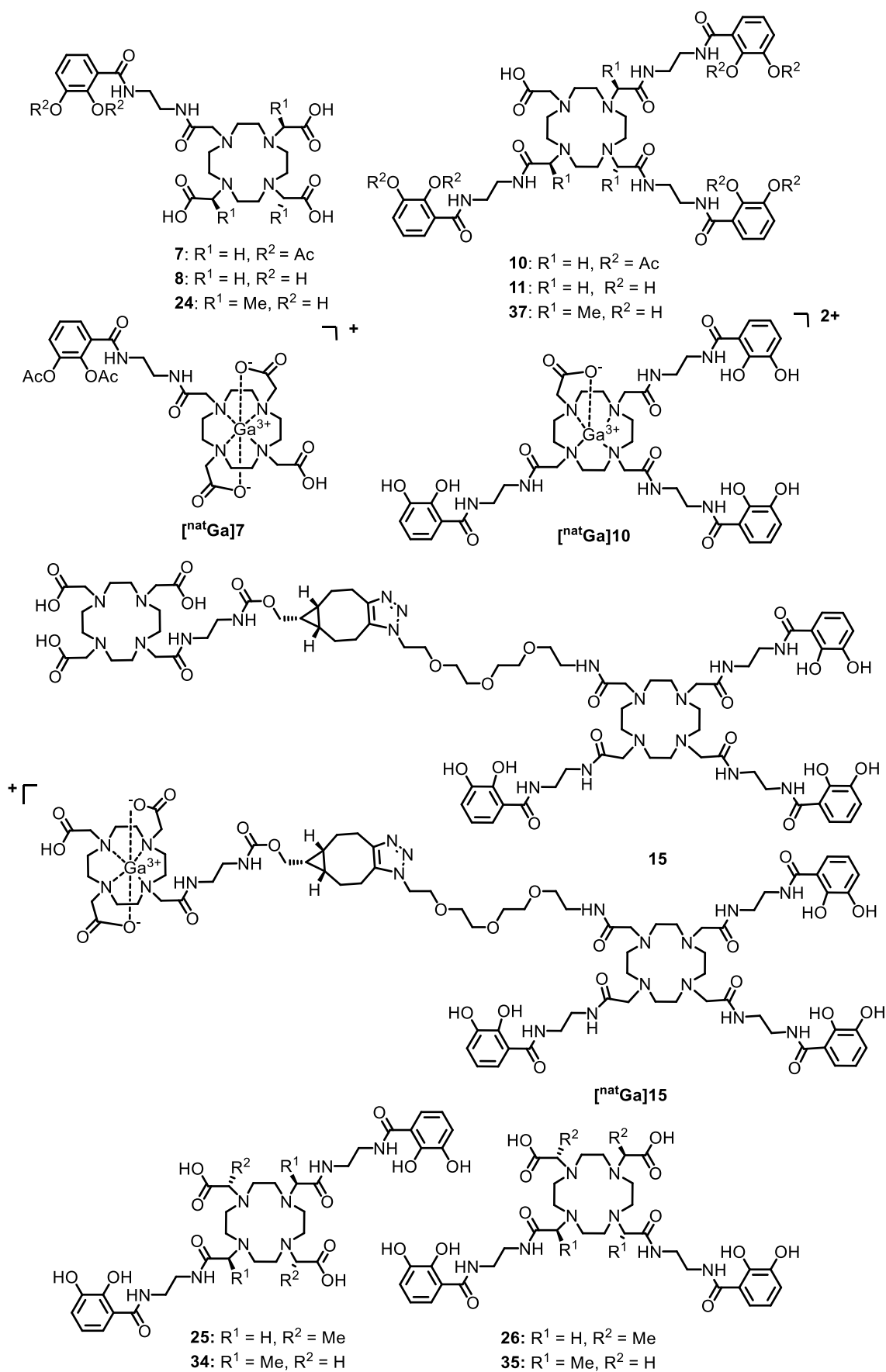


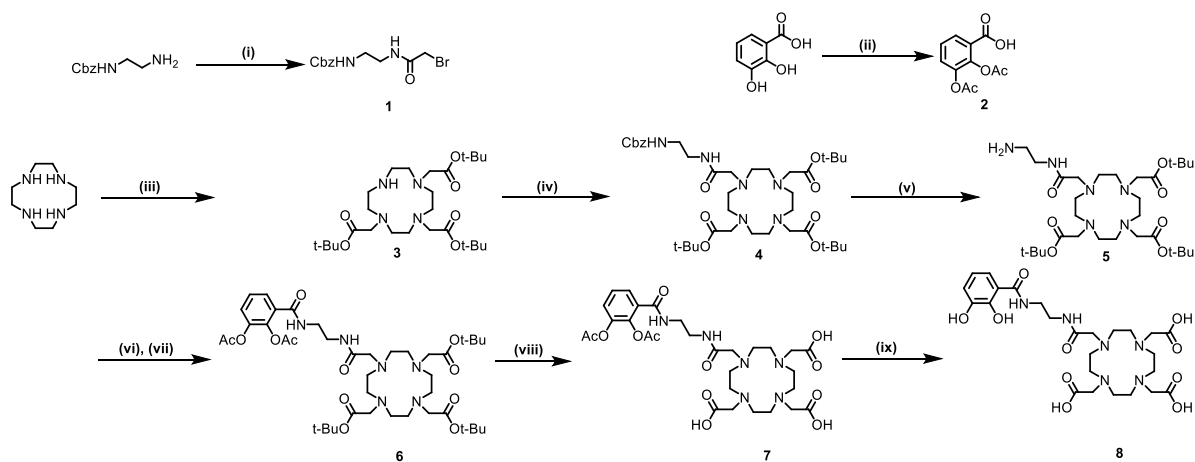
Figure 3.1 Structures of artificial siderophores investigated in this study.

The metal-free ligands – referred to as ‘precursors’ - were obtained by slow, sequential addition of the appropriate equivalents of alkyl bromide and base in acetonitrile with near to complete conversion and high purity. Depending on the choice of the initial substitution reaction, this strategy led to 1:3 or 3:1 catechol:carboxylate ratios.

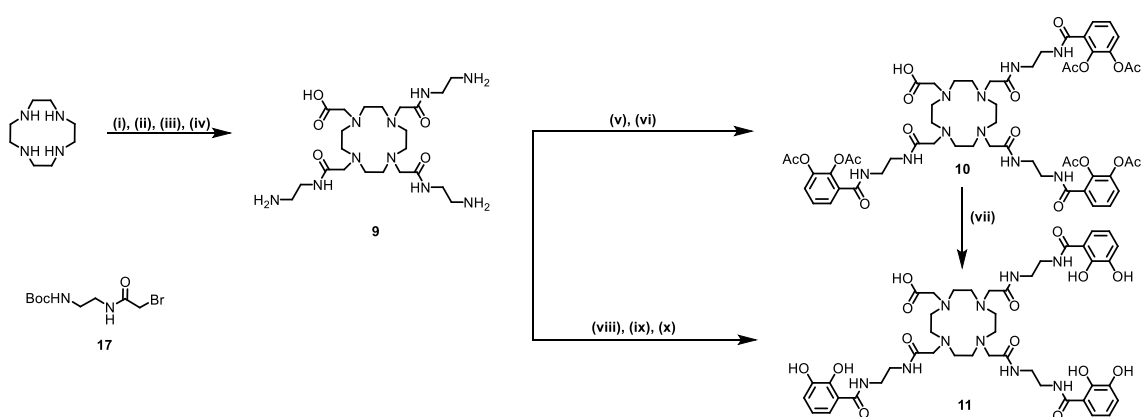
The synthesis of mono-catechol siderophore analogues started with the reaction of cyclen and *tert*-butyl bromoacetate to yield **3** (Figure 3.2A). The trisubstituted cyclen **3** was used as a crude product and reacted with the linker **1** under basic conditions to attach the fourth arm in 55% yield over two steps. Subsequently free amine **5** could be afforded after hydrogenolysis of the Cbz protecting group with Pd/C under H₂ atmosphere in 92% yield. The primary amine of **5** was reacted with the *in situ*-generated acid chloride of **2** in a two-phase Schotten-Baumann reaction to the desired amide **6** in 30% yield, which was subsequently deprotected with 50% TFA/AcOH to give the acetylated mono-catechol **7**. The free catechol **8** was then obtained by transacetylation with 20% DIPEA in MeOH. In order to obtain tri-catechol siderophores, cyclen was reacted first with the bromoacetamide **17** and subsequently with benzyl 2-bromoacetate under basic conditions, followed by a Boc group removal/hydrogenation sequence (Figure 3.2B). In this manner, intermediate **9** was obtained within four steps. The amine **9** was reacted with the freshly prepared acid chloride of **2** in a Schotten-Baumann reaction to give the acetylated precursor **10** in 32% isolated yield within six synthetic steps. A similar sequence with **9** and the acid chloride of 2,3-bis(benzyloxy)benzoic acid, followed by hydrogenolysis, yielded precursor **11** with free catechols. This compound could also be obtained by transacetylation of **10** with 20% DIPEA in MeOH in 31% overall yield within seven synthetic steps. The two *cis*- and *trans*-substituted di-catecholates **34** and **35** were obtained as an inseparable mixture by similar reaction sequences; the same was true for the regioisomers **25** and **26** that were alpha-methylated at the free carboxylic acids (Supporting Information, Figure S3.1 and Figure S3.2).

The synthesis of the DOTA tris-catechol conjugate **15**, offering three carboxylates and three catechols, commenced by reacting 2-(2-(2-(2-azidoethoxy)ethoxy)ethoxy)ethyl-1-amine with bromoacetyl bromide to afford linker **12** (Figure 3.2C). Cyclen and secondary bromides **17** and **12** were employed in a similar three-step sequence as shown above to give **13**. The DOTAM **13** and freshly prepared acid chloride of **2** yielded siderophore **14** in 36% yield within 6 steps. Transacetylation of **14** with 20% DIPEA in MeOH, followed by strain-promoted azide alkyne cycloaddition (SPAAC) with commercial **BCN-DOTA** yielded DOTA tris-catechol precursor **15** in 26% overall yield over 9 synthetic steps.

(A)



(B)



(C)

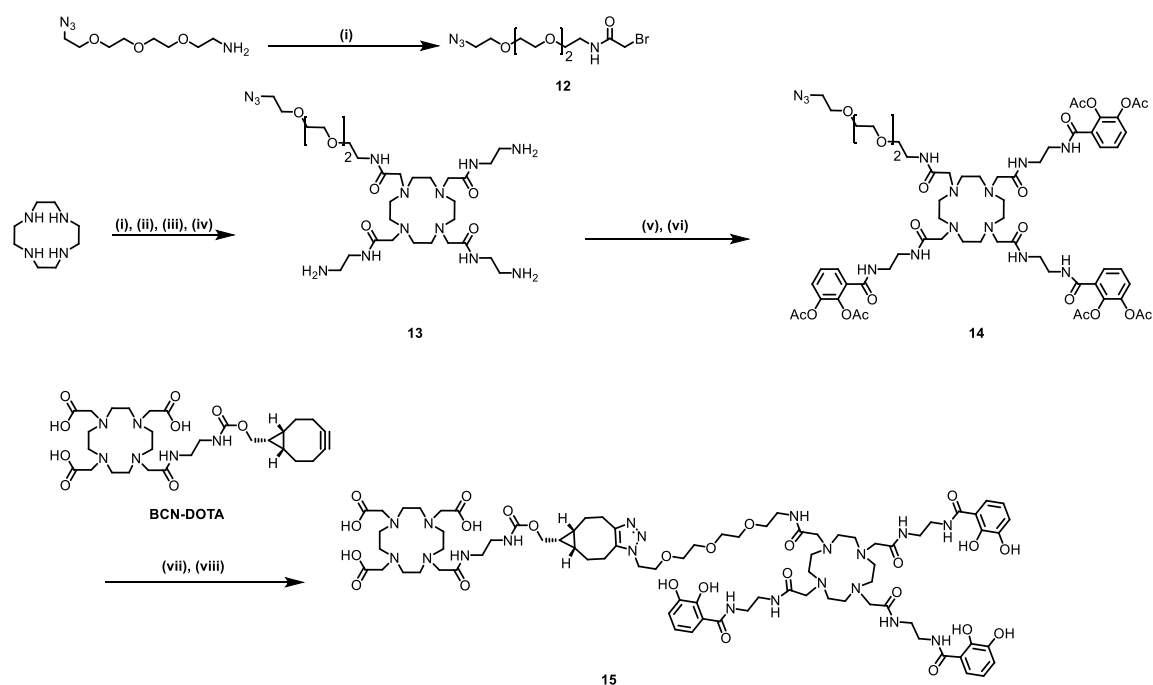


Figure 3.2 Synthesis of siderophore-based PET imaging agents. (A) Synthesis of precursors **7** and **8** from cyclen: (i) bromoacetyl bromide, K₂CO₃, DCM/H₂O (1:1), 3 hours, 21 °C, 87%, (ii) Ac₂O, DMAP, Et₃N, THF, 5 h, 29 °C, 86%, (iii) ^tBu 2-bromoacetate, NaOAc, DMA, 20 h, 23 °C, quant., (iv) **1**, K₂CO₃,

MeCN, 1 h, 22 °C, 63% , (v) 0.1 mol% Pd/C, H₂, MeOH, 1 h, 22 °C, 92%, (vi) **2**, oxalylchloride, DCM/DMF, 1 h, 0 °C to 22 °C, (vii) KHCO₃, H₂O/1,4-dioxane, 0.5 h, 23 °C, 30%, (viii) 50% TFA, DCM/AcOH, 25 h, 23 °C (1:1), 20%, (ix) 20% DIPEA in MeOH, 1 h, 22 °C, 60%. (B) Synthesis of precursors **10** and **11** from cyclen: (i) **17**, NaOAc, DMA, 20 h, 21 °C, (ii) benzyl-2-bromo-acetate, K₂CO₃, MeCN, 22 h, 23 °C, (iii) 25% TFA, DCM, 3 h, 24 °C, (iv) 0.1 mol% Pd/C, H₂, MeOH, 2 h, 21 °C, 99% within four steps, (v) **2**, oxalylchloride, DCM/DMF, 1 h, 0 °C – 20 °C, (vi) KHCO₃, H₂O/1,4-dioxane, 0.5 -1 h, 0 °C to 20 °C, 35% within two steps, (vii) 20% DIPEA, MeOH, 4 h, 25 °C, quant., (viii) 2,3-bis(benzyloxy)benzoic acid, oxalylchloride, DCM/DMF, 1 h, 0 °C – 20 °C, (ix) KHCO₃, H₂O/1,4-dioxane, 0.5 -1 h, 0 °C to 20 °C (x) 0.1 mol% Pd/C, H₂, MeOH, 2 h, 21 °C, 10% within three steps. (C) Synthesis of precursor **15** from cyclen: (i) bromoacetyl bromide, K₂CO₃, DCM/H₂O (1:1), 3 hours, 0-25 °C, 91%, (ii) **17**, NaOAc, DMA, 20 h, 21 °C, (iii) **12**, K₂CO₃, MeCN, 22 h, 23 °C, (iv) 25% TFA, DCM, 3 h, 24 °C, quant. within 4 steps, (v) **2**, oxalylchloride, DCM/DMF, 1 h, 0 °C – 20 °C (vi) KHCO₃, H₂O/1,4-dioxane, 0.5 -1 h, 0 °C to 20 °C, 39% within two steps. (vii) 20% DIPEA, MeOH, 2 h, 25 °C, (viii) **BCN-DOTA**, MeOH/DMSO, 1xPBS, 25 °C, 80% over two steps.

3.2.1 Gallium complexation

The ability of the cyclen-based siderophores to complex gallium ions was tested with the mono-catecholate **7**, the tris-catecholate **11** and the DOTA tris-catechol **15**. Using a 0.5 M NaOAc buffer and GaCl₃, 'cold' Ga-complexes could be readily prepared on an intermediate scale at 95-100 °C in 10 minutes and yields of 18-84% (Figure 3.3A). The ¹H-NMR spectra of **7**, **11** and **15** were featured by a much better resolution in the region of 3.0 to 4.1 ppm upon introduction of the Ga³⁺ cation, due to the metal loading into the cyclen moiety (Figure 3.3B, Figure S3.3 and Figure S3.4). According to previous studies, the metal-DOTA complex formation is a two-step process (Kasprzyk and Wilkins, 1982; Wang et al., 1992). Initially, a reversible adduct (type I complex) forms, followed by protonation/deprotonation reactions and a slow-forming, but stable 'type II complex' that has the metal fully coordinated.⁴² Studies suggest, the slow kinetics of metal-DOTA complex formation is caused, in part, by the dynamics of conversion between isomers of metal-DOTA compounds (Desreux, 1980). Thus, the rate of metal-DOTA complexation is much higher at elevated temperature or with more flexible macrocycles because the rate of conformational change between isomers is more rapid.⁴³ This leads to the formation of a more rigid structure with magnetically nonequivalent, geminal hydrogen atoms, which is reflected by the characteristic multiplet pattern for the involved methylene hydrogens.⁴²

The carboxylic acid groups and macrocycle nitrogen protons can undergo protonation/deprotonation reactions during gallium-68 complex formation. The formation of the fully coordinated metal complex is therefore highly pH dependent. As described in the literature, the chemical shifts of the carbon-bonded protons near the sites of

3.2.2 Growth recovery capabilities of cyclen-based siderophore analogues

Next, we tested whether the artificial siderophores were able to enter bacterial cells in free as well as in Ga^{3+} -complexed form. For this purpose, a surrogate assay that measured the compound-mediated delivery of iron into bacteria based on growth recovery was applied (Figure 3.4A).³⁶ The ΔentA and ΔentB mutants of *E. coli* BW25113, that cannot biosynthesize their endogenous siderophore enterobactin (ENT), were unable to grow under iron-depleted conditions as well as under Fe^{3+} supplemented conditions (Figure 3.4B and Figure S3.5A, DMSO control). Because these strains are reliant on exogenous siderophores to grow under iron-limited conditions, the exogenous addition of the natural siderophore ENT (10 μM) restored the growth of the *E. coli* ΔentA and ΔentB mutants. Remarkably, also the supplementation of artificial DOTAM-based siderophore analogues (10 μM) fully rescued the growth in seven out of eleven cases for both mutant strains. The most efficient growth recovery was observed for the DOTA tris-catechol **15**, as well as the tris-catechol **10** and **11**. Also the di-catechols **25/26** and **34/35** were able to relieve iron deficiency. In contrast, the mono-catechols were generally less potent. Interestingly, also [^{nat}Ga]**11** was accepted as a siderophore and exhibited a potency that was comparable to the uncomplexed analog **11**. A less pronounced, but still measurable growth recovery can also be found for the mono-catechols **7** and [⁶⁹Ga]**7**. The deacetylated mono-catechol **8** was found to be more efficient than **7** in the *E. coli* ΔentA mutant. The effect of α -methyl substituents can be assessed by comparing the methylated monocatechol **8** with its unmethylated congener **24**. Likewise, the methylated triscatechol **37** can be compared to the unmethylated **10**. In both cases, the methyl-substitution led to an impairment of growth recovery, indicating a decreased uptake of the complexes. In sum, these results demonstrate that the cyclen-based probes can shuttle Fe^{3+} into the bacterial cell, indicating their internalization, even when they are loaded with a Ga^{3+} cation. Further growth recovery data in the siderophore-deficient *P. aeruginosa* strain $\Delta\text{pvd} \Delta\text{pch}$ (see Figure S3.5B) shows a significant increase in efficiency for compound **7** compared to the *E. coli* mutants. Compounds **8**, **10** and **15** were found to exhibit retained activity in the double knockout mutant. The (increased) efficiency of all 4 compounds across bacterial species. The growth recovery in siderophore-deficient mutants mimics the long-term iron supply to the bacteria and does not correspond ideally to the short-term accumulation of our siderophore mimics in relevant bacterial strains during 60 min of PET imaging. Short-term uptake experiments with radiolabeled siderophore analogues under iron-reduced conditions would resemble the actual *in vivo* situation better. Particularly interesting remains a comparison of the taken-up tracer into wild type and siderophore-deficient strains, as this is a measure for the minimum (wildtype) and maximum (mutant) possible tracer uptake. The release of Fe-(III) from the Fe-siderophore analogue happens according to literature in the periplasm or cytoplasm of the bacteria. This redox reaction is mediated either by (i) intracellular

Fe-siderophore reductases or (ii) Fe-siderophore hydrolases.^{44 45} For example, the tri-catechol siderophore enterobactin ($E_{1/2} = -790$ mV), first undergoes a lactone cleavage by esterases/hydrolases. The ester hydrolysis reduces the complex stability, and consequently elevates the redox potential enough for the reduction of Fe-(III) to Fe-(II) with natural reductants as NAD(P)H ($E_{1/2} = -320$ mV).⁴⁶ Some studies have also mentioned acidification⁴⁷, the introduction of Fe-(II) traps or an increased lipophilic environment as ways to alter redox-potentials within cells.⁴⁴

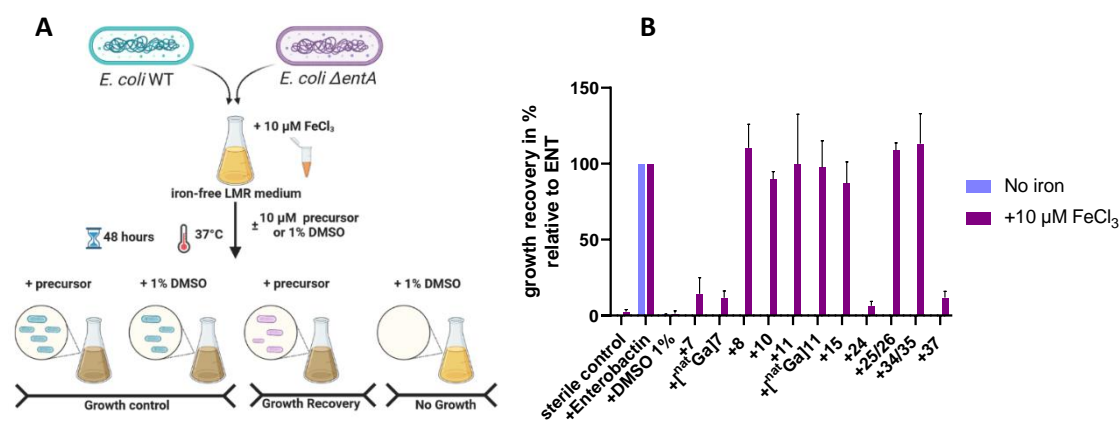


Figure 3.4 Growth recovery assay in siderophore-deficient *E. coli* mutants. (A) Principle of growth recovery assay, created using biorender and (B) growth recovery in the enterobactin (ENT) – deficient strain *E. coli* $\Delta entA$ in the presence of 10 μM compound \pm 10 μM FeCl_3 was assessed after incubation for 48 hours at 37 °C by $\text{OD}_{600\text{nm}}$ measurement in a plate reader. Bacteria were either grown in iron-depleted (no iron) or 10 μM FeCl_3 -supplemented, phosphate-buffered LMR medium ($n = 3$). The growth relative to ENT and the wildtype growth is plotted; error bars correspond to \pm standard deviation (SD).

As the DOTAM siderophore lacks a hydrolysable backbone, we assume, the release takes place *via* a combination mechanism of (i) a cellular alteration of the redox potential, and hereinafter (ii) an enzymatic reduction-release of the Fe-(III) from our triscatechol siderophores. For mono- and di-catechol siderophores with a much weaker redox potential, a simple reductase-based release should be sufficient.

3.2.3 Chemical stability and cytotoxicity

The chemical stability of the Ga^{3+} -free precursors **7**, **8**, **24**, **11**, **37**, and **34/35** was measured in PBS at 37 °C over a period from 24 to 96 hours by LC/UV/MS (see Figure S3.6). All compounds showed a stability of at least 60% over 4 hours under the given conditions, which is deemed as sufficient for PET measurements (Figure S3.6A). For prodrugs, the acetyl group

stability gradually declined, and no acetylated compound could be detected after 24 hours (Figure S3.6B), which is in accordance with previously published data.³⁶ The cellular cytotoxicity of Ga³⁺-free precursors **7**, **8**, **11**, **15**, **24**, **25/26**, **34/35**, and **37** as well as Ga³⁺-complexed siderophores [^{nat}Ga]**7** and [^{nat}Ga]**10** was tested in the five eukaryotic cell lines L929, A549, KB-3-1, MCF-7 and FS4-LTM. All compounds were classified as non-cytotoxic up to concentrations of 100 μM (Table ST3.1).

3.2.4 Radiochemical synthesis

Representative mono-, di- and tri-catecholates (**7**, **25/26**, **34/35**, **10**, **11**, **15**), that induced growth recovery, exhibited good stability in PBS and showed no cytotoxic effects, were selected for radiochemical labeling with gallium-68. For manual labelling, 30 - 50 nmol precursor were mixed with unprocessed gallium-68 chloride. The complexation process was assessed by (i) the labelling efficiency (LE), defined as percentage of ⁶⁸Ga-incorporation in relation to a respective starting activity and precursor amounts, (ii) the radiochemical yield (RCY), defined as the amount of activity (decay corrected) in the product expressed as the percentage (%) of related starting activity, and (iii) the radiochemical purity (RCP), defined as the proportion of the total radioactivity in the sample which is present as the desired radiolabeled species.⁴⁸ The precursor **15** reached the highest values for LE (97.8%), RCP (84.3%) and RCY (56.7%), followed by the mono-catechol **7** and the tri-catechol **10** (Figure 3.5A). Interestingly, **11** demonstrated dramatically decreased LE and RCP compared to the acetylated prodrug **10**. Likewise, the complexation of **8** with 'cold' gallium ions was less efficient than that of **7** (data not shown). Stable complexes with enterobactin mimics such as TREN-CAM (tripodal enterobactin analogue-catecholate coordinating moieties), which resisted transchelation even with 1000-fold excess of desferrioxamine, are evidence for the gallium-68 complexing ability of catechols.⁴⁹ In contrast these compounds, our siderophore analogue possess two chelation centers –at the catechol units and at the cyclen moiety. The competition of the latter for gallium, likely prevents an immediate, stable complex formation with catechol(s) and/or cyclen. Therefore, we introduced transient masking groups (acetyl) at the catechols, to facilitate the rapid formation of stable gallium-68 complexes at the cyclen unit. Our assumption is reflected by the difference in RCY and LE/RCC between compounds. The significantly higher LE/RCC and RCY for [⁶⁸Ga]**10**, compared to the deacetylated tracer [⁶⁸Ga]**11**, support our assumptions. Because a fast complexation is imperative due to the short half-life of gallium-68, the precursor **11** was deselected. In contrast, **15** with a spatially separated DOTA moiety achieved high LE, RCP and RCY without acetylated groups. The dicatecholates **25/26** and **34/35** had rather low RCPs and RCYs. Because **25/26** and **34/35** had the additional drawback of being regioisomeric mixtures, the dicatecholates were no longer pursued. Thus, we

conclude that the spacial separation of an optimal ^{68}Ga -chelator (DOTA) from the iron-chelating DOTAM siderophore facilitates the formation of stable ^{68}Ga -complexes. Based on the radiochemical data, the three siderophores **7**, **10** and **15** were selected for further studies.

The radiochemical synthesis of [^{68}Ga]**7**, [^{68}Ga]**10** and [^{68}Ga]**15** was first optimized manually regarding e.g. EtOH content, heating time, pH value and purification cartridges (Table ST3.2 in the Supporting Information). Based on the manual procedure, the precursors were complexed on an automated synthesis module to minimize radioactive exposure, standardize the complexation conditions and corresponding RCP/RCY for *in vivo* studies (Figure 3.5B). 30 nmol of **7** could be labelled within 8 minutes and purified via a $^1\text{C}18$ light cartridge, while precursor **15** was labelled within 6 minutes and purified via a HLB light cartridge. Precursor **10** needed 25 minutes of synthesis time. The longer time might be attributed to the presence of only one free carboxylate in the cyclen and increased steric hindrance by the side groups.

The highest RCYs were afforded by [^{68}Ga]**15** and [^{68}Ga]**7**, while [^{68}Ga]**7** reached the highest purity. The lipophilicity of all three ^{68}Ga -complexed tracers was determined in an octanol/water matrix, with [^{68}Ga]**7** being the most hydrophilic ($\log D = -3.3$) and [^{68}Ga]**15** notably more lipophilic ($\log D = -1.6$, Figure 3.5C). The stability of the radiotracers in PBS and in human serum at 37 °C was evaluated by radio chromatograms directly after synthesis for two hours (Figure 3.5D-F and Figure S3.7). As found for the uncomplexed precursors, all three compounds were >80% stable in PBS for two hours. However, [^{68}Ga]**7** and [^{68}Ga]**10** displayed some instability in serum: For [^{68}Ga]**7**, $19.1 \pm 6.2\%$ gallium-68 were released after two hours of incubation. Moreover, the tracer deacetylated, resulting in $58.9 \pm 22.0\%$ deacetylated [^{68}Ga]**7** within 2 hours. $91.4 \pm 1.8\%$ of [^{68}Ga]**10** were deacetylated in serum after two hours. Stepwise enzymatic deacetylation in human serum, and hence release of the free catechol moieties of both complexes over the course of two hours, was accompanied by a shift to smaller (more polar) retention times (see Figure S3.7A and C right), corresponding to the conversion of the prodrug to the active drug. As [^{68}Ga]**15** did not bear any acetyl groups, deacetylated metabolites were not observed, but a more lipophilic metabolite was formed after 2 hours (see Figure S3.7B). Still, $80.8 \pm 0.8\%$ [^{68}Ga]**15** remained stable for more than two hours in serum.

While [^{68}Ga]**15** displayed comparably high RCY and tracer stability to other bacteria-specific PET tracers.^{12, 18, 25, 29, 31, 32} [^{68}Ga]**7** could be further improved installing four carboxylate donor groups or the smaller NOTA chelator for future molecules to form more stable gallium-68 complexes.⁵⁰ Free catechol-assisted transchelation or complex hydrolysis in biological was successfully masked by the introduction of transient protection groups. Deacetylation of the catechol moieties took place over ca. 6 hours in PBS (pH 7.4) as demonstrated in Figure S3.6B and in our previous study.^{36, 51} However, stability and radio HPLC data of [^{68}Ga]**7** (Figure 3.5

and Figure S3.7), together with literature studies suggest a more rapid reaction to the free catechol in blood than in PBS.⁵² Therefore alternative masking groups with higher stability, e.g. sialylethers or acetals, should be evaluated with respect to species-specific higher hydrolase activities.⁵³

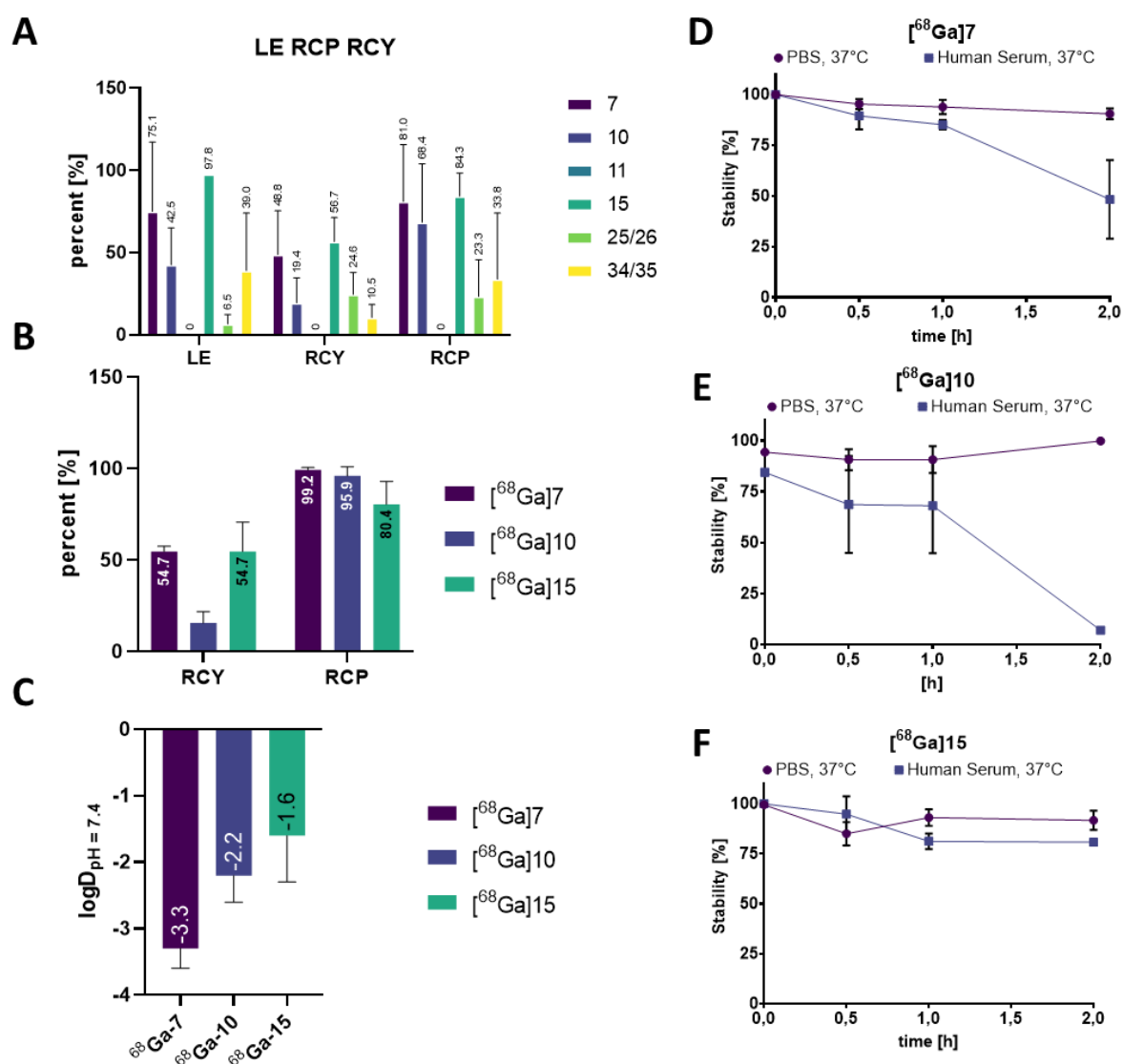


Figure 3.5. Radiochemical and physicochemical parameters and stability of gallium-68 complexes. (A) The Labelling Efficiency (LE), Radiochemical Yield (RCY) and Radiochemical Purity (RCP) of siderophores manually complexed with [⁶⁸Ga] are shown, min. n=3, error bars indicate ± SD. (B) RCP and RCY for automated radiochemical synthesis of [⁶⁸Ga]7, [⁶⁸Ga]10, [⁶⁸Ga]15 on an automatic synthesis module with 30 nmol precursor, min. n=3, error bars indicate ± SD. (C) LogD_{7.4} values were determined in an octanol/water system, min. n=3, error bars indicate ± SD. (D-F) Stability data of [⁶⁸Ga]7, [⁶⁸Ga]10, [⁶⁸Ga]15 in PBS (pH = 7.4) and human serum at 37 °C, detected by radio-HPLC runs in intervals of 30 minutes and subsequent integration of the respective peaks, min. n=3, error bars indicate ± SD. Acetylated and deacetylated forms are both considered.

3.2.5 Biodistribution studies in mice

The biodistribution properties of [⁶⁸Ga]7, [⁶⁸Ga]10 and [⁶⁸Ga]15 were tested in healthy, male C57Bl/6N mice (n = 6 per tracer). For this purpose, 12.8 ± 2 MBq (0.35 ± 0.05 mCi) [⁶⁸Ga]7, 10.8 ± 1.6 MBq (0.3 ± 0.04 mCi) [⁶⁸Ga]15 or 10.7 ± 1.5 MBq (0.29 ± 0.04 mCi) [⁶⁸Ga]10 was administered via a catheter in the lateral tail vein (i.v. injection). The tracer accumulation was monitored over 60 minutes by dynamic PET/CT scans in 32 frames. [⁶⁸Ga]7 exhibited almost exclusively renal clearance with low blood pool retention and fast clearance from examined organs (Figure 3.6A). In the last frame, unspecific tracer uptake in the healthy muscle tissue was negligible (0.05 ± 0.01 %ID/g, Figure 3.6B). [⁶⁸Ga]15 showed a similar kinetic compared to [⁶⁸Ga]7, i.e. a rapid, mainly renal clearance and a low blood pool retention, but exhibited a higher liver accumulation (Figure 3.6D), correlating well with its higher lipophilicity. The uptake into healthy muscle amounted to 0.34 ± 0.05 %ID/g (Figure 3.6E).

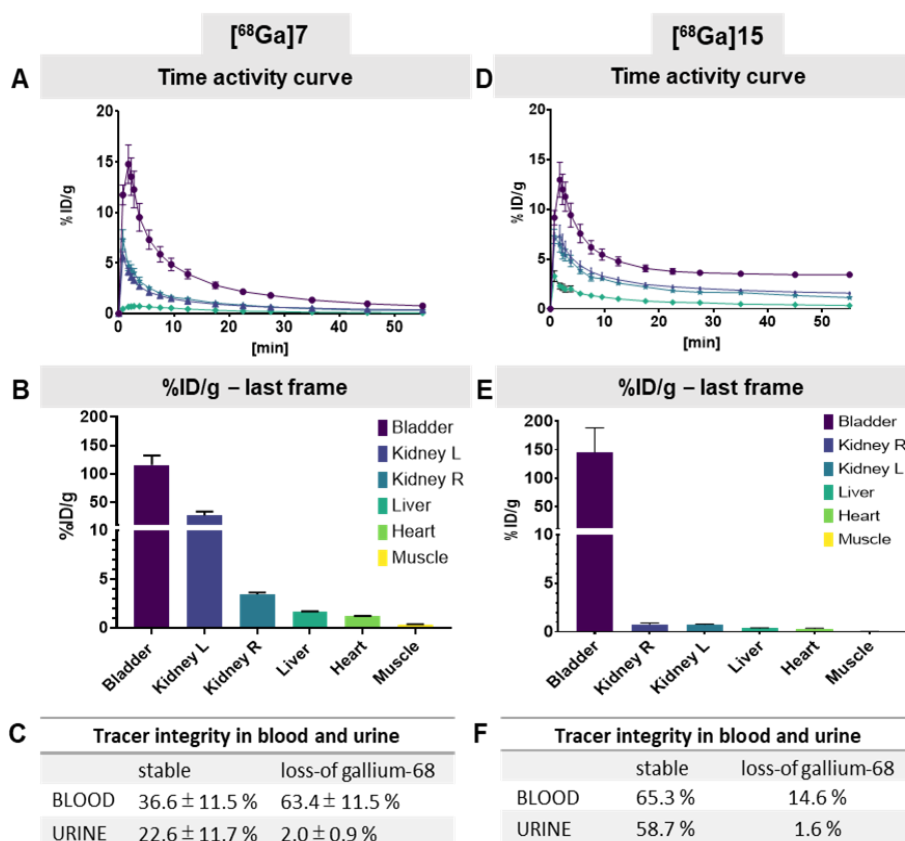


Figure 3.6. Biodistribution of [⁶⁸Ga]7 (left side, A-C) and [⁶⁸Ga]15 (right side, D-E) in male C57Bl/6N mice over 60 min of dynamic PET imaging. (A+D) Time activity curves (TAC) display the biodistribution of [⁶⁸Ga]7 or [⁶⁸Ga]15 tracers for six organs (left and right kidney, bladder, liver, heart and muscle) in the course of one hour of dynamic PET/CT imaging (n = 6, error bars indicate ± SD). In (B+E) the % injected dose / organ weight during the last time frame (50-60 min) of dynamic PET/CT scan (%ID/g), is plotted, n=6, error bars indicate ± SD. (C+F) Tracer integrity or loss of gallium-68 in blood and urine samples (each n=6, error calculated as ± SD) after 60 minutes of dynamic PET/CT scan, determined by radio-HPLC measurements.

[⁶⁸Ga]10 was excreted via the kidneys and liver, but showed a higher background activity in blood, with longer average retention periods in the respective imaged organs (Figure S3.8). The non-specific uptake of **[⁶⁸Ga]10** in healthy muscle during the last 10 minutes of imaging amounted to $0.5 \pm 0.09\%$ ID/g. Only $36.6 \pm 11.5\%$ of **[⁶⁸Ga]7** could be detected in blood after one hour of imaging, as $63.4\% \pm 11.5\%$ free gallium-68 were formed instead. In urine the tracer was mainly detected in its deacetylated, active form (ca. 75.4%), with loss of gallium-68 amounting to $2.0 \pm 0.9\%$ and the acetylated, intact **[⁶⁸Ga]7** to $22.6 \pm 11.7\%$ (Figure 3.6C). Stable **[⁶⁸Ga]15** was detected in blood as well as in urine, while the loss of ⁶⁸Ga was higher in blood (14.6%) than in urine (1.6%) Only $1.3 \pm 1.5\%$ acetylated **[⁶⁸Ga]10** could be detected in blood and mostly degraded to free ⁶⁸Ga ($95.4 \pm 3.5\%$), while the tracer was stable in urine with $42.1\% \pm 35.1\%$, accompanied by a loss of ⁶⁸Ga of $29.8 \pm 25.1\%$ (Figure S3.8). Because **[⁶⁸Ga]10** exhibited an immense loss of gallium-68, an increased liver uptake and the highest unspecific uptake in healthy muscle, it was not considered for the subsequent infection model.

3.2.6 PET/CT imaging of *E. coli* infected muscle vs. sterile-inflamed muscle in mice

The best suited tracers **[⁶⁸Ga]7** and **[⁶⁸Ga]15** were tested in an *in vivo* infection model. In order to evaluate whether the tracers could differentiate between a bacterial infection and a sterile inflammation, 3×10^7 CFU's of *E. coli* were injected into the *Musculus gastrocnemius* of the left leg, and 27 μ g lipopolysaccharide (LPS) were injected into the right leg. LPS induced a sterile inflammatory reaction, which should not be detectable by tracers that specifically visualize bacteria. Twenty hours after this challenge, 11.6 ± 0.8 MBq (0.31 ± 0.02 mCi) **[⁶⁸Ga]15** or 11.8 ± 1.5 MBq (0.32 ± 0.04 mCi) **[⁶⁸Ga]7** were injected into six mice per tracer, respectively, and dynamic PET scans were acquired.

[⁶⁸Ga]7 showed a rapid clearance in the infection setting, as already observed in uninfected mice. A higher uptake of the tracer into the substantially enlarged infected muscle compared to the inflamed muscle was evident by visual inspection of the PET scan (Figure 3.7A and Supplementary Video S3.V1). The tracer accumulated rapidly in both legs within the first 10 minutes, but the subsequent decrease was faster in the sterile-inflamed muscle (Figure 3.7B). Semi-quantitative analysis, based on the sum of regions of interest (ROIs) of the last half hour of dynamic PET scan, showed an increased uptake of **[⁶⁸Ga]7** into the infected muscle of 0.67 ± 0.05 %ID/g in comparison to the sterile-inflamed muscle (0.36 ± 0.06 %ID/g uptake, $p < 0.0001$; Figure 3.7D). The accumulated dose %ID/g is 11-fold higher in the infected muscle than in the healthy muscle (see Figure 3.6). This indicates that **[⁶⁸Ga]7**, despite its structural simplicity, can distinguish between bacterial infections, sterile inflammation and healthy tissue *in vivo*. The autoradiographic examination of the dissected muscles confirmed the PET scan

results, as an increased uptake of the tracer into the infected vs. the inflamed muscle was clearly visible (Figure 3.7C).

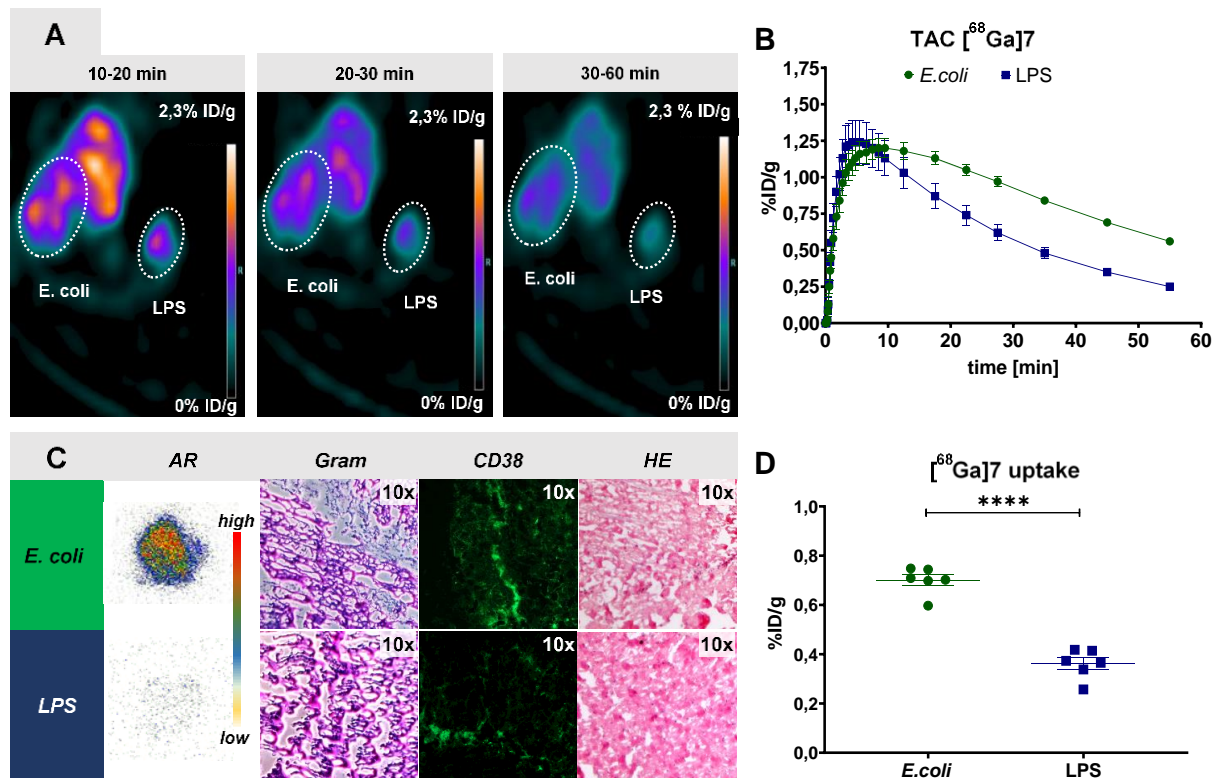


Figure 3.7. *In vivo* PET imaging in mice infected with *E. coli* with [⁶⁸Ga]7. (A) 3.0 x 10⁷ CFUs *E. coli* (ATCC47076) were administered *i.m.* into the left leg, and 27 µg LPS were administered *i.m.* into the right leg 24 hours before imaging (n = 6 animals, male C57Bl/6N mice). [⁶⁸Ga]7 was prepared directly prior to the imaging experiment and injected *i.v.* into the tail vein. Dynamic PET scans were performed for 60 min with a using a micro PET/CT (transaxial view displayed, further data and video compilation are in the Supporting Information). (B) Time-activity curves (TAC) of decay-corrected [⁶⁸Ga]7, error bars are ± SD. (C) Dissected *Musculus gastrocnemius* after 60 min of PET/CT scan were imaged by autoradiography (AR), underwent Gram staining for bacteria (blue areas), immune histology with an anti-CD38 antibody (CD38) for macrophages (green fluorescence), and hematoxylin and eosin stain for cells and tissue. The upper row shows images of the *E. coli*-infected left muscle, while the lower row shows images of the LPS-injected right muscle. (D) The accumulated dose %ID/g of [⁶⁸Ga]7 uptake over the course of the last 30 minutes of dynamic PET/CT scans was 1.9-fold higher in *E. coli*-infected compared to LPS-injected muscles (****: p-value <0.0001)

Furthermore, Gram staining of the dissected muscles confirmed the presence of bacteria in the infected muscle, whereas expectedly, no bacteria were detected in the sterile LPS inflammation. On the contrary, immune staining with an antiCD38 antibody identified invasion of macrophages in both muscles (Figure 3.7C).

For the DOTA tris-catechol [⁶⁸Ga]15, tracer clearance in *E. coli* / LPS-challenged mice was as rapid as in non-infected animals. Similar to [⁶⁸Ga]7, an increased uptake into the infected muscle was visible 15 minutes after injection (Figure 3.8 and Supplementary Video SV2). A semi-quantitative analysis of the last frame revealed that the uptake into the *E. coli*-infected muscle amounted to 0.51 ± 0.18 %ID/g, 1.7-fold higher than into the sterile-inflamed muscle (0.30 ± 0.09 %ID/g; $p = 0.035$; Figure 3.8D). The autoradiographic imaging of the dissected muscle also confirmed a higher uptake of [⁶⁸Ga]15 into the *E. coli*-infected muscle (Figure 3.8C). In comparison to [⁶⁸Ga]7, a lower %ID/g over time could be accumulated, but a differentiation between infected and sterile-inflamed muscle was possible. Autoradiographic images of the dissected muscles confirmed the PET/CT results, and even showed a stronger difference between the infected muscle and the muscle with sterile LPS inflammation. Gram staining confirmed the presence of bacteria in the infected muscle, while no bacteria were detected in the sterile LPS inflammation. Expectedly, immune staining with an antiCD38 antibody identified invasion of macrophages in both muscles.

The CD38-positive stains in in Figure 3.7 and 3.8 for both, the *E. coli* infection and the sterile inflammation, figuratively depicts the inability of the immune system to distinguish a surface antigen from live bacteria. In general, but even more in an infection or inflammation scenario, the host limits the bioavailability of free iron is in the order of $\sim 10^{-18}$ M, by a manifold of strategies to avoid the access of non-host processes.⁵⁴ During LPS-induced, sterile inflammation, literature indeed confirms an anemic environment establishes at the injection site with low Hb and even lower iron content in Hb, as well as elevated levels hepcidin.^{55 56} An enrichment of our siderophore analogues in the absence of bacteria therefore would have to occur *via* unspecific host or immune cell uptake. This kind of unspecific accumulation was not indicated by e.g. unusually high blood pool or muscle tissue retention in the biodistribution studies depicted in Figure 3.6. Moreover, the targeted TonB-dependent siderophore uptake machinery is unique to prokaryotes^{57, 58} and internalization through bacterial siderophore receptors should occur much faster than unspecific uptake by host cells, supported by the significant localization of our compounds to the site of infection. However, the unspecific tracer accumulation by host cells and potentially a lower S/N ratio would need further exploration in a competition assay.

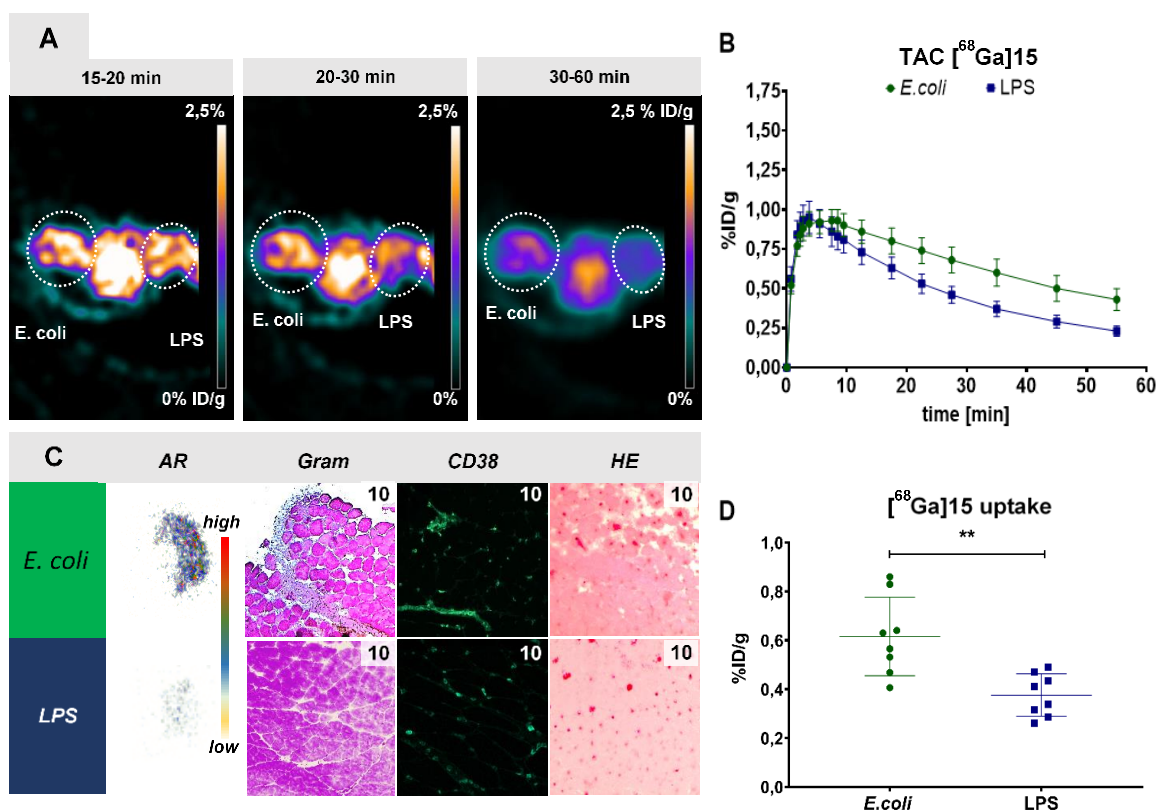


Figure 3.8. *In vivo* PET imaging in mice infected with *E. coli* with [⁶⁸Ga]15. (A) 2.2×10^7 CFUs *E. coli* were administered *i.m.* into the left leg, and 27 μ g LPS was administered *i.m.* into the right leg 24 hours before imaging ($n = 6$ animals, male C57Bl/6N mice). [⁶⁸Ga]15 was prepared directly prior to the imaging experiment and injected *i.v.* into the tail vein. Dynamic PET scans were performed for 60 min with a using a micro PET/CT (transaxial view displayed, further data and video compilation are in the Supporting Information). (B) Time-activity curves (TAC) of decay-corrected [⁶⁸Ga]15, error bars are \pm SD. (C) Dissected *Musculus gastrocnemius* after 60 min of PET/CT scan were imaged by autoradiography (AR), underwent Gram staining for bacteria (blue areas), immune histology with an anti-CD38 antibody (CD38) for macrophages (green fluorescence), and hematoxylin and eosin stain for cells and tissue. The upper row shows images of the *E. coli*-infected left muscle, while the lower row shows images of the LPS-injected right muscle. (D) The accumulated dose %ID/g of [⁶⁸Ga]15 over the course of the last 30 minutes of dynamic PET/CT scans was 1.7-fold higher in *E. coli*-infected compared to LPS-injected muscles (**: p -value < 0.0035).

Taken together, both tracers, [⁶⁸Ga]7 and [⁶⁸Ga]15, could reliably distinguish an *E. coli* infection from a LPS-induced sterile inflammation. The observed accumulation of our tracers is based on the expression of bacterial siderophore uptake systems not just for their native siderophores but also for so-called xenosiderophores solely synthesized by other pathogens or generated in the laboratory.⁵⁹ Previous approaches with e.g. natural siderophores, failed to accumulate sufficiently in other bacterial strains than in the parent species.⁶⁰ Our siderophore

analogues target the catechol-specific outer membrane siderophore receptors (OMRs) unique to prokaryotes, known to be expressed for example in *P. aeruginosa* (*PfeA*)^{61, 62}, *E. coli* and *K. pneumoniae* (*FepA*)^{63, 64}. Also studies indicate the pathogens *S. aureus*⁵⁹, *S. typhimurium* and *Y. enterocolitica* able to hijack catechol-based xenosiderophores for their iron- supply.⁶⁵ Consequently, uptake of our tracer(s) can only occur, if catechol-recognizing OMRs are expressed in the targeted species. A recent, well-designed example, screened various prokaryotes for enrichment of their gallium-68 labelled desferrioxamine tracer (targeting hydroxamate OMRs, e.g. *FpvA*), and could confirm their *in vitro* results by the visualization of *P. aeruginosa* and *S. aureus* infections *in vivo*.³² Expectedly no uptake of their tracer into *K. pneumoniae*, *C. albicans* and *E. coli* was found. In line with our and other preceding results,⁴ this emphasizes the interconnectedness of the pathogens' expressed siderophore receptors with the choice of an optimal iron chelating moiety permitting the effective accumulation at the site of infection. Towards the limited semi-synthetic modifiability of sensitive, natural siderophores, our robust and modular DOTA(M) synthesis enables the attachment of a range of iron chelators as well as combinations thereof. Our lead compounds as well as future programs would benefit from *in vitro* and *in vivo* tracer experiments with a wider panel of pathogens, including bacteria lacking the siderophore uptake machinery, to their specificity towards prevalent OMRs and bacterial strains.

3.3 Conclusion

We have expanded the suite of applications for artificial, cyclen-based siderophores to PET imaging, in order to enable the monitoring of infections in large animals. The compounds were synthesized via robust and scalable synthetic pathways in up to eight steps in a modular manner and discriminated through a suite of chemical and biological assays (Figure S3.9). Notably, the compounds could simultaneously host a ⁶⁸Ga³⁺ for PET imaging in their cyclen core and still serve as efficient xenosiderophores in *E. coli*. A reduced number of catechols clearly led to lower growth recovery. However, two and even one catechol are capable of a growth recovery; this finding is in line with the fact that many siderophore-antibiotic conjugates employ a single bidentate iron-binding moiety to enhance their uptake.³³ The α -methyl variants did neither improve bacterial growth recovery nor radiochemical labeling, and therefore seems redundant in the scaffolds investigated here. For six selected precursors, manual and automated radiochemical synthesis procedures were established successfully to yield the respective ⁶⁸Ga-complexed PET tracers. Two bacteria-targeted PET tracers, [⁶⁸Ga]7 and [⁶⁸Ga]15, displayed favorable biodistribution and stability properties and could reliably distinguish *E. coli* infections from LPS-induced, sterile inflammation in mice. While active bacterial uptake should be superior in the DOTA tris-catechol [⁶⁸Ga]15, the ease of synthesis but also the imaging data speak for [⁶⁸Ga]7. These compounds expand the yet limited arsenal

of molecular probes for bacterial imaging in large animals. In particular, we found that addressing the bacterial iron uptake system with non-natural, structurally rather simple siderophores is a viable and efficient strategy to visualize infections *in vivo*. Compared to previous siderophore-PET probes, the separation of iron and PET-tracer binding sites allows to also accommodate other metal cations (e.g. ^{111}In or ^{64}Cu) that might fit less well into the siderophore binding site that was optimized for iron. The versatile scaffold, well-amenable to further modifications,^{37, 66, 67} allows to fine-tune properties, and/or to introduce additional functionalities like antibiotic active moieties to obtain full bacteria-targeted theranostics. Indeed, a structural optimization is indicated to further improve parameters like tracer stability *in vivo* or enrichment in bacteria. The findings also pave the way for siderophore-based PET-imaging in larger, non-rodent species.

3.4 Experimental section

3.4.1 Chemical Synthesis

Chemical and reagents were purchased from commercial vendors (TCI, Carl Roth, Baker and Sigma-Aldrich), if not stated otherwise, and employed without further purification in the below synthetic procedures. For synthesis, solvents with purity grade 99.5%, extra dry, absolute, AcroSeal™, ACROS Organics™ were used. Work up procedures and purifications solvents were either HPLC or p. A. grade. Glassware was oven-dried prior to synthesis. Reaction progress was controlled by thin layer chromatography (TLC) or Liquid Chromatography-coupled Mass Spectrometry (LCMS). All compounds had purity $\geq 95\%$ as determined by high-performance liquid chromatography (UV detection) and $^1\text{H}/^{13}\text{C}$ -NMR analysis.

benzyl (2-(2-bromoacetamido)ethyl)carbamate (1)

According to a literature procedure from K. Ferreira To a white suspension of *N*-Cbz-ethylenediamine (504 mg, 2.6 mmol, 1.0 eq) in DCM (1 mL) a solution of K_2CO_3 (786 mg, 5.7 mmol, 2.2 eq) in MilliQ H_2O (4 mL) and a solution of bromo acetyl bromide (270 μL , 3.1 mmol, 1.2 eq) in DCM (4 mL) was added dropwise at 0 °C. The solution was stirred vigorously at 0 °C. The reaction was equilibrated to 21 °C and continued stirring at 21 °C for 1h. The phases were separated, and the organic phase was dried over Na_2SO_4 and concentrated *in vacuo*. The crude product **1** was obtained as a white solid and used without any further purification (715 mg, acc. to LCMS min. 96%, 87%).

$^1\text{H-NMR}$ (500 MHz, CDCl_3): δ = 7.36 – 7.28 (m, 7H), 5.11 (s, 2H), 5.05 (dd, J = 43.2, 18.1 Hz, 2H), 3.83 (s, 2H), 3.44 – 3.37 (m, 4H).

ESI-HRMS: **1**: calculated $\text{C}_{12}\text{H}_{16}\text{BrN}_2\text{O}_3^+$ $[\text{M}+\text{H}]^+$: 315.0346, measured: $[\text{M}+\text{H}]^+$: 315.0337 (Δ = 0.9 ppm).

2,3-diacetoxybenzoic acid (2)

According to modified literature procedure from K. Ferreira⁶⁸, 2,3-Dihydroxybenzoic Acid (1.29 g, 8.4 mmol, 1.0 eq) and DMAP (97 mg, 0.8 mmol, 0.1 eq) were dissolved in THF (25 mL). Then TEA (7.0 mL, 50.4 mmol, 6.0 eq) and Ac_2O (2.4 mL, 25.2 mmol, 3.0 eq) were added sequentially to the flask. After stirring for 4 h at 29 °C, the solvent was removed *via* rotary evaporation and the residue was dissolved in CHCl_3 (50 mL) and washed with HCl (0.5 M, 2x50 mL). The organic phase was dried over Na_2SO_4 and the solvent was removed *in vacuo*. Product **2** was dried under high vacuum overnight and obtained as a crude, beige solid (1.73 g, 7.3 mmol, 86 %).

¹H NMR (500 MHz, CDCl₃): δ = 7.98 (dd, *J* = 9.4, 3.1 Hz, 1H), 7.48 – 7.41 (dd, 1H, *J* = 7.9 Hz), 7.36 (t, *J* = 10.2, 5.8 Hz, 1H), 2.34 (s, 3H), 2.33 (d, *J* = 4.3 Hz, 3H).

ESI-HRMS: 2: C₁₁H₁₀O₆Na⁺ calculated [M+Na]⁺: 261.0369, measured [M+Na]⁺: 261.0371 (Δ = 0.2 ppm).

tri-*tert*-butyl 2,2',2''-(1,4,7,10-tetraazacyclododecane-1,4,7-triyl)triacetate (3)

According to a literature procedure from K. Ferreira⁶⁸, to a suspension of cyclen (104 mg, 0.6 mmol, 1.0 eq) and NaOAc (159 mg, 1.9 mmol, 3.3 eq) in DMA (0.8 mL) a solution of *tert*-butyl-bromo acetate (371 mg, 1.9 mmol, 3.3 eq) in DMA (1.0 mL, 250 μ L/h) was added via a syringe pump. The reaction mixture was stirred for 18 h at 21 °C and a KHCO₃-solution (100 mL, 0.5 M in H₂O) was added. The two-phase mixture was extracted with DCM (3 x 50 mL). The combined organic extracts were washed with brine (100 mL) and dried over Na₂SO₄, filtered and concentrated *in vacuo*. The obtained clear oil **3** (302 mg, 0.58 mmol, 98%) was used without any further purification.

¹H NMR (500 MHz, MeCN-d₃): δ = 3.41 – 3.27 (m, 6H), 2.94 (m, 4H), 2.87 – 2.75 (m, 12H), 2.16 (bs, 1H), 1.45 – 1.43 (bs, 27H).

ESI-HRMS: 3: C₂₆H₅₁N₄O₆⁺ calculated [M+H]⁺: 515.3802, measured [M+H]⁺: 515.3820 (Δ = 1.8 ppm).

tri-*tert*-butyl-2,2',2''-(10-(2-((2-(((benzyloxy)carbonyl)amino)ethyl)amino)-2-oxoethyl)-1,4,7,10-tetraazacyclododecane-1,4,7-triyl)triacetate (4)

According to a literature procedure from K. Ferreira.⁶⁸ To a suspension of **3** (100 mg, 194 μ mol, 1.0 eq) and K₂CO₃ (111 mg, 803 μ mol, 4.1 eq) in MeCN (3 mL) a solution of **1** in MeCN (1 mL) was added. The reaction was stirred at 22 °C for 1.5 h, and the reaction progress was monitored by LCMS. The suspension was filtered and the filtrate was concentrated to dryness, to obtain a crude, yellow oil of **4** (170 mg), which was employed without further purification in the next step.

¹H NMR (500 MHz, MeCN-d₃): δ = 8.96 (s, 1H), 7.39 – 7.33 (m, 5H), 6.17 (s, 1H), 5.03 (s, 2H), 3.25 – 3.15 (m, 10H), 2.95 (m, 2H), 2.79 (dd, *J* = 15.1, 5.6 Hz, 8H), 2.64 (s, 4H), 2.48 (s, 4H), 1.45 – 1.40 (bs, 27H) ppm.

tri-*tert*-butyl-2,2',2''-(10-(2-((2-aminoethyl)amino)-2-oxoethyl)-1,4,7,10-tetraazacyclododecane-1,4,7-triyl)triacetate (5)

Compound **4** (145 mg, 194 μ mol, 1.0 eq) was dissolved in anhydrous MeOH (0.5 mL), degassed with Argon balloons and Pd/C (6 mg, 57 μ mol, 0.3 eq) was added under an Argon atmosphere. Subsequently, H₂ filled balloons were inserted into the reaction solution and the reaction was stirred for 2 h at 23 °C. Then the catalyst was removed by filtration, the filtrate was concentrated to dryness *via* rotary evaporation and crude product **5** was obtained as a yellow solid (112 mg, 182 μ mol, 92%), which was employed in the next step without further purification.

¹H NMR (500 MHz, MeOH-d₄): δ = 8.44 (s, 2H), 3.66 (d, *J* = 9.2 Hz, 6H), 3.59 (d, *J* = 11.6 Hz, 2H), 3.50 (t, *J* = 6.0 Hz, 2H), 3.06 (dd, *J* = 13.6, 7.6 Hz, 18H), 1.50 (bs, 27H) ppm.

ESI-HRMS: 5: C₃₀H₅₉N₆O₇⁺ calculated [M+H]⁺: 615.4439, measured [M+H]⁺: 615.4443 (Δ = 0.4 ppm).

tri-*tert*-butyl-2,2',2''-(10-(2-((2-(2,3-diacetoxybenzamido)ethyl)amino)-2-oxoethyl)-1,4,7,10-tetraazacyclododecane-1,4,7-triyl)triacetate (6)

According to a modified procedure from K. Ferreira⁶⁸ et al., high vacuum-dried **2** (27 mg, 115 μ mol, 1.1 eq) was dissolved in anhydrous DCM/DMF (2 / 0.2 mL) and oxalylchloride was added at 0 °C (20 μ L, 230 μ mol, 2.2 eq) slowly under Argon atmosphere. The resulting reaction was equilibrated to room temperature and continued stirring for 2 hours at 22 °C. The formation of the acid chloride was tested via in situ formation of the corresponding methyl ester in anhydrous MeOH and visualization by TLC (PE:EtOAc - 1:1). After completion, the solvent was removed and the residue was dried under high vacuum for minimum 2 hours or overnight at ambient temperature. Then, a solution of **5** (64 mg, 104 μ mol, 1.0 eq) dissolved in KHCO₃ (1 M, 500 μ L, pH 8.5-9.0) was cooled to 0 °C before the acid chloride, dissolved in dry 1,4-dioxane (500 μ L), was added dropwise under vigorous stirring while the pH was monitored. After the addition, the reaction continued stirring for 30 min at 22 °C and the solvent was removed by rotary evaporation (water bath maximum 30 °C). The residue was dissolved in MeCN/milliQ water, filtered over a syringe filter and purified by RP-HPLC (C18-phenomenex, 40 min gradient from 10-60 % MeCN/H₂O 1 % AcOH). Product containing fractions were identified by LCMS and compound **6** (29 mg, 35 μ mol, 33 %) as well as the mono-acetylated product (5 mg, 6 μ mol, 6 %) could be obtained as white solids.

¹H NMR (700 MHz, MeCN-d₃): δ = 7.54 (d, *J* = 7.2 Hz, 1H), 7.36 – 7.30 (m, 2H), 3.46 (m, 2H), 3.38 (m, 4H), 3.30 (m, 6H), 2.81 (m, 12H), 2.70 (m, 4H), 2.26 (t, *J* = 3.6 Hz, 6H), 1.43 (bs, 27H) ppm.

ESI-HRMS: $C_{41}H_{67}N_6O_{12}^+$ calculated $[M+H]^+$: 835.4819, measured $[M+H]^+$: 835.4836 ($\Delta = 0.17$ ppm).

2,2',2''-(10-(2-((2-(2,3-diacetoxybenzamido)ethyl)amino)-2-oxoethyl)-1,4,7,10-tetraazacyclododecane-1,4,7-triyl)triacetic acid (7)

To a solution of **6** (22 mg, 26 μ mol, 1.0 eq) in DCM (250 μ L) were added AcOH (99%, 250 μ L) and TFA (500 μ L) at 0 °C. The reaction was stirred for 25h at 23 °C. The solvent was removed *in vacuo*, the residue was purified by RP-HPLC (C18 phenomenex, 40 min gradient: 10-40% MeCN/H₂O 1.0% AcOH) and compound **7** could be obtained as a white solid (4 mg, 6 μ mol, 23%).

¹H NMR (700 MHz, MeOH-d₄): $\delta = 7.58$ (dd, $J = 7.5, 1.8$ Hz, 1H), 7.40 – 7.33 (m, 2H), 3.86 (m, 4H), 3.76 (m, 2H), 3.71 – 3.58 (m, 2H), 3.57 – 3.41 (m, 3H), 3.39 – 3.32 (m, 6H), 3.30 – 3.11 (m, 10H), 2.29 (s, 3H), 2.28 (s, 3H).

¹³C NMR (176 MHz, MeOH-d₄): $\delta = 170.0, 169.9, 168.4, 162.95, 162.7, 144.6, 141.78, 131.8, 127.6, 127.2, 127.0, 119.0, 117.3, 55.8, 40.2, 40.1, 20.5, 20.4$.

ESI-HRMS: 7: $C_{29}H_{43}N_6O_{12}^+$ calculated $[M+H]^+$: 667.2932, measured $[M+H]^+$: 667.2938 ($\Delta = 0.6$ ppm).

Gallium-2,2',2''-(10-(2-((2-(2,3-diacetoxybenzamido)ethyl)amino)-2-oxoethyl)-1,4,7,10-tetraazacyclododecane-1,4,7-triyl)triacetate ([^{nat}Ga]7)

Compound **7** (2.8 mg, 4.2 μ mol, 1.0 eq) was dissolved in NaOAc buffer (0.5 M, pH = 4.5, 0.4 mL) and a solution of ^{nat}GaCl₃ (3.7 mg, 21 μ mol, 5.0 eq) in NaOAc buffer (0.2 mL) was added. The reaction was vortexed for 10 seconds and then heated to 95 °C for 10 min. Subsequently, [^{nat}Ga]7 was purified by RP-HPLC (C18 phenomenex, 40 min gradient 10-30 % MeCN/H₂O, 1 % AcOH) and could be obtained as a white solid (2.6 mg, 3.5 μ mol, 84 %). **¹H NMR (700 MHz, D₂O):** $\delta = 7.55 - 7.52$ (m, 1H), 7.47 – 7.41 (m, 2H), 4.02 – 3.94 (m, 2H), 3.87 – 3.75 (m, 6H), 3.64 (s, 2H), 3.62 – 3.55 (m, 2H), 3.45 (ddd, $J = 30.3, 16.8, 9.5$ Hz, 8H), 3.34 – 3.22 (m, 8H), 2.34 (s, 3H), 2.32 (s, 3H) ppm.

¹³C NMR (176 MHz, D₂O): $\delta = 175.7, 173.4, 172.3, 171.8, 171.3, 168.5, 167.9, 142.3, 139.3, 129.6, 127.6, 126.4, 126.3, 71.3, 66.5, 62.3, 61.6, 59.3, 57.3, 57.1, 54.6, 54.4, 38.9, 38.2, 19.8, 19.0, 16.3$ ppm.

ESI-HRMS: [^{nat}Ga]7: $C_{29}H_{40}GaN_6O_{12}^+$ calculated $[M+H]^+$: 733.1953, measured $[M+H]^+$: 733.1962 ($\Delta = 0.9$ ppm).

2,2',2''-(10-(2-((2-(2,3-dihydroxybenzamido)ethyl)amino)-2-oxoethyl)-1,4,7,10-tetraazacyclododecane-1,4,7-triyl)triacetic acid (8)

To a solution of acetylated compound **7** (44 mg, 70 μmol , 1.0 eq) in anhydrous MeOH (0.8 mL), cooled to 0 °C, DIPEA (0.2 mL) was added, the 20% solution was equilibrated to 22 °C and continued stirring for 4 hours. After removal of the solvent and purification by RP-HPLC (C18-phenomenex, 40 min gradient: 0-20% MeCN/H₂O 0.1% HCOOH) and lyophilization product **8** could be obtained as a white solid (22 mg, 38 μmol , 60%).

¹H NMR (700 MHz, MeOH-d₄): δ = 7.37 (dd, J = 8.1, 1.4 Hz, 1H), 6.91 (dd, J = 7.8, 1.4 Hz, 1H), 6.71 (t, J = 8.0 Hz, 1H), 3.75 (s, 4H), 3.59 (s, 2H), 3.55 (t, J = 5.8 Hz, 2H), 3.50 – 3.34 (m, 11H), 3.04 (d, J = 29.9 Hz, 8H) ppm.

¹³C NMR (176 MHz, MeOH-d₄): δ = 173.2, 171.1, 170.6, 168.6, 149.2, 145.9, 118.2, 118.1, 117.7, 115.3, 56.1, 55.6, 53.2, 51.1, 50.6, 48.9, 48.5, 38.7, 38.6 ppm.

ESI-HRMS: 8: C₂₅H₃₉N₆O₁₀⁺ calculated [M+H]⁺: 583.2721, measured [M+MeCN+H]⁺: 583.2713 (Δ = 0.8 ppm). calculated [M+2H]²⁺: 292.1397, measured [M+2H]²⁺: 292.1402 (Δ = 0.5 ppm).

di-tert-butyl-(((2,2'-(4-(2-((2-((tert-butoxycarbonyl)amino)ethyl)amino)-2-oxoethyl)-1,4,7,10-tetraazacyclododecane-1,7 diyl)bis(acetyl)) bis(azanediy)) bis(ethane-2,1-diyl))dicarbamate (9a)

To a suspension of cyclen (40 mg, 0.23 mmol, 1.0 eq) and NaOAc (63 mg, 0.77 mmol, 3.3 eq) in DMA (1 mL) was added a solution of **17** (215 mg, 0.77 mmol, 3.3 eq) in DMA (1 mL) *via* a syringe pump (0.25 mL/h). The suspension was stirred for 20 h at 25 °C and subsequently a KHCO₃ solution was added and the two-phase solution was extracted with DCM (3 x 100 mL). The combined organic extracts were dried over Na₂SO₄, concentrated to dryness and **9a** was obtained as a crude, yellow oil (229 mg) and used in the next step without any purification. Compound **9a** was prepared according to a modified literature procedure.⁶⁸

ESI-HRMS: 8: calculated C₃₅H₆₉N₁₀O₉⁺ [M+H]⁺ = 773.5242, measured [M+H]⁺ = 773.5262 (Δ = 2 ppm).

2-(4,7,10-tris(2-((2-aminoethyl)amino)-2-oxoethyl)-1,4,7,10-tetraazacyclododecan-1-yl)acetic acid (9)

To a suspension of compound **8** (110 mg, 142 μmol , 1.0 eq) and K_2CO_3 (39 mg, 284 μmol , 2.0 eq) in MeCN (0.5 mL), was added *o*-benzyl-bromoacetate (34 μL , 213 μmol , 1.5 eq) in MeCN (0.5 mL) and the reaction continued stirring for 1 hour at 28 °C. After completion, the suspension was filtered, and the filtrate was concentrated under reduced pressure. The residue was dissolved in DCM (0.75 mL) and TFA (0.25 mL) was added at 0 °C. The reaction was stirred at ambient temperature for 2 hours. Then the solvent was removed and the residue was dissolved in MeOH (0.5 mL) under H_2 atmosphere, Pd/C (3 mg, 25 μmol , 0.17 eq) was added in Ar-degassed MeOH (0.5 mL) and stirred under H_2 atmosphere for 1 h at 25 °C. The catalyst was removed over a syringe filter and the filtrate was evaporated to dryness to yield **9** as a yellow oil (69 mg, 85% pure acc. to LCMS, 99%) which was used without any further purification in the next step.

ESI-HRMS: 9: calculated $\text{C}_{22}\text{H}_{47}\text{N}_{10}\text{O}_5^+$ $[\text{M}+\text{H}]^+ = 531.3724$, measured $[\text{M}+\text{H}]^+$: 531.3736 ($\Delta = 1.2$ ppm).

2-(4,7,10-tris(2-((2-(2,3-diacetoxybenzamido)ethyl)amino)-2-oxoethyl)-1,4,7,10-tetraazacyclododecan-1-yl)acetic acid (10)

Compound **10** was prepared according to a modified literature procedure.⁶⁸ To a solution of **2** (104 mg, 436 μmol) in DCM (400 μL) and DMF (100 μL) was added oxalylchloride (74 μL , 872 μmol) at 0 °C and the orange solution was stirred at 20 °C for 1 h. Then the reaction mixture was concentrated and dried under vacuum for 2 hours. To a solution of **9** (100 mg, 104 μmol , 1 eq) in KHCO_3 (3.0 mL, 0.5 M in H_2O) was added dropwise a solution of the acid chloride in anhydrous 1,4-dioxane (3.0 mL) at 0 °C over 10 min. After the addition, the mixture was stirred at 20 °C for 0.5 h. After concentration via rotary evaporation at 30 °C, the orange solid was suspended in MeCN with 1% AcOH, filtered and purified by RP-HPLC (C18 phenomenex, 40-min-long gradient from 5 to 40 % MeCN/ H_2O , 1% AcOH). Product containing fractions were identified by LCMS and lyophilized to yield white solid **10** (45 mg, 37.8 μmol , 36 %).

^1H NMR (700 MHz, $\text{DMSO}-d_6$): $\delta = 8.55$ (bs, 3H), 8.15 (bs, 3H), 7.49 (dd, $J = 12.6, 4.5$ Hz, 3H), 7.37 – 7.33 (m, 6H), 3.59 – 3.43 (m, 4H), 3.25 – 2.94 (m, 19H), 2.81 (d, $J = 77.4$ Hz, 8H), 2.62 – 2.54 (m, 4H), 2.27 (s, 9H), 2.21 (s, 9H), 1.91 (s, 2H) ppm.

^{13}C NMR (176 MHz, CD_3CN): $\delta = 171.8, 169.8, 169.7, 169.5, 169.4, 166.3, 166.3, 163.0, 144.4, 141.6, 141.6, 140.8, 131.9, 131.7, 127.6, 127.5, 127.4, 127.3, 126.8, 126.6, 62.4, 62.2, 59.2, 57.9, 54.5, 52.8, 51.7, 49.5, 41.3, 40.6, 39.9, 39.7, 21.0, 20.9, 20.9, 20.8$ ppm.

ESI-HRMS: 10: C₅₅H₇₂N₁₀O₂₀²⁺ [M+2H]²⁺: calculated: 596.2456, [M+2H]²⁺ measured: 596.2458 (Δ = 0.2 ppm).

2-(4,7,10-tris(2-((2-(2,3-bis(benzyloxy)benzamido)ethyl)amino)-2-oxoethyl)-1,4,7,10-tetraazacyclododecan-1-yl)acetic acid (11a)

Prepared according to a modified literature procedure.⁶⁸ To a solution of catechol **2** (135 mg, 0.4 mmol, 3.3 eq) in DCM (1.0 mL) and DMF (0.1 mL) at 0 °C was added oxalylchloride (69 μL, 0.8 mmol, 6.6 eq) and the solution was stirred for 2 h at 24 °C. The formation of the acid chloride was monitored by TLC (generation of the MeOH ester in dry MeOH & DCM/MeOH 1% running solvent). After completion, the solvent was removed *in vacuo* and the acid chloride was dried overnight under high vacuum. A solution of amine **9** (65 mg, 0.1 mmol, 1.0 eq) in KHCO₃ (1 M in milliQ H₂O, 1 mL) was cooled to 0 °C before the acid chloride of **2** was added dropwise, dissolved in anhydrous 1,4-dioxane (0.5 mL) at 0 °C. During the addition the pH was monitored closely. After the addition, the yellow solution was equilibrated to 22 °C and continued stirring at that temperature for 1 hour. Product **11a** was purified by RP-HPLC (C18-phenomenex, 40 min gradient: 20-85% MeCN/H₂O, 1% AcOH) and could be afforded as a white solid (24 mg, 16 μmol, 13%).

¹H NMR (700 MHz, DMSO-d₆): δ = 8.52 (bs, 2H), 8.27 (t, 2H), 8.23 (t, 1H), 8.18 (s, 1H), 7.80 (bs, 1H), 7.1-7.5 (m, 39H), 5.18 (d, 6H), 4.99 (d, 6H), 3.0-3.9 (m, 32H), 1.26 (m, 2H) ppm.

¹³C NMR (176 MHz, DMSO-d₆): δ = 166.1, 151.6, 145.2, 137.0, 136.8, 130.80, 128.5, 128.4, 128.3, 128.2, 128.0, 128.0, 127.8, 124.17, 75.16, 70.17 ppm.

ESI-HRMS: 11a: C₈₅H₉₆N₁₀O₁₄²⁺ calculated [M+2H]²⁺:740.3548, measured [M+2H]²⁺: 740.3561 (Δ =1.3 ppm).

2-(4,7,10-tris(2-((2-(2,3-dihydroxybenzamido)ethyl)amino)-2-oxoethyl)-1,4,7,10-tetraazacyclododecan-1-yl)acetic acid (11)

Prepared according to a previously established literature procedure.⁶⁸ To a solution of **11a** (25 mg, 11 μmol, 1.0 eq) in Ar-degassed, anhydrous MeOH (0.5 mL) was added Pd/C (3 mg, 3 μmol, 0.17 eq) in anhydrous, degassed MeOH (0.5 mL). The reaction stirred under H₂ atmosphere for 1 h at 22 °C. The catalyst was removed by filtration over a syringe filter and the reaction was concentrated to dryness to yield **11** (11 mg, 12 μmol, 75%) as a clear oil. Alternatively, the same product could be obtained by a transacetylation procedure: Acetylated compound **10** (5 mg, 4 μmol, 1.0 eq) was stirred in anhydrous MeOH with 20% (v/v) anhydrous DIPEA, added at 0 °C, for 4 hours at 25 °C. Solvent and base were removed by rotary

evaporation and the residue was dried overnight under high vacuum to yield **11** as a clear oil (3.94 mg, 4 μ mol, quant.) in quantitative yield.

^1H NMR (700 MHz, MeOH- d_4): δ = 7.21 – 7.20 (m, 3H), 6.93 (dd, J = 3.9, 2.5 Hz, 3H), 6.72 (m, J = 3.8 Hz, 3H), 3.60 – 3.51 (m, 12H), 3.35 (d, J = 5.3 Hz, 12H), 3.25 – 3.16 (m, 12H) ppm.

^{13}C NMR (176 MHz, MeOH- d_4): δ = 172.06, 162.37, 162.16, 150.26, 147.55, 120.02, 119.99, 119.94, 119.10, 119.03, 117.08, 117.03, 57.62, 56.44, 40.83, 39.91 ppm.

ESI-HRMS: 11: $\text{C}_{43}\text{H}_{59}\text{N}_{10}\text{O}_{14}^+$ calculated $[\text{M}+\text{H}]^+ = 939.4207$, measured $[\text{M}+\text{H}]^+ = 939.4220$ ($\Delta = 1.3$ ppm).

Gallium-(III)-(2-(4,7,10-tris(2-((2-(2,3-dihydroxybenzamido)ethyl)amino)-2-oxoethyl)-1,4,7,10-tetraazacyclododecan-1-yl)acetate) ($[\text{natGa}]\mathbf{11}$)

To a solution of **11** (11 mg, 12 μ mol, 1.0 eq) in NaOAc buffer (0.5 M, pH = 4.5, 0.5 mL) was added a solution of GaCl_3 (10 mg, 59 μ mol, 5.0 eq) in NaOAc buffer (0.2 mL). The components were vortexed for 30 sec and heated to 95 $^\circ\text{C}$ for 10 min. After 10 min and 20 min additional equivalents of GaCl_3 (each 5.0 eq) were added. The mixture was filtered over a syringe filter and purified via HPLC (40 min gradient: 0-20 % MeCN in H_2O with 0.1 % TFA) to yield $[\text{natGa}]\mathbf{11}$ (2.2 mg, 3.4 μ mol, 18 %) as a white solid.

^1H NMR (700 MHz, MeOH- d_4): δ = 7.19 – 7.14 (m, 3H), 6.94 – 6.92 (m, 3H), 6.73 – 6.69 (m, 3H), 3.91 – 3.83 (m, 6H), 3.81 (d, J = 16.4 Hz, 2H), 3.75 – 3.71 (m, 2H), 3.69 (d, J = 16.4 Hz, 2H), 3.67 – 3.63 (m, 2H), 3.50 (m, J = 17.8, 13.2, 7.2, 3.3 Hz, 8H), 3.42 – 3.36 (m, 8H), 3.29 – 3.08 (m, 6H) ppm.

^{13}C NMR (176 MHz, MeOH- d_4): δ = 174.07, 173.84, 172.70, 172.11, 172.05, 168.93, 162.34, 162.14, 150.16, 149.23, 147.31, 147.25, 120.06, 119.91, 119.85, 119.36, 118.77, 118.64, 117.31, 117.00, 116.70, 60.93, 57.90, 57.48, 56.00, 55.42, 49.00, 46.97, 43.94, 43.49, 40.63, 39.92, 38.39, 28.12, 17.34, 17.17.

N-(2-(2-(2-(2-azidoethoxy)ethoxy)ethyl)-2-bromoacetamide (12)

Amino PEG₃ Azide linker (550 mg, 2.52 mmol, 1.0 eq) was dissolved in 100 mL DCM at 0 $^\circ\text{C}$. Then K_2CO_3 (417.95 mg, 3.05 mmol, 1.2 eq) dissolved in H_2O (50 mL) was added in one portion. Bromo acetyl bromide (610 mg, 3.02 mmol, 1.2 eq) was dissolved in DCM (25 mL) and added dropwise at 0 $^\circ\text{C}$. After stirring for 15 minutes at 0 $^\circ\text{C}$, the ice bath was removed, and the two-phase solution continued stirring for 1 hour at 23 $^\circ\text{C}$. The phases were separated, and the aqueous phase was extracted with DCM (2 x 40 mL). The combined organic extracts

were dried over Na₂SO₄ and concentrated *in vacuo*. The residue was dried under high vacuum overnight yielding **12** as a slightly yellow oil (773.36 mg, 2.29 mmol, 91%) which was used without further purification in the next step.

¹H NMR (500 MHz, CDCl₃): δ = 6.91 (bs, 1H), 3.87 (s, 2H), 3.67 (m, 10 H), 3.59 (t, 2H), 3.49 (m, 2H), 3.39 (m, 2H) ppm.

¹³C NMR (100 MHz, CDCl₃): δ = 165.7, 70.9, 70.8, 70.6, 70.2, 69.5, 53.6, 50.8, 40.1, 29.3 ppm.

ESI-HRMS: 12: C₁₀H₂₀BrN₄O₄⁺ - calculated [M+H]⁺ = 339.0662 measured [M+H]⁺ = 339.0663 (Δ = 0.1 ppm).

2,2',2''-(10-(14-azido-2-oxo-6,9,12-trioxa-3-azatetradecyl)-1,4,7,10tetraazacyclododecane-1,4,7-triyl) tris(N-(2-aminoethyl)acetamide) (13)

Prepared according to a modified literature procedure.⁶⁸ Linker **12** (302 mg, 0.89 mmol, 1.15 eq) was dissolved in MeCN (2.5 mL) and added to a stirred suspension of **9a** (600 mg, 0.776 mmol, 1.0 eq) and K₂CO₃ (429 mg, 3.11 mmol, 4.0 eq) in MeCN (7.5 mL). The reaction continued stirring overnight at 22 °C. The reaction progress was monitored by LCMS and after full conversion, the reaction mixture was filtered and dried for 1h *in vacuo* to obtain a crude beige solid. The residue was dissolved in DCM (75 mL) and washed with water and brine (each 2x 50 mL), then dried over Na₂SO₄. The solvent was removed by rotary evaporation and the residue was dried under high vacuum for 30 minutes. Then DCM (5 mL) and TFA (4 mL) were added at 0 °C, the reaction was equilibrated to room temperature and continued stirring at 24 °C for three hours. After full conversion, the solvent was removed by rotary evaporation, the residue was dried overnight under high vacuum and crude **13** (229 mg, 0.313 mmol, 40% over two steps) was obtained as a beige oil. **¹H NMR (MeOH-d₄, 700 MHz):** δ = 4.57 (s, 4H), 3.68 (m, 8H), 3.62 (m, 2H), 3.52 (t, J = 4.9 Hz, 2H), 3.41 (t, J = 5.5 Hz, 2H), 3.16 (m, J = 6.4 Hz, 8H), 3.07 (t, J = 5.9 Hz, 8H), 3.06 (s, 4H), 2.92 (s, 4H), 2.15 (s, 4H), 2.08 (s, 4H) ppm.

N,N',N''-(((2,2',2''-(10-(2-oxo-14-(112,312-triaz-2-en-1-yl)-6,9,12-trioxa-3-azatetradecyl)-1,4,7,10-tetraazacyclododecane-1,4,7-triyl)tris(acetyl))tris(azanediyl))tris(ethane-2,1-diyl))tris(2,3-dihydroxybenzamide) (14)

Oxalylchloride (250 μL, 2.92 mmol, 9.0 eq) was added to a stirred solution of **2** (386 mg, 1.62 mg, 5.0 eq) in dry DCM/DMF (500 μL/50 μL) at 0 °C under Ar conditions. The suspension was stirred for 2 h at 22 °C and the reaction progress was checked by TLC. Subsequently, the solvent was removed by rotary evaporation and the residue was dried under high vacuum

overnight to yield a dark brown solid. 1,4-dioxane (1.2 mL) was added and the suspension was added dropwise to a solution of **13** (237 mg, 0.32 μ mol, 1.0 eq) in 1 M K_2CO_3 on ice. The pH was kept constant by addition of minute amounts of sat. K_2CO_3 solution when required. The reaction mixture was equilibrated to 23 °C and continued stirring for 1 hour at that temperature. Subsequently, the mixture was extracted with DCM (3x 100 mL), the combined organic extracts were dried over Na_2SO_4 and the solvent was removed *in vacuo*. The residue was taken up in MeCN/H₂O 1:1 (2.5 mL) and purified by RP-HPLC (C18 phenomenex, 40 min gradient 0-35% MeCN/H₂O 1% AcOH). Product containing fractions were identified by LCMS and lyophilized to obtain **14** (175 mg, 0.126 mmol, 39%) as a white solid.

¹H-NMR (500 MHz, MeOH-d₄): δ = 7.48 (m, 3H), 7.36 – 7.31 (m, 6H), 3.68 – 3.59 (m, 16H), 3.58 – 3.56 (m, 2H), 3.53 – 3.50 (m, 2H), 3.48 – 3.46 (m, 4H), 3.38 (m, 12H), 3.05 – 2.73 (m, 16H), 2.30 – 2.28 (m, 9H), 2.27 – 2.25 (m, 9H) ppm.

¹³C-NMR (176 MHz, MeOH-d₄): δ = 180.2, 175.2, 172.2, 171.9, 163.1, 162.9, 151.3, 148.5, 147.2, 130.7, 129.0, 121.7, 121.2, 120.8, 120.0, 119.3, 119.2, 119.1, 118.3, 117.9, 117.4, 117.2, 117.1, 113.9, 71.7, 71.6, 71.6, 71.6, 71.5, 71.3, 71.2, 71.1, 71.1, 70.5, 70.4, 66.9, 66.1, 62.6, 57.5, 54.5, 54.1, 52.8, 51.8, 49.0, 43.0, 40.2, 39.9, 39.7, 39.5, 24.2, 20.7, 19.8, 18.6, 17.8, 17.4, 17.3, 17.2, 14.0, 10.6 ppm.

ESI-HRMS: 14: $C_{63}H_{87}N_{14}O_{22}^{+}$ - calculated $[M+H]^+ = 1391.6113$ measured $[M+H]^+ = 1391.6165$ ($\Delta = 5.2$ ppm).

2,2',2''-(10-(2-oxo-2-(((5aR,6aS)-1-(2-oxo-1-(4,7,10-tris(2-((2,3-dihydroxybenzamido)ethyl)amino)-2-oxoethyl)-1,4,7,10-tetraazacyclododecan-1-yl)-6,9,12-trioxa-3-azatetradecan-14-yl)-1,4,5,5a,6,6a,7,8octahydrocyclopropa[5,6]cycloocta[1,2-d][1,2,3]triazol-6yl)methoxy)carbonyl)amino)ethyl)amino)ethyl)-1,4,7,10-tetraazacyclododecane-1,4,7-triyl)triacetic acid (15)

Azido DOTAM **14** (30 mg, 0.02 mmol, 1.0 eq) was dissolved in MeOH (800 μ L) and DIPEA (200 μ L) was added at 0 °C. The ice bath was removed, the reaction was stirred for 4 hours at 25 °C and then the solvent was removed by rotary evaporation. The residue was dried under high vacuum overnight to remove residual DIPEA to yield a beige oil. A mixture of 1xPBS (pH 7.4)/DMSO (300 μ L each) and **BCN-DOTA** (20.14 mg, 0.03 mmol, 1.5 eq) in 400 μ L MeOH were added. The reaction was stirred overnight at 25 °C, the reaction progress was controlled by LCMS. After completion, the organic solvent was removed as much as possible by rotary evaporation. The residual liquid was filtered and injected into the RP-HPLC (C18 phenomenex,

40 min gradient 0-30% MeCN/H₂O 0.1% HCOOH). Product containing fractions were identified by LCMS and lyophilized to dryness to yield **15** (30 mg, 0.02 mmol, 80%) as a colorless oil.

¹H-NMR (700 MHz, DMSO-d₆): δ = 13.12 – 12.19 (bs, 1H), 9.53 – 9.07 (s, 1H), 8.85 (d, *J* = 17.4 Hz, 3H), 8.19 (m, 6H), 7.69 (m, 1H), 7.43 (m, 1H), 7.26 (d, *J* = 8.0 Hz, 3H), 6.92 – 6.89 (m, 3H), 6.65 (dd, *J* = 11.3, 4.5 Hz, 3H), 4.40 – 4.37 (m, 2H), 4.05 – 3.99 (m, 2H), 3.79 (m, 2H), 3.72 (m, 2H), 3.56 – 3.51 (m, 4H), 3.49 (m, 4H), 3.48 – 3.46 (m, 4H), 3.46 – 3.44 (m, 8H), 3.42 (m, 6H), 3.39 – 3.37 (m, 8H), 3.34 (m, 4H), 3.30 (dd, *J* = 5.5 Hz, 8H), 3.25 (dd, *J* = 10.1, 4.4 Hz, 4H), 3.16 – 3.14 (m, 2H), 3.11 (s, 2H), 3.01 – 2.95 (m, 14H), 2.84 (bs, 8H), 2.76 – 2.72 (m, 2H), 2.67 (m, 4H), 2.12 – 2.05 (m, 2H), 1.56 – 1.50 (m, 2H), 1.09 (dd, *J* = 16.8, 8.4 Hz, 1H), 0.91 – 0.89 (m, 1H) ppm.

¹³C-NMR (176 MHz, DMSO-d₆): δ = 181.3, 181.2, 179.4, 172.6, 165.9, 159.1, 155.7, 155.7, 152.7, 143.3, 128.3, 127.4, 126.7, 124.5, 124.5, 79.5, 79.2, 79.2, 79.1, 78.9, 78.8, 78.8, 78.7, 78.4, 78.4, 78.3, 70.9, 70.8, 65.7, 64.5, 64.3, 64.2, 60.5, 59.8, 59.5, 59.3, 56.7, 48.3, 48.2, 47.9, 47.6, 47.3, 34.8, 31.7, 31.4, 30.7, 28.6, 28.1, 26.8, 9.6 ppm.

ESI-HRMS: 15: C₈₀H₁₂₂N₂₀O₂₅²⁺ calculated [M+2H]²⁺: 881.4439 measured [M+2H]²⁺: 881.4325 (Δ = 1.4 ppm).

Gallium-2,2',2''-(10-(2-oxo-2-((2-(((5aR,6aS)-1-(2-oxo-1-(4,7,10-tris(2-((2,3-dihydroxybenzamido)ethyl)amino)-2-oxoethyl)-1,4,7,10-tetraazacyclododecan-1-yl)-6,9,12-trioxa-3-azatetradecan-14-yl)-1,4,5,5a,6,6a,7,8-octahydrocyclopropa[5,6]cycloocta[1,2-d][1,2,3]triazol-6-yl)methoxy)carbonyl)amino)ethyl)amino)ethyl)-1,4,7,10-tetraazacyclododecane-1,4,7-triyl)triacetate ([^{nat}Ga]15)

15 (10 mg, 0.006 mmol, 1.0 eq) was dissolved in 200 μL DMSO and ^{nat}GaCl₃ (2 mg, 0.011 mmol, 2 eq), dissolved in NaOAc buffer, was added at 23 °C. The reaction was heated to 100 °C under vigorous stirring. The complexation progress was monitored by LCMS - after full conversion (ca. 10 minutes), the solution was filtered and subsequently injected into the RP-HPLC (C18 phenomenex, 40 min gradient 2-30% MeCN/H₂O, 0.1% HCOOH). Product containing fractions were identified by LCMS and lyophilized to dryness, yielding the complex [^{nat}Ga]15 as a white solid (7.9 mg, 0.004 mmol, 76%).

¹H-NMR (700 MHz, MeOH-d₄): δ = δ 7.34 – 7.07 (dd, J = 7.8, 1.3 Hz, 3H), 6.93 (dd, J = 7.8, 1.3 Hz, 3H), 6.79 – 6.63 (t, J = 8.3 Hz, 3H), 3.66 – 3.61 (m, 24H), 3.60 – 3.58 (m, 4H), 3.57 – 3.53 (q, 8H), 3.48 – 3.43 (t, J = 5.96 Hz, 8H), 3.41 (m, 8H), 3.38 – 3.35 (t, J = 5.96 Hz, 8H), 2.94 (m, 28H), 2.21 (m, 1H), 1.61 (m, 1H), 1.08 (m, 1H) ppm.

¹³C-NMR (176 MHz, MeOH-d₄): δ = 171.83, 169.47, 150.38, 147.50, 119.76, 119.70, 118.76, 116.77, 71.61, 71.56, 71.50, 71.26, 71.07, 70.38, 58.29, 57.72, 57.48, 53.18, 52.89, 51.77, 49.00, 40.39, 40.17, 40.13, 17.28 ppm.

benzyl (R)-2-bromopropanoate (16)

Compound **16** was prepared according to a literature procedure from Mao et al.⁶⁹ To a solution of the (R)-2-bromo-propionic acid (400 mg, 2.61 mmol, 1.0 eq) and DCC (648 mg, 3.14 mmol, 1.2 eq) in Et₂O (5 mL) a solution of DMAP (16 mg, 0.13 mmol, 0.05 eq) and BnOH (326 μ L, 3.14 mmol, 1.2 eq) in Et₂O (2 mL) was added and the reaction was stirred overnight. The next morning, the reaction was concentrated *in vacuo* and **16** (528 mg, 2.17 mmol, 83 %) could be obtained via silica gel chromatography (0-1% EtOAc in PE bp 40-60 °C) as a colorless oil.

¹H NMR (500 MHz, CDCl₃): δ = 7.39 – 7.32 (m, 5H), 5.21 (t, J = 2.0 Hz, 2H), 4.45 – 4.38 (m, 1H), 1.84 (d, J = 6.9 Hz, 3H) ppm.

tert-butyl (2-(2-bromoacetamido)ethyl)carbamate (17)

According to a literature procedure from K. Ferreira⁶⁸ et al, to a solution of *N*-Boc-ethylendiamine (4.0 mL, 25 mmol, 1.0 eq) in DCM (120 mL), a solution of K₂CO₃ (4.2 g, 30 mmol, 1.2 eq) in H₂O (90 mL) was added and the two-phase mixture was cooled to 0 °C. A solution of bromo acetyl bromide (2.6 mL, 30 mmol, 1.2 eq) in DCM (90 mL) was added dropwise over 30 minutes at 0 °C and the reaction mixture was stirred for 1.5 h at 21 °C. The phases were separated, and the aqueous phase was extracted with DCM (3 x 100 mL). The organic extracts were washed with H₂O (2x200 mL), brine (2x100 mL) and dried over Na₂SO₄. After removal of the solvent, product **17** was obtained as a white solid (6.5 g, 23 mmol, 93 %) which was used crude in the next step.

¹H NMR (500 MHz, CDCl₃): δ = 7.09 (s, 1H), 4.87 (s, 1H), 3.86 (s, 2H), 3.42 – 3.37 (m, 2H), 3.34 – 3.29 (m, 2H), 1.45 (s, 9H) ppm.

¹³C NMR (176 MHz, CDCl₃): δ = 166.5, 79.9, 41.4, 39.8 28.4 ppm.

ESI-HRMS: 17: C₉H₁₈BrN₂O₃⁺ calculated [M+H]⁺: 281.0494, measured [M+H]⁺: 281.0502 (Δ = 0.8 ppm).

dibenzyl-2,2'-(1,4,7,10-tetraazacyclododecane-1,7-diyl)(2S,2'S)-dipropionate (18)

dibenzyl-2,2'-(1,4,7,10-tetraazacyclododecane-1,4-diyl)(2S,2'S)-dipropionate (19)

tribenzyl-2,2',2''-(1,4,7,10-tetraazacyclododecane-1,4,7-triyl)(2S,2'S,2''S)-tripropionate (20)

To a suspension of cyclen (50 mg, 0.29 mmol, 1.0 eq) und NaOAc (79 mg, 0.96 mmol, 3.3 eq) in DMA (0.5 mL) a solution of **16** (233 mg, 0.96 mmol, 3.3 eq) in DMA (1.0 mL) was added *via* a syringe pump (300 μ L/h). The suspension was stirred for 20 h at 28 °C, washed with KHCO₃ solution (2x50 mL, 0.5 M) and extracted with CHCl₃ (3x50 mL). The combined organic extracts were dried over Na₂SO₄ and the solvent was removed under reduced pressure. Products were obtained as an inseparable mixture of di- (**18/19**) and tri-substituted (**20**) compounds (180 mg) respectively and employed in the next step without purification.

LCMS: 18/19: m/z = 497.66 [M+H]⁺, t_R = 0.53 min. **20:** m/z = 659.85 [M+H]⁺; t_R = 0.99 min.

dibenzyl-2,2'-(4,10-bis(2-((2-aminoethyl)amino)-2-oxoethyl)-1,4,7,10-tetraazacyclododecane-1,7-diyl)(2S,2'S)-dipropionate (21)

dibenzyl-2,2'-(7,10-bis(2-((2-aminoethyl)amino)-2-oxoethyl)-1,4,7,10-tetraazacyclododecane-1,4-diyl)(2S,2'S)-dipropionate (22)

tribenzyl-2,2',2''-(10-(2-((2-aminoethyl)amino)-2-oxoethyl)-1,4,7,10-tetraazacyclododecane-1,4,7-triyl)(2S,2'S,2''S)-tripropionate (23)

To a suspension of **18**, **19** und **20** (142 mg, ca. 0.22 mmol, 1.0 eq) and K₂CO₃ (149 mg, 1.08 mmol, 5.0 eq) in MeCN (1.5 mL), **17** (182 mg, 0.65 mmol, 3.0 eq) was added in MeCN (0.5 mL) and the suspension was stirred for 1 h at 28 °C. The reaction was filtered and the solvent was removed and dried under reduced pressure and the crude mixture was separated by RP-HPLC (C18 phenomenex, 40 min gradient, 10-60% MeCN/H₂O, 0.1% HCOOH). A mixture of **21/22** (21 mg, 0.023 mmol, 11%) was obtained as a white solid. Several attempts to separate the regioisomers **21/22** by RP-HPLC failed. In addition, pure **23** (25 mg, 0.0291 mmol, 13%) was obtained as a white solid.

21/22:

¹H NMR (500 MHz, DMSO-d₆): δ = 7.36 (m, 10H), 5.11 (s, 4H), 5.09 (s, 2H), 3.62 (m, J = 17.2 Hz, 2H), 3.62 (m, J = 55.3 Hz, 2H), 3.53 (m, 4H), 3.12 (m, 2H), 2.95 (m, 10H), 2.76 (m, 12 H), 1.36 (s, 6H), 1.33 (s, 18H) ppm.

ESI-HRMS: 21/22: C₄₆H₇₃N₈O₁₀⁺ calculated [M+H]⁺: 897.5443, measured [M+H]⁺: 897.5456 (Δ = 1.3 ppm).

23:

¹H NMR (500 MHz, DMSO-d₆): δ = 7.36 – 7.33 (m, 15H), 5.14 (s, J = 2.8 Hz, 2H), 5.10 (s, J = 1.5 Hz, 2H), 5.09 (s, 2H), 3.47 – 3.43 (m, 2H), 3.25 – 3.16 (m, 2H), 3.10 (m, J = 12.5, 6.3 Hz, 2H), 3.04 – 2.99 (m, 2H), 2.96 (m, J = 5.9 Hz, 2H), 2.82 (m, 2H), 2.76 (m, J = 14.7 Hz, 2H), 2.69 (m, J = 4.2 Hz, 4H), 2.66 (m, 4H), 1.34 (s, 9H), 1.02 (m, J = 6.8 Hz, 6H) ppm.

¹³C NMR (176 MHz, DMSO-d₆): δ = 173.2, 173.2, 170.9, 170.9, 170.9, 170.9, 168.5, 168.5, 166.8, 163.0, 155.6, 154.9, 154.9, 136.1, 136.1, 136.0, 136.0, 135.6, 135.6, 128.4, 128.4, 128.1, 128.1, 128.0, 128.0, 127.9, 127.9, 127.9, 127.9, 77.6, 77.6, 65.8, 65.8, 65.2, 65.2, 61.1, 61.0, 55.5, 53.7, 53.7, 52.9, 52.3, 52.1, 51.3, 51.3, 49.6, 49.0, 48.6, 47.3, 46.91, 39.5, 38.5, 38.5, 28.1, 28.1, 11.8, 11.4 ppm.

tribenzyl-2,2',2''-(10-(2-((2-(2,3-diacetoxybenzamido)ethyl)amino)-2-oxoethyl)-1,4,7,10-tetraazacyclododecane-1,4,7-triyl)(2S,2'S,2''S)-tripropionate (24a)

23 (21 mg, 24 μ mol, 1.0 eq) was dissolved in DCM (0.75 mL) and TFA was added at 0 °C (0.25 mL). The solution continued stirring for 2 h at 28 °C. After completion, the reaction was concentrated to dryness and dried under HV overnight to yield **23a** as a clear oil (18.6 mg, 24 μ mol, quant.). To a solution of **2** (6 mg, 26 μ mol, 1.1 eq) in DCM (200 μ L) and DMF (50 μ L), oxalylchloride (5 μ L, 57 μ mol, 2.2 eq) was added at 0 °C and the reaction was stirred for 2 h at 22 °C. The formation of the acid chloride was monitored as previously described. After removal of the solvent, the acid chloride was dried under high vacuum. A solution of **23a** (21 mg, 24 μ mol, 1.0 eq) in KHCO₃ (1 M, 0.5 mL) was cooled to 0 °C before the acid chloride was added dropwise in 1,4-dioxane (0.1 mL), while monitoring the pH staying in a range of 8.5-9. The resulting beige solution was stirred for 30 min at 22 °C and the solvent was removed by rotary evaporation at maximum 30 °C water bath temperature. The residue was dissolved in DCM (50 mL) and washed with sat. NaHCO₃ solution and water (each 3x50 mL), the organic phase was dried over Na₂SO₄. The solvent was removed *in vacuo* and the residue dried

overnight under high vacuum, yielding crude product **24a** as a clear oil (2.5 mg, 3 μ mol, 12%).

LCMS: $m/z = 979.45$ $[M+H]^+$; $t_R = 1.35$ min.

ESI-HRMS: 23a: $C_{42}H_{59}N_6O_7^+$ calculated $[M+H]^+$: 759.4439, measured $[M+H]^+$: 759.4454 ($\Delta = 1.5$ ppm).

1H NMR (700 MHz, MeOH- d_4): $\delta = 7.45$ - 7.33 (m, 18H), 5.14 (m, 6H), 3.64 (m, 2H), 3.48-3.43 (m, 2H), 3.07 (m, 3H), 3.07 (s, 3H), 2.95 (m, .91 (s, 3H), 2.28-2.22 (m, 8H), 2.22-2.19 (m, 4H), 1.72-1.70 (d, 3H), 1.52-1.34 (m, 6H) ppm.

(2S,2'S,2''S)-2,2',2''-(10-(2-((2-(2,3-dihydroxybenzamido)ethyl)amino)-2-oxoethyl)-1,4,7,10-tetraazacyclododecane-1,4,7-triyl)tripropionic acid (24)

To a solution of **24a** (6.5 mg, 7 μ mol, 1.0 eq) in Ar-degassed, anhydrous MeOH (0.5 mL) Pd/C (0.1 mg, 1.2 μ mol, 0.17) was added. The suspension was stirred for 1 hour under an H_2 atmosphere at 22 $^\circ C$. The catalyst was removed by filtration over a syringe filter and the solvent was removed under reduced pressure. The solid was taken up in MeOH (0.8 mL) and DIPEA (0.2 mL) was added at 0 $^\circ C$. The solution was stirred for 1 h at 22 $^\circ C$ and concentrated to dryness. HPLC purification of the product mixture (C18 phenomenex, 40 min gradient 0-30% MeCN/ H_2O , 0.1 % TFA) yielded **24** (2.5 mg, 4 μ mol, 57%) as a white solid.

1H NMR (700 MHz, MeOH- d_4): $\delta = 7.25 - 7.20$ (m, 1H), 6.94 (m, 2H), 6.74 (m, 2H), 4.01 - 3.36 (m, 17H), 3.21 - 3.01 (m, 8H), 1.54 (d, 3H), 1.42 - 1.36 (d, 3H), 1.33 - 1.28 (d, 3H).

ESI-HRMS: 24: $C_{28}H_{45}N_6O_{10}^+$ calculated $[M+H]^+$: 625.3191, measured $[M+H]^+$: 625.3199 ($\Delta = 0.8$ ppm).

(((2,2'-(4,10-bis((S)-1-(benzyloxy)-1-oxopropan-2-yl)-1,4,7,10-tetraazacyclododecane-1,7-diyl)bis(acetyl))bis(azanediy))bis(ethane-2,1-diyl))bis(azanediy))bis(carbonyl))bis(benzene-3,1,2-triyl) tetraacetate (25a)

(((2,2'-(7,10-bis((S)-1-(benzyloxy)-1-oxopropan-2-yl)-1,4,7,10-tetraazacyclododecane-1,4-diyl)bis(acetyl))bis(azanediy))bis(ethane-2,1-diyl))bis(azanediy))bis(carbonyl))bis(benzene-3,1,2-triyl) tetraacetate (26a)

21/22 (21 mg, 23 μ mol, 1 eq) was dissolved in DCM (0.75 mL) and TFA was added at 0 $^\circ C$ (0.25 mL). The solution continued stirring for 2 h at 28 $^\circ C$, was then concentrated to dryness and dried under HV overnight to yield a clear oil (18.7 mg, 23 μ mol, quant.). To a solution of **2** (11 mg, 50 μ mol, 2.2 eq) in DCM (500 μ L) and DMF (50 μ L), oxalylchloride (18.9 μ L, 101.2 μ mol, 4.4 eq) was added at 0 $^\circ C$ and the solution was stirred for 1 h at 22 $^\circ C$. The formation of

the acid chloride was monitored as previously described. After removal of the solvent, the acid chloride was dried under high vacuum for at least 1 hour. A solution of **21a** and **22a** (18.7 mg, 23 μmol , 1.0 eq) in KHCO_3 (1 M in MilliQ water, 1 mL) was cooled to 0 °C and the acid chloride was added dropwise in anhydrous 1,4-dioxane (0.1 mL) while monitoring the pH to stay in the range of 8.5-9. The resulting yellow solution was stirred for 30 min at 22 °C and the solvent was removed under reduced pressure at max. 30 °C water bath temperature. The residue was dissolved in DCM (50 mL) and washed with sat. NaHCO_3 , water (each 3x50 mL) and dried over Na_2SO_4 . The solvent was removed *in vacuo*, dried overnight at ambient temperature, yielding the product **25a/26a** (24.33 mg, 21.4 μmol , 93%) as a clear oil. The crude was employed, without further purification, in the next step.

LCMS: $m/z = 1138.34$ [$\text{M}+\text{H}^+$]; $t_R = 1.22$ min.

ESI-HRMS: **21a/22a** $\text{C}_{36}\text{H}_{57}\text{N}_8\text{O}_6^+$ calculated [$\text{M}+\text{H}^+$]: 697.4395, measured [$\text{M}+\text{H}^+$]: 697.4402 ($\Delta = 0.7$ ppm).

^1H NMR (700 MHz, DMSO- d_6): $\delta = 8.53 - 8.19$ (m, 4H), 7.47 (m, 2H), 7.43 - 7.29 (m, 16H), 5.14 - 5.08 (m, 4H), 3.83 - 3.53 (m, 7H), 3.39 (m, 2H), 3.32 - 3.23 (m, 8H), 2.4-3.2 (m, 6H), 2.67-3.2 (m, 15H), 2.22 - 2.16 (s, 6H), 1.36 (s, 1H), 1.29 - 1.21 (m, 6H) ppm.

(2S,2'S)-2,2'-(4,10-bis(2-((2-(2,3-dihydroxybenzamido)ethyl)amino)-2-oxoethyl)-1,4,7,10-tetraazacyclododecane-1,7-diyl)dipropionic acid (25)

(2S,2'S)-2,2'-(7,10-bis(2-((2-(2,3-dihydroxybenzamido)ethyl)amino)-2-oxoethyl)-1,4,7,10-tetraazacyclododecane-1,4-diyl)dipropionic acid (26)

To a solution of **25a/26a** (50 mg, 44 μmol , 1.0 eq) in anhydrous MeOH under Ar atmosphere (0.5 mL), Pd/C (0.8 mg, 0.7 μmol , 0.17 eq) was added in Ar-degassed MeOH (0.5 mL). The reaction continued stirring for 2 h at 22 °C under an H_2 atmosphere. The mixture was filtered, and the solvent was removed under reduced pressure. The residue was dissolved in MeOH (0.8 mL) and DIPEA (0.2 mL) was added at 0 °C. The reaction was stirred for 1 h at 23 °C and the solvent was evaporated to dryness. The residue was purified by RP-HPLC (C18 phenomenex, 40 min gradient, 10-30% MeCN/ H_2O , 0.1% TFA). **25/26** could not be separated, and a mixture of **25/26** (1.2 mg, 1.5 μmol , 3%) was obtained as a white solid.

^1H NMR (700 MHz, DMSO- d_6): $\delta = 9.02$ (d, $J = 64.0$ Hz, 3H), 8.24 - 7.86 (m, 2H), 7.49 - 7.19 (s, 2H), 6.88 (m, 2H), 6.65 (m, 2H), 3.6 (s, 2H), 3.40 (m, 4H), 3.25 - 2.62 (m, 19H), 2.21 (s, 1H), 2.08 (d, $J = 8.4$ Hz, 2H), 1.24 - 1.12 (m, 6H) ppm.

ESI-HRMS: 25/26: C₃₆H₅₃N₈O₁₂⁺ calculated [M+H]⁺: 789.3785, measured [M+H]⁺: 789.3788 (Δ = 0.3 ppm).

***tert*-butyl (R)-(2-(2-bromopropanamido)ethyl)carbamate (27)**

The product was prepared according to a literature procedure from Moore et al.⁷⁰ (*R*)-2-bromopropanoic acid (168 mg, 1.1 mmol, 1.1 eq) and HATU (380 mg, 1.0 mmol, 1.0 eq) were suspended in DCM (3 mL) and DMF (0.75 mL) and stirred for 5 minutes at 21 °C. Then *N*-Boc-ethylendiamine (158 μ L, 1.0 mmol, 1.0 eq) and DIPEA (170 μ L, 1.0 mmol, 1.0 eq) were added slowly subsequently to the reaction mixture and continued stirring for 4 h at 25 °C. The solvent was removed under reduced pressure. The residue was taken up in EA (20 mL), washed with HCl (pH = 3, 2x15 mL), sat. NaHCO₃ (2x15 mL) and brine (15 mL). The organic phase was dried over Na₂SO₄ and the solvent was removed *in vacuo*. Product **27** was obtained as a white solid (318 mg, 1.07 μ mol, 97%) and used directly in the next step.

¹H NMR (500 MHz, CDCl₃): δ = 7.00 (bs, 1H), 4.86 (bs, 1H), 4.38 (q, *J* = 7.0 Hz, 1H), 3.40 – 3.35 (m, 2H), 3.32 (d, *J* = 5.6 Hz, 2H), 1.87 (d, *J* = 7.1 Hz, 3H), 1.45 (s, 9H) ppm.

¹³C NMR (176 MHz, CDCl₃): δ = 170.2, 157.1, 80.1, 44.9, 41.8, 39.9, 28.5, 23.2 ppm.

di-*tert*-butyl-(((2*S*,2'*S*)-2,2'-(1,4,7,10-tetraazacyclododecane-1,7-diyl)bis(propanoyl))bis(azanediyl))bis(ethane-2,1-diyl))dicarbamate (29)

di-*tert*-butyl-(((2*S*,2'*S*)-2,2'-(1,4,7,10-tetraazacyclododecane-1,4-diyl)bis(propanoyl))bis(azanediyl))bis(ethane-2,1-diyl))dicarbamate (30)

di-*tert*-butyl-(((2*S*,2'*S*)-2,2'-(4-((*S*)-1-((2-((*tert*butoxycarbonyl)amino)ethyl)amino)-1-oxopropan-2-yl)-1,4,7,10-tetraazacyclododecane-1,7-diyl)bis(propanoyl))bis(azanediyl))bis(ethane-2,1-diyl))dicarbamate (31)

To a suspension of cyclen (16 mg, 93 μ mol, 1.0 eq) and NaOAc (25 mg, 308 μ mol, 3.3 eq) in MeCN (1 mL) was added a solution of (*R*)-**27** (91 mg, 308 μ mol, 3.3 eq) at 22 °C in DMA (1 mL) *via* a syringe pump (0.25 mL/h). The suspension was stirred for 72 h at 25 °C, filtered and the solvent was removed under reduced pressure. The residue was dissolved in MeCN (0.5 mL) and K₂CO₃ (100 mg, 723 μ mol) was added. Then a solution of *O*-benzyl bromo acetate (31 μ L, 198 μ mol, 4.4 eq) in MeCN (0.5 mL) was added and the mixture was stirred for 1 hour at 22 °C. The mixture was filtered, and the reaction concentrated *in vacuo* and **29/30** (27 mg, 45 μ mol, 48%) as well as the tri-substitution **31** (7 mg, 8 μ mol, 9%) were obtained as a clear oil. Compound **29/30** could not be separated by multiple RP-HPLC attempts and were employed like this in the next step.

29/30:

¹H NMR (500 MHz, DMSO-d₆): δ = 7.50 – 7.19 (m, 10H), 5.14 – 5.07 (s, 4H), 3.32 (m, 4H), 3.10 (m, J = 14.9, 8.8 Hz, 4H), 2.99 (m, 6H), 2.76 (m, J = 25.6, 18.5 Hz, 6H), 2.67 – 2.52 (m, 8H), 1.37 – 1.35 (m, 18H), 1.25 – 1.16 (m, 6H).

ESI-HRMS: 29/30: C₄₆H₇₃N₈O₁₀⁺ calculated [M+H]⁺: 897.5443, measured [M+H]⁺: 897.5465 (Δ = 2.2 ppm).

31:

¹H NMR (500 MHz, DMSO-d₆): δ = 7.97 (d, J = 70.8 Hz, 4H), 7.37 – 7.35 (m, 5H), 5.10 (s, 2H), 3.18 – 3.13 (m, 4H), 3.09 (m, J = 12.6, 6.3 Hz, 6H), 2.99 (m, J = 5.6 Hz, 6H), 2.81 (m, J = 24.0 Hz, 4H), 2.63 (m, J = 4.2 Hz, 4H), 2.59 (m, J = 9.7, 7.9 Hz, 4H), 1.36 (s, 33H), 1.20 (d, J = 7.0 Hz, 3H).

ESI-HRMS: 31: C₄₇H₈₃N₁₀O₁₁⁺ calculated [M+H]⁺ = 963.6236, measured [M+H]⁺ = 963.6235 (Δ = 0.1 ppm).

dibenzyl-2,2'-(4,10-bis((S)-1-((2-aminoethyl)amino)-1-oxopropan-2-yl)-1,4,7,10-tetraazacyclododecane-1,7-diyl)diacetate (32)

dibenzyl-2,2'-(7,10-bis((S)-1-((2-aminoethyl)amino)-1-oxopropan-2-yl)-1,4,7,10-tetraazacyclododecane-1,4-diyl)diacetate (33)

29/30 was dissolved in DCM (0.75 mL) and TFA (0.25 mL) was added at 0 °C. Then the solution was stirred for 1 hour at 22 °C. The reaction was concentrated to dryness to afford a mixture **32/33** as a white solid (21 mg, 31 μ mol, 68 %) and employed without further purification in the next step.

ESI-HRMS: 32: C₃₆H₅₇N₈O₆⁺ calculated [M+H]⁺: 697.4394, measured [M+H]⁺: 697.4402 (Δ = 0.8 ppm).

((((((2S,2'S)-2,2'-(4,10-bis(2-(benzyloxy)-2-oxoethyl)-1,4,7,10-tetraazacyclododecane-1,7-diyl)bis(propanoyl))bis(azanediyl))bis(ethane-2,1-diyl))bis(azanediyl))bis(carbonyl))bis(benzene-3,1,2-triyl) tetraacetate (34a)

((((((2S,2'S)-2,2'-(7,10-bis(2-(benzyloxy)-2-oxoethyl)-1,4,7,10-tetraazacyclododecane-1,4-diyl)bis(propanoyl))bis(azanediyl))bis(ethane-2,1-diyl))bis(azanediyl))bis(carbonyl))bis(benzene-3,1,2-triyl) tetraacetate (35a)

To a solution of **2** (7 mg, 31 μ mol, 2.2 eq) in DCM (200 μ L) and DMF (50 μ L) was added oxalylchloride (5 μ L, 62 μ mol, 4.4 eq) at 0 °C and the solution was stirred for 1 h at 22 °C. The formation of the acid chloride was monitored as previously described. The acid chloride was concentrated under reduced pressure and dried min 1 h under high vacuum. A solution of **32/33** in KHCO₃ (1 M in MilliQ water, 500 μ L) was cooled to 0 °C before the acid chloride was added dropwise in anhydrous 1,4-dioxane (200 μ L), while monitoring the pH. The resulting yellow solution was stirred for 30 min at 22 °C and the solvent was removed by rotary evaporation (water bath: 30 °C). The residue was taken up in MeCN/MilliQ water (1 mL, 1:1) and purified by RP-HPLC (C18 phenomenex 40 min gradient, 30-50% MeCN/H₂O, 1% AcOH) and **34a/35a** could be obtained as a white solid (12 mg, 11 μ mol, 75%).

LCMS: m/z = 1138.35 [M+H⁺]; *t*_R = 1.27 min.

34a/35a:

¹H NMR (500 MHz, DMSO-d₆): δ = 8.39 (m, 3H), 8.16 – 7.99 (m, 3H), 7.45 (dd, *J* = 7.5, 1.6 Hz, 3H), 7.37 – 7.35 (m, 16H), 5.09 (s, *J* = 3.8 Hz, 4H), 3.22 (m, 16H), 2.94 (m, 4H), 2.77 (m, 4H), 2.59 (m, 10H), 2.27 (s, 9H), 2.20 – 2.19 (m, 9H), 1.16 (d, *J* = 5.6 Hz, 6H).

ESI-HRMS: 34a/35a: C₅₈H₇₄N₈O₁₆²⁺ calculated [M+2H]²⁺: 569.2605, measured [M+2H]²⁺: 569.2586 (Δ = 1.9 ppm).

2,2'-(4,10-bis((S)-1-((2-(2,3-dihydroxybenzamido)ethyl)amino)-1-oxopropan-2-yl)-1,4,7,10-tetraazacyclododecane-1,7-diyl)diacetic acid (34)

2,2'-(7,10-bis((S)-1-((2-(2,3-dihydroxybenzamido)ethyl)amino)-1-oxopropan-2-yl)-1,4,7,10-tetraazacyclododecane-1,4-diyl)diacetic acid (35)

To a solution of **34a** und **35a** (12 mg, 11 μmol , 1.0 eq) in anhydrous MeOH (0.5 mL) under Ar atmosphere, was added Pd/C (0.3 mg, 0.3 μmol , 0.17 eq) in dry MeOH (0.5 mL). The reaction continued stirring under H₂ atmosphere for 1.5 h at 25 °C. The reaction was filtered, and the solvent was removed under reduced pressure. The product mixture was purified via RP-HPLC (C18 phenomenex, 40 min gradient, 10-30% MeCN/H₂O, 0.1% TFA) and **34/35** (2.1 mg, 2.7 μmol , 19%) could be obtained as white solids.

34/35:

¹H NMR (700 MHz, MeOH-d₄): δ = 7.38 – 7.20 (m, 2H), 6.98 – 6.86 (m, 2H), 6.77 – 6.70 (m, 2H), 4.17 – 3.32 (m, 16H), 3.27 – 2.82 (m, 14H), 1.34 – 1.28 (m, 12H) ppm.

ESI-HRMS: 34/35: C₃₆H₅₃N₈O₁₂⁺ calculated [M+H]⁺ = 789.3785, measured [M+H]⁺ = 789.3790 (Δ = 0.5 ppm)

benzyl-2-(4,7,10-tris((S)-1-((2-aminoethyl)amino)-1-oxopropan-2-yl)-1,4,7,10-tetraazacyclododecan-1-yl)acetate (36)

To a suspension of **31** (7 mg, 8 μmol , 1.0 eq) and K₂CO₃ (5 mg, 36 μmol , 4.4 eq) in MeCN (0.3 mL) was added o-benzyl bromo acetate (12 μL , 18 μmol , 2.2 eq) in MeCN (0.2 mL). The reaction stirred for 1 h at 22 °C. After completion, the reaction was filtered and concentrated to dryness under reduced pressure. The residue was taken up in DCM (0.75 mL) and TFA (0.25 mL) was added at 0 °C. The reaction was stirred for 1 h at 22 °C, then solvent was removed by rotary evaporation and **36** could be obtained as a crude, white solid (1.7 mg, 3 μmol , 32%).

ESI-HRMS: 36: C₃₂H₅₉N₁₀O₅⁺ calculated [M+H]⁺: 663.4670, measured [M+H]⁺: 663.4665 (Δ = 0.5 ppm).

2-(4,7,10-tris((S)-1-((2-aminoethyl)amino)-1-oxopropan-2-yl)-1,4,7,10-tetraazacyclododecan-1-yl)acetic acid (37a)

To a solution of **36** (6.4 mg, 10 μmol , 1.0 eq) in dry MeOH (0.5 mL) under Argon atmosphere was added Pd/C (0.2 mg, 1.7 μmol , 0.17 eq) in anhydrous, degassed MeOH (0.5 mL). The reaction continued stirring under an H₂ atmosphere for 1 h at 22 °C. The suspension was filtered and product **37a** was obtained after concentration by rotary evaporation (6 mg, 10 μM , quant.) and was directly used in the next step without further purification.

ESI-HRMS: 37a: C₂₅H₅₃N₁₀O₅⁺ calculated [M+H]⁺: 573.4202, measured [M+H]⁺: 573.4199 (Δ = 0.3 ppm).

2-(4,7,10-tris((S)-1-((2-(2,3-bis(benzyloxy)benzamido)ethyl)amino)-1-oxopropan-2-yl)-1,4,7,10-tetraazacyclododecan-1-yl)acetic acid (37b)

To a solution of **2** (6 mg, 11 μmol , 3.3 eq) in DCM (200 μL) and DMF (50 μL) was added oxalylchloride (3 μL , 35 μmol , 6.6 eq) at 0 °C and the reaction continued stirring at 22 °C for 1 h. The formation of the acid chloride was monitored as previously described. After removal of the solvent, the acid chloride was dried under high vacuum for minimum 1 h. A solution of the amine **37a** (3 mg, 5 μmol , 1.0 eq) in KHCO₃ (1 M in milliQ water, 0.5 mL) was cooled to 0 °C before the acid chloride was added in 1,4-dioxane (0.1 mL), while the pH value was monitored closely. The obtained yellow solution continued stirring for 30 min at 22 °C and was concentrated under reduced pressure. Compound **37b** was HPLC-purified (C18 phenomenex, 40 min gradient, 40-70% MeCN/H₂O, 1% AcOH) and white solid **37b** could be obtained (2.5 mg, 2.03 μmol , 19%).

¹H NMR (500 MHz, MeCN-d₃): δ = 8.08 (s, 2H), 7.84-7.77 (bs, 2H), 7.77-7.73 (bs, 1H), 7.67-7.59 (bs, 3H), 7.54 (m, 3H), 7.30 (m, 6H), 3.51-3.46 (bs, 2H), 3.45-3.33 (m, 10H), 3.26-3.03 (m, 12H), 2.90-2.77 (bs, 3H), 2.67-2.57 (bs, 8H), 2.26 (s, 9H), 2.24 (s, 3H), 2.23 ppm (s, 6H).

¹³C NMR (176 MHz, MeCN-d₃): δ = 171.8, 169.8, 169.7, 169.5, 169.4, 166.3, 166.3, 163.0, 144.4, 141.6, 141.6, 140.8, 131.9, 131.7, 127.6, 127.5, 127.4, 127.3, 126.8, 126.6, 62.4, 62.2, 59.2, 57.9, 54.5, 52.8, 51.7, 49.5, 41.3, 40.6, 39.9, 39.7, 21.0, 20.9, 20.9, 20.8 ppm.

2-(4,7,10-tris((S)-1-((2-(2,3-dihydroxybenzamido)ethyl)amino)-1-oxopropan-2-yl)-1,4,7,10-tetraazacyclododecan-1-yl)acetic acid (37)

To a solution of **37b** (2.5 mg, 2.03 μmol , 1.0 eq) in dry MeOH (0.8 mL) and DIPEA (0.2 mL) was added and the reaction continued stirring for 2 h at 22 °C. The mixture was filtrated over a syringe filter and the eluate was HPLC-purified (C18 phenomenex, 40 min gradient, 5-35 % MeCN/H₂O, 0.1% TFA). Product containing fractions were identified by LCMS and lyophilized to yield product **37** (0.9 mg, 0.9 μmol , 56%) as a white solid.

LCMS: $m/z = 491.24$ [$M/2+H^+$]; $t_R = 0.86$ min.

¹H NMR (500 MHz, DMSO-d₆): $\delta = 8.22$ (m, 2H), 7.60 – 7.31 (m, 4H), 6.86 (m, 2H), 6.66 – 6.56 (m, 6H), 3.41 – 3.36 (m, 10H), 3.17 (m, 10H), 2.91 – 2.84 (m, 10H), 2.65 (m, 10H), 1.19 (d, $J = 6.4$ Hz, 9H) ppm.

ESI-HRMS: C₄₆H₆₆N₁₀O₁₄²⁺ calculated [$M+2H$]²⁺: 491.2410 measured [$M+2H$]²⁺: 491.2376 ($\Delta = 3.4$ ppm).

3.4.2 Animal Experiments

All animal experiments were conducted according to German animal welfare law (animal experiment application no. 15-2418), as well as the guide lines of the European parliament in order to protect the animals used for scientific studies (2010/63/ EU).

Funding

The presented work was supported by a “Kekulé-Stipendium” of the “Fonds der chemischen Industrie (VCI)”, as well as with a grant from the Joint Programming Initiative on Antimicrobial Resistance (JPI AMR, grant number: 01KI1825).

Acknowledgements

We thank Anja Sanders, Petra Felsch, Nele Hermann, and Ayлина Glasenapp for their help with animal experiments. We also thank Dr. Annika Heß for preparation of the cryo-sections, and Zekiye Korkmaz for her support with bacterial cultures, as well as Dr. Kevin Ferreira for his support on DOTAM synthesis. Furthermore, we thank Ulrike Beutling for the measurement of HRMS samples and Christel Kakoschke for the measurement of NMR samples.

Abbreviations

DOTAM	1,4,7,10-tetraazacyclododecane-1,4,7,10-tetraacetic amide;
DOTA	2,2',2'',2'''-(1,4,7,10-Tetraazacyclododecane-1,4,7,10-tetrayl)tetraacetic acid
BCN-DOTA	2,2',2'''-(10-(4-((2-(((1R,8S,9s)-bicyclo[6.1.0]non-4-yn-9-ylmethoxy)carbonyl)amino)ethyl)amino)-1-carboxy-4-oxobutyl)-1,4,7,10-tetraazacyclododecane-1,4,7-triyl)triacetic acid
SPAAC	Strain-promoted azide-alkyne cycloaddition
ENT	Enterobactin
LE	Labelling Efficiency
RCY	Radiochemical yield
RCP	Radiochemical purity

References

1. Interagency Coordination Group on Antimicrobial Resistance. No time to wait: securing the future from drug-resistant infections. <https://www.who.int/publications/i/item/no-time-to-wait-securing-the-future-from-drug-resistant-infections>, June 2022.
2. Theuretzbacher, U.; Gottwalt, S.; Beyer, P.; Butler, M.; Czaplewski, L.; Lienhardt, C.; Moja, L.; Paul, M.; Paulin, S.; Rex, J. H.; Silver, L. L.; Spigelman, M.; Thwaites, G. E.; Paccaud, J. P.; Harbarth, S., Analysis of the clinical antibacterial and antituberculosis pipeline. *Lancet Infect. Dis.* **2019**, *19* (2), e40-e50.
3. Tacconelli, E.; Carrara, E.; Savoldi, A.; Harbarth, S.; Mendelson, M.; Monnet, D. L.; Pulcini, C.; Kahlmeter, G.; Kluytmans, J.; Carmeli, Y.; Ouellette, M.; Outtersson, K.; Patel, J.; Cavalieri, M.; Cox, E. M.; Houchens, C. R.; Grayson, M. L.; Hansen, P.; Singh, N.; Theuretzbacher, U.; Magrini, N., Discovery, research, and development of new antibiotics: the WHO priority list of antibiotic-resistant bacteria and tuberculosis. *Lancet Infect. Dis.* **2018**, *18* (3), 318-327.
4. Mota, F.; Ordonez, A. A.; Firth, G.; Ruiz-Bedoya, C. A.; Ma, M. T.; Jain, S. K., Radiotracer development for bacterial imaging. *J. Med. Chem.* **2020**, *63* (5), 1964-1977.
5. Wang, X.; Murthy, N., Bacterial imaging comes of age. *Sci. Transl. Med.* **2014**, *6* (259), 259fs43.
6. Palestro, C. J.; Love, C.; Miller, T. T., Diagnostic imaging tests and microbial infections. *Cell. Microbiol.* **2007**, *9* (10), 2323-2333.
7. Zhuang, H.; Alavi, A., 18-Fluorodeoxyglucose positron emission tomographic imaging in the detection and monitoring of infection and inflammation. *Semin. Nucl. Med.* **2002**, *32* (1), 47-59.
8. Fletcher, J. W.; Djulbegovic, B.; Soares, H. P.; Siegel, B. A.; Lowe, V. J.; Lyman, G. H.; Coleman, R. E.; Wahl, R.; Paschold, J. C.; Avril, N.; Einhorn, L. H.; Suh, W. W.; Samson, D.; Delbeke, D.; Gorman, M.; Shields, A. F., Recommendations on the use of ¹⁸F-FDG PET in oncology. *J. Nucl. Med.* **2008**, *49* (3), 480-508.
9. Sollini, M.; Lauri, C.; Boni, R.; Lazzeri, E.; Erba, P. A.; Signore, A., Current status of molecular imaging in infections. *Curr Pharm Des* **2018**, *24* (7), 754-771.
10. Li, J.; Zheng, H.; Fodah, R.; Warawa, J. M.; Ng, C. K., Validation of 2-(18)F-Fluorodeoxysorbitol as a potential radiopharmaceutical for imaging bacterial infection in the lung. *J. Nucl. Med.* **2018**, *59* (1), 134-139.

11. Weinstein, E. A.; Ordonez, A. A.; DeMarco, V. P.; Murawski, A. M.; Pokkali, S.; MacDonald, E. M.; Klunk, M.; Mease, R. C.; Pomper, M. G.; Jain, S. K., Imaging *Enterobacteriaceae* infection *in vivo* with ¹⁸F-fluorodeoxyisotom positron emission tomography. *Sci. Transl. Med.* **2014**, *6* (259), 259ra146.
12. Martínez, M. E.; Kiyono, Y.; Noriki, S.; Inai, K.; Mandap, K. S.; Kobayashi, M.; Mori, T.; Tokunaga, Y.; Tiwari, V. N.; Okazawa, H.; Fujibayashi, Y.; Ido, T., New radiosynthesis of 2-deoxy-2-[¹⁸F]fluoroacetamido-d-glucopyranose and its evaluation as a bacterial infections imaging agent. *Nucl. Med. Biol.* **2011**, *38* (6), 807-817.
13. Ferenci, T., The recognition of maltodextrins by *Escherichia coli*. *Eur. J. Biochem.* **1980**, *108* (2), 631-636.
14. Jones, S. A.; Jorgensen, M.; Chowdhury, F. Z.; Rodgers, R.; Hartline, J.; Leatham, M. P.; Struve, C.; Krogfelt, K. A.; Cohen, P. S.; Conway, T., Glycogen and Maltose utilization by *Escherichia coli* O157:H7 in the mouse intestine. *Infect. Immun.* **2008**.
15. Shelburne, S. A.; Sumbly, P.; Sitkiewicz, I.; Okorafor, N.; Granville, C.; Patel, P.; Voyich, J.; Hull, R.; DeLeo, F. R.; Musser, J. M., Maltodextrin utilization plays a key role in the ability of group A *Streptococcus* to colonize the oropharynx. *Infect. Immun.* **2006**, *74* (8), 4605-4614.
16. Axer, A.; Hermann, S.; Kehr, G.; Clases, D.; Karst, U.; Fischer-Riepe, L.; Roth, J.; Fobker, M.; Schäfers, M.; Gilmour, R.; Faust, A., Harnessing the maltodextrin transport mechanism for targeted bacterial imaging: Structural requirements for improved *in vivo* stability in tracer design. *ChemMedChem* **2018**, *13* (3), 241-250.
17. Ning, X.; Lee, S.; Wang, Z.; Kim, D.; Stubblefield, B.; Gilbert, E.; Murthy, N., Maltodextrin-based imaging probes detect bacteria *in vivo* with high sensitivity and specificity. *Nat. Mater.* **2011**, *10* (8), 602-7.
18. Ning, X.; Seo, W.; Lee, S.; Takemiya, K.; Rafi, M.; Feng, X.; Weiss, D.; Wang, X.; Williams, L.; Camp, V. M.; Eugene, M.; Taylor, W. R.; Goodman, M.; Murthy, N., PET imaging of bacterial infections with fluorine-18-labeled maltohexaose. *Angew. Chem. Int. Ed. Engl.* **2014**, *53* (51), 14096-101.
19. Bunschoten, A.; Welling, M. M.; Termaat, M. F.; Sathekge, M.; van Leeuwen, F. W. B., Development and prospects of dedicated tracers for the molecular imaging of bacterial infections. *Bioconj. Chem.* **2013**, *24* (12), 1971-1989.
20. Zhang, Z.; Ordonez, A. A.; Wang, H.; Li, Y.; Gogarty, K. R.; Weinstein, E. A.; Daryaei, F.; Merino, J.; Yoon, G. E.; Kalinda, A. S.; Mease, R. C.; Iuliano, J. N.; Smith-Jones, P. M.; Jain, S. K.; Tonge, P. J., Positron emission tomography imaging

- with 2-[¹⁸F]F-p-aminobenzoic acid detects *Staphylococcus aureus* infections and monitors drug response. *ACS Infect. Dis.* **2018**, 4 (11), 1635-1644.
21. El-ghany, E. A.; Amin, A. M.; El-kawy, O. A.; Amin, M., Technetium-99m labeling and freeze-dried kit formulation of levofloxacin (L-Flox): a novel agent for detecting sites of infection. *J. Labelled Comp. Radiopharm.* **2007**, 50 (1), 25-31.
 22. Palestro, C.; Love, C.; Caprioli, R.; Marwin, S.; Richardson, H.; Haight, J.; Tronco, G.; Pugliese, P.; Bhargava, K., Phase II study of ^{99m}Tc-ciprofloxacin uptake in patients with high suspicion of osteomyelitis. *J. Nucl. Med.* **2006**, 47 (suppl 1), 152P.
 23. Essouissi, I.; Darghoutha, F.; Saied, N. M.; Saidi, M.; Kanoun, A.; Saidi, M., Radiolabeling, quality control, and biodistribution of ^{99m}Tc-sulfadiazine as an infection imaging agent. *Radiochemistry* **2015**, 57 (3), 307-311.
 24. le Roux, J.; Rubow, S.; Ebenhan, T.; Wagener, C., An automated synthesis method for ⁶⁸Ga-labelled ubiquicidin 29–41. *J. Radioanal. Nucl. Chem.* **2020**, 323 (1), 105-116.
 25. Renick, P. J.; Mulgaonkar, A.; Co, C. M.; Wu, C.-Y.; Zhou, N.; Velazquez, A.; Pennington, J.; Sherwood, A.; Dong, H.; Castellino, L.; Öz, O. K.; Tang, L.; Sun, X., Imaging of actively proliferating bacterial infections by targeting the bacterial metabolic footprint with d-[5-¹¹C]-glutamine. *ACS Infect. Dis.* **2021**, 7 (2), 347-361.
 26. Faraldo-Gómez, J. D.; Sansom, M. S. P., Acquisition of siderophores in Gram-negative bacteria. *Nat. Rev. Mol. Cell Biol.* **2003**, 4 (2), 105-116.
 27. Holden, V. I.; Bachman, M. A., Diverging roles of bacterial siderophores during infection. *Metallomics* **2015**, 7 (6), 986-995.
 28. Tseng, B. S.; Zhang, W.; Harrison, J. J.; Quach, T. P.; Song, J. L.; Penterman, J.; Singh, P. K.; Chopp, D. L.; Packman, A. I.; Parsek, M. R., The extracellular matrix protects *Pseudomonas aeruginosa* biofilms by limiting the penetration of tobramycin. *Environ. Microbiol.* **2013**, 15 (10), 2865-2878.
 29. Welling, M. M.; Hensbergen, A. W.; Bunschoten, A.; Velders, A. H.; Roestenberg, M.; van Leeuwen, F. W. B., An update on radiotracer development for molecular imaging of bacterial infections. *Clin. Transl. Imaging* **2019**, 7 (2), 105-124.
 30. Petrik, M.; Haas, H.; Laverman, P.; Schrettl, M.; Franssen, G. M.; Blatzer, M.; Decristoforo, C., ⁶⁸Ga-triacetylfusarinine C and ⁶⁸Ga-ferrioxamine E for *Aspergillus* infection imaging: uptake specificity in various microorganisms. *Molecular imaging and biology : MIB : the official publication of the Academy of Molecular Imaging* **2014**, 16 (1), 102-8.

31. Petrik, M.; Umlaufova, E.; Raclavsky, V.; Palyzova, A.; Havlicek, V.; Haas, H.; Novy, Z.; Dolezal, D.; Hajduch, M.; Decristoforo, C., Imaging of *Pseudomonas aeruginosa* infection with Ga-68 labelled pyoverdine for positron emission tomography. *Sci. Rep.* **2018**, *8* (1), 15698.
32. Petrik, M.; Umlaufova, E.; Raclavsky, V.; Palyzova, A.; Havlicek, V.; Pfister, J.; Mair, C.; Novy, Z.; Popper, M.; Hajduch, M.; Decristoforo, C., ⁶⁸Ga-labelled desferrioxamine-B for bacterial infection imaging. *Eur. J. Nucl. Med. Mol. Imaging* **2021**, *48* (2), 372-382.
33. Klahn, P.; Bronstrup, M., Bifunctional antimicrobial conjugates and hybrid antimicrobials. *Nat. Prod. Rep.* **2017**, *34* (7), 832-885.
34. Portsmouth, S.; van Veenhuizen, D.; Echols, R.; Machida, M.; Ferreira, J. C. A.; Ariyasu, M.; Tenke, P.; Nagata, T. D., Cefiderocol versus imipenem-cilastatin for the treatment of complicated urinary tract infections caused by Gram-negative uropathogens: a phase 2, randomised, double-blind, non-inferiority trial. *Lancet Infect. Dis.* **2018**, *18* (12), 1319-1328.
35. Wu, J. Y.; Srinivas, P.; Pogue, J. M., Cefiderocol: A novel agent for the management of multidrug-resistant Gram-Negative organisms. *Infect. Dis. Ther.* **2020**, *9* (1), 17 – 40.
36. Ferreira, K.; Hu, H.-Y.; Fetz, V.; Prochnow, H.; Rais, B.; Müller, P. P.; Brönstrup, M., Multivalent siderophore–DOTAM conjugates as theranostics for imaging and treatment of bacterial infections. *Angew. Chem. Int. Ed.* **2017**, *56* (28), 8272-8276.
37. Stasiuk, G. J.; Long, N. J., The ubiquitous DOTA and its derivatives: the impact of 1,4,7,10-tetraazacyclododecane-1,4,7,10-tetraacetic acid on biomedical imaging. *Chem. Commun.* **2013**, *49* (27), 2732-46.
38. Kubíček, V.; Havlíčková, J.; Kotek, J.; Tircsó, G.; Hermann, P.; Tóth, E.; Lukes, I., Gallium(III) complexes of DOTA and DOTA-monoamide: kinetic and thermodynamic studies. *Inorg. Chem.* **2010**, *49* (23), 10960-9.
39. Aime, S.; Botta, M.; Garda, Z.; Kucera, B. E.; Tircso, G.; Young, V. G.; Woods, M., Properties, solution state behavior, and crystal structures of chelates of DOTMA. *Inorg. Chem.* **2011**, *50* (17), 7955-7965.
40. Ji, C.; Miller, P. A.; Miller, M. J., Iron Transport-Mediated Drug Delivery: Practical syntheses and *in vitro* antibacterial studies of tris-catecholate siderophore–aminopenicillin conjugates reveals selectively potent antipseudomonal activity. *J. Am. Chem. Soc.* **2012**, *134* (24), 9898-9901.

41. Ohi, N.; Aoki, B.; Kuroki, T.; Matsumoto, M.; Kojima, K.; Nehashi, T., Semisynthetic beta-lactam antibiotics. III. Effect on antibacterial activity and comt-susceptibility of chlorine-introduction into the catechol nucleus of 6-[(R)-2-[3-(3,4-dihydroxybenzoyl)-3-(3-hydroxypropyl)-1-ureido]-2- phenylacetamido]penicillanic acid. *J. Antibiot. (Tokyo)* **1987**, *40* (1), 22-8.
42. Broan, C. J.; Cox, J. P. L.; Craig, A. S.; Katakya, R.; Parker, D.; Harrison, A.; Randall, A. M.; Ferguson, G., Structure and solution stability of indium and gallium complexes of 1,4,7-triazacyclononanetriacetate and of yttrium complexes of 1,4,7,10-tetraazacyclododecanetetraacetate and related ligands: kinetically stable complexes for use in imaging and radioimmunotherapy. X-ray molecular structure of the indium and gallium complexes of 1,4,7-triazacyclononane-1,4,7-triacetic acid. *J. Chem. Soc. Perkin Trans. 2* **1991**, (1), 87-99.
43. Keire, D. A.; Kobayashi, M., NMR studies of the metal-loading kinetics and acid-base chemistry of DOTA and butylamide-DOTA. *Bioconjug. Chem.* **1999**, *10* (3), 454-463.
44. Hider, R. C.; Kong, X., Chemistry and biology of siderophores. *Nat. Prod. Rep.* **2010**, *27* (5), 637-657.
45. Harrington, J. M.; Crumbliss, A. L., The redox hypothesis in siderophore-mediated iron uptake. *BioMetals* **2009**, *22* (4), 679-689.
46. Greenwood, K. T.; Luke, R. K. J., Enzymatic hydrolysis of enterochelin and its iron complex in *Escherichia coli* K-12. Properties of enterochelin esterase. *Biochim. Biophys. Acta* **1978**, *525* (1), 209-218.
47. Abergel, R. J.; Clifton, M. C.; Pizarro, J. C.; Warner, J. A.; Shuh, D. K.; Strong, R. K.; Raymond, K. N., The siderocalin/enterobactin interaction: A link between mammalian immunity and bacterial iron transport. *J. Am. Chem. Soc.* **2008**, *130* (34), 11524-11534.
48. Coenen, H. H.; Gee, A. D.; Adam, M.; Antoni, G.; Cutler, C. S.; Fujibayashi, Y.; Jeong, J. M.; Mach, R. H.; Mindt, T. L.; Pike, V. W.; Windhorst, A. D., Open letter to journal editors on: International Consensus Radiochemistry Nomenclature Guidelines. *Ann. Nucl. Med.* **2018**, *32* (3), 236-238.
49. Joaqui-Joaqui, M. A.; Pandey, M. K.; Bansal, A.; Raju, M. V. R.; Armstrong-Pavlik, F.; Dundar, A.; Wong, H. L.; DeGrado, T. R.; Pierre, V. C., Catechol-based functionalizable ligands for gallium-68 positron emission tomography imaging. *Inorg. Chem.* **2020**, *59* (17), 12025-12038.

50. Tsionou, M. I.; Knapp, C. E.; Foley, C. A.; Munteanu, C. R.; Cakebread, A.; Imberti, C.; Eykyn, T. R.; Young, J. D.; Paterson, B. M.; Blower, P. J.; Ma, M. T., Comparison of macrocyclic and acyclic chelators for gallium-68 radiolabelling. *RSC Adv.* **2017**, *7* (78), 49586-49599.
51. Wright, C. I., The enzymatic deacetylation of heroin and related mophine derivatives by blood serum. **1941**, *71* (2), 164-177.
52. Welch, W. D.; Bawdon, R. E., Cefotaxime metabolism by hemolyzed blood: quantitation and inhibition of the deacetylation reaction. *Diagn. Microbiol. Infect. Dis.* **1986**, *4* (2), 119-124.
53. Bahar, F. G.; Ohura, K.; Ogihara, T.; Imai, T., Species difference of esterase expression and hydrolase activity in plasma. *J. Pharm. Sci.* **2012**, *101* (10), 3979-3988.
54. Braun, V.; Hantke, K.; Köster, W., Bacterial iron transport: mechanisms, genetics, and regulation. *Met. Ions Biol. Syst.* **1998**, *35*, 67-145.
55. Huang, P.; Wang, J.; Lin, X.; Yang, F. F.; Tan, J. H., Effects of IL-10 on iron metabolism in LPS-induced inflammatory mice via modulating hepcidin expression. *Eur. Rev. Med. Pharmacol. Sci.* **2017**, *21* (15), 3469-3475.
56. Finberg, K. E., Ironing out an approach to alleviate the hypoferremia of acute inflammation. *Haematologica* **2021**, *106* (2), 326-328.
57. Miethke, M.; Marahiel, M. A., Siderophore-based iron acquisition and pathogen control. *Microbiol. Mol. Biol. Rev.* **2007**, *71* (3), 413-451.
58. Schalk, I. J.; Yue, W. W.; Buchanan, S. K., Recognition of iron-free siderophores by TonB-dependent iron transporters, *Mol. Microbiol.* **2004**, *54* (1), 14-22.
59. Sheldon, J. R.; Heinrichs, D. E., Recent developments in understanding the iron acquisition strategies of Gram positive pathogens. *FEMS Microbiol. Rev.* **2015**, *39* (4), 592-630.
60. Petrik, M.; Umlaufova, E.; Raclavsky, V.; Palyzova, A.; Havlicek, V.; Haas, H.; Novy, Z.; Dolezal, D.; Hajduch, M.; Decristoforo, C., Imaging of *Pseudomonas aeruginosa* infection with Ga-68 labelled pyoverdine for positron emission tomography. *Sci. Rep.* **2018**, *8* (1), 15698.
61. Dean, C. R.; Neshat, S.; Poole, K., PfeR, an enterobactin-responsive activator of ferric enterobactin receptor gene expression in *Pseudomonas aeruginosa*. *J. Bacteriol.* **1996**, *178* (18), 5361-5369.

62. Moynié, L.; Milenkovic, S.; Mislin, G. L. A.; Gasser, V.; Malloci, G.; Baco, E.; McCaughan, R. P.; Page, M. G. P.; Schalk, I. J.; Ceccarelli, M.; Naismith, J. H., The complex of ferric-enterobactin with its transporter from *Pseudomonas aeruginosa* suggests a two-site model. *Nat. Commun.* **2019**, *10* (1), 3673.
63. Usher, K. C.; Özkan, E.; Gardner, K. H.; Deisenhofer, J., The plug domain of FepA, a TonB-dependent transport protein from *Escherichia coli* binds its siderophore in the absence of the transmembrane barrel domain. *Proc. Natl. Acad. Sci.* **2001**, *98* (19), 10676-10681.
64. Kumar, A.; Chakravorty, S.; Yang, T.; Majumdar, A.; Newton, S.; Klebba, P., Fluorescence spectroscopic analysis of TonB-dependent transport in *Klebsiella pneumoniae*. *J. Bacteriol.* **2019**, *33* (S1), 635.12-635.12.
65. Rabsch, W.; Winkelmann, G., The specificity of bacterial siderophore receptors probed by bioassays. *Biol. Met.* **1991**, *4* (4), 244-50.
66. Kriemen, E.; Holzapfel, M.; Ruf, E.; Rehbein, J.; Maison, W., Synthesis and structural analysis of 1,4,7,10-tetraazacyclododecane-1,4,7,10-tetraazidoethylacetic acid (DOTAZA) complexes. *Eur. J. Inorg. Chem.* **2015**, *2015* (32), 5368-5378.
67. Kriemen, E.; Ruf, E.; Behrens, U.; Maison, W., Synthesis of 1,4,7,10-tetraazacyclododecan-1,4,7,10-tetra-azidoethylacetic acid (dotaza) and related "clickable" DOTA derivatives. *Chem. Asian J.* **2014**, *9* (8), 2197-2204.

Supplementary material

General chemistry methods

Reagents were purchased from commercial vendors, if not stated otherwise, and employed without further purification in the below synthetic procedures. For synthesis, only solvents with purity grade 99.5%, extra dry, absolute, AcroSeal™, ACROS Organics™ were used. For work up procedures and purifications solvents with purity grade “HPLC grade“ or p.A. were employed. Glassware was dried at 120 °C in an oven for minimum 24 h prior to being used for synthesis. Reaction progress was controlled by thin layer chromatography (TLC) or Liquid Chromatography-coupled Mass Spectrometry (LCMS).

Purification of products by silica gel chromatography (Normal Phase Liquid Chromatography - NPLC) was conducted with the Reveleris® X2 Chromatography System with pre-packed one-time usage cartridges (Reveleris® Flash Cartridges Silica 40µm) from Büchi® Labortechnik GmbH. Samples were loaded on the pre-packed columns either in liquid form or *via* a solid loader, immobilized on silica from Merck KGaA® (Silicagel 60, 1.15111.1000, 15-40 µm). Reverse-Phase High Pressure Liquid Chromatography (RP-HPLC) was performed with a Phenomenex Gemini C18 RP-column 00G-4436-NO, 10 µm, 110 A, 250×10.00 mm (flow rate 5 mL/min, max. loading 10 mg crude) or a Phenomenex Gemini C18 RP-column 00G-4435-PO-AX, 5 µm, 110 A, 250×21.20 mm (flow rate 10 mL/min, max. loading 100 mg crude) coupled to a Thermo Fisher Scientific® Dionex Ultimate 3000 HPLC-System. The gradients and additives are stated in the respective synthetic procedures. Product containing fractions were identified by LCMS and lyophilized to dryness. Thin Layer Chromatography (TLC) was conducted with DC Silica gel 60 F₂₅₄ plates from Merck KGaA® The employed solvent mixture are stated in the respective synthetic procedures. For Nuclear Magnetic Resonance (NMR) Bruker Avance III or Bruker Avance III HD instruments were employed. ¹H NMR spectra were recorded at 500 MHz or 700 MHz, ¹³C NMR spectra were recorded at 126 MHz and 176 MHz. The chemical shifts are stated in parts per million (ppm) relative to the solvent signal. Peak multiplicity is given in short as follows: s (singlet), bs (broad singlet), d (doublet), t (triplet), q (quartet), m (multiplet), dd (doublet of doublet), tt (triplet of triplet). LCMS was conducted with an Agilent® 1100 HPLC System with a DAD detector and an API 150 EX Quadrupole Mass Detector with Electro Spray Ionization (ESI) (MeCN/H₂O + 0.1 % formic acid) or with a Dionex Ultimate 3000 HPLC System with a DAD Detector and a Bruker® Amazon Ion Trap Mass Detector with ESI coupling. High Resolution Mass Spectroscopy (HRMS) was conducted with a Dionex® Ultimate 3000 HPLC System equipped with a DAD Detector and a Bruker® MAXIS HD QTOF Mass Detector with ESI.

Chemistry figures

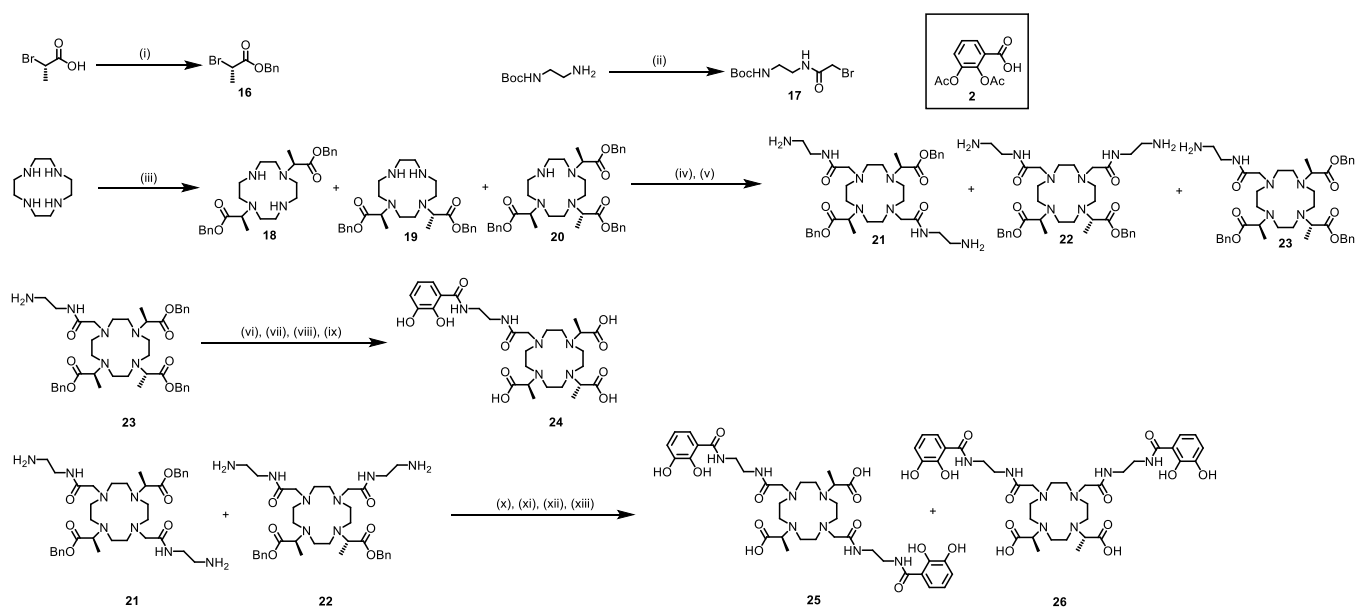


Figure S3.1. Synthesis of DOTA-based, α -methyl-, mono- and dicatechol siderophores 24, 25 and 26 from cyclen. (i) BnOH, DCC, DMAP, Et₂O, 2 h, 26 °C, 83%, (ii) bromo acetyl bromide, K₂CO₃, DCM/H₂O, 1.5 h, 22 °C, 93%, (iii) **16**, NaOAc, DMA, 20 h, 28 °C, , (iv) **17**, K₂CO₃, MeCN, 1 h, (v) 25% TFA, DCM, 18 h, 28 °C, yield in two steps **21/22** = 39% and **23** = 13%, (vi) **2**, oxalylchloride, DCM/DMF, 1 h, 22 °C, (vii) KHCO₃, H₂O/1,4-dioxane, 0.5 h, 0-22 °C, (viii) 0.1 mol% Pd/C, H₂, MeOH, 1 h, 23 °C, (viii) 20% DIPEA, MeOH, 1 h, 23 °C, yield within four steps **23**, (ix) **2**, oxalylchloride, DCM/DMF, 1 h, 22 °C, (x) KHCO₃, H₂O/1,4-dioxane, 0.5 h, 0-22 °C, (xi) 0.1 mol% Pd/C, H₂, MeOH, 1 h, 23 °C, (xii) 20% DIPEA, MeOH, 1 h, 23 °C, 3% yield over four steps.

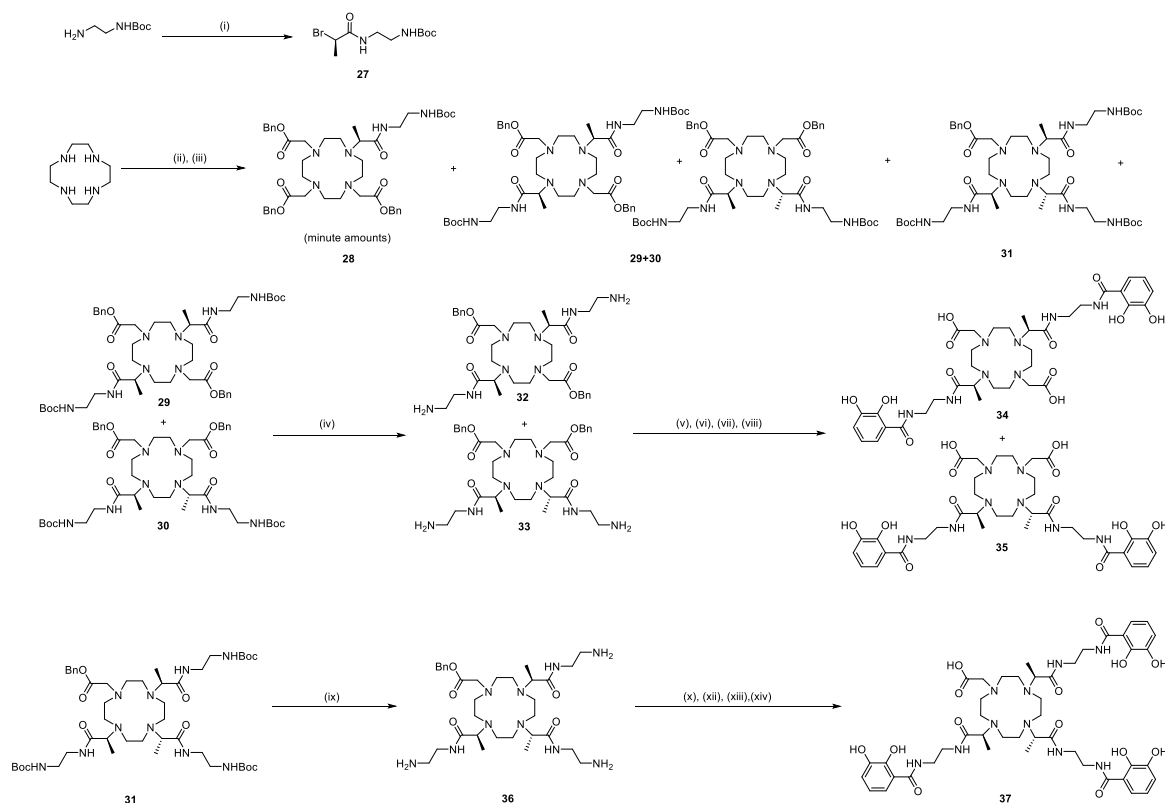


Figure S3.2. **Synthesis of cyclen-based, α -methyl-, di- and tri-catechol siderophores **34**, **35** and **37** from cyclen.** (i) (R)-2-bromopropanoic acid, HATU, DIPEA, DCM/DMF, 4 h, 25 °C, 93% . (ii) **27**, NaOAc, 35 °C, DMA, 72 h, **29/30** = 48%, **31** = 9%, (iii) benzyl-2-bromoacetate, K₂CO₃, MeCN, 1 h, 27 °C (iv) 25% TFA, DCM, 1 h, 27 °C, 68% yield, (v) **2**, oxalylchloride, DCM/DMF, 1 h, 22 °C, (vi) KHCO₃, H₂O/1,4-dioxane, 0.5 h, 0-22 °C, (vii) 0.1 mol% Pd/C, H₂, MeOH, 1 h, 23 °C, (viii) 20% DIPEA, MeOH, 1 h, 23 °C, 75% over 4 steps, (ix) 25% TFA, DCM, 1 h, 27 °C, 32% yield, (x) **2**, oxalylchloride, DCM/DMF, 1 h, 22 °C, (xi) KHCO₃, H₂O/1,4-dioxane, 0.5 h, 0-22 °C, (xii) 0.1 mol% Pd/C, H₂, MeOH, 1 h, 23 °C, (xiii) 20% DIPEA, MeOH, 1 h, 23 °C, 17% yield over four steps.

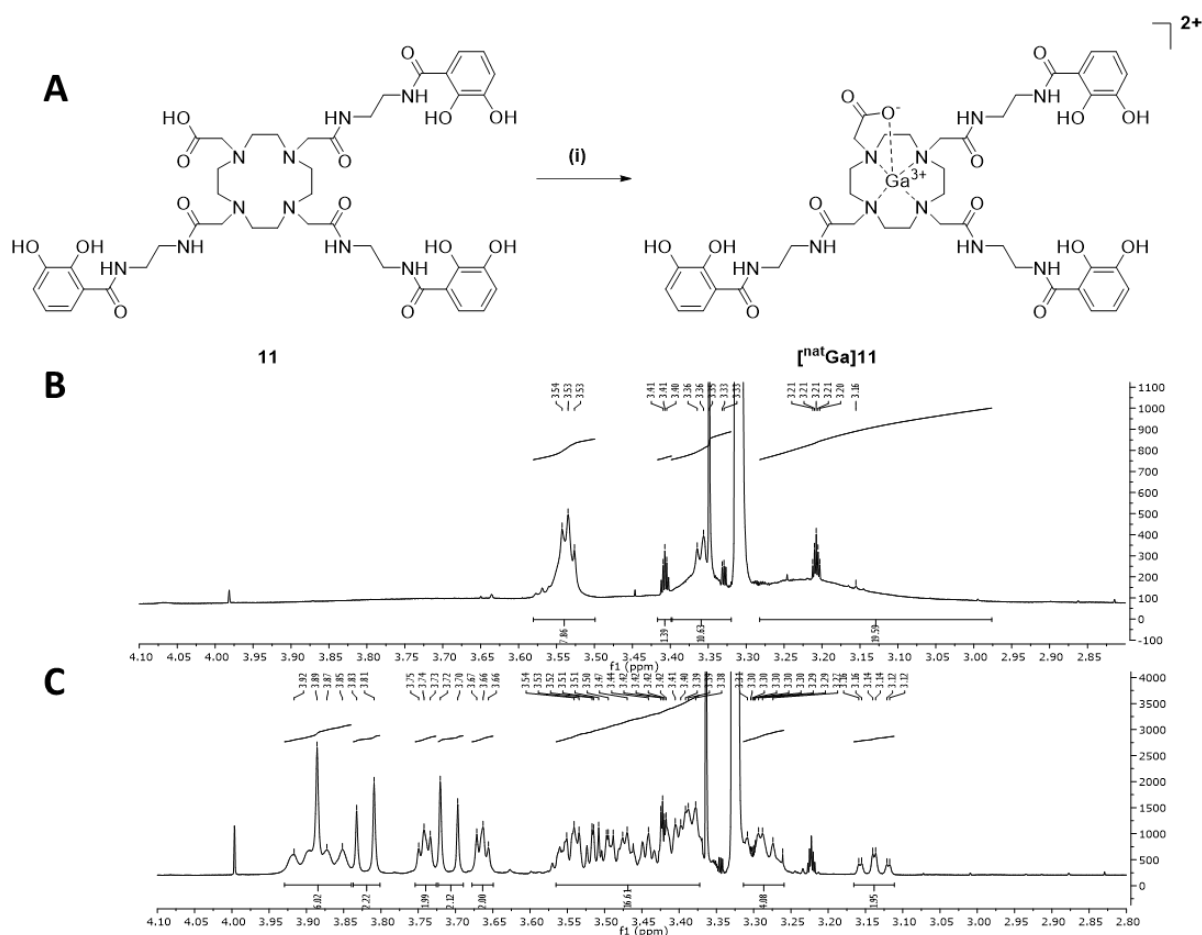


Figure S3.3. Formation of the ‘cold’ Ga-complex $[\text{natGa}]11$. (A) Reaction conditions: (i) GaCl_3 , 0.5 M NaOAc buffer, pH 4.5, 95 °C, 10 minutes, 18%. (B) $^1\text{H-NMR}$ spectrum of **11** in the alkyl region (2.8-4.1 ppm) of the cyclen ring. (C) Characteristic reorganization of the $^1\text{H-NMR}$ spectrum after of Ga^{3+} incorporation to yield complex $[\text{natGa}]11$, complex geometry with overall charge [2+] and without the preferred octahedral complex geometry in the DOTA variants. Structure may involve binding by one additional catechol group or adjacent amide (not depicted).

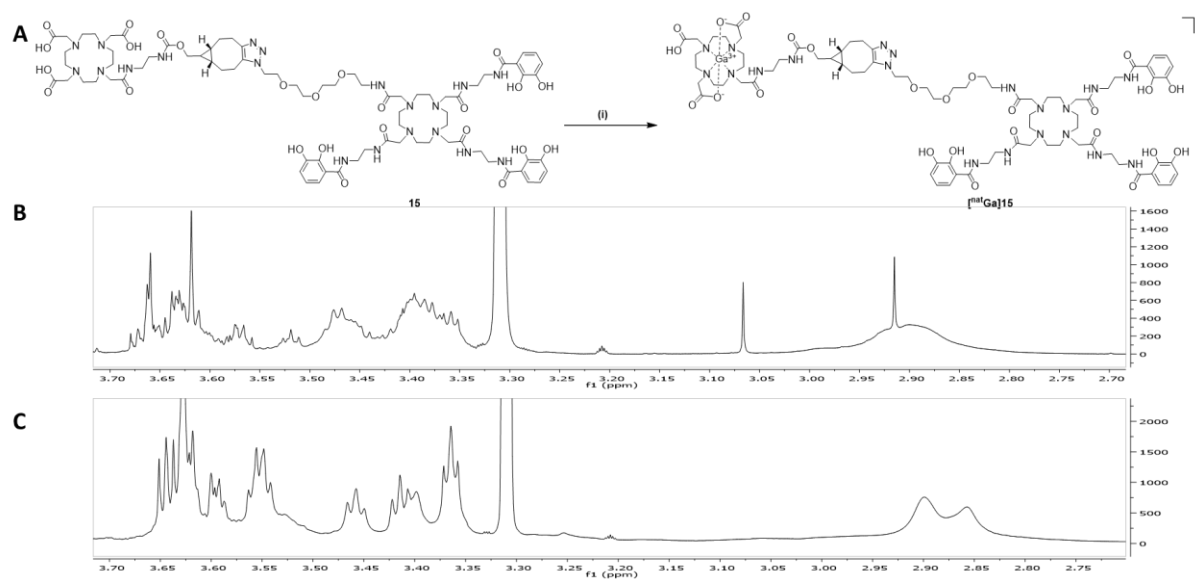


Figure S3.4. Formation of the ‘cold’ Ga-complex $[\text{natGa}]15$. (A) Reaction conditions: (i) natGaCl_3 , 0.5 M NaOAc buffer, pH 4.5, 95 °C, 10 minutes, 76%. (B) $^1\text{H-NMR}$ spectrum of **15** in the alkyl region (2.7-3.7 ppm) of the cyclen ring. (C) Characteristic reorganization of the $^1\text{H-NMR}$ spectrum after of Ga^{3+} incorporation to yield complex $[\text{natGa}]15$.

Biological methods

Growth recovery assay in siderophore-deficient *E. coli* mutants

I. Pre-Cultures of cells

The *E. coli* wild type strain BW25113 and the mutant strains JW0588-1 (“**ΔentA**”) and JW0587-1 (“**ΔentB**”) were grown in 1x LB medium (5 mL) overnight at 37 °C and 180 rpm. The *E. coli* mutants were always grown in presence of 50 µg/mL Kanamycin. The next morning the overnight inoculum was diluted 1:100 in 20 mL LB-medium, and grown to $OD_{600nm} = 0.5$ within 1-2 h at 37 °C and 180 rpm. The same assay was performed for the *P. aeruginosa* wildtype strain **PAO1** and the mutant strain **PAO1 ΔpvdD ΔpchE-F**.

II. Preparation of the iron-free bacteria-suspension

15 ml of the dilution culture were pelleted by centrifugation at 4.500 g, 5 min and 4 °C. The supernatant was discarded and the pellet was washed twice with iron-free 1xLMR (5 mL) or 1x PBS. The OD_{600nm} of the bacterial suspension was adjusted 0.01 with iron-free 1x LMR with Glycerol as carbon source.

III. Preparation and dilution of the compounds

The 10 mM compound stock in DMSO were diluted 1:500 either with the iron-free or iron-containing (20 µM) LMR to yield a 20 µM compound concentration. The dilution was prepared under a laminar flow bench with sterile medium, sterile microcentrifuge tubes and sterile filtered iron solutions.

The microcentrifuge tubes were vortexed and the tubes were incubated on an Eppendorf® shaker at 600 rpm, 25 °C overnight. The complex formation was indicated by a slight purple color of compounds with iron in 1xLMR. The control solution of siderophore containing no iron did not show any coloring. The tubes were collected from the shaker in the morning, and 25 µL of the 20 µM pre-complexed compound was added per well into a 384 well plate under a laminar flow bench.

IV. Addition of the bacteria-suspension on micro titer-plates

25 µL of bacterial suspension with a $OD_{600nm}=0.01$ in iron-free 1x LMR with Glycerol as carbon source was added to the compound in the plate in a 1:1 dilution to yield the final 10 µM compound concentration as well as a final 10 µM iron-concentration (or iron-free). Empty wells were filled with 50µL 1x LMR with glycerol as a sterile control, the plate was sealed with parafilm and incubated in a humid chamber at 37 °C for 48 h. Then the OD_{600nm} was determined with a plate UV-Vis spectrometer.

Preparation of 10xLMR stock

The following salts were dissolved in 500 mL of milliQ-H₂O and the solution was adjusted to pH = 7.4 with a sterile-filtered 1 M NaOH solution and subsequently autoclaved.

Salt	Stock concentration [mol/L]	Molecular Weight [g/mol]	Amount [g]
KH_2PO_4	1.76	136.09	119.76
$NaOH$	1	40.0	20.0
$(NH_4)_2SO_4$	0.126	132.14	8.3

10xLMR medium was diluted 1:10 in sterile milliQ-H₂O and 2 mL of sterile filtered 1 M MgSO₄ and 2 mL autoclaved glycerol were added to 1 L of 1 x LMR. Then 2 mL of the **trace metal solution** were added to 1 L of 1 x LMR and the pH was adjusted with a sterile-filtered 1 M NaOH solution to pH 7.4.

Preparation of the trace metal solution (TMS)

The following salts were dissolved in milliQ H₂O, except for the iron salts, which were dissolved in 0.1 M HCl. All solutions were filter-sterilized.

Salt	Stock concentration	Volume TMS	Final concentration
$CaCl_2$	1 M	0.2 ml	20 mM
$MnCl_2 \times 4 H_2O$	1 M	0.1 ml	10 mM
$ZnSO_4 \times 7 H_2O$	1 M	0.1 ml	10 mM
$CoCl_2 \times 6 H_2O$	0.2 M	0.1 ml	2 mM
$CuCl_2$	0.1M	0.2 ml	2 mM
$NiCl_2 \times 6 H_2O$	0.2 M	0.1 ml	2 mM
$Na_2MoO_4 \times 2 H_2O$	0.1 M	0.2 ml	2 mM
Na_2SeO_3	0.1M	0.2 ml	2 mM
H_3BO_4	0.1 M	0.2 ml	2 mM
H_2O	-	3.5 ml	-

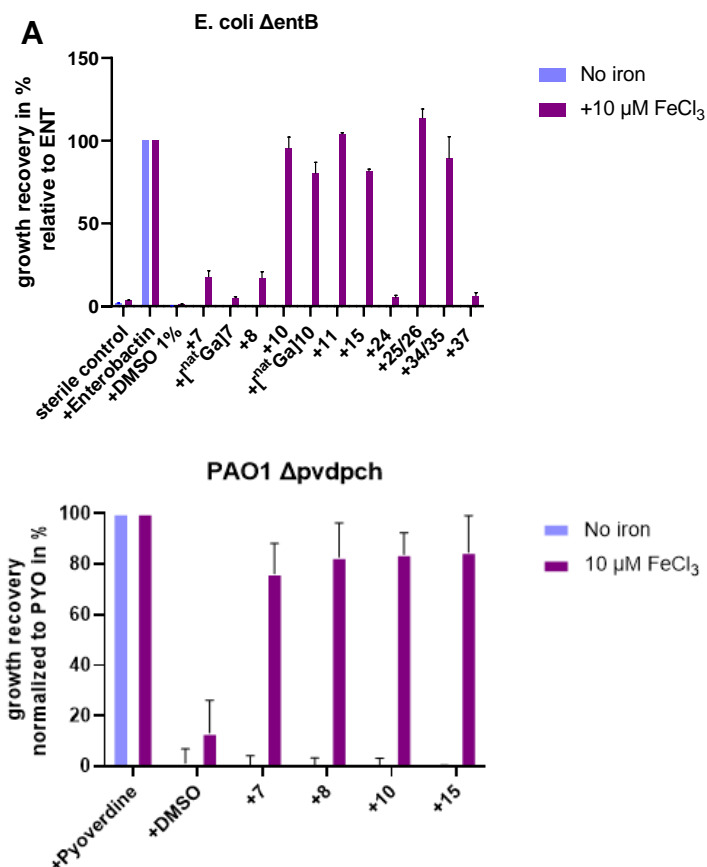


Figure S3.5. (A) Growth recovery assay in siderophore-deficient mutant *E. coli* Δ entB. Growth recovery in the enterobactin (ENT) – deficient strain *E. coli* Δ entB in the presence of 10 μ M compound \pm 10 μ M FeCl₃ was assessed after incubation for 48 hours at 37 °C by OD_{600nm} measurement in a well plate reader. Bacteria were either grown in iron-depleted (no iron) or 10 μ M FeCl₃-supplemented, phosphate-buffered LMR medium (n = 3). The growth relative to ENT and wildtype growth is plotted; error bars correspond to \pm Standard Deviation (SD). **(B) Growth recovery assay in siderophore-deficient mutant *P. aeruginosa* Δ pvdD Δ pchE-F.** Growth recovery in the pyoverdine, pyochelin – deficient strain *P. aeruginosa* Δ pvdD Δ pchE-F in the presence of 10 μ M compound \pm 10 μ M FeCl₃ was assessed after incubation for 48 hours at 37 °C by OD_{600nm} measurement in a well plate reader. Bacteria were either grown in iron-depleted (no iron) or 10 μ M FeCl₃-supplemented, phosphate-buffered LMR medium (n = 3). The growth relative to pyoverdine and wildtype growth is plotted; error bars correspond to \pm Standard Deviation (SD).

Chemical stability of the precursors in PBS

Before the biological testing, the stability of precursors **8**, **11**, **23**, was evaluated at biological standard conditions (37 °C, pH = 7.4) for total time frame of 96 hours. For the acetylated siderophores **13** and **16**, the stability of the acetyl groups at the catechol(s) was evaluated over a time frame of 24 hours. In addition, the stability of all de-acetylated compounds was evaluated. The testing was conducted for all groups in 1xPBS at a starting concentration of 10 μ M at $t = 0$. Compounds were incubated at 37 °C and 600 rpm for the whole course of the experiment. Samples for LC/MS analysis were taken at 1, 2, 4, 6 und 24 hours past $t = 0$.

The stability of the acetyl groups was evaluated for **7** und **10** over a time frame of 24 h – while samples for LCMS analysis were taken at 1, 2, 4, 6 und 24 hours past $t = 0$. The ratio of the acetylated to de-acetylated compound was obtained by integration of the UV trace (254 nm), division of the area under the curve $AUC(t_{1-24})$ by $AUC(t_0)$ and obtaining the respective ratio. Each experiment is the result of two independent replicates and the MS trace served to confirm the compounds identify at a specific retention time on the LCMS.

The general compound stability was probed over a time frame from 1 to 96 hours and samples were taken at 1, 2, 4, 6, 24 and 96 hours past $t = 0$. The procedure and calculation remained as explained above, all compounds were tested at a start concentration of 10 μ M in BS, stocks dissolved 10 mM in DMSO.

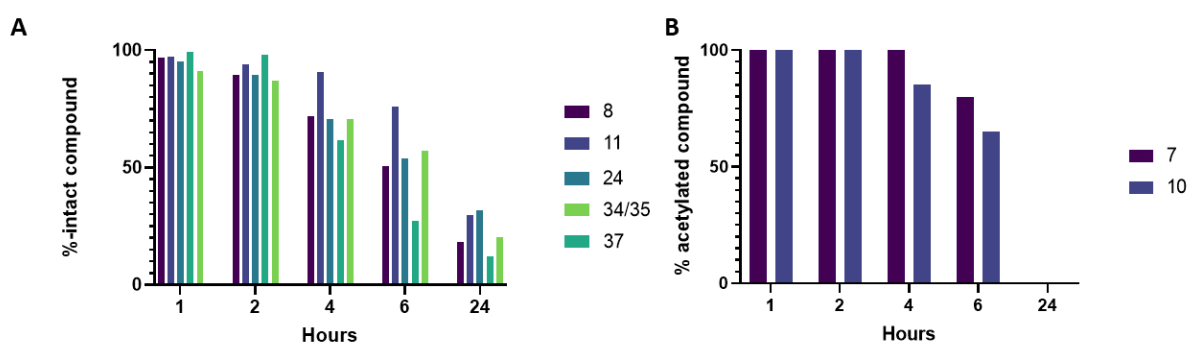


Figure S3.6. Chemical stability of cyclen-based siderophores. (A) Percentage of intact compound compared to initial peak area at $t = 0$ after 1, 2, 4, 6 or 24 hours of incubation in PBS (pH 7.4) at 37 °C, determined by LC/UV/MS measurements and subsequent integration of the UV peaks (254 and 220 nm). (B) Percentage of acetylated compounds **7** and **10** compared to $t = 0$ after 1, 2, 4, 6 or 24 hours of incubation in PBS (pH 7.4) at 37 °C, as detected by LC/UV/MS measurements and subsequent integration of the UV peaks (254 and 220 nm).

Cytotoxicity assay

The effect of compounds on cell viability was probed with a WST-1 assay, according to previously published procedures.^{1,2} The following immortalized cell lines were used: Mouse fibroblast cell line **L929** (DSM ACC 2), human cervix carcinoma cell line **KB-3-1** (DSM ACC 158), human breast cancer cell line **MCF-7** (DSM ACC 115), human lung carcinoma cell line **A549** (DSM ACC 107) and a conditional immortalized human fibroblast cell line **FS4-LTM** (InScreenex Pub No.: US2011/0189142 A2). Briefly, the subconfluent cells were washed with 1x PBS, trypsinized and resuspended in Dulbecco's modified eagle medium that contained 5% FBS (L929, KB-31, A-549, FS4-LTM) or Roswell Park Memorial Institute medium that contained 5% FBS, 0.5% Minimum Essential medium Non-Essential Amino Acids, Gibco (MEM NEAA), 0.5% GlutaAC (Gibco) and insulin at 5 µg/mL (MCF-7). 25 µL of serial dilutions of the test compounds were added to 25 µL of a cell suspension (1500 cells for KB-31, A-549, L929 and 3000 cells for MCF-7) in 384 well microtiter plates (final concentration range: 100, 50, 25, 12.5, 6.25, 3.125, 1.56, 0.78, 0.39, 0.2 µM). Blank and solvent controls were incubated under identical conditions. The compounds were incubated for 24 h for the FS4-LTM cells and 5 days for the remaining cell lines. After the incubation period 3 µL WST-1 (ready-to-use solution from Roche) were added. The incubation time of the plates, which were briefly shaken at 37 °C, varied between the cell lines from 20 min for KB-3-1 up to 2 h for MCF-7 before measuring the absorption at 450 nm and reference at 600 nm with the Infinite 200 PRO Plate Reader (TECAN). The percentage of viable cells was calculated with respect to the solvent control (100% viability). EC₅₀ values were determined with GraphPad Prism 8.

Table ST3.1: Cytotoxicity of compounds in a WST-1-based assay in five eukaryotic cell lines.

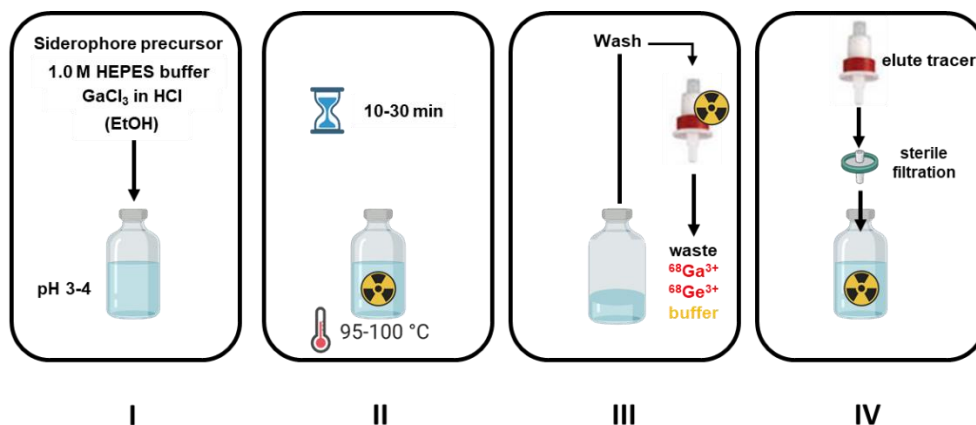
Given values indicate sensitivity of the cell line at a given compound concentration in μM , auranofin and staurosporine served as positive controls.

Compound	L929	A549	KB-3-1	MCF-7	FS4-LTM
Auranofin	1.15	6.04	0.67	1.58	1.02
Staurosporine	< 0.02	< 0.02	< 0.02	< 0.02	0.15
7	> 100	> 100	> 100	> 100	> 100
8	> 100	> 100	> 100	> 100	> 100
10	> 100	> 100	> 100	> 100	> 100
11	> 100	> 100	> 100	> 100	> 100
15	>100	>100	>100	>100	>100
24	> 100	> 100	> 100	> 100	> 100
25/26	> 100	> 100	84	> 100	> 100
34/35	> 100	> 100	> 100	> 100	> 100
37	> 100	> 100	> 100	49	> 100
[⁶⁹Ga]7	> 100	75	73	> 100	> 100
[⁶⁹Ga]10	75	> 100	> 100	> 100	> 100

Radiochemical procedures

Radiochemical synthesis of ^{68}Ga -complexed PET tracers

The radiochemical synthesis (RCS) was conducted in general without post-processing. The gallium-68 eluate was complemented with a certain amount of commercial 1.0 M HEPES buffer (ABX, Radeberg, Germany, Product No. SC-01-HBS) to adjust the pH to the desired value of 3.5. 30-50 nmol precursor were subsequently added and the complexation mixture was heated to the appropriate temperature. After the respective reaction time the reaction was cooled to room temperature. For the following purification *via* a cartridge, the reaction solution was diluted 1:1 with water. The cartridge was pre-conditioned following manufacturers recommendations. Once the solution had been loaded onto the cartridge (see Scheme S1), the latter was washed with 3-5 mL water or a 5% EtOH-solution in water to remove non-coordinated gallium-68 from the resin. The ^{68}Ga -complexed tracer was then eluted from the cartridge with an EtOH solution (30-100% in water). The alcohol was evaporated at 110 °C and a nitrogen gas flow of 1-2 bar in a closed V-vial equipped with a ventilation filter. Typically, the tracer was dissolved in 50-100 μL 0.9% isotonic saline solution. For *in vivo* studies in wildtype mice, the tracer was filter sterilized.



Scheme S3.1. General workflow for the synthesis of gallium-68 complexed PET tracers for *in vivo* applications.

Radiosynthesis for tracers evaluated in *in vivo* studies, was performed on a GRP 3V module (SCINTOMICS GmbH, Fürstenfeldbruck, Germany). In general, the gallium-68 eluate was directly eluted into a evacuated 10 mL vial and transferred by the dispenser into the reactor, where the precursor in 300 μL 1.0 M HEPES had been premixed. Subsequently, the reactor was heated to the respective, pre-set temperature and continued at this temperature for the required synthesis time. Afterwards, a purification into a SPE cartridge was conducted and the

tracer was eluted from the resin, according to the previously described procedure into a V-vial. The EtOH was removed accordingly, and the activity concentration was adjusted according to the above described procedure. The pH values of the formulated tracers ranged between pH = 5-6.8 with a residual EtOH content of 0-5%.

Generators	Post-processing	pH-value of the resulting $^{68}\text{GaCl}_3$ solution
GalliEO	No	Elution: 1.1 mL 0.1 M HCl, pH = 2.5
GalliAd	No	Elution: 1.1 mL 0.1 M HCl, pH = 2.5

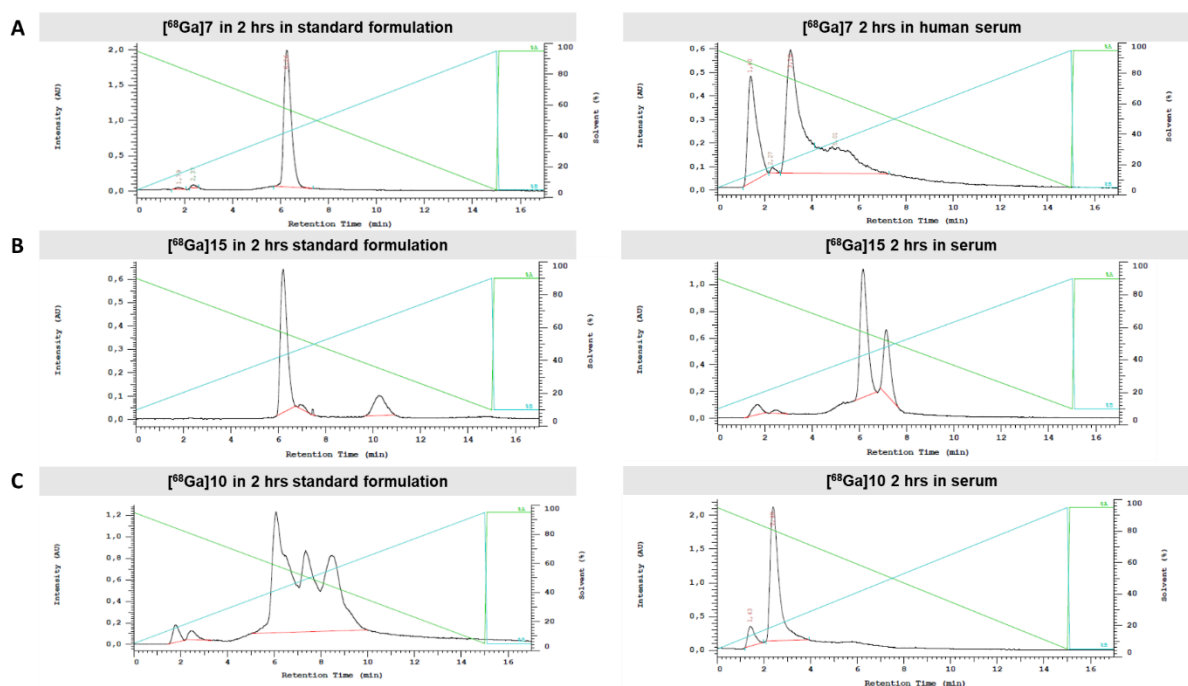


Figure S3.7. Radiochemical stability of ^{68}Ga -complexes (A) $[^{68}\text{Ga}]7$; (B) $[^{68}\text{Ga}]15$; (C) $[^{68}\text{Ga}]10$ in standard formulation (left panels) or in human serum (right panels) for 2 hours. Each radio-HPLC represents a characteristic sample from at least three independent experiments.

Table ST3.2. Evaluated SPE cartridges for purification of bacteria specific PET tracers: The table shows the recovery rates of the respective tracers, minimum recovery rate was set to 60% (green). Rates between 50-60% were regarded as moderate (orange) and rates below 50% were not acceptable (red). White field = no tested, waste = product did not show retention on the cartridge, SPE = product could not be eluted from the cartridge.

	[⁶⁸ Ga]7	[⁶⁸ Ga]10	[⁶⁸ Ga]11	[⁶⁸ Ga]15	[⁶⁸ Ga]34	[⁶⁸ Ga]35
^t C-18 light	>60			70.1		
HR-P						
HILIC						4.5
LiChrolut EN	65.0				52.6	19.2
HR-X		6.6				
SiOH-Diol		waste				
SiOH		SPE				
Envi Carb Plus			SPE			
C18ec		57.1			66.3	SPE
Ps-H+		4.4				
HLB		66.9		68.7		>100

Procedure for [⁶⁸Ga]7

For the manual synthesis, unprocessed gallium-68 eluate (approx. 300-500 MBq; 8.12 – 13.52 mCi) was mixed with 30 nmol **7** and 300 µL 1.5 M HEPES and heated for 10 minutes at 100°C with pH = 3.5. The reaction solution was diluted with water, loaded onto a ¹²C18 light cartridge (Waters GmbH, Eschborn, Germany, article no. WAT036805) and the complexed tracer was eluted with 1 mL 50% EtOH solution in water. The automated method is based on the described, manual complexation. The labelling time amounted to only 8 minutes at 125°C and a ¹²C-18 light cartridge was employed, from which the product was eluted with 1 mL 50% EtOH in a sterile pointed-bottom vessel. For animal studies, the alcohol was removed under a nitrogen gas flow at 110 °C and the residual tracer was diluted with 0.9% isotonic saline solution. The product could be afforded with a radio chemical yield (RCY) of 49.3 ± 24.7 % (n = 10).

Characterization: HPLC

Column	Gemini C6-Phenyl; 100x 4.6 mm (Phenomenex, Aschaffenburg, Germany)	
Solvent A	water	
Solvent B	acetonitrile	
Flow	1 mL/min	
Wavelength	254 nm	
Gradient	0-15 min	5% B to 95% B
	15-17 min	5% B
t _R	4.58 min (dead time 2.0 min)	

Procedure for [⁶⁸Ga]15

For the manual synthesis, unprocessed gallium-68 eluate (approx. 300-500 MBq; 8.12–13.52 mCi) was mixed with 30 nmol **15** und 300 µL 1.5 M HEPES at a pH of 3.5 for 10 minutes at 100°C. The reaction solution was diluted with water, loaded onto a HLB cartridge (Waters GmbH, Eschborn, Germany, article no. 186005125) and the complexed tracer was eluted with 1 mL 50 % EtOH solution in water. The automated method is based on the described, manual complexation procedure. The labelling time amounted to only 6 minutes at 125°C and a HLB cartridge was employed, from which the product was eluted with 0.9 mL 50% EtOH in a sterile pointed-bottom vessel. For animal studies, the alcohol was removed under a nitrogen gas flow at 110 °C and the residual tracer was diluted with 0.9% isotonic saline solution. The product could be afforded with a radiochemical yield (RCY) of 60,6 ± 16,1 % (n = 6).

Characterization: HPLC

Column	Gemini C6-Phenyl; 100x 4,6 mm (Phenomenex, Aschaffenburg, Germany)	
Solvent A	water	
Solvent B	acetonitrile	
Flow	1 mL/min	
Wavelength	254 nm	
Gradient	0-15 min	10% B -90% B
	15-17 min	10% B
t _R	4.27 min (dead time 2.0 min)	

Procedure for [⁶⁸Ga]11

For the manual synthesis, 300 µL unprocessed gallium-68 eluate (70.6 MBq; 1.91 mCi) was supplemented with 50 nmol **11**, 48 µL Ethanol and 80 µL 1.5 M HEPES at a pH = 3.5 and heated for 25 minutes to 100 °C. The reaction solution was diluted with water and loaded onto a HLB column. The product was eluted with 1 mL 100 % EtOH and the tracer could be obtained with a RCY of 49.4 % (n = 2).

Characterization: HPLC

Column	Gemini C6-Phenyl; 100x 4,6 mm Phenomenex, Aschaffenburg, Germany)	
Solvent A	water + 0,1 % AcOH	
Solvent B	acetonitrile + 0,1 % AcOH	
Flow	0.8 mL/min	
Wavelength	254 nm	
Gradient	0-10 min	5% B
	10-35 min	5% B-95% B
	35-40 min	95% B-5% B
t _R	14.9 min (dead time 2.0 min)	

Procedure for [⁶⁸Ga]10

For the manual synthesis, 300 µL unprocessed gallium-68 eluate were supplemented with 50 nmol **10**, 550 µL EtOH and 300 µL 1.5 M HEPES at a pH = 3.5 and heated for 30 minutes to 100 °C. The reaction was diluted with water and loaded onto a HLB cartridge to eluate the product with 500 µL 100% EtOH. The tracer was obtained with a RCY of 24.6 ± 13.3 % (n = 4).

For the automated method the reaction mixture was composed as follows: 1.1 mL generator eluate (approx. 300-500 MBq; 8.12 – 13.52 mCi), 550 µL EtOH, 300 µL HEPES and 60 nmol **10**. The labelling time was 25 minutes at 125 °C and the product was purified via HLB cartridge, while the product was eluted from the resin with 1 mL 100% EtOH in a pointed-bottom vial. For animal studies, the EtOH was reduced under a nitrogen gas flow at 110 °C and the tracer was diluted with 0.9% isotonic saline solution. The tracer could be obtained with a RCY of 19.4 ± 15.2 % (n = 19)

Characterization: HPLC

Column	Gemini C6-Phenyl; 100x 4,6 mm (Phenomenex, Aschaffenburg, Germany)	
Solvent A	water	
Solvent B	acetonitrile	
Flow	1 mL/min	
Wavelength	254 nm	
Gradient	0-15 min	5% B - 95% B
	15-17 min	5% B
t _R	4,69 min (dead time 2,0 min)	

Procedure for [⁶⁸Ga]25/26

For the manual synthesis, 300 µL unprocessed gallium-68 eluate (99.19 MBq; 2.68 mCi) were supplemented with 50 nmol **25/26** and 80 µL 1.5 M HEPES at a pH = 3.5 and heated for 15 minutes to 100 °C. The reaction was diluted with water and loaded onto a C18 ec cartridge (Macheray-Nagel GmbH & Co. KG, Düren, Germany, 730011) to eluate the product with 500 µL 100% EtOH. The tracer could be obtained with a RCY of 24.6 ± 13.3 % (n = 4).

Characterization: HPLC

Column	Gemini C6-Phenyl; 100x 4.6 mm (Phenomenex, Aschaffenburg, Germany)	
Solvent A	70 mM phosphate puffer (pH = 2.5)	
Solvent B	acetonitrile	
Flow	1 mL/min	
Wavelength	254 nm	
Gradient	0-20 min	5% B-95% B
	20-25 min	95% B -5% B
t _R	5.9 min (dead time 2.0 min)	

Procedure for [⁶⁸Ga]34/35

For the manual synthesis, 500 µL unprocessed gallium-68 eluate (122 MBq; 3.30 mCi) were supplemented with 50 nmol **35**, 285 µL EtOH and 125 µL 1.5 M HEPES at a pH = 3.5 and heated for 30 minutes to 100 °C. The reaction was diluted with water and loaded onto a HLB cartridge to eluate the product with 1 mL 100% EtOH. The tracer could be obtained with a RCY 10.5 ± 7.9 % (n = 6).

Characterization: HPLC

Column	Gemini C6-Phenyl; 100x 4.6 mm Phenomenex, Aschaffenburg, Germany)	
Solvent A	water	
Solvent B	MeOH	
Flow	1 mL/min	
Wavelength	254 nm	
Gradient	0-15 min	5% B-95% B
	15-17 min	95% B -5% B
t _R	3,2 min (dead time 2.0 min)	

Stability and logD determination of ⁶⁸Ga-complexed PET tracers

Determination of tracer stability was conducted by HPLC analysis employing a UV as well as a radio detector. 300 µL PBS or human serum were kept in a heating block at 37 °C, and 2-3 MBq (0.05 – 0.08 mCi) of the respective tracer were added, vortexed for 10 seconds and HPLC samples of 100-200 kBq (0.003 – 0.005 mCi) were taken at 0 minutes, 30 minutes, 1 hour und 2 hours after another 10 seconds of vortexing. The samples were analyzed with their respective HPLC column and method. Uncoordinated ⁶⁸Ga was always detected in the injection peak ($t_R = 0$).

The hydrophilicity was determined with the „shake flask method“. 700 µL 1xPBS (pH=7.4) and *n*-Octanol were pipetted in a 2 mL reaction vial. Followed by the addition of 250 kBq (0.007 mCi) of the respective tracer, the emulsion was vortexed for 2 minutes. Subsequently, the phases were separated by centrifugation for 5 minutes at 12 000 rpm, transferred to two different tubes and the activity was measured in a gamma counter (2470 WIZARD2® Automatic Gamma Counter, PerkinElmer, Waltham, MA, USA). The distribution co-efficient logD was calculated *via* the following equation:

$$\log D_{pH\ 7.4} = \log \left(\frac{[cpm\ in\ Octanol]}{[cpm\ in\ PBS]} \right)$$

All logD experiments were carried out in triplicates.

Animal experiments

Biodistribution studies of ⁶⁸Ga-complexed tracers in healthy wildtype mice

The tracers were first evaluated in healthy, living wildtype mice. Healthy mice (n = 8) were anesthetized with isoflurane (Start: 3% isoflurane with 3% Oxygen L/min; then 1.5% with 0.6 L/min Oxygen). A catheter was introduced into the tail vein, while the mouse was held on a warming bed with a temperature of 37 °C. The animals were imaged in a small animal double bed in the small animal PET scanner. The scanner was focused on the heart of the mouse while imaging. Then 12.8 ± 2 MBq (0.35 ± 0.05 mCi) [⁶⁸Ga]7, 10.8 ± 1.6 MBq (0.3 ± 0.04 mCi) [⁶⁸Ga]15 or 10.7 ± 1.5 MBq (0.29 ± 0.04 mCi) [⁶⁸Ga]10 with maximum 150 µL injection volume were given via the catheter in the lateral tail vein. In the following, 100 µL 0.9% isotonic saline solution with heparin was injected. The tracer accumulation was monitored over 60 minutes of dynamic PET scan in 32 frames. These frames were separated as follows: 5x2s, 4x5s, 3x10s, 8x 30s, 5x 60s, 4x300s and 3x600s over a span of 60 minutes. During the scan, the respiratory and heart frequency of the animals were monitored as well and a final 10-minute CT scan was recorded after the 60 minutes of dynamic PET scan to overlay the morphological details with the PET scan. Four mice were killed by cervical dislocation and heart, lung, stomach, liver, gall bladder, intestine, muscle, kidney, spleen, testicles, blood, and urine were transferred in tared γ counter tubes, weighted and measured in the γ counter. The counts per minute (cpm) were decay corrected and transferred in Becquerel.

The relative activity (percent) was then divided by the mass of the organ in gram (g). The pictures were calculated by a 3D OSEM/MAP algorithm ($\beta = 0.01$, OSEM iterations = 2, MAP iterations = 18) reconstructed in a 256x256x159 matrix (0.39 x 0.39 x 0.80 mm). The shown pictures were all decay and background corrected. The evaluation was performed with the Inveon Research Workplace Software® and regions of interest (ROIs) were defined around the kidney, liver, heart, and the muscles. For each frame and time point the tracer biodistribution could be generated in the respective organ yielding a time over activity curve (TAC). The data was shown as % injected dose per tissue weight (%ID/g) and analyzed during in the last frame (50-60 min). All experiments are in accordance with the guidelines of the European Directive 2013/63/EU as well as German national laws and are approved by the local authorities and the institutional animal care and use committee. Animals were purchased from Charles River and allowed to settle for minimum 7 days. Mice were housed at 23°C 12 under a 12-hrs light cycles and had free access to food and water. All investigated animals were 8-10 weeks old. In order to prevent suffering, time periods between injection of the bacteria and euthanasia were no longer than 24 hours. Pain treatment was administered via water after bacteria injection.

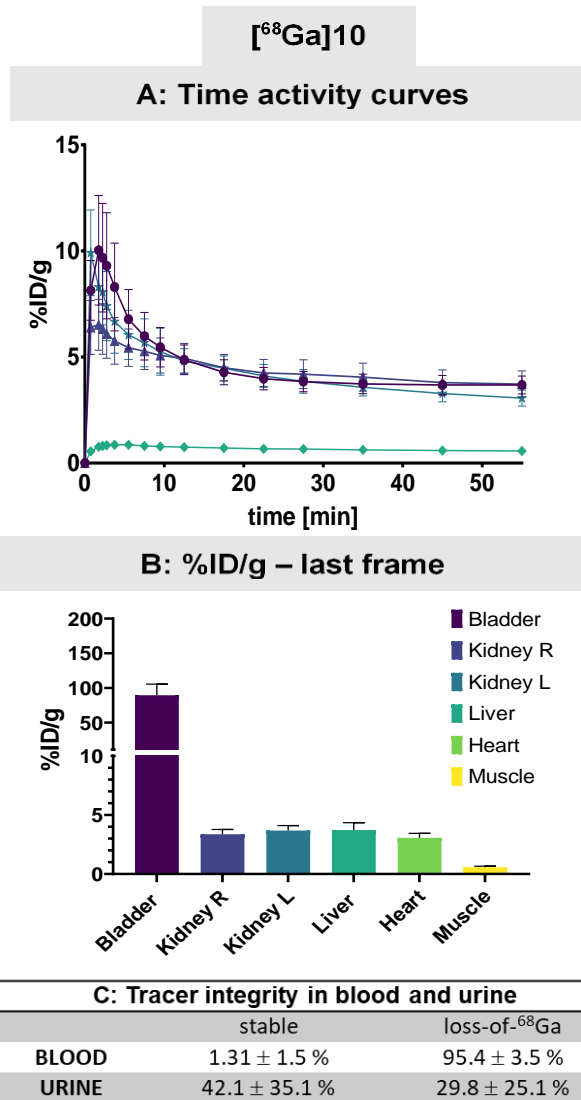


Figure S3.8. Biodistribution data of [⁶⁸Ga]10 in male C57Bl/6N mice over 60 min of dynamic PET imaging. (A) Time activity curves (TAC) display the biodistribution of [⁶⁸Ga]10 for six organs (left and right kidney, bladder, liver, heart and muscle) in the course of one hour of dynamic PET/CT imaging (n = 6, error bars indicate ± SD). In (B) the % injected dose / organ weight during the last time frame (50-60 min) of dynamic PET/CT scan (%ID/g), is plotted for [⁶⁸Ga]10, n=6, error bars indicate ± SD. (C) Tracer integrity or loss-of- gallium-68 for [⁶⁸Ga]10 in blood and urine samples (each n=6, error calculated as ± SD) after 60 minutes of dynamic PET/CT scan, determined by radio-HPLC measurements.

Dynamic PET imaging of *E. coli*-infected / LPS-injected wildtype mice

Bacterial inoculum generation and work-up

E. coli (ATCC47076) cultures were grown in LB medium (700 μ L overnight culture in 30 mL fresh LB medium) at 37 °C and 130 rpm in a shaking incubator. For the infection experiment with [⁶⁸Ga]15 bacteria were grown till OD_{600nm} = 0.500 and for the experiment with [⁶⁸Ga]7 till OD_{600nm} = 0.675. 100 μ L of each culture were taken for the determination of the live germ count. The residual culture was centrifuged for 15 minutes at 5000 rpm and 4 °C. The pellet was washed with 90 μ L ice-cold 0.9 % isotonic saline solution, centrifuged 10 minutes at 11000 rpm and 4 °C and the supernatant was discarded. The pellet was re-suspended in 90 μ L 0.9 % isotonic saline solution and stored until further usage on ice.

Injection of the bacteria or LPS into the muscles of healthy wildtype mice

After preparation of the final bacterial suspension, the mice were anesthetized (Start: 3 % isoflurane with 3 % Oxygen L/min; then 1.5-2 % isoflurane, 0.6-2.0 % L/min Oxygen) and kept on a warming bed. A 0.9 mg/mL LPS solution was prepared in 0.9% saline solution, 90 μ L of this solution were filled bubble-free in a Hamilton syringe, which was equipped subsequently with 27G needle with a mark 5 mm after the end. The right hind leg was slightly stretched and the *M. gastrocnemius* was fixated. The catheter was introduced posteriori fibular till the mark on the needle into the muscle of the right leg and 30 μ L of the solution were administered. For the injection of the bacteria a comparable procedure was employed. The bacteria suspension was re-suspended and filled bubble-free into the Hamilton syringe, the needle was attached and 30 μ L of the bacterial solution was injected in the same manner into the left *M. gastrocnemius*. The table below shows the administered amount of LPS or bacteria for the respective tracer:

Tracer	bacteria in [CFU]	LPS in [μ g]
[⁶⁸ Ga]15	2.27·10 ⁷	27
[⁶⁸ Ga]7	3.00·10 ⁷	27

After the injection, the mice were allowed to wake up and the drinking water of the mice was supplemented with 0.1 mg/mL Tramadol to reduce any pain as a result of the injections to a minimum.

Dynamic PET/CT scan procedure

The PET scans were conducted 20 hours after the injection of the bacteria/LPS. For this experiment 11.6 ± 0.8 MBq (0.31 ± 0.02 mCi) [^{68}Ga]15 und 11.8 ± 1.5 MBq (0.32 ± 0.04 mCi) [^{68}Ga]7 were injected respectively and a dynamic PET scan was acquired. Followed by a short CT scan and immediate cervical dislocation under deep anesthesia. The *M. gastrocnemius* was removed from each leg and employed in auto radiographic measurements. The 3D reconstructed pictures of the PET/CT scan were analyzed in the unit %ID/g, for this the scans from 30 to 60 minutes were cumulated and based on the PET image, ROIs were defined around the respective muscle.

Ex vivo autoradiographic measurements of dissected muscles

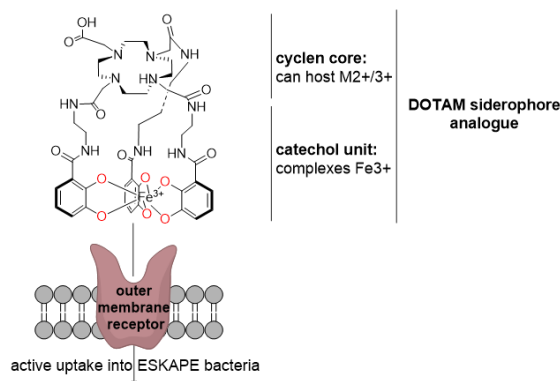
For the sampling of the muscle, the fur of the leg was removed completely, the joints fixated and starting from the Achilles tendon the muscle could be removed from the fibula. The muscle was cleaned from fascia and surrounding tissue, residual hair was removed with a Leukosil tape. The muscle was washed twice with 1xPBS and snap frozen under liquid nitrogen in Tissue Tek® O.C.T™. Closely spaced parallel tissue slices were prepared, with a layer thickness of 10 μm , and subjected immediately either to autoradiographic measurements or 6 μm thick slices were prepared for histological staining and kept frozen at -80 °C. 2-3 slices were placed for each analysis on a clean microscopy slide – for autoradiographic measurements the slides were placed on a phosphorescence plate and exposed for 1.5 hours. Afterwards the plate was analyzed by a phosphorous scanner.

Immunology stains

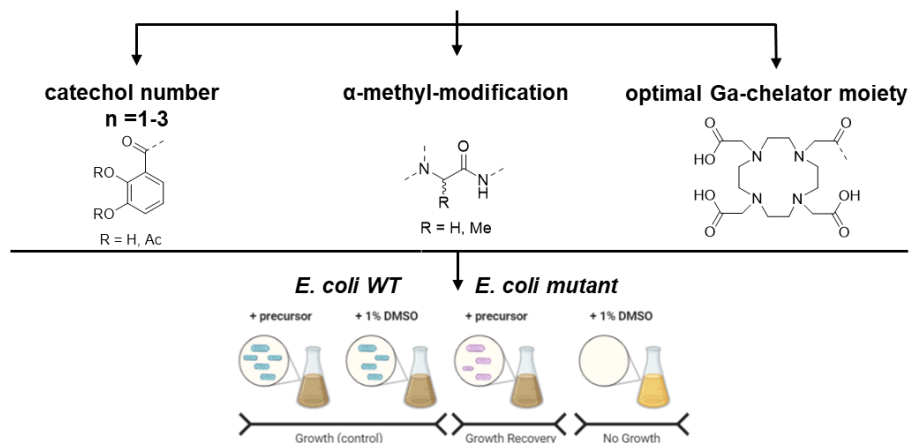
Tissue slices were prepared as described for *ex vivo* autoradiographic measurements. Adjacent sections (6 μm) were taken for histology and immunological staining. Slices were placed onto glass slides and stored at $-20\text{ }^{\circ}\text{C}$ until histological and immunological staining. For histological and immunological staining, tissue slices were air-dried and fixed in $-20\text{ }^{\circ}\text{C}$ methanol (10 min), and tissue was permeabilized with 0.1% Triton X-100 (5 min, Sigma-Aldrich, Germany). After blocking using 3% goat serum in 1xPBS (30 min), corresponding histological and immunological staining were conducted. Gram staining was performed using the BBL Gram Stain Kit (Becton, Dickinson and Company; Franklin Lakes, USA) following the manufacture's protocol. Immunostaining for CD38 (macrophages) was conducted using a mouse anti-CD38 antibody (Novus Biologicals, USA) as primary antibody. A secondary goat anti-mouse antibody (Eugene, Oregon, USA) labeled with AlexaFluor488 (AF488) was used for fluorescent microscopy. Hematoxylin/eosin (HE) staining defined general morphology and was performed using hematoxylin QS (Vektor, Burlingame-USA) and eosin Y (Sigma-Aldrich, Germany). All images were recorded using an "Olympus BX40 microscope" equipped with a "Zeiss AxioCam digital camera" and an "Olympus Hg-lamp" (BH2-RFL-T3).

Assay tree for compound design and selection

1. Bacteria-specific uptake of the synthetic DOTAM siderophore analogue in ESKAPE pathogens^[1]



2. Chemical synthesis of DOTAM variants with modifications presumed to be beneficial for Ga-complexation



3. Screening of compounds in *E. coli* mutants for growth recovery
positive outcome: 8, 10, 11, 15, 24/25, 35/36 – incl. [^{nat}Ga] complexes
4. In parallel: [^{nat}Ga] complexation with GaCl₃ and complex isolation
positive outcome: 7, 10, 15
negative outcome: 8, 11, 24/25, 35/36 - minor complex formation with [^{nat}Ga] excess
5. Cytotoxicity / chemical stability
positive outcome: all compounds, incl. [^{nat}Ga] complexes
6. Radiochemical synthesis of [⁶⁸Ga] tracers RCY, LE, RCP assessment, logD (<0), complex stability in PBS & human serum
positive outcome: 7, (10), 15
negative outcome: 8, 11, 24/25, 35/36 – no complex formation w. shortfall of [⁶⁸Ga]
7. Biodistribution studies in healthy C57Bl/6N
positive outcome: 7 and 15
negative outcome: 10 – loss of [⁶⁸Ga], high liver and heart uptake
8. *In vivo* PET imaging in mice infected with *E. coli* and injected with LPS
positive outcome: 7 and 15



Figure S3.9. Schematic workflow and assay tree for compound design and selection.

Supplementary References

1. Interagency coordination group on antimicrobial resistance. No time to wait: securing the future from drug-resistant infections. <https://www.who.int/publications/i/item/no-time-to-wait-securing-the-future-from-drug-resistant-infections>, June 2022.
2. Theuretzbacher, U.; Gottwalt, S.; Beyer, P.; Butler, M.; Czaplewski, L.; Lienhardt, C.; Moja, L.; Paul, M.; Paulin, S.; Rex, J. H.; Silver, L. L.; Spigelman, M.; Thwaites, G. E.; Paccaud, J. P.; Harbarth, S., Analysis of the clinical antibacterial and antituberculosis pipeline. *Lancet Infect. Dis.* **2019**, *19* (2), e40-e50.

4. Publication 2: Antibiotic conjugates with an artificial MECAM-based siderophore are potent agents against Gram-positive and Gram-negative bacterial pathogens

This chapter has been published as a peer-reviewed article in a scientific journal:

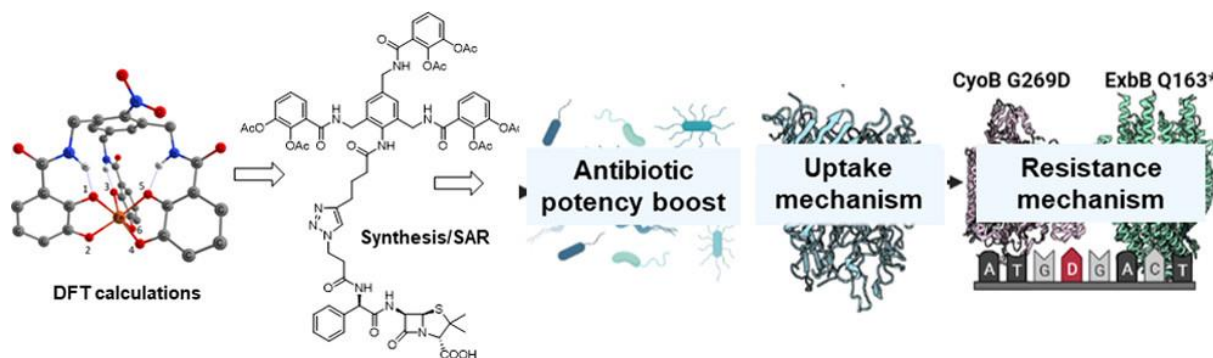
Lukas Pinkert, Yi-Hui Lai, Carsten Peukert, Sven-Kevin Hotop, Bianka Karge, Lara Marie Schulze, Jörg Grunenberg and Mark Brönstrup

„Antibiotic conjugates with an artificial MECAM-based siderophore are potent agents against Gram-positive and Gram-negative bacterial pathogens”.

Journal of Medicinal Chemistry, **2021**, 64, 20, 15440-15460.

DOI: 10.1021/acs.jmedchem.1c01482

Table of content graphic



b

Abstract

The development of novel drugs against Gram-negative bacteria represents an urgent medical need. To overcome their outer cell membrane, we synthesized conjugates of antibiotics and artificial siderophores based on the MECAM core, which are imported by bacterial iron uptake systems. Structures, spin states and iron binding properties were predicted *in silico* using density functional theory. The capability of MECAM to function as an effective artificial siderophore in *E. coli* was proven in microbiological growth recovery and bioanalytical assays. Following a linker optimization focused on transport efficiency, five β -lactam and one daptomycin conjugates were prepared. The most potent conjugate **27** showed growth inhibition of Gram-positive and Gram-negative multidrug-resistant pathogens at nanomolar concentrations. The uptake pathway of MECAMs was deciphered by knockout mutants and highlighted the relevance of FepA, CirA, and Fiu. Resistance against **27** was mediated by a mutation in the gene encoding ExbB, which is involved in siderophore transport.

4.1 Introduction

The rising resistance of human pathogenic bacteria to clinically used antibiotics has become a worldwide health problem that is associated with severe medical and economic consequences. It is striking that in a consensus list on the most critical pathogens, established by the WHO,¹ top priority was assigned to Gram-negative bacteria, i.e. drug resistant congeners of *Acinetobacter baumannii*, *Pseudomonas aeruginosa* and *Enterobacteriaceae*. The fact that therapeutic options against them are particularly limited² is due to their outer cell membrane, which represents a tight, impermeable biological barrier against antibiotic agents.³⁻⁵ A promising strategy to enhance translocation across the outer cell membrane is to embark on bacterial internalization systems, like those for siderophore transport.⁶ Siderophores are small molecule iron chelators synthesized and secreted by prokaryotes. Iron-loaded siderophores are actively transported across the bacterial outer membrane, thus satisfying the bacterial demand for iron.^{7, 8} In a so-called “Trojan Horse” strategy,⁹ antibiotic molecules have been conjugated to siderophores and thereby reach much higher intracellular concentrations compared to the free drugs.^{10, 11} After decades of research and development, a successful clinical validation of this principle has been reached with the siderophore-containing cephalosporin ‘*Cefiderocol*’ (*Fetroja*®), which has recently obtained market authorization.^{12, 13}

Enterobactin (**1**), the main siderophore of *Escherichia coli*,^{14, 15} possesses a chiral trilactone core that provides a pre-orientation of the three iron-chelating catechol groups (Scheme 4.1), thus minimizing molecular strain when forming an octahedral complex with ferric iron. Hence, it is one of strongest natural iron binders known, and became the prototype model for siderophore uptake and conjugation studies.^{16, 17} Because the synthetic access to enterobactin conjugates is demanding at large scale, and because the trilactone backbone is reported to be unstable,¹⁸ we aimed to replace enterobactin’s trilactone core by more durable, synthetic moieties. The principal feasibility of this approach has been demonstrated by Miller and others,^{16, 19-24} we qualified the DOTAM core **2** as a suitable scaffold recently.²⁵ In many cases, the catechols are masked as acetylated prodrugs in order to avoid *in vivo* deactivation of the iron chelating units by catechol-O-methyltransferases.²⁶ In this study, we explored a simple benzene ring to accommodate three arms for iron binding and a fourth arm for antibiotic payload attachment. In early reports, 1,3,5-N,N',N''-tris-(2,3-dihydroxybenzoyl)-triaminomethylbenzene (MECAM, **3**, Figure 4.1)^{27, 28} has been shown to effectively transport ferric iron through the outer membrane of Gram-negative *E. coli* into the periplasmic space.^{29, 30} In this study, we systematically varied the linkers branching from the benzene core, synthesized first MECAM-based antibiotic conjugates, and characterized their structural, microbiological and antibiotic properties, as well as their uptake routes and resistance mechanisms *in E. coli*.

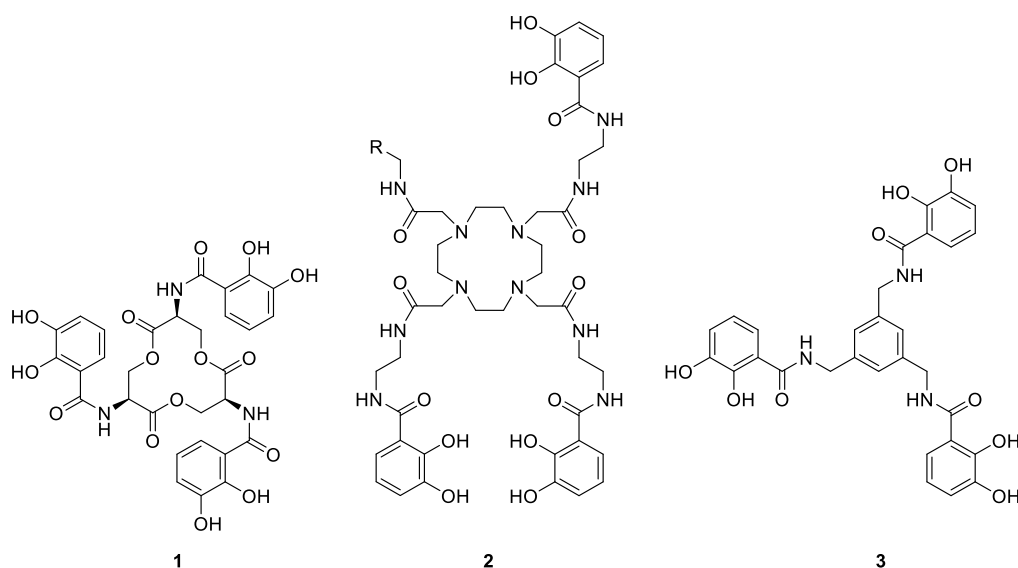


Figure 4.1. Chemical structures of enterobactin (**1**), and artificial siderophores with DOTAM- (**2**), and MECAM-based (**3**) cores.

4.2 Results

4.2.1 The MECAM scaffold is amenable to structural variations and functionalization

MECAM, the starting point for our studies, already possessed three catechol units for iron binding. Because the attachment of a fourth arm was required to install an antibiotic payload via a linker³¹, we chose to introduce a nitro group for this purpose, whose subsequent reduction should give rise to an easily accessible amine function. The acyl-protected siderophore **8** was synthesized starting from 1,3,5-tris(bromomethyl)benzene **7** by nitration, a tri-fold amine substitution, and the attachment of acid chloride **6**. To assess the roles of the nitro group and of the acetyl protecting groups, compounds **9** – **11** were prepared as well (Figure 4.2). In order to investigate whether structural modifications of MECAM had an impact on its iron transport capabilities, we designed a set of derivatives with increasing distances between the aromatic core and the iron chelating units. While elongation of the MECAM catechol arms may decrease conformational strain in the respective ferric iron complexes, the growing number of degrees of freedom render the formation of such complexes entropically unfavorable at the same time. To elucidate the structural boundaries for bioactive siderophores, four compounds **12** – **15** were synthesized, thereby covering arm length between three atoms (as in **8**) and seven atoms (as in **15**) linking the central and the peripheral phenyl rings (Schemes S4.1 – S4.3). Furthermore, three MECAM-derived congeners **16** – **18** could be obtained, in which the 1,3,5-substitution pattern is replaced by a 1,2,3-substitution pattern, thus increasing steric demand and changing symmetry properties (Figure S4.4 – S4.5).

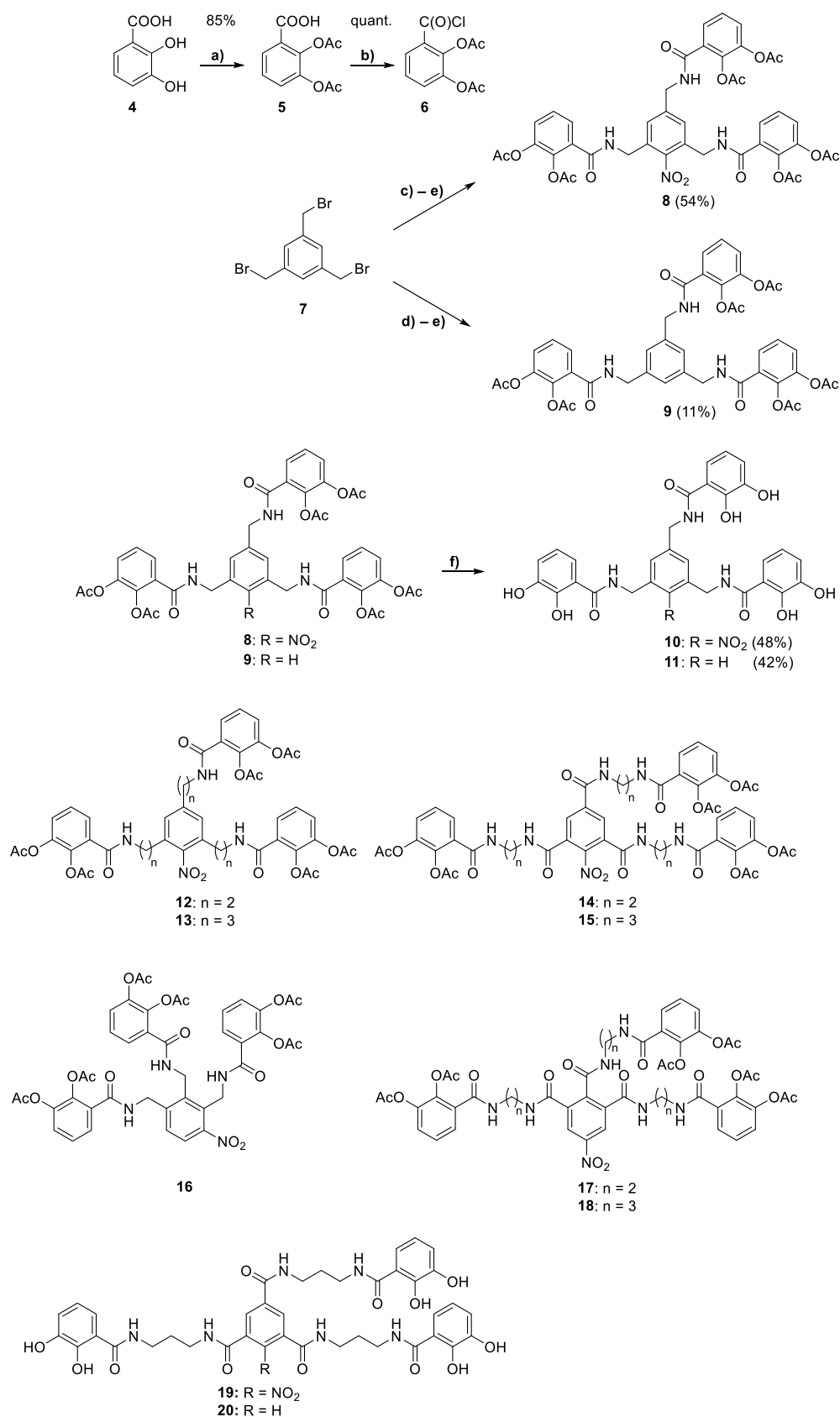


Figure 4.2. Syntheses of MECAM siderophores **8** – **11**, and structures of the final products **12** – **20**. Reagents and conditions: (A) Ac₂O, DMAP, NEt₃, reflux, 3 h; (B) (COCl)₂, DMF, CH₂Cl₂, 0 °C → rt, 2.5 h; (C) HNO₃, H₂SO₄, 0 °C → rt, 1 d; (D) NH_{3(aq)}, EtOH, THF, rt, 1 d; (E) **6**, KHCO₃, H₂O, 1,4-dioxane, 0 °C → rt; (F) KOH_(aq), rt, 1 h.

4.2.2 MECAM-based siderophores bind iron in different spin states

The structural and energetic properties of the synthetic siderophores were examined next. Since we were especially interested in the impact of linker length on iron coordination, the substances with the shortest and longest distances between aromatic core and catechol units, **10**, **19** and **20** (Figure 4.2) were studied *in silico* by density functional theory (DFT) applying the hybrid version of the TPSS functional.³² The TPSS functional provides only 10% exact exchange, reducing the large systematic error in other functionalities when it comes to the description of the electronic configuration in transition metal complexes. Since an *ab initio* prediction of the thermodynamic stabilities in solution would be far too challenging because of the structural variance in our studied systems, we additionally characterized the stability (or lability) of the Fe-O contacts by computing all relevant relaxed force constants.^{33, 34} As the hydroxyl groups of catechols were fully deprotonated, the complexes had an overall charge state of -3. After a manual conformational search followed by individual geometry optimizations, we ended up with relaxed structures for the iron-siderophore complexes exemplified here for the siderophore **10** (Figure 4.1A). All octahedral ferric iron complexes were found to represent minima of the potential energy surface characterized by additional calculations of the second energy derivatives (no imaginary frequencies). In the octahedral ferric iron complex **10**, the distances between ferric iron and oxygen atoms differ between the 2- and 3-positions of the three catechols, the latter ones adopting values close to 2.0 Å (Table S4.1). Due to the formation of an intramolecular hydrogen bond,³⁵ electron density is withdrawn from the oxygens in 2-positions (O1, O3, and O5 in Table S4.1), resulting in an Fe-O bond elongations of ca. 0.1 Å. Correspondingly, our calculated relaxed force constants are lower and the kinetic lability should be more pronounced for these FeO distances. Our findings imply that the iron complex with siderophore **10** nearly adapts an ideal C₃-symmetry (Figure 4.1A). In a second step total energies were computed for the Fe(III) *high-spin* and *low-spin* adducts of **10**, **19** and **20** as well for some natural siderophore-iron complexes (Figure S4.1), respectively. To our knowledge, octahedral *low-spin* complexes have not been reported for any siderophore so far in the literature. And indeed, our analysis of common natural siderophores and of **10** depicted an energetic preference of the *high-spin* configuration. To our surprise, the synthetic siderophore **19** was found to favor the *low-spin* state ($\Delta E (hs - ls) = 41.9$ kJ/mol) as the electronic ground state of the complexed iron(III) ion. This finding is of importance, since a low-spin ground state should be associated with a pronounced kinetic stability of the complex (see the analysis below). A direct conformational influence of the aromatic nitro group (note the two additional stabilizing NH \leftrightarrow O(nitro) interactions, Figure S4.1) on the electronic ground state of the complex is apparent, because the respective desnitro analog **20** again has a *high-spin* ground state ($\Delta E (hs - ls) = -38.5$ kJ/mol). We speculate that in solution these additional intramolecular hydrogen bonds will be weakened. Nevertheless,

siderophore **19** seems to be a good starting point, which might lead to a new class of kinetic stabilized *low-spin* siderophores. The iron–oxygen distances of **19** and **20** are smaller and more homogeneous for the *low-spin* state when compared to the respective *high-spin* complexes (Table S4.1). The force constants, indicators of the kinetic lability of weakly bound complexes, are significantly higher, suggesting that the low-spin configuration is kinetically more inert. The average force constant of 0.97 N/cm for the preferred high-spin configuration of **20** is comparable to the value of 0.95 N/cm that was recently reported for the natural siderophore enterobactin.³⁶ The average relaxed force constant of **19** is higher (1.16 N/cm, + 0.19 N/cm compared to **20**) in the high-spin state, and this difference is even more pronounced in the preferred low-spin state of **19** (2.01 N/cm, + 0.31 compared to **20**). Thus, the unusual preference of the low-spin configuration is reflected by relatively strong and covalent siderophore-iron bonds.

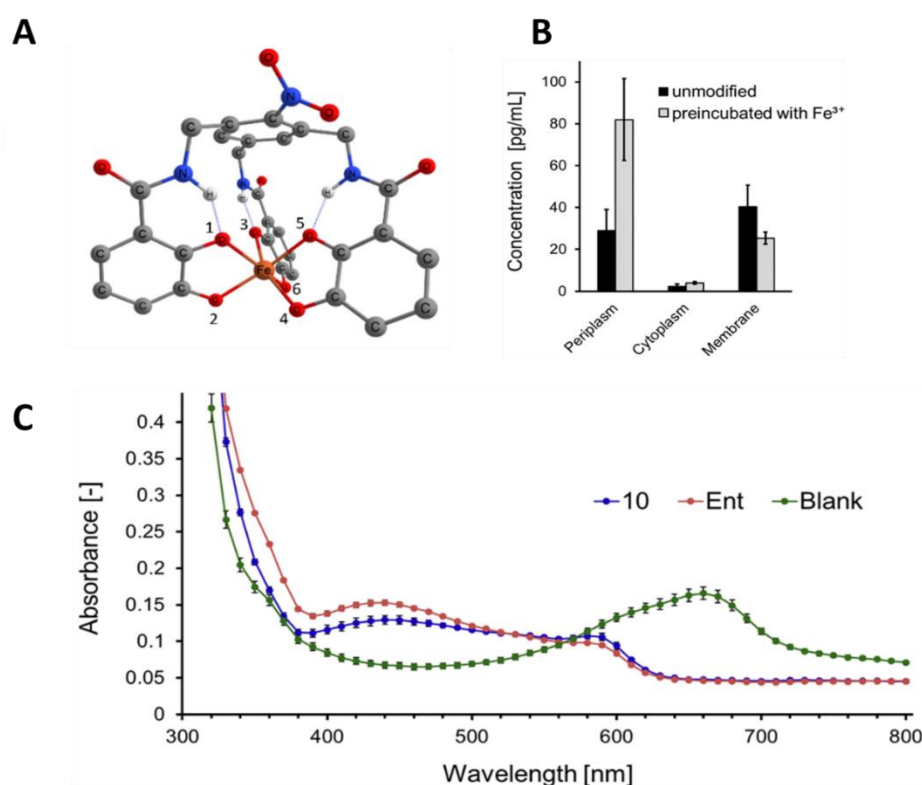


Figure 4.3. Characterization of **10**. (A) Calculated DFT-structure of ferric iron complex in stick representation with colorized atoms of carbon (grey), oxygen (red), and iron as well as nitrogen (blue). (B) Absorption spectra of an Fe³⁺-CAS solution following addition of **10** or enterobactin (Ent). (C) Intracellular concentration of **10** in *E. coli*. Following the incubation of *E. coli* with **10** (with or w/o Fe³⁺), bacterial subcompartments were fractionated, and the amount of **10** was quantified by LC-MS/MS. Compound **10** was mainly present in the periplasm and membranes, but barely in the cytoplasm.

The length of the linker had no impact on the average Fe-O bond length, as reflected by identical values of 2.04 Å for the high-spin complexes of **10** and **20**, and also their average force constants were comparable (1.03 N/cm vs. 0.97 N/cm, respectively). However, the distortion from an ideal C_3 -symmetry was larger for the siderophores with longer linkers. Next, the ability of MECAM siderophores **10** to form stable complexes with ferric iron was probed experimentally in a colorimetric assay utilizing chrome azurol S (CAS). CAS is a red dye, which forms blue complexes with ferric iron. The withdrawal of ferric iron from CAS by strong iron chelators like the positive control enterobactin results in a colorimetric shift from blue to red. We observed that the absorption maximum of CAS-Fe³⁺ at around 660 nm, corresponding to a blue color, vanished after the addition of **10** (Figure 4.1C). This demonstrates that the nitro compound **10** was capable of chelating a ferric iron.

4.2.3 MECAM-based siderophores transport iron into the periplasm via FepA

The ability to bind iron is a necessary, but not sufficient condition to serve as an artificial siderophore for Gram-negative bacteria. To probe whether the compounds would function as a siderophore, a growth recovery assay with an *E. coli* Δ entA strain was conducted. This strain is not able to biosynthesize its endogenous siderophore enterobactin and thus is only able to grow under iron-limited conditions when a suitable (xeno-)siderophore is added (Figure 4.2A, DMSO and enterobactin controls). Each of the compounds **8** – **11** restored growth sufficiently, illustrating the aptitude of MECAM to serve as an iron carrier for *E. coli* in its free and its acetylated prodrug form (Figure 4.2A). The growth recovery assay with the artificial siderophores **8** and **12** – **18** showed that only compounds **8** and **16**, possessing the shortest linkers between the aromatic ring and catechol units, were accepted as xenosiderophores by *E. coli* (Figure 4.2B). For siderophores **19** and **20**, deacetylated congeners of compound **15**, the ability to form complexes with ferric iron had been observed (*v.i.*). Thus, increasing the distances between core moiety and catechol units appears to rather hamper active transport through the outer membrane than impede complex formation. Since the synthesis of MECAM **8** proved to be more convenient than the preparation of the 1,2,3-substituted derivative **16**, we decided to stick to the former in the following studies. To pinpoint receptors involved in siderophore uptake, growth recovery assays were conducted in double knockout strains that harbor a gene deletion for one outer membrane receptor and another one for *entA*. The Δ entA Δ fepA strain showed a growth defect in the presence of the positive control enterobactin (Figure 4.2C). This demonstrates that *fepA* is a key molecule involved in enterobactin uptake, in line with literature findings¹⁵. A growth defect was also observed in the Δ entA Δ fepA strain following treatment with **8**. In contrast, **8** still enabled growth recovery in Δ entA Δ fecA, Δ entA Δ fhuA, Δ entA Δ cirA, and Δ entA Δ fiu strains (Figure 4.2C). To further confirm the role of FepA in **8** uptake, FepA

receptors were reintroduced by expressing a plasmid encoding full-length FepA in $\Delta entA\Delta fepA$ strain, followed by a growth recovery assay under supplementation of **8** (Figure 4.2D). The level of *fepA* expression was monitored by real-time PCR (Figure 4.2E).

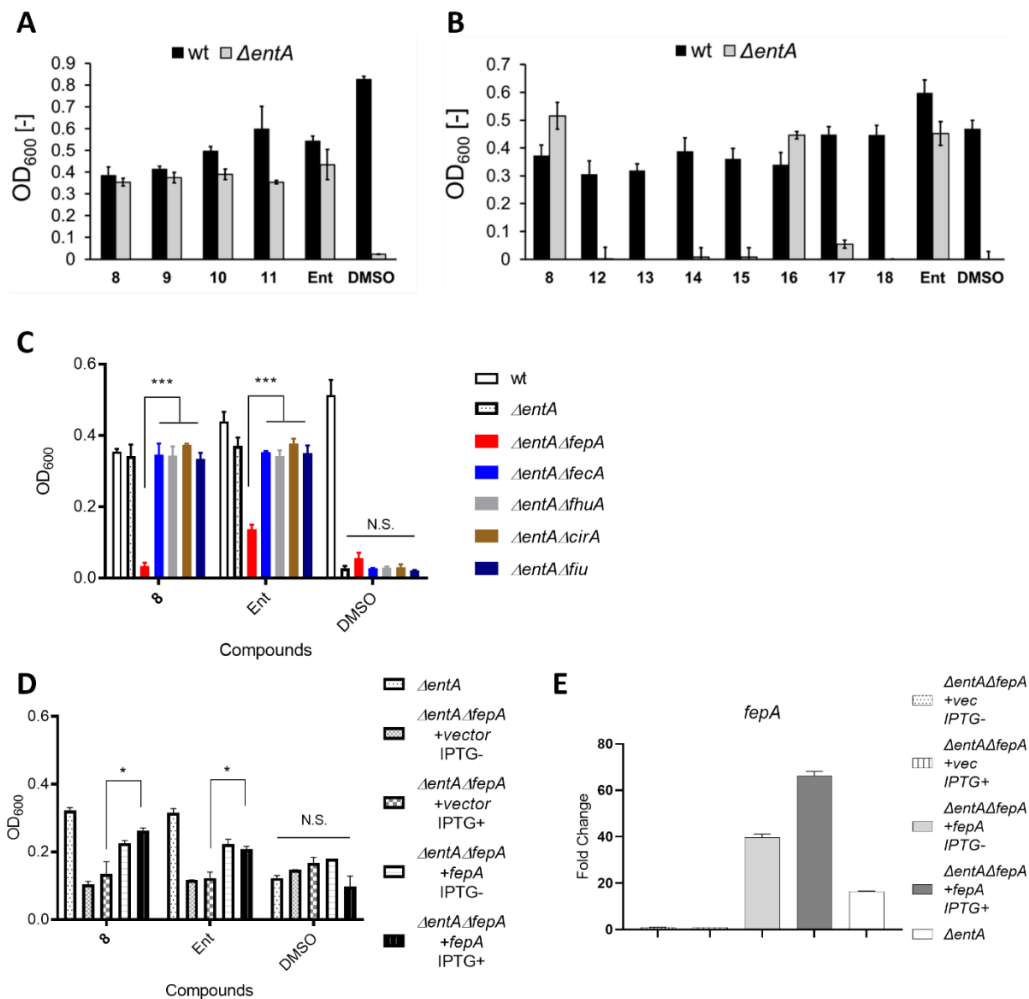


Figure 4.4. FepA is required for uptake of **8** in *E. coli*. Growth recovery assays with cultures of *E. coli* wt, single or double knockout strains that were treated with artificial siderophores, enterobactin or DMSO and grown under iron-deficient conditions. (A) Treatment with MECAM-based compounds **8** – **11**. (B) Treatment with longer chain and 1,2,3 substituted analogs **12** – **18**. (C) Treatment of outer membrane receptor deficient strains with **8**, enterobactin (Ent) or DMSO. (D) Treatment of strains harboring an IPTG-driven *fepA* expression plasmid or a vector control with **8**, enterobactin or DMSO. (E) RNA expression of *fepA* from cultures in (D) followed by real-time PCR. Gene expression was normalized against the reference gene *rpoB* and given as relative to $\Delta entA\Delta fepA$ + vec control. Bars represent the means and standard deviations of one representative experiment done in triplicate. Results shown are means and standard deviations of one representative experiment done in triplicate. * $p < 0.05$ and *** $P < 0.001$ (Student *t* test). Ent = enterobactin. Vec = vector. Complementation of FepA in $\Delta entA\Delta fepA$ strain rescued growth under treatment with **8** in iron-limited condition. These results demonstrate that FepA is the essential receptor for uptake of **8**, whereas FecA, FhuA, CirA, and Fiu are dispensable.

4.2.4 MECAM- β -lactam conjugate **27** inhibits the growth of MDR pathogens

For the design of siderophore-antibiotic conjugates, it is crucial to know the main site of subcellular accumulation, in order to assure a sufficient engagement of the antibiotic target. To measure accumulation, we applied a cell fractionation assay coupled with mass spectrometry detection.³⁷ Following a growth recovery assay of **10**, the *E. coli* cells from the restored colony were perforated employing an osmotic shock procedure. After releasing the periplasmic fraction via centrifugation, an additional sonication step resulted in complete cell lysis, yielding separate membrane and cytoplasmic fractions after centrifugation. Quantifying the content of **10** in these three fractions with mass spectrometry revealed compound enrichment in the membrane and periplasmic fractions, while a low compound concentration was detected in the cytoplasm (Figure 4.3B). The findings from the fractionation experiment suggest that antibiotics with periplasmic targets might reach their site of action and were preferably selected for conjugation to the MECAM siderophore. This renders the usage of non-cleavable linkers possible, reducing synthetic and stability problems compared to cleavable linkers. The reduction of the nitro group to the aniline **21**, followed by the attachment of a terminal alkyne, gave **22**, which was suitable for subsequent payload installation via a copper(I)-catalyzed alkyne-azide cycloaddition (CuAAC). Additionally, the deacetylated congener **23** was also prepared (Figure 4.5). In order to evaluate the extent by which a more sterically demanding linker might affect the ability of MECAM-derived xenosiderophores to translocate ferric iron into Gram-negative bacteria, a phenyl residue branching off close to the core motif was installed to yield **24** (Figure 4.5, Scheme S4.7). While the artificial siderophores **22** and **23** were functional in the growth recovery assay, growth could not be restored when **24** was applied (Figure S4.2). Thus, a linear, sterically unhindered linker appears to be necessary to maintain sufficient iron transport characteristics. We next decided to attach the amino-penicillins ampicillin and amoxicillin for the creation of MECAM-antibiotic conjugates, because they address a periplasmic target, and their primary amino groups constitute a viable attachment point according to previous studies.¹¹ The two amino-penicillins were first equipped with a terminal azide to yield derivatives **25** and **26** (Scheme S4.8) and then linked to **22** and **23** via CuAAC to afford the four MECAM conjugates **27** – **30** (Figure 4.5). It is known that replacing an unpolar alkyl linker by a more hydrophilic polyethylene glycol (PEG) linker can have a strong impact on the antibacterial activity of siderophore-drug conjugates.¹⁹

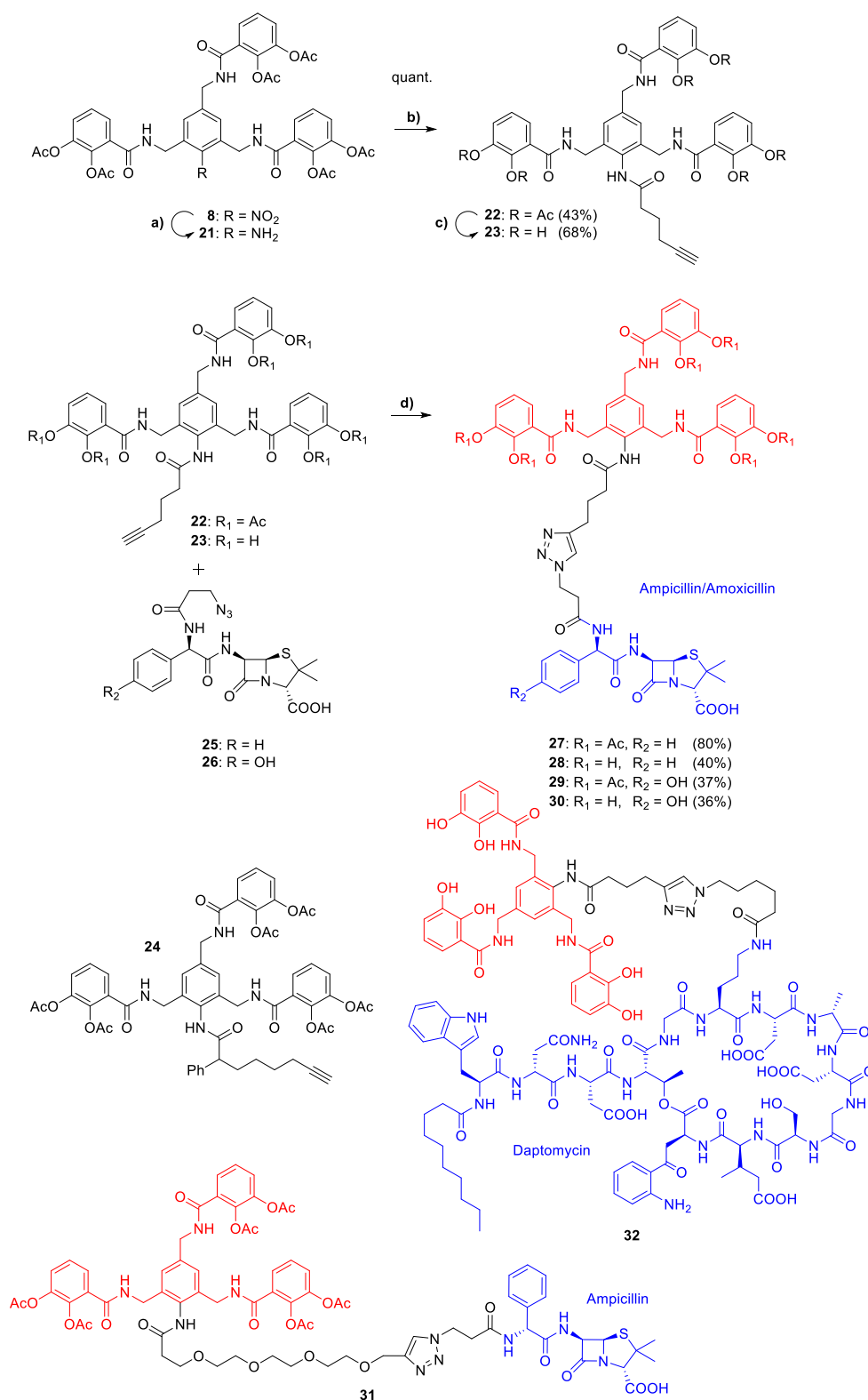


Figure 4.5. Syntheses of intermediates **21** – **23**, MECAM-amino-penicillin conjugates **27** – **30** and chemical structures of **24**, **31**, and the MECAM-daptomycin conjugate **32**. Reagents and conditions: a) Zn, AcOH, EtOH, THF, 0 °C → rt, 30 min; b) 5-hexynoic acid, isobutyl chloroformate, NMM, THF, 0 °C → rt, 1 d; c) NEt₃, MeOH, 0 °C → rt, 2.5 h. d) CuSO₄, sodium ascorbate, (TBTA), H₂O, DMF, rt, 2 – 3 h. In full conjugates, the antibiotic, linker, and siderophore moieties are labeled in blue, black and red, respectively.

Conjugate **31** comprising a PEG linker was synthesized in order to compare its activity with the four afore-mentioned congeners **27 – 30** (Figure 4.3, Scheme S4.9). Siderophore-antibiotic conjugates **27 – 32** were tested in minimal inhibitory concentration (MIC) assays against bacteria of the so-called ESKAPE panel, that comprises the clinically relevant pathogens *S. aureus*, *K. pneumoniae*, *A. baumannii*, *P. aeruginosa*, *E. faecium* and *Enterobacter* sp. To compare conjugated with unconjugated molecules on a molar level, all values are given in µg/ml. Significant inhibition of *K. pneumoniae* and *P. aeruginosa* could not be observed with any conjugate. Conjugates **28 – 31** all prevented growth of *E. coli* at concentrations that were 12–24 fold lower than those of unconjugated ampicillin or amoxicillin (Table 4.1). This result provides a proof of concept that MECAM-based artificial siderophores indeed enhanced the antibiotic activity. However, the spectrum of most conjugates was small: **29-31** inhibited only *E. coli*, and **28** was active against *S. aureus* in addition. The efficacy of **31** bearing a PEG linker was substantially lower than that of the corresponding **27** with an alkyl linker against all strains. In fact, **27** was the most potent compound in the panel, as it inhibited the Gram-negative *E. coli* and *A. baumannii*, but also the Gram-positive *S. aureus* and *E. faecium* pathogens at nanomolar concentrations. While the enhanced activity of conjugates bearing acetyl protected catechol moieties is in agreement with previous findings,^{24, 25} the superiority of ampicillin vs. amoxicillin in siderophore conjugates is surprising. Compound **27** thereby shows an advantage in comparison with cefiderocol, which is active against Gram-negative bacteria exclusively. In addition, we examined the antibacterial activity of **27** against clinically relevant uropathogenic, enteroaggregative, enteroinvasive, enteropathogenic, and enterotoxigenic *E. coli* strains as well as against Methicillin-resistant *S. aureus* (MRSA), and again found that **27** was at least 8 and 16-fold more potent than free ampicillin in *E. coli* and MRSA, respectively (Table S4.2).

4.2.5 MECAM-daptomycin conjugate **32** is active against multidrug-resistant pathogens

In order to expand the range of antibiotics used in our MECAM conjugates, the lipopeptide daptomycin was selected. Its activity, based on bacterial cell membrane perforation and depolarization, makes it a potent antibiotic against Gram-positive pathogens, whereas it is completely inactive against Gram-negative pathogens due to its large size – unless being actively transported. Thus representing an ideal test candidate for siderophore transport, daptomycin was derivatised with ε-azido-hexanoic acid at the side chain of its ornithine residue, and subsequently coupled to conjugate **32** (Figure 4.5, Scheme S4.10 – S4.11). Daptomycin conjugate **32** was less potent against Gram-positive *S. aureus* and *E. faecium* than free daptomycin, and inactive against *E. coli*, *P. aeruginosa*, and *K. pneumoniae*. However, **32** inhibited the growth of *A. baumannii* with an MIC of 4.4 µM, whereas free daptomycin was

completely inactive (Table 4.1). These findings are in line with recent data reported by Miller and coworkers, who demonstrated successful daptomycin transport with *A. baumannii*'s siderophore fimsbactin and artificial congeners.^{22, 38} Albeit the selectivity for certain bacterial species remains to be understood, it is notable that MECAM-based siderophores mediate the translocation of a very large lipopeptide cargo across the outer membrane.

Table 4.1. Minimal inhibitory concentrations (MICs) of **27** – **32** against bacterial pathogens ^a.

Strain	27	28	29	30	31	32	amp	amox	cef	dapto
<i>E. coli</i>	≤0.090	0.89 ± 0.0	1.4 ± 0.0	0.87 ± 0.0	0.81 ± 0.48	>64	19 ± 5.4	18 ± 5.2	0.042 ± 0.026	>64
<i>S. aureus</i>	0.12 ± 0.06	5.3 ± 1.6	>46	>56	>64	8.7 ± 3.1	>183	>175	>85	0.36 ± 0.19
<i>A. baumannii</i>	≤0.09	>57	>46	>56	>64	4.4 ± 1.5	>183	>175	0.053 ± 0.029	>39
<i>E. faecium</i>	0.62 ± 0.51	>57	>46	>56	>64	13 ± 0	2.7 ± 1.2	1.3 ± 0.76	>85	0.62 – 2.5 ^b

^a Ampicillin (amp), amoxicillin (amox), cefiderocol (cef), daptomycin (dapto) were used as standard antibiotics. ^b Ref 39. MICs (average ± s.d., 3-9 biological replicates) were determined by a curve-fitting procedure and expressed in μM.

4.2.6 The uptake of **27** in *E. coli* depends on three receptors

To understand the role of the siderophore uptake pathway for the activity of **27** against *E. coli*, different knockout strains were treated with **27** (Table 4.2). Strains with single deletions of catecholate receptor genes such as *fepA*, *cirA*, or *fiu* as well as the double knockout strains $\Delta fepA\Delta cirA$, $\Delta fepA\Delta fiu$, $\Delta cirA\Delta fiu$ remained susceptible to **27**. However, the triple knockout of *fepA*, *cirA* and *fiu* conferred resistance to **27**. Similarly, only a triple knockout of *fepA*, *cirA* and *fiu* was found to be resistant to cefiderocol,⁴⁰ even though a remarkable 64-fold increase in the MIC of cefiderocol was observed in the $\Delta cirA\Delta fiu$ strain. Moreover, we examined the influence of downstream components of the catechol siderophore pathway on anti-microbial activities of **27** (Table 4.2). The outer membrane receptors are coupled to a complex of TonB, ExbB and ExbD, that provide the energy for active transport.⁶ Both **27** and cefiderocol were inactive against a $\Delta tonB$ strain. Interestingly, a $\Delta exbB$ strain was fully resistant to **27**, but displayed (weakened) sensitivity to cefiderocol (Table 4.2), indicating that ExbB might play a specific role in **27**-mediated antibacterial activity against *E. coli*. On the other hand, depletion of *fepB*, a periplasmic protein responsible for shutting corresponding cargo from catechol receptors to ABC transporters in the inner membrane,⁶ led to a merely two-fold increase of

MIC in **27**. To investigate whether the siderophore import system located at the inner membrane is required, the antibacterial activity of **27** was examined in a $\Delta fepD$ strain. The $\Delta fepD$ strain, defective in catechol import from inner membrane to cytoplasm, was susceptible to **27**, suggesting that transporting **27** into the periplasm space was sufficient for antibacterial activity. This is in line with the finding that **8** mostly accumulates in periplasm (Figure 4.3), and with the fact that the target of ampicillin is located there. In summary, the results suggest that **27** can be taken up by FepA, CirA, and Fiu catechol receptors in *E. coli*; the TonB-coupling of these receptors is essential, whereas the transfer from the periplasm to the cytosol is not.

4.2.7 The truncation of ExbB at Q163 induces resistance to **27** in *E. coli*

To investigate the resistance mechanism towards **27** in *E. coli*, resistant clones in *E. coli* K-12 BW25113 were generated by serial passaging under **27** challenge. Four clones survived 21 passages and exhibited MICs $>12 \mu\text{M}$ (Figure 4.6A). To exclude that the clones became intrinsically drug-resistant, e.g. by overexpressing efflux pumps, they were tested against ampicillin, kanamycin or cefiderocol, and found to retain sensitivity against those reference antibiotics (Table S4.3). The genomic DNA of the four clones was isolated, followed by whole genome sequencing. Mapping the sequences of the parental control and four resistant clones to the reference genome *E. coli* BW25113 (GenBank: CP009273.1) containing 4,631,469 base pairs led to the identification two single nucleotide mutations among the four resistant clones (Table S4.3 and Table S4.4). Firstly, a single nucleotide mutation observed in all clones was a replacement of guanine to adenine at position 806 in the gene encoding cytochrome bo(3) ubiquinol oxidase subunit I (*cyoB*) (Table S4.3). This point mutation results in an exchange of glycine to aspartate at position 269 (G269D) in the expressed protein. *cyoABCD* genes encode and form a terminal cytochrome bo oxidase complex that is the main terminal oxidase in the aerobic respiratory chain in *E. coli* and catalyzes the four-electron reduction of molecular oxygen to water.^{41, 42} Besides, the cytochrome bo terminal oxidase serves as supplier of PMF, and also CyoB itself was reported to contribute to PMF generation.^{42, 43}

Table 4.2. Minimal inhibitory concentrations (MICs) of **27** against *E. coli* wild type and knockout strains.^a

Strain	MIC (μM)		
	27	amp	cef
<i>wt</i> ^b	1.5	46	0.33
ΔfepA	>12	46	0.17
ΔcirA	2.9	46	0.66
Δfiu	1.5	46	0.66
$\Delta\text{fepA}\Delta\text{cirA}$	1.5	46	0.17
$\Delta\text{fepA}\Delta\text{fiu}$	1.5	46	0.66
$\Delta\text{cirA}\Delta\text{fiu}$	2.9	46	21
$\Delta\text{fepA}\Delta\text{cirA}\Delta\text{fiu}$	>12	46	>21
ΔtonBb	>12	46	>21
ΔexbB	>12	46	5.3
ΔfepB	2.9	46	0.083
ΔfepD	1.5	46	0.083

^a Ampicillin (amp) and cefiderocol (cef) were used as standard antibiotics. MICs were the minimal concentrations of indicated antibiotics in μM displaying no growth determined by visual inspection. ^b *wt* = *E. coli* BW25113.

The second nucleotide mutation, found in the third and fourth clone, incorporated thymine instead of cytosine at position 487 in the gene-biopolymer transport protein *exbB*, which is a component of the Ton machinery.^{44, 45} *ExbB* serves as a supplier of PMF that is required for a conformational change of *TonB* and the outer membrane receptor in order to facilitate siderophore uptake.^{46, 47} The point mutation leads to a stop codon mutation from glutamine (Q163*) of the expressed protein. Both *CyoB* G269D and *ExbB* Q163* have not been reported in previous studies. Given that *ExbB* forms a complex with *TonB* to facilitating the siderophore uptake,⁴⁵ we examined whether the resistance towards **27** resulted from an impaired siderophore uptake. All resistant clones are able to grow in iron-limited condition (Figure 4.3B), indicating that the uptake of enterobactin is functional in resistant clones. Moreover, to evaluate whether **27** resistant (**27**^R) clones are able to uptake **8**, the *entA* gene was deleted in full-length in all four clones, which were then submitted to growth recovery assays. The growth of ΔentA , **27**^R clones was recovered upon supplementation with **8** and also with the positive control enterobactin (Figure 4.6C). This demonstrates that the siderophore uptake system was still functional in **27**^R clones.

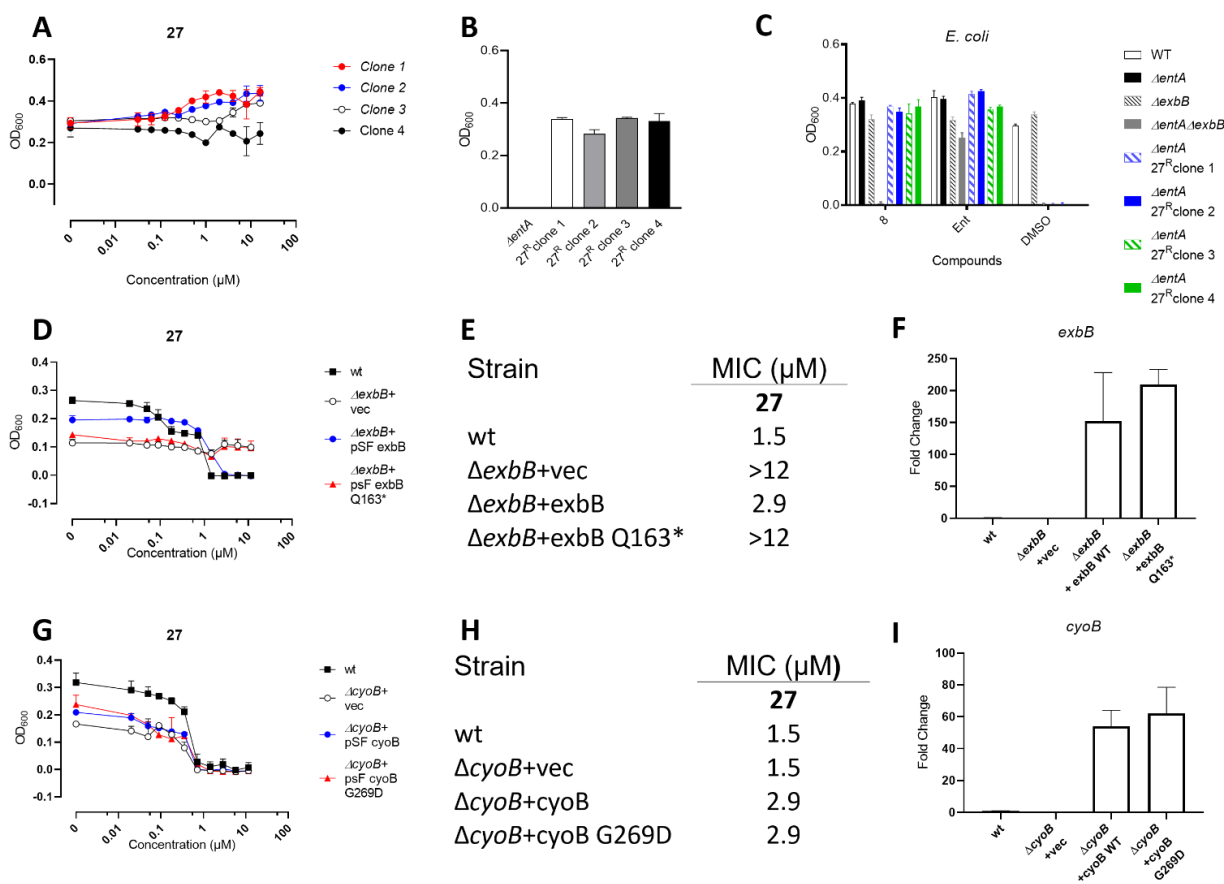


Figure 4.6. Mechanism of resistance against **27** in *E. coli*. (A) The antibacterial activity of **27** against four **27**^R clones was assessed after 24-hour treatment in iron-limited MHB. (B-C) The siderophore uptake system is functional in clones resistant to **27**. (B) Growth of $\Delta entA$ strain and four **27**^R clones in LMR medium under iron-limited conditions. (C) Growth recovery of indicated strains treated with 8, Ent or DMSO in iron-limited LMR medium for 48 h. (D-I) Over-expression of ExbB163*, but not of CyoB G269D, induces resistance to **27** in *E. coli*. The antibacterial activity of **27** (D) and a summary of MICs (E) against $\Delta exxB$ strains with a plasmid for the expression of wild-type ExbB, Q163*-truncated ExbB, or with vector control. MIC assays were conducted as mentioned in (A). (F) RNA expression of *exbB* from the cultures shown in (D). Representative results of n = 2. The antibacterial activity of **27** (G) and a summary of MICs (H) against $\Delta cyoB$ strains with a plasmid for the expression of wild-type CyoB, CyoB mutated at G269D, or with vector control. (I) RNA expression of *cyoB* from the cultures shown in (G). Gene expression was normalized against the reference gene *rpoB* and given as relative to wt control. Results shown are means and standard deviations of one representative experiment done in triplicate. Vec: vector control. Ent = enterobactin. Representative results of n = 3.

In contrast, double knockout strains of *entA* and full-length *exbB* showed no growth recovery in the presence of **8**. The fact that neither CyoB G269D nor ExbB Q163* impaired the uptake of enterobactin or **8** demonstrates that the siderophore uptake system in **27^R** clones is still functional. To validate that the CyoB G269D and ExbB Q163* variants were causal for resistance towards **27**, the respective mutated genes were reintroduced by plasmids into Δ *cyoB* and Δ *exbB* strains, respectively. Over-expression of ExbB Q163* in a Δ *exbB* clone was sufficient to confer resistance against **27** up to 12 μ M, while strains over-expressing either wild type ExbB or vector control were susceptible to **27** (Figure 4.6D and 4.6E). The expression efficiency was confirmed by real-time qPCR (Figure 4.6F). However, reintroducing either wild type CyoB or CyoB G269D on a plasmid into the Δ *cyoB* strain did not confer resistance to **27** (Figure 4.6G and 4.6H). The complementation efficiency was confirmed by real-time qPCR (Figure 4.6I). When cultures from **27^R** clones no. 1 and 2, carrying only one mutation site in *cyoB*, were further passaged, they returned sensitive to **27**, and the MIC was restored to 1.5 μ M (Figure S4.6). This reverse susceptibility to **27** was not observed in **27^R** clones carrying mutations in the *exbB* gene. A further whole-genome sequence analysis (Table S4.5) confirmed that no additional genetic mutation occurred among those “recovery” clones, i.e. the G269D mutation was still present. In summary, a mutation in ExbB was causal for sustained resistance formation against **27**, whereas the CyoB resistance mutation was transient.

4.3 Discussion and conclusion

In this study, we qualified the artificial enterobactin mimic MECAM as a functional and versatile scaffold for siderophore conjugation. The synthesis of a series of MECAM analogs allowed deriving structure activity relationships, and the structural and electronic properties were calculated by quantum chemistry. Its ferric iron complex was structurally and electronically characterized by quantum-chemically computing structural and energetic properties as well as the relaxed siderophore-Fe (III) force constants (compliance constants) at the DFT level of theory. The prediction of an unprecedented and kinetically stable ferric iron low-spin complex raises the interesting question whether the spin ground state of the iron-siderophore complex might be an additional, hitherto overseen factor in siderophore biology. Notably, spin changes at iron have been highlighted as important for reactivity in the context of iron-mediated oxidation processes.⁴⁸ A combination of chemical synthesis, bioanalytical and microbiological assays in the model pathogen *E. coli* led to the selection of the preferred artificial siderophore, and to the conjugation of standard antibiotics. MECAM conjugates led to a potentiation of activity of the β -lactam ampicillin, and they could transport the bulky lipopeptide daptomycin into *Acinetobacter baumannii*. Compound **27** inhibited the growth of Gram-negative as well as Gram-positive strains at nanomolar concentrations. The enhanced activity of **27** against S.

aureus cannot be explained by an outer membrane-spanning transporter due to the absence of this membrane. However, siderophore transport into Gram-positive bacteria involves a membrane-anchored binding protein closely located to an ABC transporter that internalizes siderophores.⁷ Thus, we hypothesize that conjugate binding to this protein might increase the local β -lactam concentration and thereby the antibacterial potency of the siderophore conjugate compared to free ampicillin.

The dependence of siderophore conjugate uptake on the expression of single receptors, that may lead to fast resistance formation, has been an often-mentioned concern.^{11, 49, 50} This study demonstrates that only a triple knockout of three catecholate receptors (FepA, CirA, and Fiu) conferred resistance to **27** in *E. coli* (Table 4.2), suggesting that **27** is able to use multiple siderophore receptors for its uptake. We hypothesize that the use of artificial siderophores, combining iron binders with a simple core scaffold, may exert advantages with respect to a broader receptor specificity. However, the unconjugated **8** was only transported by FepA (Figure 4.4), which highlights that outer membrane receptors differentiate between compound **27** and **8**. The observation that TonB and ExbB deletion strains were resistant to **27** implies that Ton-coupled transport indeed plays a key role in the anti-bacterial activity of **27**. In addition to experiments with defined knockout strains, we investigated induced resistance upon exposure to **27**, and found a mutation in *exbB*, resulting in a truncated Q163* protein. The causal role of this mutation was proven by the observation that a complementation of ExbB Q163*, but not wild type of ExbB, into a $\Delta exbB$ strain conferred resistance to **27**. Previous studies showed that ExbB is an integral cytoplasmic membrane (CM) protein with three transmembrane domains.^{46, 51} It is believed that ExbB has three functions: as a scaffold on stabilizing the structure of Ton machinery, supplier of proton motive force (PMF) for conformational changes of TonB and the associated outer membrane receptor, and signal transduction.^{46, 47} ExbB Q163* is a truncated form of ExbB lacking the third transmembrane domain (TMD3) and the cytoplasmic carboxy-terminus. By site-directed mutagenesis, Baker *et al.* found key residues located in the three TMDs of ExbB and proposed that TMD 1 mainly interacts with the TMD of TonB, TMD 2 interacts with ExbD, whereas TMD 3 is involved in signal transduction. The fact that resistant clones with ExbB Q163* mutation were able to take up either enterobactin or **8** (Figure 4.6) suggests that the truncated form of ExbB Q163* is not essential for siderophore uptake in general, but specifically mediates entry of **27** into *E. coli*. While the mechanism behind this is not understood, the finding again highlights that 'free' and conjugated siderophore mimics behave differently.

The protein CyoB (cytochrome bo(3) ubiquinol oxidase subunit I) functions as the major terminal oxidase in the aerobic respiratory chain of *E. coli* and contributes to PMF generation.^{52, 53} However, the reintroduction of CyoB G269D into a $\Delta cyoB$ strain did not lead to a restoration

of resistance to **27** (Figure 4.3). Besides, cultures from **27^R** clones with only one mutation site in *cyoB* returned sensitive to **27** after a few (MIC = 1.45 μ M) passages (Table S4.5). This transient resistance allows bacteria to temporarily survive upon antibiotic exposure.⁵⁴ A previous study from Lázár et al. revealed that mutations of CyoB contribute to aminoglycoside resistance via the reduction of PMF in presence of other mutations in other genes.⁵⁵ Considering that CyoB G269D mutation existed in all **27^R** clones, CyoB G269D might impede the uptake of **27** by reducing the membrane potential as well as PMF, even though a CyoB G269D alone is not sufficient for sustained resistance to **27**. Thus, the formation of ExbB163*, but not CyoB G269D, played an essential role in resistance formation in *E. coli*. While previous resistance studies focused mainly on outer membrane receptors for siderophores, this work highlights the importance of additional components, albeit also related to uptake to the periplasm. In contrast, downstream transport into cytoplasm was not relevant, in line with the antibiotic mechanism of **27**. In summary, the data qualify the versatile MECAM scaffold as a transporter of antibiotic cargo, and they highlight the potential of artificial siderophores as “Trojan Horses” to fight multidrug-resistant bacteria.

4.4 Experimental section

4.4.1 General chemistry methods

Commercially obtained chemicals were used without any further purification. All organic solvents possessed HPLC-grade purity. Dried solvents were used unless water was part of the solvent mixture or the total amount of solvent in the reaction was bigger than 30 mL. Dichloromethane was dried over molecular sieve (4 Å). All other dried solvents were purchased in a water-free form. Reactions requiring dried solvents were conducted in twofold baked out glassware under a nitrogen atmosphere. Removal of organic solvents was conducted on rotational evaporators at 30 °C. For the removal of water, a temperature of 40 °C was applied. Lyophilisation of compounds was conducted on an Alpha 2–4 LSCbasic (Christ) lyophilizer after freezing compound solutions in liquid nitrogen. Centrifugations were performed on a Universal 32 R (Hettich) centrifuge. Absolute reaction yields are given only after the neat compound was analyzed by NMR spectroscopy. Yields of unpurified compounds were only calculated in order to allow stoichiometric calculations for the next synthetic step. In these cases, absolute overall yields are given with the final step of the respective synthesis. All compounds had purities $\geq 95\%$ as determined by high-performance liquid chromatography (UV detection) and $^1\text{H}/^{13}\text{C}$ -NMR analysis.

4.4.2 Synthetic Procedures

Compound 5

To a solution of 2,3-dihydroxybenzoic acid (**4**, 4.00 g, 26.0 mmol, 1 eq) and 4-(dimethylamino)-pyridine (318 mg, 2.60 mmol, 0.1 eq.), acetic anhydride (7.37 mL, 7.96 g, 77.9 mmol, 3 eq.) and triethylamine (21.6 mL, 15.8 g, 156 mmol, 6 eq.) were added. The reaction mixture was refluxed for 3 h, cooled to rt and the solvent was removed. The residue was washed with cold hydrochloric acid (0.5 M) and cold saturated sodium chloride solution (2 × 75 mL each) and dried over sodium sulfate. After removing the solvent and drying *in vacuo*, **5** was obtained as a brownish solid (5.27 g, 22.1 mmol, 85%) and used for the preparation of **6** without further purification.

Compound 6

Oxalyl chloride (566 µL, 838 mg, 6.6 mmol, 2 eq.) was added dropwise to a solution of **5** (786 mg, 3.30 mmol, 1 eq.) in dichloromethane (20 mL) and dimethylformamide (200 µL) over a time of 5 min at 0 °C. The reaction was stirred for 10 min at 0 °C, warmed to rt and stirred for 2.5 h. After removing the solvent, crude product **6** was dried *in vacuo* overnight and used in subsequent reactions without further purification.

Compound 8a

Tris(bromomethyl)benzene (**7**, 1.67g, 4.68 mmol) was added in small portions to a mixture of nitric acid (65%) and concentrated sulfuric acid (10 mL each) at 0 °C. The reaction mixture was warmed to rt, stirred 1 d, poured on ice, and extracted with ethyl acetate (2 × 25 mL). The combined organic layers were washed with saturated solutions of sodium hydrogen carbonate and sodium chloride (2 × 30 mL each) and dried over sodium sulfate. After removing the solvent and drying *in vacuo*, **7a** was obtained as a light yellow solid (1.72 g, 4.28 mmol, 91%) and used in subsequent reactions without further purification.

Compound 8

An aqueous solution of ammonia (30%, 10 mL) was added dropwise to a solution of **8a** (402 mg, 1.00 mmol, 1 eq.) in tetrahydrofuran and ethanol (5 mL each). The reaction mixture was stirred overnight. After removing the solvent and drying *in vacuo*, the residue was solved in aqueous sodium hydrogen carbonate solution (0.5 M, 20 mL). Compound **6** (3.3 mmol, 3.3 eq.) in 1,4-Dioxane (20 mL) was added to this solution at 0 °C over a time of 15 min. The

reaction mixture was warmed to rt, mixed with ice, and extracted with ethyl acetate (3 × 30 mL). The combined organic layers were washed with saturated solutions of sodium hydrogen carbonate and sodium chloride (2 × 75 mL each) and dried over sodium sulfate. After removing the solvent, **8** was obtained by purification via automatic flash chromatography (CH₂Cl₂/MeOH) as a light yellow solid (510 mg, 586 μmol, 59% over 3 steps).

TLC R_f = 0.21 (CH₂Cl₂/MeOH = 20:1)

¹H-NMR (700 MHz, DMSO-d₆): δ [ppm] = 2.17 (s, 3 H), 2.19 (s, 6 H), 2.28 (s, 3 H), 2.29 (s, 6 H), 4.42 (d, J = 5.7 Hz, 4 H), 4.46 (d, J = 5.7 Hz, 2 H), 7.25 (t, J = 7.9 Hz, 1 H), 7.32 (t, J = 7.9 Hz, 2 H), 7.37 (dd, J = 8.1, 1.4 Hz, 1 H), 7.39 (dd, J = 8.1, 1.5 Hz, 2 H), 7.41 (s, 2 H), 7.46 (dd, J = 7.8, 1.5 Hz, 1 H), 7.48 (dd, J = 7.7, 1.5 Hz, 2 H), 9.02 (t, J = 5.8 Hz, 2 H), 9.06 (t, J = 6.0 Hz, 1 H).

¹³C-NMR (176 MHz, DMSO-d₆): δ [ppm] = 20.2, 20.3, 38.8, 42.0, 125.6, 125.8, 126.0, 126.1, 126.2, 126.3, 130.1, 130.3, 131.4, 140.2, 140.2, 142.7, 142.8, 147.0, 164.8, 164.8, 167.9, 167.9, 168.3.

C₄₂H₃₈N₄O₁₇ (870.78), exact mass: 870.2232.

ESI-HRMS (m/z): [M + Na]⁺ calc. for C₄₂H₃₈N₄NaO₁₇: 893.2130; found: 893.2119.

Compound **9**

An aqueous solution of ammonia (30%, 2.4 mL) was added dropwise to a solution of 1,3,5-tris(bromomethyl)benzene (**7**, 89.0 mg, 250 μmol, 1 eq.) in tetrahydrofuran and ethanol (1.2 mL each). The reaction mixture was stirred for 2.5 h and the resulting precipitate was filtered off. After removing the solvent and drying *in vacuo* the residue was solved in aqueous sodium hydrogen carbonate solution (0.5 M, 5 mL). Compound **6** (875 μmol, 3.5 eq.) in 1,4-Dioxane (4 mL) was added to this solution at 0 °C. The reaction mixture was stirred at 0 °C for 5 min, mixed with ice, and extracted with ethyl acetate (3 × 10 mL). The combined organic layers were washed with saturated sodium chloride solution (2 × 20 mL) and dried over sodium sulfate. After removing the solvent, **9** was obtained by purification via HPLC as a white solid (23.4 mg, 28.3 μmol, 11% over 2 steps).

¹H-NMR (500 MHz, DMSO-d₆): δ [ppm] = 2.17 (s, 9 H), 2.28 (s, 9 H), 4.39 (d, J = 5.9 Hz, 6 H), 7.15 (s, 3 H), 7.32 (t, J = 7.9 Hz, 3 H), 7.37 (dd, J = 8.1, 1.7 Hz, 3 H), 7.49 (dd, J = 7.6, 1.7 Hz, 3 H), 8.94 (t, J = 6.0 Hz, 3 H).

¹³C-NMR (125 MHz, DMSO-d₆): δ [ppm] = 20.2, 20.3, 42.4, 124.5, 125.4, 126.0, 126.3, 130.8, 139.5, 140.1, 142.8, 164.5, 167.9, 168.3.

C₄₂H₃₉N₃O₁₅ (825.78), exact mass: 618.1598.

ESI-HRMS (*m/z*): [M + H]⁺ calc. for C₄₂H₄₀N₃O₁₅: 826.2459; found: 826.2453.

Compound 10

Compound **8** (26.1 mg, 30.0 μmol) was stirred in aqueous potassium hydroxide solution (1 M, 15 mL) for 1 h. The reaction mixture was acidified with hydrochloric acid (1 M) and extracted with ethyl acetate (25 mL). The combined organic layer was decanted and dried over sodium sulfate. After removing the solvent, **10** was obtained by purification via HPLC as a white solid (9.0 mg, 14.5 μmol, 48%).

¹H-NMR (500 MHz, DMSO-*d*₆): δ [ppm] 4.50 (d, *J* = 5.5 Hz, 6 H), 6.63 (t, *J* = 7.9 Hz, 1 H), 6.68 (t, *J* = 8.0 Hz, 2 H), 6.89 – 6.95 (m, 3 H), 7.21 (dd, *J* = 8.2, 1.3 Hz, 1 H), 7.25 (dd, *J* = 8.2, 1.3 Hz, 2 H), 7.44 (s, 2 H), 9.14 (s_{br}, 1 H), 9.21 (s_{br}, 2 H), 9.33 (t, *J* = 5.7 Hz, 2 H), 9.39 (t, *J* = 6.0 Hz, 1 H) 12.15 (s_{br}, 2 H), 12.37 (s_{br}, 1 H).

¹³C-NMR (125 MHz, DMSO-*d*₆): δ [ppm] = 38.6, 41.9, 114.9, 115.0, 117.2, 117.5, 118.0, 118.2, 118.9, 119.0, 126.5, 131.5, 142.6, 146.1, 147.2, 149.2, 149.5, 169.8, 169.9.

C₃₀H₂₆N₄O₁₁ (618.56), exact mass: 618.1598.

ESI-HRMS (*m/z*): [M + H]⁺ calc. for C₃₀H₂₇N₄O₁₁: 641.1496; found: 641.1509.

Compound 11

Compound **9** (4.12 mg, 5.00 μmol) was stirred in aqueous potassium hydroxide solution (1 M, 2 mL) for 90 min. The reaction mixture was acidified with hydrochloric acid (2 M) and extracted with ethyl acetate (3 × 5 mL). The combined organic layers were dried over sodium sulfate. After removing the solvent, **11** was obtained by purification via HPLC as a white solid (1.20 mg, 2.08 μmol, 42%).

¹H-NMR (500 MHz, DMSO-*d*₆): δ [ppm] = 4.46 (d, *J* = 8.2 Hz, 6 H), 6.67 (t, *J* = 8.0 Hz, 3 H), 6.91 (dd, *J* = 7.8, 1.3 Hz, 3 H), 7.19 (s, 3 H), 7.29 (dd, *J* = 8.2, 1.3 Hz, 3 H), 9.14 (s_{br}, 3 H), 9.34 (t, *J* = 6.0 Hz, 3 H), 12.63 (s, 3 H).

¹³C-NMR (125 MHz, DMSO-*d*₆): δ [ppm] = 42.3, 114.9, 117.2, 118.0, 118.9, 124.9, 139.4, 146.2, 149.7, 169.7.

C₃₀H₂₇N₃O₉ (573.56), exact mass: 573.1747.

ESI-HRMS (*m/z*): [M + H]⁺ calc. for C₃₀H₂₈N₃O₉: 574.1826; found: 574.1819.

Compound 12a

Sodium cyanide (2.18 g, 43.2 mmol, 12 eq.), a saturated solution of sodium hydrogen carbonate (10 mL) and water (10 mL) were added to a solution of tris(bromomethyl)benzene (1.28 g, 3.60 mmol, 1 eq.) in tetrahydrofuran (10 mL). The solution was stirred 3 h and hydrochloric acid (1 M, ca. 38 mL) was carefully added via a droplet funnel until a pH of 6 was reached. The solution was stirred 2 h and the resulting precipitate was removed via centrifugation, taken up in acetonitrile. The solution was dried over sodium sulfate. After removing the solvent and drying *in vacuo*, **12a** was obtained as a light yellow solid (630 mg, 3.23 mmol, 90%) and used for the synthesis of **12b** without further purification.

Compound 12b

To a solution of potassium hydroxide (25%) in water (8 mL) and ethanol (4 mL), **12a** (605 mg, 3.10 mmol) was added. This solution was heated to 100 °C in a sealed glass vial and stirred overnight. The solution was poured on ice water (ca. 100 mL) and acidified to pH \approx 1 with hydrochloric acid (6 M). After the addition of saturated sodium chloride solution, the mixture was extracted with ethyl acetate (5 \times 50 mL) and the combined organic layers were dried over sodium sulfate. After removing the solvent and drying *in vacuo*, **12b** was obtained as a light yellow solid (700 mg, 2.78 mmol, 90%) and used for the synthesis of **12c** without further purification.

Compound 12c

A solution of **12b** (698 mg, 2.77 mmol, 1 eq.), trimethylorthoformate (909 μ mol, 882 mg, 8.31 mmol, 3.3 eq.), and a few drops of concentrated sulfuric acid in methanol (16 mL) was heated to 72 °C in a sealed glass vial and stirred for 18 h. After removing the solvent, the residue was taken up in ethyl acetate (25 mL). The organic layer was washed with saturated solutions of sodium hydrogen carbonate and sodium chloride (2 \times 25 mL each) and dried over sodium sulfate. After removing the solvent and drying *in vacuo*, **12c** was obtained as a light yellow oil (708 mg, 2.41 mmol, 87%) and used for the synthesis of **12d** without further purification.

Compound 12d

Lithium aluminium hydride (369 mg, 9.72 mmol, 4.5 eq.) was added to a solution of **12c** (635 mg, 2.16 mmol, 1 eq.) in tetrahydrofuran (10 mL). The reaction mixture was stirred for 4 h, carefully quenched with a saturated solution of potassium sodium tartrate and filtered over a celite frit. The filter cake was repeatedly washed with diethyl ether and methanol and the combined organic layers were dried over sodium sulfate. After removing the solvent **12d** was obtained by purification via flash chromatography (CH₂Cl₂/MeOH 20:1 → 15:1 → 10:1) as a white solid (190 mg, 904 μmol, 30% over four steps)

TLC R_f = 0.15 (CH₂Cl₂/MeOH = 20:1)

¹H-NMR (500 MHz, Methanol-d₄): δ [ppm] = 2.77 (t, J = 7.0 Hz, 6 H), 3.74 (t, J = 7.0 Hz, 6 H), 6.94 (s, 3 H).

¹³C-NMR (125 MHz, Methanol-d₄): δ [ppm] = 40.4, 64.4, 128.8, 140.5.

C₁₂H₁₈O₃ (210.27), exact mass: 210.1256.

ESI-HRMS (m/z): [M + Na]⁺ calc. for C₁₂H₁₈NaO₃: 233.1154; found: 233.1148.

Compound 12e

A solution of **12d** (174 mg, 828 μmol) in hydrobromic acid (45%, 10 mL) was heated to 125 °C in a sealed glass vial, stirred 5 h and stirred over night while slowly cooling to rt. The solution was poured on ice and extracted with ethyl acetate (3 × 40 mL). The combined organic layers were washed with saturated solutions of sodium hydrogen carbonate and sodium chloride (2 × 50 mL each) and dried over sodium sulfate. After removing the solvent **12e** was obtained by purification via flash chromatography (PE/EA 100:1 → 50:1) as a white solid (237 mg, 594 μmol, 72%)

TLC R_f = 0.46 (PE/EA = 20:1)

¹H-NMR (500 MHz, CDCl₃): δ [ppm] = 3.15 (t, J = 7.6 Hz, 6 H), 3.57 (t, J = 7.6 Hz, 6 H), 6.97 (s, 3 H).

¹³C-NMR (125 MHz, CDCl₃): δ [ppm] = 32.7, 39.1, 127.6, 139.6.

Compound **12f**

Compound **12e** (39.9 mg, 100 μmol) was added to a vigorously stirred mixture of nitric acid (65%, 500 μL) and concentrated sulfuric acid (1 mL) in small portions at 0 °C. The reaction mixture was stirred for 2 h at 0 °C and quenched with ice water. The mixture was extracted with ethyl acetate (2 \times 10 mL). The combined organic layers were washed with saturated solutions of sodium hydrogen carbonate and sodium chloride (2 \times 20 mL each) and dried over sodium sulfate. After removing the solvent **12f** was obtained by purification via flash chromatography (PE/EA 20:1 \rightarrow 15:1) as a white solid (12.2 mg, 27.5 μmol , 28%)

TLC R_f = 0.21 (PE/EA = 20:1)

$^1\text{H-NMR}$ (500 MHz, CDCl_3): δ [ppm] = 3.14 (t, J = 7.3 Hz, 4 H), 3.23 (t, J = 7.1 Hz, 2 H), 3.58 (t, J = 7.3 Hz, 4 H), 3.60 (t, J = 7.3 Hz, 2 H), 7.29 (s, 2 H).

$^{13}\text{C-NMR}$ (125 MHz, CDCl_3): δ [ppm] = 31.0, 31.8, 34.9, 38.4, 130.5, 131.1, 141.6, 150.0.

Compound **12**

An aqueous solution of ammonia (30%, 300 μL) was added dropwise to a solution of **12f** (12.0 mg, 27.0 μmol , 1 eq.) in tetrahydrofuran and ethanol (150 μL each). The reaction mixture heated to 90 °C in a sealed glass vial and stirred overnight. After removing the solvent and drying *in vacuo* the residue was solved in aqueous sodium hydrogen carbonate solution (0.5 M, 750 μL). Compound **6** (108 μmol , 4 eq.) in 1,4-dioxane (500 μL) was added to this solution dropwise at 0 °C. The reaction mixture was warmed to rt, stirred for 15 min, mixed with ice, and extracted with ethyl acetate (3 \times 5 mL). The combined organic layers were dried over sodium sulfate. After removing the solvent, **12** was obtained by purification via HPLC as a white solid (5.50 mg, 6.03 μmol , 22% over 2 steps).

$^1\text{H-NMR}$ (700 MHz, DMSO-d_6): δ [ppm] = 2.19 (s, 3 H), 2.19 (s, 6 H), 2.27 (s, 3 H), 2.28 (s, 6 H), 2.74 (t, J = 7.4 Hz, 4 H), 2.85 (t, J = 7.1 Hz, 2 H), 3.42 (dd, J = 13.8, 6.7 Hz, 4 H), 4.46 (dd, J = 13.3, 6.9 Hz, 2 H), 7.27 (s, 2 H), 7.34 – 7.40 (m, 7 H), 7.40 – 7.44 (m, 2 H), 8.45 (t, J = 5.6 Hz, 1 H), 8.52 (t, J = 5.6 Hz, 2 H).

$^{13}\text{C-NMR}$ (176 MHz, DMSO-d_6): δ [ppm] = 20.1, 20.2, 20.3, 30.3, 34.4, 39.6, 40.1, 125.3, 125.4, 125.9, 125.9, 126.2, 129.3, 130.3, 130.8, 131.0, 140.0, 140.0, 142.2, 142.8, 149.8, 164.6, 164.6, 167.7, 168.3.

$\text{C}_{45}\text{H}_{44}\text{N}_4\text{O}_{17}$ (912.86), exact mass: 912.2701.

ESI-HRMS (m/z): $[\text{M} + \text{H}]^+$ calc. for $\text{C}_{45}\text{H}_{45}\text{N}_4\text{O}_{17}$: 913.2780; found: 913.2774.

Compound **13a**

Triethyl phosphonoacetate (2.28 g, 10.2 mmol, 3.3 eq.) was added to a mixture of sodium hydride (60% in mineral oil, 432 mg, 10.8 mmol, 3.5 eq.) in tetrahydrofuran (24 mL) min at 0 °C over a time of 15 with a syringe pump. The reaction mixture was warmed to rt and stirred for 30 min. 1,3,5-triformyl benzene (500 mg, 3.08 mmol, 1 eq.) in tetrahydrofuran (6 mL) was added at 0 °C and the reaction mixture was sonicated for 10 min, stirred over night at rt and quenched with 2-propanol and ice. After removing the solvent the residue was taken up in dichloromethane (25 mL) and hydrochloric acid (1 M, 25 mL). After separating the phases, the aqueous layer was extracted with dichloromethane (25 mL) and the combined organic layers were washed with water and a saturated solution of sodium chloride (2 × 40 mL each) and dried over sodium sulfate. After removing the solvent and drying *in vacuo*, **13a** (1.05 g, 2.82 mmol, 92%) was obtained and used for the synthesis of **13b** without further purification.

Compound **13b**

A solution of **13a** (1.05 g, 2.82 mmol) in methanol (30 mL) was flushed with nitrogen for 10 min. Palladium on charcoal (10%, 105 mg) was added and the reaction mixture was flushed with hydrogen for 10 min, stirred under a hydrogen atmosphere for 16 h and filtered over a celite frit. The filter cake was washed with methanol and the filtrate was dried over sodium sulfate. After removing the solvent and drying *in vacuo*, **13b** (1.02 g, 2.70 mmol, 96%) was obtained and used for the synthesis of **13c** without further purification.

Compound **13c**

Compound **13b** (1.02 g, 2.70 mmol, 1 eq.) in tetrahydrofuran (10 mL) was added to a mixture of lithium aluminium hydride (307 mg, 8.10 mmol, 3 eq.) in tetrahydrofuran (10 mL) at 0 °C over a time of 30 min with a syringe pump. The reaction mixture was warmed to rt, quenched with hydrochloric acid (1 M, 20 mL) at 0 °C and filtered over a celite frit. The solution was extracted with dichloromethane (4 × 20 mL) and the combined organic layers were dried over sodium sulfate. After removing the solvent and drying *in vacuo*, **13c** (438 mg, 1.74 mmol, 64%) was obtained and used for the synthesis of **13d** without further purification.

Compound **13d**

Triphenylphosphine dibromide (4.40 g, 10.4 mmol, 6 eq.) was added to a vigorously stirred solution of **13c** (438 mg, 1.74 mmol, 1 eq.) in dichloromethane (10 mL). The solution was stirred overnight and the solvent was removed. The residue was taken up in petrol ether (75 mL) vigorously stirred for 30 min. The precipitate was removed via centrifugation. After removing the solvent and drying *in vacuo*, **13d** (319 mg, 723 μ mol, 23% over 4 steps) was obtained by purification via flash chromatography (PE/EA 50:1) as a colourless oil.

TLC R_f = 0.32 (PE/EA = 50:1)

$^1\text{H-NMR}$ (500 MHz, CDCl_3): δ [ppm] = 2.14 – 2.21 (m, 6 H), 2.72 – 2.78 (m, 6 H), 3.42 (t, 6.6 Hz, 6 H), 6.91 (s, 3 H).

$^{13}\text{C-NMR}$ (125 MHz, CDCl_3): δ [ppm] = 33.1, 33.8, 34.1, 126.6, 140.9.

Compound **13e**

Compound **13d** (44.1 mg, 100 μ mol) was added to a vigorously stirred mixture of nitric acid (50%, 500 μ L) and concentrated sulfuric acid (500 μ L) in small portions at 0 °C. The reaction mixture was stirred for 11 h at 0 °C and 4.5 h at rt and poured on ice water. The mixture was extracted with ethyl acetate (2 \times 10 mL). The combined organic layers were washed with saturated solutions of sodium hydrogen carbonate and sodium chloride (2 \times 15 mL each) and dried over sodium sulfate. After removing the solvent and drying *in vacuo*, **13e** (29.0 mg, 59.7 μ mol, 60%) was obtained and used for the synthesis of **13** without further purification.

Compound **13**

An aqueous solution of ammonia (30%, 1 mL) was added dropwise to a solution of **13e** (29.0 mg, 59.7 μ mol, 1 eq.) in tetrahydrofuran (500 μ L) and ethanol (100 μ L). The reaction mixture heated to 90 °C in a sealed glass vial and stirred overnight. After removing the solvent and drying *in vacuo* the residue was solved in aqueous sodium hydrogen carbonate solution (0.5 M, 2 mL). Compound **6** (209 μ mol, 3.5 eq.) in 1,4-dioxane (2 mL) was added to this solution dropwise at 0 °C. The reaction mixture was stirred for 5 min at 0 °C and 10 min at rt, mixed with ice, and extracted with ethyl acetate (3 \times 8 mL). The combined organic layers were washed with saturated solutions of sodium hydrogen carbonate and sodium chloride (2 \times 15 mL each) and dried over sodium sulfate. After removing the solvent, **13** was obtained by purification via HPLC as a white solid (14.0 mg, 14.7 μ mol, 15% over 3 steps).

¹H-NMR (700 MHz, DMSO-*d*₆): δ [ppm] = 1.72 – 1.78 (m, 4 H), 1.78 – 1.83 (m, 2 H), 2.21 (s, 9 H), 2.29 (s, 9 H), 2.52 – 2.56 (m, 4 H), 2.64 – 2.68 (m, 2 H), 3.19 – 3.24 (m, 6 H), 7.24 (s, 2 H), 7.34 – 7.39 (m, 6 H), 7.41 – 7.45 (m, 3 H), 8.41 – 8.47 (m, 3 H).

¹³C-NMR (176 MHz, DMSO-*d*₆): δ [ppm] = 20.2, 20.2, 20.3, 28.1, 30.2, 30.4, 32.1, 38.5, 38.6, 125.3, 125.9, 125.9, 126.2, 128.2, 131.2, 131.2, 132.7, 139.9, 140.0, 142.8, 144.7, 149.1, 164.6, 167.7, 167.8, 168.3.

C₄₈H₅₀N₄O₁₇ (954.94), exact mass: 954.3171.

ESI-HRMS (*m/z*): [M + Na]⁺ calc. for C₄₈H₅₀N₄NaO₁₇: 977.3069; found: 977.3063.

2-Nitrobenzene-1,3,5-tricarboxylic acid

Potassium permanganate (23.7 g, 150 mmol, 10 eq.) was added to a solution of 2-nitromesitylene (2.48 g, 15 mmol, 1 eq.), sodium hydrogen carbonate (5.04 g, 60 mmol, eq.), and aliquat 336 (0.5 mL) in water (80 mL) over a time of 15 min in small portions. The reaction mixture was refluxed for 3 d and filtered over a celite pad. The filtrate was acidified with concentrated hydrochloric acid (20 mL) and extracted with diethyl ether (5 × 100 mL). The combined organic layers were dried over sodium sulfate. After removing the solvent and drying *in vacuo*, 2-nitrobenzene-1,3,5-tricarboxylic acid was obtained as a white solid (834 mg, 3.27 mmol, 22%).

¹H-NMR (500 MHz, DMSO-*d*₆): δ [ppm] = 8.61 (s, 2 H), 14.01 (s_{br}, 1 H).

¹³C-NMR (125 MHz, DMSO-*d*₆): δ [ppm] = 125.2, 132.9, 135.2, 150.6, 163.3, 164.5.

Compound 14a

EDCI (61.3 mg, 320 μmol, 3.2 eq.) and HOBt (43.2 mg, 32.0 mmol, 3.2 eq.) were added to a solution of 2-nitrobenzene-1,3,5-tricarboxylic acid (25.5 mg, 100 μmol, 1 eq.) and diisopropylamine (87.0 μL, 64.6 mg, 500 μmol, 5 eq.) in dimethylformamide (2 mL). The solution was stirred for 1 h at 0 °C and *tert*-butyl *N*-(2-aminoethyl)carbamate (52.9 mg, 330 μmol, 3.3 eq.) was added dropwise. The solution was stirred over night at rt, quenched with water and extracted with ethyl acetate (3 × 5 mL). The combined organic layers were washed with hydrochloric acid (1 M, 10 mL), saturated sodium hydrogen carbonate solution (10 mL), and saturated sodium chloride solution (3 × 10 mL). After removing the solvent and drying *in vacuo*, **14a** was obtained and used for the synthesis of **14** without further purification.

Compound **14**

Trifluoroacetic acid (1 mL) was added to a solution of **14a** (100 μ mol, 1 eq.) in dichloromethane (3 mL) at 0 °C over a time of 15 min with a syringe pump. The solution was stirred for 30 min at 0 °C and 30 min at rt. After the addition of toluene (4 mL), the solvent was removed and the residue was dried *in vacuo*. The residue was solved in aqueous sodium hydrogen carbonate solution (0.5 M, 4 mL). Compound **6** (400 μ mol, 4 eq.) in 1,4-dioxane (4 mL) was added to this solution at 0 °C over a time of 15 min. The reaction mixture was stirred at 0 °C for 5 min, warmed to rt, mixed with ice, and extracted with ethyl acetate (3 \times 5 mL). The combined organic layers were washed with saturated solutions of sodium hydrogen carbonate and sodium chloride (2 \times 10 mL each) and dried over sodium sulfate. After removing the solvent, **14** was obtained by purification via HPLC as a white solid (9.90 mg, 9.50 μ mol, 10% over three steps).

¹H-NMR (700 MHz, DMSO-*d*₆): δ [ppm] = 2.20 (s, 3 H), 2.23, (s, 6 H), 2.28 (s, 3 H), 2.28 (s, 6 H), 3.36 (s_{br}, 8 H), 3.39 (dd, *J* = 12.8, 6.4 Hz, 2 H), 3.45 (dd, *J* = 12.6, 6.2 Hz, 2 H), 7.35 – 7.39 (m, 6 H), 7.49 – 7.53 (m, 3 H), 8.22 (s, 2 H), 8.48 (t, *J* = 5.4 Hz, 2 H), 8.50 (t, *J* = 5.7 Hz, 1 H), 8.86 (t, *J* = 5.6 Hz, 1 H), 9.00 (t, *J* = 5.2 Hz, 2 H),

¹³C-NMR (176 MHz, DMSO-*d*₆): δ [ppm] = 20.2, 20.2, 20.3, 38.5, 38.6, 38.8, 39.1, 125.5, 125.5, 126.1, 126.1, 126.2, 126.2, 128.9, 130.7, 130.8, 131.1, 136.5, 140.1, 140.1, 142.8, 142.9, 147.9, 164.0, 164.0, 164.8, 167.8, 168.3, 168.3.

C₄₈H₄₇N₇O₂₀ (1041.93), exact mass: 1041.2876.

ESI-HRMS (*m/z*): [M + H]⁺ calc. for C₄₈H₄₈N₇O₂₀: 1042.2954; found: 1042.2958.

Compound **15a**

EDCI (61.3 mg, 320 μ mol, 3.2 eq.) and HOBt (43.2 mg, 32.0 mmol, 3.2 eq.) were added to a solution of 2-nitrobenzene-1,3,5-tricarboxylic acid (25.5 mg, 100 μ mol, 1 eq.) and diisopropylamine (87.0 μ L, 64.6 mg, 500 μ mol, 5 eq.) in dimethylformamide (2 mL). The solution was stirred for 1 h at 0 °C and *tert*-butyl *N*-(3-aminopropyl)carbamate (57.5 mg, 330 μ mol, 3.3 Äq.) in dimethylformamide (500 μ L) was added dropwise. The solution was stirred over night at rt, quenched with water and extracted with ethyl acetate (3 \times 5 mL). The combined organic layers were washed with hydrochloric acid (1 M, 10 mL), saturated sodium hydrogen carbonate solution (10 mL), and saturated sodium chloride solution (3 \times 10 mL).

After removing the solvent and drying *in vacuo*, **15a** was obtained and used for the synthesis of **15** without further purification.

Compound **15**

Trifluoroacetic acid (1 mL) was added to a solution of **15a** (100 μ mol, 1 eq.) in dichloromethane (3 mL) at 0 °C over a time of 10 min with a syringe pump. The solution was stirred for 30 min at 0 °C and 30 min at rt. After the addition of toluene (4 mL), the solvent was removed and the residue was dried *in vacuo*. The residue was solved in aqueous sodium hydrogen carbonate solution (0.5 M, 4 mL). **6** (400 μ mol, 4 eq.) in 1,4-dioxane (4 mL) was added to this solution at 0 °C over a time of 15 min. The reaction mixture was stirred at 0 °C for 5 min, warmed to rt, mixed with ice, and extracted with ethyl acetate (3 \times 5 mL). The combined organic layers were washed with saturated solutions of sodium hydrogen carbonate and sodium chloride (2 \times 10 mL each) and dried over sodium sulfate. After removing the solvent, **15** was obtained by purification via HPLC as a white solid (12.5 mg, 11.5 μ mol, 12% over three steps).

¹H-NMR (700 MHz, DMSO- d_6): δ [ppm] = 1.70 – 1.79 (m, 6 H), 2.23 (s, 3 H), 2.23 (s, 6 H), 2.28 (s, 3 H), 2.28 (s, 6 H), 3.2 – 3.29 (m, 10 H), 3.36 (dd, J = 13.0, 6.7 Hz, 2 H), 7.34 – 7.39 (m, 6 H), 7.43 – 7.47 (m, 3 H), 8.16 (s, 2 H), 8.37 – 8.41 (m, 3 H), 8.87 (t, J = 5.6 Hz, 1 H), 8.96 (t, J = 5.7 Hz, 2 H).

¹³C-NMR (176 MHz, DMSO- d_6): δ [ppm] = 20.2, 20.2, 20.3, 28.8, 28.9, 36.8, 37.0, 37.2, 37.5, 125.3, 125.3, 125.9, 126.2, 126.3, 128.6, 131.1, 131.2, 131.4, 136.3, 139.9, 140.0, 132.8, 142.8, 147.9, 163.6, 163.9, 164.6, 167.8, 168.3.

C₅₁H₅₃N₇O₂₀ (1084.01), exact mass: 1083.3345.

ESI-HRMS (m/z): [M + H]⁺ calc. for C₅₁H₅₄N₇O₂₀: 1084.3424; found: 1084.3418.

Compound **16a**

1,2,3-Trimethylbenzene (90%, 741 μ L, 601 mg, 5.00 mmol, 1 eq.) was added to a solution of *N*-bromosuccinimide (3.54 g, 20.0 mmol, 4 eq.) in tetrachloromethane (15 mL). The reaction mixture was irradiated with a halogen lamp in a sealed glass vial, heated to 80 °C and stirred over night. The mixture was filtered and the filtrate was dried over sodium sulfate. After removing the solvent, **16a** was obtained by purification via automatic flash chromatography (PE/EA) but still obtained slight impurities. These were removed by washing the product with petrol ether and sonicating the mixture. After decanting and drying *in vacuo*, **16a** was obtained as a white solid (1.56 g, 4.38 mmol, 88%).

TLC $R_f = 0.24$ (PE)

$^1\text{H-NMR}$ (500 MHz, CD_2Cl_2): δ [ppm] = 4.65 (s, 4 H), 4.84 (s, 2 H), 7.46 (dd, $J = 8.6, 6.6$ Hz, 1 H), 7.37 – 7.40 (m, 2 H).

$^{13}\text{C-NMR}$ (125 MHz, CD_2Cl_2): δ [ppm] = 25.3, 30.5, 130.2, 132.3, 136.2, 138.7.

Compound **16b**

16a (2.18 g, 6.09 μmol) in dichloromethane (6 mL) was added to nitric acid (100%, 3.5 mL) in dichloromethane (2 mL) at $-40\text{ }^\circ\text{C}$ over a time of 2 h with a syringe pump. The temperature was kept strictly under $-40\text{ }^\circ\text{C}$ throughout the addition of the acid. The solution was stirred for 15 min at $-40\text{ }^\circ\text{C}$ and poured on ice. After the separation of the phases the aqueous layer was extracted with dichloromethane (4×10 mL) and the combined organic layers were dried over sodium sulfate. After removing the solvent, **16b** (875 mg, 2.18 mmol, 36%) was obtained together with its nitration regioisomer by purification via automatic flash chromatography (PE/EA).

TLC $R_f = 0.07$ (PE)

$^1\text{H-NMR}$ (500 MHz, CDCl_3): δ [ppm] = 4.61 (s, 2 H), 4.81 (s, 2 H), 4.83 (s, 2 H), 7.53 (d, $J = 8.4$ Hz, 1 H), 7.85 (d, $J = 8.4$ Hz, 1 H).

$^{13}\text{C-NMR}$ (125 MHz, CDCl_3): δ [ppm] = 22.4, 23.2, 28.0, 125.4, 131.9, 131.9, 132.2, 142.8, 149.7.

Compound **16**

An aqueous solution of ammonia (30%, 1 mL) was added dropwise to a solution of **16b** (20.1 mg, 50 μmol , 1 eq.) in tetrahydrofuran and ethanol (500 μL each). The reaction mixture was stirred for 2.5 h. After removing the solvent and drying *in vacuo*, the residue was solved in aqueous sodium hydrogen carbonate solution (0.5 M, 2 mL). Compound **6** (200 μmol , 4 eq.) in 1,4-dioxane (2 mL) was added to this solution at $0\text{ }^\circ\text{C}$ over a time of 15 min with a syringe pump. The reaction mixture was warmed to rt, mixed with ice, and extracted with ethyl acetate (3×5 mL). The combined organic layers were washed with a saturated solution of sodium chloride (2×100 mL) and dried over sodium sulfate. After removing the solvent, **16** was obtained by purification via HPLC as a white solid (12.8 mg, 14.7 μmol , 29% over 2 steps). It still contained ca. 10% of the respective nitration regioisomer.

¹H-NMR (700 MHz, DMSO-d₆): δ [ppm] = 2.14 (s, 3 H), 2.17 (s, 6 H), 2.26 (s, 3 H), 2.27 (s, 3 H), 2.29 (s, 3 H), 4.59 (d, *J* = 5.8 Hz, 2 H), 4.70 (t, *J* = 4.6 Hz, 4 H), 7.28 – 7.43 (m, 8 H), 7.50 (d, *J* = 8.5 Hz, 1 H), 7.55 (dd, *J* = 7.2, 2.1 Hz, 1 H), 7.86 (d, *J* = 8.5 Hz, 1 H), 8.76 (t, *J* = 5.0 Hz, 1 H), 8.78 (t, *J* = 4.9 Hz, 1 H), 9.08 (t, *J* = 5.9 Hz, 1 H).

¹³C-NMR (176 MHz, DMSO-d₆): δ [ppm] = 20.0, 20.0, 20.2, 20.3, 36.4, 36.5, 40.1, 123.2, 125.5, 125.6, 125.7, 125.9, 126.0, 126.1, 126.1, 126.1, 126.3, 127.2, 130.3, 130.6, 130.6, 131.0, 137.0, 140.0, 140.1, 142.8, 142.8, 143.8, 150.0, 164.4, 164.9, 167.7, 167.8, 167.9, 168.2, 168.2, 168.3.

C₄₂H₃₈N₄O₁₇ (870.78), exact mass: 870.2232.

ESI-HRMS (*m/z*): [M + H]⁺ calc. for C₄₂H₃₉N₄O₁₇: 871.2310; found: 871.2303

Compound 17a

Oxalyl chloride (690 μL, 1.02 g, 8.00 mmol, 4 eq.) was added to a solution of 5-Nitro-1,2,3-benzenetricarboxylic acid (510 mg, 2.00 mmol, 1 eq.) in dichloromethane (20 mL) and dimethylformamide (1 mL) at 0 °C over a time of 15 min with a syringe pump. The solution was stirred for 5 min at 0 °C and 20 min at rt. After removing the solvent and drying in vacuo, the residue was taken up in dichloromethane (20 mL). *Tert*-Butyl N-(2-aminoethyl)carbamate (1.04 mL, 1.06 g, 6.60 mmol, 3.3 eq.) and triethylamine (2.22 mL, 1.62 g, 16 mmol, 8 eq.) were added dropwise at 0 °C. The solution was stirred for 10 min at 0 °C and 30 min at rt. After removing the solvent, the residue was taken up in ethyl acetate (25 mL). The organic layer was washed with saturated solutions of sodium hydrogen carbonate and sodium chloride (2 × 25 mL each). The combined organic layers were re-extracted with ethyl acetate (2 × 25 mL) and dried over sodium sulfate. After removing the solvent and drying *in vacuo*, **17a** was obtained by purification via automatic flash chromatography (CH₂Cl₂/MeOH 30:1 → 20:1 → 10:1) as a light yellow solid (150 mg, 220 μmol, 11%).

TLC *R_f* = 0.22 (CH₂Cl₂/MeOH = 20:1)

¹H-NMR (700 MHz, DMSO-d₆): δ [ppm] = 1.38 (s, 9 H), 1.38 (s, 18 H), 3.06 – 3.16 (m, 8 H), 3.24 (dd, *J* = 11.5, 5.7 Hz, 4 H), 6.53 (t, *J* = 5.7 Hz, 1 H), 6.87 (t, *J* = 5.9 Hz, 2 H), 8.31 (t, *J* = 5.4 Hz, 1 H), 8.41 (s, 2 H), 8.65 (t, *J* = 5.4 Hz, 2 H).

¹³C-NMR (176 MHz, DMSO-d₆): δ [ppm] = 28.2, 28.2, 38.9, 39.3, 39.8, 77.7, 77.7, 123.4, 137.4, 141.4, 146.1, 155.4, 155.7, 165.5, 165.7.

C₃₀H₄₇N₇O₁₁ (681.74), exact mass: 681.7440.

ESI-HRMS (*m/z*): [M + H]⁺ calc. for C₃₀H₄₈N₇O₁₁: 682.3412; found: 682.3406.

Compound **17**

Trifluoroacetic acid (3.5 mL) was added to a solution of **17a** (150 mg, 220 μ mol, 1 eq.) in dichloromethane (10.5 mL) at 0 °C over a time of 15 min with a syringe pump. The solution was stirred for 30 min at 0 °C and 15 min at rt. After the addition of toluene (11 mL), the solvent was removed and the residue was dried *in vacuo*. The residue was solved in aqueous sodium hydrogen carbonate solution (0.5 M, 20 mL). Compound **6** (770 μ mol, 3.5 eq.) in 1,4-dioxane (20 mL) was added to this solution at 0 °C. The reaction mixture was stirred at 0 °C for 30 min, warmed to rt, mixed with ice, and extracted with ethyl acetate (3 \times 25 mL). The combined organic layers were washed with saturated sodium chloride solution (2 \times 50 mL) and dried over sodium sulfate. After removing the solvent, **17** was obtained by purification via HPLC as a white solid (124 mg, 119 μ mol, 54% over two steps).

¹H-NMR (500 MHz, DMSO-*d*₆): δ [ppm] = 2.21 (s, 6 H), 2.23 (s, 3 H), 2.28 (s, 9 H), 3.23 – 3.29 (m, 2 H), 3.29 – 3.39 (m, 10 H), 7.30 – 7.39 (m, 6 H), 7.53 (dd, *J* = 6.6, 2.8 Hz, 2 H), 7.56 (dd, *J* = 7.4, 1.9 Hz, 1 H), 8.18 (t, *J* = 5.7 Hz, 1 H), 8.41 – 8.47 (m, 3 H), 8.45 (s, 2 H), 8.76 (t, *J* = 5.4 Hz, 2 H).

¹³C-NMR (125 MHz, DMSO-*d*₆): δ [ppm] = 20.2, 20.2, 20.3, 38.6, 38.6, 38.7, 39.1, 123.6, 125.4, 126.0, 126.1, 130.7, 130.8, 137.2, 140.1, 140.2, 141.4, 142.8, 142.8, 146.2, 164.4, 164.8, 165.6, 165.9, 167.8, 168.3.

C₄₈H₄₇N₇O₂₀ (1041.93), exact mass: 1041.2876.

ESI-HRMS (*m/z*): [M + H]⁺ calc. for C₄₈H₄₈N₇O₂₀: 1042.2954; found: 1042.2941.

Compound **18a**

Oxalyl chloride (172 μ L 254 mg, 400 μ mol, 5 eq.) was added to a solution of 5-Nitro-1,2,3-benzenetricarboxylic acid (102 mg, 2.00 mmol, 1 eq.) in dichloromethane (7 mL) and dimethylformamide (150 μ L) at 0 °C dropwise. The solution was stirred for 30 min at 0 °C and 1 h at rt. After removing the solvent and drying *in vacuo*, the residue was taken up in dichloromethane (5 mL). To this solution, a solution of *tert*-butyl *N*-(3-aminopropyl)carbamate (230 mg, 1.32 mmol, 3.3 eq.) and triethylamine (333 μ L, 243 g, 2.4 mmol, 6 eq.) in dichloromethane (5 mL) was added dropwise at 0 °C over a time of 30 min. The solution was stirred for 1.5 h at 0 °C, quenched with ice and washed with hydrochloric acid (1 M) and saturated sodium chloride solution (15 mL each). The combined organic layers were re-extracted with dichloromethane (40 mL) and dried over sodium sulfate. After removing the solvent and drying *in vacuo*, **18a** was obtained by purification via automatic flash

chromatography (CH₂Cl₂/MeOH 30:1 → 20:1 → 10:1) as a light yellow solid (97.0 mg, 134 μmol, 34%).

¹H-NMR (500 MHz, DMSO-d₆): δ [ppm] = 1.38 (s, 27 H), 1.53 (dt, *J* = 14.2, 7.2 Hz, 2 H), 1.57 – 1.63 (m, 4 H), 2.95 – 3.02 (m, 6 H), 3.10 (dd, *J* = 13.0, 6.6 Hz, 2 H), 3.20 (dd, *J* = 12.9, 6.7 Hz, 4 H), 6.70 (t, *J* = 5.7 Hz, 1 H), 6.77 (t, *J* = 5.7 Hz, 2 H), 8.13 (t, *J* = 5.5 Hz, 1 H), 8.31 (s, 2 H), 8.41 (t, *J* = 5.6 Hz, 2 H).

¹³C-NMR (125 MHz, DMSO-d₆): δ [ppm] = 28.2, 28.8, 29.2, 36.7, 37.0, 37.4, 37.4, 77.4, 77.5, 123.1, 137.5, 141.2, 146.1, 155.6, 165.3, 165.4.

Compound 18

Trifluoroacetic acid (2 mL) was added to a solution of **18a** (72.4 mg, 100 μmol, 1 eq.) in dichloromethane (6 mL) at 0 °C over a time of 15 min with a syringe pump. The solution was stirred for 30 min at 0 °C and 30 min at rt. After the addition of toluene (8 mL), the solvent was removed and the residue was dried *in vacuo*. The residue was solved in aqueous sodium hydrogen carbonate solution (0.5 M, 10 mL). Compound **6** (350 μmol, 3.5 eq.) in 1,4-dioxane (6 mL) was added to this solution at 0 °C over a time of 20 min with a syringe pump. The reaction mixture was stirred at rt for 80 min, mixed with ice, and extracted with ethyl acetate (3 × 20 mL). The combined organic layers were washed with saturated sodium chloride solution (2 × 40 mL) and dried over sodium sulfate. After removing the solvent, **18** was obtained by purification via HPLC as a white solid (11.1 mg, 10.2 μmol, 10% over two steps).

¹H-NMR (700 MHz, DMSO-d₆): δ [ppm] = 1.63 – 1.68 (m, 2 H), 1.69 – 1.74 (m, 4 H), 2.23 (s, 9 H), 2.27 (s, 3 H), 2.28 (s, 6 H), 3.16 – 3.21 (m, 2 H), 3.24 – 3.30 (m, 10 H), 7.32 – 7.38 (m, 6 H), 7.44 – 7.47 (m, 3 H), 8.23 (t, *J* = 5.8 Hz, 1 H), 8.28 (t, *J* = 5.8 Hz, 1 H), 8.35 (s, 2 H), 8.33 – 8.37 (m, 2 H), 8.50 (t, *J* = 5.6 Hz, 2 H).

¹³C-NMR (176 MHz, DMSO-d₆): δ [ppm] = 20.2, 20.3, 28.3, 28.7, 36.7, 36.7, 37.0, 123.2, 125.3, 125.9, 126.2, 126.2, 131.1, 131.2, 137.5, 139.4, 141.3, 142.8, 146.2, 164.5, 164.6, 165.3, 165.5, 167.8, 167.9, 168.3, 168.3.

C₅₁H₅₃N₇O₂₀ (1084.01), exact mass: 1083.3345.

ESI-HRMS (*m/z*): [M + H]⁺ calc. for C₅₁H₅₄N₇O₂₀: 1084.3424; found: 1084.3408.

Compound **19a**

EDCI (2.11 g, 11.0 mmol, 1.1 eq.) and HOBt (1.49 g, 11.0 mmol, 1.1 eq.) were added to a solution of 2,3-dimethoxybenzoic acid (1.82 g, 10.0 mmol, 1 eq.) and *N,N*-diisopropylethylamine (3.50 mL, 2.59 g, 20 mmol, 2 eq.) in Dimethylformamide (20 mL) at 0 °C. The solution was stirred for 5 min at 0 °C and 90 min at rt. *Tert*-butyl *N*-(3-aminopropyl)carbamate (1.92 g, 11.0 mmol, 1.1 eq.) in dimethylformamide (5 mL) was added at 0 °C over a time of 10 min with a syringe pump. The solution was stirred over night at rt, quenched with ice water and extracted with ethyl acetate (3 × 30 mL). The combined organic layers were washed with hydrochloric acid (1 M) and saturated sodium chloride solution (2 × 75 mL each) and dried over sodium sulfate. After removing the solvent and drying *in vacuo*, **19a** was obtained and used for the synthesis of **19b** without further purification.

Compound **19b**

Hydrogen chloride (4 M in 1,4-dioxane, 24 mL) was carefully added to **19a** at 0 °C. The solution was stirred for 2 h at rt. After removing the solvent, the residue was taken up in water, frozen in liquid nitrogen and lyophilized. An aqueous solution of sodium hydroxide (2 M) was added until a pH value between 10 and 11 was reached. The resulting solution was again frozen in liquid nitrogen and lyophilized. The residue was taken up in acetone and ethyl acetate and sonicated. The precipitate was filtered off. After removing the solvent and drying *in vacuo*, **19b** was obtained as an amber-colored oil (1.98 g, 8.31 mmol, 83% over two steps)

¹H-NMR (500 MHz, DMSO-*d*₆): δ [ppm] = 1.76 – 1.84 (m, 2 H), 2.81 – 2.87 (m, 2 H), 3.28 – 3.34 (m, 2 H), 3.77 (s, 3 H), 3.83 (s, 3 H), 7.07 – 7.13 (m, 1 H), 7.12 (t, *J* = 9.0 Hz, 1 H), 7.16 (dd, *J* = 7.7, 2.2 Hz, 1 H), 7.83 (s_{br}, 2 H), 8.36 (t, *J* = 5.9 Hz, 1 H).

¹³C-NMR (125 MHz, DMSO-*d*₆): δ [ppm] = 27.4, 35.9, 36.7, 55.9, 60.9, 114.7, 120.4, 124.0, 130.1, 146.1, 152.5, 166.0.

C₁₂H₁₈N₂O₃ (238.29), exact mass: 238.1317.

ESI-HRMS (*m/z*): [M + H]⁺ calc. for C₁₂H₁₉N₂O₃: 239.1396; found: 239.1391.

Compound **19c**

EDCI (121 mg, 630 μmol, 3.5 eq.) was added to a solution of 2-nitrobenzene-1,3,5-tricarboxylic acid (45.9 mg, 180 μmol, 1 eq.) and *N,N*-diisopropylethylamine (377 μL, 279 mg, 2.16 mmol, 12 eq.) in dimethylformamide (2 mL) at 0 °C. The solution was stirred for 5 min at

0 °C and HOBt (85.1 mg, 630 μ mol, 3.5 eq.) was added. The solution was stirred for 90 min at rt and the hydrochloride of **19b** (198 mg, 720 μ mol, 4 eq.) in dimethylformamide (2 mL) was added at 0 °C over a time of 10 min with a syringe pump. The solution was stirred over night at rt. 1,4-dioxane was added and the solution was frozen in liquid nitrogen and lyophilized. Compound **19c** was obtained by purification via HPLC as a white solid (42.5 mg, 46.6 μ mol, 26%)

¹H-NMR (500 MHz, Methanol-*d*₄): δ [ppm] = 1.85 – 2.94 (m, 6 H), 3.43 – 3.49 (m, 6 H), 3.49 – 3.54 (m, 6 H), 3.87 (s, 9 H), 3.88 (s, 3 H), 3.89 (s, 6 H), 7.09 – 7.16 (m, 6 H), 7.31 (dd, J = 7.4, 2.0 Hz, 1 H), 7.34 (dd, J = 7.4, 2.1 Hz, 2 H), 8.20 (s, 2 H), 8.59 (t, J = 5.9 Hz, 1 H), 8.62 (t, J = 6.0 Hz, 2 H).

¹³C-NMR (125 MHz, Methanol-*d*₄): δ [ppm] = 30.4, 30.5, 38.0, 38.2, 38.5, 38.8, 56.7, 62.1, 116.7, 116.8, 122.5, 122.6, 125.5, 125.5, 129.3, 129.4, 130.2, 133.3, 138.5, 148.8, 148.9, 149.8, 154.4, 166.7, 167.2, 168.8, 168.9.

C₄₅H₅₃N₇O₁₄ (915.95), exact mass: 915.3650.

ESI-HRMS (m/z): [M + Na]⁺ calc. for C₄₅H₅₃N₇NaO₁₄: 938.3548; found: 938.3540.

Compound **19**

Boron tribromide (1 M in dichloromethane, 436 μ L, 436 μ mol, 18 eq.) was added dropwise to a solution of **19c** (22.2 mg, 24.2 μ mol, 1 eq.) in dichloromethane (5 mL) at –78 °C. The reaction mixture was stirred at –78 °C for 1 h, slowly warmed to rt, quenched with ice water and methanol, and extracted with ethyl acetate (3 \times 15 mL). The combined organic layers were dried over sodium sulfate. After removing the solvent **19** was obtained by purification via HPLC as a brownish solid (10.4 mg, 12.5 μ mol, 52%).

¹H-NMR (500 MHz, DMSO-*d*₆): δ [ppm] = 1.73 – 1.87 (m, 6 H), 3.28 (dd, J = 12.5, 6.3 Hz, 4 H), 3.32 – 3.42 (m, 8 H), 6.68 (t, J = 7.9 Hz, 3 H), 6.91 (d, J = 7.6 Hz, 3 H), 7.27 (d, J = 8.0 Hz, 3 H), 8.16 (s, 2 H), 8.76 – 8.83 (m, 3 H), 8.89 (t, J = 5.2 Hz, 1 H), 8.98 (t, J = 5.4 Hz, 2 H), 9.14 (s_{br}, 3 H), 12.72 (s_{br}, 3 H).

¹³C-NMR (125 MHz, DMSO-*d*₆): δ [ppm] = 28.7, 28.9, 36.8, 36.9, 37.3, 37.5, 115.0, 115.0, 117.1, 117.9, 118.8, 128.7, 131.4, 136.3, 146.2, 147.9, 149.6, 149.7, 163.7, 163.9, 169.8, 169.6.

C₃₉H₄₁N₇O₁₄ (831.69), exact mass: 831.2711.

ESI-HRMS (m/z): [M + H]⁺ calc. for C₃₉H₄₂N₇O₁₄: 832.2790; found: 832.2783.

Compound **20a**

EDCI (121 mg, 630 μ mol, 3.5 eq.) was added to a solution of 1,3,5-tricarboxylic acid (37.8 mg, 180 μ mol, 1 eq.) and *N,N*-diisopropylethylamine (377 μ L, 279 mg, 2.16 mmol, 12 eq.) in dimethylformamide (3 mL) at 0 °C. The solution was stirred for 5 min at 0 °C and HOBt (85.1 mg, 630 μ mol, 3.5 eq.) was added. The solution was stirred for 2.5 h at rt and the hydrochloride of **19b** (198 mg, 720 μ mol, 4 eq.) in dimethylformamide (2 mL) was added at 0 °C over a time of 10 min with a syringe pump. The solution was stirred over night, quenched with ice and hydrochloric acid (1 M), and extracted with ethyl acetate (5 \times 10 mL). The precipitate from the organic layers was collected and solved in acetone. The combined organic layers were dried over sodium sulfate. After removing the solvent **20a** was obtained by purification via flash chromatography (CH₂Cl₂/MeOH 20:1 \rightarrow 15:1 \rightarrow 10:1) as a white solid (38.2 mg, 43.9 μ mol, 24%).

TLC R_f = 0.20 (CH₂Cl₂/MeOH = 20:1)

¹H-NMR (500 MHz, Methanol-d₄): δ [ppm] = 1.91 (p, J = 6.6 Hz, 6 H), 3.51 (td, J = 13.3, 6.6 Hz, 12 H), 3.86 (s, 9 H), 3.88 (s, 9 H), 7.08 – 7.15 (m, 6 H), 7.32 (dd, J = 7.4, 2.1 Hz, 3 H), 8.43 (s, 3 H).

¹³C-NMR (125 MHz, Methanol-d₄): δ [ppm] = 30.6, 38.3, 38.7, 56.7, 62.1, 116.7, 122.5, 125.5, 129.4, 130.0, 136.8, 148.8, 154.4, 168.8, 168.9.

C₄₅H₅₄N₆O₁₂ (870.96), exact mass: 870.3800.

ESI-HRMS (m/z): [M + Na]⁺ calc. for C₄₅H₅₄N₆NaO₁₂: 893.3697; found: 893.3690.

Compound **20**

Boron tribromide (1 M in dichloromethane, 3.75 mL, 3.75 mmol, 18 eq.) was added dropwise to a solution of **20a** (181 mg, 208 μ mol, 1 eq.) in dichloromethane (10 mL) at –78 °C. The reaction mixture was stirred at –78 °C for 1 h, slowly warmed to rt over night. Since conversion was not complete, another batch of boron tribromide (1 M in dichloromethane, 1.25 mL, 1.25 mmol, 6 eq.) was added at –78 °C. The reaction mixture was stirred at –78 °C for 1 h, slowly warmed to rt over night, quenched with ice water and methanol, and extracted with ethyl acetate (25 mL). The precipitate from the organic layers was collected and solved in methanol. The combined organic layers were dried over sodium sulfate. After removing the solvent **20** was obtained by purification via HPLC as a brownish solid (67.5 mg, 85.8 μ mol, 41%).

¹H-NMR (500 MHz, DMSO-*d*₆): δ [ppm] = 1.83 (p, *J* = 7.0 Hz, 6 H), 3.32 – 3.40 (m, 12 H), 6.68 (t, *J* = 8.0 Hz, 3 H), 6.90 (dd, *J* = 7.8, 1.4 Hz, 3 H), 7.27 (dd, *J* = 8.2, 1.4 Hz, 3 H), 8.42 (s, 3 H), 8.76 (t, *J* = 5.7 Hz, 3 H), 8.81 (t, *J* = 5.7 Hz, 3 H), 9.11 (s_{br}, 3 H), 12.75 (s_{br}, 3 H).

¹³C-NMR (125 MHz, DMSO-*d*₆): δ [ppm] = 29.0, 36.9, 37.3, 115.0, 117.0, 117.9, 118.8, 128.4, 135.0, 146.2, 149.6, 165.6, 169.7.

C₃₉H₄₂N₆O₁₂ (786.80), exact mass: 786.2861.

ESI-HRMS (*m/z*): [M + H]⁺ calc. for C₃₉H₄₃N₆O₁₂: 787.2939; found: 787.2934.

Compound **21**

Zinc dust (574 mg, 7.79 mmol, 15 eq.) was added to a solution of **8** (510 mg, 586 μmol, 1 eq.) in tetrahydrofuran (4 mL), ethanol (3.2 mL), and acetic acid (800 μL) at 0 °C. The reaction mixture was stirred for 10 min at 0 °C and 20 min at rt. It was filtered over celite and the precipitate was washed with ethyl acetate. The organic layer was washed with saturated solutions of sodium hydrogen carbonate and sodium chloride (2 × 30 mL each) and dried over sodium sulfate. After removing the solvent, crude product **21** was dried *in vacuo* and used in subsequent reactions without further purification.

Compound **22**

N-methylmorpholine (257 μL, 237 mg, 2.34 mmol, 4 eq.) and isobutyl chloroformate (224 μL, 240 mg, 1.76 mmol, 3 eq.) were added to a solution of 5-hexynoic acid (226 μL, 230 mg, 2.05 mmol, 3.5 Äq.) in tetrahydrofuran (6 mL) dropwise at 0 °C, whereupon a white precipitate formed immediately. The reaction mixture was stirred 10 min at 0 °C and 90 min at rt. Compound **21** (586 μmol, 1 eq.) in tetrahydrofuran (5 mL) was added at 0 °C over a time of 10 min with a syringe pump at 0 °C. The reaction mixture was stirred over night at rt, quenched with ice and saturated sodium hydrogen carbonate solution (ca. 5 mL each), and extracted with ethyl acetate (3 × 10 mL). The organic layer was washed with hydrochloric acid (0.1 M) and saturated solutions of sodium hydrogen carbonate and sodium chloride (2 × 25 mL each) and dried over sodium sulfate. After removing the solvent, **22** was obtained by purification via automatic flash chromatography (CH₂Cl₂/MeOH) as a white solid (233 mg, 249 μmol, 43%).

TLC *R_f* = 0.19 (CH₂Cl₂/MeOH = 20:1)

¹H-NMR (700 MHz, DMSO-*d*₆): δ [ppm] = 1.80 (p, *J* = 7.2 Hz, 2 H), 2.16 (s, 3 H), 2.17 (s, 6 H), 2.25 (td, *J* = 7.1, 2.6 Hz, 2 H), 2.28 (s, 3 H), 2.28 (s, 6 H), 2.51 (t, *J* = 7.5 Hz, 2 H), 2.81 (t, *J* = 2.6 Hz, 1 H), 4.33 (s_{br}, 4 H), 4.38 (d, *J* = 5.9 Hz, 2 H), 7.21 (s, 2 H), 7.23 (t, *J* = 7.9 Hz, 1 H),

7.31 (t, $J = 7.9$ Hz, 2 H), 7.35 (dd, $J = 8.1, 1.5$ Hz, 1 H), 7.38 (dd, $J = 8.1, 1.5$ Hz, 2 H), 7.44 (dd, $J = 7.8, 1.5$ Hz, 1 H), 7.53 (dd, $J = 7.7, 1.5$ Hz, 2 H), 8.78 (t, $J = 6.0$ Hz, 2 H), 8.94 (t, $J = 6.0$ Hz, 1 H), 9.54 (s, 1 H).

$^{13}\text{C-NMR}$ (176 MHz, DMSO- d_6): δ [ppm] = 17.5, 20.2, 20.3, 24.1, 34.1, 39.1, 42.2, 71.6, 84.0, 124.6, 125.4, 125.5, 126.0, 126.1, 126.2, 130.6, 130.6, 131.8, 153.8, 137.5, 140.1, 132.8, 164.5, 164.7, 167.8, 167.9, 168.3, 171.1.

$\text{C}_{48}\text{H}_{46}\text{N}_4\text{O}_{16}$ (934.91), exact mass: 934.2909.

ESI-HRMS (m/z): $[\text{M} + \text{H}]^+$ calc. for $\text{C}_{48}\text{H}_{47}\text{N}_4\text{O}_{16}$: 935.2987; found: 935.2985.

Compound 23

Triethylamine (1 mL) was added to a solution of **22** (80 mg, 85.6 μmol) in methanol (3 mL) dropwise at 0 °C. This solution was stirred 5 min at 0 °C and 2.5 h at rt, quenched with ice, acidified with hydrochloric acid (2 M) and extracted with ethyl acetate (3 \times 3 mL). The combined organic layers were dried over sodium sulfate. After removing the solvent, **23** was obtained by purification via HPLC as a white solid (39.5 mg, 57.9 μmol , 68%).

$^1\text{H-NMR}$ (700 MHz, DMSO- d_6): δ [ppm] = 1.79 (p, $J = 7.2$ Hz, 2 H), 2.24 (td, $J = 7.1, 2.6$ Hz, 2 H), 2.49 – 2.53 (m, 2 H), 2.81 (t, $J = 2.6$ Hz, 1 H), 4.40 (d, $J = 5.9$ Hz, 2 H), 4.43 (s_{br}, 4 H), 6.60 (t, $J = 7.9$ Hz, 1 H), 6.67 (t, $J = 7.9$ Hz, 2 H), 6.88 (dd, $J = 7.8, 1.3$ Hz, 1 H), 6.92 (dd, $J = 7.8, 1.3$ Hz, 2 H), 7.19 – 7.21 (m, 1 H), 7.20 (s, 2 H), 7.29 (dd, $J = 8.2, 1.3$ Hz, 2 H), 9.15 (s_{br}, 3 H), 9.15 (t, $J = 6.0$ Hz, 2 H), 9.32 (t, $J = 7.2$ Hz, 1 H), 9.57 (s, 1 H), 12.52 (s_{br}, 2 H), 12.57 (s_{br}, 1 H).

$^{13}\text{C-NMR}$ (176 MHz, DMSO- d_6): δ [ppm] = 17.5, 24.1, 34.1, 39.0, 42.1, 71.6, 84.0, 114.9, 115.1, 117.1, 117.3, 117.9, 118.0, 118.8, 118.9, 124.8, 132.1, 135.9, 137.4, 146.1, 146.2, 149.5, 149.6, 169.7, 169.8, 171.2.

$\text{C}_{36}\text{H}_{34}\text{N}_4\text{O}_{10}$ (682.69), exact mass: 682.2275.

ESI-HRMS (m/z): $[\text{M} + \text{Na}]^+$ calc. for $\text{C}_{36}\text{H}_{34}\text{N}_4\text{NaO}_{10}$: 705.2173; found: 705.2170.

Compound 24a

Lithium-bis(trimethylsilyl)amide (1 M in tetrahydrofuran, 22 mL, 22 mmol, 1.1 eq.) was added to a solution of methyl-2-phenyl acetate (2.82 mL, 3.00 g, 20.0 mmol, 1 eq.) in tetrahydrofuran (50 mL) over a time of 20 min with a syringe pump at -50 °C. The reaction mixture was stirred for 1 h at -50 °C, warmed to -20 °C, and 6-iodo-1-hexyne (2.90 mL, 4.58 g, 22.0 mmol, 1.1 eq.) in tetrahydrofuran (5 mL) was added over a time of 20 min with a syringe

pump. The reaction mixture was warmed to 0 °C, stirred for 1 h, quenched with ice, and mixed with saturated ammonium chloride solution (50 mL). After separation of the phases, the aqueous layer was extracted with diethyl ether (2 × 50 mL) and the combined organic layers were dried over sodium sulfate. After removing the solvent crude product **24a** was dried *in vacuo* and for the synthesis of **24b** without further purification.

Compound **24b**

Potassium hydroxide (1.68 g, 30.0 mmol, 1.5 eq.) was added to a solution of **24a** (20.0 mmol, 1 eq.) in methanol (100 mL) and water (2 mL). The reaction mixture was refluxed over night and cooled to room temperature. After removing the solvent the crude product was taken up in water (30 mL) and washed with diethyl ether. The aqueous layer was acidified with hydrochloric acid (6 M) to pH ≈ 1 and extracted with diethyl ether (3 × 30 mL). The combined organic layers were dried over sodium sulfate. After removing the solvent **24b** was obtained by purification via flash chromatography (CH₂Cl₂/MeOH 100:0 → 99:1 → 97:3, 1% AcOH) as a white solid (3.08 g, 14.2 mmol, 71%).

¹H-NMR (500 MHz, DMSO-d₆): δ [ppm] = 1.19 – 1.27 (m, 1 H), 1.27 – 1.36 (m, 1 H), 1.39 – 1.49 (m, 2 H), 1.60 – 1.69 (m, 1 H), 1.90 – 1.99 (m, 1 H), 2.11 (td, *J* = 7.0, 2.6 Hz, 2 H), 2.70 (t, 2.6 Hz, 1 H), 3.48 (t, *J* = 7.6 Hz, 1 H), 7.22 – 7.26 (m, 1 H), 7.27 – 7.34 (m, 4 H), 12.3 (s, 1 H).

¹³C-NMR (125 MHz, DMSO-d₆): δ [ppm] = 17.6, 26.3, 27.7, 32.5, 50.8, 71.2, 84.3, 126.8, 127.7, 128.4, 139.7, 174.8.

C₁₄H₁₆O₂ (216.28)

Compound **24c**

Oxalyl chloride (1.72 mL, 2.54 g, 20.0 mmol, 2 eq.) was added to a solution of **22b** (2.16 g, 10.0 mmol, 1 eq.) in dichloromethane (10 mL) over a time of 10 min with a syringe pump. After the addition of one drop of dimethylformamide the solution was stirred for 1 h. The solvent was removed while stirring *in vacuo* under stirring using a cooling trap. The residue was taken up in tetrahydrofuran (20 mL) and triethylamine (5.50 mL, 4.05 g, 40.0 mmol, 4 eq.) was added at 0 °C. The solution was stirred for 2 h at 0 °C and the resulting precipitate was filtered off over a Schlenk-frit. The solvent was distilled off at 110 °C and the residue was purified via distillation at 3 mbar at a temperature of 110 °C increasing to 150 °C. Compound **24c** was isolated from the main run as a yellow oil (433 mg, 2.18 mmol, 22%). Since Ketene **24c** was instable under atmospheric conditions, all work steps were conducted under Schlenk conditions.

¹H-NMR (500 MHz, CDCl₃): δ [ppm] = 1.54 – 1.67 (m, 4 H), 1.88 (t, *J* = 2.7 Hz, 1 H), 2.16 (td, *J* = 6.8, 2.6 Hz, 2 H), 2.34 – 2.38 (m, 2 H), 6.94 – 7.02 (m, 3 H), 7.21 – 7.25 (m, 2 H),

¹³C-NMR (125 MHz, CDCl₃): δ [ppm] = 18.2, 23.2, 27.1, 28.0, 39.2, 68.7, 84.0, 124.1, 124.3, 129.0, 132.5, 204.6.

C₁₄H₁₄O (198.27)

Compound **24**

Compound **24c** (65.4 mg, 330 μmol, 1.2 eq.) in tetrahydrofuran (800 μL) was added to a solution of **21** (231 mg, 275 μmol, 1 eq.) in tetrahydrofuran (2 mL) at 0 °C. The solution was stirred for 10 min at 0 °C and over night at rt. Another batch of **24c** (32.7 mg, 165 μmol, 0.6 eq.) was added and the solution was stirred over night. After removing the solvent, the crude product was purified via flash chromatography (CH₂Cl₂/MeOH 80:2 → 80:3). Since the purity of the target compound was not adequate, **24** was obtained by further purification via HPLC as a white solid (80.0 mg, 77.0 μmol, 28%).

TLC *R_f* = 0.29 (CH₂Cl₂/MeOH = 80:3)

¹H-NMR (700 MHz, DMSO-*d*₆): δ [ppm] = 1.34 – 1.40 (m, 1 H), 1.41 – 1.47 (m, 1 H), 1.47 – 1.57 (m, 2 H), 1.69 – 1.75 (m, 1 H), 2.08 – 2.14 (m, 1 H), 2.14 (s, 3 H), 2.14 – 2.17 (m, 2 H), 2.16 (s, 6 H), 2.27 (s, 3 H), 2.29 (s, 6 H), 2.68 (t, *J* = 2.6 Hz, 1 H), 3.80 (dd, *J* = 8.6, 6.6 Hz, 1 H), 4.18 (s_{br}, 4 H), 4.36 (d, *J* = 5.9 Hz, 2 H), 7.15 (s, 2 H), 7.20 (t, *J* = 7.9 Hz, 1 H), 7.22 – 7.26 (m, 1 H), 7.28 – 7.35 (m, 5 H), 7.38 (dd, *J* = 8.1, 1.4 Hz, 2 H), 7.41 (dd, 7.8, 1.5 Hz, 1 H), 7.44 (d, *J* = 7.2 Hz, 2 H), 7.50 (d, *J* = 6.1 Hz, 2 H), 8.70 (s_{br}, 2 H), 8.93 (t, *J* = 6.0 Hz, 1 H), 9.79 (s, 1 H).

¹³C-NMR (176 MHz, DMSO-*d*₆): δ [ppm] = 17.6, 20.1, 20.3, 26.5, 27.8, 32.1, 38.8, 42.2, 51.4, 71.1, 84.4, 124.0, 125.4, 125.6, 126.0, 126.0, 126.2, 126.8, 127.6, 128.4, 130.5, 130.6, 131.2, 135.8, 137.7, 140.1, 140.1, 140.6, 142.8, 142.8.

C₅₆H₅₄N₄O₁₆ (1039.06), exact mass: 1038.3535.

ESI-HRMS (*m/z*): [M + H]⁺ calc. for C₅₆H₅₅N₄O₁₆: 1039.3613 found: 1039.3605.

Compound 25a

Sodium azide (3.25 g, 50 mmol, 5 eq.) was added to a solution of 3-bromoproionic acid (1.53 g, 10 mmol, 1 eq.) in water (20 mL). The solution was stirred for 4 h at rt, carefully acidified with hydrochloric acid to pH \approx 1, and extracted with ethyl acetate (3 \times 30 mL). The combined organic layers were washed with saturated sodium chloride solution (50 mL) and dried over sodium sulfate. After removing the solvent **25a** was obtained as a pale yellow oil (1.04 g, 9.00 mmol, 90%).

Compound 25

N-methylmorpholine (5.50 μ L, 5.06 mg, 50 μ mol, 1 eq.) and isobutyl chloroformate (6.36 μ L, 6.83 mg, 50 μ mol, 1 eq.) were added to a solution of **25a** (7.75 mg, 50 μ mol, 1 eq.) in tetrahydrofuran (2 mL) at 0 $^{\circ}$ C, whereupon a white precipitate formed immediately. The reaction mixture was stirred for 2 h at 0 $^{\circ}$ C. A solution of ampicillin (11.2 mg, 55 μ mol, 1.1 eq.) and triethylamine (20.0 μ L, 14.5 mg, 144 μ mol, 2.87 eq.) in tetrahydrofuran (1 mL) and water (200 μ L) was added at 0 $^{\circ}$ C. The reaction mixture was stirred for 1 h at 0 $^{\circ}$ C and for 1 h at rt. After removing the solvent the residue was taken up in water (ca. 4 mL) and acidified with hydrochloric acid (1 M) to pH \approx 2. The resulting suspension was extracted with ethyl acetate (3 \times 5 mL) and the combined organic layers were washed with saturated sodium chloride solution (15 mL) and dried over sodium sulfate. After removing the solvent **25** was obtained by purification via HPLC as a white solid (13.3 mg, 29.8 μ mol, 60%).

$^1\text{H-NMR}$ (500 MHz, DMSO- d_6): δ [ppm] = 1.41 (s, 3 H), 1.56 (s, 3 H), 2.54 (td, J = 6.3, 2.3, 2 H), 3.46 – 3.55 (m, 2 H), 4.21 (s, 1 H), 5.40 (d, J = 4.0 Hz, 1 H), 5.52 (dd, J = 7.8, 4.0 Hz, 1 H), 5.77 (d, J = 8.2 Hz, 1 H), 7.24 – 7.29 (m, 1 H), 7.30 – 7.35 (m, 2 H), 7.43 (d, J = 7.3 Hz, 2 H), 8.73 (d, J = 8.2 Hz, 1 H), 9.16 (d, J = 7.9 Hz, 1 H), 13.32 (s_{br} , 1 H).

$^{13}\text{C-NMR}$ (125 MHz, DMSO- d_6): δ [ppm] = 26.6, 30.4, 34.2, 46.9, 55.4, 58.1, 63.7, 67.2, 70.3, 127.1, 127.5, 128.2, 138.1, 168.9, 169.3, 170.0, 173.4.

$\text{C}_{19}\text{H}_{22}\text{N}_6\text{O}_5\text{S}$ (446.48), exact mass: 446.1372.

ESI-HRMS (m/z): $[\text{M} + \text{H}]^+$ calc. for $\text{C}_{19}\text{H}_{23}\text{N}_6\text{O}_5\text{S}$: 447.1451; found: 447.1445.

Compound **26**

N-methylmorpholine (165 μ L, 152 mg, 1.50 μ mol, 1 eq.) and isobutyl chloroformate (191 μ L, 205 mg, 150 μ mol, 1 eq.) were added to a solution of **25a** (233 mg, 1.50 mmol, 1 eq.) in tetrahydrofuran (10 mL) at 0 °C, whereupon a white precipitate formed immediately. The reaction mixture was stirred for 30 min at 0 °C and for 30 min at rt. A solution of amoxicillin (603 mg, 1.65 mmol, 1.1 eq.) and triethylamine (627 μ L, 455 mg, 4.50 mmol, 3 eq.) in tetrahydrofuran (5 mL) and water (1 mL) was added at 0 °C. The reaction mixture was stirred for 30 min at 0 °C and for 30 min at rt. After removing the solvent the residue was taken up in ice water and acidified with hydrochloric acid (1 M) to pH \approx 2. The resulting suspension was extracted with ethyl acetate (3 \times 10 mL) and the combined organic layers were washed with saturated sodium chloride solution (30 mL) and dried over sodium sulfate. After removing the solvent, **26** was obtained by purification via automatic flash chromatography over a reversed-phase column as a white solid (123 mg, 266 μ mol, 18%).

¹H-NMR (500 MHz, DMSO-*d*₆): δ [ppm] = 1.42 (s, 3 H), 1.56 (s, 3 H), 2.45 – 2.55 (m, 2 H), 3.45 – 3.54 (m, 2 H), 4.21 (s, 1 H), 5.39 (d, *J* = 4.1 Hz, 1 H), 5.52 (dd, *J* = 8.0, 4.1 Hz, 1 H), 5.60 (d, *J* = 8.1 Hz, 1 H), 6.66 – 6.71 (m, 2 H), 7.17 – 7.23 (m, 2 H), 8.57 (d, *J* = 8.1 Hz, 1 H), 8.98 (d, *J* = 8.0 Hz, 1 H), 9.37 (s_{br}, 1 H), 13.33 (s_{br}, 1 H).

¹³C-NMR (125 MHz, DMSO-*d*₆): δ [ppm] = 26.6, 30.3, 34.2, 46.9, 54.9, 80.0, 63.7, 67.2, 70.3, 114.9, 128.3, 128.3, 156.8, 168.9, 169.1, 170.5, 173.6.

C₁₉H₂₂N₆O₆S (462.48), exact mass: 462.1322.

ESI-HRMS (*m/z*): [M + H]⁺ calc. for C₁₉H₂₃N₆O₆S: 463.1400; found: 463.1395.

Compound **27**

TBTA (2.65 mg, 5.00 μ mol, 0.5 eq.) in dimethylformamide (50 μ L) was added to a solution of **22** (18.7 mg, 20.0 μ mol, 2 eq.) and **25** (4.46 mg, 10.0 μ mol, 1 eq.) in dimethylformamide (400 μ L) and PBS buffer (100 μ L). A mixture of copper(II) sulfate (400 μ g, 2.50 μ mol, 0.25 eq.) and sodium ascorbate (990 μ g, 5.00 μ mol, 0.5 eq.) in water (100 μ L) was added. This step was repeated after stirring for 45 min at rt and the solution was again stirred for 45 min at rt. Another batch of TBTA (2.65 mg, 5.00 μ mol, 0.5 eq.) in dimethylformamide (50 μ L) was added to the solution. An identical amount of the mixture consisting of copper(II) sulfate and sodium ascorbate in water (*v.s.*) was added. This step was repeated after stirring for 45 min at rt. After another 45 min of stirring at rt **27** was obtained by purification of the solution via HPLC as a white solid (11.0 mg, 7.96 μ mol, 80%).

¹H-NMR (700 MHz, DMSO-*d*₆): δ [ppm] = 1.40 (s, 3 H), 1.54 (s, 3 H), 1.89 – 1.95 (m, 2 H), 2.15 (s, 6 H), 2.16 (s, 3 H), 2.28 (s, 3 H), 2.28 (s, 6 H), 2.46 (t, *J* = 7.5 Hz, 2 H), 2.67 (t, *J* = 7.6 Hz, 2 H), 2.79 – 2.85 (m, 1 H), 2.86 – 2.92 (m, 1 H), 4.17 (s, 1 H), 4.34 (s_{br}, 4 H), 4.38 (d, *J* = 5.8, Hz, 2 H), 4.51 (td, *J* = 13.7, 7.0 Hz, 2 H), 5.38 (d, *J* = 3.9 Hz, 1 H), 5.50 (dd, *J* = 7.8, 4.0 Hz, 1 H), 5.73 (d, *J* = 8.1 Hz, 1 H), 7.21 (s, 2 H), 7.23 (t, *J* = 7.9 Hz, 1 H), 7.26 (t, *J* = 7.2 Hz, 1 H), 7.30 (t, *J* = 7.9 Hz, 4 H), 7.33 – 7.39 (m, 5 H), 7.44 (dd, *J* = 7.7, 1.4 Hz, 1 H), 7.52 (dd, *J* = 7.7, 1.4 Hz, 2 H), 7.76 (s, 1 H), 8.73 (d, *J* = 8.1 Hz, 1 H), 8.78 (t, *J* = 6.0 Hz, 2 H), 8.94 (t, *J* = 6.0 Hz, 1 H), 9.16 (d, *J* = 7.8 Hz, 1 H), 9.51 (s, 1 H), 13.30 (s_{br}, 1 H).

¹³C-NMR (176 MHz, DMSO-*d*₆): δ [ppm] = 20.1, 20.2, 20.3, 24.8, 25.1, 26.7, 30.4, 34.9, 35.2, 39.1, 42.2, 45.6, 55.4, 58.0, 63.8, 67.1, 69.8, 121.9, 124.6, 125.4, 125.5, 126.0, 126.0, 126.1, 126.2, 127.0, 127.5, 128.2, 130.6, 130.7, 131.8, 135.8, 137.5, 138.0, 140.1, 140.1, 142.8, 146.2, 164.5, 164.7, 167.8, 167.9, 168.3, 168.9, 168.9, 169.9, 171.5, 173.3.

C₆₇H₆₈N₁₀O₂₁S (1381.39), exact mass: 1380.4281.

ESI-HRMS (*m/z*): [M + H]⁺ calc. for C₆₇H₆₉N₁₀O₂₁S: 1381.4359; found: 1381.4366.

Compound **28**

TBTA (2.65 mg, 5.00 μmol, 0.5 eq.) in dimethylformamide (50 μL) was added to a solution of **23** (13.7 mg, 20.0 μmol, 2 eq.) and **25** (4.46 mg, 10.0 μmol, 1 eq.) in dimethylformamide (400 μL) and PBS buffer (100 μL). A mixture of copper(II) sulfate (400 μg, 2.50 μmol, 0.25 eq.) and sodium ascorbate (990 μg, 5.00 μmol, 0.5 eq.) in water (100 μL) was added. This step was repeated after stirring for 45 min at rt and the solution was again stirred for 45 min at rt. Another batch of TBTA (2.65 mg, 5.00 μmol, 0.5 eq.) in dimethylformamide (50 μL) was added to the solution. An identical amount of the mixture consisting of copper(II) sulfate and sodium ascorbate in water (*v.s.*) was added. This step was repeated after stirring for 45 min at rt. After another 45 min of stirring at rt **28** was obtained by purification of the solution via HPLC as a white solid (4.50 mg, 3.98 μmol, 40%).

¹H-NMR (700 MHz, DMSO-*d*₆): δ [ppm] = 1.40 (s, 3 H), 1.54 (s, 3 H), 1.88 – 1.94 (m, 2 H), 2.46 (t, *J* = 7.5 Hz, 2 H), 2.66 (t, *J* = 7.6 Hz, 2 H), 2.79 – 2.84 (m, 1 H), 2.86 – 2.92 (m, 1 H), 4.19 (s, 1 H), 4.40 (d, *J* = 5.8, Hz, 2 H), 4.44 (s_{br}, 4 H), 4.47 – 4.55 (m, 2 H), 5.39 (d, *J* = 4.0 Hz, 1 H), 5.51 (dd, *J* = 7.9, 4.0 Hz, 1 H), 5.73 (d, *J* = 8.1 Hz, 1 H), 6.60 (t, *J* = 7.9 Hz, 1 H), 6.67 (t, *J* = 7.9 Hz, 2 H), 6.88 (dd, *J* = 7.8, 1.3 Hz, 1 H), 6.92 (dd, *J* = 7.8, 1.2 Hz, 2 H), 7.18 – 7.21 (m, 1 H), 7.20 (s, 2 H), 7.23 – 7.27 (m, 1 H), 7.27 – 7.31 (m, 4 H), 7.33 – 7.36 (m, 2 H), 7.75 (s, 1 H), 8.72 (d, *J* = 8.1 Hz, 1 H), 9.08 (s_{br}, 1 H), 9.13 – 9.18 (m, 5 H), 9.32 (t, *J* = 6.0 Hz, 1 H), 9.54 (s, 1 H), 12.52 (s, 2 H), 12.57 (s, 1 H), 13.32 (s_{br}, 1 H).

¹³C-NMR (176 MHz, DMSO-d₆): δ [ppm] = 24.8, 25.1, 26.6, 30.3, 34.8, 35.2, 38.9, 42.1, 45.6, 55.4, 58.1, 63.7, 67.2, 70.3, 114.9, 115.1, 117.1, 117.3, 117.9, 118.0, 118.8, 118.9, 121.9, 124.8, 127.0, 127.5, 128.1, 132.1, 135.9, 137.4, 138.0, 146.1, 146.2, 146.2, 149.5, 149.6, 168.9, 168.9, 169.7, 169.8, 169.9, 171.5, 173.3.

C₅₅H₅₆N₁₀O₁₅S (1129.17), exact mass: 1128.3647.

ESI-HRMS (*m/z*): [M + H]⁺ calc. for C₅₅H₅₇N₁₀O₁₅S: 1129.3726; found: 1129.3713.

Compound **29**

A mixture of copper(II) sulfate (800 μg, 5.00 μmol, 0.25 eq.) and sodium ascorbate (1.98 mg, 10.0 μmol, 0.5 eq.) in water (100 μL) was added to a solution of **22** (28.0 mg, 30.0 μmol, 1.5 eq.) and **26** (9.25 mg, 20.0 μmol, 1 eq.) in dimethylformamide (500 μL). The solution was stirred for 30 min at rt. The addition of an equal mixture of copper(II) sulfate and sodium ascorbate in water was repeated three times. After each addition, the solution was stirred for 30 min. Compound **29** was obtained by purification of the solution via HPLC as a white solid (10.5 mg, 7.51 μmol, 38%).

¹H-NMR (700 MHz, DMSO-d₆): δ [ppm] = 1.42 (s, 3 H), 1.56 (s, 3 H), 1.91 – 1.97 (m, 2 H), 2.16 (s, 6 H), 2.17 (s, 3 H), 2.29 (s, 3 H), 2.29 (s, 6 H), 2.47 (t, *J* = 7.5 Hz, 2 H), 2.68 (t, *J* = 7.6 Hz, 2 H), 2.77 – 2.83 (m, 1 H), 2.83 – 2.88 (m, 1 H), 4.20 (s, 1 H), 4.35 (s_{br}, 4 H), 4.39 (d, *J* = 5.8 Hz, 2 H), 4.47 – 4.51 (m, 2 H), 5.40 (d, *J* = 4.0 Hz, 1 H), 5.52 (dd, *J* = 8.0, 4.1 Hz, 1 H), 5.58 (d, *J* = 7.9 Hz, 1 H), 6.68 (d, *J* = 8.6 Hz, 2 H), 7.16 (d, *J* = 8.6 Hz, 2 H), 7.22 (s, 2 H), 7.24 (t, *J* = 7.9 Hz, 1 H), 7.31 (t, *J* = 7.9 Hz, 2 H), 7.35 (dd, *J* = 8.1, 1.5 Hz, 1 H), 7.38 (dd, *J* = 8.1, 1.5 Hz, 2 H), 7.45 (dd, *J* = 7.8, 1.4 Hz, 1 H), 7.53 (dd, *J* = 7.7, 1.5 Hz, 2 H), 7.78 (s, 1 H), 8.59 (d, *J* = 7.9 Hz, 1 H), 8.79 (t, *J* = 6.0 Hz, 2 H), 8.95 (t, *J* = 6.0 Hz, 1 H), 9.02 (d, *J* = 8.0 Hz, 1 H), 9.38 (s, 1 H), 9.51 (s, 1 H), 13.30 (s_{br}, 1 H).

¹³C-NMR (176 MHz, DMSO-d₆): δ [ppm] = 20.1, 20.2, 20.3, 24.7, 25.1, 26.6, 30.2, 34.9, 35.2, 39.1, 42.2, 45.6, 55.0, 58.0, 63.7, 67.2, 70.3, 114.9, 121.9, 124.6, 125.4, 125.5, 126.0, 126.0, 126.1, 126.2, 128.1, 128.3, 130.6, 130.6, 131.8, 135.8, 137.5, 140.1, 140.1, 142.8, 146.2, 156.8, 164.5, 164.7, 167.8, 167.9, 168.3, 168.7, 168.9, 170.4, 171.5, 173.5.

C₆₇H₆₈N₁₀O₂₂S (1397.39), exact mass: 1396.4230.

ESI-HRMS (*m/z*): [M + H]⁺ calc. for C₆₇H₆₉N₁₀O₂₂S: 1397.4309; found: 1397.4285.

Compound **30**

A mixture of copper(II) sulfate (800 μg , 5.00 μmol , 0.25 eq.) and sodium ascorbate (1.98 mg, 10.0 μmol , 0.5 eq.) in water (100 μL) was added to a solution of **23** (20.5 mg, 30.0 μmol , 1.5 eq.) and **26** (9.25 mg, 20.0 μmol , 1 eq.) in dimethylformamide (500 μL). The solution was stirred for 30 min at rt. The addition of an equal mixture of copper(II) sulfate and sodium ascorbate in water was repeated three times. After each addition, the solution was stirred for 30 min. Compound **30** was obtained by purification of the solution via HPLC as a white solid (8.50 mg, 7.42 μmol , 37%).

$^1\text{H-NMR}$ (700 MHz, DMSO-d_6): δ [ppm] = 1.42 (s, 3 H), 1.56 (s, 3 H), 1.90 – 1.96 (m, 2 H), 2.47 (t, $J = 7.4$ Hz, 2 H), 2.67 (t, $J = 7.6$ Hz, 2 H), 2.77 – 2.83 (m, 1 H), 2.83 – 2.88 (m, 1 H), 4.19 (s, 1 H), 4.41 (d, $J = 5.8$ Hz, 2 H), 4.44 (s_{br} , 4 H), 4.47 – 4.55 (m, 2 H), 5.40 (d, $J = 4.0$ Hz, 1 H), 5.52 (dd, $J = 8.0, 4.0$ Hz, 1 H), 5.88 (d, $J = 7.9$ Hz, 1 H), 6.61 (t, $J = 7.9$ Hz, 1 H), 6.68 (t, $J = 8.0$ Hz, 4 H), 6.89 (d, $J = 7.3$ Hz, 1 H), 6.93 (d, $J = 7.8$ Hz, 2 H), 7.15 (d, $J = 8.6$ Hz, 2 H), 7.21 (d, $J = 7.6$ Hz, 1 H), 7.21 (s, 2 H), 7.30 (d, $J = 7.7$ Hz, 2 H), 7.77 (s, 1 H), 8.59 (d, $J = 7.9$ Hz, 1 H), 9.01 (d, $J = 8.0$ Hz, 1 H), 9.09 (s_{br} , 1 H), 9.13 – 9.18 (m, 4 H), 9.33 (t, $J = 6.0$ Hz, 1 H), 9.38 (s, 1 H), 9.55 (s, 1 H), 12.53 (s, 2 H), 12.58 (s, 1 H), 13.23 (s_{br} , 1 H).

$^{13}\text{C-NMR}$ (176 MHz, DMSO-d_6): δ [ppm] = 24.7, 25.1, 26.6, 30.2, 34.8, 35.2, 39.1, 42.1, 45.6, 55.0, 58.0, 63.7, 67.2, 70.3, 114.9, 115.1, 117.1, 117.3, 117.9, 118.0, 118.8, 118.9, 121.9, 124.8, 128.1, 128.3, 132.1, 135.9, 137.4, 146.1, 146.2, 146.2, 149.5, 149.6, 156.8, 168.7, 168.9, 169.7, 169.8, 170.4, 171.5, 173.5.

$\text{C}_{55}\text{H}_{56}\text{N}_{10}\text{O}_{16}\text{S}$ (1145.17), exact mass: 1144.3596.

ESI-HRMS (m/z): $[\text{M} + \text{H}]^+$ calc. for $\text{C}_{55}\text{H}_{57}\text{N}_{10}\text{O}_{16}\text{S}$: 1145.3675; found: 1145.3663

Compound **31a**

N-methylmorpholine (44.0 μL , 40.5 mg, 400 μmol , 4 eq.) and isobutyl chloroformate (32.0 μL , 34.1 mg, 250 μmol , 2.5 eq.) were added to a solution of 4,7,10,13-tetraoxahexadec-15-ynoic acid (78.1 mg, 300 μmol , 3 eq.) in tetrahydrofuran (3 mL) at 0 $^\circ\text{C}$, whereupon a white precipitate formed immediately. The reaction mixture was stirred for 10 min at 0 $^\circ\text{C}$ and 90 min at rt. Compound **21** (100 μmol , 1 eq.) in tetrahydrofuran (1 mL) was added at 0 $^\circ\text{C}$ over a time of 5 min with a syringe pump. The reaction mixture was stirred over night at rt, quenched with ice and saturated sodium hydrogen carbonate solution, and extracted with ethyl acetate (3 \times 5 mL). The organic layer was washed with hydrochloric acid (0.1 M) and saturated solutions of sodium hydrogen carbonate and sodium chloride (2 \times 25 mL each) and dried over

sodium sulfate. After removing the solvent, **31a** was obtained by purification via HPLC as a white solid (14.5 mg, 13.4 μmol , 13% over 2 steps).

$^1\text{H-NMR}$ (700 MHz, DMSO-d_6): δ [ppm] = 2.16 (s, 3 H), 2.17 (s, 6 H), 2.28 (s, 3 H), 2.28 (s, 6 H), 2.62 (t, $J = 6.2$ Hz, 2 H), 3.41 (t, $J = 2.4$ Hz, 1 H), 3.46 – 3.54 (m, 12 H), 3.74 (t, $J = 6.2$ Hz, 2 H), 4.12 (d, $J = 2.4$ Hz, 2 H), 4.35 (s_{br} , 4 H), 4.38 (d, $J = 5.9$ Hz, 2 H), 7.20 (s, 2 H), 7.23 (t, $J = 7.9$ Hz, 1 H), 7.31 (t, $J = 7.9$ Hz, 2 H), 7.34 (dd, $J = 8.1, 1.5$ Hz, 1 H), 7.38 (dd, $J = 8.1, 1.5$ Hz, 2 H), 7.44 (dd, $J = 7.8, 1.5$ Hz, 1 H), 7.52 (dd, $J = 7.7, 1.5$ Hz, 2 H), 8.74 (t, $J = 6.0$ Hz, 2 H), 8.94 (t, $J = 6.0$ Hz, 1 H), 9.56 (s, 1 H).

$^{13}\text{C-NMR}$ (176 MHz, DMSO-d_6): δ [ppm] = 20.1, 20.2, 20.3, 36.4, 39.1, 42.2, 57.5, 67.0, 68.5, 69.4, 69.6, 69.6, 69.7, 69.7, 77.1, 80.3, 124.6, 125.4, 125.5, 126.0, 126.0, 126.1, 126.2, 130.6, 130.7, 131.8, 136.0, 137.6, 140.1, 142.8, 142.8, 164.5, 164.6, 167.8, 167.9, 168.3, 170.0.

$\text{C}_{54}\text{H}_{58}\text{N}_4\text{O}_{20}$ (1083.07), exact mass: 1082.3644.

ESI-HRMS (m/z): $[\text{M} + \text{Na}]^+$ calc. for $\text{C}_{54}\text{H}_{58}\text{N}_4\text{NaO}_{20}$: 1105.3542 found: 1105.3532.

Compound 31

A mixture of copper(II) sulfate (200 μg , 1.25 μmol , 0.17 eq.) and sodium ascorbate (500 μg , 2.50 μmol , 0.33 eq.) in water (50 μL) was added to a solution of **31a** (10.8 mg, 10.0 μmol , 1.33 eq.) and **25** (3.30 mg, 7.5 μmol , 1 eq.) in dimethylformamide (200 μL). The solution was stirred for 30 min at rt. The addition of an equal mixture of copper(II) sulfate and sodium ascorbate in water was repeated three times. After each addition, the solution was stirred for 30 min. Compound **31** was obtained by purification of the solution via HPLC as a white solid (9.0 mg, 5.88 μmol , 78%).

$^1\text{H-NMR}$ (700 MHz, DMSO-d_6): δ [ppm] = 1.41 (s, 3 H), 1.54 (s, 3 H), 2.16 (s, 3 H), 2.16 (s, 6 H), 2.28 (s, 3 H), 2.28 (s, 6 H), 2.61 (t, $J = 6.1$ Hz, 2 H), 2.81 – 2.93 (m, 2 H), 3.45 – 3.54 (m, 12 H), 3.73 (t, $J = 6.2$ Hz, 2 H), 4.18 (s, 1 H), 4.35 (s_{br} , 4 H), 4.38 (d, $J = 5.8$ Hz, 2 H), 4.47 (s, 2 H), 4.50 – 4.58 (m, 2 H), 5.38 (d, $J = 4.0$ Hz, 1 H), 5.50, (dd, $J = 7.8, 4.0$ Hz, 1 H), 5.72 (d, $J = 8.1$ Hz, 1 H), 7.20 (s, 2 H), 7.22 (t, $J = 7.9$ Hz, 1 H), 7.26 (t, $J = 7.2$ Hz, 1 H), 7.30 (t, $J = 7.5$ Hz, 2 H), 7.31 (t, $J = 7.9$ Hz, 2 H), 7.33 – 7.36 (m, 3 H), 7.37 (dd, $J = 8.1, 1.4$ Hz, 2 H), 7.44 (dd, $J = 7.7, 1.3$ Hz, 1 H), 7.52 (dd, $J = 7.7, 1.4$ Hz, 2 H), 7.96 (s, 1 H), 8.72 – 8.76 (m, 3 H), 8.94 (t, $J = 6.0$ Hz, 1 H), 9.16 (d, $J = 7.8$ Hz, 1 H), 9.58 (s, 1 H), 13.38 (s_{br} , 1 H).

¹³C-NMR (176 MHz, DMSO-d₆): δ [ppm] = 20.1, 20.1, 20.3, 26.6, 30.4, 35.1, 36.4, 39.1, 42.2, 45.7, 55.4, 58.1, 63.4, 63.8, 67.0, 67.2, 68.9, 69.6, 69.6, 69.7, 69.8, 70.5, 123.9, 124.6, 125.4, 125.5, 126.6, 126.6, 126.1, 126.2, 127.0, 127.5, 128.2, 130.6, 130.7, 131.8, 136.0, 137.6, 137.9, 140.1, 142.8, 142.8, 143.7, 164.5, 164.6, 167.8, 167.9, 168.3, 168.8, 168.9, 169.9, 170.0, 173.3.

C₇₃H₈₀N₁₀O₂₅S (1529.55), exact mass: 1528.5017.

ESI-HRMS (*m/z*): ([M + 2 H]²⁺/2) calc. for C₇₃H₈₂N₁₀O₂₅S: 765.2587; found: 765.2588.

Compound **32a**

6-Azidohexanoic acid (24.3 mg, 154 μmol, 5 eq.) und *N*-Hydroxysuccinimide (18.5 mg, 161 μmol, 5.2 Äq.) were dried *in vacuo* for 20 min and solved in dichloromethane (2 mL). *N,N*-Dicyclohexylcarbodiimide (33.1 mg, 161 μmol, 5.2 Äq.) was added to this solution at 0 °C. The reaction mixture was stirred for 3 h at rt and filtered over celite. Pyridine (15.0 μL, 14.7 mg, 185 μmol, 6 eq.) and daptomycin (50.0 mg, 30.9 μmol, 1 eq.), both solved in dimethyl sulfoxide (4 mL), were added to the filtered solution. The reaction mixture was stirred over night at rt, frozen in liquid nitrogen, and lyophilized. Compound **32a** was obtained by purification of the residue via HPLC as a white solid (23.6 mg, 13.4 μmol, 43%).

¹H-NMR (700 MHz, Methanol-d₄): δ [ppm] = 0.89 (t, *J* = 7.2 Hz, 3 H), 0.95 (d, *J* = 6.8 Hz, 3 H), 1.18 – 1.27 (m, 10 H), 1.23 (d, *J* = 6.5 Hz, 3 H), 1.27 – 1.32 (m, 3 H), 1.35 (d, *J* = 7.1 Hz, 3 H), 1.36 – 1.41 (m, 2 H), 1.47 – 1.52 (m, 2 H), 1.55 – 1.64 (m, 6 H), 1.65 – 1.72 (m, 1 H), 1.82 – 1.89 (m, 1 H), 2.09 – 2.15 (m, 1 H), 2.15 – 2.22 (m, 4 H), 2.23 – 2.27 (m, 1 H), 2.29 – 2.36 (d, *J* = 9.1 Hz, 1 H), 2.43 (dd, *J* = 15.6, 4.2 Hz, 1 H), 2.49 – 2.59 (m, 3 H), 2.75 (dd, *J* = 17.1, 8.7 Hz, 1 H), 2.80 (dd, *J* = 17.0, 7.5 Hz, 1 H), 2.90 – 2.96 (m, 2 H), 3.12 (dd, *J* = 14.4, 7.1 Hz, 1 H), 3.18 – 3.25 (m, 3 H), 3.28 (t, *J* = 6.9 Hz, 2 H), 3.49 (dd, *J* = 17.7, 4.5 Hz, 1 H), 3.70 (d, *J* = 14.1 Hz, 1 H), 3.74 – 3.80 (m, 2 H), 3.84 (d, *J* = 16.9 Hz, 1 H), 3.90 – 4.00 (m, 2 H), 4.17 (d, *J* = 16.8 Hz, 1 H), 4.23 (q, *J* = 7.0 Hz, 1 H), 4.33 (t, *J* = 7.3 Hz, 1 H), 4.48 (*J* = 7.7 Hz, 1 H), 4.59 (dt, *J* = 12.2, 5.8 Hz, 2 H), 4.62 – 4.64 (m, 1 H), 4.65 – 4.69 (m, 2 H), 4.78 – 4.81 (m, 1 H), 5.06 – 5.10 (m, 1 H), 5.33 – 5.37 (m, 1 H), 6.52 – 6.56 (m, 1 H), 6.70 (dd, *J* = 8.4, 0.8 Hz, 1 H), 6.97 – 7.01 (m, 1 H), 7.05 – 7.09 (m, 1 H), 7.14 (s, 1 H), 7.21 (ddd, *J* = 8.4, 7.0, 1.4 Hz, 1 H), 7.32 (d, *J* = 8.1 Hz, 1 H), 7.55 (d, *J* = 7.9 Hz, 1 H), 7.65 (d, *J* = 8.2 Hz, 1 H).

¹³C-NMR (176 MHz, Methanol-*d*₄): δ [ppm] = 14.6, 15.7, 16.4, 17.3, 23.9, 26.7, 26.8, 26.9, 27.6, 28.3, 29.7, 29.8, 30.5, 30.6, 30.7, 33.2, 34.5, 36.2, 36.2, 36.4, 36.8, 37.0, 37.2, 39.5, 39.9, 42.7, 43.8, 44.3, 48.9, 49.8, 50.7, 51.2, 51.4, 51.9, 52.3, 52.5, 55.5, 56.4, 57.4, 57.7, 63.6, 72.1, 110.8, 112.5, 116.6, 118.0, 118.5, 119.5, 120.0, 122.6, 125.0, 128.9, 132.5, 136.3, 138.1, 152.9, 171.0, 171.6, 171.8, 172.3, 172.4, 172.7, 172.9, 173.4, 173.8, 173.8, 173.9, 174.2, 174.2, 174.4, 174.9, 175.1, 175.8, 176.2, 176.2, 176.6, 200.6.

C₇₈H₁₁₀N₂₀O₂₇ (1759.85), exact mass: 1758.7849.

ESI-HRMS (*m/z*): ([M + 2 H]²⁺/2) calc. for C₇₈H₁₁₂N₂₀O₂₇: 880.4003; found.: 880.4005.

Compound **32**

A mixture of copper(II) sulfate (680 μg, 4.25 μmol, 0.5 eq.) and sodium ascorbate (1.69 mg, 8.50 μmol, 1 eq.) in water (50 μL) was added to a solution of **23** 11.6 mg, 17.0 μmol, 2 eq.) and **32a** (15.0 mg, 8.50 μmol, 1 eq.) in water (1 mL) and dimethylformamide (300 μL). The solution was stirred for 30 min at rt. The addition of an equal mixture of copper(II) sulfate and sodium ascorbate in water was repeated three times. After each addition, the solution was stirred for 30 min. Compound **32** was obtained by purification of the solution via HPLC as a white solid (16.9 mg, 6.93 μmol, 82%).

¹H-NMR (700 MHz, Methanol-*d*₄): δ [ppm] = 0.88 (t, *J* = 7.2 Hz, 3 H), 0.94 (d, *J* = 6.8 Hz, 3 H), 1.15 – 1.31 (m, 18 H), 1.33 (d, *J* = 7.1 Hz, 3 H), 1.45 – 1.51 (m, 2 H), 1.51 – 1.55 (m, 1 H), 1.55 – 1.61 (m, 3 H), 1.63 – 1.69 (m, 1 H), 1.79 – 1.87 (m, 3 H), 1.99 – 2.05 (m, 2 H), 2.09 – 2.19 (m, 5 H), 2.22 – 2.26 (m, 1 H), 2.35 (s_{br}, 1 H), 2.43 (dd, *J* = 15.7, 4.3 Hz, 1 H), 2.49 – 2.60 (m, 5 H), 2.71 – 2.82 (m, 4 H), 2.89 (dd, *J* = 17.1, 4.7 Hz, 1 H), 2.94 (dd, *J* = 17.0, 5.9 Hz, 1 H), 3.12 (dd, *J* = 14.3, 7.2 Hz, 1 H), 3.16 (t, *J* = 7.0 Hz, 2 H), 3.22 (dd, *J* = 114.2, 7.9 Hz, 1 H), 3.47 (dd, *J* = 17.6, 4.3 Hz, 1 H), 3.68 (d, *J* = 14.7 Hz, 1 H), 3.74 – 3.79 (m, 2 H), 3.87 (t, *J* = 15.1 Hz, 2 H), 3.94 (d, *J* = 16.9 Hz, 1 H), 4.13 (d, *J* = 18.2 Hz, 1 H), 4.22 (q, *J* = 7.0 Hz, 1 H), 4.28 – 4.34 (m, 3 H), 4.47 (t, *J* = 7.6 Hz, 1 H), 4.51 – 4.58 (m, 7 H), 4.60 (t, *J* = 5.6 Hz, 1 H), 4.62 – 4.67 (m, 3 H), 4.77 – 4.80 (m, 1 H), 5.04 – 5.09 (m, 1 H), 5.32 – 5.37 (m, 1 H), 6.53 (t, *J* = 7.6 Hz, 1 H), 6.55 (t, *J* = 8.8 Hz, 1 H), 6.68 (t, *J* = 7.9 Hz, 3 H), 6.90 (dd, *J* = 7.8, 1.4 Hz, 1 H), 6.92 (dd, *J* = 7.8, 1.3 Hz, 2 H), 6.98 (t, *J* = 7.2 Hz, 1 H), 7.06 (t, *J* = 7.6 Hz, 1 H), 7.13 (s, 1 H), 7.15 (dd, *J* = 8.1, 1.2 Hz, 1 H), 7.18 (dd, *J* = 8.1, 1.1 Hz, 2 H), 7.19 – 7.22 (m, 1 H), 7.31 (d, *J* = 7.6 Hz, 1 H), 7.38 (s, 2 H), 7.54 (d, *J* = 7.9 Hz, 1 H), 7.64 (d, *J* = 8.4 Hz, 1 H), 7.65 (s, 1 H).

¹³C-NMR (176 MHz, Methanol-d₄): δ [ppm] = 14.6, 15.7, 16.5, 17.4, 23.9, 26.0, 26.4, 26.6, 26.8, 26.9, 27.1, 28.3, 29.7, 30.5, 30.6, 30.7, 31.1, 33.2, 34.5, 36.4, 36.5, 36.8, 37.0, 39.5, 39.9, 41.1, 42.6, 43.6, 43.8, 44.3, 48.9, 49.9, 50.8, 51.1, 51.3, 51.4, 51.9, 52.4, 55.5, 56.6, 57.4, 57.8, 63.5, 72.2, 110.8, 112.5, 116.6, 116.7, 116.7, 118.1, 118.5, 118.8, 118.9, 119.5, 119.8, 119.9, 120.0, 122.6, 123.6, 125.0, 128.4, 128.9, 132.5, 133.9, 136.2, 137.6, 138.1, 140.1, 147.4, 147.5, 148.5, 150.5, 152.8, 171.0, 171.6, 171.7, 171.8, 171.9, 172.3, 172.5, 172.7, 173.0, 173.4, 173.8, 174.0, 174.3, 174.4, 174.9, 175.1, 175.7, 175.8, 176.1, 176.3, 176.6, 200.6.

C₁₁₄H₁₄₄N₂₄O₃₇ (2442.54), exact mass: 2441.0124. **ESI-HRMS** (*m/z*): ([M + 2 H]²⁺/2) calc. for C₁₁₄H₁₄₆N₂₄O₃₇: 1222.0157; found.: 1222.0159.

Abbreviations

Amp,	ampicillin;
Amox,	amoxicillin;
Cef,	cefiderocol;
Dapto,	daptomycin;
Ent,	Enterobactin;
MIC,	minimal inhibitory concentration.

Funding

This project was funded by the DFG (grant number: BR 3572/4-1) and the Joint Program Initiative on Antimicrobial Resistance (JPI AMR, grant number: 01KI1825). C.P. thanks the “Fonds der chemischen Industrie” for a scholarship.

Acknowledgments

The authors thank Christel Kakoschke and Ulrike Beutling for their support with NMR and HRMS analytics and Tanja Schickschneit for microbiological experiments.

References

1. Tacconelli, E.; Carrara, E.; Savoldi, A.; Harbarth, S.; Mendelson, M.; Monnet, D. L.; Pulcini, C.; Kahlmeter, G.; Kluytmans, J.; Carmeli, Y.; Ouellette, M.; Outtersson, K.; Patel, J.; Cavalieri, M.; Cox, E. M.; Houchens, C. R.; Grayson, M. L.; Hansen, P.; Singh, N.; Theuretzbacher, U.; Magrini, N.; Aboderin, A. O.; Al-Abri, S. S.; Awang Jalil, N.; Benzonana, N.; Bhattacharya, S.; Brink, A. J.; Burkert, F. R.; Cars, O.; Cornaglia, G.; Dyar, O. J.; Friedrich, A. W.; Gales, A. C.; Gandra, S.; Giske, C. G.; Goff, D. A.; Goossens, H.; Gottlieb, T.; Guzman Blanco, M.; Hryniewicz, W.; Kattula, D.; Jinks, T.; Kanj, S. S.; Kerr, L.; Kieny, M.-P.; Kim, Y. S.; Kozlov, R. S.; Labarca, J.; Laxminarayan, R.; Leder, K.; Leibovici, L.; Levy-Hara, G.; Littman, J.; Malhotra-Kumar, S.; Manchanda, V.; Moja, L.; Ndoye, B.; Pan, A.; Paterson, D. L.; Paul, M.; Qiu, H.; Ramon-Pardo, P.; Rodríguez-Baño, J.; Sanguinetti, M.; Sengupta, S.; Sharland, M.; Si-Mehand, M.; Silver, L. L.; Song, W.; Steinbakk, M.; Thomsen, J.; Thwaites, G. E.; van der Meer, J. W. M.; Van Kinh, N.; Vega, S.; Villegas, M. V.; Wechsler-Fördös, A.; Wertheim, H. F. L.; Wesangula, E.; Woodford, N.; Yilmaz, F. O.; Zorzet, A., Discovery, research, and development of new antibiotics: the WHO priority list of antibiotic-resistant bacteria and tuberculosis. *Lancet. Infect. Dis.* **2018**, *18* (3), 318 – 327.
2. Theuretzbacher, U.; Gottwalt, S.; Beyer, P.; Butler, M.; Czaplewski, L.; Lienhardt, C.; Moja, L.; Paul, M.; Paulin, S.; Rex, J. H.; Silver, L. L.; Spigelman, M.; Thwaites, G. E.; Paccaud, J. P.; Harbarth, S., Analysis of the clinical antibacterial and antituberculosis pipeline. *Lancet Infect. Dis.* **2019**, *19* (2), e40-e50.
3. Zgurskaya, H. I.; Rybenkov, V. V., Permeability barriers of Gram-negative pathogens. *Ann. Acad. Sci.* **2020**, *1459* (1), 5-18.
4. Masi, M.; Refregiers, M.; Pos, K. M.; Pages, J. M., Mechanisms of envelope permeability and antibiotic influx and efflux in Gram-negative bacteria. *Nat. Microbiol.* **2017**, *2*, 17001.
5. Bassetti, M.; Ginocchio, F.; Mikulska, M., New treatment options against gram-negative organisms. *Crit. Care* **2011**, *15*, 215.
6. Hider, R. C.; Kong, X., Chemistry and biology of siderophores. *Nat. Prod. Rep.* **2010**, *27* (5), 637-657.
7. Krewulak, K. D.; Vogel, H. J., Structural biology of bacterial iron uptake. *Biochim. Biophys. Acta* **2008**, *1778* (9), 1781-1804.
8. Miethke, M.; Marahiel, M. A., Siderophore-based iron acquisition and pathogen control. *Microbiol. Mol. Biol. Rev.* **2007**, *71* (3), 413 – 451.

9. Gorska, A.; Sloderbach, A.; Marszall, M. P., Siderophore-drug complexes: potential medicinal applications of the 'Trojan horse' strategy. *Trends Pharmacol. Sci.* **2014**, *35* (9), 442 – 449.
10. Negash, K. H.; Norris, J. K. S.; Hodgkinson, J. T., Siderophore-antibiotic conjugate design: New drugs for bad bugs? *Molecules* **2019**, *24* (18).
11. Klahn, P.; Bronstrup, M., Bifunctional antimicrobial conjugates and hybrid antimicrobials. *Nat. Prod. Rep.* **2017**, *34* (7), 832-885.
12. Wu, J. Y.; Srinivas, P.; Pogue, J. M., Cefiderocol: A novel agent for the management of multidrug-resistant Gram-negative organisms. *Infect. Dis. Ther.* **2020**, *9* (1), 17 – 40.
13. Portsmouth, S.; van Veenhuizen, D.; Echols, R.; Machida, M.; Ferreira, J. C. A.; Ariyasu, M.; Tenke, P.; Nagata, T. D., Cefiderocol versus imipenem-cilastatin for the treatment of complicated urinary tract infections caused by Gram-negative uropathogens: a phase 2, randomised, double-blind, non-inferiority trial. *Lancet Infect. Dis.* **2018**, *18* (12), 1319-1328.
14. Pollack, J. R.; Neilands, J., Enterobactin, an iron transport compound from *Salmonella typhimurium*. *Biochem. Biophys. Res. Commun.* **1970**, *38* (5), 989 – 992.
15. Raymond, K. N.; Dertz, E. A.; Kim, S. S., Enterobactin: an archetype for microbial iron transport. *Proc. Natl. Acad. Sci. U.S.A.* **2003**, *100* (7), 3584 – 3588.
16. Perraud, Q.; Moynie, L.; Gasser, V.; Munier, M.; Godet, J.; Hoegy, F.; Mely, Y.; Mislin, G. L. A.; Naismith, J. H.; Schalk, I. J., A key role for the periplasmic PfeE esterase in iron acquisition via the siderophore enterobactin in *Pseudomonas aeruginosa*. *ACS Chem. Biol.* **2018**, *13* (9), 2603 – 2614.
17. Zheng, T.; Nolan, E. M., Evaluation of (acyloxy)alkyl ester linkers for antibiotic release from siderophore-antibiotic conjugates. *Bioorg. Med. Chem. Lett.* **2015**, *25* (21), 4987 – 4991.
18. Raines, D. J.; Moroz, O. V.; Blagova, E. V.; Turkenburg, J. P.; Wilson, K. S.; Duhme-Klair, A. K., Bacteria in an intense competition for iron: Key component of the *Campylobacter jejuni* iron uptake system scavenges enterobactin hydrolysis product. *Proc. Natl. Acad. Sci.* **2016**, *113* (21), 5850-5855.
19. Neumann, W.; Sassone-Corsi, M.; Raffatellu, M.; Nolan, E. M., Esterase-catalyzed siderophore hydrolysis activates an enterobactin-ciprofloxacin conjugate and confers targeted antibacterial activity. *J. Am. Chem. Soc.* **2018**, *140* (15), 5193 – 5201.

20. Zheng, T.; Nolan, E. M., Enterobactin-mediated delivery of beta-lactam antibiotics enhances antibacterial activity against pathogenic *Escherichia coli*. *J. Am. Chem. Soc.* **2014**, *136* (27), 9677-9691.
21. Paulen, A.; Hoegy, F.; Roche, B.; Schalk, I. J.; Mislin, G. L. A., Synthesis of conjugates between oxazolidinone antibiotics and a pyochelin analogue. *Bioorg. Med. Chem. Lett.* **2017**, *27* (21), 4867 – 4870.
22. Ghosh, M.; Miller, P. A.; Mollmann, U.; Claypool, W. D.; Schroeder, V. A.; Wolter, W. R.; Suckow, M.; Yu, H.; Li, S.; Huang, W.; Zajicek, J.; Miller, M. J., Targeted antibiotic delivery: selective siderophore conjugation with daptomycin confers potent activity against multidrug resistant *Acinetobacter baumannii* both *in vitro* and *in vivo*. *J. Med. Chem.* **2017**, *60* (11), 4577 – 4583.
23. Liu, R.; Miller, P. A.; Vakulenko, S. B.; Stewart, N. K.; Boggess, W. C.; Miller, M. J., A synthetic dual drug sideromycin induces gram-negative bacteria to commit suicide with a Gram-positive antibiotic. *J. Med. Chem.* **2018**, *61* (9), 3845 – 3854.
24. Ji, C.; Miller, M. J., Chemical syntheses and *in vitro* antibacterial activity of two desferrioxamine B-ciprofloxacin conjugates with potential esterase and phosphatase triggered drug release linkers. *Bioorg. Med. Chem.* **2012**, *20* (12), 3828-3836.
25. Ferreira, K.; Hu, H. Y.; Fetz, V.; Prochnow, H.; Rais, B.; Muller, P. P.; Bronstrup, M., Multivalent Siderophore-DOTAM conjugates as theranostics for imaging and treatment of bacterial infections. *Angew. Chem. Int. Ed.* **2017**, *56* (28), 8272-8276.
26. Ohi, N.; Aoki, B.; Kuroki, T.; Matsumoto, M.; Kojima, K.; Nehashi, T., Semisynthetic beta-lactam antibiotics. III. Effect on antibacterial activity and comt-susceptibility of chlorine-introduction into the catechol nucleus of 6-[(R)-2-[3-(3,4-dihydroxybenzoyl)-3-(3-hydroxypropyl)-1-ureido]-2- phenylacetamido]penicillanic acid. *J. Antibiot.* **1987**, *40* (1), 22-28.
27. Harris, W. R.; Weigl, F. L.; Raymond, K. N., Synthesis and evaluation of an enterobactin model compound. 1,3,5-tris-(2,3-dihydroxybenzoylamino)methyl)benzene and its iron(III) complex. *J. Chem. Soc.* **1979**, (4), 177 – 178.
28. Venuti, M. C.; Rastetter, W. H.; Neilands, J. B., 1,3,5-Tris(N,N',N''-2,3-dihydroxybenzoyl)amino-methylbenzene, a synthetic iron chelator related to enterobactin. *J. Med. Chem.* **1979**, *22* (2), 123 – 124.
29. Heidinger, S.; Braun, V.; Pecoraro, V. L.; Raymond, K. N., Iron supply to *Escherichia coli* by synthetic analogs of enterochelin. *J. Bacteriol.* **1983**, *153* (1), 109 – 115.

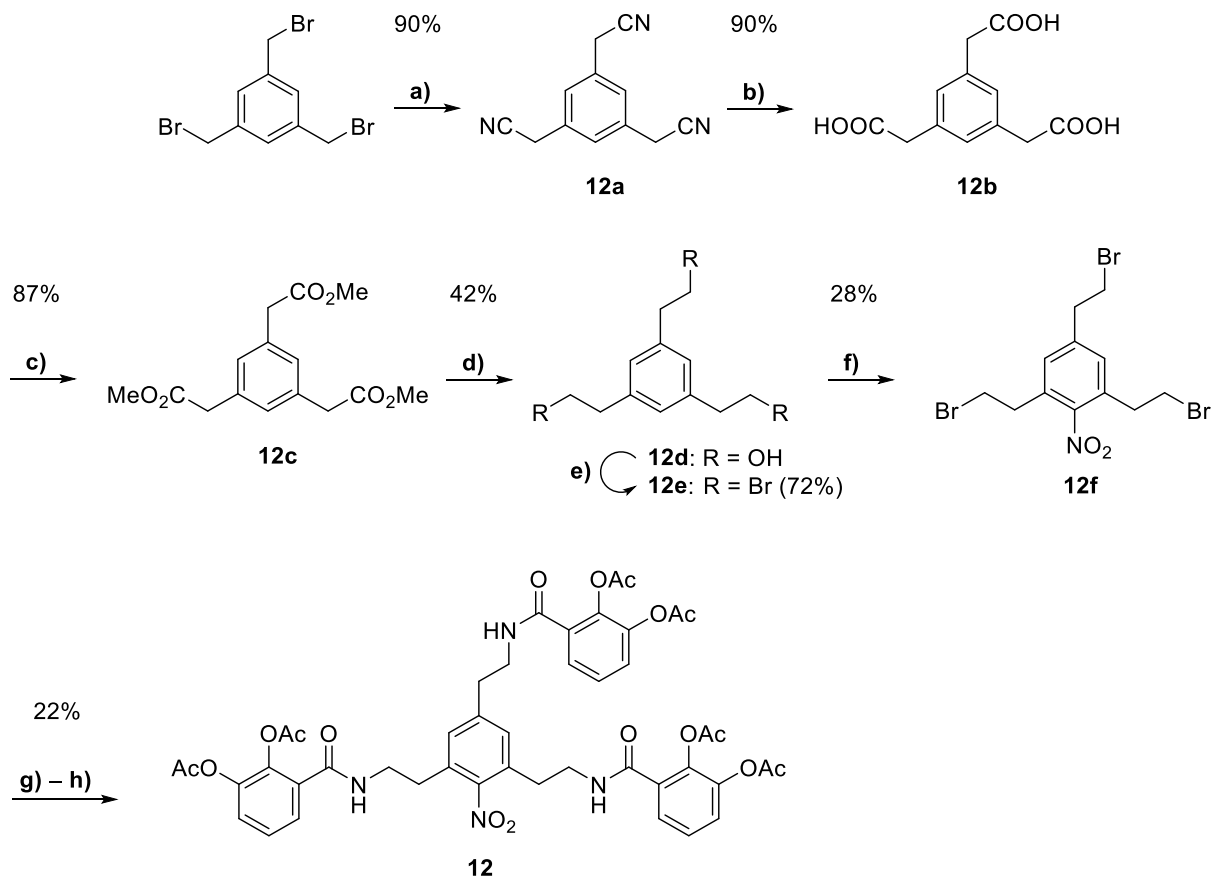
30. Matzanke, B. F.; Ecker, D. J.; Yang, T. S.; Huynh, B. H.; Muller, G.; Raymond, K. N., *Escherichia coli* iron enterobactin uptake monitored by Mossbauer spectroscopy. *J. Bacteriol.* **1986**, *167* (2), 674 – 680.
31. Kong, H.; Cheng, W.; Wei, H.; Yuan, Y.; Yang, Z.; Zhang, X., An overview of recent progress in siderophore-antibiotic conjugates. *Eur. J. Med. Chem.* **2019**, *182*, 111615.
32. Tao, J.; Perdew, J. P.; Staroverov, V. N.; Scuseria, G. E., Climbing the density functional ladder: nonempirical meta-generalized gradient approximation designed for molecules and solids. *Phys. Rev. Lett.* **2003**, *91* (14), 146401.
33. Grunenberg, J., The interstitial carbon of the nitrogenase FeMo cofactor is far better stabilized than previously assumed. *Angew. Chem. Int. Ed.* **2017**, *56* (25), 7288-7291.
34. Markopoulos, G.; Grunenberg, J., Predicting kinetically unstable C-C bonds from the ground-state properties of a molecule. *Angew. Chem. Int. Ed.* **2013**, *52* (40), 10648-10651.
35. Abergel, R. J.; Warner, J. A.; Shuh, D. K.; Raymond, K. N., Enterobactin protonation and iron release: structural characterization of the salicylate coordination shift in ferric enterobactin. *J. Am. Chem. Soc.* **2006**, *128* (27), 8920 – 8931.
36. Zscherp, R.; Coetzee, J.; Vornweg, J.; Grunenberg, J.; Herrmann, J.; Müller, R.; Klahn, P., Biomimetic enterobactin analogue mediates iron-uptake and cargo transport into *E. coli* and *P. aeruginosa*. *Chem. Sci.* **2021**, *12*, 10179-10190.
37. Prochnow, H.; Fetz, V.; Hotop, S. K.; García-Rivera, M. A.; Heumann, A.; Brönstrup, M., Subcellular quantification of uptake in Gram-negative bacteria. *Anal. Chem.* **2019**, *91* (3), 1863-1872.
38. Ghosh, M.; Lin, Y.-M.; Miller, P. A.; Möllmann, U.; Boggess, W. C.; Miller, M. J., Siderophore conjugates of daptomycin are potent inhibitors of carbapenem resistant strains of *Acinetobacter baumannii*. *ACS Infect. Dis.* **2018**, *4* (10), 1529 – 1535.
39. El-Mady, A.; Mortensen, J. E., The bactericidal activity of ampicillin, daptomycin, and vancomycin against ampicillin-resistant *Enterococcus faecium*. *Diag. Mic. Inf. Dis.* **1991**, *14* (2), 141 – 145.
40. Sato, T.; Yamawaki, K., Cefiderocol: Discovery, chemistry, and *in vivo* profiles of a novel siderophore cephalosporin. *Clin. Infect. Dis.* **2019**, *69* (Suppl 7), S538-S543.
41. Puustinen, A.; Finel, M.; Haltia, T.; Gennis, R. B.; Wikstrom, M., Properties of the two terminal oxidases of *Escherichia coli*. *Biochemistry* **1991**, *30* (16), 3936-3942.

42. Thomas, J. W.; Puustinen, A.; Alben, J. O.; Gennis, R. B.; Wikstrom, M., Substitution of asparagine for aspartate-135 in subunit I of the cytochrome bo ubiquinol oxidase of *Escherichia coli* eliminates proton-pumping activity. *Biochemistry* **1993**, 32 (40), 10923-10928.
43. Abramson, J.; Riistama, S.; Larsson, G.; Jasaitis, A.; Svensson-Ek, M.; Laakkonen, L.; Puustinen, A.; Iwata, S.; Wikström, M., The structure of the ubiquinol oxidase from *Escherichia coli* and its ubiquinone binding site. *Nat. Struc. Biol.* **2000**, 7 (10), 910-917.
44. Braun, V., Surface signaling: novel transcription initiation mechanism starting from the cell surface. *Arch. Microbiol.* **1997**, 167 (6), 325-331.
45. Faraldo-Gómez, J. D.; Sansom, M. S., Acquisition of siderophores in gram-negative bacteria. *Nat. Rev. Mol. Cell Biol.* **2003**, 4 (2), 105-116.
46. Baker, K. R.; Postle, K., Mutations in *Escherichia coli* ExbB transmembrane domains identify scaffolding and signal transduction functions and exclude participation in a proton pathway. *J. Bacteriol.* **2013**, 195 (12), 2898-2911.
47. Skare, J. T.; Ahmer, B. M.; Seachord, C. L.; Darveau, R. P.; Postle, K., Energy transduction between membranes. TonB, a cytoplasmic membrane protein, can be chemically cross-linked *in vivo* to the outer membrane receptor FepA. *J. Biol. Chem.* **1993**, 268 (22), 16302-16308.
48. Shaik, S.; Kumar, D.; de Visser, S. P.; Altun, A.; Thiel, W., Theoretical perspective on the structure and mechanism of cytochrome P450 enzymes. *Chem. Rev.* **2005**, 105 (6), 2279-2328.
49. Kim, A.; Kutschke, A.; Ehmann, D. E.; Patey, S. A.; Crandon, J. L.; Gorseth, E.; Miller, A. A.; McLaughlin, R. E.; Blinn, C. M.; Chen, A.; Nayar, A. S.; Dangel, B.; Tsai, A. S.; Rooney, M. T.; Murphy-Benenato, K. E.; Eakin, A. E.; Nicolau, D. P., Pharmacodynamic Profiling of a siderophore-conjugated monocarbam in *Pseudomonas aeruginosa*: assessing the risk for resistance and attenuated efficacy. *Antimicrob. Agents Chemother.* **2015**, 59 (12), 7743-7752.
50. Tomaras, A. P.; Crandon, J. L.; McPherson, C. J.; Banevicius, M. A.; Finegan, S. M.; Irvine, R. L.; Brown, M. F.; O'Donnell, J. P.; Nicolau, D. P., Adaptation-based resistance to siderophore-conjugated antibacterial agents by *Pseudomonas aeruginosa*. *Antimicrob. Agents Chemother.* **2013**, 57 (9), 4197-4207.
51. Kopp, D. R.; Postle, K., The intrinsically disordered region of ExbD is required for signal transduction. *J. Bacteriol.* **2020**, 202 (7).

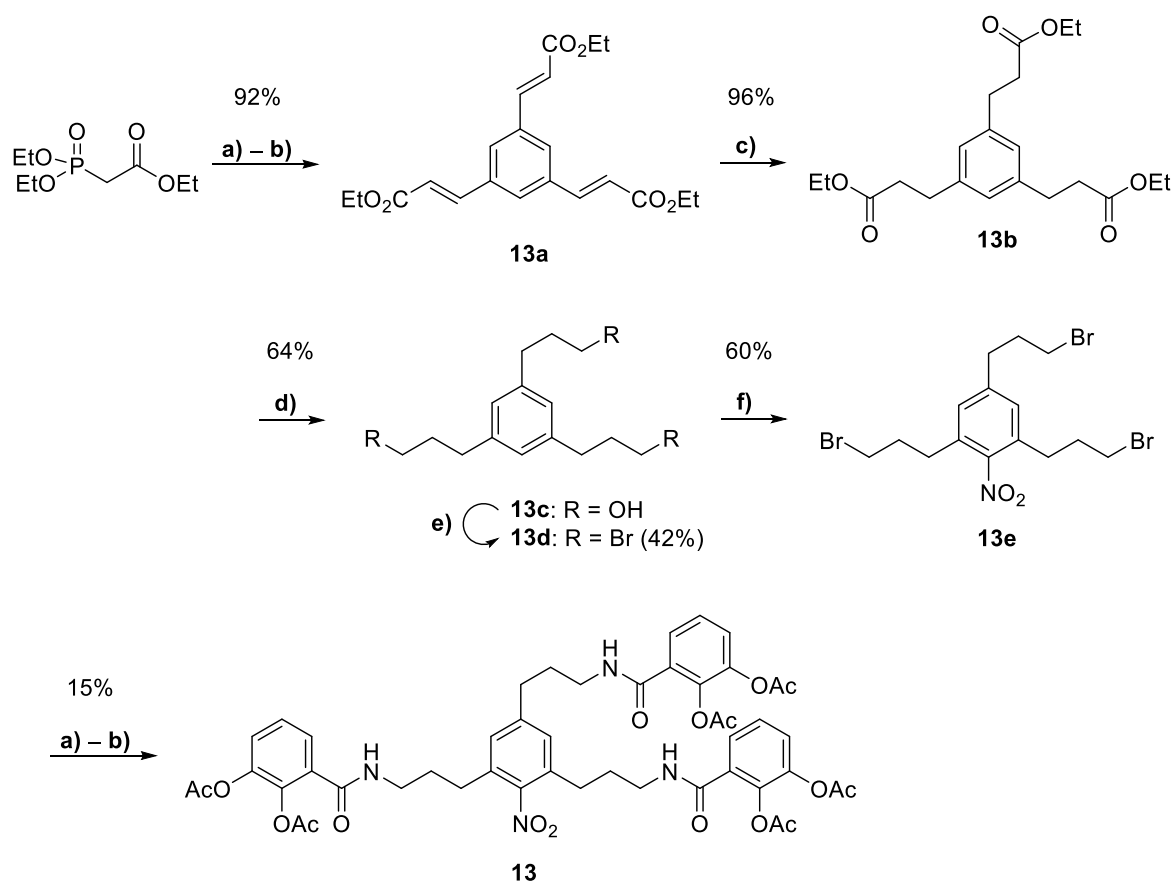
52. Wikström, M.; Bogachev, A.; Finel, M.; Morgan, J. E.; Puustinen, A.; Raitio, M.; Verkhovskaya, M.; Verkhovsky, M. I., Mechanism of proton translocation by the respiratory oxidases. The histidine cycle. *Biochim. Biophys. Acta* **1994**, *1187* (2), 106-111.
53. Price, C. E.; Driessen, A. J. M., Biogenesis of membrane bound respiratory complexes in *Escherichia coli*. *Biochim. Biophys. Acta, Mol. Cell Res.* **2010**, *1803* (6), 748-766.
54. Keren, I.; Kaldalu, N.; Spoering, A.; Wang, Y.; Lewis, K., Persister cells and tolerance to antimicrobials. *FEMS Microbiol. Lett.* **2004**, *230* (1), 13-18.
55. Lázár, V.; Pal Singh, G.; Spohn, R.; Nagy, I.; Horváth, B.; Hrtyan, M.; Busa-Fekete, R.; Bogos, B.; Méhi, O.; Csörgő, B.; Pósfai, G.; Fekete, G.; Szappanos, B.; Kégl, B.; Papp, B.; Pál, C., Bacterial evolution of antibiotic hypersensitivity. *Mol. Syst. Biol.*

Supplementary Information

Schemes, Figures and Tables

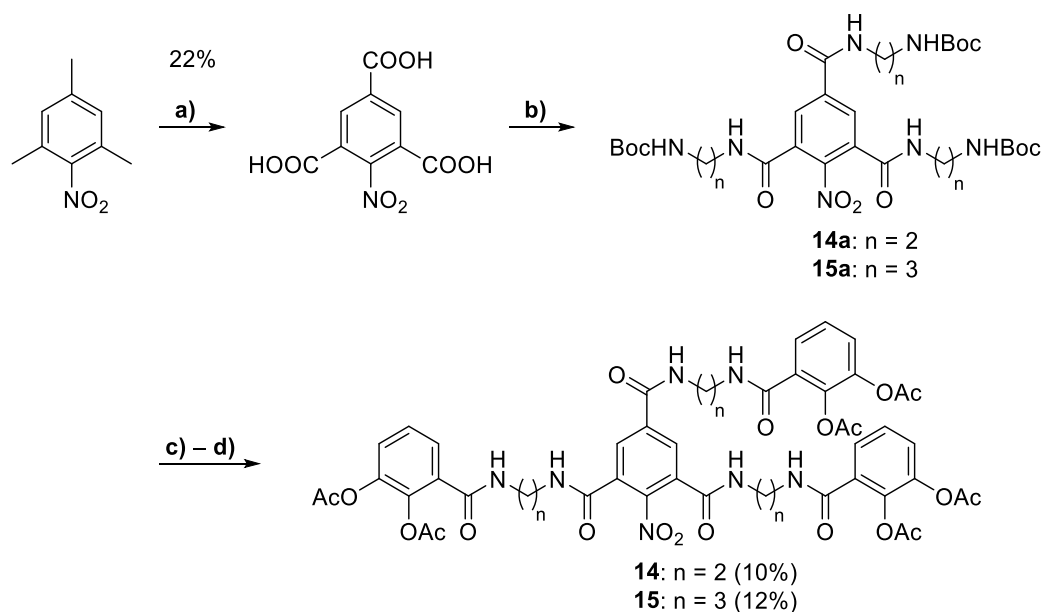
Scheme S4.1. Synthesis of **12**.

Reagents and conditions: a) NaCN, NaHCO₃, THF, H₂O, rt, 3 h; b) NaOH(aq), EtOH, 100 °C, 1 d; c) TMOF, H₂SO₄, MeOH, 72 °C, 18 h; d) LiAlH₄, THF, rt, 4 h; e) HBr(aq), 125 °C, 5 h; f) HNO₃, H₂SO₄, 0 °C, 2 h; g) NH₃(aq), EtOH, THF, 90 °C, 1 d; h) 6, KHCO₃, H₂O, 1,4-dioxane, 0 °C \rightarrow rt. Related to scheme 2.



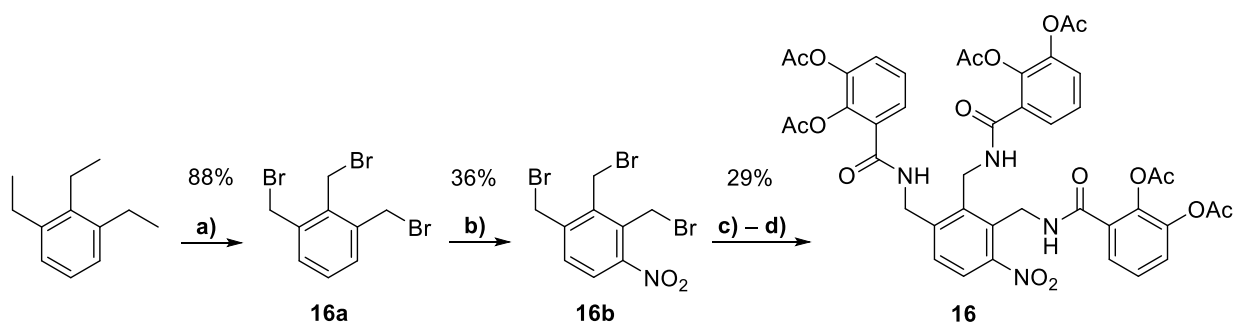
Scheme S4.1. Synthesis of **13**.

Reagents and conditions: a) NaH, THF 0 °C, → rt, 45 min; b) Trimesaldehyde, THF, 0 °C → rt, 1 d; c) H₂, Pd/C, MeOH, rt, 1 d; d) LiAlH₄, THF, 0 °C → rt; e) PBr₂Ph₃, CH₂Cl₂, rt, 1 d; f) HNO₃, H₂SO₄, 0 °C → rt, 16 h; g) NH₃(aq), EtOH, THF, 90 °C, 1 d; h) **6**, KHCO₃, H₂O, 1,4-dioxane, 0 °C → rt. Related to scheme 4.2.



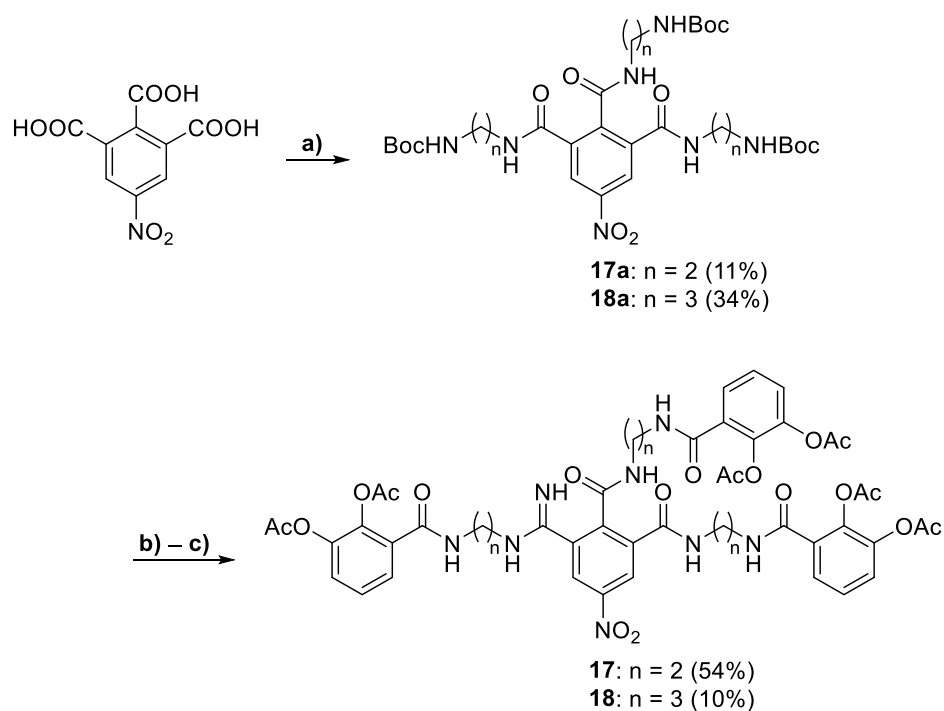
Scheme S4.2. Syntheses of **14** and **15**.

Reagents and conditions: a) KMnO_4 , NaHCO_3 , Aliquat 336, H_2O , reflux, 3 d; b) *tert*-butyl *N*-(2-aminoethyl)carbamate / *tert*-butyl *N*-(3-aminopropyl)carbamate, EDCI, HOBT, DIPEA, DMF, $0\text{ }^\circ\text{C} \rightarrow \text{rt}$, 1 d; c) TFA, CH_2Cl_2 , $0\text{ }^\circ\text{C} \rightarrow \text{rt}$, 1 h; d) **6**, KHCO_3 , H_2O , 1,4-dioxane, $0\text{ }^\circ\text{C} \rightarrow \text{rt}$. Related to scheme 2.



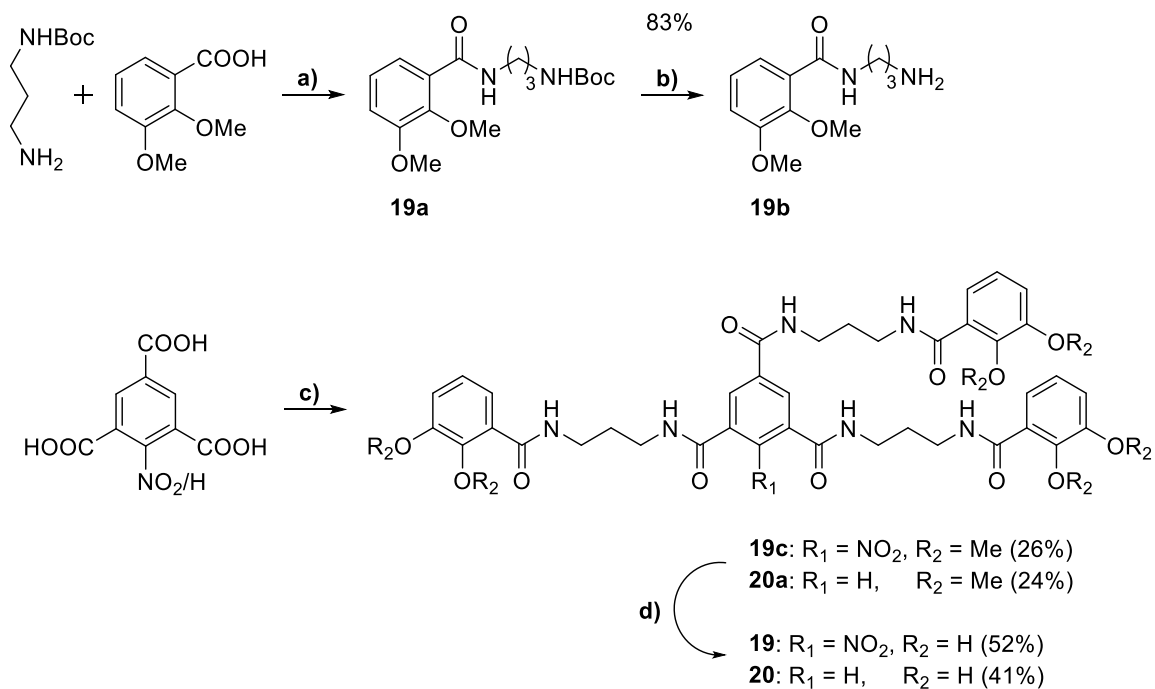
Scheme S4.3. Synthesis of **16**.

Reagents and conditions: a) NBS, hv, CCl_4 , $80\text{ }^\circ\text{C}$, 1 d; b) HNO_3 , CH_2Cl_2 , $-40\text{ }^\circ\text{C}$, 2 h; c) $\text{NH}_3(\text{aq})$, EtOH, THF, rt, 2.5 h; d) **6**, KHCO_3 , H_2O , 1,4-dioxane, $0\text{ }^\circ\text{C} \rightarrow \text{rt}$. Related to scheme 4.2.



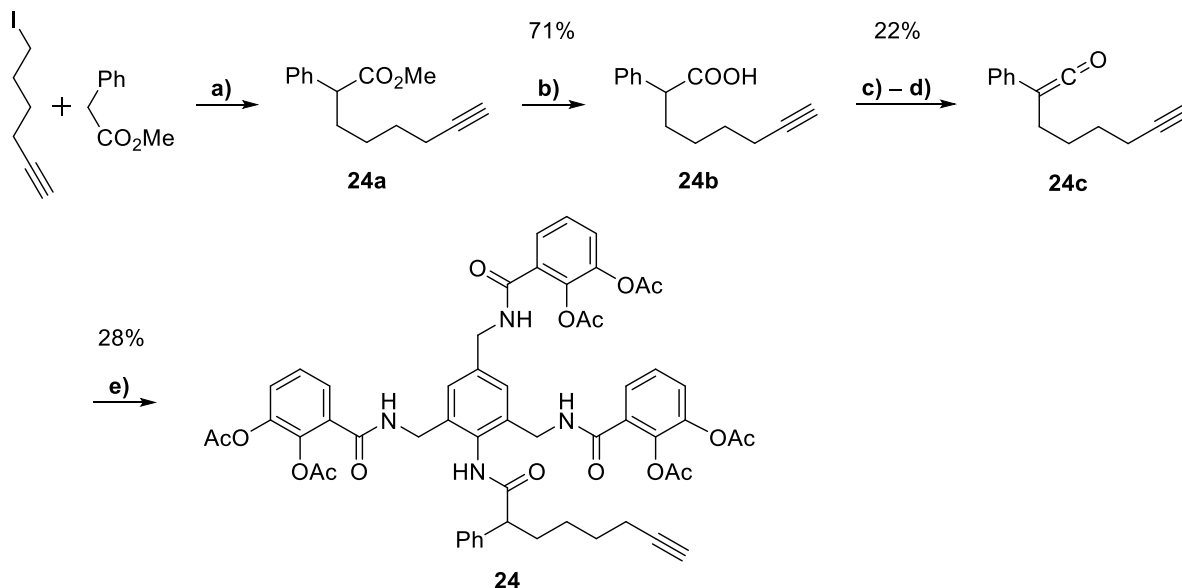
Scheme S4.4. Syntheses of **17** and **18**.

Reagents and conditions: a) $(\text{COCl})_2$, DMF CH_2Cl_2 , $0\text{ }^\circ\text{C} \rightarrow \text{rt}$, 1.5 h, *tert*-butyl *N*-(2-aminoethyl)carbamate / *tert*-butyl *N*-(3-aminopropyl)carbamate; b) TFA, CH_2Cl_2 , $0\text{ }^\circ\text{C} \rightarrow \text{rt}$, 1 h; c) 6, KHCO_3 , H_2O , 1,4-dioxane, $0\text{ }^\circ\text{C} \rightarrow \text{rt}$. Related to scheme 4.2.



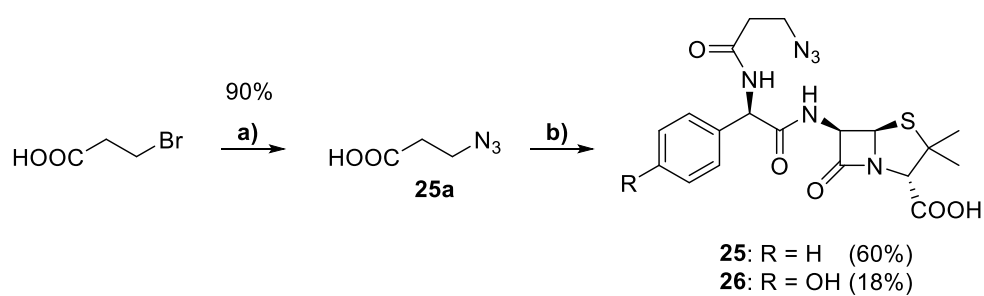
Scheme S4.5. Synthesis of **19** and **20**.

Reagents and conditions: a) EDCI, HOBT, DMF, 0 °C → rt, 2.5 h; b) HCl(aq), 0 °C → rt, 2 h; c) **19b**, EDCI; HOBT, DMF, 0 °C → rt, 1 d; d) BBr_3 , CH_2Cl_2 , -78 °C → rt, 1 d. Related to scheme 4.2.



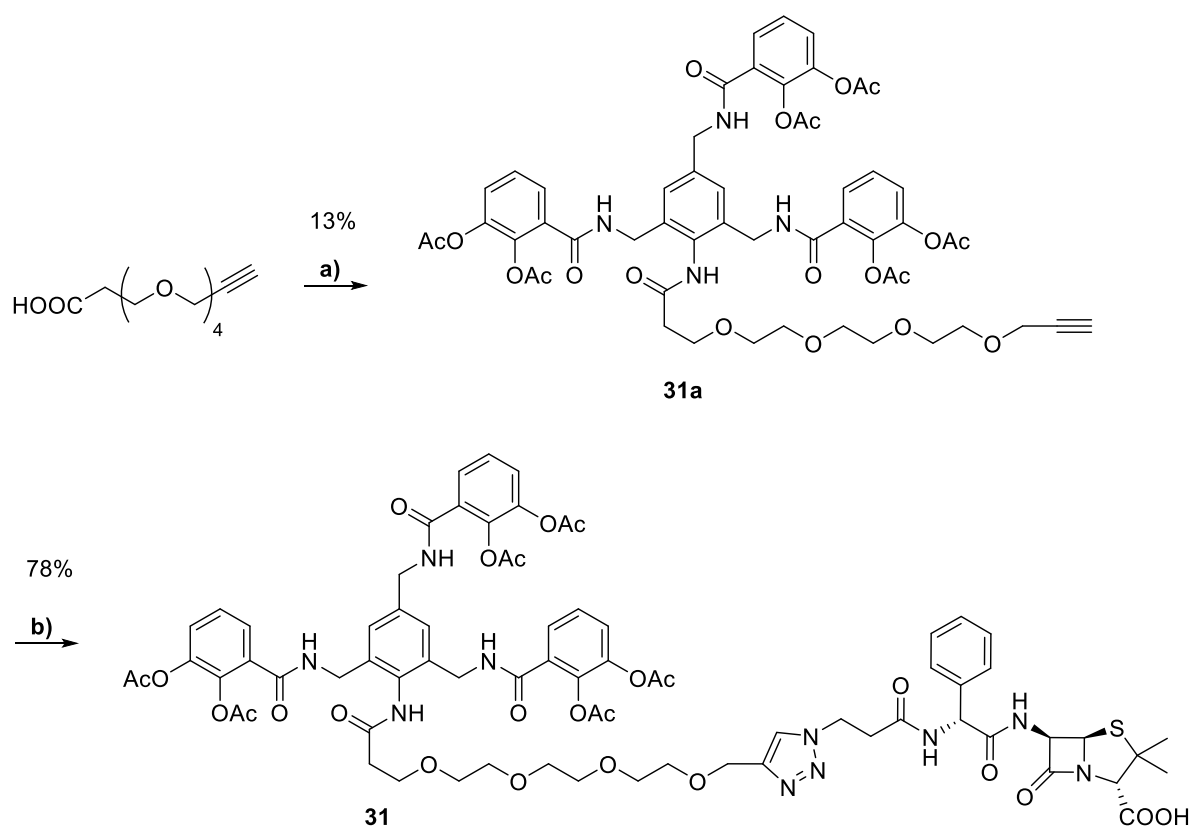
Scheme S4.6. Synthesis of **24**.

Reagents and conditions: a) LiHMDS, THF, -50 °C → -20 °C → 0 °C, 2.5 h; b) KOH, MeOH, reflux, 1 d; c) $(\text{COCl})_2$, DMF, CH_2Cl_2 , rt, 1 h; d) Et_3N , THF; 0 °C, 2 h; e) **19**, THF, 0 °C → rt, 2 d. Related to scheme 3



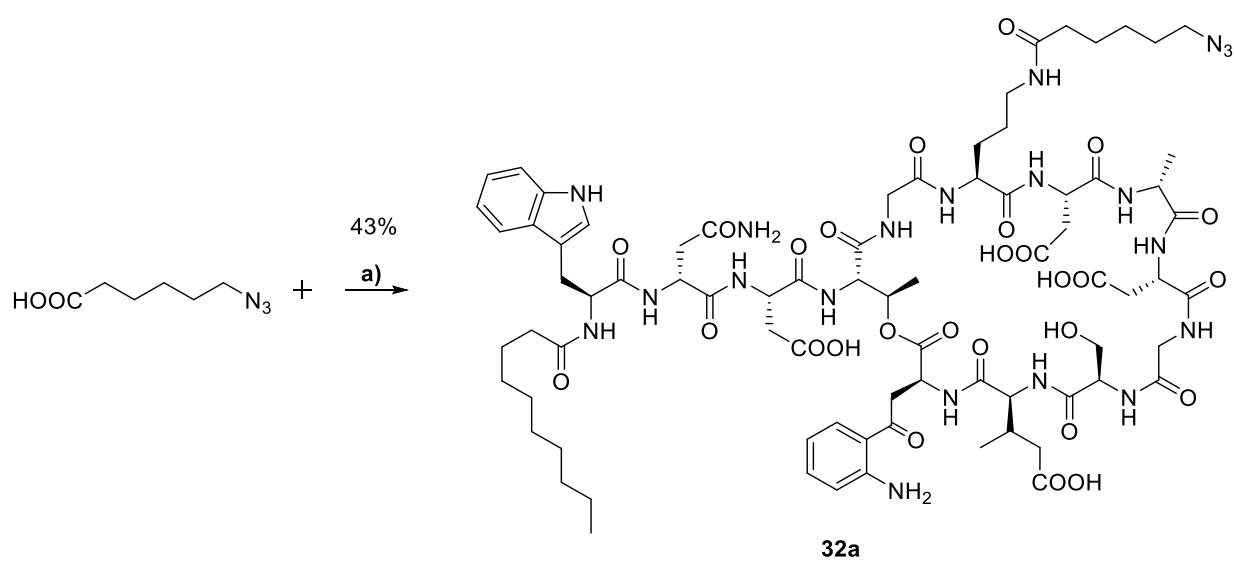
Scheme S4.7. Syntheses of **25** and **26**.

Reagents and conditions: a) NaN₃, H₂O, rt, 4 d; b) NMM, isobutyl chloroformate, ampicillin/amoxicillin, THF, 0 °C → rt, 4 h. Related to scheme 4.3.



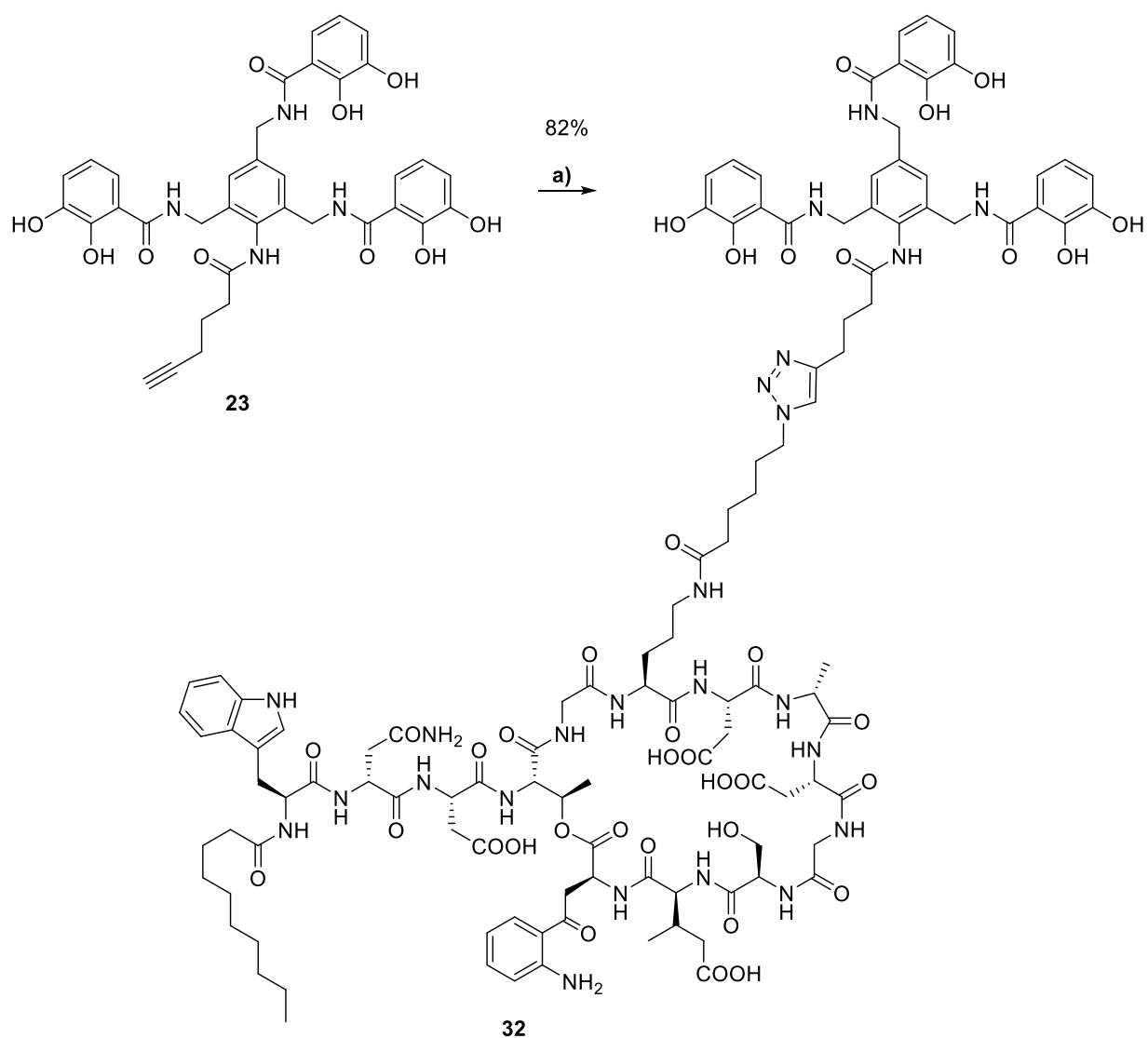
Scheme S4.8. Synthesis of **31**.

Reagents and conditions: a) **21**, isobutyl chloroformate, NMM, THF, 0 °C → rt, 1 d; b) **25**, CuSO₄, sodium ascorbate, H₂O, DMF, rt, 2 h. Related to scheme 4.3.

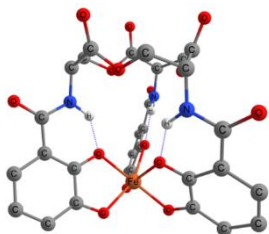
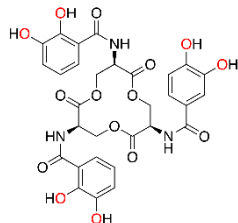


Scheme S4.9. Synthesis of **32a**.

Reagents and conditions: a): Daptomycin, NHS, DCC, pyridine, CH_2Cl_2 , DMSO, $0\text{ }^\circ\text{C} \rightarrow \text{rt}$, 1 d. Related to scheme 4.3.

**Scheme S4.10.** Synthesis of **32**.

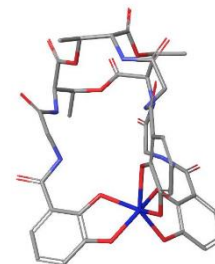
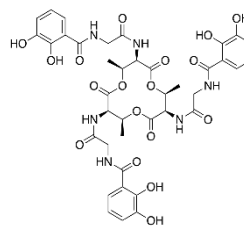
Reagents and conditions: a): **32a**, CuSO₄, sodium ascorbate, H₂O, DMF, rt, 2 h. Related to scheme 4.3.

Enterobactin

ΔE (hs-Is): -65.74 kJ/mol

E (hs): -3711.89426 a.u.

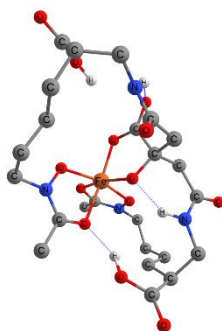
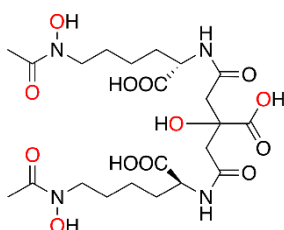
E (Is): -3711.86922 a.u.

Bacillibactin

ΔE (hs-Is): -42.64 kJ/mol

E (hs): -3872.18317 a.u.

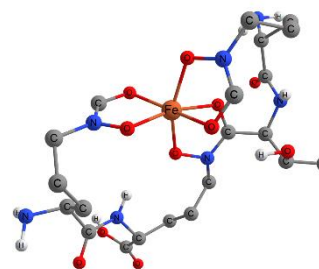
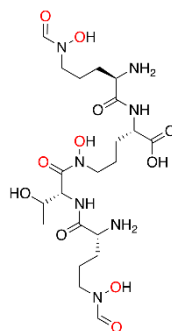
E (Is): -3872.16693 a.u.

Aerobactin

ΔE (hs-Is): -62.04 kJ/mol

E (hs) -3397.05476 a.u.

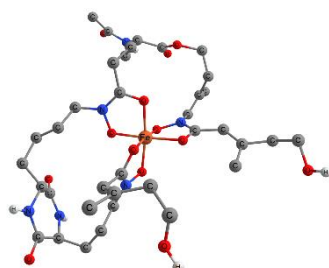
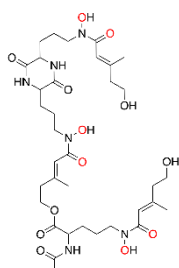
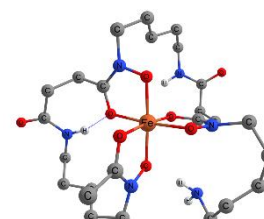
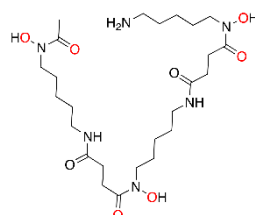
E (Is) -3397.03113 a.u.

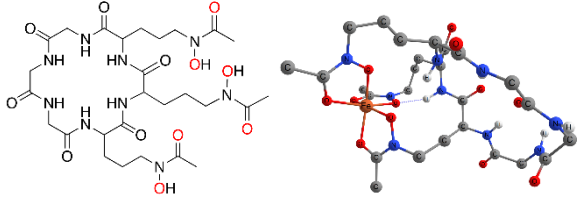
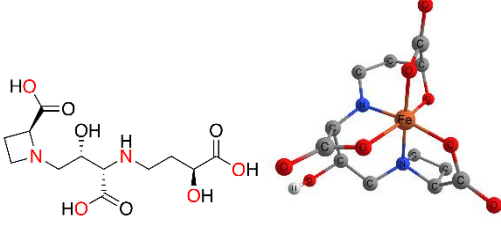
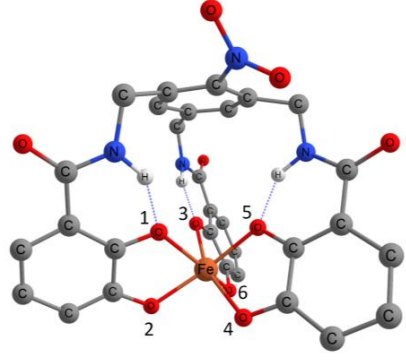
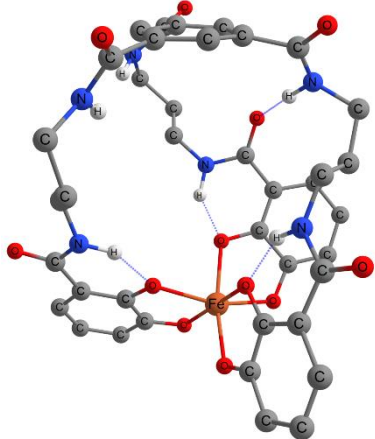
Coelichelin

ΔE (hs-Is): -62.10 kJ/mol

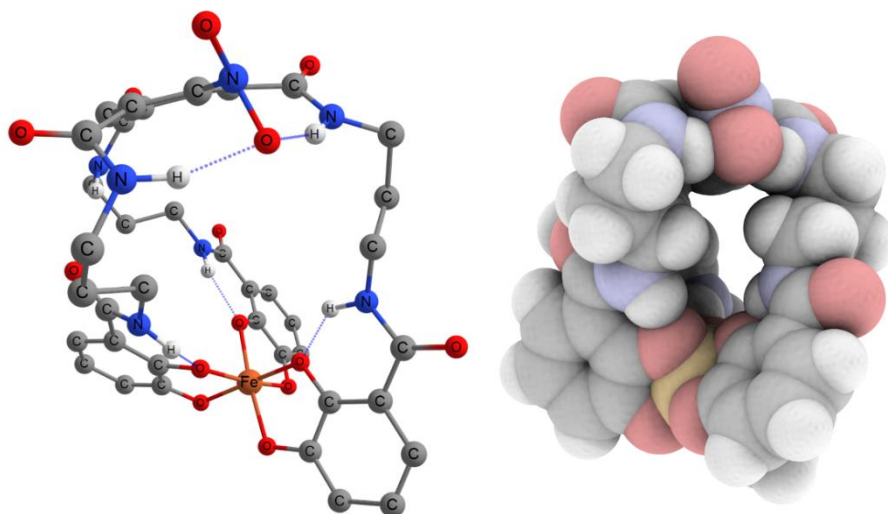
E (hs): -3296.33711 a.u.

E (Is): -3296.31347 a.u.

Coprogen**Desferrioxamine B**

<p>ΔE (hs-Is): -16.22 kJ/mol</p> <p>E (hs): -3975.08965 a.u.</p> <p>E (Is): -3975.08347 a.u.</p>	<p>ΔE (hs-Is): -19.45 kJ/mol</p> <p>E (hs): -3173.84055 a.u.</p> <p>E (Is): -3173.83314 a.u.</p>
<p>Ferrichrome A</p>  <p>ΔE (hs-Is): -22.89 kJ/mol</p> <p>E (hs): -3713.47881 a.u.</p> <p>E (Is): -3713.47009 a.u.</p>	<p>Mugineic Acid</p>  <p>ΔE (hs-Is): -43.76 kJ/mol</p> <p>E (hs): -2441.28499 a.u.</p> <p>E (Is): -2441.30166 a.u.</p>
<p>10</p>  <p>ΔE (hs-Is): -52.34 kJ/mol</p> <p>E (hs): -3780.54629 a.u.</p> <p>E (Is): -3780.52897 a.u.</p>	<p>20</p>  <p>ΔE (hs-Is): -38.47 kJ/mol</p> <p>E (hs): -4003.02760 a.u.</p> <p>E (Is): -4003.01300 a.u.</p>

19



ΔE (hs-ls): 41.92 kJ/mol (ls is ground state)

E (hs): -4208.31783 a.u.

E (ls): -4208.33380 a.u.

Figure S4.1. Structures and differences in the sum of electronic and zero-point energies between high-spin and low-spin states of natural siderophore ferric iron-complexes.

Structures were computed at the DFT (tpssh/dz) level of theory. The 2D-structures of each siderophore, as well as the computed global minima of the complexes are depicted. Hydrogen atoms attached to carbon are omitted for clarity. A negative sign for ΔE is connected with a high-spin ground state. Starting points for our conformational scans were experimental coordinates in the case of enterobactin,¹ coprogen,² desferrioxamin,³ ferrichrome,⁴ and mugineic acid (analogous Co(III)-complex)⁵.

Coordinates for ground state *low-spin* iron siderophore **19** complex optimized at utpssh/tz level of theory.

6	4.019122000	-1.108012000	1.995113000
6	4.356893000	0.242383000	1.851906000
6	4.945436000	0.671222000	0.644450000
6	5.097370000	-0.232421000	-0.428060000
6	4.690484000	-1.558031000	-0.270820000
6	4.145221000	-2.006600000	0.934654000
6	3.863882000	1.130513000	2.978454000
6	3.519223000	-3.362214000	1.083148000
6	5.318153000	0.163896000	-1.872235000
8	5.763660000	-0.634464000	-2.700537000
8	3.653451000	-4.050070000	2.096558000
8	3.755853000	0.691069000	4.128688000
7	3.420655000	2.352374000	2.594182000
7	2.729072000	-3.730549000	0.026788000
7	4.758648000	1.354624000	-2.220426000
7	-0.581353000	3.426416000	1.227757000
7	-1.185730000	-2.929917000	1.618813000
7	0.715919000	-0.033727000	-2.697504000
6	-1.323768000	4.516714000	0.871627000
6	-2.188939000	-3.236264000	2.486064000
6	0.630090000	-1.392311000	-2.683741000
8	-0.982129000	5.674079000	1.158084000
8	1.635818000	-2.125648000	-2.660184000
8	-2.110061000	-4.162921000	3.307326000
6	-3.403231000	-2.367459000	2.385505000
6	-2.536205000	4.242185000	0.038100000
6	-0.755011000	-1.943541000	-2.733678000
6	-2.960173000	2.954000000	-0.364276000
6	-3.978911000	2.815088000	-1.361878000
6	-4.629926000	3.945561000	-1.860401000
6	-4.249973000	5.217991000	-1.405341000

6	-3.217945000	5.359628000	-0.483943000
6	-0.946466000	-3.250871000	-3.230178000
6	-2.211816000	-3.823779000	-3.252942000
6	-3.326052000	-3.134054000	-2.742363000
6	-3.164238000	-1.852396000	-2.211840000
6	-1.874206000	-1.238120000	-2.250408000
6	-3.560047000	-1.320508000	1.451968000
6	-4.767466000	-0.560352000	1.415432000
6	-5.787817000	-0.824319000	2.329527000
6	-5.622659000	-1.858796000	3.266599000
6	-4.457516000	-2.615365000	3.288289000
8	-2.455154000	1.811352000	0.059096000
8	-4.216882000	1.576267000	-1.764257000
8	-1.840854000	0.000201000	-1.765291000
8	-4.126313000	-1.116251000	-1.677679000
8	-2.660782000	-0.934457000	0.556138000
8	-4.811160000	0.380295000	0.481937000
26	-3.368848000	0.309320000	-0.699141000
6	4.158776000	1.525216000	-3.535683000
6	1.976944000	0.671441000	-2.489590000
6	1.795942000	-4.848537000	0.131965000
6	0.341342000	-4.380454000	0.303717000
6	0.099000000	-3.604447000	1.607942000
6	0.804907000	3.557689000	1.656194000
6	1.085072000	3.069593000	3.084364000
6	2.580078000	3.170604000	3.453061000
7	5.389286000	2.035754000	0.480359000
8	4.385425000	2.865962000	0.098256000
8	6.589217000	2.217978000	0.073584000
6	2.902749000	0.641843000	-3.717731000
1	3.577994000	-1.429336000	2.931810000
1	4.753214000	-2.208258000	-1.137238000
1	3.603301000	2.661801000	1.621123000

1	2.544130000	-3.057120000	-0.712671000
1	4.438585000	1.992325000	-1.475827000
1	-0.934173000	2.521151000	0.916593000
1	-1.351045000	-2.144448000	0.989406000
1	-0.153354000	0.449718000	-2.473052000
1	-5.410278000	3.813791000	-2.606285000
1	-4.757113000	6.101285000	-1.791068000
1	-2.876877000	6.337070000	-0.157902000
1	-0.071588000	-3.791454000	-3.578060000
1	-2.341747000	-4.831157000	-3.645357000
1	-4.312715000	-3.590261000	-2.719761000
1	-6.694993000	-0.225808000	2.292643000
1	-6.419886000	-2.069913000	3.978224000
1	-4.315662000	-3.425832000	3.996348000
1	3.899242000	2.585042000	-3.626903000
1	1.724787000	1.702568000	-2.224068000
1	2.128650000	-5.441749000	0.986530000
1	1.879314000	-5.463623000	-0.771718000
1	-0.323570000	-5.252506000	0.271785000
1	0.067301000	-3.754235000	-0.551318000
1	0.118434000	-4.270746000	2.471838000
1	0.887889000	-2.856761000	1.742982000
1	1.054470000	4.617870000	1.570537000
1	1.438171000	3.004234000	0.954208000
1	0.496868000	3.668710000	3.791043000
1	0.763214000	2.028732000	3.195762000
1	2.738732000	2.833846000	4.479470000
1	2.913250000	4.213531000	3.374681000
1	4.895005000	1.288401000	-4.309517000
1	2.500804000	0.234976000	-1.635570000
1	2.348126000	0.976833000	-4.604023000
1	3.205433000	-0.393249000	-3.888334000

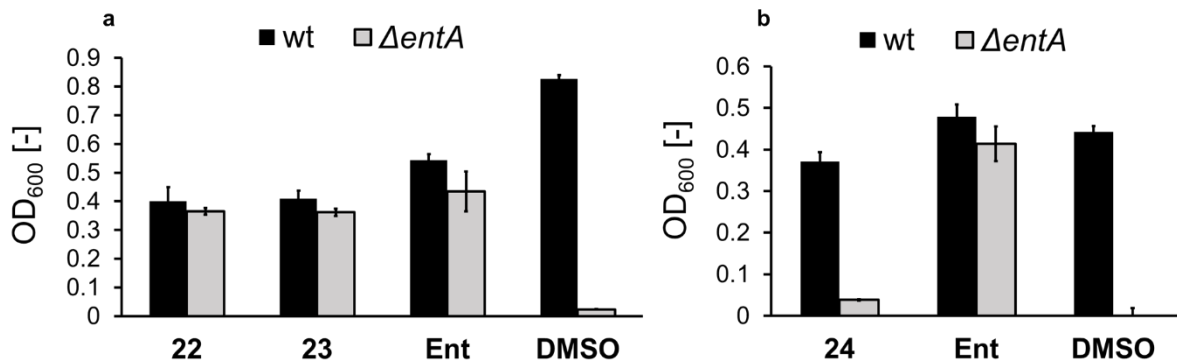


Figure S4.2. Growth recovery assay with compounds 22 – 23 (a) and 24 (b). Related to scheme 3. *E. coli* BW25113 (wild type, wt) and $\Delta entA$ cultures were treated with DMSO (solvent control), enterobactin (Ent) or indicated compounds in iron-limited medium. The growth of *E. coli* strains was determined by the OD₆₀₀ after 48-hour compound treatment.

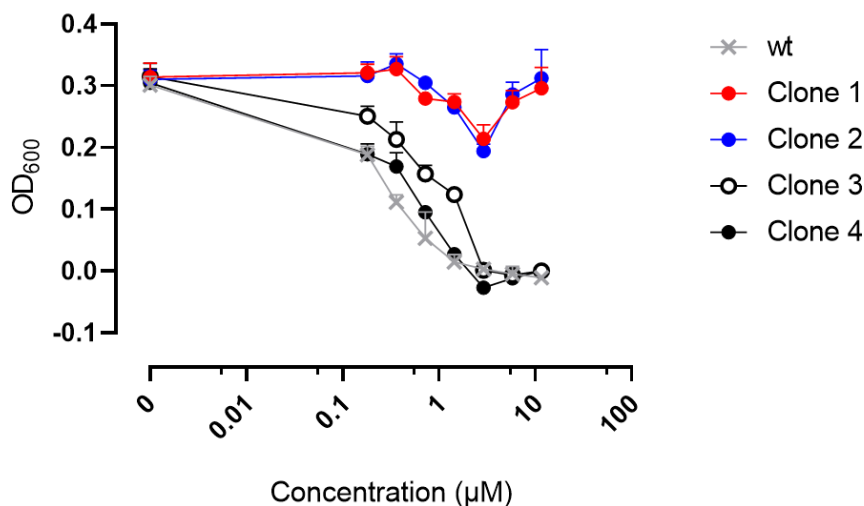


Figure S4.3. Further passages of 27^R clone 3 and clone 4 recover sensitivity against **27**. Related to Figure 4.3. Cultures from four 27^R clones were inoculated from glycerol stock at -80 °C. Glycerol stocks from four original 27^R clones were plated on MHB plates and incubated overnight at 37 °C. The colonies from plates were picked and inoculated for overnight cultures, followed by MIC assay procedure as mentioned in Figure 4.3. MIC assay against indicated new clones derived from original four 27^R clones with **27** were assessed by OD_{600nm} measurement after 24-hour antibiotic treatment in iron-limited MHB.

Table S4.1. Calculated distances and force constants of Fe–O contacts (O1 – O6) in ferric iron complexes of compounds (cpd) **10**, **19** and **20**. Related to figure 4.1. Averaged values (avg) are given additionally. The preferred spin configuration is indicated in bold.

cpd	Distances (Fe–O) [Å]						Force constants (Fe–O) [N/cm]					
	10		19		20		10		19		20	
spin state	high-spin	<i>low-spin</i>	<i>high-spin</i>	low-spin	high-spin	<i>low-spin</i>	high-spin	<i>low-spin</i>	<i>high-spin</i>	low-spin	high-spin	<i>low-spin</i>
O1	2.10	1.97	1.90	1.88	2.10	1.92	0.75	1.59	1.35	2.00	0.71	1.58
O2	2.00	1.91	1.86	1.86	1.97	1.88	1.19	1.92	1.57	2.16	1.33	2.01
O3	2.08	1.94	1.93	1.91	2.10	1.94	0.86	1.60	0.90	1.77	0.67	1.47
O4	1.99	1.96	1.87	1.88	2.02	1.91	1.24	2.02	1.46	2.01	1.02	1.73
O5	2.08	1.95	2.12	1.90	2.07	1.92	0.85	1.72	0.62	1.82	0.82	1.70
O6	2.01	1.94	2.01	1.85	1.97	1.91	1.26	2.11	1.07	2.29	1.29	1.73
avg	2.04	1.96	1.94	1.88	2.04	1.91	1.03	1.82	1.16	2.01	0.97	1.70

Table S4.2. Minimal inhibitory concentrations (MICs) of **27** against pathogenic *E. coli* and clinical isolate strain of *S. aureus*. Related to table 4.1.

MIC (µM)	27	amp
<i>E. coli</i> UPEC 536	0.72 (1 µg/mL)	23 (8 µg/mL)
<i>E. coli</i> EAEC 17-2	0.36 (0.5 µg/mL)	5.7 (2 µg/mL)
<i>E. coli</i> EIEC 12860	1.5 (2 µg/mL)	11 (4 µg/mL)
<i>E. coli</i> EPEC E2348/69	0.36 (0.5 µg/mL)	11 (4 µg/mL)
<i>E. coli</i> ETEC O6:H-117/86	0.72 (1 µg/mL)	11 (4 µg/mL)
<i>S. aureus</i> MRSA N315	5.8 (8 µg/mL)	92 (32 µg/mL)

Amp: ampicillin. UPEC: uropathogenic *E. coli*. EAEC: enteroaggregative *E. coli*. EIEC: enteroinvasive *E. coli*. EPEC: enteropathogenic *E. coli*. ETEC: enterotoxigenic *E. coli*. MRSA: methicillin-resistant *S. aureus*.

Table S4.3. Single nucleotide variants and antimicrobial susceptibility of 27-resistant clones.

Clone	Type of variant	Gene	Mutation (DNA)	Mutation (protein)	MIC (μM)		
					amp	kan	cef
Clone 1	SNP	cyoB	G > A	Gly269Asp	46 (16 $\mu\text{g}/\text{mL}$)	4.1 (2 $\mu\text{g}/\text{mL}$)	0.17 (0.13 $\mu\text{g}/\text{mL}$)
	SNP	exbB	C > T	Gln163*			
Clone 2	SNP	cyoB	G > A	Gly269Asp	46 (16 $\mu\text{g}/\text{mL}$)	4.1 (2 $\mu\text{g}/\text{mL}$)	0.17 (0.13 $\mu\text{g}/\text{mL}$)
	SNP	exbB	C > T	Gln163*			
Clone 3	SNP	cyoB	G > A	Gly269Asp	46 (16 $\mu\text{g}/\text{mL}$)	4.1 (2 $\mu\text{g}/\text{mL}$)	0.17 (0.13 $\mu\text{g}/\text{mL}$)
Clone 4	SNP	cyoB	G > A	Gly269Asp	46 (16 $\mu\text{g}/\text{mL}$)	4.1 (2 $\mu\text{g}/\text{mL}$)	0.17 (0.13 $\mu\text{g}/\text{mL}$)

SNP: Single nucleotide polymorphism. amp: ampicillin. kan: kanamycin. cef: cefiderocol.

Table S4.4. Summary of statistical results of whole genome sequencing for four clones resistant to 27.

	Number of fragments	Average length (bp)	Total base count	Average depth	Percentage coverage of reference genome
Parental genome					
Fragment	1004273	301	301272850	53.3	100
Written	996322				
Non-written	851				
Clone 1					
Fragments	1420630	300	404550050	75.3	100
Written	1409359				
Non-written	1286				
Clone 2					
Fragments	1308499	300	373231276	69.5	100
Written	1299605				
Non-written	1347				
Clone 3					
Fragments	1518924	300	428039546	80.5	100
Written	1505838				
Non-written	1389				
Clone 4					
Fragments	1451979	300	418014672	77.1	100
Written	1442124				
Non-written	1912				

Table S4.5. Summary of statistical results of whole genome sequencing for recovery clones.

	Number of fragments	Average length (bp)	Total base count	Average depth	Percentage coverage of reference genome
Recover-Clone 1 (from 27^R clone 3)					
Fragments	495639	301	126417775	26.4	100
Written	494434				
Non-written	162				
Recover-Clone 2 (from 27^R clone 4)					
Fragments	678482	301	144121524	36.2	100
Written	676259				
Non-written	322				

General chemistry methods

Thin-layer chromatography (TLC)

TLC-plates (Silica gel 60 F₂₅₄, on aluminum or glass, respectively) manufactured by Merck were used for thin-layer chromatography. The retention factor R_f is used to depict the ratio of compound and solvent front. Detection was performed under UV irradiation ($\lambda = 254$ nm). Furthermore, staining solutions of vanillin (5 g vanillin, 50 mL concentrated sulfuric acid, 100 mL glacial acetic acid, 850 mL methanol) and potassium permanganate (2 g KMnO₄, 6.5 g K₂CO₃, 200 mL H₂O) were used.

Column chromatography

Preparative column chromatography was performed on silica gel (Si 60, 40 – 63 μ m, manufactured by Merck) under increased pressure (flash-chromatography). Utilized solvents are given after the respective retention factor.

Automatic column chromatography

Automatic preparative column chromatography was performed on a Grace Reveleris® X2 (Büchi) system. Automatic preparative column chromatography over a C18 column (reversed-phase) was performed on a Pure C-850 (Büchi) system.

HPLC

HPLC purifications were performed on a Dionex Ultimate (Thermo Fisher Scientific) system. HPLC Columns (Phenomenex) of the following specifications were used:

-Luna 5 μ m, 100 Å, 00G-4252-PO-AX.

-Gemini 10 μ m, 110 Å, 00G-4436-PO.

-Gemini 10 μ m, 110 Å, 00G-4436-NO.

Characterization of synthesized compounds

All final compounds were fully characterized (¹H-, ¹³C-NMR spectra, ESI-HRMS, retention factors in case of chromatographic purification). The spectra are available in a supplemental file.

NMR spectroscopy

An Avance III 500 system (BRUKER) equipped with a PABBO BB/¹⁹F-¹H/D Z-GRD probehead (500 MHz for ¹H, 125 MHz for ¹³C spectra) and an Avance III HD 700 system (BRUKER) equipped with a cryo platform and a CPTCI ¹H-¹³C/¹⁵N/D Z-GRD probehead (700 MHz for ¹H, 176 MHz for ¹³C spectra) were used for NMR measurements at room temperature. Substances

were solved in deuterated solvents prior to the measurements. Chemical shifts δ are given in parts per million (ppm). Multiplicities are denoted by the following abbreviations: s (singlet), d (doublet), t (triplet), q (quartet), p (quintet) as well as combinations of those. Further abbreviations are: s_{br} (broad singlet) and m (multiplet). All spectra are interpreted as first-order spectra. Coupling constants J are given in Hertz (Hz) and refer to ^1H - ^1H -couplings.

Mass spectrometry

ESI-HRMS spectra were measured on a UHR-TOF spectrometer (Bruker maXis HD™, Bremen, Germany). Samples were directly injected by an Ultimate 3000RS Autosampler (Thermo Fisher Scientific). The mass-to-charge ratio m/z is given for each measurement.

DFT calculations

Calculations of all quantum mechanical raw data including the secondary derivations of energy values in the Cartesian coordinate system were conducted using the Gaussian 09 program.⁶ Hybrid functional TPSSh, containing 10% of Hartree-Fock exchange, was used.⁷ Determination of conformational states, geometry optimization and calculations of Cartesian force constants were executed applying the def2-SV(P).⁸ Geometry optimizations were conducted for *high-spin* as well as for *low-spin* states of the respective ferric iron complexes. In order to calculate the kinetic stability of iron-oxygen bonds, our own COMPLIANCE code was used, which gives the relaxed force constants for all atom-atom contacts automatically using Cartesian force constants as input.^{9, 10}

Iron(III)-chrome azurol S assay

The iron(III)-chrome azurol S assay was conducted following a known procedure.¹¹ All glassware needed for the assay was cleaned with concentrated hydrochloric acid and milliQ water. Water (few mL) and aqueous solutions of iron(III) chloride (1 mM in 10 mM HCl, 150 μL) and chrome azurol S (2 mM, 750 μL) were added to an aqueous solution of hexadecyltrimethylammonium bromide (HDTMA, 10 mM, 600 μL). A buffer solution consisting of piperazine (431 mg, 5 mmol) and concentrated hydrochloric acid (625 μL) in water (5 mL) was added. The resulting solution was diluted to a total volume of 10 mL. The stock solution used for the assay was generated by further addition of 5-sulfosalicylic acid dihydrate (10.2 mg, 40 μmol) Solutions of **10** and enterobactin (15 μM , 120 μL each) as well as water (40 μL) were added to 40 μL of stock solution. The assay was conducted in triplicates in CellBIND®-96-well plates (Corning). Absorbances were determined after 17 h using an Infinite® 200 PRO (Tecan) spectrometer in a wavelength range from 300 to 800 nm.

General biological methods

Strains, Media and Materials

MHB medium was used for the Gram-negative strains *Escherichia coli* (DSM11116, BW25113, indicated gene modification strains, and pathogenic strains), *Klebsiella Pneumoniae* (DSM11678), *Acinetobacter baumannii* (DSM30007), and *Pseudomonas aeruginosa* (DSM24068), while TSY medium was used for the Gram-positive strains *Staphylococcus aureus* (DSM11822, N315) and *Enterococcus faecium* (DSM20477). The strains used in this study are listed below.

Bacteria	Strains	Source
<i>Escherichia coli</i>	BW25113	Coli Genetic Stock Center (CGSC)
<i>Escherichia coli</i>	$\Delta entA$	CGSC
<i>Escherichia coli</i>	$\Delta fepA$	CGSC
<i>Escherichia coli</i>	$\Delta tonB$	Horizon
<i>Escherichia coli</i>	$\Delta cyoB$	Horizon
<i>Escherichia coli</i>	$\Delta exbB$	Horizon
<i>Escherichia coli</i>	$\Delta fepB$	This paper
<i>Escherichia coli</i>	$\Delta fepD$	This paper
<i>Escherichia coli</i>	$\Delta entA \Delta fepA$	This paper
<i>Escherichia coli</i>	$\Delta entA \Delta fecA$	This paper
<i>Escherichia coli</i>	$\Delta entA \Delta fhuA$	This paper
<i>Escherichia coli</i>	$\Delta entA \Delta cirA$	This paper
<i>Escherichia coli</i>	$\Delta entA \Delta fiu$	This paper
<i>Escherichia coli</i>	$\Delta fepA \Delta cirA$	This paper
<i>Escherichia coli</i>	$\Delta fepA \Delta fiu$	This paper
<i>Escherichia coli</i>	$\Delta cirA \Delta fiu$	This paper
<i>Escherichia coli</i>	$\Delta fepA \Delta cirA \Delta fiu$	This paper
<i>Escherichia coli</i>	UPEC 536	Obtained from Prof. Petra Dersch, University of Münster (formerly HZI)
<i>Escherichia coli</i>	EAEC 17-2	Obtained from Prof. Petra Dersch, University of Münster (formerly HZI)
<i>Escherichia coli</i>	EIEC 12860	Obtained from Prof. Petra Dersch, University of Münster (formerly HZI)
<i>Escherichia coli</i>	EPEC E2348/69	Obtained from Prof. Petra Dersch, University of Münster (formerly HZI)
<i>Escherichia coli</i>	ETEC O6:H- 117/86	Obtained from Prof. Petra Dersch, University of Münster (formerly HZI)

<i>Escherichia coli</i>	DSM1116	German Collection of Microorganisms and Cell Cultures GmbH (DSMZ)
<i>Klebsiella pneumoniae</i>	DSM11678	DSMZ
<i>Acinetobacter baumannii</i>	DSM30007	DSMZ
<i>Pseudomonas aeruginosa</i>	DSM24068	DSMZ
<i>Staphylococcus aureus</i>	DSM11822	DSMZ
<i>Staphylococcus aureus</i>	MRSA N315 (NR-45898)	BEI Resources
<i>Enterococcus faecium</i>	DSM20477	DSMZ

Plasmids

The sources of plasmids were mentioned above. To generate protein-expressing plasmids, sequences encoding FepA, CyoB and ExbB were amplified from chromosomal DNA of wild type or compound **27** resistant clones by PCR amplification. FepA sequence was cloned into BamHI and HindIII sites of pQE 80L vector (Qiagen Cat# 32943). CyoB and ExbB sequences were cloned into XhoI and XbaI sites of pSF-OXB15 vector (Sigma-Aldrich Cat # OGS558). The primers used for PCR amplification are listed below.

Primer	Sequence
BamHI-fepA F	CGCGGATCCATGAACAAGAAGATTCATTC
HindIII-fepA R	CCCAAGCTTTCAGAAGTGGGTGTTTACGC
XhoI-cyoB F	CCGCTCGAGATGTTTCGGAAAATTATCACTTGATG
XbaI-cyoB R	GCTCTAGATCAGTTGCCATTTTTTCAGCCCTGCC
XhoI-exbB F	CCGCTCGAGGTGGGTAATAATTTAATGCAGACGG
XbaI-exbB R	GCTCTAGATTATCCTGCGCGTAATTTTTGTGCG

Recombineering/Lambda red-mediated gene deletion

Gene deletion was conducted via lambda red recombineering in *E. coli* wild type BW25113 or indicated strains. Targeted genes on the corresponding locus were replaced by homologous recombination with chloramphenicol cassette with FRT sequence which is flanked by 50 base pairs of upstream and downstream of the targeted gene. Chloramphenicol cassette was amplified from pKD3¹² by PCR with the primers containing corresponding upstream and downstream of the gene sequence. The primers are listed below. For expression of lambda red system, the plasmid pKD46, encoding lambda red genes with araBAD promoter, was transformed into the target strain and grown at 30 ° C. Strain with pKD46 were further grown until the early exponential phase (OD₆₀₀ = 0.2) followed by the induction of "lambda red" proteins Gam, Exo and Beta by supplementation of 0.2 % arabinose. Bacterial cultures were grown up to an OD₆₀₀ of 0.6 and transformed with the PCR product. The transformed cells were recovered for 2 hours at 37 ° C. and then selected on an agar plate with chloramphenicol (25 µg/mL). Indicated gene deletion strains were obtained and checked by colony PCR with the primers listed below.

Primer	Sequence
entA-K-F	AACCCGACCATCGACGCCTGGTGGAAAGCTACTCTCCCGCGAGGTGAAATAGTGTA GGCTGGAGCTGCTTC
entA-K-R	GCTGGTGGCGTTCAGTTCGTTCGAGCGTTAAATGGCGTTTCCAGATCATGCATGGG AATTAGCCATGGTCC
fepA-K-F	CCGCATCCGGCATGAACGACGCGCACTTTGTCAACAATCTGACGTTAGCAGTGTA GGCTGGAGCTGCTTC
fepA-K-R	CGACCATGCCCGACAGTTGCAATTCGTGGCAAAAATGCAGGAATAAAACAATGGG AATTAGCCATGGTCC
fecA-K-F	CAACATAATCACATTCCAGCTAAAAGCCCGGCAAGCCGGGCGTTAACACAGTGTA GGCTGGAGCTGCTTC
fecA-K-R	TTCTCGTTTCGACTCATAGCTGAACACAACAAAAATGATGATGGGGAAGGTATGGGA ATTAGCCATGGTCC
fhuA-K-F	ATAATCATTCTCGTTTACGTTATCATTCACTTTACATCAGAGATATACCAGTGTAGG CTGGAGCTGCTTC
fhuA-K-R	AACAGCCAACCTTGTAATGGGCACGGAAATCCGTGCCCAAAAGAGAAAATGGG AATTAGCCATGGTCC
K-fepB-F	CGCAGGTGACAGCGTCCGACAGTTAATGCTTAAAACAGCGCCTTAAGCCTGTGTA GGCTGGAGCTGCTTC
K-fepB-R	AATTTGTCATTACGCCCTTAACCTTATTAATAACAGGAAGCTGATTTGTGATGGGAA TTAGCCATGGTCC
K-fepD-F	GGTGATGAGTAATCGGCGAGAGACGTAAATCATGCACCACCTCGCGTTTTGTGTA GGCTGGAGCTGCTTC
K-fepD-R	AAATAAGATCGATAACGATAATTAATTTATTATCATGGAAGTTCGTATGATGGGAA TTAGCCATGGTCC
K-fecD-F	ACCGTCAGATTTTCAGTTCGTAAAGTCATTTATCGCATTCTCACAAGCAAGTGTAGG CTGGAGCTGCTTC
K-fecD-R	GCGCTGATTGGCAGCCCTTGCTTTGTCTGGCTTGTGAGGAGGCGAGGATGATGGG AATTAGCCATGGTCC
K-fhuB-F	GCAATGCACTTTGTGCGCGTTCTGGATAACGCCATCGGAGGTAAAGCGTGGTGTA GGCTGGAGCTGCTTC
K-fhuB-R	CAGGCGTACAGGGCCGTTATATGGAAAAATTAACGGCTCTGCTTTCTCAAATGGGA ATTAGCCATGGTCC

K-cirA-F	GCAGTATTTACTGAAGTGAAAGTCCGCCCGTCGCCGGGCATCTTCTCAGTGTAGG CTGGAGCTGCTTC
K-cirA-R	TGTGAGCGATAACCCATTTTATTTTCGTAGTTACCTCATGGAGATATGGAATGGGAA TTAGCCATGGTCC
K-fiu-F	GTACATCATACAATTTCTCCAAAAGTGGGGCCTGCGCCCCACATCTGAAGTGTAG GCTGGAGCTGCTTC
K-fiu-R	TTTCTCGTGGCAGTGAAAATTTCAACATATAAGAAAAAGTCACCTGCAAAATGGGA ATTAGCCATGGTCC
entA-C-F	AACCCGACCA TCGACGCCTG
entA-C-R	GCTGGTGGCGTTCAGTTCGT
fepA-C-F	CCGCATCCGG CATGAACGAC GCGCA
fepA-C-R	CGACCATGCCCGACAGTTGCAATTC
fecA-C-F	CAACATAATC ACATTCCAGC TAAAA
fecA-C-R	TTCTCGTTTCTGACTCATAGCTGAACA
fhuA-C-F	ATAATCATTG TCGTTTACGT TATCA
fhuA-C-R	AACAGCCAACTTGTGAAATGGGCAC
C-fepB-F	CGCAGGTGACAGCGTCCGACAGTTA
C-fepB-R	AATTTGTCATTACGCCCTTAACCTT
C-fepD-F	GGTGATGAGTAATCGGCGAGAGACG
C-fepD-R	AAATAAGATCGATAACGATAATTAA
C-fecD-F	ACCGTCAGATTTTCAGTTCGTAAAG
C-fecD-R	GCGCTGATTGGCAGCCCTTGCTTTG
C-fhuB-F	GCAATGCACTTTGTGCGCGTTCTGG
C-fhuB-R	CAGGCGTACAGGGCCGTTATATGGA
C-cirA-F	GCAGTATTTA CTGAAGTGAA AGTCC
C-cirA-R	TGTGAGCGATAACCCATTTTATTTT
C-fiu-F	GTACATCATA CAATTTCTCC AAAAA
C-fiu-R	TTTCTCGTGGCAGTGAAAATTTCA

Growth Recovery Assay (GRA)

The LMR medium needed for the assay was prepared according to a literature procedure. It contained monopotassium phosphate (176 mM), sodium hydroxide (100 mM), ammonium sulfate (12.6 mM), magnesium sulfate (2 mM), and glycerol (0.2 % v/v). To one liter of this solution, 2 mL of a trace element solution (listed below) was added.

Substance	Concentration	Final concentration
CaCl ₂	20 mM	40 μM
MnCl ₂ × 4 H ₂ O, ZnSO ₄ × 7 H ₂ O	10 mM	20 μM
CoCl ₂ × 6 H ₂ O, CuCl ₂ , NiCl ₂ × 6 H ₂ O, Na ₂ MoO ₄ × 2 H ₂ O, Na ₂ SeO ₃ , H ₃ BO ₄	2 mM	4 μM

The Fe³⁺-concentration was adjusted to 0.1 μM using iron(III) chloride hexahydrate. All solutions were autoclaved prior to their use. *Escherichia coli* strains BW25113 and Δ *entA* were cultivated overnight in MHB medium, until an OD₆₀₀-value of 0.5 was reached. Bacteria were partitioned by centrifugation (8000 g, 5 min) and washed by threefold centrifugation (8000 g, 5 min) in PBS buffer solution. An OD₆₀₀-value of 0.01 was set up by dilution with LMR medium. The assay was conducted in 96-well plates in triplicates. To 148.5 μL of the bacterial suspension, 1.5 μL of siderophore solution (1 mM in DMSO, neat DMSO for negative control) was added, resulting in a final compound concentration of 10 μM in each case. Neat LMR medium was used as a blank. The well plates were sealed with parafilm and incubated at 37 °C for 48 h. OD₆₀₀-values were determined using a well plate spectrometer. Blank values were subtracted from the raw values to obtain final data.

Cell Fractionation Assay

Primarily, a GRA with compound **10** was conducted according to the procedure described above. Kanamycin (50 μM) was used for the incubation in LMR medium over night. The incubation proceeded, until an OD_{600} -value of one was reached. Since therefore the assay had to be conducted on a bigger scale (5 mL of LMR-Medium with a final siderophore concentration of 50 μM), falcon tubes were used for incubation instead of well plates. The assay was conducted using iron(III) chloride hexahydrate as described above or with iron(III) pre-complexation of compound **10**. For the latter, iron(III) chloride hexahydrate was not added to the medium but instead was added to the solution of compound **10** and incubated over night before applying. The obtained bacterial colonies were used for a cell fractionation assay coupled with mass spectrometry detection, according to a known literature procedure.¹³

Minimal inhibitory concentration assay against bacterial pathogens

The assay was conducted in 384-well plates using an epMotion[®] pipetting robot in triplicates. Generic and iron-limited nutrition media were used. Iron-limited nutrition media were prepared by adding 100 g of Chelex[®] (Hercules) resin to a liter of generic medium. This mixture was stirred for 2 h, and the resin was removed by filtration (0.2 μm). Sodium chloride, magnesium sulfate and zinc sulfate heptahydrate were added to yield final respective cation concentrations of 200 μM , 93 μM , and 10 μM , respectively. The pH value was brought to 7.4 with hydrochloric acid. The iron-limited media were sterilized by filtration (0.2 μm).

All ESKAPE panel strains were cultivated in generic nutrition medium overnight. The cultures were diluted by a factor of 100 with generic nutrition medium and cultivated again for 5 h. Bacteria were partitioned by centrifugation (4500 g, 0 °C, 5 min), washed three times with iron-limited medium, and diluted with the respective iron-limited nutrition medium to an OD_{600} value of 0.005.

For MICs in EAKAPE panel, starting from conjugate stock solutions (6.4 mg in DMSO), maximum concentrations of 64 $\mu\text{g}/\text{mL}$ and 6.4 $\mu\text{g}/\text{mL}$, respectively, were prepared by dilution with iron-limited media. For testing MICs in *E. coli* BW25113, genomically modified, and clinical isolate strains in Table S4.2, maximum concentrations of conjugate 16 $\mu\text{g}/\text{mL}$ were prepared as mentioned above. From here, twofold dilution series with iron-limited media were established for each conjugate. For daptomycin and its conjugate **32**, a CaCl_2 concentration of 110 $\mu\text{g}/\text{mL}$ was added to the medium. The efficacy of the conjugates was compared to the respective free antibiotics ampicillin and amoxicillin, and with the state-of-the-art siderophore conjugate cefiderocol. DMSO in iron-limited medium at the respective maximum dilution series concentration was used as the negative control. Neat medium was used as a blank. As

additional positive controls, linezolid was used against *Staphylococcus aureus*, amikacin against *Pseudomonas aeruginosa*, and ciprofloxacin against the remaining ESKAPE panel strains. The well plates were sealed with parafilm and incubated at 37 °C for 24 h. OD₆₀₀ values were determined using a well plate spectrometer. Averaged blank values as well as the respective background value were subtracted from the raw values. MICs shown in Table 4.1 were determined by a curve-fitting procedure using the Graph Pad Prism program and expressed in µM. MICs shown in Table 4.2, Table S4.2 and Figure 4.3 were the minimal concentrations of indicated antibiotics displaying OD₆₀₀ = 0 determined by visual inspection and expressed in µM.

Generation of clones resistant to 27 and bioinformatic analysis of whole genome sequences

To render *E. coli* K-12 BW25113 resistant against **27**, cell suspensions with a cell density equal to 10⁸ CFU/ml were grown in chelating Mueller-Hinton broth as mentioned before containing conjugate **27** in a concentration of 2 x MIC (2.9 µM) at 37 °C under shaking (180 rpm). Cultures that displayed visible growth after 24h (OD₆₀₀ > 0.1 units) were exposed to higher drug concentrations. Four of the original cultures survived 21 passages. To exclude general drug-resistant clones, resistant clones were subject to ampicillin, kanamycin or cefiderocol, and the clones that were only resistant to **27** were selected. Genomic DNA was isolated from the resistant clones and from the parental strain control using the DNeasy Blood and Tissue Kit (Qiagen). The whole-genome sequence analysis was performed by the Genome Analytics Research Group at the Helmholtz Centre for Infection Research.

According to the manufacturer's protocols, the library was generated from 0.2 mg DNA for PCR amplification with 4 cycles by applying NEBNext Ultra II FS DNA Library Prep Kit for Illumina (New England BioLabs). The libraries were sequenced on an Illumina MiSeq system (600 cycle) using MiSeq Reagent Kit v3 with an average of 1 million reads per DNA sample, paired-end mode, 2 x300 bp read length, and ~100x genome coverage. Libraries of DNA fragments with an average length of 580 bp were prepared according to the manufacturer's instructions. Sequences were quality controlled and adapter clipped by using the fastq-mcf tool of ea-utils.¹⁴ The sequences of parental control and four resistant clones were mapped to the reference genome *E. coli* BW25113 (GenBank: CP009273.1)¹⁵ to find substitutions and insertions/deletions.

Protein expression in *E. coli*

To prepare electro-competent cells, overnight cultures of *E. coli* $\Delta FepA$, $\Delta cyoB$, and $\Delta exbB$ were diluted into $OD_{600} = 0.1$ and grown in 10 mL LB, and then harvested when reaching the exponential phase ($OD_{600} = 0.5$). Bacterial pellets were harvested for ten minutes and then washed in ddH₂O three times and in 10 % sterile glycerol for two times by centrifugation (6000 g, 4 °C). The supernatant was discarded and the pellet is resuspended in 1 mL 10 % sterile glycerol (4°C) and again centrifuged (6000 g, 4°C, 15 min). 100 μ L aliquots of this bacteria solution were prepared for further electroporation.

By electroporation, pQE FepA, pSF CyoB, or pSF ExbB were transformed into strains $\Delta FepA$, $\Delta cyoB$ and $\Delta exbB$, respectively. Transformed cells were spread onto kanamycin (50 μ g/mL)-containing LB agar plates and grown overnight at 37°C. For protein expression of CyoB and ExbB, a single colony of bacteria was picked followed by inoculation as mentioned. For FepA protein expression, cells were grown with the addition of 1 mM isopropyl β -D-thiogalactopyranoside (IPTG) for protein induction. The effectiveness of overexpression was determined by real-time PCR. All constructs were verified by PCR amplification, restriction enzyme analysis and sequencing.

Quantitative RT-PCR

Total RNAs from bacteria pellets were isolated via RNAeasy Mini Kit (Qiagen) following the manufacturer's recommendations. 2500 ng of total RNA was reverse-transcribed to cDNA using RevertAid H Minus First Strand cDNA Synthesis Kit (Thermo Scientific) following the manufacturer's instructions. To determine the amount of cDNA by qPCR, 100 ng cDNA was mixed with primers and amplified using LightCycler® 480 SYBR Green I Master (Roche, Cat# 04887352001) following the manufacturer's instructions. The program for real-time was set as follows: 95°C for 10 min, 40 cycles of 95°C for 15 seconds, annealing temperature (60°C) for 1 minute, and 72°C for 15 seconds. The real-time PCR was performed using Roche LightCycler® 480 system. All values of interesting genes were normalized to the housekeeping gene- *rpoB* mRNA as an internal control using the $2^{-\Delta\Delta Ct}$ method, where $\Delta\Delta Ct = \Delta Ct$ test sample (Ct target gene-Ct internal control) - ΔCt untreated wild type sample (Ct target gene-Ct internal control). All data were presented as fold change relative to the untreated wild type sample. Expression levels of the target genes were presented as mean \pm s.d (standard deviation). Primers used to detect specific mRNA are listed below.

Primer	Sequence
fepA-F	GGAATACGCGAGTTACGGGT
fepA-R	ACCGTCTGTATCGCCAGAAC
rpoB-F	TCCGTATTCCCGATTCAGAG
rpoB-R	TCACCAGACGCAGTTTAACG
cyoB-q-F	ATGTTCCGAAAATTATCACT
cyoB-q-R	CTTACCGAAGTAAGTGATCA
exbB-q-F	GTGGGTAATAATTTAATGCA
exbB-q-R	AAGAAGATTGCCAGGTGAC
exB735-F	TTAAAGCGATGCTGGGTGAT

Quantification and Statistical Analysis

OD₆₀₀ values and quantitative RT-PCR results are presented as averages \pm s.d. The significance of differences between averages was assessed using the Student *t* test.

Supplementary References

1. Johnstone, T. C.; Nolan, E. M., Determination of the molecular structures of ferric enterobactin and ferric enantioenterobactin using racemic crystallography. *J. Am. Chem. Soc.* **2017**, *139* (42), 15245-15250.
2. Hossain, M. B.; Jalal, M. A. F.; Benson, B. A.; Barnes, C. L.; Van der Helm, D., Structure and conformation of two coprogen-type siderophores. Neocoprogen I and neocoprogen II. *J. Am. Chem. Soc.* **1987**, *109* (16), 4948-4954.
3. Dhungana, S.; White, P. S.; Crumbliss, A. L., Crystal structure of ferrioxamine B: a comparative analysis and implications for molecular recognition. *J. Biol. Inorg. Chem.* **2001**, *6* (8), 810-8.
4. Van der Helm, D.; Baker, J. R.; Eng-Wilmot, D. L.; Hossain, M. B.; Loghry, R. A., Crystal structure of ferrichrome and a comparison with the structure of ferrichrome A. *J. Am. Chem. Soc.* **1980**, *102* (12), 4224-4231.
5. Mino, Y.; Ishida, T.; Ota, N.; Inoue, M.; Nomoto, K.; Takemoto, T.; Tanaka, H.; Sugiura, Y., Mugineic acid-iron(III) complex and its structurally analogous cobalt(III) complex: characterization and implication for absorption and transport of iron in gramineous plants. *J. Am. Chem. Soc.* **1983**, *105* (14), 4671-4676.
6. M. J. Frisch, G. W. T., H. B. Schlegel, G. E. Scuseria, M. A. Robb, J. R. Cheeseman, G. Scalmani, V. Barone, G. A. Petersson, H. Nakatsuji, X. Li, M. Caricato, A. Marenich, J. Bloino, B. G. Janesko, R. Gomperts, B. Mennucci, H. P. Hratchian, J. V. Ortiz, A. F. Izmaylov, J. L. Sonnenberg, D. Williams-Young, F. Ding, F. Lipparini, F. Egidi, J. Goings, B. Peng, A. Petrone, T. Henderson, D. Ranasinghe, V. G. Zakrzewski, J. Gao, N. Rega, G. Zheng, W. Liang, M. Hada, M. Ehara, K. Toyota, R. Fukuda, J. Hasegawa, M. Ishida, T. Nakajima, Y. Honda, O. Kitao, H. Nakai, T. Vreven, K. Throssell, J. A. Montgomery, Jr., J. E. Peralta, F. Ogliaro, M. Bearpark, J. J. Heyd, E. Brothers, K. N. Kudin, V. N. Staroverov, T. Keith, R. Kobayashi, J. Normand, K. Raghavachari, A. Rendell, J. C. Burant, S. S. Iyengar, J. Tomasi, M. Cossi, J. M. Millam, M. Klene, C. Adamo, R. Cammi, J. W. Ochterski, R. L. Martin, K. Morokuma, O. Farkas, J. B. Foresman, and D. J. Fox *Wallingford CT* **2016**, (Revision A.02).
7. Tao, J.; Perdew, J. P.; Staroverov, V. N.; Scuseria, G. E., Climbing the density functional ladder: nonempirical meta-generalized gradient approximation designed for molecules and solids. *Phys. Rev. Lett.* **2003**, *91* (14), 146401.
8. Schäfer, A.; Horn, H.; Ahlrichs, R., Fully optimized contracted gaussian basis sets for atoms Li to Kr. *J. Chem. Phys.* **1992**, *97* (4), 2571 – 2577.
9. Brandhorst, K.; Grunenberg, J., How strong is it? The interpretation of force and compliance constants as bond strength descriptors. *Chem. Soc. Rev.* **2008**, *37* (8), 1558 –1567.

10. Brandhorst, K.; Grunenberg, J., Efficient computation of compliance matrices in redundant internal coordinates from Cartesian Hessians for nonstationary points. *J. Chem. Phys.* **2010**, *132* (18), 184101.
11. Schwyn, B.; Neilands, J. B., Universal chemical assay for the detection and determination of siderophores. *Anal. Biochem.* **1987**, *160*, 47 – 56.
12. Datsenko, K. A.; Wanner, B. L., One-step inactivation of chromosomal genes in *Escherichia coli* K-12 using PCR products. *Proc. Natl. Acad. Sci.* **2000**, *97* (12), 6640-6645.
13. Prochnow, H.; Fetz, V.; Hotop, S. K.; García-Rivera, M. A.; Heumann, A.; Brönstrup, M., Subcellular quantification of uptake in Gram-negative bacteria. *Anal. Chem.* **2019**, *91* (3), 1863-1872.
14. Aronesty, E. e.-u. 'Command-line tools for processing biological sequencing data'. <https://github.com/ExpressionAnalysis/ea-utils>
15. Snippy, T. S. Fast bacterial variant calling from NGS reads.

5. Publication 3: Enzyme-activated, chemiluminescent siderophore-dioxetane probes enable the selective and highly sensitive detection of bacterial pathogens

This chapter has been published as a peer-reviewed article in a scientific journal:

Carsten Peukert, Sachin Popat Gholap, Ori Green, Lukas Pinkert, Joop van den Heuvel, Marco van Ham, Doron Shabat und Mark Brönstrup.

“Enzyme-activated, chemiluminescent siderophore-dioxetane probes enable the selective and highly sensitive detection of bacterial pathogens”.

Angewandte Chemie International, **2022**, e202201423,

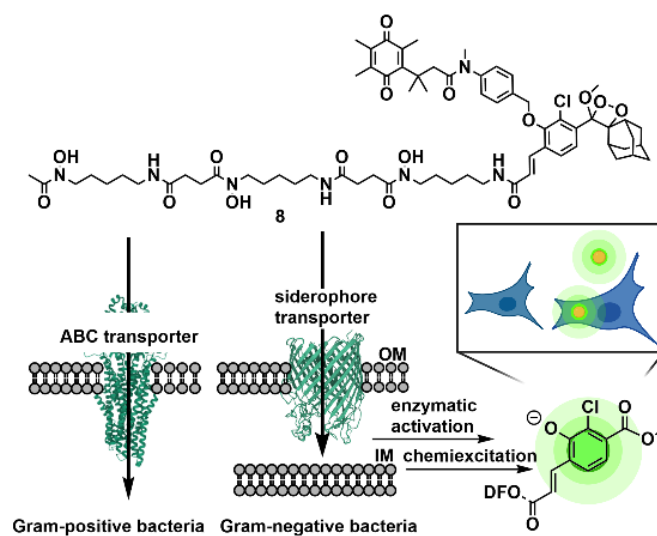
DOI: 10.1002/anie.202201423

This article was also published as a German version (see below), translated by the first author C.P and can be accessed with the credentials below:

“Enzymaktivierte, chemilumineszente Siderophor-Dioxetan-Sonden ermöglichen den selektiven und hochempfindlichen Nachweis von bakteriellen Krankheitserregern”, *Angewandte Chemie*, **2022**, e202201423.

DOI: 10.1002/ange.202201423

Table of content graphic



Abstract

The sensitive detection of bacterial infections is a prerequisite for their successful treatment. The use of a chemiluminescent readout was so far hampered by an insufficient probe enrichment at the pathogens. We coupled siderophore moieties, that harness the unique iron transport system of bacteria, with enzyme-activatable dioxetanes and obtained seven trifunctional probes with high signal-to-background ratios ($S/B = 426-859$). Conjugates with efficient iron transport capability into bacteria were identified through a growth recovery assay. All ESKAPE pathogens were labelled brightly by desferrioxamine conjugates, while catechols were weaker due to self-quenching. Bacteria could also be detected inside lung epithelial cells. The best probe **8** detected 9.1×10^3 CFU/mL of *S. aureus* and 5.0×10^4 CFU/mL of *P. aeruginosa*, while the analogous fluorescent probe **10** was 200-307fold less sensitive. This qualifies siderophore dioxetane probes for the selective and sensitive detection of bacteria.

5.1 Introduction

The escalating resistance of pathogenic bacteria to clinically employed antibiotics has become a global problem in the health care sector with severe economic and medical repercussions.¹ The timely and specific diagnosis of a bacterial infection remains a crucial factor for its tailored and successful treatment.² The common procedures for detection and susceptibility testing are based on optimized microbiological methods in automated, central labs. However, a further shortening of analysis times and the establishment of simple, point-of-care solutions are subject to intense research efforts. A special, growing area concerns the detection of infections *in vivo* by molecular imaging techniques.^{4,5} Radioactively-labelled PET or SPECT tracers visualize infections at deep body sites, but the high costs and demands on infrastructure prevent their broad usage in everyday clinical practice. A simple detection method, that is also amenable to point-of-care applications, exploits the detection of chemiluminescence in the visible light range. Such probes require no external light source and reach excellent sensitivities and signal-to-background (S/B) ratios.^{6, 7} Turn-on chemiluminescent phenolic dioxetanes, first discovered by Schaap and coworkers,⁸⁻¹⁰ were significantly improved recently through the introduction of an electron-withdrawing group at the aromatic ring. This resulted in activatable probes that are brightly emissive in aqueous environments and applicable in biological systems.¹¹⁻¹³ Lately, we functionalized dioxetanes for the detection of *Mycobacterium tuberculosis* as well as for bacterial carbapenemases and β -lactamases.^{14, 15} However, a broad detection of both Gram-negative and -positive bacteria that does not rely on the secretion of resistance enzymes like β -lactamases remained elusive so far. One cause for this is the hampered intracellular accumulation and activation of such probes, impeded by impervious bacterial cell walls.¹⁷ To alleviate this, an enhanced translocation into prokaryotes can be achieved by hijacking their siderophore-based iron transport systems.¹⁸ Siderophores are low molecular mass iron chelators that are recognized by chelator-specific transporters which translocate them over the bacterial membrane to satiate the pathogen's iron demand.¹⁹ Because these transport systems are exclusively found in prokaryotes and not in mammalian cells,^{18, 19} they have been exploited as molecular 'Trojan Horses', designed to smuggle siderophore-conjugated antibiotics, dyes or radioactive labels inside bacterial cells.^{20, 21} Recently, we introduced the MECAM (1,3,5-*N,N,N'*-tris-(2,3-dihydroxybenzoyl)-tri amino methyl benzene) and DOTAM (1,4,7,10-tetra azacyclododecane-1,4,7,10-tetra acetic amide) cores as artificial siderophores for bacterial imaging and antibacterial therapy.^{22, 23} We also demonstrated the ability of gallium-68-labelled DOTAM derivatives to act as bacteria-specific PET tracers *in vivo*.²⁴ In this study, we aimed to establish bright and selective probes for the detection of a broad spectrum of clinically relevant bacterial pathogens based on a chemiluminescent mode of detection, with superior properties compared to fluorescent probes.

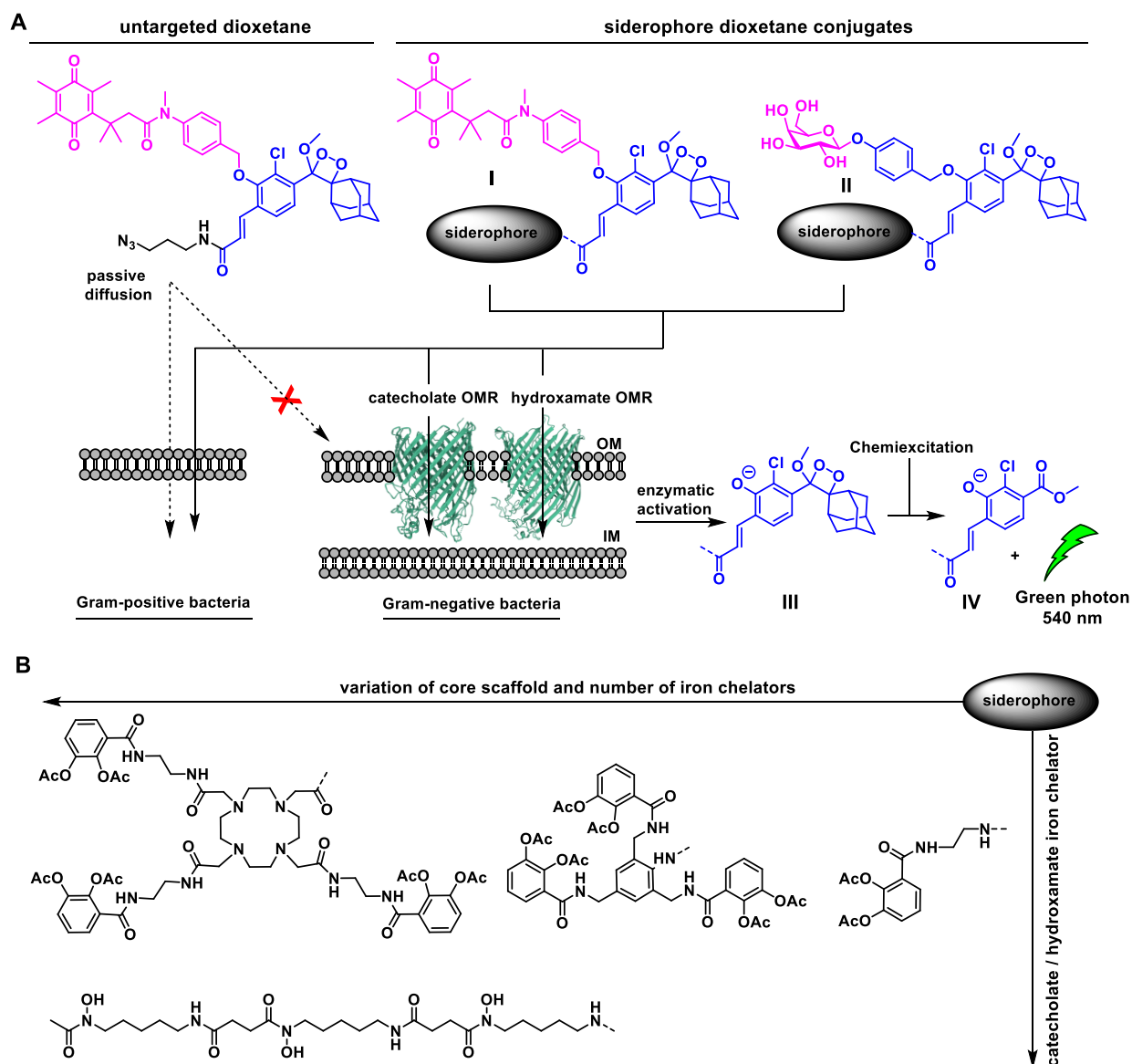


Figure 5.1. Design concept for bacteria-targeting chemiluminescent dioxetanes. (A) Untargeted dioxetanes diffuse into Gram-positive bacteria, but uptake into Gram-negative bacteria and activation is minor or absent due to their double-layered cell membrane. Conjugation to siderophores enables active uptake via bacterial siderophore transporters (structures PDB: 1FEP and 1FCP). Subsequent enzymatic activation via the trigger moiety (pink), followed by the self-immolation of the excited phenolate **IV** yields a bright luminescence emission. (B) Structural variations of the siderophores with regard to their core, the number and the chemical nature of iron-chelating groups. OM = outer membrane, IM = inner membrane, OMR = outer membrane receptor.

5.2 Results and Discussion

In order to obtain sensitive and bacteria-specific imaging probes with broad spectrum activity, we combined three functionalities in one molecule, i.e. a siderophore vector, which is effectively internalized, an enzyme-trigger combination with widespread occurrence in Gram-positive and Gram-negative bacteria that serves to release the third component, a latest generation dioxetane moiety for bright chemiluminescence (Figure 5.1). For the siderophore part, DOTAM- and MECAM-based synthetic cores with catecholate chelators^{24, 23} and the natural desferrioxamine (DFO) with hydroxamate chelators were chosen and attached to the dioxetane's acrylic acid moiety.

For a triggered release, the two bicomponent systems β -galactosidase & β -galactose or quinone oxidoreductase & trimethyl lock (TML) were chosen. β -Galactosidases occur in *E. coli*, *A. baumannii*, *K. pneumoniae* as well as in some Gram-positive strains. In addition, colorimetric tests for β -galactosidase based on the hydrolysis of 2-nitrophenyl β -D-galactopyranoside (ONPG), were also found to be positive in the presence of β -glucuronidases,^{25, 26} indicating a broad substrate tolerance. Secondly, the TML trigger has been successfully employed as a self-immolative linker in antibiotic siderophore conjugates, with activities in pathogens of the so-called ESKAPE panel (*E. faecium*, *S. aureus*, *K. pneumoniae*, *A. baumannii*, *P. aeruginosa*, and *Enterobacter sp.*)²¹ The TML release is mediated by quinone oxidoreductases, which are commonly found in a range of bacteria.²⁷ We envisaged the following cascade of events (Figure 5.1A): After internalization of the iron-loaded siderophore, a cleavage of the β -glycosidic bond with subsequent elimination of the 4-ethylphenol spacer (**I**) releases the phenolate dioxetane (**III**).²⁸ In the second approach, the reduction of the trimethyl lock yields a hydroquinone that would undergo a sterically induced lactonization, eliminate the *para*-aminobenzyl alcohol spacer (**II**) and thus release the phenolate dioxetane (**III**).²⁹ This phenolate would swiftly decompose under elimination of 2-adamantanone in a chemical excitation process and yield the excited benzoate ester (**IV**), which decays to its ground state with concurrent release of energy in the form of a green photon. Thus, bacterial uptake of the probe and its subsequent activation by the live bacteria would be detected as a chemiluminescent signal. The synthesis of the free dioxetanes **1-2** that served as controls, and the siderophore dioxetane probes **3-9** was performed as summarized in Figure 5.2.

In brief, the enoether **13** could be obtained by reacting phenol **11** with the benzyl bromide **12**. Amide couplings at the acrylic acid moiety, combined with the oxidation of the olefin with singlet oxygen, yielded the dioxetanes **1-2** and the monocatechol dioxetane **7** over two to three synthetic steps. The DOTAM- and MECAM-based dioxetanes **3-6** were synthesized either through a sequence of copper-catalyzed azide-alkyne cycloaddition (CuAAC) followed by

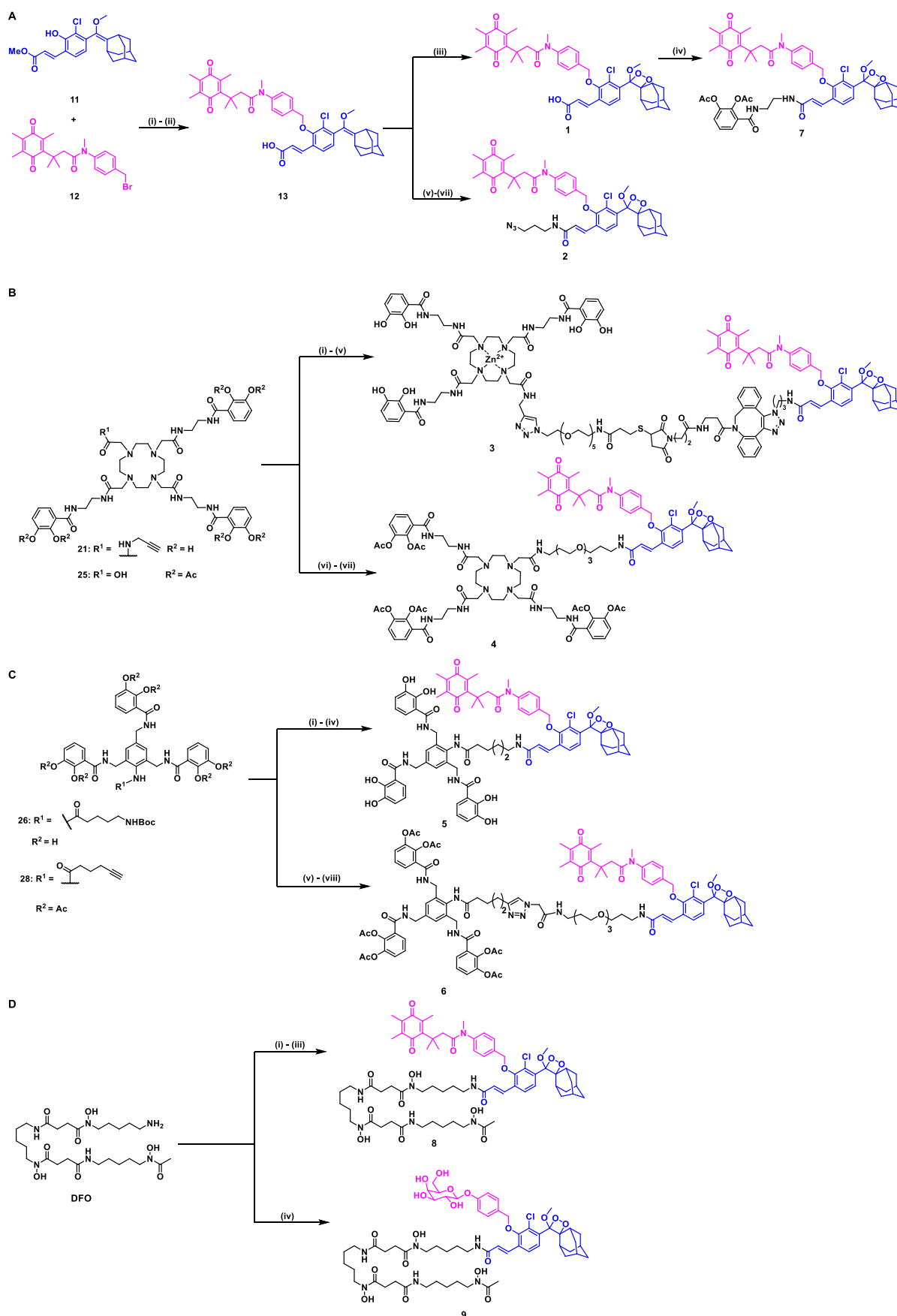


Figure 5.2. Synthesis of dioxetanes **1-2** and siderophore dioxetane probes **3-9**. (A) See also Figures S5.1, S5.2 and S5.6. (i) K_2CO_3 , DMF, 50 °C, 2 h, (ii) LiOH, THF:H₂O (2:1), 50 °C, 2 h, 67% over 2 steps, (iii) cat. methylene blue, O₂, yellow light, DCM/DMF (9:1), 20 min, 67% (iv) **31**, *iso*-butyl chloroformate,

N-methylmorpholine (NMM); THF, 0-25 °C, 2 h, then NMM, THF, 0-25 °C, 1 h, 43%, (v) NHS, DCC, DCM, 1.5 h, (vi) 3-azidopropan-1-amine, DMF, 30 min, 69% over 2 steps, (vii) cat. methylene blue, O₂, yellow light, DCM/DMF (9:1), 20 min, 85%, (B) See also Figures S5.2 and S5.3. (i) **21**, Zn(OAc)₂, DMSO/H₂O (2:1), 23 °C, 5 min, then **20** in DMSO, 5 min, 23 °C; then sodium ascorbate/CuSO₄, THPTA, 1xPBS pH 7.4, 23 °C, 1 h, 76% (ii) 50% TFA, anhydrous DCM, TIPS, 2 h, 25 °C, Et₂O wash then centrifuge 4500 rcf, 15 min, 0 °C (iii) **23**, 1 M HEPES buffer pH 7.5, DMF (1:1), overnight, 25 °C, 96% over 2 steps, (iv) **2a**, MeOH, overnight, 25 °C, quantitative, (v) cat. methylene blue, DCM/DMF (1:9), O₂, yellow light, 10 min, 85%, (vi) **25**, *iso*-butyl-chloroformate, NMM, THF, 0-23 °C, 2 h, then **24**, NMM, THF, 0-23 °C, 1 h, 67% (vii) cat. methylene blue, O₂, yellow light, DCM/DMF (1:9), 1% AcOH, 25 °C, 30 min, 47%, (C) See also Figures S5.4 and S5.5. (i) **26**, TFA, DCM, 1 h, (ii) **16**, NHS, DCC, DCM, (iii) TEA, DMF, yield over 3 steps 59%, (iv) cat. methylene blue, O₂, yellow light, DCM:DMF (9:1), 30 min, 84%, (v) **28**, 2-azido acetic acid, sodium ascorbate, CuSO₄, THPTA, DMSO, 1xPBS pH 7.4, 24 °C, 3 h, 1% AcOH, 74%, (vi) *iso*-butyl chloroformate, NMM, THF, 0-23 °C, 2 h, (vii) **24**, NMM, THF, 0-23 °C, 1 h, 67% (viii) cat. methylene blue, O₂, yellow light, DCM/DMF (1:9), 1% AcOH, 25 °C, 30 min, 63%, (D) See also Figures S5.7 and S5.8. (i) **13**, DCC, NHS, 1.5 h, (ii) desferrioxamine (DFO) mesylate salt, TEA, DMF, 30 min, (iii) cat. methylene blue, O₂, yellow light, DCM, 5 min, 52% over 3 steps. (iv) **32**, TEA, DMF, 40%. For more details and substrate structures, see the Supporting Information.

mixed-anhydride amide coupling, or a strain-promoted azide-alkyne cycloaddition (SPAAC), with subsequent oxidation to the dioxetane. The DFO siderophore was linked to the acrylic acid moiety of enoether **13** via its primary amine, and successive dioxygenation afforded **8**. In a similar manner, the previously synthesized acrylic acid **32**³⁰ was coupled to DFO to yield probe **9**. In total, two free dioxetanes and seven siderophore dioxetane probes were synthesized in up to nine steps for the longest linear sequence. First, we evaluated the activation of the free and the conjugated dioxetanes **1-9**. The incubation of **1-8** with NaBH₄ (1 mM) or of **9** with β-galactosidase (1.5 EU/mL) produced a bright chemiluminescent signal, clearly distinct from the unactivated control (Figure 5.3, Figure S5.9).

The acrylic acid dioxetane **1** showed a 2-4 fold higher light emission compared to all other tested compounds (Figure 5.3A). However, the probes **2-9**, with an acrylic amide instead of the acid, generally had a two to four - fold higher S/B ratio than **1** (Figure 5.3B). As reported before, an electron-withdrawing acrylic acid moiety at the phenoxy dioxetane drastically increased light emission compared to Schaap's probes.³¹ Consistently, a more electron-rich acrylic amide at the same position decreased light emission while improving the probes stability. Upon addition of the activators, both DFO dioxetanes showed an immediate chemiluminescence emission, which reached its maximum after 5-10 minutes and then declined gradually (Figure 5.3C-D). On average, the DFO probe **8** had a similar intensity as dioxetane **2** and was 2-3 fold brighter than the catechol siderophores **3-7** (Figure 5.3A). According to literature data, luminol- as well as electro-generated chemiluminescence can be

effectively quenched by catechol or quinone addition in solution by either a concurrent radical-mediated, a direct excited-state, or a redox-mediated quenching mechanism.^{32, 33, 34} We hypothesized that the reduced chemiluminescence for **3-7** might be due to intra- or intermolecular quenching by the siderophore's catechol groups. To test this, we incubated **1** with three different catechols (Q1 with free, Q2 with unstable, acetylated or Q3 with stable, methylated phenol moieties) in a three-fold excess to reproduce the stoichiometry of a triscatecholate siderophore (Figure 5.4A). Chemiluminescence required the presence of both **1** and of the activator NaBH₄ (Figure 5.4 and Figure S5.14). The highest luminescence was observed for the unquenched condition (Figure 5.4B, red curve). Pronounced signal reductions were observed for the addition of free catechol Q1 and, to a smaller extent, for the acetylated catechol Q2 (purple and green curves). The addition of Q3 (orange curve), resulted in a slight, non-significantly reduced overall signal. Thus, free phenol groups, which may also be generated by acetyl cleavage from Q2, displayed more significant quenching than methyl ethers. Because an intermolecular quenching was possible, it is likely that also an intramolecular process is operative in **3-7** (potential mechanisms are outlined in Scheme S1).

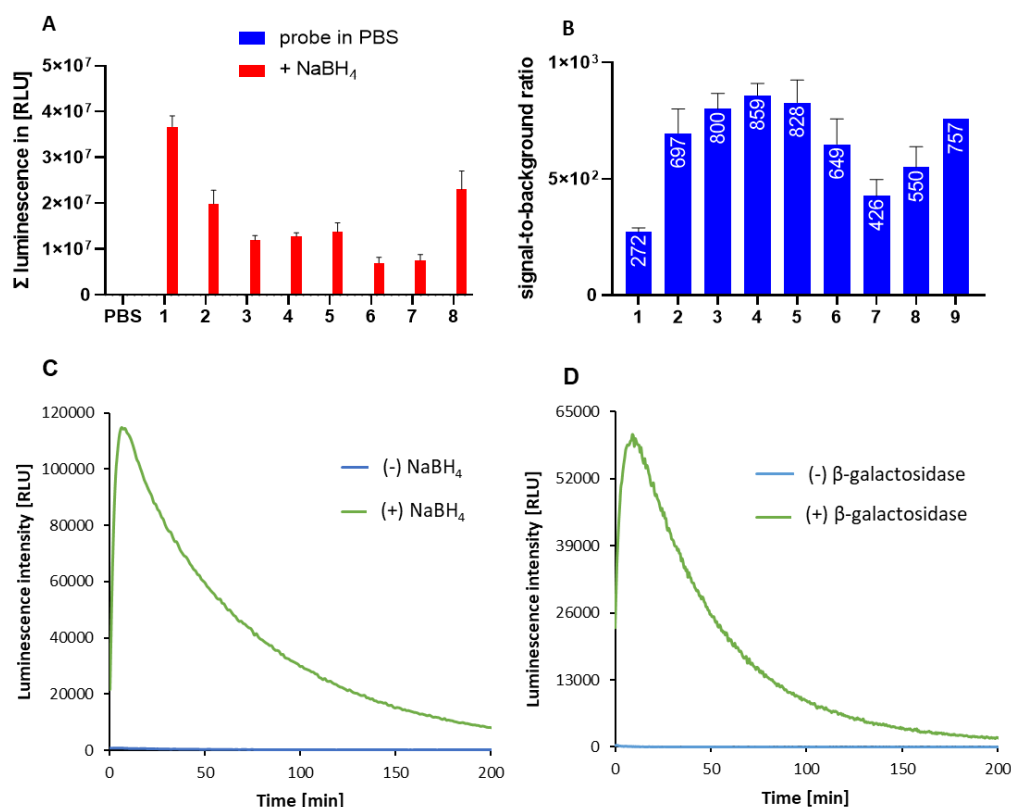


Figure 5.3. *In vitro* chemiluminescence induction. (A) Total light emission for quinone oxidoreductase-triggered dioxetanes **1-2** and siderophore-conjugates **3-9** ± 1 mM NaBH₄, n = 3, error bars ± standard error of mean (SEM). (B) Signal-to-background (S/B) ratios for **1-9**, n = 3, error bars ± SEM. (C) Chemiluminescence kinetic profiles following *in vitro* activation of **8** in PBS at pH 7.4 ± 1 mM NaBH₄. (D) Chemiluminescence kinetic profiles following *in vitro* activation of **9** in PBS at pH 7.4 ± β-galactosidase [1.5 EU/mL].

We also note that a similar photon-induced electron transfer (PET) quenching effect by free catechol was reported for the excited state of fluorescence dyes; this effect was blocked upon acylation.³⁵ In summary, the data suggest a catechol-mediated chemiluminescence quenching and thus explain the observed lower intensities for **3-7**.

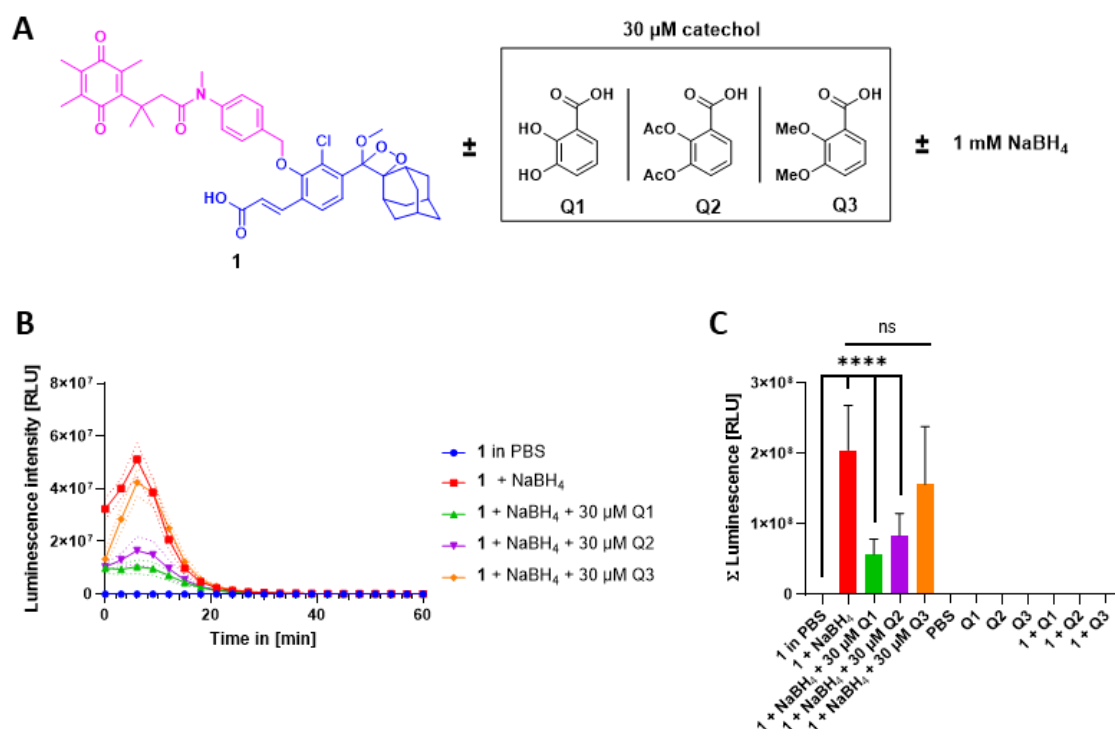


Figure 5.4. Quenching of dioxetane chemiluminescence by catechols. (A) Reagents were **1** (10 μM) in PBS at pH 7.4, \pm 30 μM quencher Q₁ (2,3-dihydroxybenzoic acid), Q₂ (2,3-diacetoxybenzoic acid) or Q₃ (dimethoxybenzoic acid), \pm 1 mM NaBH₄ as a chemical activator. (B) Chemiluminescence kinetic profiles and (C) summed chemiluminescence over 60 minutes in [RLU] for 10 μM probe **1** \pm 30 μM quencher Q₁, Q₂ or Q₃ and \pm 1 mM NaBH₄ as a chemical activator, including controls (Q_x + **1**, Q_x, PBS), n = 3, error bars correspond to \pm standard error of mean (SEM). Controls are shown in Figure S5.9A.

In order to demonstrate that the TML moiety and a subsequent chemiluminescence signal in **8** can not only be triggered chemically, but also enzymatically, the probe was incubated with two bacterial NADH-dependent quinone oxidoreductases, one from a Gram-negative and one from a Gram-positive species. *E. coli* quinone oxidoreductase 2 (QOR2) was obtained by homologous expression in *E. coli*, while the diaphorase from *Clostridium kluyveri* was commercially available (Figure S5.12).³⁶ Methyl benzoquinone (MBQ) served as positive control substrate for both enzymes, and the obtained k_{cat} and K_{m} values for MBQ reduction by both enzymes were similar to previously reported values (Tables S5.1 and S5.2, Figure S5.11

and S5.13). Fitting of the data to the Michaelis Menten equation showed that diaphorase and QOR2 readily reduced probe **8** (V_{max} of 9.5 and 19.35 $\mu\text{M}/\text{min}$, respectively. Enzyme addition also lead to a bright luminescence signal over five hours that was significantly larger than the control in the absence of enzymes (Figures S5.11 B/C and S5.13 B/C). The higher V_{max} , k_{cat} and K_m values for the activation of **8** with QOR2 are reflected by the increased chemiluminescence signals compared to the incubation with diaphorase. A sequence homology search (pBLAST) for QOR2 from *E. coli* and the commercial diaphorase yielded more than 200 sequences from various bacterial genera express similar proteins such as *Klebsiella*, *Pseudomonas*, *Shigella*, *Salmonella*, *Acinetobacter*, *Clostridium*, *Staphylococcus* (Supplementary Data File). This finding supports the potential for the activation of **8** by a broad range of pathogens. Next, we investigated whether the siderophore dioxetane conjugates retained their ability to enter bacterial cells through siderophore transporters, which is a prerequisite for their activation and excitation. For this purpose, a complementation assay that measured the conjugate-mediated delivery of ferric iron into bacteria was applied. The *E. coli* ΔentA and *P. aeruginosa* ΔpvdD $\Delta\text{pchE-F}$ strains cannot biosynthesize their endogenous siderophores enterobactin (ENT) or pyoverdine/ pyochelin (PYO/PCH), respectively and thus are unable to grow under iron-restricted conditions, except when a suitable (xeno-) siderophore is added (Figure 5.5).

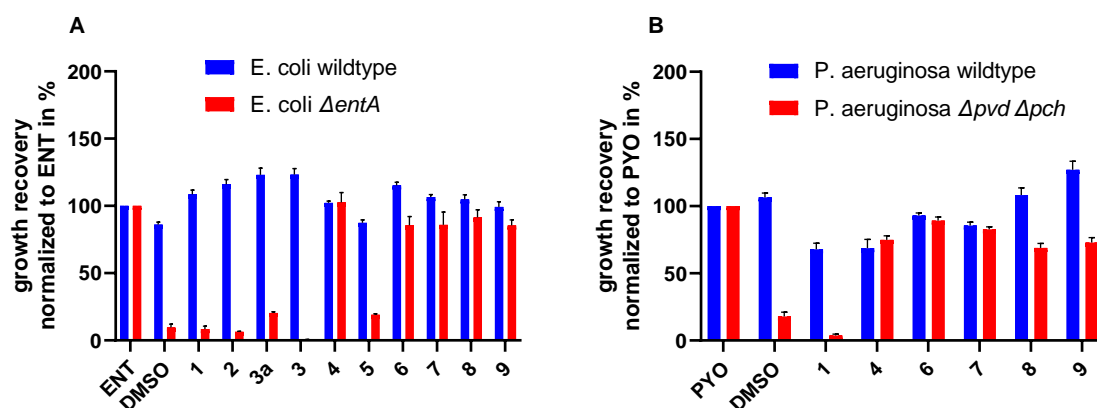


Figure 5.5 Probe-induced growth recovery in siderophore-deficient *E. coli* and *P. aeruginosa* mutants. (A) Growth recovery in the *E. coli* wildtype and enterobactin (ENT) – deficient strain ΔentA . The relative growth normalized to ENT is plotted in %. (B) Growth recovery in the *P. aeruginosa* wildtype and pyoverdine, pyochelin (PYO/PCH) – deficient strain (ΔpvdD $\Delta\text{pchE-F}$). The relative growth, normalized to PYO is plotted in %. All bacteria were grown in phosphate-buffered LMR medium and incubated in the presence of 10 μM compound (or 1% DMSO) and 10 μM FeCl_3 for 48 hours at 37 $^\circ\text{C}$, $n = 3$. Error bars correspond to \pm standard error of mean (SEM)

The exogenous addition of the respective natural siderophores, restored the growth in both mutants. The solvent control as well as the free dioxetanes **1** and **2** did not foster bacterial growth. The DOTAM dioxetane **3** was unable to complement iron-deficiency, and the corresponding deoxygenated enolether 3a performed only slightly better (Figure 5.5A). In contrast, five conjugates (**4**, **6-9**) restored bacterial growth efficiently in both mutant strains. Compound **5** showed a less pronounced, but still detectable growth. The robust growth recovery of **4** and **6-9** in *E. coli* was confirmed in *P. aeruginosa* (Figure 5.5B). The results indicate the probe's capability to shuttle ferric iron into the bacteria in the absence and also in the presence of natural siderophores, hereby proving that the necessary condition of their import is fulfilled. Given the small amounts administered as a single dose, we do not expect the probes to aggravate infections, even when applied *in vivo*. Probes with proven ability to transport iron into bacteria, i.e. the siderophore dioxetane conjugates **4**, **6**, **7**, **8**, **9** and control dioxetane **2**, were selected to visualize ESKAPE pathogens by chemiluminescence in iron-depleted, cation-adjusted medium (IDCAM) in kinetic experiments over 20 hours (Figure 5.6 and S5.15). Analogous to the *in vitro* results, the probes had good S/B ratios (not shown) and remained stable in the medium for 20 hours. A mediocre signal was observed for the free dioxetane **2** only in the presence of Gram-positive bacteria, while no chemiluminescence could be detected in Gram-negative bacteria (Figure 5.6E-F and Figure S5.16). As mentioned in the introduction, the double-layered cell wall of Gram-negative bacteria acts as a tight barrier, preventing efficient dioxetane accumulation and activation. In contrast, all five siderophore conjugates displayed a strong activation by at least three out of the six tested ESKAPE bacteria. DOTAM probe **4** and MECAM probe **6** were activated by *E. coli*, *A. baumannii*, *S. aureus*, and a lower signal for *P. aeruginosa* and *K. pneumoniae* was observed (Figure S5.10A-B). Monocatechol probe **7** showed chemiluminescence for *K. pneumoniae*, *A. baumannii* and the two Gram-positive strains. Commonly, the catechol probes reached their maximum intensity within 15-30 minutes after onset, then declined 10^3 - 10^5 fold within 5-7 hours. We assume that the time delay of the signal reflected a lag and delay phase of bacterial growth after their exposure to the IDCAM medium, while the following exponential growth led to enhanced chemiluminescence.³⁷ The DFO dioxetanes **8** and **9** both showed a bright signal for all six bacteria, with a two- to four-fold higher intensity for the Gram-negative strains (Figure 5.6A-D). The TML trigger of probe **8** achieved higher luminescence intensities on average than probe **9** carrying a β -galactosidase trigger.

A similar complementation assay with the chromogenic substrate *ortho*-nitrophenyl- β -D-galacto-pyranoside was conducted, as only a subset of the bacterial strains was reported to hydrolyze β -glycosidic bonds.³⁸⁻⁴³ A shift from colorless to bright yellow ($\lambda_{\text{Ex}} = 400$ nm) due to the release of the *ortho*-nitro phenol was observed for all strains, thus confirming a unanimous β -galactosidase activity with broad substrate tolerance (Figure S5.17).⁴⁴

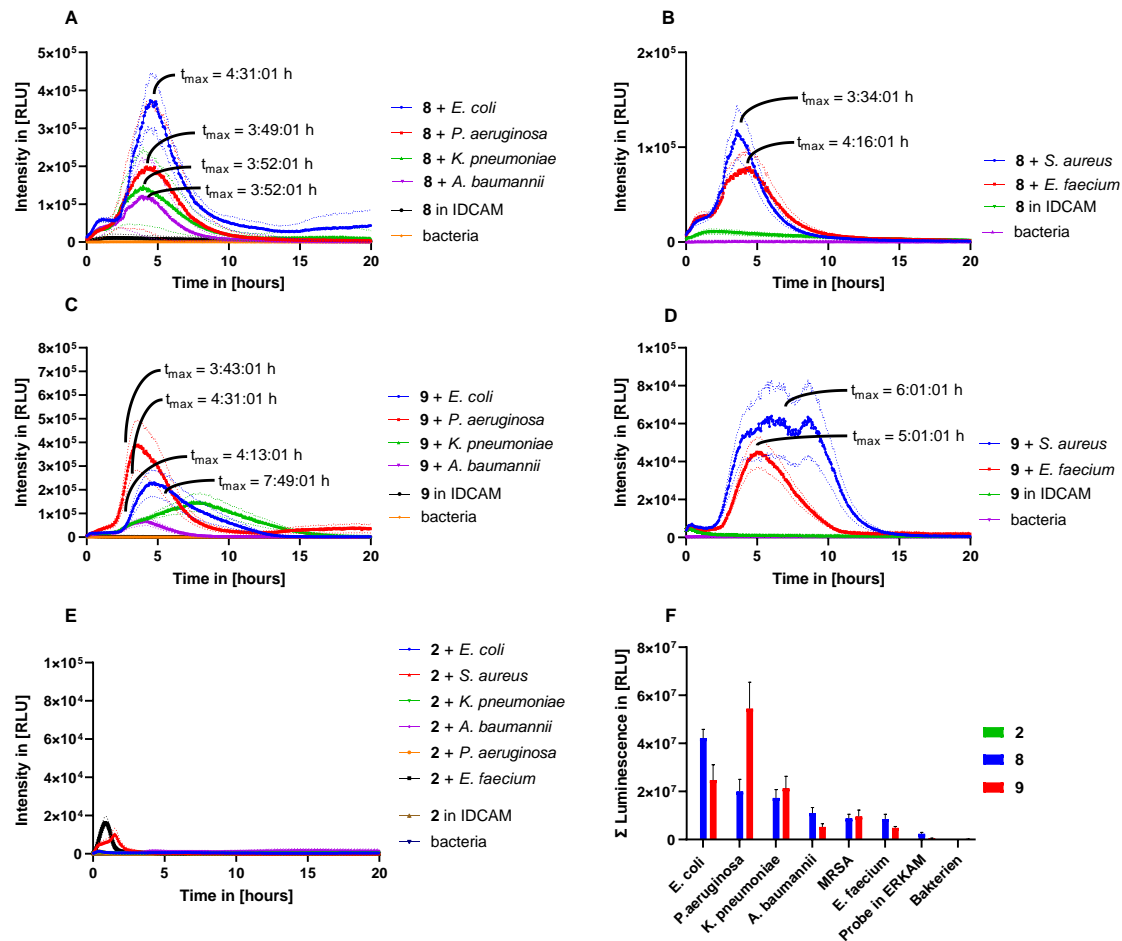


Figure 5.6. Chemiluminescence kinetics in bacterial pathogens. (A) Probe **8** ± Gram-negative bacteria (*E. coli*, *P. aeruginosa*, *K. pneumoniae*, *A. baumannii*). (B) Probe **8** ± Gram-positive bacteria (*E. faecium*, *S. aureus*). (C) Probe **9** ± Gram-negative bacteria (*E. coli*, *P. aeruginosa*, *K. pneumoniae*, *A. baumannii*). (D) Probe **9** ± Gram-positive bacteria (*E. faecium*, *S. aureus*). (E) Control **2** ± Gram-positive and -negative bacteria (*E. faecium*, *S. aureus*, *E. coli*, *P. aeruginosa*, *K. pneumoniae*, *A. baumannii*). Dotted lines correspond to the ± standard error of mean (SEM), (n = 3). (F) Total photon count of **2**, **8** and **9** over 20 h. All experiments n = 3, final probe concentration of 10 μM in iron-depleted, cation-adjusted medium (IDCAM). The error bars correspond to the ± standard error of the mean (SEM). t_{max} indicates the time point with the highest luminescence signal.

Next, we verified the stability of **8** and **9** in the bacterial culture supernatant, in order to underpin their activation merely inside bacteria. Bacteria are known to secrete enzymes into the surrounding to promote the extracellular decomposition of macromolecules into smaller products, than can then be taken up as nutrients. Therefore, an extracellular secretion and unspecific activation by microbial enzymes seems possible.^{45, 46} TML-triggered **8** remained inactive and stable in the presence of all supernatants (Figure S5.18A-B). In contrast, **9** showed luminescence in *K. pneumoniae* supernatant, that was ~20-fold weaker compared to the incubation with the live pathogen. An OD_{600nm} measurement after 20 hours excluded a

bacterial contamination as the source for this lower probe activation (Figure S5.18E). No induction was observed by culture supernatants from the other ESKAPE pathogens (Figure S5.18C-D). Based on the superior stability properties in the culture supernatant, probe **8** was selected as a frontrunner within the set. We synthesized an analogous fluorescent probe **10** with umbelliferone as the fluorescent reporter (Figure 5.7A) to compare its efficiency *in vitro* and upon bacterial incubation with that of **8**. In PBS, a high background signal was observed, and upon activation with NaBH₄ the fluorescent signal rapidly reached its characteristic plateau (Figure 5.7A).

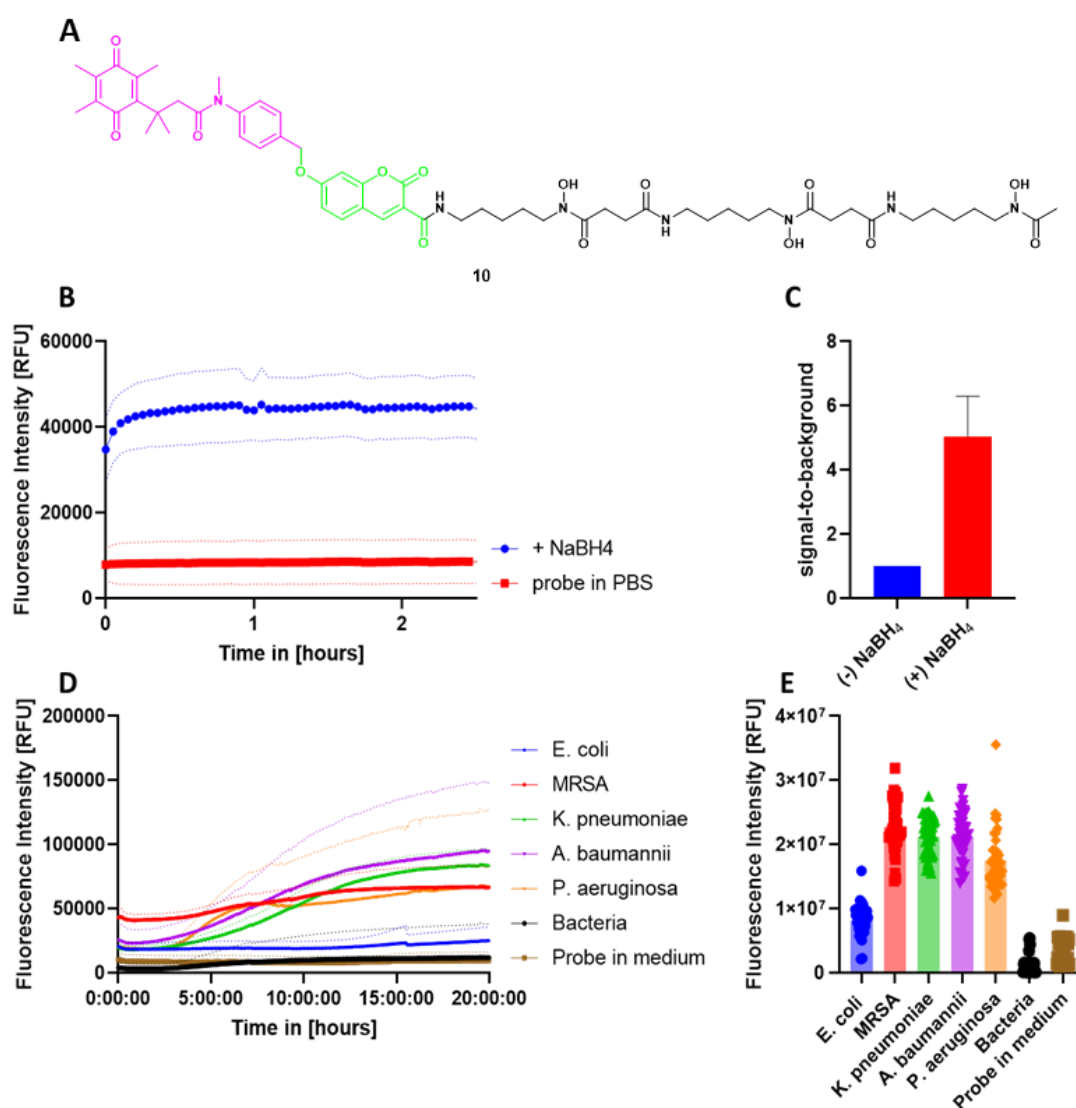


Figure 5.7. Characterization of turn-on fluorescent TML-coumarin DFO conjugate **10**. (A) Structure of **10**. The siderophore is shown in black, the coumarin dye in green and the TML trigger in pink. (B) Fluorescence kinetics after chemical activation of **10** (10 μM) ± 1 mM NaBH₄ in PBS at pH 7.4 over 2.5 hours. n = 3, dotted lines depict ± standard error of mean (SEM). (C) Signal-to-background ratio of 10 ± 1 mM NaBH₄. Error bars correspond to ± SEM. (D) Fluorescence kinetic profiles of **10** (10 μM) ± bacterial pathogens, n = 4, dotted lines depict ± SEM. (E) Summed fluorescence intensities, n = 4, error ± SEM.

The S/B ratio of **10** was 110-fold lower than for the analogous chemiluminescent probe **8** and more than 40-fold lower compared to dioxetane **2**, which had the lowest ratio amongst all compounds (Figure 5.7B-C). The higher background of many biological samples in the blue-cyan visible light range, where the umbelliferon of **10** is emissive, did not allow a direct comparison of the chemiluminescence and fluorescence outputs. However, also when directly comparing fluorescent emissions of **8** vs. **10** at 540 nm, we found that the fluorescent S/B ratio for **8** was 15-fold higher compared to that of **10** (Figure S5.10). In bacteria, **10** was activated by four out of five tested ESKAPE pathogens, with a minor activation in *E. coli*, and reached its plateau after seven to ten hours. The proportion of average background signal for the fluorescent probe in the presence of Gram-negative bacteria was more than twice as high ($23.9 \pm 11.0\%$) compared to the chemiluminescent counterparts **8** and **9** ($8.5 \pm 6.6\%$). Overall, the comparisons demonstrate a clear superiority of chemiluminescent vs. fluorescent modes of detection. Both DFO probes showed a bright luminescence signal for all ESKAPE pathogens, including critical pathogens from the WHO priority list.⁴⁷ As mentioned above, the prerequisite for a luminescence signal is the recognition and internalization through a chelator-specific siderophore receptor, followed by subsequent activation. The broad scope of both probes are probably due to the wide prevalence of ferrioxamine siderophore transporters i.e. FhuD2 in *S. aureus*,⁴⁸ FoxA in *P. aeruginosa*,⁴⁹ FhuE in *E. coli* or *A. baumannii*,^{50, 51} as well as in *K. pneumoniae*.⁵² Upon cation-DFO supplementation, previous studies revealed an increased pathogen growth, effects on biofilm formation and a modulated severity of infection. Taken together, these results indicate the acceptance of DFO as a xenosiderophore with multifaceted modes-of-action.^{53,54} Additionally, a screening with gallium-68-complexed DFO in various strains confirmed the accumulation of the latter in a broad-spectrum of clinical, prokaryotic pathogens.⁵⁵

Some opportunistic pathogens can adapt smoothly to various environments and persist within cells of the host, e.g. in infections of the lung.^{56, 57} To demonstrate the applicability of the best probe **8** for the detection of intracellular pathogens, an infection model in confluent A549 human lung epithelial cells (LECs) was applied (Figure 5.8A). Cells were infected with the facultative intracellular pathogens *P. aeruginosa* or *S. aureus* in iron-depleted medium at a multiplicity of infection of 10 with $9.52\text{-}9.92 \times 10^5$ CFUs. After 1.5 h, the extracellular bacteria were removed either by a rigorous washing step or treatment with gentamicin, that lacks the ability to penetrate into mammalian cells.⁵⁸ Then the pre-incubated siderophore probe (10 μM) was added to detect residual bacteria. Moreover, we monitored whether any probe was unspecifically activated by uninfected LECs. The presence of intracellularly residing bacteria after the infection was verified by lysis, plating and subsequent colony forming unit (CFU) counting of the serially diluted cell lysates (Figure 5.8E).

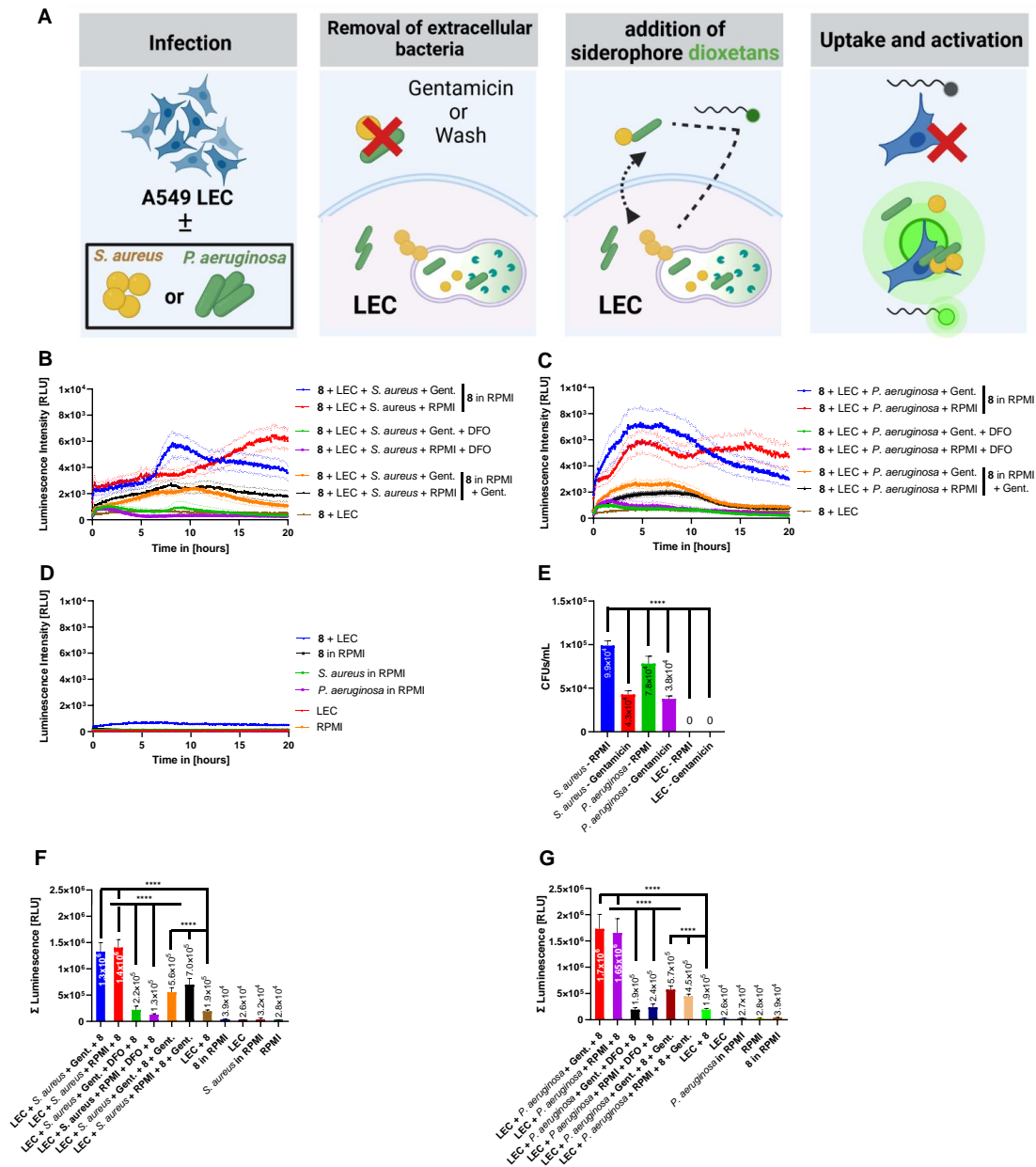


Figure 5.8. Detection of intracellular bacteria in A549 lung epithelial cells. (A) Experimental workflow for A549 lung epithelial cell (LEC) infection and subsequent bacterial chemiluminescence imaging of *P. aeruginosa* or methicillin-resistant *S. aureus* at a multiplicity of infection (MOI) of 10. (B) Chemiluminescence kinetic profiles of LECs infected with *S. aureus* followed by gentamicin treatment or a thorough wash and incubation with **8**. (C) Chemiluminescence kinetic profiles of LECs infected with *P. aeruginosa* followed by gentamicin treatment or a thorough wash and incubation with **8**. (D) Chemiluminescence kinetic profiles of LECs treated with gentamicin or with a thorough wash and incubated with **8**. (E) Quantification of intracellular bacteria after infection of A549 LECs with *S. aureus* or *P. aeruginosa*. (F) Summed luminescence values for *S. aureus* treatments including controls. (G) Summed luminescence values for *P. aeruginosa* treatments including controls. Dotted lines and error bars correspond to \pm standard error of mean (SEM), $n = 3-6$. All experiments in iron-depleted, cation-adjusted medium (IDCAM). The summed intensities in (F) and (G) were compared by two-way ANOVA (****, $p < 0.0001$). Gent. = gentamicin.

In a previous study by Son *et al.*, unconjugated **1** was readily activated *in vitro* by NQO1, an eukaryotic quinone oxidoreductase, which is overexpressed in A549 cells.²⁹ Indeed, incubation of **1** with sterile or bacteria-infected LECs resulted in bright luminescence (Figure S5.19A). Thus, the unconjugated dioxetane was unable to distinguish eukaryotic cells from a prokaryotic infection. In contrast, **8**, essentially a siderophore-conjugated **1**, showed a 10.000-fold lower signal in the presence of sterile LECs. However, bacteria-infected LECs showed bright activation and had five- to eight-fold higher luminescence intensities compared to baseline (Figure 5.8B- D). This difference became even more apparent when comparing the respective summed luminescence values (Figure 5.8F-G). Similar correlations between the treatment groups were found for a fluorescent readout of the weak benzoate fluorophore **IV** ($\lambda_{\text{Ex}} = 340$ nm), which was formed following chemiexcitation (Figure S5.20 and Figure 5.1), while the kinetics with an increasing emission reflected the accumulation of the fluorophore over time. Two further experimental groups were studied. The permanent addition of gentamicin to the RPMI medium restricted extracellular bacterial growth even after the probe addition; this led to a 2-3 fold reductions of chemiluminescence compared to gentamicin-free incubations (Figure 5.8B-C and F-G). Secondly, bacterial transporters were blocked with a tenfold excess of free DFO before and during infection; this led to 7-11 fold reductions of chemiluminescence compared to DFO-free incubations (Figure 5.8B-C and F-G). These findings underline the siderophore's key role for an efficient translocation and activation via the bacterial iron transport systems. In sum, all events that yielded a bright probe activation were infection- and siderophore-dependent, and thus demonstrated the probe's ability to distinguish even small amounts of bacteria from sterile host cells. A comparable curve shape and similar intensity was seen for the DOTAM probe **4**, while monocatechol **7** reached even higher luminosity values (Figure S5.19). In either case, an infection was required to obtain a signal. Previous studies reported that the free DFO siderophore accumulated randomly by fluid-phase endocytosis into mammalian cells. This process was assumed to be much slower than the active transport by bacterial siderophore transporters.⁵⁹ The induction of luminescence by the bacteria alone took several hours (Figure 5.6), and an even slower onset of signals would be expected for intracellular bacteria within LECs.

As the opposite, i.e. an instant luminescence signal was observed, we hypothesize that the probes were not activated by bacteria within LECs, but by small amounts of released enzymes. These may stem from the bacteria, or also from the LECs, as bacterial infections have been reported to cause membrane damage and a spill of NQO1 from the mammalian cells' cytosol.⁶⁰ Taken together, this renders siderophore dioxetane conjugates promising candidates for the

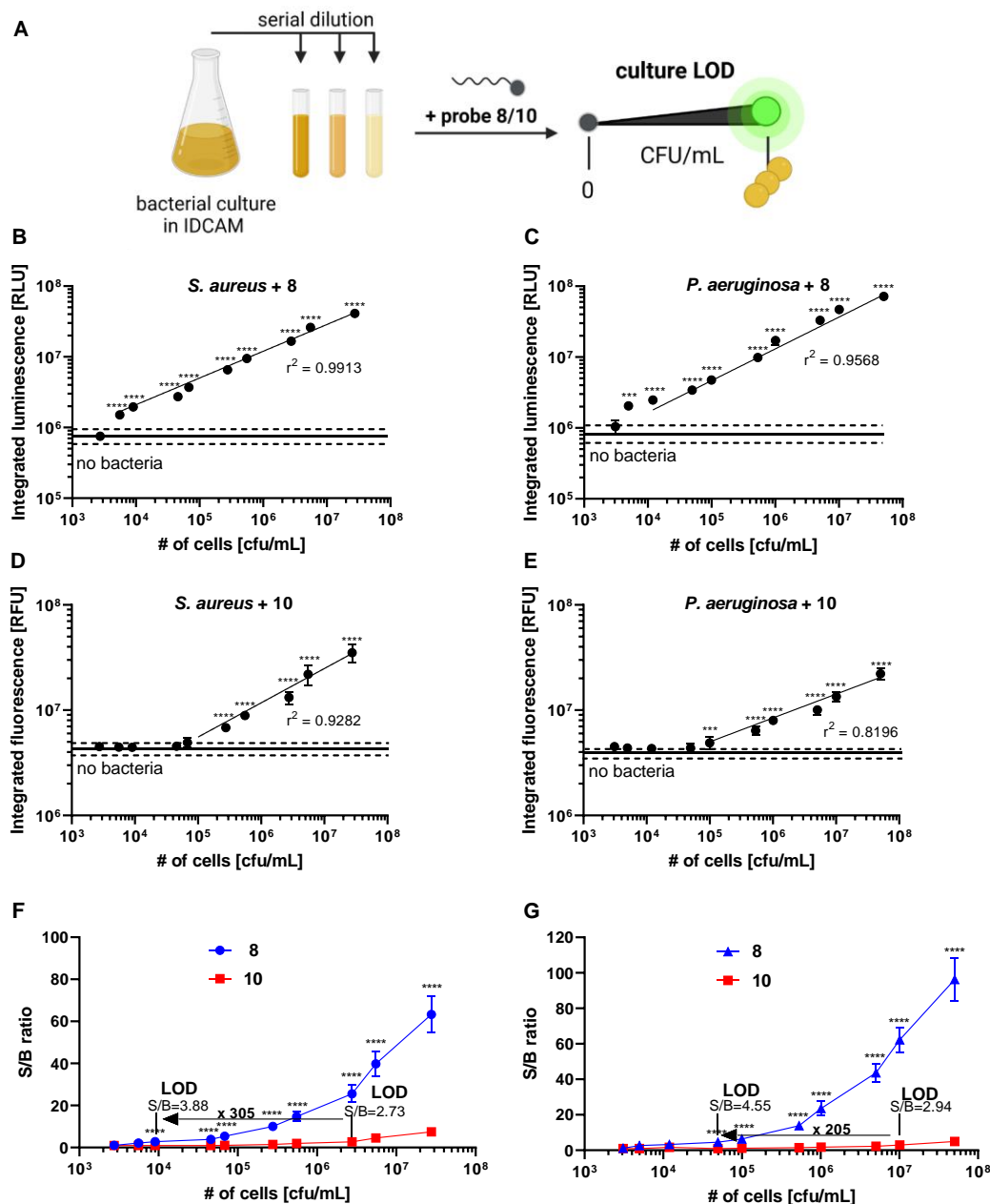


Figure 5.9. LOD determination of siderophores probes.(A) To determine the limit of detection (LOD), cultures of *S. aureus* or *P. aeruginosa* were iron-starved, then serially diluted in iron-depleted, cation adjusted medium and then incubated with chemiluminescent probe **8** or fluorescent probe **10** (10 μ M each). Total integrated signal after 24 h of incubation of (B) **8** with *S. aureus*, (C) **8** with *P. aeruginosa*, (D) **10** with *S. aureus* and (E) **10** with *P. aeruginosa* (mean \pm SEM, n = 4) is shown. Horizontal lines show the mean signal of probe in medium \pm SEM (dashed) of control samples lacking bacteria. Best-fit lines show linear regressions of the log-transformed data. For all experiments, each sample was compared to the no-bacteria control by one-way ANOVA (***, p=0.001-0.005, **** p<0.0001). The signal-to-background (S/B) ratios were plotted against different *S. aureus* (F) and *P. aeruginosa* (G) concentrations for the two probes. The S/B ratios of the two probes were compared by two-way ANOVA (****, p < 0.0001).

in vitro detection of bacteria, but also for the sensitive monitoring of bacterial infections in tissues. For a potential use of the probes as a diagnostic tool to detect bacteria, the ability to detect only small numbers of CFUs, such as usually found in medical samples, is important. To this end, the limits of detection (LODs) of live *S. aureus* and *P. aeruginosa* bacteria by chemiluminescent **8** and its fluorescent analog **10** were determined under iron-depleted conditions. Optical density (OD_{600}) measurements were linked to numbers of living bacteria by CFU counting through plating after iron starvation (see the Supporting Information). *S. aureus* or *P. aeruginosa* bacteria were starved for ferric iron and subsequently serially diluted in IDCAM prior to incubation with 10 μ M probe (Figure 5.9A). After 24 hours of luminescence (Figure 5.9B/C) or fluorescence (Figure 5.9D/E) recording, the signals were integrated and plotted against the previously obtained bacterial count using logarithmic scales. Best fit lines showed a linear decline of the signal upon reduction of the initial CFUs/mL for all tested strains and probes. Chemiluminescent **8** displayed a later decline of the summed signal at lower bacterial concentrations than observed for the fluorescent probe **10**, and hence could detect a smaller number of Gram-positive or -negative pathogens. From the summed values, the signal-to-background (S/B) ratios for each probe could be calculated and were plotted against the logarithmic bacterial concentration (Figure 5.9F/G). Remarkably, **8** exhibited a LOD value of 9.1×10^3 CFU/mL for *S. aureus*, while **10** could minimally detect 2.8×10^6 CFU/mL of the same pathogen. Similarly, **8** exhibited an LOD value of 5.0×10^4 CFU/mL for *P. aeruginosa*, while **10** reliably detected 1.0×10^7 CFU/mL. The strongly enhanced sensitivity of **8** (305- and 205-fold, respectively) demonstrates a clear sensitivity advantage of chemiluminescent siderophore dioxetane probes for the detection of bacterial pathogens compared to fluorescent analogs. The ability to detect bacterial pathogens at low abundance in a clinical setting was probed by spiking *S. aureus* and *P. aeruginosa* at their LOD into sterile, human plasma, followed by addition of **8**. The luminescence (and also the fluorescence) signals were significantly higher in the presence of both prokaryotes compared to **8** in sterile plasma (Figure S5.21). Thus, the probe displayed sufficient stability in a complex biological environment to enable bacterial pathogen detection. Previous microbiological studies demonstrated that the bacterial CFU counts recovered from clinical samples (e.g. blood of patients) were commonly low.⁶¹ PCR-based methods have shown lower LODs (30-700 CFU/mL), but fail to distinguish DNA from live vs. dead bacteria or debris.⁶² Microfluidic methods, which employ antibody-coated microspheres and subsequent optical analysis to identify bacteria generally, had LOD values in a similar range (10^3 - 10^5 CFU/mL) as **8**.⁶³ A commercial bacterial viability kit (BacLight®) with fluorescent reagents exhibited a LOD with more than 10^6 CFU/mL of bacteria.⁶⁴ Compared to previous chemiluminescent probes for the detection of *Salmonella*, *Listeria* and *Mycobacteria*, **8** detected a similar bacterial concentration range (10^3 to 10^4 CFU/mL).^{14, 17}

5.3 Conclusion

In this study, we expanded the application of artificial siderophores as functional and versatile targeting entities to the chemiluminescent imaging of bacterial infections. DOTAM- and MECAM-based siderophore mimics were conjugated to enzyme-triggered dioxetanes in up to nine synthetic steps. All probes showed bright luminescence and very high S/B ratios *in vitro*, but hydroxamates were superior to catecholates due to the quenching effects of the latter. Notably, five siderophore conjugates retained their ability to shuttle iron into the bacterial cell, thereby enabling the reliable detection of a broad range of Gram-negative and Gram-positive pathogens. The advantages of a chemiluminescent vs. fluorescent detection principle of bacterial pathogens manifested in higher S/B ratios *in vitro* and in cells, that translated in lower limits of detection. Moreover, **4**, **7** and **8** succeeded to detect facultative intracellular pathogens in bacteria-infected LECs, and remained inactive when incubated with uninfected host cells. The study suggests that siderophore dioxetane conjugates may find valuable applications for the detection of microbes in food quality control as well as in the healthcare sector. It is a good basis to examine trigger-siderophore combinations more systematically and optimize them for high conjugate enrichment. In addition, the probe's performance across a broader panel of clinically relevant, drug-sensitive and drug-resistant clinical isolates per strain needs to be investigated further. Future projects will also include the development of IR-shifted dioxetane siderophore conjugates, which permit the broad-spectrum, chemiluminescent *in vivo* imaging of bacteria in rodent infection models. Beyond practical perspectives, the study illustrates how a molecular targeting can significantly improve the sensitivity and specificity of drug delivery. It also underlines the attractiveness and potential of the bacterial siderophore uptake system as an entry gate for the transport of cargo.

Acknowledgement

We thank Kirsten Harmrolfs and Christel Kakoschke for the measurement of NMR samples and Ulrike Beutling for the mass spectrometric measurement of probes and protein samples. We express our gratitude to Till Orth for help with siderophore synthesis and Bianka Karge, Aditya Shekhar, Virginia Njau and Mario Vetter for microbiology and cell cultivation support. We are also grateful to Vadim Korotkov and Hazel Fuchs for helpful comments and discussions on the manuscript. We thank Anja Meier for help with the timsTOF measurement of protein samples.

Funding information

We acknowledge funding by the DFG (grant number: BR 3572/4-1) and the Joint Program Initiative on Antimicrobial Resistance (JPI AMR, grant number: 01KI1825). C. P. thanks the “Fonds der chemischen Industrie” for a scholarship and L. P. was funded by the DFG project number BR 3572/4-1. D.S. thanks the Ministry of Health, ERA-NET, for funding.

Conflict of interest

The authors declare no conflict of interest.

Keywords

Siderophores • chemiluminescence • imaging • bacterial diagnostics • drug delivery

References

1. Butler, M. S.; Gigante, V.; Sati, H.; Paulin, S.; Al-Sulaiman, L.; Rex, J. H.; Fernandes, P.; Arias, C. A.; Paul, M.; Thwaites, G. E.; Czaplewski, L.; Alm, R. A.; Lienhardt, C.; Spigelman, M.; Silver, L. L.; Ohmagari, N.; Kozlov, R.; Harbarth, S.; Beyer, P., Analysis of the clinical pipeline of treatments for drug-resistant bacterial infections: Despite progress, more action is needed. *Antimicrob. Agents Chemother.* **2022**, *66* (3), e0199121.
2. Årdal, C.; Balasegaram, M.; Laxminarayan, R.; McAdams, D.; Outterson, K.; Rex, J. H.; Sumpradit, N., Antibiotic development — economic, regulatory and societal challenges. *Nat. Rev. Microbiol.* **2020**, *18* (5), 267-274.
3. Caliendo, A. M.; Gilbert, D. N.; Ginocchio, C. C.; Hanson, K. E.; May, L.; Quinn, T. C.; Tenover, F. C.; Alland, D.; Blaschke, A. J.; Bonomo, R. A.; Carroll, K. C.; Ferraro, M. J.; Hirschhorn, L. R.; Joseph, W. P.; Karchmer, T.; MacIntyre, A. T.; Reller, L. B.; Jackson, A. F., Better tests, better care: Improved diagnostics for infectious diseases. *Clin. Infect. Dis.* **2013**, *57* (suppl_3), S139-S170.
4. Wang, X.; Murthy, N., Bacterial imaging comes of age. *Sci. Transl. Med.* **2014**, *6* (259), 243-259.
5. Nieuwlaat, R.; Mbuagbaw, L.; Mertz, D.; Burrows, L. L.; Bowdish, D. M. E.; Moja, L.; Wright, G. D.; Schünemann, H. J., Coronavirus disease 2019 and antimicrobial resistance: Parallel and interacting health emergencies. *Clin. Infect. Dis.* **2020**, *72* (9), 1657-1659.
6. Dodeigne, C.; Thunus, L.; Lejeune, R., Chemiluminescence as diagnostic tool. A review. *Talanta* **2000**, *51* (3), 415-439.
7. Hananya, N.; Green, O.; Blau, R.; Satchi-Fainaro, R.; Shabat, D., A highly efficient chemiluminescence probe for the detection of singlet oxygen in living cells. *Angew. Chem. Int. Ed.* **2017**, *56* (39), 11793-11796.
8. Schaap, A. P.; Handley, R. S.; Giri, B. P., Chemical and enzymatic triggering of 1,2-dioxetanes. 1: Aryl esterase-catalyzed chemiluminescence from a naphthyl acetate-substituted dioxetane. *Tet. Lett.* **1987**, *28* (9), 935-938.
9. Schaap, A. P.; Chen, T.-S.; Handley, R. S.; DeSilva, R.; Giri, B. P., Chemical and enzymatic triggering of 1,2-dioxetanes. 2: fluoride-induced chemiluminescence from *tert*-butyldimethylsilyloxy-substituted dioxetanes. *Tet. Lett.* **1987**, *28* (11), 1155-1158.

10. Schaap, A. P.; Sandison, M. D.; Handley, R. S., Chemical and enzymatic triggering of 1,2-dioxetanes. 3: Alkaline phosphatase-catalyzed chemiluminescence from an aryl phosphate-substituted dioxetane. *Tet. Lett.* **1987**, 28 (11), 1159-1162.
11. Roth-Konforti, M. E.; Bauer, C. R.; Shabat, D., Unprecedented sensitivity in a probe for monitoring cathepsin B: Chemiluminescence microscopy cell-imaging of a natively expressed enzyme. *Angew. Chem. Int. Ed.* **2017**, 56 (49), 15633-15638.
12. Ye, S.; Hananya, N.; Green, O.; Chen, H.; Zhao, A. Q.; Shen, J.; Shabat, D.; Yang, D., A highly selective and sensitive chemiluminescent probe for real-time monitoring of hydrogen peroxide in cells and animals. *Angew. Chem. Int. Ed.* **2020**, 59 (34), 14326-14330.
13. Hananya, N.; Reid, J. P.; Green, O.; Sigman, M. S.; Shabat, D., Rapid chemiexcitation of phenoxy-dioxetane luminophores yields ultrasensitive chemiluminescence assays. *Chem. Sci.* **2019**, 10 (5), 1380-1385.
14. Babin, B. M.; Fernandez-Cuervo, G.; Sheng, J.; Green, O.; Ordonez, A. A.; Turner, M. L.; Keller, L. J.; Jain, S. K.; Shabat, D.; Bogoyo, M., Chemiluminescent protease probe for rapid, sensitive, and inexpensive detection of live *Mycobacterium tuberculosis*. *ACS Cent. Sci.* **2021**, 7 (5), 803-814.
15. Das, S.; Ihssen, J.; Wick, L.; Spitz, U.; Shabat, D., Chemiluminescent carbapenem-based molecular probe for detection of carbapenemase activity in live bacteria. *Chem. Eur. J.* **2020**, 26 (16), 3647-3652.
16. Gholap, S. P.; Yao, C.; Green, O.; Babjak, M.; Jakubec, P.; Malatinský, T.; Ihssen, J.; Wick, L.; Spitz, U.; Shabat, D., Chemiluminescence detection of hydrogen sulfide release by β -lactamase-catalyzed β -lactam biodegradation: Unprecedented pathway for monitoring β -lactam antibiotic bacterial resistance. *Bioconj. Chem.* **2021**, 32 (5), 991-1000.
17. Roth-Konforti, M.; Green, O.; Hupfeld, M.; Fieseler, L.; Heinrich, N.; Ihssen, J.; Vorberg, R.; Wick, L.; Spitz, U.; Shabat, D., Ultrasensitive detection of *Salmonella* and *Listeria monocytogenes* by small-molecule chemiluminescence probes. *Angew. Chem. Int. Ed.* **2019**, 58 (30), 10361-10367.
18. Hider, R. C.; Kong, X., Chemistry and biology of siderophores. *Nat. Prod. Rep.* **2010**, 27 (5), 637-657.
19. Miethke, M.; Marahiel, M. A., Siderophore-based iron acquisition and pathogen control. *Microbiol. Mol. Biol. Rev.* **2007**, 71 (3), 413-451.

20. Klahn, P.; Brönstrup, M., Bifunctional antimicrobial conjugates and hybrid antimicrobials. *Nat. Prod. Rep.* **2017**, *34* (7), 832-885.
21. Ji, C.; Miller, M. J., Siderophore–fluoroquinolone conjugates containing potential reduction-triggered linkers for drug release: synthesis and antibacterial activity. *BioMetals* **2015**, *28* (3), 541-551.
22. Ferreira, K.; Hu, H.-Y.; Fetz, V.; Prochnow, H.; Rais, B.; Müller, P. P.; Brönstrup, M., Multivalent siderophore–DOTAM conjugates as theranostics for imaging and treatment of bacterial infections. *Angew. Chem. Int. Ed.* **2017**, *56* (28), 8272-8276.
23. Pinkert, L.; Lai, Y.-H.; Peukert, C.; Hotop, S.-K.; Karge, B.; Schulze, L. M.; Grunenberg, J.; Brönstrup, M., Antibiotic conjugates with an artificial MECAM-based siderophore are potent agents against Gram-positive and Gram-negative bacterial pathogens. *J. Med. Chem.* **2021**, *64* (20), 15440-15460.
24. Peukert, C.; Langer, L. N. B.; Wegener, S. M.; Tutov, A.; Bankstahl, J. P.; Karge, B.; Bengel, F. M.; Ross, T. L.; Brönstrup, M., Optimization of artificial siderophores as ⁶⁸Ga-complexed PET tracers for in vivo imaging of bacterial infections. *J. Med. Chem.* **2021**, *64* (16), 12359-12378.
25. Hansen, W.; Yourassowsky, E., Detection of β -glucuronidase in lactose-fermenting members of the family *Enterobacteriaceae* and its presence in bacterial urine cultures. *J. Clin. Microbiol.* **1984**, *20* (6), 1177-1179.
26. Gadelle, D.; Raibaud, P.; Sacquet, E., β -Glucuronidase activities of intestinal bacteria determined both *in vitro* and *in vivo* in gnotobiotic rats. *Appl. Environ. Microbiol.* **1985**, *49* (3), 682-685.
27. Yagi, T., Bacterial NADH-quinone oxidoreductases. *J. Bioenerg. Biomembr.* **1991**, *23* (2), 211-225.
28. Green, O.; Eilon, T.; Hananya, N.; Gutkin, S.; Bauer, C. R.; Shabat, D., Opening a gateway for chemiluminescence cell imaging: Distinctive methodology for design of bright chemiluminescent dioxetane probes. *ACS Cent. Sci.* **2017**, *3* (4), 349-358.
29. Son, S.; Won, M.; Green, O.; Hananya, N.; Sharma, A.; Jeon, Y.; Kwak, J. H.; Sessler, J. L.; Shabat, D.; Kim, J. S., Chemiluminescent probe for the *in vitro* and *in vivo* imaging of cancers over-expressing NQO1. *Angew. Chem. Int. Ed.* **2019**, *58* (6), 1739-1743.

30. Eilon-Shaffer, T.; Roth-Konforti, M.; Eldar-Boock, A.; Satchi-Fainaro, R.; Shabat, D., *ortho*-Chlorination of phenoxy 1,2-dioxetane yields superior chemiluminescent probes for *in vitro* and *in vivo* imaging. *Org. Biomol. Chem.* **2018**, *16* (10), 1708-1712.
31. Hananya, N.; Shabat, D., Recent advances and challenges in luminescent imaging: Bright outlook for chemiluminescence of dioxetanes in water. *ACS Cent. Sci.* **2019**, *5* (6), 949-959.
32. Dongqin, Y.; Yanyan, H.; Yanyan, S.; Funan, C., Determination of catechol in water based on gold nanocluster-catalyzed chemiluminescence. *J. Lum.* **2017**, *187*, 186-192.
33. He, Y.; Huang, G.; Cui, H., Quenching the chemiluminescence of acridinium ester by graphene oxide for label-free and homogeneous DNA detection. *ACS Appl. Mat. Int.* **2013**, *5* (21), 11336-11340.
34. McCall, J.; Alexander, C.; Richter, M. M., Quenching of electrogenerated chemiluminescence by phenols, hydroquinones, catechols, and benzoquinones. *Anal. Chem.* **1999**, *71* (13), 2523-2527.
35. Kim, T.-I.; Kim, D.; Bouffard, J.; Kim, Y., Rapid, specific, and ultrasensitive fluorogenic sensing of phosgene through an enhanced PeT mechanism. *Sens. Actuators B Chem.* **2019**, *283*, 458-462.
36. Kim, I.-K.; Yim, H.-S.; Kim, M.-K.; Kim, D.-W.; Kim, Y.-M.; Cha, S.-S.; Kang, S.-O., Crystal structure of a new type of NADPH-dependent quinone oxidoreductase (QOR2) from *Escherichia coli*. *J. Mol. Biol.* **2008**, *379* (2), 372-384.
37. Rolfe, M. D.; Rice, C. J.; Lucchini, S.; Pin, C.; Thompson, A.; Cameron, A. D. S.; Alston, M.; Stringer, M. F.; Betts, R. P.; Baranyi, J.; Peck, M. W.; Hinton, J. C. D., Lag phase is a distinct growth phase that prepares bacteria for exponential growth and involves transient metal accumulation. *J. Bacteriol.* **2012**, *194* (3), 686-701.
38. BacDive, K. p. s. p. C., *Klebsiella pneumoniae subsp. pneumoniae* C122, [10.13145/bacdive4955.20211221.6](https://pubmed.ncbi.nlm.nih.gov/10.13145/bacdive4955.20211221.6) accessed 17.01.2022.
39. BacDive, *Staphylococcus aureus* DSM 11822, [10.13145/bacdive14461.20211221.6](https://pubmed.ncbi.nlm.nih.gov/10.13145/bacdive14461.20211221.6) accessed 17.01.2022.
40. BacDive, *Pseudomonas aeruginosa* PAO, [10.13145/bacdive12763.20211221.6](https://pubmed.ncbi.nlm.nih.gov/10.13145/bacdive12763.20211221.6) accessed 17.01.2022.
41. BacDive, *E. coli* W [10.13145/bacdive4428.20211221.6](https://pubmed.ncbi.nlm.nih.gov/10.13145/bacdive4428.20211221.6) accessed 17.01.2022.

42. BacDive, *Enterococcus faecium* DSM 20477 10.13145/bacdive5301.20211221.6 accessed 17.01.2022.
43. BacDive, *Acinetobacter baumannii* 2208 10.13145/bacdive8093.20211221.6 accessed 17.01.2022.
44. Flores, M.; Ford, E. G.; Janda, J. M., Value of the o-nitrophenyl-beta-D-galactopyranoside test to differentiate among the aerobic actinomycetes. *J. Clin Microbiol.* **1990**, 28 (9), 2142-2144.
45. Cezairliyan, B.; Ausubel, F. M., Investment in secreted enzymes during nutrient-limited growth is utility dependent. *Proc. Natl. Acad. Sci.* **2017**, 114 (37), E7796-E7802.
46. Aristoteli, L. P.; Willcox, M. D. P., Mucin degradation mechanisms by distinct *Pseudomonas aeruginosa* isolates *in vitro*. *Infect. Immun.* **2003**, 71 (10), 5565-5575.
47. Tacconelli, E.; Carrara, E.; Savoldi, A.; Harbarth, S.; Mendelson, M.; Monnet, D. L.; Pulcini, C.; Kahlmeter, G.; Kluytmans, J.; Carmeli, Y.; Ouellette, M.; Outtersson, K.; Patel, J.; Cavaleri, M.; Cox, E. M.; Houchens, C. R.; Grayson, M. L.; Hansen, P.; Singh, N.; Theuretzbacher, U.; Magrini, N., Discovery, research, and development of new antibiotics: The WHO priority list of antibiotic-resistant bacteria and tuberculosis. *Lancet Infect. Dis.* **2018**, 18 (3), 318-327.
48. Podkova, K. J.; Briere, L.-A. K.; Heinrichs, D. E.; Shilton, B. H., Crystal and solution structure analysis of FhuD2 from *Staphylococcus aureus* in multiple unliganded conformations and bound to ferrioxamine-B. *Biochemistry* **2014**, 53 (12), 2017-2031.
49. Josts, I.; Veith, K.; Tidow, H., Ternary structure of the outer membrane transporter FoxA with resolved signaling domain provides insights into TonB-mediated siderophore uptake. *Elife* **2019**, 8, 1-15.
50. Grinter, R.; Lithgow, T., Determination of the molecular basis for coprogen import by Gram-negative bacteria. *IUCrJ* **2019**, 6 (Pt 3), 401-411.
51. Funahashi, T.; Tanabe, T.; Mihara, K.; Miyamoto, K.; Tsujibo, H.; Yamamoto, S., Identification and characterization of an outer membrane receptor gene in *Acinetobacter baumannii* required for utilization of desferricoprogen, rhodotorulic acid, and desferrioxamine B as xenosiderophores. *Biol. Pharm. Bull* **2012**, 35 (5), 753-760.
52. Khimji, P. L.; Miles, A. A., Microbial iron-chelators and their action on *Klebsiella* infections in the skin of guinea-pigs. *Br. J. Exp. Pathol.* **1978**, 59 (2), 137-147.
53. Robins-Browne, R. M.; Prpic, J. K., Effects of iron and desferrioxamine on infections with *Yersinia enterocolitica*. *Infect. Immun.* **1985**, 47 (3), 774-779.

54. Banin, E.; Lozinski, A.; Brady, K. M.; Berenshtein, E.; Butterfield, P. W.; Moshe, M.; Chevion, M.; Greenberg, E. P.; Banin, E., The potential of desferrioxamine-gallium as an anti-*Pseudomonas* therapeutic agent. *Proc. Natl. Acad. Sci. U.S.A.* **2008**, *105* (43), 16761-16766.
55. Petrik, M.; Umlaufova, E.; Raclavsky, V.; Palyzova, A.; Havlicek, V.; Pfister, J.; Mair, C.; Novy, Z.; Popper, M.; Hajduch, M.; Decristoforo, C., ⁶⁸Ga-labelled desferrioxamine-B for bacterial infection imaging. *Eur. J. Nucl. Med. Mol. Imaging* **2021**, *48* (2), 372-382.
56. Faure, E.; Kwong, K.; Nguyen, D., *Pseudomonas aeruginosa* in chronic lung infections: How to adapt within the host? *Front. Immunol.* **2018**, *9* (2416), 100-109.
57. Defres, S.; Marwick, C.; Nathwani, D., MRSA as a cause of lung infection including airway infection, community-acquired pneumonia and hospital-acquired pneumonia. *Eur. Respir. J.* **2009**, *34* (6), 1470-1476.
58. Schwab, J. C.; Mandell, G. L., The importance of penetration of antimicrobial agents into cells. *Infect. Dis. Clin. North Am.* **1989**, *3* (3), 461-467.
59. Cable, H.; Lloyd, J. B., Cellular uptake and release of two contrasting iron chelators. *J. Pharm. Pharmacol.* **2010**, *51* (2), 131-134.
60. Labbé, K.; Saleh, M., Cell death in the host response to infection. *Cell Death Differ.* **2008**, *15* (9), 1339-1349.
61. Wilson, M. L., Critical factors in the recovery of pathogenic microorganisms in blood. *Clin. Microbiol. Infect.* **2020**, *26* (2), 174-179.
62. Bacconi, A.; Richmond, G. S.; Baroldi, M. A.; Laffler, T. G.; Blyn, L. B.; Carolan, H. E.; Frinder, M. R.; Toleno, D. M.; Metzgar, D.; Gutierrez, J. R.; Massire, C.; Rounds, M.; Kennel, N. J.; Rothman, R. E.; Peterson, S.; Carroll, K. C.; Wakefield, T.; Ecker, D. J.; Sampath, R.; Gilligan, P. H., Improved sensitivity for molecular detection of bacterial and candida infections in blood. *J. Clin. Microbiol.* **2014**, *52* (9), 3164-3174.
63. Kim, J. S.; Anderson, G. P.; Erickson, J. S.; Golden, J. P.; Nasir, M.; Ligler, F. S., Multiplexed detection of bacteria and toxins using a microflow cytometer. *Anal. Chem.* **2009**, *81* (13), 5426-5432.
64. Robertson, J.; McGoverin, C.; Vanholsbeeck, F.; Swift, S., Optimization of the protocol for the LIVE/DEAD® BacLight™ bacterial viability kit for rapid determination of bacterial load. *Front. Microbiol.* **2019**, *10* (801), 801-814.

Supporting Information

General chemical information

All reactions requiring anhydrous conditions were performed under an argon atmosphere. All reactions were carried out at room temperature unless stated otherwise. All general reagents, including salts and solvents, were purchased from Sigma-Aldrich, Acros Organics or comparable and employed without further purification in the below synthetic procedures. Chemicals and solvents were either p. A. grade or purified by standard techniques. For work up procedures and purifications, solvents with purity grade HPLC grade or p. A. were employed. Glassware was dried at 120 °C in an oven for minimum 24 h prior to being used for synthesis. Indicated yields are calculated based on substance purity $\geq 95\%$ analyzed by NMR spectroscopy and liquid chromatography mass spectrometry (LCMS).

Thin-layer chromatography (TLC)

Reaction progress was controlled by thin layer chromatography (TLC) or Liquid Chromatography-coupled Mass Spectrometry (LCMS). TLC silica gel plates were Merck® 60 F254 and compounds were visualized by irradiation with UV light. The retention factor R_f is the ratio of compound running distance divided by the distance of the solvent front, (detection: $\lambda = 254$ nm).

Column chromatography (FC)

Preparative normal phase purifications were performed with silica gel Merck® 60 (particle size 0.040-0.063 mm), eluent given in parentheses.

Reverse-phase HPLC (RP-HPLC)

RP-HPLC was performed on a Dionex Ultimate system from Thermo Fisher Scientific® with the HPLC columns indicated below. The eluent is specified in parentheses for the respective synthetic procedure. Two columns (both C18, 250x4.6mm) were used.

- Luna C18, 5 μm , 100 Å, 00G-4252-PO-AX
- Gemini C18, 10 μm , 110 Å, 00G-4436-PO

Characterization of synthetic compounds

All final compounds were characterized by ^1H -, ^{13}C -NMR spectra and mass spectrometry and the spectra are added in the appendix.

NMR spectroscopy

An Bruker Avance III 500 system with a PABBO BB/19F-1H/D Z-GRD probe head (500 MHz for ¹H, 125 MHz for ¹³C spectra) and an Avance III HD 700 system (BRUKER) equipped with a cryo platform and a CPTCI 1H-13C/15N/D Z-GRD probe head (700 MHz for ¹H, 176 MHz for ¹³C spectra) was used for NMR measurements. Substances were dissolved in deuterated solvents prior to the measurements and chemical shifts δ are given in parts per million (ppm). Multiplicities are stated as follows: s (singlet), d (doublet), t (triplet), q (quartet), p (quintet) and combinations of the latter. Further included are bs (broad singlet) and m (multiplet). All spectra are interpreted as first-order spectra and coupling constants *J* are given in Hertz (Hz), which refer to 1H-1H-couplings.

Mass spectrometry

Mass spectra (MS) were measured on Waters Xevo TQD. High-resolution mass spectrometry (HRMS) was performed via a Dionex Ultimate 3000 HPLC system (Thermo Fisher Scientific, Dreieich, Germany) equipped with a DAD detector and a QTOF mass detector with electrospray ionization (ESI) (Bruker maxis HD, Bremen, Germany). Samples were directly injected via an Ultimate 3000RS autosampler (Thermo Fisher Scientific, Dreieich, Germany). The mass-to-charge ratio *m/z* is indicated.

Light irradiation

Light irradiation for photochemical reactions was performed with a LED PAR38 lamp (19W, 3000K) for the indicated time frames and temperatures.

Chemiluminescence or fluorescence measurement

Chemiluminescence was recorded on a Molecular Devices Spectramax i3x, a SpectraMax M, a Biotek® synergy 5 or a Tecan® SPARK plate reader.

Abbreviations

ACN - Acetonitrile, **DCC** - *N, N*-dicyclohexylcarbodiimide, **NHS** - *N*-hydroxysuccinimide, **DCM** - dichloromethane, **DMF** - *N, N*-dimethylformamide, **DMSO** - dimethyl sulfoxide, **EtOAc** - ethyl acetate, **Hex** - hexane, **TFA** - trifluoroacetic acid, **TEA** - triethylamine, **THF** - tetrahydrofuran, **TMSCl** - trimethylsilyl chloride, **PBS** - phosphate-buffered saline, **HBTU** - 3-[bis(dimethylamino)methyl]imidazolium hexafluorophosphate, **iBuCF** - isobutyl-chloroformate.

Supplementary Figures

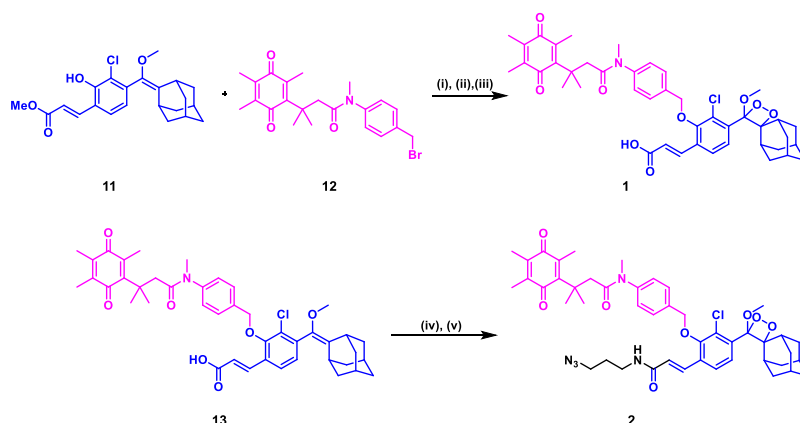


Figure S5.1. Synthesis of dioxetanes **1** and **2**.^{1, 2} (i) K_2CO_3 , DMF, 50 °C, 2 h, 67% (ii) LiOH, THF:H₂O (2:1), 50 °C, 2 h, 67% over 2 steps, (iii) cat. methylene blue, O₂, yellow light, DCM/DMF (9:1), 20 min (iv) NHS, DCC, DCM, 1.5 h, 3-azidopropan-1-amine, DMF, 30 min, 69%, (v) cat. methylene blue, O₂, yellow light, DCM/DMF (9:1), 20 min, 85%.

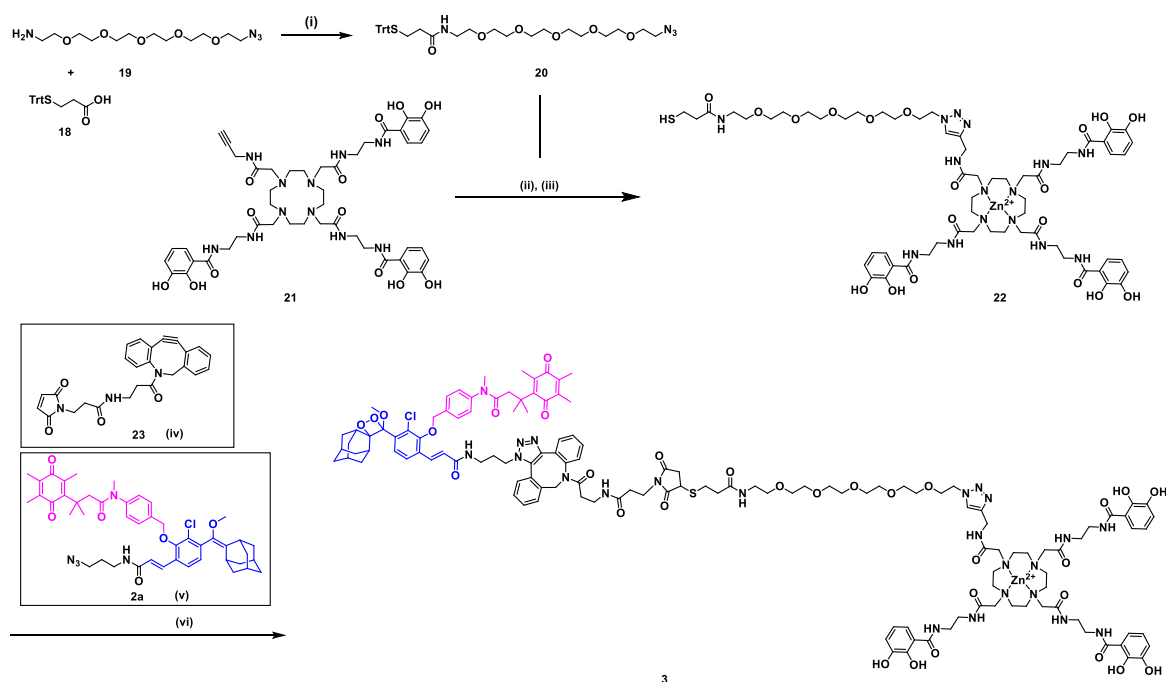


Figure S5.2. Synthesis of DOTAM dioxetane **3**. (i) HATU, DCM, DMF, 0-23 °C, 76%, (ii) **21**, Zn(OAc)₂, DMSO/H₂O (2:1), 23 °C, 5 min, then **20** in DMSO, 5min, 23 °C; then sodium ascorbate/CuSO₄, THPTA, 1xPBS pH 7.4, 23 °C, 1 h, 76%, (iii) 50% TFA, anhydrous DCM, TIPS, 2 h, 25 °C, Et₂O wash then centrifuge 4500 rcf, 15 min, 0 °C (iv) 1 M HEPES buffer pH 7.5, DMF (1:1), overnight, 25 °C, 96% over 2 steps, (v) MeOH, overnight, 25 °C, quant., (vi) cat. methylene blue, DCM/DMF (1:9), oxygen, yellow light, 10 min, 87%.

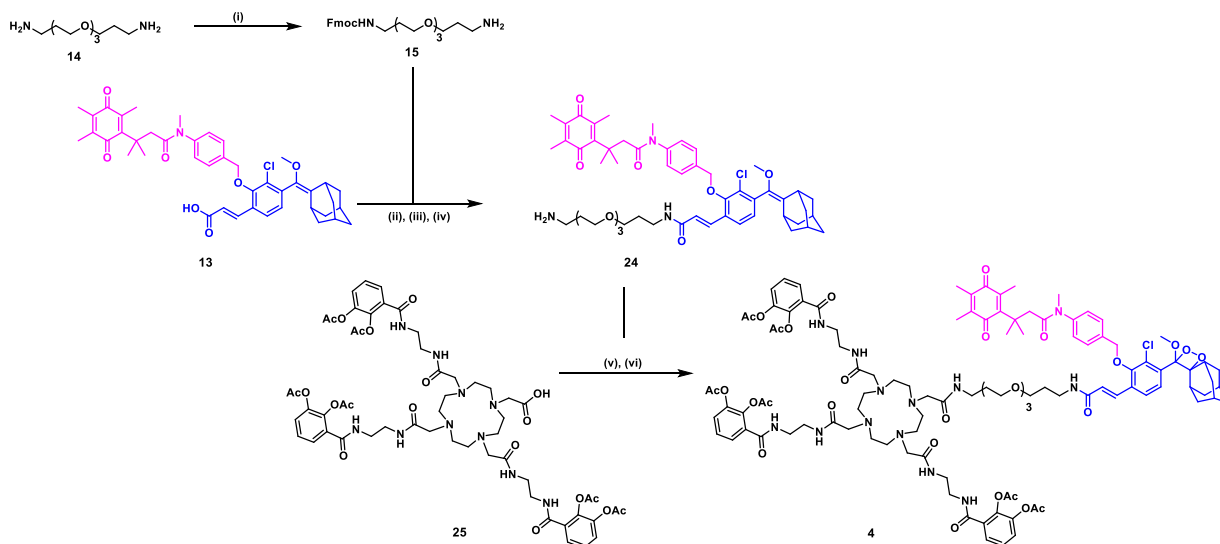


Figure S5.3. Synthesis of DOTAM dioxetane **4**. (i) Fmoc-OSu, TEA, DMF, 53% (ii) NHS, DCC, DCM, 1.5 h, (iii) **15**, DMF, 30 min, 63% over 2 steps, (iv) piperidine, DMF, 23 °C, 3 h, 84%, (v) *iso*-butylchloroformate, *N*-methyl-morpholine (NMM), THF, 0-23 °C, 2h, then **24**, NMM, THF, 0-23 °C, 1 h, 67%, (vi) cat. methylene blue, oxygen, yellow light, DCM/DMF (1:9), 1% AcOH, 25 °C, 30 min, 47%.

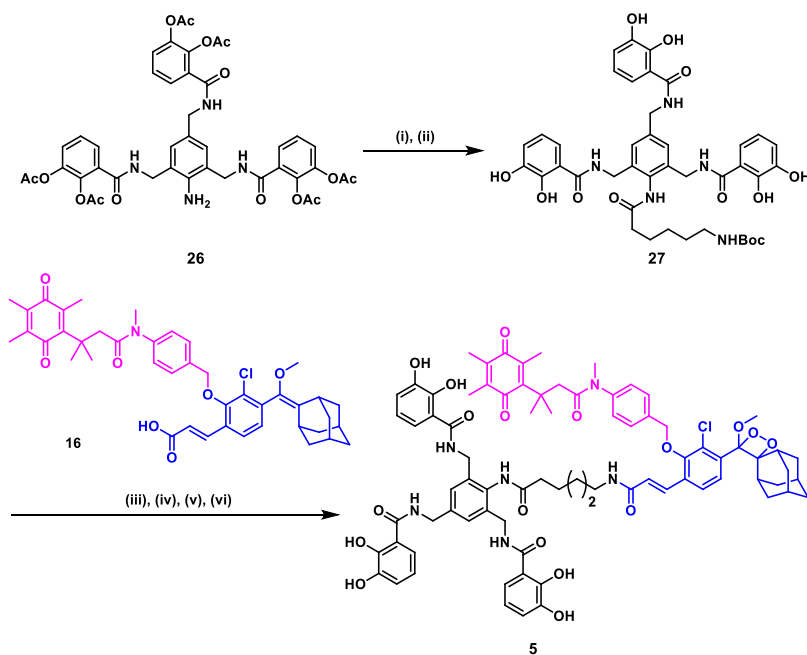


Figure S5.4. Synthesis of MECAM dioxetane **5**. (i) 6-((*tert*-butoxycarbonyl)amino)hexanoic acid, THF, NMM, then *iso*-butyl chloroformate, (ii) MeOH, TEA, 0-25 °C, 30% over 2 steps, (iii) TFA, DCM, 1 h, (iv) **16**, NHS, DCC, DCM, (v) TEA, DMF, yield over 2 steps 59%, (vi) cat. methylene blue, O₂, yellow light, DCM:DMF (9:1), 30 min, 69%.

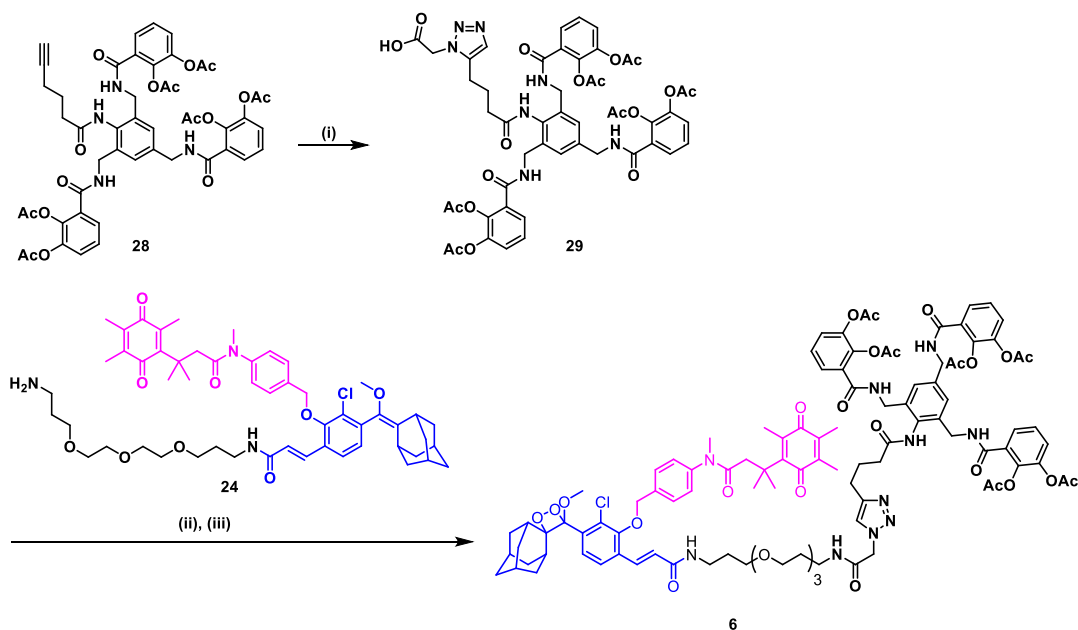


Figure S5.5. Synthesis of MECAM dioxetane **6**. (i) 2-azido acetic acid, sodium ascorbate, CuSO_4 , THPTA, DMSO, 1xPBS pH 7.4, 24 °C, 3 h, 1% AcOH, 74%, (ii) *iso*-butyl chloroformate, NMM, THF, 0-23 °C, 2h, then **24**, NMM, THF, 0-23 °C, 1 h, 67% (iii) cat. methylene blue, oxygen, yellow light, DCM/DMF (1:9), 1% AcOH, 25 °C, 30 min, 42% over two steps.

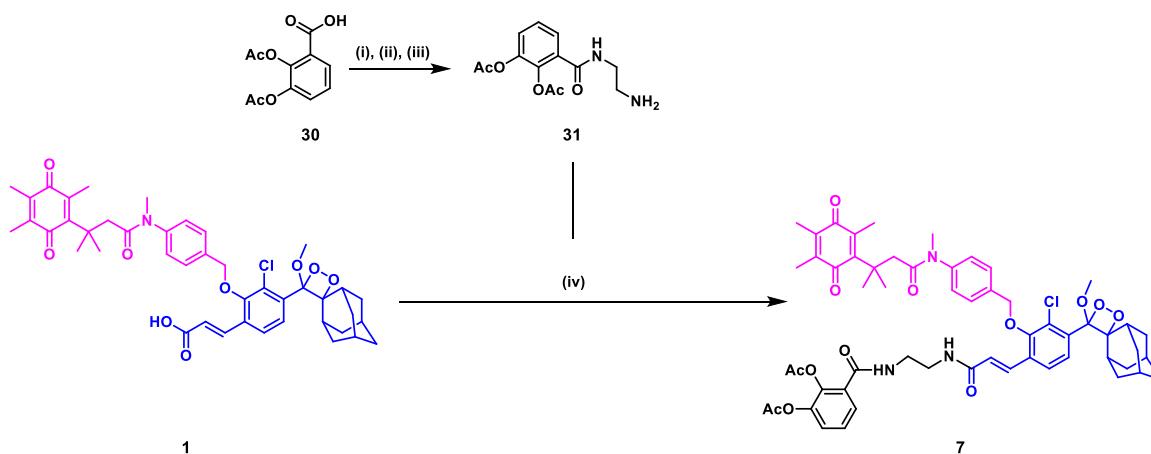


Figure S5.6. Synthesis of mono catechol dioxetane **7**. (i) *N*-Boc ethylene diamine, DCM/DMF, 0-25 °C, 1 h, then high vacuum, 2 h, 24 °C, (ii) sat. NaHCO_3 , 1,4-dioxane, 0-24 °C, (iii) 25% TFA, 10% AcOH, in dry DCM, 0-25 °C, 67% o 3 S, (iv) **31**, *iso*-butyl chloroformate, NMM; THF, 0-25 °C, 2 h, then NMM, THF, 0-25 °C, 1 h, 43% over 3 steps.

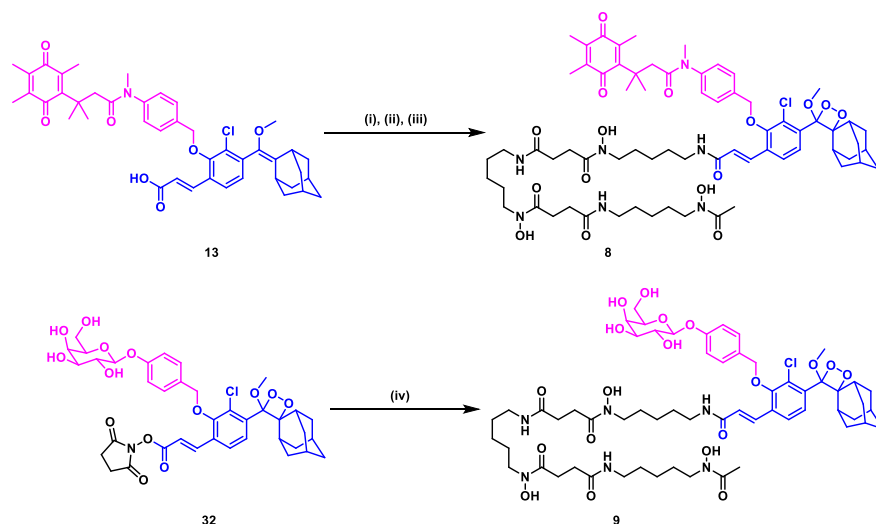


Figure S5.7. Synthesis of desferrioxamine dioxetane probes **8** and **9**. (i) DCC, NHS, 1.5 h, (ii) desferrioxamine mesylate salt, TEA, DMF, 30 min, (iii) cat. methylene blue, O₂, hv, DCM, 5 min, 52% over 3 steps. (iv) desferrioxamine mesylate salt, TEA, DMF, 40%.

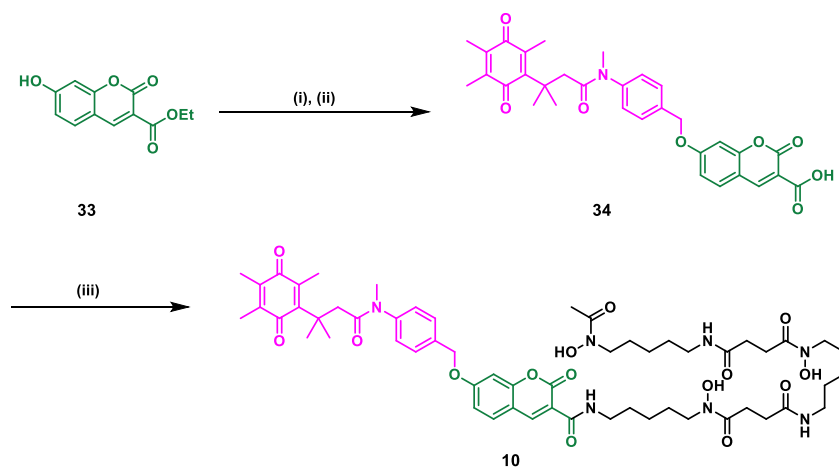
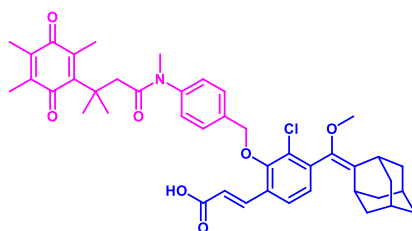


Figure S5.8. Synthesis of fluorescence turn-on probe **10**. (i) **12**, DMF, 50 °C, 3h, (ii) LiOH, THF/H₂O (3:1), 50 °C, 3h, 51% over 2 steps, (iii) HBTU, 2,4,6-collidine, desferrioxamine mesylate salt, DMF:DMSO (2:1), 60 °C, 3 h, 63%.

Synthesis Procedures

Dioxetane Synthesis

(E)-3-(4-(((1*r*,3*r*,5*R*,7*S*)-adamantan-2-ylidene)(methoxy)methyl)-3-chloro-2-((4-(*N*,3-dimethyl-3-(2,4,5-trimethyl-3,6-dioxocyclohexa-1,4-dien-1-yl)butanamido)benzyl)oxy)phenyl)acrylic acid **13**^{1 3}



Chemical Formula: C₄₃H₄₈ClNO₇
 Exact Mass: 725,3119
 Molecular Weight: 726,3070

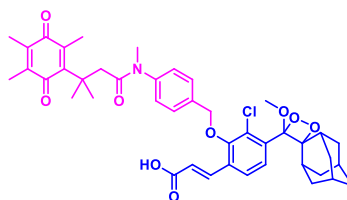
Compound **11**¹ (200 mg, 0.52 mmol, 1 eq) and K₂CO₃ (142 mg, 1.03 mmol, 2 eq) were dissolved in DMF (3 mL) and stirred for 10 min followed by addition of compound **12**¹ (233 mg, 0.54 mmol, 1.05 eq). The reaction mixture was then stirred for 2 h at 50 °C with the reaction progress being monitored by TLC analysis (Hex/EtOAc: 90:10). Upon completion, the solvent was removed and the crude mixture was directly used for the next step without further purification. A mixture of THF:H₂O (2:1, 3 mL) and LiOH (41 mg, 1.03 mmol, 2 eq) was then added. The resulting mixture was stirred at 50 °C for an additional 2 h. When full hydrolysis was inferred on the basis of TLC analysis (Hex:EtOAc, 60:40), the mixture was diluted with EtOAc (100 mL) and washed with 0.5 M HCl (50 mL). The organic layer was separated off, washed with brine, dried over Na₂SO₄ and evaporated under reduced pressure. The crude product was then purified using silica column chromatography (Hex/EtOAc, 60:40) to elute **13** as a yellow solid (0.249 g, 67%).

¹H NMR (400 MHz, CDCl₃) δ 8.04 (d, *J* = 16.2 Hz, 1H), 7.59 (d, *J* = 7.6 Hz, 2H), 7.50 (d, *J* = 7.9 Hz, 1H), 7.24 (d, *J* = 7.8 Hz, 2H), 7.13 (d, *J* = 8.0 Hz, 1H), 6.48 (d, *J* = 16.2 Hz, 1H), 5.06 (s, 2H), 3.36 (s, 3H), 3.29 (s, 1H), 3.17 (s, 3H), 2.77 (s, 2H), 2.10 (s, 4H), 2.06 – 1.65 (m, 18H), 1.31 (s, 6H).

¹³C NMR (101 MHz, CDCl₃) δ 191.46, 187.84, 172.41, 170.74, 153.98, 144.22, 143.67, 140.95, 139.42, 138.97, 138.07, 136.58, 135.93, 133.09, 130.29, 129.96, 129.38, 128.24, 127.78, 125.45, 119.49, 75.64, 57.52, 47.80, 39.35, 38.83, 38.29, 37.34, 37.16, 33.15, 29.89, 28.63, 28.47, 14.24, 12.87, 12.24.

MS (ESI) calculated for $C_{43}H_{49}ClNO_7^+$ ($[M+H]^+$): $m/z = 725.3$; experimental = 726.5.

Compound 1¹

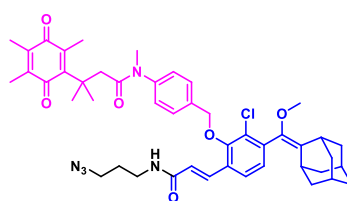


Chemical Formula: $C_{43}H_{48}ClNO_9$
 Exact Mass: 757,3018
 Molecular Weight: 758,3050

This compound was synthesized according to Son et al.¹

HRMS (ESI) calculated for $C_{43}H_{49}ClNO_9^+$ $[M+H]^+$: $m/z = 758.3090$, experimental = 758.3090,
 δ [ppm] = 0.0 ppm

(*N*-(4-((3-(((1*r*,3*r*,5*R*,7*S*)-Adamantan-2-ylidene)(methoxy)methyl)-6-((*E*)-3-((3-azidopropyl)amino)-3-oxoprop-1-en-1-yl)-2-chlorophenoxy)methyl)phenyl)-*N*,3-dimethyl-3-(2,4,5-trimethyl-3,6-dioxocyclohexa-1,4-dien-1-yl)butanamide) 2a



Chemical Formula: $C_{46}H_{54}ClN_5O_6$
 Exact Mass: 807,3763
 Molecular Weight: 808,4170

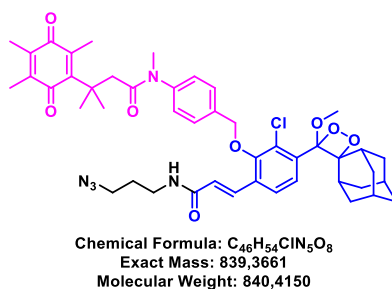
To the solution of compound **13** (100 mg, 0.14 mmol, 1 eq) in DCM (5 mL) was added NHS (24 mg, 0.21 mmol, 1.5 eq) followed by DCC (43 mg, 0.21 mmol, 1.5 eq) and stirred for 1.5 h at room temperature. Upon completion, the reaction mixture was filtered and the solvent was removed. The crude was dissolved in DMF (1 ml) and 3-azidopropylamine (21 mg, 0.21 mmol, 1.5 eq) followed by a drop of TEA. The reaction was monitored by RP-HPLC (90-100% ACN/H₂O, 20 min). Upon completion, the reaction mixture was concentrated by evaporation under reduced pressure. The crude product was purified by silica column chromatography to elute **2a** as a yellow solid (77 mg, 69%).

¹H NMR (400 MHz, CDCl₃) δ 8.14 (d, *J* = 16.2 Hz, 1H), 7.56 (d, *J* = 7.9 Hz, 2H), 7.49 (d, *J* = 8.0 Hz, 1H), 7.23 (d, *J* = 8.1 Hz, 2H), 7.15 (d, *J* = 8.0 Hz, 1H), 6.63 (d, *J* = 16.2 Hz, 1H), 5.06 (d, *J* = 2.1 Hz, 2H), 3.36 (s, 3H), 3.29 (s, 2H), 3.16 (s, 3H), 2.90 (s, 9H), 2.76 (s, 2H), 2.09 (s, 4H), 2.03 – 1.71 (m, 15H), 1.30 (s, 6H).

¹³C NMR (101 MHz, CDCl₃) δ 191.41, 187.85, 172.60, 169.42, 162.00, 154.73, 154.37, 144.26, 144.08, 139.91, 139.31, 138.08, 136.60, 135.70, 133.45, 130.48, 130.12, 128.84, 128.34, 127.82, 125.76, 114.04, 75.78, 57.61, 47.72, 39.36, 39.19, 38.83, 38.34, 37.42, 37.16, 33.17, 29.93, 28.61, 28.46, 25.82, 14.21, 12.83, 12.19.

MS (ESI) calculated for C₄₆H₅₅ClN₅O₆⁺ [M+H]⁺: *m/z* = 807.4, experimental = 808.9.

(*N*-4-((6-((*E*)-3-((3-Azidopropyl)amino)-3-oxoprop-1-en-1-yl)-2-chloro-3-((1*r*,3*r*,5*r*,7*r*)-4'-methoxyspiro[adamantane-2,3'-[1,2]dioxetan]-4'-yl)phenoxy)methyl)phenyl)-*N*,3-dimethyl-3-(2,4,5-trimethyl-3,6-dioxocyclohexa-1,4-dien-1-yl)butanamide) 2



Enol Ether **2a** (5 mg, 6 μmol, 1.0 eq) and a catalytic amount of methylene blue (ca. 0.2 mg) were dissolved in 1 mL of DCM:DMF (9:1) in a septum-capped screw cap tube. The solution was saturated with oxygen (5 min) while stirring at 300 rpm, then the reaction was irradiated with a yellow light for 20 min. The reaction was monitored by LCMS and upon completion, the DCM was removed by rotary evaporation at 30 °C in the dark. The residue was filtered and purified by preparative RP-HPLC (C18 phenomenex. 40 min gradient, 20-100% ACN/H₂O, 0.1% HCOOH, 220 nm). The product containing fractions were identified by LC-MS (*t* = 2,492 min) and lyophilized to yield product **2** (4.39 mg, 5 μmol, 85%) as a yellow solid.

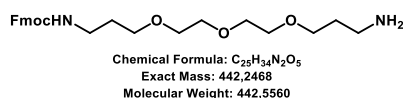
¹H NMR (700 MHz, DMSO-*d*₆): δ (ppm) = 8.28-8.26 (t, *J*=5.63Hz, 1H), 7.67-7.65 (d, *J*=15.43 Hz, 1H), 7.67-7.57 (m, 3H), 7.31-7.30 (d, *J*=6.21 Hz, 2H), 7.17-7.16 (d, *J*=8.15 Hz, 1H), 6.69-6.67 (d, *J*=15.91 Hz, 1H), 5.01-4.99 (d, *J*=9.90 Hz, 2H), 3.40 (t, *J*=6.60 Hz, 2H), 3.29 (s, 3H), 3.25-

3.24 (m, 5H), 3.19 (bs, 1H), 3.06 (bs, 2H), 2.66 (bs, 1H), 2.50 (s, 3H), 2.02-2.00 (bs, 1H), 1.93-1.90 (m, 10 H), 1.81-1.73 (m, 10H), 1.24 (bs, 6H).

¹³C NMR (176 MHz, DMSO-d₆): δ (ppm) = 190.33, 186.87, 164.63, 154.93, 152.55, 143.70, 139.43, 136.71, 136.32, 135.17, 132.02, 130.21, 130.15, 129.82, 128.70, 127.89, 127.45, 125.04, 124.72, 74.87, 56.53, 48.46, 46.85, 38.49, 38.15, 37.74, 36.46, 36.15, 32.42, 29.04, 28.41, 28.06, 27.71, 27.55, 13.71, 12.60, 11.73.

HRMS (ESI) calculated for C₄₆H₅₅ClN₅O₈⁺ ([M+H]⁺): m/z = 840.3733 experimental: m/z = 840.3733, δ [ppm] = 4.8 ppm.

(9H-fluoren-9-yl)methyl(3-(2-(2-(3-aminopropoxy)ethoxy)ethoxy)propyl)carbamate **15**

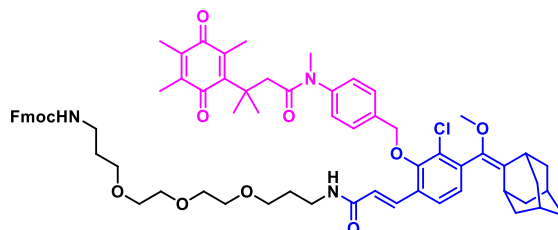


To the solution of 4,7,10-Trioxa-1,13-tridecanediamine **14** (100 mg, 0.45 mmol, 1 eq) in DMF (1 mL) was added NEt₃ (0.127 mL, 0.91 mmol, 2 eq) followed by a solution of Fmoc-OSu (153 mg, 0.45 mmol, 1 eq) in DMF (1 mL) at 0 °C. The reaction was monitored by RP-HPLC (50-100% ACN in water, 20 min). Upon completion, the reaction mixture was concentrated by evaporation under reduced pressure and purified using RP-HPLC (50-100% ACN/H₂O, 20 min) to afford compound **15** (106 mg, 53% yield) as a colorless liquid.

¹H NMR (400 MHz, MeOD): δ = 7.79 (d, *J* = 7.5 Hz, 2H), 7.63 (d, *J* = 7.4 Hz, 2H), 7.39 (t, *J* = 7.4 Hz, 2H), 7.30 (td, *J* = 7.4, 0.8 Hz, 2H), 4.36 (d, *J* = 6.8 Hz, 2H), 4.20 (t, *J* = 6.7 Hz, 1H), 3.66 – 3.55 (m, 10H), 3.52 – 3.45 (m, 2H), 3.18 (t, *J* = 6.8 Hz, 2H), 3.05 (t, *J* = 5.8 Hz, 2H), 1.90 – 1.85 (m, 2H), 1.82 – 1.67 (m, 2H).

¹³C NMR (101 MHz, MeOD): δ = 157.71, 127.54, 126.88, 124.85, 119.69, 70.08, 69.75, 69.07, 68.27, 66.30, 38.82, 37.70, 29.58, 26.75. MS (ES⁺): m/z calc. for C₂₅H₃₄N₂O₅: 442.3; found: 443.3 [M+H]⁺.

((9H-Fluoren-9-yl)methyl((E)-17-(4-(((1r,3r,5R,7S)-adamantan-2ylidene)(methoxy)methyl)-3-chloro-2-((4-(N,3-dimethyl-3-(2,4,5-trimethyl-3,6-dioxocyclohexa-1,4-dien-1-yl)butanamido)benzyl)oxy)phenyl)-15-oxo-4,7,10-trioxa-14-azaheptadec-16-en-1-yl)carbamate) 17



Chemical Formula: C₆₈H₈₀ClN₃O₁₁
 Exact Mass: 1149,5481
 Molecular Weight: 1150,8480

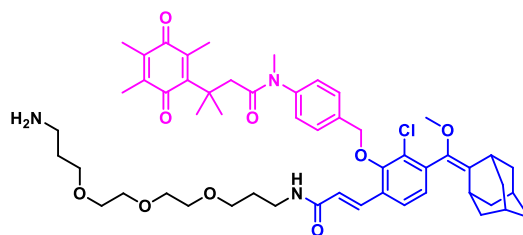
To the solution of compound **13** (100 mg, 0.14 mmol, 1 eq) in DCM (5 mL) was added NHS (24 mg, 0.21 mmol, 1.5 eq) followed by DCC (43 mg, 0.21 mmol, 1.5 eq) and stirred for 1.5 h at room temperature. Upon completion, the reaction mixture was filtered and the solvent was removed. The crude mixture was dissolved in DMF (1 ml) and compound **15** (93 mg, 0.21 mmol, 1.5 eq) was added followed by a drop of Et₃N. The reaction was monitored by RP-HPLC (90-100% ACN/H₂O, 20 min). Upon completion, the reaction mixture was concentrated by evaporation under reduced pressure. The crude product was purified by silica column chromatography to elute **17** as a yellow solid (100 mg, 0.087 mmol, 63%).

¹H NMR (400 MHz, CDCl₃) δ 7.95 (d, *J* = 15.7 Hz, 1H), 7.90 (d, *J* = 8.4 Hz, 1H), 7.75 (d, *J* = 7.5 Hz, 2H), 7.64 (d, *J* = 7.8 Hz, 2H), 7.59 (d, *J* = 7.4 Hz, 2H), 7.39 (t, *J* = 7.4 Hz, 2H), 7.29 (t, *J* = 7.4 Hz, 2H), 7.23 (d, *J* = 8.1 Hz, 2H), 6.68 (s, 1H), 6.53 (d, *J* = 15.7 Hz, 1H), 5.35 (t, *J* = 5.2 Hz, 1H), 4.92 (s, 2H), 4.39 (d, *J* = 6.8 Hz, 2H), 4.21 (t, *J* = 6.7 Hz, 1H), 3.68 – 3.55 (m, 10H), 3.51 (dt, *J* = 11.8, 5.8 Hz, 4H), 3.32 – 3.25 (m, 2H), 3.23 (s, 3H), 3.15 (s, 3H), 3.03 (s, 1H), 2.77 (s, 1H), 2.32 (d, *J* = 11.9 Hz, 1H), 2.10 (s, 3H), 2.00 (s, 3H), 1.96 (s, 3H), 1.88 – 1.61 (m, 15H), 1.47 (d, *J* = 12.7 Hz, 1H), 1.30 (t, *J* = 16.6 Hz, 8H).

¹³C NMR (101 MHz, CDCl₃) δ 191.35, 187.87, 172.24, 165.61, 165.26, 156.70, 155.02, 153.46, 144.29, 144.15, 143.78, 141.46, 139.60, 137.87, 137.59, 136.35, 136.15, 134.44, 132.53, 132.32, 130.40, 130.10, 129.90, 129.13, 127.97, 127.81, 127.71, 127.47, 127.17, 125.17, 124.96, 123.88, 120.10, 111.93, 96.53, 75.37, 75.22, 70.55, 70.26, 70.10, 69.54, 66.57, 39.38, 39.18, 38.78, 38.57, 38.46, 38.28, 37.21, 36.73, 34.05, 33.79, 33.12, 32.79, 32.39, 31.74, 31.70, 29.88, 29.84, 29.57, 28.98, 28.60, 26.32, 25.99, 14.21, 12.89, 12.24.

MS (ES⁺): *m/z* calc. for C₆₈H₈₀ClN₃O₁₁: 1150.8; found: 1173.0 [M+H]⁺.

(N-(4-((3-(((1*r*,3*r*,5*R*,7*S*)-Adamantan-2-ylidene)(methoxy)methyl)-6-((*E*)-1-amino-15-oxo-4,7,10-trioxa-14-azaheptadec-16-en-17-yl)-2-chlorophenoxy)methyl)phenyl)-N,3-dimethyl-3-(2,4,5-trimethyl-3,6-dioxocyclohexa-1,4-dien-1-yl)butanamide) 24



Chemical Formula: C₅₃H₇₀ClN₃O₉
 Exact Mass: 927,4801
 Molecular Weight: 928,6050

Compound **17** (20 mg, 0.022 mmol, 1.0 eq), was dissolved in DMF (1 mL) and piperidine (3 μ L) was added. The reaction was monitored by LCMS and upon completion, the compound was purified by RP-HPLC (C18, phenomenex, 40 min gradient 20-100% ACN/H₂O, 0.1% HCOOH, 220 nm). The product containing fractions were identified by LCMS and lyophilized to dryness, yielding pure amine **24** (16.9 mg, 0.018 mmol, 84%) as a yellow powder.

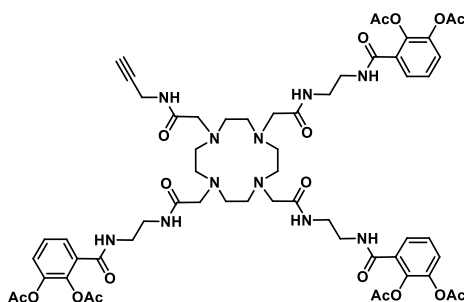
¹H NMR (700 MHz, MeOH-d₄): δ (ppm) = 7.87-7.85 (d; J=14.35 Hz, 1H), 7.64-7.63 (d, J=7.97 Hz, 2H), 7.60-7.59 (d, J=9.25 Hz, 1H), 7.29-7.28 (d, J=7.97 Hz, 2H), 7.14-7.13 (d, J=9.25 Hz, 1H), 6.67-6.65 (d, J=15.94 Hz, 1H), 5.09 (bs, 2H), 3.67-3.64 (m, 6H), 3.62 (m, 4H), 3.56 (t, J=6.38 Hz, 2H), 3.41 (t, J=6.7 Hz, 2H), 3.32 (m, 3H), 3.26 (m, 1H), 3.14 (bs, 2H), 3.07 (t, J=6.38 Hz, 2H), 2.75 (t, J=6.7 Hz, 2H), 2.09-2.08 (m, 4H), 1.99-1.96 (m, 10H), 1.90-1.89 (m, 6H), 1.85 (m, 4H), 1.80 (m, 2H), 1.75-1.73 (m, 1H), 1.31 (bs, 6H).

¹³C NMR (176 MHz, MeOH-d₄): δ (ppm) = 192.41, 188.91, 174.13, 170.39, 168.32, 156.29, 154.76, 145.39, 144.84, 141.20, 139.10, 138.87, 137.92, 137.82, 135.61, 133.18, 131.87, 131.74, 130.99, 129.36, 128.80, 126.15, 124.50, 76.44, 71.73, 71.57, 71.38, 71.28, 71.25, 71.19, 70.56, 69.86, 57.57, 40.34, 40.16, 39.87, 39.72, 39.49, 38.28, 38.15, 37.66, 34.60, 31.23, 30.74, 29.99, 29.85, 29.12, 28.41, 14.51, 12.93, 12.13.

HRMS (ESI) calculated for (C₅₃H₇₁ClN₃O₉)⁺ ([M+H]⁺): m/z = 928.4872, experimental = 928.4887, δ [ppm] = 1.3 ppm

DOTAM and DOTAM dioxetane conjugates

(((2,2'-(7-(2-((2-(3-acetoxy-2-hydroxybenzamido)ethyl)amino)-2-oxoethyl)-10-(2-oxo-2-(prop-2-yn-1-ylamino)ethyl)-1,4,7,10-tetraazacyclododecane-1,4-diyl)bis(acetyl))bis(azanediy))bis(ethane-2,1-diyl))bis(azanediy))bis(carbonyl))bis(benzene-3,1,2-triyl) tetraacetate **21a**



Chemical Formula: $C_{58}H_{73}N_{11}O_{19}$

Exact Mass: 1227,5084

Molecular Weight: 1228,2800

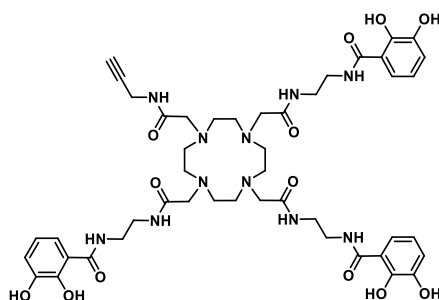
Over 5 steps over the longest linear sequence DOTAM siderophore **21a** was prepared according to our previously established procedures, first reported by Ferreira *et al.* and modified by Peukert *et al* (100.5 mg, 0.0818 mmol, 52% over 5 steps starting from cyclen).^{4, 5}

¹H NMR (700 MHz, DMSO- d_6): δ (ppm) = 8.50 (bs, 1H), 8.39 (bs, 3H), 8.22 – 8.10 (m, 3H), 7.46 (dd, $J = 7.4$ Hz, 1.8 Hz, 3H), 7.39 – 7.32 (m, 6H), 3.90 – 3.89 (m, 2H), 3.45 – 3.34 (m, 12H), 3.28 – 2.94 (m, 24H), 2.52 (t, $J = 1.9$ Hz, 1H), 2.28 (s, 9H), 2.22 (s, 9H).

¹³C NMR (176 MHz, DMSO- d_6): δ [ppm] = 170.6, 170.0, 169.4, 168.5, 149.8, 146.3, 118.7, 117.7, 117.2, 115.0, 81.0, 72.9, 62.2, 57.7, 54.9, 38.9, 38.0, 27.9, 20.4.

HRMS (ESI) calculated for $C_{58}H_{74}N_{11}O_{19}^+$ ($[M+H]^+$): $m/z = 1228.51570$, experimental: 1228.5160, δ [ppm] = 0.08, calculated for $C_{58}H_{75}N_{11}O_{19}^{2+}$ ($[M+2H]^{2+}$): $m/z = 614.76149$, experimental: 614.7615, δ [ppm] = 0.02.

N,N',N''*-(((2,2',2''-(10-(2-oxo-2-(prop-2-yn-1-ylamino)ethyl)-1,4,7,10-tetraazacyclododecane-1,4,7-triyl)tris(acetyl))tris(azanediyl))tris(ethane-2,1-diyl))tris(2,3-dihydroxybenzamide) **21*



Chemical Formula: $C_{46}H_{61}N_{11}O_{13}$

Exact Mass: 975,4450

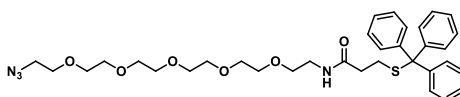
Molecular Weight: 976,0580

21a (100 mg, 0.0818 mmol, 1.0 eq) was dissolved in anhydrous MeOH (8 mL) and 20% DIPEA (2 mL, v/v) was added at 0 °C. The reaction continued stirring at 24 °C for 2 hours and was purified by RP-HPLC (40 min gradient 5-40% ACN/H₂O, 0.1% HCOOH, C18 phenomenex, 220 nm). Product containing fractions were identified by LCMS, lyophilized to dryness to yield siderophore **21** (76.13 mg, 0.078 mmol, 95%), according to our previously reported procedure.⁵

¹H NMR (700 MHz, DMSO-*d*₆): δ (ppm) = 8.92 (s, 3H), 8.50 (s, 1H), 8.31 – 8.05 (m, 3H), 7.23 (dd, *J* = 8.0 Hz, 1.2 Hz, 3H), 6.89 (ddd, *J* = 7.7 Hz, 3.5 Hz, 1.3 Hz, 3H), 6.66 – 6.62 (m, 3H), 3.90 (d, *J* = 1.9 Hz, 2H), 3.37 (s, 6H), 3.24 – 3.05 (m, 12H), 3.04 (t, *J* = 2.5 Hz, 1H), 3.04 – 2.50 (m, 18H).

¹³C NMR (176 MHz, DMSO-*d*₆): δ [ppm] = 170.3, 169.9, 164.5, 164.4, 150.0, 150.0, 146.4, 118.6, 117.6, 117.6, 117.3, 115.0, 81.1, 72.9, 57.3, 57.1, 52.5, 38.9, 38.0, 27.9.

HRMS (ESI) calculated for $C_{46}H_{62}N_{11}O_{13}^+$ ([M+H]⁺): *m/z* = 976.45231, experimental: 976.4525, δ [ppm] = 0.19, calculated for $C_{46}H_{61}N_{11}NaO_{13}^+$ ([M+Na]⁺): *m/z* = 998.43425, experimental: 998.4347, δ [ppm] = 0.45.

***N*-(17-azido-3,6,9,12,15-pentaoxaheptadecyl)-3-(tritylthio)propanamide 20**

Chemical Formula: C₃₄H₄₄N₄O₆S
 Exact Mass: 636,2982
 Molecular Weight: 636,8080

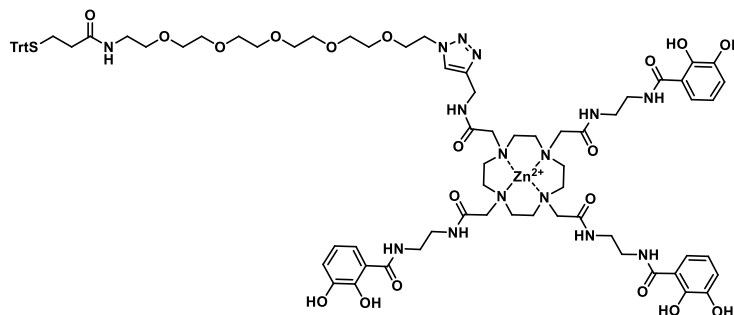
3-Tritylsulfanylpropanoic acid **18** (300.0 mg, 0.861 mmol, 1.0 eq.) was dissolved in anhydrous DCM (25 mL) and DMF (5 mL). Then HATU (818.4 mg, 2.152 mmol, 2.5 eq.) was added, dissolved in anhydrous DMF (10 mL). The solution was cooled to 0 °C and 17-azido-3,6,9,12,15-pentaoxaheptadecan-1-amine **19** (290.1 mg, 263.8 μL, 0.947 mmol, 1.1 eq.) was added in dry DMF (10 mL) at 0 °C. Dry TEA (348.5 mg, 477.4 μL, 3.444 mmol, 4.0 eq.) was added over 10 min dropwise at 0 °C. The reaction continued stirring at 0 °C for 30 min, allowed to warm to room temperature and continued stirring for an additional 20 h at 23 °C. After completion of the reaction, controlled by LCMS, the solution was concentrated by rotary evaporation. The residue was taken up in EtOAc (50 mL) and washed with 1 M HCl (2 x 25 mL), sat. NaHCO₃ (2 x 25 mL), brine (2 x 25 mL) and dried over Na₂SO₄. The solvent was removed by rotary evaporation, the residue was dissolved in ACN/H₂O/MeOH (5mL) and purified by RP-HPLC (40 min gradient, 65-95% ACN/H₂O, 0.1% HCOOH, 220 nm). The product containing fractions were identified by LCMS and lyophilized to dryness to yield product **20** as a white solid, (418.0 mg, 0.656 mmol, 76%).

¹H NMR (500 MHz, DMSO-d₆): δ (ppm) = 7.88 (t, *J* = 5.6 Hz, 1H), 7.34 – 7.31 (m, 12H), 7.24 (dd, *J* = 8.8 Hz, 4.5 Hz, 3H), 3.59 (t, *J* = 4.8 Hz, 2H), 3.56 – 3.48 (m, 12H), 3.40 – 3.35 (m, 4H), 3.18 (q, *J* = 5.6 Hz, 2H), 2.26 (t, *J* = 7.3 Hz, 2H), 2.17 (t, *J* = 7.3 Hz, 2H).

¹³C NMR (126 MHz, DMSO-d₆) δ (ppm) = 170.1, 144.5, 129.1, 128.0, 126.7, 69.9, 69.8, 69.7, 69.7, 69.6, 69.3, 69.1, 66.0, 50.0, 38.6, 33.9, 27.5.

HRMS (ESI) calculated for C₃₄H₄₅N₄O₆S⁺ ([M+H]⁺): *m/z* = 637.30544, experimental: 637.3054, δ [ppm] = 0.06 calculated for C₃₄H₄₄N₄NaO₆S⁺ ([M+Na]⁺): *m/z* = 659.28738, experimental: 659.2873, δ [ppm] = 0.12.

Zn²⁺-N,N',N''-(((2,2',2''-(10-(2-Oxo-2-(((1-(5-oxo-1,1,1-triphenyl-9,12,15,18,21-pentaoxa-2-thia-6-azatricosan-23-yl)-1H-1,2,3-triazol-4-yl)methyl)amino)ethyl)-1,4,7,10-tetraazacyclododecane-1,4,7-triyl)tris(acetyl))tris(azanediyl))tris(ethane-2,1-diyl))tris(2,3-dihydroxybenzamide) **22**



Chemical Formula: C₈₀H₁₀₅N₁₅O₁₉SZn²⁺

Exact Mass: 1675,6712

Molecular Weight: 1678,2449

22 was prepared by an adapted version of our previously established procedure.⁶

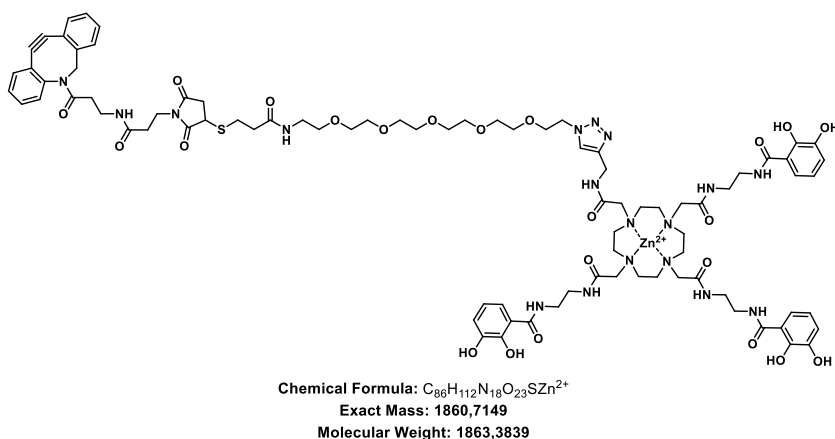
21 (92.0 mg, 0.094 mmol, 1.5 eq.) was dissolved under Argon atmosphere in DMSO (2 mL). Zinc acetate (41.4 mg, 0.188 mmol, 3.0 eq.), dissolved in milliQ H₂O (2 mL), was added and the solution was stirred at 23 °C for 5 min. **20** (40.0 mg, 0.063 mmol, 1.0 eq.), dissolved in DMSO (2 mL), was added to the solution. CuSO₄ (5.0 mg, 0.031 mmol, 0.5 eq., - dissolved in PBS (0.5 mL) and sodium ascorbate (12.4 mg, 0.063 mmol, 1.0 eq. - dissolved in PBS (1 mL)), was added to the CuSO₄ solution. A white precipitate formed immediately. THPTA (6.8 mg, 0.016 mmol, 0.25 eq., - dissolved in PBS (0.5 mL), was added to the suspension and the turbidity disappeared. The solution was added to the reaction under Argon atmosphere and was stirred at 23 °C for 1 h. The reaction progress was controlled by LCMS and after completion, the solution was filtered over cotton wool and purified by RP-HPLC (40 min gradient, collect all, 5-35% ACN/H₂O, 0.1% HCOOH, 220 nm). The product containing fractions were identified by LCMS and lyophilized to dryness to yield product **22** as a white solid (80.0 mg, 0.042 mmol, 76%).

¹H NMR (700 MHz, DMSO-d₆): δ [ppm] = 10.32 – 9.39 (m, 3H), 9.04 (bs, 3H), 8.49 (bs, 1H), 8.21 (bs, 1H), 7.97 – 7.82 (m, 3H), 7.35 – 7.33 (m, 1H), 7.33 – 7.29 (m, 12H), 7.25 – 7.24 (m, 3H), 7.23 – 7.21 (m, 3H), 6.84 – 6.70 (m, 3H), 6.54 – 6.32 (m, 3H), 4.43 (t, *J* = 5.0 Hz, 2H), 4.38 (s, 2H), 3.75 (t, *J* = 4.8 Hz, 2H), 3.47 – 3.45 (m, 16H), 3.36 (t, *J* = 5.9 Hz, 2H), 3.31 – 3.24 (m, 12H), 3.14 (q, *J* = 5.7 Hz, 2H), 2.99 – 2.52 (m, 24H), 2.23 (t, *J* = 7.4 Hz, 2H), 2.15 (t, *J* = 7.4 Hz, 2H).

^{13}C NMR (176 MHz, DMSO- d_6) δ (ppm) = 172.3, 171.5, 170.1, 169.7, 169.6, 165.0, 147.5, 147.2, 144.5, 143.6, 129.1, 128.0, 126.7, 123.7, 118.0, 117.9, 116.6, 115.7, 115.4, 115.3, 114.4, 69.7, 69.7, 69.6, 69.5, 69.0, 68.7, 66.0, 55.6, 50.5, 49.4, 40.4, 40.0, 38.6, 38.0, 37.6, 34.6, 33.9, 27.5.

HRMS (ESI) calculated for $(\text{C}_{80}\text{H}_{107}\text{N}_{15}\text{O}_{19}\text{SZn}^{2+})^{2+}$ ($[\text{M}+2\text{H}]^{2+}$): $m/z = 838.84290$, experimental: 838.8427, δ [ppm] = 0.24.

Zn²⁺-N,N',N''-(((2,2',2''-(10-(2-(((1-(21-(((1-(3-((3-(11,12-Dihydro-1115,1215-dibenzo[b,f]azocin-5(6H)-yne)-3-oxopropyl) amino)-3-oxopropyl)-2,5-dioxopyrrolidin-3-yl)thio)-19-oxo-3,6,9,12,15-pentaoxa-18-azahenicosyl)-1H-1,2,3-triazol-4-yl)methyl)amino)-2-oxoethyl)-1,4,7,10-tetraazacyclododecane-1,4,7-triyl)tris(acetyl))tris(azanediyl))tris(ethane-2,1-diyl))tris(2,3-dihydroxybenzamide) 35



Tritylthiol **22** (15.0 mg, 8.938 μmol , 1.0 eq.) was dissolved in dry DCM (3 mL), and TFA (1 mL), as well as TIPS (100 μL), were added at 0 $^{\circ}\text{C}$. An immediate color change from slightly yellow to neon orange was observed. The reaction was stirred at 23 $^{\circ}\text{C}$ for 2 h and the reaction progress was controlled by LCMS. After full deprotection, the reaction was transferred in a 50 mL Falcon, the solvent was removed by rotary evaporation and the residue was dried for 10 minutes. The residue was washed with ice-cold Et_2O (3 x 50 mL), centrifuged (4500 rpm, 20 min, -20 $^{\circ}\text{C}$) and the supernatant was decanted after each washing step. The light brown solid was dried for 1 hour *in vacuo* before the next step yielding free thiol **35a**. The residue was dissolved in DMF and 1M HEPES buffer pH 7.4 was added (each 1 mL). The slightly turbid, yellow reaction continued stirring overnight at 23 $^{\circ}\text{C}$. The next morning, the reaction was acidified with 1% AcOH, filtered over a cotton wool filter and injected into the RP-HPLC (220

nm, 40 min gradient, 5-50% ACN/H₂O, 0.1% HCOOH). The product containing fractions were identified by LCMS and lyophilized to dryness to yield strained alkyne **35**.

Zn²⁺-N,N',N''-(((2,2',2''-(10-(2-(((1-(21-Mercapto-19-oxo-3,6,9,12,15-pentaoxa-18-azahenicosyl)-1H-1,2,3-triazol-4-yl)methyl)amino)-2-oxoethyl)-1,4,7,10-tetraazacyclododecane-1,4,7-triyl)tris(acetyl))tris(azanediyl))tris(ethane-2,1-diyl))tris(2,3-dihydroxybenzamide) 35a

¹H NMR (700 MHz, DMSO-d₆): δ (ppm) = 12.45 (bs, 3H), 9.17 (t, *J* = 5.2 Hz, 1H), 8.91 (t, *J* = 5.3 Hz, 1H), 8.87 (t, *J* = 5.4 Hz, 2H), 8.80 (t, *J* = 5.4 Hz, 3H), 7.98 – 7.95 (m, 1H), 7.23 (dd, *J* = 8.2 Hz, 1.1 Hz, 3H), 7.12 – 6.99 (m, 1H), 6.91 (ddd, *J* = 7.8 Hz, 4.4 Hz, 1.3 Hz, 3H), 6.67 (ddd, *J* = 7.9 Hz, 4.3 Hz, 2.1 Hz, 3H), 4.45 (t, *J* = 5.2 Hz, 2H), 4.42 (s, 2H), 3.77 (t, *J* = 5.3 Hz, 2H), 3.48 – 3.46 (m, 16H), 3.45 – 3.40 (m, 12H), 3.38 (t, *J* = 6.9 Hz, 2H), 3.34 (t, *J* = 6.7 Hz, 2H), 3.31 – 2.78 (m, 24H), 2.73 – 2.72 (m, 2H), 2.63 (q, *J* = 7.0 Hz, 2H), 2.37 (t, *J* = 7.0 Hz, 1H).

¹³C NMR (176 MHz, DMSO-d₆) δ [ppm] = 171.4, 171.3, 170.7, 170.6, 170.4, 170.2, 170.0, 149.5, 149.4, 149.4, 146.2, 143.3, 136.1, 135.8, 134.6, 130.0, 129.4, 129.1, 128.4, 126.3, 126.2, 123.7, 118.9, 118.3, 118.0, 117.4, 117.4, 116.6, 115.2, 115.0, 113.3, 69.8, 69.7, 69.6, 69.5, 69.1, 69.1, 69.1, 68.7, 65.0, 56.2, 55.9, 55.8, 55.7, 54.9, 50.9, 50.8, 50.4, 49.5, 40.4, 40.0, 39.1, 39.0, 38.6, 38.6, 38.6, 38.2, 38.2, 36.0, 35.8, 35.3, 35.2, 34.9, 34.7, 34.6, 34.0, 33.9, 30.8, 30.7, 26.6, 25.7, 23.3, 20.0, 19.4, 19.3, 19.0, 17.9, 17.3, 15.2, 12.7, 12.1, 9.7.

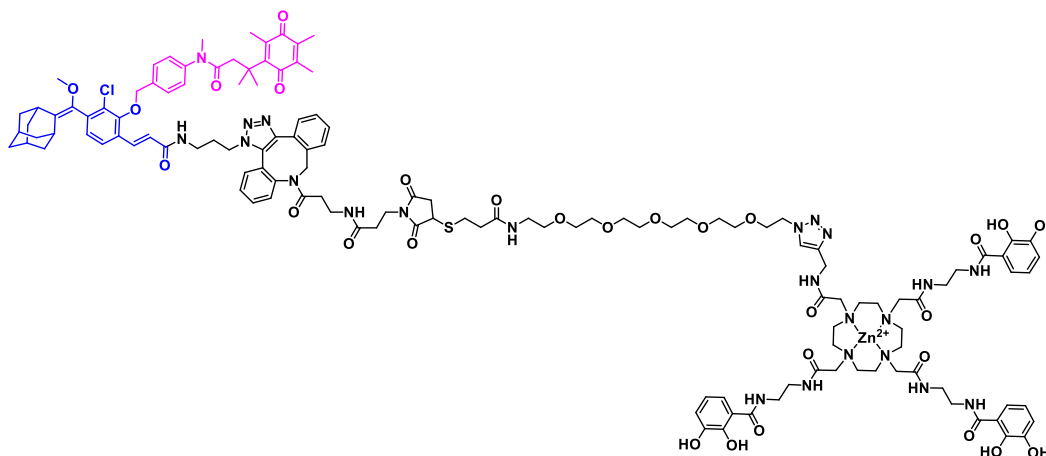
Compound 35

¹H NMR (700 MHz, DMSO) δ (ppm) = 9.05 (m, 4H), 8.87 (m, 3H), 7.95 (m, 1H), 7.80 (m, 1H), 7.62 (dd, *J* = 8.96 Hz, 17.92 Hz, 1H), 7.46 (m, 2H), 7.38 (t, *J* = 7.38 Hz, 1H), 7.34 (t, *J* = 7.56 Hz, 1H), 7.30 (d, *J* = 7.56 Hz, 1H), 7.23 (m, 5H), 7.06 (d, *J* = 8.96 Hz, 2H), 7.00 (d, *J* = 8.08 Hz, 2H), 6.88 (d, *J* = 7.38 Hz, 5H), 6.61 (t, *J* = 7.56 Hz, 5H), 4.45 (m, 4H), 4.42 (bs, 2H), 3.91 (m, 1H), 3.76 (m, 4H), 3.64 (s, 3H), 3.48 (m, 8H), 3.47 (m, 6H), 3.46 (m, 4H), 3.45 (m, 4H), 3.43 (m, 4H), 3.39 (m, 10H), 3.19 (q, *J* = 5.27 Hz, 11.25 Hz, 4H), 3.11 (m, 2H), 2.99 (m, 4H), 2.90 (m, 2H), 2.83 (m, 2H), 2.68 (m, 4H), 2.54 (m, 2H), 2.40 (m, 2H), 2.34 (t, *J* = 6.85 Hz, 2H), 2.18 (d, *J* = 6.85 Hz, 6H).

^{13}C NMR (176 MHz, DMSO): δ (ppm) = 176.35, 174.74, 172.00, 171.29, 170.55, 170.22, 170.14, 169.89, 169.00, 163.20, 157.72, 157.55, 157.38, 151.40, 148.38, 146.49, 146.46, 146.43, 146.24, 146.21, 143.31, 136.03, 135.71, 134.56, 132.36, 129.92, 129.53, 129.36, 128.96, 128.22, 128.05, 127.72, 126.81, 126.17, 125.21, 123.69, 122.45, 121.43, 119.98, 118.27, 117.48, 116.55, 115.15, 114.30, 108.06, 69.74, 69.69, 69.56, 69.49, 69.09, 69.06, 68.67, 55.76, 55.72, 55.63, 54.91, 54.84, 49.39, 40.02, 38.56, 38.00, 35.86, 35.22, 35.09, 34.99, 34.93, 34.61, 34.53, 33.98, 32.84, 26.57, 21.05, 19.36, 19.00, 1.15.

HRMS (ESI) calculated for $(\text{C}_{56}\text{H}_{114}\text{N}_{18}\text{O}_{23}\text{SZn}^{2+})^{2+}$ ($[\text{M}+2\text{H}]^{2+}$): $m/z = 931.3647$ experimental: 931.3681, δ [ppm] = 3.4 ppm

Zn²⁺-N,N',N''-(((2,2',2''-(10-(2-(((1-(21-((1-(3-((3-(1-(3-((E)-3-(4-(((1r,3r,5R,7S)-Adamantan-2-ylidene)(methoxy)methyl)-3-chloro-2-((4-(N,3-dimethyl-3-(2,4,5-trimethyl-3,6-dioxocyclohexa-1,4-dien-1-yl)butanamido)benzyl)oxy)phenyl) acrylamido)propyl)-1,9-dihydro-8H-dibenzo[b,f][1,2,3]triazolo[4,5-d]azocin-8-yl)-3-oxopropyl)amino)-3-oxopropyl)-2,5-dioxopyrrolidin-3-yl)thio)-19-oxo-3,6,9,12,15-pentaoxa-18-azahenicosyl)-1H-1,2,3-triazol-4-yl)methyl)amino)-2-oxoethyl)-1,4,7,10-tetraazacyclododecane-1,4,7-triyl)tris(acetyl))tris(azanediy))tris(ethane-2,1-diyl))tris(2,3-dihydroxybenzamide) 3a



Chemical Formula: $\text{C}_{132}\text{H}_{166}\text{ClN}_{23}\text{O}_{25}\text{SZn}^{2+}$
 Exact Mass: 2668,0912
 Molecular Weight: 2671,8009

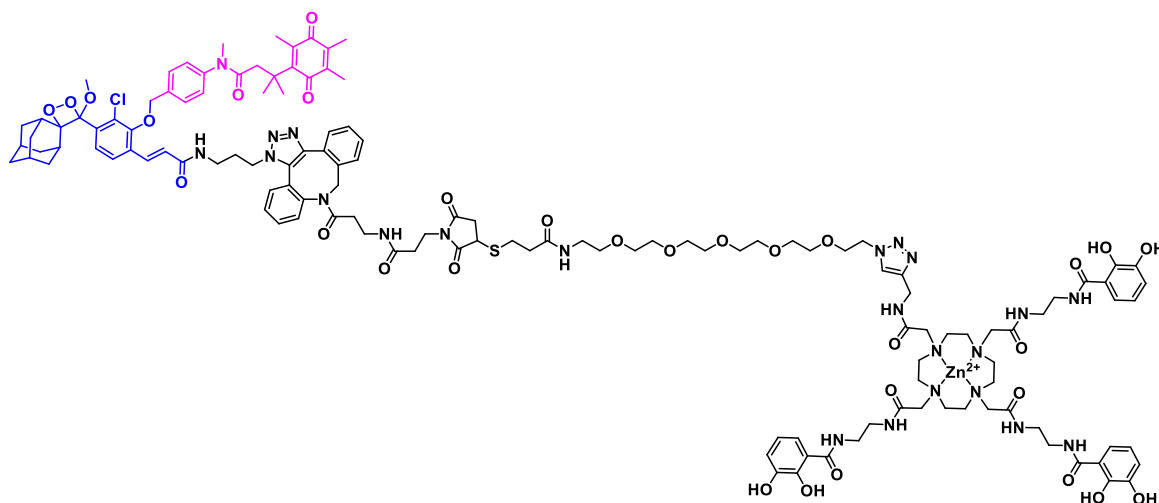
Strained alkyne **35** (8 mg, 4.5 μmol , 1.0 eq) was dissolved in anhydrous MeOH (2 mL) and under stirring azide **2a** (4.01 mg, 5 μmol , 1.1 eq) was added in anhydrous MeOH (2 mL). The solution continued stirring overnight at 25 °C in the dark. The next morning the reaction was concentrated *in vacuo* and the purity was assessed by LCMS. Washing with ice-cold ether (2x 5 mL) removed minor impurities. The residue was dried to yield the crude product **3a** as a

slightly beige oil, (>95% pure by LCMS) and was employed without further purification directly in the next step (11.61 mg, 4.5 μ mol, quant.).

$^1\text{H NMR}$ (700 MHz, DMSO) δ 8.20 (m, 1H), 7.98 (m, 1H), 7.92 (s, 1H), 7.84 (m, 1H), 7.66-7.50 (m, 11H), 7.39-7.17 (m, 13H), 6.75 (m, 2H), 6.69 (t, $J=17.27$ Hz, 1H), 6.43 (m, 2H), 5.96-5.85 (dd, $J=17.27$ Hz, 56.6 Hz, 1H), 5.00-4.94 (m, 2H), 4.54 (m, 1H), 4.47-4.43 (m, 4H), 4.38-4.32 (m, 4H), 3.91 (m, 1H), 3.76 (t, $J=6.25$ Hz, 2H), 3.48-3.45 (m, 16H), 3.44 (m, 6H), 3.42-3.38 (t, $J=7.2$ Hz, 12H), 3.24 (m, 8H), 3.18 (m, 4H), 3.12 (m, 2H), 3.05 (bs, 2H), 2.97 (m, 2H), 2.91 (m, 6H), 2.83 (m, 2H), 2.65 (m, 2H), 2.52 (m, 4H), 2.40 (m, 2H), 2.22 (q, $J=7.2$ Hz, 2H) 2.01 (m, 4H), 1.91 (m, 12H), 1.81 (m, 10H), 1.74 (m, 2H), 1.66 (m, 2H), 1.50 (m, 1H), 1.21 (bs, 6H).

HRMS (ESI) calculated for $(\text{C}_{132}\text{H}_{169}\text{ClN}_{23}\text{O}_{29}\text{SZn}^{2+})^{2+}$ ($[\text{M}+3\text{H}]^{3+}$): $m/z = 890.3710$
experimental: 890.3652, δ [ppm] = 5.8 ppm

Zn²⁺- N,N',N''-(((2,2',2''-(10-(2-(((1-(21-(((1-(3-(((1-(3-((E)-3-(3-Chloro-2-((4-(N,3-dimethyl-3-(2,4,5-trimethyl-3,6-dioxocyclohexa-1,4-dien-1-yl)butanamido)benzyl)oxy)-4'-((1r,3r,5r,7r)-4'-methoxyspiro[adamantane-2,3'-[1,2]dioxetan]-4'-yl)phenyl)acrylamido)propyl)-1,9-dihydro-8H-dibenzo[b,f][1,2,3]triazolo[4,5-d]azocin-8-yl)-3-oxopropyl)amino)-3-oxopropyl)-2,5-dioxopyrrolidin-3-yl)thio)-19-oxo-3,6,9,12,15-penta-18-azahenicosyl)-1H-1,2,3-triazol-4-yl)methyl) amino)-2-oxoethyl)-1,4,7,10-tetraazacyclododecane-1,4,7-triyl)tris(acetyl))tris(azanediy))tris(ethane-2,1-diyl))tris(2,3-dihydroxybenzamide) 3



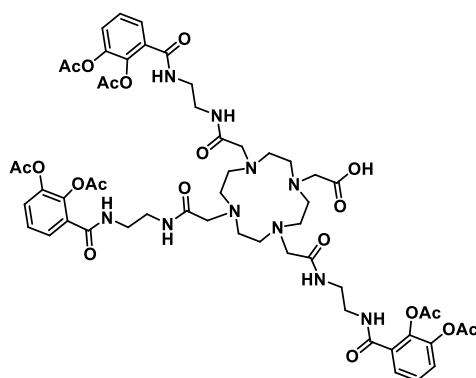
Chemical Formula: C₁₃₂H₁₆₆ClN₂₃O₃₁SZn²⁺
 Exact Mass: 2700,0810
 Molecular Weight: 2703,7989

Enolether **3a** (5 mg, 1.9 μmol, 1 eq) and a catalytic amount of methylene blue (0.37 mg, 1 μmol, 0.6 eq) were dissolved in DCM:DMF (5 mL, 9:1) in a septum-capped screw cap tube. The solution was pre-saturated with oxygen gas (5 min). Then the reaction was irradiated with yellow light for 20 min at 23 °C and the reaction progress was monitored by LCMS. Upon LCMS indicated completion, the DCM was removed by rotary evaporation at 30 °C. The residue was diluted in ACN:H₂O (1:1, 1 mL), then purified by preparative RP-HPLC (40 min gradient, 20-100% ACN/H₂O, 0.1% HCOOH) to yield siderophore dioxetane **3** as a beige solid (4.38 mg, 1.7 μmol, 87%).

¹H NMR (700 MHz, DMSO) δ 8.36 (m, 1H), 8.21 (m, 1H), 8.15 (m, 1H), 7.97 (m, 1H), 7.93 (m, 1H), 7.88 (m, 1H), 7.82 (m, 1H), 7.66-7.46 (m, 10H), 7.40-7.16 (m, 13H), 6.84 (bs, 2H), 6.69 (m, 1H), 5.96-5.85 (dd, J=19.0 Hz, 56.08 Hz), 4.97 (m, 2H), 4.56-4.34 (m, 8H), 3.91 (m, 1H), 3.76 (m, 2H), 3.51 (m, 4H), 3.75 (m, 10H), 3.48 (m, 10H), 3.413 (m, 7H), 3.37 (m, 12H), 3.24 (s, 4H), 3.19 (m, 4H), 3.12 (m, 4H), 3.05 (bs, 2H), 2.98 (m, 6H), 2.90 (m, 2H), 2.82 (m, 1H), 2.65 (m, 6H), 2.20 (m, 3H), 2.01 (m, 4H), 1.91 (m, 13H), 1.76 (m, 8H), 1.50 (m, 1H), 1.23 (bs, 4H), 1.21 (bs, 6H).

HRMS (ESI) calculated for $(C_{132}H_{168}ClN_{23}O_{31}SZn^{2+}Na^+)^{3+}$ ($[M+2H+Na]^{3+}$): $m/z = 908.3616$, experimental: 908,3643, δ [ppm] = 2.7 ppm

2-(4,7,10-tris(2-((2-(2,3-diacetoxybenzamido)ethyl)amino)-2-oxoethyl)-1,4,7,10-tetraazacyclododecan-1-yl)acetic acid **25**



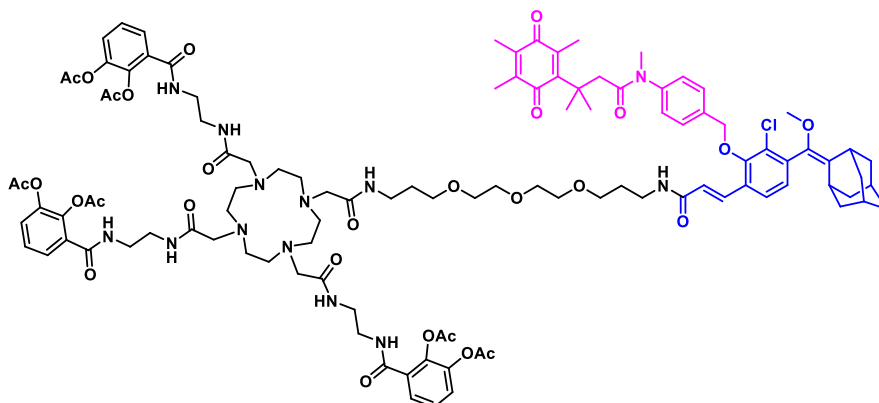
Chemical Formula: $C_{55}H_{70}N_{10}O_{20}$
 Exact Mass: 1190,4768
 Molecular Weight: 1191,2150

Acid DOTAM siderophore **25** was afforded according to our previously published procedure.⁵

1H NMR (700 MHz, DMSO- d_6): δ (ppm) = 8.32-8.09 (m, 6H), 7.22-7.07 (m, 9H), 3.83 (s, 9H), 3.75 (s, 9H), 3.61-3.37 (m, 8H), 3.26-2.57 (m, 28H).

^{13}C NMR (176 MHz, DMSO): δ (ppm) = 172.03, 171.99, 170.61, 170.52, 170.25, 170.17, 168.57, 168.32, 168.26, 168.13, 167.85, 167.81, 167.67, 166.71, 165.65, 164.62, 164.58, 164.54, 164.49, 142.83, 142.58, 140.21, 140.18, 139.17, 138.55, 131.73, 130.71, 130.66, 130.61, 130.56, 126.72, 126.25, 126.17, 126.10, 125.42, 125.33, 124.89, 124.29, 57.71, 57.12, 53.11, 51.65, 50.29, 47.80, 34.23, 21.05, 20.69, 20.58, 20.47, 20.43, 20.38, 20.34, 20.25, 20.13, 19.99, 1.15.

(((2,2'-(7-(2-((2-(2,3-DiAcetoxy-benzamido)ethyl)amino)-2-oxoethyl)-10-((E)-20-(4-((Z)-((1r,5R,7S)-adamantan-2-ylidene)(methoxy)methyl)-3-chloro-2-((4-(N,3-dimethyl-3-(2,4,5-trimethyl-3,6-dioxocyclohexa-1,4-dien-1-yl)butanamido)benzyl)oxy)phenyl)-2,18-dioxo-7,10,13-trioxa-3,17-diazaicos-19-en-1-yl)-1,4,7,10-tetraazacyclododecane-1,4-diyl)bis(acetyl))bis(azanediy))bis(ethane-2,1-diyl))bis(azanediy))bis(formyl))bis(benzene-3,1,2-triyl)tetraacetate **4a**



Chemical Formula: $C_{108}H_{138}ClN_{13}O_{28}$
 Exact Mass: 2099,9463
 Molecular Weight: 2101,8050

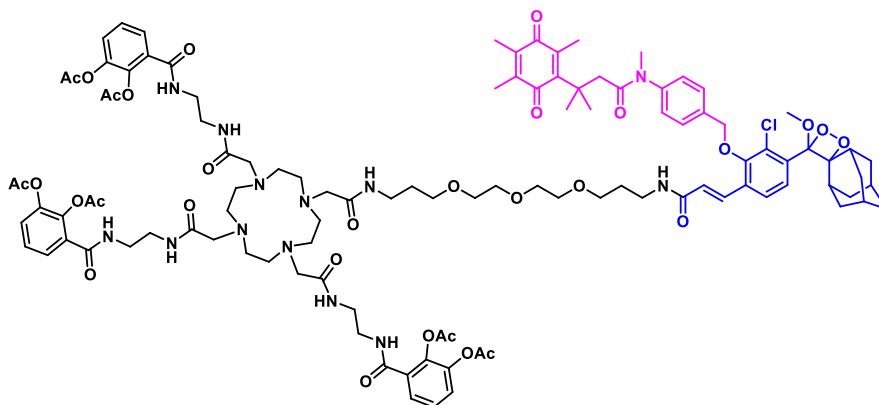
The acid DOTAM **25** (7.5 mg, 0.007 mmol, 1.5 eq) was dissolved under an Argon atmosphere in anhydrous THF (500 μ L) and NMM (100 μ L) was added, after cooling to 0 $^{\circ}$ C. Then *iso*-butyl chloroformate (0.96 μ L, 0.007 mmol, 0.95 eq) was added to the reaction and the solution became turbid instantly. The reaction stirred 5 min at 0 $^{\circ}$ C and 55 min at 23 $^{\circ}$ C. Then the amine **24** (6.72 mg, 0.007 mmol, 1.0 eq) was added under Argon conditions dissolved in an anhydrous THF/NMM mixture (100 μ L/500 μ L) and was added dropwise at 0 $^{\circ}$ C to the mixed anhydride. The reaction cleared and continued stir at 0 $^{\circ}$ C for 5 minutes and 1 hour at 23 $^{\circ}$ C. The reaction progress was monitored by LCMS. After complete conversion, AcOH (100 μ L) were added, the majority of the organic solvent was removed by rotary evaporation (30 $^{\circ}$ C water bath). The residue was diluted with ACN (1 mL) and purified by RP-HPLC (40 min. gradient from 20-99% ACN/H₂O, 1% AcOH, 220 nm). A product containing fractions was identified by LCMS and lyophilized to yield enolether **4a** (9.48 mg, 0.005 mmol, 67%) as a yellow solid.

¹H NMR (700 MHz, CD₂Cl₂) δ (ppm) = 7.86-7.70 (m, 2H), 7.62-7.46 (m, 8H), 7.38-7.13 (m, 9H), 7.08-6.93 (m, 3H), 6.78 (m, 1H), 6.59-6.57 (d, J=14.84 Hz, 1H), 5.32-5.02 (bs, 2H), 3.93 (m, 2H), 3.59-3.55 (m, 8H), 3.53-3.50 (m, 4H), 3.46 (m, 4H), 3.41 (m, 4H), 3.31 (s, 4H), 3.25 (m, 2H), 3.12 (m, 4H), 2.95 (m, 4H), 2.87 (m, 4H), 2.74 (m, 2H), 2.64 (s, 2H), 2.27 (s, 9H), 2.25 (m, 6H), 2.08 (s, 9H), 1.97 (m, 4H), 1.95 (m, 8H), 1.86 (m, 4H), 1.80 (m, 7H), 1.75 (s, 3H), 1.71 (m, 2H), 1.30 (s, 2H), 1.29 (s, 6H), 1.26 (s, 4H).

DEPT (176 MHz, CD₂Cl₂): δ (ppm) = 214.30, 213.79, 134.45, 130.39, 128.34, 126.85, 126.23, 124.04, 118.38, 79.46, 75.54, 70.62, 70.28, 69.83, 64.46, 57.32, 50.72, 47.80, 46.04, 43.95, 42.43, 40.49, 39.50, 39.34, 38.90, 37.39, 34.01, 33.40, 30.15, 30.06, 29.42, 28.90, 28.74, 28.60, 26.49, 24.49, 24.07, 23.21, 20.77, 14.20, 12.81, 12.10, 11.50, 11.26, 8.64.

HRMS (ESI) calculated for (C₁₀₈H₁₄₀ClN₁₃O₂₈)²⁺ ([M+2H]²⁺): m/z = 1050.9840, experimental = 1050.9849, δ [ppm] = 0.9 ppm, calculated for (C₁₀₈H₁₄₃ClN₁₄O₂₈)²⁺ ([M+H+NH₄]²⁺): m/z = 1059.4937, experimental = 1059.4949, δ [ppm] = 1.2 ppm, calculated for (C₁₀₈H₁₃₉ClN₁₃O₂₈K)²⁺ ([M+H+K]²⁺): m/z = 1069.9583, experimental = 1069.9593, δ [ppm] = 1.0 ppm.

(((2,2'-(7-(2-((2-(2,3-Diacetoxy-benzamido)ethyl)amino)-2-oxoethyl)-10-((E)-20-(3-chloro-2-((4-(N,3-dimethyl-3-(2,4,5-trimethyl-3,6-dioxocyclohexa-1,4-dien-1-yl)butanamido)benzyl)oxy)-4-((1r,5R,7S)-4'-methoxyspiro[adamantane-2,3'-[1,2]dioxetan]-4'-yl)phenyl)-2,18-dioxo-7,10,13-trioxa-3,17-diazaicos-19-en-1-yl)-1,4,7,10-tetraazacyclododecane-1,4-diyl)bis(acetyl))bis(azanediy))bis(ethane-2,1-diyl))bis(azanediy))bis(formyl))bis(benzenene-3,1,2-triyl) tetraacetate 4



Chemical Formula: $C_{108}H_{138}ClN_{13}O_{30}$
 Exact Mass: 2131,9361
 Molecular Weight: 2133,8030

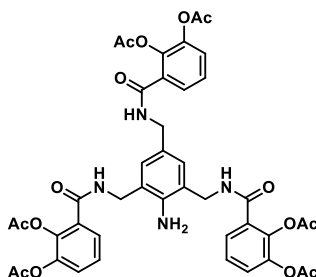
Enolether **4a** (8 mg) and a catalytic amount of methylene blue were dissolved in DCM:DMF (9:1, 5 mL). Acetic acid (5 μ L) was added to prevent deacetylation. The solution was presaturated with oxygen gas (5 min) while stirring at 300 rpm. Then the reaction was irradiated with yellow light for 20 min at 23 °C. Upon completion, the DCM was removed by rotary evaporation (30 °C) and the product was purified by preparative RP-HPLC (220nm, 20-99% ACN/H₂O, 1% AcOH, 40 min. linear gradient). The product containing fractions were identified by LCMS and lyophilized to dryness to yield conjugate **4** (4.29 mg, 0.002 mmol, 47%) as a beige solid.

¹H NMR (700 MHz, CD₃CN+1% AcOH-d₃): δ (ppm) = 7.86-7.84 (d, J=9.23 Hz, 2H), 7.73-7.68 (m, 2H), 7.56 (m, 4H), 7.51-7.49 (m, 4H), 7.33-7.31 (m, 6H), 7.25 (m, 2H), 7.19 (m, 2H), 6.65-6.62 (d, J=16.2 Hz, 2H), 4.98 (bs, 2H), 3.55 (m, 4H), 3.53 (m, 6H), 3.49 (m, 4H), 3.41 (m, 4H), 3.34 (m, 4H), 3.18 (m, 4H), 3.09 (m, 2H), 2.92 (m, 2H), 2.69 (m, 2H), 2.26 (m, 10H), 2.23 (m, 6H), 2.05 (s, 4H), 2.03 (m, 1H), 1.99 (m, 2H), 1.97 (s, 2H), 1.92 (m, 4H), 1.76 (m, 12H), 1.66 (m, 12H), 1.38 (m, 2H), 1.34 (m, 2H), 1.31 (m, 6H), 1.27 (m, 12H).

HRMS (ESI) calculated for $(C_{108}H_{143}ClN_{13}O_{30})^{3+}$ ([M+H+NH₄]²⁺): m/z = 1031.4624, experimental = 1031.4638, δ [ppm] = 1.4 ppm, calculated for $(C_{112}H_{146}ClN_{15}O_{30})^{2+}$ ([M+2H+ACN]²⁺): m/z = 1084.4889, experimental = 1084.4916, δ [ppm] = 2.7 ppm.

MECAM and MECAM dioxetane conjugates

(((5-((2,3-Diacetoxy-benzamido)methyl)-4-amino-1,3-phenylene)bis(methylene))bis(azanediy))bis(carbonyl)) bis(benzene-3,1,2-triyl)tetraacetate **26**



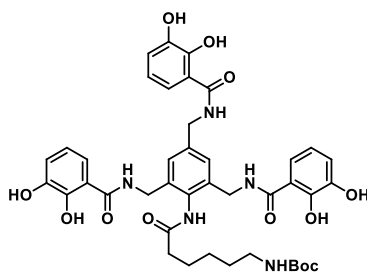
Chemical Formula: $C_{42}H_{40}N_4O_{15}$
 Exact Mass: 840,24902
 Molecular Weight: 840,79500

26 was prepared according to an established procedure reported by Pinkert.⁷

$^1\text{H NMR}$ (500 MHz, DMSO-d_6): δ [ppm] = 8.84 (t, $J = 6.1$ Hz, 2H), 8.75 (t, $J = 6.0$ Hz, 1H), 7.48 (dd, $J = 7.5$ Hz, 1.8 Hz, 2H), 7.45 (dd, $J = 7.6$ Hz, 1.7 Hz, 1H), 7.37 (dd, $J = 8.1$ Hz, 1.9 Hz, 2H), 7.35 (dd, $J = 8.2$ Hz, 1.8 Hz, 1H), 7.33 (t, $J = 7.8$ Hz, 2H), 7.30 (t, $J = 7.8$ Hz, 1H), 7.01 (s, 2H), 5.12 (s, 2H), 4.28 (d, $J = 6.0$ Hz, 4H), 4.25 (d, $J = 5.9$ Hz, 2H), 2.27 (s, 9H), 2.16 (s, 3H), 2.14 (s, 6H).

$^{13}\text{C NMR}$ (126 MHz, DMSO-d_6) δ [ppm] = 168.3, 168.3, 167.8, 167.8, 164.8, 164.3, 142.8, 142.6, 140.1, 140.0, 131.0, 130.8, 127.8, 126.3, 126.1, 126.1, 126.0, 125.9, 125.5, 125.3, 122.0, 42.1, 30.4, 20.8, 20.3, 20.2, 20.1.

HRMS (ESI) calculated for $C_{42}H_{41}N_4O_{15}^+$ ($[\text{M}+\text{H}]^+$): $m/z = 841.25630$, experimental: 841.2562, δ [ppm] = 0.12.

***tert*-Butyl (6-oxo-6-((2,4,6-tris((2,3-dihydroxybenzamido)methyl) phenyl)amino) hexyl) carbamate 27**Chemical Formula: C₄₁H₄₇N₅O₁₂

Exact Mass: 801,3221

Molecular Weight: 801,8500

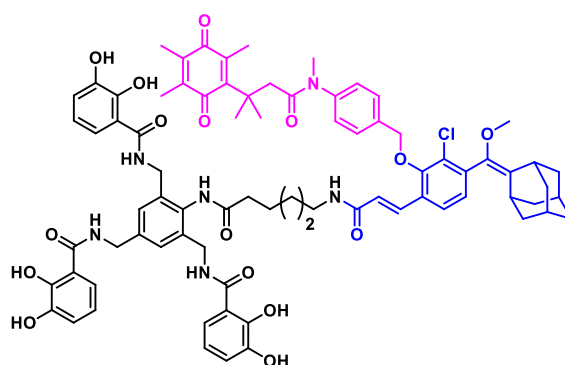
6-Boc-amino hexanoic acid (246 mg, 1.07 μ mol, 3.5 eq) was dissolved in THF (6 mL) and NMM was added (167 μ L, 1.52 μ mol, 5.0 eq). The solution was cooled to 0 °C and stirred for 10 minutes at that temperature. The ice-bath was removed and the turbid reaction continued stirring for 60 minutes at ambient temperature. Then the aniline **26** (256 mg, 3.01 μ mol, 1.0 eq) was dissolved in THF (6 mL) and added at 0 °C over 10 minutes with a syringe pump. The reaction continued stirring overnight, while equilibrating to ambient temperature. Quenching was performed by the addition of ice and sat. NaHCO₃ (8 mL each), then EtOAc was added (3x10 mL). The combined organic extracts were washed with 0.1 M HCl, sat. NaHCO₃, brine (each 2x30 mL) and were dried over Na₂SO₄. The solvent was removed *in vacuo* to yield crude amide **27a**, which was dissolved in MeOH (6 mL). Then TEA (2 mL) was added at 0 °C and the ice bath was removed. The reaction was stirred for 2.5 h at ambient temperature. The solvent was removed by rotary evaporation and the residue was purified by RP-HPLC (40 min gradient, 10-70% ACN/H₂O, 0.1% HCOOH, 220 nm) Product containing fractions were identified by LCMS and lyophilized to dryness to yield deacetylated product **27** (71.3 mg, 88 μ mol, 30% over 2 steps) as a beige oil.

¹H NMR (500 MHz, MeOD) δ 7.18 (dd, *J* = 8.1, 1.4 Hz, 1H), 7.14 (dd, *J* = 8.1, 1.4 Hz, 1H), 6.92 (dd, *J* = 7.9, 1.4 Hz, 1H), 6.90 (dd, *J* = 7.9, 1.4 Hz, 1H), 6.68 (t, *J* = 8.0 Hz, 1H), 3.01 (t, *J* = 6.8 Hz, 1H), 2.49 (t, *J* = 7.5 Hz, 1H), 1.74 – 1.66 (m, 1H), 1.48 (dt, *J* = 13.7, 7.0 Hz, 1H). 1.40 (bs, 9H)

¹³C NMR (126 MHz, MeOD) δ 176.30, 171.78, 171.58, 158.72, 150.50, 147.49, 147.45, 140.12, 137.56, 133.83, 128.24, 119.93, 119.87, 119.84, 119.79, 118.88, 118.74, 116.69, 79.98, 43.64, 41.34, 41.03, 37.21, 30.81, 28.92, 27.82, 26.65.

HRMS (ESI) calculated for $C_{41}H_{48}N_5O_{12}^+$ ($[M+H]^+$): $m/z = 802.3293$, experimental: 802.3317, δ [ppm] = 2.4 ppm.

N,N',N''-((2-(6-((E)-3-(4-(((1r,3r,5r,7r)-Adamantan-2-yl)(methoxy)methyl)-3-chloro-2-((4-(N,3-dimethyl-3-(2,4,5-trimethyl-3,6-dioxocyclohexa-1,4-dien-1-yl)butanamido)benzyl)oxy)phenyl)acrylamido)hexanamido)benzene-1,3,5-triyl)tris(methylene))tris(2,3-dihydroxybenzamide) 5a

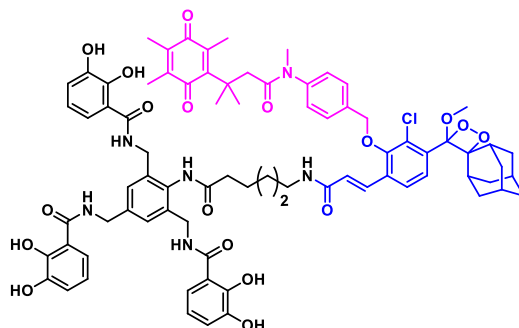


Chemical Formula: $C_{79}H_{86}ClN_6O_{16}$
 Exact Mass: 1408,5711
 Molecular Weight: 1410,0250

Compound **27** (30 mg, 0.038 mmol, 1 eq) was dissolved in TFA:DCM (1:1, 1 mL) and stirred for 1 h at 23 °C. The reaction was monitored by RP-HPLC (30-100% ACN in water, 20 min). Upon completion, the mixture was concentrated by evaporation under reduced pressure. Besides, the equimolar amount NHS ester of compound **13** was prepared according to the procedure explained in the preparation of compound **2a**. Then, the crude residue of compound **9** and the NHS ester were added together in DMF (1 mL). After the addition of a drop of TEA, the reaction was stirred for 30 min at room temperature. The reaction was monitored by RP-HPLC (50-100% ACN/H₂O, 20 min). Upon completion, the reaction mixture was concentrated by evaporation under reduced pressure and purified using RP-HPLC (50-100% ACN/H₂O, 20 min) to afford compound **5a** (31 mg, 59% yield) as a yellow solid.

MS (ESI): calculated for $C_{79}H_{86}ClN_6O_{16}^+$ $[M+H]^+$: $m/z = 1408.6$, experimental = 1410.3.

N,N',N''-((2-(6-((E)-3-(3-Chloro-2-((4-(N,3-dimethyl-3-(2,4,5-trimethyl-3,6-dioxocyclohexa-1,4-dien-1-yl)butanamido)benzyl)oxy)-4-((1R,3S,4'S,5S,7S)-4'-methoxyspiro[adamantane-2,3'-[1,2]dioxetan]-4'-yl)phenyl)acrylamido)hexanamido)benzenene-1,3,5-triyl)tris(methylene))tris(2,3-dihydroxybenzamide) 5



Chemical Formula: $C_{79}H_{85}ClN_6O_{18}$
 Exact Mass: 1440,5609
 Molecular Weight: 1442,0230

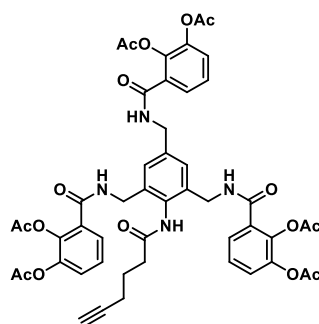
Enol ether **5a** (9 mg, 6 μ mol, 1.0 eq) and a catalytic amount of methylene blue (0.5 mg, 1.5 μ mol, 0.25 eq) were dissolved in 5 mL of DCM/DMF (9:1). The solution was presaturated with oxygen gas (5 min). Then the reaction was irradiated under O_2 atmosphere with yellow light for 30 min. The reaction was monitored by LCMS, and upon complete conversion, the DCM was removed by rotary evaporation at 30 $^{\circ}C$. The product was purified by preparative RP-HPLC (40 min linear gradient, 20-100% ACN/H₂O, 0.1% HCOOH, 220 nm). The product containing fractions were identified by LCMS and lyophilized to yield MECAM dioxetane **5** (6.3 mg, 4 μ mol, 69%) as a slightly yellow solid.

1H NMR (700 MHz, ACN- d_3): δ (ppm) = 8.79 (bs, 1H), 8.03-8.02 (t, $J_{08.02Hz}$, 2H), 7.85 (t, $J_{06.48Hz}$, 1H), 7.65-7.63 (d, $J=15.80Hz$, 1H), 7.52-7.48 (m, 3H), 7.33 (s, 2H), 7.21-7.20 (d, $J=6.48Hz$, 2H), 7.17-7.16 (d, $J=6.08 Hz$, 1H), 7.09-7.05 (m, 3H), 6.96-6.93 (m, 3H), 6.80 (m, 1H), 6.72-6.69 (m, 3H), 6.60-6.58 (d, $J=15.80Hz$, 1H), 4.97 (bs, 2H), 4.48 (d, $J=8.10 Hz$, 6H), 3.34 (bs, 1H), 3.29-3.26 (q, $J=6.08, 8.10 Hz$, 2H), 3.07 (bs, 2H), 2.67 (bs, 1H), 2.49 (t, $J=9.32 Hz$, 2H), 2.25 (bs, 2H), 2.09 (bs, 6H), 2.04-2.03 (m, 6H), 1.90 (m, 4H), 1.88 (m, 2H), 1.86 (m, 1H), 1.85-1.84 (m, 2H), 1.75 (m, 2H), 1.71 (m, 2H), 1.62-1.60 (m, 2H), 1.56 (m, 2H), 1.45-1.43 (m, 2H), 1.27 (s, 6H), -1.25 (s, 5H), 0.88 (s, 1H).

¹³C NMR (176 MHz, CD₃CN): δ (ppm) = 188.35, 188.26, 188.23, 171.05, 170.90, 156.00, 150.60, 150.58, 150.55, 150.54, 146.89, 146.81, 145.38, 145.35, 145.33, 145.31, 145.29, 144.53, 144.49, 144.48, 142.25, 139.15, 136.94, 136.93, 136.87, 136.81, 134.13, 134.06, 133.47, 133.33, 133.08, 131.19, 131.17, 131.14, 128.65, 128.63, 128.60, 128.58, 119.40, 119.39, 119.36, 118.26, 115.28, 79.10, 78.91, 78.73, 76.15, 75.41, 56.37, 42.95, 40.65, 39.85, 38.84, 37.77, 36.73, 33.87, 30.33, 30.28, 30.25, 29.78, 28.76, 28.66, 28.49, 27.09, 26.53, 25.81, 14.30, 12.90, 12.03, 11.66.

HRMS (ESI) calculated for C₇₉H₅₁ClN₆O₁₈⁺ ([M+H]⁺): m/z = 1440.5609 experimental: m/z = 1440.5632, δ [ppm] = 2.2 ppm

(((5-((2,3-Diacetoxy-benzamido)methyl)-4-(hex-5-ynamido)-1,3-phenylene)bis(methylene))bis(azanediyl))bis(carbonyl))bis(benzene-3,1,2-triyl)tetraacetate 28



Chemical Formula: C₄₈H₄₆N₄O₁₆
 Exact Mass: 934,29088
 Molecular Weight: 934,90800

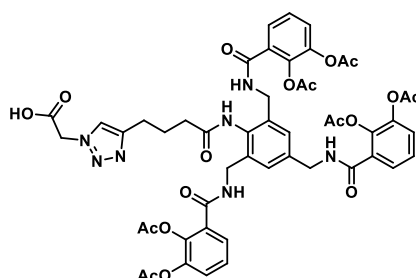
28 was prepared according to an established procedure reported by Pinkert.⁷

¹H NMR (700 MHz, DMSO-d₆): δ [ppm] = 9.54 (s, 1H), 8.94 (t, *J* = 6.1 Hz, 1H), 8.77 (t, *J* = 6.0 Hz, 2H), 7.52 (dd, *J* = 7.7 Hz, 1.6 Hz, 2H), 7.44 (dd, *J* = 7.7 Hz, 1.6 Hz, 1H), 7.38 (dd, *J* = 8.1 Hz, 1.6 Hz, 2H), 7.34 (dd, *J* = 8.1 Hz, 1.6 Hz, 1H), 7.31 (t, *J* = 7.8 Hz, 2H), 7.23 (t, *J* = 7.9 Hz, 1H), 7.20 (s, 2H), 4.38 (d, *J* = 5.9 Hz, 2H), 4.33 (bs, 4H), 2.81 (t, *J* = 2.6 Hz, 1H), 2.52 – 2.51 (m, 2H), 2.28 (s, 6H), 2.28 (s, 3H), 2.25 (td, *J* = 7.1 Hz, 2.7 Hz, 2H), 2.17 (s, 6H), 2.16 (s, 3H), 1.80 (p, *J* = 7.2 Hz, 2H).

^{13}C NMR (176 MHz, DMSO- d_6) δ [ppm] = 173.96, 171.16, 168.30, 167.91, 167.85, 164.70, 164.57, 142.85, 140.16, 137.57, 135.86, 131.81, 130.67, 130.63, 126.20, 126.12, 126.07, 126.04, 125.55, 125.43, 124.64, 84.00, 83.82, 71.65, 71.64, 48.60, 42.23, 39.52, 34.17, 32.39, 24.14, 23.49, 20.35, 20.18, 17.48, 17.14.

HRMS (ESI) ($[M+2H]^{2+}$): m/z = 468.15272, experimental: 468.1527, δ [ppm] = 0.04.

2-(4-(4-Oxooxo-4-((2,4,6-tris((2,3-diacetoxybenzamido)methyl)phenyl)amino)butyl)-1H-1,2,3-triazol-1-yl)acetic acid 29



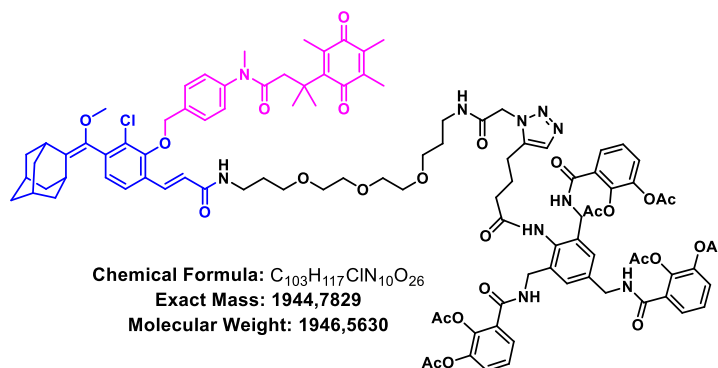
Chemical Formula: $\text{C}_{50}\text{H}_{49}\text{N}_7\text{O}_{18}$

Exact Mass: 1035,3134

Molecular Weight: 1035,9730

28 (20 mg, 0.021 mmol, 1.0 eq) was dissolved in DMSO (1 mL) and PBS was added (400 μL), followed by AcOH (10 μL). Then 2-azido-acetic acid (12.97 mg, 0.128 mmol, 6 eq) was added in DMSO (500 μL). Sodium ascorbate (4.24 mg, 0.021 mmol, 1.0 eq) and CuSO_4 (3.41 mg, 0.021 mmol, 1.0 eq) were dissolved in a DMSO/PBS mixture (500/100 μL). Upon addition of the reductant, the blue color of the sulfate vanished and the solution turned white and turbid. When the ligand THPTA (11.14 mg, 0.021, 1.0 eq) was added, the suspension cleared and added to the reaction at 24 $^\circ\text{C}$. The reaction continued stirring for 3 h. Upon completion, AcOH (100 μL), DCM (100 mL) and brine (100 mL) were added. The phases were separated and the organic phase was washed with milliQ water:brine (1:1, 2x50 mL), then with milliQ (1x50 mL) and sat. NaHCO_3 (2x50 mL). The organic phase was dried over anhydrous Na_2SO_4 and the reaction was concentrated by rotary evaporation, to yield the crude product as a colorless oil (16.3 mg, 0.016 mmol, 74%), which was used without further purification in the next step.

(((5-((2-Acetoxy-3-methoxybenzamido)methyl)-4-(4-(1-((E)-20-(4-(((1*r*,3*r*,5*R*,7*S*)-adamantan-2-ylidene)(methoxy)methyl)-3-chloro-2-((4-(N,3-dimethyl-3-(2,4,5-trimethyl-3,6-dioxocyclohexa-1,4-dien-1-yl)butanamido)benzyl)oxy)phenyl)-2,18-dioxo-7,10,13-trioxa-3,17-diazaicos-19-en-1-yl)-1*H*-1,2,3-triazol-5-yl)butanamido)-1,3-phenylene)bis(methylene))bis(azanediyl))bis(carbonyl))bis(benzene-3,1,2-triyl)tetraacetate **6a**



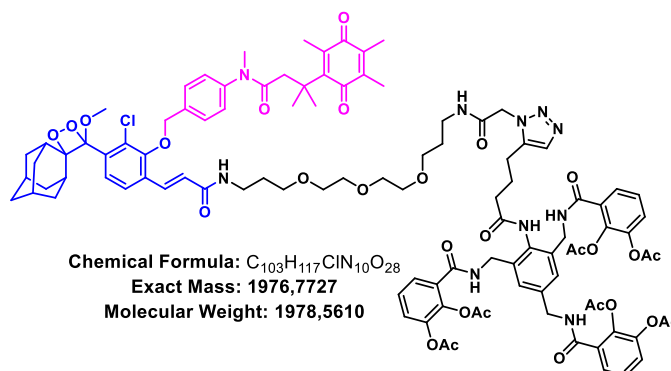
Acid **29** (7.5 mg, 0.007 mmol, 1.5 eq) was dissolved under an Argon atmosphere in anhydrous THF (500 μ L) and NMM (100 μ L) was added, after cooling the solution to 0 $^{\circ}$ C. Then *iso*-butylchloroformate (0.96 μ L, 0.007 mmol, 0.95 eq) was added to the reaction and the solution turned turbid instantly. The reaction stirred 5 min at 0 $^{\circ}$ C and 55 min at 23 $^{\circ}$ C. Then the amine **24** (6.72 mg, 0.007 mmol, 1.0 eq) was added under Argon conditions in an anhydrous THF/NMM (500/100 μ L) and was added dropwise at 0 $^{\circ}$ C. The reaction cleared and continued stir at 0 $^{\circ}$ C for 5 minutes and 1 hour at 23 $^{\circ}$ C. After complete conversion, AcOH (100 μ L) were added, the majority of the organic solvent was removed by rotary evaporation (30 $^{\circ}$ C). The residue was diluted with ACN and filtered over a syringe filter to be purified by RP-HPLC (40 min. gradient from 20-99% ACN/H₂O, 1% AcOH, 220 nm). A product containing fractions were identified by LCMS and lyophilized to dryness to yield enolether **6a** (9.48 mg, 0.005 mmol, 67%) as a yellow solid.

¹H NMR (700 MHz, CD₂Cl₂): δ (ppm) = 7.63-7.62 (d, J = 7.28 Hz, 1H), 7.57-7.56 (m, 2H), 7.55-7.53 (m, 2H), 7.43 (m, 1H), 7.41 (m, 2H), 7.39 (m, 4H), 7.37 (m, 1H), 7.36 (m, 1H), 7.35 (m, 1H), 7.34 (m, 1H), 7.32 (m, 1H), 7.31 (m, 1H), 7.28 (m, 8H), 5.11-5.09 (d, J = 13.85 Hz, 2H), 4.88-4.82 (q, J = 15.98 Hz, 24.15 Hz, 4H), 4.50 (d, J = 5.15 Hz, 2H), 4.45 (bs, 8H), 3.71-3.69 (d, J = 13.14 Hz, 2H), 3.25 (m, 2H), 3.11 (m, 2H), 2.84 (t, J = 7.28 Hz, 4H), 2.61 (t, J = 7.69 Hz, 4H), 2.46 (m, 2H), 2.25 (s, 24H), 2.13 (m, 6H), 2.07 (s, 6H), 2.04 (s, 9H), 2.02 (s, 13H), 1.94 (m, 2H).

¹³C NMR (176 MHz, CD₂Cl₂): δ (ppm) = 176.03, 174.93, 174.39, 174.31, 172.70, 169.16, 169.11, 168.98, 168.89, 168.85, 167.19, 166.34, 166.27, 166.16, 166.07, 165.86, 165.78, 151.41, 148.62, 148.14, 147.65, 143.64, 143.60, 142.56, 140.83, 140.78, 138.78, 138.46, 136.12, 135.93, 134.49, 133.59, 133.48, 133.27, 132.78, 130.57, 130.53, 130.49, 130.43, 130.39, 130.30, 130.14, 129.73, 129.36, 129.09, 128.70, 128.65, 128.44, 127.74, 127.64, 127.21, 127.14, 127.11, 127.02, 126.70, 126.64, 126.59, 126.16, 124.21, 123.94, 123.74, 123.57, 122.96, 122.01, 121.95, 121.31, 120.07, 115.11, 109.84, 108.23, 91.53, 56.20, 53.48, 53.04, 49.05, 43.55, 43.43, 41.05, 40.98, 40.93, 36.14, 36.01, 35.39, 35.27, 35.18, 34.72, 33.67, 30.26, 25.63, 25.55, 25.26, 24.91, 21.07, 20.94, 20.92, 20.74, 20.64, 20.63, 20.55, 20.51, 20.40, 20.29, 20.18, 20.07.

HRMS (ESI) calculated for (C₁₀₃H₁₂₀ClN₁₀O₂₆)³⁺ ([M+3H]³⁺): m/z =649.2682, experimental = 649.2697, δ [ppm] = 1.5 ppm

(((5-((2,3-Diacetoxy-benzamido)methyl)-4-(4-(1-((E)-20-(3-chloro-2-((4-(N,3-dimethyl-3-(2,4,5-trimethyl-3,6-dioxocyclohexa-1,4-dien-1-yl)butanamido)benzyl)oxy)-4-((1r,3r,5r,7r)-4'-methoxyspiro[adamantane-2,3'-[1,2]dioxetan]-4'-yl)phenyl)-2,18-dioxo-7,10,13-trioxa-3,17-diazaicos-19-en-1-yl)-1H-1,2,3-triazol-5-yl)butanamido)-1,3-phenylene)bis(methylene))bis(azanediy))bis(carbonyl))bis(benzenene-3,1,2-triyl) tetraacetate **6**

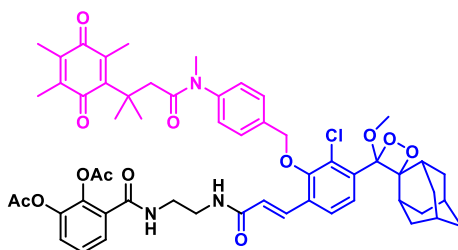


Enolether **6a** (8 mg, 0.004 mmol, 1.0 eq) and a catalytic amount of methylene blue (0.66 mg, 0.0021, 0.5 eq) were dissolved in DCM/DMF (9:1- 5 mL). Acetic acid (5 μ L) was added to prevent deacetylation. The solution was presaturated with oxygen gas (5 min). Then the reaction was irradiated with yellow light for 20 min under O₂ atmosphere. Upon completion, the DCM was removed by rotary evaporation at 30 °C and the product was purified by RP-HPLC (40 min gradient, 20-100% ACN/H₂O, 1% AcOH, 220 nm). The product containing fractions were identified by LCMS and lyophilized to dryness to yield conjugate **6** (4.29 mg, 0.002 mmol, 63%) as a slightly yellow solid.

¹H NMR (700 MHz, CD₃CN+1% AcOH-d₃): δ (ppm) = 7.64-7.62 (d, J=8.78 Hz, 1H), 7.53 (m, 2H), 7.52 (m, 2H), 7.50 (m, 2H), 7.45-7.43 (m, 2H), 7.42-7.40 (m, 2H), 7.38 (m, 2H), 7.34-7.33 (m, 4H), 7.31 (m, 4H), 7.29 (m, 4H), 5.08-4.97 (dd, J=14.84 Hz, 2H), 4.84 (s, 2H), 4.47 (t, J=5.44 Hz, 6H), 4.43 (bs, 6H), 3.69-3.67 (d, J=14.18Hz, 2H), 3.14-3.12 (m, 3H), 2.79 (t, J=8.08 Hz, 4H), 2.55 (t, J=8.08 Hz, 4H), 2.25 (m, 2H), 2.25 (bs, 9H), 2.24 (bs, 9H), 2.23 (m, 3H), 2.09 (m, 2H), 2.07 (m, 22H), 1.98 (s, 5H).

HRMS (ESI) calculated for (C₁₀₃H₁₂₀ClN₁₀O₂₈)³⁺ ([M+3H]³⁺): m/z = 659.9315, experimental = 659.9341, δ [ppm] = 2.6 ppm, calculated for (C₁₀₃H₁₁₉ClN₁₀O₂₈Na)³⁺ ([M+2H+Na]³⁺): m/z = 667.2588, experimental = 667.2596, δ [ppm] = 0.8 ppm, calculated for (C₁₀₃H₁₁₈ClN₁₀O₂₈Na₂)³⁺ ([M+H+2Na]³⁺): m/z = 674.5866, experimental = 674.5823, δ [ppm] = 4.3 ppm.

3-((2-((E)-3-(3-Chloro-2-((4-(N,3-dimethyl-3-(2,4,5-trimethyl-3,6-dioxocyclohexa-1,4-dien-1-yl)butanamido)benzyl)oxy)-4-((1r,3r,5r,7r)-4'-methoxyspiro[adamantane-2,3'-[1,2]dioxetan]-4'-yl)phenyl)acrylamido)ethyl) carbamoyl)-1,2-phenylene diacetate 7



Chemical Formula: C₅₆H₆₂ClN₃O₁₃

Exact Mass: 1019,3971

Molecular Weight: 1020,5700

Catechol **30** (12.56 mg, 0.053 mmol, 2.0 eq) was dissolved under Argon atmosphere in a mixture of DCM/DMF (9:1, 2 mL) and cooled to 0 °C. Then oxalylchloride (9.52 µL, 0.105 mmol, 4.0 eq) was added dropwise at 0 °C under vigorous stirring and the brown suspension was stirred 5 min at that temperature. The ice bath was removed and the reaction continued stirring 1h at 25 °C. The reaction progress was monitored by TLC (quench in MeOH, DCM w. 1% MeOH vs acid). Upon completion, the reaction was evaporated to dryness to yield crude acid chloride as an orange-brown solid, which was dried further under a high vacuum for 2 h at 24 °C. The *N*-Boc ethylendiamine (8.45 mg, 0.053 mmol, 2.0 eq) was dissolved in a mixture of anhydrous 1,4-dioxane (5 mL) and sat. NaHCO₃ (10 mL) and cooled to 0 °C. The acid chloride was dissolved in anhydrous 1,4-dioxane (15 mL) and added dropwise the amine in the basic buffer. The pH was monitored with pH paper closely. After the addition was complete, the two-phase solution continued stirring at 0 °C for 5 min and was equilibrated to ambient temperature afterwards for 1 h. Then DCM (100 mL) was added and the phases were separated, the organic phase was washed with sat. NaHCO₃ (2x50 mL) and 1M HCl (2x50 mL), then dried over Na₂SO₄. The solvent was removed in vacuo and the residue dissolved in anhydrous DCM (15 mL), AcOH (5 mL) and at 0 °C TFA (5 mL) was added. The reaction was stirred at ambient temperature for 1 h and was then concentrated by rotary evaporation and dried under a high vacuum to yield the crude amine **31** as a beige oil (9.95, 0,0355 mmol, 67%). Meanwhile, the dioxetane **1** was dissolved in anhydrous THF and NMM (2 mL / 10 µL) was added in the dark at 0 °C under Argon atmosphere. Then *iso*-butyl-chloroformate (3.42 µL, 0.026 mmol, 1.0 eq) was added and the reddish reaction solution turned turbid instantly. The reaction continued stirring at 25 °C for 30 min, then the amine was added at 0 °C dropwise to the reaction over 5 min. The reaction continued stirring at that temperature for 5 min, before it was equilibrated to ambient temperature and stirred for 50 min 25 °C. 30 µL of AcOH were added, the reaction was filtered and purified by RP-HPLC (40 min gradient, 20-99% ACN/H₂O, 1% AcOH, 220

nm). Product containing fractions were identified by LCMS and lyophilized to dryness, to yield monocatechol dioxetane **7** as a beige solid (11.7 mg, 0.011 mmol, 43%).

Compound 31

¹H NMR (500 MHz, DMSO-d₆+1% AcOH-d₃): δ (ppm) = 7.95 (m, 3H), 7.60-7.58 (m, 1H), 7.40-7.38 (m, 2H), 3.43 (t, J=5.77 Hz, 2H), 2.94 (m, 2H), 2.28 (s, 3H), 2.23 (s, 3H).

¹³C NMR (126 MHz, DMSO-d₆+1% AcOH-d₃): δ (ppm) = 172.06, 168.37, 167.90, 165.24, 165.15, 162.38, 142.94, 140.28, 130.19, 130.14, 127.18, 126.35, 126.22, 125.83, 124.97, 115.12, 38.33, 38.25, 36.90, 35.83, 30.81, 25.17, 20.67, 20.52, 20.42, 20.35, 20.32, 20.20, 20.05.

HRMS (ESI) calculated for (C₁₃H₁₆N₂O₅)³⁺ ([M+H]⁺): m/z = 281.1131, experimental = 281.1132, δ [ppm] = 0.1 ppm.

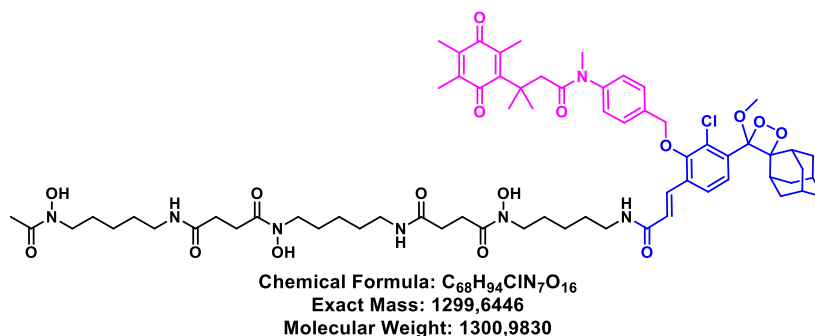
Compound 7

¹H NMR (700 MHz, CD₃CN+1% AcOH-d₃): δ (ppm) = 7.86-7.84 (m, 1H), 7.78-7.75 (m, 1H), 7.71-7.70, 7.67 (m, 1H), 7.58-7.53 (m, 1H), 7.39 (m, 1H), 7.32 (m, 1H), 7.25 (m, 2H), 6.67-6.57 (dd, J=16.42 Hz, 57.47 Hz, 2H), 5.35 (t, J=5.37 Hz, 1H), 4.98 (bs, 2H), 3.91-3.89 (q, J=2.91 Hz, 3.28 Hz, 4H), 3.49 (m, 4H), 3.18 (m, 2H), 3.09 (m, 2H), 2.92 (m, 1H), 2.69 (m, 2H), 2.25 (s, 3H), 2.23 (s, 3H), 2.15 (t, J=4.98 Hz, 2H), 2.05 (bs, 4H), 2.04 (m, 2H), 2.02 (m, 2H), 1.75 (m, 1H), 1.69 (m, 2H), 1.63 (m, 2H), 1.55 (m, 2H), 1.27 (bs, 6H).

HRMS (ESI) calculated for (C₅₆H₆₃ClN₃O₁₃)⁺ ([M+H]⁺): m/z = 1020.4043, experimental = 1020.4039, δ [ppm] = 0.4 ppm.

Desferrioxamine dioxetane conjugates

N1-(5-((E)-3-(3-Chloro-4-(4-(N,3-dimethyl-3-(2,4,5-trimethyl-3,6-dioxocyclohexa-1,4-dien-1-yl)butanamido)benzyl)oxy)-4-((1r,3r,5r,7r)-4'-methoxyspiro[adamantane-2,3'-[1,2]dioxetan]-4'-yl)phenyl)acrylamido)pentyl)-N1-hydroxy-N4-(5-(N-hydroxy-4-((5-(N-hydroxyacetamido)pentyl)amino)-4-oxobutanamido)pentyl)succinamide 8



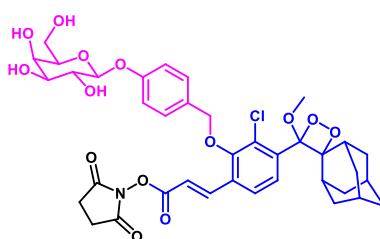
Compound **13** (50 mg, 0.069 mmol, 1.0 eq) was dissolved in DCM (5 mL), followed by the addition of NHS (89 mg, 0.77 mmol, 1.5 eq) and DCC (159 mg, 0.77 mmol, 1.5 eq) and stirred for 1.5 h at room temperature. Upon completion, the reaction mixture was filtered and the solvent was removed. The crude compound were dissolved in DMF (1 ml) and the desferrioxamine mesylate salt (48 mg, 0.072 mmol, 1.05 eq) followed by a drop of TEA was added. The reaction was monitored by RP-HPLC (30-100% ACN/H₂O, 20 min). Upon completion, the reaction mixture was concentrated by evaporation under reduced pressure. The crude compound was dissolved in DCM:DMF (4:1, 10 mL) and a catalytic amount (~2 mg) of methylene blue were added. Oxygen gas was bubbled through the solution while irradiating with yellow light for 10 minutes. The reaction progress was monitored by RP-HPLC. Upon completion, the solvent was removed and the crude mixture was then purified by preparative RP-HPLC (30-100% ACN/H₂O, 0.1 % TFA, 20 min) to afford compound **8** as a yellow solid (47 mg, 52%).

¹H NMR (400 MHz, MeOD) δ 7.88 (d, *J* = 8.4 Hz, 1H), 7.83 (d, *J* = 15.9 Hz, 1H), 7.74 (d, *J* = 8.4 Hz, 1H), 7.63 (d, *J* = 7.6 Hz, 2H), 7.28 (d, *J* = 7.6 Hz, 2H), 6.73 (d, *J* = 15.8 Hz, 1H), 5.02 (s, 2H), 3.59 (dt, *J* = 14.0, 7.1 Hz, 6H), 3.34 – 3.27 (m, 3H), 3.22 – 3.09 (m, 10H), 2.95 (s, 1H), 2.75 (t, *J* = 6.7 Hz, 6H), 2.44 (t, *J* = 7.0 Hz, 4H), 2.36 (d, *J* = 12.0 Hz, 1H), 2.08 (s, 3H), 2.07 (s, 3H), 1.96 (d, *J* = 11.1 Hz, 8H), 1.77 – 1.56 (m, 14H), 1.50 (dd, *J* = 13.2, 6.1 Hz, 6H), 1.40 – 1.23 (m, 12H).

^{13}C NMR (101 MHz, MeOD) δ 190.89, 187.47, 173.53, 173.09, 172.60, 172.14, 166.41, 154.82, 153.93, 143.85, 143.36, 137.58, 136.28, 134.43, 133.43, 132.24, 131.22, 130.17, 128.72, 127.32, 124.85, 124.33, 111.52, 95.92, 75.11, 39.18, 38.92, 37.94, 36.23, 33.66, 32.27, 31.82, 31.52, 31.29, 30.13, 28.56, 27.66, 27.54, 26.25, 25.92, 23.59, 23.50, 18.91, 13.07, 11.51, 10.71.

MS (ES+): m/z calc. for $\text{C}_{68}\text{H}_{94}\text{ClN}_7\text{O}_{16}$: 1299.6; found: 1301.3 $[\text{M}+\text{H}]^+$.

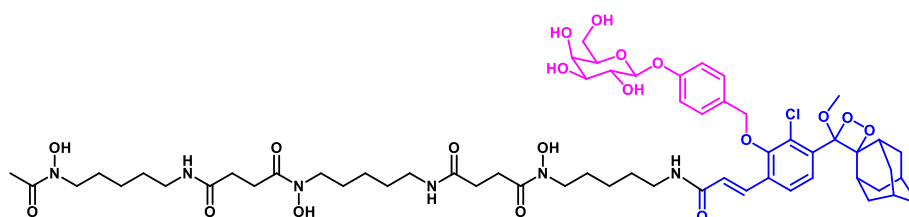
Compound 32



Chemical Formula: $\text{C}_{38}\text{H}_{42}\text{ClNO}_{14}$
Exact Mass: 771,2294
Molecular Weight: 772,1970

Compound **32** was synthesized as previously described by Eilon-Schaffer et al.³

N1-(5-((E)-3-(3-Chloro-4-((1r,3r,5S,7S)-4'-methoxyspiro[adamantane-2,3'-[1,2]dioxetan]-4'-yl)-2-((4-(((2S,3R,4S,5R,6R)-3,4,5-trihydroxy-6-(hydroxymethyl) tetrahydro-2H-pyran-2-yl)oxy)benzyl)oxy)phenyl)acrylamido)pentyl)-N1-hydroxy-N4-(5-(N-hydroxy-4-((5-(N-hydroxyacetamido)pentyl)amino)-4-oxobutanamido)pentyl)succinamide 9

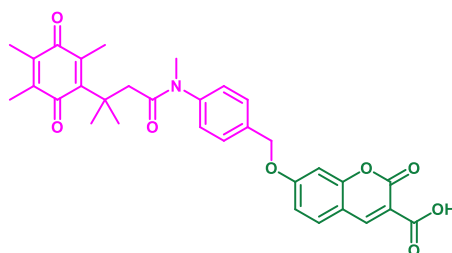


Chemical Formula: $\text{C}_{59}\text{H}_{85}\text{ClN}_6\text{O}_{19}$
Exact Mass: 1216,5558
Molecular Weight: 1217,8020

Compound **32**³ (30 mg, 0.039 mmol, 1.0 eq) and desferrioxamine mesylate salt (27 mg, 0.041 mmol, 1.05 eq) were dissolved in DCM (10 ml) and a drop of TEA was added. The reaction was monitored by RP-HPLC (30-100% ACN/ H_2O , 20 min). Upon completion, the reaction mixture was concentrated by evaporation under reduced pressure and purified using RP-HPLC (30-100% ACN/ H_2O , 20 min) to afford compound **9** (19 mg, 40%) as a yellow solid.

MS (ESI): calculated for $C_{59}H_{86}ClN_6O_{19}^+$ $[M/2+H]^+$: $m/z = 1216.6$, experiment = 609.9.

7-((4-(N,3-Dimethyl-3-(2,4,5-trimethyl-3,6-dioxocyclohexa-1,4-dien-1yl)butanamido)benzyl) oxy) -2-oxo-2H-chromene-3-carboxylic acid 34



Chemical Formula: $C_{32}H_{31}NO_8$
 Exact Mass: 557,2050
 Molecular Weight: 557,5990

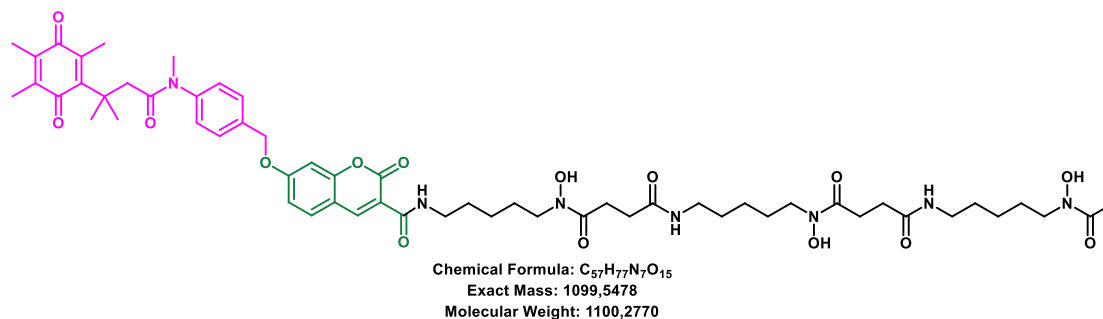
Compound **33** (100 mg, 0.43 mmol, 1.0 eq) and K_2CO_3 (118 mg, 0.86 mmol, 2.0 eq) were dissolved in DMF (2 mL) and stirred for 10 min before compound **12**³ (203 mg, 0.47 mmol, 1.1 eq) was added to the mixture. The reaction mixture was then stirred for 3 h at 50 °C with the reaction progress being monitored by TLC analysis (Hex/EtOAc: 2:1). Upon completion, the solvent was removed and the crude mixture was used for the next step. A mixture of THF:H₂O (2:1, 3 mL) and LiOH (21 mg, 0.86 mmol, 2.0 eq) were then added. The resulting mixture was stirred at 50 °C for an additional 2 h. Full hydrolysis was inferred on the basis of TLC analysis (Hex:EtOAc, 4:6). Upon completion, the reaction mixture was concentrated by evaporation under reduced pressure and purified using RP-HPLC (30-100% ACN/H₂O, 20 min) to afford compound **34** (19 mg, 51%) as a yellow solid.

¹H NMR (400 MHz, CDCl₃) δ 8.87 (s, 1H), 7.69 (d, $J = 8.7$ Hz, 1H), 7.53 (d, $J = 7.5$ Hz, 2H), 7.27 (d, $J = 8.5$ Hz, 2H), 7.12 (d, $J = 8.6$ Hz, 1H), 7.02 (s, 1H), 5.24 (s, 2H), 3.17 (s, 3H), 2.76 (s, 2H), 2.09 (s, 3H), 1.98 (s, 3H), 1.95 (s, 3H), 1.30 (s, 6H).

¹³C NMR (101 MHz, CDCl₃) δ 191.42, 187.79, 172.63, 165.14, 164.54, 163.40, 157.08, 154.33, 151.41, 144.18, 143.41, 138.28, 136.90, 134.92, 132.07, 129.19, 128.02, 115.73, 112.80, 111.30, 101.88, 70.47, 47.90, 38.30, 37.47, 28.71, 14.25, 12.78, 12.19.

MS (ES⁺): m/z calc. for $C_{32}H_{31}NO_8$: 557.2; found: 558.4 $[M+H]^+$.

N1-(5-(7-((4-(N,3-Dimethyl-3-(2,4,5-trimethyl-3,6-dioxocyclohexa-1,4-dien-1-yl)butanamido)benzyl)oxy)-2-oxo-2H-chromene-3-carboxamido)pentyl)-N1-hydroxy-N4-(5-(N-hydroxy-4-((5-(N-hydroxyacetamido)pentyl)amino)-4-oxobutanamido)pentyl)succinamide 10



To a stirred solution of compound **34** (20 mg, 0.036 mmol, 1.0 eq) in DMF (1 mL) was added 2,4,6-collidine (14 μ L, 0.11 mmol, 3.0 eq) and HBTU (20 mg, 0.053 mmol, 1.5 eq). The reaction was stirred for 10 min before addition of desferrioxamine mesylate salt (27 mg, 0.039 mmol, 1.1 eq) with 2,4,6-collidine (10 μ L, 0.071 mmol, 2.0 eq) in DMSO (0.5 mL). The reaction mixture was stirred for 3 h at 60 °C with the reaction progress being monitored by RP-HPLC (30-100% ACN in water, 20 min). Upon completion, the reaction mixture was concentrated by evaporation under reduced pressure and purified using RP-HPLC (30-100% ACN/H₂O, 20 min) to afford compound **10** (25 mg, 63%) as an off-white solid.

¹H NMR (700 MHz, DMSO): δ = 9.61 (t, J = 16.3 Hz, 3H), 8.83 (s, 1H), 8.63 (t, J = 4.84 Hz, 1H), 7.94-7.93 (d, J = 8.91 Hz, 2H), 7.77-7.76 (q, J = 4.84, 10.06 Hz, 2H), 7.59 (m, 2H), 7.34 (m, 2H), 7.24 (s, 1H), 7.15-7.14 (d, J = 7.45 Hz, 1H), 5.30 (s, 2H), 3.48-3.44 (m, 8H), 3.31-3.29 (q, J = 6.68, 12.98 Hz, 2H), 3.06 (bs, 2H), 3.01-2.98 (m, 4H), 2.66 (bs, 1H), 2.57 (m, 4H), 2.26 (t, J = 4.24 Hz, 4H), 2.02 (s, 3H), 1.96 (s, 3H), 1.92-1.90 (m, 6H), 1.58-1.45 (m, 10H), 1.40-1.35 (m, 5H), 1.30-1.25 (m, 2H), 1.23 (m, 10H).

¹³C NMR (176 MHz, DMSO): δ = 190.33, 186.84, 171.95, 171.27, 170.10, 163.24, 161.28, 160.85, 158.06, 157.86, 156.00, 154.82, 147.58, 143.51, 143.28, 136.75, 135.24, 131.58, 129.44, 127.56, 115.20, 114.07, 112.38, 101.14, 69.65, 50.15, 47.04, 46.90, 46.75, 40.00, 38.93, 38.39, 37.71, 36.63, 29.87, 28.79, 28.71, 28.58, 28.09, 27.55, 26.00, 23.53, 23.47, 23.10, 22.71, 21.03, 20.32, 13.70, 12.57, 11.72.

MS (ES⁺): m/z calc. for C₅₇H₇₇N₇O₁₅: 1099.6; found: 1098.9 [M-H]⁺.

Biological Assays

All steps were conducted under a laminar flow bench with autoclaved buffers and reagents or filter-sterilized solutions. Compounds were dissolved in sterile, cell culture-grade DMSO.

Chemical probe activation

The probe was diluted 1:1000 from 10 mM stocks in DMSO to 10 μ M in 1xPBS pH 7.4, pre-incubated for 45 min in the dark and 99 μ L were distributed per well in a 96-well white luminescence plate without coating. NaBH₄ was dissolved 100 mM in PBS pH 7.4 and 1 μ L was added to the respective wells with a multichannel pipette. The plate was sealed with a transparent foil and the luminescence signal [relative luminescence units - RLU] was recorded in a plate reader for 150 min. The data evaluation and plots were done with Microsoft Excel 2016 and GraphPad Prism 9 respectively. Negative controls (background) were probe in PBS pH 7.4 stock, as well as pure PBS pH 7.4.

For the fluorescent probe a similar protocol was carried out and the fluorescence was recorded in a 96-well black fluorescence plate without coating. The plate was sealed and the fluorescence signal [relative fluorescence units - RFU] was recorded in a plate reader (monochromator, excitation 400 nm, emission 540 nm, bandwidth 20 nm).

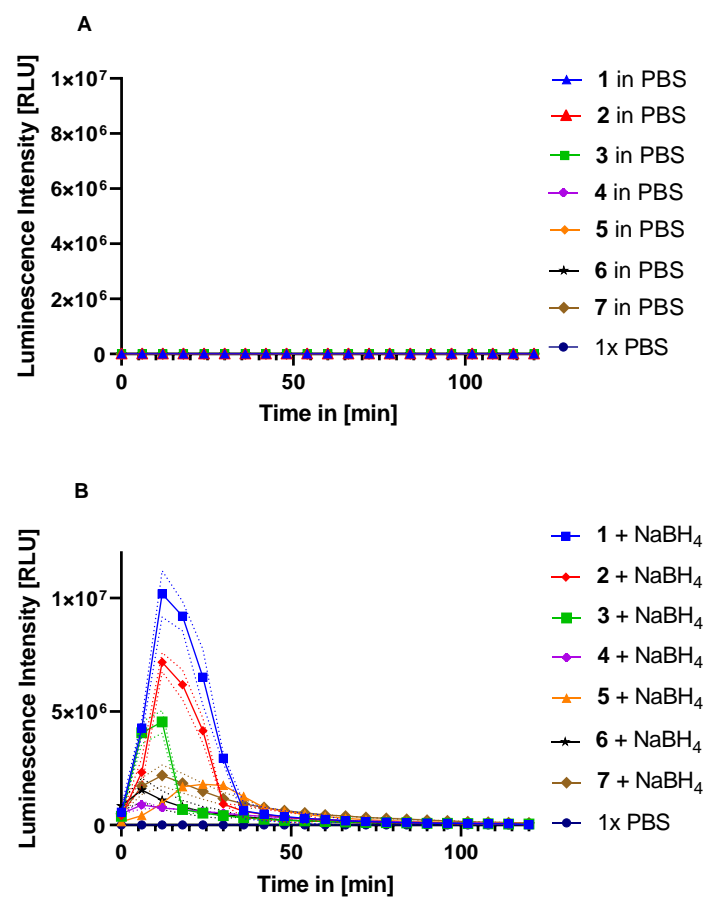


Figure S5.9. Kinetic curves of the *in vitro* activation of quinone oxidoreductase-triggered dioxetanes. Luminescence of the control probe **2** and siderophore-conjugates **3-7** \pm 1 mM NaBH_4 is plotted. Panel (A) shows the probe without activator in 1xPBS (pH 7.4), and panel (B) shows the curves upon addition of the activator. $n = 3$, dotted lines correspond to \pm standard error of mean (SEM).

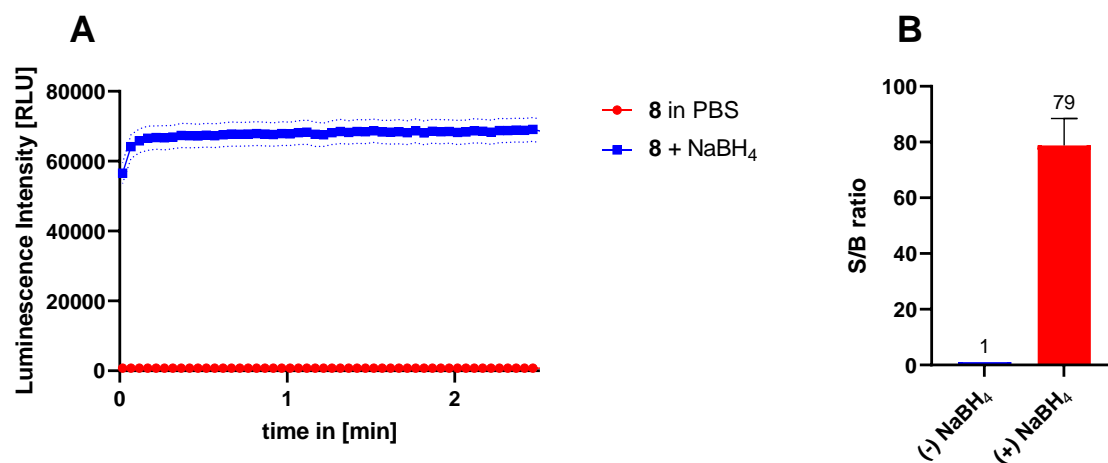


Figure S5.10. Increase of fluorescence following the chemical activation of **8**. (A) Fluorescence kinetic of **8** (Ex 400 nm, Em 540 nm) in 1xPBS (pH 7.4) \pm NaBH₄ (1 mM) for 150 min. (B) S/B ratios of **8** \pm NaBH₄ (1 mM). All experiments $n = 3$, dotted lines or error bars correspond to \pm standard error of mean (SEM).

β -Galactosidase probe activation

The probe was diluted 1:1000 from 10 mM stocks in DMSO to 10 μ M in PBS pH 7.4, pre-incubated for 45 min in the dark and then distributed 99 μ L per well (technical triplicates) in a 96-well non-transparent, white luminescence plate without coating. β -galactosidase was dissolved in PBS pH 7.4 and 1.5 EU/mL were added to the respective wells with a multichannel pipette. The plate was sealed with a transparent foil and the luminescence was recorded immediately in a plate reader for 120 min. The data evaluation and plots with statistical comparisons were done with Microsoft Excel 2016 and GraphPad Prism 9 respectively. Negative controls (background) were probe in PBS pH 7.4 stock, as well as pure PBS pH 7.4.

Diaphorase probe activation

The protocol was conducted according to existing protocols.^{8, 9} All stock dilutions were performed with sterile-filtered 50 mM K_3PO_4 buffer (pH 7.0, reduction of quinone autoxidation), from reagent or compound stocks in water or cell culture grade DMSO under a laminar flow bench. Dioxetane probe **8** was pre-incubated 60 min prior to enzyme kinetic or chemiluminescence measurement at 25 °C and 330 rpm in the dark. The dioxetane probe was diluted with an excess β -NADH (30 mM stock in sterile milliQ water, from Sigma, final 250 μ M) in phosphate buffer to yield four substrate concentrations (0.1, 0.05, 0.03, 0.025 mM for luminescence and seven substrate concentrations (0.1, 0.08, 0.05, 0.03, 0.025, 0.01, 0.001 mM) for enzyme kinetic measurement. The reaction was started by the addition of the diaphorase from *Clostridium kluyveri* (2.5 mg/mL stock in phosphate buffer pH 7.0, from Sigma, D5540-100UN, 5 μ g/mL final) and the initial oxidation rate of β -NADH was determined by measuring the absorbance at 340 nm. The apparent K_m , V_{max} and k_{cat} values were calculated over a range of seven substrate concentrations by plotting the velocities over the substrate concentration to the Michaelis-Menten equation. All kinetic measurements were performed at least three times with 16 technical replicates. As a positive control, the same protocol was conducted with methyl benzoquinone (MBQ), which was reported to be reduced by quinone oxidoreductases.⁸ For the luminescence measurement the plate was sealed with a transparent film and the measurement was conducted in a white 384 well plates in a plate reader (measure every 3 min total time 5 h, medium shaking, no filter). The data was evaluated using Microsoft Excel 2016 and GraphPad Prism 9.

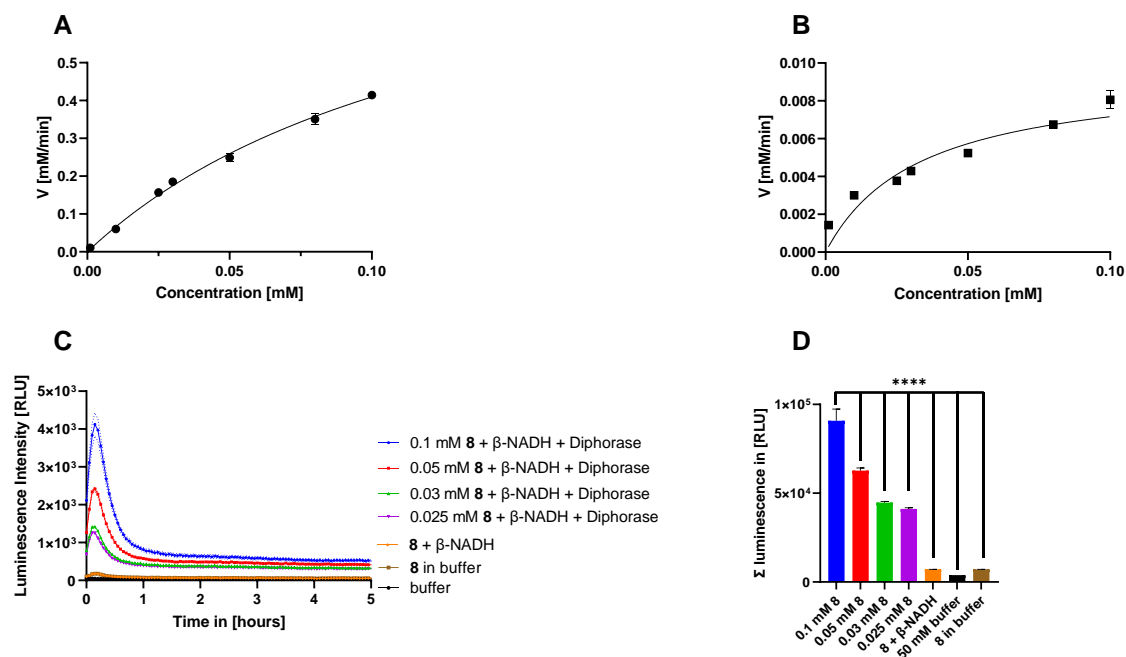


Figure S5.11. Kinetic characterization of diaphorase-catalysed reduction of **8** and MBQ. **(A)** Initial velocities were obtained for varied concentrations of methyl benzoquinone (MBQ) in the presence of diaphorase (5 μ g/mL) and β -NADH (250 μ M) in phosphate buffer (pH 7.0). **(B)** Initial velocities were obtained for varied concentrations of probe **8** in the presence of diaphorase (5 μ g/mL) and β -NADH (250 μ M) in phosphate buffer (pH 7.0). Data points are the average of three experiments. Best fit lines showed an $R^2 > 0.9-0.7$ and their slopes were significantly different from zero ($p < 0.005$), error bars correspond to \pm standard error of mean (SEM). **(C)** Chemiluminescence curves and **(D)** Summed chemiluminescence values for different concentrations of **8** \pm diaphorase (5 μ g/mL) and β -NADH (250 μ M) in phosphate buffer (pH 7.0). Dotted lines or error bars correspond to \pm standard error of mean (SEM). For the summed experiments, each group was compared to the no-enzyme control *via* one-way ANOVA (**** $p < 0.0001$).

Table S5.1. Determination of enzymatic parameters for the reduction of **8** or MBQ^a with diaphorase.

Compound	Diaphorase [μ g/mL]	V_{\max} [μ M/min]	K_m [μ M]	k_{cat} [s^{-1}]
MBQ	5	97.03	137	9594
8	5	9.5	32.7	93.84

a) MBQ = methyl benzoquinone, $n = 3$. All measurements at 25 $^{\circ}\text{C}$ and pH 7.0.

Recombinant production and characterization of QOR2

Cloning of ytfG (qor2) into pET28c

The *ytfG* gene (uniprot code P39315, QOR2_ECOLI) was purchased from GenScript in a pUC57 vector (pUC57-*ytfG*) and amplified (midiprep, ampR). The sequences of the full vector and the *ytfG* gene can be found below. The *ytfG* gene was amplified by PCR, gel-purified, extracted and cloned into a pET28c vector, containing a kanamycin (kan) resistance gene and an *N*-terminal HisTag sequence. In detail, the pET28c vector and the PCR-amplified *ytfG* gene were digested with restriction enzymes (NcoI, NotI) and subsequently purified. The fragments were ligated O/N at 16°C using Roche ligase and transformed into *E. coli*. Single colonies were screened on LB-kan plates. A single colony was isolated, sequenced and the clone pET28c-*N*-His-Tev-*ytfG* (sequence below) was amplified by midiprep.

QOR2 expression and isolation

The pET28c-*N*-His-Tev-*ytfG* clone was transformed in Rosetta2™ (DE3) competent *E. coli* cells (Novagen®, BL21 derivatives, genomic chloramphenicol – cm resistance). The bacteria were cultured in terrific broth (TB) medium (+kan, +cm). The overnight culture was diluted with TB medium (1:100, +kan, +cm) and the culture was grown until an OD_{600nm} ~ 1.0. Then the *ytfG* (synonym QORB, QOR2) expression was initiated with IPTG (isopropyl-β-D-thiogalactopyranoside, 250 μM final) at 37 °C and 140 rpm. The culture continued shaking for 4 hours and was harvested by centrifugation (16.000 g, 20 min, 4 °C). The pellet was resuspended in lysis buffer (2mM MgCl₂, cOmplete™ mini EDTA-free protease inhibitor cocktail Roche®, 1 mg/mL DNase in 50 mM Tris-HCl pH 7.4, 300 mM NaCl buffer), filtered through a tissue membrane and lysed in two cycles with a flow through homogenizer (Avestin, Emulsiflex C3 Homogenizer) cooled by ice. The lysate was separated from cell debris by centrifugation (2 x 16.000 g, 20 min, 4 °C). Each time the supernatant was transferred to a new tube. The protein of interest was purified by Ni²⁺ affinity chromatography (HisTrap™ High Performance, GE Healthcare; Buffer A: 20 mM Tris pH 7.4, 300 mM NaCl; Buffer B: 20 mM Tris pH 7.4, 300 mM NaCl, 500 mM imidazole, filter-sterilized). The column was washed with increasing concentrations of imidazole (20 mM and 40 mM Imidazole). The bound QOR2 was eventually eluted with 250 mM imidazole. Further purification and buffer exchange was performed by size exclusion chromatography (SEC – sephadex 75, 10/300GL, 20 mM KH₂PO₄/K₂HPO₄ pH 7.5, 150 mM NaCl buffer) and ion exchange chromatography (DEAE sepharose, Buffer A: 50 mM KH₂PO₄/K₂HPO₄, 0.1 mM EDTA pH 7.5, Buffer B: buffer A + 1 M NaCl). Fractions from each purification were concentrated with Vivaspin (Sartorius) 10K MCOW centrifugal concentrators between subsequent purification steps. The purification process was monitored by SDS-PAGE (Mini-PROTEAN TGX™, anykD gradient gel, Biorad®) and Western Blot analysis (monoclonal IgG anti-His, Novagen®, 70796-3, Batch 3683778,

then IgG H&L AP Conjugates Promega® S372B as secondary antibody and finally stained using NBT/BCIP substrate (Promega) as recommend by the supplier).

Protein sequence confirmation by tryptic digest and timsTOF mass spectrometry

Proteins were separated by SDS-PAGE and identified in a peptide mass fingerprinting approach. For that, protein bands were cut from the SDS-PAGE gel, gel slices were washed three times with Milli-Q water and dehydrated with 100% acetonitrile. The gel is shown in Figure S5.12C (DEAE column). Proteins were reduced with 5 mM TCEP / 0.05 M TEAB for 60 min at 56°C and subsequently alkylated with 1.5 mM MMTS / 0.05 M TEAB for 30 min at room temperature, followed by dehydration with 100% acetonitrile and drying by using a Speedvac. Proteins were digested into peptides using 80 ng trypsin (Progema) in 40 µl Milli-Q at 37°C overnight. Peptide extraction was performed by subsequent steps using 100% acetonitrile, 5% formic acid and 100% acetonitrile. Combined peptide fractions were dried using a Speedvac and resolved in 0.1% formic acid. Samples were loaded onto EvoTips using manufacturer's guidelines and measured using a Evosep I HPLC (Evosep) connected to a timsTOFPro mass spectrometer with PASEF (Bruker Daltonics, Bremen, Germany). The standard Evosep "15 sample per day" method and Bruker "PASEF method for short gradients" methods were used for peptide analyses. Raw MS/MS data files were processed by using the PEAKS studio Xpro software and searched against the QORB sequence or the *Escherichia coli* (strain K12) UniProt database. The following search parameters were used: Enzyme, Trypsin; Max Missed Cleavages, 1; Fixed Modifications, Beta-methylthiolation (C); Variable Modifications, Oxidation (M); Parent Mass Error Tolerance, 20 ppm; Fragment Mass Error Tolerance, 0.03 Da. The sequence coverage of the respective bands is shown in Figure S5.12D and in the appendix. The *N*-terminal HisTag could only be detected after initial NiNTA purification. The HisTag was found to be cleaved over the time of the purification procedures and after the DEAE column, the QOR2 protein without tag and a *N*-terminally shortened QOR2 version were detected. The DEAE fraction with the greatest purity, in lane 2 in Figure S5.12C, was thus employed for enzyme and chemiluminescence kinetics.

ESI-TOF whole protein mass spectrometry

Before LC/MS measurement buffer exchange (phosphate removal) of the DEAE fractions was performed by repeated washing through 10K centrifugal columns with a tris NaCl buffer (5 mM Tris, 30 mM NaCl). The whole protein mass was determined by LC/MS with a 1290 Agilent UPLC-system (binary high gradient pump, DAD-detector, Xbridge column: BEH300 C4 3.5 μ m 4, 6x50 mm (Waters, Eschborn, Germany) column temperature: 40 °C, solvent A: water 0.1% HCOOH, solvent B: ACN 0.1% HCOOH, flow rate 900 μ l/min), with a 30 minute gradient (0 to 1 min 1% B, 23 min 100% B, then column wash with 100% B and returning to the starting conditions with 1%B, total: 30 min), coupled to a TOF mass spectrometer (maxis HD UHR, Bruker Daltonics, Bremen, Germany). The mass spectrometric acquisition parameters were set as follows: ESI with a scan range: 500 – 4000 m/z, positive ion polarity, capillary voltage: 4500 V, nebulizer pressure: 4.0 bar dry heater: 200°C dry gas: 9.0 l/min, transfer time: 115 μ s, prepulse storage: 30 μ s.

The DEAE fraction displayed in the SDS-PAGE lane II in Figure 5.12C was characterized. The highest peaks have, when deconvoluted, a neutral mass of 30756 Da, which corresponds to amino acids 11Ser-306Asn of recombinant *E. coli* His-QOR2. Side peaks have masses of 30581 Da, 30667 Da, 30895 Da, 31031 Da, corresponding to the sequences 13Gly-306Asn, 12Ser-306Asn, 10His-306Asn, and 9His-306 Asn, respectively. The data demonstrate that lane II contained the recombinant full-length protein with a partially degraded His-tag.

Gene and protein sequences

pUC57-*ytfG* vector from GenScript

```
TCGCGCGTTTCGGTGATGACGGTGAAAACCTCTGACACATGCAGCTCCCGGAGACGGT
CACAGCTTGTCTGTAAGCGGATGCCGGGAGCAGACAAGCCCGTCAGGGCGCGTCAGC
GGGTGTTGGCGGGTGTCCGGGCTGGCTTA ACTATGCGGCATCAGAGCAGATTGTACTG
AGAGTGCACCATATGCGGTGTGAAATACCGCACAGATGCGTAAGGAGAAAATACCGCAT
CAGGCGCCATTCGCCATTCAGGCTGCGCAACTGTTGGGAAGGGCGATCGGTGCGGGC
CTCTTCGCTATTACGCCAGCTGGCGAAAGGGGGATGTGCTGCAAGGCGATTAAGTTGG
GTAACGCCAGGGTTTTCCAGTCACGACGTTGTAAAACGACGGCCAGTGAATTCGAGCT
CGGTACCTCGCGAATGCATCTAGATCCATGGGCCACCATCATCACCATCACCATCACAG
CAGCGGCGAGAATCTTTATTTTCAGGGCGCTATCGCTATTACTGGTGCCACTGGCCAAC
TTGGTCACTATGTTATTGAATCCTTGATGAAAACGGTTCCTGCCAGCCAAATAGTGGCTA
TCGTTTCGTAATCCGGCAAAGCCCAAGCCCTGGCAGCACAAGGCATTACCGTGCGTCA
GGCTGACTACGGCGATGAAGCCGCACTGACATCTGCACTTCAGGGAGTGAAAAACTA
CTGCTGATCTCTTCCAGCGAAGTGGGTCAACGTGCCCCGCAGCATCGTAATGTTATTAA
```

TGCCGCAAAGGCGGCTGGCGTGAAATTTATCGCTTATACCAGCCTGCTACATGCAGATA
CCTCCCCGCTCGGCCTCGCCGATGAGCACATCGAGACGGAGAAAATGCTGGCTGATTC
TGGCATCGTTTACACCCTGCTGCGCAACGGCTGGTACAGCGAAAACCTCGCCAGC
GCCCCGGCAGCACTGGAACACGGCGTATTTATCGGTGCGGCGGGCGATGGCAAATC
GCCTCAGCAACGCGGGCAGATTATGCGGCAGCTGCGGCACGCGTGATTAGCGAAGCC
GGTCACGAAGGCAAGGTTTACGAACTGGCGGGCGATAGTGCCTGGACGTTGACACAGT
TAGCGGCAGAGCTGACCAAACAGAGCGGCAAACAGGTTACCTATCAAATCTGAGCGA
AGCCGATTTCCGCCGCGGCACTGAAAAGCGTCCGACTGCCCGACGGACTGGCGGATAT
GCTGGCGGATTCTGACGTTGGCGCATCGAAAGGCGGTCTGTTTGATGACAGCAAAACA
CTTAGCAAATTGATTGGCCACCCAACGACAACGTTAGCCGAAAGCGTAAGCCATCTTTT
TAATGTTAATAACTAAAAGCTTGCGGCCGCATCGGATCCCGGGCCCGTCCGACTGCAGA
GGCCTGCATGCAAGCTTGGCGTAATCATGGTCATAGCTGTTTCCTGTGTGAAATTGTTAT
CCGCTCACAATTCCACACAACATACGAGCCGGAAGCATAAAGTGTAAGCCTGGGGTG
CCTAATGAGTGAGCTAACTCACATTAATTGCGTTGCGCTCACTGCCCGCTTTCCAGTCG
GGAAACCTGTGCTGCCAGCTGCATTAATGAATCGGCCAACGCGCGGGGAGAGGCGGTT
TGCGTATTGGGCGCTCTTCCGCTTCCCTCGCTCACTGACTCGCTGCGCTCGGTCTGTTCCG
GCTGCGGCGAGCGGTATCAGCTCACTCAAAGGCGGTAATACGGTTATCCACAGAATCA
GGGATAACGCAGGAAAGAACATGTGAGCAAAAGGCCAGCAAAAGGCCAGGAACCGTA
AAAAGGCCGCGTTGCTGGCGTTTTTCCATAGGCTCCGCCCCCTGACGAGCATCACAA
AATCGACGCTCAAGTCAGAGGTGGCGAAACCCGACAGGACTATAAAGATACCAGGCG
TTTCCCCTGGAAGCTCCCTCGTGCGCTCTCCTGTTCCGACCCTGCCGCTTACCGGATA
CCTGTCCGCCTTTCTCCCTTCGGGAAGCGTGGCGCTTTCTCATAGCTCACGCTGTAGGT
ATCTCAGTTCGGTGTAGGTCGTTTCGCTCCAAGCTGGGCTGTGTGCACGAACCCCCCGT
TCAGCCCGACCGCTGCGCCTTATCCGGTAACTATCGTCTTGAGTCCAACCCGGTAAGAC
ACGACTTATCGCCACTGGCAGCAGCCACTGGTAACAGGATTAGCAGAGCGAGGTATGT
AGGCGGTGCTACAGAGTTCTTGAAGTGGTGGCCTAACTACGGCTACACTAGAAGAACA
GTATTTGGTATCTGCGCTCTGCTGAAGCCAGTTACCTTCGGAAAAAGAGTTGGTAGCTC
TTGATCCGGCAAACAAACCACCGCTGGTAGCGGTGGTTTTTTTTGTTTGCAAGCAGCAGA
TTACGCGCAGAAAAAAGGATCTCAAGAAGATCCTTTGATCTTTTCTACGGGGTCTGAC
GCTCAGTGGAACGAAAACCTCACGTTAAGGGATTTTGGTCATGAGATTATCAAAAAGGAT
CTTCACCTAGATCCTTTTAAATTAATAAATGAAGTTTTAAATCAATCTAAAGTATATATGAGT
AACTTGGTCTGACAGTTACCAATGCTTAATCAGTGAGGCACCTATCTCAGCGATCTGTC
TATTTGTTTCATCCATAGTTGCCTGACTCCCCGTCGTGTAGATAACTACGATACGGGAG
GGCTTACCATCTGGCCCCAGTGCTGCAATGATACCGCGAGACCCACGCTCACCGGCTC
CAGATTTATCAGCAATAAACCAGCCAGCCGGAAGGGCCGAGCGCAGAAGTGGTCCTGC
AACTTTATCCGCCTCCATCCAGTCTATTAATTGTTGCCGGGAAGCTAGAGTAAGTAGTTC
GCCAGTTAATAGTTTTCGCAACGTTGTTGCCATTGCTACAGGCATCGTGGTGTACGCT

CGTCGTTTGGTATGGCTTCATTCAGCTCCGGTCCCAACGATCAAGGCGAGTTACATGA
TCCCCATGTTGTGCAAAAAGCGGTTAGCTCCTTCGGTCCTCCGATCGTTGTCAGAAG
TAAGTTGGCCGCAGTGTTATCACTCATGGTTATGGCAGCACTGCATAATTCTTACTGT
CATGCCATCCGTAAGATGCTTTTCTGTGACTGGTGAGTACTCAACCAAGTCATTCTGAGA
ATAGTGTATGCGGCGACCGAGTTGCTCTTGCCCGGCGTCAATACGGGATAATACCGCG
CCACATAGCAGAACTTTAAAAGTGCTCATCATTGGAAAACGTTCTTCGGGGCGAAAAC
CTCAAGGATCTTACCGCTGTTGAGATCCAGTTCGATGTAACCCACTCGTGCACCCAACT
GATCTTCAGCATCTTTTACTTTACCAGCGTTTCTGGGTGAGCAAAAACAGGAAGGCAA
AATGCCGCAAAAAGGGAATAAGGGCGACACGGAAATGTTGAATACTCATACTCTTCCT
TTTTCAATATTATTGAAGCATTATCAGGGTTATTGTCTCATGAGCGGATACATATTTGAA
TGTATTTAGAAAAATAACAAATAGGGGTTCCGCGCACATTTCCCGAAAAGTGCCACCT
GACGTCTAAGAAACCATTATTATCATGACATTAACCTATAAAAATAGGCGTATCACGAGG
CCCTTTCGTC

ytfG gene insert sequence

CCATGGGCCACCATCATCACCATCACCATCACAGCAGCGGCGAGAATCTTTATTTTCAG
GGCGCTATCGCTATTACTGGTGCCACTGGCCAACTTGGTCACTATGTTATTGAATCCTT
GATGAAAACGGTTCCTGCCAGCCAAATAGTGGCTATCGTTTCGTAATCCGGCAAAAGCCC
AAGCCCTGGCAGCACAAGGCATTACCGTGCGTCAGGCTGACTACGGCGATGAAGCCGC
ACTGACATCTGCACTTCAGGGAGTGGAAAACTACTGCTGATCTCTTCCAGCGAAGTGG
GTCAACGTGCCCGCAGCATCGTAATGTTATTAATGCCGCAAAGGCGGCTGGCGTGAA
ATTTATCGCTTATACCAGCCTGCTACATGCAGATACCTCCCCGCTCGGCCTCGCCGATG
AGCACATCGAGACGGAGAAAATGCTGGCTGATTCTGGCATCGTTTACACCCTGCTGCG
CAACGGCTGGTACAGCGAAAACCTCGCCAGCGCCCCGGCAGCACTGGAACACGG
CGTATTTATCGGTGCGGCGGGCGATGGCAAATCGCCTCAGCAACGCGGGCAGATTAT
GCGGCAGCTGCGGCACGCGTGATTAGCGAAGCCGGTCACGAAGGCAAGGTTTACGAA
CTGGCGGGCGATAGTGCCTGGACGTTGACACAGTTAGCGGCAGAGCTGACCAAACAGA
GCGGCAAACAGGTTACCTATCAAATCTGAGCGAAGCCGATTTCCGCGCGGCACTGAA
AAGCGTCGGACTGCCCGACGGACTGGCGGATATGCTGGCGGATTCTGACGTTGGCGC
ATCGAAAGGCGGTCTGTTTGATGACAGCAAAACACTTAGCAAATTGATTGGCCACCCAA
CGACAACGTTAGCCGAAAGCGTAAGCCATCTTTTTAATGTTAATAACTAAAAGCTTGCGG
CCGC

pET28c-*N-His-Tev-ytfG* expression vector

TGGCGAATGGGACGCGCCCTGTAGCGGCGCATTAAAGCGCGGGCGGGTGTGGTGGTTAC
GCGCAGCGTGACCGCTACACTTGCCAGCGCCCTAGCGCCCGCTCCTTTTCGCTTTCTTC
CCTTCCTTTCTCGCCACGTTTCGCCGGCTTTCCCCGTCAAGCTCTAAATCGGGGGCTCCC
TTTAGGGTTCCGATTTAGTGCTTTACGGCACCTCGACCCCAAAAACTTGATTAGGGTG
ATGGTTCACGTAGTGGGCCATCGCCCTGATAGACGGTTTTTCGCCCTTTGACGTTGGAG
TCCACGTTCTTTAATAGTGGACTCTTGTTCCAACTGGAACAACACTCAACCCTATCTCG
GTCTATTCTTTTGATTTATAAGGGATTTTGCCGATTTTCGGCCTATTGGTTAAAAAATGAGC
TGATTTAACAAAAATTTAACGCGAATTTTAACAAAATATTAACGTTTACAATTTACAGGTGG
CACTTTTCGGGGAAATGTGCGCGGAACCCCTATTTGTTTATTTTTCTAAATACATTCAAAT
ATGTATCCGCTCATGAATTAATTCTTAGAAAACTCATCGAGCATCAAATGAAACTGCAA
TTTATTCATATCAGGATTATCAATACCATATTTTTGAAAAAGCCGTTTCTGTAATGAAGGA
GAAACTCACCGAGGCAGTTCATAGGATGGCAAGATCCTGGTATCGGTCTGCGATTCC
GACTCGTCCAACATCAATACAACCTATTAATTTCCCCTCGTCAAAAATAAGGTTATCAAG
TGAGAAATCACCATGAGTGACGACTGAATCCGGTGAGAATGGCAAAGTTTATGCATTT
CTTTCCAGACTTGTTCAACAGGCCAGCCATTACGCTCGTCATCAAATCACTCGCATCAA
CCAAACCGTTATTCATTTCGTGATTGCGCCTGAGCGAGACGAAATACGCGATCGCTGTTA
AAAGGACAATTACAAACAGGAATCGAATGCAACCGGCGCAGGAACACTGCCAGCGCAT
CAACAATATTTTCACCTGAATCAGGATATTCTTCTAATACCTGGAATGCTGTTTTCCCGG
GGATCGCAGTGGTGAGTAACCATGCATCATCAGGAGTACGGATAAAATGCTTGATGGTC
GGAAGAGGCATAAATTCCGTCAGCCAGTTTAGTCTGACCATCTCATCTGTAACATCATTG
GCAACGCTACCTTTGCCATGTTTCAGAAACAACCTCTGGCGCATCGGGCTTCCCATACAA
TCGATAGATTGTGCGCACCTGATTGCCCGACATTATCGCGAGCCCATTTATACCCATATAA
ATCAGCATCCATGTTGGAATTTAATCGCGCCCTAGAGCAAGACGTTTCCCGTTGAATAT
GGCTCATAACACCCCTTGTATTACTGTTTATGTAAGCAGACAGTTTTATTGTTTCATGACC
AAAATCCCTTAACGTGAGTTTTCGTTCCACTGAGCGTCAGACCCCGTAGAAAAGATCAA
AGGATCTTCTTGAGATCCTTTTTTTCTGCGCGTAATCTGCTGCTTGCAAACAAAAAACC
ACCGCTACCAGCGGTGGTTTGTTTGCCGGATCAAGAGCTACCAACTCTTTTTCCGAAGG
TAACTGGCTTCAGCAGAGCGCAGATACCAAATACTGTCCTTCTAGTGTAGCCGTAGTTA
GGCCACCACTTCAAGAACTCTGTAGCACCGCCTACATACCTCGCTCTGCTAATCCTGTT
ACCAGTGGCTGCTGCCAGTGGCGATAAGTCGTGTCTTACCGGGTTGGACTCAAGACGA
TAGTTACCGGATAAGGCGCAGCGGTCCGGCTGAACGGGGGGTTCGTGCACACAGCCC
AGCTTGAGCGAACGACCTACACCGAACTGAGATACCTACAGCGTGAGCTATGAGAAA
GCGCCACGCTTCCCGAAGGGAGAAAGGCGGACAGGTATCCGGTAAGCGGCAGGGTCCG
GAACAGGAGAGCGCACGAGGGAGCTTCCAGGGGAAACGCCTGGTATCTTTATAGTCC
TGTCGGGTTTTCGCCACCTCTGACTTGAGCGTCGATTTTTGTGATGCTCGTCAGGGGGG
CGGAGCCTATGAAAAACGCCAGCAACGCGGCCTTTTTACGGTTCCTGGCCTTTTGCTG

GCCTTTTGCTCACATGTTCTTTCTGCGTTATCCCCTGATTCTGTGGATAACCGTATTAC
CGCCTTTGAGTGAGCTGATACCGCTCGCCGCAGCCGAACGACCGAGCGCAGCGAGTC
AGTGAGCGAGGAAGCGGAAGAGCGCCTGATGCGGTATTTTCTCCTTACGCATCTGTGC
GGTATTTACACCCGCATATATGGTGCACCTCTCAGTACAATCTGCTCTGATGCCGCATAGT
TAAGCCAGTATACTCCGCTATCGCTACGTGACTGGGTCATGGCTGCGCCCCGACAC
CCGCCAACACCCGCTGACGCGCCCTGACGGGCTTGTCTGCTCCCGGCATCCGCTTACA
GACAAGCTGTGACCGTCTCCGGGAGCTGCATGTGTGAGAGGTTTTACCGTCATCACC
GAAACGCGCGAGGCAGCTGCGGTAAAGCTCATCAGCGTGGTCGTGAAGCGATTACAG
ATGTCTGCCTGTTTCATCCGCGTCCAGCTCGTTGAGTTTCTCCAGAAGCGTTAATGTCTG
GCTTCTGATAAAGCGGGCCATGTTAAGGGCGGTTTTTCTGTTTGGTCACTGATGCCT
CCGTGTAAGGGGGATTTCTGTTTCATGGGGTAATGATACCGATGAAACGAGAGAGGAT
GCTCACGATACGGGTTACTGATGATGAACATGCCCGTTACTGGAACGTTGTGAGGGTA
AACAACTGGCGGTATGGATGCGGCGGGACCAGAGAAAAATCACTCAGGGTCAATGCCA
GCGCTTCGTTAATACAGATGTAGGTGTTCCACAGGGTAGCCAGCAGCATCCTGCGATG
CAGATCCGGAACATAATGGTGCAGGGCGCTGACTTCCGCGTTTCCAGACTTTACGAAAC
ACGGAAACCGAAGACCATTTCATGTTGTTGCTCAGGTCGCAGACGTTTTGCAGCAGCAGT
CGCTTCACGTTGCTCGGTATCGGTGATTTCATTCTGCTAACCCAGTAAGGCAACCCCGC
CAGCCTAGCCGGGTCTCAACGACAGGAGCACGATCATGCGCACCCGTGGGGCCGCC
ATGCCGGCGATAATGGCCTGCTTCTCGCCGAAACGTTTGGTGGCGGGACCAGTGACGA
AGGCTTGAGCGAGGGCGTGCAAGATTCCGAATACCGCAAGCGACAGGCCGATCATCGT
CGCGCTCCAGCGAAAGCGGTCTCGCCGAAAATGACCCAGAGCGCTGCCGGCACCTG
TCCTACGAGTTGCATGATAAAGAAGACAGTCATAAGTGCGGCGACGATAGTCATGCCCC
GCGCCCACCGGAAGGAGCTGACTGGGTTGAAGGCTCTCAAGGGCATCGGTGAGATC
CCGGTGCCTAATGAGTGAGCTAACTTACATTAATTGCGTTGCGCTCACTGCCCGCTTTC
CAGTCGGGAAACCTGTGCTGCCAGCTGCATTAATGAATCGGCCAACGCGCGGGGAGAG
GCGGTTTGCATATTGGGCGCCAGGGTGGTTTTTCTTTTACCAGTGAGACGGGCAACA
GCTGATTGCCCTTACCGCCTGGCCCTGAGAGAGTTGCAGCAAGCGGTCCACGCTGGT
TTGCCCCAGCAGGCGAAAATCCTGTTTGATGGTGGTTAACGGCGGGATATAACATGAGC
TGTCTTCGGTATCGTTCGATCCCACTACCGAGATATCCGCACCAACGCGCAGCCCGGA
CTCGGTAATGGCGCGCATTGCGCCCAGCGCCATCTGATCGTTGGCAACCAGCATCGCA
GTGGGAACGATGCCCTCATTACGATTTGCATGGTTTGTGAAAACCGGACATGGCACT
CCAGTCGCCTTCCCGTTCCGCTATCGGCTGAATTTGATTGCGAGTGAGATATTTATGCC
AGCCAGCCAGACGCAGACGCGCCGAGACAGAACTTAATGGGCCCGCTAACAGCGCGA
TTTGCTGGTGACCAATGCGACCAGATGCTCCACGCCAGTCGCGTACCGTCTTCATG
GGAGAAAATAATACTGTTGATGGGTGTCTGGTCAGAGACATCAAGAAATAACGCCGGAA
CATTAGTGACGGCAGCTTCCACAGCAATGGCATCCTGGTCATCCAGCGGATAGTTAATG
ATCAGCCCCTGACGCGTTGCGCGAGAAGATTGTGCACCGCCGCTTTACAGGCTTCGA

CGCCGCTTCGTTCTACCATCGACACCACCACGCTGGCACCCAGTTGATCGGCGCGAGA
TTTAATCGCCGCGACAATTTGCGACGGCGCGTGCAGGGCCAGACTGGAGGTGGCAAC
GCCAATCAGCAACGACTGTTTGCCCGCCAGTTGTTGTGCCACGCGGTTGGGAATGTAAT
TCAGCTCCGCCATCGCCGCTTCCACTTTTTCCCGCGTTTTTCGCAGAAACGTGGCTGGCC
TGGTTCACCACGCGGGAAACGGTCTGATAAGAGACACCGGCATACTCTGCGACATCGT
ATAACGTTACTGGTTTCACATTCACCACCCTGAATTGACTCTCTTCCGGGCGCTATCATG
CCATACCGCGAAAGGTTTTGCGCCATTCGATGGTGTCCGGGATCTCGACGCTCTCCCTT
ATGCGACTCCTGCATTAGGAAGCAGCCCAGTAGTAGGTTGAGGCCGTTGAGCACCGCC
GCCGCAAGGAATGGTGCATGCAAGGAGATGGCGCCCAACAGTCCCCCGGCCACGGGG
CCTGCCACCATACCCACGCCGAAACAAGCGCTCATGAGCCCGAAGTGGCGAGCCCGAT
CTTCCCATCGGTGATGTGCGCGATATAGGCGCCAGCAACCGCACCTGTGGCGCCGGT
GATGCCGGCCACGATGCGTCCGGCGTAGAGGATCGAGATCTCGATCCCGCGAAATTA
TACGACTCACTATAGGGGAATTGTGAGCGGATAACAATCCCCTCTAGAAATAATTTTGT
TTAACTTTAAGAAGGAGATATACCATGGGCCACCATCATCACCATCACCATCACAGCAG
CGGCGAGAATCTTTATTTTCAGGGCGCTATCGCTATTACTGGTGCCACTGGCCAACTTG
GTCACTATGTTATTGAATCCTTGATGAAAACGGTTCCTGCCAGCCAAATAGTGGCTATCG
TTCGTAATCCGGCAAAGGCCAAGCCCTGGCAGCACAAGGCATTACCGTGCGTCAGGC
TGACTACGGCGATGAAGCCGCACTGACATCTGCACTTCAGGGAGTGGAAAACTACTG
CTGATCTCTTCCAGCGAAGTGGGTCAACGTGCCCCGCGAGCATCGTAATGTTATTAATGC
CGCAAAGGCGGCTGGCGTGAAATTTATCGTTATACCAGCCTGCTACATGCAGATACCT
CCCCGCTCGGCCTCGCCGATGAGCACATCGAGACGGAGAAAATGCTGGCTGATTCTGG
CATCGTTTACACCCTGCTGCGCAACGGCTGGTACAGCGAAAATACCTCGCCAGCGCC
CCGGCAGCACTGGAACACGGCGTATTTATCGGTGCGGGCGGGCGATGGCAAATCGCCT
CAGCAACGCGGGCAGATTATGCGGCAGCTGCGGCACGCGTGATTAGCGAAGCCGGTC
ACGAAGGCAAGGTTTACGAACTGGCGGGCGATAGTGCCTGGACGTTGACACAGTTAGC
GGCAGAGCTGACCAAACAGAGCGGCAAACAGGTTACCTATCAAATCTGAGCGAAGCC
GATTCGCCGCGGCACTGAAAAGCGTCGGACTGCCCGACGGACTGGCGGATATGCTG
GCGGATTCTGACGTTGGCGCATCGAAAGGCGGTCTGTTTGATGACAGCAAACACTTAG
CAAATTGATTGGCCACCCAACGACAACGTTAGCCGAAAGCGTAAGCCATCTTTTTAATGT
TAATAACTAAAAGCTTGCGGCCGCACTCGAGCACCACCACCACCACCCTGAGATCCG
GCTGCTAACAAAGCCCGAAAGGAAGCTGAGTTGGCTGCTGCCACCGCTGAGCAATAAC
TAGCATAACCCCTTGGGGCCTCTAAACGGGTCTTGAGGGGTTTTTTGCTGAAAGGAGGA
ACTATATCCGGAT

native *E. coli* QOR2 protein sequence

MIAITGATGQLGHYVIESLMKTVPASQIVAIVRNPAKAQALAAQGITVRQADYGDEAALTSAL
 QGVEKLLLISSSEVGQRAPQHRNVINA AKAAGVKFIAYTSLLHADTSPLGLADEHIETEKMLA
 DSGIVYTLLRNGWYSENYLASAPAALEHG VFIGAAGDGKIASATRADYAAAAARVISEAGHE
 GKVYELAGDSAWTLTQLAAELTKQSGKQVTYQNLSEADFAAALKSVGLPDGLADMLADSDV
 GASKGGLFDDSKTLSKLIGHPTTTLAESVSHLFNVNN

native *E. coli* QOR2 protein sequence, with amino acid numbering

10 20 30 40 50 60
 MIAITGATGQ LGHYVIESLM KTVPASQIVA IVRNPAKAQA LAAQGITVRQ ADYGDEAALT

70 80 90 100 110 120
 SALQGVEKLL LISSSEVGQR APQHRNVINA AKAAGVKFIA YTSLLHADTS PLGLADEHIE

130 140 150 160 170 180
 TEKMLADSGI VYTLLRNGWY SENYLASAPA ALEHG VFIGA AGDGKIASAT RADYAAAAAR

190 200 210 220 230 240
 VISEAGHEGK VYELAGDSAW TLTQLAAELT KQSGKQVTYQ NLSEADFAAA LKSVGLPDGL

250 260 270 280
 ADMLADSDVG ASKGGLFDDSKTLSKLIGHPTTTLAESVSH LFNVNN

recombinant *E. coli* His-QOR2 protein sequence

MGHHHHHHHSSGENLYFQGAIITGATGQLGHYVIESLMKTVPASQIVAIVRNPAKAQALA
 AQGITVRQADYGDEAALTSALQGVEKLLLISSSEVGQRAPQHRNVINA AKAAGVKFIAYTSLL
 HADTSPLGLADEHIETEKMLADSGIVYTLLRNGWYSENYLASAPAALEHG VFIGAAGDGKIAS
 ATRADYAAAAARVISEAGHEGK VYELAGDSAWTLTQLAAELTKQSGKQVTYQNLSEADFAA
 ALKSVGLPDGLADMLADSDVGASKGGLFDDSKTLSKLIGHPTTTLAESVSHLFNVNN

recombinant *E. coli* His-QOR2 protein sequence, with amino acid numbering

10 20 30 40 50 60
MGHHHHHHHH SSGENLYFQG AIAITGATGQ LGHYVIESLM KTVPASQIVA IVRNPAKAQA

70 80 90 100 110 120
LAAQGIVRQ ADYGDEAALT SALQGVEKLL LISSEVGQR APQHRNVINA AKAAGVKFIA

130 140 150 160 170 180
YTSLHADTS PLGLADEHIE TEKMLADSGI VYTLRNGWY SENYLASAPA ALEHGFIGA

190 200 210 220 230 240
AGDGKIASAT RADYAAAAAR VISEAGHEGK VYELAGDSAW TLTQLAAELT
KQSGKQVTYQ

250 260 270 280 290 300
NLSEADFAAA LKSVGLPDGL ADMLADSDVG ASKGGLFDDS KTLKLIHHP TTTLAESVSH

LFNVNN

QOR2 probe activation

The protocol was conducted according to previously published studies.^{8, 9} All stock dilutions were performed with sterile-filtered 50 mM $\text{KH}_2\text{PO}_4/\text{K}_2\text{HPO}_4$ buffer (pH 7.0, reduction of quinone autoxidation), from reagent or compound stocks in water or cell culture grade DMSO under a laminar flow bench. Dioxetane probe **8** was pre-incubated 60 min prior to enzyme kinetic or chemiluminescence measurement at 25 °C and 330 rpm in the dark. The dioxetane probe was diluted with NADH (Sigma) in buffer to yield a range of seven substrate concentrations (0.1, 0.08, 0.05, 0.03, 0.025, 0.01, 0.001 mM for luminescence and for enzyme kinetic measurements) and an excess of NADH (250 μM). The DEAE fraction with the greatest purity, in lane 2 in Figure S5.12C, was employed for kinetic measurements. The reaction was started by the addition of QOR2 (stock 0.1 mg/mL in buffer, final 1.25 $\mu\text{g}/\text{mL}$) and the initial oxidation rate of NADH at 340 nm was determined (5-12 seconds). The apparent K_m , V_{max} and k_{cat} values were determined over a range of seven substrate concentrations by fitting the data to the Michaelis Menten equation. All kinetic measurements were performed at least three times. As a positive control, the same protocol was conducted with methyl benzoquinone (MBQ), which was previously reported to be reduced by quinone oxidoreductases.⁸ For the luminescence measurement, the plate was sealed with a transparent film. The measurement was conducted in white or transparent 384 well plates in a plate reader (every 3 min, total time 5 h, medium shaking, no filter). The data were evaluated using Microsoft Excel 2016 and GraphPad Prism 9.

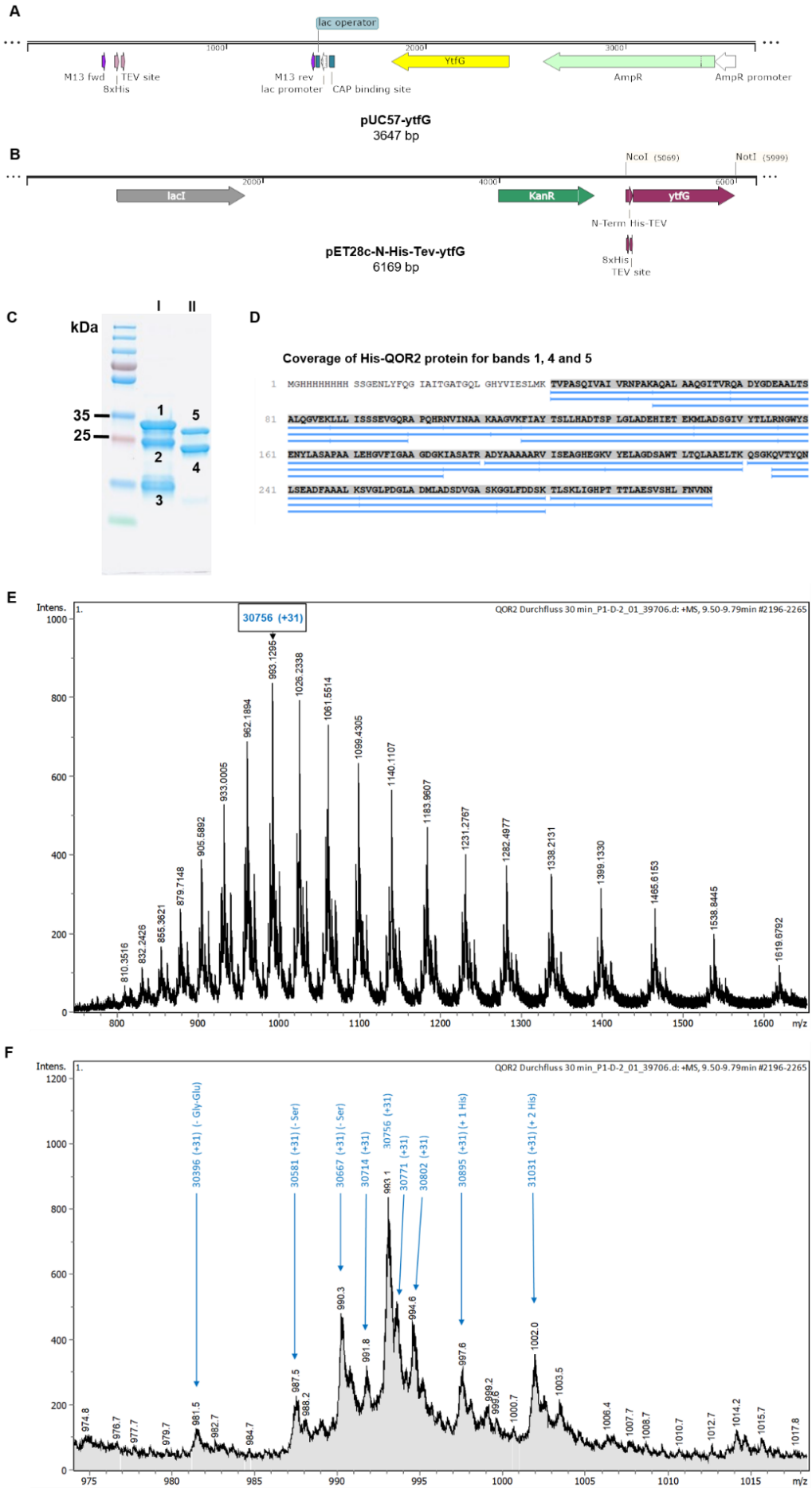


Figure S5.12. Expression, purification and characterization of QOR2 from *E. coli* BL21 Rosetta 2 cultures. **(A)** Plasmid maps of pUC57-*ytfG* and pET28c-*N-His-Tev-ytfG* **(B)**, **(C)** SDS-PAGE of QOR2 containing fractions from the DEAE column, stained with either ReadyBlue representative example of optimized expression. Lane **I**: retained fractions on the column, high salt buffer affected running behaviour, lane **II**: flow through, low salt buffer. Bands **1-5** were excised and subjected to in gel tryptic digestion with subsequent tims-TOF MS/MS measurement. **(D)** Sequence coverage of gel bands **1**, **4** and **5** matched with His-QOR2 (this paper) and native QOR2 (Uniprot: P39315). **(E)** and **(F)**. Whole protein mass determination by UPLC-ESI-TOF mass spectrometry of DEAE fraction displayed in the SDS-PAGE lane **II** in **(C)**. **(E)** Full mass spectrum. **(F)** Zoom into the region of 974-1018 Da of the spectrum shown in **(E)**, covering the charge state +31. The highest peaks have, when deconvoluted, a neutral mass of 30756 Da, which corresponds to amino acids 11Ser-306Asn of recombinant *E. coli* His-QOR2.

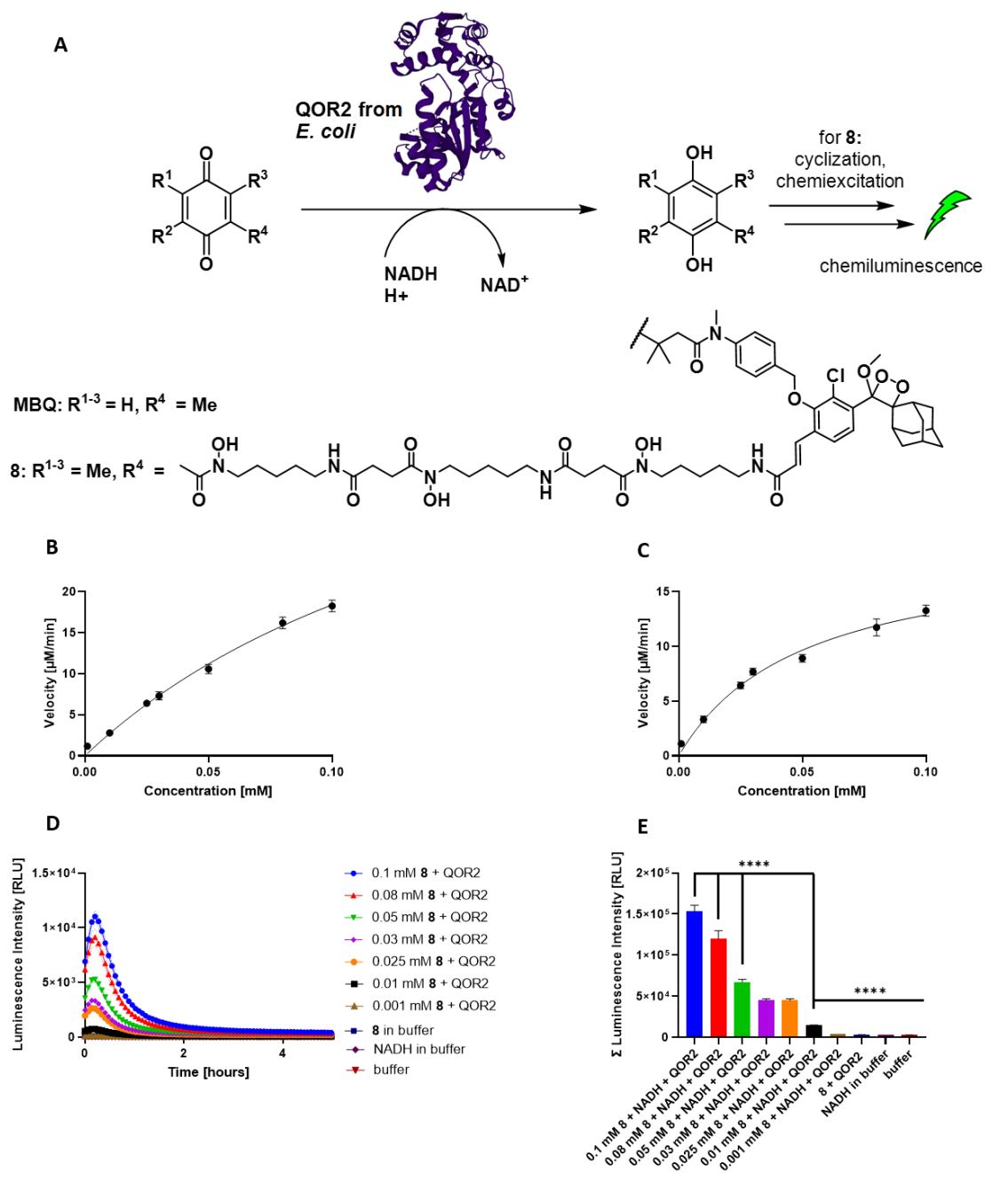


Figure S5.13. Quinone oxidoreductase-catalysed reduction of **8**. **(A)** Reduction catalysed by the *E. coli* quinone oxidoreductase QOR2 for methyl benzoquinone (MBQ) or probe **8**. **(B)** Initial velocities were obtained for varied concentrations of methyl benzoquinone (MBQ) in the presence of QOR2 (1.25 µg/mL) and NADH (250 µM) in phosphate buffer (pH 7.0). **(C)** Initial velocities were obtained for varied concentrations of probe **8** in the presence of QOR2 (1.25 µg/mL) and NADH (250 µM) in phosphate buffer (pH 7.0). Data points are the average of three experiments. Best fit lines showed an $R^2 > 0.7$, and their slopes were significantly different from zero ($p < 0.005$), error bars correspond to \pm standard error of mean (SEM). **(D)** Chemiluminescence curves and **(E)** Summed chemiluminescence intensities for different concentrations of **8** \pm QOR2 (1.25 µg/mL) and NADH (250 µM) in phosphate buffer (pH 7.0). Dotted lines or error bars correspond to \pm standard error of mean (SEM). For the summed experiments, each group was compared to the no-bacteria control *via* one-way ANOVA (**** $p < 0.0001$).

Table S5.2. Determination of key enzymatic parameters for the reduction of 8 or MBQ^{a)} with QOR2.

Compound	QOR2 [$\mu\text{g/mL}$]	V_{max} [$\mu\text{M/min}$]	K_{m} [μM]	k_{cat} [s^{-1}]
MBQ	1.25	51.65	180.4	1275
8	1.25	19.35	50.11	477.7

a) MBQ = methyl benzoquinone, n = 3. All measurements at 25 °C and pH 7.0.

Quenching experiment

Probe 1 was diluted 1:1000 in 10 mL PBS pH 7.4 to yield a 10 μM assay concentration and pre-incubated for 45 min at 25 $^{\circ}\text{C}$ and 1000 rpm. The quenchers Q1 (2,3-dihydroxy benzoic acid), Q2 (2,3-diacetoxy benzoic acid) and Q3 (2,3-dimethoxy benzoic acid) were dissolved in DMSO to yield a 100 mM stock. 100 μL per well of the pre-incubated probe 1 were distributed into a non-treated, white 96-well plate. The quenchers Q1, Q2 and Q3 were diluted 1:100 ($c = 1 \text{ mM}$, 1 mL in PBS pH 7.4) and 3 μL of the dilution were either added to the probe in PBS ($C_{\text{final}} = 30 \mu\text{M}$) or into plain PBS. Then either 1 μL of the inducer (NaBH_4 100mM in PBS) or 1 μL of plain PBS was added to the respective wells. The plate was sealed with a transparent foil and the luminescence was recorded for 120 min (measure every 3min, shaking 30 sec, 25 $^{\circ}\text{C}$). The results are evaluated, plotted and analyzed with Microsoft Excel 2016 and GraphPad Prism 9.

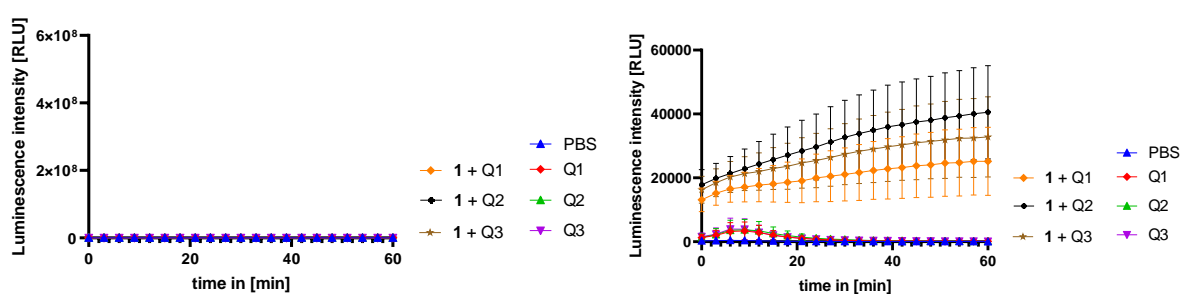
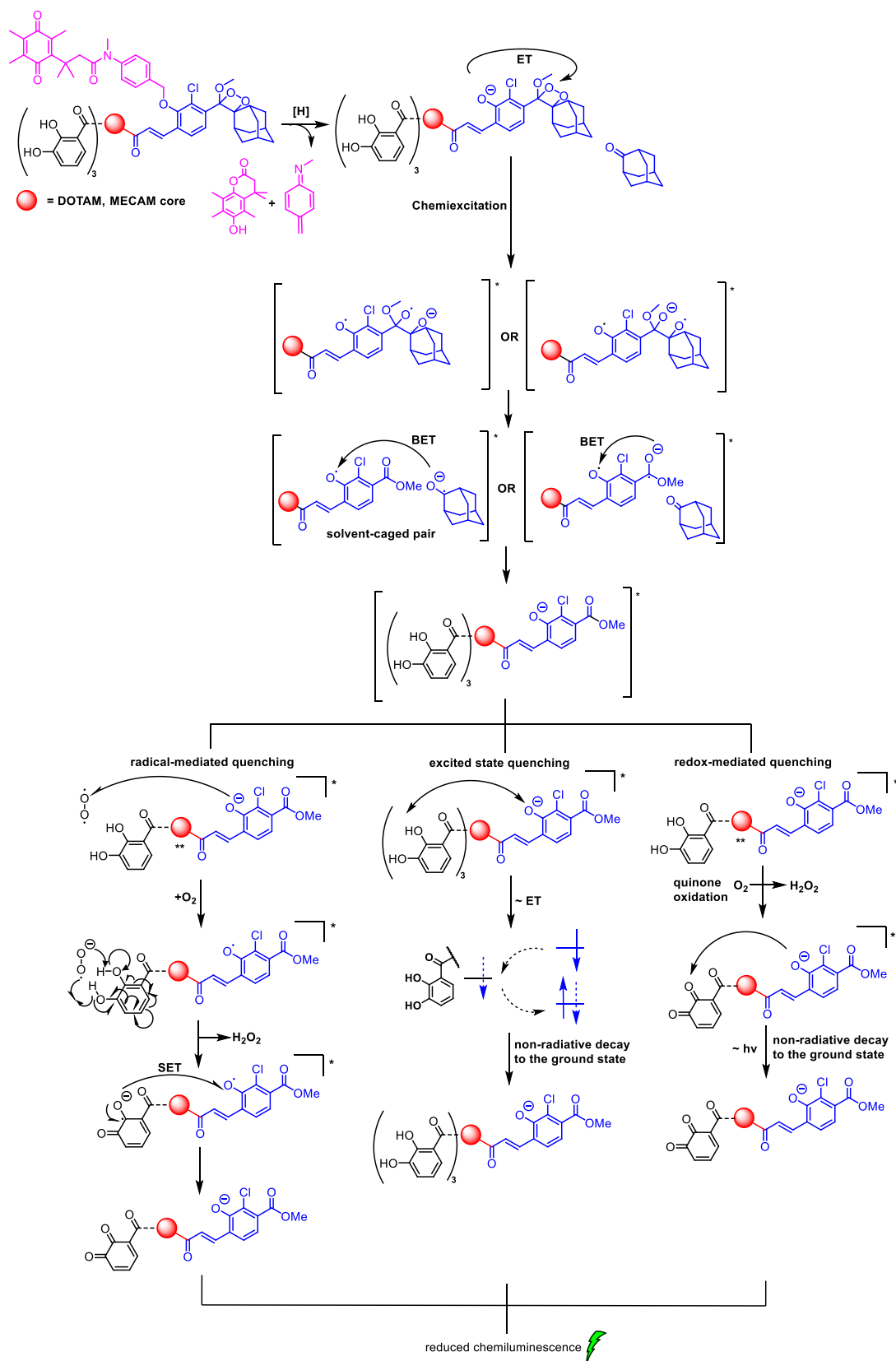


Figure S5.14. Chemiluminescence kinetic profiles of 1 in PBS at pH 7.4, $\pm 30 \mu\text{M}$ quencher Q₁ (= 2,3-dihydroxybenzoic acid), Q₂ (= 2,3-diacetoxybenzoic acid) or Q₃ (= dimethoxybenzoic acid) over 60 minutes in [RLU], including controls (Q_x + 1, Q_x, PBS). Probes were pre-incubated in PBS at pH 7.4 prior to use. The left panels has a y-axis scale identical to that of Figure 5.4, while the y-axis is zoomed on the right panel. $n = 3$, error bars correspond to \pm standard error of mean (SEM).



Scheme S5.1. Hypothetical chemiluminescence quenching by a radical-mediated, excited state or redox-mediated mechanism. ** mark a simplification of the triscatechol siderophore for drawing purposes. ET = electron transfer, BET = back electron transfer, SET = single electron transfer.

Growth recovery assay

The growth recovery assay was conducted after a procedure originally described by C. Peukert and L. Langer *et al*, narrated in part below.⁵

The *E. coli* wild type strain BW25113 and the mutant strain JW0588-1 (“ Δ entA”) was grown in LB medium (5 mL) overnight at 37 °C and 180 rpm. The *E. coli* mutants were always grown in presence of 50 µg/mL Kanamycin. The *P. aeruginosa* WT strain PAO1 and the mutant strain PAO1 Δ pvdD Δ pchE-F were grown in 1x LB medium (5 mL overnight at 37 °C and 180 rpm. The next morning the overnight inoculums were diluted 1:100 in 20 mL LB medium, and grown to OD_{600nm}= 0.5 within 1-2 h at 37 °C and 180 rpm.

15 ml of the dilution culture were pelleted by centrifugation at 4.500 g, 5 min and 4 °C. The supernatant was discarded and the pellet was washed twice with iron-free 1xLMR (5 mL) or 1x PBS. The OD_{600nm} of the bacterial suspension was adjusted 0.01 with iron-free 1x LMR with Glycerol as carbon source.

The 10 mM compound stocks in DMSO were diluted 1:500 ± iron with LMR (20 µM FeCl₃ or none) to yield a 20 µM compound concentration. The dilution was prepared under a laminar flow bench with sterile medium, sterile microcentrifuge tubes and sterile filtered iron solutions. The microcentrifuge tubes were vortexed and 50 µL of the 20 µM compound in LMR medium ± iron was added / well into a 96-well, half-area plates under a laminar flow bench.

50 µL of bacterial suspension with a OD_{600nm}=0.01 in iron-free 1x LMR with glycerol as carbon source was added to the compound in the plate in a 1:1 dilution to yield the final 10 µM compound concentration ± a 10 µM iron-concentration (or iron-free). Empty wells were filled with 50µL 1x LMR, the plate was sealed with parafilm and incubated in a humid chamber at 37 °C for 48 h. The OD_{600nm} was determined with a plate UV-Vis spectrometer, the data was exported to Microsoft Excel 2016 and data evaluation was conducted with GraphPad Prism 9.

ESKAPE pathogen iron starvation

This protocol was applied for all chemiluminescence assays and fluorescence assays with siderophore compounds before incubation with the probe. Overnight cultures (5 mL) were prepared in MHB or TSY-CHELEX medium at 37 °C and 180 rpm. The day inoculum (5 mL) was grown till an OD_{600nm} = 0.3-0.5, then centrifuged and the pellet was washed with PBS (pH 7.4, 3x5, 4000 rcf, 5 min, 4 °C). The pellet(s) were resuspended in LMR medium (5 mL, no iron, see 'Growth recovery assay'). The cultures were starved for 24 h at 37 °C, 180 rpm. Then bacteria were harvested by centrifugation (4000 rcf, 5 min, 4 °C) and washed with PBS. Their OD_{600nm} was adjusted with iron-depleted, cation-adjusted medium (IDCAM) to the desired value and employed in the subsequent assay.

ESKAPE pathogen luminescence assay

Bacteria from the ESKAPE panel, indicated in the table below, were grown from their corresponding glycerol stocks according to the protocol for 'ESKAPE pathogen iron starvation'. After iron starvation, cultures were resuspended in the appropriate IDCAM and adjusted to an $OD_{600nm} = 0.04$.

Strain	DSMZ-#	Antibiotic resistance^a	Medium
<i>Escherichia coli</i>	DSM11116	Penicillin G, Oxacillin	MHB
<i>Staphylococcus aureus</i>	DSM11822	Aztreonam, Oxacillin	TSY
<i>Klebsiella pneumoniae</i>	DSM11678	-	MHB
<i>Acinetobacter baumannii</i>	DSM30007	Penicillin G, Oxacillin, Ampicillin, Cefalotin, Cefazolin	MHB
<i>Pseudomonas aeruginosa</i>	DSM24068	Penicillin G, Oxacillin, Ampicillin, Mezlocillin, Cefalotin, Cefazolin, Cefotaxime	MHB
<i>Enterococcus faecium</i>	DSM20477	Oxacillin, Aztreonam	TSY

a: list incomplete, more information on the bacdive website with the DSMZ#

The dioxetane or siderophore dioxetane probes (10 mM in DMSO) were diluted in IDCAM (MHB- or TSY-CHELEX) to yield a 20 μ M intermediate solution, which was pre-incubated in the dark at room temperature for 45 minutes at 300 rpm on an Eppendorf shaker. 75 μ L of the 20 μ M probe solution were distributed into a sterile 96well luminescence plate (untreated, white, non-transparent). Control wells were either filled with bacterial suspension or 20 μ M probe in medium and adjusted to the appropriate concentration or OD_{600nm} with IDCAM. 75 μ L bacterial suspension ($OD_{600nm} = 0.04$) was added with a multichannel pipette to the wells, to yield a final 10 μ M probe concentration and a final bacterial $OD_{600nm} = 0.02$. The plate was sealed with a transparent foil and put into the luminescence reader (Read: 20:00:00 h, 30 seconds shaking low, read every 3 minutes, filter = hole). Luminescence curves were exported to Excel, further data processing and plotting was done with Microsoft Excel 2016 and GraphPad Prism 9.

CHELEX treatment for preparation of media⁷

The medium was treated with CHELEX 100 resin (BioRad®, catalog-#: 1422822) to deplete cations. 100g CHELEX resin was weight in per liter of MHB or TSY medium, and stirred with the media for 2 h at room temperature. The resin was removed by filtration medium was filter-sterilized *via* a 0.2 μm bottle top filter. Sterile filtered trace elements were added, as described, before under a laminar flow bench and pH was adjusted to 7.4 with sterile HCl or NaOH.

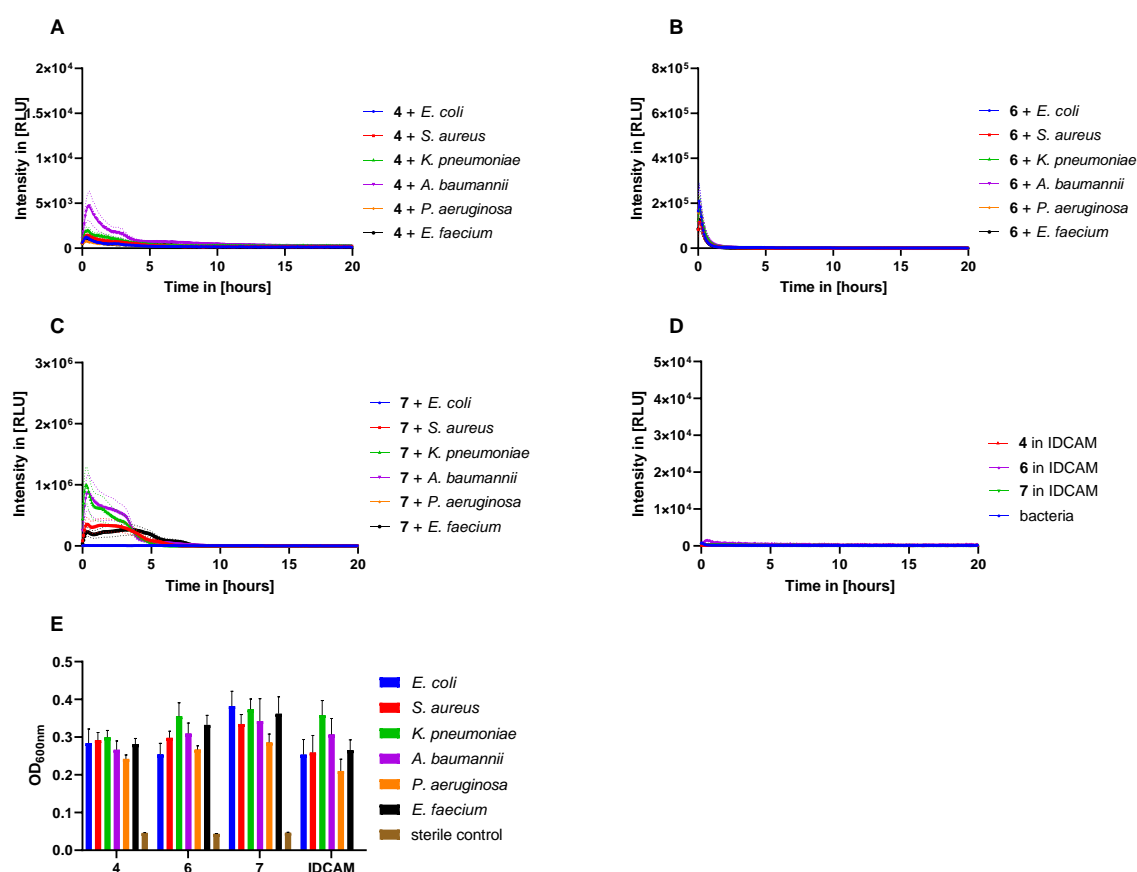


Figure S5.15. ESKAPE luminescence assay with DOTAM dioxetane **4** and MECAM dioxetane **6** and mono catechol **7**. (A) Chemiluminescence kinetic profiles of **4** ± ESKAPE pathogens in iron-depleted, cation-adjusted medium (IDCAM). (B) Chemiluminescence kinetic profiles of **6** ± ESKAPE pathogens in IDCAM. (C) Chemiluminescence kinetic profiles of **7** ± ESKAPE pathogens in iron-depleted, cation-adjusted medium (IDCAM). (D) Chemiluminescence kinetic profiles of **4**, **6** and **7** or bacteria in plain IDCAM, (n = 3). (E) OD_{600nm} values after 20 h of luminescence imaging, grouped by probe or condition. All experiments n = 3, 10 μM final probe concentration. Probes were pre-incubated prior to use. Dotted lines or error bars correspond to \pm standard error of mean (SEM).

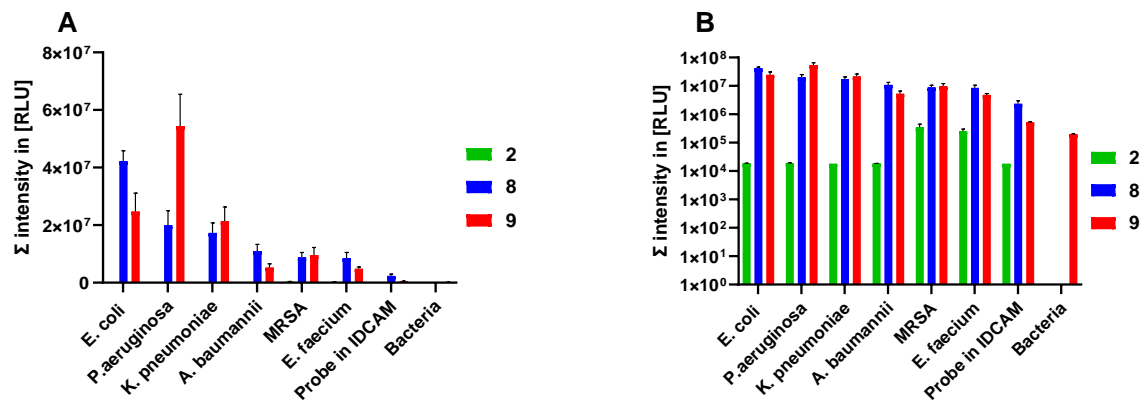


Figure S5.16. Total photon count of **2**, **8** and **9** over 20 h. The left panel (**A**) has a y-axis scale identical to that of Figure 5.6, while the y-axis is changed to a log-scale on the right panel (**B**). $n = 3$, error bars correspond to \pm standard error of mean (SEM). All experiments $n = 3$, final probe concentration of 10 μM in iron-depleted, cation-adjusted medium (IDCAM).

OPNG assay for β -galactosidase/-glucuronidase activity

Bacteria from the ESKAPE panel (strain details see above), were grown in 5 mL LB overnight cultures at 37 °C and 180 rpm from their corresponding glycerol stocks. The next morning, the cultures were centrifuged (4000 g, 5 min, 4 °C) and the supernatant was discarded - the pellet was washed trice with PBS (5 mL) and subsequently centrifuged. Finally, the pellet was resuspended in LMR medium (10 μ M FeCl₃) and the OD₆₀₀ was adjusted to 0.04.

OPNG was dissolved in LMR (+10 μ FeCl₃) by ultrasound sonication for 5 min at 24 °C, to yield a 20 μ M solution. The LMR medium \pm 10 μ M OPNG was added into a 96-well, half-area plate and the bacterial suspension was added on top, to yield an OD_{600nm} = 0.02. The plate was incubated overnight at 500 rpm and 37 °C, sealed with a transparent film, in a shaker. After 20 h, the film was removed, a picture was taken and the absorption (320-1000 nm) was recorded with a plate spectrometer (SPARK, TECAN®). The data was evaluated by Microsoft Excel 2016, and plotted with GraphPad Prism 8 and Microsoft PowerPoint 2016.

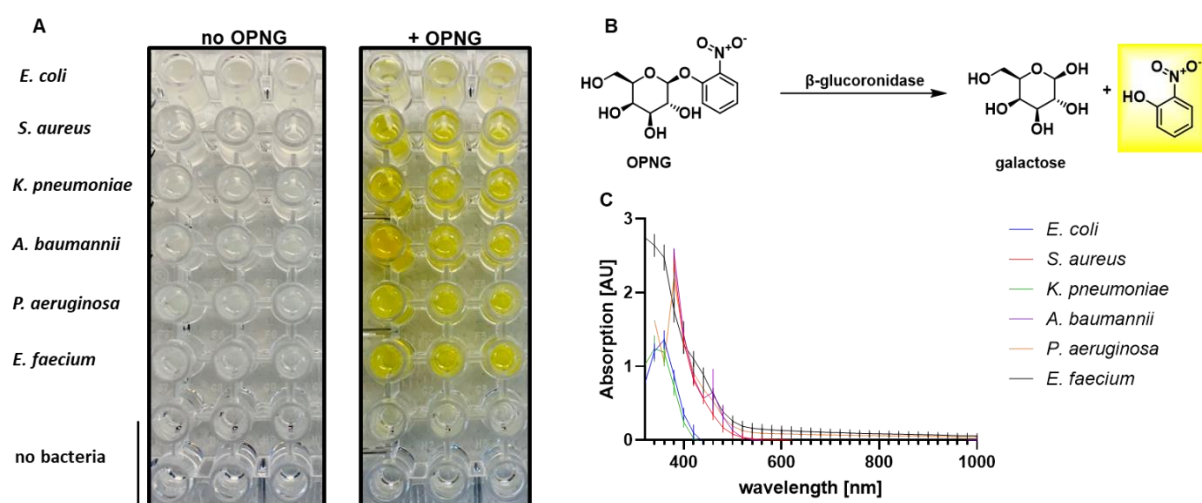


Figure S5.17. Detection of β -galactosidase/-glucuronidase activity in ESKAPE pathogens. **(A)** Representative picture of OPNG assay (\pm 10 μ M OPNG). Endpoint outcome with ESKAPE bacteria after 20 h, conducted in iron-depleted, cation-adjusted medium (IDCAM – LMR with 10 μ M iron), n = 2. **(B)** Enzymatic conversion of the chromogenic *ortho*-nitrophenyl- β -galactoside (OPNG) substrate to galactose and *ortho*-nitro phenol. **(C)** Spectral absorption from 320-1000 nm of OPNG assay endpoint with ESKAPE bacteria after 20 h, conducted in IDCAM (LMR with 10 μ M iron), n = 2, AU = arbitrary units, n = 2.

Probe stability in culture supernatant from ESKAPE pathogens.

Bacteria from the ESKAPE panel (details see above), were grown in 5 mL LB overnight cultures at 37°C and 180 rpm from their corresponding glycerol stocks. The next morning, the cultures were centrifuged (4000 g, 5 min, 4 °C) and the supernatant was discarded - the pellet was washed trice with PBS (5 mL) and subsequently centrifuged. Finally, the pellet was resuspended in CHELEX-MHB or -TSY medium (iron-depleted, cation-adjusted medium, MHB for Gram-negative, TSY for Gram-positive bacteria) and the OD₆₀₀ was adjusted to 0.1 with the indicated medium. The day cultures were grown in 5 mL culture tubes at 37 °C and 180 rpm until a maximum OD_{600nm} = 0.5-1.0. Then the cultures were centrifuged (4000 g, 5 min, 4 °C) and each supernatant from each strain was sterile-filtered over a new Sartorius Minisart™ Plus Syringe Filter (220 µm, 3 filtrations / supernatant / bacterium) and collected in a new 15 mL falcon tube after each filtration step.

In the meanwhile, the probe (10 mM in DMSO) was diluted in IDCAM (MHB- or TSY-CHELEX) to yield a 20 µM intermediate solution. This solution was pre-incubated in the dark at room temperature for 45 minutes at 300 rpm in an Eppendorf shaker. 75 µL of this solution were added per well in a sterile white 96-well luminescence plate (untreated). Control wells were either filled with just (i) sterile-filtered bacterial supernatant or just (ii) 20 µM probe in the medium. Then 75 µL of the sterile-filtered bacterial supernatant was added per well with a multichannel pipette, to yield a final 10 µM probe concentration. The plate was sealed with a transparent foil and put instantly into the luminescence reader (Read: 20:00:00 h, 30 seconds shaking, read every 3 minutes, filter = hole). Luminescence curves were exported to Excel, further data processing and plotting was done with Microsoft Excel 2016 and GraphPad Prism 9. The supernatant was transferred well-by-well to a fresh transparent 96-well plate and subsequently the OD_{600nm} was measured to assure no growth occurred. For control wells, only plain medium was added.

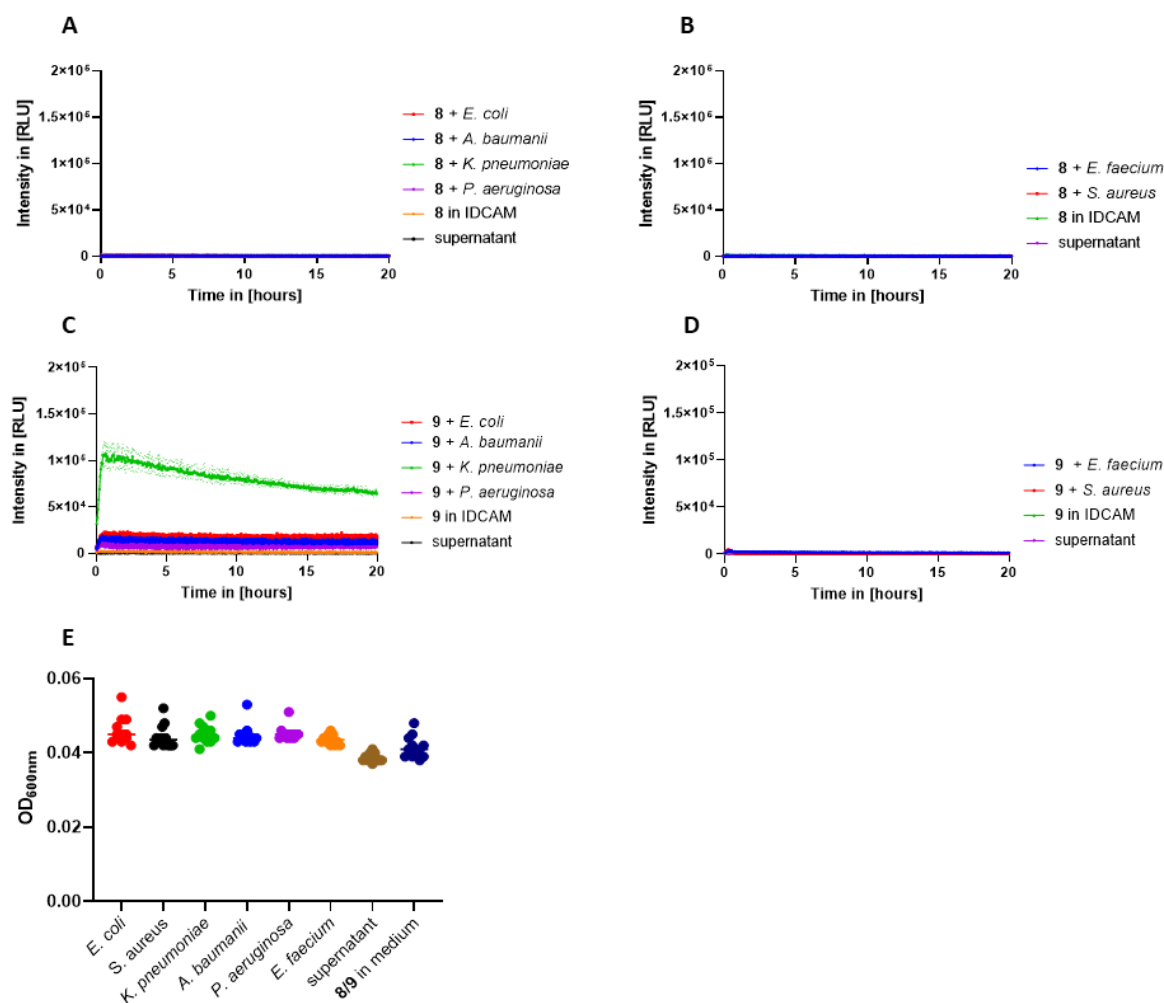


Figure S5.18. Probe stability in the bacterial culture supernatant. **(A)** Chemiluminescence kinetic profiles of **8** (10 μ M) incubated with culture supernatant from Gram-negative bacteria or with plain medium. **(B)** Chemiluminescence kinetic profiles of **8** (10 μ M) incubated with culture supernatant from Gram-positive bacteria or with plain medium. **(C)** Chemiluminescence kinetic profiles of **9** (10 μ M) incubated with culture supernatant from Gram-negative pathogens or with plain medium. **(D)** Chemiluminescence kinetic profiles of **9** (10 μ M) incubated with culture supernatant from Gram-positive bacteria or with plain medium. **(E)** OD_{600nm} values after 20 h of luminescence imaging, grouped by bacterium or assay condition. Individual replicates are plotted, ($n = 3$). Probes were pre-incubated in plain medium prior to use. Dotted lines correspond to \pm standard error of mean (SEM), $n = 3$ for all experiments.

***In vitro* fluorescence activation**

Probe **10** (10 mM stock in DMSO) was diluted in 1x PBS pH 7.4 to yield a 10 μ M intermediate solution. Then 99 μ L of the 10 μ M **10** solution was per well into a 96well black bottom plate and probe only wells were filled with +1 μ L PBS instead of activator. Then 1 μ L NaBH₄ (100 mM) was added with a multichannel pipette to the respective well. The plate was sealed with a transparent foil and put into the luminescence reader (Read: 150 min, every 3 minutes, 30 sec shaking medium, λ_{Ex} = 360 nm, λ_{Em} = 460 nm, top read). Fluorescence curves were exported to Excel, further data processing and plotting was done with Excel and GraphPad Prism 8/9.

Fluorescence ESKAPE assay

Bacteria from the ESKAPE panel (see table above), were grown from their corresponding glycerol stocks according to the protocol for 'ESKAPE pathogen iron starvation'. After iron starvation, cultures were resuspended in the appropriate IDCAM and adjusted to an OD_{600nm} = 0.04. The probe **10** (10 mM stock in DMSO) was diluted in the respective iron-depleted, cation-adjusted medium (IDCAM) to yield a 20 μ M intermediate solution. Then 75 μ L 20 μ M **10** solution was distributed into each well of a 96well black bottom plate and probe only wells were filled with 75 μ L medium instead of bacteria). 75 μ L bacterial suspension (OD₆₀₀ = 0.04) was transferred into the respective well to yield a final 10 μ M probe concentration and a bacterial OD₆₀₀ = 0.02. The plate was sealed with a transparent foil and put into the luminescence reader (Read: 20:00:00 h, every 3 minutes, 30 sec shaking medium, λ_{Ex} = 360 nm, λ_{Em} = 460 nm, top read). Fluorescence curves were exported to Excel, further data processing and plotting was done with Microsoft Excel 2016 and GraphPad Prism 9.

Chemiluminescent detection of *S. aureus* or *P. aeruginosa* in A549 LECs

The day before the experiment, lung epithelial cells (LECs, A549, obtained from DSMZ, ACC 107) were washed twice with sterile PBS, detached with trypsin, and seeded in RPMI medium (+10% FBS) into white, collagen coated 96-well plates. This was done 24 h prior to infection to achieve 80% confluence (50 000 cells/well, after 24h: 100 000 cells/well) the next day. LECs were grown overnight at 5% CO₂ and 37 °C. On the day of the experiment, a visual inspection of the medium color confirmed that no contamination had occurred.

Bacteria were grown from their corresponding glycerol stocks according to the protocol for 'ESKAPE pathogen iron starvation'. After iron starvation, cultures were resuspended in the appropriate IDCAM and adjusted to an OD_{600nm} = 0.04. Finally, the pellet was resuspended in CHELEX-RPMI medium w/o FBS (treated as described above) and the OD₆₀₀ was adjusted to 0.1 with the indicated medium. The day cultures were grown at 37 °C and 180 rpm until a maximum OD₆₀₀ = 0.5-1.0. Then the cultures were centrifuged (4000 g, 5 min, 4 °C) and the pellet was washed trice with 1xPBS. Finally, the bacterial pellet was resuspended in RPMI-CHELEX medium w/o FBS and the OD_{600nm} was adjusted to 0.3 with RMPI w/o FBS.

The LEC-seeded wells were divided into three groups (i) bacteria-infected and gentamicin-treated (50 µg/mL), (ii) bacteria-infected and washed, (iii) controls:

- (i) Bacteria-infected and gentamicin-treated: The medium was removed and the cells were washed with 150 µL RPMI-CHELEX medium w/o FBS / well. Cells were infected at a MOI (multiplicity of infection) of ~ 10 each, as determined by CFU counting, for MRSA (951000 CFUs) and *P. aeruginosa* (992000 CFUs) respectively. The bacterial dilution in RPMI-CHELEX medium was carefully added to the respective wells. The plate was sealed and incubated for 1.5 h at 37 °C at 5% CO₂. After the incubation, the medium was removed, and the wells were washed once with 150 µL RPMI-CHELEX medium w/o FBS / well. Then 150 µL RPMI with a final gentamicin concentration of 50 µg/mL was added for 1.5 hours to the wells. After 1.5 hours of incubation, the supernatant was removed and the cells were thoroughly but gently washed with RPMI-CHELEX w/o FBS (6 x 150 µL).
- (ii) Bacteria-infected and washed: The medium was removed and the cells were washed with 150 µL RPMI-CHELEX medium w/o FBS / well. Cells were infected at a MOI (multiplicity of infection) of ~ 10 each, as determined by CFU counting, for MRSA (951000 CFUs) and *P. aeruginosa* (992000 CFUs) respectively. The bacterial dilution in RPMI-CHELEX medium was carefully added to the respective wells. The plate was sealed and incubated for 1.5 h at 37 °C at 5% CO₂. After 1.5 hours of incubation, the supernatant was removed and the cells were thoroughly but gently washed with RPMI-CHELEX w/o FBS (6 x 150 µL).

- (iii) Controls: LECs were either infected as described under (i) and (ii), but a probe was not added. In other controls, the cells were left uninfected (3x 150 μ L wash RPMI w/o FBS, then the probe was added or not.

Meanwhile the probes were pre-incubated (10 μ M) in sterile RPMI-CHELEX w/o FBS for 45 min. at ambient temperature and 300 rpm in the dark. The plate reader was pre-heated and set up as well. Then 150 μ L of the probe (10 μ M), bacteria or plain medium RPMI-CHELEX w/o FBS was added to the respective wells with a multichannel pipette. The plate was quickly sealed with a transparent film, and the luminescence kinetic was recorded in a plate reader (t = min. 20 h, filter: hole, read interval: 3 min, T = 37 °C, low shaking). The values were exported to Microsoft Excel 2016 and plotted using GraphPad Prism 9. The supernatant/medium was transferred well-by-well to a fresh transparent 96-well plate, and subsequently the OD_{600nm} was measured to assure that the uninfected control wells exhibited no growth due to contaminations.

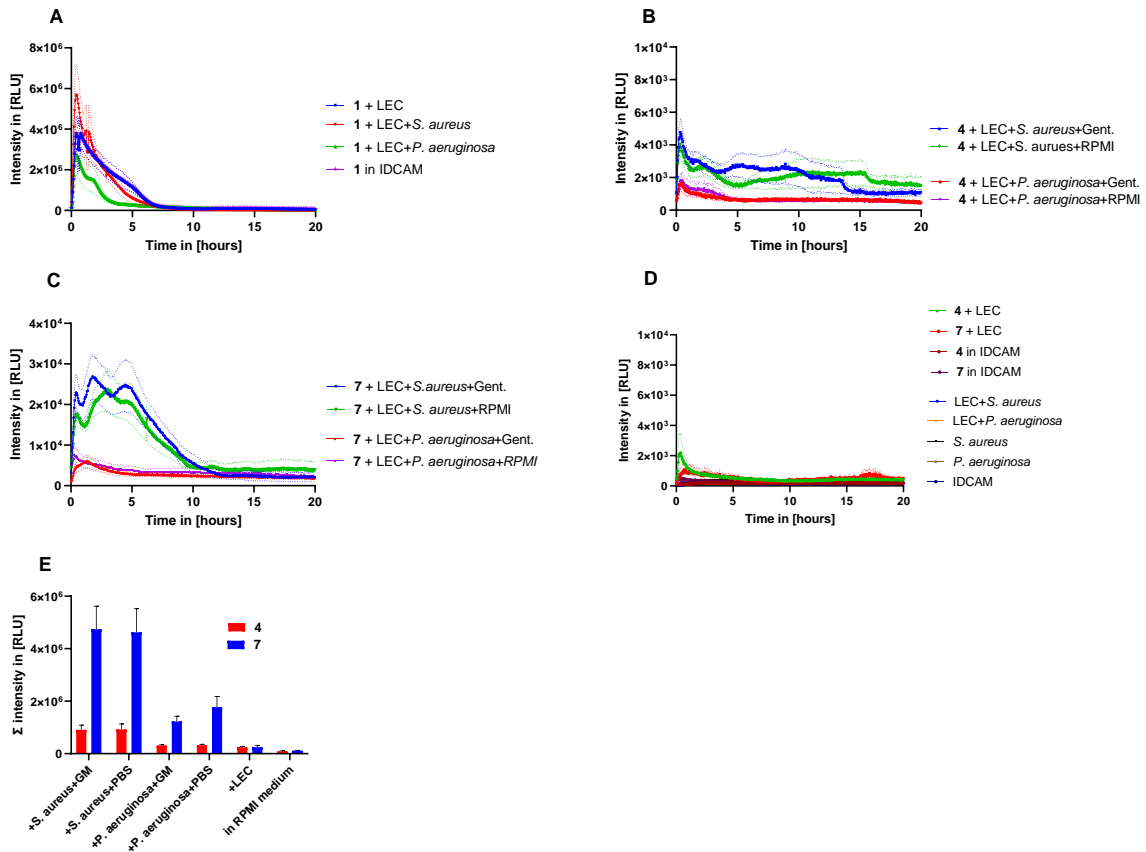


Figure S5.19. Detection of intracellular bacteria in A549 lung epithelial cells (LECs). **(A)** Chemiluminescence kinetic profile of LECs infected with *S. aureus* (MRSA, MOI = 10) or *P. aeruginosa* (PAO7, MOI = 10) followed by a 50 µg/mL gentamicin treatment or a thorough PBS wash and incubated for 20 hours with 1 in IDCAM. **(B)** Chemiluminescence kinetic profile of LECs infected with *S. aureus* or *P. aeruginosa*, followed by a 50µg/mL gentamicin treatment or a thorough PBS wash and incubated for 20 hours with 4 in IDCAM. **(C)** Chemiluminescence kinetic profile of LECs infected with *S. aureus* and *P. aeruginosa* followed by a 50 µg/mL gentamicin treatment or a thorough PBS wash and incubated for 20 hours with probe 7 in IDCAM. **(D)** Assay controls in medium. **(F)** OD_{600nm} after 24 h of luminescence assay, grouped by assay condition and employed probe, error bars correspond to ± SEM. **(E)** Total photon count of probes 4 and 7, as well as assay controls during 20 h of luminescence imaging. Probes were pre-incubated prior to use. Dotted lines correspond to ± standard error of mean (SEM), n = 3 for all experiments.

Fluorescent detection of *S. aureus* or *P. aeruginosa* in A549 LECs

The same protocol as for the “chemiluminescent detection of “*S. aureus* or *P. aeruginosa* in A549 LECs” was carried out and the plate was subjected to fluorescence kinetic in a plate reader (t = min. 20 h, monochromator, Excitation: 400 nm, Emission: 540 nm, band width 20 nm, read interval: 3 min, T = 37 °C, low shaking). Afterwards the values were exported to Microsoft Excel 2016 and plotted using GraphPad Prism 9. The supernatant/medium was transferred well-by-well to a fresh transparent 96-well plate and subsequently the OD_{600nm} was measured to assure no growth occurred in the control wells.

Uptake and activation of 8 in the presence of DFO

The same protocol as for the “chemiluminescent or fluorescent detection of *S. aureus* or *P. aeruginosa* in A549 LECs” was carried out, but with addition of 100 µM DFO (100 mM stock in DMSO) in RPMI-CHELEX, added 3 h before the infection. The DFO was also added to the bacterial day culture and during bacterial iron starvation at the same concentration. After the antibiotic treatment or wash sequence the extracellular DFO was removed and the probe 8 (10 µM) was added in RPMI-CHELEX medium. Then the chemiluminescence/fluorescence kinetic was recorded in a plate reader (t = min. 20 h, luminescence with filter: hole and fluorescence: monochromator with Ex: 400 nm, Em: 540 nm, band width 20 nm, read interval: 3 min, T = 37 °C, low shaking). Afterwards the values were exported to Microsoft Excel 2016 and plotted using GraphPad Prism 9. The supernatant/medium was transferred well-by-well to a fresh transparent 96-well plate and subsequently the OD_{600nm} was measured to assure no growth occurred in the control wells.

Detection of *S. aureus* or *P. aeruginosa* in A549 LECs with extracellular gentamicin

The same protocol as for the “chemiluminescent or fluorescent detection of *S. aureus* or *P. aeruginosa* in A549 LECs” was carried out, but 50 µg/mL gentamicin in RPMI-CHELEX was added after the antibiotic treatment or wash sequence together with probe **8** (10 µM) in RPMI-CHELEX medium. Then the plate was subjected to a chemiluminescence/fluorescence kinetic in a plate reader (t = min. 20 h, luminescence with filter: hole and fluorescence: monochromator with excitation: 400 nm, emission: 540 nm, bandwidth 20 nm, read interval: 3 min, T = 37 °C, low shaking). Afterwards the values were exported to Microsoft Excel 2016 and plotted using GraphPad Prism 9.

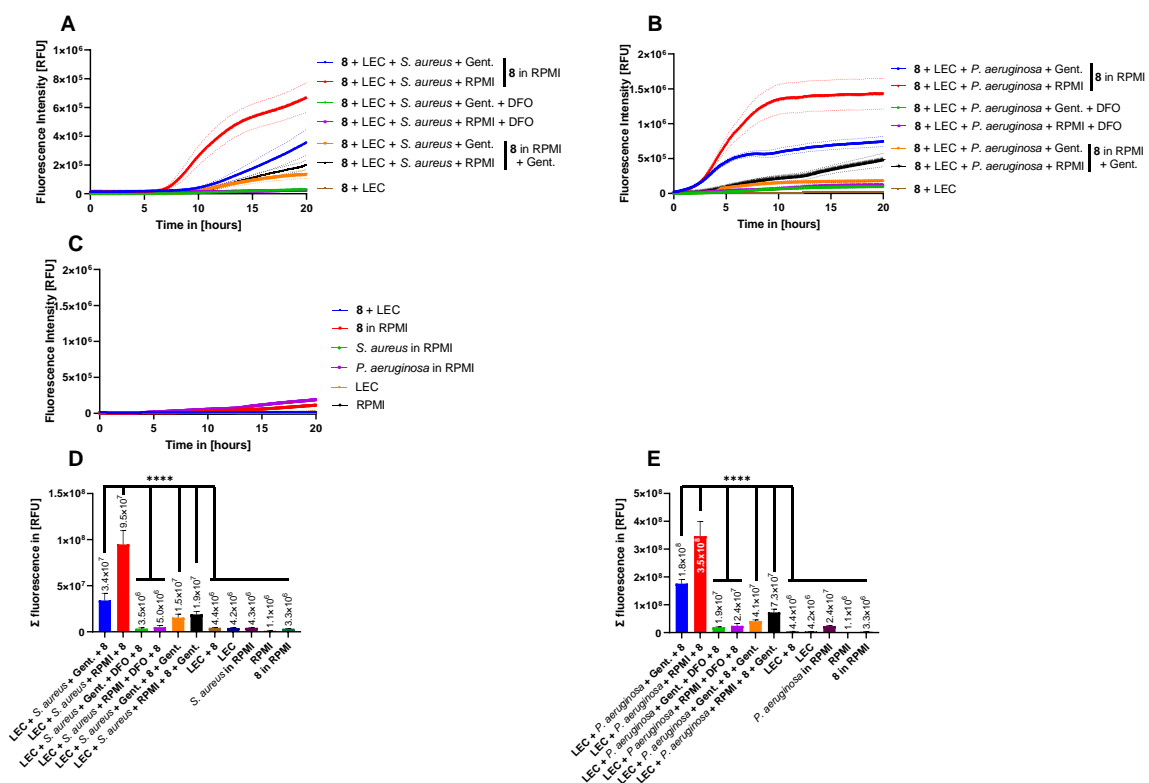


Figure S5.20. Fluorescent detection of intracellular bacteria in A549 lung epithelial cells. (A) Fluorescence kinetic profiles of LECs infected with *S. aureus* followed by gentamicin treatment or a thorough PBS wash and incubation with **8**. (B) Fluorescence kinetic profiles of LECs infected with *P. aeruginosa* followed by gentamicin treatment or a thorough PBS wash and incubation with **8**. (C) Fluorescence kinetic profiles of control conditions. (D) Summed fluorescence values for *S. aureus* treatments including controls. (E) Summed fluorescence values for *P. aeruginosa* treatments including controls. Dotted lines and error bars correspond to \pm standard error of mean (SEM), n = 3. All experiments in iron-depleted, cation-adjusted medium (IDCAM). The summed intensities in (D) and (E) were compared *via* two-way ANOVA (****; p < 0.0001).

Evaluation of LEC infection by CFU counting

The same protocol as for the “chemiluminescent / fluorescent detection of *S. aureus* or *P. aeruginosa* in A549 LECs” was carried out. After the gentamicin treatment or RPMI-CHELEX wash, the wells were washed once with PBS and the supernatant was removed. Then 0.1% Triton-X100 in 1xPBS (pH 7.4) was added to the wells and incubated for 2 minutes. By careful resuspension, the cells were detached and lysed. Immediate serial dilution (10-10⁸ fold) in 24-well plates with subsequent plating on TSY (*S. aureus*) or MHB (*P. aeruginosa*) agar plates in small drops and incubation for min. 10 h at 37 °C allowed CFU counting the next day. The values were collected in Microsoft Excel 2016 and plotted using GraphPad Prism 9.

CFU determination

The bacteria (*S. aureus* and *P. aeruginosa*) were grown in TSY/MHB-CHELEX for 4-6 hour over the day at 37°C and 110 rpm. Plates with MHB or TSY agar were poured and pre-dried under a laminar flow bench before plating of the bacteria. The bacteria cultures were washed (3x 5 mL PBS pH 7.4, 4000 rcf, 5 min, 4 °C) and after the last washing step diluted with LMR medium (see growth recovery assay) to an OD_{600 nm} = 0.2-0.5. The bacteria were starved in iron-free LMR medium for 24 h at 37 °C and 110 rpm. The starved cultures were diluted with iron-free LMR to an OD_{600 nm} = 0.3 and grown for max. 4 hours (5 mL culture) or an OD_{600 nm} below 1. The culture was washed (3x 5 mL PBS pH 7.4, 4000 rcf, 5 min, 4 °C) and serially diluted in 0.9% saline for CFU counting.

OD_{600nm}	0.5	0.1	0.05	0.01	0.005	0.001	0.0005	0.0001	0.00005	0.00001
Dilution	-	(1:5)	(1:2)	(1:5)	(1:2)	(1:5)	(1:2)	(1:5)	(1:2)	(1:5)

2x 5 x 10 µL drops were placed on one quarter of the plate and soaked in under a laminar flow bench to dry with half open cover. Afterwards the plates were turned upside down and incubated at room temperature overnight. Colonies were counted the next day on a SchuettBiotech colony counter, the numbers were collected and extrapolated in Excel assuming a linear relationship:

OD _{600nm}	CFU/mL
<i>S. aureus</i> (OD _{600 nm} = 0.5)	2.76x10 ⁷
<i>P. aeruginosa</i> (OD _{600 nm} = 0.5)	5.06x10 ⁷

Limit of detection

The bacteria (*S. aureus* and *P. aeruginosa*) were grown in TSY/MHB-CHELEX for 4-6 hours over the day at 37°C and 110 rpm. Plates with MHB or TSY agar were poured and pre-dried under a laminar flow bench before plating of the bacteria. The bacteria cultures were washed (3x 5 mL PBS pH 7.4, 4000 rcf, 5 min, 4 °C) and after the last washing step diluted with LMR medium (see growth recovery assay) to an $OD_{600\text{ nm}} = 0.2-0.5$. The bacteria were starved in iron-free LMR medium for 24 h at 37 °C and 110 rpm. The starved cultures were diluted with iron-free LMR to an $OD_{600\text{ nm}} = 0.3$ and grown for max. 4 hours (5 mL culture) or an $OD_{600\text{ nm}}$ below 1. The culture was washed (3x 5 mL PBS pH 7.4, 4000 rcf, 5 min, 4 °C) and serially diluted in TSY/MHB-CHELEX for the assay. Probes were pre-incubated in the respective medium timely before usage for 45 min at room temperature. Bacterial dilutions were distributed in a 96-well white or black plate (no treatment) with a multi-channel pipette under the laminar flow bench. 50 μ L of the pre-incubated 20 μ M compound solution was added to the bacteria (10 μ M final concentration). The plate was sealed with a transparent film and the luminescence/fluorescence kinetic was started for 24 h at 37 °C (medium shaking, measurement every 3 minutes). Appropriate assay controls included a bacterial control without probe (1% DMSO) as well as probe in the plain medium. The data analysis was performed in Microsoft Excel 2016 and GraphPad Prism by plotting the integrated luminescence values over the previously obtained CFU/mL on a logarithmic scale. Best-fit curves were performed for the range of integrated signals that showed a linear dependency and were significantly different from values of the probe in plain medium ($p < 0.0001-0.01$), as tested by one-way ANOVA. S/B-ratios were calculated by division of the bacteria-treated values through the probe signal in the plain medium. S/B ratios from probes **8** and **10** for the same pathogen were plotted in one graph over the CFU/mL (log-scale) to obtain the LOD, as the concentration of bacteria that could be reliably distinguished from probe signal without bacteria and had an S/B ratio > 2.0 .

Detection of bacteria in human plasma

Overnight cultures of PAO7 and MRSA (strain details see above) were grown in MHB-CHELEX or TSY-CHELEX medium (5 mL) overnight at 37 °C and 180 rpm from their corresponding glycerol stocks. The next day, the cultures were harvested by centrifugation (4000 g, 5 min, 4 °C) and the supernatant was discarded. The pellet was washed with PBS (3x5 mL) and subsequently centrifuged (4000 g, 5 min, 4 °C). The pellet was resuspended in the respective, fresh IDCAM (5 mL) and the OD₆₀₀ was adjusted to 0.1. The cultures were grown at 37 °C and 180 rpm until a max. OD₆₀₀ = 0.5-1.0. Then the cultures were harvested by centrifugation (4000 g, 5 min, 4 °C) and the pellet was washed trice with 1xPBS. The pellet was resuspended in 1xPBS and the OD_{600nm} was adjusted to 0.002 (*P. aeruginosa*) and to 0.001 (*S. aureus*) with sterile human plasma in sodium EDTA (prod-# ABIN5706551, antikoerper-online, mixed sex, IgG and heme normal, without preservative). 25 µL of the bacterial dilution were added per well in a sterile, white 96-well half area plate. 25 µL probe **8** (20 µM, pre-incubated in plasma at 23°C in the dark) were added. This 1:1 dilution yielded a starting CFU/mL in the range of the LOD (~10⁶ and 10³ CFU/mL respectively) and a 10 µM final probe concentration. The plate was sealed with a transparent film. Subsequently the luminescence and fluorescence were imaged for 20 h (37 °C, shaking, measurement every 3 min, luminescence filter: hole, fluorescence excitation 400, emission 540 nm). 10 µM probe in plasma, bacteria in plasma and plain plasma were used as controls. Simultaneously the probe dilution in plasma and plain plasma controls (100 µl each) were plated on LB agar plates and no growth was observed 48 h after incubation at 37 °C.

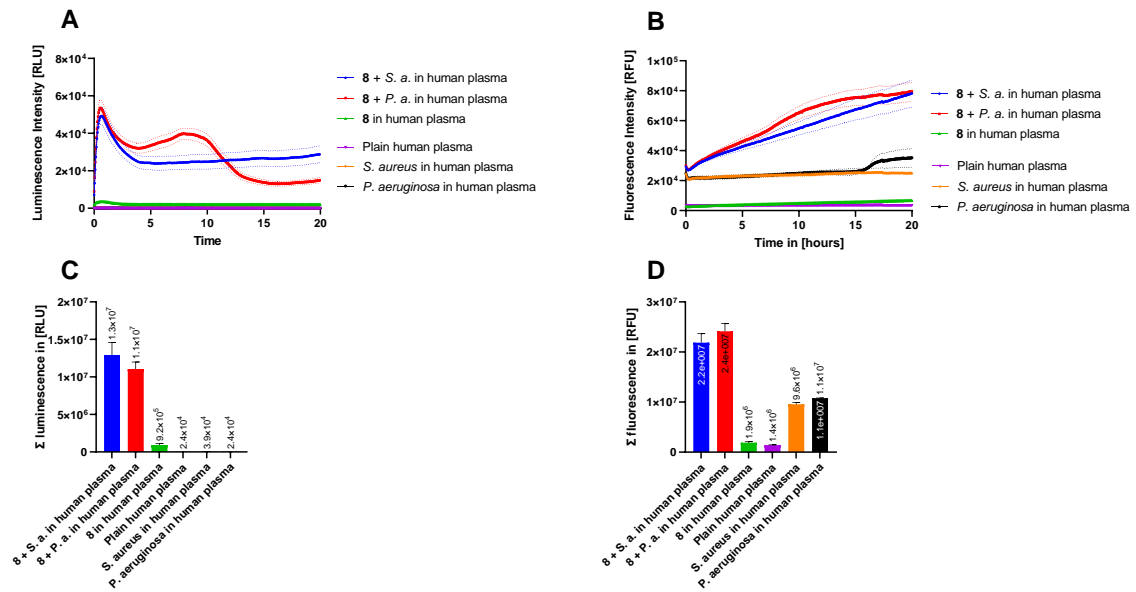


Figure S5.21. Detection of bacteria in human plasma. (A) Luminescence intensities of probe **8** (10 μ M) in human plasma in the presence or absence of *S. aureus* or *P. aeruginosa* (10^5 CFU/mL) including assay controls. (B) Fluorescence intensities of probe **8** (10 μ M) in human plasma in the presence or absence of *S. aureus* or *P. aeruginosa* (10^5 CFU/mL) including assay controls. (C) Summed luminescence intensities and (D) Summed fluorescence intensities. Dotted lines or error bars correspond to \pm standard error of mean (SEM), n = 3. A one-way ANOVA statistical test of the summed values confirmed significant different means between groups with p < 0.0001; ****.

Author Contributions

C.P. performed chemical synthesis, conducted biological assays and wrote the manuscript. L.P. conducted chemical synthesis. S.P.G. and O.G. conducted chemical synthesis and wrote the manuscript. J.V.H. conducted protein purification and optimization. M.V.H. conducted timsTOF MS/MS data acquisition and evaluation. M.B. conceptualized the study, coordinated the research and wrote the manuscript. D.S. conceptualized the study and wrote the manuscript. All authors analyzed the results, participated in the final revision of the manuscript, and gave approval for publication.

Supplementary references

1. S. Son, M. Won, O. Green, N. Hananya, A. Sharma, Y. Jeon, J. H. Kwak, J. L. Sessler, D. Shabat, J. S. Kim, *Angew. Chem. Int. Ed.* **2019**, *58*, 1739-1743.
2. O. Green, T. Eilon, N. Hananya, S. Gutkin, C. R. Bauer, D. Shabat, *ACS Cent. Sci.* **2017**, *3*, 349-358.
3. T. Eilon-Shaffer, M. Roth-Konforti, A. Eldar-Boock, R. Satchi-Fainaro, D. Shabat, *Org. Biomol. Chem.* **2018**, *16*, 1708-1712.
4. A. K. Ferreira, Gottfried Wilhelm Leibniz Universität Hannover, Dissertation **2018**; bK. Ferreira, H.-Y. Hu, V. Fetz, H. Prochnow, B. Rais, P. P. Müller, M. Brönstrup, *Angew. Chem. Int. Ed.* **2017**, *56*, 8272-8276.
5. C. Peukert, L. N. B. Langer, S. M. Wegener, A. Tutov, J. P. Bankstahl, B. Karge, F. M. Bengel, T. L. Ross, M. Brönstrup, *J. Med. Chem.* **2021**, *64*, 12359-12378.
6. K. Ferreira, H.-Y. Hu, V. Fetz, H. Prochnow, B. Rais, P. P. Müller, M. Brönstrup, *Angew. Chem. Int. Ed.* **2017**, *56*, 8272-8276.
7. L. Pinkert, Y.-H. Lai, C. Peukert, S.-K. Hotop, B. Karge, L. M. Schulze, J. Grunenberg, M. Brönstrup, *J. Med. Chem.* **2021**, *64*, 15440-15460.
8. I.-K. Kim, H.-S. Yim, M.-K. Kim, D.-W. Kim, Y.-M. Kim, S.-S. Cha, S.-O. Kang, *J. Mol. Biol.* **2008**, *379*, 372-384.
9. C. F. Gonzalez, D. F. Ackerley, S. V. Lynch, A. Martin, *J. Biol. Chem.* **2005**, *280*, 22590-22595.

6. Publication 4 : Uptake mechanisms and regulatory responses to MECAM- and DOTAM-based artificial siderophores and their antibiotic conjugates in *Pseudomonas aeruginosa*

This chapter has been published as a peer-reviewed article in a scientific journal:

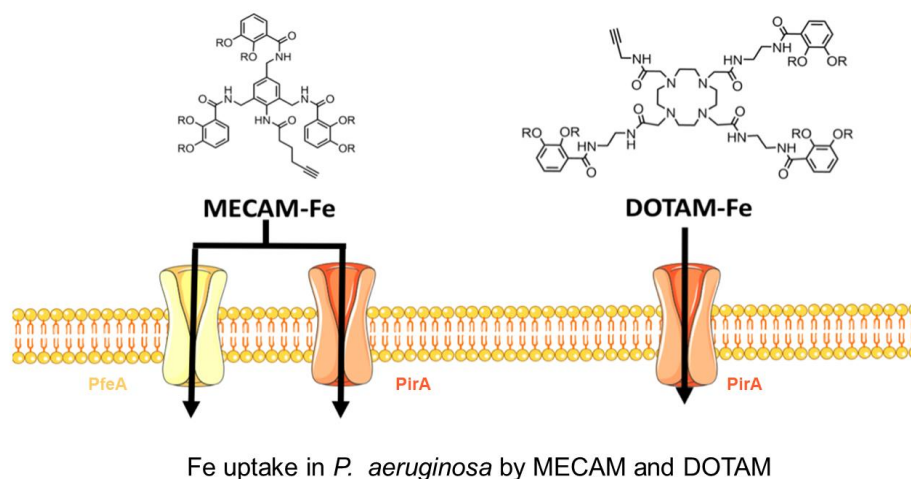
Sarah Fritsch, Véronique Gasser, Carsten Peukert, Lukas Pinkert, Lauriane Kuhn, Quentin Perraud, Vincent Normant, Mark Brönstrup and Isabelle J. Schalk.

"Uptake mechanisms and regulatory responses to MECAM- and DOTAM-based artificial siderophores and their antibiotic conjugates in *Pseudomonas aeruginosa*".

ACS Infectious Diseases, **2022**, 8, 6, 1134-1146

DOI: 10.1021/acsinfecdis.2c00049

Table of content graphic



Fe uptake in *P. aeruginosa* by MECAM and DOTAM

Abstract

The development of new antibiotics against Gram-negative bacteria has to deal with the low permeability of the outer membrane. This obstacle can be overcome by utilizing siderophore-dependent iron uptake pathways as entrance routes for antibiotic uptake. Iron-chelating siderophores are actively imported by bacteria, and their conjugation to antibiotics allows smuggling the latter into bacterial cells. Synthetic siderophore mimetics based on MECAM (1,3,5-*N,N',N''*-tris-(2,3-dihydroxybenzoyl)-triaminomethylbenzene) and DOTAM (1,4,7,10-tetrakis(carbamoylmethyl)-1,4,7,10-tetraazacyclododecane) cores, both chelating iron via catechol groups, have been recently applied as versatile carriers of functional cargo. In the present study, we show that MECAM and the MECAM-ampicillin conjugate **3** transport iron into *Pseudomonas aeruginosa* cells via the catechol-type outer membrane transporters PfeA and PirA and DOTAM solely via PirA. Differential proteomics and quantitative real-time polymerase chain reaction (qRT-PCR) showed that MECAM import induced the expression of *pfeA*, whereas **3** led to an increase in the expression of *pfeA* and *ampc*, a gene conferring ampicillin resistance. The presence of DOTAM did not induce the expression of *pirA* but upregulated the expression of two zinc transporters (*cntO* and PA0781), pointing out that bacteria become zinc starved in the presence of this compound. Iron uptake experiments with radioactive ^{55}Fe demonstrated that import of this nutrient by MECAM and DOTAM was as efficient as with the natural siderophore enterobactin. The study provides a functional validation for DOTAM- and MECAM-based artificial siderophore mimetics as vehicles for the delivery of cargo into Gram-negative bacteria.

6.1 Introduction

There is an urgent need to find new antibiotics to counter bacterial antibiotic resistance and the situation is particularly alarming for Gram-negative bacteria. The challenge associated with Gram-negative bacteria is the presence of an additional, outer membrane that reduces drug penetration compared to Gram-positive bacteria. Nutrient import pathways involving TonB-dependent transporters (TBDT) are promising entrance routes to deliver antibiotic drugs into Gram-negative bacteria. These TBDTs are embedded in the outer membrane and have a β -barrel structure with a lumen that is closed by the *N*-terminal region of the transporter forming a plug.¹ The substrate binding site is usually specific for a family of structurally related compounds. Uptake of the substrate depends on the proton motive force, that is transmitted by coupling the TBDT with the TonB protein anchored in the inner membrane in complex with two other inner membrane proteins ExbB and ExbD.²⁻⁶

TBDTs are involved in the import of essential nutrients as vitamin B12, oligosaccharides and biological metals, but have been mostly investigated for their ability to import ferric iron *via* siderophores.^{1,7-11} Ferric iron (the iron form present in aerobic conditions) is poorly soluble in aqueous solutions and poorly bioavailable in the host during infections, because it is mainly protein-bound. To increase access to ferric iron, bacteria produce and secrete siderophores who serve to sequester iron from the environment and transport it back into bacteria *via* TBDTs.¹² Siderophores are small molecules and are usually classified in four groups according to the nature of the dentates used to chelate the ferric iron: hydroxamates (such as ferrioxamine B or ferrichrome), catecholate (enterobactin), carboxylate (rhizobactin) and mixed siderophores (pyoverdine).^{12,13} Siderophore are also characterized by a strong affinity for iron, which, in the case of enterobactin (ENT), can reach values up to 10^{42} M^{-1} .^{14,15} Often the bacteria produce their own siderophores, but can as well use siderophores produced by other microorganisms in a piracy strategy.¹⁶⁻¹⁸ The opportunist pathogen *P. aeruginosa* produces the two endogenous siderophores pyoverdine (PVD) and pyocheline (PCH)¹⁹, while many chelators from other pathogens can be hijacked as so-called xenosiderophores (Table S6.1). For each of these siderophores or xenosiderophores, *P. aeruginosa* expresses a specific TBDT and other proteins allowing the dissociation of iron from the chelator.^{17,18,20,21} These iron uptake pathways are generally expressed at very low levels and bacteria only induce the expression of the most efficient pathway(s) for iron acquisition, depending on the iron sources present.¹⁰ Under iron-restricted condition, *P. aeruginosa* detects the presence of xenosiderophores in its environment using sigma and anti-sigma factors, two component systems, and transcriptional regulators of the AraC family (Table S6.1).^{10,12-14} This transcriptional regulators activate in the presence of ferri-xenosiderophores the transcription of the gene encoding the (xeno-)siderophore-corresponding TBDTs as well as genes encoding other proteins involved in the pathway.

When the intracellular iron concentration reaches a certain level, the transcriptional regulator Fur represses the transcription of all genes involved in iron import.¹¹ Numerous studies show that these iron import pathways can be used to smuggle antibiotics into bacteria through a 'Trojan Horse' approach.^{22–25} If the antibiotic is linked covalently to siderophore units, it is internalized together with the bound ferric iron into the bacterial cell^{22,25–30}. The first antibiotic on the market that chelates iron and enters pathogenic cells via the iron uptake pathways is cefiderocol, a cephalosporin-catechol conjugate.^{31–33} Siderophores coupled to fluorescent probes or to probes chelating gallium-68 nuclide can also be used to visualize, detect or identify microbial pathogens during infections in animals.^{34–38}

The respective TBDTs allowing the accumulation of these antibiotic-siderophore conjugates have not been identified in most cases. The goal of the present work was to evaluate the ability of two siderophore mimetics based on the MECAM (1,3,5-N,N',N''-tris-(2,3-dihydroxybenzoyl)-triaminomethylbenzene) (**1**) and DOTAM (1,4,7,10-Tetrakis(carbamoylmethyl)-1,4,7,10-tetraazacyclododecane) (**4**) scaffolds (Figure 6.1),^{35,39,40} (I) to transport iron and antibiotics into *P. aeruginosa* cells, (II) to identify the transporters involved and (III) to evaluate the modulation of its different iron uptake pathways in the presence of these vectors and their corresponding antibiotic conjugates. MECAM **1** is an analogue of ENT, a tris-catechol-like siderophore produced by *E. coli* that is used as a xenosiderophore by *P. aeruginosa*.^{4,17,41,42} We also examined the MECAM-ampicillin conjugate **3**, which has a minimal inhibitory concentration lower than 90 nM on *E. coli* and *A. baumannii* growth and no activity on *P. aeruginosa*.⁴⁰ Ampicillin is usually inactive on *P. aeruginosa* strains due to the low permeability of the outer membrane and its ability to induce the expression of the β -lactamase AmpC.⁴³ The (DOTAM)-based siderophore **4** is a bifunctional compound with two separate metal binding sites, one for iron at the catechol units and a second one at the cyclen.³⁵ This vector has been linked either to an antibiotic (daptomycin; compound **6**) or to a DOTA unit commonly used for a radionuclide chelation (compound **7**). Conjugate **7** was found to be suitable for positron emission tomography (PET) imaging and was able to discern *E. coli* infection from a lipopolysaccharide-triggered, sterile inflammation.³⁹ For both vectors MECAM and DOTAM, the deacetylated and acetylated forms were tested, as the acetylated forms avoid *in vivo* deactivation of the iron chelating units by catechol-O-methyltransferases.⁴⁴ Because the antibiotic conjugates had no antimicrobial activity on *P. aeruginosa* (Table S6.2), they were used here as tools to study uptake mechanisms and responses.

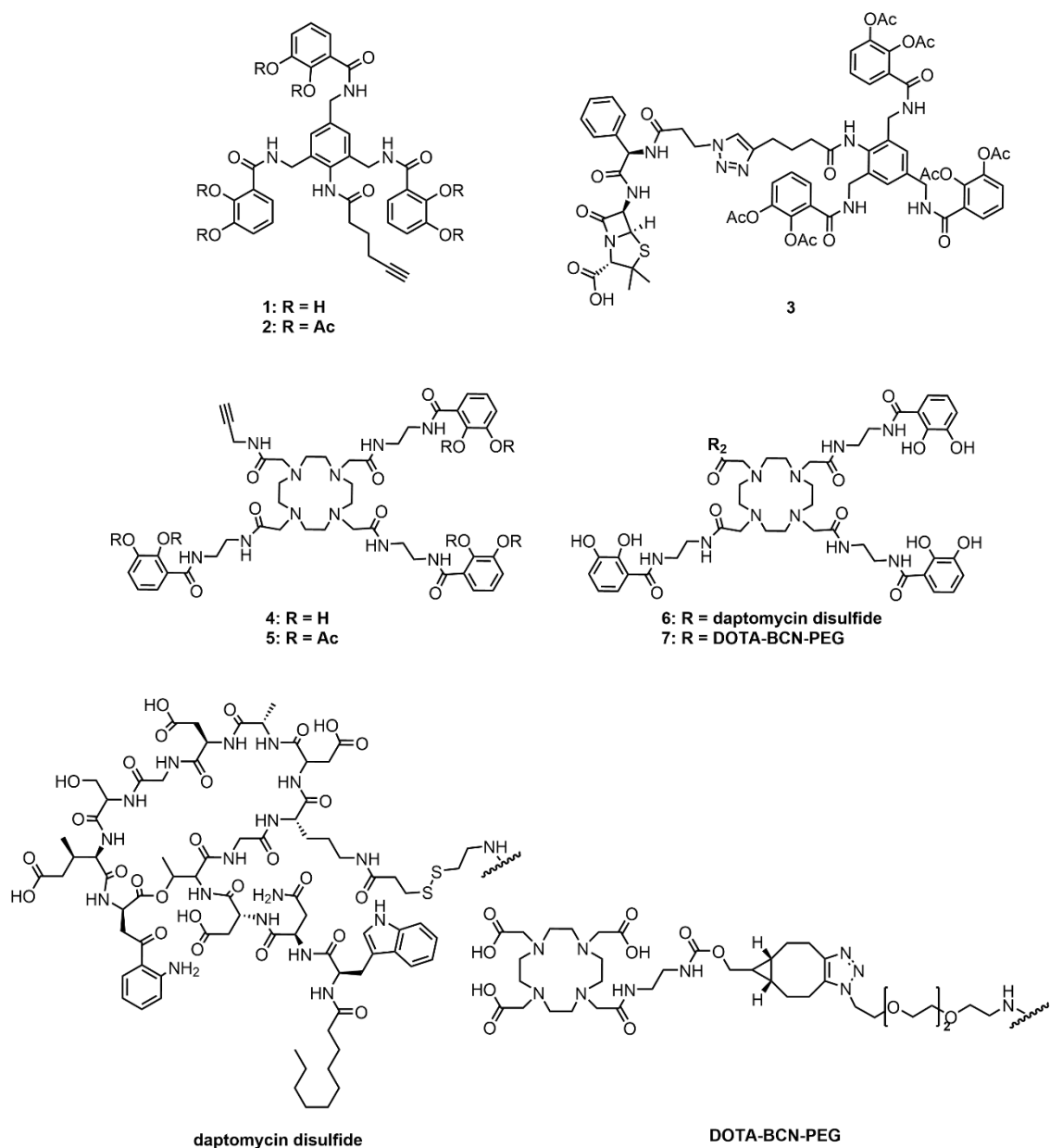


Figure 6.1. Structures of MECAM (**1/2**), DOTAM (**4/5**) and the conjugates **3**, **6** and **7**.

6.2 Results and Discussion

6.2.1 MECAM- and DOTAM-based artificial siderophores compete for ferric iron with PVD.

In order to investigate whether MECAM and DOTAM could compete for iron with *P. aeruginosa*'s endogeneous siderophores PVD and PCH, a fluorescence assay was applied. PVD, which has a higher affinity for ferric iron than PCH (K_a of $10^{30.8} \text{ M}^{-1}$ for PVD vs 10^{18} M^{-1} for PCH), emits fluorescence at 447 nm in its apo form upon excitation at 400 nm (pH 7.0), whereas the PVD-Fe complex is non-fluorescent.⁴⁵⁻⁴⁷ Non-fluorescent PVD-Fe (10 μM) was incubated with increasing concentrations of MECAM (**1**), DOTAM (**4**), the corresponding

conjugates, and the positive control siderophores ENT and ferrichrome (FERRI)¹⁷ (Figure 6.2). A complete removal of ferric iron from PVD was only observed for ENT at concentrations of approximately 20 μM as previously described, ferrichrome was unable to completely remove iron from PVD at the tested concentrations.¹⁷ These results are consistent with the siderophores' affinity for iron: K_a of 10^{49} M^{-1} for ENT¹⁵, 10^{29} M^{-1} for ferrichrome⁴⁸, and $10^{30.8} \text{ M}^{-1}$ for PVD.⁴⁵ The normalized fluorescence values of **1** and **4** indicate that these two siderophores exhibited a similar efficiency in removing iron from PVD, but they were less efficient than FERRI or ENT (Figure 6.2A). The linkage of an antibiotic moiety to either of the siderophore conjugates **3**, **6** or **7** did not significantly affect their iron chelation properties (Figures 6.2B and 6.2C).

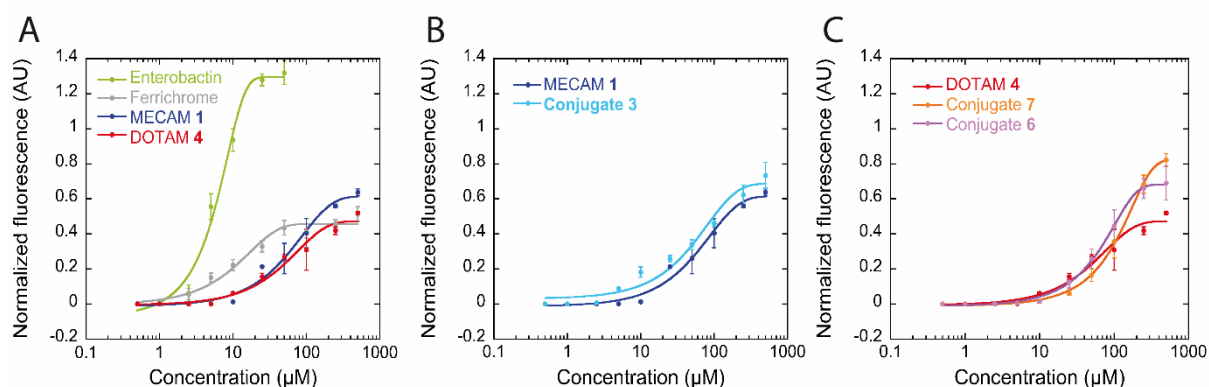


Figure 6.2. Iron scavenging from PVD-Fe by MECAM- and DOTAM-based siderophores. PVD-Fe at 10 μM was incubated with increasing concentrations of siderophores or conjugates for 48 h in 100 mM HEPES pH 7.4. Apo PVD formation was followed by monitoring its fluorescence at 447 nm (excitation at 400 nm). In panel A, the experiment was also carried out exactly in the same conditions with ENT and ferrichrome to compare the iron scavenging properties of compounds **1**, **3** (panel B), **4**, **6** and **7** (panel C). Standard deviations were calculated from three independent experiments.

6.2.2 MECAMs 1-3 induce changes in expression of iron uptake-associated proteins in *P. aeruginosa*.

Because MECAM-ampicillin **3** showed no antibiotic effect on *P. aeruginosa* cells, the compound was suited as a tool to investigate the phenotypic adaptation of *P. aeruginosa* to its presence using quantitative proteomics. *P. aeruginosa* adapts the expression of its different iron import pathways according to environmental stimuli such as natural or synthetic siderophores.^{17,20,42,49–52} Cells were grown over 8 h in iron-restricted medium (CAA medium, iron concentration = 20 nM (acc. to our previous work⁵³) in the absence or presence of **1-3** and analyzed by differential proteomics (Figure 6.3 for compounds **1** and **3** and Figure S6.1 for

compound **2**). The deacetylated and acetylated forms of MECAM (**1/ 2**) strongly induced the expression of the TBDT PfeA. A moderate overexpression of PirA was observed in the case of MECAM **2** (Figure 6.3C). PfeA and PirA have been described in the literature as the TBDTs for ferric iron uptake by ENT in *P. aeruginosa*.^{4,41,42,54} Their transcription is regulated by their corresponding two-component systems, with the sensor PfeS and the transcriptional regulator PfeR for *pfeA* and PirS (sensor) and PirR (transcriptional regulator) for *pirA* (Figure S6.2).^{17,42,55} For example, to induce *pfeA* transcription, ferri-ENT, after its uptake across the outer membrane, interacts in the bacterial periplasm with PfeS, which then releases PfeR to activate *pfeA* transcription. In analogy, an induction of *pfeA* expression in the presence of **1** and **2** provides clear evidence that both compounds were able to cross *P. aeruginosa*'s outer membrane to interact with PfeS in the bacterial periplasm. An increased expression of FemA (yersiniabactin TBDT) was also observed in the presence of **1** and **2**, albeit with low statistical significance (Figure 6.3C and S6.1C). The presence of **3** also induced the expression of PfeA, but to a lower extent compared to **1** and **2**, whereas PirA expression remained unchanged. In parallel, the expression of proteins involved in ferric iron uptake by PCH was repressed by **1-3** (Figure 6.3D), whereas proteins associated with the PVD pathway were not affected (Figure 3F). Notably, **3** also led to a strong induction of AmpC (Figure 6.3E). The protein data for **1** and **3** were confirmed by RT-qPCR for the corresponding genes *pfeA*, *fptA*, *fpvA* and *ampC* (Figure S6.3). Overall, **1-3** induced the transcription and expression of the gene encoding PfeA, suggesting that (i) the transporter was able to import the iron-loaded compounds **1-3** into *P. aeruginosa* cells and that (ii) **1-3** were able to activate the two-component system PfeS/PfeR (Figure S6.2). This phenotypic adaptation of the iron uptake pathway was accompanied by a repression of genes involved in the PCH-dependent iron uptake pathway, which forced the bacteria to preferentially use **1-3** to access extracellular iron. The induction of *ampC* expression suggests that the absence of antibiotic activity of **3** is due to the serine- β -lactamase activity of AmpC, which hydrolysed the β -lactam ring of MECAM-ampicillin.

6.2.3 MECAM **1** and conjugate **3** transport ⁵⁵Fe into *P. aeruginosa* cells mainly via PfeA and to a lower extent via PirA.

In order to evaluate the ability of **1** and the corresponding conjugate **3** to transport iron into *P. aeruginosa* cells, the compounds were loaded with radioactive ⁵⁵Fe and exposed to a $\Delta pvdF\Delta pchA$ *P. aeruginosa* mutant, that is unable to produce the endogenous siderophores PVD and PCH.⁵¹ This mutant was used to avoid any uptake of ⁵⁵Fe via the endogenous siderophores. The experiment was also carried out with *pirA*- and *pfeA*-deficient mutants of $\Delta pvdF\Delta pchA$ (Table S6.3), as these genes encode TBDTs involved in iron acquisition by **1-3** (Figure 6.3) and by ENT.^{42, 54, 56}

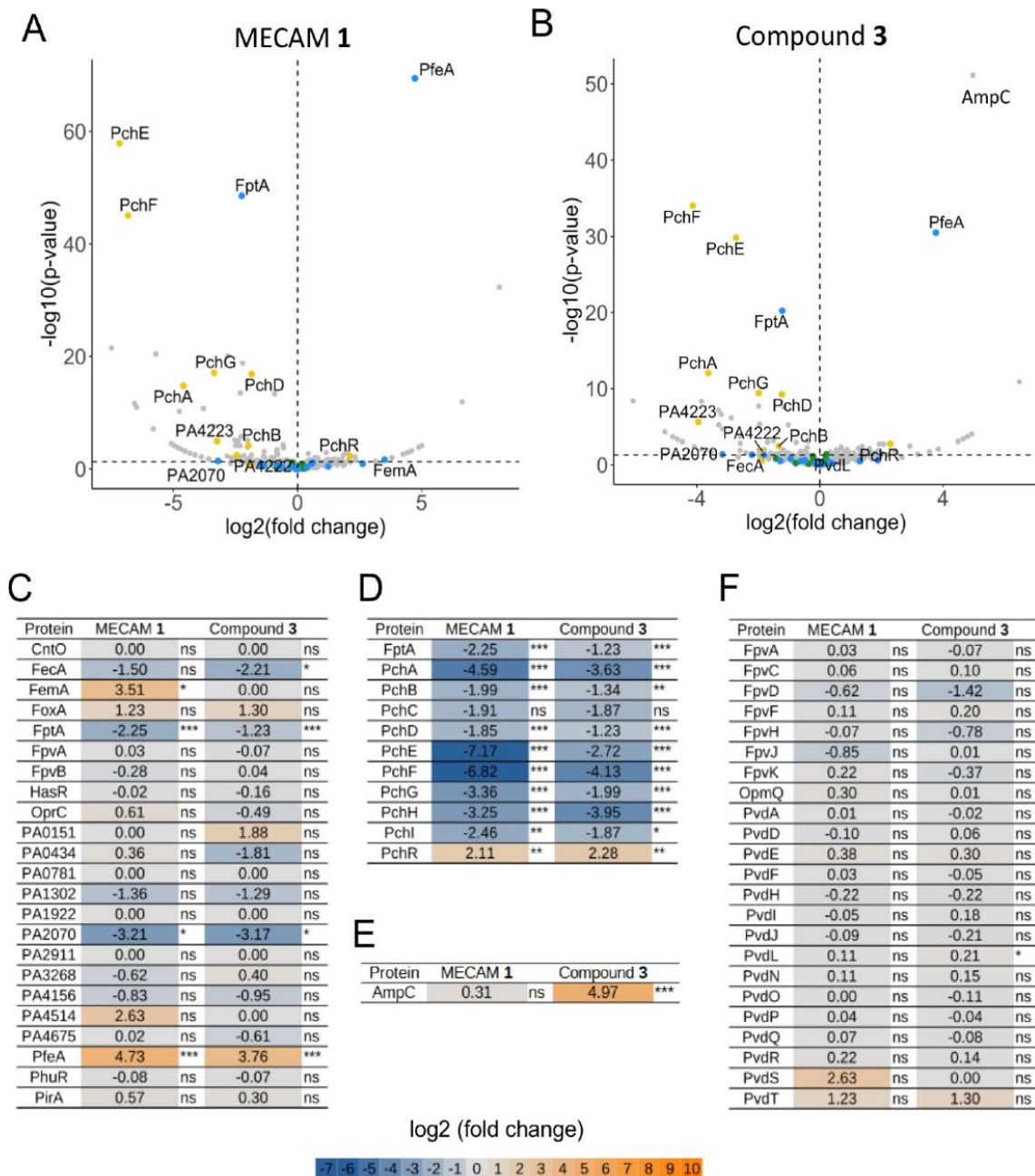


Figure 6.3. Modulation of protein expression in *P. aeruginosa* in the presence of MECAMs 1 and 3. Proteomic analyses were performed on *P. aeruginosa* PAO1 strains grown overnight in CAA medium supplemented with 10 μ M 1 (A) or 3 (B). Log₂-fold changes in protein abundances and corresponding -log₁₀-transformed p-values relative to untreated control samples are shown in volcano plots. Proteins of the PCH pathway are represented by yellow dots, those of the PVD pathway by green dots, and the TBDTs by blue dots. C, D, E and F show heat maps of log₂-fold changes in TBDT proteins (C), proteins involved in the PCH pathway (D), AmpC protein (E) and proteins of the PVD pathway (F). The darker the shade of blue, the more expression of the protein is repressed; the darker the shade of orange, the more expression of the protein is induced. NS: data not significant; *p < 0.05, **p < 0.01, and ***p < 0.001. Data for 2 are presented in Figure S6.1.

Bacteria were grown under iron starvation conditions in order to induce the expression of iron uptake pathways. Both **1** and its corresponding conjugate **3** transported between 250 and 270 pmol ^{55}Fe per $\text{OD}_{600\text{ nm}}$ after 1 h incubation, whereas around 200 pmol ^{55}Fe per $\text{OD}_{600\text{ nm}}$ were imported in the presence of ENT (Figure 6.4A). This indicates that **1** and **3** were at least as efficient as the natural siderophore ENT with respect to uptake of iron in *P. aeruginosa* cells. The ^{55}Fe uptake by **1** and **3** was completely abolished in the presence of the protonophore inhibitor carbonyl cyanide m-chlorophenyl hydrazine (CCCP). Because CCCP inhibits any TonB-dependent uptake in bacteria,^{57,58} this finding indicates that the uptake of **1** and **3** was not due to passive diffusion *via* porins, but due to an energy-dependent transport relying on TonB. The deletion of the gene *pirA* did not affect ^{55}Fe uptake by **1**, but deletion of *pfeA* resulted in an 80% decrease of ^{55}Fe uptake at 2 h. This indicates that uptake of iron by MECAM occurs essentially *via* PfeA. In the case of **3**, *pfeA* and *pirA* deletions had inhibitory effects of 50% and 22%, respectively. In conclusion, these data show that **1** and **3** were able to transport iron as efficiently as ENT into *P. aeruginosa* cells, with PfeA being the major TBDT involved, while PirA served as a secondary transporter.

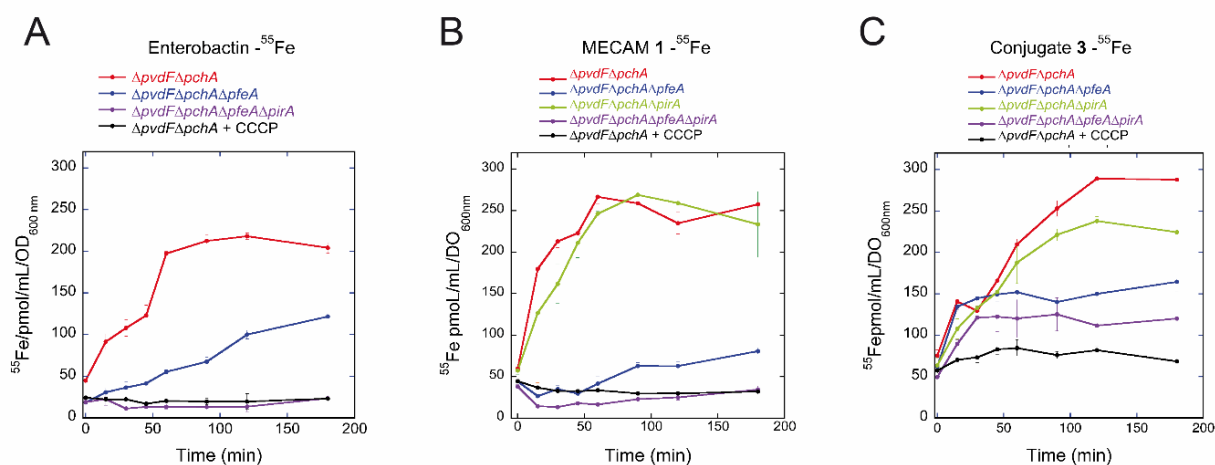


Figure 6.4. ^{55}Fe uptake in *P. aeruginosa* strains mediated by the siderophores enterobactin, **1** and **3**. *P. aeruginosa* $\Delta pvdF\Delta pchA$ and its isogenic $\Delta pfeA$ and $\Delta pirA$ mutants, grown in iron-restricted CAA medium and in the presence of 10 μM ENT (A), **1** (B) or **3** (C) to induce the corresponding uptake pathway, were incubated with 500 nM ENT- ^{55}Fe (A), **1**- ^{55}Fe (B) or **3**- ^{55}Fe (C). The amount of ^{55}Fe taken up into the bacteria was measured as a function of time. As a control, the experiment was repeated in the presence of the protonophore CCCP (200 μM). Errors bars were calculated from three independent biological replicates.

6.2.4 PirA efficiently replaces PfeA in iron uptake via 1 and 3.

Next, we sought to determine whether the deletion of *pfeA* or/and *pirA* would have an inhibitory effect on *P. aeruginosa* growth in iron-restricted conditions in the presence of these two compounds. If a given gene deletion leads to a growth inhibition in the presence of the tested siderophore, the knocked-out gene is involved in iron acquisition by the tested siderophore.⁵⁸ We used a strain with a $\Delta pvdF\Delta pchA$ background that was unable to produce the siderophores PVD and PCH, and the corresponding $\Delta pfeA$ and $\Delta pirA$ mutants (Table S6.3). $\Delta pvdF\Delta pchA$ is able to grow in an iron-deficient environment probably using citrate as a siderophore or iron reduction systems with import of ferrous iron through the *feoABC* system.^{59–61} $\Delta pvdF\Delta pchA$ was grown in CAA medium $\pm 10 \mu\text{M}$ of **1** or **3**. The presence of an excess of **1** or **3** chelates all iron traces present in the growth medium making this metal no longer accessible for low affinity import systems. If growth of $\Delta pvdF\Delta pchA$ is observed in the presence of **1** or **3**, it demonstrates that the bacteria can access iron *via* these two iron chelators.

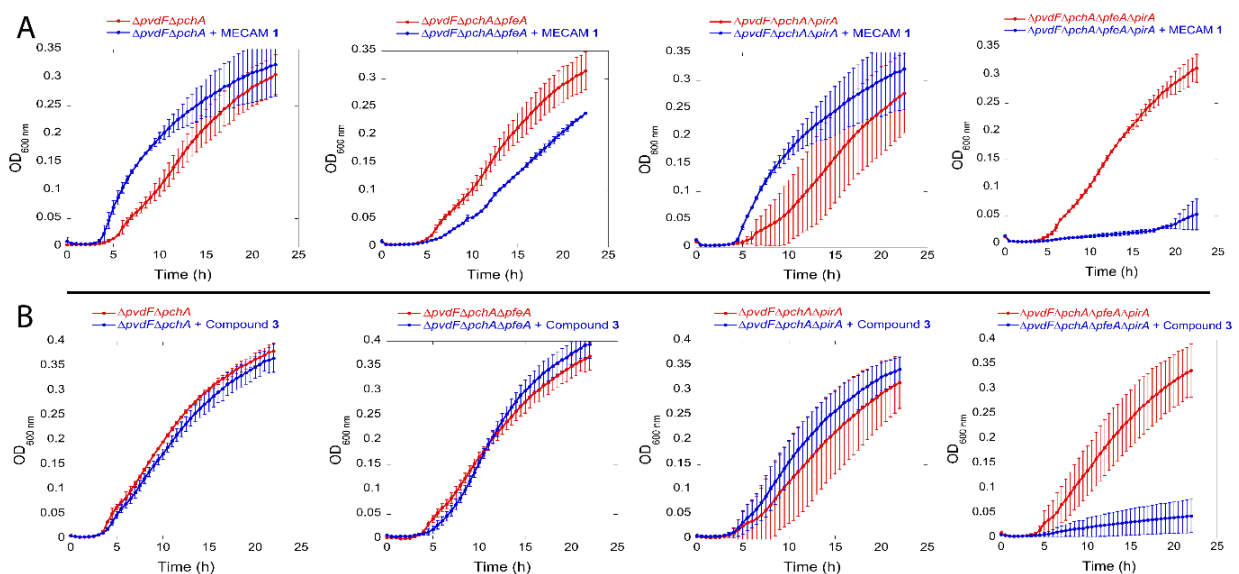


Figure 6.5. Growth of TBDDT-deficient *P. aeruginosa* mutants in the presence of **1** or **3**. A PVD and PCH-deficient strain of *P. aeruginosa* ($\Delta pvdF\Delta pchA$) and its corresponding TBDDT deletion mutants were used. Strains were grown in CAA medium in the absence (kinetics in red) or presence (kinetics in blue) of $10 \mu\text{M}$ **1** (A) or **3** (B). Growth was followed by monitoring the optical density (OD) at 600 nm. Errors bars were calculated from three independent biological replicates.

This is illustrated in Figure S6.4 with bacillibactin, a catechol type siderophore unable to be used by *P. aeruginosa* cells to import iron: in the presence of 10 μ M bacillibactin a strong growth inhibition is observed. Moreover, the presence of 1 or 3, the single deletion of *pfeA* slightly affected bacterial growth, whereas the single deletion of *pirA* had no effect (Figure 6.5). In contrast, the deletion of both *pfeA* and *pirA* completely abolished bacterial growth. These results confirm that PfeA is the major TBDT involved in iron acquisition by 1 and 3. However, if *pfeA* was deleted PirA replaced PfeA efficiently. The same mechanism has been described for iron uptake by ENT, where PirA played a key role only if PfeA was absent.⁴²

6.2.5 Gene expression modulation in *P. aeruginosa* grown in the presence of DOTAM 4 and conjugates 6 and 7.

The same proteomic strategy as described above was used to examine genes expression changes in *P. aeruginosa* PAO1 in the presence of the DOTAM-based siderophore 4 and the corresponding conjugates 6 and 7 (Figure 6.6). We were surprised to notice that none of the three compounds induced the expression of TBDTs involved in iron uptake to *P. aeruginosa* cells. Instead, the presence of 4 and 7 increased the expression of CntO and PA0781 (ZnuD), two TBDTs involved in Zn uptake. This was confirmed by RT-qPCR analysis (Figure S6.5). CntO imports zinc *via* the metallophore pseudopaline,^{9,62,63} while ZnuD transports zinc ions without the help of any metal chelator.^{64, 65} These data suggest that 4 and 7 chelated zinc, and bacteria became zinc starved or that 4 and 7 can somehow induce the expression of these two genes via a transcriptional regulator. Compound 6 did not exhibit this effect. In addition, the expression of proteins of the PCH pathway was repressed by all three compounds. This suggests that less PCH-Fe complexes were formed, probably because 4, 6 and 7 chelated iron.

6.2.6 Deletion of *pirA* inhibits bacterial growth in the presence of DOTAM.

For the DOTAM-based siderophores 4, 6 and 7, ⁵⁵Fe uptake assays could not be carried out due to precipitation of the compounds and hence significant background noise in the radioactivity signal. In consequence, only the growth assay under iron restricted conditions has been used to test for iron transport of DOTAM and its conjugates into bacteria and to identify the potentially TBDTs involved. $\Delta pvdF\Delta pchA$, the *P. aeruginosa* strain unable to produce PVD and PCH, grew with the same efficiency in the absence or presence of 10 μ M of 4, indicating that bacteria were able to use this compound to access iron (Figure 6.7). However, growth in the presence of 4 was completely abrogated upon deletion of the *pirA* gene, while the *pfeA* knockout had no effect. This finding implies that 4 transported iron exclusively via PirA.

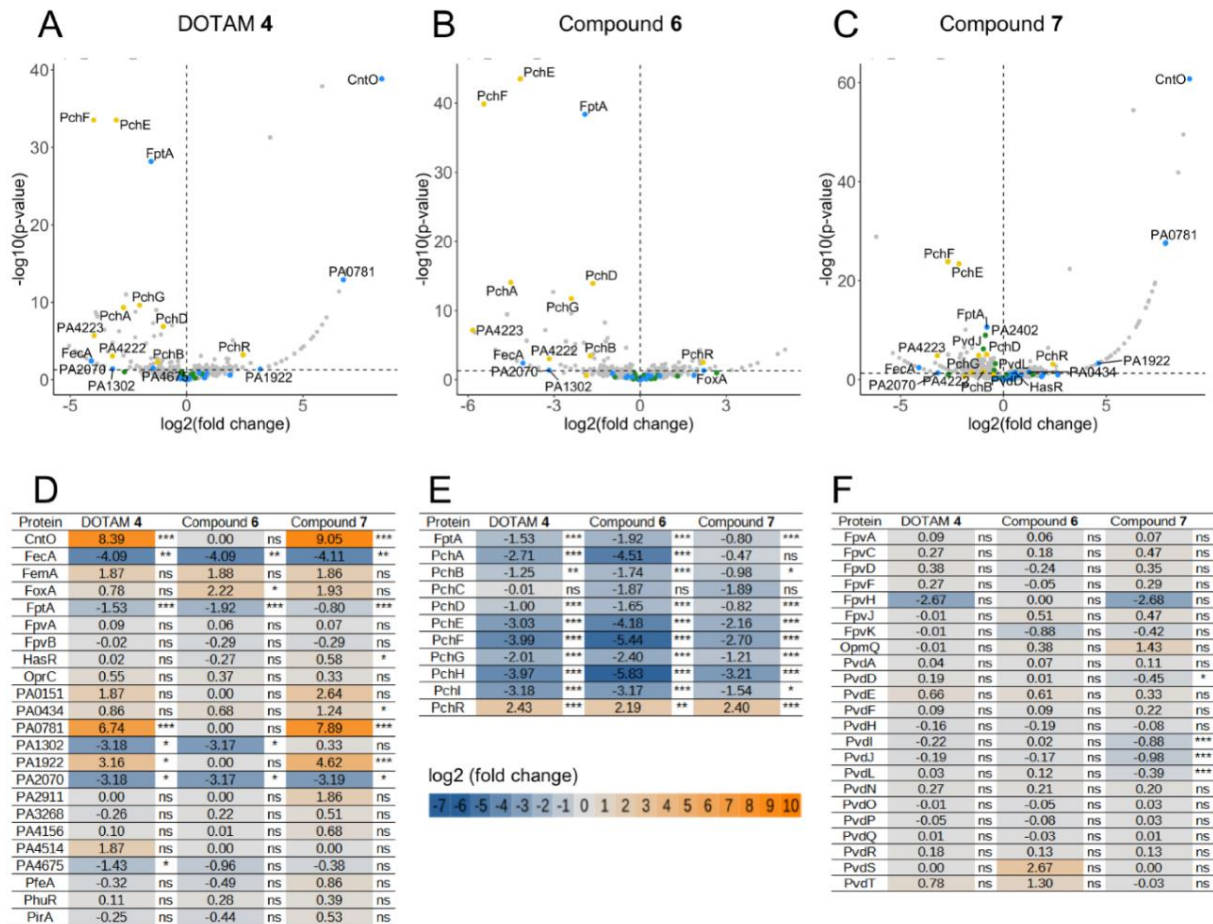


Figure 6.6. Modulation of protein expression in *P. aeruginosa* in the presence of DOTAM-based siderophore 4 and the associated conjugates 6 and 7. Proteomic analyses were performed on *P. aeruginosa* PAO1 strains grown overnight in CAA medium supplemented with 10 μ M of DOTAM-based siderophores 4 (A), 6 (B) or 7 (C). Log₂-fold changes in protein abundances and corresponding -log₁₀-transformed p-values relative to untreated control samples are shown in volcano plots. Proteins of the PCH pathway are represented by yellow dots, those of the PVD pathway by green dots, and the TBBDTs by blue dots. C, D, E and F show heat maps of log₂-fold changes in TBBDT proteins (C), proteins involved in the PCH pathway (D), AmpC protein (E) and proteins of the PVD pathway (F). The darker the shade of blue, the more expression of the protein is repressed; the darker the shade of orange, the more expression of the protein is induced. NS: data not significant; *p < 0.05, **p < 0.01, and ***p < 0.001. Data for 5 are presented in Figure S6.

In the presence of **6** or **7**, $\Delta pvdF\Delta pchA$ growth was decreased by 63% and 82%, respectively, compared to the growth in the absence of any compounds. This indicating that **6** and **7** were not efficient in making iron accessible to *P. aeruginosa* cells, although the compounds were able to chelate iron (Figure 6.2). The residual growth observed with **6** appears to be PirA dependent, as the mutation of *pirA* gene abolished almost the growth completely. In

conclusion, iron is transported by DOTAM 4 into *P. aeruginosa* cells by PirA, but this uptake ability is affected by the presence of the payloads incorporated in 6 and 7.

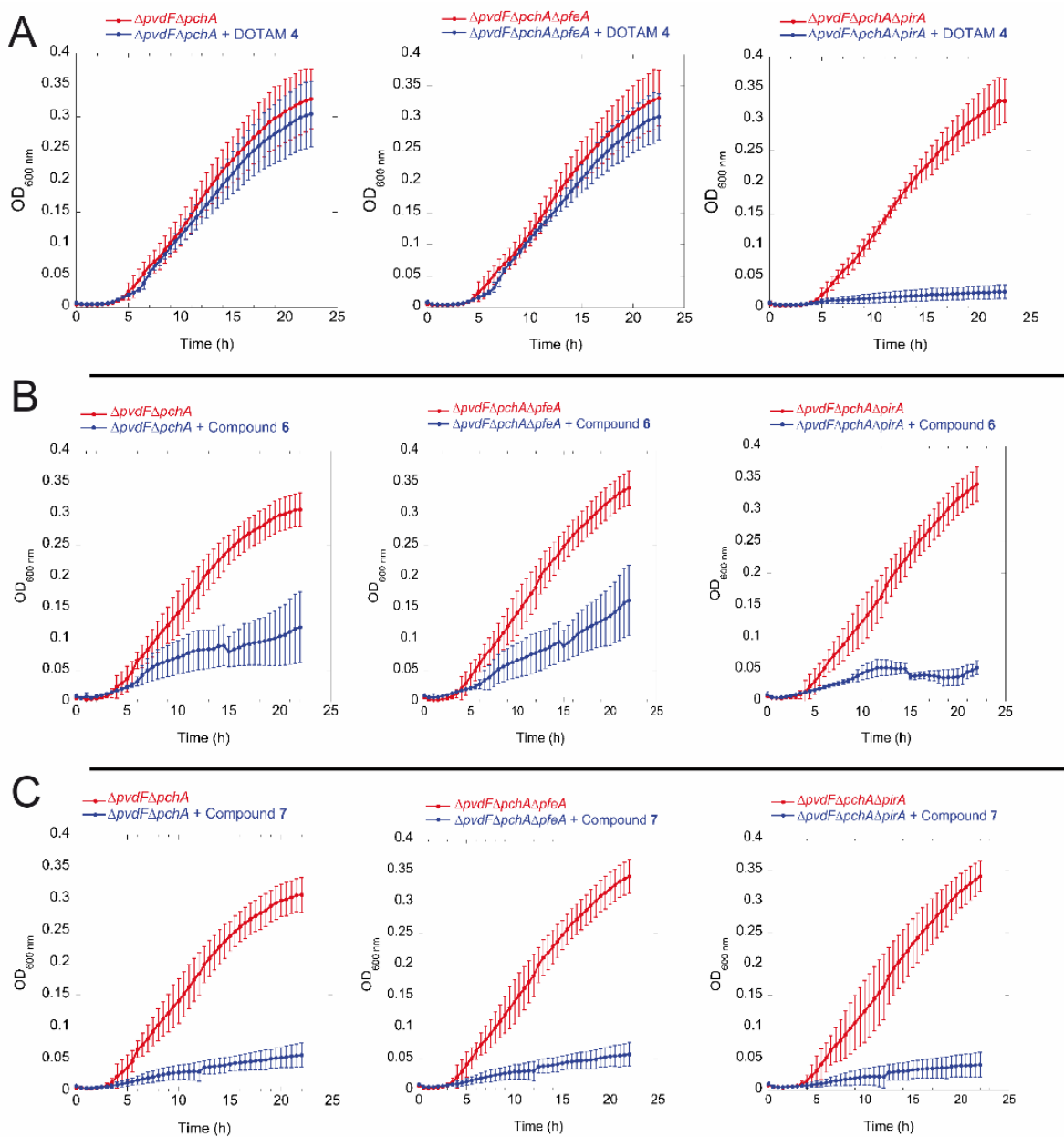


Figure 6.7. Growth of TBDDT-deficient *P. aeruginosa* mutants in the presence of DOTAM-based siderophores 4, 6 and 7. A PVD and PCH-deficient strain of *P. aeruginosa* ($\Delta pvdF\Delta pchA$) and its corresponding TBDDT deletion mutants were used. Strains were grown in CAA medium in the absence (kinetics in red) or presence (kinetics in blue) of 10 μ M 4 (A), 6 (B) or 7 (C). Growth was followed by monitoring the optical density (OD) at 600 nm. Errors bars were calculated from three independent biological replicates.

6.3 Discussion

Bacteria possess the ability to use artificial siderophores to access iron, and antibiotics can be linked to these compounds in order to enhance their transport across the bacterial membranes.^{22,28–30} The use of synthetic siderophores and their antibiotic conjugates is possible, because bacteria often entertain a large panel of TBDTs involved in iron acquisition with different substrate specificities.^{66–68} *P. aeruginosa* has at least 15 genes encoding TBDTs involved in iron acquisition by siderophores and xenosiderophores.^{17,69} According to the present work, MECAM behaves in a similar way as ENT with respect to iron uptake in *P. aeruginosa* cells, except that MECAM seems to have a lower affinity for ferric ion chelation than ENT (Figure 6.2).

In the literature, PfeA is considered as the major and PirA as a secondary TBDT for ferri-ENT.^{42, 54} Here, we observed that ferri-MECAM was mostly imported across the outer membrane by PfeA, but if this transporter was not expressed, PirA assumed the role very effectively (Figure 6.5). To date, the natural siderophore transported by PirA has not been identified, but it has been shown that PirA was able to import iron via catecholamines such as the neuromediators L-DOPA and norepinephrine.⁵⁸ The coupling of MECAM to ampicillin did not change its ability to chelate iron and transport it into *P. aeruginosa* cells via PfeA or PirA (Figures 6.4 and 6.5). However, PirA seems to be more relevant for the uptake of ferric **3** than for ferric **1**, suggesting that the presence of the antibiotic slightly affected the affinity of PfeA for **3** (Figure 6.4). Moreover, iron was effectively dissociated from **1** and **3**, as demonstrated by the growth of *P. aeruginosa* unable to produce its own siderophores PVD and PCH (Figure 6.5). If the iron remained chelated by MECAM in the bacteria, making it non-bioavailable, growth would be significantly affected.

The presence of **1-3** had several effects on the proteome of *P. aeruginosa*. First, the three compounds induced a strong expression of PfeA. This has also been reported previously by us for ENT, but also for another synthetic triscatechol siderophore, free or coupled with linezolid.^{51, 52} The fact that both the MECAM and MECAM-ampicillin compounds induce the expression of the gene encoding their transporter PfeA is a clear advantage for the uptake of antibiotics by this transporter via a Trojan horse strategy, because translocation gets amplified. The conjugation to ampicillin did not affect the ability of MECAM to be translocated through the TBDTs PfeA and PirA and to interact with the sensor PfeS. In contrast, MECAM **1/2** and **3** were unable to interact with PirS and activate the transcription of *pirA*. The induction of PfeA expression went hand in hand with a repression of proteins involved in the PCH-dependent iron uptake pathway, suggesting that *P. aeruginosa* cells will use MECAM or the conjugate MECAM-ampicillin to acquire iron rather than its own siderophore PCH. However, the expression of the proteins of the PVD-dependent iron uptake pathway was not affected; in

contrast, the presence of ENT in the same growth conditions repressed both the PCH and the PVD pathways.^{17, 51, 52} and we assume that this is due to the higher iron affinity of ENT compared to the MECAMs **1-3**. Such phenotypic adaptation of *P. aeruginosa* cells to the presence of different xenosiderophores with different affinities for iron has already been described previously with ENT, vibriobactin, ferrichrome, nocardamine and yersiniabactin.^{17,18} The observation that the effects on *P. aeruginosa* proteome obtained with MECAMs **1** and **2** were similar indicates that both compounds exert similar siderophore effects, and that the acetyl groups protecting the catechol groups in MECAM **2** were hydrolyzed in the bacterial growth media, as found for many other acetyl-protected catechols.^{35, 44} The presence of **3** in *P. aeruginosa* also induced the expression of *ampC*, which explains the absence of antibiotic activity for this conjugate. Thus, *P. aeruginosa* developed a resistance mechanism targeting the antibiotic and not at the expression level of the iron import pathways used by the vector. This illustrates that the vectorization of antibiotics by siderophores will not necessarily prevent the development of resistance against the antibiotic component.

All these data show that MECAM is a promising vector for the import of cargo into *P. aeruginosa* cells via the PfeA and PirA TBDTs. It should be kept in mind that ENT in *P. aeruginosa* cells is hydrolyzed in the bacterial periplasm and not in the cytoplasm, with this siderophore certainly never entering the cytoplasm;⁷⁰ also MECAM was shown to reach the periplasm, not the cytoplasm.⁴⁰ Consequently, to combat *P. aeruginosa*, it seems more promising to conjugate MECAM with antibiotics addressing targets in the periplasm. Along this line, a conjugate of MECAM to the relatively bulky cyclic lipopeptide daptomycin was recently prepared.⁴⁰ It showed promising activity against *A. baumannii*, but not against *P. aeruginosa*. Thus, it might be interesting to vectorise smaller, linear antimicrobial peptides affecting the integrity of the internal membrane by the MECAM core.

The DOTAM **4** has two metal binding sites, one triscatecholate site to chelate iron and the cyclen-based site, that has been used for chelating e.g. lanthanides, zinc³⁵ or radioactive gallium-68 for bacteria-specific PET imaging.^{35,39} The competition experiment for iron with PVD showed that this vector had an affinity for iron that was comparable to MECAM. Proteomics data show that DOTAMs **4**, **5** and **7** chelated zinc very efficiently, as their presence induced an increase in the expression of two TBDTs involved in zinc acquisition, CntO and PA0781 (ZnuD). According to *P. aeruginosa* genome,⁶⁹ no transcriptional regulating sigma factors or two-component systems are associated to *cntO* and *PA0781* genes. Consequently the induction of the expression of these two zinc transporters is probably due to zinc starvation and involves the transcriptional regulator Zur^{64,71} and not to the interaction of DOTAM with the sensor of some two-component system as shown above for MECAM. Compounds **4**, **5** and **7** certainly chelate zinc in the environment of the bacteria, rendering bacterial cells zinc deficient.

The upregulating effect was not observed with the DOTAM-daptomycin **6** compound, suggesting that the presence of the antibiotic affects the ability of the DOTAM moiety to chelate zinc. According to the growth experiments with the strain unable to produce the endogenous siderophores PVD and PCH, DOTAM **4/5** imports iron into *P. aeruginosa* cells only through the TBDT PirA. PirA apparently recognizes substrates of relatively variable structures, since it imports ferric complexes with ENT, but also with catecholamines such as the neuromediators L-DOPA and norepinephrine.⁵⁸ The common motif is the coordination of iron by the catechols. Expression of *pirA* is inducible in the same way as *pfeA* by a two-component system with PirS being the sensor and PirR the regulator (Figure S6.2). Since no induction of expression was observed in the presence of **4/5**, this molecule was probably not recognized by the sensor PirS. The presence of **4/5** in the environment of *P. aeruginosa* repressed the expression of proteins of the PCH pathway and had no effect on the PVD pathway, probably because the affinity for ferric iron of these compounds is higher than that of PCH and lower than that of PVD. This effect on the expression of the PCH pathway indicates that the bacteria used less PCH to access iron and favor the use of DOTAM molecules. Indeed, a previous study on the adaptation of the expression of the iron import pathways of *P. aeruginosa* grown in the presence of 10 μ M ENT, vibriobactin, ferrichrome, yersiniabactin, or nocardamine had already shown the important of the tested siderophores' affinity for ferric iron on the expression levels of the corresponding uptake pathways^{17,72}. *P. aeruginosa* adjusts the expression of its various iron-uptake pathways to match the competition for iron between the siderophores present.

While **4** could restore growth, the ability of **6** and **7** to import iron into *P. aeruginosa* cells was limited, as the PVD/PCH-deficient pathogen hardly grew in the presence of these compounds. Also the recognition of the molecules by PirA was affected, possibly due to their relative size. It remains interesting to test DOTAM conjugates with smaller payloads.

In conclusion, the present study provides insights how hexacoordinating artificial siderophores import iron and conjugated cargo into the Gram-negative pathogen *P. aeruginosa*. While such mimetics have advantages with respect to synthetic access and variability compared to natural siderophores, their functionality is often only assessed by global phenotypic experiments such as MIC assays that reflect an overlay of multiple parameters. Here, we demonstrate iron stealing from endogenous siderophores, efficient iron transport into *P. aeruginosa*, identify the involved transporters and their regulation, and also show the limitations of these processes when the vectors carry a payload. All these data show that MECAM is a promising vector for antibiotic import into the periplasm of *P. aeruginosa*.

Keywords

Antibiotic vectorization, Trojan horse, *Pseudomonas aeruginosa*, siderophores, iron uptake, outer membrane transporters

Materials and Methods

Chemical Methods

The protonophore carbonyl cyanide m-chlorophenylhydrazone (CCCP) was purchased from Sigma-Aldrich, and $^{55}\text{FeCl}_3$ was purchased from Perkin Elmer. Pyoverdine (PVD) was purified from *P. aeruginosa* PAO1 culture supernatants as described previously.⁷³ Enterobactin (ENT) and ferrichrome (FERRI) were purchased from Sigma-Aldrich. The MECAM siderophores **1**, **2**, and **3** were synthesized as described previously.⁴⁰ DOTAM siderophores **4** and **5** were synthesized as described in Ferreira et al.³⁵ and conjugate **7** was synthesized as described in Peukert et al.³⁹ The synthesis of DOTAM conjugate **6** is described in the Supplemental Materials.

Bacterial strains and growth conditions

The *P. aeruginosa* PAO1 strains used in this study are listed in Table S6.3. For all experiments presented below, bacteria were first grown in LB medium overnight at 30°C, and then washed and resuspended in iron-deficient CAA (casamino acid) medium containing 5g l⁻¹ low-iron CAA (Difco), 1.46 g l⁻¹ K₂HPO₄ 3H₂O and 0.25 g l⁻¹ MgSO₄ 7H₂O and grown overnight at 30°C. Afterwards, the bacteria were grown a second time overnight in CAA medium at 30°C in the presence of 10 μM of siderophores, vectors or conjugates if required for the experiment.

Iron scavenging from PVD-Fe.

Compounds were prepared in stock solutions at 10 mM in DMSO (compounds **1**, **3**, **4**, **6** and **7**) or water (PVD, ENT and FERRI). PVD-Fe at 10 μM in 100 μL of HEPES buffer (100 mM, pH 7.4) was incubated at 25 °C for 48 h in the presence of increasing concentrations of ENT, FERRI, **1**, **3**, **4**, **6**, or **7**, and PVD fluorescence was monitored at 447 nm (excitation at 400 nm).¹⁷ The data were normalized using the formula $(F_{\text{MEASURED}} - F_{\text{PVD-Fe}})/(F_{\text{PVD}} - F_{\text{PVD-Fe}})$, F_{MEASURED} being the fluorescence measured for each experimental condition, $F_{\text{PVD-Fe}}$ the fluorescence of 10 μM PVD-Fe, and F_{PVD} the fluorescence of 10 μM PVD.

Quantitative real-time PCR on bacteria grown in the presence of compounds 1-7

This RT-qPCR assay was carried out as described previously^{17,51} on PAO1 cells grown in CAA medium the presence of 10 μM of compounds 1-7. The primers used are listed in Table S6.4. An aliquot of 2.5×10^8 cells from this culture was added to two volumes of RNAprotect Bacteria Reagent (Qiagen) and exactly the same protocol was used as previously described.¹⁷ Primer efficiency was determined using serially diluted genomic DNA and the double ΔC_T method was used to analyze qPCR data.

Iron uptake

Enterobactin-⁵⁵Fe, vectors-⁵⁵Fe and conjugates-⁵⁵Fe complexes were prepared at ⁵⁵Fe concentrations of 50 μM , with a compound:iron (mol:mol) ratio of 20:1 as described previously.⁵¹ *P. aeruginosa* strains were successively grown an overnight in LB broth, followed by an overnight in CAA medium and at last an overnight in CAA medium with either 10 μM ENT, MECAM 1 or MECAM conjugate 3. All these successive cultures were carried out at 30°C. The bacteria were subsequently used for ⁵⁵Fe uptake kinetics as described previously⁵¹ in the absence and presence of 200 μM CCCP (a proton motive force inhibitor).⁵⁷

Growth assays in iron-restricted conditions

For *P. aeruginosa* growth assays in microplates, bacteria were grown as described above: a first overnight culture at 30°C in 10 mL of LB broth, afterwards bacteria were washed and a second overnight culture was carried out in 20 mL CAA medium at 30°C. Bacteria were then washed, resuspended in CAA medium at an optical density of 0.02 at 600 nm and distributed in the wells of a 96-well plate (Greiner, U-bottomed microplate) in the absence or presence of 10 μM of compounds 1, 3, 4, 6 and 7. The plate was incubated at 30 °C, with shaking, in a TECAN microplate reader (Infinite M200, Tecan) and bacterial growth was monitored at OD_{600 nm}. The presented data are the mean of three replicates for each measurement.

Author Contributions

I.J., V.G. and M.B. conceived the idea and designed the experiments. C.P. and L.P. synthesized all the compounds synthetic siderophores and conjugates. S.F. performed bacterial cultures, ⁵⁵Fe uptake assays and iron competition with PVD, V.G. performed RT-qPCR assays. L.K. performed proteomic assays and L.K. and Q.P. proteome data analyzes. I.J.S, C.P and M.B. wrote the manuscript.

Abbreviations used

DOTAM,	tetrapodal 1,4,7,10-tetraazacyclododecane-1,4,7,10-tetraacetic amide;
CAA,	casamino acid;
CCCP,	carbonyl cyanide- <i>m</i> -chlorophenylhydrazone;
ENT,	enterobactin ;
FERRI,	ferrichrome;
PCH,	pyochelin;
PVD,	pyoverdine;
RT-qPCR ,	quantitative reverse transcription polymerase chain reaction;
TBDT,	TonB-dependent transporters.

Acknowledgements

This work was partially funded by the *Centre National de la Recherche Scientifique*, a grant from the Joint Programming Initiative on Antimicrobial Resistance (JPI AMR, grant number: 01KI1825) and the Interdisciplinary Thematic Institute (ITI) InnoVec (Innovative Vectorization of Biomolecules, IdEx, ANR-10-IDEX-0002) and SFRI (ANR-20-SFRI-0012). The mass spectrometry instrumentation at the IBMC was funded by the University of Strasbourg, IdEx “Equipelement mi-lourd” 2015. The equipment at the IPHC was partly funded by the French Proteomics Infrastructure (ProFI; ANR-10-INSB-08-03). QP had a fellowship from the associations Vaincre la Mucoviscidose and Gregory Lemarchal. CP had a Kekulé stipend from the ‘Verband der chemischen Industrie’, and LP was funded by the DFG project number BR 3572/4-1.

References

1. Schalk, I. J.; Mislin, G. L. A.; Brillet, K. Structure, function and binding selectivity and stereoselectivity of siderophore-iron outer membrane transporters. *Curr. Top. Membr.* **2012**, 69, 37–66.
2. Celia, H.; Noinaj, N.; Zakharov, S. D.; Bordignon, E.; Botos, I.; Santamaria, M.; Barnard, T. J.; Cramer, W. A.; Lloubes, R.; Buchanan, S. K. Structural insight into the role of the ton complex in energy transduction. *Nature* **2016**, 538 (7623), 60–65.
3. Celia, H.; Botos, I.; Ni, X.; Fox, T.; De Val, N.; Lloubes, R.; Jiang, J.; Buchanan, S. K. Cryo-EM structure of the bacterial ton motor subcomplex Exbb-Exbd provides information on structure and stoichiometry. *Commun. Biol.* **2019**, 2, 358.
4. Moynié, L.; Milenkovic, S.; Mislin, G. L. A.; Gasser, V.; Mallocci, G.; Baco, E.; McCaughan, R. P.; Page, M. G. P.; Schalk, I. J.; Ceccarelli, M.; Naismith, J. H. The complex of ferric-enterobactin with its transporter from *Pseudomonas aeruginosa* suggests a two-site model. *Nat. Commun.* **2019**, 10 (1), 3673.
5. Josts, I.; Veith, K.; Tidow, H. Ternary Structure of the outer membrane transporter Foxa with resolved signalling domain provides insights into Tonb-mediated siderophore uptake. *eLife* **2019**, 8, e48528.
6. Celia, H.; Noinaj, N.; Buchanan, S. K. Structure and stoichiometry of the TonB molecular motor. *Int. J. Mol. Sci.* **2020**, 21 (2).
7. Schauer, K.; Gouget, B.; Carriere, M.; Labigne, A.; de Reuse, H. Novel nickel transport mechanism across the bacterial outer membrane energized by the TonB/ExbB/ExbD machinery. *Mol. Microbiol.* **2007**, 63 (4), 1054–1068.
8. Schauer, K.; Rodionov, D. A.; de Reuse, H. New substrates for Tonb-dependent transport: Do we only see the “tip of the iceberg”? *T. Biochem. Sci.* **2008**, 33 (7), 330–338.
9. Lhospice, S.; Gomez, N. O.; Ouerdane, L.; Brutesco, C.; Ghssein, G.; Hajjar, C.; Liratni, A.; Wang, S.; Richaud, P.; Bleves, S.; Ball, G.; Borezée-Durant, E.; Lobinski, R.; Pignol, D.; Arnoux, P.; Voulhoux, R. *Pseudomonas aeruginosa* zinc uptake in chelating environment is primarily mediated by the metallophore pseudopaline. *Sci. Rep.* **2017**, 7 (1), 17132.
10. Pieńko, T.; Czarnecki, J.; Równicki, M.; Wojciechowska, M.; Wierzba, A. J.; Gryko, D.; Bartosik, D.; Trylska, J. Vitamin b12-peptide nucleic acids use the Btub receptor to pass through the *Escherichia coli* outer membrane. *Biophys. J.* **2021**, 120 (4), 725–737.

11. Monge, E. C.; Gardner, J. G. Efficient chito-oligosaccharide utilization requires two TonB-dependent transporters and one hexosaminidase in *Cellvibrio japonicus*. *Mol. Microbiol.* **2021**, 116 (2), 366–380.
12. Hider, R. C.; Kong, X. Chemistry and biology of siderophores. *Nat. Prod. Rep.* **2011**, 27 (5), 637–657.
13. Boukhalfa, H.; Crumbliss, A. L. Chemical aspects of siderophore mediated iron transport. *BioMetals* **2002**, 15 (4), 325–339.
14. Hider, R. Siderophore mediated absorption of iron. *Struct. Bonding* **1984**, 58, 28.
15. Loomis, L.; Raymond, K. N. Solution equilibria of enterobactin complexes. *Inorg. Chem.* **1991**, 30, 906–911.
16. Galet, J.; Deveau, A.; Hôtel, L.; Frey-Klett, P.; Leblond, P.; Aigle, B. *Pseudomonas fluorescens* pirates both ferrioxamine and ferricoelichelin siderophores from *Streptomyces ambofaciens*. *Appl. Environ. Microbiol.* **2015**, 81 (9), 3132–3141.
17. Perraud, Q.; Cantero, P.; Roche, B.; Gasser, V.; Normant, V. P.; Kuhn, L.; Hammann, P.; Mislin, G. L. A.; Ehret-Sabatier, L.; Schalk, I. J. Phenotypic adaption of *Pseudomonas aeruginosa* by hacking siderophores produced by other microorganisms. *Mol. Cell Proteomics* **2020**, 19 (4), 589–607.
18. Normant, V.; Josts, I.; Kuhn, L.; Perraud, Q.; Fritsch, S.; Hammann, P.; Mislin, G. L. A.; Tidow, H.; Schalk, I. J. Nocardamine-dependent iron uptake in *Pseudomonas aeruginosa*: Exclusive involvement of the FoxA outer membrane transporter. *ACS Chem. Biol.* **2020**.
19. Schalk, I. J.; Rigouin, C.; Godet, J. n Overview of siderophore biosynthesis among fluorescent pseudomonads and new insights into their complex cellular organization. *Environ. Microbiol.* **2020**, 22 (4), 1447–1466.
20. Llamas, M. A.; Mooij, M. J.; Sparrius, M.; Vandenbroucke-Grauls, C. M.; Ratledge, C.; Bitter, W. Characterization of five novel *Pseudomonas aeruginosa* cell-surface signalling systems. *Mol. Microbiol.* **2008**, 67 (2), 458–472.
21. Hannauer, M.; Barda, Y.; Mislin, G. L.; Shanzer, A.; Schalk, I. J. The ferrichrome uptake pathway in *Pseudomonas aeruginosa* involves an iron release mechanism with acylation of the siderophore and a recycling of the modified desferrichrome. *J. Bacteriol.* **2010**, 192, 1212–1220.

22. Mislin, G. L. A.; Schalk, I. J. Siderophore-dependent iron uptake systems as gates for antibiotic Trojan horse strategies against *Pseudomonas aeruginosa*. *Metallomics* **2014**, 6 (3), 408–420.
23. Schalk, I. J.; Mislin, G. L. A. Bacterial iron uptake pathways: Gates for the import of bactericide compounds. *J. Med. Chem.* **2017**, 60 (11), 4573–4576.
24. Schalk, I. J. Siderophore-antibiotic conjugates: Exploiting iron uptake to deliver drugs into bacteria. *Clin. Microbiol. Infect.* **2018**, 24 (8), 801–802.
25. Negash, K. H.; Norris, J. K. S.; Hodgkinson, J. T. Siderophore-antibiotic conjugate design: New drugs for bad bugs? *Molecules* **2019**, 24 (18), E3314.
26. Zheng, T.; Bullock, J. L.; Nolan, E. M. Siderophore-mediated cargo Delivery to the cytoplasm of *Escherichia coli* and *Pseudomonas aeruginosa*: Syntheses of monofunctionalized enterobactin scaffolds and evaluation of enterobactin-cargo conjugate uptake. *J. Am. Chem. Soc.* **2012**, 134 (44), 18388–18400.
27. Zheng, T.; Nolan, E. M. Enterobactin-mediated delivery of beta-lactam antibiotics enhances antibacterial activity against pathogenic *Escherichia coli*. *J. Am. Chem. Soc.* **2014**, 136 (27), 9677–9691.
28. Górska, A.; Sloderbach, A.; Marszał, M. P. Siderophore-drug complexes: Potential medicinal applications of the “Trojan Horse” strategy. *Trends Pharmacol. Sci.* **2014**, 35 (9), 442–449.
29. Miller, M. J.; Liu, R. Design and syntheses of new antibiotics inspired by nature’s quest for iron in an oxidative climate. *Acc. Chem. Res.* **2021**, 54 (7), 1646–1661.
30. Sargun, A.; Gerner, R. R.; Raffatellu, M.; Nolan, E. M. Harnessing iron acquisition machinery to target *Enterobacteriaceae*. *J. Infect. Dis.* **2021**, 223 (12 Suppl 2), S307–S313.
31. Choi, J. J.; McCarthy, M. W. Cefiderocol: A novel siderophore cephalosporin. *Expert Opin. Investig. Drugs* **2018**, 27 (2), 193–197.
32. Silva, J. T.; López-Medrano, F. Cefiderocol, a new antibiotic against multidrug-resistant Gram-negative bacteria. *Rev. Esp. Quimioter* **2021**, 34 Suppl 1, 41–43.
33. Syed, Y. Y. Cefiderocol: A review in serious Gram-negative bacterial infections. *Drugs* **2021**, 81 (13), 1559–1571.

34. Auletta, S.; Galli, F.; Lauri, C.; Martinelli, D.; Santino, I.; Signore, A. Imaging bacteria with radiolabeled quinolones, cephalosporins and siderophores for imaging infection: A systematic review. *Clin. Transl. Imaging* **2016**, 4, 229–252.
35. Ferreira, K.; Hu, H.-Y.; Fetz, V.; Prochnow, H.; Rais, B.; Müller, P. P.; Brönstrup, M. Multivalent siderophore-DOTAM conjugates as theranostics for imaging and treatment of bacterial infections. *Angew. Chem. Int. Ed. Engl.* **2017**, 56 (28), 8272–8276.
36. Dutta, J.; Naicker, T.; Ebenhan, T.; Kruger, H. G.; Arvidsson, P. I.; Govender, T. Synthetic approaches to radiochemical probes for imaging of bacterial infections. *Eur J. Med. Chem.* **2017**, 133, 287–308.
37. Petrik, M.; Pfister, J.; Misslinger, M.; Decristoforo, C.; Haas, H. Siderophore-based molecular imaging of fungal and bacterial infections-current status and future perspectives. *J. Fungi (Basel)* **2020**, 6 (2), E73.
38. Petrik, M.; Umlaufova, E.; Raclavsky, V.; Palyzova, A.; Havlicek, V.; Pfister, J.; Mair, C.; Novy, Z.; Popper, M.; Hajduch, M.; Decristoforo, C. ⁶⁸Ga-labelled desferrioxamine-B for bacterial infection imaging. *Eur. J. Nucl. Med. Mol. Imaging* **2021**, 48 (2), 372–382.
39. Peukert, C.; Langer, L. N. B.; Wegener, S. M.; Tutov, A.; Bankstahl, J. P.; Karge, B.; Bengel, F. M.; Ross, T. L.; Brönstrup, M. Optimization of artificial siderophores as ⁶⁸Ga-complexed PET tracers for *in vivo* imaging of bacterial infections. *J. Med. Chem.* **2021**, 64 (16), 12359–12378.
40. Pinkert, L.; Lai, Y.-H.; Peukert, C.; Hotop, S.-K.; Karge, B.; Schulze, L. M.; Grunenberg, J.; Brönstrup, M. Antibiotic conjugates with an artificial MECAM-based siderophore are potent agents against Gram-positive and Gram-negative bacterial pathogens. *J. Med. Chem.* **2021**, 64 (20), 15440–15460.
41. Dean, C. R.; Poole, K. Cloning and characterization of the ferric enterobactin receptor gene (PfeA) of *Pseudomonas aeruginosa*. *J. Bacteriol.* **1993**, 175 (2), 317–324.
42. Gasser, V.; Kuhn, L.; Hubert, T.; Aussel, L.; Hammann, P.; Schalk, I. J. The esterase PfeE, the achilles' heel in the battle for iron between *Pseudomonas aeruginosa* and *Escherichia coli*. *Int. J. Mol. Sci.* **2021**, 22 (6), 2814.
43. Livermore, D. M. Multiple Mechanisms of antimicrobial resistance in *Pseudomonas aeruginosa*: Our worst nightmare? *Clin. Infect. Dis.* **2002**, 34 (5), 634–640.
44. Ohi, N.; Aoki, B.; Kuroki, T.; Matsumoto, M.; Kojima, K.; Nehashi, T. Semisynthetic beta-lactam antibiotics. III. Effect on antibacterial activity and comt-susceptibility of

- chlorine-introduction into the catechol nucleus of 6-[(R)-2-[3-(3,4-dihydroxybenzoyl)-3-(3-hydroxypropyl)-1-ureido]-2-phenylacetamido]penicillanic acid. *J. Antibiot.* (Tokyo) **1987**, 40 (1), 22–28.
45. Albrecht-Gary, A. M.; Blanc, S.; Rochel, N.; Ocacktan, A. Z.; Abdallah, M. A. Bacterial iron transport: Coordination properties of pyoverdine, a peptidic siderophore of *Pseudomonas aeruginosa*. *Inorg. Chem.* **1994**, 33, 6391–6402.
 46. Folschweiller, N.; Gallay, J.; Vincent, M.; Abdallah, M. A.; Pattus, F.; Schalk, I. J. The interaction between pyoverdine and its outer membrane receptor in *Pseudomonas aeruginosa* leads to different conformers: A time-resolved fluorescence study. *Biochemistry* **2002**, 41 (49), 14591–14601.
 47. Brandel, J.; Humbert, N.; Elhabiri, M.; Schalk, I. J.; Mislin, G. L. A.; Albrecht-Garry, A.-M. Pyochelin, a Siderophore of *Pseudomonas Aeruginosa*: Physicochemical characterization of the iron(III), copper(II) and zinc(II) complexes. *Dalton Trans.* **2012**, 41 (9), 2820–2834.
 48. Anderegg, G.; L'Eplattenier, F.; Schwarzenbach, G. Hydroxamatkomplexe III. Eisen(III)-Austausch zwischen Sideraminen und Komplexonen. Diskussion der Bildungskonstanten der Hydroxamatkomplexe. *Hel. Chim. Act.* **1963**, 46 (4), 1409–1422.
 49. Llamas, M. A.; Sparrius, M.; Kloet, R.; Jimenez, C. R.; Vandenbroucke-Grauls, C.; Bitter, W. The heterologous siderophores ferrioxamine B and ferrichrome activate signaling pathways in *Pseudomonas aeruginosa*. *J. Bacteriol.* **2006**, 188 (5), 1882–1891.
 50. Llamas, M. A.; Imperi, F.; Visca, P.; Lamont, I. L. Cell-Surface Signaling in *Pseudomonas*: stress responses, iron transport, and pathogenicity. *FEMS Microbiol. Rev.* **2014**, 38 (4), 569–597.
 51. Gasser, V.; Baco, E.; Cunrath, O.; August, P. S.; Perraud, Q.; Zill, N.; Schleberger, C.; Schmidt, A.; Paulen, A.; Bumann, D.; Mislin, G. L. A.; Schalk, I. J. Catechol siderophores repress the pyochelin pathway and activate the enterobactin pathway in *Pseudomonas aeruginosa*: An opportunity for siderophore-antibiotic conjugates development. *Environ. Microbiol.* **2016**, 18 (3), 819–832.
 52. Perraud, Q.; Cantero, P.; Munier, M.; Hoegy, F.; Zill, N.; Gasser, V.; Mislin, G. L. A.; Ehret-Sabatier, L.; Schalk, I. J. Phenotypic adaptation of *Pseudomonas aeruginosa* in the presence of siderophore-antibiotic conjugates during epithelial cell infection. *Microorganisms* **2020**, 8 (11).

53. Cunrath, O.; Geoffroy, V. A.; Schalk, I. J. Metallome of *Pseudomonas aeruginosa*: A role for siderophores. *Environ. Microbiol.* **2016**, 18 (10), 3258–3267.
54. Ghysels, B.; Ochsner, U.; Mollman, U.; Heinisch, L.; Vasil, M.; Cornelis, P.; Matthijs, S. The *Pseudomonas aeruginosa* PirA gene encodes a second receptor for ferri-enterobactin and synthetic catecholate analogues. *FEMS Microbiol. Lett.* **2005**, 246 (2), 167–174.
55. Dean, C. R.; Poole, K. Expression of the ferric enterobactin receptor (PfeA) of *Pseudomonas aeruginosa*: Involvement of a two-component regulatory system. *Mol. Microbiol.* **1993**, 8 (6), 1095–1103.
56. Moynié, L.; Luscher, A.; Rolo, D.; Pletzer, D.; Tortajada, A.; Weingart, H.; Braun, Y.; Page, M. G. P.; Naismith, J. H.; Köhler, T. Structure and function of the PiuA and PirA siderophore-drug receptors from *Pseudomonas aeruginosa* and *Acinetobacter baumannii*. *Antimicrob. Agents Chemother.* **2017**, 61 (4).
57. Clément, E.; Mesini, P. J.; Pattus, F.; Abdallah, M. A.; Schalk, I. J. The binding mechanism of pyoverdine with the outer membrane receptor FpvA in *Pseudomonas aeruginosa* is dependent on its iron-loaded status. *Biochemistry* **2004**, 43, 7954–7965.
58. Perraud, Q.; Kuhn, L.; Fritsch, S.; Graulier, G.; Gasser, V.; Normant, V.; Hammann, P.; Schalk, I. J. Opportunistic use of catecholamine neurotransmitters as siderophores to access iron by *Pseudomonas aeruginosa*. *Environ. Microbiol.* 2020.
59. Cox, C. D. Iron uptake with ferripyochelin and ferric citrate by *Pseudomonas aeruginosa*. *J. Bacteriol.* 1980, 142, 581–587.
60. Marshall, B.; Stintzi, A.; Gilmour, C.; Meyer, J.-M.; Poole, K. Citrate-mediated iron uptake in *Pseudomonas aeruginosa*: Involvement of the citrate-inducible FecA receptor and the FeoB ferrous iron transporter. *Microbiology* **2009**, 155 (Pt 1), 305–315.
61. Seyedmohammad, S.; Fuentealba, N. A.; Marriott, R. A. J.; Goetze, T. A.; Edwardson, J. M.; Barrera, N. P.; Venter, H. Structural model of FeoB, the iron transporter from *Pseudomonas aeruginosa*, predicts a cysteine lined, GTP-gated pore. *Biosci. Rep.* **2016**, 36 (2), e00322.
62. McFarlane, J. S.; Lamb, A. L. Biosynthesis of an opine metallophore by *Pseudomonas aeruginosa*. *Biochemistry* **2017**, 56 (45), 5967–5971.
63. Hermansen, G. M. M.; Hansen, M. L.; Khademi, S. M. H.; Jelsbak, L. Intergenic evolution during host adaptation increases expression of the metallophore pseudopaline in *Pseudomonas aeruginosa*. *Microbiology* **2018**, 164 (8), 1038–1047.

64. Pederick, V. G.; Eijkelkamp, B. A.; Begg, S. L.; Ween, M. P.; McAllister, L. J.; Paton, J. C.; McDevitt, C. A. ZnuA and zinc homeostasis in *Pseudomonas aeruginosa*. *Sci. Rep.* **2015**, 5, 13139.
65. Calmettes, C.; Ing, C.; Buckwalter, C. M.; El Bakkouri, M.; Chieh-Lin Lai, C.; Pogoutse, A.; Gray-Owen, S. D.; Pomès, R.; Moraes, T. F. The Molecular mechanism of zinc acquisition by the neisserial outer-membrane transporter ZnuD. *Nat. Commun.* **2015**, 6.
66. Kingsley, R.; Rabsch, W.; Stephens, P.; Roberts, M.; Reissbrodt, R.; Williams, P. H. Iron supplying systems of *Salmonella* in diagnostics, epidemiology and infection. *FEMS Immunol. Med. Microbiol.* **1995**, 11 (4), 257–264.
67. Braun, V. Iron uptake by *Escherichia coli*. *Front. Biosci.* **2003**, 8, 1409–1421.
68. Cornelis, P.; Dingemans, J. *Pseudomonas aeruginosa* adapts its iron uptake strategies in function of the type of infections. *Front. Cell Infect Microbiol.* **2013**, 3, 75.
69. Winsor, G. L.; Griffiths, E. J.; Lo, R.; Dhillon, B. K.; Shay, J. A.; Brinkman, F. S. L. Enhanced annotations and features for comparing thousands of *Pseudomonas* genomes in the *Pseudomonas* genome database. *Nucleic Acids Res.* **2016**, 44 (D1), D646-653.
70. Perraud, Q.; Moynié, L.; Gasser, V.; Munier, M.; Godet, J.; Hoegy, F.; Mély, Y.; Mislin, G. L. A.; Naismith, J. H.; Schalk, I. J. A Key role for the periplasmic PfeE esterase in iron acquisition via the siderophore enterobactin in *Pseudomonas aeruginosa*. *ACS Chem. Biol.* **2018**, 13 (9), 2603–2614.
71. Outten, C. E.; Tobin, D. A.; Penner-Hahn, J. E.; O'Halloran, T. V. Characterization of the metal receptor sites in *Escherichia coli* Zur, an ultrasensitive zinc(II) metalloregulatory protein. *Biochemistry* **2001**, 40 (35), 10417–10423.
72. Normant, V.; Josts, I.; Kuhn, L.; Perraud, Q.; Fritsch, S.; Hammann, P.; Mislin, G. L. A.; Tidow, H.; Schalk, I. J. Nocardamine-dependent iron uptake in *Pseudomonas aeruginosa*: Exclusive involvement of the FoxA outer membrane transporter. *ACS Chem. Biol.* **2020**, 15 (10), 2741–2751.
73. Demange, P.; Bateman, A.; Mertz, C.; Dell, A.; Piémont, Y.; Abdallah, M. A. Bacterial siderophores: Structures of pyoverdines Pt, siderophores of *Pseudomonas Tolaasii* NCPPB 2192, and pyoverdines Pf, siderophores of *Pseudomonas fluorescens* CCM 2798. Identification of an unusual natural amino acid. *Biochemistry* **1990**, 29 (50), 11041–11051.

74. Bouyssié, D.; Hesse, A.-M.; Mouton-Barbosa, E.; Rompais, M.; Macron, C.; Carapito, C.; Gonzalez de Peredo, A.; Couté, Y.; Dupierris, V.; Burel, A.; Menetrey, J.-P.; Kalaitzakis, A.; Poisat, J.; Romdhani, A.; Burlet-Schiltz, O.; Cianférani, S.; Garin, J.; Bruley, C. Proline: An efficient and user-friendly software suite for large-scale proteomics. *Bioinformatics* **2020**, 36 (10), 3148–3155.
75. Gregori, J.; Sanchez, A.; Villanueva, J. MSMSTests: LC-MS/MS differential expression tests; *Bioconductor version: Release (3.9)*, **2019**.
76. Vizcaíno, J. A.; Csordas, A.; del-Toro, N.; Dienes, J. A.; Griss, J.; Lavidas, I.; Mayer, G.; Perez-Riverol, Y.; Reisinger, F.; Ternent, T.; Xu, Q.-W.; Wang, R.; Hermjakob, H. 2016 Update of the PRIDE database and its related tools. *Nucleic Acids Res.* **2016**, 44 (D1), D447-456.

Supporting information

General chemical information

Commercially available chemicals were used directly in the below stated procedures, without any further purification. All employed organic solvents possessed min. ACS or HPLC-grade purity. Dried solvents were used unless water was part of the reaction mixture and other dried solvents were purchased in a water-free form. Reactions with dried solvents were conducted in oven-dried glassware under a nitrogen atmosphere. Removal of organic solvents was conducted on rotational evaporators at 30 °C.

Reverse-Phase High Pressure Liquid Chromatography (RP-HPLC) was performed with a Phenomenex Gemini C18 RP-column 00G-4436-NO, 10 µm, 110 Å, 250×10.00 mm (flow rate 5 mL/min, max. loading 10 mg crude) or a Phenomenex Gemini C18 RP-column 00G-4435-PO-AX, 5 µm, 110 Å, 250×21.20 mm (flow rate 10 mL/min, max. loading 100 mg crude) coupled to a Thermo Fisher Scientific® Dionex Ultimate 3000 HPLC-System.

The gradients and additives are stated in the respective synthetic procedures. For Nuclear Magnetic Resonance (NMR) Bruker Avance III or Bruker Avance III HD instruments were employed.

¹H NMR spectra were recorded at 500 MHz or 700 MHz, ¹³C NMR spectra were recorded at 126 MHz and 176 MHz. The chemical shifts are stated in parts per million (ppm) relative to the solvent signal. Peak multiplicity is given in short as follows: s (singlet), bs (broad singlet), d (doublet), t (triplet), q (quartet), m (multiplet), dd (doublet of doublet), tt (triplet of triplet).

Lyophilisation of HPLC-purified compounds was conducted on an Alpha 2–4 LSCbasic (Christ) lyophilizer after freezing compound solutions in liquid nitrogen. Absolute reaction yields are given after the pure compound was analyzed by NMR spectroscopy and yields of unpurified compounds were calculated in order to allow stoichiometric calculations for the next synthetic step. High Resolution Mass Spectroscopy (HRMS) was conducted with a Dionex® Ultimate 3000 HPLC System equipped with a DAD Detector and a Bruker® MAXIS HD QTOF Mass Detector with ESI.

All biologically tested compounds had purities ≥ 95% as determined by high-performance liquid chromatography (UV detection) and ¹H-/¹³C-NMR analysis.

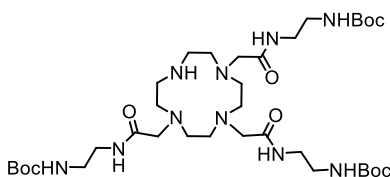
Synthesis procedures

Compounds **1-3** were synthesized according to.¹

Compounds **4-5** were synthesized according to.²

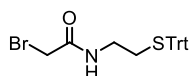
Compound **7** was synthesized according to.³

Compound **8**



Compound **8** was synthesized according to previously established procedures by K. Ferreira et al and Peukert, Langer et al.^{2,3}

Compound **9**



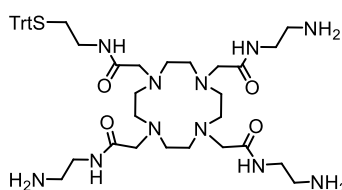
The HCl salt of 2-trityl-thio-1-ethylamin (1.5 g, 4.214 mmol, 1.0 eq) was dissolved in DCM (100 mL) at 0 °C. Then K₂CO₃ (698.97 mg, 5.057 mmol, 1.2 eq) was added in milliQ water (50 mL) in one portion followed by 2-bromoacetyl bromide (441 μL, 5.057 mmol, 1.2 eq) in DCM (50 mL) was added dropwise at 0 °C and stirred at that temperature for 15 minutes. The ice bath was removed and the two-phase solution continued stirring for 2 hours at 23 °C. The phases were separated and the aqueous phase was extracted with DCM (2x50 mL). The combined organic extracts were dried over Na₂SO₄ and concentrated to yellow crystals *in vacuo*. The residue was dried under high vacuum overnight, yielding crude compound **9** a slight yellow powder (1.786 g, 4.027 mmol, 96%).

¹H-NMR (700 MHz, DMSO-d₆): δ = 8.35 (t, J = 5.75 Hz, 1H), 7.35-7.32 (m, 6H), 7.32-7.30 (m, 6H), 7.25 (m, 3H), 3.79 (s, 2H), 3.01-2.98 (q, J = 6.96, 12.88 Hz, 2H), 2.22-2.20 (t, J = 7.90 Hz, 2H).

¹³C NMR (176 MHz, DMSO-d₆): δ = 165.9, 144.4, 129.1, 128.1, 127.8, 127.5, 126.8, 66.0, 38.0, 31.1, 29.3.

HRMS (ESI(+)): m/z = calcd. for C₂₃H₂₂BrNNaOS [M+Na]⁺: 462.0498, found: 462.0494 (Δ = 0.4 ppm).

Compound 10

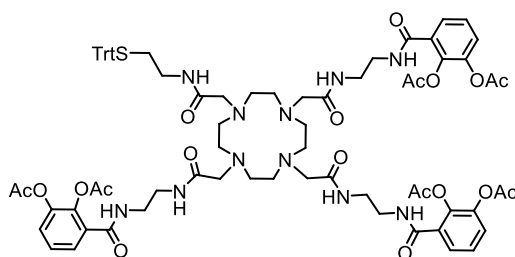


To a suspension of **8** (600 mg, 0.776 mmol, 1.0 eq) and K₂CO₃ (429.12 mg, 3.105 mmol, 4.0 eq) in ACN (5 mL) bromide **9** was added (681.6 mg, 1.552 mmol, 2.0 eq) solution in DCM (2.5 mL) at 23 °C and the pale yellow suspension was stirred overnight at 23 °C. Upon completion, the reaction was filtered, the solvent was removed by rotary evaporation and the residue concentrated under high vacuum to yield a crude, yellow oil. The oil was dissolved in wet (!) DCM (3 mL) and then TFA (1 ml) was added dropwise at 0 °C. The reaction turned neon yellow upon slow addition. After the addition was complete, the reaction continued stirring at 0 °C for 5 minutes and then at 23 °C for two hours. The solvent was removed by rotary evaporation and the obtained residues was dissolved in an ACN/H₂O mixture (1:1, 1200 μL), filtered over a syringe filter and purified by RP-HPLC (C18 phenomenex, 220 nm, 2-45% ACN/H₂O, 0.1% HCOOH). Product containing fractions were identified by LCMS and lyophilized to dryness to yield the product **10** as a yellow oil (232.0 mg, 0.279 mmol, 84%).

¹H NMR (700 MHz, MeOH-d₄): δ = 7.39-7.38 (d, J = 7.69 Hz, 6H), 7.31-7.25 (t, J = 7.15 Hz, 6H), 7.24-7.23 (t, J = 7.15 Hz, 3H), 4.26-3.77 (m, 4H), 3.74-3.34 (m, 17H), 3.24-2.90 (m, 17H), 2.42 (t, J = 7.20 Hz, 2H).

¹³C-NMR (176 MHz, MeOH-d₄): δ = 163.5, 163.3, 163.1, 162.93, 146.2, 130.9, 129.2, 128.2, 120.8, 119.1, 117.5, 115.8, 68.2, 56.4, 55.7, 39.8, 38.39, 38.1, 32.7, 29.00.

Compound 11



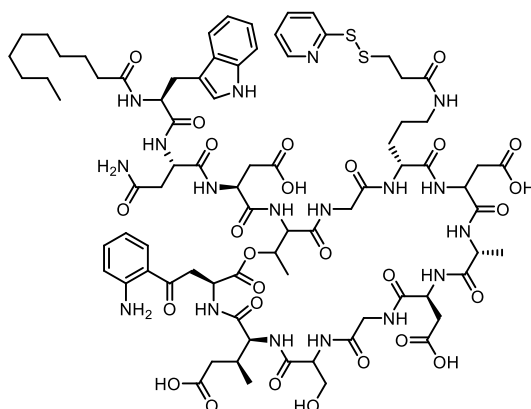
2,3-diacetoxybenzoic acid (232.4 mg, 0.976 mmol, 3.5 eq) was obtained according to our previously published standard procedure and converted to the acid chloride with oxalylchloride (77.4 μ L, 0.976 mmol, 3.5 eq) in DCM/DMF (500/100 μ L) under Argon conditions.²⁰⁷ The acid chloride was dried under high vacuum overnight. Amine **10** (232 mg, 0.279 mmol, 1.0 eq) was dissolved in milliQ water (1 mL) and sat. NaHCO_3 (5 mL) was added, until a pH of 8.5 was reached. The solution was cooled to 0 °C and the acid chloride was dissolved in dry 1,4-dioxane (5 mL) and added dropwise at that temperature in portions of 1 mL to the amine. After the addition of each milliliter, the pH was controlled and adjusted again to min. 8.0. After the addition, the ice bath was removed and the pale yellow-white suspension continued stirring at 23 °C for 30 minutes. After 1 h the reaction extracted with ethyl acetate (3x50 mL) and dried over Na_2SO_4 . The combined organic extracts were evaporated to dryness by rotary evaporation at 30 °C and with addition of conc. acetic acid (1 mL). And the residue was taken up in ACN/ H_2O (1:1) and purified by RP-HPLC (C18 phenomenex, 220 nm, 40-min gradient 10-50% ACN/ H_2O , 1% AcOH). The product containing fractions were identified by LCMS and lyophilized to dryness to yield siderophore **11** as a beige powder (128 mg, 0.086 mmol, 31%).

$^1\text{H-NMR}$ (700 MHz, DMSO-d_6): δ = 8.38 (s, 3H), 8.24-8.00 (m, 4H), 7.46-7.45 (m, 3H), 7.37-7.36 (m, 3H), 7.34-7.29 (m, 3H), 7.24-7.22 (m, 3H), 3.25-3.21 (m, 15H), 3.06-3.03 (q, J = 6.49, 12.51 Hz, 2H), 2.95-2.82 (m, 8H), 2.80-2.52 (m, 15H), 2.27 (s, 9H), 2.20 (s, 9H).

$^{13}\text{C NMR}$ (176 MHz, DMSO-d_6) δ 172.06, 168.62, 168.53, 168.31, 168.20, 167.80, 164.72, 144.41, 142.85, 140.12, 130.75, 129.06, 128.34, 128.06, 126.78, 126.16, 126.07, 125.47, 65.93, 38.10, 37.29, 31.47, 21.09, 20.57, 20.54, 20.44, 20.36, 20.26, 19.94.

HRMS (ESI(+)): m/z = calcd. for $\text{C}_{76}\text{H}_{91}\text{N}_{11}\text{O}_{19}\text{S}$ $[\text{M}+2\text{H}]^{2+}$: 746.8101, found: 746.8105 (Δ = 0.4 ppm)

Compound 12

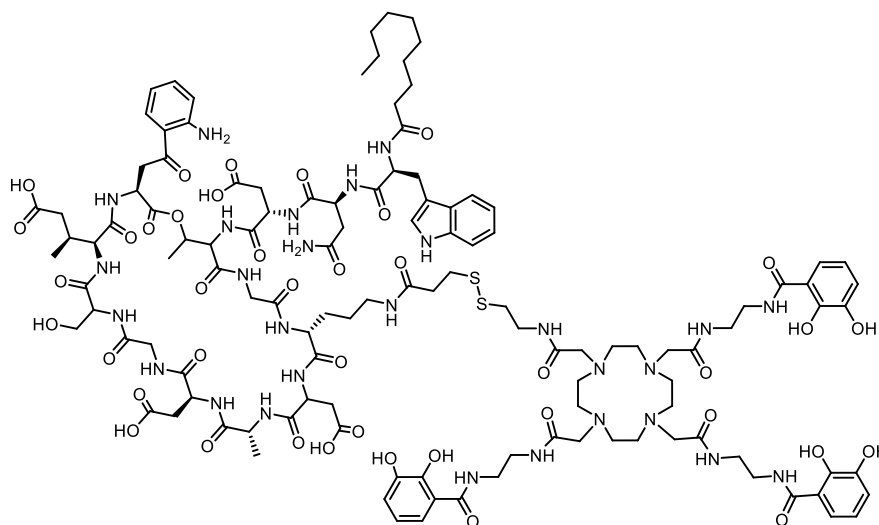


Daptomycin (from across organics, 15 mg, 0.009 mmol, 1.0 eq) was dissolved in DMSO (1.3 mL) and then dry pyridine (30 μ L) was added under argon atmosphere. The solution stirred at 25 $^{\circ}$ C for 5 minutes and clarified. SPDP (3.18 mg, 0.010 mmol, 1.1 eq) was added in DMSO (200 μ L) and the solution continued stirring overnight at 25 $^{\circ}$ C. The base was removed by rotary evaporation as much as possible and the residue was purified by RP-HPLC (C18 phenomenex, 220 nm, 40 min gradient 10-70% ACN/H₂O 0.1% HCOOH). The product containing fractions were identified by LCMS and lyophilized to dryness to yield amide 12 (13.9 mg, 0.008 mmol, 83%).

¹H NMR (700 MHz, DMSO-d₆): δ = 12.21 (t, J = 95.44 Hz, 4H), 10.75 (s, 1H), 8.45-8.41 (m, 3H), 8.32 (m, 3H), 8.21 (s, 1H), 8.11 (m, 2H), 7.98 (m, 2H), 7.87 (t, J = 4.29 Hz, 1H), 7.83-7.81 (m, 1H), 7.76-7.71 (m, 3H), 7.56-7.55 (d, J = 7.77 Hz, 1H), 7.31-7.26 (m, 2H), 7.24-7.21 (m, 2H), 7.14-7.06 (m, 3H), 7.04 (t, J = 6.70 Hz, 1H), 6.95 (t, J = 7.76 Hz, 1H), 6.86 (s, 1H), 6.74-6.73 (d, J = 8.57 Hz, 1H), 6.51 (t, J = 7.64 Hz, 1H), 5.03 (t, J = 4.69 Hz, 1H), 4.88-4.77 (m, 2H), 4.61-4.47 (m, 8H), 4.40-4.38 (q, J = 6.97, 14.74 Hz, 1H), 4.22-4.20 (q, J = 6.56, 12.73 Hz, 1H), 4.10 (t, J = 6.56 Hz, 2H), 3.75 (m, 3H), 3.58 (m, 3H), 3.05-2.98 (m, 6H), 2.92-2.88 (q, J = 9.24, 14.74 Hz, 1H), 2.81-2.71 (ddd, J = 6.97, 16.61, 50.78, 67.39 Hz, 2H), 2.66-2.54 (m, 7H), 2.47-2.25 (m, 8H), 2.02 (m, 2H), 1.91 (m, 1H), 1.67 (m, 1H), 1.52-1.34 (m, 6H), 1.24-1.18 (m, 10H), 1.14 (m, 5H), 1.08-1.07 (d, J = 6.16 Hz, 6H), 0.84-0.81 (m, 6H).

¹³C NMR (176 MHz, DMSO-d₆): δ = 173.5, 173.1, 172.9, 171.9, 171.8, 171.6, 171.4, 171.4, 170.9, 170.4, 170.1, 169.7, 168.8, 167.7, 159.2, 151.1, 149.5, 137.8, 136.0, 131.3, 127.2, 123.7, 121.1, 120.8, 119.08, 118.3, 118.1, 116.9, 115.9, 111.2, 109.9, 69.9, 61.9, 55.5, 54.1, 53.1, 50.2, 49.7, 49.4, 42.4, 41.7, 40.4, 38.2, 37.8, 37.0, 35.7, 35.56, 35.3, 35.0, 34.6, 34.1, 31.2, 28.8, 28.7, 28.7, 28.6, 27.1, 25.3, 24.9, 22.1, 16.9, 14.8, 13.9.

Compound 6



Compound **11** (8 mg, 0.005 mmol, 1.0 eq) was dissolved in 20% DIPEA in anhydrous MeOH (full volume = 3 mL) at 0 °C and stirred for 4 h at 25 °C. Then the solvent was removed by rotary evaporation at 30 °C and the brownish residue was dried under high vacuum overnight. Then the residue was dissolved in a mixture of TFA/DCM/TIPS (1/0.05/1 mL), added dropwise at 0 °C and warmed to 25 °C over 5 minutes. After full conversion, the solvent was removed *in vacuo* and the residue was washed with petrolether (bp 40-60 °C, 3x1 mL) and dried again overnight high vacuum. Then DMSO and DMF (600 μ L each) were added, followed by sat. NaHCO₃ (200 μ). Then compound **12** (9.6 mg, 0.006 mmol, 1.2 eq) was added, dissolved in DMSO/DMF (1:1, 400 μ L). The reaction was stirred for 4 h at 25 °C and then 1,4-dioxane (10x the volume) was added, the mixture frozen in liquid nitrogen in a falcon and lyophilized to dryness. The residue was purified by RP-HPLC (C18 phenomenex, 220nm, 40 min gradient 10-80% ACN/water, 0.1% HCOOH), product containing fractions were identified by LCMS and lyophilized to dryness to yield compound **3** as a beige solid (9.76 mg, 0.004 mmol, 67%).

¹H NMR (700 MHz, DMSO-d₆): δ = 12.59 (s, 3H), 12.43-11.97 (m, 4H), 10.75 (s, 1H), 9.15 (s, 3H), 8.77 (t, J = 5.06 Hz, 3H), 8.42 (m, 2H), 8.32-8.22 (m, 8H), 8.12 (m, 3H), 7.99-7.98 (d, J = 7.08 Hz, 2H), 7.86 (m, 1H), 7.74-7.71 (m, 2H), 7.56-7.55 (d, J = 7.76 Hz, 1H), 7.31-7.29 (m, 2 H), 7.23-7.22 (d, J = 8.77 Hz, 4H), 7.14 (d, J = 2.02 Hz, 1 H), 7.10 (bs, 1H), 7.04 (t, J = 7.76 Hz, 1H), 6.95 (t, J = 7.08 Hz, 1 H), 6.91-6.90 (d, J = 8.09 Hz, 3H), 6.86 (bs, 1H), 6.74-6.73 (d, J = 8.77 Hz, 1 H), 6.67 (t, J = 6.74 Hz, 3H), 6.51 (t, J = 7.76 Hz, 1 H), 5.04 (bs, 1H), 4.84-4.80 (m, 2H), 4.62-4.48 (m, 7), 4.40-4.37 (q, J = 7.08, 13.83 Hz, 1H), 4.21-4.20 (d, J = 5.73 Hz, 1H), 4.12-4.08 (m, 2H), 3.80-3.70 (m, 4H), 3.60-3.58 (m, 4H), 3.50-3.38 (m, 16H), 3.04-3.03 (m, 4H), 2.95-2.71 (m, 24H), 2.63-2.53 (m, 3H), 2.47-2.22 (m, 8H), 2.04-1.99 (m, 2H), 1.93-1.89 (m, 1H), 1.67-1.66 (m, 1H), 1.54-1.52 (m, 1H), 1.47-1.45 (m, 1H), 1.41 (m, 1H), 1.34 (m, 2H), 1.25-1.18 (m, 11H), 1.14 (m, 4H), 1.08-1.07 (d, J = 6.28 Hz, 5H), 0.85-0.81 (m, 7H).

¹³C NMR (176 MHz, DMSO-d₆) δ 174.0, 173.4, 172.4, 172.3, 172.0, 171.9, 171.4, 170.9, 170.6, 170.4, 170.4, 169.59, 158.2, 151.6, 150.0, 146.7, 136.5, 131.8, 127.7, 124.2, 121.3, 119.3, 118.8, 118.7, 118.6, 118.4, 117.7, 117.4, 116.4, 115.5, 115.0, 111.7, 110.3, 70.5, 62.4, 56.6, 54.7, 51.4, 50.7, 50.2, 49.9, 40.9, 39.2, 38.7, 38.6, 38.3, 37.5, 37.2, 35.7, 35.5, 34.3, 31.7, 29.3, 29.2, 29.1, 29.1, 27.6, 25.9, 25.4, 22.6, 21.5, 20.9, 17.5, 15.3, 14.4.

DEPT (176 MHz, DMSO-d₆): δ = 134.5, 131.3, 123.7, 120.8, 118.8, 118.3, 118.1, 117.9, 117.2, 116.9, 114.5, 111.21, 70.0, 61.9, 56.2, 55.5, 54.7, 54.2, 53.1, 50.9, 50.2, 49.7, 49.4, 49.1, 42.3, 41.8, 40.4, 38.7, 38.3, 38.1, 37.9, 37.0, 36.7, 35.7, 35.5, 35.2, 35.0, 33.8, 32.8, 31.3, 28.8, 28.7, 28.7, 28.6, 27.1, 25.4, 24.9, 22.1, 17.0, 14.8, 14.0, 0.1.

HRMS (ESI(+)): m/z = calcd. for C₁₂₀H₁₆₉N₂₈O₄₀S₂ [M+3H]³⁺: 902.0369, found: 902.0492, (Δ = 12.3 ppm), m/z = calcd. for C₁₂₀H₁₆₈N₂₈O₄₀S₂ [M+2H]²⁺: 1352.5702, found: 1352.5706, (Δ = 0.4 ppm).

MIC assay in iron-depleted, cation-adjusted MHB

The assay was conducted as described by Pinkert et al with *P. aeruginosa* PAO7.¹

Daptomycin requires Ca²⁺ for exerting its antimicrobial effect. Therefore, the medium was supplemented, according to previously published studies, with 110 µg/mL CaCl₂ (trace metal).^{4,}

⁵

The DOTAM-daptomycin conjugate was tested together with free daptomycin (AcrosOrganics™) and cefiderocol and ciprofloxacin as controls, see Table below.

No antimicrobial activity was observed for compound 6 nor for free daptomycin in PAO7, in coherence with previous studies.

The control antibiotics displayed values in the expected range.

Supplementary tables

Table S6.1. TBDTs of *P. aeruginosa* PAO1 potentially involved in iron acquisition and siderophore or xenosiderophore their recognize. In the third column, the transcriptional regulators regulating the transcription of the genes encoding TBDTs: in green AraC transcriptional regulators; in blue, anti-sigma and sigma factors; and in grey, two-component systems.

TBDT	Siderophore or xenosiderophore	Transcriptional regulators
FptA	Pyochelin	PchR
FpvA	Pyoverdine	FpvI/FpvR/PvdS
FpvB	Pyoverdine	
ChtA	aerobactin, rhizobactin and schizokinen	
FvbA	Vibriobactin	
PfeA	Enterobactin	PfeS/PfeR
PirA	Enterobactin Catechol siderophore	PirS/PirR
CirA	Catechol siderophore	
FecA	Citrate	FecR/FecI
FemA	Mycobactin	FemR/FemI
FiuA	Ferrichrome	FiuR/FiuI
FoxA	Ferrioxamine Nocardamine Desferioxamine B	FoxR/FoxI
HasR	Heme	HasI/HasS
HxuA	Heme	HxuR/HxuI
PhuR	Heme	
PiuA	Unknown function	
OptI	Unknown function	

OptO	Unknown function	
PfuA	Unknown function	
Sppr	Unknown function	
PA0151	Unknown function	
PA0192	Unknown function	
PA0434	Unknown function	
PA0781	Unknown function	
PA1365	Unknown function	
PA1613	Unknown function	
PA2070	Unknown function	
PA2089	Unknown function	
PA2289	Unknown function	
PA2590	Unknown function	
PA2911	Unknown function	
PA3268	Rhizobactin, Staphilobactin	

Table S6.2. MIC values of daptomycin and DOTAM daptomycin conjugate **6** with control antibiotics.

Compound	MIC in PAO7 [$\mu\text{g/mL}$]	References
<i>Compound 6</i>	>64	This work
<i>Daptomycin</i>	>64	This work
<i>Ciprofloxacin</i>	6.3 \pm 0	This work
<i>Cefiderocol (Fetroja®)</i>	0.16 \pm 0	6

Table S6.3. Strains used in this study.

Strains and plasmids	Collection ID	Relevant characteristics	Reference
PAO1		<i>P. aeruginosa</i> wild-type strain	
$\Delta pvdF\Delta pchA$	PAS28 3	PAO1; <i>pvdF</i> and <i>pchA</i> chromosomally deleted	7
$\Delta pvdF\Delta pchA\Delta pfeA$	PAS29 4	PAO1; <i>pvdF</i> , <i>pchA</i> and <i>pfeA</i> chromosomally deleted	7
$\Delta pvdF\Delta pchA\Delta pirA$	PAS34 8	PAO1; <i>pvdF</i> , <i>pchA</i> and <i>pirA</i> chromosomally deleted	8
$\Delta pvdF\Delta pchA\Delta pfeA\Delta pirA$	PAS35 1	PAO1; <i>pvdF</i> , <i>pchA</i> , <i>pfeA</i> and <i>pirA</i> chromosomally deleted	8

Table S6.4. Oligonucleotides used in this study for RT-qPCR.

Oligonucleotides	Sequence (5' to 3')
uvrD F	CTACGGTAGCGAGACCTACAACAA
uvrD R	GCGGCTGACGGTATTGGA
fpvA F	AGCCGCCTACCAGGATAAGC
fpvA R	TGCCGTAATAGACGCTGGTTT
fptA F	GCGCCTGGGCTACAAGATC
fptA R	CCGTAGCGGTTGTTCCAGTT
pfeA F	GCCGAGACCAGCGTGAAC
pfeA R	GGCCGGATTTCGATCTTGTT
pirA F	GCCTGAACGCTTCCCAA
pirA R	TGAAGGCCCGTGCGATA
ampC F	CCTGGCCGTAGCCATCAG
ampC R	CGGCCGTCCTCTTTTCA
cntO F	TGATGGGCCTCGAGTACGA
cntO R	GCGCGACGGGATGCTA
PA0781 F	TGGCTGGCCTTCGTCAAG
PA0781 R	GTCGCGCAGGATCGAACT

Supplementary figures

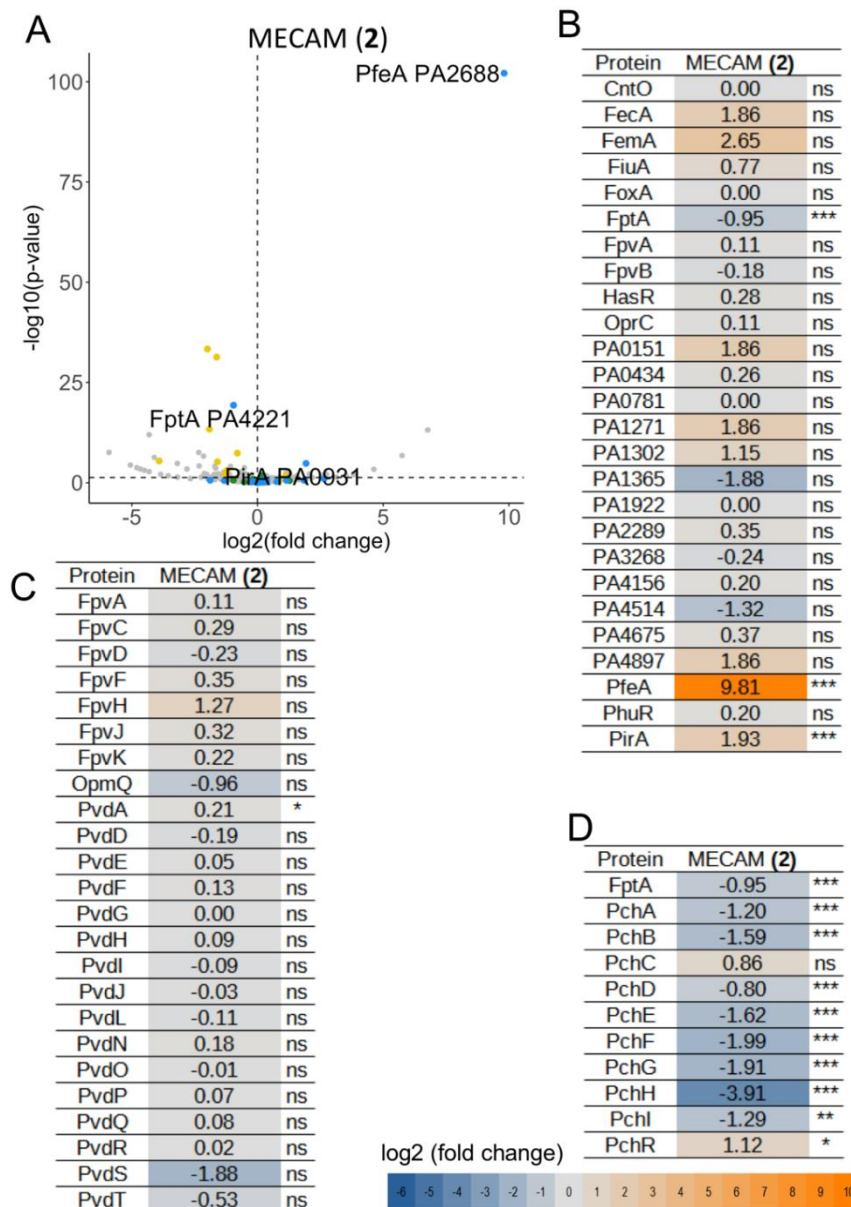


Figure S6.1. Proteomic analyses of *P. aeruginosa* PAO1 cells grown under iron-limited conditions (CAA medium) in the absence or presence of MECAM 2. Proteomic analyses were performed on *P. aeruginosa* PAO1 strains grown overnight in CAA medium supplemented, or not, with 10 μ M MECAM 2 (A). Average values measured in CAA in the absence of any supplementation are plotted against average values measured in CAA supplemented with either 10 μ M MECAM 2. Median values represent the median of the relative intensity of each protein, normalized against all proteins detected by shotgun analysis ($n = 3$). The proteins of the PCH pathway are represented by yellow dots, those of the PVD pathway by green dots, and the TBDTs by blue dots. B, C and D show the heat maps: TBDTs present in *P. aeruginosa* genome (B), proteins involved in the PVD pathway (C) and proteins of the PCH pathway (D). The darker the shade of blue, the more expression of the protein was repressed; the darker the shade of orange, the more expression of the protein was induced. NS: data not significant; * $p < 0.05$, ** $p < 0.01$, and *** $p < 0.001$.

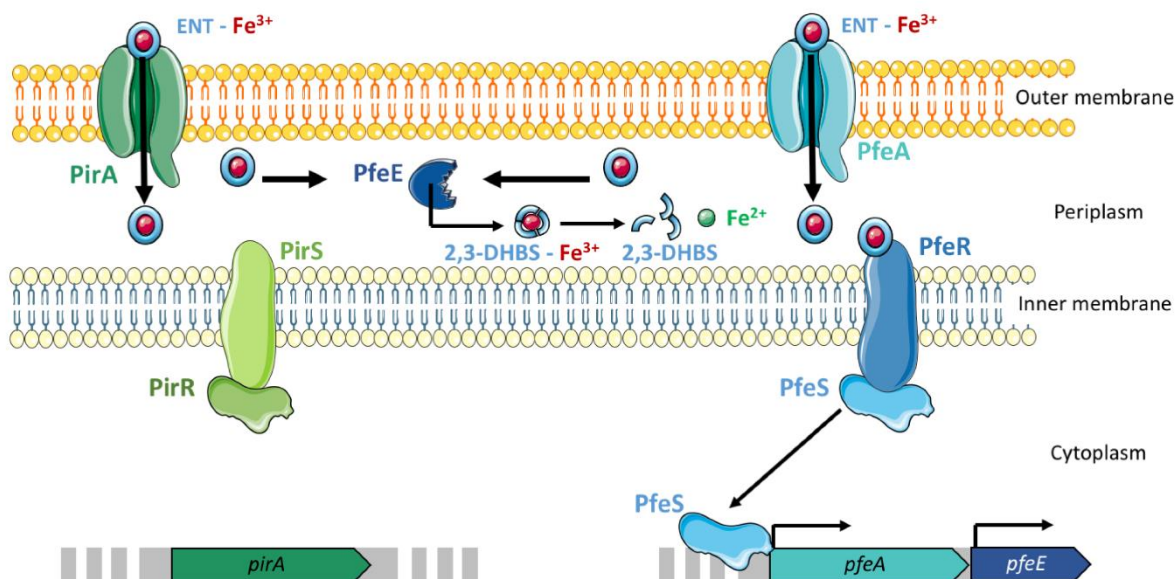


Figure S6.2. ENT-dependent iron uptake pathways in *P. aeruginosa*. Ferri-ENT is transported across the outer membrane by PfeA. If PfeA is not expressed, PirA can take over this uptake.⁸⁻¹¹ In the periplasm, PfeE hydrolyses Ferri-ENT into three molecules of 2,3-DHBS, which still stay in complex with iron.¹² An iron reduction by an unidentified reductase is necessary to release iron from the chelating catechol groups.¹² The inner membrane transporter of ferrous iron has not been identified yet. The transcription of *pfeA* and *pfeE* is activated by the two-component system PfeS/PfeR.^{8, 13, 14} Ferri-ENT binds in the bacterial periplasm to the sensor PfeS, which releases the transcriptional regulator PfeR. *pirA* has also its transcription regulated by a two-component system PirS/PirR, but apparently the presence of ferri-ENT does not strongly activate this system.^{14, 15}

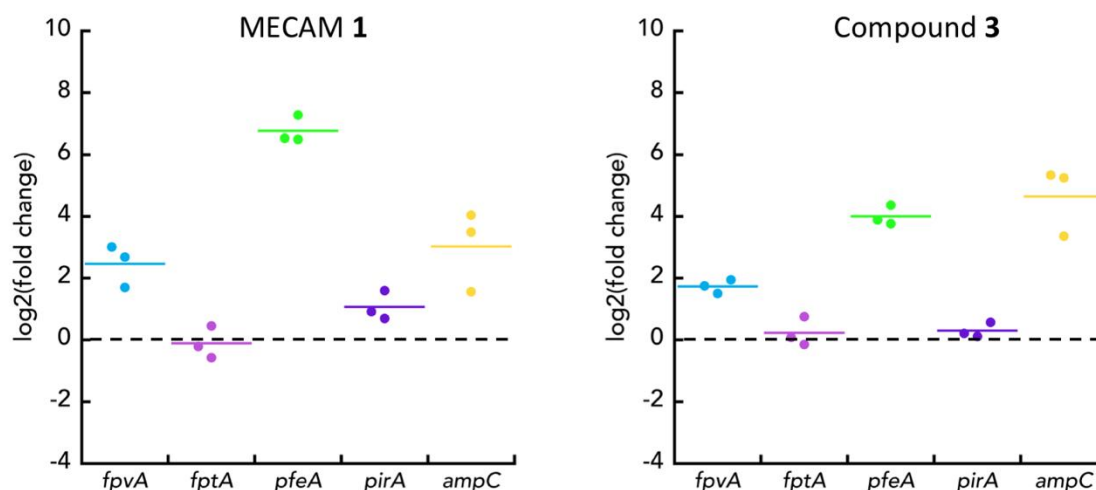


Figure S6.3. Transcription of the *fpvA*, *fptA*, *pfeA*, *pirA*, and *ampC* genes in the presence of 1 or 3. RT-qPCR was performed on RNA isolated from *P. aeruginosa* PAO1 cells grown in CAA medium in the absence or presence of 10 μ M MECAM 1 or compound 3, during 8 h. The results are given as the ratio between the values obtained in the presence of 10 μ M MECAM 1 or compound 3 over those obtained in the absence of the compounds. *pfeA* and *pirA* encode TBDTs involved in ENT-Fe uptake^{9,10}, *fpvA*, the TBDT of PVD-Fe¹⁶, *fptA* of PCH-Fe¹⁷ and *ampC* encodes the β -lactamase AmpC.¹⁸ For both panels, the data are normalized relative to the reference gene *uvrD* and are representative of three independent experiments.

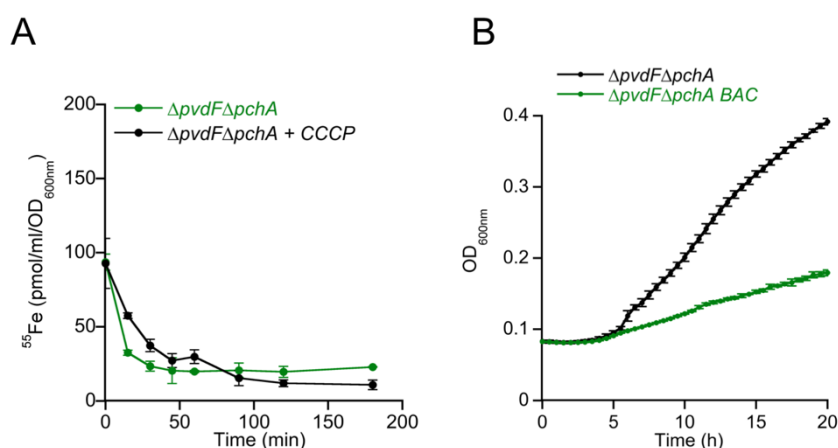


Figure S6.4. A. ⁵⁵Fe uptake in $\Delta pvdF\Delta pchA$ cells in the presence of bacillibactin. ⁵⁵Fe uptake was carried out as in Figure 4 with 500 nM bacillibactin-⁵⁵Fe; for kinetic in green the cells were pretreated with CCCP. The data show no ⁵⁵Fe uptake in *P. aeruginosa* cells in the presence of bacillibactin indicating that the pathogen is unable to use this siderophore to access iron. **B. Growth of $\Delta pvdF\Delta pchA$ in the absence (black) or presence (green) of 10 μ M bacillibactin.** The growth experiment was carried out as described in Figure 5.

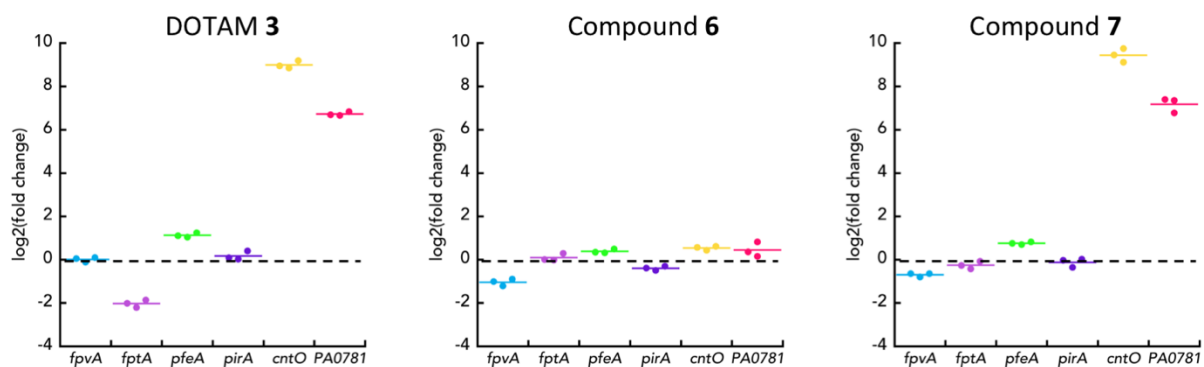


Figure S6.5. Analysis of changes in the transcription of the *fpvA*, *fptA*, *pfeA*, *pirA*, *cntO* and *PA0781* genes in the presence of DOTAM 4 or compounds 6 and 7. RT-qPCR was performed on RNA isolated from *P. aeruginosa* PAO1 cells grown in CAA medium in the absence or presence of 10 μ M DOTAM 3 or compounds 6 and 7, during 8 h. The results are given as the ratio between the values obtained in the presence of 10 μ M MECAM 1 or compound 3 over those obtained in the absence of the compounds. *pfeA* and *pirA* encode TBDTs involved in ENT-Fe uptake,^{9,10} *fpvA*, the TBDT of PVD-Fe,¹⁶ *fptA* of PCH-Fe¹⁷ and *ampC* encodes the β -lactamase AmpC.¹⁸ For both panels, the data are normalized relative to the reference gene *uvrD* and are representative of three independent experiments.

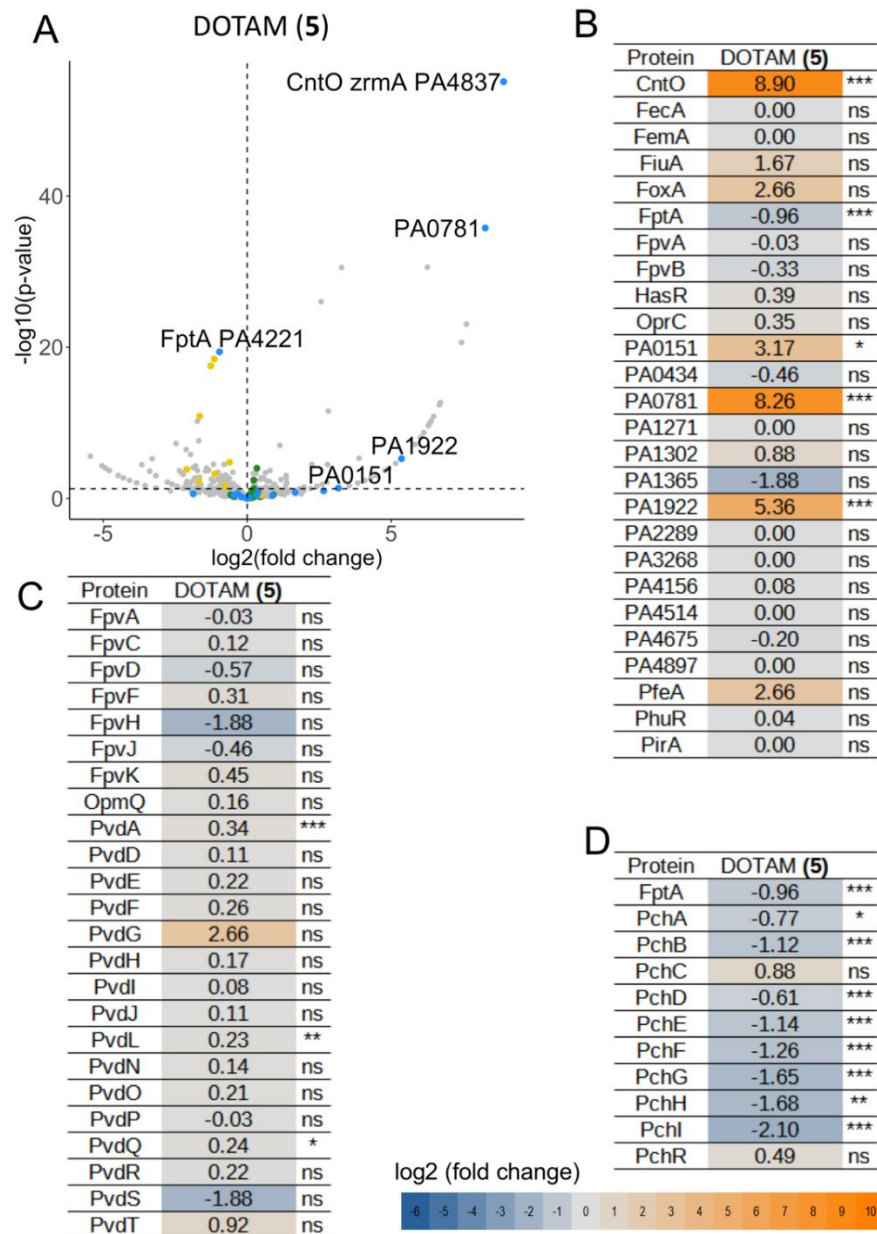


Figure S6.6. Proteomic analyses of *P. aeruginosa* PAO1 cells grown under iron-limited conditions (CAA medium) in the absence or presence of DOTAM 5. Proteomic analyses were performed on *P. aeruginosa* PAO1 strains grown overnight in CAA medium supplemented, or not, with 10 μ M DOTAM 5 (A). Average values measured in CAA in the absence of any supplementation are plotted against average values measured in CAA supplemented with either 10 μ M DOTAM 5. Median values represent the median of the relative intensity of each protein, normalized against all proteins detected by shotgun analysis ($n = 3$). The proteins of the PCH pathway are represented by yellow dots, those of the PVD pathway by green dots, and the TBDTs by blue dots. B, C and D show the heat maps: TBDTs present in *P. aeruginosa* genome (B), proteins involved in the PVD pathway (C) and proteins of the PCH pathway (D). The darker the shade of blue, the more expression of the protein is repressed; the darker the shade of orange, the more expression of the protein is induced. NS: data not significant; * $p < 0.05$, ** $p < 0.01$, and *** $p < 0.001$.

Supplementary references

1. Pinkert, L.; Lai, Y.-H.; Peukert, C.; Hotop, S.-K.; Karge, B.; Schulze, L. M.; Grunenberg, J.; Brönstrup, M. Antibiotic conjugates with an artificial MECAM-based siderophores are potent agents against Gram-positive and Gram-negative bacterial pathogens. *J. Med. Chem.* **2021**, 64 (20), 15440–15460.
2. Ferreira, K.; Hu, H.-Y.; Fetz, V.; Prochnow, H.; Rais, B.; Müller, P. P.; Brönstrup, M. Multivalent siderophore-DOTAM conjugates as theranostics for imaging and treatment of bacterial infections. *Angew. Chem. Int. Ed.* **2017**, 56 (28), 8272–8276.
3. Peukert, C.; Langer, L. N. B.; Wegener, S. M.; Tutov, A.; Bankstahl, J. P.; Karge, B.; Bengel, F. M.; Ross, T. L.; Brönstrup, M. Optimization of artificial siderophores as ⁶⁸Ga-complexed PET tracers for *in vivo* imaging of bacterial infections. *J. Med. Chem.* **2021**, 64 (16), 12359–12378.
4. Ghosh, M.; Miller, P. A.; Möllmann, U.; Claypool, W. D.; Schroeder, V. A.; Wolter, W. R.; Suckow, M.; Yu, H.; Li, S.; Huang, W.; Zajicek, J.; Miller, M. J. Targeted antibiotic delivery: Selective siderophore conjugation with daptomycin confers potent activity against multidrug resistant *Acinetobacter baumannii* both *in vitro* and *in vivo*. *J. Med. Chem.* **2017**, 60 (11), 4577–4583.
5. Ghosh, M.; Lin, Y.-M.; Miller, P. A.; Möllmann, U.; Boggess, W. C.; Miller, M. J. Siderophore conjugates of daptomycin are potent inhibitors of carbapenem resistant strains of *Acinetobacter baumannii*. *ACS Infect. Dis.* **2018**, 4 (10), 1529–1535.
6. Lee, Y. R.; Yeo, S. Cefiderocol, a new siderophore cephalosporin for the treatment of complicated urinary tract infections caused by multidrug-resistant pathogens: preclinical and clinical pharmacokinetics, pharmacodynamics, efficacy and safety. *Clin. Drug Investig.* **2020**, 40 (10), 901–913.
7. Gasser, V.; Baco, E.; Cunrath, O.; August, P. S.; Perraud, Q.; Zill, N.; Schleberger, C.; Schmidt, A.; Paulen, A.; Bumann, D.; Mislin, G. L. A.; Schalk, I. J. Catechol siderophores express the pyochelin pathway and activate the enterobactin pathway in *Pseudomonas aeruginosa*: An opportunity for siderophore-antibiotic conjugates development. *Environ. Microbiol.* **2016**, 18 (3), 819–832.
8. Gasser, V.; Kuhn, L.; Hubert, T.; Aussel, L.; Hammann, P.; Schalk, I. J. The esterase PfeE, the achilles' heel in the battle for iron between *Pseudomonas aeruginosa* and *Escherichia coli*. *Int. J. Mol. Sci.* **2021**, 22 (6), 2814.

9. Dean, C. R.; Poole, K. Cloning and characterization of the ferric enterobactin receptor gene (PfeA) of *Pseudomonas aeruginosa*. *J. Bacteriol.* **1993**, 175 (2), 317–324.
10. Ghysels, B.; Ochsner, U.; Mollman, U.; Heinisch, L.; Vasil, M.; Cornelis, P.; Matthijs, S. The *Pseudomonas aeruginosa* pirA gene encodes a second receptor for ferri-enterobactin and synthetic catecholate analogues. *FEMS Microbiol. Lett.* **2005**, 246 (2), 167–174.
11. Moynié, L.; Milenkovic, S.; Mislin, G. L. A.; Gasser, V.; Mallocci, G.; Baco, E.; McCaughan, R. P.; Page, M. G. P.; Schalk, I. J.; Ceccarelli, M.; Naismith, J. H. The complex of ferric-enterobactin with its transporter from *Pseudomonas aeruginosa* suggests a two-site model. *Nat. Commun.* **2019**, 10 (1), 3673.
12. Perraud, Q.; Moynié, L.; Gasser, V.; Munier, M.; Godet, J.; Hoegy, F.; Mély, Y.; Mislin, G. L. A.; Naismith, J. H.; Schalk, I. J. A key role for the periplasmic PfeE esterase in iron acquisition via the siderophore enterobactin in *Pseudomonas aeruginosa*. *ACS Chem. Biol.* **2018**, 13 (9), 2603–2614.
13. Dean, C. R.; Poole, K. Expression of the ferric enterobactin receptor (PfeA) of *Pseudomonas aeruginosa*: Involvement of a two-component regulatory system. *Mol. Microbiol.* 1993, 8 (6), 1095–1103.
14. Perraud, Q.; Cantero, P.; Roche, B.; Gasser, V.; Normant, V. P.; Kuhn, L.; Hammann, P.; Mislin, G. L. A.; Ehret-Sabatier, L.; Schalk, I. J. Phenotypic adaption of *Pseudomonas aeruginosa* by hacking siderophores produced by other microorganisms. *Mol. Cell Proteomics* **2020**, 19 (4), 589–607.
15. Winsor, G. L.; Griffiths, E. J.; Lo, R.; Dhillon, B. K.; Shay, J. A.; Brinkman, F. S. L. Enhanced annotations and features for comparing thousands of *Pseudomonas* genomes in the *Pseudomonas* genome database. *Nucleic Acids Res.* **2016**, 44 (D1), D646-653.
16. Poole, K.; Neshat, S.; Krebes, K.; Heinrichs, D. E. Cloning and nucleotide sequence analysis of the ferri pyoverdine receptor gene FpvA of *Pseudomonas aeruginosa*. *J. Bacteriol.* 1993, 175 (15), 4597–4604.
17. Ankenbauer, R. G.; Quan, H. N. FptA, the Fe(III)-pyochelin receptor of *Pseudomonas aeruginosa*: A phenolate siderophore receptor homologous to hydroxamate siderophore receptors. *J. Bacteriol.* **1994**, 176 (2), 307–319.
18. Yahav, D.; Giske, C. G.; Grāmatniece, A.; Abodakpi, H.; Tam, V. H.; Leibovici, L. New β -lactam- β -lactamase inhibitor combinations. *Clin. Microbiol. Rev.* **2020**, 34 (1), e00115-20.

7. Publication 5: Trojan Horse siderophore conjugates induce *P. aeruginosa* suicide and qualify the TonB protein as a novel antibiotic target

This chapter was uploaded as a preprint on ChemRxiv™:

Carsten Peukert*, Véronique Gasser*, Till Orth*, Sarah Fritsch, Vincent Normant, Olivier Cunrath, Isabelle Schalk, Mark Brönstrup

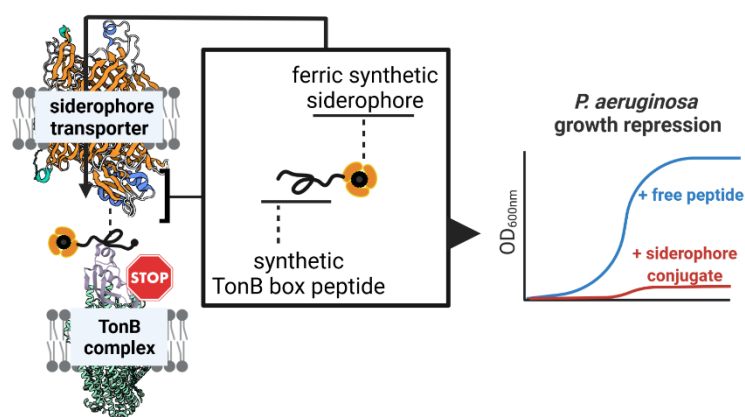
"Trojan Horse siderophore conjugates induce *P. aeruginosa* suicide and qualify the TonB protein as a novel antibiotic target".

ChemRxiv, **2022**

DOI: 10.26434/chemrxiv-2022-9zvfx

* these authors contributed equally

Table of Content graphic



Abstract

Rising infection rates with multidrug-resistant bacterial pathogens such as *Pseudomonas* combined with a shallow antibiotic pipeline urgently call for antibiotics with novel modes of action. Herein, we identify the inner membrane protein TonB, motor of active uptake in Gram negative bacteria, as a novel target in antimicrobial therapy. The interaction of the TonB box, the periplasmic *N*-terminal domain of ferri-siderophore transporters, with the inner membrane protein TonB is crucial for the internalization of essential bacterial metabolites. Overexpression of a TonB box-containing peptide fragment in *P. aeruginosa* resulted in a growth repression, even in the presence of ferric heme as an iron source. The coupling of three TonB box peptides to synthetic DOTAM and MECAM siderophores with covalent or cleavable linkers of varying length and attachment sites yielded a panel of 24 conjugates in up to 32 synthetic steps. The transporters mediating iron uptake through these conjugates were identified by molecular approaches and transporter knockout mutants to be PfeA and PirA. The conjugates **11**, **13** and **17** repressed bacterial growth in *P. aeruginosa* strains with minimal inhibitory concentrations of 0.5, 4 and 0.1 μM , respectively. The study illustrates a variant of cellular suicide therapy where a transporter imports its own inhibitor; it also demonstrates that artificial siderophores are capable to import large cargo with molecular weights of up to 4 kDa, and suggests that TonB constitutes an attractive target for antimicrobial therapy.

7.1 Introduction

Due to antibiotic overuse and a shallow antibiotic pipeline, nosocomial infections with multidrug-resistant (MDR) Gram-negative bacteria, e.g. *Pseudomonas aeruginosa* or *E. coli*, become increasingly difficult to treat.^{1, 2, 3} Moreover, newly approved antimicrobials are largely derivatives of existing classes, while novel modes of action are scarce.^{4, 5} ‘Critical’ pathogens on the WHO’s priority list are all Gram-negative bacteria, mainly because they effectively prevent the accumulation of antibiotics by their double-layered cell membranes, that operate as a tight biological barrier.⁶ The ‘Trojan Horse’ strategy outsmarts this hurdle by hijacking prokaryotic nutrient transport systems to increase the penetration of a variety of payloads (e.g. dyes, radioactive labels and antibiotics), to image and treat infections.^{7, 8} A key nutrient of prokaryotes is iron, which fulfills numerous enzymatic and metabolic functions, enabling bacterial growth and pathogenicity. Bacteria evade iron limitation in the host organism through the import of heme and ferric iron. In the latter case this implies the synthesis and secretion of small, organic iron chelators, so-called siderophores (Greek for ‘iron carriers’).⁹ After iron sequestration from host proteins, the ferric siderophore complexes are recaptured via specific outer membrane transporters called TonB-dependent transporters (TBDTs, Figure 7.1A).¹⁰ Ferric siderophores constitute cargo for TBDTs, but also other nutrients like heme, carbohydrates, nickel complexes and vitamin B₁₂ are transported by TBDTs.¹¹ Interestingly, TBDTs have also been parasitized by bacteriophages and colicins to board the bacterial cell.¹² These transporters are unique to prokaryotes and present an unparalleled gateway to shuttle antibiotics inside bacterial pathogens.¹³ This was demonstrated by the recently approved siderophore-cephalosporin antibiotic cefiderocol (Fetroja®).¹⁴ The ability to transport even large cargo into bacteria is best illustrated by microcin MccE492, a natural product that consists of an 84 aa peptide chain attached via a sugar linkage to a triscatecholate chelator originating from enterobactin.¹⁵ MccE492 exerts its antimicrobial effect at the cytoplasmic membrane after import. The application of natural siderophores as molecular targeting entities is in part hampered by their challenging synthetic access, their chemical lability as well as in some cases by their limited bacterial spectrum.^{16, 17, 18, 19} Fortunately, much like piracy, prokaryotes seize so-called ‘xenosiderophores’ (siderophores produced by other organisms or even synthetic siderophore mimetics), to satisfy their iron demand.²⁰ Along those lines, we established enterobactin analogues based on synthetic DOTAM and MECAM scaffolds as robust, readily accessible and variable vectors for bacterial imaging and antibacterial therapy in Gram-negative and Gram-positive bacteria.^{21, 22, 23}

TBDTs are composed of a 22 β -barrel inserted into the outer membrane, a plug domain that closes the channel formed by the barrel, and the TonB box.^{10,24,25} The incoming ferric siderophore from the extracellular space binds to a specific site on the plug domain, promoting the protein-protein interaction (PPI) between the TBDT's TonB box sequence and the TonB protein, that is anchored in the inner membrane and protrudes into the periplasm.²⁶ Located at the N-terminus of the TBDTs, the TonB box is a semiconserved stretch of five to seven amino acids that serves as a signature sequence for this transporter family. TonB is in complex with two other proteins ExbB and ExbD in the inner membrane (stoichiometry of 1:5:2 for TonB:ExbB:ExbD) and forms a molecular motor that uses the proton gradient of the inner membrane to convey energy to TBDTs, allowing the active transport of nutrients into the periplasmic space.²⁷ Like a lock-and-key principle, the PPI between TonB and the TonB box of the TBDT promotes a conformational change in the transporter and permits the internalization of an iron-siderophore complex into the periplasm.²⁶ *P. aeruginosa* has three genes in its genome coding for TonB proteins (TonB1, TonB2 and TonB3), with solely TonB1 interacting with the TBDTs involved in iron or heme acquisition.²⁸ Moreover, the number of TonB proteins is very limited in relation to the different TBDTs in the outer membrane, implying a strong competition of TBDTs for TonB binding.²⁹ In previous studies, bacterial virulence, TonB-mediated colicin killing and ϕ 80 phage infection could be reduced significantly by the treatment of *E. coli* with a species-specific, small TonB box consensus peptide (ETVIV), that was small enough to be internalized by polypeptide transporters.³⁰ However, an effect was only observed for high concentrations (>100 μ M).

In this study, we aimed to explore the disruption of the TBDT-TonB interaction as a novel principle in antimicrobial therapy, with a proof-of-concept in the challenging pathogen *P. aeruginosa*. First, a conditional overexpression of a soluble TonB box peptide demonstrated the antimicrobial potential of this strategy. Secondly, a pharmacological approach was pursued by conjugating TonB box peptides of varying length to siderophore mimics, to enable accumulation at their target site inside the bacterial cell. Similar to the natural microcins, an essential cellular machinery was preyed to import its own destroyer (Figure 7.1B).

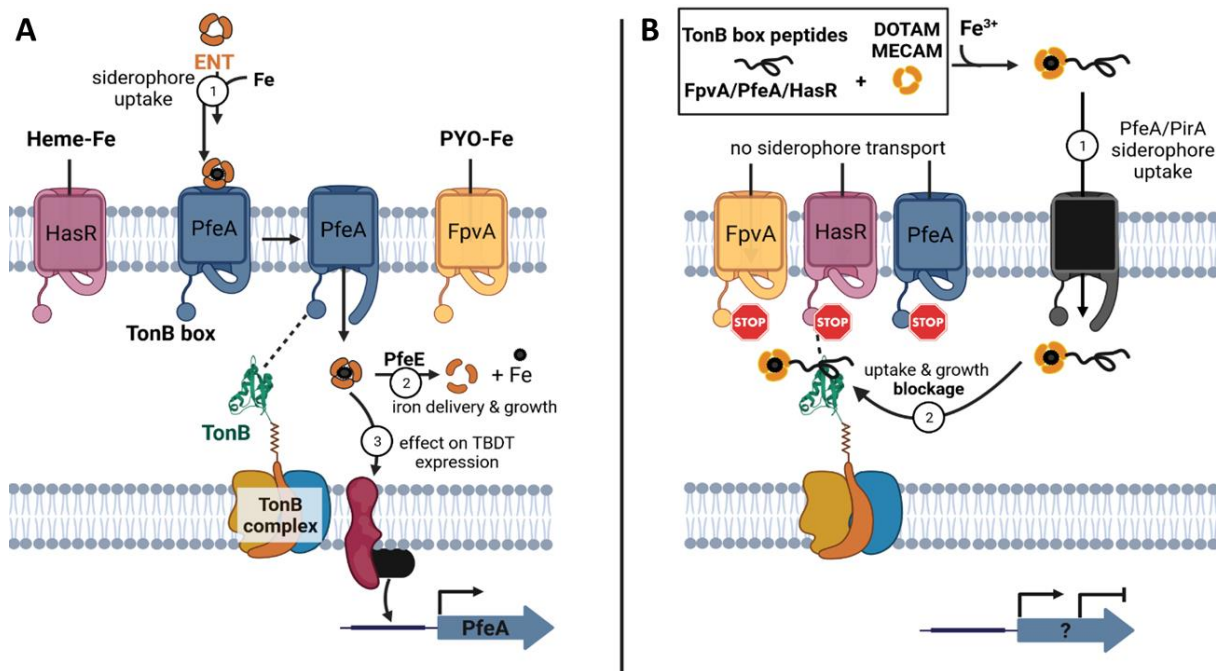


Figure 7.1 Iron delivery by enterobactin (ENT) and envisioned suicide TonB siderophore strategy. (A) Iron chelators like heme, enterobactin (ENT) or pyoverdine (PYO) are recognized by their TonB-dependent transporters (TBDTs) HasR, PfeA and FpvA in *P. aeruginosa*. In the case of ferri-enterobactin, after internalization, the esterase PfeE hydrolyzes the siderophore to get release of iron. A fraction of ferri-enterobactin interacts with the two component system PfeS/PfeR regulating the transcription of *pfeA* and *pfeE* (B) Schematic depiction of the competitive inhibition of the TonB-TonB box interaction by peptide siderophore conjugates. Synthetic siderophores DOTAM or MECAM are coupled to TonB box peptides originating from the FpvA, PfeA, or HasR. The bacteria-specific vectors are transported into the periplasm and inhibit TonB function, thereby inhibiting uptake of additional iron or heme and consequently repressing bacterial growth

7.2 Results and discussion

7.2.1 HasR TonB box peptide fragment overexpression induces growth reduction in *P. aeruginosa*

The Has system of *P. aeruginosa* extracts lipophilic heme from hemoglobin or hemopexin by a secreted hemophore to form a heme-hemophore complex, which is subsequently recognized by the TBDT HasR.^{31, 32} Until recently, the TonB box location within the amino acid sequence of HasR remained unknown. We pinpointed the TonB box of *P. aeruginosa* HasR by pBLAST alignment with a HasR homolog from *Serratia marcescens*. The TonB box in *S. marcescens* is located between the regulatory extension domain and the plug domain (Supplementary Figure S7.2).³³ Because these domains are highly conserved between species, we assumed that the TonB box of *P. aeruginosa* is located in the homologous region, and accordingly identified the peptide sequence ¹³⁰DLVQMSPSV¹³⁰ as the putative TonB box in *P. aeruginosa*.

A 172 amino acid fragment, containing the potential HasR TonB box, was cloned with a periplasmic localization sequence into a vector under the control of an arabinose promoter (*araC/pbad*, see SI) to yield the pMMB190-*araC-pbad-hasR*-His6 plasmid (Supplementary Figure S7.2). Transformed *P. aeruginosa* PAO1 bacteria were cultured in low iron (20 nM) casamino acid (CAA) medium with or without an induction with arabinose (1%) and with or without 0.25 μ M heme (Figure 7.2). As expected, addition of heme stimulated *P. aeruginosa* growth in CAA medium, indicating that bacteria used heme as an iron source (red curve). Bacterial growth was reduced upon arabinose-induced peptide expression under both growth conditions, with and without heme. This suggests that the HasR TonB box peptide bound to the inner membrane TonB protein, subsequently interfered with TonB-dependent heme internalization as well as probably with the pyoverdine and/or pyochelin-dependent iron uptake pathways used by the PAO1 strain when grown in the absence of heme. Thus, less efficient iron sequestration resulted in a growth reduction. A similar study with overexpressing the N-terminal domain of FpvA (regulating and TonB box domains) showed an inhibition of ^{55}Fe uptake by pyoverdine (PYO).³⁴ To examine the feasibility to construct a consensus sequence for TonB boxes within *Pseudomonas*, the sequence identified for HasR was compared with those for the transporter PfeA, that imports triscatecholate xenosiderophores like enterobactin (ENT), and for FpvA, that recognizes the endogenous siderophore PYO.^{35, 36} However, the conservation between the curated sequences of FpvA (FPVA_PSEAE), PfeA (PFEA_PSEAE) and HasR (Q9HYJ7_PSEAE) retrieved from the UniProt database was low (score ≤ 0.3 , black frame, Supplementary Figure S7.2).³⁷

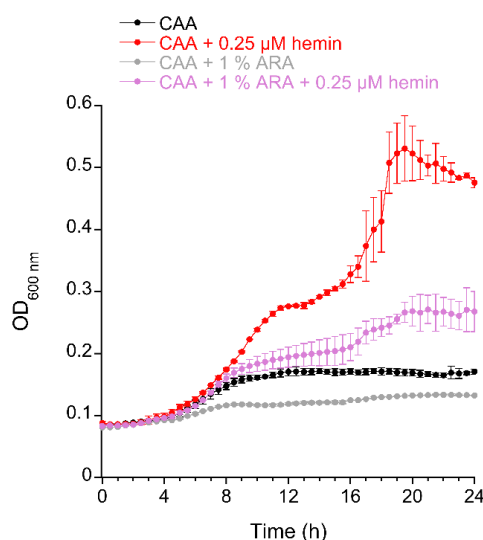


Figure 7.2. Growth of *P. aeruginosa* PAO1 transformed with pMMB190-*araC-pbad-hasR*-His₆ plasmid. The transformed bacteria were grown in CAA medium in the presence or not of 0.25 μ M hemin and with or without arabinose (ARA, 1%) induction to induce the peptide expression. Bacterial growth is followed by monitoring optical density at 600 nm ($\text{OD}_{600 \text{ nm}}$). Errors bars were calculated from three independent biological replicates.

In summary, the bioinformatics and microbiological data suggest that a TonB box peptide without transporter association can compete for TonB binding and prevent a vital PPI interaction, consequently inhibiting siderophore uptake. As a consensus sequence between the different TBBDTs of *P. aeruginosa* could not be identified, the individual sequences were employed for follow-up experiments.

7.2.2 Design and synthesis of TonB box peptide DOTAM and MECAM siderophore conjugates

Next, we aimed to induce the growth inhibition, observed with the *N*-terminal HasR overexpression, through a pharmacological intervention with synthetic TonB box peptides. These were designed to compete for the TonB-TBBDT protein-protein interaction. The lack of a consensus sequence of the employed TBBDTs required the separate synthesis of the three corresponding peptides. Each peptide was afforded in a long and a short form, with either four to five (long) or one framing amino acid (short) around the TonB box (Figure 7.3B, 9-10 aa, bold). The peptides were too large for a passive permeation through porins or the lipid bilayer and thus required the conjugation to siderophore mimics as molecular 'Trojan Horses' to allow their penetration into the bacterial periplasm. Siderophores were attached to the *N*- or the *C*-terminus of the peptide by covalent or cleavable linkers. The artificial siderophores based on DOTAM (1,4,7,10-tetraazacyclododecane-1,4,7,10-tetraacetic amide) or MECAM (1,3,5-*N,N,N'*-tris-(2,3-dihydroxybenzoyl)-triaminomethylbenzene) scaffolds were equipped with an alkyne handle for copper-catalyzed click chemistry according to established procedures (Figure 7.3C).^{22, 23} Starting from cyclen **43**, DOTAM siderophores **1** and **2** were prepared over four (38%) or five (30%) steps for the longest linear sequence, respectively (Scheme S1-S2). MECAM siderophores **3** and **4** were obtained from trisbromo-methylbenzene **47** over five (37%) or six steps (34%) in the longest linear sequence (Scheme S3). The peptides were synthesized on the solid phase using Fmoc-chemistry. More side product formation was observed for the HasR and FpvA peptides than for the PfeA peptides. This was attributed to the aspartic acid (D) and methionine (M) aa in their sequence, which are known to display i.e. succinamide formation³⁸ or oxidation to the sulfoxide under the reaction conditions.³⁹ In addition, also the unconjugated control peptides **5-10** were afforded (Schemes S5-S7, Table S7.1). For the synthesis of covalent conjugates, a N₃-PEG₇-CO₂H linker was attached at the *C*- or *N*-terminus of the peptide to permit the conjugation to **1-4** by copper-catalyzed azide alkyne additions (CuAAC). A *C*-terminal K(Dde) amino acid allowed the regioselective linker introduction after deprotection of the ϵ -amino function with hydrazine in THF/MeOH.⁴⁰ This yielded the DOTAM conjugates **11-21** and the MECAM conjugates **22-30** (Scheme S8-S10). In the case of **20** and **31**, the catechols were masked as acetylated prodrugs in order to avoid *in vivo* deactivation of the iron chelating units by catechol-*O*-methyltransferases. Pyridyl

disulfide chemistry was applied in the synthesis of the cleavable conjugates **21** and **32** that allowed an intracellular, reductive release of the peptide, thereby reducing steric hindrance of the siderophore (Scheme S10-11). The monocatechol-modified peptides **33** and **34** were constructed to reduce the overall molecular weight and still retain a TBDT-based internalization through a single chelator unit (Scheme S11). Taken together, 24 covalent or cleavable siderophore conjugates with a molecular weight of 3-4 kDa could be constructed in up to 32 synthetic steps. All conjugates were characterized by $^1\text{H-NMR}$ and high resolution mass spectrometry, exemplary molecules also by $^{13}\text{C-NMR}$, HSQC-NMR and tandem mass spectrometry (see the Supporting Information).

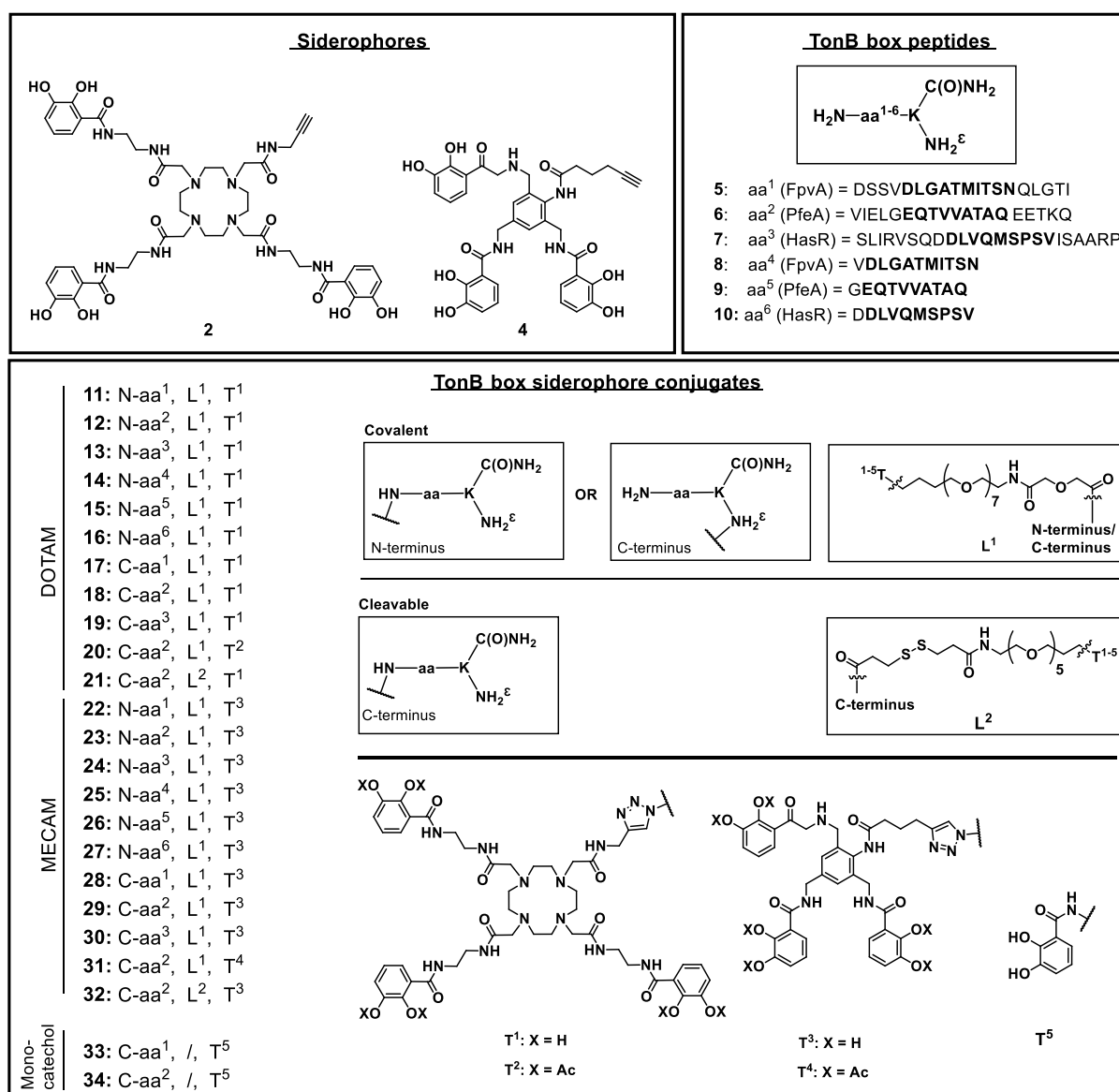


Figure 7.3. Structures of the DOTAM and MECAM siderophores **2** and **4**, TonB box peptides **5-10**, and siderophore-peptide conjugates **11-34**. The conjugates consist of a siderophore unit (T_x) that is linked via a covalent or a cleavable disulfide unit (L_x) to the *N*-terminus or the *C*-terminus of the peptide (aa_x).

7.2.3 Peptide siderophore conjugates show antimicrobial effects in *P. aeruginosa*

The siderophores **2** and **4**, the peptides **5-10** and the siderophore conjugates **11-34** were evaluated for their antimicrobial activity in *P. aeruginosa* wild type and in siderophore-deficient *P. aeruginosa* mutant strains ($\Delta pvdF \Delta pchA$). The $\Delta pvdF \Delta pchA$ mutant cannot biosynthesize its endogenous siderophores pyoverdine and pyochelin to access iron but probably uses low affinity iron uptake pathways like iron assimilation via citrate or an iron reduction process with uptake of Fe^{3+} by the FeoAB system. During an infection bacteria face an iron-starvation, as the host restrict iron access of the pathogens by nutritional immunity.⁴¹ In order to test close to the *in vivo* infection conditions, all assays were conducted in iron-depleted CAA medium (20 nM iron).^{42, 43} Along those lines, differential proteomics have shown that iron uptake pathways are solely expressed in *P. aeruginosa* cells under iron restricted conditions.⁴⁴ Compounds were first evaluated for the lowest compound concentration preventing visible bacterial growth in a standard minimal inhibitory concentration (MIC). In a second step, for a selection of compounds the ability to slow down bacterial growth was also evaluated.

MICs were determined after 24 and 48 h culture, as bacterial growth in iron-restricted conditions is slower than in an iron rich medium. While the positive control gentamicin exhibited an activity in the expected range, the free peptides **5-10** did not induce any growth inhibition (24 and 48 h). Also the free DOTAM and MECAM siderophores **2** and **4**, all MECAM conjugates as well as the monocatechols **33** and **34** remained inactive (Table 7.1). In contrast, several DOTAM conjugates inhibited bacterial growth. In particular, the long *N*-terminally linked conjugates **11** (FpvA), **12** (PfeA) and **13** (HasR) showed MICs of 0.5, 0.5 and 4 μ M, respectively at 24 h. The most potent growth inhibition (MIC = 0.1 μ M) was observed for **17**, that differs from **11** by its *C*-terminal (rather than *N*-terminal) linkage of the long FpvA-derived peptide. A moderate MIC of 8 μ M was obtained for **21** that carries a cleavable linker to a long, PfeA-derived peptide. At 48 h, growth was recovered for conjugates **14**, **17** and **21**, but not for **11** and **12**. Possibly the peptide payloads exhibit an antimicrobial activity due an interaction with TonB, but over time either an adaptation of the bacteria or a degradation of the peptide payload by proteases takes place.⁴⁵ An attempt to increase the antimicrobial efficacy through a combination treatment of *N*- or *C*-terminal peptide siderophore conjugates did not result in a potency boost (data not shown). All compounds were inactive in the wildtype strain *P. aeruginosa* PAO1.

We reasoned that the high steric demand of the peptide payload might reduce the chelator's affinity for iron, thereby reducing uptake and antimicrobial activity. Therefore, the ability of the conjugates to sequester ferric iron was tested with chrome azurol S (CAS), whose color shifts from blue (iron bound state) to bright red upon iron decomplexation. A color change was not

observed for the free peptides, while the siderophores **2** and **4** showed a clear color shift in the range from 300 to 800 nm, in line with previous reports (Supplementary Figure S7.3 and Table S7.9).^{21, 22} Notably, all siderophore-peptide conjugates retained their ability to complex iron. From the experiments it becomes apparent that iron binding was possible, but the affinity may not be sufficient to compete with the wildtype siderophore PYO for ferric iron and to confer growth inhibition.

Table 7.1. MIC values in *P. aeruginosa* $\Delta pvdF\Delta pchA$ strain for siderophores **2** and **4**, peptides **5-10** and peptide-siderophore conjugates **11-34**.

Compound number	Description	MIC after 24 h	MIC after 48 h
-	Gentamicin	1	4
5	FpvA (l)	>64	>64
6	PfeA (l)	>64	>64
7	HasR (l)	>64	>64
8	FpvA (s)	>64	>64
9	PfeA (s)	>64	>64
10	HasR (s)	>64	>64
2	DOTAM	64	64
11	FpvA (l)- <i>N</i> -DOTAM	0.5	1
12	PfeA (l)- <i>N</i> -DOTAM	0.5	1
13	HasR (l)- <i>N</i> - DOTAM	4	32
14	FpvA (s)- <i>N</i> -DOTAM	32	>64
15	PfeA (s)- <i>N</i> -DOTAM	32	32
16	HasR (s)- <i>N</i> - DOTAM	>64	>64
17	FpvA (l)- <i>C</i> -DOTAM	0.1	>64
18	PfeA (l)- <i>C</i> -DOTAM	>64	>64
19	HasR (l)- <i>C</i> -DOTAM	>64	>64
20	PfeA (l)- <i>C</i> -DOTAM-OAc	>64	>64
21	PfeA (l)- <i>DS</i> - <i>C</i> -DOTAM	8	>64

4	MECAM	>64	>64
22	FpvA (l)-N-MECAM	>64	>64
23	PfeA (l)-N-MECAM	>64	>64
24	HasR (l)-N-MECAM	>64	>64
25	FpvA (s)-N-MECAM	>64	>64
26	PfeA (s)-N-MECAM	>64	>64
27	HasR (s)-N-MECAM	>64	>64
28	FpvA (l)-C-MECAM	>64	>64
29	PfeA (l)-C-MECAM	>64	>64
30	HasR (l)-C-MECAM	>64	>64
31	PfeA (l)-C-MECAM-OAc	>64	>64
32	PfeA (l)-DS-C-MECAM	>64	>64
33	FpvA-C-catechol	>64	>64
34	PfeA-C-catechol	>64	>64

MIC values were determined after 24 h and 48 h growth and are the mean of three independent experiments. (l) = long peptide, 20-24 aa, (s) = short peptide, 11-12 aa, C/N = C/N-terminal, DS = disulfide. Values are given in [μ M], n = 3.

7.2.4 Peptide-siderophore conjugates enter the bacterial periplasm

Previously, we have employed ^{55}Fe uptake assays to demonstrate that MECAM or DOTAM have the ability to shuttle iron into bacteria through the TBDTs PfeA and PirA, or through PirA only, respectively.⁴⁶ Unfortunately, small precipitations of iron loaded conjugates prohibited the execution of ^{55}Fe uptake assays with DOTAM and MECAM peptide conjugates with a sufficiently strong ^{55}Fe signal-to-noise ratio (data not shown). Consequently we exploited the property of ferri-siderophores to interact with the two component system PfeS/PfeR and induce *pfeA* transcription. Upon binding of periplasmic ferri-siderophore to the PfeS sensor at the inner membrane, the transcriptional regulator PfeR is released, upregulating the transcription of the *pfeA* gene.^{47,48} Induction of *pfeA* transcription in the presence of the conjugates indicates the penetration of the compounds, since an interaction with PfeS can occur only in the periplasm. We have recently shown that unconjugated MECAM induced the transcription and expression of *pfeA* by interacting with PfeS.⁴⁶ This induction was accompanied by a transcription repression of the genes involved in acquisition of iron by the siderophore pyochelin (PCH).⁴⁶

The PYO and PCH-deficient $\Delta pvdF\Delta pchA$ strain was grown over eight hours in iron-restricted CAA medium in the absence or presence of the peptides, free DOTAM and MECAM cores, and a selection of conjugates (**11**, **12**, **13**, **17**, **22** and **28**, each at 10 μ M). The expression of the genes encoding *pfeA* (ferri-ENT TBDT),³⁶ *pirA* (ferri-ENT and ferri-catecholamines TBDT),^{49, 50} *fpvA* (ferri-PYO TBDT),²⁴ and *fptA* (ferri-PCH TBDT)^{51, 35, 52} was analyzed by differential quantitative real-time PCR (qRT-PCR) (Figure 7.4). Expectedly, the cores **2** and **4** showed a one to six (log2)fold induction of *pfeA* transcription in the PAO1 wildtype and $\Delta pvdF\Delta pchA$ mutant.⁴⁶ The free peptides **5-10** had no effect. For all tested MECAM and DOTAM conjugates, an induction of *pfeA* transcription was observed. This verifies their translocation into the periplasm and their interaction with the sensor PfeS at the inner membrane. The MECAM conjugates induced the transcription of *pfeA* with the same efficiency as the MECAM vector **4** alone. The DOTAM conjugates displayed an even stronger *pfeA* transcription induction than the free DOTAM vector **2**. None of the vectors or conjugates had a significant effect on *pirA* transcription. The transcription of *pirA*, such as of *pfeA*, is regulated by a two component system, namely PirS/PirR. Apparently the MECAM and DOTAM conjugates were able to bind to PfeS and induce a release of PfeR, but not to PirS.

All compounds, vectors and conjugates also induced a repression of *fptA* transcription. Interestingly, the highest fold changes concerning induction of *pfeA* and repression of *fptA* transcription were seen for the inactive MECAM conjugates, whilst the DOTAM conjugates generally had lower effects. This is probably due to a higher iron affinity of MECAM compared to DOTAM compounds. This adjustment of *pfeA* and *fptA* transcription indicates that the $\Delta pvdF\Delta pchA$ strain adapted its TBDT expression for optimal iron acquisition via the conjugates in its surrounding. We also checked the ability of **11** to modulate the transcription of *pfeA*, *pirA*, *fpvA* and *fptA* in the PAO1 wildtype strain. However, their transcription was unaffected, possibly due to a higher efficacy of PYO and PCH to access iron than the larger **11**. In summary, both MECAM and DOTAM conjugates were able to cross the outer membrane of *P. aeruginosa*, because they induced a phenotypic adaptation of the bacteria (\uparrow *pfeA* transcription, \downarrow *fptA* transcription). Consequently, we conclude that the antibiotic activity of the DOTAM conjugates was not due to iron sequestration by the compounds outside bacterial cells, but caused by internalized peptides, and probably an interaction of the peptides with TonB. All together these data indicate that the self-internalizing suicide Trojan horse mechanism is operational.

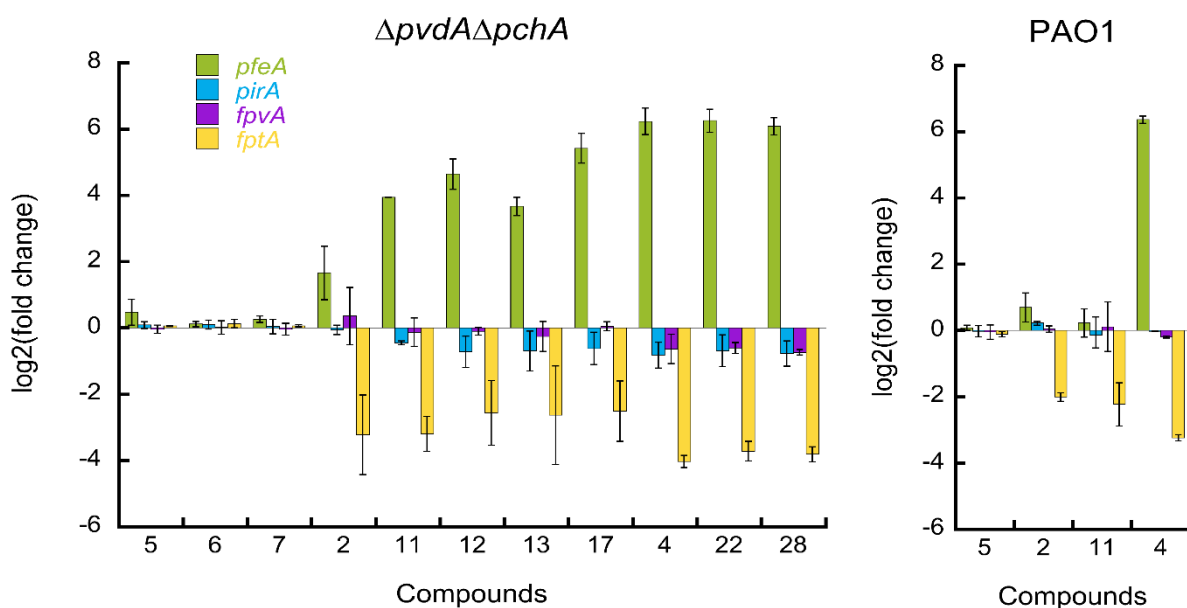


Figure 7.4. Modulation of TBDT gene expression by conjugates. *P. aeruginosa* $\Delta pvdF\Delta pchA$ cells were grown for 8 h in the presence or absence of test compounds (10 μ M). The transcription of *pfeA*, *pirA*, *fpvA* and *fptA* was followed by qRT-PCR.⁴² *pfeA* encodes the ferri-ENT TBDT,^{53,36} *pirA* the ferri-ENT and ferri-catecholamines TBDT^{49, 50} *fpvA* the ferri-PYO TBDT²⁴ and *fptA* the ferri-PCH TBDT.^{51, 52} For the OD_{600 nm} values, see the supporting information.

7.2.5 The transporters PfeA and PirA mediate the entry of conjugates in *P. aeruginosa* cells

Next, we aimed to elucidate the TBDT(s) involved in conjugate uptake. For this purpose, the growth of the *P. aeruginosa* $\Delta pvdF\Delta pchA$ strain was compared to strains that carried additional TBDT deletions of (i) *pfeA*, (ii) *pirA* or (iii) *pfeA* and *pirA*. For compounds that do not exert antimicrobial activities, a growth reduction after TBDT knock-out proves that the missing siderophore transporter was crucial for the internalization of ferric chelates and thus permitted bacterial growth.^{54, 46} The free peptides **5-7** exerted no effect (Figure 7.5). The growth of DOTAM-based conjugates was hardly impaired by missing PfeA, but a strong growth inhibition was observed for all mutants lacking PirA, indicating that all these compounds enter the cells through this TBDT. For MECAM-based conjugates the single deletion of PirA had no significant effect, whereas a lack of PfeA delayed growth slightly, in particular for the free MECAM **4** and the conjugate **29**. Interestingly, the dual knockout of *pfeA* and *pirA* genes led to a complete growth inhibition for all MECAM compounds, indicating that these compounds entered *P. aeruginosa* cells by both PfeA and PirA. This result also indicates that one receptor was able to rescue when the other receptor was absent or not functional. The data are in agreement with our recent finding that the MECAM core and a MECAM-ampicillin conjugate are transported into *P. aeruginosa* cells via PfeA and PirA, whereas DOTAM is solely internalized

via PirA.⁴⁶ We conclude that the transport mechanisms of the artificial siderophores were not altered by the conjugation of large peptidic cargo in the kilodalton range, and that the MECAM conjugates enter bacteria by either PfeA or PirA and the DOTAM conjugates by PirA.

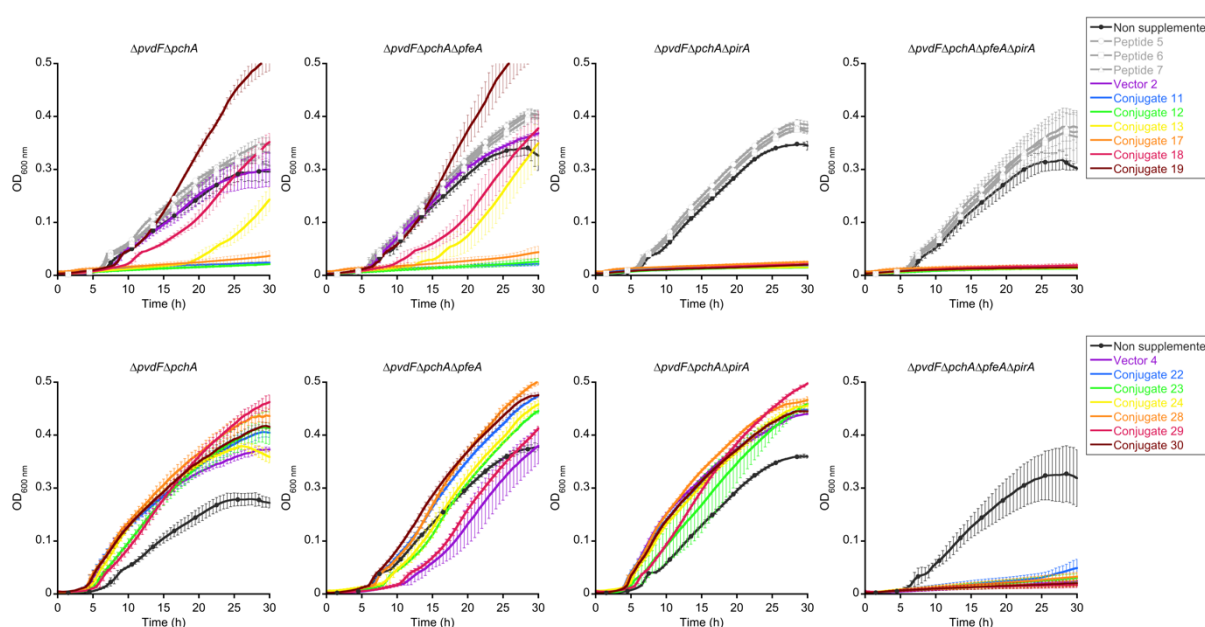


Figure 7.5. Growth kinetics of *P. aeruginosa* *pfeA* and *pirA* mutants in the presence of the conjugates. The PYO and PCH-deficient strain of *P. aeruginosa* ($\Delta pvdF\Delta pchA$) and its corresponding *pfeA* and *pirA* deletion mutants were used. Strains were grown in CAA medium in the absence or presence of 10 μ M peptides 5-7, DOTAM 2, MECAM 4 or the conjugates 11-13, 17-19, 22-24 and 28-30. Growth was followed by monitoring the optical density (OD) at 600 nm. Errors bars were calculated from three independent biological replicates.

7.3 Conclusion

In this study, we propose the disturbance of the interaction between TBDTs involved in the uptake of nutrient across the outer membrane of Gram negative bacteria and the TonB protein as a novel strategy to inhibit bacterial growth. A systematic attachment of siderophores to TonB box polypeptides from three TBDTs, coupled via cleavable or covalent linkers at the N- or C-terminus of the peptide to various of the targeting vectors (DOTAM and MECAM), yielded a diverse compound collection of two mono catechol peptides and 24 full siderophore conjugates. With molecular weights of up to 4 kDa, these are, to the best of our knowledge, among the largest synthetic siderophore conjugates. Their iron complexation capabilities were demonstrated by the CAS test. Growth recovery assays and their ability to induce the transcription of *pfeA* via the two component system PfeS/PfeR proved that all compounds were able to enter the periplasm of *P. aeruginosa*. All MECAM conjugates were internalized by PfeA

and PirA TBDTs, and DOTAM conjugates by PirA. A notable growth delay or inhibition, attributed to ferric siderophore internalization, was observed solely for DOTAM conjugates. The five conjugates **11**, **12**, **13**, **17** and **21** displayed antimicrobial activity in siderophore-deficient *P. aeruginosa* strains, and the most potent analogs **11** and **17** reached MICs of 0.5 and 0.1 μM , respectively. Based on the above data, we derive the following preliminary structure activity relationships (SAR) (Supplementary Figure S7.4). Because all active compounds were based on the triscatecholate DOTAM vector, it was obviously better suited than MECAM. Conjugates with FpvA-originating peptides were more active compared to the equivalent congeners carrying sequences from PfeA and HasR. The active congeners had an *N*-terminal linkage rather than a *C*-terminal disulfide linker, and the longer peptides were superior to shorter ones.

Together, these results demonstrate the capability of MECAM and DOTAM to transport large cargo in the kilodalton range into bacteria. While first evidence in this direction has been obtained for the prototype natural product microcin MccE492, the data suggest that also artificial siderophores, coupled to synthetic linkers and peptides, can be employed. We realized the first siderophore 'Trojan Horse' antibiotics that target and disrupt a protein-protein interaction in the bacterial periplasm. Instead of satiating the pathogen's appetite for iron, the TonB box peptide payload competes with the TBDTs for TonB and thereby prevents the internalization of further ferric chelates. Thus, the study illustrates a variant of cellular suicide where a transporter imported its own inhibitor. Perturbing the TonB-TBBDT interaction is a novel principle to interfere with the pathogen's iron homeostasis and growth, yielding a decreased metabolism and fitness, and the conjugates described herein support the validity of the target. At this stage, structural information of the TonB box - TonB interaction at a molecular level would be beneficial to improve the understanding why only a subset of the conjugates was active. From here, it appears attractive to initiate a search for less complex small molecules that interfere with the PPI in future studies.

Funding information

The presented work was supported by a 'Kekulé-Stipendium' of the 'Fonds der chemischen Industrie (VCI)', as well as with a grant from the Joint Programming Initiative on Antimicrobial Resistance (JPI AMR, grant number: 01KI1825). We also acknowledge the Interdisciplinary Thematic Institute (ITI) InnoVec (Innovative Vectorization of Biomolecules, IdEx, ANR-10-IDEX-0002).

Conflict of interest

The authors declare no conflict of interest.

Acknowledgements

We thank Ulrike Beutling for the measurement of HRMS samples and Christel Kakoschke as well as Kirsten Harmrolfs for the measurement of NMR samples. We are thankful for helpful comments on the manuscript by Hazel Fuchs, Anna Vetter und Vadim Korotkov.

Abbreviations

TBDT - TonB-dependent transporters,

PMF - proton-motive force,

aa - amino acid;

DOTAM - 1,4,7,10-tetraazacyclododecane-1,4,7,10-tetraacetic amide;

MECAM - 1,3,5-*N,N,N'*-tris-(2,3-dihydroxybenzoyl)-triaminomethylbenzene,

PPI - protein-protein interactions;

SAR - structure activity relationship;

PCH - pyochelin;

PYO - pyoverdine;

CAS - chrome azurol S;

MIC - minimal inhibitory concentration;

CAA - casamino acid;

CuAAC - copper-catalyzed azide alkyne cycloaddition;

ENT - enterobactin;

MDR - multidrug-resistant.

References

1. Tacconelli, E.; Carrara, E.; Savoldi, A.; Harbarth, S.; Mendelson, M.; Monnet, D. L.; Pulcini, C.; Kahlmeter, G.; Kluytmans, J.; Carmeli, Y.; Ouellette, M.; Outtersson, K.; Patel, J.; Cavalieri, M.; Cox, E. M.; Houchens, C. R.; Grayson, M. L.; Hansen, P.; Singh, N.; Theuretzbacher, U.; Magrini, N., Discovery, research, and development of new antibiotics: the WHO priority list of antibiotic-resistant bacteria and tuberculosis. *Lancet Infect. Dis.* **2018**, *18* (3), 318-327.
2. Murray, C. J. L.; Ikuta, K. S.; Sharara, F.; Swetschinski, L.; Robles Aguilar, G.; Gray, A.; Han, C.; Bisignano, C.; Rao, P.; Wool, E.; Johnson, S. C.; Browne, A. J.; Chipeta, M. G.; Fell, F.; Hackett, S.; Haines-Woodhouse, G.; Kashef Hamadani, B. H.; Kumaran, E. A. P.; McManigal, B.; Agarwal, R.; Akech, S.; Albertson, S.; Amuasi, J.; Andrews, J.; Aravkin, A.; Ashley, E.; Bailey, F.; Baker, S.; Basnyat, B.; Bekker, A.; Bender, R.; Bethou, A.; Bielicki, J.; Boonkasidecha, S.; Bukosia, J.; Carneiro, C.; Castañeda-Orjuela, C.; Chansamouth, V.; Chaurasia, S.; Chiurchiù, S.; Chowdhury, F.; Cook, A. J.; Cooper, B.; Cressey, T. R.; Criollo-Mora, E.; Cunningham, M.; Darboe, S.; Day, N. P. J.; De Luca, M.; Dokova, K.; Dramowski, A.; Dunachie, S. J.; Eckmanns, T.; Eibach, D.; Emami, A.; Feasey, N.; Fisher-Pearson, N.; Forrest, K.; Garrett, D.; Gastmeier, P.; Giref, A. Z.; Greer, R. C.; Gupta, V.; Haller, S.; Haselbeck, A.; Hay, S. I.; Holm, M.; Hopkins, S.; Iregbu, K. C.; Jacobs, J.; Jarovsky, D.; Javanmardi, F.; Khorana, M.; Kissoon, N.; Kobeissi, E.; Kostyanov, T.; Krapp, F.; Krumkamp, R.; Kumar, A.; Kyu, H. H.; Lim, C.; Limmathurotsakul, D.; Loftus, M. J.; Lunn, M.; Ma, J.; Mturi, N.; Munera-Huertas, T.; Musicha, P.; Mussi-Pinhata, M. M.; Nakamura, T.; Nanavati, R.; Nangia, S.; Newton, P.; Ngoun, C.; Novotney, A.; Nwakanma, D.; Obiero, C. W.; Olivas-Martinez, A.; Olliaro, P.; Ooko, E.; Ortiz-Brizuela, E.; Peleg, A. Y.; Perrone, C.; Plakkal, N.; Ponce-de-Leon, A.; Raad, M.; Ramdin, T.; Riddell, A.; Roberts, T.; Robotham, J. V.; Roca, A.; Rudd, K. E.; Russell, N.; Schnall, J.; Scott, J. A. G.; Shivamallappa, M.; Sifuentes-Osornio, J.; Steenkeste, N.; Stewardson, A. J.; Stoeva, T.; Tasak, N.; Thaiprakong, A.; Thwaites, G.; Turner, C.; Turner, P.; van Doorn, H. R.; Velaphi, S.; Vongpradith, A.; Vu, H.; Walsh, T.; Waner, S.; Wangrangsimakul, T.; Wozniak, T.; Zheng, P.; Sartorius, B.; Lopez, A. D.; Stergachis, A.; Moore, C.; Dolecek, C.; Naghavi, M., Global burden of bacterial antimicrobial resistance in 2019: a systematic analysis. *The Lancet* **2022**, *399* (10325), 629-655.
3. Thaden, J. T.; Park, L. P.; Maskarinec, S. A.; Ruffin, F.; Fowler, V. G.; Duin, D. v., Results from a 13-year prospective cohort study show increased mortality associated with bloodstream infections caused by *Pseudomonas aeruginosa* compared to other bacteria. *Antimicrob. Agents Chemother.* **2017**, *61* (6), e02671-16.

4. Butler, M. S.; Gigante, V.; Sati, H.; Paulin, S.; Al-Sulaiman, L.; Rex, J. H.; Fernandes, P.; Arias, C. A.; Paul, M.; Thwaites, G. E.; Czaplewski, L.; Alm, R. A.; Lienhardt, C.; Spigelman, M.; Silver, L. L.; Ohmagari, N.; Kozlov, R.; Harbarth, S.; Beyer, P., Analysis of the clinical pipeline of treatments for drug resistant bacterial infections: despite progress, more action is needed. *Antimicrob. Agents Chemother.* **2022**, Aac0199121.
5. Theuretzbacher, U.; Gottwalt, S.; Beyer, P.; Butler, M.; Czaplewski, L.; Lienhardt, C.; Moja, L.; Paul, M.; Paulin, S.; Rex, J. H.; Silver, L. L.; Spigelman, M.; Thwaites, G. E.; Paccaud, J. P.; Harbarth, S., Analysis of the clinical antibacterial and antituberculosis pipeline. *Lancet Infect. Dis.* **2019**, *19* (2), e40-e50.
6. Breidenstein, E. B. M.; de la Fuente-Núñez, C.; Hancock, R. E. W., *Pseudomonas aeruginosa*: all roads lead to resistance. *Trends Microbiol.* **2011**, *19* (8), 419-426.
7. Klahn, P.; Bronstrup, M., Bifunctional antimicrobial conjugates and hybrid antimicrobials. *Nat. Prod. Rep.* **2017**, *34* (7), 832-885.
8. Miller, M. J.; Liu, R., Design and syntheses of new antibiotics inspired by nature's quest for iron in an oxidative climate. *Acc. Chem. Res.* **2021**, *54* (7), 1646-1661.
9. Hider, R. C.; Kong, X., Chemistry and biology of siderophores. *Nat. Prod. Rep.* **2010**, *27* (5), 637-657.
10. Schalk, I. J.; Mislin, G. L. A.; Brillet, K., Chapter two - structure, function and binding selectivity and steoselectivity of siderophore-ion outer membrane transporters. *Curr. Top. Membr.*, Argüello, J. M.; Lutsenko, S., Eds. Academic Press: 2012; Vol. 69, pp 37-66.
11. Schauer, K.; Rodionov, D. A.; de Reuse, H., New substrates for TonB-dependent transport: do we only see the 'tip of the iceberg'? *Trends Biochem. Sci.* **2008**, *33* (7), 330-338.
12. Hickman, S. J.; Cooper, R. E. M.; Bellucci, L.; Paci, E.; Brockwell, D. J., Gating of TonB-dependent transporters by substrate-specific forced remodelling. *Nat. Comm.* **2017**, *8* (1), 14804.
13. Schalk, I. J.; Mislin, G. L. A., Bacterial Iron Uptake Pathways: Gates for the import of bactericide compounds. *J. Med. Chem.* **2017**, *60* (11), 4573-4576.
14. Wu, J. Y.; Srinivas, P.; Pogue, J. M., Cefiderocol: A novel agent for the management of multidrug-resistant Gram-negative organisms. *Infect. Dis. Ther.* **2020**, *9* (1), 17 – 40.
15. Duquesne, S.; Destoumieux-Garzón, D.; Peduzzi, J.; Rebuffat, S., Microcins, gene-encoded antibacterial peptides from enterobacteria. *Nat. Prod. Rep.* **2007**, *24* (4), 708-34.
16. Neumann, W.; Sassone-Corsi, M.; Raffatellu, M.; Nolan, E. M., Esterase-catalyzed siderophore hydrolysis activates an enterobactin-ciprofloxacin conjugate and confers targeted antibacterial activity. *J. Am. Chem. Soc.* **2018**, *140* (15), 5193 – 5201.

17. Raines, D. J.; Moroz, O. V.; Blagova, E. V.; Turkenburg, J. P.; Wilson, K. S.; Duhme-Klair, A. K., Bacteria in an intense competition for iron: Key component of the *Campylobacter jejuni* iron uptake system scavenges enterobactin hydrolysis product. *Proc. Natl. Acad. Sci.* **2016**, *113* (21), 5850-5855.
18. Mashiach, R.; Meijler, M. M., Total synthesis of pyoverdine D. *Org. Lett.* **2013**, *15* (7), 1702-1705.
19. Petrik, M.; Umlaufova, E.; Raclavsky, V.; Palyzova, A.; Havlicek, V.; Haas, H.; Novy, Z.; Dolezal, D.; Hajduch, M.; Decristoforo, C., Imaging of *Pseudomonas aeruginosa* infection with Ga-68 labelled pyoverdine for positron emission tomography. *Sci. Rep.* **2018**, *8* (1), 15698.
20. Perraud, Q.; Cantero, P.; Roche, B.; Gasser, V.; Normant, V. P.; Kuhn, L.; Hammann, P.; Mislin, G. L. A.; Ehret-Sabatier, L.; Schalk, I. J., Phenotypic adaption of *Pseudomonas aeruginosa* by hacking siderophores produced by other microorganisms* *Mol. Cell. Proteomics* **2020**, *19* (4), 589-607.
21. Ferreira, K.; Hu, H.-Y.; Fetz, V.; Prochnow, H.; Rais, B.; Müller, P. P.; Brönstrup, M., Multivalent siderophore–DOTAM conjugates as theranostics for imaging and treatment of bacterial infections. *Angew. Chem. Int. Ed.* **2017**, *56* (28), 8272-8276.
22. Pinkert, L.; Lai, Y.-H.; Peukert, C.; Hotop, S.-K.; Karge, B.; Schulze, L. M.; Grunenberg, J.; Brönstrup, M., Antibiotic conjugates with an artificial MECAM-Based siderophore are potent agents against Gram-positive and Gram-negative bacterial pathogens. *J. Med. Chem.* **2021**, *64* (20), 15440-15460.
23. Peukert, C.; Langer, L. N. B.; Wegener, S. M.; Tutov, A.; Bankstahl, J. P.; Karge, B.; Bengel, F. M.; Ross, T. L.; Brönstrup, M., Optimization of artificial siderophores as ⁶⁸Ga-complexed PET tracers for *in vivo* imaging of bacterial infections. *J. Med. Chem.* **2021**, *64* (16), 12359-12378.
24. Brillet, K.; Journet, L.; Célia, H.; Paulus, L.; Stahl, A.; Pattus, F.; Cobessi, D., A β strand lock exchange for signal transduction in TonB-dependent transducers on the basis of a common structural motif. *Structure* **2007**, *15* (11), 1383-1391.
25. Llamas, M. A.; Mooij, M. J.; Sparrius, M.; Vandenbroucke-Grauls, C. M. J. E.; Ratledge, C.; Bitter, W., Characterization of five novel *Pseudomonas aeruginosa* cell-surface signalling systems. *Mol. Microbiol.* **2008**, *67* (2), 458-472.
26. Celia, H.; Noinaj, N.; Zakharov, S. D.; Bordignon, E.; Botos, I.; Santamaria, M.; Barnard, T. J.; Cramer, W. A.; Lloubes, R.; Buchanan, S. K., Structural insight into the role of the Ton complex in energy transduction. *Nature* **2016**, *538* (7623), 60-65.
27. Ratliff, A. C.; Buchanan, S. K.; Celia, H., Ton motor complexes. *Curr. Opin. Struct. Biol.* **2021**, *67*, 95-100.

28. DiRita, V. J.; Takase, H.; Nitanaï, H.; Hoshino, K.; Otani, T., Requirement of the *Pseudomonas aeruginosa tonB* gene for high-affinity iron acquisition and infection. *Infect. Immun.* **2000**, *68* (8), 4498-4504.
29. Higgs, P. I.; Larsen, R. A.; Postle, K., Quantification of known components of the *Escherichia coli* TonB energy transduction system: TonB, ExbB, ExbD and FepA. *Mol. Microbiol.* **2002**, *44*.
30. Tuckman, M.; Osburne, M. S., *In vivo* inhibition of TonB-dependent processes by a TonB box consensus pentapeptide. *J. Bacteriol.* **1992**, *174* (1), 320-323.
31. Zygiel, E. M.; Obisesan, A. O.; Nelson, C. E.; Oglesby, A. G.; Nolan, E. M., Heme protects *Pseudomonas aeruginosa* and *Staphylococcus aureus* from calprotectin-induced iron starvation. *J. Biol. Chem.* **2021**, *296*, 100160.
32. Smith, A. D.; Modi, A. R.; Sun, S.; Dawson, J. H.; Wilks, A., Spectroscopic determination of distinct heme ligands in outer-membrane receptors PhuR and HasR of *Pseudomonas aeruginosa*. *Biochemistry* **2015**, *54* (16), 2601-2612.
33. Létoffé, S.; Wecker, K.; Delepierre, M.; Delepelaire, P.; Wandersman, C., Activities of the *Serratia marcescens* heme receptor HasR and isolated plug and beta-barrel domains: The beta-barrel forms a heme-specific channel. *J. Bacteriol.* **2005**, *187* (13), 4637-45.
34. Nader, M.; Journet, L.; Meksem, A.; Guillon, L.; Schalk, I. J., Mechanism of ferripyoverdine uptake by *Pseudomonas aeruginosa* outer membrane transporter FpvA: No diffusion channel formed at any time during ferrisiderophore uptake. *Biochemistry* **2011**, *50* (13), 2530-2540.
35. Cobessi, D.; Celia, H.; Folschweiller, N.; Schalk, I. J.; Abdallah, M. A.; Pattus, F., The crystal structure of the pyoverdine outer membrane receptor FpvA from *Pseudomonas aeruginosa* at 3.6Å resolution. *J. Mol. Biol.* **2005**, *347* (1), 121-134.
36. Moynié, L.; Milenkovic, S.; Mislin, G. L. A.; Gasser, V.; Mallocci, G.; Baco, E.; McCaughan, R. P.; Page, M. G. P.; Schalk, I. J.; Ceccarelli, M.; Naismith, J. H., The complex of ferric-enterobactin with its transporter from *Pseudomonas aeruginosa* suggests a two-site model. *Nat. Comm.* **2019**, *10* (1), 3673.
37. Zimmermann, L.; Stephens, A.; Nam, S.-Z.; Rau, D.; Kübler, J.; Lozajic, M.; Gabler, F.; Söding, J.; Lupas, A. N.; Alva, V., A completely reimplemented MPI bioinformatics toolkit with a new HHpred server at its core. *J. Mol. Biol.* **2018**, *430* (15), 2237-2243.
38. Capasso, S.; Mazzarella, L.; Sica, F.; Zagari, A.; Salvadori, S., Spontaneous cyclization of the aspartic acid side chain to the succinimide derivative. *J. Chem. Soc. Chem. Comm.* **1992**, (12), 919-921.
39. Schilter, D., Thiol oxidation: A slippery slope. *Nat. Rev. Chem.* **2017**, *1* (2), 0013.

40. Díaz-Mochón, J. J.; Bialy, L.; Bradley, M., Full orthogonality between Dde and Fmoc: The direct synthesis of PNA–peptide conjugates. *Org. Lett.* **2004**, *6* (7), 1127-1129.
41. Cassat, James E.; Skaar, Eric P., Iron in infection and immunity. *Cell Host & Microbe* **2013**, *13* (5), 509-519.
42. Gasser, V.; Baco, E.; Cunrath, O.; August, P. S.; Perraud, Q.; Zill, N.; Schleberger, C.; Schmidt, A.; Paulen, A.; Bumann, D.; Mislin, G. L. A.; Schalk, I. J., Catechol siderophores repress the pyochelin pathway and activate the enterobactin pathway in *Pseudomonas aeruginosa*: an opportunity for siderophore–antibiotic conjugates development. *Environ. Microbiol.* **2016**, *18* (3), 819-832.
43. Cunrath, O.; Geoffroy, V. A.; Schalk, I. J., Metallome of *Pseudomonas aeruginosa*: A role for siderophores. *Environ. Microbiol.* **2016**, *18* (10), 3258-3267.
44. Perraud, Q.; Cantero, P.; Munier, M.; Hoegy, F.; Zill, N.; Gasser, V.; Mislin, G. L. A.; Ehret-Sabatier, L.; Schalk, I. J., Phenotypic adaptation of *Pseudomonas aeruginosa* in the presence of siderophore-antibiotic conjugates during epithelial cell infection. *Microorganisms* **2020**, *8* (11), 1820.
45. Culp, E.; Wright, G. D., Bacterial proteases, untapped antimicrobial drug targets. *J. Antibiot.* **2017**, *70* (4), 366-377.
46. Fritsch, S.; Gasser, V.; Peukert, C.; Pinkert, L.; Kuhn, L.; Perraud, Q.; Normant, V.; Brönstrup, M.; Schalk, I., Uptake mechanisms and regulatory responses to MECAM- and DOTAM-based artificial siderophores and their antibiotic conjugates in *Pseudomonas aeruginosa*. *ACS Infect. Dis.* **2022**, *8*, 6, 1134-1146.
47. Dean, C. R.; Neshat, S.; Poole, K., PfeR, an enterobactin-responsive activator of ferric enterobactin receptor gene expression in *Pseudomonas aeruginosa*. *J. Bacteriol.* **1996**, *178* (18), 5361-5369.
48. Gasser, V.; Kuhn, L.; Hubert, T.; Aussel, L.; Hammann, P.; Schalk, I. J., The esterase PfeE, the achilles' Hheel in the battle for Iron between *Pseudomonas aeruginosa* and *Escherichia coli*. *Int. J. Mol. Sci.* **2021**, *22* (6), 2814.
49. Ghysels, B.; Ochsner, U.; Möllman, U.; Heinisch, L.; Vasil, M.; Cornelis, P.; Matthijs, S., The *Pseudomonas aeruginosa pirA* gene encodes a second receptor for ferrienterobactin and synthetic catecholate analogues. *FEMS Microbiol. Lett.* **2005**, *246* (2), 167-174.
50. Perraud, Q.; Kuhn, L.; Fritsch, S.; Graulier, G.; Gasser, V.; Normant, V.; Hammann, P.; Schalk, I. J., Opportunistic use of catecholamine neurotransmitters as siderophores to access iron by *Pseudomonas aeruginosa*. *Environ. Microbiol.* **2022**, *24* (2), 878-893.
51. Ankenbauer, R. G.; Quan, H. N., FptA, the Fe(III)-pyochelin receptor of *Pseudomonas aeruginosa*: A phenolate siderophore receptor homologous to hydroxamate siderophore receptors. *J. Bacteriol.* **1994**, *176* (2), 307-319.

52. Cobessi, D.; Celia, H.; Pattus, F., Crystal structure at high resolution of ferric-pyochelin and its membrane receptor FptA from *Pseudomonas aeruginosa*. *J. Molec. Biol.* **2005**, *352* (4), 893-904.
53. Dean, C. R.; Poole, K., Cloning and characterization of the ferric enterobactin receptor gene (pfeA) of *Pseudomonas aeruginosa*. *J. Bacteriol.* **1993**, *175* (2), 317-324.
54. Perraud, Q.; Cantero, P.; Roche, B.; Gasser, V.; Normant, V. P.; Kuhn, L.; Hammann, P.; Mislin, G. L. A.; Ehret-Sabatier, L.; Schalk, I. J., Phenotypic adaption of *Pseudomonas aeruginosa* by hacking siderophores produced by other microorganisms*. *Mol. Cell. Proteom.* **2020**, *19* (4), 589-607.

Supporting information

General chemical information

Unless otherwise mentioned, reagents were purchased and used without further purification. All employed solvents for workups and purifications were HPLC purity grade. Solid-phase peptide synthesis (SPPS) was performed on an automated Syro Multiple Peptide Synthesizer (MultiSynTech, Witten, Germany) with a Rapp TentaGel® S RAM resin (Rapp Polymere, Tübingen, Germany). Centrifugations were performed on a Universal 32 R centrifuge (Hettich).

With the exception of biphasic reactions or reactions in water, all reactions were carried out in anhydrous solvents. Moisture-sensitive reactions were carried out oven-dried glassware under argon atmosphere. Reaction progress was monitored by TLC (silica gel 60 F₂₅₄, on aluminum/glass, Merck®).

Automatic preparative column chromatography was performed on a Grace Reveleris® X2 instrument (Büchi®) with disposable columns (Reveleris® Flash Cartridges Silica 40 µm, Büchi).

Purifications by RP-HPLC were performed on a Pure C-850 (Büchi) or Dionex Ultimate (Thermo Fisher Scientific) on a phenomenex Gemini C18 RP-column 00G-4436-NO, 10 µm, 110 A, 250×10.00 mm (5 mL/min) or phenomenex Gemini C18 RP-column 00G-4435-PO-AX, 5 µm, 110 A, 250×21.20 mm (10 mL/min). Substances were subsequently freeze-dried on an Alpha 2-4 LSCbasic (Christ) instrument.

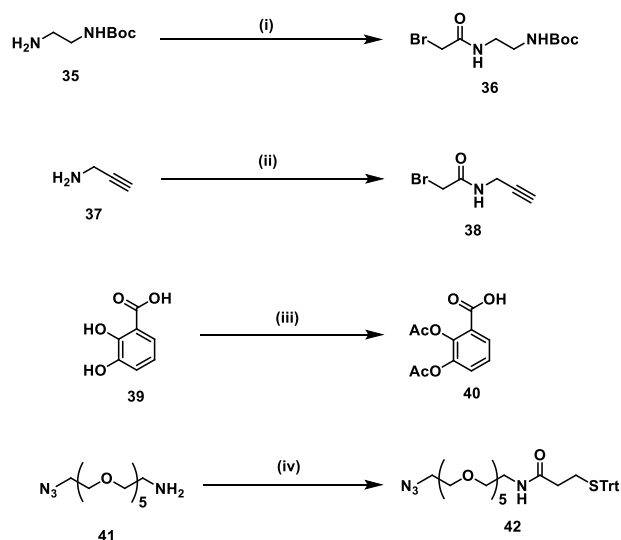
High resolution mass spectrometry (HRMS) was performed using a Dionex Ultimate 3000 HPLC system equipped with a DAD detector and a Bruker maxis HD QTOF mass detector with electrospray ionization (ESI). Samples were injected directly *via* an Ultimate 3000RS autosampler (Thermo Fisher Scientific). The mass-to-charge ratios (*m/z*) are indicated.

All isolated compounds were characterized by ¹H-, ¹³C-NMR spectra, and/or ESI-HRMS.

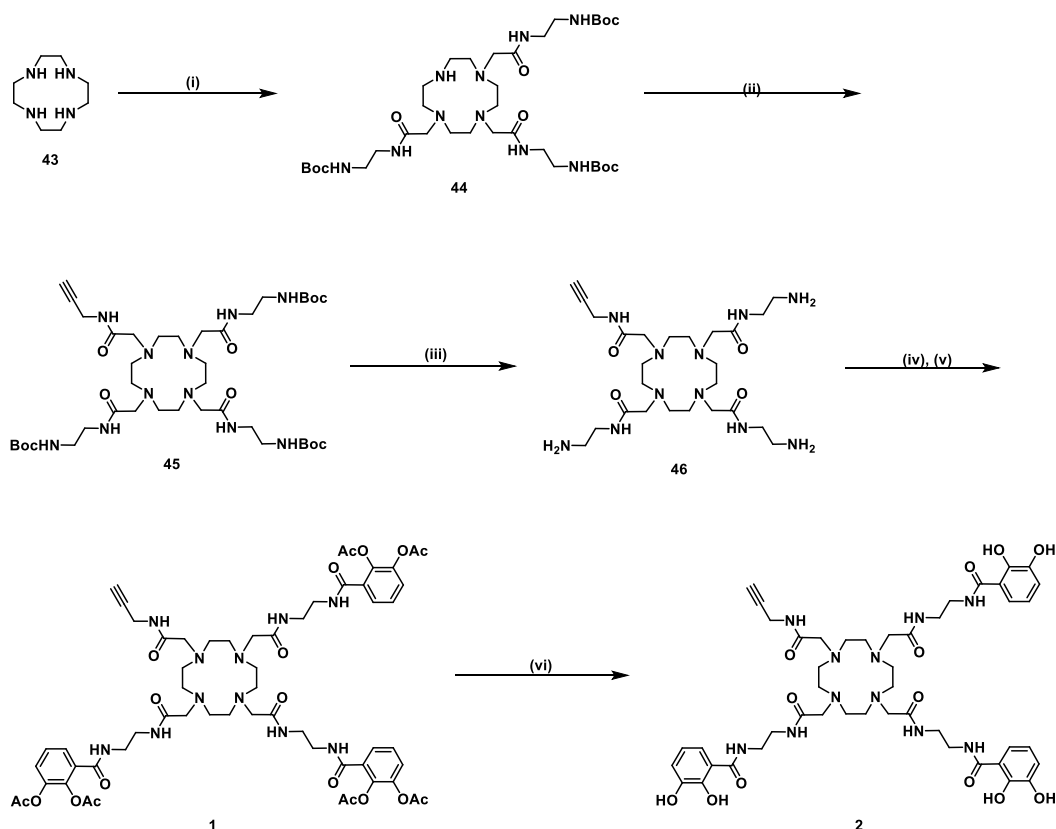
Yields are calculated based on substance purity ≥95% as confirmed by NMR and MS.

NMR spectra were acquired on Advance III 500 with the probe head PABBO BB/19F-1H/D Z-GRD (500 MHz for ¹H, 125 MHz for ¹³C), and Advance III HD 700 with cryo platform and the probe head CPTCI 1H-13C/15N/D Z-GRD (700 MHz for ¹H, 176 MHz for ¹³C) from Bruker. The measured substances were dissolved in the respective deuterated solvent and the chemical shifts δ are given in ppm. Multiplicities of the individual signals are as follows: s (singlet), d (doublet), t (triplet), q (quartet), quint (quintet) and combinations thereof, dd (doublet of doublet), tt (triplet of triplet), dt (doublet of triplet), td (triplet of doublet), etc. Others include: bs (broad singlet) and m (multiplet). All spectra were interpreted as first order spectra. The coupling constants *J* are given in hertz (Hz) and refer to ¹H-¹H couplings.

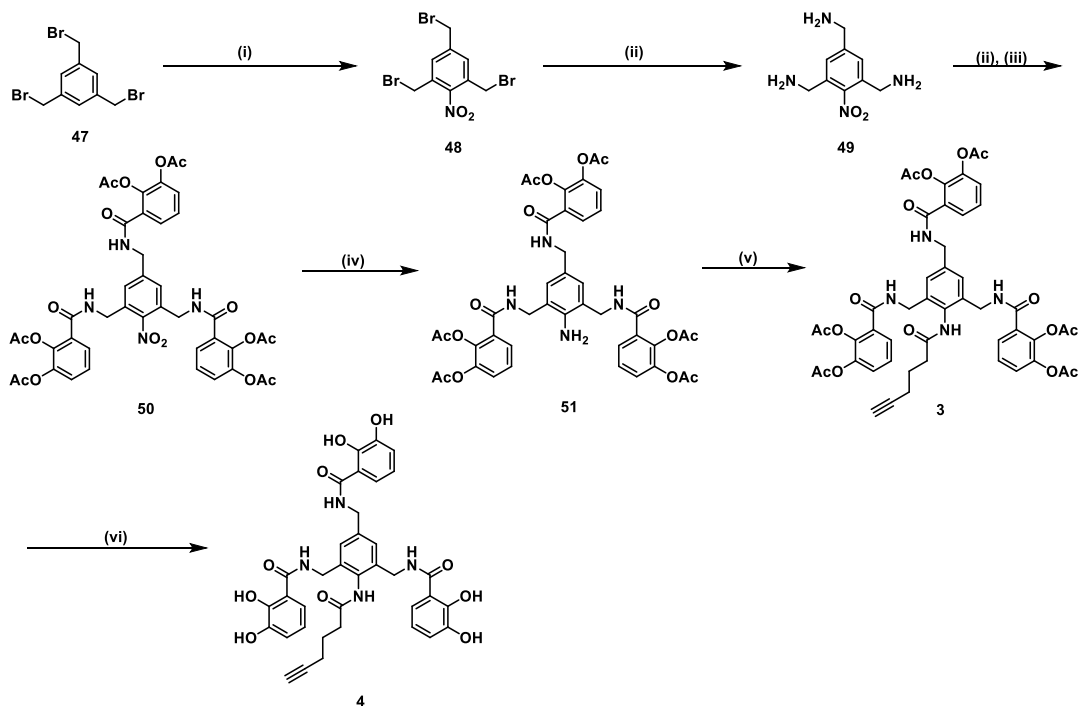
Chemistry figures, schemes and tables



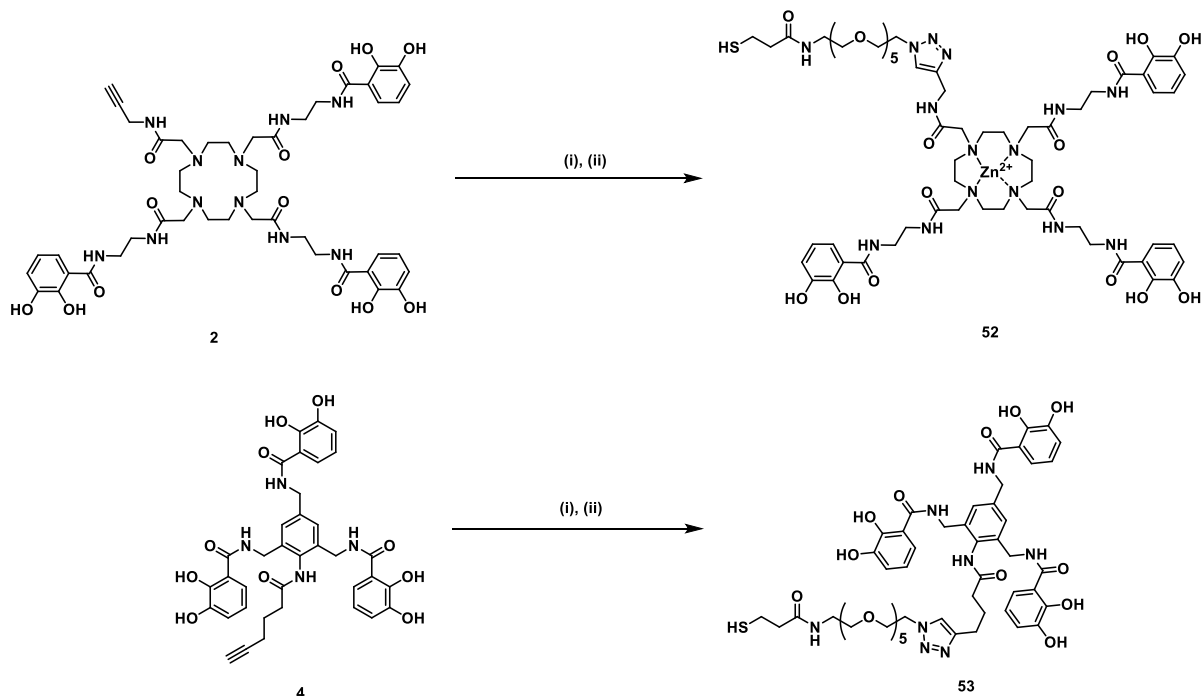
Scheme S7.1. Synthesis of siderophore building blocks **36**, **38**, **40**, **42** and **44**. (i) BrCH_2COBr , K_2CO_3 , $\text{H}_2\text{O}/\text{CH}_2\text{Cl}_2$, 0-23 °C, 95% (ii) $\text{BrCH}_2\text{C}(\text{O})\text{Br}$, K_2CO_3 , $\text{H}_2\text{O}/\text{CH}_2\text{Cl}_2$, 0-23 °C, 72%, (iii) BrCH_2COBr , K_2CO_3 , $\text{H}_2\text{O}/\text{CH}_2\text{Cl}_2$, 0-23 °C, 2h, 81%, (iv) Ac_2O , TEA, DMAP, THF, 23-60 °C, 21 °C, 96%, (v) $(\text{C}_6\text{H}_5)_3\text{CS}(\text{CH}_2)_2\text{COOH}$, HATU, TEA, $\text{CH}_2\text{Cl}_2/\text{DMF}$, 23 °C, 21 h, 76%.



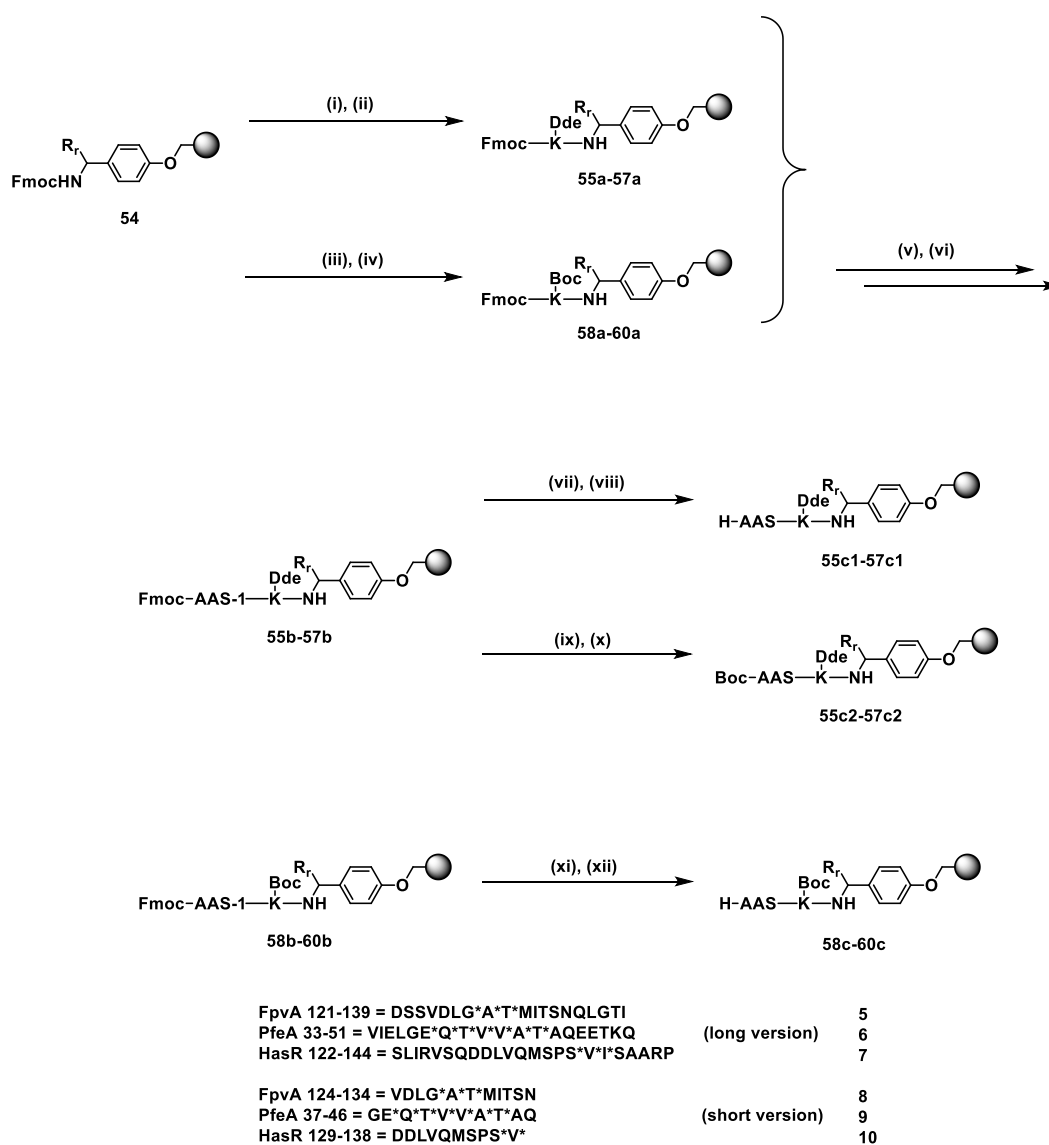
Scheme S7.2. Synthesis of DOTAM siderophores **1** and **2**. (i) **36**, NaOAc, ACN, 23 °C, 21 h, (ii) **38**, K_2CO_3 , ACN, 23 °C, 21 h, (iii) 25% TFA, DCM, 0-23 °C, 4 h, 82% over three steps, (iv) **40**, $(\text{COCl})_2$, DCM/DMF, 0-23 °C, 3 h, (v) NaHCO_3 , $\text{H}_2\text{O}/1,4\text{-dioxane}$, 0-23 °C, 6 h, (vi) 20% DIPEA, MeOH, 0-23 °C, 4 h, 80% over 3 steps.



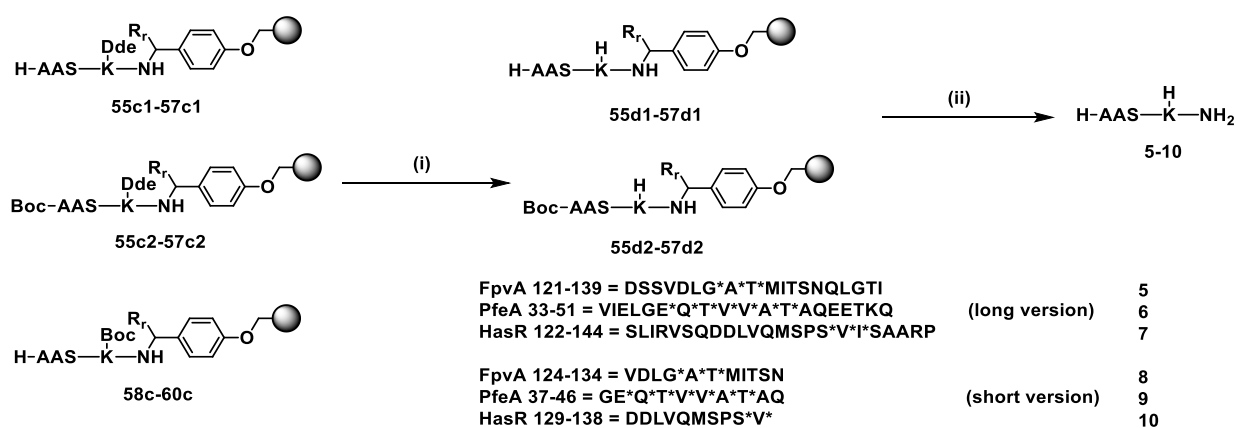
Scheme S7.3. Synthesis of MECAM siderophores **3** and **4**. (i) HNO_3 (50%), H_2SO_4 , 0-23 °C, 48 h, 98%, (ii) NH_4OH (30%), THF/EtOH, 23 °C, 21 h, (iii) **40**, $(\text{COCl})_2$, DCM/DMF, 0-23 °C, 3 h, (iv) NaHCO_3 , $\text{H}_2\text{O}/1,4\text{-dioxane}$, 0-23 °C, 6 h, over two steps 68%, (v) Zn dust, AcOH, THF/EtOH, 0-23 °C, 1 h, (vi) 6-hexynoic acid, *i*BuCF, NMM, THF, 0-23 °C, 6 h, over two steps 56%, (vii) 20% DIPEA, MeOH, 0-23 °C, 4 h, 90%.



Scheme S7.4. Synthesis of thio-DOTAM (**53**) and MECAM (**53**) derivatives. (i) $\text{Zn}(\text{CH}_3\text{COO})_2$, DMSO/ H_2O , 23 °C, 5 min, then **44**, DMSO, 23 °C, 5 min, then CuSO_4 , sodium ascorbate, THPTA, PBS pH 7.4, 23 °C, 1 h, 76%, (ii) 25% TFA, TIPS, DCM, 0-23 °C, 2 h, 94%. (iii) **44**, DMSO/ H_2O , 23 °C, 5 min, then CuSO_4 , sodium ascorbate, THPTA, PBS, 23 °C, 1 h, 82%, (iv) 25% TFA, TIPS DCM, 0-23 °C, 2 h, 90%.



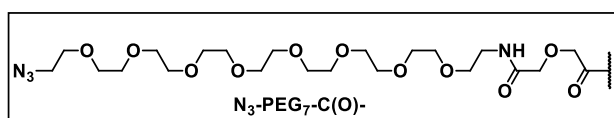
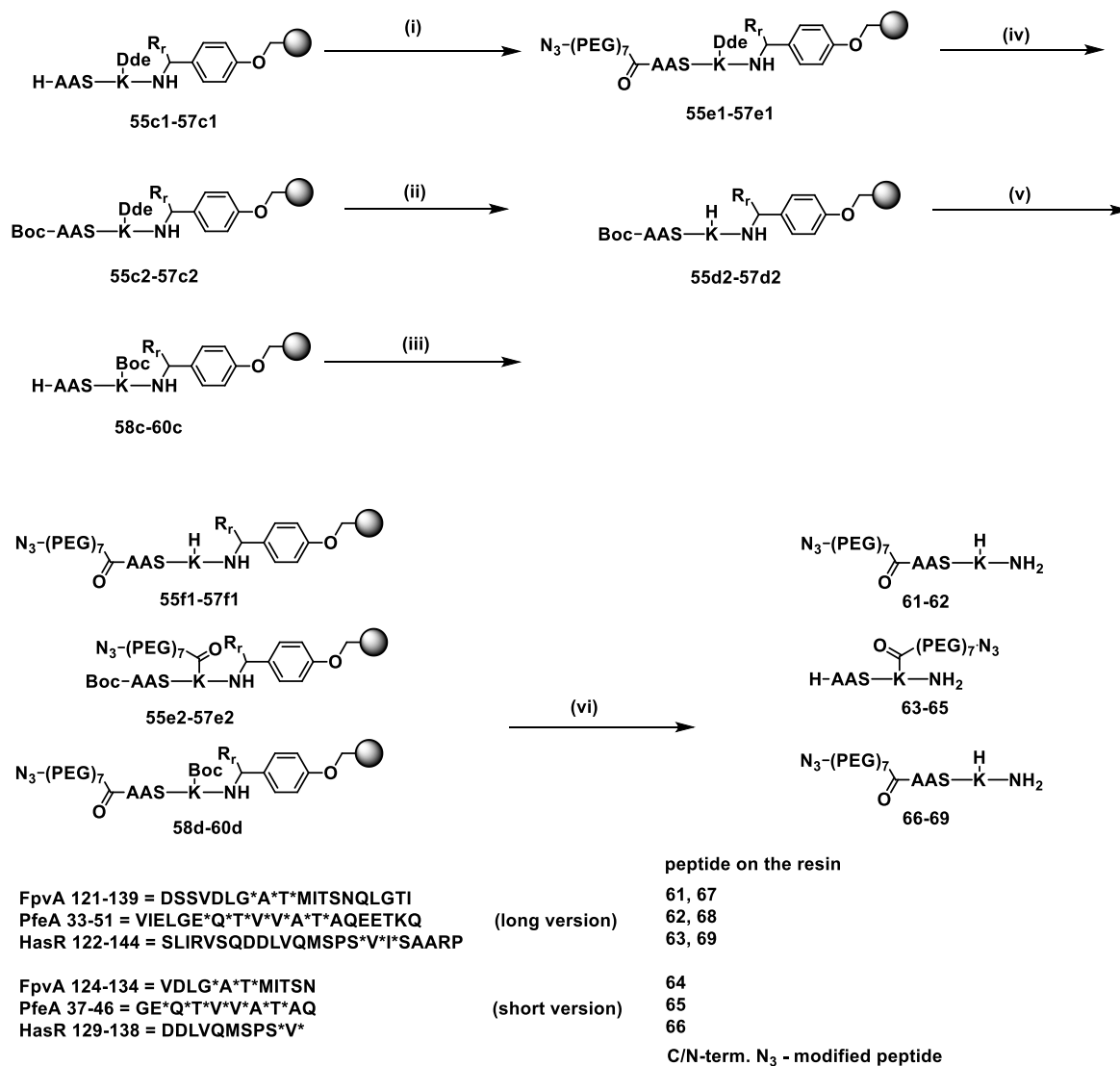
Scheme S7.5 Synthesis of (unmodified) peptide precursors *via* SPPS. * = mark complicated couplings determined by *Peptide Companion* (1.25 CoshiSoft/PeptiSearch, 2000) and were performed with double coupling and capping. For the long peptide sequences, an Fmoc- or Boc-protected amino acid at the α -amino group was introduced as the terminal amino acid. (i) piperidine, DMF, 23 °C, 10 min, (ii) Fmoc-Lys(Dde)-OH, HATU, DIPEA, DMF, 23 °C, 1 h, (iii) piperidine, DMF, 23 °C, 10 min, (iv) Fmoc-Lys(Boc)-OH, HATU, DIPEA, DMF, 23 °C, 1 h, (v) piperidine, DMF, 23 °C, 10 min, (vi) protected Fmoc-aa, HCTU, DIPEA, DMF, 23 °C, 1 h, (vii) piperidine, DMF, 23 °C, 10 min, (viii) protected Fmoc-Aa, HCTU, DIPEA, DMF, 23 °C, 1 h, (ix) piperidine, DMF, 23 °C, 10 min, (x) piperidine, DMF, 23 °C, 10 min, (xi) protected Boc-Aa, HATU, DIPEA, DMF, 23 °C, 1 h, (xii) piperidine, DMF, 23 °C, 10 min.



Scheme S7.6 Synthesis of unmodified peptides **5-10**. * = mark complicated couplings determined by Peptide Companion (1.25 CoshiSoft/PeptiSearch, 2000) and were performed with double coupling and capping. For the long peptide sequences, a Fmoc- or Boc-protected amino acid at the α -amino group was introduced as the terminal amino acid. (i) 1.0 M hydrazine in THF, 23 °C, 3 h, (ii) 95% TFA, 3% TIPS, 2% H₂O, 23 °C, 3 h, over 12 to 26 steps 8-52%.

Table S7.1 Synthesis characteristics of the unmodified peptides **5-10**, (l) = long peptide, (s) = short peptide.

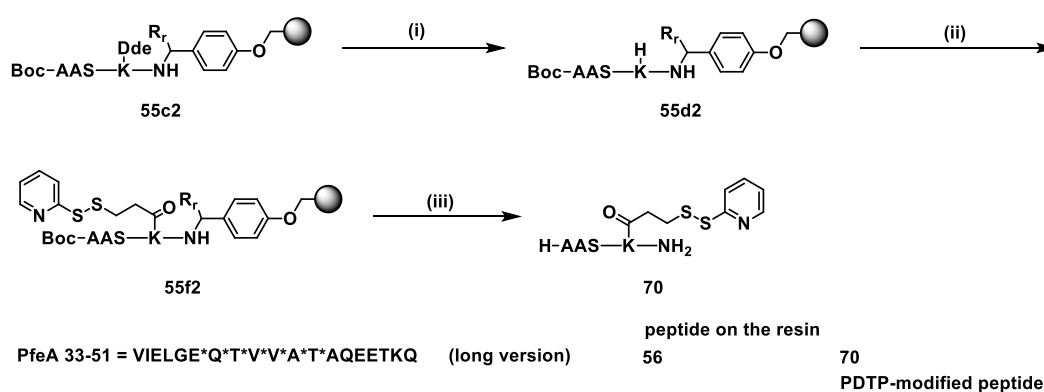
#	Peptides	aa	Cycles	Time t [h]	Steps	Yield [%]	Yield/step [%]
5	<i>FpvA</i> (l)	20	23	34	22	16	92
6	<i>PfeA</i> (l)	20	27	39	22	27	94
7	<i>HasR</i> (l)	24	27	38	26	12	92
8	<i>FpvA</i> (s)	12	15	21	13	33	92
9	<i>PfeA</i> (s)	11	18	25	12	52	95
10	<i>HasR</i> (s)	11	13	19	12	36	92



Scheme S7.7 Syntheses of *N*- & *C*-terminal PEG-modified peptides **61-69**. (i) N₃-PEG₇-CO₂H, HOBt, HATU, NMM, DMF, 23 °C, 21 h, (ii) 1.0 M hydrazine in THF, DMF, 23 °C, 3 h, (iii) N₃-PEG₇-CO₂H, HOBt, HATU, NMM, DMF, 23 °C, 21 h, (iv) 1.0 M hydrazine in THF, DMF, 23 °C, 3 h, (v) N₃-PEG₇-CO₂H, HOBt, HATU, NMM, DMF, 23 °C, 21 h, (vi) 95% TFA; 3% TIPS, 2% H₂O, 23 °C, 3 h, synthesized over 13 – 27 steps with 3 – 33% overall yield.

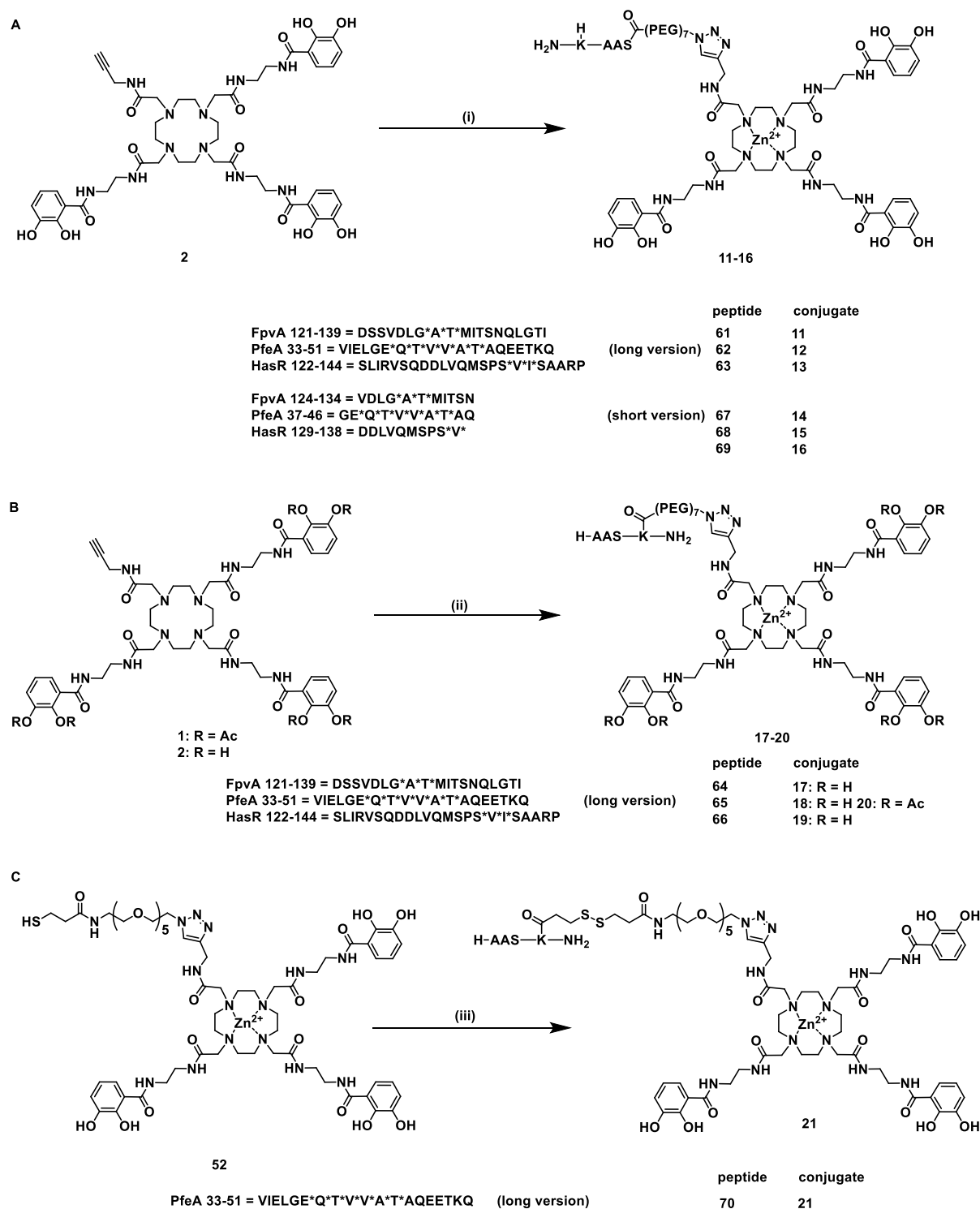
Table S7.2. Comparison of the PEG-modified peptides **61-69**. aa= amino acid, (l) = long peptide, (s) = short peptide.

#	Peptides	aa	Cycles	time <i>t</i> [h]	Steps	Yield [%]	Yield/step [%]
61	<i>FpvA</i> (l) N-term	20	23	55	23	11	91
62	<i>PfeA</i> (l) N-term	20	27	60	23	21	93
63	<i>HasR</i> (l) N-term	24	27	59	27	10	92
64	<i>FpvA</i> (l) C-term	20	23	55	23	12	91
65	<i>PfeA</i> (l) C-term	20	27	60	23	23	94
66	<i>HasR</i> (l) C-term	24	27	59	27	12	92
67	<i>FpvA</i> (s) N-term	12	15	42	14	24	90
68	<i>PfeA</i> (s) N-term	11	18	46	13	33	92
69	<i>HasR</i> (s) N-term	11	13	40	13	15	86



Scheme S7.8 Synthesis of C-terminal PDTP-modified *PfeA* 33-51 peptide **70**. (i) 1.0 M hydrazine, in THF, DMF, 23 °C, 3 h, (ii) 3-(pyridin-2-yl)disulfaneyl)propanoic acid, HOBt, HATU, NMM, DMF, 23 °C, 21 h, (iii) 95% TFA, 3% TIPS, 2% H₂O, 23 °C, 3 h, over three steps 11%.

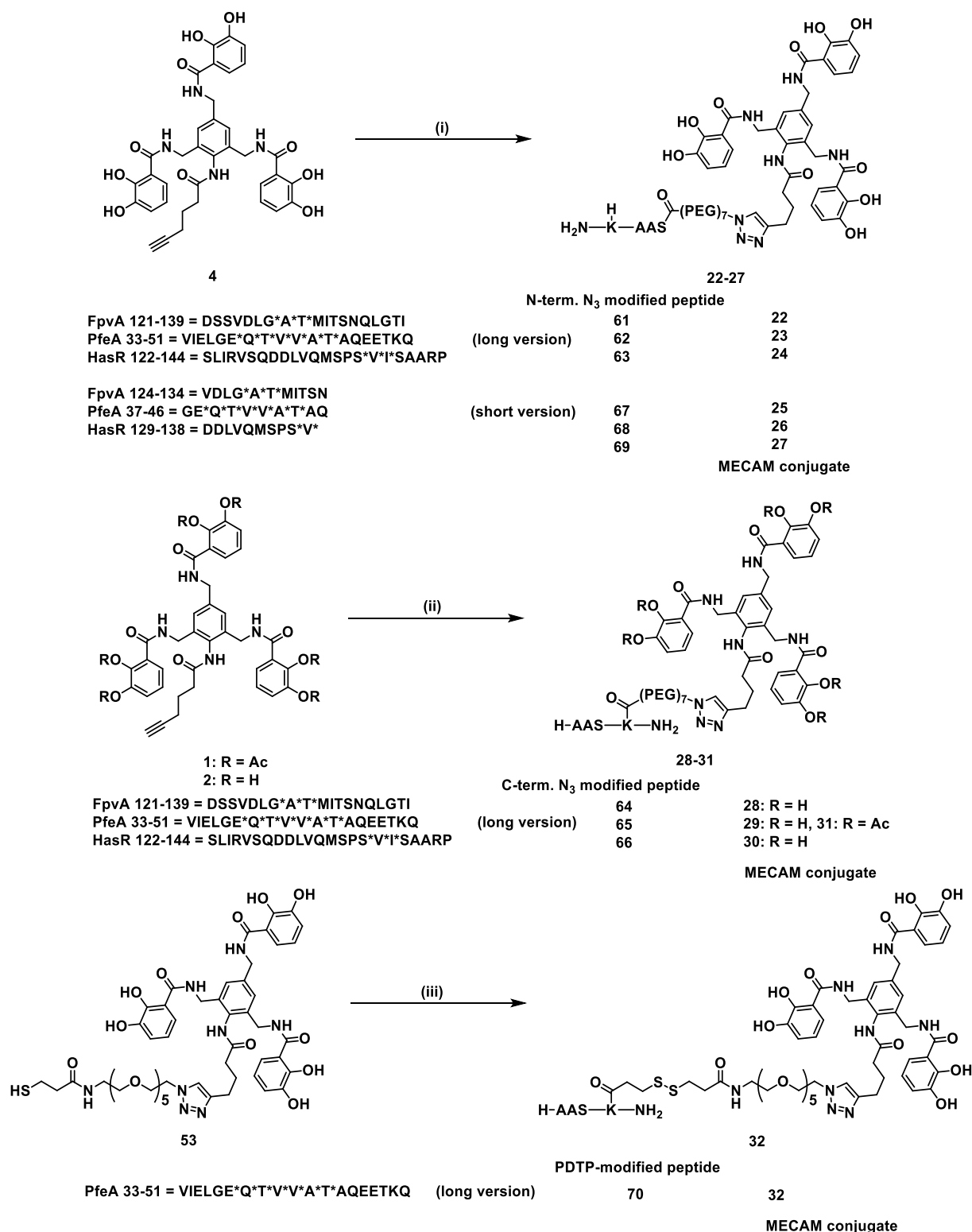
Conjugate synthesis



Scheme S7.9. Synthesis of the siderophore *TonB* box peptide conjugates. (A) Long and short, *N*-terminal peptide DOTAM conjugates: (i) Zn(OAc)₂, DMSO/H₂O, 23°C, 5 min, **61/62/63/67/68/69** in DMSO, 5 min, 23 °C, CuSO₄, sodium ascorbate, THPTA, PBS pH 7.4, 23 °C, 3 h, 81-99%. (B) Long, *C*-terminal peptide DOTAM conjugates: (ii) Zn(OAc)₂, DMSO/H₂O, 23°C, 5 min, **64/65/66** in DMSO, 5 min, 23 °C, CuSO₄, sodium ascorbate, THPTA, PBS pH 7.4, 23 °C, 3 h, 79-99%. (C) Long, disulfide, *C*-terminal peptide DOTAM conjugates: (iii) **70**, HEPES buffer pH 7.4, DMF/DMSO, 23 °C, 72 h, 76%. * indicate complicated coupling reactions.

Table S7.3: Overview over the yields of the peptide DOTAM siderophore conjugates **11-21** for the final CuAAC. l = long, s = short peptide.

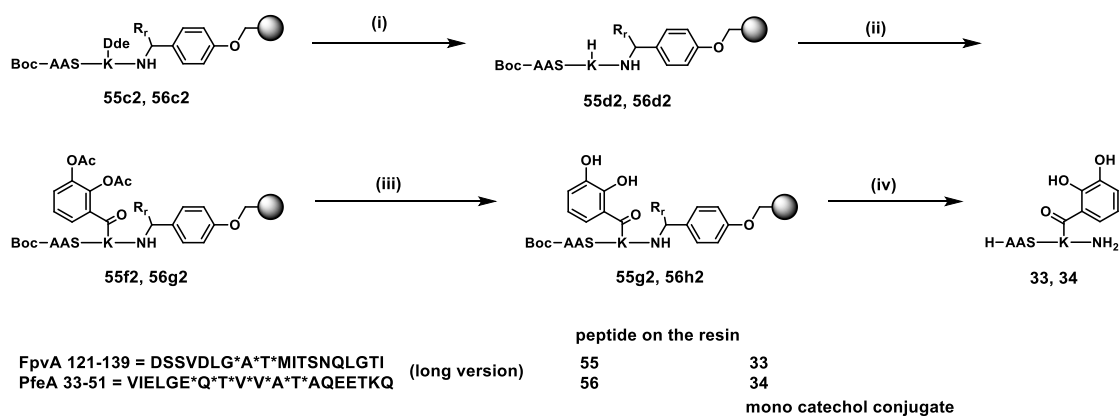
#	Peptide	Siderophore	Conjugation	Yield [%]
11	<i>FpvA</i> 121-139	DOTAM	N-term PEG	91
12	<i>PfeA</i> 33-51	DOTAM	N-term PEG	99
13	<i>HasR</i> 122-144	DOTAM	N-term PEG	87
14	<i>FpvA</i> 124-134	DOTAM	N-term PEG	91
15	<i>PfeA</i> 37-46	DOTAM	N-term PEG	96
16	<i>HasR</i> 129-138	DOTAM	N-term PEG	81
17	<i>FpvA</i> 121-139	DOTAM	C-term PEG	94
18	<i>PfeA</i> 33-51	DOTAM	C-term PEG	99
19	<i>HasR</i> 122-144	DOTAM	C-term PEG	79
20	<i>PfeA</i> 33-51	DOTAM	C-term PEG	82
21	<i>PfeA</i> 33-51	DOTAM	C-term disulfide	76



Scheme S7.10. Conjugation of the TonB box containing peptides to the MECAM siderophores. (i) **61/62/63/67/68/69**, DMSO, H₂O, 23 °C, 5 min, CuSO₄, sodium ascorbate, THPTA, PBS pH 7.4, 23 °C, 1 h, 86-97%, (ii) **64/65/66**, DMSO, H₂O, 23 °C, 5 min, CuSO₄, sodium ascorbate, THPTA, PBS pH 7.4, 23 °C, 1 h, 85-95%, (iii) **70**, HEPES buffer pH 7.4, DMF, DMSO, 23 °C, 48 h, 78%.* indicates a complicated coupling.

Table S7.4: Overview over the yields of peptide MECAM siderophore conjugates **22-32** for the final CuAAC. l = long, s = short peptide.

#	Peptide	Siderophore	Conjugation	Yield [%]
22	<i>FpvA</i> (l)	MECAM	N-term PEG	95
23	<i>PfeA</i> (l)	MECAM	N-term PEG	97
24	<i>HasR</i> (l)	MECAM	N-term PEG	86
25	<i>FpvA</i> (s)	MECAM	N-term PEG	88
26	<i>PfeA</i> (s)	MECAM	N-term PEG	96
27	<i>HasR</i> (s)	MECAM	N-term PEG	86
28	<i>FpvA</i> (l)	MECAM	C-term PEG	95
29	<i>PfeA</i> (l)	MECAM	C-term PEG	96
30	<i>HasR</i> (l)	MECAM	C-term PEG	85
31	<i>PfeA</i> (l)	MECAM	C-term PEG	80
32	<i>PfeA</i> (l)	MECAM	C-term disulfide	78



Scheme S7.11: Syntheses of C-terminal mono catechol-modified peptides **33** and **34**. (i) 1.0 M hydrazine in THF, DMF, 23 °C, 3 h, (ii) **40**, HOBt, HATU, NMM, DMF, 0-23 °C, 21 h, (iii) 20% DIPEA, MeOH, 0-23 °C, 4 h, (iv) 95% TFA, 3% TIPS, 2% H₂O, 23 °C, 3 h, over 24 steps to 15%.

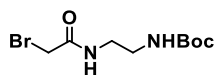
Table S7.5: Comparison of yields of the mono catechol-modified peptides **33** and **34**. aa = amino acids, (l) = long peptide, (s) = short peptide.

#	Peptides	aa	Cycle s	Time <i>t</i> [h]	Total steps	Yield [%]	Yield/step [%]
33	<i>FpvA</i> (l) C-term	20	23	59	24	9	90
34	<i>PfaA</i> (l) C-term	20	27	64	24	15	92

Synthesis instructions

Siderophore synthesis

Compound 36^{1, 2}



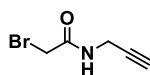
Chemical Formula: C₉H₁₇BrN₂O₃
 Exact Mass: 280,0423
 Molecular Weight: 281,1500

Tert-Butyl *N*-(2-aminoethyl)carbamate **35** (6.0 g, 37.4 mmol., 5.9 mL, 1.0 eq) was dissolved in DCM (150 mL) and K₂CO₃ (20.7 g, 149.8 mmol, 4.0 eq) was added, dissolved in MilliQ H₂O (100 mL). The two-phase solution was cooled to 0 °C and 2-bromoacetyl bromide (5.2 mL, 59.9 mmol, 1.6 eq.) in DCM (150 mL) was added over 10 min dropwise at 0 °C under vigorous stirring. The reaction continued stirring at 0 °C for 30 min, allowed to warm to room temperature and continued stirring for 90 min at 23 °C. The phases were separated and the aqueous phase was extracted with DCM (2 x 100 mL). The combined organic phases were washed with 1 M HCl (2 x 100 mL), sat. NaHCO₃ (2 x 100 mL) and brine (2 x 100 mL) and dried over Na₂SO₄. The solvent was removed by rotary evaporation to yield product **36** as a white solid (10.0 g, 35.6 mmol, 95%).

¹H NMR (500 MHz, CDCl₃): δ [ppm] = 7.14 (*bs*, 1H), 4.97 (*bs*, 1H), 3.84 (*s*, 2H), 3.37 (*q*, *J* = 5.4 Hz, 2H), 3.29 (*q*, *J* = 4.7 Hz, 2H), 1.43 (*s*, 9H).

¹³C NMR (126 MHz, CDCl₃) δ [ppm] = 166.5, 156.9, 80.1, 41.6, 40.0, 29.0, 28.5.

HRMS (ESI) calculated for C₉H₁₈BrN₂O₃⁺ ([M+H]⁺): *m/z* = 281.0495 experimental: 281.0493, δ [ppm] = 0.2, calculated for C₉H₁₇BrN₂NaO₃⁺ ([M+Na]⁺): *m/z* = 303.0315, experimental: 303.0313, δ [ppm] = 0.2.

Compound 38¹

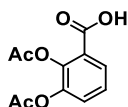
Chemical Formula: C₅H₆BrNO
 Exact Mass: 174,9633
 Molecular Weight: 176,0130

Prop-2-yn-1-amine **37** (5.8 mL, 90.8 mmol, 1.0 eq) was dissolved in DCM (150 mL) and K₂CO₃ (50.2 g, 363.1 mmol, 4.0 eq) was added, dissolved in MilliQ H₂O (100 mL). The two-phase solution was cooled to 0 °C and 2-bromoacetyl bromide (12.7 mL, 145.2 mmol, 1.6 eq) in DCM (150 mL) was added over 10 min dropwise at 0 °C under vigorous stirring. The reaction mixture was stirred at 0 °C for 30 min. After this time, the mixture was allowed to warm to room temperature and stirred for another 90 min at 23 °C. The phases were separated and the aqueous phase was extracted with DCM (2 x 100 mL). The combined organic extracts were washed with 1 M HCl (2 x 100 mL), sat. NaHCO₃ (2 x 100 mL), brine (2 x 100 mL) and dried over Na₂SO₄. The solvent was removed by rotary evaporation to yield product **38** as a brown solid (11.5 g, 65.1 mmol, 72%).

¹H NMR (500 MHz, CDCl₃): δ [ppm] = 6.87 (bs, 1H), 4.07 (dd, *J* = 5.4 Hz, 2.6 Hz, 2H), 3.87 (s, 2H), 2.27 (t, *J* = 2.6 Hz, 1H).

¹³C NMR (126 MHz, CDCl₃) δ [ppm] = 165.5, 78.7, 72.2, 30.0, 28.7.

HRMS (ESI) calculated for C₅H₇BrNO⁺ ([M+H]⁺): *m/z* = 175.9706, experimental: 175.9705, δ [ppm] = 0.1.

Compound 40¹

Chemical Formula: C₁₁H₁₀O₆

Exact Mass: 238,0477

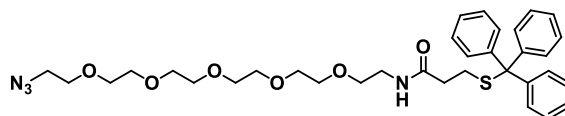
Molecular Weight: 238,1950

2,3-Dihydroxybenzoic acid **39** (25.0 g, 162.2 mmol, 1.0 eq) was suspended in THF (200 mL) and Ac₂O (46.0 mL, 486.6 mmol, 3.0 eq) and TEA (90.0 mL, 648.8 mmol, 4.0 eq), as well as DMAP (1.98 g, 16.2 mmol, 0.1 eq), were added sequentially. The precipitate dissolved after a few minutes of stirring at 23 °C; then the reaction mixture was heated to 60 °C and stirred for 20 h at that temperature. The next morning, as much of the solvent as possible was removed by rotary evaporation (clear beige solution) and the residue was dissolved in DCM (500 mL). The organic phase was washed with 1 M HCl (4 x 100 mL), brine (1 x 100 mL) and then dried over Na₂SO₄. The solvent was removed *in vacuo* to yield product **40** as a crude, beige solid (37.0 g, 155.3 mmol, 96%).

¹H NMR (500 MHz, DMSO-d₆): δ [ppm] = 13.23 (*bs*, 1H), 7.81 (*dd*, *J* = 8.0 Hz, 1.7 Hz, 1H), 7.51 (*dd*, *J* = 8.0 Hz, 1.7 Hz, 1H), 7.41 (*t*, *J* = 8.0 Hz, 1H), 2.30 (*s*, 3H), 2.26 (*s*, 3H).

¹³C NMR (126 MHz, DMSO-d₆) δ [ppm] = 168.3, 168.1, 165.1, 143.2, 142.1, 128.5, 127.7, 126.3, 125.8, 20.4, 20.3.

HRMS (ESI) calculated for C₁₁H₁₁O₆⁺ ([M+H]⁺): *m/z* = 239.0550, experimental: 239.0550, δ [ppm] = 0.0, calculated for C₁₁H₁₄NO₆⁺ ([M+NH₄]⁺): *m/z* = 256.0816, experimental: 256.0816, δ [ppm] = 0.0, calculated for C₁₁H₁₀NaO₆⁺ ([M+Na]⁺): *m/z* = 261.0370, experimental: 261.0370, δ [ppm] = 0.0.

Compound 42^{3,4}Chemical Formula: C₃₄H₄₄N₄O₆S

Exact Mass: 636,2982

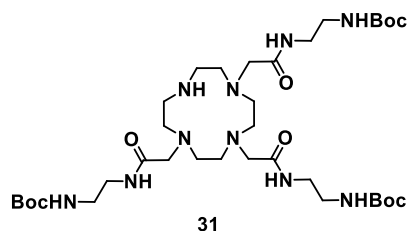
Molecular Weight: 636,8080

3-Tritylsulfanylpropanoic acid (300.0 mg, 0.861 mmol, 1.0 eq) was dissolved in anhydrous DCM (25 mL) and DMF (5 mL). Then HATU (818.4 mg, 2.152 mmol, 2.5 eq) was added, dissolved in anhydrous DMF (10 mL). The solution was cooled to 0 °C and 17-azido-3,6,9,12,15-pentaoxaheptadecan-1-amine **42** (263.8 μL, 0.947 mmol, 1.1 eq) was added in dry DMF (10 mL) at 0 °C. Dry TEA (477.4 μL, 3.444 mmol, 4.0 eq) was added over 10 min dropwise at 0 °C. The reaction continued stirring at 0 °C for 30 min, allowed to warm to room temperature and continued stirring for an additional 20 h at 23 °C. After completion of the reaction, controlled by LCMS, the solution was concentrated by rotary evaporation. The residue was taken up in EtOAc (50 mL) and washed with 1 M HCl (2 x 25 mL), sat. NaHCO₃ (2 x 25 mL), brine (2 x 25 mL) and dried over Na₂SO₄. The solvent was removed by rotary evaporation, the residue was dissolved in ACN/MilliQ H₂O/MeOH and purified by RP-HPLC (C18 phenomenex, 220 nm, collect all, 65-95% ACN/MilliQ H₂O, 0.1% HCOOH). The product containing fractions were identified by LCMS and lyophilized to dryness to yield product **26** as a white solid (418.0 mg, 0.656 mmol, 76%).

¹H NMR (500 MHz, DMSO-d₆): δ [ppm] = 7.88 (t, *J* = 5.6 Hz, 1H), 7.34 – 7.31 (m, 12H), 7.24 (dd, *J* = 8.8 Hz, 4.5 Hz, 3H), 3.59 (t, *J* = 4.8 Hz, 2H), 3.56 – 3.48 (m, 12H), 3.40 – 3.35 (m, 4H), 3.18 (q, *J* = 5.6 Hz, 2H), 2.26 (t, *J* = 7.3 Hz, 2H), 2.17 (t, *J* = 7.3 Hz, 2H).

¹³C NMR (126 MHz, DMSO-d₆) δ [ppm] = 170.1, 144.5, 129.1, 128.0, 126.7, 69.9, 69.8, 69.7, 69.7, 69.6, 69.3, 69.1, 66.0, 50.0, 38.6, 33.9, 27.5.

HRMS (ESI) calculated for C₃₄H₄₅N₄O₆S⁺ ([M+H]⁺): *m/z* = 637.3054, experimental: 637.3054, δ [ppm] = 0.0 calculated for C₃₄H₄₈N₅O₆S⁺ ([M+NH₄]⁺): *m/z* = 654.3320, experimental: 654.3319, δ [ppm] = 0.1 calculated for C₃₄H₄₄N₄NaO₆S⁺ ([M+Na]⁺): *m/z* = 659.2874, experimental: 659.2873, δ [ppm] = 0.1.

Compound **44**^{1, 2}

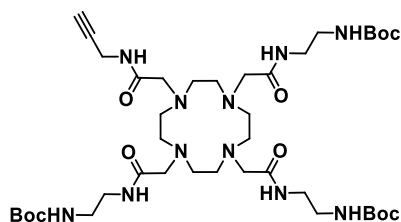
Chemical Formula: C₃₅H₆₈N₁₀O₉
 Exact Mass: 772,5171
 Molecular Weight: 772,9900

1,4,7,10-Tetraazacyclododecane **43** (186.0 mg, 1.080 mmol, 1.0 eq) and NaOAc (354.3 mg, 4.319 mmol, 4.0 eq) were suspended in ACN (75 mL) and stirred at 23 °C for 5 min. **36** (1.00 g, 3.563 mmol, 3.3 eq) was added dropwise with a syringe pump (6 mL/h, 24 mL, 4 h total) under vigorous stirring at 23 °C over 4 h. The syringe pump was removed and the reaction continued stirring at 23 °C for 16 h and the reaction progress was monitored by LCMS. After completion of the reaction the suspension was filtered and the solvent was removed by rotary evaporation and *in vacuo* to yield product **44** as a colorless oil in quantitative yield without the need for further purification.

¹H NMR (500 MHz, DMSO-d₆): δ [ppm] = 8.75 (s, 1H), 8.21 – 7.94 (m, 2H), 6.80 (s, 3H), 3.34 – 2.52 (m, 34H), 2.07 (s, 1H), 1.37 (s, 27H).

¹³C NMR (126 MHz, DMSO-d₆): δ [ppm] = 170.5, 166.1, 155.7, 155.6, 77.7, 57.8, 55.6, 54.2, 50.8, 49.2, 45.0, 38.8, 38.7, 29.5, 28.2.

HRMS (ESI) calculated for C₃₅H₆₉N₁₀O₉⁺ ([M+H]⁺): m/z = 773.5244, experimental: 773.5249, δ [ppm] = 0.5, calculated for C₃₅H₆₈N₁₀NaO₉⁺ ([M+Na]⁺): m/z = 795.5063, experimental: 795.5066, δ [ppm] = 0.3.

Compound 45^{1, 2}Chemical Formula: C₄₀H₇₃N₁₁O₁₀

Exact Mass: 867,5542

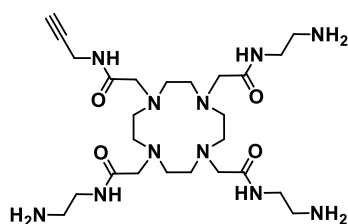
Molecular Weight: 868,0910

44 (834.6 mg 1.080 mmol, 1.0 eq) and K₂CO₃ (597.0 mg, 4.319 mmol, 4.0 eq) were suspended in ACN (75 mL) and the suspension was stirred at 23 °C for 5 min. **20** (342.1 mg, 1.943 mmol, 1.8 eq) was dissolved in ACN (25 mL) and added dropwise over 10 min to the suspension. The reaction was stirred vigorously at 23 °C for 20 h and the reaction progress was monitored by LCMS. The reaction was filtered after completeness and the solvent was removed by rotary evaporation and *in vacuo* to yield product **45** as a light brown solid in quantitative yield without the need for further purification.

¹H NMR (500 MHz, DMSO-d₆): δ [ppm] = 8.72 (s, 3H), 8.34 – 7.87 (m, 3H), 6.81 (s, 1H), 4.04 (s, 1H), 3.91 – 2.80 (m, 38H), 1.38 (s, 27H).

¹³C NMR (126 MHz, DMSO-d₆): δ [ppm] = 166.0, 165.8, 155.7, 80.4, 77.7, 73.4, 42.6, 42.3, 29.0, 28.5, 28.2.

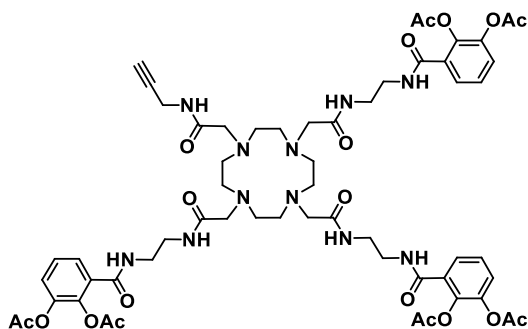
HRMS (ESI) calculated for C₄₀H₇₄N₁₁O₁₀⁺ ([M+H]⁺): m/z = 868.5615, experimental: 868.5612, δ [ppm] = 0.3, calculated for C₄₀H₇₅N₁₁O₁₀²⁺ ([M+2H]²⁺): m/z = 434.7844, experimental: 434.7845, δ [ppm] = 0.1.

Compound 46^{1, 2}Chemical Formula: C₂₅H₄₉N₁₁O₄

Exact Mass: 567,3969

Molecular Weight: 567,7400

45 (937.2 mg, 1.080 mmol, 1.0 eq) was dissolved in DCM (75 mL) and cooled to 0 °C. TFA (25 mL) was added slowly to yield a 25% TFA solution in DCM, which changed the color of the solution to a neon yellow. The reaction was stirred at 23 °C for 4 h and the reaction progress was monitored by LCMS. After completion of the reaction the solvent was removed by rotary evaporation and *in vacuo* to yield product **46** (500.0 mg, 0.881 mmol, 82% crude) as a transparent, yellow to brown oil. The residue was used crude directly in the next step without further purification.

Compound 1^{1, 2}Chemical Formula: C₅₈H₇₃N₁₁O₁₉

Exact Mass: 1227,5084

Molecular Weight: 1228,2800

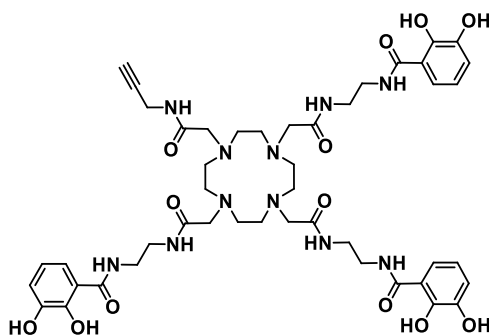
40 (740.1 mg, 3.107 mmol, 3.6 eq) was dissolved under an argon atmosphere in dry DCM (8 mL) and dry DMF (2 mL) and cooled to 0 °C. Oxalyl chloride (666.3 μL, 7.768 mmol, 9.0 eq) was added dropwise over the septum at 0 °C and the reaction was stirred 10 more minutes after the addition was finished. The reaction was allowed to warm to room temperature and stirred at 23 °C for an additional 3 h and the reaction progress was checked *via* TLC. For this, an aliquot of the reaction was quenched with MeOH to form the corresponding methyl ester. The differential running behavior on TLC indicated the formation of the desired acid chloride, compared to the starting material at the bottom of the TLC. After completion, the solvent was removed by rotary evaporation, the purity was checked *via* NMR, and the residue was dried overnight *in vacuo*.

The next morning **46** (490.0 mg, 0.863 mmol, 1.0 eq) was dissolved in MilliQ H₂O (50 mL) and the pH was carefully adjusted with NaHCO₃ solution (0.5 M) to ca. 8.5. The reaction mixture was cooled to 0 °C. The formed acid chloride **40** was dissolved in 1,4-dioxane (50 mL) and was added dropwise to the reaction mixture at 0 °C for 60 min. The pH was monitored during the addition and was adjusted otherwise with a NaHCO₃ solution (0.5 M) to 8.5 during the addition and more to pH 7.0 towards the end of the addition. After the addition was completed, the reaction progress was monitored by LCMS, while the reaction was allowed to equilibrate to room temperature and stirred at 23 °C for an additional 4 h. After completion, the suspension was extracted with DCM (4 x 100 mL or until the organic phase became colorless) and the combined organic phases were washed with sat. NaHCO₃ (2 x 100 mL), brine (2 x 100 mL) and dried over Na₂SO₄. The solvent was removed by rotary evaporation. The residue dissolved in ACN/MilliQ H₂O with 1% AcOH to delay further deacetylation and purified by RP-HPLC (C18 phenomenex, 220 nm, collect all, 30-60% ACN/MilliQ H₂O, 1% AcOH). The product containing fractions were identified by LCMS and lyophilized to dryness to yield compound **1** as a white solid (485.0 mg, 0.395 mmol, 46%).

¹H NMR (700 MHz, DMSO-d₆): δ [ppm] = 8.50 (bs, 1H), 8.39 (bs, 3H), 8.22 – 8.10 (m, 3H), 7.46 (dd, *J* = 7.4 Hz, 1.8 Hz, 3H), 7.39 – 7.32 (m, 6H), 3.90 – 3.89 (m, 2H), 3.45 – 3.34 (m, 12H), 3.28 – 2.94 (m, 24H), 2.52 (t, *J* = 1.9 Hz, 1H), 2.28 (s, 9H), 2.22 (s, 9H).

¹³C NMR (176 MHz, DMSO-d₆): δ [ppm] = 170.6, 170.0, 169.4, 168.5, 149.8, 146.3, 118.7, 117.7, 117.2, 115.0, 81.0, 72.9, 62.2, 57.7, 54.9, 38.9, 38.0, 27.9, 20.4.

HRMS (ESI) calculated for C₅₈H₇₄N₁₁O₁₉⁺ ([M+H]⁺): *m/z* = 1228.5157, experimental: 1228.5160, δ [ppm] = 0.3, calculated for C₅₈H₇₅N₁₁O₁₉²⁺ ([M+2H]²⁺): *m/z* = 614.7614, experimental: 614.7615, δ [ppm] = 0.1.

Compound 2^{1,2}Chemical Formula: C₄₆H₆₁N₁₁O₁₃

Exact Mass: 975,4450

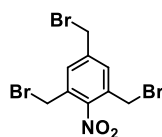
Molecular Weight: 976,0580

1 (485.0 mg, 0.395 mmol, 1.0 eq) was dissolved in MeOH (1.6 mL) and cooled to 0 °C. DIPEA was added (0.4 mL), the reaction was allowed to warm to room temperature and continued stirring at 23 °C for 3 h. The reaction progress was controlled by LCMS. After completion of the reaction, the solvent was removed by rotary evaporation, the residue was taken up in ACN/MilliQ and purified by RP-HPLC (C18 phenomenex, 220 nm, collect all, 5-35% ACN/MilliQ H₂O, 0.1% HCOOH). The product containing fractions were identified by LCMS and lyophilized to dryness to yield product **2** as a white solid (310.0 mg, 0.318 mmol, 80%).

¹H NMR (700 MHz, DMSO-d₆): δ [ppm] = 8.92 (s, 3H), 8.50 (s, 1H), 8.31 – 8.05 (m, 3H), 7.23 (dd, *J* = 8.0 Hz, 1.2 Hz, 3H), 6.89 (ddd, *J* = 7.7 Hz, 3.5 Hz, 1.3 Hz, 3H), 6.66 – 6.62 (m, 3H), 3.90 (d, *J* = 1.9 Hz, 2H), 3.37 (s, 6H), 3.24 – 3.05 (m, 12H), 3.04 (t, *J* = 2.5 Hz, 1H), 3.04 – 2.50 (m, 18H).

¹³C NMR (176 MHz, DMSO-d₆) δ [ppm] = 170.3, 169.9, 164.5, 164.4, 150.0, 150.0, 146.4, 118.6, 117.6, 117.6, 117.3, 115.0, 81.1, 72.9, 57.3, 57.1, 52.5, 38.9, 38.0, 27.9.

HRMS (ESI) calculated for C₄₆H₆₂N₁₁O₁₃⁺ ([M+H]⁺): *m/z* = 976.4523, experimental: 976.4525, δ [ppm] = 0.2, calculated for C₄₆H₆₁N₁₁NaO₁₃⁺ ([M+Na]⁺): *m/z* = 998.4343, experimental: 998.4347, δ [ppm] = 0.4.

Compound 48⁵Chemical Formula: C₉H₈Br₃NO₂

Exact Mass: 398,8105

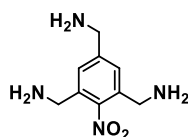
Molecular Weight: 401,8800

HNO₃ (50%, 18 mL) and H₂SO₄ (95%, 18 mL) were mixed and cooled to 0 °C. 1,3,5-tris(bromomethyl)benzene **47** (3.0 g, 8.406 mmol, 1.0 eq) was added in small portions to the mixture at 0 °C over 10 min. The reaction was stirred vigorously at 0 °C for 6 h, was subsequently allowed to warm to room temperature and stirred at 23 °C for additional 42 h. The reaction progress was controlled by TLC. The reaction was quenched with MilliQ H₂O (100 mL) after completeness and extracted with EtOAc (3 x 150 mL). The combined organic phases were washed with sat. NaHCO₃ (3 x 100 mL), brine (3 x 100 mL) and dried over Na₂SO₄. The solvent was removed by rotary evaporation and *in vacuo* to yield product **48** as a light yellow solid (3.3 g, 8.211 mmol, 98%).

TLC: R_f (**47** - PE/EtOAc = 10:1) = 0.90, R_f (**48** - PE/EtOAc = 10:1) = 0.72.

¹H NMR (500 MHz, DMSO-d₆): δ [ppm] = 7.81 (s, 2H), 4.75 (s, 2H), 4.70 (s, 4H).

¹³C NMR (126 MHz, DMSO-d₆) δ [ppm] = 148.4, 142.3, 132.8, 131.4, 31.5, 27.5.

Compound 49⁵

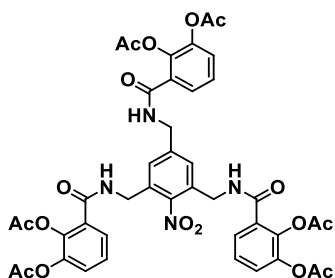
Chemical Formula: C₉H₁₄N₄O₂
 Exact Mass: 210,1117
 Molecular Weight: 210,2370

48 (3.3 g, 8.211 mmol, 1.0 eq) was dissolved in THF (30 mL) and EtOH (30 mL), then NH₄OH (30%, 30 mL) was added dropwise with a syringe pump (30 mL/h, 30 mL, 1 h total) under vigorous stirring at 23 °C for 1 h. The reaction mixture continued stirring at 23 °C for 20 h and the reaction progress was controlled by LCMS. After completion of the reaction the solvent was removed by rotary evaporation and *in vacuo* to yield product **49** as a light brown solid in quantitative yield without the need for further purification.

¹H NMR (500 MHz, DMSO-d₆): δ [ppm] = 7.99 (s, 2H), 4.15 (s, 2H), 4.14 (s, 4H).

¹³C NMR (126 MHz, DMSO-d₆): δ [ppm] = 148.7, 138.1, 132.1, 128.4, 41.6, 38.8.

HRMS (ESI) calculated for C₉H₁₅N₄O₂⁺ ([M+H]⁺): m/z = 211,1190, experimental: 211.1190, δ [ppm] = 0.0.

Compound 50⁵

Chemical Formula: C₄₂H₃₈N₄O₁₇
 Exact Mass: 870,2232
 Molecular Weight: 870,7770

40 (7.0 g, 29.6 mmol, 3.6 eq) was dissolved under argon atmosphere in anhydrous DCM (40 mL) and DMF (10 mL), then cooled to 0 °C. Oxalyl chloride (6.3 mL, 73.903 mmol, 9.0 eq.) was added at 0 °C and the reaction continued stirring at 0 °C for 10 minutes after the addition was finished. The reaction was equilibrated to 23 °C and was stirred at that temperature for 3 h. The reaction progress was checked *via* TLC. For this, an aliquot of the reaction was quenched with MeOH to form the corresponding methyl ester. The differential running behavior on TLC indicated the formation of the desired acid chloride, compared to the starting material

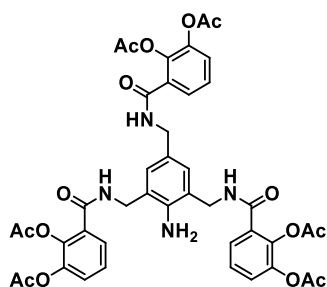
at the bottom of the TLC. After completion, the solvent was removed by rotary evaporation, the purity was checked *via* NMR, and the residue was dried overnight *in vacuo*.

The next morning **49** (1.7 g, 8.211 mmol, 1.0 eq) was dissolved in MilliQ H₂O (200 mL), the pH was adjusted with NaHCO₃ solution (0.5 M) to 8.5 and the reaction mixture was cooled to 0 °C. The vacuum dried acid chloride was dissolved in anhydrous 1,4-dioxane (100 mL) and added dropwise to the reaction mixture at 0 °C for 60 min. The pH was controlled during the addition and was adjusted otherwise with NaHCO₃ solution (0.5 M) to 8.5 during the addition and more to pH 7.0 towards the end of the addition. After the addition was completed, the reaction was equilibrated to 23 °C and continued stirring for an additional 4 h. The reaction progress was controlled by LCMS. After completion, the suspension was extracted with EtOAc (4 x 200 mL or until the organic phase became colorless) and the combined organic extracts were washed with sat. NaHCO₃ (2 x 200 mL), brine (2 x 200 mL) and dried over Na₂SO₄. After addition of 1% AcOH, the solvent was removed by rotary evaporation and purified by RP-Flash (EcoFlex, C18 particle size: 50 µm spherical, 20 g, 220 nm, collect all, 30-80% ACN/MilliQ H₂O, 1% AcOH). The product containing fractions were identified by LCMS and lyophilized to dryness to yield product **50** as a light brown solid (4.8 g, 5.57 mmol, 68%).

¹H NMR (500 MHz, DMSO-d₆): δ [ppm] = 9.07 (t, *J* = 6.0 Hz, 1H), 9.02 (t, *J* = 5.8 Hz, 2H), 7.48 (dd, *J* = 7.7 Hz, 1.6 Hz, 2H), 7.46 (dd, *J* = 7.7 Hz, 1.5 Hz, 1H), 7.42 (s, 2H), 7.39 (dd, *J* = 8.1 Hz, 1.6 Hz, 2H), 7.37 (dd, *J* = 8.1 Hz, 1.6 Hz, 1H), 7.33 (t, *J* = 7.9 Hz, 2H), 7.25 (t, *J* = 7.9 Hz, 1H), 4.45 (d, *J* = 5.7 Hz, 2H), 4.42 (d, *J* = 5.7 Hz, 4H), 2.29 (s, 6H), 2.29 (s, 3H), 2.20 (s, 6H), 2.18 (s, 3H).

¹³C NMR (126 MHz, DMSO-d₆) δ [ppm] = 168.3, 167.9, 167.9, 164.9, 164.8, 147.0, 142.9, 142.7, 140.2, 131.5, 130.3, 130.1, 126.3, 126.2, 126.1, 126.1, 125.8, 125.7, 42.0, 38.8, 20.4, 20.2.

HRMS (ESI) calculated for C₄₂H₃₉N₄O₁₇⁺ ([M+H]⁺): *m/z* = 871.2305, experimental: 871.2304, δ [ppm] = 0.1, calculated for C₄₂H₄₂N₅O₁₇⁺ ([M+NH₄]⁺): *m/z* = 888.2570, experimental: 888.2569, δ [ppm] = 0.1, calculated for C₄₂H₃₈N₄NaO₁₇⁺ ([M+Na]⁺): *m/z* = 893.2124, experimental: 893.2125, δ [ppm] = 0.1.

Compound 51⁵Chemical Formula: C₄₂H₄₀N₄O₁₅

Exact Mass: 840,2490

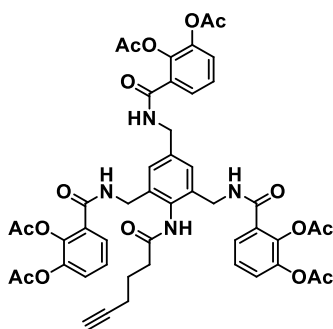
Molecular Weight: 840,7950

15 (3.0 g, 3.445 mmol, 1.0 eq) was dissolved under argon atmosphere in anhydrous THF (12 mL), anhydrous EtOH (9.6 mL) and AcOH (2.4 mL), then Zn dust (3.4 g, 51.7 mmol, 15.0 eq) was added at 0 °C. The reaction was stirred at 0 °C for 10 min and was allowed to warm to room temperature and continued stirring at 23 °C for 45 min. The reaction progress was controlled by LCMS. After completion, the reaction mixture was filtered over a pad of Celite which was washed with EtOAc until the organic phase occurred colorless. The combined organic phases were washed with sat. NaHCO₃ (2 x 150 mL) and brine (2 x 150 mL) and dried over Na₂SO₄. The solvent was removed by rotary evaporation and *in vacuo* to yield product **51** as a light brown solid in quantitative yield without the need for further purification.

¹H NMR (500 MHz, DMSO-d₆): δ [ppm] = 8.84 (t, *J* = 6.1 Hz, 2H), 8.75 (t, *J* = 6.0 Hz, 1H), 7.48 (dd, *J* = 7.5 Hz, 1.8 Hz, 2H), 7.45 (dd, *J* = 7.6 Hz, 1.7 Hz, 1H), 7.37 (dd, *J* = 8.1 Hz, 1.9 Hz, 2H), 7.35 (dd, *J* = 8.2 Hz, 1.8 Hz, 1H), 7.33 (t, *J* = 7.8 Hz, 2H), 7.30 (t, *J* = 7.8 Hz, 1H), 7.01 (s, 2H), 5.12 (s, 2H), 4.28 (d, *J* = 6.0 Hz, 4H), 4.25 (d, *J* = 5.9 Hz, 2H), 2.27 (s, 9H), 2.16 (s, 3H), 2.14 (s, 6H).

¹³C NMR (126 MHz, DMSO-d₆) δ [ppm] = 168.3, 168.3, 167.8, 167.8, 164.8, 164.3, 142.8, 142.6, 140.1, 140.0, 131.0, 130.8, 127.8, 126.3, 126.1, 126.1, 126.0, 125.9, 125.5, 125.3, 122.0, 42.1, 30.4, 20.8, 20.3, 20.2, 20.1.

HRMS (ESI) calculated for C₄₂H₄₁N₄O₁₅⁺ ([M+H]⁺): *m/z* = 841.2563, experimental: 841.2562, δ [ppm] = 0.1, calculated for C₄₂H₄₀N₄NaO₁₅⁺ ([M+Na]⁺): *m/z* = 863.2382, experimental: 863.2381, δ [ppm] = 0.1.

Compound 3⁵

Chemical Formula: C₄₈H₄₆N₄O₁₆
 Exact Mass: 934,2909
 Molecular Weight: 934,9080

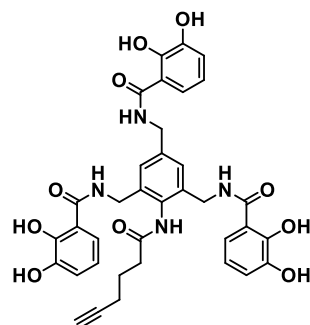
Hex-5-ynoic acid (81.7 μ L, 0.758 mmol, 2.2 eq) was dissolved under an argon atmosphere in dry THF (3.6 mL) and cooled to 0 °C. NMM (229.8 μ L, 2.067 mmol, 6.0 eq) and *iso*-butyl chloroformate (89.6 μ L, 0.689 mmol, 2.0 eq) were added dropwise at 0 °C, which immediately resulted in the formation of a white precipitate. The reaction was stirred 10 more minutes at 0 °C, then it was allowed to warm to room temperature and stirred at 23 °C for an additional 90 min. **51** (289.7 mg, 0.345 mmol, 1.0 eq) was dissolved in dry THF (6 mL), then added dropwise at 0 °C to the reaction, which continued stirring for 10 minutes at 0 °C. The reaction was equilibrated to 23 °C and stirred 5 h at that temperature, while the reaction progress was controlled by LCMS. After completion or when overreaction was increasingly observed by LCMS, the suspension was quenched by the addition of H₂O (5 mL) and sat. NaHCO₃ (5 mL). The phases were separated, the aqueous phase was extracted with EtOAc (3 x 25 mL). The combined organic extracts were washed with 0.1 M HCl (2 x 50 mL), sat. NaHCO₃ (2 x 50 mL), brine (2 x 50 mL) and dried over Na₂SO₄. The solvent was removed by rotary evaporation. The residue was taken up in ACN/MilliQ H₂O with 1% AcOH to delay further deacetylation and purified by RP-HPLC (C18 phenomenex, 220 nm, collect all, 30-70% ACN/MilliQ H₂O, 1% AcOH). The product containing fractions were identified by LCMS and lyophilized to dryness to yield product **3** as a white solid (180.0 mg, 0.193 mmol, 56%).

¹H NMR (700 MHz, DMSO-d₆): δ [ppm] = 9.54 (s, 1H), 8.94 (t, J = 6.1 Hz, 1H), 8.77 (t, J = 6.0 Hz, 2H), 7.52 (dd, J = 7.7 Hz, 1.6 Hz, 2H), 7.44 (dd, J = 7.7 Hz, 1.6 Hz, 1H), 7.38 (dd, J = 8.1 Hz, 1.6 Hz, 2H), 7.34 (dd, J = 8.1 Hz, 1.6 Hz, 1H), 7.31 (t, J = 7.8 Hz, 2H), 7.23 (t, J = 7.9 Hz, 1H), 7.20 (s, 2H), 4.38 (d, J = 5.9 Hz, 2H), 4.33 (bs, 4H), 2.81 (t, J = 2.6 Hz, 1H), 2.52 – 2.51 (m, 2H), 2.28 (s, 6H), 2.28 (s, 3H), 2.25 (td, J = 7.1 Hz, 2.7 Hz, 2H), 2.17 (s, 6H), 2.16 (s, 3H), 1.80 (p, J = 7.2 Hz, 2H).

¹³C NMR (176 MHz, DMSO-d₆) δ [ppm] = 174.0, 171.2, 168.3, 167.9, 167.9, 164.7, 164.6, 142.9, 140.2, 137.6, 135.9, 131.8, 130.7, 130.6, 126.2, 126.1, 126.1, 126.0, 125.6, 125.4, 124.6, 84.0, 83.8, 71.7, 71.6, 48.6, 42.2, 34.2, 32.4, 24.1, 23.5, 20.4, 20.2, 17.5, 17.1.

HRMS (ESI) calculated for $C_{48}H_{47}N_4O_{16}^+$ ($[M+H]^+$): $m/z = 935.2982$, experimental: 935.2979, δ [ppm] = 0.3, calculated for $C_{48}H_{46}N_4NaO_{16}^+$ ($[M+Na]^+$): $m/z = 957.2801$, experimental: 957.2797, δ [ppm] = 0.4, calculated for $C_{48}H_{48}N_4O_{16}^{2+}$ ($[M+2H]^{2+}$): $m/z = 468.1527$, experimental: 468.1527, δ [ppm] = 0.0, calculated for $C_{48}H_{46}N_4Na_2O_{16}^{2+}$ ($[M+Na_2]^{2+}$): $m/z = 490.1347$, experimental: 490.1345, δ [ppm] = 0.2.

Compound 4⁵



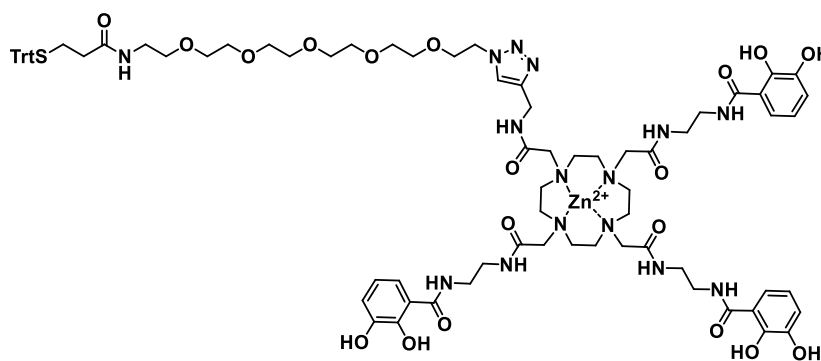
Chemical Formula: $C_{36}H_{34}N_4O_{10}$
 Exact Mass: 682,2275
 Molecular Weight: 682,6860

3 (500.0 mg, 0.535 mmol, 1.0 eq) was dissolved in MeOH (4.8 mL) and cooled to 0 °C. DIPEA was added (1.2 mL), the reaction was allowed to warm to room temperature and stirred at 23 °C for 3 h. The reaction progress was controlled by LCMS. After completion, the solvent was removed by rotary evaporation, the residue was taken up in ACN/MilliQ and purified by RP-HPLC (C18 phenomenex, 220 nm, collect all, 25-65% ACN/MilliQ H₂O, 0.1% HCOOH). The product containing fractions were identified by LCMS and lyophilized to dryness to yield product **4** as a white solid (330.0 mg, 0.483 mmol, 90%).

¹H NMR (500 MHz, DMSO-*d*₆): δ [ppm] = 12.54 (s, 3H), 9.58 (s, 1H), 9.33 (t, $J = 6.2$ Hz, 1H), 9.16 (t, $J = 6.1$ Hz, 2H), 9.14 (bs, 3H), 7.29 (dd, $J = 8.2$ Hz, 1.3 Hz, 2H), 7.21 (s, 2H), 7.19 (dd, $J = 8.2$ Hz, 1.4 Hz, 1H), 6.92 (dd, $J = 7.8$ Hz, 1.2 Hz, 2H), 6.89 (dd, $J = 7.8$ Hz, 1.2 Hz, 1H), 6.67 (t, $J = 7.9$ Hz, 2H), 6.61 (t, $J = 7.9$ Hz, 1H), 4.46 (d, $J = 6.1$ Hz, 2H), 4.41 (d, $J = 6.0$ Hz, 4H), 2.81 (t, $J = 2.6$ Hz, 1H), 2.54 – 2.50 (m, 2H), 2.25 (td, $J = 7.1$ Hz, 2.6 Hz, 2H), 1.79 (p, $J = 7.2$ Hz, 2H).

¹³C NMR (126 MHz, DMSO-*d*₆) δ [ppm] = 171.2, 169.8, 169.8, 149.7, 149.5, 146.2, 146.2, 137.5, 135.9, 132.1, 124.8, 118.9, 118.9, 118.1, 118.0, 117.3, 117.1, 115.1, 114.9, 84.0, 71.7, 42.2, 39.0, 34.1, 24.2, 17.5.

HRMS (ESI) calculated for $C_{36}H_{35}N_4O_{10}^+$ ($[M+H]^+$): $m/z = 683.2348$, experimental: 683.2346, δ [ppm] = 0.2, calculated for $C_{36}H_{34}N_4NaO_{10}^+$ ($[M+Na]^+$): $m/z = 705.2167$, experimental: 705.2164, δ [ppm] = 0.3.

Compound 52a¹

Chemical Formula: C₈₀H₁₀₅N₁₅O₁₉SZn²⁺

Exact Mass: 1675,6712

Molecular Weight: 1678,2449

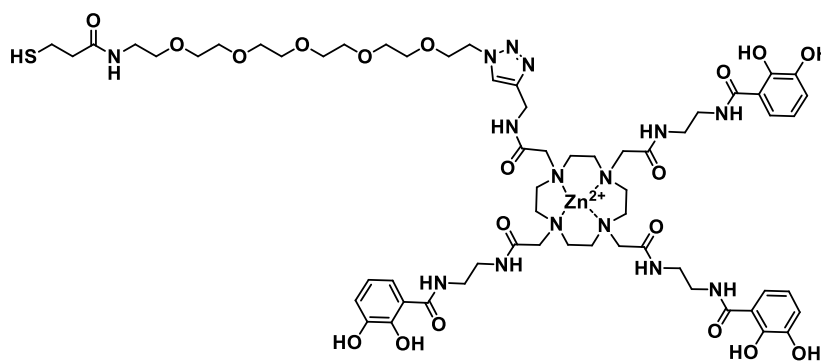
2 (92.0 mg, 0.094 mmol, 1.5 eq) was dissolved under argon atmosphere in DMSO (2 mL) zinc acetate (41.4 mg, 0.188 mmol, 3.0 eq), dissolved in MilliQ H₂O (2 mL), was added and the solution was stirred at 23 °C for 5 min. **26** (40.0 mg, 0.063 mmol, 1.0 eq), dissolved in DMSO (2 mL), was added to the solution. CuSO₄ (5.0 mg, 0.031 mmol, 0.5 eq in 0.5 mL PBS) and sodium ascorbate (12.4 mg, 0.063 mmol, 1.0 eq - in 1xPBS 1 mL), was added to the CuSO₄ solution, whereupon a white precipitate formed immediately. THPTA (6.8 mg, 0.016 mmol, 0.25 eq -in 0.5 mL PBS), was added to the suspension. The suspension was added under argon atmosphere to the reaction. The reaction was stirred at 23 °C for 1 h and the reaction progress was controlled by LCMS. After completion, the solution was filtered over cotton wool and purified by RP-HPLC (C18 phenomenex, 220 nm, collect all, 5-35% ACN/MilliQ H₂O, 0.1% HCOOH). The product containing fractions were identified by LCMS and lyophilized to dryness to yield product **52a** as a white solid (80.0 mg, 0.042 mmol, 76%).

¹H NMR (700 MHz, DMSO-d₆): δ [ppm] = 10.32 – 9.39 (m, 3H), 9.04 (bs, 3H), 8.49 (bs, 1H), 8.21 (bs, 1H), 7.97 – 7.82 (m, 3H), 7.35 – 7.33 (m, 1H), 7.33 – 7.29 (m, 12H), 7.25 – 7.24 (m, 3H), 7.23 – 7.21 (m, 3H), 6.84 – 6.70 (m, 3H), 6.54 – 6.32 (m, 3H), 4.43 (t, *J* = 5.0 Hz, 2H), 4.38 (s, 2H), 3.75 (t, *J* = 4.8 Hz, 2H), 3.47 – 3.45 (m, 16H), 3.36 (t, *J* = 5.9 Hz, 2H), 3.31 – 3.24 (m, 12H), 3.14 (q, *J* = 5.7 Hz, 2H), 2.99 – 2.52 (m, 24H), 2.23 (t, *J* = 7.4 Hz, 2H), 2.15 (t, *J* = 7.4 Hz, 2H).

¹³C NMR (176 MHz, DMSO-d₆) δ [ppm] = 172.3, 171.5, 170.1, 169.7, 169.6, 165.0, 147.5, 147.2, 144.5, 143.6, 129.1, 128.0, 126.7, 123.7, 118.0, 117.9, 116.6, 115.7, 115.4, 115.3, 114.4, 69.7, 69.7, 69.6, 69.5, 69.0, 68.7, 66.0, 55.6, 50.5, 49.4, 40.4, 40.0, 38.6, 38.0, 37.6, 34.6, 33.9, 27.5.

HRMS (ESI) calculated for (C₈₀H₁₀₇N₁₅O₁₉SZn²⁺)²⁺ ([M+2H]²⁺): *m/z* = 838.8429, experimental: 838.8427, δ [ppm] = 0.2, calculated for (C₈₀H₁₀₆N₁₅NaO₁₉SZn²⁺)²⁺ ([M+H+Na]²⁺): *m/z* = 849.8339, experimental: 849.8337, δ [ppm] = 0.2.

Compound 52



Chemical Formula: $C_{61}H_{91}N_{15}O_{19}SZn^{2+}$

Exact Mass: 1433,5617

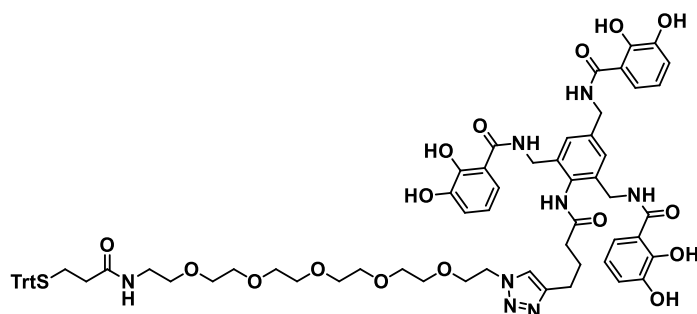
Molecular Weight: 1435,9239

52a (15.0 mg, 8.938 μ mol, 1.0 eq) was dissolved in dry DCM (1.5 mL), TFA (1.5 mL) and TIPS (75 μ L) were added (immediate shift from slightly yellow to neon-yellow/orange was observed) and the reaction was stirred at 23 $^{\circ}$ C for 2 h. The reaction progress was controlled by LCMS and after completion, the solvent was removed by rotary evaporation. The residue was washed with ice cold diethyl ether (2 x 50 mL), centrifuged (4500 rpm, 15 min, -20 $^{\circ}$ C) and decanted after each washing step. The residue dried *in vacuo* to yield product **52** as a light brown solid (12.0 mg, 8.357 mmol, 94%).

1H NMR (700 MHz, DMSO- d_6): δ [ppm] = 12.45 (bs, 3H), 9.17 (t, J = 5.2 Hz, 1H), 8.91 (t, J = 5.3 Hz, 1H), 8.87 (t, J = 5.4 Hz, 2H), 8.80 (t, J = 5.4 Hz, 3H), 7.98 – 7.95 (m, 1H), 7.23 (dd, J = 8.2 Hz, 1.1 Hz, 3H), 7.12 – 6.99 (m, 1H), 6.91 (ddd, J = 7.8 Hz, 4.4 Hz, 1.3 Hz, 3H), 6.67 (ddd, J = 7.9 Hz, 4.3 Hz, 2.1 Hz, 3H), 4.45 (t, J = 5.2 Hz, 2H), 4.42 (s, 2H), 3.77 (t, J = 5.3 Hz, 2H), 3.48 – 3.46 (m, 16H), 3.45 – 3.40 (m, 12H), 3.38 (t, J = 6.9 Hz, 2H), 3.34 (t, J = 6.7 Hz, 2H), 3.31 – 2.78 (m, 24H), 2.73 – 2.72 (m, 2H), 2.63 (q, J = 7.0 Hz, 2H), 2.37 (t, J = 7.0 Hz, 1H).

^{13}C NMR (176 MHz, DMSO- d_6) δ [ppm] = 171.4, 171.3, 170.7, 170.6, 170.4, 170.2, 170.0, 149.5, 149.4, 149.4, 146.2, 143.3, 136.1, 135.8, 134.6, 130.0, 129.4, 129.1, 128.4, 126.3, 126.2, 123.7, 118.9, 118.3, 118.0, 117.4, 117.4, 116.6, 115.2, 115.0, 113.3, 69.8, 69.7, 69.6, 69.5, 69.1, 69.1, 69.1, 68.7, 65.0, 56.2, 55.9, 55.8, 55.7, 54.9, 50.9, 50.8, 50.4, 49.5, 40.4, 40.0, 39.1, 39.0, 38.6, 38.6, 38.6, 38.2, 38.2, 36.0, 35.8, 35.3, 35.2, 34.9, 34.7, 34.6, 34.0, 33.9, 30.8, 30.7, 26.6, 25.7, 23.3, 20.0, 19.4, 19.3, 19.0, 17.9, 17.3, 15.2, 12.7, 12.1, 9.7.

HRMS (ESI) calculated for $(C_{61}H_{92}N_{15}O_{19}SZn^{2+})^+$ ($[M+H]^+$): m/z = 1434.5690, experimental: 1434.5695, δ [ppm] = 0.5, calculated for $(C_{61}H_{91}N_{15}NaO_{19}SZn^{2+})^+$ ($[M+Na]^+$): m/z = 1456.5509, experimental: 1456.5504, δ [ppm] = 0.5, calculated for $(C_{61}H_{93}N_{15}O_{19}SZn^{2+})^{2+}$ ($[M+2H]^{2+}$): m/z = 717.78812, experimental: 717.7880, δ [ppm] = 0.2, calculated for $(C_{61}H_{92}N_{15}NaO_{19}SZn^{2+})^{2+}$ ($[M+H+Na]^{2+}$): m/z = 728.7791, experimental: 728.7793.

Compound 53a⁵

Chemical Formula: C₇₀H₇₈N₈O₁₆S

Exact Mass: 1318,5256

Molecular Weight: 1319,4940

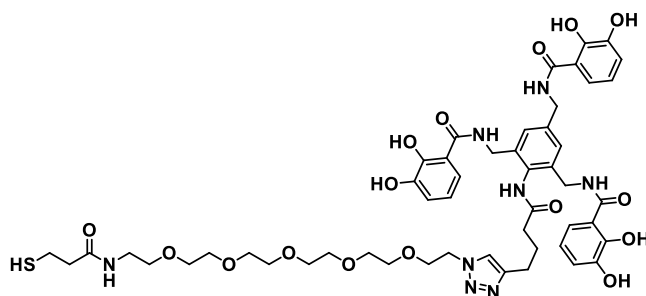
4 (80.4 mg, 0.118 mmol, 1.5 eq) was dissolved under argon atmosphere in DMSO (2 mL) and MilliQ H₂O (2 mL). **26** (50.0 mg, 0.079 mmol, 1.0 eq), dissolved in DMSO (2 mL), was added to the solution. CuSO₄ (5.0 mg, 0.031 mmol, 0.5 eq - in 0.5 mL PBS) and sodium ascorbate (12.4 mg, 0.063 mmol, 1.0 eq., in 1 mL PBS), were combined, whereupon a white solid precipitated immediately. THPTA (6.8 mg, 0.016 mmol, 0.25 eq - in 0.5 mL PBS), was added to the suspension. The suspension was then added under argon atmosphere to the reaction. The reaction was stirred at 23 °C for 1 h and the reaction progress was controlled by LCMS. After completion, the solution was filtered over cotton wool and purified by RP-HPLC (C18 phenomenex, 220 nm, collect all, 50-90% ACN/MilliQ H₂O, 0.1% HCOOH). The product containing fractions were identified by LCMS and lyophilized to dryness to yield product **53a** as a white solid (85.0 mg, 0.064 mmol, 82%).

¹H NMR (700 MHz, DMSO-d₆): δ [ppm] = 12.57 (s, 1H), 12.52 (s, 2H), 9.57 (s, 1H), 9.33 (t, *J* = 5.9 Hz, 1H), 9.19 (s, 1H), 9.16 (t, *J* = 5.9 Hz, 2H), 9.12 (s, 1H), 7.87 (t, *J* = 5.6 Hz, 1H), 7.83 (s, 1H), 7.36 – 7.27 (m, 15H), 7.25 (t, *J* = 1.4 Hz, 1H), 7.24 – 7.23 (m, 1H), 7.23 (t, *J* = 1.6 Hz, 1H), 7.22 – 7.21 (m, 2H), 7.21 (dd, *J* = 8.3 Hz, 1.2 Hz 1H) 6.92 (d, *J* = 7.8 Hz, 2H), 6.89 (d, *J* = 7.8 Hz, 1H), 6.67 (t, *J* = 7.9 Hz, 2H), 6.61 (t, *J* = 8.0 Hz, 1H), 4.46 – 4.45 (m, 4H), 4.42 (d, *J* = 5.7 Hz, 2H), 3.78 (t, *J* = 5.2 Hz, 2H), 3.50 – 3.49 (m, 2H), 3.46 – 3.45 (m, 16H), 3.36 (t, *J* = 5.6 Hz, 2H), 3.15 (q, *J* = 5.6 Hz, 2H), 2.70 (t, *J* = 7.3 Hz, 2H), 2.47 (t, *J* = 7.3 Hz, 2H), 2.24 (t, *J* = 7.4 Hz, 2H), 2.16 (t, *J* = 7.4 Hz, 2H), 1.95 (p, *J* = 7.3 Hz, 2H).

¹³C NMR (176 MHz, DMSO-d₆) δ [ppm] = 171.6, 170.2, 169.8, 169.8, 149.7, 149.6, 146.2, 146.2, 144.5, 137.5, 136.0, 132.8, 132.2, 129.1, 128.1, 126.8, 124.9, 122.3, 118.9, 118.1, 118.0, 117.4, 117.2, 115.1, 115.0, 69.8, 69.7, 69.7, 69.6, 69.1, 68.8, 66.0, 49.3, 42.2, 39.1, 38.6, 34.9, 33.9, 27.5, 25.3, 24.8.

HRMS (ESI) calculated for C₇₀H₇₉N₈O₁₆S⁺ ([M+H]⁺): *m/z* = 1319.5329, experimental: 1319.5332, δ [ppm] = 0.3, calculated for C₇₀H₇₈N₈NaO₁₆S⁺ ([M+Na]⁺): *m/z* = 1341.5149, experimental: 1341.5149, δ [ppm] = 0.0.

Compound 53



Chemical Formula: $C_{51}H_{64}N_8O_{16}S$

Exact Mass: 1076,4161

Molecular Weight: 1077,1730

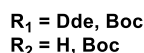
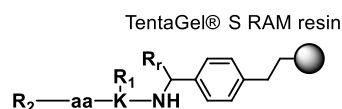
52 (25.0 mg, 18.9 μ mol, 1.0 eq) was dissolved in dry DCM (1.5 mL) and TFA (1.5 mL) and TIPS (75 μ L) were added, while an immediate shift from slight yellow to neon-yellow/orange was observed. The reaction was stirred at 23 °C for 2 h. After complete conversion, the solvent was removed by rotary evaporation. The residue was washed with ice-cold diethyl ether (2 x 50 mL), centrifuged (4500 rpm, 15 min, -20 °C) and dried *in vacuo* to yield product **53** as a light yellow solid (18.3 mg, 17.0 μ mol, 90%).

¹H NMR (700 MHz, DMSO- d_6): δ [ppm] = 12.52 (s, 2H), 9.56 (s, 1H), 9.32 (t, J = 6.1 Hz, 1H), 9.16 (t, J = 6.0 Hz, 2H), 7.94 (t, J = 5.4 Hz, 1H), 7.84 (s, 1H), 7.29 (dd, J = 8.2 Hz, 1.1 Hz, 2H), 7.21 (s, 2H), 7.20 (dd, J = 8.3 Hz, 1.2 Hz, 1H), 6.92 (dd, J = 7.8 Hz, 1.3 Hz, 2H), 6.89 (dd, J = 7.8 Hz, 1.3 Hz, 1H), 6.67 (t, J = 7.9 Hz, 2H), 6.61 (t, J = 7.9 Hz, 1H), 4.51 – 4.44 (m, 4H), 4.40 (d, J = 5.8 Hz, 2H), 3.79 (t, J = 5.4 Hz, 2H), 3.53 – 3.49 (m, 2H), 3.48 – 3.44 (m, 16H), 3.39 (t, J = 5.9 Hz, 2H), 3.20 (q, J = 5.8 Hz, 2H), 2.70 (t, J = 7.6 Hz, 2H), 2.63 (dd, J = 14.9 Hz, 7.0 Hz, 2H), 2.47 (t, J = 7.5 Hz, 2H), 2.37 (t, J = 7.0 Hz, 2H), 2.23 (t, J = 8.0 Hz, 1H), 1.94 (p, J = 7.6 Hz, 2H).

¹³C NMR (176 MHz, DMSO- d_6) δ [ppm] = 171.6, 170.4, 169.8, 169.8, 149.7, 149.6, 146.3, 146.2, 146.2, 137.5, 136.0, 132.2, 124.9, 122.4, 118.9, 118.9, 118.1, 118.0, 117.4, 117.2, 115.1, 115.0, 69.8, 69.8, 69.8, 69.7, 69.6, 69.1, 68.8, 49.3, 42.2, 39.2, 39.1, 38.6, 34.9, 25.3, 24.8, 20.0, 17.4.

HRMS (ESI) calculated for $C_{51}H_{65}N_8O_{16}S^+$ ($[M+H]^+$): m/z = 1077.4234, experimental: 1077.4234, δ [ppm] = 0.0, calculated for $C_{51}H_{64}N_8NaO_{16}S^+$ ($[M+Na]^+$): m/z = 1099.4053, experimental: 1099.4055, δ [ppm] = 0.2, calculated for $C_{51}H_{66}N_8O_{16}S^{2+}$ ($[M+2H]^{2+}$): m/z = 539.2153, experimental: 539.2154, δ [ppm] = 0.1, calculated for $C_{51}H_{65}N_8NaO_{16}S^{2+}$ ($[M+H+Na]^{2+}$): m/z = 550.2063, experimental: 550.2065, δ [ppm] = 0.2, calculated for $C_{51}H_{67}N_8O_{16}S^+$ ($[M+3H]^+$): m/z = 359.8126, experimental: 359.8127, δ [ppm] = 0.1.

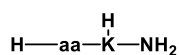
General procedure for peptide synthesis



	FpvA 121-139 = DSSVDLG*A*T*MITSNQLGTI	
	PfeA 33-51 = VIELGE*Q*T*V*V*A*T*AQEETKQ	(long version)
	HasR 122-144 = SLIRVSQDDLVMSPS*V*I*SAARP	
aa sequence	FpvA 124-134 = VDLG*A*T*MITSN	
	PfeA 37-46 = GE*Q*T*V*V*A*T*AQ	(short version)
	HasR 129-138 = DDLVMSPS*V*	

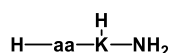
Solid-phase peptide synthesis (SPPS) was performed in a 50.0 μmol scale in 5 mL tubes with on an automated Syro Multiple Peptide Synthesizer (MultiSynTech, Witten, Germany) on Rapp TentaGel® S RAM resin **54** (Rapp Polymere, Tübingen, Germany). Couplings were performed with HCTU (206.9 mg, 500.0 μmol , 10.0 eq., in 1.0 mL DMF)/DIPEA (176.0 μL , 1.035 mmol, 20.7 eq). The C-terminal amino acid for all peptides was either Fmoc-Lys(Dde)-OH, Fmoc-Lys(Boc)-OH and was coupled manually to the resin, followed by manual deprotection with first 40% piperidine in DMF (1.2 mL/tube, 2 min) and second 20% piperidine in DMF (1.2 mL/tube, 8 min). The remaining SPPS was performed automated on the previously mentioned peptide synthesizer. For the automated procedure, amino acids were dissolved freshly with the help of ultrasound sonication in NMP (500.0 μmol , 10.0 eq, 0.5 M). HCTU (25.1 g, 60.0 mmol, 1200.0 eq) was dissolved in DMF (120.0 mL), DIPEA (25.0 mL, 147.0 mmol, 2940.0 eq) was bottled, piperidine (80.0 mL, 808.0 mmol, 16160.0 eq) was prepared in DMF (120 mL), acetic anhydride (5 mL, 52.9 mmol, 1058.0 eq) and DMF (5000 mL) were bottled separately and were provided to the peptide synthesizer. Complicated couplings, indicated by an asterisk in the amino acid sequence above (*), were performed through a double coupling followed by capping with acetic anhydride (75.0 μL , 793.4 μmol , 15.9 eq)/DIPEA (15.0 μL , 88.2 μmol , 1.8 eq) in DMF (1410 μL) of potentially unreacted free α -amino groups. Side chain protection groups of the amino acids were as follows: Arg: Pmc; Asn, Cys, Gln and His: Trt; Asp, Glu, Ser, Thr and Tyr: *t*Bu; Lys and Trp: Boc. For the peptides with C-terminal PEG derivatization amino acids with a Boc-protecting group at the α -amino function were incorporated at the N-terminus, to allow for simultaneous resin cleavage, deprotection of side chains and the N-terminus.

General procedure for global deprotection and resin cleavage



	FpvA 121-139 = DSSVDLG*A*T*MITSNQLGTI	
	PfeA 33-51 = VIELGE*Q*T*V*V*A*T*AQEETKQ	(long version)
	HasR 122-144 = SLIRVSQDDLVMSPS*V*I*SAARP	
aa sequence	FpvA 124-134 = VDLG*A*T*MITSN	
	PfeA 37-46 = GE*Q*T*V*V*A*T*AQ	(short version)
	HasR 129-138 = DDLVMSPS*V*	

For C-terminal peptides, a Dde group was present at the ϵ -amino function at the C-terminal lysine, which was removed on the resin (50.0 μmol , 1.0 eq) by a treatment with hydrazine (8.0 eq) in THF (1.0 M, 0.4 mL) further diluted in DMF (1.6 mL) at 23 °C for 3 h. The crude peptides were simultaneously cleaved from the resin and deprotected globally by a 3 h treatment with 2.0 mL of a deprotection solution (1.9 mL TFA, 60 μL triisopropylsilane, 40 μL MilliQ H₂O) at 23 °C. The cleaved and deprotected peptides were precipitated with ice cold *t*-butylmethyl ether, centrifuged (4500 rpm, 30 min, -20 °C) and the supernatant was discarded. The remaining pellets were taken up in ACN/MilliQ H₂O containing 0.1% TFA and were purified by RP-HPLC (C18 phenomenex, 220 nm, collect all, 5-50% ACN/MilliQ H₂O, 0.1% TFA). The product containing fractions were identified by LCMS and lyophilized to dryness to yield the peptides as white solids.

FpvA 121-139 peptide 5

aa: DSSVDLG*A*T*MITSNQLGTI

Chemical Formula: C₈₅H₁₄₈N₂₄O₃₂S

Exact Mass: 2049,04122

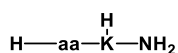
Molecular Weight: 2050,31500

5 (16.7 mg, 8.145 μmol, 16%) was prepared following the general procedures for peptide synthesis and global deprotection and resin cleavage.

¹H NMR (700 MHz, DMSO-d₆): δ [ppm] = 12.64 (s), 8.62 (d, *J* = 7.9 Hz), 8.29 (d, *J* = 7.4 Hz), 8.20 – 8.10 (m), 8.07 (t, *J* = 5.7 Hz), 8.05 (t, *J* = 5.7 Hz), 7.97 (t, *J* = 7.6 Hz), 7.93 (d, *J* = 7.7 Hz), 7.90 – 7.85 (m), 7.84 (d, *J* = 8.4 Hz), 7.80 (d, *J* = 7.8 Hz), 7.76 (d, *J* = 8.2 Hz), 7.73 (d, *J* = 8.6 Hz), 7.67 (d, *J* = 8.2 Hz), 7.63 (t, *J* = 6.8 Hz), 7.45 (s), 7.22 (s), 7.19 (s), 7.03 (s), 6.98 (s), 6.80 (s), 5.23 – 4.74 (m), 4.66 – 4.64 (m), 4.48 – 4.09 (m), 4.07 – 4.01 (m), 4.00 – 3.94 (m), 3.81 (d, *J* = 5.8 Hz), 3.79 (d, *J* = 5.6 Hz), 3.76 – 3.51 (m), 2.87 (d, *J* = 3.9 Hz), 2.84 (d, *J* = 3.8 Hz), 2.78 – 2.70 (m), 2.68 (d, *J* = 8.8 Hz), 2.65 (d, *J* = 8.8 Hz), 2.60 – 2.52 (m), 2.49 – 2.35 (m), 2.19 – 2.02 (m), 2.00 – 1.82 (m), 1.81 – 1.69 (m), 1.68 – 1.57 (m), 1.55 – 1.39 (m), 1.36 – 1.22 (m), 1.21 (d, *J* = 7.0 Hz), 1.15 – 0.99 (m), 0.90 – 0.76 (m).

¹³C NMR (176 MHz, DMSO-d₆) δ [ppm] = 174.2, 173.5, 172.6, 172.5, 172.3, 172.0, 171.9, 171.4, 171.3, 171.2, 171.2, 171.1, 170.9, 170.8, 170.6, 170.1, 170.0, 169.9, 169.9, 169.8, 169.7, 169.1, 168.4, 168.1, 69.9, 66.8, 66.7, 66.5, 61.8, 61.7, 61.4, 58.3, 58.0, 57.7, 57.4, 57.4, 57.1, 55.4, 55.2, 55.1, 52.8, 52.2, 51.8, 51.5, 51.5, 50.0, 49.5, 49.1, 48.2, 42.2, 42.0, 40.7, 40.5, 40.0, 38.8, 36.7, 36.4, 36.3, 35.8, 32.3, 31.5, 31.2, 30.8, 29.3, 27.6, 27.2, 26.6, 24.3, 24.2, 24.0, 23.1, 23.1, 22.3, 21.5, 21.5, 19.7, 19.5, 19.4, 19.1, 18.2, 17.7, 15.4, 15.4, 14.7, 11.2, 11.0.

HRMS (ESI) calculated for C₈₅H₁₅₀N₂₄O₃₂S²⁺ ([M+2H]²⁺): *m/z* = 1025.5279, experimental: 1025.5278, δ [ppm] = 0.1, calculated for C₈₅H₁₄₉N₂₄NaO₃₂S²⁺ ([M+H+Na]²⁺): *m/z* = 1036.5189, experimental: 1036.5188, δ [ppm] = 0.1, calculated for C₈₅H₁₅₁N₂₄O₃₂S⁺ ([M+3H]³⁺): *m/z* = 684.0210, experimental: 684.0210, δ [ppm] = 0.0.

PfeA 33-51 peptide 6

aa: VIELGE*Q*T*V*V*A*T*AQEETKQ

Chemical Formula: C₉₄H₁₆₂N₂₆O₃₄

Exact Mass: 2199,17468

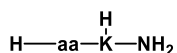
Molecular Weight: 2200,47800

6 (29.3 mg, 13.315 μmol, 27%) was prepared following the general procedures for peptide synthesis and global deprotection and resin cleavage.

¹H NMR (700 MHz, DMSO-d₆): δ [ppm] = 12.23 (s), 8.36 (d, *J* = 8.5 Hz), 8.23 – 8.14 (m), 8.08 – 8.01 (m), 8.00 (d, *J* = 7.3 Hz), 7.98 – 7.90 (m), 7.88 (d, *J* = 8.1 Hz), 7.80 (d, *J* = 7.9 Hz), 7.76 (d, *J* = 7.7 Hz), 7.73 (d, *J* = 7.8 Hz), 7.71 – 7.61 (m), 7.29 (d, *J* = 7.2 Hz), 7.26 (s), 7.05 (s), 6.79 (s), 6.77 (s), 5.10 – 4.80 (m), 4.38 – 4.09 (m), 4.07 (t, *J* = 7.6 Hz), 4.04 – 3.94 (m), 3.81 (d, *J* = 5.9 Hz), 3.78 (d, *J* = 5.7 Hz), 3.69 – 3.65 (m), 3.63 (d, *J* = 5.5 Hz), 2.79 – 2.71 (m), 2.34 – 2.06 (m), 2.05 – 1.83 (m), 1.82 – 1.40 (m), 1.39 – 1.24 (m), 1.22 (t, *J* = 7.2 Hz), 1.15 – 1.06 (m), 1.05 – 0.97 (m), 0.93 – 0.77 (m).

¹³C NMR (176 MHz, DMSO-d₆) δ [ppm] = 174.1, 174.1, 174.0, 173.9, 173.9, 173.5, 172.6, 172.3, 171.7, 171.5, 171.4, 171.1, 171.1, 171.1, 170.8, 170.7, 170.5, 170.0, 169.9, 168.7, 167.8, 66.6, 66.5, 58.3, 58.3, 58.0, 57.7, 57.1, 57.0, 52.7, 52.4, 52.2, 52.1, 51.8, 51.7, 51.0, 48.6, 48.4, 41.9, 41.0, 40.0, 38.7, 36.6, 31.5, 31.4, 31.4, 31.0, 30.6, 30.2, 30.1, 30.1, 30.1, 30.0, 27.7, 27.6, 27.6, 27.5, 27.2, 27.1, 26.7, 26.7, 24.4, 24.1, 23.1, 22.2, 22.2, 21.5, 19.6, 19.5, 19.4, 19.2, 18.3, 18.3, 18.1, 17.9, 17.9, 17.6, 15.1, 11.0.

HRMS (ESI) calculated for C₉₄H₁₆₄N₂₆O₃₄⁺ ([M+2H]²⁺): *m/z* = 1100.5941, experimental: 1100.5940, δ [ppm] = 0.1.

HasR 122-144 peptide 7aa: SLIRVSQDDLQMS^{*}VS^{*}I^{*}SAARPChemical Formula: C₁₁₁H₁₉₄N₃₄O₃₅S

Exact Mass: 2595,41665

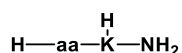
Molecular Weight: 2597,03600

7 (15.6 mg, 6.007 μmol, 12%) was prepared following the general procedures for peptide synthesis and global deprotection and resin cleavage.

¹H NMR (700 MHz, DMSO-d₆): δ [ppm] = 12.36 (s), 8.52 (d, *J* = 8.1 Hz), 8.17 (d, *J* = 7.4 Hz), 8.13 (d, *J* = 7.8 Hz), 8.11 – 8.08 (m), 8.06 (d, *J* = 7.3 Hz), 8.03 – 7.85 (m), 7.81 (d, *J* = 8.0 Hz), 7.77 (d, *J* = 8.2 Hz), 7.73 – 7.43 (m), 7.25 (s), 7.21 – 7.17 (m), 7.01 (s), 6.81 (s), 6.76 (s), 5.48 (bs), 5.15 – 4.77 (m), 4.58 – 4.01 (m), 3.88 – 3.83 (m), 3.74 (d, *J* = 4.2 Hz), 3.72 (d, *J* = 4.1 Hz), 3.70 – 3.49 (m), 3.15 – 3.04 (m), 2.80 – 2.73 (m), 2.72 – 2.65 (m), 2.53 – 2.34 (m), 2.19 – 2.02 (m), 1.99 – 1.02 (m), 0.93 – 0.68 (m).

¹³C NMR (176 MHz, DMSO-d₆) δ [ppm] = 174.1, 173.9, 173.9, 173.6, 172.1, 171.9, 171.9, 171.8, 171.8, 171.4, 171.1, 171.0, 171.0, 170.9, 170.8, 169.9, 169.8, 169.2, 166.6, 156.7, 61.6, 61.4, 61.4, 60.6, 59.7, 59.6, 57.8, 57.6, 57.0, 55.4, 55.0, 54.2, 53.3, 52.2, 51.6, 51.3, 50.0, 49.8, 49.7, 48.3, 48.1, 47.1, 46.9, 40.6, 40.5, 40.4, 40.0, 39.9, 39.8, 39.6, 39.5, 39.4, 39.3, 39.2, 38.8, 36.7, 36.2, 36.0, 32.2, 31.5, 31.1, 30.5, 30.4, 29.4, 29.2, 29.1, 28.2, 27.7, 27.2, 27.0, 26.6, 24.5, 24.3, 24.0, 23.2, 23.2, 23.1, 22.5, 22.3, 21.6, 21.5, 19.2, 19.2, 18.2, 18.2, 17.9, 17.8, 17.8, 15.3, 14.7, 11.0.

HRMS (ESI) calculated for C₁₁₁H₁₉₈N₃₄O₃₅S⁺ ([M+4H]⁺): *m/z* = 649.8614, experimental: 649.8607, δ [ppm] = 0.7.

FpvA 124-134 peptide 8aa: **VDLG*A*T*MITSN**Chemical Formula: C₅₂H₉₃N₁₅O₁₈S

Exact Mass: 1247,65437

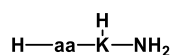
Molecular Weight: 1248,46300

8 (20.3 mg, 16.260 μmol, 33%) was prepared following the general procedures for peptide synthesis and global deprotection and resin cleavage.

¹H NMR (700 MHz, DMSO-d₆): δ [ppm] = 12.56 (s), 8.69 (d, *J* = 7.3 Hz), 8.24 (d, *J* = 7.7 Hz), 8.20 (d, *J* = 7.5 Hz), 8.14 – 8.07 (m), 8.06 (t, *J* = 5.9 Hz), 7.99 (d, *J* = 8.5 Hz), 7.92 – 7.85 (m), 7.82 – 7.77 (m), 7.72 (s), 7.44 (s), 7.26 (s), 7.23 (s), 7.20 – 7.16 (m), 7.11 (s), 7.08 (s), 6.98 (s), 4.97 (s), 4.67 – 4.61 (m), 4.52 – 4.47 (m), 4.44 – 4.36 (m), 4.34 – 4.32 (m), 4.29 (dd, *J* = 8.3 Hz, 3.8 Hz), 4.26 – 4.21 (m), 4.18 (dd, *J* = 8.3 Hz, 4.3 Hz), 4.10 – 4.04 (m), 4.03 – 3.95 (m), 3.72 (d, *J* = 5.8 Hz), 3.69 (d, *J* = 5.7 Hz), 3.67 (d, *J* = 5.9 Hz), 3.65 – 3.62 (m), 3.59 – 3.42 (m), 2.80 – 2.71 (m), 2.60 – 2.51 (m), 2.48 – 2.35 (m), 2.11 – 2.02 (m), 1.95 – 1.87 (m), 1.81 – 1.69 (m), 1.66 – 1.58 (m), 1.53 – 1.38 (m), 1.35 – 1.23 (m), 1.21 (d, *J* = 7.0 Hz), 1.12 – 1.06 (m), 1.02 (dd, *J* = 11.1 Hz, 6.3 Hz), 0.91 (dd, *J* = 10.2 Hz, 6.9 Hz), 0.86 (d, *J* = 6.6 Hz), 0.83 – 0.77 (m).

¹³C NMR (176 MHz, DMSO-d₆) δ [ppm] = 173.6, 172.4, 172.3, 171.8, 171.7, 171.1, 170.9, 170.7, 170.3, 170.2, 169.8, 169.8, 168.3, 167.7, 66.6, 66.5, 61.8, 58.3, 57.7, 57.2, 57.1, 54.8, 52.3, 51.8, 51.4, 50.1, 49.6, 48.1, 41.9, 40.5, 40.0, 38.8, 36.6, 36.2, 35.9, 32.2, 30.7, 29.9, 29.3, 26.5, 24.3, 24.0, 23.2, 22.2, 21.3, 19.7, 19.3, 18.3, 18.1, 17.5, 15.4, 14.6, 10.9.

HRMS (ESI) calculated for C₅₂H₉₄N₁₅O₁₈S⁺ ([M+H]⁺): *m/z* = 1248.6617, experimental: 1248.6610, δ [ppm] = 0.7, calculated for C₅₂H₉₄N₁₅NaO₁₈S²⁺ ([M+H+Na]²⁺): *m/z* = 635.8254, experimental: 635.8249, δ [ppm] = 0.5, calculated for C₅₂H₉₃N₁₅Na₂O₁₈S²⁺ ([M+2Na]²⁺): *m/z* = 646.8164, experimental: 646.8158, δ [ppm] = 0.6, calculated for C₅₂H₉₆N₁₅O₁₈S³⁺ ([M+3H]³⁺): *m/z* = 416.8921, experimental: 416.8918, δ [ppm] = 0.3.

PfeA 37-46 peptide 9

aa: GE*Q*T*V*V*A*T*AQ

Chemical Formula: C₄₇H₈₃N₁₅O₁₇

Exact Mass: 1129,60914

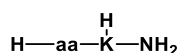
Molecular Weight: 1130,26900

9 (31.6 mg, 25.957 μmol, 52%) was prepared following the general procedures for peptide synthesis and global deprotection and resin cleavage.

¹H NMR (700 MHz, DMSO-d₆): δ [ppm] = 12.14 (s), 8.54 (d, *J* = 7.9 Hz), 8.31 (d, *J* = 7.5 Hz), 8.06 (d, *J* = 6.8 Hz), 8.05 – 7.97 (m), 7.94 – 7.88 (m), 7.82 – 7.68 (m), 7.63 (d, *J* = 8.6 Hz), 7.29 (s), 7.25 (s), 7.05 (s), 6.78 (d, *J* = 5.4 Hz), 4.93 (s), 4.45 – 4.38 (m), 4.37 – 4.31 (m), 4.28 – 4.23 (m), 4.21 – 4.07 (m), 4.02 – 3.97 (m), 3.60 – 3.56 (m), 2.88 (s), 2.80 – 2.70 (m), 2.28 – 2.19 (m), 2.18 – 2.06 (m), 1.99 – 1.84 (m), 1.78 – 1.64 (m), 1.54 – 1.48 (m), 1.33 – 1.24 (m), 1.21 (dd, *J* = 11.4 Hz, 7.1 Hz), 1.02 (dd, *J* = 10.1 Hz, 6.4 Hz), 0.90 – 0.75 (m).

¹³C NMR (176 MHz, DMSO-d₆) δ [ppm] = 173.9, 173.9, 173.4, 172.5, 172.4, 171.3, 171.0, 171.0, 170.7, 170.6, 169.9, 169.7, 165.9, 162.4, 66.5, 66.5, 58.1, 58.1, 57.8, 57.6, 52.6, 52.3, 52.1, 51.8, 48.4, 48.3, 40.2, 40.0, 38.8, 31.6, 31.4, 31.4, 30.7, 30.3, 30.0, 27.9, 27.7, 27.6, 26.7, 22.2, 19.6, 19.5, 19.2, 18.2, 18.0, 18.0, 18.0.

HRMS (ESI) calculated for C₄₇H₈₄N₁₅O₁₇⁺ ([M+H]⁺): *m/z* = 1130.6164, experimental: 1130.6154, δ [ppm] = 1.0, calculated for C₄₇H₈₃N₁₅NaO₁₇⁺ ([M+Na]⁺): *m/z* = 1152.5984., experimental: 1152.5980, δ [ppm] = 0.4, calculated for C₄₇H₈₅N₁₅O₁₇²⁺ ([M+2H]²⁺): *m/z* = 565.8119, experimental: 565.8118, δ [ppm] = 0.1, calculated for C₄₇H₈₆N₁₅O₁₇³⁺ ([M+3H]³⁺): *m/z* = 377.5437, experimental: 377.5436, δ [ppm] = 0.1.

HasR 129-138 peptide 10

aa: DDLVQMSPS*V*

Chemical Formula: C₅₁H₈₈N₁₄O₁₈S

Exact Mass: 1216,61217

Molecular Weight: 1217,40500

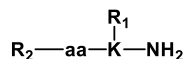
10 (21.7 mg, 17.825 μmol, 36%) was prepared following the general procedures for peptide synthesis and global deprotection and resin cleavage.

¹H NMR (700 MHz, DMSO-d₆): δ [ppm] = 12.67 (s), 8.77 (d, *J* = 7.7 Hz), 8.20 (s), 8.10 (d, *J* = 6.8 Hz), 8.05 (t, *J* = 8.5 Hz), 8.00 – 7.95 (m), 7.84 (d, *J* = 8.1 Hz), 7.75 (s), 7.68 (d, *J* = 8.5 Hz), 7.63 (d, *J* = 8.1 Hz), 7.26 (s), 7.19 (s), 7.15 (s), 7.12 (s), 7.03 (s), 6.77 (s), 4.61 (td, *J* = 8.2 Hz, 4.7 Hz), 4.56 (q, *J* = 6.8 Hz), 4.44 – 4.33 (m), 4.30 – 4.26 (m), 4.23 – 4.19 (m), 4.16 – 4.03 (m), 3.97 – 3.34 (m), 3.15 – 2.99 (m), 2.84 (dd, *J* = 17.8 Hz, 3.3 Hz), 2.78 – 2.73 (m), 2.70 (dd, *J* = 16.9 Hz, 4.5 Hz), 2.66 (dd, *J* = 17.9 Hz, 9.0 Hz), 2.56 – 2.35 (m), 2.12 – 2.01 (m), 1.98 – 1.80 (m), 1.78 – 1.40 (m), 1.35 – 1.22 (m), 1.10 (s), 0.87 (dd, *J* = 6.5 Hz, 5.4 Hz), 0.84 – 0.78 (m).

¹³C NMR (176 MHz, DMSO-d₆) δ [ppm] = 173.9, 173.5, 171.8, 171.8, 171.4, 171.1, 171.0, 170.8, 170.6, 170.4, 170.0, 169.3, 169.1, 167.9, 61.5, 61.4, 59.6, 58.1, 57.5, 55.3, 53.3, 52.3, 52.2, 51.6, 51.4, 49.8, 48.8, 47.1, 43.7, 40.4, 40.0, 38.7, 36.0, 35.6, 32.2, 31.5, 31.1, 30.6, 30.2, 29.5, 29.1, 27.8, 26.6, 24.4, 24.2, 23.1, 22.4, 21.6, 19.2, 19.2, 18.2, 17.8.

HRMS (ESI) calculated for C₅₁H₈₉N₁₄O₁₈S⁺ ([M+H]⁺): *m/z* = 1217.6195, experimental: 1217.6194, δ [ppm] = 0.1, calculated for C₅₁H₈₈N₁₄NaO₁₈S⁺ ([M+Na]⁺): *m/z* = 1239.6014, experimental: 1239.6006, δ [ppm] = 0.8, calculated for C₅₁H₉₀N₁₄O₁₈S²⁺ ([M+2H]²⁺): *m/z* = 609.3134, experimental: 609.3136, δ [ppm] = 0.2, calculated for C₅₁H₈₉N₁₄NaO₁₈S²⁺ ([M+H+Na]²⁺): *m/z* = 620.3043, experimental: 620.3047, δ [ppm] = 0.4, calculated for C₅₁H₈₈N₁₄Na₂O₁₈S²⁺ ([M+2Na]²⁺): *m/z* = 631.2953, experimental: 631.2949, δ [ppm] = 0.4.

General procedure for the *N*-*C*-terminal modification, global deprotection and resin cleavage



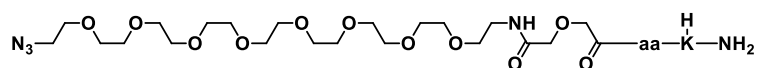
R₁ = H, CO-(PEG)₇-N₃, 3-(Pyridin-2-yl)disulfanyl)propionyl, 2,3-Dihydroxybenzoyl
 R₂ = CO-(PEG)₇-N₃, H

	FpvA 121-139 = DSSVDLG*A*T*MITSNQLGTI	
	PfeA 33-51 = VIELGE*Q*T*V*V*A*T*AQEETKQ	(long version)
	HasR 122-144 = SLIRVSQDDLQMSPS*V*I*SAARP	
aa sequences	FpvA 124-134 = VDLG*A*T*MITSN	
	PfeA 37-46 = GE*Q*T*V*V*A*T*AQ	(short version)
	HasR 129-138 = DDLVQMSPS*V*	

N-terminal coupling with N₃-(PEG)₇-COOH (83.2 mg, 150 μmol, 3.0 eq) was performed after manual deprotection of the *N*-terminal Fmoc group cleavage of the peptide chain (50.0 μmol, 1.0 eq) on the resin with HOBt (30.6 mg, 200.0 μmol, 4.0 eq), HATU (85.6 mg, 225.0 μmol, 4.5 eq), and NMM (0.2 mL) activation in threefold excess at 23 °C for 21 h in DMF (1.8 mL). The Dde group, if present, was removed on the resin by a treatments with hydrazine (8.0 eq.) in THF (1.0 M) (0.4 mL) in DMF (1.6 mL) at 23 °C for 3 h.

C-terminal coupling with N₃-(PEG)₇-COOH (83.2 mg, 150 μmol, 3.0 eq), PDTP (32.3 mg, 150 μmol, 3.0 eq) or **40** (35.7 mg, 150 μmol, 3.0 eq) was performed after the Dde deprotection procedure described in *General procedure for global deprotection and resin cleavage* after the same procedure as stated above for the *N*-terminal modification. For *C*-terminal coupling with **40**, the reagents were added dropwise at 0 °C. After the coupling with **40**, deacetylation was performed with DIPEA (0.4 mL) in MeOH (1.6 mL) at 0 °C for 3 h. The crude peptides were cleaved from the resin and globally deprotected as described in *General procedure for global deprotection and resin cleavage*. After precipitation with ice-cold *t*-butylmethyl ether and centrifugation (4500 rpm, 30 min, -20 °C) the resulting crude peptides were taken up in ACN/MilliQ H₂O containing 0.1% TFA and were purified by RP-HPLC (C18 phenomenex, 220 nm, collect all, 5-50% ACN/MilliQ H₂O, 0.1% TFA). The product containing fractions were identified by LCMS and lyophilized to dryness to yield the PEG-modified peptides as white solids.

Compound 61



aa: DSSVDLG*A*T*MITSNQLGTI

Chemical Formula: C₁₀₇H₁₈₈N₂₈O₄₃S

Exact Mass: 2585,31058

Molecular Weight: 2586,89400

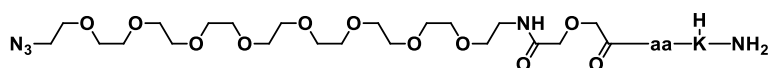
61 (4.8 mg, 5.721 μmol, 11%) was prepared following the general procedures for peptide synthesis, *N*-/*C*-terminal modification and global deprotection with the *FpvA* 121-139 C-term Dde peptide or *FpvA* 121-139 C-term Boc peptide and N₃-(PEG)₇-COOH.

¹H NMR (700 MHz, DMSO-d₆): δ [ppm] = 12.33 (s), 8.28 (d, *J* = 8.1 Hz), 8.23 (s), 8.16 (d, *J* = 7.6 Hz), 8.11 – 8.01 (m), 7.99 (t, *J* = 5.6 Hz), 7.96 (d, *J* = 7.3 Hz), 7.93 (d, *J* = 7.4 Hz), 7.88 (d, *J* = 8.0 Hz), 7.87 – 7.82 (m), 7.80 (d, *J* = 7.4 Hz), 7.76 (d, *J* = 8.0 Hz), 7.70 (d, *J* = 8.2 Hz), 7.67 (d, *J* = 7.9 Hz), 7.60 (s), 7.44 (s), 7.22 (s), 7.19 (s), 7.04 (s), 7.02 (s), 6.99 (s), 6.80 (s), 5.12 – 4.80 (m), 4.68 (dd, *J* = 13.5 Hz, 7.7 Hz), 4.57 – 4.50 (m), 4.45 – 3.91 (m), 3.83 – 3.77 (m), 3.75 – 3.47 (m), 3.44 (t, *J* = 6.0 Hz), 3.40 – 3.14 (m), 3.09 (dd, *J* = 14.4 Hz, 7.2 Hz), 2.78 – 2.52 (m), 2.47 – 2.36 (m), 2.27 (s), 2.15 – 2.02 (m), 2.00 – 1.19 (m), 1.17 (t, *J* = 7.3 Hz), 1.15 – 1.05 (m), 1.02 (dd, *J* = 9.5 Hz, 5.9 Hz), 0.94 (s), 0.86 (dd, *J* = 11.9 Hz, 6.5 Hz), 0.84 – 0.75 (m).

¹³C NMR (176 MHz, DMSO-d₆) δ [ppm] = 174.0, 173.4, 173.3, 172.8, 172.4, 172.4, 172.2, 171.9, 171.9, 171.8, 171.3, 171.1, 171.0, 170.8, 170.8, 170.7, 170.5, 170.4, 170.0, 169.9, 169.8, 169.0, 168.8, 168.3, 70.3, 70.1, 69.8, 69.8, 69.7, 69.6, 69.3, 68.9, 66.7, 66.7, 66.6, 66.5, 61.7, 61.4, 58.2, 57.9, 57.6, 57.4, 57.2, 57.2, 57.0, 55.0, 55.0, 54.9, 52.7, 52.1, 51.7, 51.4, 51.4, 51.3, 50.0, 49.9, 49.4, 49.0, 48.6, 48.1, 45.8, 42.6, 42.2, 41.9, 40.6, 40.4, 40.2, 38.7, 38.1, 36.6, 36.4, 36.2, 32.2, 31.5, 31.2, 30.6, 29.7, 29.3, 27.9, 27.5, 27.1, 26.5, 24.2, 24.1, 23.9, 23.1, 23.0, 22.2, 21.5, 19.6, 19.5, 19.3, 19.1, 19.0, 18.2, 17.7, 17.3, 15.4, 15.3, 14.6, 11.2, 11.2, 10.9, 8.7.

HRMS (ESI) calculated for C₁₀₇H₁₉₀N₂₈O₄₃S²⁺ ([M+2H]²⁺): *m/z* = 1293.6626, experimental: 1293.6622, δ [ppm] = 0.4, calculated for C₁₀₇H₁₉₁N₂₈O₄₃S²⁺ ([M+3H]³⁺): *m/z* = 862.7775, experimental: 862.7777, δ [ppm] = 0.2.

Compound 62



aa: VIELGE*Q*T*V*V*A*T*AQEETKQ

Chemical Formula: C₁₁₆H₂₀₂N₃₀O₄₅

Exact Mass: 2735,44403

Molecular Weight: 2737,05700

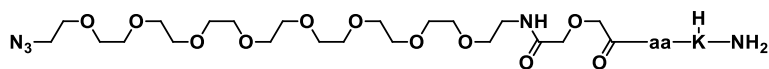
62 (29.1 mg, 10.632 μmol, 21%) was prepared following the general procedures for peptide synthesis, *N*-/*C*-terminal modification and global deprotection with the *PfeA* 33-51 *C*-term Dde peptide or *PfeA* 33-51 *C*-term Boc peptide and N₃-(PEG)₇-COOH.

¹H NMR (700 MHz, DMSO-*d*₆): δ [ppm] = 12.08 (s, 1H), 8.20 – 8.15 (m), 8.08 – 8.02 (m), 8.02 – 7.98 (m), 7.97 (d, *J* = 7.2 Hz), 7.95 – 7.85 (m), 7.79 (d, *J* = 8.0 Hz), 7.76 (d, *J* = 7.7 Hz), 7.73 (d, *J* = 7.9 Hz), 7.69 (bs), 7.65 (d, *J* = 8.3 Hz), 7.29 (s), 7.27 (s), 7.24 (s), 7.05 (s), 6.79 (s), 6.77 (s), 4.99 – 4.86 (m), 4.39 – 4.07 (m), 4.05 – 3.92 (m), 3.79 (dd, *J* = 16.5 Hz, 5.5 Hz), 3.67 – 3.51 (m), 3.50 (s), 3.43 (t, *J* = 6.0 Hz), 3.40 – 3.38 (m), 3.26 (q, *J* = 5.9 Hz), 3.19 – 3.15 (m), 2.76 (t, *J* = 7.3 Hz), 2.34 – 2.05 (m), 2.02 – 1.83 (m), 1.82 – 1.25 (m), 1.23 – 1.19 (m), 1.04 (dd, *J* = 11.7 Hz, 6.3 Hz), 1.01 (d, *J* = 6.3 Hz), 0.86 (d, *J* = 6.6 Hz), 0.85 – 0.77 (m).

¹³C NMR (176 MHz, DMSO-*d*₆) δ [ppm] = 174.1, 174.1, 174.0, 174.0, 173.9, 173.9, 173.4, 172.7, 172.3, 171.7, 171.5, 171.5, 171.4, 171.1, 171.1, 170.8, 170.7, 170.6, 170.0, 170.0, 168.9, 168.8, 168.7, 70.3, 70.2, 69.8, 69.8, 69.7, 69.7, 69.6, 69.3, 68.9, 66.5, 66.4, 58.3, 58.3, 58.0, 57.8, 57.2, 56.8, 52.7, 52.7, 52.6, 52.4, 52.2, 52.1, 51.7, 51.7, 51.0, 50.0, 48.6, 48.4, 41.9, 41.0, 40.0, 38.7, 38.1, 38.0, 36.4, 31.5, 31.5, 31.4, 31.3, 31.0, 30.6, 30.5, 30.2, 30.1, 30.0, 29.0, 27.7, 27.6, 27.4, 27.2, 27.2, 27.0, 26.7, 26.6, 24.4, 24.0, 23.1, 22.4, 22.2, 21.5, 19.6, 19.5, 19.4, 19.2, 19.2, 18.3, 18.2, 18.1, 17.9, 17.9, 15.2, 14.0, 11.0.

HRMS (ESI) calculated for C₁₁₆H₂₀₄N₃₀O₄₅²⁺ ([M+2H]²⁺): *m/z* = 1368.7292, experimental: 1368.7312, δ [ppm] = 1.0, calculated for C₁₁₆H₂₀₅N₃₀O₄₅³⁺ ([M+3H]³⁺): *m/z* = 912.8220, experimental: 912.8232 δ [ppm] = 1.2.

Compound 63



aa: SLIRVSQDDLQMSPS*V*I*SAARP

Chemical Formula: C₁₃₃H₂₃₄N₃₈O₄₆S

Exact Mass: 3131,68601

Molecular Weight: 3133,61500

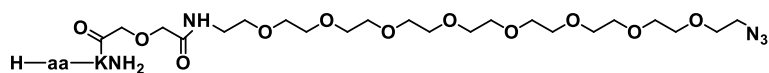
63 (16.0 mg, 5.106 μmol, 10%) was prepared following the general procedures for peptide synthesis, *N*-*C*-terminal modification and global deprotection with the *HasR* 122-144 *C*-term Dde peptide or *HasR* 122-144 *C*-term Boc peptide and N₃-(PEG)₇-COOH.

¹H NMR (700 MHz, DMSO-*d*₆): δ [ppm] = 12.36 (s), 8.52 (d, *J* = 8.1 Hz), 8.48 (d, *J* = 8.3 Hz), 8.40 – 7.27 (m), 7.25 (s), 7.21 (s), 7.19 (s), 7.12 (s), 7.05 (s), 7.00 (s), 6.81 (s), 6.79 (s), 6.76 (s), 5.21 – 4.06 (m), 4.00 (s), 3.98 (s), 3.74 (d, *J* = 4.2 Hz), 3.72 (d, *J* = 4.3 Hz), 3.66 – 3.24 (m), 3.17 (s), 3.15 – 3.00 (m), 2.96 (s), 2.89 – 2.51 (m), 2.49 – 2.33 (m), 2.27 (s), 2.16 – 2.02 (m), 1.99 – 1.14 (m), 1.12 (s), 1.10 – 1.01 (m), 0.94 (s), 0.90 – 0.75 (m).

¹³C NMR (176 MHz, DMSO-*d*₆) δ [ppm] = 174.0, 173.9, 173.6, 172.8, 172.0, 171.7, 171.7, 171.5, 171.4, 171.4, 171.2, 171.0, 171.0, 170.8, 170.8, 170.7, 170.6, 170.3, 170.2, 170.2, 170.1, 170.0, 169.9, 169.8, 169.7, 169.7, 169.5, 169.4, 169.2, 169.1, 168.9, 166.6, 166.1, 157.5, 156.7, 73.6, 73.0, 72.9, 72.8, 70.3, 70.2, 69.8, 69.8, 69.7, 69.6, 69.3, 68.9, 61.6, 61.6, 61.5, 61.4, 60.6, 60.5, 59.6, 59.6, 59.5, 57.6, 57.3, 57.3, 56.9, 56.8, 56.7, 55.3, 54.9, 54.5, 54.2, 53.3, 52.7, 52.5, 52.3, 52.2, 52.1, 52.0, 51.6, 51.3, 51.2, 51.1, 50.0, 50.0, 49.9, 49.6, 49.5, 48.2, 48.1, 48.1, 47.0, 46.9, 46.8, 42.6, 42.5, 41.2, 40.6, 40.6, 40.5, 40.5, 40.4, 38.7, 38.2, 36.7, 36.6, 36.4, 36.3, 36.3, 36.0, 35.8, 32.2, 31.5, 31.3, 31.3, 31.1, 30.9, 30.8, 30.5, 30.4, 30.4, 29.8, 29.4, 29.2, 29.1, 28.3, 28.3, 28.2, 28.1, 27.9, 27.7, 27.1, 27.0, 26.6, 26.5, 25.0, 24.5, 24.3, 24.2, 24.1, 24.1, 24.1, 24.0, 24.0, 23.9, 23.2, 23.1, 22.6, 22.5, 22.5, 22.3, 22.2, 22.1, 21.8, 21.6, 21.5, 21.5, 19.2, 19.1, 19.0, 18.2, 18.0, 17.9, 17.8, 17.8, 17.6, 17.4, 15.3, 15.2, 14.6, 12.3, 10.9.

HRMS (ESI) calculated for C₁₃₃H₂₃₇N₃₈O₄₆S³⁺ ([M+3H]³⁺): *m/z* = 1044.90261, experimental: 1044.9013, δ [ppm] = 1.25, calculated for C₁₃₃H₂₃₈N₃₈O₄₆S⁴⁺ ([M+4H]⁴⁺): *m/z* = 783.92878, experimental: 783.9286 δ [ppm] = 0.23.

Compound 64



aa: DSSVDLG*A*T*MITSNQLGTI

Chemical Formula: C₁₀₇H₁₈₈N₂₈O₄₃S

Exact Mass: 2585,31058

Molecular Weight: 2586,89400

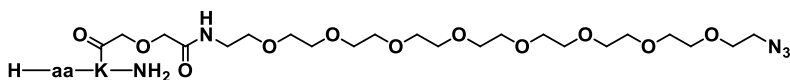
64 (15.7 mg, 6.069 μ mol, 12%) was prepared following the general procedures for peptide synthesis, *N*-*C*-terminal modification and global deprotection with the *FpvA* 121-139 *N*-term Boc C-term Dde peptide and N₃-(PEG)₇-COOH.

¹H NMR (700 MHz, DMSO-*d*₆): δ [ppm] = 12.64 (s), 8.62 (d, *J* = 7.7 Hz), 8.36 (d, *J* = 7.5 Hz), 8.29 (d, *J* = 7.4 Hz), 8.19 – 8.10 (m), 8.09 – 8.02 (m), 7.98 – 7.94 (m), 7.92 (d, *J* = 7.4 Hz), 7.90 – 7.83 (m), 7.81 – 7.78 (m), 7.76 (d, *J* = 8.1 Hz), 7.74 (d, *J* = 8.6 Hz), 7.71 – 7.64 (m), 7.62 (s), 7.44 (s), 7.25 – 7.15 (m), 7.05 – 6.94 (m), 6.82 – 6.75 (m), 5.17 – 4.80 (m), 4.59 – 4.09 (m), 4.06 – 3.89 (m), 3.83 – 3.48 (m), 3.44 (t, *J* = 5.9 Hz), 3.42 – 3.38 (m), 3.28 (q, *J* = 6.0 Hz), 3.17 (s), 3.08 (dd, *J* = 13.3 Hz, 6.8 Hz), 2.88 – 2.82 (m), 2.77 – 2.63 (m), 2.60 – 2.53 (m), 2.50 – 2.35 (m), 2.27 (s, 1H), 2.14 – 2.03 (m), 2.00 – 1.82 (m), 1.81 – 1.17 (m), 1.16 – 0.98 (m), 0.94 (s), 0.90 – 0.76 (m).

¹³C NMR (176 MHz, DMSO-*d*₆) δ [ppm] = 174.0, 174.0, 173.5, 173.4, 173.4, 172.8, 172.4, 172.4, 172.4, 172.2, 171.8, 171.8, 171.3, 171.2, 171.1, 171.0, 171.0, 170.8, 170.7, 170.6, 170.6, 170.4, 170.0, 170.0, 169.9, 169.8, 169.8, 169.7, 169.5, 169.0, 168.9, 168.7, 168.4, 168.3, 167.8, 73.2, 72.9, 70.3, 70.2, 69.8, 69.8, 69.7, 69.6, 69.3, 68.9, 66.7, 66.7, 66.6, 66.5, 61.8, 61.7, 61.7, 61.4, 58.2, 57.8, 57.6, 57.2, 57.2, 57.0, 55.1, 55.0, 55.0, 52.7, 52.4, 52.3, 52.1, 52.1, 51.7, 51.3, 51.3, 50.0, 49.9, 49.4, 48.9, 48.8, 48.6, 48.1, 42.6, 42.5, 42.2, 42.1, 41.9, 40.7, 40.5, 40.4, 40.1, 40.0, 38.7, 38.1, 38.0, 36.7, 36.5, 36.5, 36.4, 36.3, 35.7, 35.5, 32.3, 31.5, 31.2, 30.8, 29.7, 29.3, 28.9, 28.1, 27.9, 27.6, 27.5, 27.1, 26.5, 24.3, 24.2, 24.1, 24.0, 23.9, 23.1, 23.0, 22.8, 22.7, 22.2, 21.5, 21.5, 19.6, 19.5, 19.3, 19.3, 19.1, 18.2, 17.6, 17.3, 15.4, 15.3, 14.6, 11.2, 11.2, 10.9.

HRMS (ESI) calculated for C₁₀₇H₁₉₀N₂₈O₄₃S²⁺ ([M+2H]²⁺): *m/z* = 1293.6626, experimental: 1293.6626, δ [ppm] = 0.0, calculated for C₁₀₇H₁₈₉N₂₈NaO₄₃S²⁺ ([M+H+Na]²⁺): *m/z* = 1304.6535, experimental: 1304.6535, δ [ppm] = 0.0, calculated for C₁₀₇H₁₉₁N₂₈O₄₃S³⁺ ([M+3H]³⁺): *m/z* = 862.7775, experimental: 862.7777, δ [ppm] = 0.2, calculated for C₁₀₇H₁₉₂N₂₈O₄₃S⁴⁺ ([M+4H]⁴⁺): *m/z* = 647.3349, experimental: 647.3351, δ [ppm] = 0.2.

Compound 65



aa: VIELGE*Q*T*V*V*A*T*AQEETKQ

Chemical Formula: C₁₁₆H₂₀₂N₃₀O₄₅

Exact Mass: 2735,44403

Molecular Weight: 2737,05700

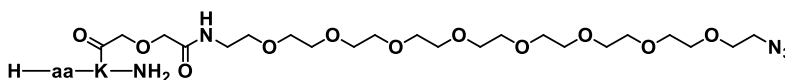
65 (31.3 mg, 11.436 μ mol, 23%) was prepared following the general procedures for peptide synthesis, *N*-/*C*-terminal modification and global deprotection with the *PfeA* 33-51 *N*-term Boc *C*-term Dde peptide and N₃-(PEG)₇-COOH.

¹H NMR (700 MHz, DMSO-*d*₆): δ [ppm] = 12.08 (s), 8.36 (d, *J* = 8.5 Hz), 8.21 (d, *J* = 8.0 Hz), 8.19 – 8.15 (m), 8.07 – 8.01 (m), 8.00 (d, *J* = 7.3 Hz), 7.96 – 7.86 (m), 7.78 (d, *J* = 7.7 Hz), 7.76 (d, *J* = 7.8 Hz), 7.73 (d, *J* = 7.9 Hz), 7.66 – 7.62 (m), 7.32 (s), 7.27 (s), 7.23 (s), 7.01 (s), 6.81 – 6.74 (m), 4.92 (bs), 4.89 (bs), 4.40 – 4.08 (m), 4.03 – 3.90 (m), 3.81 (d, *J* = 5.8 Hz), 3.79 (d, *J* = 5.7 Hz), 3.70 – 3.65 (m), 3.63 (d, *J* = 5.4 Hz), 3.62 – 3.58 (m), 3.57 – 3.48 (m), 3.44 (t, *J* = 6.0 Hz), 3.39 – 3.38 (m), 3.28 (q, *J* = 5.9 Hz), 3.17 (s), 3.09 (dd, *J* = 13.8 Hz, 7.1 Hz), 2.76 (dd, *J* = 12.7 Hz, 6.6 Hz), 2.33 – 1.83 (m), 1.80 – 1.24 (m), 1.21 (t, *J* = 6.2 Hz), 1.11 – 0.99 (m), 0.90 (t, *J* = 7.6 Hz), 0.86 (d, *J* = 6.6 Hz), 0.85 – 0.79 (m).

¹³C NMR (176 MHz, DMSO-*d*₆) δ [ppm] = 174.1, 174.0, 174.0, 173.9, 173.8, 173.5, 172.5, 172.4, 172.3, 171.5, 171.4, 171.3, 171.2, 171.0, 171.0, 171.0, 170.7, 170.6, 170.5, 169.8, 169.8, 169.8, 168.7, 168.7, 168.5, 167.6, 70.2, 70.2, 69.8, 69.8, 69.7, 69.6, 69.3, 68.9, 66.6, 66.5, 58.1, 58.1, 58.1, 57.8, 57.6, 57.1, 56.9, 52.5, 52.5, 52.4, 52.3, 52.0, 51.9, 51.7, 51.6, 51.0, 50.0, 48.6, 48.4, 48.3, 41.8, 41.0, 40.0, 38.8, 38.1, 38.1, 36.6, 31.7, 31.5, 31.5, 31.4, 31.1, 30.6, 30.3, 30.2, 30.1, 30.0, 30.0, 30.0, 29.0, 27.8, 27.7, 27.6, 27.5, 27.3, 27.2, 27.2, 26.6, 24.4, 24.0, 23.1, 22.7, 22.1, 21.5, 19.5, 19.4, 19.2, 18.3, 18.2, 18.0, 18.0, 17.9, 17.6, 15.1, 11.0.

HRMS (ESI) calculated for C₁₁₆H₂₀₄N₃₀O₄₅²⁺ ([*M*+2*H*]²⁺): *m/z* = 1368.7293, experimental: 1368.7299, δ [ppm] = 0.6, calculated for C₁₁₆H₂₀₅N₃₀O₄₅³⁺ ([*M*+3*H*]³⁺): *m/z* = 912.8220, experimental: 912.8232, δ [ppm] = 1.2.

Compound 66



aa: SLIRVSQDDLVMSPS*V*I*SAARP

Chemical Formula: C₁₃₃H₂₃₄N₃₈O₄₆S

Exact Mass: 3131,68601

Molecular Weight: 3133,61500

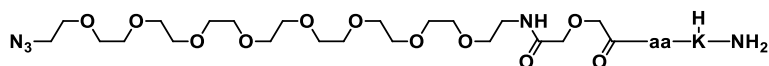
66 (18.6 mg, 5.936 μ mol, 12%) was prepared following the general procedures for peptide synthesis, *N*-*C*-terminal modification and global deprotection with the *HasR* 122-144 *N*-term Boc *C*-term Dde peptide and N₃-(PEG)₇-COOH.

¹H NMR (700 MHz, DMSO-*d*₆): δ [ppm] = 12.33 (s), 8.53 (d, *J* = 8.1 Hz), 8.48 (d, *J* = 8.2 Hz), 8.38 – 7.45 (m), 7.40 – 7.17 (m), 7.03 – 6.95 (m), 6.83 – 6.72 (m), 5.48 (t, *J* = 4.7 Hz), 5.40 (s), 5.10 – 4.89 (m), 4.79 (d, *J* = 7.7 Hz), 4.58 – 4.05 (m), 3.95 – 3.83 (m), 3.76 – 3.20 (m), 3.17 (s), 3.15 – 2.51 (m), 2.47 – 2.33 (m), 2.27 (s), 2.20 – 1.01 (m), 0.94 (s), 0.91 – 0.74 (m).

¹³C NMR (176 MHz, DMSO-*d*₆) δ [ppm] = 174.0, 173.8, 173.6, 173.6, 172.8, 172.0, 171.7, 171.7, 171.7, 171.4, 171.4, 171.2, 171.0, 171.0, 171.0, 170.8, 170.8, 170.8, 170.8, 170.7, 170.6, 170.2, 170.2, 170.0, 170.0, 169.8, 169.8, 169.7, 169.7, 169.2, 169.1, 168.7, 168.5, 166.6, 166.1, 156.7, 73.6, 73.0, 72.8, 70.3, 70.2, 69.8, 69.8, 69.7, 69.6, 69.3, 68.9, 61.6, 61.6, 61.5, 61.4, 60.6, 60.5, 59.6, 59.6, 59.5, 59.5, 59.5, 57.7, 57.6, 57.2, 57.2, 56.9, 56.8, 56.7, 55.3, 55.3, 54.9, 54.9, 54.2, 53.3, 52.7, 52.5, 52.4, 52.3, 52.2, 52.2, 52.0, 51.6, 51.2, 51.2, 51.1, 50.0, 49.9, 49.6, 49.5, 48.1, 48.1, 47.0, 46.9, 46.8, 42.6, 41.2, 40.6, 40.6, 40.5, 40.5, 40.4, 40.0, 38.7, 38.2, 38.1, 36.7, 36.3, 36.0, 35.8, 32.2, 31.5, 31.3, 31.3, 31.1, 30.9, 30.9, 30.5, 30.4, 29.8, 29.4, 29.2, 29.1, 29.1, 29.0, 29.0, 29.0, 28.7, 28.3, 28.3, 28.2, 28.1, 27.9, 27.7, 27.7, 27.2, 27.1, 27.0, 26.6, 25.0, 24.5, 24.3, 24.2, 24.1, 24.1, 24.0, 23.1, 22.8, 22.6, 22.5, 22.3, 22.1, 21.7, 21.6, 21.5, 21.5, 19.2, 19.1, 18.2, 18.1, 18.0, 17.9, 17.8, 17.8, 17.8, 17.4, 15.3, 15.3, 14.6, 14.0, 10.9.

HRMS (ESI) calculated for C₁₃₃H₂₃₇N₃₈O₄₆S³⁺ ([M+3H]³⁺): *m/z* = 1044.9026, experimental: 1044.9043, δ [ppm] = 1.7, calculated for C₁₃₃H₂₃₈N₃₈O₄₆S⁴⁺ ([M+4H]⁴⁺): *m/z* = 783.9288, experimental: 783.9303, δ [ppm] = 1.5, calculated for C₁₃₃H₂₃₉N₃₈O₄₆S⁵⁺ ([M+5H]⁵⁺): *m/z* = 627.3445, experimental: 627.3454, δ [ppm] = 0.9.

Compound 67



aa: VDLG*A*T*MITSN

Chemical Formula: C₇₄H₁₃₃N₁₉O₂₉S

Exact Mass: 1783,92373

Molecular Weight: 1785,04200

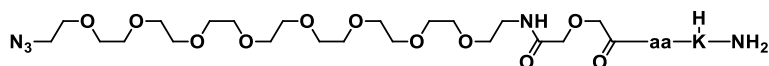
67 (21.2 mg, 11.876 μmol, 24%) was prepared following the general procedures for peptide synthesis, *N*-/*C*-terminal modification and global deprotection with the *FpvA* 124-134 C-term Boc peptide and N₃-(PEG)₇-COOH.

¹H NMR (700 MHz, DMSO-*d*₆): δ [ppm] = 12.39 (s), 8.40 (d, *J* = 7.5 Hz), 8.18 (d, *J* = 7.5 Hz), 8.08 (t, *J* = 5.8 Hz), 8.05 (t, *J* = 5.8 Hz), 7.98 (d, *J* = 8.5 Hz), 7.92 (d, *J* = 7.6 Hz), 7.89 – 7.82 (m), 7.82 (d, *J* = 7.5 Hz), 7.80 (dd, *J* = 8.0 Hz, 3.9 Hz), 7.67 (s), 7.44 (s), 7.24 (s), 7.08 (s), 6.99 (s), 5.11 (t, *J* = 5.5 Hz), 4.98 (d, *J* = 4.8 Hz), 4.87 (d, *J* = 5.1 Hz), 4.57 (dd, *J* = 13.8 Hz, 7.7 Hz), 4.50 (dd, *J* = 13.9 Hz, 6.6 Hz), 4.44 – 4.36 (m), 4.33 (dd, *J* = 13.1 Hz, 5.7 Hz), 4.30 (dd, *J* = 8.3 Hz, 3.9 Hz), 4.26 – 4.16 (m), 4.10 – 4.05 (m), 4.04 – 3.96 (m), 3.94 (s), 3.72 – 3.62 (m), 3.61 – 3.59 (m), 3.57 – 3.46 (m), 3.43 (t, *J* = 6.0 Hz), 3.40 – 3.38 (m), 3.26 (q, *J* = 6.0 Hz), 2.79 – 2.70 (m), 2.58 (dd, *J* = 15.7 Hz, 6.6 Hz), 2.54 – 2.51 (m), 2.49 – 2.35 (m), 1.97 (q, *J* = 6.7 Hz), 1.95 – 1.88 (m), 1.82 – 1.70 (m), 1.64 – 1.56 (m), 1.54 – 1.38 (m), 1.36 – 1.23 (m), 1.21 (d, *J* = 7.0 Hz), 1.16 – 1.05 (m), 1.02 (dd, *J* = 10.6 Hz, 6.3 Hz), 0.95 – 0.77 (m).

¹³C NMR (176 MHz, DMSO-*d*₆) δ [ppm] = 173.6, 172.4, 172.2, 171.9, 171.8, 171.1, 170.9, 170.7, 170.6, 170.5, 170.1, 169.8, 169.8, 168.9, 168.3, 70.4, 70.2, 69.8, 69.8, 69.7, 69.6, 69.3, 68.9, 66.5, 66.5, 61.8, 58.2, 57.7, 57.1, 57.0, 54.8, 52.3, 51.8, 51.4, 50.0, 50.0, 49.4, 48.1, 41.9, 40.6, 40.0, 38.7, 38.1, 36.6, 36.2, 35.7, 32.2, 30.8, 30.7, 29.3, 27.2, 26.5, 24.3, 24.0, 23.1, 22.2, 21.4, 19.6, 19.3, 19.1, 18.2, 18.0, 15.3, 14.6, 10.9.

HRMS (ESI) calculated for C₇₄H₁₃₅N₁₉O₂₉S²⁺ ([M+2H]²⁺): *m/z* = 892.9691, experimental: 892.9687, δ [ppm] = 0.4, calculated for C₇₄H₁₃₄N₁₉NaO₂₉S²⁺ ([M+H+Na]²⁺): *m/z* = 903.9601, experimental: 903.9599, δ [ppm] = 0.2, calculated for C₇₄H₁₃₃N₁₉Na₂O₂₉S²⁺ ([M+2Na]²⁺): *m/z* = 914.9511, experimental: 914.9512, δ [ppm] = 0.1, calculated for C₇₄H₁₃₆N₁₉O₂₉S³⁺ ([M+3H]³⁺): *m/z* = 595.6485, experimental: 595.6484, δ [ppm] = 0.1.

Compound 68



aa: GE*Q*T*V*V*A*T*AQ

Chemical Formula: C₆₉H₁₂₃N₁₉O₂₈

Exact Mass: 1665,87849

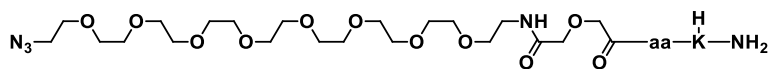
Molecular Weight: 1666,84800

68 (27.8 mg, 16.678 μmol, 33%) was prepared following the general procedures for peptide synthesis, *N*-/*C*-terminal modification and global deprotection with the *PfeA* 37-46 *C*-term Boc peptide and N₃-(PEG)₇-COOH.

¹H NMR (700 MHz, DMSO-*d*₆): δ [ppm] = 12.08 (s), 8.25 (t, *J* = 6.0 Hz), 8.15 (d, *J* = 7.6 Hz), 8.10 (d, *J* = 7.9 Hz), 8.05 (dd, *J* = 12.8 Hz, 6.6 Hz), 7.99 (d, *J* = 7.5 Hz), 7.92 (d, *J* = 7.0 Hz), 7.90 (d, *J* = 8.5 Hz), 7.87 (d, *J* = 8.3 Hz), 7.76 (d, *J* = 8.1 Hz), 7.73 – 7.68 (m), 7.62 (d, *J* = 8.6 Hz), 7.31 – 7.24 (m), 7.06 (s), 6.78 (s), 6.76 (s), 4.98 (d, *J* = 4.7 Hz), 4.89 (d, *J* = 4.7 Hz), 4.36 (p, *J* = 7.1 Hz), 4.33 – 4.23 (m), 4.19 – 4.08 (m), 4.03 – 3.94 (m), 3.80 (d, *J* = 6.1 Hz), 3.61 – 3.58 (m), 3.56 – 3.48 (m), 3.44 (t, *J* = 6.1 Hz), 3.40 – 3.38 (m), 3.28 (q, *J* = 6.0 Hz), 2.78 – 2.71 (m), 2.27 – 2.19 (m), 2.16 – 2.05 (m), 2.01 – 1.84 (m), 1.78 – 1.64 (m), 1.56 – 1.47 (m), 1.34 – 1.25 (m), 1.23 (d, *J* = 7.1 Hz), 1.21 (d, *J* = 7.0 Hz), 1.03 (d, *J* = 6.3 Hz), 1.01 (d, *J* = 6.4 Hz), 0.84 (d, *J* = 2.4 Hz), 0.83 (d, *J* = 2.4 Hz), 0.82 (d, *J* = 6.8 Hz).

HRMS (ESI) calculated for C₅₉H₁₂₅N₁₉O₂₈²⁺ ([*M*+2*H*]²⁺): *m/z* = 833.9465, experimental: 833.9459, δ [ppm] = 0.6, calculated for C₅₉H₁₂₄N₁₉NaO₂₈²⁺ ([*M*+*H*+*Na*]²⁺): *m/z* = 844.9375, experimental: 844.9372, δ [ppm] = 0.3, calculated for C₅₉H₁₂₃N₁₉Na₂O₂₈²⁺ ([*M*+2*Na*]²⁺): *m/z* = 855.9285, experimental: 855.9285, δ [ppm] = 0.0, calculated for C₅₉H₁₂₆N₁₉O₂₈³⁺ ([*M*+3*H*]³⁺): *m/z* = 556.3001, experimental: 556.3002, δ [ppm] = 0.1.

Compound 69



aa: DDLVQMSPS*V*

Chemical Formula: C₇₃H₁₂₈N₁₈O₂₉S

Exact Mass: 1752,88153

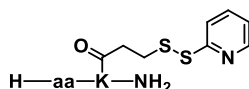
Molecular Weight: 1753,98400

69 (12.8 mg, 7.298 μ mol, 15%) was prepared following the general procedures for peptide synthesis, *N*-/*C*-terminal modification and global deprotection with the *HasR* 129-138 *C*-term Boc peptide and N₃-(PEG)₇-COOH.

¹H NMR (700 MHz, DMSO-*d*₆): δ [ppm] = 12.33 (s), 8.28 (t, *J* = 8.0 Hz), 8.09 (d, *J* = 6.8 Hz), 8.04 – 7.98 (m), 7.96 (d, *J* = 8.0 Hz), 7.822 (d, *J* = 8.1 Hz), 7.73 (d, *J* = 8.0 Hz), 7.71 – 7.65 (m), 7.64 (d, *J* = 8.5 Hz), 7.59 (d, *J* = 8.2 Hz), 7.26 (s), 7.15 (s), 7.04 (s), 6.76 (s), 5.10 – 5.04 (m), 4.62 (td, *J* = 8.2 Hz, 5.0 Hz), 4.56 (q, *J* = 6.8 Hz), 4.52 (dd, *J* = 13.4 Hz, 7.6 Hz), 4.41 – 4.33 (m), 4.30 – 4.25 (m), 4.23 – 4.10 (m), 3.99 – 3.92 (m), 3.73 – 3.65 (m), 3.64 – 3.49 (m), 3.44 (t, *J* = 6.1 Hz), 3.40 – 3.38 (m), 3.27 (q, *J* = 6.1 Hz), 2.79 – 2.67 (m), 2.61 – 2.51 (m), 2.46 – 2.36 (m), 2.13 – 2.01 (m), 1.97 – 1.82 (m), 1.79 – 1.63 (m), 1.60 – 1.38 (m), 1.37 – 1.21 (m), 1.14 – 1.07 (m), 0.89 – 0.79 (m).

HRMS (ESI) calculated for C₇₃H₁₃₀N₁₈O₂₉S²⁺ ([M+2H]²⁺): *m/z* = 877.4480, experimental: 877.4486, δ [ppm] = 0.6, calculated for C₇₃H₁₃₃N₁₉O₂₉S²⁺ ([M+H+NH₄]²⁺): *m/z* = 885.9613, experimental: 885.9613, δ [ppm] = 0.0, calculated for C₇₃H₁₂₉N₁₈NaO₂₉S²⁺ ([M+H+Na]²⁺): *m/z* = 888.4390, experimental: 888.4395, δ [ppm] = 0.5, calculated for C₇₃H₁₂₈N₁₈Na₂O₂₉S²⁺ ([M+2Na]²⁺): *m/z* = 899.4300, experimental: 899.4305, δ [ppm] = 0.5, calculated for C₇₃H₁₃₁N₁₈O₂₉S³⁺ ([M+3H]³⁺): *m/z* = 585.3011, experimental: 585.3018, δ [ppm] = 0.7.

Compound 70



aa: VIELGE*Q*T*V*V*A*T*AQEETKQ

Chemical Formula: $C_{102}H_{169}N_{27}O_{35}S_2$

Exact Mass: 2396,17158

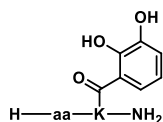
Molecular Weight: 2397,74800

70 (12.7 mg, 5.297 μ mol, 11%) was prepared following the general procedures for peptide synthesis, *N*-/*C*-terminal modification and global deprotection with the *PfeA* 33-51 *N*-term Boc *C*-term Dde peptide and PDTP.

1H NMR (700 MHz, DMSO- d_6): δ [ppm] = 12.10 (s), 8.47 – 8.43 (m), 8.37 (d, J = 8.4 Hz), 8.20 (d, J = 8.0 Hz), 8.18 – 8.14 (m), 8.09 – 8.02 (m), 7.99 (d, J = 7.3 Hz), 7.97 – 7.90 (m), 7.88 (d, J = 8.1 Hz), 7.82 (td, J = 8.0 Hz, 1.7 Hz), 7.79 (d, J = 7.7 Hz), 7.76 – 7.74 (m), 7.72 (d, J = 8.1 Hz), 7.69 (bs), 7.63 (d, J = 8.3 Hz), 7.31 (s), 7.28 (s), 7.25 – 7.23 (m), 7.01 (s), 6.78 (s), 6.77 (s), 4.93 (bs), 4.71 – 4.65 (m), 4.45 (d, J = 5.8 Hz), 4.42 (d, J = 5.8 Hz), 4.39 – 4.05 (m), 4.04 – 3.99 (m), 3.97 (dd, J = 10.9 Hz, 6.1 Hz), 3.80 (d, J = 5.8 Hz), 3.78 (d, J = 5.5 Hz), 3.71 – 3.66 (m), 3.64 (d, J = 5.4 Hz), 3.20 – 3.11 (m), 3.03 – 2.97 (m), 2.80 – 2.73 (m), 2.60 – 2.52 (m), 2.48 (s), 2.47 (s), 2.41 – 2.07 (m), 2.04 – 1.83 (m), 1.81 – 1.25 (m), 1.24 – 1.18 (m), 1.11 – 0.97 (m), 0.90 (t, J = 6.9 Hz), 0.86 (d, J = 6.6 Hz), 0.84 – 0.78 (m).

HRMS (ESI) calculated for $C_{102}H_{171}N_{27}O_6S_2^{2+}$ ($[M+2H]^{2+}$): m/z = 1199.0930, experimental: 1199.0925, δ [ppm] = 0.5, calculated for $C_{102}H_{172}N_{27}O_6S_2^{3+}$ ($[M+3H]^{3+}$): m/z = 799.7311, experimental: 799.7309, δ [ppm] = 0.20, calculated for $C_{102}H_{173}N_{27}O_6S_2^{4+}$ ($[M+4H]^{4+}$): m/z = 600.0502 experimental: 600.0500, δ [ppm] = 0.2, calculated for $C_{102}H_{174}N_{27}O_6S_2^{5+}$ ($[M+5H]^{5+}$): m/z = 480.2416, experimental: 480.2415, δ [ppm] = 0.1.

Compound 33



aa: DSSVDLG*A*T*MITSNQLGTI

Chemical Formula: C₉₂H₁₅₂N₂₄O₃₅S

Exact Mass: 2185,05726

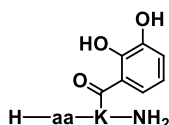
Molecular Weight: 2186,42100

33 (9.6 mg, 4.391 μmol, 9%) was prepared following the general procedures for peptide synthesis, *N*-*C*-terminal modification and global deprotection with the *FpvA* 121-139 *N*-term Boc *C*-term Dde peptide and catechol **40**.

¹H NMR (700 MHz, DMSO-*d*₆): δ [ppm] = 12.82 (s), 9.13 (s), 8.75 (t, *J* = 5.5 Hz), 8.64 – 8.55 (m), 8.37 – 8.31 (m), 8.28 (d, *J* = 7.4 Hz), 8.27 – 8.25 (m), 8.16 (d, *J* = 7.4 Hz), 8.14 (d, *J* = 7.6 Hz), 8.11 – 7.94 (m), 7.92 (d, *J* = 7.7 Hz), 7.90 – 7.76 (m), 7.72 (d, *J* = 8.5 Hz), 7.68 (d, *J* = 8.1 Hz), 7.45 (s), 7.25 (dd, *J* = 8.2 Hz, 1.4 Hz), 7.23 (s), 7.18 (s), 7.17 (s), 7.03 – 6.94 (m), 6.89 (dd, *J* = 7.8 Hz, 1.3 Hz), 6.79 (s), 6.66 (t, *J* = 7.9 Hz), 5.20 – 5.06 (m), 4.98 (s), 4.88 (s), 4.66 – 3.92 (m), 3.83 – 3.50 (m), 3.24 (dd, *J* = 12.9 Hz, 7.0 Hz), 2.97 (dd, *J* = 12.8 Hz, 7.0 Hz), 2.91 – 2.81 (m), 2.72 (dd, *J* = 16.7 Hz, 5.9 Hz), 2.69 – 2.62 (m), 2.61 – 2.55 (m), 2.54 (s), 2.48 – 2.34 (m), 2.18 (t, *J* = 7.3 Hz), 2.14 – 2.02 (m), 2.00 (s), 1.99 – 1.81 (m), 1.78 (s), 1.76 – 1.70 (m), 1.68 – 1.19 (m), 1.15 – 1.04 (m), 1.02 – 0.98 (m), 0.94 – 0.75 (m).

HRMS (ESI) calculated for C₉₂H₁₅₄N₂₄O₃₅S²⁺ ([*M*+2*H*]²⁺): *m/z* = 1093.5359, experimental: 1093.5365, δ [ppm] = 0.6, calculated for C₉₂H₁₅₃N₂₄NaO₃₅S²⁺ ([*M*+*H*+*Na*]²⁺): *m/z* = 1104.5269, experimental: 1104.5264, δ [ppm] = 0.5, calculated for C₉₂H₁₅₅N₂₄O₃₅S³⁺ ([*M*+3*H*]³⁺): *m/z* = 729.3597, experimental: 729.3597, δ [ppm] = 0.0.

Compound 34



aa: VIELGE*Q*T*V*V*A*T*AQEETKQ

Chemical Formula: C₁₀₁H₁₆₆N₂₆O₃₇

Exact Mass: 2335,19072

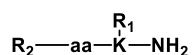
Molecular Weight: 2336,58400

34 (17.4 mg, 7.447 μmol, 15%) was prepared following the general procedures for peptide synthesis, *N*-/*C*-terminal modification and global deprotection with the *PfeA* 33-51 *N*-term Boc *C*-term Dde peptide and catechol **40**.

¹H NMR (700 MHz, DMSO-d₆): δ [ppm] = 12.80 (s), 12.09 (s), 9.12 (s), 8.76 (t, *J* = 5.6 Hz), 8.36 (d, *J* = 8.5 Hz), 8.21 (d, *J* = 8.0 Hz), 8.19 – 8.15 (m), 8.03 (dd, *J* = 14.7 Hz, 7.6 Hz), 8.00 (d, *J* = 7.3 Hz), 7.97 – 7.87 (m), 7.79 (d, *J* = 7.6 Hz), 7.72 (d, *J* = 8.0 Hz), 7.63 (d, *J* = 8.3 Hz), 7.33 (s), 7.29 – 7.21 (m), 7.02 (s), 6.90 (dd, *J* = 7.8 Hz, 1.4 Hz), 6.81 – 6.74 (m), 6.67 (t, *J* = 7.9 Hz), 4.93 (s), 4.89 (s), 4.40 – 4.08 (m), 4.03 – 3.94 (m), 3.80 (d, *J* = 5.9 Hz), 3.78 (d, *J* = 4.4 Hz), 3.69 – 3.65 (m), 3.63 (d, *J* = 5.5 Hz), 3.50 (s), 3.25 (dd, *J* = 13.0 Hz, 7.1 Hz), 2.76 (t, *J* = 7.3 Hz), 2.61 – 2.52 (m), 2.47 (s), 2.41 – 2.08 (m), 2.06 – 1.83 (m), 1.80 – 1.42 (m), 1.39 – 1.19 (m), 1.11 – 0.99 (m), 0.94 (s), 0.90 (d, *J* = 7.3 Hz), 0.89 (d, *J* = 7.1 Hz), 0.86 (d, *J* = 6.6 Hz), 0.85 – 0.78 (m).

HRMS (ESI) calculated for C₁₀₁H₁₆₈N₂₆O₃₇²⁺ ([M+2H]²⁺): *m/z* = 1168.6026, experimental: 1168.6046, δ [ppm] = 2.0, calculated for C₁₀₁H₁₆₇N₂₆NaO₃₇²⁺ ([M+H+Na]²⁺): *m/z* = 1179.5936, experimental: 1179.5953, δ [ppm] = 1.7, calculated for C₁₀₁H₁₆₆N₂₆Na₂O₃₇²⁺ ([M+2Na]²⁺): *m/z* = 1190.5846, experimental: 1190.5853, δ [ppm] = 0.7, calculated for C₁₀₁H₁₆₉N₂₆O₃₇³⁺ ([M+3H]³⁺): *m/z* = 779.4042, experimental: 779.4054, δ [ppm] = 1.2, calculated for C₁₀₁H₁₇₀N₂₆O₃₇⁴⁺ ([M+4H]⁴⁺): *m/z* = 584.8050, experimental: 584.8062, δ [ppm] = 1.2.

General procedure for CuAAC with DOTAM 1 or 2



R₁ = H, CO-(PEG)₇-(1,2,3-Triazole)-Zn DOTAM
 R₂ = CO-(PEG)₇-(1,2,3-Triazole)-Zn DOTAM, H

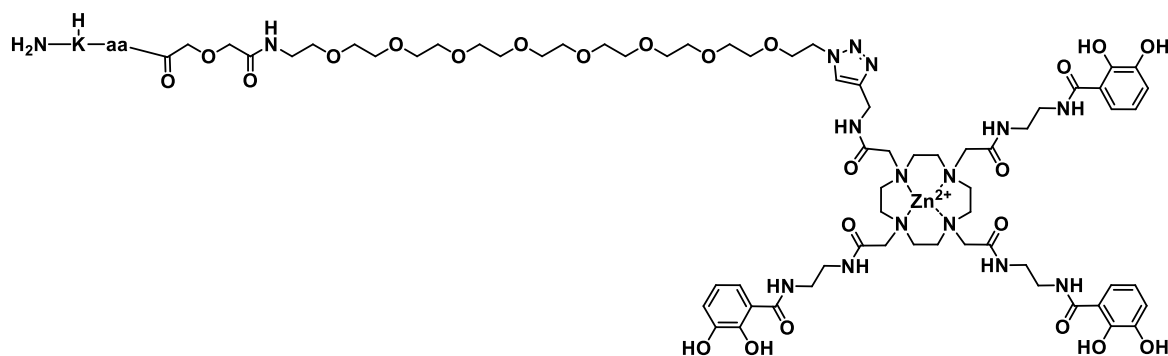
FpvA 121-139 = DSSVDLG*A*T*MITSNQLGTI
 PfeA 33-51 = VIELGE*Q*T*V*V*A*T*AQEETKQ
 HasR 122-144 = SLIRVSQDDLVMSPS*V*I*SAARP

aa sequence

FpvA 124-134 = VDLG*A*T*MITSN
 PfeA 37-46 = GE*Q*T*V*V*A*T*AQ
 HasR 129-138 = DDLVQMSPS*V*

11-21 were prepared adapted from an established procedure reported by Ferreira *et al.*¹

1 or **2** (2.5 eq) was dissolved under an argon atmosphere in DMSO (1 mL) and zinc acetate (5.0 eq), dissolved in MilliQ H₂O (1 mL), was added and the solution was stirred at 23 °C for 5 min. In case **2** was used, acetic acid was added (1%, 40 μL) to prevent deacetylation. PEG-modified peptide (**61-69**) (1.0 eq), dissolved in DMSO (1 mL), was added to the solution. CuSO₄ (0.5 eq.) was dissolved in PBS (pH 7.4, 0.3 mL) and sodium ascorbate (1.0 eq), dissolved in PBS (pH 7.4, 0.4 mL) was added to the CuSO₄ solution, whereupon a white solid precipitated immediately. THPTA (0.25 eq), dissolved in PBS (pH 7.4, 0.3 mL) was added to the suspension and under Ar atmosphere to the reaction. The reaction was stirred at 23 °C for 1 h and the reaction progress was controlled by LCMS. After completion of the reaction the solution was filtered over cotton wool and purified by RP-HPLC (C18 phenomenex, 220 nm, collect all, 5-35% ACN/MilliQ H₂O, 0.1% HCOOH). The product containing fractions were identified by LCMS and lyophilized to dryness to yield product **11-21** as white solids.

Compound 11 (Fpva 121-139 N-term (PEG)₇-Zn²⁺-DOTAM)

aa: DSSVDLG*A*T*MITSNQLGTI

Chemical Formula: C₁₅₃H₂₄₉N₃₉O₅₆SZn²⁺

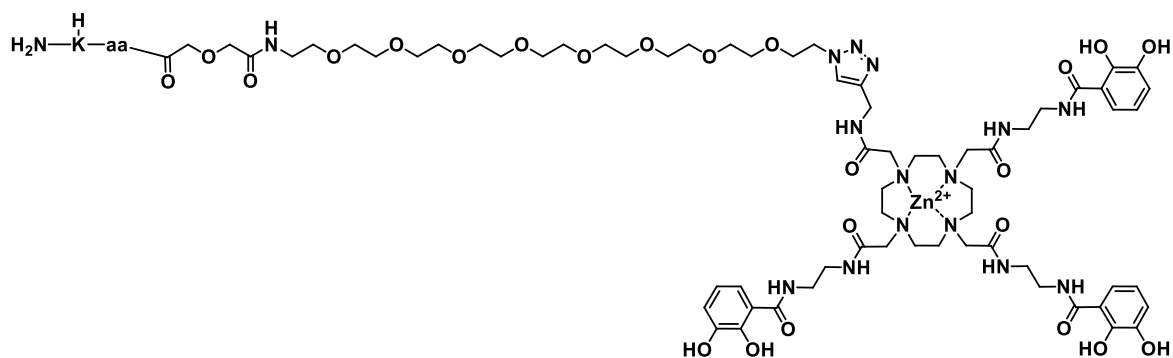
Exact Mass: 3624,68366

Molecular Weight: 3628,33090

11 (36.0 mg, 9.9 μmol, 91%) was prepared following the general procedure for CuAAC with DOTAM **2** (26.7 mg, 27.4 μmol, 2.5 eq) and peptide **61** (30.0 mg, 11.0 μmol, 1.0 eq).

¹H NMR (700 MHz, DMSO-*d*₆): δ [ppm] = 9.36 (s), 9.02 (s), 8.62 – 8.57 (m), 8.55 – 8.51 (m), 8.44 – 8.39 (m), 8.37 – 8.29 (m), 8.26 (s), 8.22 – 8.10 (m), 8.09 – 7.75 (m), 7.72 (d, *J* = 7.8 Hz), 7.55 (d, *J* = 7.3 Hz), 7.51 – 7.44 (m), 7.28 – 7.20 (m), 7.18 (s), 7.02 (s), 6.98 (s), 6.87 – 6.81 (m), 6.80 (s), 6.56 (t, *J* = 7.6 Hz), 4.61 (q, *J* = 6.7 Hz), 4.56 – 4.47 (m), 4.44 (t, *J* = 5.1 Hz), 4.40 (s), 4.39 – 4.36 (m), 4.34 – 4.27 (m), 4.26 – 4.20 (m), 4.17 – 4.11 (m), 4.09 – 3.96 (m), 3.94 (d, *J* = 5.1 Hz), 3.92 (s), 3.85 – 3.58 (m), 3.55 (dd, *J* = 10.6 Hz, 5.6 Hz), 3.52 – 3.20 (m), 3.14 (q, *J* = 6.3 Hz), 3.02 – 2.85 (m), 2.74 (t, *J* = 7.4 Hz), 2.71 – 2.55 (m), 2.54 (s), 2.48 – 2.35 (m), 2.15 – 2.02 (m), 1.95 – 1.87 (m), 1.84 – 1.71 (m), 1.68 – 1.58 (m), 1.56 – 1.40 (m), 1.37 (s), 1.35 – 1.26 (m), 1.25 (d, *J* = 7.0 Hz), 1.15 – 0.98 (m), 0.87 (d, *J* = 6.6 Hz), 0.85 – 0.76 (m).

HRMS (ESI) calculated for (C₁₅₃H₂₅₂N₃₉O₅₆SZn²⁺)³⁺ ([M+3H]³⁺): *m/z* = 1209.2352, experimental: 1209.2347, δ [ppm] = 0.5, calculated for (C₁₅₃H₂₅₃N₃₉O₅₆SZn²⁺)⁴⁺ ([M+4H]⁴⁺): *m/z* = 907.1782, experimental: 907.1777, δ [ppm] = 0.5, calculated for (C₁₅₃H₂₅₄N₃₉O₅₆SZn²⁺)⁵⁺ ([M+5H]⁵⁺): *m/z* = 725.9440, experimental: 725.9441, δ [ppm] = 0.1.

Compound 12 (PfeA 33-51 N-term (PEG)₇-Zn²⁺-DOTAM)

aa: VIELGE*Q*T*V*V*A*T*AQEETKQ

Chemical Formula: C₁₆₂H₂₆₃N₄₁O₅₈Zn²⁺

Exact Mass: 3774,81712

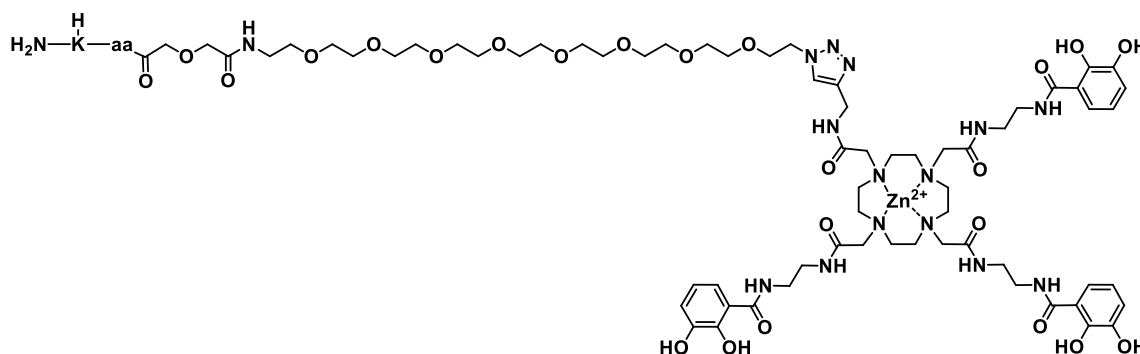
Molecular Weight: 3778,49390

12 (34.0 mg, 9.0 μmol, 99%) was prepared following the general procedure for CuAAC with DOTAM **2** (22.3 mg, 22.8 μmol, 2.5 eq) and peptide **62** (25.0 mg 9.1 μmol, 1.0 eq).

¹H NMR (700 MHz, DMSO-d₆): δ [ppm] = 8.31 (s), 8.24 (s), 8.21 – 8.13 (m), 8.11 – 7.75 (m), 7.59 (d, *J* = 8.0 Hz), 7.55 (s), 7.38 (s), 7.30 (s), 7.23 (d, *J* = 7.0 Hz), 7.20 (d, *J* = 7.3 Hz), 7.08 (s), 7.07 (s), 6.81 – 6.74 (m), 6.70 (s), 6.47 (t, *J* = 7.9 Hz), 6.42 (t, *J* = 7.4 Hz), 4.44 (t, *J* = 5.3 Hz), 4.38 (s), 4.35 – 4.24 (m), 4.23 – 3.92 (m), 3.89 (s), 3.84 (s), 3.76 (t, *J* = 5.2 Hz), 3.61 – 3.28 (m), 3.26 (q, *J* = 5.8 Hz), 3.00 – 2.80 (m), 2.73 (t, *J* = 7.5 Hz), 2.64 – 2.56 (m), 2.54 (s), 2.44 (s), 2.41 – 2.39 (m), 2.26 – 2.08 (m), 2.05 – 1.14 (m), 1.06 (dd, *J* = 12.6 Hz, 6.0 Hz), 1.02 (d, *J* = 6.1 Hz), 0.90 – 0.76 (m).

¹³C NMR (176 MHz, DMSO-d₆) δ [ppm] = 174.8, 174.8, 174.8, 174.3, 174.3, 173.9, 173.9, 173.9, 173.7, 173.7, 173.5, 172.7, 172.3, 172.0, 171.3, 171.2, 171.2, 170.9, 170.8, 170.7, 170.1, 169.9, 169.9, 168.9, 168.8, 168.7, 167.7, 164.0, 150.1, 150.0, 146.5, 146.5, 143.4, 123.7, 118.4, 118.4, 117.5, 117.5, 117.4, 117.4, 115.3, 115.3, 70.3, 70.2, 69.8, 69.7, 69.6, 69.5, 68.9, 68.7, 57.2, 56.9, 55.8, 55.7, 53.0, 52.8, 52.2, 49.4, 41.9, 40.4, 40.0, 38.1, 31.5, 30.6, 28.3, 27.4, 26.7, 26.6, 24.4, 24.1, 23.1, 22.2, 21.5, 19.6, 19.6, 19.5, 19.2, 19.2, 18.3, 18.2, 18.1, 17.9, 17.8, 15.2, 11.0.

HRMS (ESI) calculated for (C₁₆₂H₂₆₆N₄₁O₅₈Zn²⁺)³⁺ ([M+3H]³⁺): *m/z* = 1259.2797, experimental: 1259.2793, δ [ppm] = 0.4, calculated for (C₁₆₂H₂₆₇N₄₁O₅₈Zn²⁺)⁴⁺ ([M+4H]⁴⁺): *m/z* = 944.7116, experimental: 944.7114, δ [ppm] = 0.2, calculated for (C₁₆₂H₂₆₈N₄₁O₅₈Zn²⁺)⁵⁺ ([M+5H]⁵⁺): *m/z* = 755.9707, experimental: 755.9708, δ [ppm] = 0.1, calculated for (C₁₆₂H₂₆₉N₄₁O₅₈Zn²⁺)⁶⁺ ([M+6H]⁶⁺): *m/z* = 630.1435, experimental: 630.1434, δ [ppm] = 0.1.

Compound 13 (HasR 122-144 N-term (PEG)₇-Zn²⁺-DOTAM)

aa: SLIRVSQDDLVMSPS*V*I*SAARP

Chemical Formula: C₁₇₉H₂₉₅N₄₉O₅₉SZn²⁺

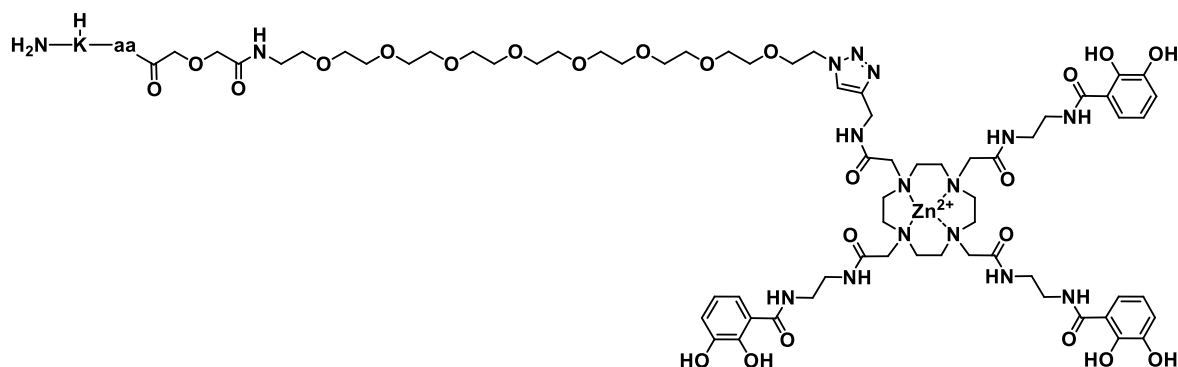
Exact Mass: 4171,05909

Molecular Weight: 4175,05190

13 (29.0 mg, 6.9 μmol, 87%) was prepared following the general procedure for CuAAC with DOTAM **2** (19.5 mg, 19.9 μmol, 2.5 eq) and peptide **63** (25.0 mg, 8.0 μmol, 1.0 eq).

¹H NMR (700 MHz, DMSO-*d*₆): δ [ppm] = 9.27 (s), 9.05 (s), 8.63 – 8.36 (m), 8.29 (s), 8.24 – 7.47 (m), 7.40 – 7.18 (m), 7.05 – 6.95 (m), 6.90 – 6.83 (m), 6.76 (s), 6.72 (s), 6.66 – 6.55 (m), 6.4 – 6.31 (m), 5.07 – 4.76 (m), 4.55 (d, *J* = 6.3 Hz), 4.45 (d, *J* = 4.9 Hz), 4.42 – 4.09 (m), 4.04 (t, *J* = 7.3 Hz), 4.00 (s), 3.97 (s), 3.92 (d, *J* = 9.4 Hz), 3.80 – 3.54 (m), 3.52 – 3.40 (m), 3.39 – 3.30 (m), 3.27 (t, *J* = 5.9 Hz), 3.13 (q, *J* = 6.3 Hz), 3.11 – 3.02 (m), 2.99 (q, *J* = 6.1 Hz), 2.91 – 2.84 (m), 2.75 (bs), 2.67 (bs), 2.64 (s), 2.54 (s), 2.49 – 2.35 (m), 2.22 – 2.01 (m), 1.98 – 1.38 (m), 1.37 (s), 1.26 – 1.00 (m), 0.90 – 0.73 (m).

HRMS (ESI) calculated for (C₁₇₉H₂₉₈N₄₉O₅₉SZn²⁺)³⁺ ([M+3H]³⁺): *m/z* = 1391.36031, experimental: 1391.3564, δ [ppm] = 2.81, calculated for (C₁₇₉H₂₉₉N₄₉O₅₉SZn²⁺)⁴⁺ ([M+4H]⁴⁺): *m/z* = 1043.77205, experimental: 1043.7701, δ [ppm] = 1.87, calculated for (C₁₇₉H₃₀₀N₄₉O₅₉SZn²⁺)⁵⁺ ([M+5H]⁵⁺): *m/z* = 835.21909, experimental: 835.2184, δ [ppm] = 0.83, calculated for (C₁₇₉H₃₀₁N₄₉O₅₉SZn²⁺)⁶⁺ ([M+6H]⁶⁺): *m/z* = 696.18379, experimental: 696.1829, δ [ppm] = 1.28.

Compound 14 (FpvA 124-134 N-term (PEG)₇-Zn²⁺-DOTAM)

aa: VDLG*A*T*MITSN

Chemical Formula: C₁₂₀H₁₉₄N₃₀O₄₂SZn²⁺

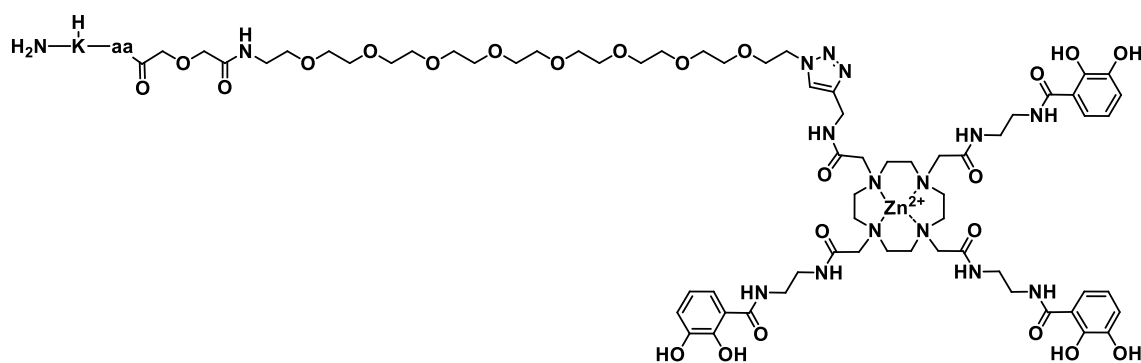
Exact Mass: 2823,29681

Molecular Weight: 2826,47890

14 (26.0 mg, 9.2 μmol, 91%) was prepared following the general procedure for CuAAC with DOTAM **2** (24.6 mg, 25.2 μmol, 2.5 eq) and peptide **67** (18.0 mg, 10.1 μmol, 1.0 eq).

¹H NMR (700 MHz, DMSO-*d*₆): δ [ppm] = 8.36 (d, *J* = 8.5 Hz), 8.21 (d, *J* = 8.0 Hz), 8.17 (t, *J* = 5.9 Hz), 8.08 – 8.03 (m), 8.00 (d, *J* = 7.3 Hz), 7.97 – 7.91 (m), 7.88 (d, *J* = 8.3 Hz), 7.81 – 7.75 (m), 7.72 (d, *J* = 7.9 Hz), 7.70 – 7.60 (m), 7.31 (s), 7.27 (s), 7.24 (s), 7.20 (s), 7.13 (s), 7.06 (s), 7.04 (bs), 7.02 (s), 6.78 (bs), 6.77 (s), 6.43 (s), 6.38 (bs), 4.39 – 4.07 (m), 4.03 – 3.99 (m), 3.97 (dd, *J* = 10.8 Hz, 5.8 Hz), 3.80 (d, *J* = 5.9 Hz), 3.78 (d, *J* = 5.7 Hz), 3.68 – 3.62 (m), 3.10 (ddd, *J* = 8.6 Hz, 6.1 Hz, 4.6 Hz), 2.99 (dd, *J* = 14.5 Hz, 7.6 Hz), 2.82 (dd, *J* = 12.5 Hz, 5.1 Hz), 2.76 (dd, *J* = 13.0 Hz, 7.2 Hz), 2.58 (s), 2.57 (s), 2.33 – 1.83 (m), 1.80 – 1.24 (m), 1.21 (t, *J* = 6.5 Hz), 1.11 – 0.99 (m), 0.90 (t, *J* = 7.3 Hz), 0.86 (d, *J* = 6.6 Hz), 0.84 – 0.79 (m).

HRMS (ESI) calculated for (C₁₂₀H₁₉₆N₃₀O₄₂SZn²⁺)²⁺ ([M+2H]²⁺): *m/z* = 1412.6557, experimental: 1412.6552, δ [ppm] = 0.5, calculated for (C₁₂₀H₁₉₇N₃₀O₄₂SZn²⁺)³⁺ ([M+3H]³⁺): *m/z* = 942.1062, experimental: 942.1065, δ [ppm] = 0.3, calculated for (C₁₂₀H₁₉₈N₃₀O₄₂SZn²⁺)⁴⁺ ([M+4H]⁴⁺): *m/z* = 706.8315, experimental: 706.8318, δ [ppm] = 0.3, calculated for (C₁₂₀H₁₉₉N₃₀O₄₂SZn²⁺)⁵⁺ ([M+5H]⁵⁺): *m/z* = 565.6666, experimental: 565.6665, δ [ppm] = 0.1.

Compound 15 (PfeA 37-46 N-term (PEG)₇-Zn²⁺-DOTAM)


86

aa: GE*Q*T*V*V*A*T*AQ

Chemical Formula: C₁₁₅H₁₈₄N₃₀O₄₁Zn²⁺

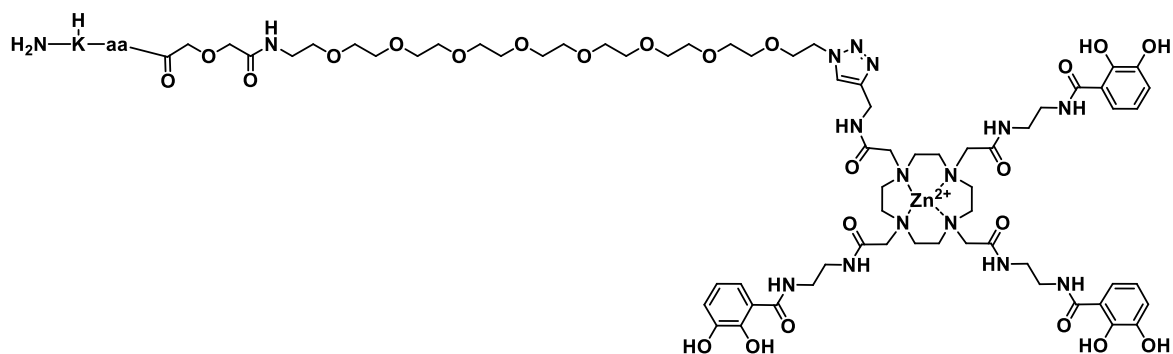
Exact Mass: 2705,25158

Molecular Weight: 2708,28490

15 (25.0 mg, 9.2 μmol, 96%) was prepared following the general procedure for CuAAC with DOTAM **2** (23.4 mg, 24.0 μmol, 2.5 eq) and peptide **68** (16.0 mg, 9.6 μmol, 1.0 eq).

¹H NMR (700 MHz, DMSO-d₆): δ [ppm] = 10.03 (s), 9.86 (s), 9.29 – 8.78 (m), 8.47 (s), 8.36 (s), 8.30 (s), 8.19 (d, *J* = 5.4 Hz), 8.11 (d, *J* = 6.4 Hz), 8.04 – 7.99 (m), 7.96 (t, *J* = 5.3 Hz), 7.92 (s), 7.91 – 7.84 (m), 7.80 (d, *J* = 7.1 Hz), 7.77 – 7.64 (m), 7.35 (s), 7.27 (s), 7.26 – 7.14 (m), 7.10 (d, *J* = 7.7 Hz), 7.05 (s), 6.94 – 6.89 (m), 6.87 (d, *J* = 7.7 Hz), 6.83 – 6.69 (m), 6.66 – 6.59 (m), 6.51 (d, *J* = 6.5 Hz), 6.48 – 6.29 (m), 4.93 – 3.88 (m), 3.82 – 3.75 (m), 3.49 – 3.42 (m), 3.38 – 3.36 (m), 3.32 – 3.27 (m), 3.01 – 2.78 (m), 2.73 (t, *J* = 7.4 Hz), 2.63 – 2.51 (m), 2.19 – 2.08 (m), 2.03 – 1.85 (m), 1.80 – 1.71 (m), 1.70 – 1.63 (m), 1.57 – 1.46 (m), 1.35 – 1.25 (m), 1.23 (t, *J* = 7.7 Hz), 1.03 (dd, *J* = 8.9 Hz, 6.4 Hz), 0.87 – 0.78 (m).

HRMS (ESI) calculated for (C₁₁₅H₁₈₆N₃₀O₄₁Zn²⁺)²⁺ ([M+2H]²⁺): *m/z* = 1353.6331, experimental: 1353.6328, δ [ppm] = 0.3, calculated for (C₁₁₅H₁₈₇N₃₀O₄₁Zn²⁺)³⁺ ([M+3H]³⁺): *m/z* = 902.7578, experimental: 902.7575, δ [ppm] = 0.3, calculated for (C₁₁₅H₁₈₈N₃₀O₄₁Zn²⁺)⁴⁺ ([M+4H]⁴⁺): *m/z* = 677.3202, experimental: 677.3200, δ [ppm] = 0.2, calculated for (C₁₁₅H₁₈₉N₃₀O₄₁Zn²⁺)⁵⁺ ([M+5H]⁵⁺): *m/z* = 542.0576, experimental: 542.0573, δ [ppm] = 0.3.

Compound 16 (HasR 129-138 N-term (PEG)₇-Zn²⁺-DOTAM)

aa: DDLVQMSPS*V*

Chemical Formula: C₁₁₉H₁₈₉N₂₉O₄₂SZn²⁺

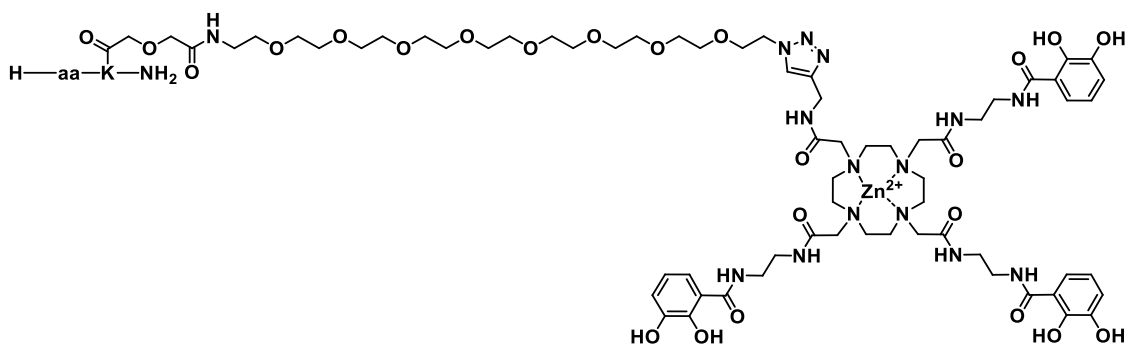
Exact Mass: 2792,25461

Molecular Weight: 2795,42090

16 (12.9 mg, 4.6 μmol, 81%) was prepared following the general procedure for CuAAC with DOTAM **2** (13.9 mg, 14.3 μmol, 2.5 eq) and peptide **69** (10.0 mg, 5.7 μmol, 1.0 eq).

¹H NMR (700 MHz, DMSO-d₆): δ [ppm] = 9.37 (s), 9.07 (s), 8.57 – 8.32 (m), 8.30 (d, *J* = 5.0 Hz), 8.20 – 8.12 (m), 8.04 – 7.90 (m), 7.82 – 7.65 (m), 7.56 – 7.46 (m), 7.40 – 7.15 (m), 7.07 (s), 7.02 (s), 6.88 – 6.62 (m), 6.56 – 6.29 (m), 5.22 – 5.00 (m), 4.62 – 3.57 (m), 3.49 – 3.48 (m), 3.17 – 2.77 (m), 2.73 (t, *J* = 6.6 Hz), 2.67 – 2.56 (m), 2.54 (s), 2.53 – 2.52 (m), 2.46 – 2.30 (m), 2.22 – 2.08 (m), 2.06 – 1.95 (m), 1.92 – 1.74 (m), 1.69 – 1.44 (m), 1.40 – 1.21 (m), 1.15 – 1.06 (m), 0.89 – 0.80 (m), 0.78 (d, *J* = 5.5 Hz).

HRMS (ESI) calculated for (C₁₁₉H₁₉₁N₂₉O₄₂SZn²⁺)²⁺ ([M+2H]²⁺): *m/z* = 1397.1346, experimental: 1397.1358, δ [ppm] = 0.8, calculated for (C₁₁₉H₁₉₀N₂₉NaO₄₂SZn²⁺)²⁺ ([M+H+Na]²⁺): *m/z* = 1408.1256, experimental: 1408.1230, δ [ppm] = 2.6, calculated for (C₁₁₉H₁₈₉N₂₉Na₂O₄₂SZn²⁺)²⁺ ([M+2Na]²⁺): *m/z* = 1419.1165, experimental: 1419.1149, δ [ppm] = 1.6, calculated for (C₁₁₉H₁₉₂N₂₉O₄₂SZn²⁺)³⁺ ([M+3H]³⁺): *m/z* = 931.7588, experimental: 931.7571, δ [ppm] = 1.7.

Compound 17 (FpvA 121-139 C-term (PEG)₇-Zn²⁺-DOTAM)

aa: DSSVDLG*A*T*MITSNQLGTI

Chemical Formula: C₁₅₃H₂₄₉N₃₉O₅₆SZn²⁺

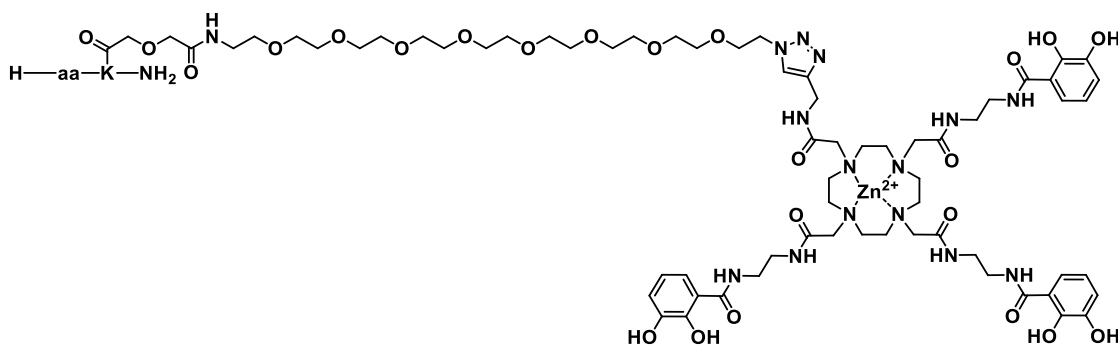
Exact Mass: 3624,68366

Molecular Weight: 3628,33090

17 (31.0 mg, 8.6 μmol, 94%). was prepared following the general procedure for CuAAC with DOTAM **2** (22.3 mg, 22.8 μmol, 2.5 eq) and peptide **64** (25.0 mg, 9.1 μmol, 1.0 eq).

¹H NMR (700 MHz, DMSO-*d*₆): δ [ppm] = 9.42 (s), 9.09 – 8.80 (m), 8.60 (s), 8.52 (s), 8.42 (s), 8.38 – 8.27 (m), 8.22 (s), 8.20 – 8.14 (m), 8.10 – 7.78 (m), 7.70 (d, *J* = 7.7 Hz), 7.65 (d, *J* = 8.5 Hz), 7.60 (d, *J* = 6.4 Hz), 7.45 (s), 7.30 – 7.19 (m), 7.16 (s), 6.99 (s), 6.98 (s), 6.84 (d, *J* = 6.9 Hz), 6.78 (s), 6.69 – 6.50 (m), 4.52 (q, *J* = 6.9 Hz), 4.48 (q, *J* = 6.8 Hz), 4.44 (t, *J* = 5.1 Hz), 4.42 – 4.37 (m), 4.36 – 4.27 (m), 4.24 (q, *J* = 6.0 Hz), 4.16 (t, *J* = 7.5 Hz), 4.15 – 3.94 (m), 3.92 (s), 3.91 (s), 3.82 – 3.28 (m), 3.27 (q, *J* = 5.9 Hz), 3.26 – 3.09 (m), 3.07 (dd, *J* = 13.3 Hz, 6.9 Hz), 2.72 – 2.55 (m), 2.54 (s), 2.47 – 2.34 (m), 2.15 – 2.07 (m), 2.07 (s), 2.06 – 1.98 (m), 1.95 – 1.91 (m), 1.90 (s), 1.87 – 1.70 (m), 1.67 – 1.32 (m), 1.30 – 1.17 (m), 1.15 – 0.99 (m), 0.87 (d, *J* = 6.5 Hz), 0.85 (d, *J* = 6.7 Hz), 0.83 – 0.75 (m).

HRMS (ESI) calculated for (C₁₅₃H₂₅₂N₃₉O₅₆SZn²⁺)³⁺ ([M+3H]³⁺): *m/z* = 1209.2352, experimental: 1209.2338, δ [ppm] = 1.4, calculated for (C₁₅₃H₂₅₃N₃₉O₅₆SZn²⁺)⁴⁺ ([M+4H]⁴⁺): *m/z* = 907.1782, experimental: 907.1775, δ [ppm] = 0.7, calculated for (C₁₅₃H₂₅₄N₃₉O₅₆SZn²⁺)⁵⁺ ([M+5H]⁵⁺): *m/z* = 725.9440, experimental: 725.9435, δ [ppm] = 0.5.

Compound 18 (PfeA 33-51 C-term (PEG)₇-Zn²⁺-DOTAM)

aa: VIELGE*Q*T*V*V*A*T*AQEETKQ

Chemical Formula: C₁₆₂H₂₆₃N₄₁O₅₈Zn²⁺

Exact Mass: 3774,81712

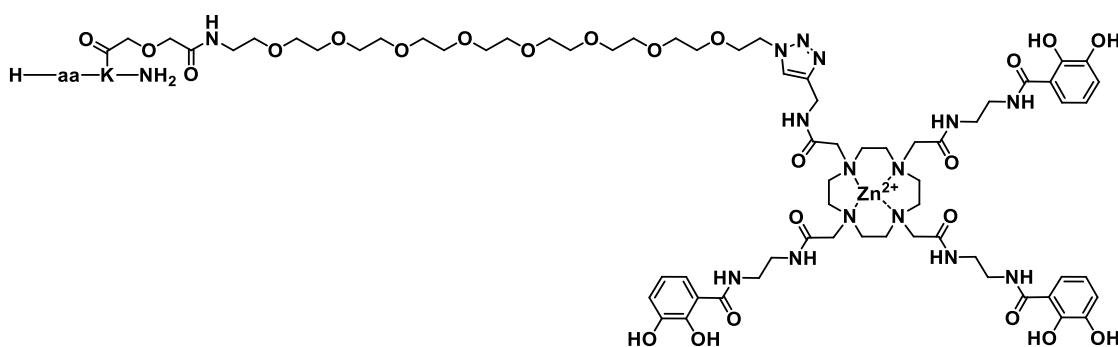
Molecular Weight: 3778,49390

18 (34.0 mg, 9.0 μmol, 99%) was prepared following the general procedure for CuAAC with DOTAM **2** (26.7 mg, 27.4 μmol, 2.5 eq) and peptide **65** (25.0 mg, 9.1 μmol, 1.0 eq).

¹H NMR (700 MHz, DMSO-d₆): δ [ppm] = 9.37 – 8.73 (m), 8.30 – 8.16 (m), 8.08 (d, *J* = 7.7 Hz), 8.04 – 7.63 (m), 7.33 (s), 7.28 (d, *J* = 12.0 Hz), 7.24 (d, *J* = 9.0 Hz), 7.02 (s), 6.86 (d, *J* = 6.7 Hz), 6.76 (d, *J* = 8.9 Hz), 6.74 (s), 6.67 – 6.53 (m), 4.52 – 4.46 (m), 4.44 (t, *J* = 5.0 Hz), 4.40 (s), 4.35 (t, *J* = 6.8 Hz), 4.26 (dd, *J* = 13.5 Hz, 7.0 Hz), 4.24 – 3.96 (m), 3.92 (d, *J* = 8.1 Hz), 3.88 – 3.52 (m), 3.50 – 3.30 (m), 3.28 (q, *J* = 5.7 Hz), 3.08 (dd, *J* = 13.2 Hz, 6.8 Hz), 3.03 – 2.89 (m), 2.75 (t, *J* = 6.6 Hz), 2.72 – 2.58 (m), 2.54 (s), 2.45 – 2.39 (m), 2.31 – 2.08 (m), 2.03 – 1.94 (m), 1.90 (s), 1.84 – 1.18 (m), 1.12 – 0.98 (m), 0.88 (d, *J* = 6.9 Hz), 0.86 (d, *J* = 6.6 Hz), 0.85 – 0.77 (m).

¹³C NMR (176 MHz, DMSO-d₆) δ [ppm] = 174.9, 174.4, 173.9, 173.9, 173.7, 172.7, 172.4, 172.1, 171.9, 171.6, 171.3, 171.1, 171.0, 170.7, 170.5, 170.1, 170.0, 169.8, 169.7, 168.8, 168.5, 164.1, 150.7, 146.7, 130.4, 123.7, 117.7, 116.8, 115.4, 70.2, 69.8, 69.7, 69.6, 69.5, 68.9, 68.7, 66.5, 66.4, 66.3, 59.2, 58.3, 58.3, 58.2, 58.0, 56.8, 55.7, 55.7, 52.8, 52.7, 52.7, 52.5, 52.0, 51.2, 49.4, 48.6, 42.0, 40.8, 40.4, 40.0, 38.1, 38.1, 36.8, 31.5, 31.5, 31.4, 30.7, 30.7, 30.5, 30.4, 30.2, 29.0, 27.6, 27.5, 27.4, 27.3, 27.3, 27.3, 26.6, 26.6, 24.4, 24.1, 23.1, 22.8, 22.0, 21.5, 21.2, 19.7, 19.6, 19.5, 19.2, 18.9, 18.4, 18.2, 17.9, 17.7, 17.3, 15.2, 11.1.

HRMS (ESI) calculated for (C₁₆₂H₂₆₆N₄₁O₅₈Zn²⁺)³⁺ ([M+3H]³⁺): *m/z* = 1259.2797, experimental: 1259.2767, δ [ppm] = 3.0, calculated for (C₁₆₂H₂₆₇N₄₁O₅₈Zn²⁺)⁴⁺ ([M+4H]⁴⁺): *m/z* = 944.7116, experimental: 944.7091, δ [ppm] = 1.5, calculated for (C₁₆₂H₂₆₈N₄₁O₅₈Zn²⁺)⁵⁺ ([M+5H]⁵⁺): *m/z* = 755.9707, experimental: 755.9697, δ [ppm] = 1.0, calculated for (C₁₆₂H₂₆₉N₄₁O₅₈Zn²⁺)⁶⁺ ([M+6H]⁶⁺): *m/z* = 630.1435, experimental: 630.1424, δ [ppm] = 1.1.

Compound 19 (HasR 122-144 C-term (PEG)₇-Zn²⁺-DOTAM)

aa: SLIRVSQDDLVMSPS*V*I*SAARP

Chemical Formula: C₁₇₉H₂₉₅N₄₉O₅₉SZn²⁺

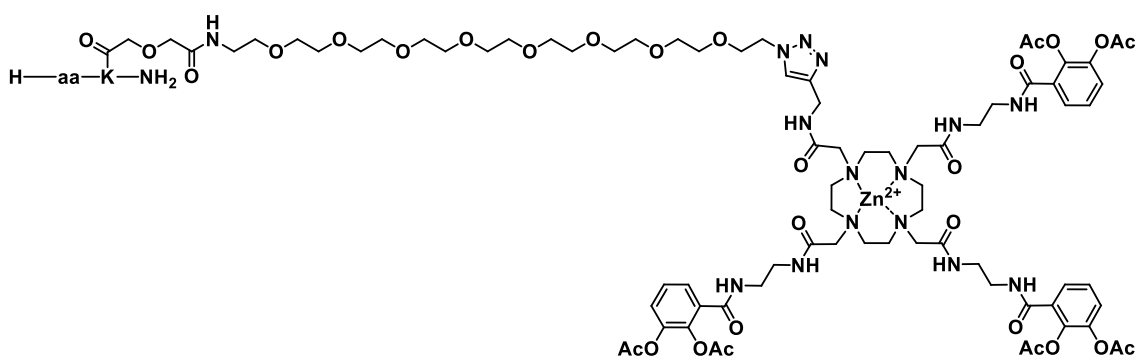
Exact Mass: 4171,05909

Molecular Weight: 4175,05190

19 (42.0 mg, 10.1 μmol, 79%) was prepared following the general procedure for CuAAC with DOTAM **2** (31.1 mg, 31.9 μmol, 2.5 eq) and peptide **66** (40.0 mg, 12.8 μmol, 1.0 eq).

¹H NMR (700 MHz, DMSO-*d*₆): δ [ppm] = 9.53 (s), 9.45 (s), 8.91 (s), 8.53 – 8.39 (m), 8.34 – 8.24 (m), 8.22 (s), 8.05 (dd, *J* = 13.4 Hz, 5.9 Hz), 8.02 – 7.78 (m), 7.76 – 7.66 (m), 7.57 (d, *J* = 7.5 Hz), 7.40 – 7.28 (m), 7.25 – 7.17 (m), 6.98 (s), 6.82 (t, *J* = 6.6 Hz), 6.75 (s), 6.71 (s), 6.55 – 6.46 (m), 4.55 (dd, *J* = 12.6 Hz, 6.2 Hz), 4.48 (dd, *J* = 11.7 Hz, 5.1 Hz), 4.44 (t, *J* = 5.2 Hz), 4.42 – 4.12 (m), 4.06 (dd, *J* = 13.5 Hz, 8.4 Hz), 4.03 (t, *J* = 7.5 Hz), 3.93 (s), 3.92 (s), 3.80 – 3.43 (m), 3.28 – 2.84 (m), 2.71 – 2.58 (m), 2.54 (s), 2.48 – 2.32 (m), 2.19 – 2.01 (m), 1.98 – 1.35 (m), 1.31 – 1.00 (m), 0.87 (d, *J* = 6.7 Hz), 0.85 – 0.73 (m).

HRMS (ESI) calculated for (C₁₇₉H₂₉₉N₄₉O₅₉SZn²⁺)⁴⁺ ([M+4H]⁴⁺): *m/z* = 1043.7721, experimental: 1043.7742, δ [ppm] = 2.1, calculated for (C₁₇₉H₃₀₀N₄₉O₅₉SZn²⁺)⁵⁺ ([M+5H]⁵⁺): *m/z* = 835.2191, experimental: 835.2201, δ [ppm] = 1.0, calculated for (C₁₇₉H₃₀₁N₄₉O₅₉SZn²⁺)⁶⁺ ([M+6H]⁶⁺): *m/z* = 696.1838, experimental: 696.1848, δ [ppm] = 1.0.

Compound 20 (PfeA 33-51 C-term (PEG)₇-Zn²⁺-DOTAM)

aa: VIELGE*Q*T*V*V*A*T*AQEETKQ

Chemical Formula: C₁₇₄H₂₇₅N₄₁O₆₄Zn²⁺

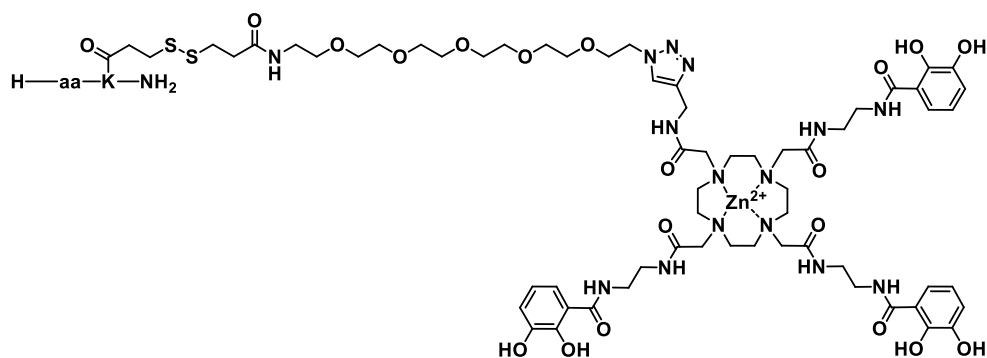
Exact Mass: 4026,88050

Molecular Weight: 4030,71590

20 (18.0 mg, 4.5 μmol, 82%) was prepared following the general procedure for CuAAC with DOTAM **1** (16.8 mg, 13.7 μmol, 2.5 eq) and peptide **62** (15.0 mg, 5.5 μmol, 1.0 eq).

¹H NMR (700 MHz, DMSO-d₆): δ [ppm] = 8.30 (s), 8.23 – 8.15 (m), 8.13 – 7.96 (m), 7.95 – 7.77 (m), 7.75 – 7.63 (m), 7.61 – 7.55 (m), 7.54 – 7.49 (m), 7.40 – 7.27 (m), 7.25 (s), 7.01 (s), 6.76 (s), 6.74 (s), 4.58 – 3.93 (m), 3.92 (d, *J* = 8.0 Hz), 3.82 – 3.67 (m), 3.53 – 3.43 (m), 3.27 (q, *J* = 6.1 Hz), 3.07 (dd, *J* = 13.3 Hz, 6.8 Hz), 2.98 (dd, *J* = 12.7 Hz, 6.6 Hz), 2.61 – 2.52 (m), 2.47 – 2.39 (m), 2.29 – 2.08 (m), 2.02 – 1.92 (m), 1.91 (s), 1.90 – 1.86 (m), 1.86 (s), 1.85 – 1.79 (m), 1.78 (s), 1.77 – 1.19 (m), 1.15 (s), 1.04 (dd, *J* = 11.0 Hz, 5.9 Hz), 1.02 (d, *J* = 6.2 Hz), 0.94 (s), 0.88 (d, *J* = 6.9 Hz), 0.86 (d, *J* = 6.6 Hz), 0.85 – 0.76 (m).

HRMS (ESI) calculated for (C₁₇₄H₂₇₈N₄₁O₆₄Zn²⁺)³⁺ ([M+3H]³⁺): *m/z* = 1343.3008, experimental: 1343.2967, δ [ppm] = 4.1, calculated for (C₁₇₄H₂₇₉N₄₁O₆₄Zn²⁺)⁴⁺ ([M+4H]⁴⁺): *m/z* = 1007.7274, experimental: 1007.7240, δ [ppm] = 3.4, calculated for (C₁₇₄H₂₈₀N₄₁O₆₄Zn²⁺)⁵⁺ ([M+5H]⁵⁺): *m/z* = 806.3834, experimental: 806.3806, δ [ppm] = 2.8, calculated for (C₁₇₄H₂₈₁N₄₁O₆₄Zn²⁺)⁶⁺ ([M+6H]⁶⁺): *m/z* = 672.1540, experimental: 672.1522, δ [ppm] = 1.8, calculated for (C₁₇₄H₂₈₂N₄₁O₆₄Zn²⁺)⁷⁺ ([M+7H]⁷⁺): *m/z* = 576.2759, experimental: 576.2750, δ [ppm] = 0.9.

Compound 21 (PfeA 33-51 C-term disulfide-(PEG)₇-Zn²⁺-DOTAM)


aa: VIELGE*Q*T*V*V*A*T*AQEETKQ

Chemical Formula: C₁₅₈H₂₅₅N₄₁O₅₄S₂Zn²⁺

Exact Mass: 3718,71900

Molecular Weight: 3722,50990

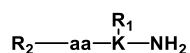
21 was prepared adapted from an established procedure reported by Song, Yang, Hall, Gurnani, and Perrier,⁶ which is a modified version of the procedures for disulfide bond formation by Bernatowicz, Matsueda and Matsueda.⁷

52 (8.2 mg, 5.687 μmol, 1.0 eq) was dissolved in DMF (1 mL) and HEPES buffer (1.0 M, 1 mL). **70** (15 mg, 6.256 μmol, 1.1 eq) was added to the solution, dissolved in DMF (1 mL), DMSO (1 mL) and HEPES buffer (1.0 M, 1 mL). The reaction was stirred at 23 °C for 72 h and the reaction progress was controlled by LCMS. The reaction was concentrated by rotary evaporation and filtered after completeness. The remains in the filter were washed with ACN (20 mL) and the solvent was removed by rotary evaporation. The residue was taken up, diluted with ACN/MilliQ H₂O, and purified by RP-HPLC (C18 phenomenex, 220 nm, collect all, 5-45% ACN/MilliQ H₂O, 0.1% HCOOH). The product containing fractions were identified by LCMS and lyophilized to dryness to yield the product **21** as a white solid. **Yield** 16.0 mg (4.298 mmol, 76%).

¹H NMR (700 MHz, DMSO-*d*₆): δ [ppm] = 9.60 (s), 8.47 – 8.36 (m), 8.29 (s), 8.27 (s), 8.23 – 8.00 (m), 7.97 – 7.54 (m), 7.42 – 7.12 (m), 7.02 (s), 6.84 – 6.79 (m), 6.77 (s), 6.73 (s), 6.54 – 6.42 (m), 4.50 – 3.95 (m), 3.80 – 3.70 (m), 3.48 (d, *J* = 3.8 Hz), 3.46 – 3.21 (m), 3.19 (q, *J* = 5.6 Hz), 3.06 (t, *J* = 7.1 Hz), 3.03 – 2.89 (m), 2.87 (t, *J* = 7.2 Hz), 2.79 – 2.70 (m), 2.66 (t, *J* = 7.4 Hz), 2.64 – 2.54 (m), 2.54 (s), 2.53 – 2.51 (m), 2.48 – 2.39 (m), 2.36 – 2.08 (m), 2.06 – 1.19 (m), 1.17 (d, *J* = 6.7 Hz), 1.14 (s), 1.09 – 0.98 (m), 0.88 (d, *J* = 6.9 Hz), 0.86 (d, *J* = 6.7 Hz), 0.85 – 0.77 (m).

HRMS (ESI) calculated for (C₁₅₈H₂₅₈N₄₁O₅₄S₂Zn²⁺)³⁺ ([M+3H]³⁺): *m/z* = 1240.5803, experimental: 1240.5800, δ [ppm] = 0.3, calculated for (C₁₅₈H₂₅₉N₄₁O₅₄S₂Zn²⁺)⁴⁺ ([M+4H]⁴⁺): *m/z* = 930.6870, experimental: 930.6872, δ [ppm] = 0.2, calculated for (C₁₅₈H₂₆₀N₄₁O₅₄S₂Zn²⁺)⁵⁺ ([M+5H]⁵⁺): *m/z* = 744.7511, experimental: 744.7511, δ [ppm] = 0.0.

General procedure for CuAAC with MECAM 3 or 4



R₁ = H, CO-(PEG)₇-(1,2,3-Triazole)-MECAM
 R₂ = CO-(PEG)₇-(1,2,3-Triazole)-MECAM, H

FpvA 121-139 = DSSVDLG*A*T*MITSNQLGTI
 PfeA 33-51 = VIELGE*Q*T*V*V*A*T*AQEETKQ
 HasR 122-144 = SLIRVSQDDLVMSPS*V*I*SAARP

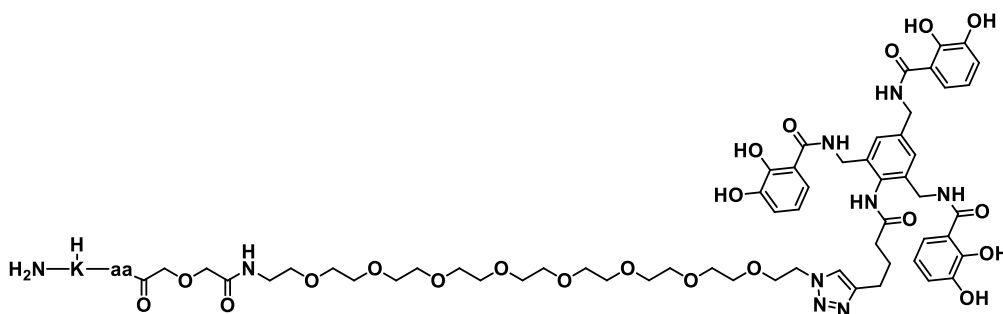
aa sequence

FpvA 124-134 = VDLG*A*T*MITSN
 PfeA 37-46 = GE*Q*T*V*V*A*T*AQ
 HasR 129-138 = DDLVMSPS*V*

Compounds **22-32** were prepared adapted from an established procedure reported by Pinkert *et al.*³

3 or **4** (2.5 eq) was dissolved under argon atmosphere in DMSO (1 mL) and MilliQ H₂O (1 mL). In case **3** was employed as starting material, acetic acid was added (1%, 40 μL) to prevent deacetylation. PEG-modified peptide (**61-70**) (1.0 eq), dissolved in DMSO (1 mL), was added to the solution. CuSO₄ (1.0 eq.) was dissolved in PBS (0.3 mL) and sodium ascorbate (2.0 eq), dissolved in PBS (0.4 mL) was added to the CuSO₄ solution, whereupon a white solid precipitated immediately. THPTA (0.5 eq), dissolved in PBS (0.3 mL) was added to the suspension. The suspension was added under argon atmosphere to the reaction. The reaction was stirred at 23 °C for 1 h and the reaction progress was controlled by LCMS. After completion of the reaction the solution was filtered over a cotton wool and purified by RP-HPLC (C18 phenomenex, 220 nm, collect all, 5-45% ACN/MilliQ H₂O, 0.1% HCOOH). The product containing fractions were identified by LCMS and lyophilized to dryness to yield products **22-32** as a white solids.

Compound 22 (FpvA 121-139 N-term-(PEG)₇-MECAM)



aa: DSSVDLG*A*T*MITSNQLGTI

Chemical Formula: C₁₄₃H₂₂₂N₃₂O₅₃S

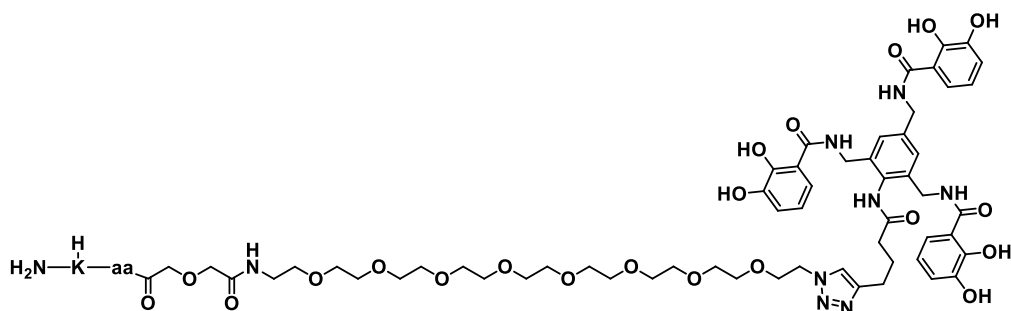
Exact Mass: 3267,53807

Molecular Weight: 3269,58000

22 (36.0 mg, 11.0 μmol, 95%) was prepared following the general procedure for CuAAC with MECAM **4** (19.8 mg, 29.0 μmol, 2.5 eq) and peptide **61** (30.0 mg, 11.6 μmol, 1.0 eq).

¹H NMR (700 MHz, DMSO-d₆): δ [ppm] = 9.59 (s), 9.38 (t, *J* = 5.3 Hz), 9.23 (s), 8.49 – 8.12 (m), 8.08 – 7.99 (m), 7.96 (d, *J* = 6.4 Hz), 7.93 (d, *J* = 6.7 Hz), 7.88 (d, *J* = 6.0 Hz), 7.83 (s), 7.81 (dd, *J* = 14.8 Hz, 8.0 Hz), 7.72 – 7.50 (m), 7.46 (s), 7.28 (d, *J* = 7.9 Hz), 7.23 (s), 7.21 (s), 7.19 (dd, *J* = 8.2 Hz, 1.2 Hz), 7.03 (s), 6.99 (s), 6.91 (d, *J* = 7.7 Hz), 6.88 (d, *J* = 7.7 Hz), 6.82 – 6.74 (m), 6.65 (t, *J* = 7.9 Hz), 6.59 (t, *J* = 7.9 Hz), 5.08 (bs), 4.99 (bs), 4.63 (dd, *J* = 14.1 Hz, 6.7 Hz), 4.60 – 4.47 (m), 4.46 (t, *J* = 5.3 Hz), 4.43 (s), 4.40 (d, *J* = 5.8 Hz), 4.39 – 3.95 (m), 3.94 (d, *J* = 5.5 Hz), 3.92 (t, *J* = 4.9 Hz), 3.79 (t, *J* = 5.3 Hz), 3.77 – 3.53 (m), 3.52 – 3.41 (m), 3.28 – 3.23 (m), 2.75 (bs), 2.69 (t, *J* = 7.6 Hz), 2.67 – 2.51 (m), 2.47 – 2.34 (m), 2.27 – 2.22 (m), 2.15 – 2.02 (m), 1.99 – 1.87 (m), 1.84 – 1.70 (m), 1.68 – 1.58 (m), 1.56 – 1.39 (m), 1.37 – 1.26 (m), 1.23 (d, *J* = 6.8 Hz), 1.22 – 0.97 (m), 0.87 (d, *J* = 6.5 Hz), 0.85 (d, *J* = 6.4 Hz), 0.84 – 0.76 (m).

HRMS (ESI) calculated for C₁₄₃H₂₂₅N₃₂O₅₃S³⁺ ([M+3H]³⁺): *m/z* = 1090.1866, experimental: 1090.1872, δ [ppm] = 0.6, calculated for C₁₄₃H₂₂₆N₃₂O₅₃S⁴⁺ ([M+4H]⁴⁺): *m/z* = 817.8918, experimental: 817.8917, δ [ppm] = 0.1.

Compound 23 (*PfeA* 33-51 *N*-term (PEG)₇-MECAM)

aa: VIELGE*Q*T*V*V*A*T*AQEETKQ

Chemical Formula: C₁₅₂H₂₃₆N₃₄O₅₅

Exact Mass: 3417,67153

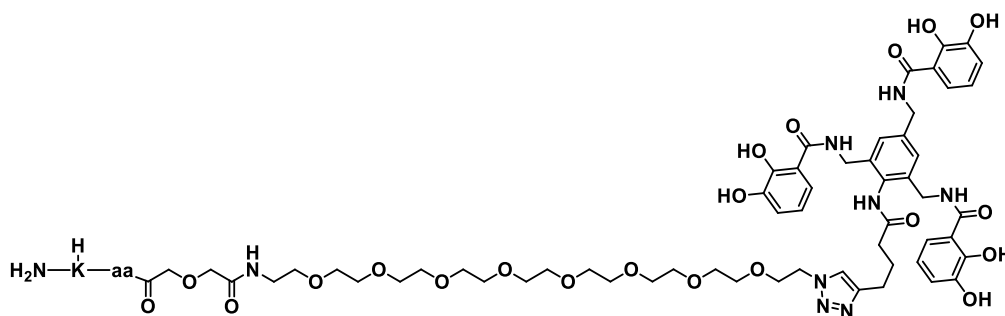
Molecular Weight: 3419,74300

23 (36.2 mg, 10.6 μmol, 97%) was prepared following the general procedure for CuAAC with MECAM **4** (18.7 mg, 27.4 μmol, 2.5 eq) and peptide **62** (30.0 mg, 11.0 μmol, 1.0 eq).

¹H NMR (700 MHz, DMSO-*d*₆): δ [ppm] = 9.62 (s), 9.42 (t, *J* = 5.3 Hz), 9.28 (s), 8.22 (s), 8.20 – 8.16 (m), 8.10 (t, *J* = 6.2 Hz), 8.05 (t, *J* = 5.6 Hz), 8.04 – 7.94 (m), 7.92 (d, *J* = 7.0 Hz), 7.88 (d, *J* = 8.8 Hz), 7.86 – 7.80 (m), 7.75 – 7.67 (m), 7.41 – 7.33 (m), 7.31 – 7.24 (m), 7.21 (s), 7.20 (dd, *J* = 6.9 Hz, 1.2 Hz), 7.06 (s), 6.89 (dd, *J* = 7.7 Hz, 0.8 Hz), 6.87 (dd, *J* = 7.8 Hz, 1.0 Hz), 6.80 – 6.73 (m), 6.64 (t, *J* = 7.9 Hz), 6.58 (t, *J* = 7.9 Hz), 4.46 (t, *J* = 5.3 Hz), 4.43 (s), 4.41 (d, *J* = 5.7 Hz), 4.37 – 4.32 (m), 4.31 – 4.02 (m), 4.00 (d, *J* = 7.4 Hz), 3.99 – 3.98 (m), 3.95 (d, *J* = 3.9 Hz), 3.93 (s), 3.79 (t, *J* = 5.3 Hz), 3.76 – 3.58 (m), 3.52 – 3.44 (m), 3.43 (t, *J* = 6.0 Hz), 3.26 (q, *J* = 5.9 Hz), 2.74 (t, *J* = 6.9 Hz), 2.69 (t, *J* = 7.6 Hz), 2.64 – 2.58 (m), 2.54 (s), 2.48 – 2.43 (m), 2.41 – 2.33 (m), 2.28 – 2.10 (m), 2.08 (s), 2.03 – 1.35 (m), 1.33 (s), 1.30 (s), 1.28 – 1.13 (m), 1.09 – 0.99 (m), 0.89 – 0.68 (m).

¹³C NMR (176 MHz, DMSO-*d*₆) δ [ppm] = 173.9, 170.5, 169.7, 163.4, 153.4, 149.8, 149.8, 146.3, 140.7, 140.7, 135.9, 135.8, 133.5, 132.0, 126.9, 125.5, 125.5, 125.2, 124.8, 124.8, 124.6, 124.4, 124.3, 124.3, 123.3, 122.3, 119.0, 118.9, 118.7, 117.9, 117.9, 117.4, 115.2, 70.3, 69.8, 69.8, 69.6, 69.6, 68.9, 68.8, 66.4, 40.4, 40.0, 31.3, 31.2, 30.7, 30.4, 29.8, 29.0, 28.7, 26.5, 25.2, 22.1, 19.2, 14.0, 11.0.

HRMS (ESI) calculated for C₁₅₂H₂₃₉N₃₄O₅₅³⁺ ([M+3H]³⁺): *m/z* = 1140.2311, experimental: 1140.2301, δ [ppm] = 1.0, calculated for C₁₅₂H₂₄₀N₃₄O₅₅⁴⁺ ([M+4H]⁴⁺): *m/z* = 855.4252, experimental: 855.4255, δ [ppm] = 0.3, calculated for C₁₅₂H₂₄₁N₃₄O₅₅⁵⁺ ([M+5H]⁵⁺): *m/z* = 684.5416, experimental: 684.5425, δ [ppm] = 0.9.

Compound 24 (HasR 122-144 N-term (PEG)₇-MECAM)


aa: SLIRVSQDDLQMSPS*V*I*SAARP

 Chemical Formula: C₁₆₉H₂₆₈N₄₂O₅₆S

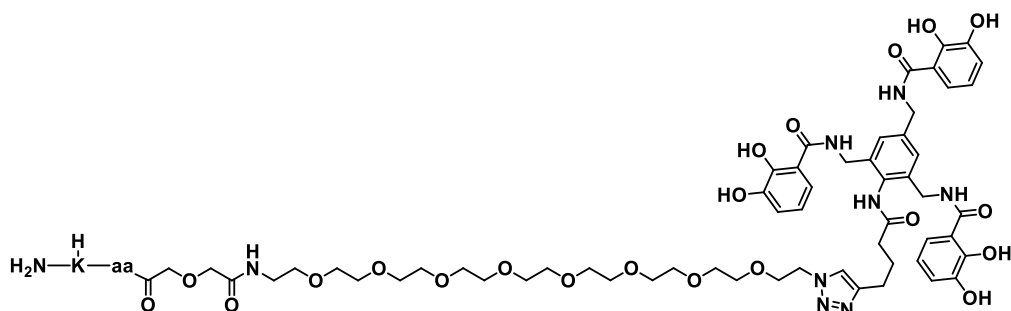
Exact Mass: 3813,91351

Molecular Weight: 3816,30100

24 (21.0 mg, 5.5 μmol, 86%) was prepared following the general procedure for CuAAC with MECAM **4** (10.9 mg, 16.0 μmol, 2.5 eq) and peptide **63** (20.0 mg, 6.4 μmol, 1.0 eq).

¹H NMR (700 MHz, DMSO-*d*₆): δ [ppm] = 9.68 (s), 9.55 (s), 9.44 (s), 8.50 (s), 8.31 (s), 8.27 (s), 8.16 (d, *J* = 6.5 Hz), 8.13 – 7.85 (m), 7.84 (s), 7.83 – 7.28 (m), 7.26 (dd, *J* = 8.1 Hz, 1.2 Hz), 7.22 (s), 7.19 (dd, *J* = 8.1 Hz, 1.4 Hz), 7.05 – 6.94 (m), 6.88 (dd, *J* = 7.4 Hz, 0.7 Hz), 6.85 (dd, *J* = 8.7 Hz, 1.0 Hz), 6.75 (s), 6.71 (s), 6.60 (t, *J* = 7.9 Hz), 6.56 (t, *J* = 7.9 Hz), 4.58 – 4.52 (m), 4.46 (t, *J* = 5.3 Hz), 4.44 – 4.02 (m), 4.00 (s), 3.97 (s), 3.96 – 3.90 (m), 3.79 (t, *J* = 5.3 Hz), 3.77 – 3.54 (m), 3.52 – 3.40 (m), 3.26 (q, *J* = 5.8 Hz), 3.17 – 2.95 (m), 2.78 (t, *J* = 2.7 Hz), 2.75 (s), 2.70 (t, *J* = 7.6 Hz), 2.68 – 2.59 (m), 2.54 (s), 2.47 (t, *J* = 7.5 Hz), 2.45 – 2.30 (m), 2.29 (t, *J* = 7.4 Hz), 2.27 – 2.20 (m), 2.18 (td, *J* = 7.1 Hz, 2.6 Hz), 2.16 – 2.07 (m), 2.06 – 2.01 (m), 2.00 (s), 1.99 – 1.93 (m), 1.90 – 1.25 (m), 1.24 – 1.17 (m), 1.14 – 1.00 (m), 0.86 (d, *J* = 6.5 Hz), 0.84 – 0.73 (m).

HRMS (ESI) calculated for C₁₆₉H₂₇₁N₄₂O₅₆S³⁺ ([M+3H]³⁺): *m/z* = 1272.3118, experimental: 1272.3114, δ [ppm] = 0.4, calculated for C₁₆₉H₂₇₂N₄₂O₅₆S⁴⁺ ([M+4H]⁴⁺): *m/z* = 954.4857, experimental: 954.4850, δ [ppm] = 0.7, calculated for C₁₆₉H₂₇₃N₄₂O₅₆S⁵⁺ ([M+5H]⁵⁺): *m/z* = 763.7900, experimental: 763.7890, δ [ppm] = 1.0, calculated for C₁₆₉H₂₇₄N₄₂O₅₆S⁶⁺ ([M+6H]⁶⁺): *m/z* = 636.6595, experimental: 636.6587, δ [ppm] = 0.8.

Compound 25 (*FpvA* 124-134 N-term (PEG)₇-MECAM)

aa: VDLG*A*T*MITSN

Chemical Formula: C₁₁₀H₁₆₇N₂₃O₃₉S

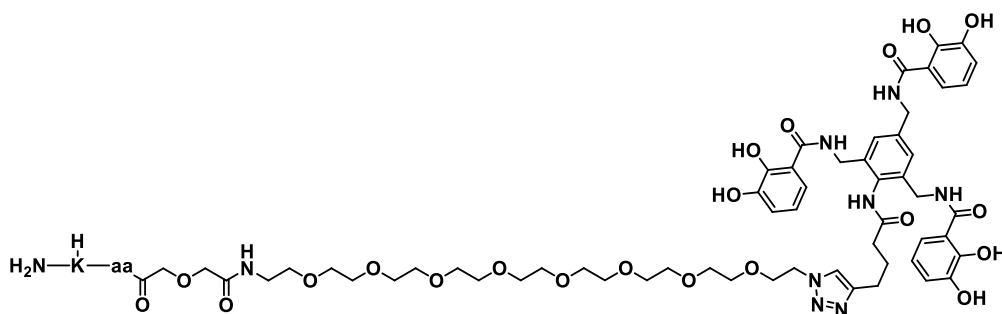
Exact Mass: 2466,15122

Molecular Weight: 2467,72800

25 (22.0 mg, 8.9 μmol, 88%) was prepared following the general procedure for CuAAC with MECAM **4** (17.2 mg, 25.2 μmol, 2.5 eq) and peptide **67** (18.0 mg, 10.1 μmol, 1.0 eq).

¹H NMR (700 MHz, DMSO-*d*₆): δ [ppm] = 9.62 (s), 9.43 (s), 9.29 (s), 8.37 (s), 8.33 (d, *J* = 7.5 Hz), 8.21 (s), 8.18 – 8.10 (m), 8.06 (t, *J* = 5.4 Hz), 7.85 – 7.78 (m), 7.83 (s), 7.73 (d, *J* = 7.9 Hz), 7.45 (s), 7.27 (dd, *J* = 8.2 Hz, 1.1 Hz), 7.22 (s), 7.21 (s), 7.19 (dd, *J* = 8.2 Hz, 1.2 Hz), 7.08 (s), 6.99 (s), 6.89 (dd, *J* = 7.8 Hz, 1.2 Hz), 6.86 (dd, *J* = 7.8 Hz, 1.3 Hz), 6.63 (t, *J* = 7.9 Hz), 6.58 (t, *J* = 7.9 Hz), 4.53 (dd, *J* = 14.2 Hz, 7.3 Hz), 4.49 (dd, *J* = 13.8 Hz, 6.7 Hz), 4.46 (t, *J* = 5.3 Hz), 4.43 (s), 4.41 (d, *J* = 5.8 Hz), 4.39 – 4.34 (m), 4.32 – 4.26 (m), 4.25 – 4.18 (m), 4.14 (dd, *J* = 15.1 Hz, 7.7 Hz), 4.12 (dd, *J* = 7.9 Hz, 4.2 Hz), 4.07 (td, *J* = 9.4 Hz, 4.4 Hz), 4.04 – 4.03 (m), 4.01 (d, *J* = 3.2 Hz), 4.00 – 3.98 (m), 3.96 (d, *J* = 6.8 Hz), 3.94 (s), 3.79 (t, *J* = 5.3 Hz), 3.75 – 3.69 (m), 3.67 – 3.61 (m), 3.56 – 3.44 (m), 3.43 (t, *J* = 6.1 Hz), 3.26 (q, *J* = 5.9 Hz), 2.75 (t, *J* = 7.1 Hz), 2.69 (t, *J* = 7.6 Hz), 2.65 – 2.51 (m), 2.48 – 2.35 (m), 2.01 (s), 1.99 – 1.88 (m), 1.85 – 1.70 (m), 1.65 – 1.58 (m), 1.56 – 1.39 (m), 1.36 – 1.28 (m), 1.26 (d, *J* = 7.0 Hz), 1.23 – 1.19 (m), 1.15 – 1.07 (m), 1.04 (d, *J* = 6.4 Hz), 1.02 (d, *J* = 6.3 Hz), 0.88 (d, *J* = 6.6 Hz), 0.87 – 0.77 (m).

HRMS (ESI) calculated for C₁₁₀H₁₇₀N₂₃O₃₉S³⁺ ([M+3H]³⁺): *m/z* = 823.0577, experimental: 823.0600, δ [ppm] = 2.3, calculated for C₁₁₀H₁₇₁N₂₃O₃₉S⁴⁺ ([M+4H]⁴⁺): *m/z* = 617.5451, experimental: 617.5460, δ [ppm] = 0.9.

Compound 26 (*PfeA* 37-46 *N*-term (PEG)₇-MECAM)

aa: GE*Q*T*V*V*A*T*AQ

Chemical Formula: C₁₀₅H₁₅₇N₂₃O₃₈

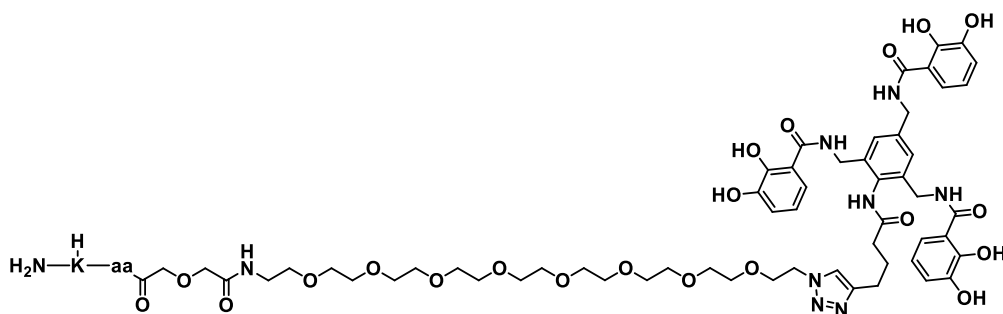
Exact Mass: 2348,10599

Molecular Weight: 2349,53400

26 (27.0 mg, 11.5 μ mol, 96%) was prepared following the general procedure for CuAAC with MECAM **4** (20.5 mg, 30.0 μ mol, 2.5 eq) and peptide **68** (20.0 mg, 12.0 μ mol, 1.0 eq).

¹H NMR (700 MHz, DMSO-*d*₆): δ [ppm] = 9.67 (s), 9.53 (s), 9.42 (s), 8.26 (t, J = 5.6 Hz), 8.17 (d, J = 7.3 Hz), 8.12 – 8.06 (m), 7.97 (d, J = 6.9 Hz), 7.93 (d, J = 6.4 Hz), 7.87 (d, J = 7.3 Hz), 7.84 (s), 7.74 (d, J = 7.7 Hz), 7.68 (d, J = 8.0 Hz), 7.30 (s), 7.27 (s), 7.26 (s), 7.25 (s), 7.22 (s), 7.19 (d, J = 8.0 Hz), 7.06 (s), 6.87 (d, J = 7.7 Hz), 6.85 (d, J = 7.8 Hz), 6.78 (s), 6.76 (s), 6.61 (t, J = 7.8 Hz), 6.56 (t, J = 7.9 Hz), 4.46 (t, J = 5.3 Hz), 4.43 (s), 4.41 (d, J = 5.7 Hz), 4.38 – 4.32 (m), 4.31 – 4.19 (m), 4.17 – 4.10 (m), 4.09 (t, J = 7.5 Hz), 4.04 – 3.99 (m), 3.98 (s), 3.96 (s), 3.79 (t, J = 5.5 Hz), 3.50 – 3.44 (m), 3.43 (t, J = 6.0 Hz), 3.27 (q, J = 5.9 Hz), 2.74 (t, J = 7.3 Hz), 2.70 (t, J = 7.6 Hz), 2.47 (t, J = 7.4 Hz), 2.23 – 2.07 (m), 2.02 – 1.85 (m), 1.79 – 1.63 (m), 1.57 – 1.46 (m), 1.35 – 1.25 (m), 1.23 (d, J = 7.2 Hz), 1.21 (d, J = 7.1 Hz), 1.03 (d, J = 6.3 Hz), 1.01 (d, J = 6.3 Hz), 0.83 (dd, J = 11.2 Hz, 6.5 Hz).

HRMS (ESI) calculated for C₁₀₅H₁₅₉N₂₃O₃₈²⁺ ([M+2H]²⁺): m/z = 1175.0603, experimental: 1175.0617, δ [ppm] = 1.4, calculated for C₁₀₅H₁₅₈N₂₃NaO₃₈²⁺ ([M+H+Na]²⁺): m/z = 1186.0512, experimental: 1186.0523, δ [ppm] = 1.1, calculated for C₁₀₅H₁₅₇N₂₃NaO₃₈²⁺ ([M+2Na]²⁺): m/z = 1197.0422, experimental: 1197.0430, δ [ppm] = 0.8, calculated for C₁₀₅H₁₆₀N₂₃O₃₈³⁺ ([M+3H]³⁺): m/z = 783.7093, experimental: 783.7104, δ [ppm] = 1.1.

Compound 27 (*HasR* 129-138 N-term (PEG)₇-MECAM)

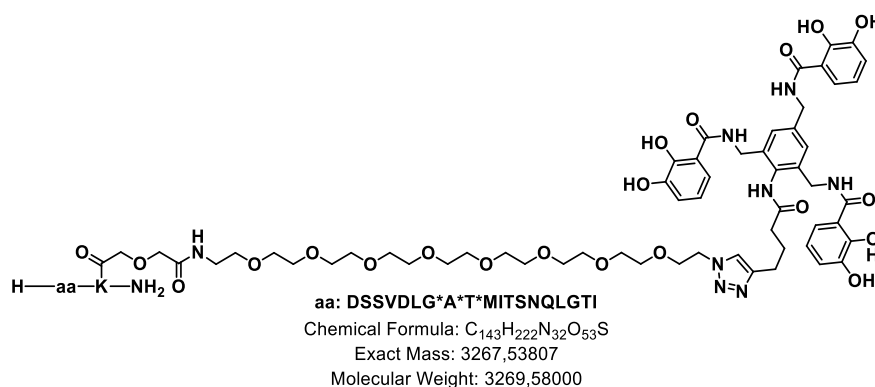
aa: DDLVQMSPS*V*

Chemical Formula: C₁₀₉H₁₆₂N₂₂O₃₉S
 Exact Mass: 2435,10902
 Molecular Weight: 2436,67000

27 (12.0 mg, 4.9 μmol, 86%) was prepared following the general procedure for CuAAC with MECAM **4** (9.7 mg, 14.3 μmol, 2.5 eq) and peptide **69** (10.0 mg, 5.7 μmol, 1.0 eq).

¹H NMR (700 MHz, DMSO-d₆): δ [ppm] = 9.61 (s), 9.41 (t, *J* = 5.7 Hz), 9.26 (t, *J* = 7.0 Hz), 8.37 (s), 8.29 (s), 8.28 (s), 8.22 (bs), 8.09 (t, *J* = 5.2 Hz), 7.96 (d, *J* = 6.6 Hz), 7.83 (s), 7.76 (d, *J* = 7.7 Hz), 7.57 (d, *J* = 6.9 Hz), 7.41 (s), 7.38 (s), 7.27 (dd, *J* = 8.1 Hz, 1.0 Hz), 7.21 (s), 7.19 (dd, *J* = 8.2 Hz, 1.2 Hz), 7.10 (s), 7.04 (s), 6.90 (dd, *J* = 7.8 Hz, 0.9 Hz), 6.87 (dd, *J* = 7.8 Hz, 1.0 Hz), 6.76 (s), 6.73 (s), 6.64 (t, *J* = 7.9 Hz), 6.58 (t, *J* = 7.9 Hz), 4.78 (d, *J* = 8.3 Hz), 4.59 – 4.52 (m), 4.46 (t, *J* = 5.3 Hz), 4.43 (bs), 4.41 (d, *J* = 5.7 Hz), 4.38 – 4.30 (m), 4.25 – 4.18 (m), 4.17 – 4.10 (m), 4.09 (t, *J* = 7.2 Hz), 4.01 (t, *J* = 7.6 Hz), 3.99 (s), 3.97 (s), 3.95 (s), 3.93 (s), 3.79 (t, *J* = 5.3 Hz), 3.69 (t, *J* = 6.0 Hz), 3.66 – 3.55 (m), 3.54 – 3.44 (m), 3.43 (t, *J* = 6.1 Hz), 3.28 – 3.26 (m), 2.77 – 2.73 (m), 2.69 (t, *J* = 7.6 Hz), 2.63 – 2.52 (m), 2.46 (t, *J* = 7.5 Hz), 2.44 – 2.36 (m), 2.21 – 2.08 (m), 2.04 (dd, *J* = 13.7 Hz, 7.2 Hz), 2.01 (s), 2.00 (s), 1.94 (p, *J* = 7.6 Hz), 1.91 – 1.72 (m), 1.70 – 1.63 (m), 1.61 – 1.43 (m), 1.40 – 1.26 (m), 1.23 (s), 1.14 (s), 1.13 (d, *J* = 2.3 Hz), 1.12 (s), 1.11 (s), 1.10 – 1.06 (m), 0.90 – 0.82 (m), 0.80 (d, *J* = 6.4 Hz).

HRMS (ESI) calculated for C₁₀₉H₁₆₄N₂₂O₃₉S²⁺ ([M+2H]²⁺): *m/z* = 1218.5618, experimental: 1218.5614, δ [ppm] = 0.4, calculated for C₁₀₉H₁₆₃N₂₂NaO₃₉S²⁺ ([M+H+Na]²⁺): *m/z* = 1229.5528, experimental: 1229.5523, δ [ppm] = 0.5, calculated for C₁₀₉H₁₆₅N₂₂O₃₉S³⁺ ([M+3H]³⁺): *m/z* = 812.7103, experimental: 812.7104, δ [ppm] = 0.1, calculated for C₁₀₉H₁₆₆N₂₂O₃₉S⁴⁺ ([M+4H]⁴⁺): *m/z* = 609.7845, experimental: 609.7845, δ [ppm] = 0.0.

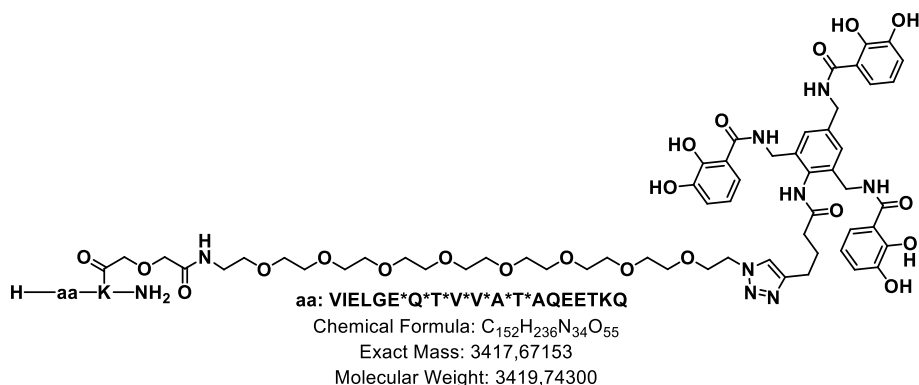
Compound 28 (FpvA 121-139 C-term (PEG)₇-MECAM)


28 (18.0 mg, 5.5 μ mol, 95%) was prepared following the general procedure for CuAAC with MECAM **4** (9.9 mg, 14.5 μ mol, 2.5 eq) and peptide **64** (15.0 mg, 5.8 μ mol, 1.0 eq).

¹H NMR (700 MHz, DMSO-*d*₆): δ [ppm] = 12.53 (bs), 9.55 (s), 9.33 (t, *J* = 6.0 Hz), 9.16 (t, *J* = 5.7 Hz), 8.57 (d, *J* = 5.7 Hz), 8.31 (d, *J* = 6.4 Hz), 8.16 (d, *J* = 7.5 Hz), 8.11 (t, *J* = 5.2 Hz), 8.07 – 8.00 (m), 7.95 (t, *J* = 8.9 Hz), 7.91 (d, *J* = 7.8 Hz), 7.89 (d, *J* = 8.0 Hz), 7.88 – 7.84 (m), 7.83 (s), 7.81 – 7.77 (m), 7.68 (d, *J* = 8.1 Hz), 7.61 (d, *J* = 8.0 Hz), 7.44 (s), 7.28 (dd, *J* = 8.2 Hz, 1.3 Hz), 7.21 (s), 7.20 (s), 7.19 (dd, *J* = 8.3 Hz, 1.4 Hz), 7.17 (s), 6.99 (s), 6.98 (s), 6.91 (dd, *J* = 7.8 Hz, 1.3 Hz), 6.88 (dd, *J* = 7.8 Hz, 1.4 Hz), 6.78 (s), 6.66 (t, *J* = 7.9 Hz), 6.60 (t, *J* = 7.9 Hz), 5.09 (s), 4.96 (s), 4.57 – 4.50 (m), 4.46 (t, *J* = 5.3 Hz), 4.44 – 4.38 (m), 4.36 (t, *J* = 7.0 Hz), 4.34 – 4.29 (m), 4.28 – 4.09 (m), 4.06 – 4.02 (m), 4.00 – 3.94 (m), 3.93 (s), 3.91 (s), 3.81 (d, *J* = 6.0 Hz), 3.79 (t, *J* = 5.3 Hz), 3.74 – 3.69 (m), 3.67 (d, *J* = 5.9 Hz), 3.65 – 3.59 (m), 3.56 – 3.53 (m), 3.51 – 3.43 (m), 3.27 (q, *J* = 6.0 Hz), 3.08 (dd, *J* = 13.3 Hz, 7.0 Hz), 2.71 (s), 2.69 (t, *J* = 7.6 Hz), 2.62 – 2.52 (m), 2.48 – 2.35 (m), 2.18 (t, *J* = 7.4 Hz), 2.13 – 2.07 (m), 2.06 – 2.01 (m), 2.01 (s), 2.00 – 1.87 (m), 1.81 – 1.70 (m), 1.67 – 1.57 (m), 1.55 – 1.35 (m), 1.32 – 1.18 (m), 1.15 – 1.05 (m), 1.02 (d, *J* = 6.4 Hz), 1.01 (dd, *J* = 6.3 Hz, 1.3 Hz), 0.87 (d, *J* = 6.6 Hz), 0.86 (d, *J* = 6.6 Hz), 0.84 – 0.75 (m).

¹³C NMR (176 MHz, DMSO-*d*₆) δ [ppm] = 174.1, 173.5, 172.5, 172.4, 172.4, 172.3, 171.9, 171.2, 171.0, 170.1, 170.0, 170.0, 169.9, 169.8, 169.7, 168.9, 168.8, 168.5, 168.4, 149.7, 149.6, 146.3, 146.2, 146.2, 137.5, 135.9, 132.2, 124.8, 122.3, 118.9, 118.8, 118.8, 118.0, 117.9, 117.3, 117.1, 115.1, 113.3, 70.3, 70.3, 70.2, 69.8, 69.7, 69.6, 69.6, 69.6, 68.9, 68.8, 57.8, 57.2, 55.0, 52.7, 52.4, 51.8, 51.5, 51.3, 49.2, 42.2, 42.1, 42.0, 40.5, 40.0, 39.0, 38.2, 38.0, 36.5, 36.3, 34.8, 32.2, 31.5, 29.3, 28.9, 27.6, 25.2, 24.8, 24.3, 24.2, 24.1, 24.0, 23.1, 23.0, 22.8, 21.5, 19.7, 19.3, 19.3, 19.1, 18.1, 17.8, 15.4, 15.3, 14.6, 11.3, 10.9.

HRMS (ESI) calculated for C₁₄₃H₂₂₅N₃₂O₅₃S³⁺ ([M+3H]³⁺): *m/z* = 1090.1866, experimental: 1090.1870, δ [ppm] = 0.4, calculated for C₁₄₃H₂₂₆N₃₂O₅₃S⁴⁺ ([M+4H]⁴⁺): *m/z* = 817.8918, experimental: 817.8931, δ [ppm] = 1.4.

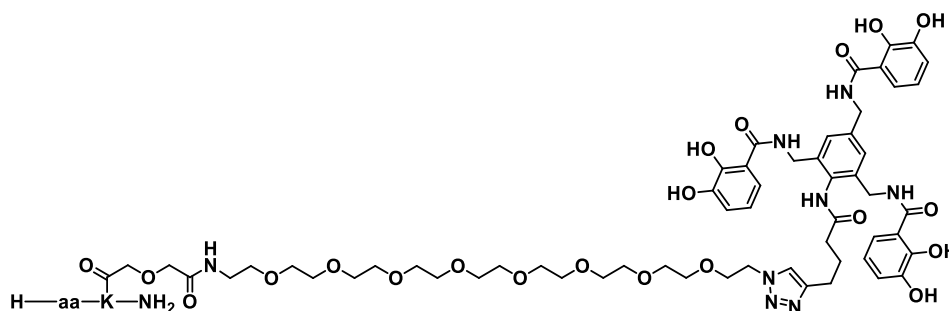
Compound 29 (*PfeA* 33-51 C-term (PEG)₇-MECAM)

29 (36.0 mg, 10.5 μ mol, 96%) was prepared following the general procedure for CuAAC with MECAM **4** (18.7 mg, 27.4 μ mol, 2.5 eq) and peptide **65** (30.0 mg, 11.0 μ mol, 1.0 eq).

¹H NMR (700 MHz, DMSO-*d*₆): δ [ppm] = 9.62 (s), 9.44 (t, *J* = 5.4 Hz), 9.31 (t, *J* = 5.7 Hz), 8.25 (d, *J* = 7.0 Hz), 8.23 – 8.15 (m), 8.12 – 8.09 (m), 8.07 (d, *J* = 6.6 Hz), 8.05 (dd, *J* = 12.4 Hz, 6.0 Hz), 7.99 (t, *J* = 5.0 Hz), 7.95 (d, *J* = 6.6 Hz), 7.92 (d, *J* = 8.0 Hz), 7.84 (bs), 7.84 (s), 7.78 (d, *J* = 7.4 Hz), 7.70 (d, *J* = 7.5 Hz), 7.31 (s), 7.29 (s), 7.27 (dd, *J* = 8.1 Hz, 1.4 Hz), 7.23 (bs), 7.21 (s), 7.19 (dd, *J* = 8.2 Hz, 1.4 Hz), 7.01 (s), 6.89 (dd, *J* = 7.8 Hz, 1.3 Hz), 6.86 (dd, *J* = 7.8 Hz, 1.4 Hz), 6.77 (d, *J* = 6.0 Hz), 6.75 (s), 6.63 (t, *J* = 7.9 Hz), 6.58 (t, *J* = 7.9 Hz), 4.46 (t, *J* = 5.4 Hz), 4.43 (bs), 4.41 (d, *J* = 5.8 Hz), 4.35 (p, *J* = 6.9 Hz), 4.31 – 4.22 (m), 4.19 – 3.97 (m), 3.93 (s), 3.91 (s), 3.79 (t, *J* = 5.4 Hz), 3.76 (d, *J* = 5.4 Hz), 3.74 (d, *J* = 5.0 Hz), 3.69 (d, *J* = 5.4 Hz), 3.67 (d, *J* = 5.3 Hz), 3.53 – 3.45 (m), 3.43 (t, *J* = 6.0 Hz), 3.28 (q, *J* = 6.0 Hz), 3.08 (dd, *J* = 13.3 Hz, 7.0 Hz), 2.75 (t, *J* = 6.8 Hz), 2.70 (t, *J* = 7.6 Hz), 2.46 (t, *J* = 7.5 Hz), 2.30 – 2.04 (m), 2.02 – 1.85 (m), 1.84 – 1.35 (m), 1.34 – 1.26 (m), 1.24 (d, *J* = 7.1 Hz), 1.23 (d, *J* = 6.9 Hz), 1.07 – 0.99 (m), 0.88 (d, *J* = 6.9 Hz), 0.86 (d, *J* = 6.6 Hz), 0.85 – 0.79 (m).

¹³C NMR (176 MHz, DMSO-*d*₆) δ [ppm] = 174.9, 174.9, 174.9, 174.5, 174.4, 173.9, 173.9, 173.9, 173.6, 172.8, 172.8, 172.8, 172.7, 172.3, 171.9, 171.8, 171.6, 171.6, 171.5, 171.2, 171.1, 171.0, 170.8, 170.7, 170.4, 170.2, 170.1, 169.6, 169.6, 168.8, 168.8, 168.5, 150.0, 150.0, 146.4, 146.4, 146.3, 137.5, 135.9, 132.2, 124.8, 122.3, 118.5, 117.6, 117.5, 117.3, 115.3, 70.2, 70.2, 69.8, 69.7, 69.6, 69.6, 68.9, 68.8, 66.5, 66.4, 66.3, 58.5, 56.7, 53.0, 52.9, 52.8, 52.7, 52.5, 52.0, 52.0, 51.1, 49.2, 48.8, 48.6, 42.1, 42.0, 40.8, 40.0, 39.0, 38.3, 38.1, 38.1, 36.8, 34.8, 31.6, 31.5, 31.5, 31.4, 31.3, 31.1, 30.6, 30.6, 30.5, 30.5, 30.5, 30.5, 30.2, 29.0, 27.6, 27.6, 27.6, 27.5, 27.4, 27.3, 27.2, 26.6, 25.2, 24.8, 24.4, 24.0, 23.1, 22.8, 22.1, 21.9, 21.5, 19.7, 19.6, 19.5, 19.2, 18.9, 18.3, 18.1, 17.9, 17.7, 17.2, 15.2, 11.1.

HRMS (ESI) calculated for C₁₅₂H₂₃₉N₃₄O₅₅³⁺ ([M+3H]³⁺): *m/z* = 1140.2311, experimental: 1140.2310, δ [ppm] = 0.1, calculated for C₁₅₂H₂₄₀N₃₄O₅₅⁴⁺ ([M+4H]⁴⁺): *m/z* = 855.4252, experimental: 855.4253, δ [ppm] = 0.1, calculated for C₁₅₂H₂₄₁N₃₄O₅₅⁵⁺ ([M+5H]⁵⁺): *m/z* = 684.5416, experimental: 684.5415, δ [ppm] = 0.1.

Compound 30 (HasR 122-144 C-term (PEG)₇-MECAM)

aa: SLIRVSQDDLVLQMSPS*V*I*SAARP

Chemical Formula: C₁₆₉H₂₆₈N₄₂O₅₆S

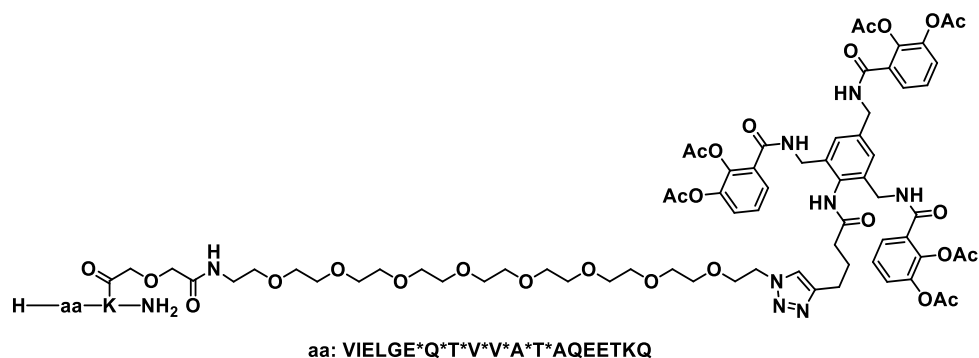
Exact Mass: 3813,91351

Molecular Weight: 3816,30100

30 (31.0 mg, 8.1 μ mol, 85%) was prepared following the general procedure for CuAAC with MECAM-OH **4** (16.3 mg, 23.9 μ mol, 2.5 eq) and peptide **66** (30.0 mg, 9.6 μ mol, 1.0 eq).

¹H NMR (700 MHz, DMSO-*d*₆): δ [ppm] = 9.67 (bs), 9.54 (bs), 9.43 (bs), 8.49 (bs), 8.32 (bs), 8.28 (s), 8.25 – 8.06 (m), 8.05 (d, *J* = 5.4 Hz), 8.03 – 7.85 (m), 7.84 (s), 7.82 (s), 7.81 – 7.50 (m), 7.47 – 7.28 (m), 7.26 (dd, *J* = 8.1 Hz, 1.2 Hz), 7.22 (s), 7.19 (dd, *J* = 8.2 Hz, 1.4 Hz), 6.98 (s), 6.87 (dd, *J* = 7.7 Hz, 0.8 Hz), 6.85 (dd, *J* = 7.7 Hz, 1.2 Hz), 6.75 (s), 6.71 (s), 6.60 (t, *J* = 7.9 Hz), 6.56 (t, *J* = 7.9 Hz), 5.05 (bs), 4.78 (d, *J* = 8.2 Hz), 4.54 (d, *J* = 6.6 Hz), 4.49 (d, *J* = 5.5 Hz), 4.46 (t, *J* = 5.3 Hz), 4.43 (d, *J* = 5.7 Hz), 4.41 (d, *J* = 6.0 Hz), 4.35 (d, *J* = 4.9 Hz), 4.33 – 4.10 (m), 4.07 (dd, *J* = 13.2 Hz, 8.7 Hz), 4.04 – 3.97 (m), 3.93 (s), 3.92 (s), 3.79 (t, *J* = 5.3 Hz), 3.72 – 3.53 (m), 3.52 – 3.42 (m), 3.29 – 3.27 (m), 3.17 – 3.01 (m), 2.78 (t, *J* = 2.7 Hz), 2.70 (t, *J* = 7.6 Hz), 2.64 – 2.58 (m), 2.54 (s), 2.48 – 2.33 (m), 2.29 (t, *J* = 7.4 Hz), 2.25 – 2.20 (m), 2.18 (td, *J* = 7.1 Hz, 2.7 Hz), 2.15 – 2.08 (m), 2.07 – 2.01 (m), 2.00 (s), 2.00 – 1.36 (m), 1.34 – 1.14 (m), 1.13 – 1.00 (m), 0.89 – 0.74 (m)

HRMS (ESI) calculated for C₁₆₉H₂₇₁N₄₂O₅₆S³⁺ ([M+3H]³⁺): *m/z* = 1272.3118, experimental: 1272.3127, δ [ppm] = 0.9, calculated for C₁₆₉H₂₇₂N₄₂O₅₆S⁴⁺ ([M+4H]⁴⁺): *m/z* = 954.4857, experimental: 954.4871, δ [ppm] = 1.4, calculated for C₁₆₉H₂₇₃N₄₂O₅₆S⁵⁺ ([M+5H]⁵⁺): *m/z* = 763.7900, experimental: 763.7907, δ [ppm] = 0.7.

Compound 31 (*PfeA* 33-51 C-term (PEG)₇-MECAM)Chemical Formula: C₁₆₄H₂₄₈N₃₄O₆₁

Exact Mass: 3669,73492

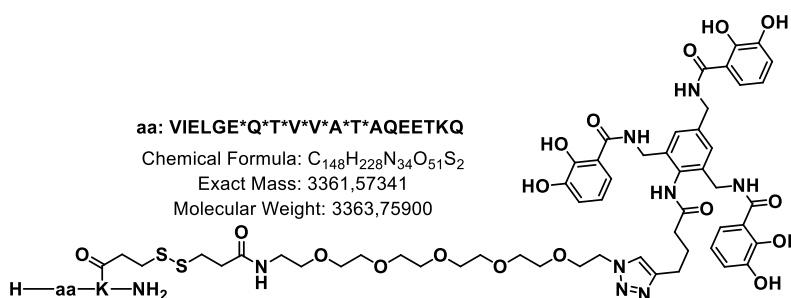
Molecular Weight: 3671,96500

31 (16.0 mg (4.4 μmol, 80%)) was prepared following the general procedure with MECAM **3** (12.8 mg, 13.7 μmol, 2.5 eq) and **65** (15.0 mg, 5.5 μmol, 1.0 eq).

¹H NMR (700 MHz, DMSO-d₆): δ [ppm] = 9.68 (s), 9.60 (s), 9.52 (d, *J* = 8.5 Hz), 8.98 – 8.91 (m), 8.84 – 8.80 (m), 8.78 (t, *J* = 5.8 Hz), 8.24 (d, *J* = 6.5 Hz), 8.21 – 8.15 (m), 8.10 – 8.01 (m), 7.99 – 7.86 (m), 7.86 (s), 7.84 (s), 7.83 (s), 7.82 – 7.78 (m), 7.77 (t, *J* = 5.3 Hz), 7.76 – 7.70 (m), 7.66 (d, *J* = 7.4 Hz), 7.54 – 7.51 (m), 7.48 (d, *J* = 1.4 Hz), 7.47 (t, *J* = 1.7 Hz), 7.46 (d, *J* = 1.4 Hz), 7.44 (d, *J* = 1.5 Hz), 7.43 (d, *J* = 1.5 Hz), 7.39 – 7.36 (m), 7.36 (d, *J* = 1.4 Hz), 7.35 (d, *J* = 1.5 Hz), 7.34 (t, *J* = 1.3 Hz), 7.33 (s), 7.32 (d, *J* = 1.4 Hz), 7.32 (s), 7.31 (d, *J* = 1.5 Hz), 7.31 (s), 7.30 – 7.26 (m), 7.25 – 7.14 (m), 7.01 (s), 6.88 – 6.72 (m), 4.51 (d, *J* = 5.4 Hz), 4.46 (t, *J* = 5.3 Hz), 4.42 – 4.37 (m), 4.36 (d, *J* = 6.5 Hz), 4.35 – 3.99 (m), 3.98 (t, *J* = 5.3 Hz), 3.93 (s), 3.91 (s), 3.79 (t, *J* = 5.3 Hz), 3.75 (d, *J* = 4.6 Hz), 3.70 – 3.64 (m), 3.55 – 3.40 (m), 3.27 (q, *J* = 5.9 Hz), 3.08 (dd, *J* = 13.3 Hz, 6.9 Hz), 2.99 (dd, *J* = 12.7 Hz, 6.7 Hz), 2.78 (t, *J* = 2.7 Hz), 2.75 (t, *J* = 6.8 Hz), 2.70 (t, *J* = 7.5 Hz), 2.62 (t, *J* = 7.6 Hz), 2.54 (s), 2.47 – 2.44 (m), 2.30 (t, *J* = 7.3 Hz), 2.28 – 2.19 (m), 2.18 (td, *J* = 7.1 Hz, 2.7 Hz), 2.18 – 2.15 (m), 2.15 (s), 2.15 (s), 2.14 – 2.07 (m), 2.03 – 1.88 (m), 1.86 (s), 1.85 – 1.79 (m), 1.78 (s), 1.77 – 1.68 (m), 1.65 (p, *J* = 7.2 Hz), 1.63 – 1.58 (m), 1.56 – 1.24 (m), 1.22 (t, *J* = 6.7 Hz), 1.10 – 0.98 (m), 0.89 (d, *J* = 6.8 Hz), 0.86 (d, *J* = 6.6 Hz), 0.85 – 0.77 (m).

¹³C NMR (176 MHz, DMSO-d₆) δ [ppm] = 174.3, 174.1, 174.0, 173.9, 173.9, 173.6, 172.5, 172.4, 172.3, 171.8, 171.5, 171.4, 171.3, 171.2, 171.1, 171.1, 171.0, 171.0, 170.9, 170.9, 170.6, 170.0, 169.9, 169.8, 169.3, 169.3, 169.3, 169.2, 169.1, 168.8, 168.8, 168.7, 168.6, 168.5, 168.3, 168.3, 168.0, 167.9, 167.8, 164.8, 164.6, 153.0, 146.3, 146.1, 142.9, 142.8, 140.2, 140.1, 139.2, 139.2, 136.1, 135.8, 135.6, 135.6, 132.5, 130.8, 130.7, 130.6, 127.1, 127.0, 127.0, 126.2, 126.1, 126.1, 126.0, 125.6, 124.8, 124.8, 124.7, 124.7, 124.6, 124.6, 122.3, 122.3, 118.1, 117.8, 117.8, 117.8, 117.8, 116.1, 116.1, 115.9, 115.9, 83.9, 71.7, 70.3, 70.2, 69.8, 69.8, 69.7, 69.7, 69.6, 68.9, 68.8, 66.6, 66.5, 58.2, 58.1, 57.9, 57.7, 57.6, 56.9, 56.8, 52.8, 52.5, 52.4, 52.1, 52.0, 51.8, 51.7, 51.7, 51.1, 51.0, 49.2, 48.4, 48.3, 41.9, 41.0, 40.9, 40.4, 40.0, 38.4, 38.2, 38.1, 36.7, 36.5, 34.9, 33.0, 32.4, 31.7, 31.5, 31.5, 31.4, 31.4, 30.6, 30.4, 30.3, 30.2, 30.1, 30.1, 29.0, 28.9, 27.7, 27.7, 27.6, 27.6, 27.4, 27.3, 27.2, 25.2, 24.8, 24.4, 24.4, 24.1, 23.5, 23.1, 23.1, 22.7, 22.7, 22.5, 21.5, 21.5, 21.1, 20.4, 20.4, 20.2, 20.1, 19.6, 19.5, 19.5, 19.3, 19.2, 18.5, 18.2, 18.0, 18.0, 18.0, 17.5, 17.2, 15.2, 15.1, 11.0, 11.0.

HRMS (ESI) calculated for C₁₆₄H₂₅₁N₃₄O₆₁³⁺ ([M+3H]³⁺): m/z = 1224.2523, experimental: 1224.2512, δ [ppm] = 1.1, calculated for C₁₆₄H₂₅₂N₃₄O₆₁⁴⁺ ([M+4H]⁴⁺): m/z = 918.4410, experimental: 918.4408, δ [ppm] = 0.2, calculated for C₁₆₄H₂₅₃N₃₄O₆₁⁵⁺ ([M+5H]⁵⁺): m/z = 734.9543, experimental: 734.9545, δ [ppm] = 0.2, calculated for C₁₆₄H₂₅₄N₃₄O₆₁⁶⁺ ([M+6H]⁶⁺): m/z = 612.6298, experimental: 612.6303, δ [ppm] = 0.5.

Compound 32 (PfeA 33-51 C-term disulfide-(PEG)₇-MECAM)


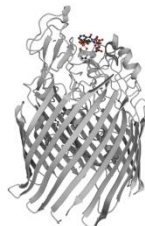
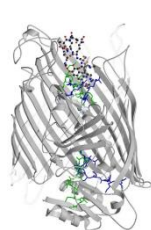
32 was prepared adapted from an established procedure reported by Song, Yang, Hall, Gurnani, and Perrier,⁶ which is a modified version of the procedures for disulfide bond formation by Bernatowicz, Matsueda and Matsueda.⁷

53 (6.1 mg, 5.7 μmol, 1.0 eq) was dissolved in DMF (1 mL) and HEPES buffer (1.0 M, 1 mL). **70** (15 mg, 6.3 μmol, 1.1 eq) was added to the solution, dissolved in DMF (1 mL), DMSO (1 mL) and HEPES buffer (1.0 M, 1 mL). The reaction was stirred at 23 °C for 48 h and the reaction progress was controlled by LCMS. The reaction was concentrated by rotary evaporation and filtered after completeness. The remains in the filter were washed with ACN (20 mL) and the solvent was removed by rotary evaporation. The residue was taken up, diluted with ACN/MilliQ H₂O, and purified by RP-HPLC (C18 phenomenex, 220 nm, collect all, 15-55% ACN/MilliQ H₂O, 0.1% HCOOH). The product containing fractions were identified by LCMS and lyophilized to dryness to yield the product **32** as a white solid. **Yield** 15.0 mg (4.5 μmol, 78%).

¹H NMR (700 MHz, DMSO-*d*₆): δ [ppm] = 9.56 (s), 9.33 (t, *J* = 6.0 Hz), 9.17 (t, *J* = 5.8 Hz), 8.33 (d, *J* = 8.4 Hz), 8.22 (d, *J* = 7.8 Hz), 8.20 – 8.14 (m), 8.04 (t, *J* = 6.8 Hz), 8.01 (t, *J* = 5.6 Hz), 7.98 – 7.86 (m), 7.83 (s), 7.78 (d, *J* = 7.0 Hz), 7.74 (d, *J* = 7.7 Hz), 7.63 (d, *J* = 7.9 Hz), 7.30 (s), 7.28 (dd, *J* = 8.2 Hz, 1.3 Hz), 7.24 (s), 7.20 (s), 7.19 (dd, *J* = 8.3 Hz, 1.4 Hz), 7.03 – 6.99 (m), 6.91 (dd, *J* = 7.8 Hz, 1.3 Hz), 6.88 (dd, *J* = 7.8 Hz, 1.3 Hz), 6.78 (s), 6.77 (s), 6.66 (t, *J* = 7.9 Hz), 6.60 (t, *J* = 7.9 Hz), 4.46 (t, *J* = 5.3 Hz), 4.43 (s), 4.40 (d, *J* = 5.8 Hz), 4.38 – 4.33 (m), 4.29 (t, *J* = 6.8 Hz), 4.25 (t, *J* = 6.3 Hz), 4.23 – 4.07 (m), 4.04 – 3.94 (m), 3.79 (t, *J* = 5.4 Hz), 3.66 (d, *J* = 5.7 Hz), 3.64 (d, *J* = 5.5 Hz), 3.62 – 3.59 (m), 3.51 (s), 3.50 – 3.49 (m), 3.48 (s), 3.47 (s), 3.46 – 3.44 (m), 3.38 (t, *J* = 6.0 Hz), 3.19 (dd, *J* = 5.8 Hz), 3.00 (dd, *J* = 12.8 Hz, 6.9 Hz), 2.87 (t, *J* = 7.1 Hz), 2.76 (t, *J* = 7.3 Hz), 2.69 (t, *J* = 7.6 Hz), 2.48 – 2.42 (m), 2.33 – 2.08 (m), 2.06 – 1.83 (m), 1.81 – 1.17 (m), 1.11 – 0.99 (m), 0.94 (s), 0.90 (d, *J* = 6.9 Hz), 0.88 (d, *J* = 6.9 Hz), 0.86 (d, *J* = 6.6 Hz), 0.85 – 0.80 (m).

HRMS (ESI) calculated for C₁₄₈H₂₃₂N₃₄O₅₁S₂⁴⁺ ([M+4H]⁴⁺): *m/z* = 841.4006, experimental: 841.4019, δ [ppm] = 1.3, calculated for C₁₄₈H₂₃₃N₃₄O₅₁S₂⁵⁺ ([M+5H]⁵⁺): *m/z* = 673.3220, experimental: 673.3218, δ [ppm] = 0.2.

Supplementary biological information

Literature information on *P. aeruginosa*'s TBDTs

no crystal structure

	FpvA	PfeA	HasR
Name	Ferripyoverdine receptor	Ferric enterobactin receptor	Heme assimilation system receptor
Uniprot #	P48632 (FPVA_PSEAE)	Q05098 (PFEA_PSEAE)	Q9HYJ7 (Q9HYJ7_PSEAE)
Genome db tag	PA2398 (fpvA)	PA2688 (pfeA)	PA3408 (hasR)
Gene	<i>fpvA</i>	<i>pfeA</i>	<i>hasR</i>
MW [kDa]	91.2	81.0	97.9
Location	OM	OM	OM
Organism	PAO1 DSM 22644	PAO1 DSM 22644	PAO1 DSM 22644
Induction	pyoverdine, under iron starvation conditions	enterobactin, iron	-
TonB box & framing aa	¹²¹ DSSVDLGATMITSN QLGTI ¹³⁹	³³ VIELGEQTVVATAQE ETKQ ⁵¹	¹²² SLIRVSQDDLVMQ SPSVISAARP ¹⁴⁴

Figure S7.1. (Top) Crystal structures of *FpvA*-PYO-Fe (PDB 2W6T) and *PfeA*-ENT-Fe (PDB 5M9B) of *P. aeruginosa*, no crystal structure determined for *HasR*.^{8 9} (Bottom) Summary on the three selected OMRs *FpvA*, *PfeA* and *HasR* regarding their name, UniProt accession numbers, Genome DB tag, gene, MW = molecular weight [Da], location = outer membrane (OM), organism, induction of TBDT expression, the TonB box and framing aa sequences.

Table S7.6 Natural and synthetic siderophores and the corresponding OMRs of *P. aeruginosa* and *E. coli*. PYO: pyoverdine, PCH: pyochelin, ENT: enterobactin.^{10, 11, 12, 13, 14, 15}

Siderophore	PYO	PCH	ENT	DOTAM	MECAM	HEME
<i>P. aeruginosa</i>	<u>FpvA</u>	<i>FptA</i>	<u>PfeA</u> , <i>PirA</i>	<i>PirA</i>	<u>PfeA</u> , <i>PirA</i>	<u>HasR</u> , <i>PhuR</i>

Biology methods

HasR plasmid construction

Enzymes were obtained from ThermoFisher Scientific. *E. coli* SM10 was used as the host strain for the plasmid. Primers are listed in Table S7 and for more information please see sections 'Cloned nucleotide / amino acid sequence' below. The DNA region encoding *araC* and *pbad* was amplified by PCR using primers 1595 and 1596. The PCR product was digested with *EcoRI* and *Sall* and inserted into corresponding sites of pMMB190 plasmid. The resulting plasmid was named pMMB190-*araC*-*pbad*. A DNA fragment corresponding to 26bp upstream of the initiator codon of *hasR* gene and 540bp of *hasR* coding sequence was amplified by PCR using primers 1589 and 1593 designed to generate *Sall* and *HindIII* sites at the 5' and 3' of the PCR product. A sequence coding for His6 was added on the 3' primer. The PCR fragment was inserted in pMMB190-*araC*-*pbad* using *Sall* and *HindIII* site to generate pMMB190-*araC*-*pbad*-*hasR*-His6.

Table S7.7. Primers used in this study.

Primer	Collection ID	Sequence (5'>3')
<i>araC</i> <i>EcoRI</i> F	1595	AAAAGAATTCCGATGCATAATGTGCCTGTCAAATGG
<i>araC</i> <i>pBAD</i> <i>Sall</i> R	1596	AAAAGTCGACGAGAGTTGCGATAAAAAGCGTCAGG
<i>hasR</i> sig pep F <i>Sall</i>	1589	AAAAGTCGACCAAACGATGGAGTGTAGGCGC
<i>hasR</i> TonB Box His6 2 R	1593	AAAAAAGCTTTCAGTGGTGGTGGTGGTGGTGCCCGG GGGTTTCCTCGAGCATGTC

Cloned nucleotide sequence

(EcoRI)GAATTCCGATGCATAATGTGCCTGTCAAATGGACGAAGCAGGGATTCTGCAAAC
 CCTATGCTACTCCGTCAAGCCGTCAATTGTCTGATTTCGTTACCAATTATGACAACTTGAC
 GGCTACATCATTCACTTTTTTCTTCACAACCGGCACGGAAGCTCGCTCGGGCTGGCCCCG
 GTGCATTTTTTAAATACCCGCGAGAAATAGAGTTGATCGTCAAACCAACATTGCGACCG
 ACGGTGGCGATAGGCATCCGGGTGGTGTCTCAAAGCAGCTTCGCCTGGCTGATACGTT
 GGTCCTCGCGCCAGCTTAAGACGCTAATCCCTAACTGCTGGCGGAAAAGATGTGACAG
 ACGCGACGGCGACAAGCAAACATGCTGTGCGACGCTGGCGATATCAAATTGCTGTCT
 GCCAGGTGATCGCTGATGTAAGCAAGCCTCGCGTACCCGATTATCCATCGGTGGAT
 GGAGCGACTCGTTAATCGCTTCCATGCGCCGACGTAACAATTGCTCAAGCAGATTTATC
 GCCAGCAGCTCCGAATAGCGCCCTTCCCCTTGCCCGGCGTTAATGATTTGCCCAAACA
 GGTCGCTGAAATGCGGCTGGTGCCTTCATCCGGGCGAAAGAACCCTGATTGGCAA
 TATTGACGGCCAGTTAAGCCATTCATGCCAGTAGGCGCGCGGACGAAAGTAAACCCAC
 TGGTGATACCATTGCGGAGCCTCCGGATGACGACCGTAGTGATGAATCTCTCCTGGCG
 GAAACAGCAAATATCACCCGGTCGGCAAACAAATTCTCGTCCCTGATTTTTACCACC
 CCCTGACCGCGAATGGTGAGATTGAGAATATAACCTTTCATTCCCAGCGGTTCGGTCGAT
 AAAAAATCGAGATAACCGTTGGCCTCAATCGGCGTTAAACCCGCCACCAGATGGGCAT
 TAAACGAGTATCCCGGCAGCAGGGGATCATTTTGCCTTCAGCCATACTTTTCATACTC
 CCGCCATTCAGAGAAGAAACCAATTGTCCATATTGCATCAGACATTGCCGTCCTGCGT
 CTTTTACTGGCTCTTCTCGCTAACCAAACCGGTAACCCCGCTTATTAAGCATTCTGTA
 ACAAAGCGGGACCAAAGCCATGACAAAAACGCGTAACAAAAGTGTCTATAATCACGGCA
 GAAAAGTCCACATTGATTATTTGCACGGCGTCACACTTTGCTATGCCATAGCATTTTTAT
 CCATAAGATTAGCGGATCCTACCTGACGCTTTTTATCGCAACTCTCGTCGAC(SalI)CAA
 ACGATGGAGTGTAGGCGCTGTC**ATGAAACATCGTGGATGGAGTGCCGTGCGAGGCGG**
TCGCAAGGGGGCGCAACTGGCCCTGGGGCTGGGCTGGTCTGCTGGGAACGGCCG
CGCTACCGCTGCATGCGCAAGACGGGGCGGACTCGGCGAGCCAGCAGCAGACCGCG
CTGCGCCGGGTCCGGCTGGACATCCCGGCACAACCGCTGAACCGCGCCCTGCTGCG
ATTCGCCGAGCAGGCCGGGTCCAGGTGTTCTTCGACAGCCAGCGTTTCGCCGGTCT
CGGCAGCGCGGCGGTGCACGGCGAATACTTGCTGGCCGACGGCCTGAGCCAGATGC
TCCAGGGCAGCCGGTGAATACCGTTCTCCGGCAAGGACCAATTGAGCCTGATCC
GCGTCAGCCAGGACGACCTGGTGCAGATGTCGCCCTCGGTGATCTCCGCCGCGCGTC
CGGACGACTGGGTCTACCAGACGCCGCATTCGGTCAGCGTGATCGGCCGCGAGCAG
ATCGAGCGCAACCCGCCGCGGCATGCCGCCGACATGCTCGAGGAAACCCCGGGCA
 CCACCACCACCACCACTGAAAGCTT(HindIII)

The colors in the nucleotide sequence above correspond to the following sequence motifs:

AraC - regulates transcription of arabinose transport and catabolic operons

Pbad – also araBp, promoter activated in the presence of arabinose.

hasR promoter, ***hasR coding sequence***, His6 Tag, Stop codon

Cloned amino acid sequence

The corresponding HasR Aa sequence can be found below:

MKHRGWSAVRGGRKGAQLALGLGLVLLGTAALPLHAQDGADSASQQQTALRRVRLDIPAQ
PLNRALLRFAEQAGVQVFFDSQRFAGLGSAAVHGEYLLADGLSQMLQGSPVEYRFSGKDQ
LSLIRVSQDDLVMSPSVISAARPDDWVYQTPHSVSVIGREQUIERNPPRHAADMLEETPG

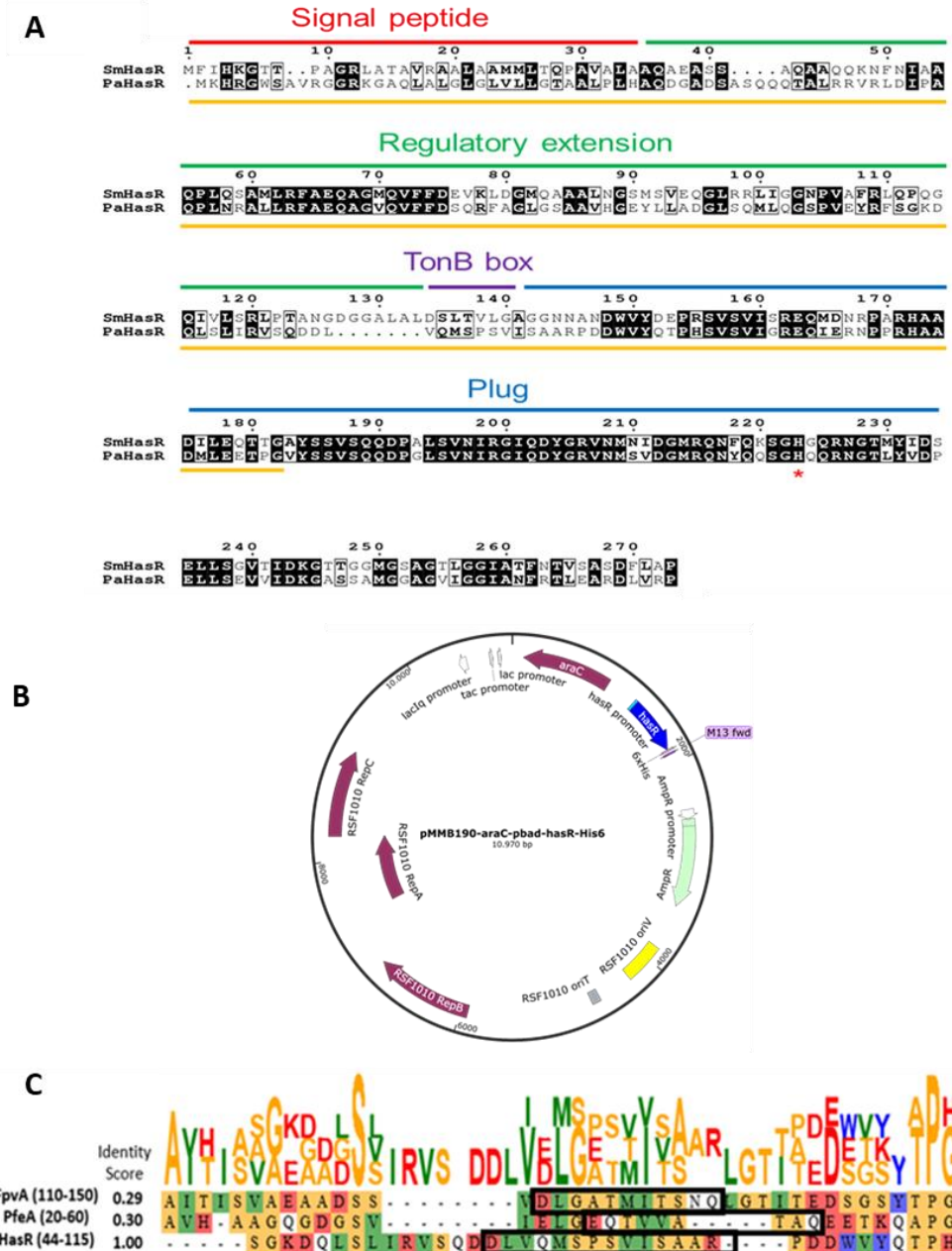


Figure S7.2. (A) Alignment of *S. marcescens* HasR (SmHasR) and *P. aeruginosa* HasR (PaHasR) N-terminal protein sequences. Black boxes indicate similar aa sequences, bold and white-boxed letters indicate an aa from a similar group (e.g. I and L or D and E). Domains of the SmHasR protein are represented by coloured lines. The TonB box (¹³⁰DSLTVLG¹³⁹) is indicated in purple. The cloned part of PaHasR protein (1-172 aa) is represented by a yellow line. The histidin residue indicated by a red-asterisk is essential for heme uptake.¹⁶ The alignment was performed using Clustal Omega and analysed with ESPrnt 3.0. **(B)** Plasmid for N-terminal HasR expression (uniprot: Q9HYJ7_PSEAE) cloned sequence: signal peptide - regulating extension - TonB box, details on cloning and sequence see above **(C)** Clustal alignment of reviewed *P. aeruginosa* TonB box sequences from FpvA (FPVA_PSEAE), PfeA (PFEA_PSEAE) and HasR (Q9HYJ7_PSEAE) from the Uniprot database with ClustalΩ.

Bacteria strain and growth conditions

The *P. aeruginosa* PAO1 bacteria expressing pMMB190-araC-pbad-*hasR*-His6 were first grown in LB medium containing carbenicillin overnight at 30°C. Then, they were washed and resuspended in iron-deficient CAA (casamino acid) medium containing 5 g.L⁻¹ low-iron CAA (Difco), 1.46 g.L⁻¹ K₂HPO₄.3H₂O and 0.25 g.L⁻¹ MgSO₄.7H₂O supplemented with carbenicillin, and grown overnight at 30°C. Afterward, bacteria were diluted at OD_{600nm} = 0.02 in fresh CAA medium with or without 1% arabinose and with or without 0.25 µM hemin in 96 well plates. Plates were incubated at 30°C, with shaking every 15 minutes in a microplate reader (Infinite M200, Tecan). Growth was followed by measuring the optical density at 600 nm every 30 minutes, for 25 h.

Table S7.8. Strains used in this study

Strain	Collection ID	Relevant characteristics	Reference
PAO1	PAO1	Wild-type strain	Stover et al. ¹⁷
PAO1 pbad- <i>hasR</i> -His6	PAS620	PAO1; pMMB190 - araC – pbad - <i>hasR</i> -His6	present work

Fe-Chrome Azurol S (CAS) assay¹

The Fe-chrome azurol S (FeCAS) assay was conducted following a known procedure¹⁸. All glassware needed for the assay was cleaned with concentrated hydrochloric acid and milliQ water. Water and aqueous solutions of iron(III) chloride (1 mM in 10 mM HCl, 150 μ L) and Chrome Azurol S (50 μ L, CAS) were added to an aqueous solution of hexadecyltrimethylammonium bromide (600 μ L HDTMA 10 mM). A buffer solution consisting of piperazine (431 mg, 5 mmol) and concentrated hydrochloric acid (625 μ L) in water (5 mL) was added. The resulting solution was diluted with dH₂O to a total volume of 10 mL. The stock solution used for the assay was generated by further addition of 5-sulfosalicylic acid dihydrate (10.2 mg, 40 μ mol). Solutions of the test compounds (15 μ M, 120 μ L each), as well as water (40 μ L) were added to 40 μ L of stock solution. The assay was conducted in technical triplicates in transparent, untreated 96-well plates. Absorbance from 300 to 800 nm was determined after 17 h using a plate reader, the curves were plotted and evaluated using Microsoft Excel 2016 and GraphPad Prism 9.

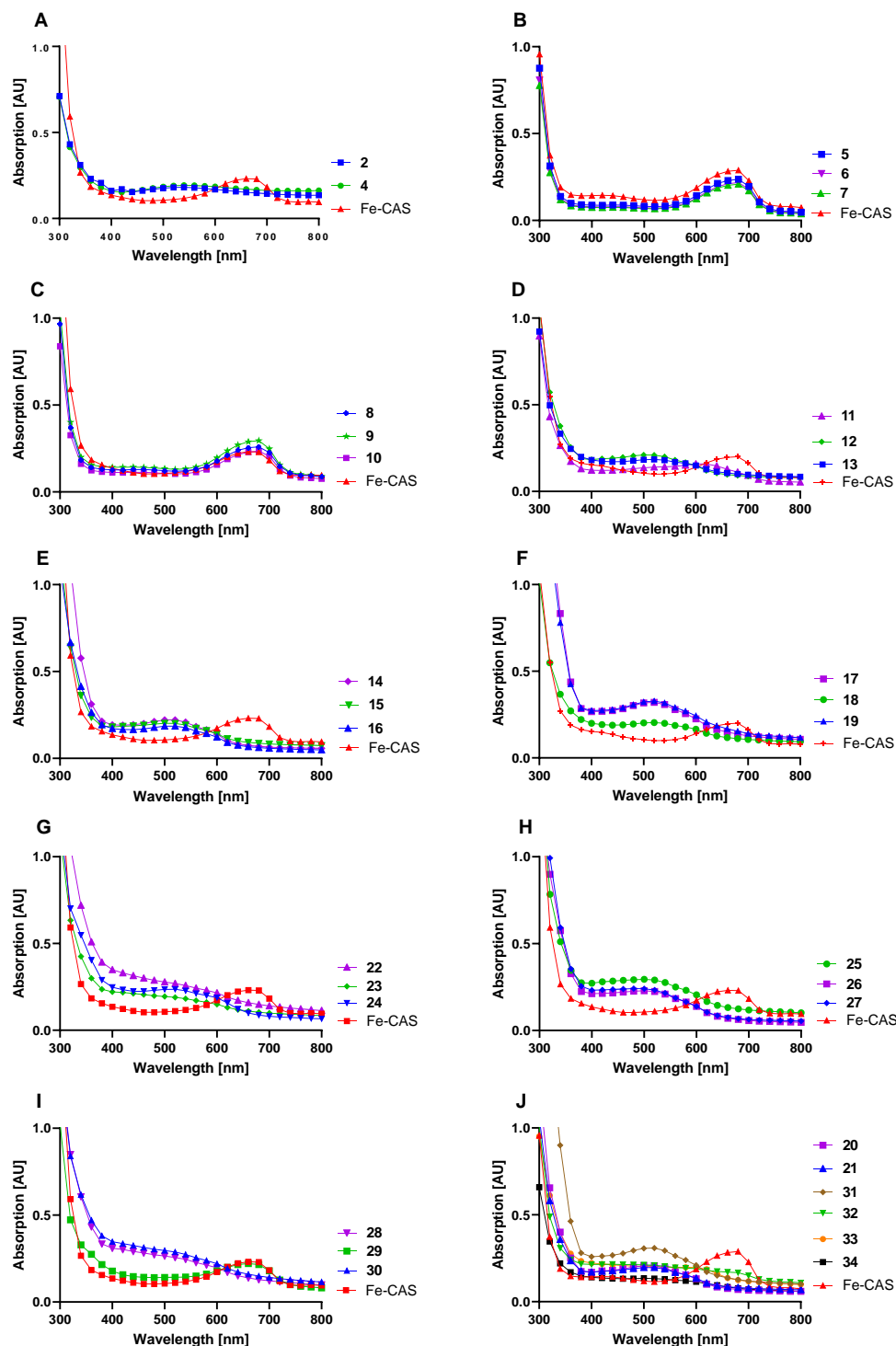


Figure S7.3. Absorbance spectra from 300-800 nm of Fe-CAS, the free unmodified TonB box peptides **5-10** and siderophore conjugates **11-34** upon incubation with the Fe-CAS complex for 17 hours. (A) DOTAM **2** and MECAM **4** (B) long, free peptides **5-7**, (C) short, free peptides **8-10**, (D) long, *N*-term. DOTAM conjugates **11-13**, (E) short, *N*-term. DOTAM conjugates **14-16**, (F) long *C*-term. DOTAM conjugates **17-18**, (G) long, *N*-term. MECAM conjugates **22-24**, (H) short, *N*-term. MECAM conjugates **25-27**, (I) long, *C*-term. MECAM conjugates **28-30**, (J) special conjugates **20, 21, 31-34**. All plots with a FeCAS reference curve, ($n = 3$).

Table S7.9. Iron-binding capability measured by the Fe-CAS assay and antimicrobial activity in mutant *P. aeruginosa* strains.

#	Name	Fe-CAS result
2	DOTAM	P
4	MECAM	P
5	FpvA (l)	N
6	PfeA (l)	N
7	HasR (l)	N
8	FpvA (s)	N
9	PfeA (s)	N
10	HasR (s)	N
11	FpvA (l)-N-D	P
12	PfeA (l)-N-D	P
13	HasR (l)-N- D	P
14	FpvA (s)-N-D	P
15	PfeA (s)-N-D	P
16	HasR (s)-N- D	P
17	FpvA (l)-C-D	P
18	PfeA (l)-C-D	P
19	HasR (l)-C-D	P
20	PfeA (l)-C-D-Ac	P
21	PfeA (l)-DS-C-D	P
22	FpvA (l)-N-M	P
23	PfeA (l)-N-M	P
24	HasR (l)-N-M	P
25	FpvA (s)-N-M	P
26	PfeA (s)-N-M	P
27	HasR (s)-N- M	P
28	FpvA (l)-C-M	P
29	PfeA (l)-C-M	P
30	HasR (l)-C-M	P
31	PfeA (l)-C-M-Ac	P
32	PfeA (l)-DS-C-M	P
33	FpvA-C-catechol	P
34	PfeA-C-catechol	P

P = positive FeCAS result, absorbance shift (blue to red), N = negative. (l) = long, (s) = short, D = DOTAM and M = MECAM, CAT = catechol.

Antimicrobial susceptibility assays

The *P. aeruginosa* strains used in this study are listed in Table S1. Evaluation of the different compounds activities was carried out in the iron-deficient CAA medium (casamino acid medium, composition: 5 g l⁻¹ low-iron CAA (Difco), 1.46 g l⁻¹ K₂HPO₄ 3H₂O, 0.25 g l⁻¹ MgSO₄ 7H₂O) using the two-fold serial dilution method with an inoculum of 10⁵ bacteria per mL. *P. aeruginosa* $\Delta pvdF\Delta pchA$ strains were first grown overnight at 37°C in LB broth, then washed and resuspended in CAA medium. The strains were grown for two successive overnight cultures at 30°C in iron-deficient CAA medium, with a dilution of the cells of 1/10. Data were reported as MIC, which reflects the lowest concentration of antibiotic that inhibits the visible cell growth after a 24 h or 48 h incubation at 30 °C.

RT-qPCR analysis in PAO1 wildtype and mutant strains

RT-PCR was used to follow specific gene transcription as previously described.^{19, 20} Bacteria (PAO1 or $\Delta pvdF\Delta pchA$) were grown in CAA medium and in 50 mL Falcons, for 8 h, at 30°C, in the presence or absence of 10 μ M of the tested compounds and with vigorous shaking. Aliquot of 2.5 x 10⁸ cells from these cultures were added to two volumes of RNAprotect Bacteria Reagent (Qiagen) and exactly the same protocol was used as previously described (Perraud *et al.*, 2020). Primers efficiency were determined using serially diluted genomic DNA and the double ΔC_T method was used to analyze qPCR data. The primers used are summarized in Table S3.

Growth kinetic in the absence and presence of vectors and conjugates.

Bacteria were first grown overnight in LB, washed and then grown in CAA at 30 °C. This culture was washed and resuspended in CAA medium at an OD_{600 nm} of 0.02 and 200 μ L was distributed in 96 well U-shaped plates (Greiner). Fresh, sterile-filtered aqueous solutions of the tested compounds were added to the different strains tested, at a final concentration of 10 μ M. OD_{600 nm} was monitored in an Infinite M200 (TECAN, Austria) plate reader for 48 h, with regular agitation and incubation temperature set to 30°C.

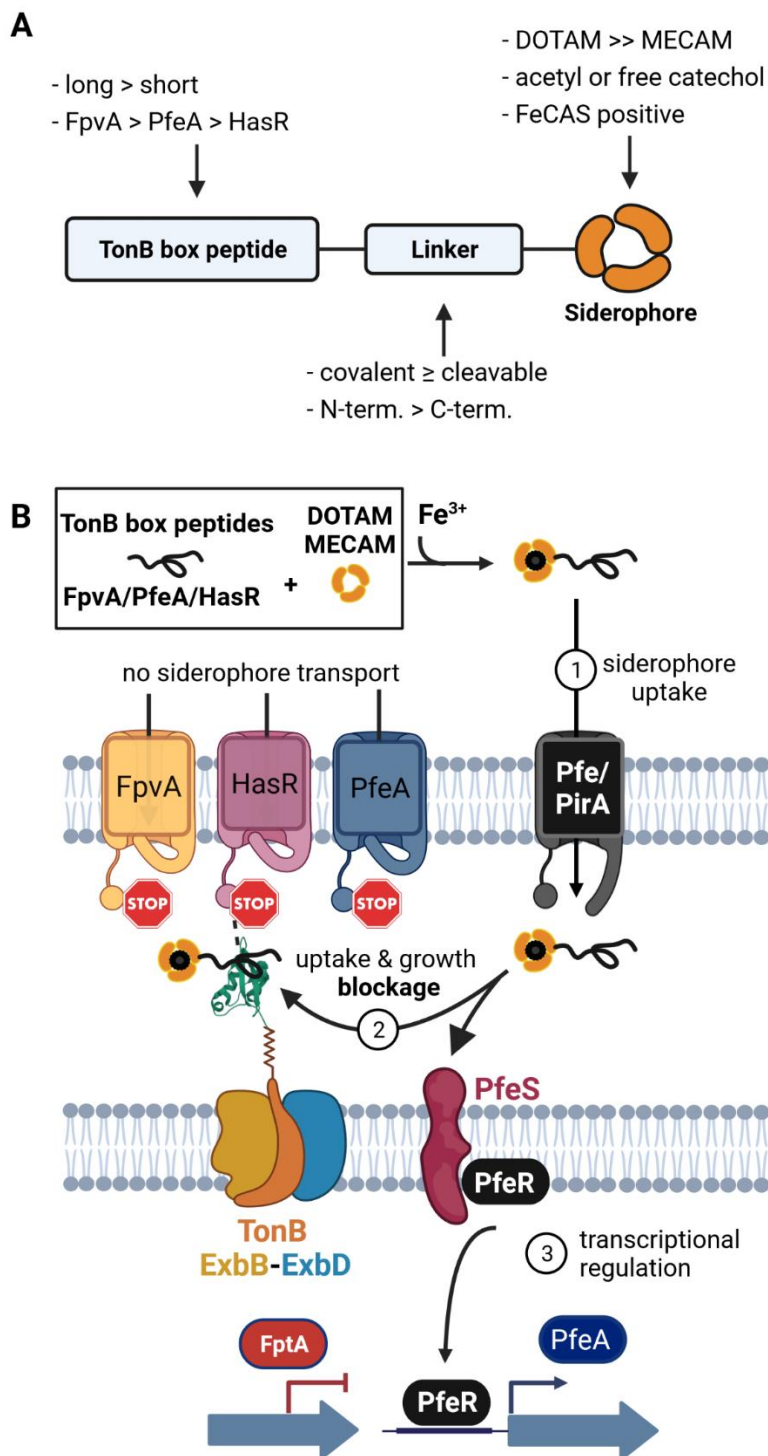


Figure S7.4. Structure activity relationships (A) and mechanistic summary (B) on TonB box peptide-siderophore conjugates.

Supplementary References

1. Ferreira, K.; Hu, H.-Y.; Fetz, V.; Prochnow, H.; Rais, B.; Müller, P. P.; Brönstrup, M., Multivalent siderophore–DOTAM conjugates as theranostics for imaging and treatment of bacterial infections. *Angew. Chem. Int. Ed.* **2017**, *56* (28), 8272-8276.
2. Peukert, C.; Langer, L. N. B.; Wegener, S. M.; Tutov, A.; Bankstahl, J. P.; Karge, B.; Bengel, F. M.; Ross, T. L.; Brönstrup, M., Optimization of artificial siderophores as ⁶⁸Ga-complexed PET tracers for *in vivo* imaging of bacterial infections. *J. Med. Chem.* **2021**, *64* (16), 12359-12378.
3. Pinkert, L.; Lai, Y.-H.; Peukert, C.; Hotop, S.-K.; Karge, B.; Schulze, L. M.; Grunenberg, J.; Brönstrup, M., Antibiotic conjugates with an artificial MECAM-Based siderophore are potent agents against Gram-positive and Gram-negative bacterial pathogens. *J. Med. Chem.* **2021**, *64* (20), 15440-15460.
4. Svedhem, S.; Hollander, C.-Å.; Shi, J.; Konradsson, P.; Liedberg, B.; Svensson, S. C. T., Synthesis of a Series of Oligo(ethylene glycol)-terminated alkanethiol amides designed to address structure and stability of biosensing interfaces. *J. Org. Chem.* **2001**, *66* (13), 4494-4503.
5. Pinkert, L. Synthese von Siderophor-Antibiotika-Konjugaten als neuartige antibakterielle Wirkstoffe. Gottfried Wilhelm Leibniz Universität Hannover, Dissertation, 2021.
6. Song, Q.; Yang, J.; Hall, S. C. L.; Gurnani, P.; Perrier, S., Pyridyl disulfide reaction chemistry: An efficient strategy toward redox-responsive cyclic peptide–polymer conjugates. *ACS Macro Lett.* **2019**, *8* (10), 1347-1352.
7. Bernatowicz, M. S.; Matsueda, R. E. I.; Matsueda, G. R., Preparation of Boc-[S-(3-nitro-2-pyridinesulfonyl)]-cysteine and its use for unsymmetrical disulfide bond formation. *Int. J. Pept. Protein Res.* **1986**, *28* (2), 107-112.
8. Moynié, L.; Milenkovic, S.; Mislin, G. L. A.; Gasser, V.; Mallocci, G.; Baco, E.; McCaughan, R. P.; Page, M. G. P.; Schalk, I. J.; Ceccarelli, M.; Naismith, J. H., The complex of ferric-enterobactin with its transporter from *Pseudomonas aeruginosa* suggests a two-site model. *Nat. Comm.* **2019**, *10* (1), 3673.
9. Brillet, K.; Journet, L.; Célia, H.; Paulus, L.; Stahl, A.; Pattus, F.; Cobessi, D., A β -strand lock exchange for signal transduction in TonB-dependent transducers on the basis of a common structural motif. *Structure* **2007**, *15* (11), 1383-1391.

10. Nikaido, H., Molecular basis of bacterial outer membrane permeability revisited. *Microbiol. Mol. Biol. Rev.* **2003**, *67* (4), 593-656.
11. Smith, A. D.; Modi, A. R.; Sun, S.; Dawson, J. H.; Wilks, A., Spectroscopic determination of distinct heme ligands in outer-membrane receptors PhuR and HasR of *Pseudomonas aeruginosa*. *Biochemistry* **2015**, *54* (16), 2601-2612.
12. Cobessi, D.; Celia, H.; Folschweiller, N.; Schalk, I. J.; Abdallah, M. A.; Pattus, F., The crystal structure of the pyoverdine outer membrane receptor FpvA from *Pseudomonas aeruginosa* at 3.6Å resolution. *J. Mol. Biol.* **2005**, *347* (1), 121-134.
13. Zheng, T.; Bullock, J. L.; Nolan, E. M., Siderophore-mediated cargo delivery to the cytoplasm of *Escherichia coli* and *Pseudomonas aeruginosa*: Syntheses of monofunctionalized enterobactin scaffolds and evaluation of enterobactin–cargo conjugate uptake. *J. Am. Chem. Soc.* **2012**, *134* (44), 18388-18400.
14. Suits, M. D. L.; Pal, G. P.; Nakatsu, K.; Matte, A.; Cygler, M.; Jia, Z., Identification of an *Escherichia coli*; O157:H7 heme oxygenase with tandem functional repeats. *Proc. Natl. Acad. Sci. U.S.A.* **2005**, *102* (47), 16955.
15. Ankenbauer, R. G.; Quan, H. N., FptA, the Fe(III)-pyochelin receptor of *Pseudomonas aeruginosa*: A phenolate siderophore receptor homologous to hydroxamate siderophore receptors. *J. Bacteriol* **1994**, *176* (2), 307-319.
16. Létoffé, S.; Wecker, K.; Delepierre, M.; Delepelaire, P.; Wandersman, C., Activities of the *Serratia marcescens* heme receptor *HasR* and isolated plug and beta-barrel domains: The beta-barrel forms a heme-specific channel. *J. Bacteriol* **2005**, *187* (13), 4637-45.
17. Stover, C. K.; Pham, X. Q.; Erwin, A. L.; Mizoguchi, S. D.; Warrenner, P.; Hickey, M. J.; Brinkman, F. S. L.; Hufnagle, W. O.; Kowalik, D. J.; Lagrou, M.; Garber, R. L.; Goltry, L.; Tolentino, E.; Westbrook-Wadman, S.; Yuan, Y.; Brody, L. L.; Coulter, S. N.; Folger, K. R.; Kas, A.; Larbig, K.; Lim, R.; Smith, K.; Spencer, D.; Wong, G. K. S.; Wu, Z.; Paulsen, I. T.; Reizer, J.; Saier, M. H.; Hancock, R. E. W.; Lory, S.; Olson, M. V., Complete genome sequence of *Pseudomonas aeruginosa* PAO1, an opportunistic pathogen. *Nature* **2000**, *406* (6799), 959-964.
18. Schwyn, B.; Neilands, J. B., Universal chemical assay for the detection and determination of siderophores. *Anal. Biochem.* **1987**, *160*, 47 – 56.
19. Gasser, V.; Baco, E.; Cunrath, O.; August, P. S.; Perraud, Q.; Zill, N.; Schleberger, C.; Schmidt, A.; Paulen, A.; Bumann, D.; Mislin, G. L. A.; Schalk, I. J., Catechol

siderophores repress the pyochelin pathway and activate the enterobactin pathway in *Pseudomonas aeruginosa*: an opportunity for siderophore–antibiotic conjugates development. *Environ. Microbiol.* **2016**, *18* (3), 819-832.

20. Gross, H.; Loper, J. E., Genomics of secondary metabolite production by *Pseudomonas* spp. *Nat. Prod. Rep.* **2009**, *26* (11), 1408-1446.

8. Publication 6: Bridging diagnostics and therapy: Towards theranostic DOTAM-based sideromycins as potent and selective effectors for bacterial imaging and antimicrobial therapy

This chapter was included as a manuscript and will soon be submitted as an article to a peer-reviewed, scientific journal:

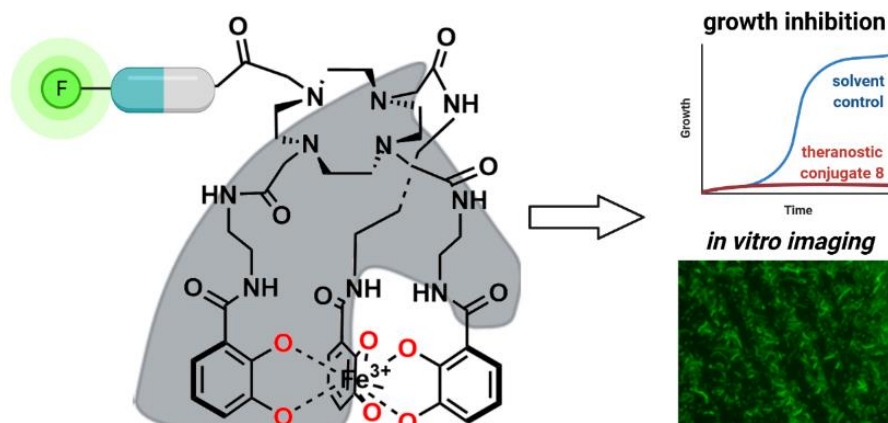
Carsten Peukert, Katharina Rox, Sven-Kevin Hotop, Bianka Karge, Mark Brönstrup

”Bridging diagnostics and therapy: Towards theranostic DOTAM-based sideromycins as potent and selective effectors for bacterial imaging and antimicrobial therapy”.

Abstract

The rise of antimicrobial resistance, especially in Gram-negative bacteria, calls for novel diagnostics and antibiotics. In order to efficiently penetrate their double layered cell membrane, we conjugated the antibiotics daptomycin, vancomycin and sorangicin A, with potent activity in Gram-positive bacteria, to catechol siderophores, which are actively internalized by the bacterial iron uptake machinery. LC-MS/MS uptake measurements of sorangicins verified that conjugation led to a 100-525 enhanced uptake into bacteria compared to the free drug. However, the transfer to the cytosol was insufficient, which explains their lack of antibiotic efficacy. In contrast, potent antimicrobial effects were observed for the daptomycin-DOTAM conjugate **7** (~1 μM) against multidrug resistant *A. baumannii*. A modification with a fluorescent cyanin-7 label aside the daptomycin warhead furnished the theranostic **13** that retained its *in vitro* antibiotic activity and obtained the ability to label a range of Gram-negative bacteria, as demonstrated by microscopy and fluorescence assays. Moreover, **13** and the cyanin-7 imaging conjugate **14** were stable in plasma and had low plasma protein binding and cytotoxicity.

Table of content graphic



8.1 Introduction

The escalating antibiotic resistance has become a major, global health challenge that will probably prevail in the decades to come. The consequences of antimicrobial resistance caused 1.27 million deaths in 2019 alone, and there is a severe economic damage in addition.¹ An innovation gap over the past 3-4 decades, that followed the so-called golden era of antibiotics, laid the foundation for this scenario.² Among the last approved and clinically used antibiotics were the oxazolidinones and the lipopeptide antibiotic daptomycin. In 2017, the World Health Organization's (WHO) published a priority list of antibiotic resistant bacteria, that named multidrug-resistant *A. baumannii*, *P. aeruginosa*, and *Enterobacteriaceae* as strains of critical concern.³ The need for novel antibiotics, drug delivery systems, and innovative bacterial diagnostics for those Gram-negative species is regarded as particularly high.⁴ Scientists have exploited bacterial transporters and their actively transported substrates to increase the accumulation of various payloads for bacterial imaging or antibacterial treatment into bacterial pathogens.⁵ Such transporters play a role in the competition for iron between a host organism and the invading pathogenic bacteria and for the outcome of an infection.^{6,7} The insolubility of Fe-(III) required prokaryotes to evolve sequestration processes that involve the active transport of so-called siderophores, iron chelators of medium molecular weight. Gram-negative bacteria, recognize ferric siderophore complexes by chelator-specific outer membrane receptors (OMR). Binding to the OMR initiates the energy-dependent translocation of the complex into the periplasm and often to the inner membrane.⁶ Many bacteria commit 'iron thievery' by hijacking the siderophores from other bacterial species (xenosiderophores); also synthetic siderophore mimics are transported by OMRs.^{8,9} To prevent the usage of their siderophores by other species, some microbes secrete covalent conjugates of antibiotic molecules and siderophores that are called sideromycins and assure important growth advantages to the producer strain. In the following, numerous groups leveraged the potential of siderophores as molecular 'Trojan Horses' to smuggle diagnostic and therapeutic payloads into the bacterial cell (Figure 8.1A), thereby overcoming the reduced permeability into Gram-negative prokaryotes. Most conjugates employed well characterized antibiotics (e.g. β -lactams) and intended to expand their antibiotic activity by an improved, bacteria-specific active uptake of the effector.¹⁰ Accordingly, siderophore conjugation may repurpose Gram-positive only antibiotics that show limited bacterial accumulation due to their high molecular weight, overall charge and lipophilicity, and unfold their efficacy to combat Gram-negative infections. The potent siderophore conjugates of the bulky lipopeptides daptomycin and teicoplanin, with nanomolar minimal inhibitory concentration (MIC) values in multidrug resistant *A. baumannii*, impressively confirmed the feasibility of the above strategy.^{11, 12, 13, 14} In some cases, the iron-binding catechol moieties were masked transiently by acetylation, to avoid *in vivo* deactivation of the iron chelator by catechol-O-methyltransferases.¹⁵

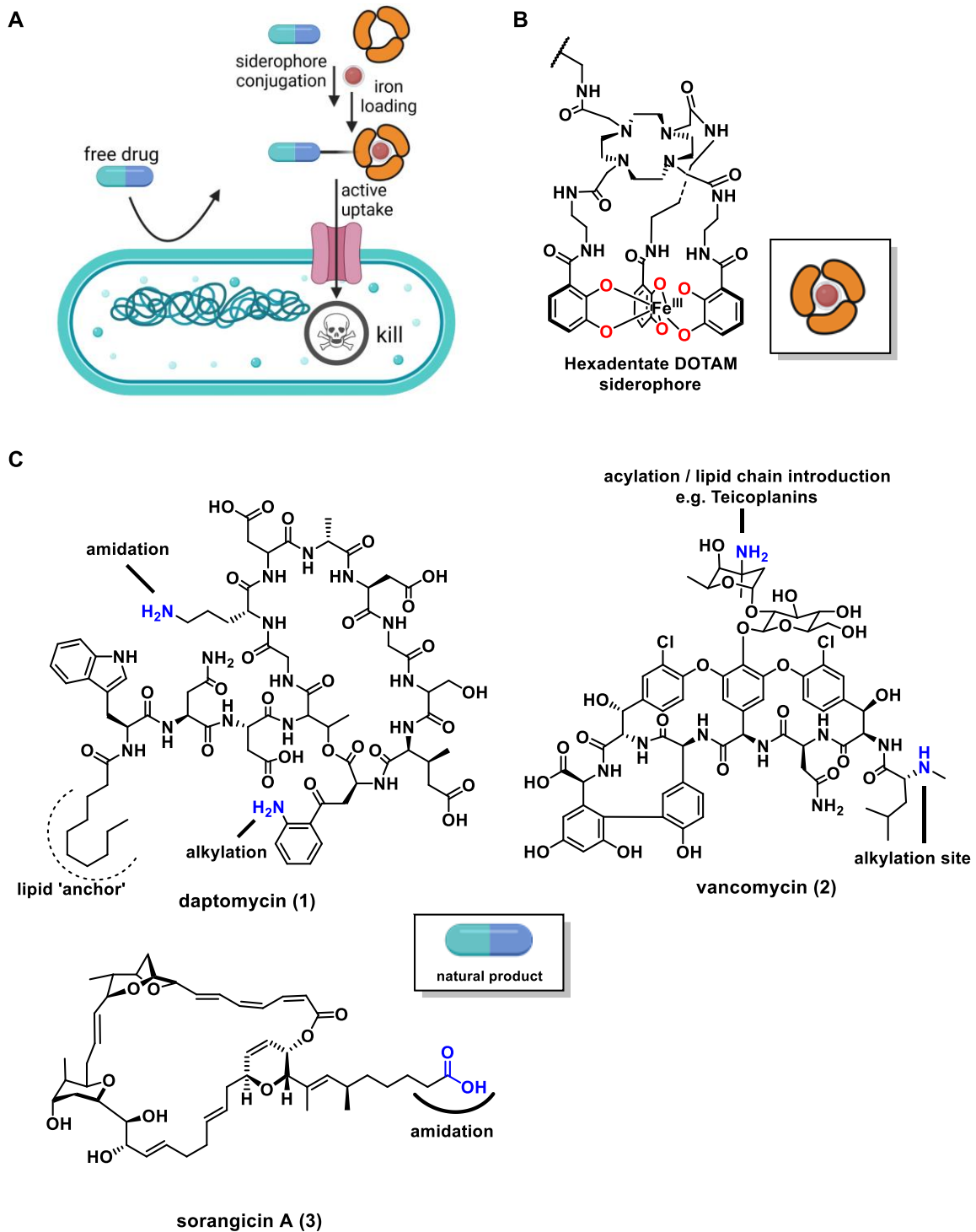


Figure 8.1. Conjugation of siderophores to natural products with exclusive activity in Gram-positive bacteria. (A) Schematic depiction of enhanced bacterial accumulation and antibiotic activity through siderophore conjugation. (B) Structure of the synthetic hexadentate DOTAM siderophore. (C) The lipopeptide daptomycin, the glycopeptide vancomycin and the macrolide sorangicin A are potent antibiotics against Gram-positive bacteria, but inactive against Gram-negative pathogens. Possible modification sites for a conjugation to 'Trojan Horses' are highlighted in blue.^{16, 17, 18}

Recently we developed the DOTAM (1,4,7,10-tetra azacyclododecane-1,4,7,10-tetra acetic acid amide) core as an effective carrier for bacteria-specific imaging as well as for bacterial killing (Figure 8.1B).^{19, 20-22} While a conjugate enrichment into pathogenic microbes via active transporters for either therapeutic or diagnostic purposes has been leveraged widely, a combination of both functionalities to yield a theranostic that can treat as well as monitor an infection herd simultaneously has remained largely unexplored.^{23, 24, 25} Therefore, we aimed to equip a potent antimicrobial with a fluorescent imaging modality to afford such a theranostic molecule. In this study, we describe the synthesis, antibiotic potential and accumulation of high molecular weight DOTAM-natural product conjugates against Gram-negative pathogens.

8.2 Results and discussion

We selected the lipopeptide antibiotic daptomycin (**1**, 1620.7 Da), the glycopeptide vancomycin (**2**, 1447.4 Da) and the macrolide sorangicin A (sorA **3**, 806.5 Da) which are all very potent antibiotics with submicromolar minimal inhibitory concentration (MIC) values, but are solely effective in Gram-positive bacteria (Figure 8.1C). In brief, daptomycin interacts with the lipid phosphatidylglycerol (PG) in a calcium-dependent manner, while its lipid anchor allows the insertion into the Gram-positive cell membrane, which disturbs intracellular homeostasis.^{26, 27, 28} Vancomycin exerts its effect in the periplasm by binding to the C-terminal D-Ala-D-Ala motif of the Gram-positive cell wall precursors leading to an inhibition of the peptidoglycan crosslinking by the transpeptidase.^{29,30} The myxobacterial natural product sorangicin inhibits, like the well-studied ansamycin rifamycin, the DNA-dependent RNA polymerase in the cytosol by blocking the RNA transcript elongation at a length of 2-3 nucleotides.³¹ Crystallographic studies indicated that sorangicin A adopts a globular structure upon binding to the bacterial RNA polymerase (RNAP).^{18, 31, 32} We hypothesized that the attachment of a full DOTAM chelator to any of the effectors could impact their target binding ability due to the steric demand of the chelator. For this reason, either a full DOTAM siderophore or a monocatechol were attached to the peripheral moieties of all effectors (Figure 8.2). The alkyne-tagged DOTAM siderophore **18** was synthesized as previously described, and the alkyne-tagged monocatechol **16** was afforded over two steps from **15** (Figure S8.1).¹⁹ Previous structure–activity relationship (SAR) studies demonstrated that amide coupling of the ornithine side chain in daptomycin was well tolerated and in turn antibacterial activity in Gram-positive bacteria was retained.²⁷ Similarly, a vancomycin modification at the peripheral disaccharide entity was found to be well tolerated.^{33,34} Therefore, daptomycin **1** and vancomycin **2** were modified at their primary amine moieties with NHS- or PFP-activated 6-azido hexanoic acid in yields of 46% and 25%, respectively, and then coupled to siderophores through copper-catalyzed azide alkyne cycloadditions (CuAACs).

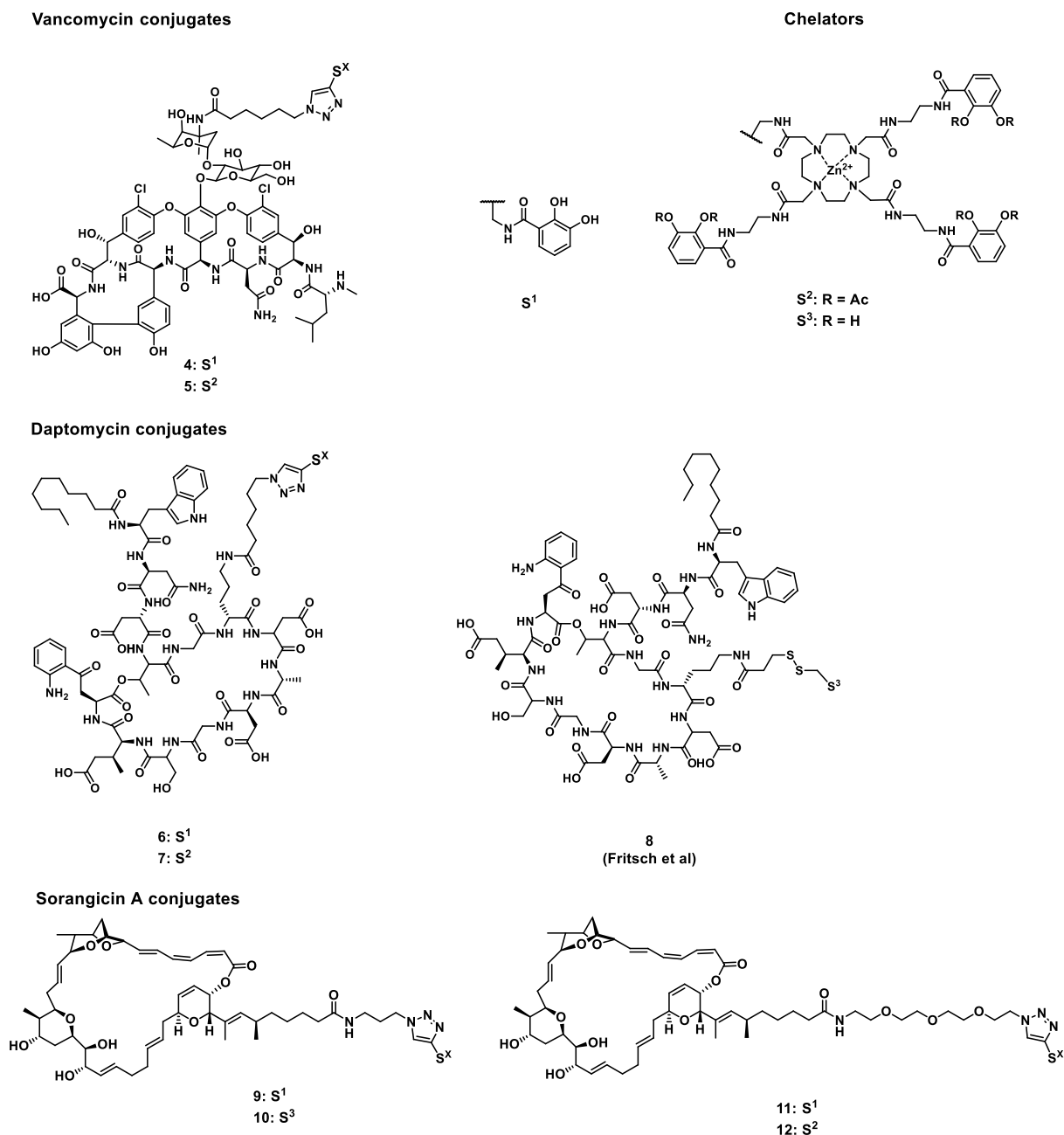


Figure 8.2. Structures of synthetic vancomycin, daptomycin and sorangicin A conjugates.

The vancomycin-DOTAM conjugate **4** and vancomycin-catechol conjugate **5** were synthesized over four to six steps with 5-20% overall yield. The daptomycin-DOTAM conjugate **6** and daptomycin-catechol conjugate **7** were synthesized over four to six steps with 23 and 19% overall yield, respectively. Also the daptomycin-DOTAM conjugate **8** with a cleavable disulfide linker could be afforded over seven steps with 17% yield, as reported recently.²² In the case of sorangicin A, the molecule's acid moiety was modified either with an azido propan-1-amine or with an azido-PEG₃-amine linker, which was then conjugated through CuAAC to **16** or **18**. The alkyl-linked monocatechol **9** and DOTAM **10** could be afforded over two steps each with 28%

and 43% overall yield, respectively. Sorangicin A conjugates with a longer NH₂-PEG₃-N₃ linker could be synthesized via a similar route with 79% (catechol **11**) and 84% (DOTAM **12**) yield over two steps. We next determined the antimicrobial activities of the conjugates that reflect their ability to translocate into bacteria, but also to inhibit their targets. The MICs of all conjugates were evaluated in iron-depleted, cation adjusted medium (IDCAM). Siderophore conjugation did not enhance the activity of vancomycin conjugates **4** and **5**. In contrast, the daptomycin-DOTAM conjugates **7** and **8** exhibited potent, single digit micromolar MICs in two MDR *A. baumannii* strains in CaCl₂ supplemented media (Table 8.1). The cleavable disulfide linker in **8** did not lead to a significant improvement in activity compared to the non-cleavable linker of **7**. In accordance with previous reports.¹² Possibly the ferric complex formation required for uptake via siderophore transporter in the case of the daptomycin monocatechol **6** only lead to a moderate increase in potency. The MICs against *S. aureus* were generally higher for the conjugates than for the unmodified drugs **1** or **2**.¹¹ Overall, the increased potency of two conjugates against *A. baumannii* demonstrates the ability of the DOTAM siderophore to improve translocation into this species. However, although a universal OMR binding motif in form of catechols was presented, activity could not be obtained against all Gram-negative bacteria.

Table 8.1. Antimicrobial activity of daptomycin **1**, vancomycin **2** and their conjugates **1-8**.^a

Strain	4	5	6	7	8	dapto	vanco	cef
<i>E. coli</i> DSM1116	>20	>20	>20	>20	>20	>20	>20	0.1
<i>S. aureus</i> DSM11822	21.8 ± 7.3	6.1 ± 2.7	14.0 ± 4.9	5.5 ± 1.9	11.8	0.3	0.5	>8.5
<i>K. pneumoniae</i> DSM11678	>20	>20	>20	>20	>20	>20	>20	0.2
<i>A. baumannii</i> DSM30007	>20	>20	12.3 ± 4.1	1.6 ± 0.6	1.48	>20	>20	0.1
<i>A. baumannii</i> DSM30008	>20	>20	>20	1.3	2.5 ± 0.7	>20	>20	0.1
<i>P. aeruginosa</i> DSM117	>20	>20	>20	>20	>20	>20	>20	0.2
<i>E. faecium</i> DSM20477	>20	>20	>20	>20	>20	0.9	0.3	>8.5

^a values in [μM], n = 3, in iron-depleted, cation adjusted medium (IDCAM), 110 μg/ml CaCl₂ addition²⁶ for the daptomycins **1**, **6-8**. Daptomycin (dapto), vancomycin (vanco) and cefiderocol (cef) were used as standard antibiotics.³⁵

The covalent chelator conjugation to the RNAP inhibitor sorangicin did not enhance activity in Gram-negative bacteria; the moderate activity of **3** against *E. coli* was even lowered by conjugation. In Gram-positive strains, **9**, **10**, **11** and **12** retained activity in comparison to unmodified sorangicin A, although the potency was lowered (Table 8.2). In general, the modification of the carboxylic acid of **3** with a linker by amide formation consistently reduced activity.

Table 8.2. Antimicrobial activity of sorangicin A (**3**) and its siderophore conjugates **9-12**.^a

Strain	9	10	11	12	sorA (3)	cef
<i>E. coli</i> DSM1116	>20	>20	>20	>20	3.13	0.1
<i>S. aureus</i> RKI	18	2	-	-	0.15	-
<i>S. aureus</i> DSM11822	37.5	0.78	6.7	3.5	0.2	>8.5
<i>A. baumannii</i> DSM30007	-	-	>20	>20	>20	0.2
<i>A. baumannii</i> DSM30008	-	-	>20	>20	>20	0.1
<i>P. aeruginosa</i> DSM117	>20	>20	>20	>20	>20	0.2
<i>E. faecium</i> DSM20477		-	6.7	3.5	0.15	>8.5

^a values in [μ M], n = 3, in iron-depleted, cation adjusted medium (IDCAM). Sorangicin A (sorA) and cefiderocol (cef) were used as standard antibiotics.

The lack of a potency boost upon chelator conjugation to sorangicins could be attributed to three major reasons: (i) The chemical modification impeded target engagement, (ii) the uptake into bacteria was inefficient or (iii) transport across the outer membrane occurred, but the conjugates could not reach the cellular compartment of their target in sufficient quantity. To investigate the latter two options, an uptake assay based on a combination of cellular fractionation with liquid chromatography coupled to mass spectrometry (LC/MS/MS) was conducted in siderophore-deficient *E. coli* Δ entA in iron-free media, with or without 10 μ M FeCl₃ supplementation.³⁶ The bacteria were incubated with **3**, **9**, or **10** (50 μ g/ml) for 10 minutes and perforated by an osmotic shock to release the periplasmic fraction by centrifugation. A sonication-centrifugation procedure yielded separate membrane and cytosolic fractions. Mass

spectrometric quantitation revealed a strong enrichment of the sorangicin A conjugates in the membrane and periplasmic fractions, with minor accumulation in the cytoplasmic fractions. The addition of ferric iron increased the accumulation of the conjugates **9** and **10** inside of the bacteria, but expectedly had no effect on the accumulation of the unmodified natural product due to the missing siderophore entity (Figure 8.3).

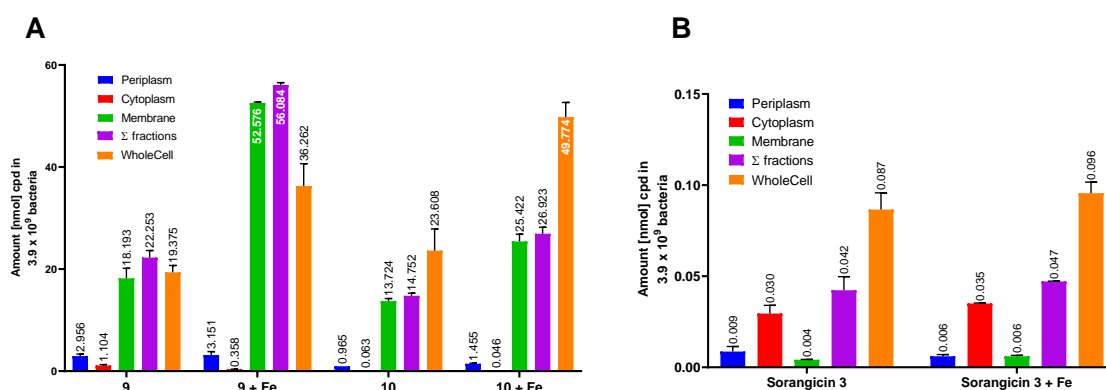


Figure 8.3. Intracellular accumulation of **3**, **9** and **10** in *E. coli*. Following the incubation of *E. coli* Δ entA with the test compounds ($\pm 10 \mu\text{M FeCl}_3$), the bacterial subcompartments were fractionated, and their amount was quantified by LC-MS/MS, $n = 2$.

Generally, the conjugation to a chelator increased compound lipophilicity and manifested in higher membrane accumulation. The comparison of the cytoplasmic amounts of the conjugates with those of the unmodified natural product **3** showed an increased accumulation of **9** (11-36-fold) and **10** (~ two fold) at their target site in the cytosol. In the periplasm **9** and **10** displayed a 100-525-fold enrichment compared to free sorangicin A. The data suggest that already the addition of a monocatechol and also of a DOTAM chelator boosted the accumulation of the natural product significantly. This underlines the general ability of the DOTAM to act as a molecular 'Trojan Horse', efficiently transporting cargo into bacterial cells. However, the relative ratio of compound amounts in the cytoplasm compared to the periplasm was lowered upon conjugation: Whereas **3** had a cytoplasm:periplasm ratio of 300-500%, we found only 11-37% for **9** and 3-7% for **10**. Because the periplasm has a much smaller volume compared to the cytoplasm, the differences in concentrations c were even more pronounced: The ratio $c_{\text{cyto}}/c_{\text{peri}}$ was 27-45:1 for **3**, but only 0.8-3:1 for **9**, and 0.2-0.5:1 for **10**. We conclude that the DOTAM-based siderophore mimics function well with respect to the transport across the outer membrane, but their efficiency with respect to the cytoplasmic delivery of sorangicins is insufficient.

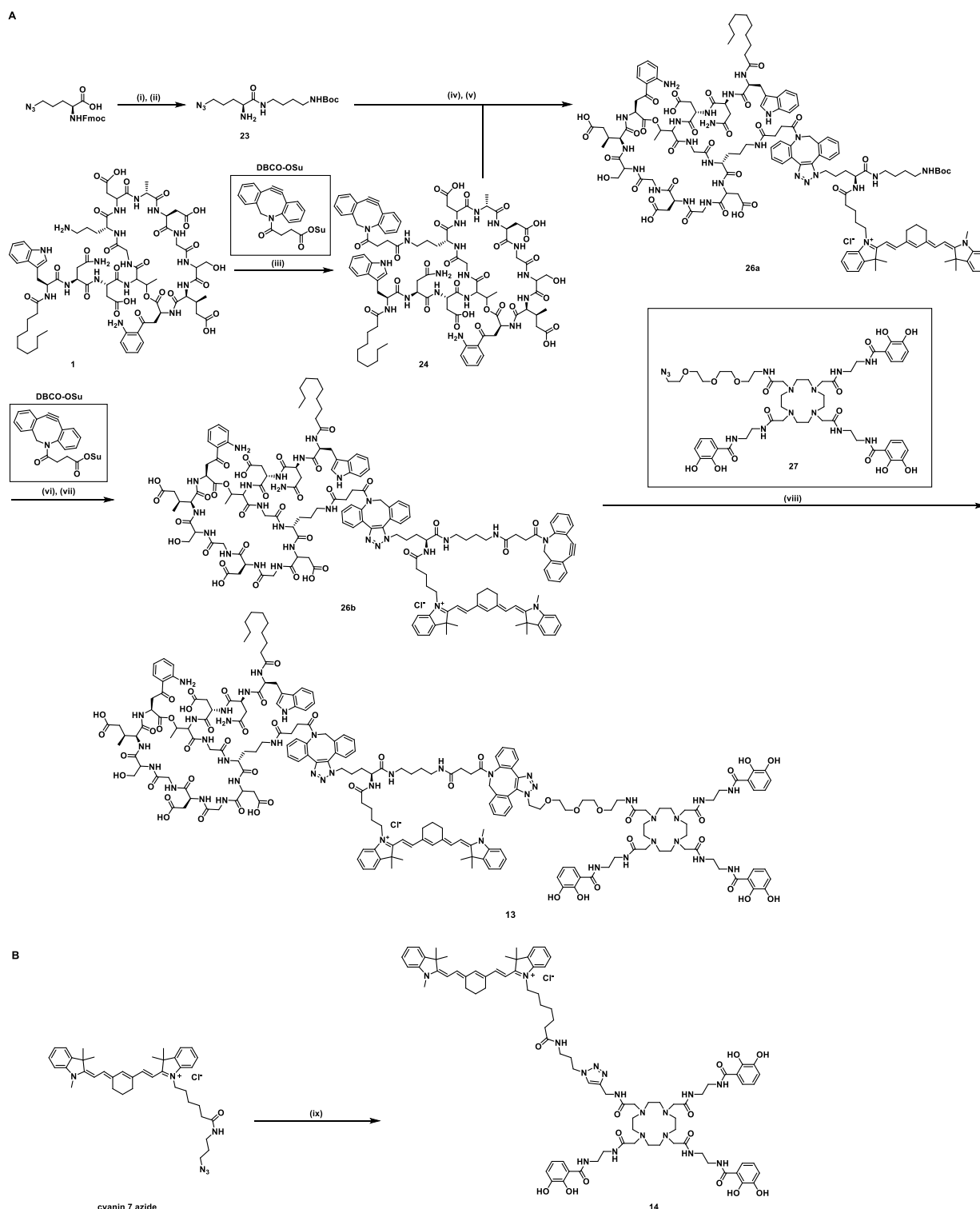


Figure 8.4. Synthesis of the DOTAM-based theranostic **13** and the imaging conjugate **14**. (A) Theranostic **13**: (i) *N*-Boc-1,6 diaminohexane, HATU, DIPEA, DCM, DMF, 22 °C, (ii) 20% diethylamine in ACN, 22 °C, 2h, 87% over two steps, (iii) **DBCO-OSu**, DIPEA, DMSO, 23 °C, overnight, crude quant., (iv) **cyanin 7-OSu**, DCM, DIPEA, 23 °C, 2 h, (v) MeOH, overnight, 23 °C, quant. over two steps, (vi) 20% TFA, DCM, 23 °C, (vii) **DBCO-OSu**, DCM, DMF, DIPEA, 23 °C, 67% over two steps, (viii) MeOH, 23 °C, overnight, 85%, (B) Imaging conjugate **14**: (ix) **19**, Zn(OAc)₂, CuSO₄, sodium ascorbate, DMF/milliQ H₂O, (1:1), TBTA, 23 °C to 30°C, 2 h, 80%.

From the first panel of compounds, we selected the potent daptomycin DOTAM conjugate **7** as a blueprint for the construction of a theranostic conjugate. In particular, we envisioned a combination of the DOTAM-conjugated daptomycin warhead with an infrared, fluorescent cyanin-7 imaging label to visualize and treat *A. baumannii* infections simultaneously (Figure 8.4). We feared the combination of a bulky DOTAM carrier, a fluorophore, together with the big polypeptide daptomycin in one conjugate would lead to significantly reduced antibiotic efficacy due to steric hindrance by the label and the siderophore. For this reason, a conjugate with a longer linker between the siderophore and the crosslinker with the attached fluorophore and antibiotic was designed to permit for an unperturbed target binding and retained activity compared to **7**. The synthesis commenced with the amide coupling with the mono-Boc-protected 1,6-diaminohexane to the artificial amino acid, whose Fmoc group was subsequently cleaved to afford amine **23**. Reaction of the primary amine with cyanin-7 active succinimidyl ester and strain-promoted azide-alkyne cycloaddition (SPAAC) with DBCO-daptomycin **24** yielded the difunctionalized fragment **26a**.

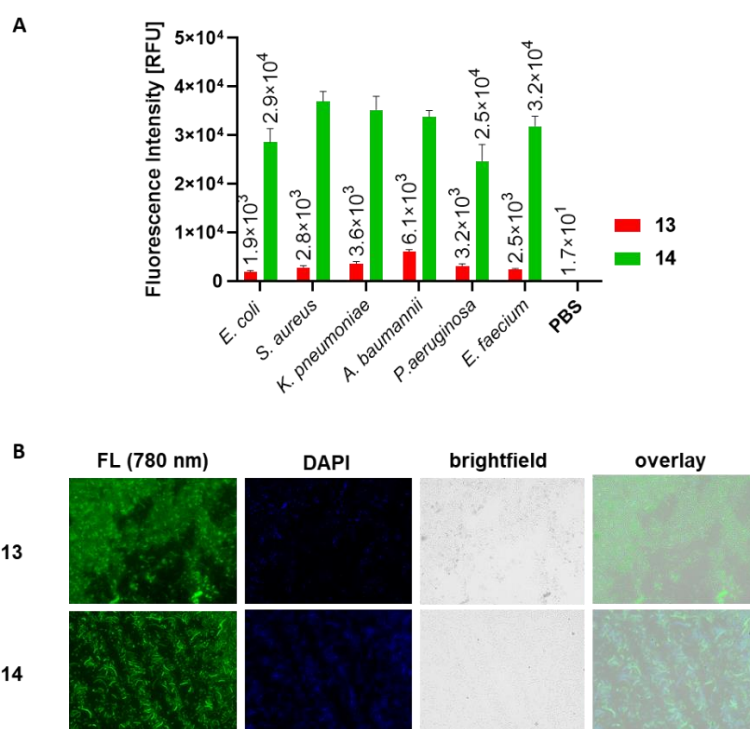


Figure 8.5. Labeling of bacterial pathogens with fluorescent DOTAM conjugates **13** and **14**. **(A)** Fluorescence intensity [RFU] of ESKAPE pathogens after incubation with **13** and **14** ($10 \mu\text{M}$) in iron-depleted, cation-adjusted medium (IDCAM), with $\lambda_{\text{Ex}}=735 \text{ nm}$, $\lambda_{\text{Em}}=780 \text{ nm}$, error bars correspond to \pm standard error of mean (SEM), $n = 3$. **(B)** Fluorescence microscopy images (FL 780 nm) of *A. baumannii* (DSM30007) after incubation with **13** and **14** ($10 \mu\text{M}$) in IDCAM. Also DAPI fluorescence, the brightfield image and the overlay of all three images are shown. Representative examples of two experiments are given. Full ESKAPE panel microscopy pictures for **14** are given in the supporting information.

Boc group cleavage and modification with *N*-hydroxy succinamide-activated DBCO gave amide **26b** in 67% yield over two steps. Another SPAAC with the previously published azido DOTAM **27** furnished the full theranostic conjugate **13** in 32% yield over seven synthetic steps for the longest linear sequence.³⁷ CuAAC of commercial cyanin-7 azide to alkyne **19** gave imaging conjugate **14** in 80% yield.

We tested whether the theranostic **13** and the imaging probe **14** were able to label iron-starved, MDR *A. baumannii*. A quantitative read-out displayed a rather homogenous fluorescence signal for **14** in all ESKAPE pathogens (*E. coli*, *S. aureus*, *K. pneumoniae*, *A. baumannii*, *P. aeruginosa*, *E. faecium*) panel. The signal from **13** with its much higher molecular weight was much lower than for **14**. Surprisingly, the theranostic had a roughly two to three fold higher fluorescence signal for its target species *A. baumannii* than for the other bacteria (p value <0.0001). The labelling of *A. baumannii* bacteria by **13** and **14** was also confirmed by fluorescence microscopy experiments (Figure 8.5). For the imaging probe **14** that gave higher intensities in the plate assay, microscopy pictures were obtained for the whole ESKAPE panel (Figure S8.5). Varying staining efficiencies were observed and in many cases, subpopulations within a given strain were labeled differentially. This heterogeneity on the single cell level might reflect varying conjugate uptake or growth phases.

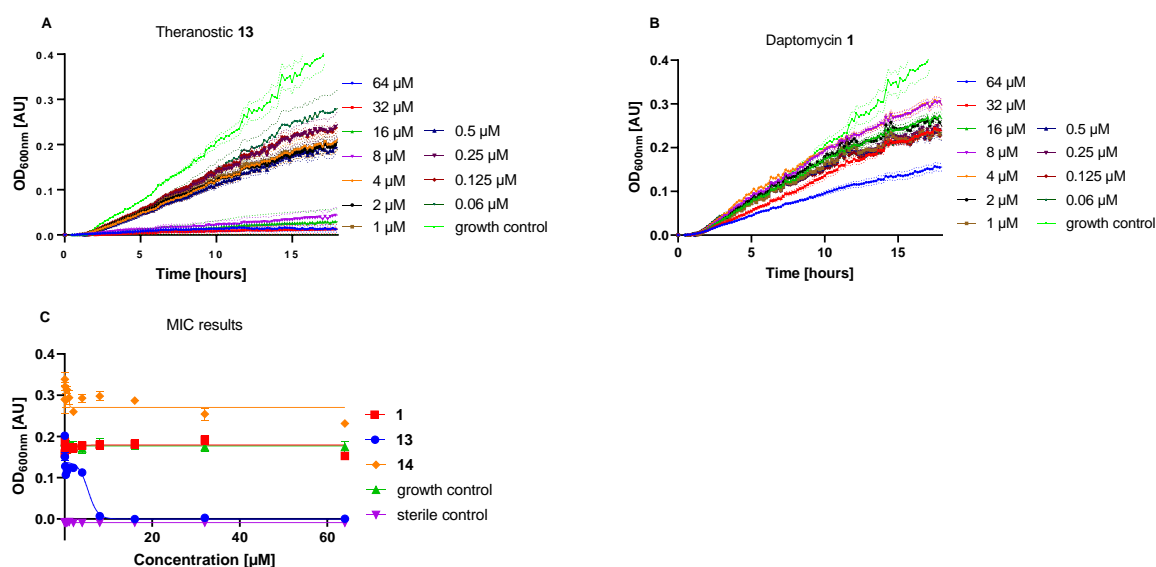


Figure 8.6 Cellular antimicrobial activity of daptomycin **1** and theranostic **13**. Growth kinetic (OD_{600nm}) of (A) theranostic **13** and (B) daptomycin **1** in iron-depleted, cation-adjusted medium (IDCAM, with 110 μg/mL CaCl₂), over 18 hours at 37 °C, dotted lines correspond to ± standard error of mean (SEM), n=3. Minimal inhibitory concentration assay of theranostic **13** (C) and free daptomycin **1** (D) in iron-depleted, cation-adjusted medium (IDCAM, with 110 μg/mL CaCl₂), without shaking at 37 °C, error bars correspond to ± standard error of mean (SEM), n=3. MIC for the positive control ciprofloxacin are deposited in Figure S8.6.

Next, we aimed to evaluate the antimicrobial activity of **13** and **14** under iron-depleted conditions against *A. baumannii* (DSM30007). Conjugates were evaluated two-fold: (i) either in an 18 hour growth kinetic with shaking or (ii) in a single endpoint measurement after 18 hours without shaking. Expectedly, **14** did not affect microbial growth, while the growth control and the control antibiotics had activity in the expected ranges (Figure S8.6). Despite the moderate growth reduction observed for free daptomycin at the highest concentration, no concentration could inhibit growth completely, confirmed by the single point measurement (Figure 8.6B and D). In contrast the theranostic **13** reduced bacterial growth prominently in the kinetic as well as in the endpoint experiment at a concentration of 8 to 16 μM . This corresponds to a ca. eight fold increase in MIC compared to conjugate **7** without the imaging label. Thus the attachment of the cyanin-7 dye had a negative effect on either target binding or accumulation. Yet the residual, potent activity against *A. baumannii* encouraged us to examine the compound for cytotoxicity, plasma protein binding and plasma stability.

Table 8.3. Plasma stability, plasma protein binding (compound **14**, **26** and **26a**) and cytotoxicity in four eukaryotic cells of the conjugates **13**, **14** and free daptomycin **1**.

	1	14	26a	26
PPB human [%]	98.75 \pm 0.1	94.53 \pm 0.5	91.56 \pm 3.7	82.60 \pm 14.2
Plasma stability				
mouse [min]	> 240	> 240	> 240	> 240
Plasma stability				
human [min]	> 240	> 240	> 240	> 240

	Cytotoxicity [μM]				
	1	13	14	staurosporin	auranofin
L929 cells	64	64	64	<0.064	0.1
A549 cells	>64	64	64	0.05	0.1
KB-3-1 cells	>64	>64	64	0.004	0.1
MCF-7 cells	>64	>64	>64	0.002	0.05

The cytotoxicity of the theranostic **13**, the imaging compound **14** and daptomycin **1** was tested in four eukaryotic cell lines L929, A549, KB-3-1, and MCF-7. All conjugates as well as daptomycin were non-cytotoxic up to concentrations $\geq 64 \mu\text{M}$. Moreover, we assessed the stability of the imaging conjugate **14** and theranostic intermediates **26/26a** as well as daptomycin **1** in mouse and human plasma to assess whether the compounds are sufficiently stable when administered *in vivo*. None of the conjugates or theranostic fragments showed liabilities with respect to plasma stability, as all compounds were stable for more than 240 min (Table 8.3). Next, we determined the plasma protein binding for human species, as only the free fraction may exert an effect as a theranostic. Whereas more than 98 % of **1** was bound to plasma proteins, imaging compound **14** showed a lower plasma protein binding of less than 95 %. Furthermore, both intermediates **26** and **26a** exhibited a plasma protein binding of around 90 % and around 82 %, respectively. Taken together the theranostic **13** and the imaging conjugate **14** showed good cellular activity with regard to labelling and therapeutic properties but also regarding stability and cytotoxicity that implies future evaluation of these compounds in *in vivo* rodent models.

8.3 Conclusion

We explored whether the antibiotic potency of three well-established classes of natural products against Gram-negative bacteria could be enhanced by conjugation to a DOTAM triscatecholate or a monocatechol unit. Most conjugates had reduced activity in Gram-positive, and also the Gram-negative activity was only enhanced in few cases. For sorangicin conjugates, we demonstrated by quantitative uptake measurements that the siderophore improved the translocation across the outer membrane significantly, but the passage across the inner membrane to the cytosol remained insufficient. The finding is in line with a general observation for most covalent siderophore conjugates, i.e. that antibiotic activity is by large poor when cytosolic targets are addressed. This implies that for siderophore conjugates acting in the cytosol, the passage across the inner membrane needs to be considered – a mechanism that is mostly not understood and neglected. Alternatively, such conjugates may require or strongly benefit from an intracellular release mechanism for the antibiotic from the carrier to assure activity. The daptomycin DOTAM conjugate **7** had potent activity against antibiotic resistant *A. baumannii* and thus was equipped with a cyanin-7 fluorophore to yield the theranostic **13**. This large conjugate retained potency and could detect, like imaging compound **14**, Gram-negative and gram-positive ESKAPE bacteria in culture. Both conjugates showed no cytotoxicity, beneficial stability and thus are interesting candidates for further *in vivo* experiments in smaller rodent infection models. In sum, we expanded the application of the DOTAM siderophore as a versatile and functional carrier even for bulky payloads such as daptomycin or sorangicin A, for therapeutic and diagnostic purposes.¹⁹ Future attempts could,

in accordance with previous studies, incorporate a radioactive label e.g. copper-64 directly at the cyclen instead of the bulky cyanin-7, which in turn would facilitate synthesis and reduce structural alterations.

Acknowledgements

We thank Dr. Kirsten Harmrolfs and Christel Kakoschke for the measurement of NMR samples and Ulrike Beutling for the mass spectrometric measurement of probes. We are thankful to Marc Stadler and the microbial drug unit at the Helmholtz Centre for Infection Research for providing us with sorangicin A.

Funding information

We acknowledge funding by the DFG (grant number: BR 3572/4-1) and the Joint Program Initiative on Antimicrobial Resistance (JPI AMR, grant number: 01KI1825). C. P. thanks the “Fonds der chemischen Industrie” for a scholarship. K.R. receives support from the German Centre for Infection Research (DZIF, former TTU 09.710, now TTU 09.719).

References

1. Murray, C. J. L.; Ikuta, K. S.; Sharara, F.; Swetschinski, L.; Robles Aguilar, G.; Gray, A.; (...); Naghavi, M., Global burden of bacterial antimicrobial resistance in 2019: a systematic analysis. *The Lancet* **2022**.
2. Theuretzbacher, U.; Gottwalt, S.; Beyer, P.; Butler, M.; Czaplewski, L.; Lienhardt, C.; Moja, L.; Paul, M.; Paulin, S.; Rex, J. H.; Silver, L. L.; Spigelman, M.; Thwaites, G. E.; Paccaud, J. P.; Harbarth, S., Analysis of the clinical antibacterial and antituberculosis pipeline. *Lancet Infect. Dis.* **2019**, *19* (2), e40-e50.
3. Tacconelli, E.; Carrara, E.; Savoldi, A.; Harbarth, S.; Mendelson, M.; Monnet, D. L.; Pulcini, C.; Kahlmeter, G.; Kluytmans, J.; Carmeli, Y.; Ouellette, M.; Outtersson, K.; Patel, J.; Cavalieri, M.; Cox, E. M.; Houchens, C. R.; Grayson, M. L.; Hansen, P.; Singh, N.; Theuretzbacher, U.; Magrini, N., Discovery, research, and development of new antibiotics: the WHO priority list of antibiotic-resistant bacteria and tuberculosis. *Lancet Infect. Dis.* **2018**, *18* (3), 318-327.
4. Fleming, K. A.; Horton, S.; Wilson, M. L.; Atun, R.; DeStigter, K.; Flanigan, J.; Sayed, S.; Adam, P.; Aguilar, B.; Andronikou, S.; Boehme, C.; Cherniak, W.; Cheung, A. N. Y.; Dahn, B.; Donoso-Bach, L.; Douglas, T.; Garcia, P.; Hussain, S.; Iyer, H. S.; Kohli, M.; Labrique, A. B.; Looi, L.-M.; Meara, J. G.; Nkengasong, J.; Pai, M.; Pool, K.-L.; Ramaiya, K.; Schroeder, L.; Shah, D.; Sullivan, R.; Tan, B.-S.; Walia, K., The *Lancet* Commission on diagnostics: transforming access to diagnostics. *The Lancet* **2021**.
5. Klahn, P.; Bronstrup, M., Bifunctional antimicrobial conjugates and hybrid antimicrobials. *Nat. Prod. Rep.* **2017**, *34* (7), 832-885.
6. Miethke, M.; Marahiel, M. A., Siderophore-based iron acquisition and pathogen control. *Microbiol. Mol. Biol. Rev.* **2007**, *71* (3), 413 – 451.
7. Kramer, J.; Özkaya, Ö.; Kümmerli, R., Bacterial siderophores in community and host interactions. *Nat. Rev. Microbiol.* **2020**, *18* (3), 152-163.
8. Ji, C.; Miller, M. J., Siderophore–fluoroquinolone conjugates containing potential reduction-triggered linkers for drug release: synthesis and antibacterial activity. *BioMetals* **2015**, *28* (3), 541-551.
9. Zheng, T.; Nolan, E. M., Enterobactin-mediated delivery of beta-lactam antibiotics enhances antibacterial activity against pathogenic *Escherichia coli*. *J. Am. Chem. Soc.* **2014**, *136* (27), 9677-9691.
10. Kim, A.; Kutschke, A.; Ehmman, D. E.; Patey, S. A.; Crandon, J. L.; Gorseth, E.; Miller, A. A.; McLaughlin, R. E.; Blinn, C. M.; Chen, A.; Nayar, A. S.; Dangel, B.; Tsai, A. S.; Rooney, M. T.; Murphy-Benenato, K. E.; Eakin, A. E.; Nicolau, D. P., Pharmacodynamic profiling of a siderophore-conjugated monocarbam in

- Pseudomonas aeruginosa*: assessing the risk for resistance and attenuated efficacy. *Antimicrob. Agents Chemother.* **2015**, *59* (12), 7743-7752.
11. Ghosh, M.; Miller, P. A.; Mollmann, U.; Claypool, W. D.; Schroeder, V. A.; Wolter, W. R.; Suckow, M.; Yu, H.; Li, S.; Huang, W.; Zajicek, J.; Miller, M. J., Targeted antibiotic delivery: Selective siderophore conjugation with daptomycin confers potent activity against multidrug resistant *Acinetobacter baumannii* both *in vitro* and *in vivo*. *J. Med. Chem.* **2017**, *60* (11), 4577 – 4583.
 12. Ghosh, M.; Lin, Y.-M.; Miller, P. A.; Möllmann, U.; Boggess, W. C.; Miller, M. J., Siderophore conjugates of aptomycin are potent Inhibitors of carbapenem resistant strains of *Acinetobacter baumannii*. *ACS Infect. Dis.* **2018**, *4* (10), 1529 – 1535.
 13. Ghosh, M.; Miller, P. A.; Miller, M. J., Antibiotic repurposing: bis-catechol- and mixed ligand (bis-catechol-mono-hydroxamate)-teicoplanin conjugates are active against multidrug resistant *Acinetobacter baumannii*. *J. Antibiot.* **2020**, *73* (3), 152-157.
 14. Pinkert, L.; Lai, Y. H.; Peukert, C.; Hotop, S. K.; Karge, B.; Schulze, L. M.; Grunenberg, J.; Brönstrup, M., Antibiotic conjugates with an artificial MECAM-based siderophore are potent agents against Gram-positive and Gram-negative bacterial pathogens. *J. Med. Chem.* **2021**, *64* (20), 15440-15460.
 15. Ohi, N.; Aoki, B.; Kuroki, T.; Matsumoto, M.; Kojima, K.; Nehashi, T., Semisynthetic beta-lactam antibiotics. III. Effect on antibacterial activity and comt-susceptibility of chlorine-introduction into the catechol nucleus of 6-[(R)-2-[3-(3,4-dihydroxybenzoyl)-3-(3-hydroxypropyl)-1-ureido]-2- phenylacetamido]penicillanic acid. *J. Antibiot.* **1987**, *40* (1), 22-28.
 16. Chow, H. Y.; Po, K. H. L.; Jin, K.; Qiao, G.; Sun, Z.; Ma, W.; Ye, X.; Zhou, N.; Chen, S.; Li, X., Establishing the structure–activity relationship of daptomycin. *ACS Med. Chem. Lett.* **2020**, *11* (7), 1442-1449.
 17. Mühlberg, E.; Umstätter, F.; Kleist, C.; Domhan, C.; Mier, W.; Uhl, P., Renaissance of vancomycin: approaches for breaking antibiotic resistance in multidrug-resistant bacteria. **2020**, *66* (1), 11-16.
 18. Jansen, R.; Schummer, D.; Irschik, H.; Höfle, G., Antibiotics from gliding bacteria, XLII. Chemical modification of sorangicin A and structure - activity relationship I: Carboxyl and hydroxyl group derivatives. *Liebigs Ann. Chem.* **1990**, *1990* (10), 975-988.
 19. Ferreira, K.; Hu, H.-Y.; Fetz, V.; Prochnow, H.; Rais, B.; Müller, P. P.; Brönstrup, M., Multivalent siderophore–DOTAM conjugates as theranostics for imaging and treatment of bacterial infections. *Angew. Chem. Int. Ed.* **2017**, *56* (28), 8272-8276.
 20. Peukert, C.; Langer, L. N. B.; Wegener, S. M.; Tutov, A.; Bankstahl, J. P.; Karge, B.; Bengel, F. M.; Ross, T. L.; Brönstrup, M., Optimization of artificial siderophores as

- ⁶⁸Ga-complexed PET tracers for *in vivo* imaging of bacterial infections. *J. Med. Chem.* **2021**, *64* (16), 12359-12378.
21. Peukert, C.; Popat Gholap, S.; Green, O.; Pinkert, L.; van den Heuvel, J.; van Ham, M.; Shabat, D.; Brönstrup, M., Enzyme-activated, chemiluminescent siderophore-dioxetane probes enable the selective and highly sensitive detection of bacterial pathogens. *Angew. Chem. Int. Ed.* **2022**, e202201423.
 22. Fritsch, S.; Gasser, V.; Peukert, C.; Pinkert, L.; Kuhn, L.; Perraud, Q.; Normant, V.; Brönstrup, M.; Schalk, I., Uptake mechanisms and regulatory responses to MECAM- and DOTAM-based artificial siderophores and their antibiotic conjugates in *Pseudomonas aeruginosa*. *ACS Infect. Dis.* **2022**.
 23. Pandey, A.; Savino, C.; Ahn, S. H.; Yang, Z.; Van Lanen, S. G.; Boros, E., Theranostic gallium siderophore ciprofloxacin conjugate with broad spectrum antibiotic potency. *J. Med. Chem.* **2019**, *62* (21), 9947-9960.
 24. Nosrati, R.; Abnous, K.; Alibolandi, M.; Mosafer, J.; Dehghani, S.; Taghdisi, S. M.; Ramezani, M., Targeted SPION siderophore conjugate loaded with doxorubicin as a theranostic agent for imaging and treatment of colon carcinoma. *Sci. Rep.* **2021**, *11* (1), 13065.
 25. Pfister, J.; Petrik, M.; Bendova, K.; Matuszczak, B.; Binder, U.; Misslinger, M.; Kühbacher, A.; Gsaller, F.; Haas, H.; Decristoforo, C., Antifungal siderophore conjugates for theranostic applications in invasive pulmonary aspergillosis using low-molecular TAFC scaffolds. *J. Fungi* **2021**, *7* (7), 558.
 26. Ho, S. W.; Jung, D.; Calhoun, J. R.; Lear, J. D.; Okon, M.; Scott, W. R.; Hancock, R. E.; Straus, S. K., Effect of divalent cations on the structure of the antibiotic daptomycin. *Eur. Biophys. J.* **2008**, *37* (4), 421-433.
 27. Heidary, M.; Khosravi, A. D.; Khoshnood, S.; Nasiri, M. J.; Soleimani, S.; Goudarzi, M., Daptomycin. *J. Antimicrob. Chemother.* **2017**, *73* (1), 1-11.
 28. Grein, F.; Müller, A.; Scherer, K. M.; Liu, X.; Ludwig, K. C.; Klöckner, A.; Strach, M.; Sahl, H.-G.; Kubitscheck, U.; Schneider, T., Ca²⁺-daptomycin targets cell wall biosynthesis by forming a tripartite complex with undecaprenyl-coupled intermediates and membrane lipids. *Nat. Commun.* **2020**, *11* (1), 1455.
 29. Wu, Z.-C.; Cameron, M. D.; Boger, D. L., Vancomycin C-terminus guanidine modifications and further insights into an added mechanism of action imparted by a peripheral structural modification. *ACS Infect. Dis.* **2020**, *6* (8), 2169-2180.
 30. Okano, A.; Isley, N. A.; Boger, D. L., Peripheral modifications of [Ψ[CH₂NH]Tpg₄]vancomycin with added synergistic mechanisms of action provide durable and potent antibiotics. *Proc. Natl. Acad. Sci.* **2017**, *114* (26), E5052-E5061.

31. Campbell, E. A.; Pavlova, O.; Zenkin, N.; Leon, F.; Irschik, H.; Jansen, R.; Severinov, K.; Darst, S. A., Structural, functional, and genetic analysis of sorangicin inhibition of bacterial RNA polymerase. *EMBO J.* **2005**, *24* (4), 674-682.
32. Jansen, R.; Schummer, D.; Irschik, H.; Höfle, G., ChemInform Abstract: Antibiotics from gliding bacteria. Part 42. Chemical modification of sorangicin A and structure-activity relationship. Part 1. Carboxyl and hydroxyl group derivatives. *ChemInform* **2010**, *22*.
33. Ge, M.; Chen, Z.; Russell, H.; Onishi, Kohler, J.; Silver, L. L.; Kerns, R.; Fukuzawa, S.; Thompson, C.; Kahne, D., Vancomycin derivatives that inhibit peptidoglycan biosynthesis without binding α -Ala- α -Ala. *Science* **1999**, *284* (5413), 507-511.
34. Kerns, R.; Dong, S. D.; Fukuzawa, S.; Carbeck, J.; Kohler, J.; Silver, L.; Kahne, D., The role of hydrophobic substituents in the biological activity of glycopeptide antibiotics. *J. Am. Chem. Soc.* **2000**, *122* (50), 12608-12609.
35. El-Mady, A.; Mortensen, J. E., The bactericidal activity of ampicillin, daptomycin, and vancomycin against ampicillin-resistant *Enterococcus faecium*. *Diag. Mic. Inf. Dis.* **1991**, *14* (2), 141 – 145.
36. Prochnow, H.; Fetz, V.; Hotop, S.-K.; García-Rivera, M. A.; Heumann, A.; Brönstrup, M., Subcellular quantification of uptake in Gram-negative bacteria. *Anal. Chem.* **2019**, *91* (3), 1863-1872.
37. Peukert, C.; Langer, L. N. B.; Wegener, S. M.; Tutov, A.; Bankstahl, J. P.; Karge, B.; Bengel, F. M.; Ross, T. L.; Brönstrup, M., Optimization of artificial siderophores as ^{68}Ga -complexed PET tracers for *in vivo* imaging of bacterial infections. *J. Med. Chem.* **2021**.
38. Rackov, G.; Shokri, R.; De Mon, M. Á.; Martínez-A., C.; Balomenos, D., The role of IFN- β during the course of sepsis progression and its therapeutic potential. *Front. Immunol.* **2017**, *8*.
39. Hughes, L. D.; Rawle, R. J.; Boxer, S. G., Choose your label wisely: Water-soluble fluorophores often interact with lipid bilayers. *PLoS one* **2014**, *9* (2), e87649.
40. Patel, N.; Cardone, K.; Grabe, D. W.; Meola, S.; Hoy, C.; Manley, H.; Drusano, G. L.; Lodise, T. P., Use of pharmacokinetic and pharmacodynamic principles to determine optimal administration of daptomycin in patients receiving standardized thrice-weekly hemodialysis. *Antimicrob. Agents Chemother.* **2011**, *55* (4), 1677-1683.
41. Flessner, M. F., Pharmacokinetic problems in peritoneal drug administration: an update after 20 years *J. Pleura and Peritoneum* **2016**, *1* (4), 183-191.
42. Ball, L.-J.; Goult, C. M.; Donarski, J. A.; Micklefield, J.; Ramesh, V., NMR structure determination and calcium binding effects of lipopeptide antibiotic daptomycin. *Org. Biomol. Chem.* **2004**, *2* (13), 1872-1878.

43. Ho, S. W.; Jung, D.; Calhoun, J. R.; Lear, J. D.; Okon, M.; Scott, W. R. P.; Hancock, R. E. W.; Straus, S. K., Effect of divalent cations on the structure of the antibiotic daptomycin. *Eur. Biophys. J.* **2008**, 37 (4), 421-433.
44. Rahim, M. I.; Weizbauer, A.; Evertz, F.; Hoffmann, A.; Rohde, M.; Glasmacher, B.; Windhagen, H.; Gross, G.; Seitz, J.-M.; Mueller, P. P., Differential magnesium implant corrosion coat formation and contribution to bone bonding. *J. Biomed. Mater. Res. Part A* **2017**, 105 (3), 697-709.

Supporting information

General chemical information

Unless otherwise mentioned, reagents were purchased and used without further purification. All employed solvents for workups and purifications were p.a. or HPLC purity grade. A Universal 32 R centrifuge (Hettich) was used for centrifugations.

Except biphasic reactions or reactions in water, all reactions were carried out with anhydrous solvents stored over molecular sieves. Moisture-sensitive reactions were carried out oven-dried glassware under argon atmosphere. The reaction progress was monitored by TLC (silica gel 60 F₂₅₄, on aluminum/glass, Merck®).

Automatic preparative column chromatography was performed on a Grace Reveleris® X2 instrument (Büchi®) with disposable columns (Reveleris® Flash Cartridges Silica 40 µm, Büchi). RP-HPLC purifications were performed on a Pure C-850 (Büchi) or Dionex Ultimate (Thermo Fisher Scientific) on a phenomenex Gemini C18 RP-column 00G-4436-NO, 10 µm, 110 A, 250×10.00 mm (5 mL/min) or phenomenex Gemini C18 RP-column 00G-4435-PO-AX, 5 µm, 110 A, 250×21.20 mm (10 mL/min). Substances were subsequently freeze-dried on an Alpha 2-4 LSCbasic (Christ) instrument.

High resolution mass spectrometry (HRMS) was performed using a Dionex Ultimate 3000 HPLC system equipped with a DAD detector and a Bruker maxis HD QTOF mass detector with electrospray ionization (ESI). Samples were injected directly *via* an Ultimate 3000RS autosampler (Thermo Fisher Scientific). The mass-to-charge ratios (*m/z*) are indicated.

NMR spectra were acquired on Advance III 500 with the probe head PABBO BB/19F-1H/D Z-GRD (500 MHz for ¹H, 125 MHz for ¹³C), and Advance III HD 700 with cryo platform and the probe head CPTCI 1H-13C/15N/D Z-GRD (700 MHz for ¹H, 176 MHz for ¹³C) from Bruker. The measured substances were dissolved in the respective deuterated solvent and the chemical shifts δ are given in ppm. Multiplicities of the individual signals are as follows: s (singlet), d (doublet), t (triplet), q (quartet), quint (quintet) and combinations thereof, dd (doublet of doublet), tt (triplet of triplet), dt (doublet of triplet), td (triplet of doublet), etc. Others include: bs (broad singlet) and m (multiplet). All spectra were interpreted as first order spectra. The coupling constants *J* are given in hertz (Hz) and refer to ¹H-¹H couplings.

All isolated compounds were characterized by ¹H-NMR (all compounds), ¹³C-NMR (molecular weight < 1300 g/mol and selected compounds) spectra, and ESI-HRMS (all compounds). The yields are calculated based on substance purity $\geq 95\%$ as confirmed by NMR and MS.

Chemistry figures, schemes and tables

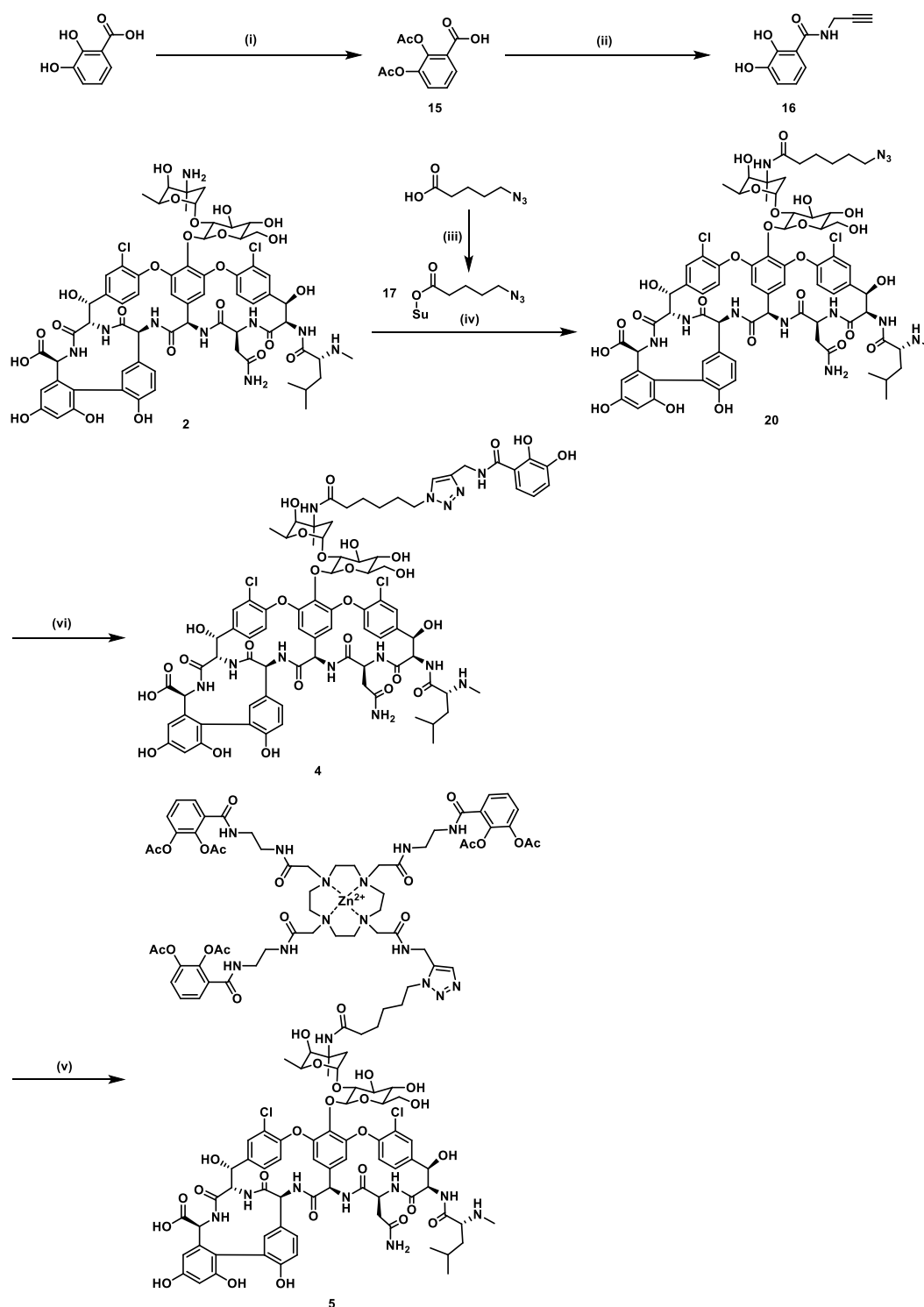


Figure S8.1. Synthesis of vancomycin monocatechol **4** and vancomycin DOTAM **5**. (i) Ac₂O, TEA, DMAP, THF, 29 °C, overnight, 79%, (ii) propargylamine, HATU, DIPEA, DCM, DMF, dropwise addition at 0 °C, 30 min, then 20% DIPEA/MEOH at 23 °C, 79%, (iii) 6-azido hexanoic acid, *N*-hydroxy succinamide, EDCI, DMF, overnight, 23 °C, 98% crude, (iv) DIPEA, DMSO at 23 °C, overnight, 25%, (v) **16**, CuSO₄, sodium ascorbate, DMF/milliQ H₂O, (1:1), TBTA, 23 °C to 30°C, 2 h, 83%, (vi) **18**, Zn(OAc)₂, CuSO₄, sodium ascorbate, DMF/milliQ H₂O, (1:1), TBTA, 23 °C to 30°C, 2 h, 22%.

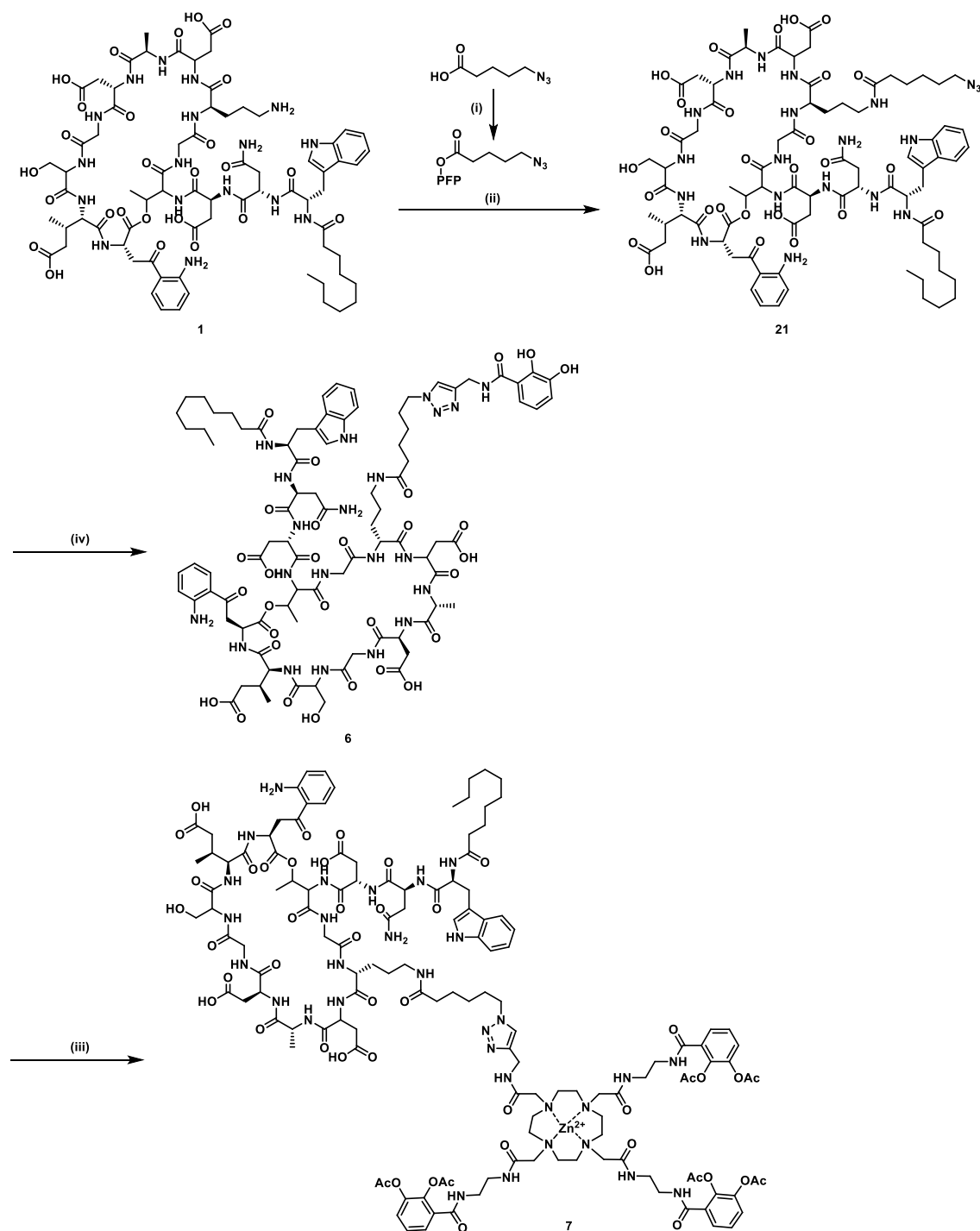


Figure S8.2. Synthesis of daptomycin catechol **6** and daptomycin DOTAM **7**. (i) pentafluorophenol, 6-azido hexanoic acid, EDCI, DMF, overnight 23 °C, quant. crude, (ii) DIPEA, DMSO, 23 °C, overnight, 46%, (iii) **16**, CuSO₄, sodium ascorbate, DMF/milliQ H₂O, (1:1), TBTA, 23 °C to 30°C, 2 h, 89%, (iv) **18**, Zn(OAc)₂, CuSO₄, sodium ascorbate, DMF/milliQ H₂O, (1:1), TBTA, 23 °C to 30°C, 2 h, 87%.

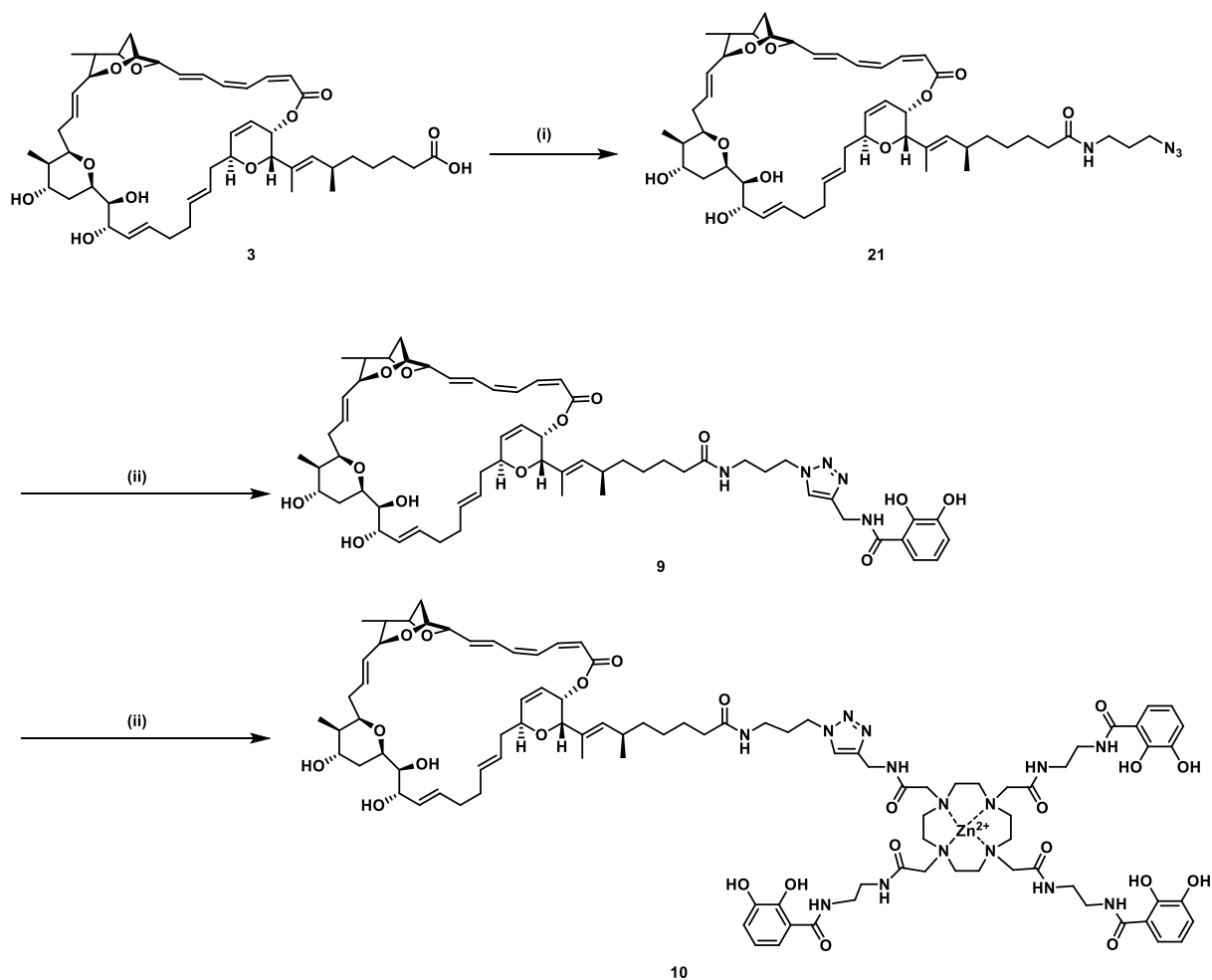


Figure S8.3. Synthesis of sorangicin A monocatechol **9** and sorangicin A DOTAM **10**. (i) 3-azido propan-1-amine, HATU, DIPEA, DCM, DMF, 23 °C, overnight, 85%, (ii) **16**, CuSO₄, sodium ascorbate, DMF/milliQ H₂O, (1:1), TBTA, 23-30°C, 2h, 21% (iii) **19**, Zn(OAc)₂, CuSO₄, sodium ascorbate, DMF/milliQ H₂O, (1:1), TBTA, 23 °C to 30°C, 2 h, 39%.

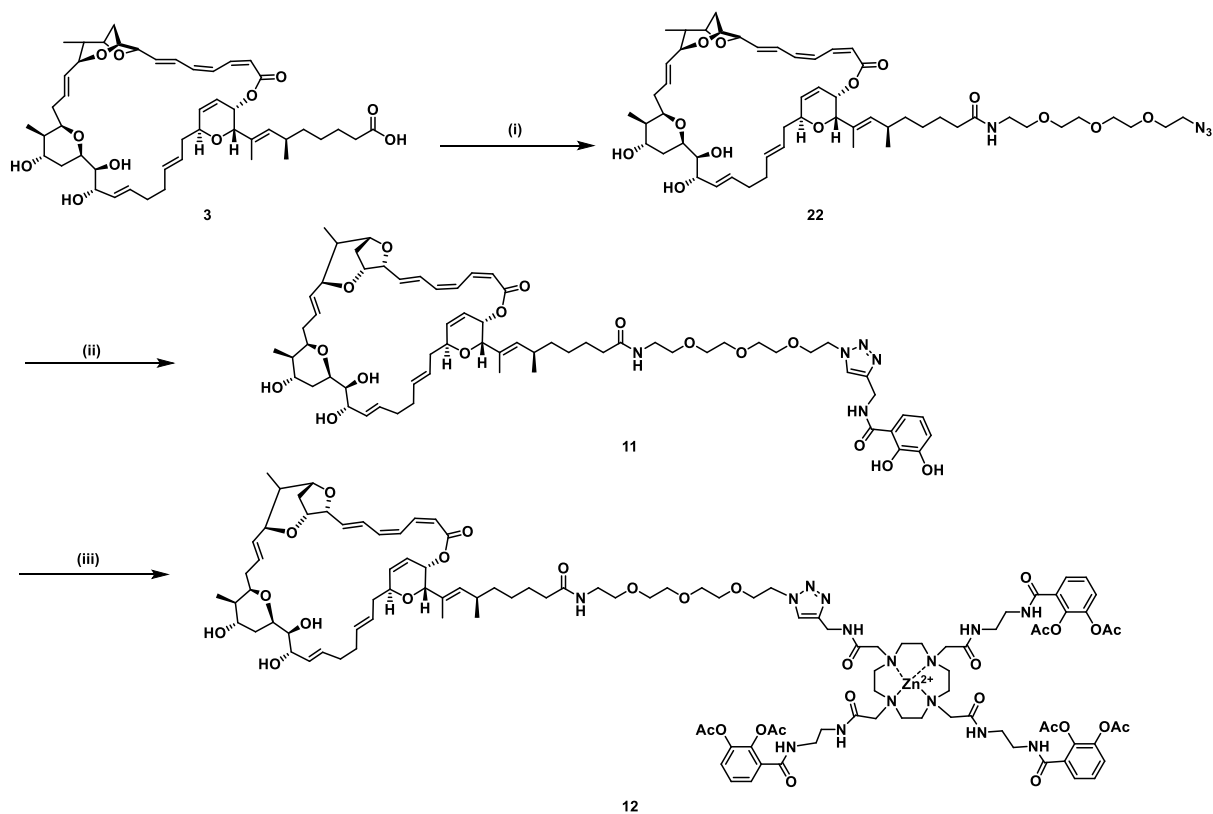
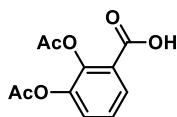


Figure S8.4. Synthesis of sorangicin A PEG CAT **11** and sorangicin A PEG DOTAM **12**. (i) N_3 -PEG₃-NH₂, HATU, DIPEA, DCM, DMF, 25 °C, overnight, 88%, (ii) **16**, CuSO₄, sodium ascorbate, DMF/milliQ H₂O, (1:1), TBTA, 23-30°C, 2h, 95% (iii) **18**, Zn(OAc)₂, CuSO₄, sodium ascorbate, DMF/milliQ H₂O, (1:1), TBTA, 23 °C to 30°C, 2 h, 90%.

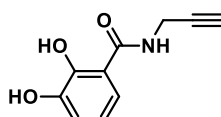
Synthesis procedures

Compound 15



Compound **15** was synthesized as published in Peukert, Langer et al.¹

Compound 16



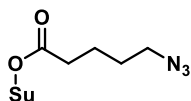
Acid **15** (100 mg, 0.42 mmol, 1.0 eq) and HATU (175.6, 0.46 mmol, 1.1 eq) were dissolved in a mixture of DCM/DMF (100 μ L each, 1:1). Then DIPEA (298.7 μ L, 1.679 mmol, 4.0 eq) was added, followed by propargylamine (23.12 mg, 0.42 mmol, 1.0 eq) addition, dropwise diluted in DCM/DMF (1:1, 100 μ L) over 10 minutes at 0 °C. Deacetylation was driven to completion by addition of MeOH (200 μ L) and DIPEA (50 μ L). The reaction mixture was concentrated in vacuo and purified by silica gel chromatography (0-100% PE/EtOAc, 15 mL/min), product containing fractions were identified by LCMS, combined and concentrated in vacuo to yield **16** as a colorless oil (63.5 mg, 0.332 mmol, 79%) that became crystalline at 0 °C.

¹H-NMR (500 MHz, CDCl₃): δ = 7.07-7.05 (ddd, *J* = 1.61, 7.72 Hz, 1H), 6.93-6.91 (ddd, *J* = 1.69, 8.35 Hz, 1H), 6.78 (t, *J* = 7.72 Hz, 1H), 6.52 (bs, 1H), 4.25 (dd, *J* = 2.5, 5.23 Hz, 2H), 2.32 (t, *J* = 2.43 Hz, 1H).

¹³C-NMR (126 MHz, CDCl₃): δ = 146.09, 119.01, 118.61, 116.23, 77.16, 72.55, 60.55, 39.74, 29.61, 14.35.

HRMS (ESI) calculated for ([M+H]⁺): *m/z* = 192.0654; experimental = 192.0655

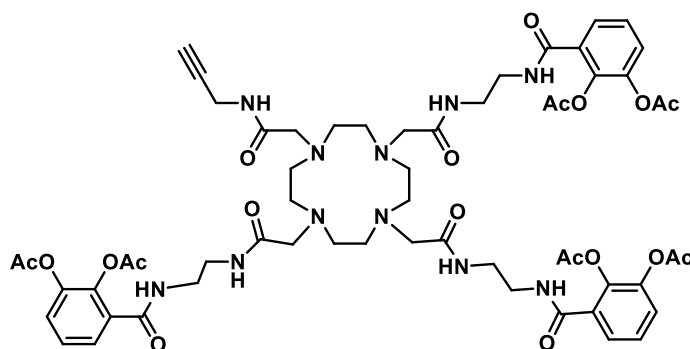
Compound 17



Acid (200 mg, 1.397 mmol, 1.0 eq) was dissolved in DMF (25 mL) and *N*-hydroxy succinamide (NHS) (169.5 mg, 1.677 mmol, 1.2 eq) as well as EDCI (401.75 mg, 2.096 mmol, 1.5 eq) were added at 0 °C. The reaction was warmed to 23 °C and the reaction continued stirring overnight at that temperature. Then ethyl acetate (EA) was added (50 mL) and the organic phase was washed with sat. NH₄Cl (1x 40 mL) and brine (1x40 mL) and dried over Na₂SO₄ and under high vacuum for 2 hours. The crude, white **17** was used without further purification in the next step (328.3 mg, 1.367 mmol, 98%).

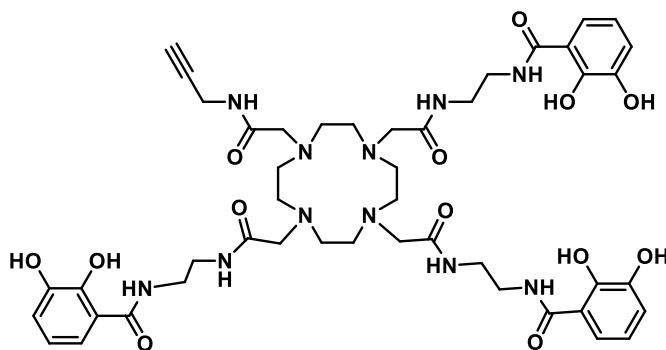
¹H-NMR (500 MHz, CDCl₃): δ = 3.34 (t, J = 6.79 Hz, 2H), 2.84 (bs, 4H), 2.66 (t, J = 7.49 Hz, 2H), 1.88-1.82 (m, 2H), 1.75-1.69 (m, 2H).

Compound 18



Compound **18** was synthesized as described previously by K. Ferreira et al.²

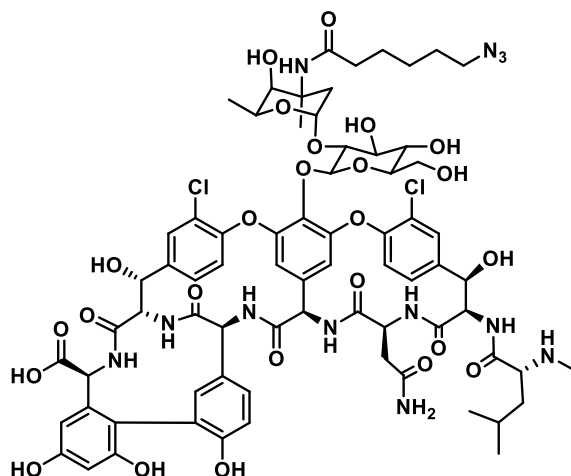
Compound 19



Compound **19** was synthesized as described previously by K. Ferreira et al.²

Vancomycin compounds

Compound 20

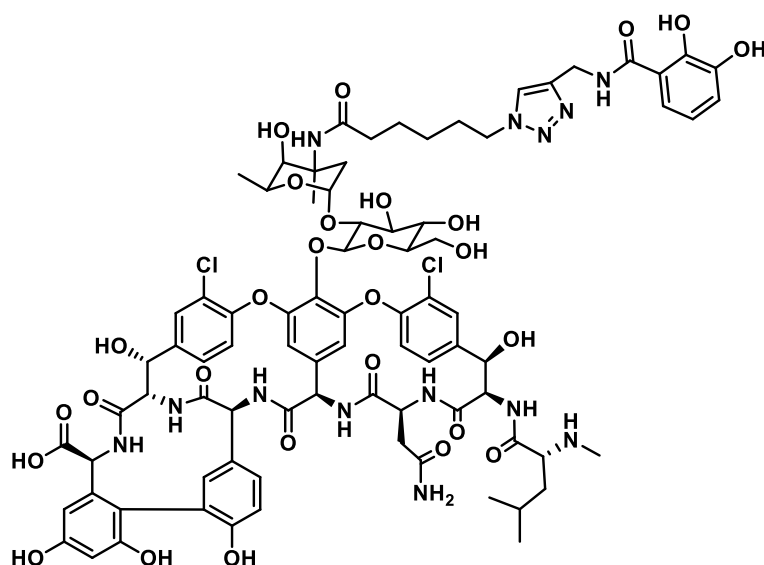


Vancomycin **2** (100 mg, 0.069 mmol, 1.0 eq) was dissolved in DMSO (300 μ L) and dissolved after stirring for 1 hour at room temperature. Then **17** (34.18 mg, 0.142 mmol, 2.0 eq) in DMSO (100 μ L) was added dropwise over two minutes under Argon atmosphere, followed by dry DIPEA (100 μ L) and the mixture continued stirring overnight at 23 $^{\circ}$ C. The next day the reaction mixture was diluted with ice cold Et₂O (80 μ L on 2 mL). The dilution was vortexed and centrifuged for 15 min at 15000 rpm at 0 $^{\circ}$ C. The supernatant was discarded and the pellet was dried under high vacuum. The crude product was dissolved in DMSO (700 μ L) and purified by RP-HPLC (15-50% ACN in H₂O 0.1% HCOOH, 220 nm). Fractions containing product were combined and lyophilized to dryness (27.35 mg, 0.017 mmol, 25%) to yield **20** as a white solid.

¹H-NMR (700 MHz, DMSO-d₆): δ = 9.43 (bs, 1H), 9.16-9.00 (m, 2H), 8.69 (m, 1H), 8.52 (m, 1H), 7.85 (s, 1H), 7.65 (bs, 3H), 7.56 (d, J = 9.07 Hz, 1H), 7.47 (m, 2H), 7.35 (d, J = 9.53 Hz, 1H), 7.20 (d, J = 9.07 Hz, 1H), 7.16 (s, 1H), 6.78 (d, J = 10.89 Hz, 1H), 6.72 (m, 2H), 6.40 (s, 1H), 6.25 (s, 1H), 5.96 (bs, 1H), 5.77 (d, J = 9.07 Hz, 1H), 5.60 (bs, 1H), 5.26 (m, 2H), 5.20 (m, 2H), 5.11 (s, 1H), 4.92 (bs, 1H), 4.68 (m, 1H), 4.44 (d, J = 9.07 Hz, 2H), 4.19 (d, J = 13.16 Hz, 1H), 3.94 (bs, 1H), 3.69 (d, 11.80 Hz, 1H), 3.55 (m, 2H), 3.44 (m, 1H), 3.27 (m, 2H), 3.18 (s, 1H), 2.64 (m, 3H), 2.15 (m, 1H), 1.90 (m, 1H), 1.71 (m, 2H), 1.62 (m, 2H), 1.30 (s, 3H), 1.07 (d, J = 6.81 Hz, 3H), 0.91 (d, J = 6.35 Hz, 3H), 0.87 (d, J = 8.17 Hz, 3H).

HRMS (ESI) calculated for ([M+2H]²⁺): m/z = 794.2596; experimental = 794.2540

Compound 4



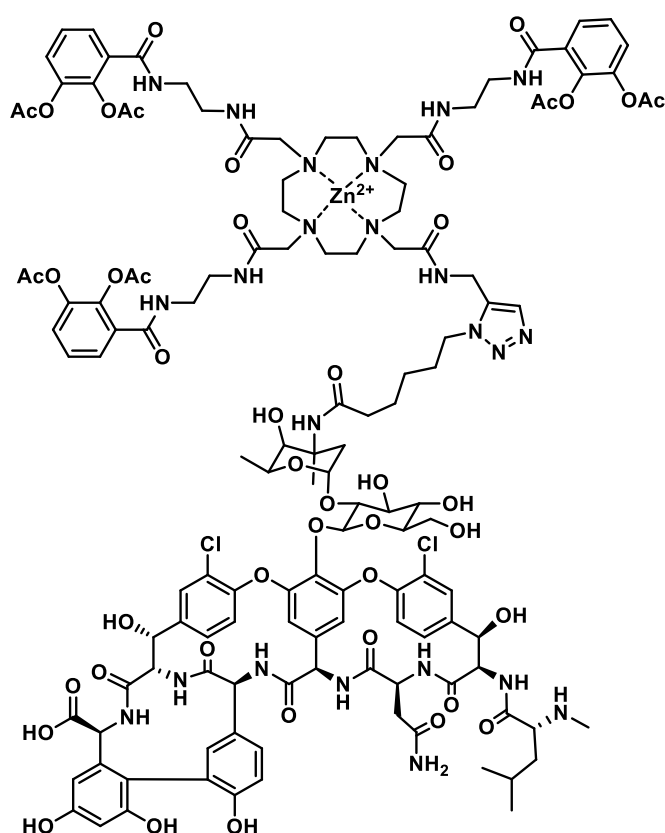
Azide **20** (8 mg, 0.005 mmol, 1.0 eq) was dissolved in DMF/H₂O 1:1 (200 μ L) and TBTA (0.27 mg, 0.001 mmol, 0.1 eq) in DMSO (10 μ L) was added. The alkyne **16** (1.94 mg, 0.01 mmol, 2.0 eq) dissolved in DMF (100 μ L) was added. Then sodium ascorbate (1.01 mg, 0.005 mmol, 1.0 eq) and CuSO₄ (0.16 mg, 0.001 mmol, 0.2 eq) dissolved in degassed milliQ H₂O (200 μ L) were added and the reaction mixture continued stirring at 25°C. The reaction solution was filtered after full conversion over a syringe filter and purified by RP-HPLC (10-65 %, ACN/H₂O, 1% AcOH, 220 nm). Product containing fractions were identified by LCMS and lyophilized to yield **4** as a white solid (11.83 mg, 0.004 mmol, 83%).

¹H-NMR (700 MHz, DMSO-d₆): δ = 9.41 (s, 1H), 9.14-9.06 (m, 2H), 8.62- 8.51 (m, 2H), 7.83 (s, 1H), 7.507.49 (d, J = 8.60 Hz, 1H), 7.45-7.44 (d, J = 11,18 Hz, 1H), 7.35-7.31 (m, 2H), 7.22-7.21 (d, J = 7.74 Hz, 1H), 7.17 (s, 1H), 6.95 (s, 1H), 6.77-6.76 (dd, J = 9.89 Hz, 1H), 6.71-6.70 (d, J = 9.03 Hz, 1H), 6.68-6.66 (d, J = 13.76 Hz, 1H), 6.39-6.38 (d, J = 6.02 Hz, 1H), 6.25 (d, J = 3.87 Hz, 1H), 5.91-5.91 (d, J = 6.45 Hz, 1H), 5.74-5.73 (m, 2H), 5.55 (s, 1H), 5.31-5.30 (d, J = 7.31 Hz, 1H), 5.27-5.26 (d, J = 7.31 Hz, 1H) 5.20 (s, 1H), 5.16-5.14 (m, 2H), 5.10-5.09 (d, J = 7.74 Hz, 1H), 5.04-5.03 (d, J = 4.73 Hz, 1H), 4.86 (bs, 1H), 4.68-4.66 (q, J = 7.74, 12.47 Hz, 1H), 4.44-4.41 (m, 4H), 4.20-4.18 (d, J = 11,18 Hz, 1H), 4.00 (t, J = 5.16 Hz, 1H), 3.69-3.67 (dd, 1H), 3.56-3.49 (m, 2H), 3.47- 3.43 (q, J = 8.60, 15.05 Hz, 1H), 3.35 (m, 2H), 3.26-3.24 (m, 1H), 3.06 (bs, 1H), 2.54 (s, 1H), 2.31(s, 3H) , 2.16-2.13 (dd, J = 6.45, 18.48 Hz, 1H), 2.02-1.91 (m, 4H), 1.91 (s, 2H), 1.81-1.78 (m, 1H), 1.74-1.70 (m, 1H), 1.47 (m, 6H), 1.40 (m, 4H), 1.04-1.03 (d, J = 6-98 Hz, 3H), 0.90-0.89 (d, J = 7.89, 3H), 0.86-0.85 (d, J = 6.53 Hz, 3H).

$^{13}\text{C-NMR}$ (176 MHz, DMSO- d_6): δ = 171.99, 171.10, 169.10, 167.81, 163.18, 157.16, 156.49, 155.05, 152.15, 151.21, 150.05, 148.34, 142.33, 136.11, 135.62, 132.02, 128.70, 127.25, 126.30, 125.54, 124.24, 121.54, 118.02, 116.19, 105.69, 104.66, 102.30, 101.15, 97.54, 77.80, 77.11, 76.66, 71.59, 71.50, 70.29, 63.23, 62.33, 62.31, 61.76, 61.29, 58.07, 56.66, 54.85, 53.86, 53.67, 50.95, 50.38, 40.42, 39.52, 35.45, 34.47, 33.76, 27.72, 24.14, 23.02, 22.44, 22.39, 21.04, 17.34.

HRMS (ESI) calculated for ($[M+2H]^{2+}$): m/z = 889.7887; experimental = 889.7898

Compound 5



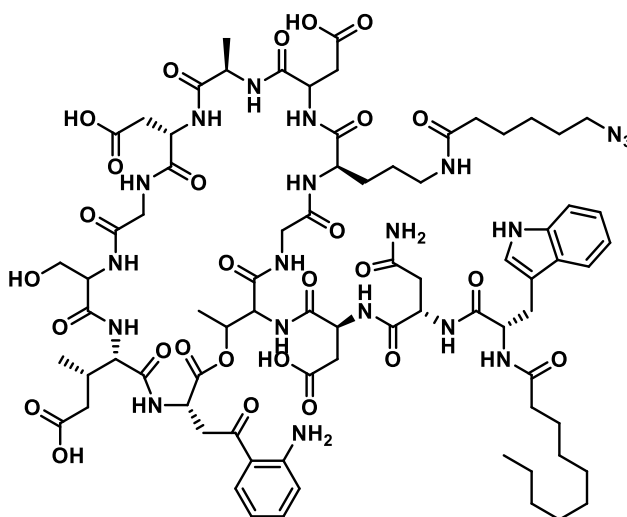
Azide **20** (53.2 mg, 0.034 mmol, 1.8 eq) was dissolved in DMF/ H_2O 1:1 (200 μL) and TBTA (1 mg, 0.002 mmol, 0.1 eq) in DMSO (10 μL) was added. The alkyne **18** (23.05 mg, 0.019 mmol, 1.0 eq) was dissolved in DMF (100 μL) and pre-complexed with $\text{Zn}(\text{OAc})_2$ (6.89 mg, 0.038 mmol, 2 eq). Then sodium ascorbate (9.29 mg, 0.047 mmol, 2.5 eq) and CuSO_4 (7.49 mg, 0.047 mmol, 2.5 eq) dissolved in degassed milliQ H_2O (200 μL) were added and the reaction mixture continued stirring at 25°C. After completion, the reaction was filtered over a syringe filter and directly injected and purified by RP-HPLC (10 to 70 %, ACN/ H_2O , 1% AcOH, 220 nm). Product containing fractions were identified by LCMS and lyophilized to yield **5** as a white solid (11.83 mg, 0.004 mmol, 22%).

¹H-NMR (700 MHz, DMSO-d₆): δ = 8.85 (m, 1H), 8.59 (m, 2H), 8.26 (m, 1H), 7.91 (m, 3H), 6.94 (m, 3H), 6.88 (m, 1H), 6.81 (m, 6H), 6.71 (m, 2H), 6.62 (s, 1H), 6.39 (s, 1H), 6.20 (d, J = 9.33 Hz, 1H), 6.16 (m, 2H), 5.83 (s, 1H), 5.70 (s, 1H), 5.34 (s, 1H), 5.18 (m, 2H), 4.98 (m, 1H), 4.76 (m, 1H), 4.68 (m, 1H), 4.64 (m, 1H), 4.60 (m, 1H), 4.53 (m, 1H), 4.49 (m, 1H), 4.11 (d, 1H), 3.87 (m, 5H), 3.67 (m, 2H), 2.91 (m, 13H), 2.67 (m, 6H), 2.45 (m, 7H), 2.13 (m, 7H), 1.72 (s, 9H), 1.65 (s, 9H), 1.45 (m, 3H), 1.35 (m, 3H), 1.15 (m, 2H), 0.92 (m, 1H), 0.83 (m, 6H), 0.67 (m, 1H), 0.48 (d, J = 5.72 Hz, 3H), 0.34 (d, J = 6.76 Hz, 3H), 0.30 (d, J = 6.37 Hz, 3H).

HRMS (ESI) calculated for ([M+3H]³⁺): m/z = 960,3210; experimental = 960.3229

Daptomycin compounds

Compound 21



6-azido hexanoic acid (2.33 mg, 0.015 mmol, 1.2 eq) and PFP (2.27 mg, 0.015 mmol, 1.2 eq) were dissolved in DCM (0.2 mL) and cooled to 0°C. DCC (3.06 mg, 0.015 mmol, 1.2 eq) was added and stirred for 10 min at 0°C. The solution was stirred at room temperature for six hours. Then solvent was evaporated under reduced pressure, the residue was diluted with water (5 mL) and extracted with DCM (2x10 mL). The solvent was removed *in vacuo* and the residue was dissolved in DMSO (100 μL). Then daptomycin (20 mg, 0.012 mmol, 1.0 eq) was added in DMSO (100 μL), followed by DIPEA (10 μL) and stirred for 2 h at 24 °C. The solvent was removed *in vacuo* and the residue was purified by RP-HPLC (10-70% ACN/H₂O, 0.1% HCOOH, 220 nm). Product containing fractions were combined and lyophilized to yield **21** as a slight yellow powder (9.9 mg, 0.006 mmol, 46%).

Daptomycin

¹H-NMR (700 MHz, MeOH-d₄): δ = 7.65 (d, J = 8.0 Hz, 1H), 7.55 (d, J = 7.9 Hz, 1H), 7.33 (d, J = 8.1 Hz, 1H), 7.21 (ddd, J = 8.4, 7.0, 1.4 Hz, 1H), 7.15 (s, 1H), 7.09 – 7.05 (m, 1H), 7.00 – 6.96 (m, 1H), 6.71 (dd, J = 8.4, 0.9 Hz, 1H), 6.58 – 6.51 (m, 1H), 5.42 (dd, J = 6.4, 3.0 Hz, 1H), 5.03 (s, 1H), 4.78 (s, 1H), 4.72 (t, J = 6.7 Hz, 1H), 4.65 (t, J = 6.7 Hz, 1H), 4.61 (t, J = 5.2 Hz, 2H), 4.58 – 4.46 (m, 3H), 4.34 (t, J = 6.8 Hz, 1H), 4.29 (q, J = 6.9 Hz, 1H), 4.05 – 3.81 (m, 6H), 3.59 – 3.47 (m, 2H), 3.27 – 3.21 (m, 1H), 3.12 (dd, J = 14.4, 7.3 Hz, 1H), 2.99 – 2.91 (m, 2H), 2.89 (dd, J = 16.5, 7.0 Hz, 1H), 2.82 (dd, J = 16.5, 5.2 Hz, 1H), 2.77 – 2.71 (m, 2H), 2.65 (ddd, J = 20.3, 15.9, 6.4 Hz, 3H), 2.52 (s, 1H), 2.41 (dd, J = 15.6, 6.5 Hz, 1H), 2.27 (dd, J = 15.9, 4.2 Hz, 1H), 2.24 – 2.14 (m, 3H), 1.88 (dd, J = 23.1, 16.3 Hz, 1H), 1.83 – 1.77 (m, 1H), 1.74 (dd, J = 15.2, 7.1 Hz, 2H), 1.54 – 1.46 (m, 2H), 1.36 (d, J = 7.1 Hz, 3H), 1.33 – 1.27 (m, 2H), 1.27 – 1.15 (m, 14H), 0.97 (d, J = 6.9 Hz, 3H), 0.89 (t, J = 7.2 Hz, 3H).

¹³C-NMR (176 MHz, MeOH-d₄) δ 199.89, 177.19, 176.43, 175.88, 175.72, 175.48, 174.97, 174.76, 174.43, 174.24, 173.76, 173.61, 173.10, 172.88, 172.26, 172.05, 152.73, 137.97, 135.86, 132.29, 128.80, 124.81, 122.45, 119.84, 119.29, 118.35, 118.08, 116.34, 112.45, 110.73, 72.19, 63.44, 58.75, 57.43, 57.07, 54.55, 52.77, 52.54, 51.00, 50.25, 44.08, 41.83, 40.28, 37.90, 37.55, 36.95, 36.73, 34.30, 33.06, 30.59, 30.47, 30.45, 30.33, 29.21, 28.20, 26.75, 24.61, 23.75, 17.11, 15.77, 14.47.

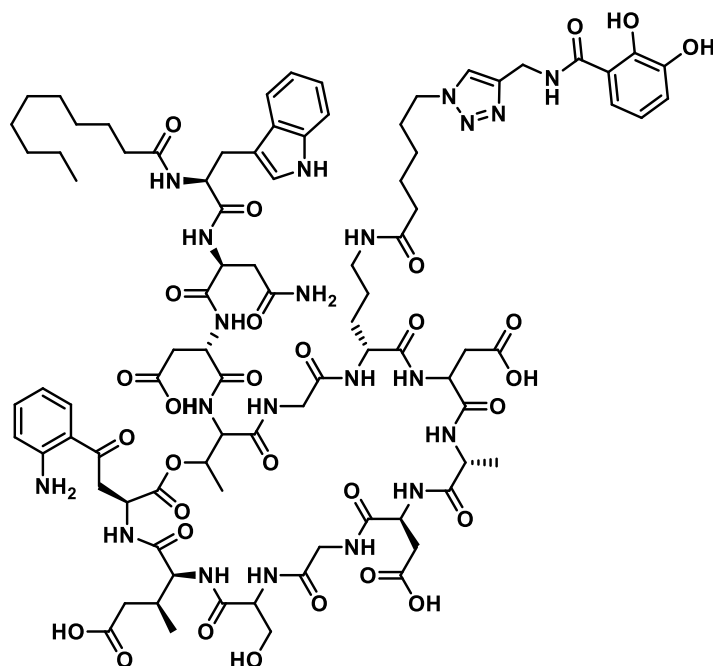
Compound 21

¹H-NMR (700 MHz, DMSO-d₆): δ = 12.21 (bs, 4H), 10.75 (s, 1H), 8.44 (s, 2H), 8.32 (m, 2H), 8.21 m, 1H), 8.11 m, 2H), 8.02 (m, 1H), 7.98 (d, J = 5.28 Hz, 1H), 7.71 (m, 3H), 7.55 (d, J = 8.80 Hz, 2H), 7.30 (m, 2H), 7.22 (t, J = 8.21 Hz, 1H), 7.14-7.10 (m, 2H), 7.04 (t, J = 8.21 Hz, 1H), 6.95, (t, J = 8.20 Hz, 1H) 6.86 (s, 1H), 6.73 (d, J = 8.21 Hz, 1H), 6.51 (t, J = 8.21 Hz, 1H), 5.57 (d, J = 10.56 Hz, 3H), 5.03 (s, 1H), 4.85 (m, 2H), 4.53 (m, 7H), 4.40 (m, 1H), 4.22 (m, 1H), 4.10 (m, 2H), 3.75 (m, 2H), 3.57 (m, 3H), 3.29 (m, 3H), 3.02 (m, 3H), 2.90 (q, J = 11.73, 15.25 Hz, 1H), 2.74 (m, 2H), 2.57 (m, 2H), 2.35 (m, 6H), 2.02 (m, 4h), 1.90 (m, 1H), 1.72 (m, 7H), 1.60 (m, 7H), 1.50 (m, 9H), 1.35 (m, 2H), 1.22 (m, 12H), 1.13 (m, 6H), 1.05(m, 6H), 0.84 (m, 6H).

¹³C-NMR (176 MHz, DMSO-d₆): δ = 173.98, 173.61, 173.32, 172.38, 172.34, 172.25, 172.03, 171.87, 171.39, 170.82, 170.65, 169.44, 168.13, 157.06, 157.04, 151.63, 136.48, 134.97, 131.74, 127.72, 124.15, 121.24, 118.82, 118.60, 117.38, 116.40, 115.00, 111.68, 110.34, 70.44, 62.43, 55.96, 54.62, 53.54, 50.98, 50.69, 50.16, 49.86, 49.71, 47.97, 42.88, 42.21, 40.90, 40.49, 38.51, 38.30, 37.51, 36.18, 35.70, 35.47, 33.82, 33.36, 31.74, 29.32, 29.22, 29.15, 29.06, 28.74, 28.48, 28.20, 27.64, 26.29, 25.89, 25.79, 25.43, 25.26, 24.93, 22.57, 17.41, 15.32, 14.44.

HRMS (ESI) calculated for $([M+3H]^{3+})$: $m/z = 587.2689$; experimental = 587.6024

Compound 6



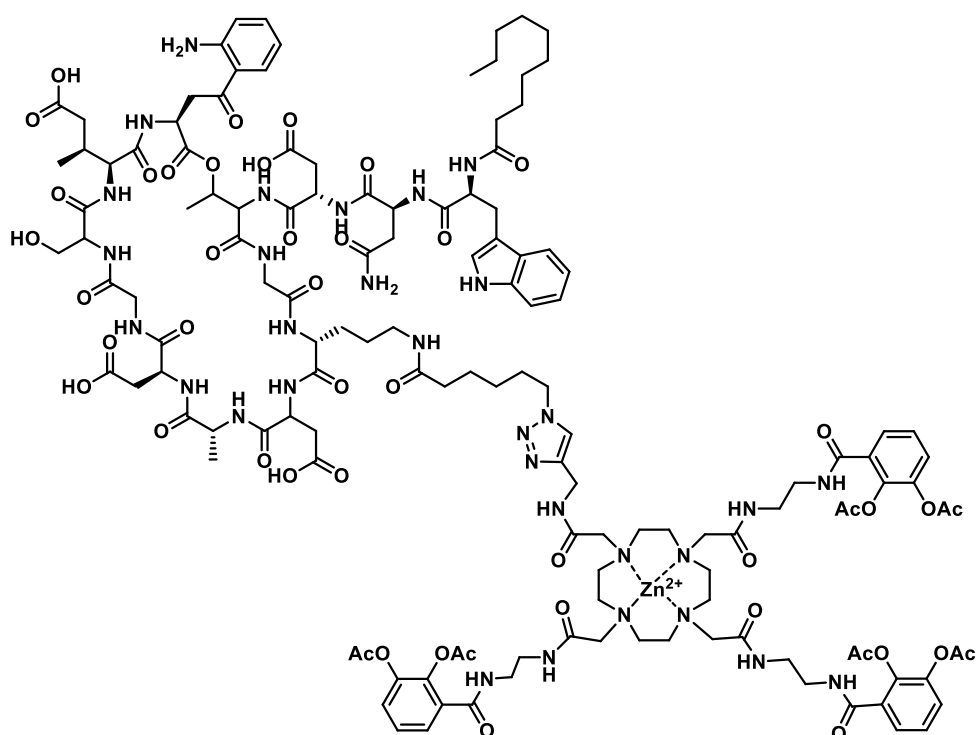
Azide **21** (7.0 mg, 0.004 mmol, 1.0 eq) was dissolved in DMF/H₂O 1:1 (200 μ L) and TBTA (1 mg, 0.002 mmol, 0.1 eq) in DMSO (10 μ L) was added. The alkyne **16** (1.52 mg, 0.008 mmol, 2.0 eq) was dissolved in DMF (100 μ L). Then sodium ascorbate (0.79 mg, 0.004 mmol, 1.0 eq) and CuSO₄ (0.13 mg, 0.001 mmol, 0.2 eq), dissolved in degassed milliQ H₂O (200 μ L), were added and the reaction mixture continued stirring at 25°C. After full conversion, the reaction was filtered over a syringe filter and purified by RP-HPLC (10-80 % ACN/H₂O, 0.1% HCOOH, 220 nm). Product containing fractions were identified by LCMS and lyophilized to yield **6** as a white, slightly yellow solid (6.9 mg, 0.004 mmol, 89%).

¹H-NMR (700 MHz, DMSO-d₆): $\delta = 12.57$ (s, 1H), 12.17 (m, 4H), 10.75 (s, 1H), 9.28 (t, J = 5.38 Hz, 1H), 9.17 (s, 1H), 8.44 (m, 2H), 8.32 (m, 3H), 8.22 (m, 1H), 8.11 (m, 1H), 7.98 (m, 3H), 7.68 (m, 3H), 7.56 (d, J = 8.06 Hz, 1H), 7.29 (m, 3H), 7.22 (t, J = 7.68 Hz, 1H), 7.14 (d, 1H), 7.10 (m, 1H), 7.04 (t, J = 7.68 Hz, 1H), 6.95-6.92 (t, J = 9.98 Hz, 1H), 6.86 (d, J = 7.68 Hz, 1H), 6.73 (bs, 1H), 6.68 (d, J = 6.04 Hz, 1H), 6.51 (t, J = 7.68 Hz, 1H), 5.03 (m, 1H), 4.60 (q, J = 7.68, 15,74 Hz, 1H), 4.56-4.52 (m, 7H), 4.48 (m, 2H), 4.38 (q, J = 8.06, 12,29 Hz, 1H), 4.29 (t, J = 7.68 Hz, 2H), 4.22 (m, 1H), 4.10 (m, 2H), 3.75 (m, 3H), 3.57 (m, 3H), 3.02 (m, 3H), 2.91 (m, 1H), 2.74 (m, 2H), 2.33 (m, 5H), 2.01 (m, 5H), 1.77 (m, 2H), 1.72 (m, 1H), 1.67 (m, 1H), 1.61 (m, 1H), 1.49 (m, 4H), 1.42 (m, 2H), 1.35 (m, 2H), 1.23 (m, 2H), 1.20 (m, 2H), 1.14 (m, 6H), 1.07 (m, 6H), 0.84 (m, 7H).

¹³C-NMR (176 MHz, DMSO-d₆): δ = 173.52, 172.87, 171.89, 171.78, 171.57, 171.42, 170.94, 170.18, 169.57, 168.98, 168.75, 167.67, 151.16, 149.54, 146.18, 144.22, 136.01, 134.50, 127.25, 123.68, 122.91, 120.78, 118.90, 118.35, 118.13, 118.02, 117.36, 116.91, 115.94, 114.93, 111.21, 109.86, 85.17, 69.98, 61.94, 54.15, 50.23, 49.68, 49.38, 49.16, 40.43, 40.01, 38.04, 37.83, 37.03, 35.71, 35.48, 35.28, 35.16, 34.99, 34.55, 33.34, 31.26, 29.58, 28.84, 28.74, 28.67, 28.58, 27.15, 25.59, 25.42, 25.31, 24.95, 24.65, 24.45, 22.09, 21.05, 16.94, 14.84, 13.96.

HRMS (ESI) calculated for ([M+3H]³⁺): m/z = 650.9550; experimental = 650.9557

Compound 7



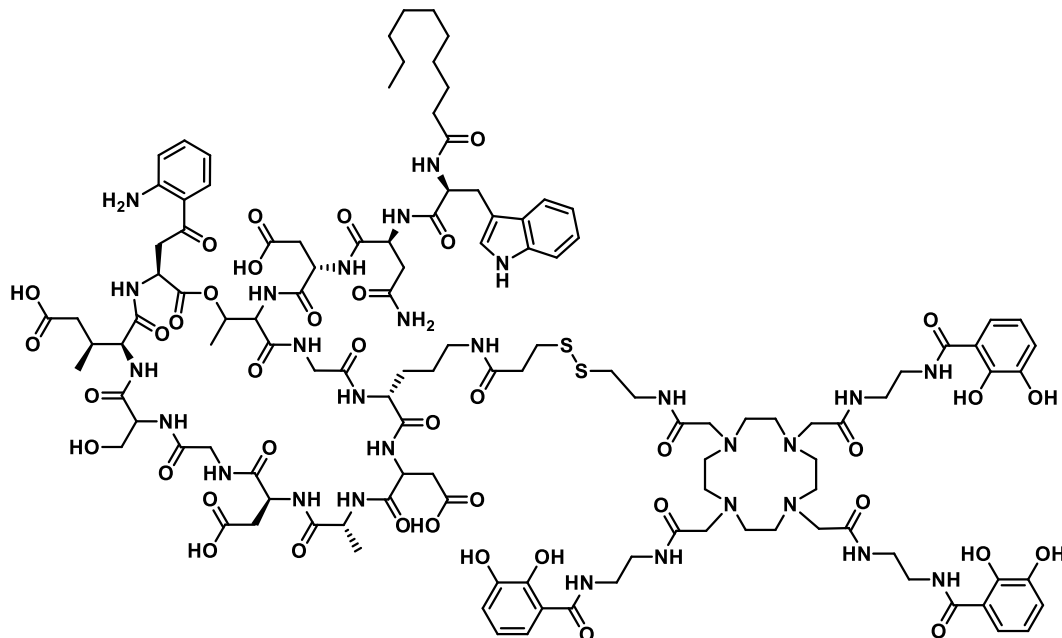
Azide **21** (7.5 mg, 0.004 mmol, 1.0 eq) was dissolved in DMF/H₂O (1:1, 200 μ L) and TBTA (1.66 mg, 0.003 mmol, 0.1 eq) in DMSO (10 μ L) was added. The alkyne **18** (10.47 mg, 0.009 mmol, 2.0 eq) was dissolved in DMF (100 μ L) and pre-complexed with Zn(OAc)₂ (9.35 mg, 0.043 mmol, 10.0 eq). Then sodium ascorbate (0.84 mg, 0.004 mmol, 1.0 eq) and CuSO₄ (0.14 mg, 0.001 mmol, 0.2 eq) dissolved in degassed DMF/H₂O (1:1, 200 μ L) were added and the reaction mixture continued stirring at 25. After full conversion, the reaction was filtered over a syringe filter and purified by RP-HPLC (10-70 %, ACN/H₂O, 1% AcOH, 220 nm). Product containing fractions were identified by LCMS and lyophilized to yield **7** as a beige solid (11.3 mg, 0.004 mmol, 87%).

¹H-NMR (700 MHz, DMSO-d₆): δ = 10.75 (s, 1H), 8.52 (m, 1H), 7.97 (m, 1H), 7.57 (d, J = 8.17 Hz, 1H), 7.50 (m, 2H), 7.36 (m, 6H), 7.30 (d, J = 8.17 Hz, 2H), 7.21 (m, 1H), 7.13 (s, 2H), 7.03 (t, J = 7.1 Hz, 1H), 6.95 (t, J = 7.1 Hz, 1H), 6.86 (s, 1H), 6.73 (d, J = 9.23 Hz, 1H), 4.59 (m, 2H), 4.40 (m, 2H), 4.25 (m, 2H), 3.70 (m, 2H), 3.00 (m, 9H), 2.70 (m, 6H), 2.27 (s, 9H), 2.21 (s, 9H), 2.01 (m, 4H), 1.73 (m, 2H), 1.58 (m, 2H), 1.45 (m, 4H), 1.33 (m, 2H), 1.28-1.24 (m, 7H), 1.19 (m, 6H), 1.14 (m, 6H), 1.08 (m, 5H), 0.89 (d, 3H), 0.84 (t, J = 8.17 Hz, 4H).

¹³C-NMR (176 MHz, MeOH-d₄): δ = 216.16, 215.53, 213.02, 212.67, 176.60, 176.42, 175.55, 173.56, 170.22, 170.03, 168.52, 168.42, 161.76, 158.41, 158.30, 152.86, 144.77, 141.91, 138.10, 131.87, 129.10, 128.95, 127.89, 127.61, 127.30, 125.00, 124.84, 122.63, 120.04, 119.47, 118.48, 118.16, 116.56, 112.56, 110.85, 103.43, 91.22, 84.52, 69.61, 65.92, 63.42, 63.32, 57.74, 57.62, 57.50, 57.37, 41.00, 40.09, 40.06, 39.82, 39.79, 39.51, 37.07, 36.75, 36.69, 36.38, 36.00, 33.20, 30.73, 30.59, 30.48, 29.65, 29.47, 29.29, 29.10, 29.01, 28.21, 27.20, 26.99, 26.78, 23.90, 23.01, 22.89, 22.61, 22.55, 22.28, 20.85, 20.59, 20.04, 17.64, 17.53, 17.43, 17.32, 15.73, 14.62, 13.39.

MS (ESI) calculated for ([M+3H]³⁺): m/z = 1017.7477; experimental = 1017.7483

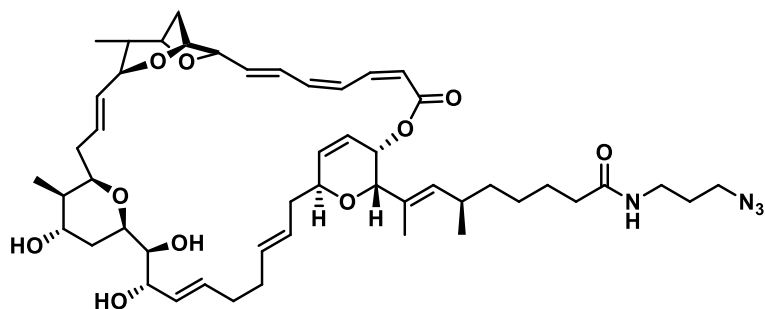
Compound 8



Compound 8 was previously published in Fritsch et al.³

Sorangicin A compounds

Compound 21



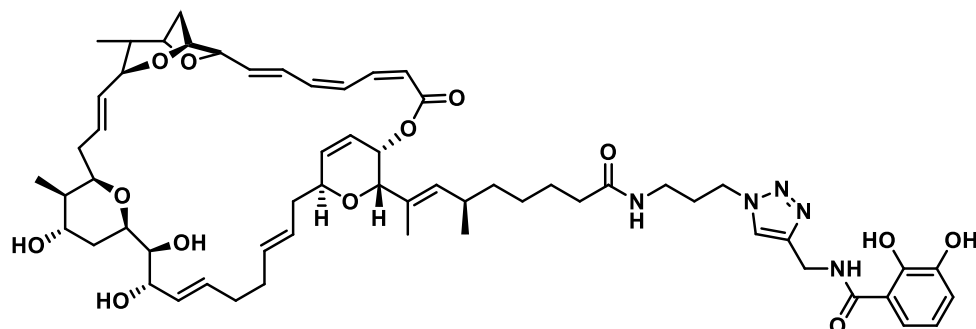
Sorangicin A **3** (16 mg, 0.02 mmol, 1.0 eq) was dissolved in dry DCM/DMF (200/100 μ l) and HATU (22.59 mg, 0.059 mmol, 3.0 eq), 3-azido-propan-1-amine (5.94 mg, 0.059 mmol, 3.0 eq) and DIPEA (21 μ L, 0.119 mmol, 6.0 eq) were added under Argon atmosphere. The mixture continued stirring for 2 hours at 24 $^{\circ}$ C, was concentrated, filtered and then purified by RP-HPLC (10-80% ACN/H₂O, 0.1% HCOOH, 220 nm). Product fractions were identified by LCMS, combined and lyophilized to yield **21** a slight yellow solid (15.01 mg, 0.017 mmol, 85%).

¹H-NMR (700 MHz, MeOH-d₄): δ = 7.17 (m, 2H), 6.99 (m, 1H), 6.44 t, J = 10.02 Hz, 1H), 6.21 (dd, J = 5.59, 15.30 Hz, 1H), 6.12 (dd, J = 2.92, 10.69 Hz, 1H), 6.02 (m, 1H), 5.74 (m, 1H), 5.60 (m, 2H), 5.54 (m, 2H), 5.50 (m, 1H), 5.37 (m, 1H), 5.32 (m, 2H), 4.58 (m, 1H), 4.40 (m, 2H), 4.29 (d, J = 6.56 Hz, 1H), 4.22 (s, 1H), 4.16 (m, 1H), 3.86 (m, 2H), 3.83 (t, J = 8.26 Hz, 1H), 3.72 (m, 2H), 3.48 (m, 1H), 3.34 (m, 3H), 3.24 (m, 3H), 2.38 (m, 2H), 2.27 (m, 1H), 2.16 (m, 5H), 2.04 (m, 5H), 1.92 (d, J = 11.17 Hz, 1H), 1.75 (m, 3H), 1.68 (m, 1H), 1.63 (s, 3H), 1.57 (m, 3H), 1.37 (m, 8H), 1.29 (m, 4H), 1.21 (m, 2H), 0.88 (m, 6H), 0.81 (d, J = 6.80 Hz, 3H).

¹³C-NMR (176 MHz, MeOH-d₄): δ = 176.63, 167.81, 139.27, 137.87, 137.09, 135.13, 134.62, 134.17, 133.81, 133.10, 132.95, 131.26, 130.17, 128.41, 127.92, 127.12, 123.87, 119.73, 118.27, 82.24, 81.34, 81.13, 77.86, 77.65, 75.43, 75.06, 74.85, 74.44, 74.33, 71.19, 66.77, 57.74, 57.62, 57.50, 56.00, 50.27, 49.67, 43.94, 42.20, 39.94, 38.72, 38.53, 37.85, 37.45, 37.28, 35.49, 34.38, 33.65, 33.15, 31.08, 29.93, 28.48, 27.29, 21.97, 18.85, 17.53, 17.41, 17.32, 17.21, 15.54, 14.56, 13.31, 11.00, 0.72, 0.60, 0.48, 0.36, 0.25.

HRMS (ESI) calculated for ([M+H]⁺): m/z = 889.5320; experimental = 889.5321

Compound 9



Azide **21** (16.4 mg, 0.037 mmol, 1.0 eq) was dissolved in DMF/H₂O 1:1 (200 μ L) and TBTA (1 mg, 0.002 mmol, 0.1 eq) in DMSO (10 μ L) was added. The alkyne **16** (3.66 mg, 0.037 mmol, 1.8 eq) was dissolved in DMF (100 μ L). Then sodium ascorbate (10.06 mg, 0.051 mmol, 2.5 eq) and CuSO₄ (8.11 mg, 0.051 mmol, 2.5 eq) dissolved in degassed water (200 μ L) were added and the reaction mixture continued stirring at 25. Then the reaction was filtered over a syringe filter and purified by RP-HPLC (10-80 %, ACN/H₂O, 0.1% HCOOH, 220 nm). Product containing fractions were identified by LCMS and lyophilized to yield **9** as a white, slightly yellow solid (8.34 mg, 0.008 mmol, 21%).

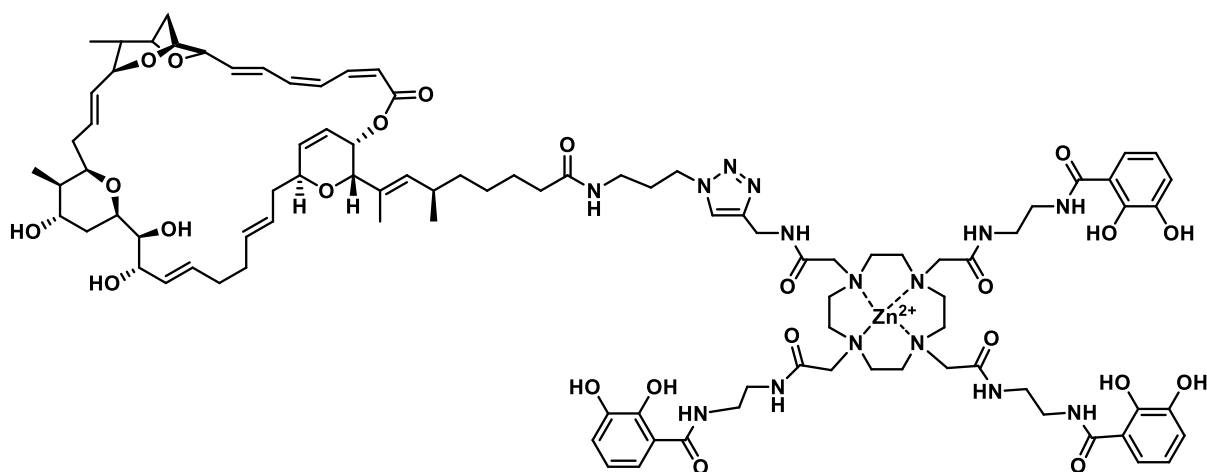
¹H-NMR (700 MHz, MeOH-d₄): δ = 7.94 (s, 1H), 7.23 (dd, *J* = 1.65, 8.57 Hz, 1H), 7.16 (m, 2H), 6.98 (m, 1H), 6.94 (dd, *J* = 1.35 7.82 Hz, 1H), 6.72 (t, *J* = 7.82 Hz, 1H), 6.43 (t, *J* = 11.28 Hz, 1H), 6.20 (dd, *J* = 4.36, 15.19 Hz, 1H), 6.12 (dd, *J* = 3.46, 9.93 Hz, 1H), 6.00 (m, 1H), 5.74 (m, 1H), 5.60 (m, 2H), 5.52 (m, 2H), 5.48 (m, 1H), 5.37 (m, 1H), 5.30 (m, 2H), 4.64 (s, 2H), 4.56 (m, 1H), 4.40 (m, 4H), 4.26 (d, *J* = 6.92 Hz, 1H), 4.20 (s, 1H), 4.17 (q, *J* = 4.81, 7.37 Hz, 1H), 3.85 (m, 2H), 3.81 (t, *J* = 8.72 Hz, 1H), 3.69 (m, 1H), 3.48 (q, *J* = 4.36, 7.82 Hz, 1H), 3.19 (t, *J* = 6.62 Hz, 2H), 2.37 (m 2H), 2.25 (m, 1H), 2.15 (m, 6H), 2.08 m, 3H), 2.03 (m, 1H), 1.92 (d, *J* = 12.18 Hz, 1H), 1.73 (m, 1H), 1.65 (ttt, 1H), 1.62 (s, 1H), 1.55 (m, 3H), 1.38 (m, 2H), 1.29 (m, 1H), 1.20 (m, 1H), 0.86 (m, 6H), 0.80 (d, *J* = 6.92 Hz, 3H).

¹³C-NMR (176 MHz, MeOH-d₄): δ = 176.72, 171.68, 167.80, 150.52, 147.54, 146.49, 139.28, 137.87, 137.08, 135.13, 134.65, 134.16, 133.80, 133.03, 132.97, 131.27, 130.10, 128.40, 127.94, 127.13, 124.82, 123.87, 119.94, 119.80, 119.72, 118.97, 116.73, 82.20, 81.34, 81.12, 77.87, 77.63, 75.40, 75.05, 74.83, 74.43, 74.31, 71.18, 66.77, 57.87, 57.75, 57.62, 57.50, 49.68, 49.51, 49.39, 49.27, 49.15, 49.03, 48.90, 48.78, 42.18, 39.94, 38.73, 38.49, 37.58, 37.44, 37.27, 35.86, 35.47, 34.40, 33.67, 33.15, 31.31, 31.16, 28.51, 27.23, 22.00, 17.65, 17.54, 17.43, 17.32, 17.21, 15.55, 14.57, 11.00.

DEPT (176 MHz, MeOH-d₄): δ = 138.85, 137.44, 136.65, 134.70, 134.22, 133.73, 133.37, 132.54, 129.67, 127.97, 127.51, 123.44, 119.51, 119.37, 119.29, 118.54, 81.77, 80.91, 80.69, 77.44, 77.20, 74.97, 74.62, 74.39, 74.00, 73.88, 70.75, 66.33, 49.00, 41.75, 39.51, 38.06, 37.15, 37.01, 35.43, 33.97, 32.72, 30.88, 28.08, 26.80, 21.56, 15.12, 14.14, 10.56.

HRMS (ESI) calculated for ([M+H]⁺): m/z = 1080.5903; experimental = 1080.5943

Compound 10



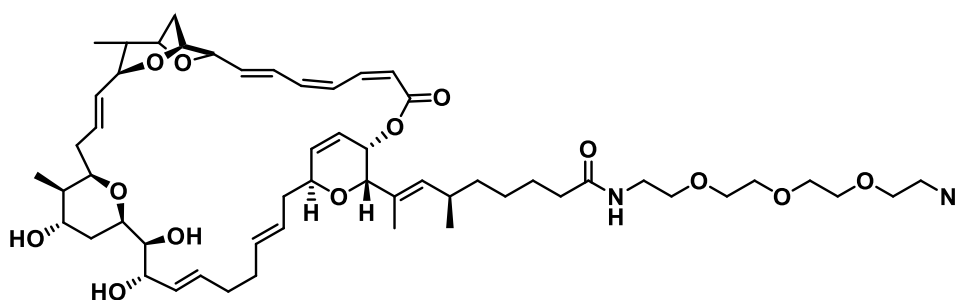
Azide **21** (27.11 mg, 0.031 mmol, 1.0 eq) was dissolved in DMF/H₂O (1:1, 200 μ L) and TBTA (1.66 mg, 0.003 mmol, 0.1 eq) in DMSO (10 μ L) was added. The alkyne **19** (23.05 mg, 0.019 mmol, 1.0 eq) dissolved in DMF (100 μ L) and pre-complexed with Zn(OAc)₂ (6.89 mg, 0.038 mmol, 2.2 eq) was added. Then sodium ascorbate (13.61 mg, 0.069 mmol, 2.2 eq) and CuSO₄ (10.97 mg, 0.069 mmol, 2.2 eq) dissolved in degassed DMF/H₂O (1:1, 200 μ L) were added and the reaction mixture continued stirring at 25 °C. Then the reaction was filtered over a syringe filter and purified by RP-HPLC (10-70 %, ACN/H₂O, 1% AcOH, 220 nm). Product containing fractions were identified by LCMS and lyophilized to yield **10** as a white solid (22.1 mg, 0.012 mmol, 39%).

¹H-NMR (700 MHz, MeOH): δ = 7.87 (s, 1H), 7.20 (m, 4H), 7.15 (m, 2H), 6.98 (m, 1H), 6.91 (m, 3H), 6.68 (m, 3H), 6.43 (t, J = 9.59 Hz, 1H), 6.22 (dd, J = 6.61, 16.20 Hz, 1H), 6.13 (dd, J = 3.64, 11.24 Hz, 1H), 6.00 (m, 1H), 5.74 (m, 1H), 5.60 (m, 2H), 5.52 (m, 2H), 5.47 (m, 1H), 5.38 (m, 2H), 5.29 (m, 2H), 5.17 (m, 1H), 4.83 (m, 5H), 4.58 (m, 7H), 4.53 (s, 2H), 4.39 (m, 2H), 4.35 (t, J = 7.60 Hz, 2H), 4.27 (d, J = 6.94 Hz, 1H), 4.18 (m, 2H), 3.85 (m, 2H), 3.81 (m, 1H), 3.69 (m, 1H), 3.53 (m, 7H), 3.45 (m, 10H), 3.41 (m, 5H), 3.15 (t, J = 7.60 Hz, 2H), 2.97 (m, 7 H), 2.72 (m, 7H), 2.35 (m, 2H), 2.25 (m, 1H), 2.15 (m, 14H), 1.91 (d, J = 10.58 Hz, 1H), 1.73 (d, J = 11.57 Hz, 1H), 1.67 (m, 1H), 1.61 (s, 3H), 1.55 (m, 3H), 1.42 (m, 1H), 1.36 (m, 1H), 1.29 (m, 2H), 1.19 (m, 3H), 0.87 (m, 6H), 0.79 (d, J = 6.61 Hz, 3H).

¹³C-NMR (176 MHz, MeOH-d₄): δ = 176.75, 173.55, 172.10, 167.83, 139.28, 137.90, 137.10, 135.20, 134.65, 134.12, 133.78, 131.29, 130.13, 128.42, 127.93, 127.10, 124.85, 123.85, 119.72, 119.21, 117.04, 82.22, 81.34, 81.15, 77.87, 77.64, 75.40, 75.06, 74.86, 74.42, 74.29, 71.20, 66.77, 57.87, 57.74, 57.62, 57.50, 57.38, 49.67, 42.17, 41.36, 41.18, 39.93, 39.82, 39.66, 38.75, 38.52, 37.46, 37.26, 35.95, 35.47, 34.42, 33.68, 33.17, 31.34, 31.18, 28.54, 27.29, 22.02, 17.64, 17.53, 17.42, 17.32, 17.21, 15.57, 14.61, 11.01.

HRMS (ESI) calculated for ([M+3H]³⁺): m/z = 643.6399; experimental = 643.4051

Compound 22



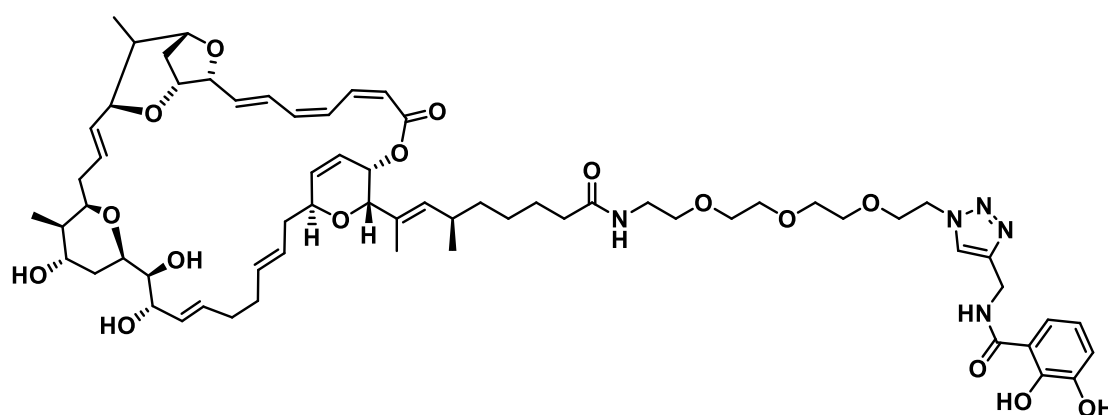
Sorangicin A **3** (15 mg, 0.019 mmol, 1.0 eq) was dissolved in dry DCM/DMF (500/50 μ L) and HATU (12.01 mg, 0.032 mmol, 1.7 eq) was added. The reaction was stirred 5 minutes at 25 $^{\circ}$ C before NH₂-PEG₃-N₃ (Sigma, 4.87 mg, 0.022 mmol, 1.2 eq) and DIPEA (9.93 μ L, 0.056 mmol, 3.0 eq) were added and the reaction was stirred overnight at ambient temperature. Then the solvent was removed under rotary evaporation and the residue was dissolved in ACN/H₂O and purified by RP-HPLC (10-80% ACN/H₂O, 0.1% HCOOH, 220 nm). The product containing fractions were lyophilized to yield amide **22** as a white powder (16.48 mg, 0.016 mmol, 88%).

¹H-NMR (700 MHz, DMSO-d₆): δ = 7.75 (t, J = 6.12 Hz, 1H), 7.11 (t, J = 11.91 Hz, 1H), 7.03 (t, J = 7.03 Hz, 1H), 6.91 (t, J = 14.63 Hz, 1H), 6.47 (t, J = 11.91 Hz, 1H), 6.21 (dd, J = 3.74, 15.65 Hz, 1H), 6.13 (dd, J = 4.08, 9.87 Hz, 1H), 5.96 (m, 1H), 5.63 (d, J = 11.91 Hz, 1H), 5.52 (m, 3H), 5.45 (m, 2H), 5.30 (m, 2H), 5.23 (d, J = 6.81 Hz, 2H), 4.49 (m, 1H), 4.42 (m, 1H), 4.37 (m, 1H), 4.33 (m, 1H), 4.18 (m, 2H), 3.94 (t, J = 4.76 Hz, 1H), 3.73 (t, J = 7.83 Hz, 1H), 3.68 (s, 1H), 3.63 (t, J = 8.85 Hz, 1H), 3.60 (t, J = 6.12 Hz, 3H), 3.55 (m, 3H), 3.52 (m, 6H), 3.49 (m, 3H), 3.38 (m, 6H), 3.28 (m, 2H), 3.17 (m, 3H), 2.29 (m, 2H), 2.08 (m, 5H), 2.01 (m, 6H), 1.92 (m, 1H), 1.80 (d, J = 10.89 Hz, 1H), 1.54 (s, 5H), 1.43 (m, 5H), 1.33 (m, 1H), 1.25 (m, 1H), 1.14 (m, 4H), 0.79 (d, J = 7.83 Hz, 3H), 0.75 (d, J = 6.81 Hz, 3H), 0.71 (d, J = 6.12 Hz, 3H).

¹³C-NMR (176 MHz, DMSO-d₆): δ = 172.36, 165.20, 137.61, 136.81, 135.84, 135.00, 132.22, 132.08, 131.85, 130.53, 130.32, 130.22, 129.53, 126.67, 125.40, 124.59, 122.37, 118.38, 80.01, 78.85, 78.44, 76.26, 75.14, 72.98, 72.73, 72.46, 72.13, 71.70, 69.79, 69.76, 69.69, 69.55, 69.25, 69.16, 68.43, 64.72, 49.98, 40.13, 40.02, 38.51, 38.42, 36.83, 36.74, 35.66, 35.45, 33.69, 32.57, 32.11, 31.08, 29.73, 26.55, 25.31, 20.79, 14.76, 13.48, 10.27, 0.11.

HRMS (ESI) calculated for ([M+H]⁺): m/z = 1007.5951; experimental = 1007.5957

Compound 11



Azide **22** (5.6 mg, 0.006 mmol, 1.0 eq) was dissolved in DMF/H₂O 1:1 (200 μ L) and TBTA (1 mg, 0.002 mmol, 0.1 eq) in DMSO (10 μ L) was added. The alkyne **16** (2.13 mg, 0.011 mmol, 2.0 eq) dissolved in DMF (100 μ L). Then sodium ascorbate (1.1 mg, 0.006 mmol, 1.0 eq) and CuSO₄ (0.18 mg, 0.001 mmol, 0.1 eq) dissolved in degassed water (200 μ L) were added and the reaction mixture continued stirring at 25°C for 30 minutes. Then the reaction was filtered over a syringe filter and purified by RP-HPLC (10-80 %, ACN/H₂O, 0.1% HCOOH, 220 nm). Product containing fractions were identified by LCMS and lyophilized to yield **11** as a white, slightly yellow solid (6.3 mg, 0.005 mmol, 95%).

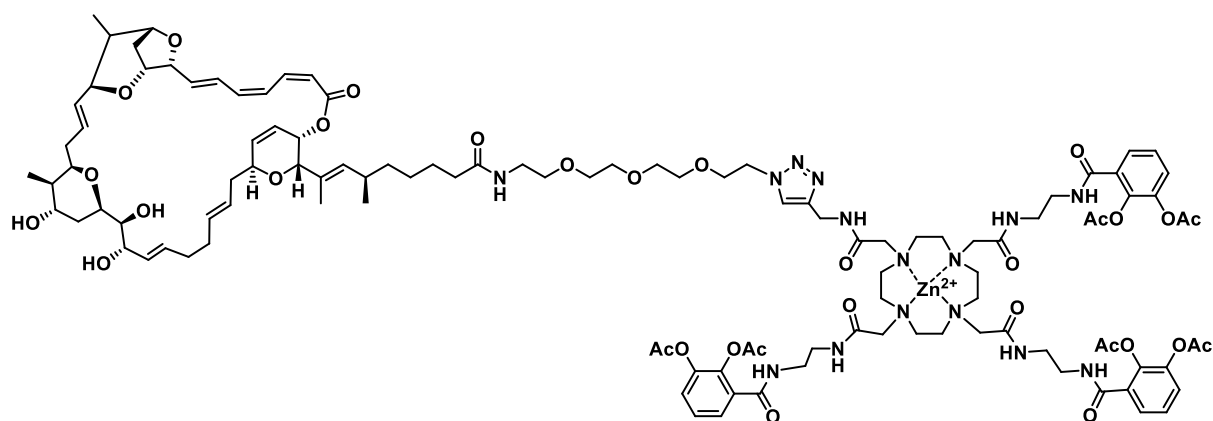
¹H-NMR (700 MHz, MeOH-d₄): δ = 7.94 (s, 1H), 7.23 (dd, J = 1.65, 8.57 Hz, 1H), 7.16 (m, 2H), 6.98 (m, 1H), 6.94 (dd, J = 1.35, 7.82 Hz, 1H), 6.72 (t, J = 7.82 Hz, 1H), 6.43 (t, J = 11.28 Hz, 1H), 6.20 (dd, J = 4.36, 15.19 Hz, 1H), 6.12 (dd, J = 3.46, 9.93 Hz, 1H), 6.00 (m, 1H), 5.74 (m, 1H), 5.60 (m, 2H), 5.52 (m, 2H), 5.48 (m, 1H), 5.37 (m, 1H), 5.30 (m, 2H), 4.64 (s, 2H), 4.56 (m, 1H), 4.40 (m, 4H), 4.26 (d, J = 6.92 Hz, 1H), 4.20 (s, 1H), 4.17 (q, J = 4.81, 7.37 Hz, 1H), 3.85 (m, 2H), 3.81 (t, J = 8.72 Hz, 1H), 3.69 (m, 1H), 3.48 (q, J = 4.36, 7.82 Hz, 1H), 3.19 (t, J = 6.62 Hz, 2H), 2.37 (m, 2H), 2.25 (m, 1H), 2.15 (m, 6H), 2.08 (m, 3H), 2.03 (m, 1H), 1.92 (d, J = 12.18 Hz, 1H), 1.73 (m, 1H), 1.65 (t, 1H), 1.62 (s, 1H), 1.55 (m, 3H), 1.38 (m, 2H), 1.29 (m, 1H), 1.20 (m, 1H), 0.86 (m, 6H), 0.80 (d, J = 6.92 Hz, 3H).

$^{13}\text{C-NMR}$ (176 MHz, MeOH-d₄): δ = 176.72, 171.68, 167.80, 150.52, 147.54, 146.49, 139.28, 137.87, 137.08, 135.13, 134.65, 134.16, 133.80, 133.03, 132.97, 131.27, 130.10, 128.40, 127.94, 127.13, 124.82, 123.87, 119.94, 119.80, 119.72, 118.97, 116.73, 82.20, 81.34, 81.12, 77.87, 77.63, 75.40, 75.05, 74.83, 74.43, 74.31, 71.18, 66.77, 57.87, 57.75, 57.62, 57.50, 49.68, 49.51, 49.39, 49.27, 49.15, 49.03, 48.90, 48.78, 42.18, 39.94, 38.73, 38.49, 37.58, 37.44, 37.27, 35.86, 35.47, 34.40, 33.67, 33.15, 31.31, 31.16, 28.51, 27.23, 22.00, 17.65, 17.54, 17.43, 17.32, 17.21, 15.55, 14.57, 11.00.

DEPT (176 MHz, MeOH-d₄): δ = 138.85, 137.44, 136.65, 134.70, 134.22, 133.73, 133.37, 132.54, 129.67, 127.97, 127.51, 123.44, 119.51, 119.37, 119.29, 118.54, 81.77, 80.91, 80.69, 77.44, 77.20, 74.97, 74.62, 74.39, 74.00, 73.88, 70.75, 66.33, 49.00, 41.75, 39.51, 38.06, 37.15, 37.01, 35.43, 33.97, 32.72, 30.88, 28.08, 26.80, 21.56, 15.12, 14.14, 10.56.

HRMS (ESI) calculated for ($[\text{M}+\text{H}]^+$): m/z = 599.8303; experimental = 599.8306

Compound 12



Azide **22** (8.0 mg, 0.008 mmol, 1.0 eq) was dissolved in DMF/H₂O (1:1, 200 μL) and TBTA (1.66 mg, 0.003 mmol, 0.1 eq) in DMSO (10 μL) was added. The alkyne **18** (19.51 mg, 0.016 mmol, 2.0 eq) was dissolved in DMF (100 μL) and pre-complexed with $\text{Zn}(\text{OAc})_2$ (17.43 mg, 0.079 mmol, 10.0 eq) in milliQ H₂O (100 μL). Then sodium ascorbate (1.57 mg, 0.008 mmol, 1.0 eq) and CuSO_4 (0.25 mg, 0.002 mmol, 0.2 eq), dissolved in degassed DMF/H₂O (1:1, 200 μL), were added and the reaction mixture continued stirring at 25 $^\circ\text{C}$. Then the reaction was filtered over a syringe filter and purified by RP-HPLC (10-70 %, ACN/H₂O, 1% AcOH, 220 nm). Product containing fractions were identified by LCMS and lyophilized to yield **12** as a white solid (16.4 mg, 0.007 mmol, 90%).

¹H-NMR (700 MHz, DMSO-d₆): δ = 7.91 (s, 1H), 7.77 (s, 1H), 7.11 (t, J = 11.95 Hz, 1H), 7.03 (t, J = 11.95 Hz, 1H), 6.91 (m, 1H), 6.65 (d, J = 6.83 Hz, 1H), 6.46 (t, J = 10.58 Hz, 1H), 6.21 (dd, J = 4.78, 14.68 Hz, 2H), 6.14 (dd, J = 4.99, 15.03 Hz, 1H), 5.95 (m, 1H), 5.61 (d, J = 11.95 Hz, 1H), 5.51 (m, 2H), 5.45 (m, 1H), 5.30 (m, 2H), 5.23 (d, J = 6.83 Hz, 2H), 4.49 (m, 1H), 4.43 (m, 2H), 4.35 (m, 3H), 4.17 (m, 2H), 3.94 (t, J = 6.83 Hz, 1H), 3.75 (m, 3H), 3.67 (m, 2H), 3.62 (t, J = 8.87 Hz, 2H), 3.53 (m, 2H), 3.45 (m, 14H), 3.37 (m, 10H), 3.17 (m, 7H), 3.00 (m, 7H), 2.82 (m, 6H), 2.45 (q, J = 7.85, 14.68 Hz, 6H), 2.28 (m, 2H), 2.10 (m, 4H), 2.00 (m, 6H), 1.90 (s, 4H), 1.79 (d, J = 10.58 Hz, 4H), 1.53 (s, 4H), 1.42 (m, 4H), 1.28 (m, 4H), 0.78 (d, J = 6.83 Hz, 3H), 0.75 (d, J = 6.83 Hz, 3H), 0.70 (d, J = 8.19 Hz, 3H).

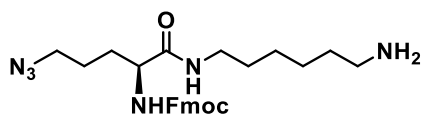
¹³C-NMR (176 MHz, DMSO-d₆): δ = 172.39, 172.09, 171.65, 169.62, 169.43, 165.18, 148.29, 143.75, 137.60, 136.80, 135.81, 134.99, 132.21, 132.07, 131.84, 130.52, 130.30, 130.20, 129.52, 126.65, 125.38, 124.57, 123.75, 122.35, 118.37, 118.02, 115.27, 115.13, 79.99, 78.84, 78.43, 76.25, 75.13, 72.97, 72.71, 72.45, 72.11, 71.69, 69.62, 69.54, 69.48, 69.11, 68.66, 68.41, 64.72, 64.08, 63.46, 60.70, 58.19, 55.51, 49.36, 48.58, 47.94, 42.06, 38.49, 38.39, 38.29, 37.24, 36.81, 36.73, 35.65, 35.43, 34.51, 33.67, 32.55, 32.10, 31.18, 31.07, 29.72, 29.17, 26.55, 25.29, 25.20, 25.15, 23.90, 22.52, 21.15, 20.78, 20.46, 20.41, 16.65, 14.91, 14.75, 13.92, 13.46, 12.17, 11.04, 10.25.

DEPT (176 MHz, DMSO-d₆): δ = 137.60, 136.80, 135.81, 134.99, 132.20, 132.06, 131.84, 130.52, 130.30, 130.19, 126.65, 125.38, 124.57, 123.75, 122.35, 118.36, 118.01, 79.99, 78.83, 78.42, 76.25, 75.12, 72.97, 72.71, 72.45, 72.11, 71.69, 69.62, 69.54, 69.48, 69.11, 68.72, 68.66, 68.41, 64.71, 64.08, 63.45, 60.70, 58.19, 55.50, 49.36, 48.57, 47.94, 42.05, 39.37, 39.23, 38.48, 38.39, 38.29, 37.93, 37.24, 36.81, 36.73, 35.65, 35.43, 35.35, 34.51, 33.67, 32.55, 32.10, 31.07, 29.72, 26.55, 25.44, 25.29, 25.20, 23.90, 22.52, 21.15, 20.78, 20.46, 20.41, 16.65, 14.91, 14.74, 13.77, 13.46, 12.17, 10.25, 10.18.

HRMS (ESI) calculated for ([M+H]⁺): m/z = 767.0154; experimental = 767.0159

Theranostic and imaging compounds

Compound 23



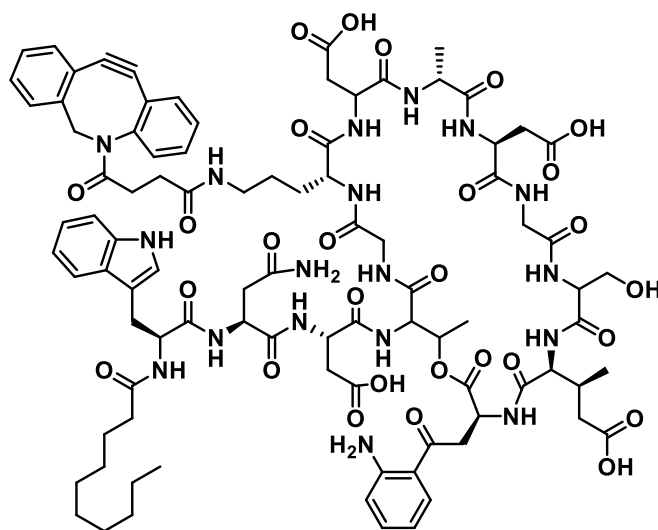
(S)-2-((((9H-fluoren-9-yl)methoxy)carbonyl)amino)-5-azidopentanoic acid (Sigma, 250 mg, 0.657 mmol, 1.0 eq) and HATU (499.8 mg, 1.314 mmol, 2.0 eq) were suspended in DCM/DMF and left stirring at 22 °C for 5 min, before the amine (148.48 mg, 0.789 mmol, 1.2 eq) and DIPEA (200 μ L) were added. The reaction continued stirring at 22 °C for 2 hours and then the solvent was removed *in vacuo* (**23a**). The residue was dried and dissolved in ACN (16 mL) before diethylamine (4 mL) was added. The 20% solution stirred for 1 hour before the solvent was removed *in vacuo*. The residue was purified by RP-HPLC (1%-35% ACN/H₂O, 0.1% AcOH) and product containing fractions were combined to yield pure title compound **23** as a beige oil (188.15 mg, 0.573 mmol, 87%).

¹H-NMR (500 MHz, DMSO-d₆): δ = 8.07 (s, 1H), 6.78 (t, J = 5.5.3 Hz, 1H), 3.33 (m, 3H), 3.06 (m, 2H), 2.89 (q, J = 7.23, 12.12 Hz, 2H), 1.59 (m, 4H), 1.37 (s, 15H).

¹³C-NMR (126 MHz, DMSO-d₆): δ = 156.07, 77.81, 53.81, 50.86, 38.67, 31.21, 28.74, 27.42, 26.88, 24.97.

HRMS (ESI) calculated for ([M+H]⁺): m/z = 479.2765; experimental = 479.2761

Compound 24



Daptomycin **1** (AcrosOrganics™, 100 mg, 0.062 mmol, 1.0 eq) was suspended in dry DMSO under argon and DIPEA (0.2 mL) was added. This allowed the full dissolution within minutes. Then DBCO-OSu (25 mg, 0.062 mmol, 1.05 eq) was added in one portion and the reaction continued stirring for two hours at 23 °C. Upon full conversion the base was removed by rotary evaporation and the residual solution purified by RP-HPLC (10-70% ACN/H₂O, 0.1% HCOOH, 220 nm). The product containing fractions were identified by LCMS and lyophilized to yield a slightly yellow powder as **24** (118.05 mg, 0.062 mmol, quant.).

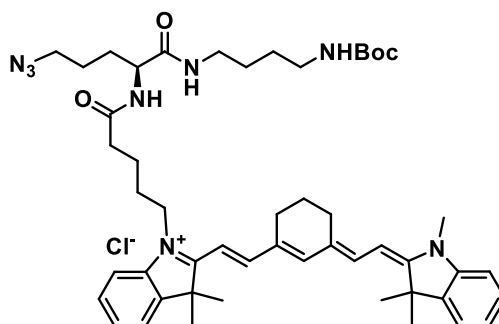
¹H-NMR (700 MHz, DMSO-d₆): δ = 7.68 (m, 4H), 7.57 (dd, J = 4.07, 7.05, 3H), 7.37 (m, 6H), 7.21 (m, 3H), 7.10-7.01 (m, 3H), 6.68 (m, 2H), 6.53 (m, 1H), 6.37 (m, 1H), 6.16 (d, J = 14.10 Hz, 2H), 5.49 (m, 1H), 4.11 (t, J = 7.59 Hz, 2H), 3.46 (d, J = 8.68 Hz, 1H), 3.09 (m, 2H), 2.95 (m, 1H), 2.57 (d, J = 4.61 Hz, 2H), 2.52 (m, 3H), 2.14 (m, 6H), 1.82 (m, 2H), 1.71 (m, 4H), 1.54 (m, 6H), 1.51 (m, 4H), 1.44 (m, 4H), 1.35 (m, 5H), 1.22 (m, 6H), 1.09 (m, 3H), 0.96 (m, 2H), 0.81 (m, 2H).

¹³C-NMR (176 MHz, DMSO-d₆): δ = 173.50, 172.85, 171.86, 171.68, 171.40, 170.94, 170.46, 170.36, 170.17, 170.07, 168.97, 168.76, 151.77, 151.14, 148.43, 136.00, 134.48, 132.37, 131.26, 129.42, 128.87, 128.08, 127.98, 127.65, 127.24, 126.76, 125.13, 123.67, 122.45, 121.37, 120.76, 118.33, 118.12, 116.89, 115.92, 114.52, 114.31, 111.20, 109.85, 108.15, 69.97, 61.89, 54.76, 54.14, 50.22, 49.66, 49.18, 38.03, 37.79, 37.01, 35.69, 35.44, 35.26, 34.98, 33.92, 31.24, 28.83, 28.73, 28.66, 28.57, 27.13, 25.39, 24.93, 24.84, 24.61, 24.51, 22.07, 16.90, 14.82, 13.95.

DEPT (176 MHz, DMSO-d₆): δ = 132.37, 131.27, 129.42, 128.87, 128.08, 127.98, 127.65, 126.75, 125.12, 123.66, 120.76, 118.33, 118.11, 114.51, 111.19, 61.88, 54.76, 54.14, 50.21, 49.66, 49.36, 39.39, 38.03, 37.79, 37.01, 35.45, 35.26, 34.98, 33.92, 31.24, 28.82, 28.73, 28.65, 28.56, 27.14, 25.39, 24.93, 24.61, 24.51, 22.07, 16.91, 14.82, 13.95.

HRMS (ESI) calculated for ([M+H]⁺): m/z = 954.4097; experimental = 954.4099

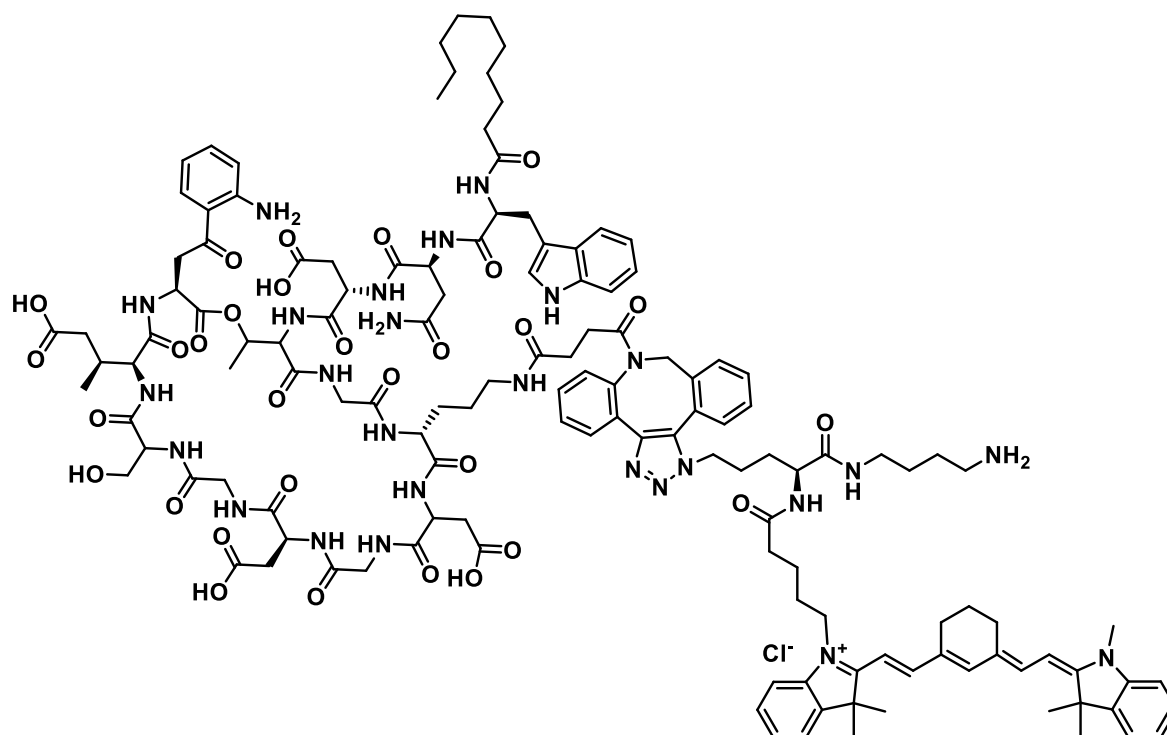
Compound **25**



Amine **24** (11.90 mg, 0.036 mmol, 1.0 eq) was dissolved in anhydrous DCM (500 μ L) under argon and DIPEA (50 μ L) was added. Then cyanin-7 succinimidylester (lumiprobe™, 24.61 mg, 0.038 mmol, 1.05 eq) was added in dry DCM (500 μ L) in the dark. The reaction continued stirring at 23 °C for two hours. The solvent was removed by rotary evaporation at 30 °C (dark) and yielded crude, pure amide (31.05 mg, 0.036 mmol, quant.) as a deep green solid **25**.

¹H-NMR (700 MHz, DMSO-d₆): δ = 7.90 (m, 1H), 7.68 (m, 3H), 7.57 (m, 2H), 7.37 (m, 4H), 7.21 (m, 2H), 6.15 (m, 2H), 4.10 (m, 2H), 3.61 (s, 3H), 3.36 (q, J = 7.00, 15.66 Hz, 2H), 3.29 (m, 5H), 3.01 (m, 2H), 2.88 (m, 1H), 2.59 (s, 3H), 2.54 (s, 1H), 1.81 (m, 2H), 1.72 (m, 2H), 1.66 (s, 13H), 1.55 (m, 2H), 1.49 (m, 2H), 1.35 (m, 10H), 1.23 (t, J = 8.66 Hz, 3H), 1.09 (bs, 7H).

¹³C-NMR (176 MHz, DMSO-d₆): δ = 172.75, 171.84, 171.36, 171.16, 170.32, 170.22, 155.56, 147.35, 142.92, 142.24, 140.82, 131.90, 131.74, 128.37, 124.53, 124.33, 122.35, 122.25, 110.85, 110.77, 100.09, 99.56, 77.31, 69.77, 62.51, 54.91, 51.99, 51.76, 50.27, 48.56, 48.52, 45.70, 43.16, 40.43, 38.21, 34.82, 33.48, 31.07, 29.50, 28.25, 27.17, 26.99, 26.91, 26.48, 26.40, 25.78, 25.43, 25.22, 24.89, 24.82, 23.37, 21.07, 7.16.

Compound **26**

25 (31.05 mg, 0.036 mmol, 1.0 eq) and **24** (103.31 mg, 0.054 mmol, 1.5 eq) were suspended in anhydrous MeOH (500 μ L) and stirred in the dark overnight at 23 $^{\circ}$ C. Then the solvent was removed and the residue was dried 1 h under high vacuum to yield **26a**. Then anhydrous DCM (400 μ L) was added under argon and the solution was cooled to 0 $^{\circ}$ C. Then TFA (20%, 100 μ L) was added dropwise at 0 $^{\circ}$ C and the reaction stirred 90 minutes under argon at that temperature, followed by 30 min at 23 $^{\circ}$ C to yield. Then the reaction was concentrated to dryness (water bath 30 $^{\circ}$ C, dark) and the residue was purified by RP-HPLC (10-50% ACN/H₂O, 0.1% HCOOH, 220 nm). Product containing fractions were identified by LCMS and lyophilized to yield **26** as a green solid (69.3 mg, 0.026 mmol, 72%).

Compound **26a** (Cy7 CL Dap DBCO)

¹H-NMR (700 MHz, DMSO-d₆): δ = 10.76 (s, 1H), 8.26 (m, 1H), 7.93 (m, 2H), 7.77 (m, 5H), 7.56 (m, 4H), 7.29 (m, 13H), 7.03 (t, J = 6.83 Hz, 1H), 6.95 (t, J = 7.07 Hz, 1H), 6.85 (bs, 1H), 6.74 (m, 2H), 6.50 (m, 1H), 6.14 (m, 1H), 4.49 (m, 5H), 3.64 (m, 8H), 3.17 (m, 16H), 3.06 (q, J = 7.42, 14.32 Hz, 10H), 2.88 (m, 5H), 2.59 (s, 3H), 2.54 (s, 2H), 2.03 (m, 7H), 1.80 (m, 2H), 1.65 (m, 12H), 1.36 (m, 18H), 1.24 (m, 6H), 1.18 (m, 13H), 1.07 (m, 4H), 0.84 (m, 4H).

¹³C-NMR (176 MHz, DMSO-d₆): δ = 174.36, 173.57, 172.81, 171.86, 171.52, 171.22, 170.43, 169.20, 157.78, 155.62, 151.18, 142.94, 142.36, 142.25, 141.18, 140.85, 136.05, 134.38, 131.95, 131.79, 129.34, 128.40, 127.29, 124.57, 124.37, 123.69, 122.38, 122.28, 120.80, 118.38, 118.18, 116.94, 116.11, 111.25, 110.88, 109.94, 100.20, 99.60, 77.44, 77.37, 69.80, 62.54, 52.02, 50.33, 50.04, 49.68, 48.62, 48.55, 48.38, 45.72, 43.20, 40.42, 40.00, 38.49, 38.26, 37.80, 35.02, 33.51, 31.28, 31.09, 31.06, 30.71, 30.03, 29.48, 28.87, 28.76, 28.69, 28.60, 28.27, 27.20, 27.02, 26.93, 26.52, 26.43, 26.19, 25.82, 25.70, 25.24, 24.98, 24.88, 24.20, 23.95, 23.37, 22.52, 22.11, 21.09, 17.11, 14.65, 13.99, 8.70, 7.18.

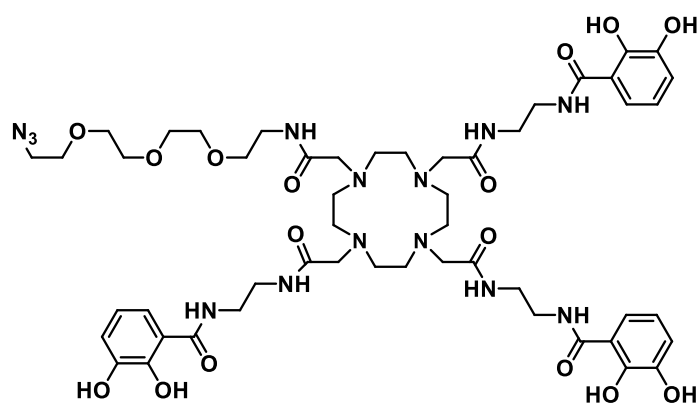
DEPT (176 MHz, DMSO-d₆): δ = 147.64, 134.15, 129.10, 128.21, 128.16, 124.33, 124.13, 123.45, 122.14, 122.03, 120.56, 118.14, 117.93, 116.70, 111.00, 110.63, 110.55, 99.95, 99.35, 69.56, 62.30, 51.78, 51.75, 51.58, 50.53, 50.09, 50.06, 49.79, 49.44, 48.37, 48.14, 45.47, 42.95, 42.86, 40.17, 39.22, 38.25, 38.02, 37.57, 36.98, 34.78, 34.68, 33.27, 31.04, 30.85, 30.82, 30.47, 29.78, 29.23, 28.86, 28.63, 28.52, 28.45, 28.36, 28.28, 28.03, 26.96, 26.78, 26.68, 26.28, 26.19, 25.95, 25.56, 25.46, 25.20, 25.00, 24.74, 24.68, 24.64, 23.96, 23.71, 23.13, 22.27, 21.87, 20.85, 13.74, 8.46, 6.93.

Compound **26**

¹H-NMR (700 MHz, DMSO-d₆): δ = 8.31 (m, 3H), 8.12 (m 1H), 7.99 (m, 2H), 7.71 (m, 8H), 7.57 (m, 5H), 7.39 (m, 5H), 7.30 (m, 2H), 7.21 (m, 4H), 7.14 (m, 1H), 7.03 (t, J = 7.38 Hz, 1H), 6.95 (t, J = 6.11 Hz, 1H), 6.87 (bs, 1H), 6.73 (d, J = 9.06 Hz, 1H), 6.52 (m, 1H), 6.15 (m, 1H), 5.75 (m, 1H), 5.26 (m, 1H), 5.04 (m, 1H), 4.87 (m, 1H), 4.50 (m, 9H), 4.24 (m 2H), 4.10 (m, 3H), 3.78 (m, 3H), 3.58 (m, 7H), 3.43 (m 3H), 3.10 (m, 10H), 3.01 (m, 3H), 2.91 (m, 2H), 2.79 (m, 3H), 2.71 (m, 1H), 2.59 (s, 4H), 2.34 (m, 7H), 2.17 (m, 3H), 1.97 (m, 6H), 1.79 (m, 3H), 1.66 (m, 14H), 1.53 (m, 6H), 1.37 (m, 8H), 1.23 (m, 5H), 1.17 (m, 21H), 1.14 (m, 4H), 1.08 (m, 4H), 0.83 (m, 6H).

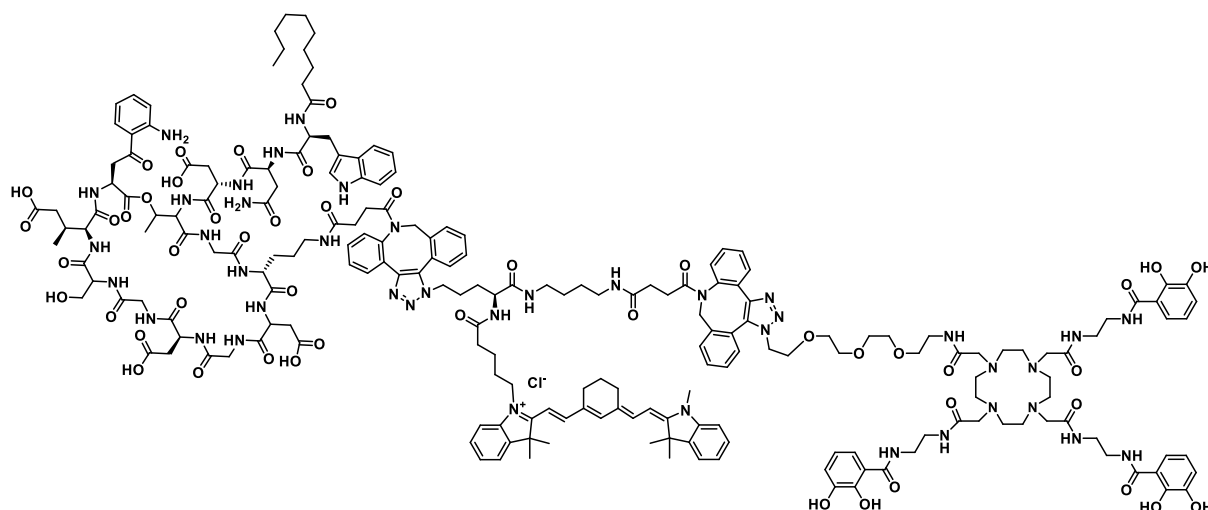
¹³C-NMR (176 MHz, DMSO-d₆): δ = 174.30, 173.53, 172.84, 172.76, 171.88, 171.78, 171.56, 171.42, 171.01, 170.22, 169.00, 168.78, 158.51, 158.30, 158.10, 157.89, 151.12, 147.89, 147.28, 143.36, 142.89, 142.25, 142.15, 140.85, 140.79, 136.02, 134.49, 132.13, 131.92, 131.72, 131.29, 128.37, 128.04, 127.25, 124.55, 124.29, 124.05, 123.69, 122.35, 122.25, 121.23, 121.13, 120.78, 120.68, 119.33, 118.34, 118.19, 118.13, 116.92, 116.54, 114.88, 114.57, 113.22, 111.22, 110.87, 110.69, 109.86, 100.17, 99.45, 90.92, 70.03, 69.77, 62.52, 61.85, 54.90, 51.99, 51.25, 50.22, 49.68, 49.39, 48.58, 48.48, 48.35, 45.72, 45.66, 43.20, 43.07, 40.42, 40.00, 38.57, 38.21, 37.91, 37.81, 37.03, 35.72, 35.44, 35.17, 34.97, 33.48, 31.25, 31.07, 30.00, 28.84, 28.74, 28.67, 28.58, 27.17, 26.97, 26.51, 26.03, 25.99, 25.93, 25.87, 25.43, 25.21, 24.93, 24.49, 24.17, 23.96, 23.33, 22.08, 21.06, 17.04, 16.94, 15.01, 14.84, 13.96, 8.60, 7.15.

DEPT (176 MHz, DMSO-d₆): δ = 131.28, 128.36, 128.04, 127.24, 124.30, 124.04, 123.68, 122.34, 122.25, 121.22, 121.12, 120.77, 120.67, 119.32, 118.33, 118.13, 116.91, 114.55, 111.21, 110.87, 109.86, 90.92, 69.77, 62.51, 54.90, 54.16, 51.98, 51.24, 50.22, 49.67, 49.39, 48.35, 45.72, 45.65, 43.06, 40.41, 38.56, 38.21, 37.90, 37.81, 37.02, 35.27, 34.97, 33.47, 31.25, 31.06, 29.99, 29.76, 28.83, 28.73, 28.66, 28.57, 27.17, 26.97, 26.50, 26.03, 25.67, 25.42, 25.21, 24.93, 24.48, 24.16, 23.95, 23.32, 22.08, 21.05, 16.93, 14.83, 13.95, 8.60, 7.15.

Compound **27**

Compound **27** was synthesized according C. Peukert, L. Langer et al.¹

Compound 13



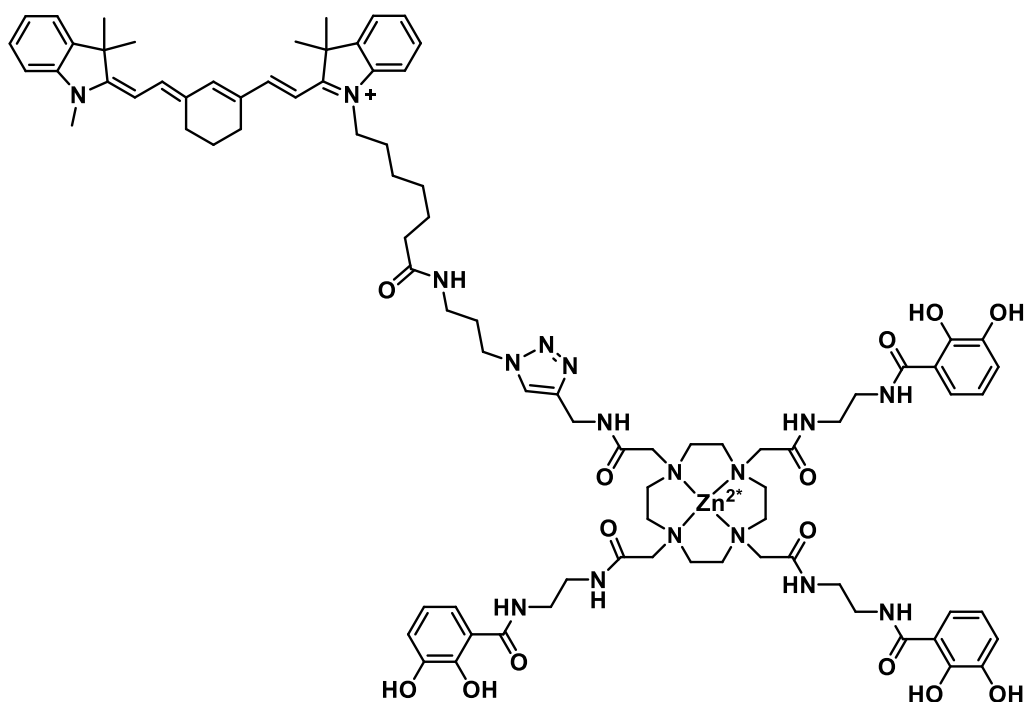
Amine **26** (69.3 mg, 0.026 mmol, 1.0 eq) was dissolved in dry DCM/DMF (5 mL, 10:1) under argon, followed by the addition of DIPEA (100 μ L) and DBCO succinimidylester (10.97 mg, 0.027 mmol, 1.05 eq) was added in one portion. The reaction continued stirring for two hours and the solvent was removed in vacuo. The residue was dried thoroughly overnight (**26b**) and meanwhile the azido DOTAM **27** (44.39 mg, 0.039 mmol, 1.5 eq) had been deacetylated with a 20% DIPEA solution in MeOH (2/8 mL respectively) and was also dried under high vacuum overnight. Then both residues were dissolved in MeOH, joined together and continued stirring in the dark at 23 $^{\circ}$ C overnight. Upon full conversion, the reaction mixture was injected into the RP-HPLC (10-80% ACN/H₂O, 0.1% HCOOH, 220 nm) and product containing fractions were identified by LCMS. Lyophilisation yielded theranostic **13** (90.7 mg, 0.022 mmol, 85%) as a green powder.

¹H-NMR (700 MHz, DMSO-*d*₆): δ = 10.75 (s, 1H), 8.88 (m, 1H), 8.34 (m, 1H), 8.16 (s, 2H), 7.93 (m, 3H), 7.82 (m, 1H), 7.67 (m, 7H), 7.56 (m, 8H), 7.46 (m, 1H), 7.36 (m, 11H), 7.19 (m, 12H), 7.03 (t, *J* = 7.76 Hz, 1H), 6.95 (t, *J* = 7.76 Hz, 1H), 6.88 (m, 3H), 6.74 (m, 1H), 6.63 (m, 2H), 6.50 (m, 1H), 6.14 (d, *J* = 14.42 Hz, 2H), 5.85 (m, 2H), 4.61 (m, 4H), 4.44 (m, 6H), 4.08 (m, 12H), 3.73 (m, 5H), 3.57 (m, 8H), 3.48 (m, 6H), 3.40 (m, 11H), 3.29 (m, 11H), 2.98 (m, 17H), 2.65 (m, 12H), 2.48 (m, 4H), 2.33 (m, 3H), 2.13 (m, 4H), 1.98 (m, 8H), 1.78 (m, 3H), 1.64 (m, 12H), 1.51 (m, 6H), 1.32 (m, 10H), 1.24 (m, 3H), 1.18 (m, 4H), 1.13 (m, 4H), 1.07 (m, 4H), 0.88 (m, 2H), 0.83 (t, *J* = 6.65 Hz, 4H).

¹³C-NMR: (176 MHz, DMSO-d₆): δ = 172.30, 171.99, 171.96, 171.75, 171.47, 171.33, 171.21, 171.16, 170.99, 170.87, 170.65, 170.59, 170.27, 169.91, 163.23, 151.12, 149.88, 147.69, 147.44, 146.28, 143.57, 142.90, 142.40, 142.30, 142.20, 142.18, 141.18, 140.80, 140.09, 136.00, 135.61, 134.66, 134.26, 134.14, 134.02, 133.95, 133.90, 132.17, 132.12, 131.90, 131.87, 131.79, 131.71, 131.59, 131.39, 131.35, 131.31, 131.15, 131.07, 130.83, 130.49, 130.37, 130.02, 129.97, 129.89, 129.51, 129.40, 129.23, 129.07, 128.66, 128.58, 128.31, 128.25, 127.41, 127.27, 126.85, 126.82, 126.76, 125.25, 124.78, 124.48, 124.45, 124.33, 124.09, 123.62, 122.30, 122.21, 120.71, 118.55, 118.35, 118.09, 117.61, 117.19, 116.82, 116.14, 114.95, 111.18, 110.77, 110.01, 100.05, 99.60, 69.99, 69.82, 69.57, 69.48, 68.90, 68.79, 68.57, 51.87, 51.76, 51.37, 51.28, 51.24, 51.19, 50.86, 50.74, 49.63, 48.57, 48.51, 48.41, 47.97, 47.51, 43.15, 40.42, 40.00, 38.22, 38.18, 38.13, 37.98, 35.08, 35.01, 34.97, 34.88, 31.25, 31.01, 30.08, 30.02, 29.92, 29.07, 28.84, 28.81, 28.72, 28.66, 28.56, 27.15, 26.98, 26.46, 26.01, 25.78, 24.96, 24.87, 23.32, 22.07, 21.04, 17.10, 15.95, 14.48, 13.94, 13.58.

DEPT(176 MHz, DMSO-d₆): δ = 155.03, 147.80, 147.74, 147.66, 147.48, 147.26, 134.23, 134.18, 134.13, 132.17, 131.85, 131.39, 130.50, 130.36, 130.02, 129.40, 129.23, 129.06, 128.65, 128.57, 128.39, 128.34, 128.24, 127.42, 127.40, 126.77, 124.45, 124.33, 123.62, 122.30, 122.22, 120.71, 119.17, 118.56, 118.35, 118.10, 117.60, 117.19, 116.82, 115.55, 111.18, 110.77, 100.11, 100.04, 99.59, 69.99, 69.81, 69.57, 69.45, 68.89, 68.79, 68.57, 51.84, 51.76, 50.86, 50.71, 48.41, 47.97, 47.56, 43.15, 40.41, 38.84, 38.52, 38.22, 38.14, 37.97, 35.11, 35.02, 34.97, 34.87, 31.24, 31.00, 30.08, 29.92, 29.07, 28.84, 28.72, 28.66, 28.56, 27.15, 26.98, 26.47, 25.77, 24.95, 23.32, 22.07, 21.03, 13.94.

HRMS (ESI) calculated for ([M+H]⁺): m/z = 1355.6458; experimental = 1355.6471

Compound **14**

Alkyne **19** (10 mg, 0.008 mmol, 1.0 eq) was dissolved in DMF/MQ water (1:1, 333 μ L), the $\text{Zn}(\text{OAc})_2$ (8.72 mg, 0.016 mmol, 2.0 eq) was added in one portion, followed by the addition of cyanin-7 azide (lumiprobe™, 10.87 mg, 0.016 mmol, 2.0 eq). After 5 min THPTA (0.71 mg, 0.002 mmol, 0.2 eq) was added followed by a mixture of sodium ascorbate (3.23 mg, 0.016 mmol, 2.0 eq) and CuSO_4 (0.26 mg, 0.002 mmol, 0.2 eq). The reaction continued stirring at 23 °C for 1 h. Then AcOH (100 μ L) was added and the reaction was purified by RP-HPLC (10-80% ACN/ H_2O , 1% AcOH, 220 nm). Product containing fractions were combined and lyophilized to yield **14** as a green powder (12.45 mg, 0.006 mmol, 80%).

$^1\text{H-NMR}$ (700 MHz, ACN- d_3): δ = 8.50 (m, 1H), 8.23 (m, 1H), 7.78 (m, 1H), 7.63 (m, 3H), 7.53 (m, 1H), 7.45 (t, J = 9.96 Hz, 3H), 7.37 (m, 3H), 7.30 (m, 5H), 7.21 (m, 5H), 7.05 (m, 2H), 6.09 (t, J = 14.09 Hz, 2H), 4.38 (m, 4H), 4.00 (m, 4H), 3.82 (s, 1H), 3.53 (s, 3H), 3.36 (m, 15H), 3.07 (m, 2H), 2.86 (m, 2H), 2.68 (m, 2H), 2.51 (bs, 5H), 2.26 (m, 12H), 2.21 (m, 6H), 2.11 (m, 2H), 1.92 (s, 18H), 1.86 (m, 2H), 1.76 (m, 2H), 1.65 (d, J = 5.10 Hz, 12H), 1.59 (m, 2H), 1.40 (m, 2H).

$^{13}\text{C-NMR}$ (176 MHz, ACN- d_3): δ = 173.97, 173.70, 171.01, 169.73, 169.65, 169.39, 168.89, 168.08, 166.45, 149.09, 144.35, 143.65, 142.13, 142.07, 141.75, 141.46, 133.25, 131.88, 129.60, 129.57, 127.54, 127.46, 127.25, 126.79, 125.68, 123.28, 123.18, 111.80, 111.57, 100.78, 79.22, 79.03, 78.85, 63.50, 56.86, 49.95, 48.67, 44.81, 43.70, 41.38, 40.44, 40.37, 40.23, 39.72, 36.97, 36.56, 32.01, 30.93, 30.08, 27.98, 27.81, 27.72, 27.17, 26.19, 24.64, 22.49, 22.42, 21.50, 21.00, 20.96, 20.89, 20.86.

DEPT (176 MHz, ACN-d₃): δ = 129.39, 129.36, 127.31, 127.26, 127.07, 127.03, 126.57, 125.46, 123.07, 122.97, 111.59, 111.36, 100.57, 63.29, 56.73, 49.74, 48.45, 44.59, 43.48, 41.17, 40.26, 40.22, 40.16, 40.02, 39.51, 36.77, 36.34, 31.79, 30.73, 29.87, 27.76, 27.60, 27.51, 26.96, 25.95, 24.45, 22.28, 22.21, 21.44, 20.81, 20.78, 20.68, 20.65.

MS (ESI) calculated for ($[M+2H]^{2+}$): m/z = 811.4436; experimental = 811.4442

General biological information

Biology figures, schemes and tables

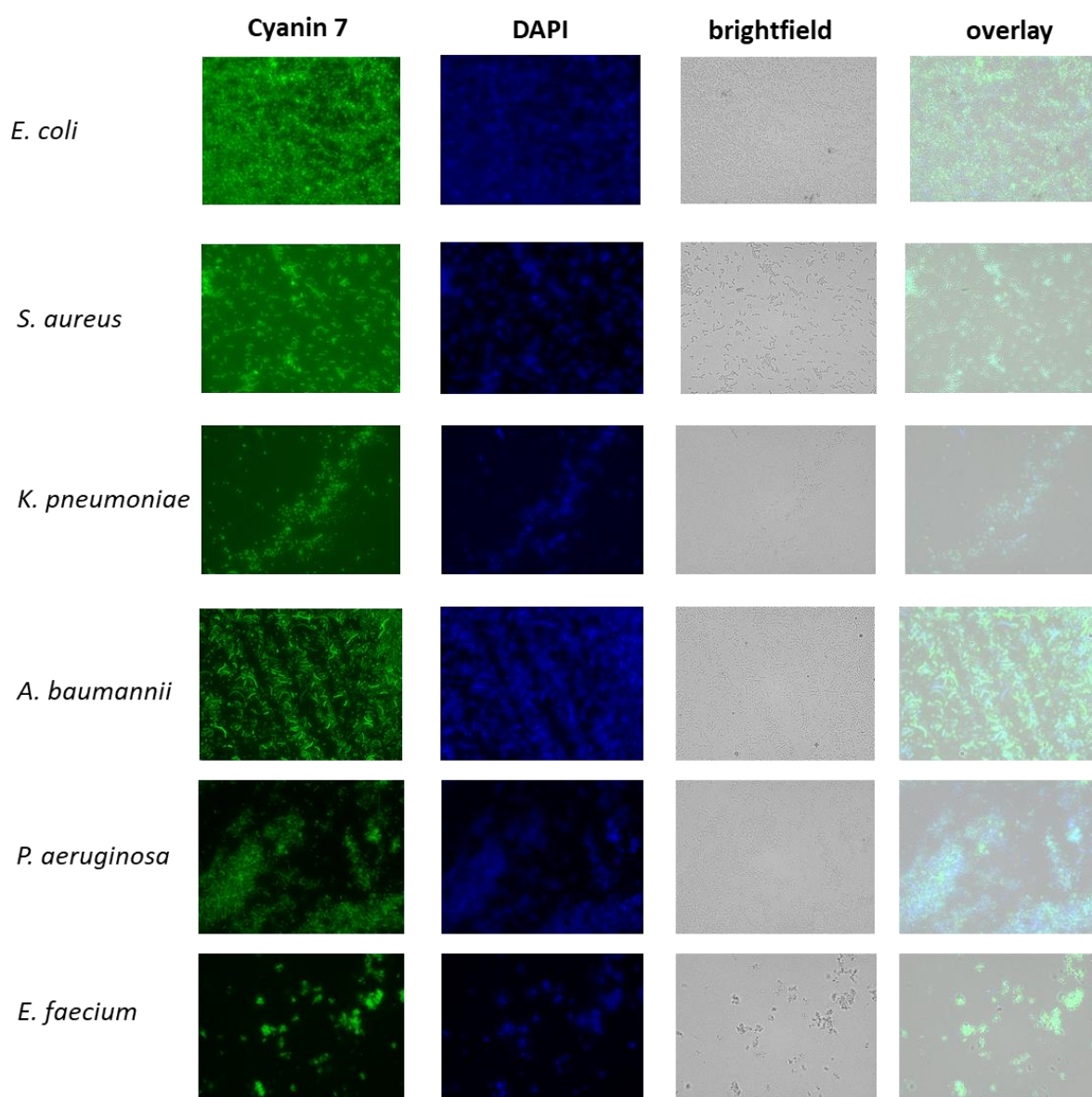


Figure S8.5: Microscopy pictures of ESKAPE pathogens after incubation with 10 μ M probe **14** for 18 hours in IDCAM. Cells were washed trice with PBS and resuspended in 4% PFA in PBS pH 7.4, then 1 μ L of a ready-to-use DAPI solution was added, samples were vortexed and stored at 4 $^{\circ}$ C in the dark until microscopy 48 hours later. Representative images of cyanin-7, DAPI and brightfield, as well as an overlay of three channels are shown from one of the three biological replicates.

MIC tests in iron-depleted, cation-adjusted medium

The minimal inhibitory concentration was determined in iron-depleted, cation-adjusted medium (IDCAM), as previously described by L. Pinkert, Y. Lai et al.⁴ Used strains are shown below.

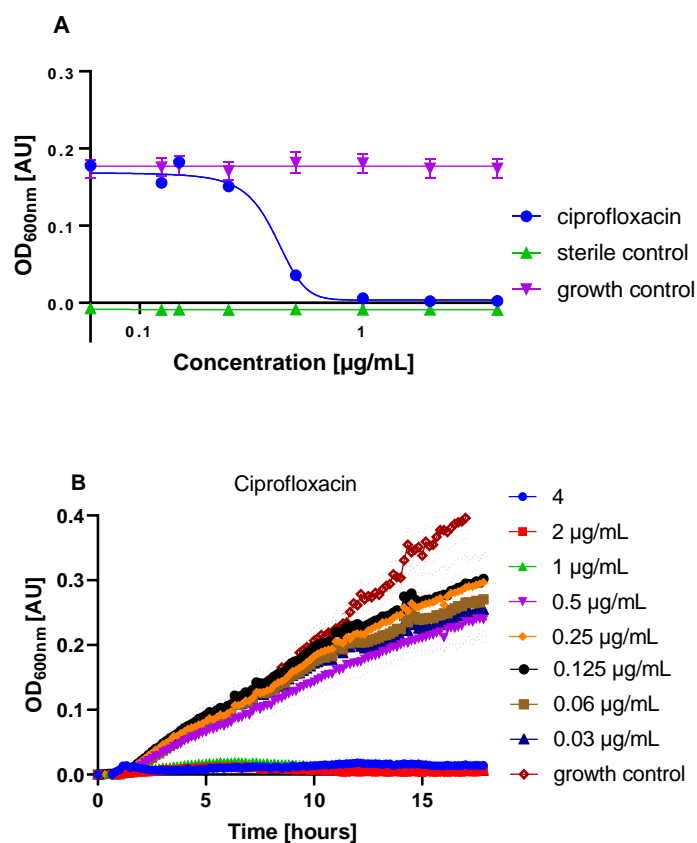


Figure S8.6. Cellular antimicrobial activity of imaging conjugate **14** in *A. baumannii*. (A) Ciprofloxacin, sterile and growth control in IDCAM of *A. baumannii* (DSM30007), in iron-depleted, cation-adjusted medium (IDCAM, with 110 µg/mL CaCl₂) (B) Growth kinetic (OD_{600nm}) of *A. baumannii* (DSM30007) in the presence of control antibiotic ciprofloxacin in IDCAM with 110 µg/mL CaCl₂ over 18 hours at 37 °C, dotted lines correspond to ± standard error of mean (SEM), n=3

Table S8.1. Bacteria used in the MIC assay.

Strain	DSMZ-#	Antibiotic Resistance	Medium
<i>Escherichia coli</i>	DSM1116	Penicillin G, Oxacillin, Vancomycin, Lincomycin, Bacitracin, Clindamycin, Linezolid, Nystatin, Quinupristin, Teicoplanin, Piperacillin	MHB
<i>Staphylococcus aureus</i>	DSM11822	Colistin, Kanamycin, Aztreonam, Oxacillin, Clindamycin, Nystatin, Lincomycin, Erythromycin, Norfloxacin, Pipedemic acid	TSY
<i>Klebsiella pneumoniae</i>	DSM11678	-	MHB
<i>Acinetobacter baumannii</i>	DSM30007	Penicillin G, Oxacillin, Ampicillin, Cefalotin, Cefazolin, Chloramphenicol, Vancomycin, Lincomycin, Pipedemic acid, Bacitracin, Clindamycin, Linezolid, Nystatin, Quinupristin, Teicoplanin,	MHB
<i>Acinetobacter baumannii</i>	DSM30008	Penicillin G, Oxacillin, Ampicillin, Cefalotin, Cefazolin, Vancomycin, Lincomycin, Linezolid, Nystatin, Quinupristin, Teicoplanin	MHB
<i>Pseudomonas aeruginosa</i>	DSM24068	Penicillin G, Oxacillin, Ampicillin, Mezlocillin, Cefalotin, Cefazolin, Cefotaxime, Chloramphenicol, Vancomycin, Erythromycin, Lincomycin, Ofloxacin, Norfloxacin, Pipedemic acid, Nitrofurantoin, Bacitracin, Kanamycin, Neomycin, Ceftriaxone, Clindamycin, Fosfomicin, Moxifloxacin, Linezolid, Nystatin, Quinupristin, Teicoplanin, Piperacillin	MHB
<i>Enterococcus faecium</i>	DSM20477	Colistin, Polymyxin B, Pipedemic acid, Nystatin, Aztreonam	TSY

Quantification of Sorangicin and derivatives in subcellular compartments of *E. coli* Δ entA

The compounds were quantified using our previously described protocol for strain cultivation, incubation, and cellular fractionation.⁵ In brief, a culture of *E. coli* Δ entA (CGSC# 11768) was grown in LB media over night. On the following day the culture was started in LB media at $OD_{600} = 0.2$ until it reached $OD_{600} = 0.8$. Cells were washed with twice with LMR media without $FeCl_3$ and centrifuged at $4500 \times g$.^{6, 7} Afterwards cells were adjusted to $OD_{600} = 1.0$ in LMR media (-/+ $10 \mu M FeCl_3$) and incubated with $50 \mu g/ml$ of respective compound for 10min. Thereafter cells were handled according to the protocol used by Prochnow *et al.*

LC/MS/MS measurements were carried out on an Agilent 1290 UHPLC (Agilent Technologies, Santa Clara, CA, USA) coupled to an AB Sciex QTrap 6500 triple quadrupole mass spectrometer (AB Sciex Germany GmbH, Darmstadt, Germany). The LC separations were conducted with a linear gradient of solvent A ($H_2O + 0.1\% HCOOH$) and solvent B (ACN + $0.1\% HCOOH$) from 1% B to 99% B within 8.5 min at a flowrate of 0.7 mL/min on a YMC - Pack TMS 100 mm \times 2.1 mm /S3- μm /12 nm column (YMC Europe, Dinslaken, Germany) equipped with a guard column. A multiple reaction monitoring (MRM) method was used for compound detection in positive and negative mode. The Q1/Q3 transition masses used for compound identification are given in Table S2 below. The reported data represent the average of two biological replicates performed on different days.

Table S8.2. MRM transitions of test compounds **3**, **9** and **10**.

Name	Mode	Q1 Mass (Da)	Q3 Mass (Da)	DP ^a (V)	CE ^a (V)	CXP ^a (V)
Caffeine (IS) ^a	positive	195,116	138,1	66	27	10
			110,1	66	31	6
540,964		90,9	16	93	14	
		79	16	123	12	
SorA_Dotam		964,607	896,4	246	49	20
			955,4	246	47	20
Glipizide (IS) ^a	negative	443,936	319,1	-66	-26	-21
			170,1	-66	-40	-7
805,359		761,4	-260	-46	-17	
		389,3	-260	-56	-21	

^a IS: internal standard; DP: declustering potential; CE: collision energy; CXP: collision cell exit potential

Cytotoxicity testing

The effect of compounds on cell viability was probed with a WST-1 assay, according to previously published procedures.^{8,9} The following immortalized cell lines were used: Mouse fibroblast cell line **L929** (DSM ACC 2), human cervix carcinoma cell line **KB-3-1** (DSM ACC 158), human breast cancer cell line **MCF-7** (DSM ACC 115), human lung carcinoma cell line **A549** (DSM ACC 107). Briefly, the subconfluent cells were washed with 1x PBS, trypsinized and resuspended in Dulbecco's modified eagle medium that contained 5% FBS (L929, KB-31, A-549, FS4-LTM) or Roswell Park Memorial Institute medium that contained 5% FBS, 0.5% Minimum Essential medium Non-Essential Amino Acids, Gibco (MEM NEAA), 0.5% GlutaAC (Gibco) and insulin at 5 µg/mL (MCF-7). 25 µL of serial dilutions of the test compounds were added to 25 µL of a cell suspension (1500 cells for KB-31, A-549, L929 and 3000 cells for MCF-7) in 384 well microtiter plates (final concentration range: 64-0 µM). Blank and solvent controls were incubated under identical conditions. The compounds (**1**, **13**, and **14**) were incubated for 24 h for the FS4-LTM cells and 5 days for the remaining cell lines. After the incubation period 3 µL WST-1 (ready-to-use solution from Roche) were added. The incubation time of the plates, which were briefly shaken at 37 °C, varied between the cell lines from 20 min for KB-3-1 up to 2 h for MCF-7 before measuring the absorption at 450 nm and reference at 600 nm with the Infinite 200 PRO Plate Reader (TECAN). The percentage of viable cells was calculated with respect to the solvent control (100% viability). EC₅₀ values were determined with GraphPad Prism 8.

Cellular fluorescence assay

The bacterial strains were used and maintained at 37°C in iron-depleted MHB (21 g/L Müller Hinton, pH 7.4, made iron-free by using CHELEX*). Before the assay, the strains were cultivated overnight in iron-free MHB at 37°C and 180 rpm. The next morning the overnight inoculum was diluted 1:25 in 10 ml iron-free MHB in 100 ml Erlenmeyer flasks with chicane.

After ca. 4 h (OD_{600nm} range 0.2 to 1.0) the inoculum was washed with 1xPBS (pH 7.4 – 3x 25 mL/tube, 4500 rcf, 5 min, 4 °C), then the pellet was diluted to an $OD_{600nm} = 0.4$ in iron-depleted MHB. The 10 mM compounds stocks in DMSO (cell culture grade) were diluted in iron-depleted to yield a 20 μ M intermediate solution and 300 μ L each were distributed into 1.5 mL tubes.

The washed bacterial suspension was added to 20 μ M compound in medium in a 1:1 dilution to yield an $OD_{600nm} = 0.2$ and a compound concentration of 10 μ M. For the solvent control, an equal amount of DMSO was diluted and added to the bacteria. Compound incubation was performed for 4 hours at 30 °C and 200 rpm on a shaker. Then bacteria were spun down and washed gently 6 times with 1 mL of 10% DMSO (v/v) in 1xPBS (pH 7.4 – 5 min, 4500 rcf, 4 °C, remove supernatant, add 1 mL, vortex 20 seconds). Low-binding tubes and tips were used and changed as often as possible, to reduce artificial fluorescence read-outs by residual dye sticking to the tubes.

The residual bacterial pellet was gently resuspended in 300 μ L fresh 10% paraformaldehyde solution (stored otherwise at -20 °C). This fixing buffer was supplemented with 3% glutaraldehyde; if the imaging facility was just S1 level, and bacteria were incubated in this mixture overnight at 4 °C. In all cases, 3 μ L of a ready-to-use solution of DAPI Rotiphorese solution was added and incubated for 30 min before pictures were taken. The imaging was performed in the fixation solution in ibidi™ 35 mm glass bottom dishes or the sample was distributed into a black 96-well transparent bottom plate (150 μ L / well) for quantitative analysis.

Plasma stability

Each compound (**1**, **14**, **26** or **26a**) dissolved in DMSO was added to pre-warmed (37 °C) mouse (pH 7.4) or human plasma (pH 7.4) to yield a final concentration of 1 µM. In addition, procaine and procainamide (dissolved in DMSO) were added to mouse or human plasma (pH 7.4) to yield a final concentration of 1 µM. Procaine served as positive control as it is unstable in mouse plasma. Procainamide served as negative control as it is stable in mouse plasma. The samples were incubated for 0, 15, 30, 60, 90, 120 and 240 min at 37 °C. At each time point, 10 µL of the respective sample was extracted with 90 µL acetonitrile containing 12.5 ng/mL caffeine as internal standard for 5 min at 2000 rpm on a MixMate vortex mixer (Eppendorf). Acetonitrile and caffeine were dispensed using a Mantis Formulatrix. The samples were centrifuged for 20 min at 2270 rcf at 4 °C and the supernatants were transferred to 96-well Greiner V-bottom plates. Next, samples were dried using N₂. Then samples were dissolved in 70 µL DMSO per well. Samples were analyzed using HPLC-MS/MS analysis as described in the respective section. Peak areas of each compound and of the internal standard were analyzed using the MultiQuant 3.0 software (AB Sciex). Peak areas of the respective compound were normalized to the internal standard peak area and to the respective peak areas at time point 0 min: $(C/D)/(A/B)$ with A: peak area of the compound at time point 0 min, B: peak area of the internal standard at time point 0 min, C: peak area of the compound at the respective time point, D: peak area of the internal standard at the respective time point. Every experiment was repeated independently at least three times.

Plasma protein binding

Plasma protein binding was assessed using the rapid equilibrium device (RED) system from ThermoFisher. Compounds **1**, **14**, **26** or **26a** were dissolved in DMSO. Naproxene served as control as it shows high plasma protein binding. Compounds were diluted in human plasma (human donors, both genders, pooled) to a final concentration of 1 μ M. Dialysis buffer and plasma samples were added to the respective chambers according to the manufacturer's protocol. The RED plate was sealed with a tape and incubated at 37 °C for 2 h at 800 rpm on an Eppendorf MixMate vortex-mixer. Then, samples were withdrawn from the respective chambers. To 25 μ L of each dialysis sample, 25 μ L of plasma and to 25 μ L of plasma sample, 25 μ L of dialysis buffer was added. Then, 150 μ L ice-cold extraction solvent (MeCN/H₂O (90:10) containing 12.5 ng/mL caffeine as internal standard) was added. Samples were incubated for 30 min on ice. Then, samples were centrifuged at 4 °C at 2270 rcf for 10 min. Supernatants were transferred to Greiner V-bottom 96-well plates and sealed with a tape. Then, samples were subjected to HPLC-MS/MS analysis as described in the section 'HPLC-MS/MS analysis'. The percentage of bound compound was calculated as follows:

$$f_{\text{bound}} = 1 - (C_{\text{buffer chamber}} / C_{\text{plasma chamber}}) * 100$$

HPLC-MS/MS analysis for plasma protein binding and plasma stability assays

Table S8.2. Quantifiers for plasma stability and binding studies.

ID	Q1 mass [Da]	Q3 mass [Da]	Time [msec]	DP [volts]	CE [volts]	CXP [volts]
Daptomycin 1 (Qtrap6500plus)	811.1	640.9	30	91	29	30
		341.1	30	91	33	16
Fragment of 14, 26 and 26a (Qtrap6500plus)	511.315	255.2	30	-55	-20	-23
		283.1	30	-55	-12	-27
		227.0	30	-55	-20	-11
Fragment of 14, 26 and 26a (Qtrap7500)	617.0	172.94	47.3	10	62	16
		372.95	47.3	10	21	32
		250.98	47.3	10	45	24
Naproxene	231.106	185.1	50	80	19	10
		170.2	50	80	33	12
Caffeine	195.024	138.0	50	80	25	14
		110.0	50	80	31	18
Procaine	236.773	100.0	30	80	21	12
		120.0	30	80	31	14
Procainamide	235.744	163.0	30	80	21	18
		120.0	30	80	39	12

Plasma protein binding samples were analyzed using an Agilent 1290 Infinity II coupled to an AB Sciex 6500plus mass spectrometer. For the plasma stability assay binding samples were analyzed using an Agilent 1290 Infinity II coupled to an AB Sciex 7500 mass spectrometer. LC conditions were as follows: column: Agilent Zorbax Eclipse Plus C18, 50x2.1 mm, 1.8 μm ; temperature: 30 $^{\circ}\text{C}$; injection volume: 5 μL per sample; flow rate: 700 $\mu\text{L}/\text{min}$. Solvents: A: H_2O + 0.1% formic acid; solvent B: 95% MeCN/5% H_2O + 0.1% formic acid. Gradient for naproxene: 99% A from 0 min until 1 min; 99 - 0% A from 1.0 until 5.5 min, 0% A until 6.0 min. Gradient for procaine and procainamide and compounds: 99% A from 0 min until 1.0 min, 99 - 0% A from 1.0 until 3.5 min, 0% A until 3.7 min. Mass transitions for controls and compounds are depicted in the table above.

Supplementary references

1. Peukert, C.; Langer, L. N. B.; Wegener, S. M.; Tutov, A.; Bankstahl, J. P.; Karge, B.; Bengel, F. M.; Ross, T. L.; Brönstrup, M., Optimization of artificial siderophores as ^{68}Ga -complexed PET tracers for *in vivo* imaging of bacterial infections. *J. Med. Chem.* **2021**, *64* (16), 12359-12378.
2. Ferreira, K.; Hu, H.-Y.; Fetz, V.; Prochnow, H.; Rais, B.; Müller, P. P.; Brönstrup, M., Multivalent siderophore–DOTAM conjugates as theranostics for imaging and treatment of bacterial infections. *Angew. Chem. Int. Ed.* **2017**, *56* (28), 8272-8276.
3. Fritsch, S.; Gasser, V.; Peukert, C.; Pinkert, L.; Kuhn, L.; Perraud, Q.; Normant, V.; Brönstrup, M.; Schalk, I. J., Uptake mechanisms and regulatory responses to MECAM- and DOTAM-based artificial siderophores and their antibiotic conjugates in *Pseudomonas aeruginosa*. *ACS Infect. Dis.* **2022**, *8*, 6, 1134-1146.
4. Pinkert, L.; Lai, Y.-H.; Peukert, C.; Hotop, S.-K.; Karge, B.; Schulze, L. M.; Grunenberg, J.; Brönstrup, M., Antibiotic conjugates with an artificial MECAM-based siderophore are potent agents against Gram-positive and Gram-negative bacterial pathogens. *J. Med. Chem.* **2021**, *64* (20), 15440-15460.
5. Prochnow, H.; Fetz, V.; Hotop, S. K.; García-Rivera, M. A.; Heumann, A.; Brönstrup, M., Subcellular quantification of uptake in Gram-negative bacteria. *Anal. Chem.* **2019**, *91* (3), 1863-1872.
6. Krasavin, M.; Parchinsky, V.; Kantin, G.; Manicheva, O.; Dogonadze, M.; Vinogradova, T.; Karge, B.; Brönstrup, M., New nitrofurans amenable by isocyanide multicomponent chemistry are active against multidrug-resistant and poly-resistant *Mycobacterium tuberculosis*. *Bioorg. Med. Chem.* **2017**, *25* (6), 1867-1874.
7. Wildermuth, R.; Speck, K.; Haut, F.-L.; Mayer, P.; Karge, B.; Brönstrup, M.; Magauer, T., A modular synthesis of tetracyclic meroterpenoid antibiotics. *Nat. Commun.* **2017**, *8* (1), 2083.

9. Publication 7: Cleavable RNA polymerase inhibitor siderophore conjugates as potent antimicrobial agents against multidrug-resistant bacteria

This chapter was included as a manuscript and will soon be submitted as an article to a peer-reviewed, scientific journal:

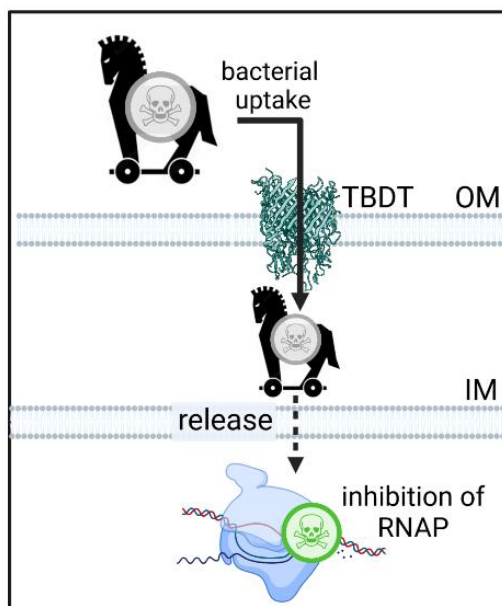
Carsten Peukert, Bianka Karge, Mark Brönstrup

"Cleavable RNA polymerase inhibitor siderophore conjugates as potent antimicrobial agents against multidrug-resistant bacteria".

Abstract

The growing antibiotic resistance, foremost in Gram-negative bacteria, requires novel therapeutic approaches. In order to overcome their double layered cell envelope and enhance the potency of the antibiotic rifamycin, we attached catechol siderophore mimics to evaluate their enrichment via the microbial iron transport machinery. As covalent modifications generally resulted in moderate to low antibiotic activity, cleavable linkers are required to permit a release of the payload inside the bacteria and lead to an unperturbed target binding. A systematic panel of cleavable siderophore-ciprofloxacin conjugates with variation at the chelator and the linker moiety was used to identify the quinone trimethyllock in conjugates **8** and **11** (MIC ≤ 1 μ M) as the superior linker system in terms of activity. Enzymatic activation assays with quinone oxidoreductases QOR2 from *E. coli* and diaphorase from *C. kluyveri* confirmed a linker activation and subsequent payload release. Finally, rifamycin SV, sorangicin A and coralopyronin A, representatives of three structurally and mechanistically different RNA polymerase inhibitor classes, were conjugated via the quinone linker to hydroxamate and catecholate hexadentate siderophores. Minimal inhibitory concentration assays in multidrug resistant, Gram-negative pathogens revealed a significant increase in antibiotic activity for the conjugates, while the free natural products or payloads remained mostly inactive.

Table of content graphic



9.1 Introduction

Drug resistance in bacteria poses an increasing threat to public health and is aggravated by the fact that few new antimicrobials pass clinical programs and progress towards approval.^{1, 2} Specifically Gram-negative microbes are a serious challenge, including four of the six ESKAPE pathogens (*E. coli*, *S. aureus*, *K. pneumoniae*, *A. baumannii*, *P. aeruginosa*, *E. faecium*), which are characterized by high intrinsic resistance to antibiotics and their ability to acquire further resistance by mutations and horizontal gene transfer.⁴ Infections with these bacteria are hard to treat with the existing arsenal of antibiotics available in the clinics.² For this reason, innovative approaches are required to develop robust drug candidates and to keep pace with the constant resistance development of multidrug resistant (MDR) pathogens. The two-membrane cell envelope of Gram-negative bacteria, which acts as a low permeability barrier, protects the pathogen against a variety of potentially harmful, bioactive molecules.^{5, 6} The outer membrane (OM), a lipid bilayer composed mostly of lipopolysaccharides, prevents the penetration of large, hydrophobic molecules. In contrast the inner membrane (IM), together with a thin peptidoglycan layer, restricts the translocation of polar compounds.⁷ The orthogonality of both membranes in combination with bacterial efflux pumps yields a barrier system that is impassable for many compounds (Figure 9.1A).⁸ Moreover, uptake studies found that the minor accumulation of e.g. rifampicin into Gram-negative bacteria directly correlated with a low antimicrobial activity against the pathogen.⁹ Despite these protective mechanisms, bacteria still require nutrients to survive and multiply in their ecological niche or a eukaryotic host organism. In this context, ferric iron is an essential nutrient, which is involved in central cellular processes such as DNA synthesis, ATP generation, oxidative stress protection and hence relates directly or indirectly to bacterial growth.¹⁰ Iron is mostly protein-bound in a eukaryotic host (e.g. heme, transferrin). Thus bacteria synthesize and secrete small molecule iron chelators, termed siderophores, in order to capture the metal from the environment.¹¹ TonB-dependent outer membrane transporters (TBDT) internalize these ferric chelates into the bacterial periplasm. Numerous studies have exploited siderophores as carrier moieties in a 'Trojan Horse' strategy, in order to actively enrich various payloads inside the bacterial pathogen.¹² Most studies focused on β -lactam conjugates that access periplasmic targets.¹³ This general principle has recently been validated clinically by the siderophore-containing cephalosporin antibiotic "cefiderocol" (Fetroja™) that recently obtained market authorization.^{14, 15} In this study we aimed to boost the potency of antibiotics acting in the cytosol towards Gram-negative bacteria by conjugation. In order to furnish potent antibiotic conjugates, we combined three functionalities in one molecule: a siderophore vector, which is effectively internalized by TBDTs, an enzymatically cleavable linker with widespread occurrence in Gram-positive and Gram-negative bacteria, that serves to release the third component, a natural product-based RNA-polymerase inhibitor (RNAP-I) (Figure 9.1B).

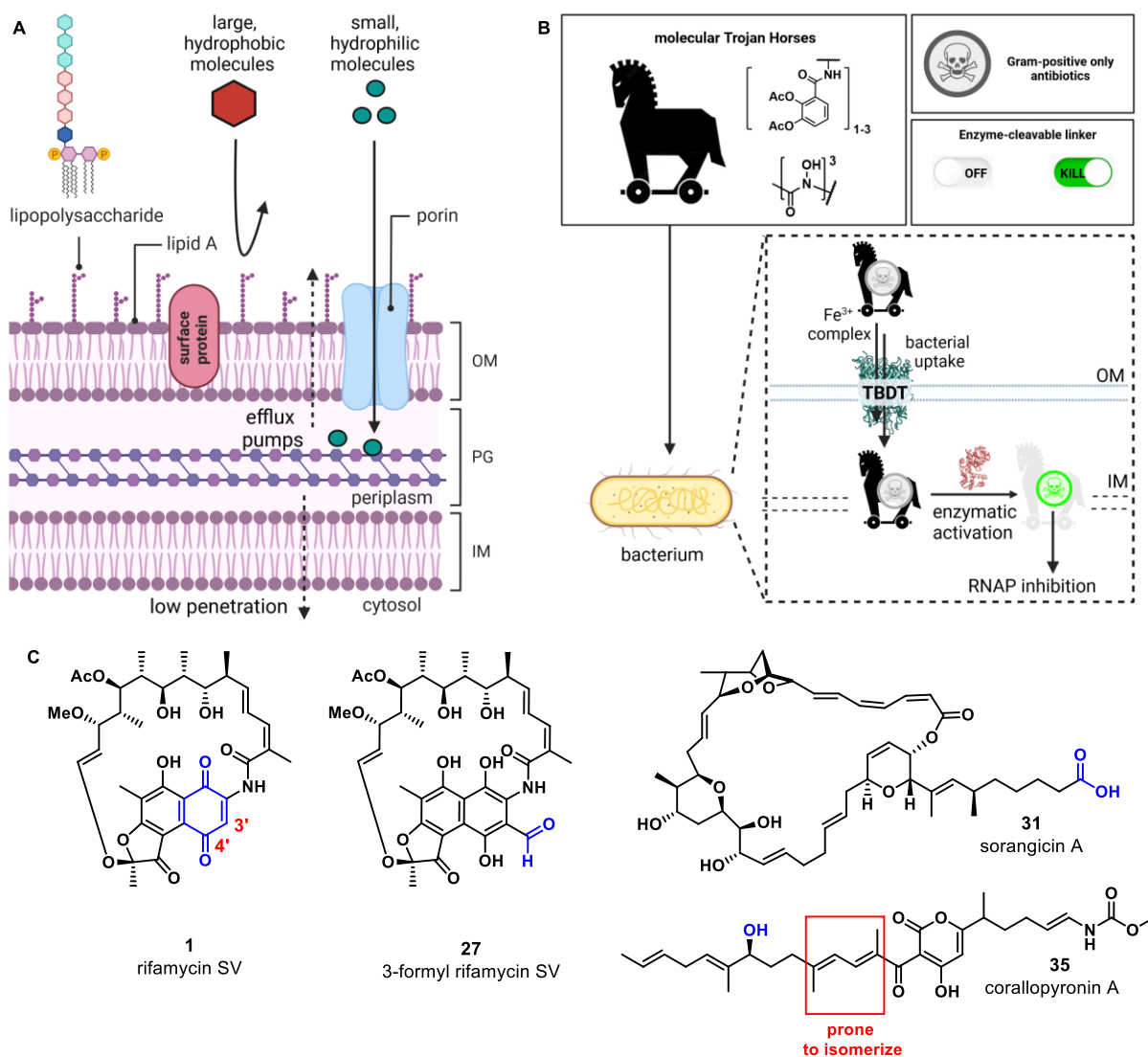


Figure 9.1. “Trojan Horse” strategy to increase the activity of antibiotics in Gram-negative pathogens. (A) Reduced permeability of the double layered, Gram-negative cell enveloped as an orthogonal, biological barrier. Graph inspired by Zhao et al.⁸ (B) Siderophore ‘Trojan Horses’ are attached through enzymatically cleavable linkers to antibiotics to restore their activity. Internalization by bacterial TonB-dependent transporters (TBDT) enables subsequent linker cleavage, payload release and antimicrobial action. (C) Structures of RNA-polymerase inhibitors (RNAP-I) rifamycin S **1** and 3-formyl rifamycin SV **27**, sorangicin A **31** and corallopyronin A **35** explored in this study. For each molecule the modification site is highlighted in blue.

To achieve this aim, we leveraged our previous synthetic advancements and mechanistic understanding on siderophore mimics as bacterial targeting agents diagnostic or therapeutic purposes.^{16, 17, 18, 19, 20} For the siderophore part, the DOTAM 1,4,7,10-tetraazacyclododecane-1,4,7,10-tetra acetic amide) and natural siderophore desferrioxamine (DFO) were chosen. Three different classes of RNAP inhibitors, represented by rifamycin S **1**, sorangicin A **31** and corallopyronin **35**, respectively, were employed as the antibiotic warheads (Figure 9.1C).

The DNA-dependent RNA polymerase (RNAP), the enzyme responsible for transcription of DNA into RNA, is the target of potent antibiotics like the ansamycin rifampicin, derived semisynthetically from rifamycin S **1** or 3-formyl-rifamycin SV **27**, which constitute a cornerstone in the treatment of tuberculosis.^{21,22} The polyketide sorangicin A (sorA, **31**), was isolated from the myxobacterium *Sorangium cellulosum* and exhibits selective, potent activity against bacterial RNAPs.^{23, 24} Despite addressing a similar binding site,²⁵ sorA was found recently to inhibit wild-type and mutant RNAPs through different mechanisms.²⁶ The third RNAP-I is corallopyronin A (corA, **35**) from *Coralloccoccus coralloides*, which could overcome rifamycin resistance by binding to the switch region of RNAP; the compound is currently in preclinical development for the treatment of filariasis.^{27, 28, 29, 30} All natural products exhibit high activities against Gram-positive bacteria, but show 100-1000 fold increased minimal inhibitory concentrations (MICs) against Gram-negative species (Table S9.1 and S9.2). Although systematic investigations for the underlying cause of this difference are missing, it was hypothesized that the difference in activity, is due to their difficulty to translocate over the double layered Gram-negative cell wall. Therefore, we aimed to exploit the active transport of siderophores to enrich these compounds in Gram-negative bacteria.

9.2 Results and Discussion

For siderophore conjugation especially mild synthetic strategies needed to be developed, as the natural products were sensitive to a range of reaction conditions in organic chemistry. For example, the lactone units of the rifamycins were prone to hydrolysis, the double bond of **35** was prone to isomerization at C5 to C8 (red box in Figure 9.1B), and the quinone moiety of **1** and **27** was redox sensitive. Thus those structural features required synthetic routes that avoided transition metal catalyzed reactions (e.g. click chemistry) or strongly acidic protection group chemistry (e.g. TFA). As the ansamycin bridge motif has been described to be important for rifamycin function, modifications generally exhibited a negative effect on the antimicrobial efficacy of the compound and cleavage of the bridge completely inactivated rifamycin.³¹ Therefore, we initially aimed to introduce a conjugation handle at the 3'/4' position of the naphthyl core (red numbers Figure 9.1B) of **1** based on existing protocols using mono TBS protected 2-amino-resorcinol **72** to give **73**. This could be reacted further to intermediate **74** by attaching an amine of choice using manganese dioxide (Figure 9.2A).³² However, the workup was found to be difficult, and the reaction generally led to low yields for the used amines (not shown). Therefore, we switched to a procedure with 4-fluoro-modified 2-amino-resorcinol **61**, developed by Genentech scientists in their synthesis of antibiotic antibody conjugates.^{33, 34} Reductive addition of **61** to **1** under protective atmosphere and subsequent re-oxidation to the quinone with oxygen and benzoquinone or TEMPO yielded fluoro-rifamycin S **2**. Upon the

nucleophilic aromatic substitution with primary amines, several linker moieties could be introduced to give the mono and dicatechol conjugated rifamycins **3** and **4**.

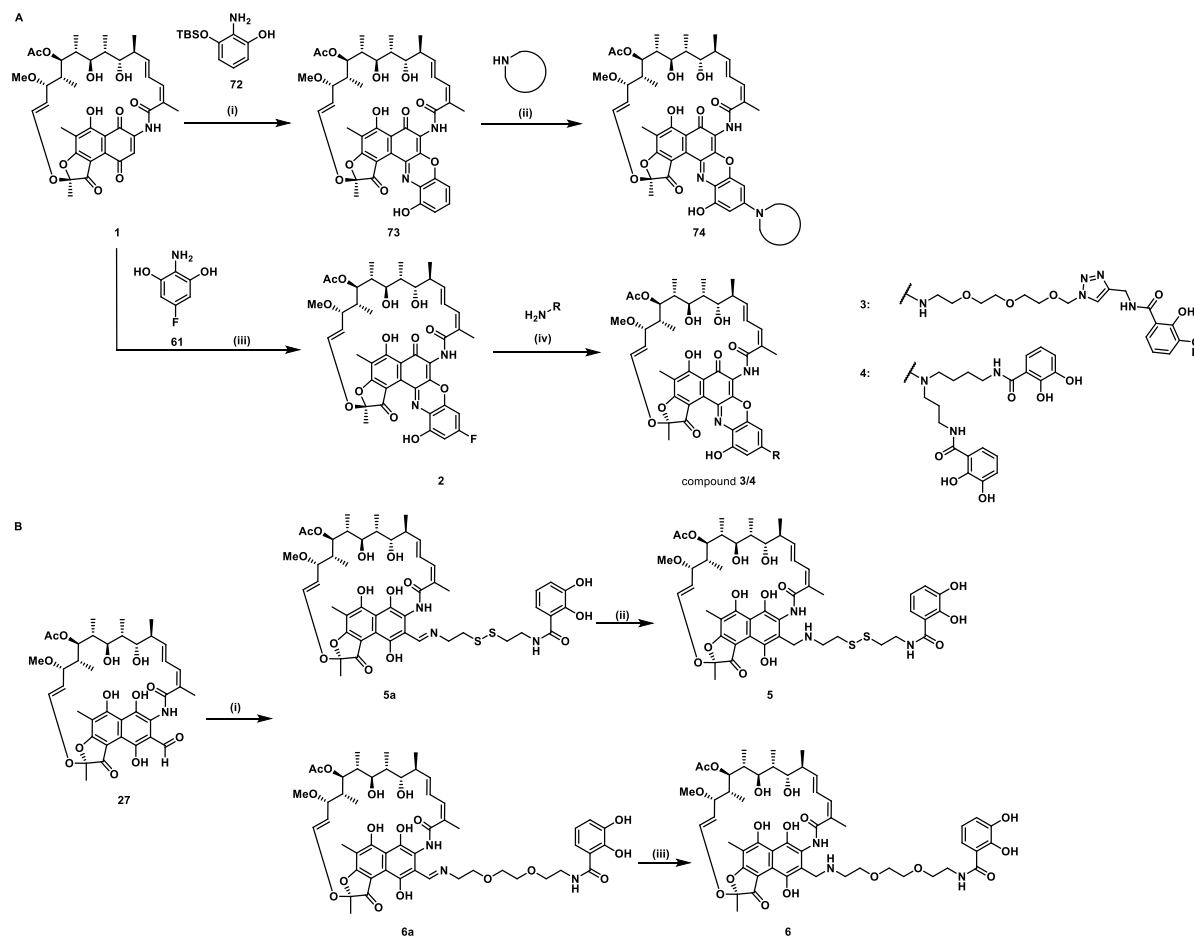


Figure 9.2. Synthesis of mono and dicatechol rifamycin derivatives **3-6**. (A) Amine-functionalized rifamycin S derivatives: (i) toluene, 22 °C, 19 h, then MnO_2 , EtOH, 22 °C, 23 h, (ii) amine, MnO_2 , 65 °C, low yield,³² (iii) **61**, argon - benzoquinone or TEMPO, oxygen, iPrOAc, 23 °C, 48 h, yield for Ar/BQ/O₂: 21% and Ar/TEMPO/O₂: 50%, (iv) DIPEA, DMSO, THF, 25-60 °C, 30-55%.³⁴ (B) Monocatechol derivatives of 3-formyl rifamycin SV **27**: (i) **40** or **41**, TEA, THF, 0-23 °C, 93-98%, (ii/iii) $NaBH(OAc)_3$, 1h, 0-23 °C, 57-79%. For detailed information, see the supporting information and Figure S9.1-S9.2.

The 3-formyl rifamycin **27** was reacted with the primary amines **40** or **41**, bearing a monocatechol unit with a disulfide linker or a covalent PEG linker, respectively, to the imines **5a** and **6a** and subsequently reduced to the amines **5** and **6** with $NaBH(OAc)_3$ in THF (Figure 9.2B). Biological testing of rifamycin **1** and its derivatives **2-6** in a minimal inhibitory concentration (MIC) assay under iron-depleted conditions **2**, **3**, **5a** and **6a** showed a retained activity against MDR *S. aureus* compared to the unmodified drug (Figure S9.17-S9.20 and Table S9.3). In MDR Gram-negative bacteria, these conjugates also exhibited a higher activity

than free, unmodified rifamycin **1** or fluoro intermediate **2**. Notably, dicatechol **3** exhibited an MIC of 500 nM in MDR *A. baumannii*, corresponding to a 4-32 fold increase in activity compared to **1** or to the fluorinated intermediate **2**. A recent study also reported that also the rifamycin derivative rifabutin was shown to exhibit a nanomolar MIC in carbapenem-resistant *A. baumannii* following uptake via the bacterium's siderophore receptor FhuE.³⁵ However, the increase of activity upon conjugation suggests that siderophore attachment, but not the ansamycin itself is responsible for the increased activity of **3** in *A. baumannii*. In sum, the bi- and tetradentate chelators could not achieve a potent, broad-spectrum antimicrobial activity. These observations are in accordance with literature findings that generally report a poor activity for most covalent conjugates with warheads aiming at cytosolic targets.³⁶ This implies that the passage of those compounds over the inner membrane needs to be considered in order to achieve a significant antimicrobial effect. Given the orthogonality of the two membranes, those conjugates may substantially benefit from an intracellular release mechanism for the antibiotic cargo to facilitate their translocation over the second membrane. We assumed that a cleavable conjugation to a hexadentate siderophore would not only enhance their accumulation but also their antibiotic activity. A second factor for the limited efficacy of **3-6** might be their reduced competitiveness towards natural triscatecholate siderophores (e.g. enterobactin) which form more stable, mononuclear iron complexes. We therefore aimed to couple a cleavable linker with siderophores that have higher coordination numbers, such as the triscatechol DOTAM (1,4,7,10-tetra azacyclododecane-1,4,7,10-tetra acetic amide) and desferrioxamine (DFO) siderophore.^{17, 19}

For a release within the pathogens, the trimethyllock (TML) linker system, which has been widely used for diagnostic probes and therapeutic conjugates in antibacterial research, was adapted.^{37, 38} In order to identify beneficial siderophore linker combinations, we used the antibiotic ciprofloxacin, with its well-established chemistry and mode of action, to optimize the chemistry and to study the effect of cleavable linkers before coupling to the more complex RNAP-inhibiting natural products. For an efficient release, a quinone based or a *para*-nitrobenzyl based linker was coupled to ciprofloxacin and then attached to monocatechol or hexadentate siderophores. Starting from 2,6-dimethylbenzene-1,4-diol and methyl 3-methylbut-2-enoate, the amino benzoquinone **51** was prepared in 8% yield over six steps based on modified literature procedures (Figure 9.3A).³⁸ Derivatization attempts with phosgene proved to be ineffective and only after extensive optimization efforts, triphosgene in toluene at 80 °C could be employed to introduce an *N*-Boc ethylenediamine linker and form the urea intermediate **52**. Ester hydrolysis, amide coupling and Boc group cleavage yielded **59a** in 51% over three steps. This key intermediate was coupled by mixed anhydride chemistry or thiourea formation to monocatechol, DOTAM or DFO siderophores (Figure 9.3B). The second linker was synthesized starting from a commercial synthetic amino acid over two steps to yield the

para-nitrobenzyl intermediate **54** in 83% yield (Figure S9.4A). Similarly ester hydrolysis, EDCI coupling of ciprofloxacin and boc group cleavage yielded key intermediate **60** over three steps in 65% yield, which was also conjugated to catechol, DOTAM or DFO siderophores (Figure S9.4B-C).

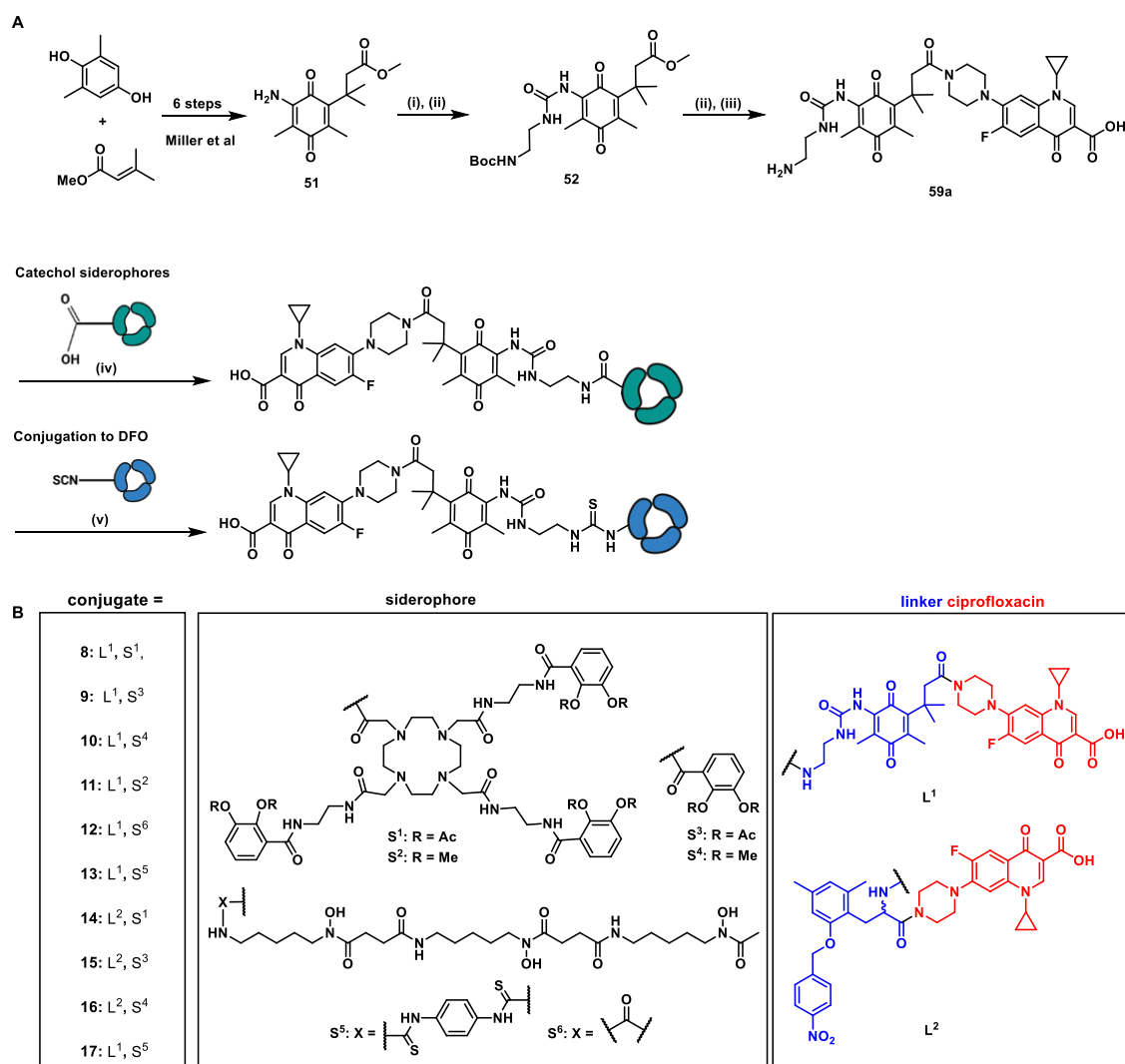


Figure 9.3. Enzymatically cleavable ciprofloxacin siderophore conjugates. (A) Exemplary synthesis of quinone based trimethyllock (TML) ciprofloxacin fragment **59a**: (i) triphosgene, anhydrous toluene, 23 - 80 °C, four hours, (ii) *N*-boc ethylenediamine, TEA, DCM, 0 - 23 °C, 59% over two steps, (iii) 1 N NaOH, MeOH/H₂O, (iv) ciprofloxacin, EDCI*HCl, HOBT, DIPEA, DCM, DMF, 0 - 23 °C, overnight, (v) 25% TFA in anhydrous DCM, 0 - 23 °C, 2 h, 51% over three steps, followed by a general strategy for conjugation to catechol siderophore units: (iv) *iso*-butylchloroformate, NMM, THF, 0-23 °C, 79-89% and desferrioxamine siderophores: (v) TEA, DMF, 23 °C, 73%. (B) Structures of synthesized monocatechol, DOTAM and desferrioxamine TML ciprofloxacin conjugates **8-17**. For detailed information on the synthetic procedures and reagents consult the supporting information.

The conjugates as well as the intermediates **52** and **59** were subjected to antimicrobial susceptibility testing under iron-depleted conditions in MDR *E. coli* to probe for the linker-siderophore combinations with the highest retained activity (Figure S9.21). Overall the hexadentate conjugates **8**, **12**, **13** and **17** exhibited a higher retained activity than the mono catechol conjugates. The quinone-based TML yielded lower MIC values than the *para*-nitrobenzyl TML analogue. The latter lacked two geminal methyl groups at the methylene, that drive the lactonization and payload release. The lower self-immolation speed and efficiency might contribute to their lower activity.

Table 9.1. MIC values^a for compounds **8** to **17**.

Compound	MW	Chelator	Linker	Payload	<i>E. coli</i>
8	1823	DOTAM	quinone	ciprofloxacin	2
9	844	CAT-Ac	quinone	ciprofloxacin	4
10	788	CAT-Me	quinone	ciprofloxacin	32
11	1655	DOTAM-Me	quinone	ciprofloxacin	>64
12	1151	DFO	quinone	ciprofloxacin	≤1
13	1387	DFO	quinone	ciprofloxacin	≤1
14	1830	DOTAM	nitro	ciprofloxacin	32
15	877	CAT-Ac	nitro	ciprofloxacin	>64
16	821	CAT-Me	nitro	ciprofloxacin	>64
17	1410	DFO	nitro	ciprofloxacin	≤1
52	451	-	quinone	-	>64
59	650	-	quinone	ciprofloxacin	2
cefiderocol	752	Cl-catechol	alkyl	cephalosporin	0.01
ciprofloxacin	331	-	-	ciprofloxacin	0.24

^a values are given in [μ M], MW = molecular weight [g/mol], CAT-Ac = 2,3-diacethoxy catechol, CAT-Me = 2,3-dimethoxy catechol, DFO = desferrioxamine, DOTAM-Me = DOTAM with methylated catechols prohibiting iron complexation.

The increased steric bulk for the DOTAM conjugates **8** and **14** also translated to a lower antibiotic activity than observed for the less strained DFO conjugates **11**, **12** and **17** with their elongated structure. In accordance with previous studies, the catechols were masked as acetylated prodrugs in order to avoid immediate deactivation of the iron chelating units by bacterial catechol-*O*-methyltransferases.³⁹ An exchange of the acetyl groups of **9** (4 μ M) with stable methyl groups as in **10** prohibited iron complexation and in turn TBDT uptake, and it decreased activity eight fold. As stated in literature, the molecular weight cut-off for unspecific uptake via bacterial porins ranges between 600-800 Da with species specific differences.^{40, 41}

Compound **10** with a molecular weight of 788 Da may still enter by passive diffusion, but less efficiently than acetylated conjugate **9**. The methylated triscatecholate conjugate **11** (1655 Da), with a molecular weight significantly above the cutoff for passive uptake, had no antimicrobial activity. This confirmed the central role of the siderophore carrier for bacterial accumulation and antimicrobial efficacy. Next, we verified whether bacterial enzymes could indeed activate the linker and release ciprofloxacin. The conjugates **11** and **13** were incubated with a quinone oxidoreductase QOR2 from *E. coli* and diaphorase from *C. kluyveri*¹⁹ in phosphate buffer (pH 7.4) at 30 °C. Analytical RP-HPLC traces were recorded at specific times and compared to a reference injection of free ciprofloxacin. Both enzymes led to a release of ciprofloxacin from the respective conjugates, and finally the less strained DFO conjugate **13** as well as the bulky DOTAM conjugate **11** were cleaved within 24 hours to show a similar result (see Figure S9.16). This is in line with our previous finding that these enzymes are able to cleave TML-based linker or trigger systems, thereby enabling the observed antimicrobial activities. All in all, the conjugates with a quinone-based TML linker retained the highest activity, and thus were selected for the conjugation of the RNAP-I payloads.

Next, reaction conditions were developed to synthesize covalent or cleavable RNAP-I siderophore conjugates. Rifamycins **1** and **27** were modified at the naphthyl core using the chemistry established above (Figure 9.2). Prior medicinal chemistry efforts at this position retained or increased the molecules antibiotic activity and even yielded potent, clinically used antibiotics like rifampicin, or rifabutin (Table S9.1 and S9.2).^{42, 43, 44, 45} As the binding site of rifampin is located within a shallow concave pocket formed by the RNAP β subunit, long azide bearing linkers were employed to reduce negative steric effects perturbing target binding (Figure 9.4A).⁴⁶

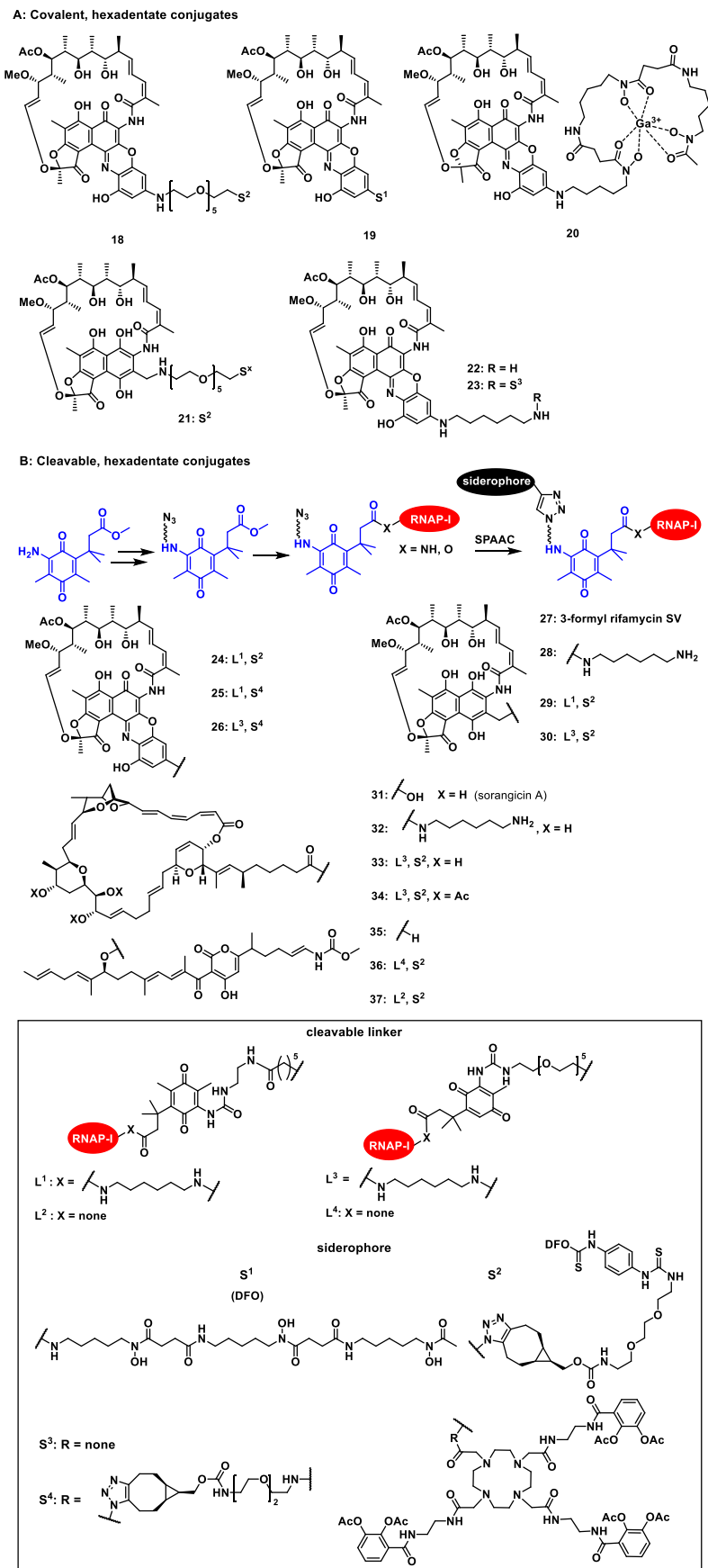


Figure 9.4. Structural overview of covalent and cleavable RNAP-I siderophore conjugates.

(A) Covalent conjugates **18-21** and **23**, including control rifamycin **22**. (B) Conjugates with a cleavable linker, top: synthesis overview, bottom: structural overview of control substances and conjugates **24-37**.

Conjugation via strain promoted azide alkyne cycloaddition (SPAAC) to alkyne DFO **47** then gave conjugates **18** and **21** in yields of 88% and 57%, respectively. Direct aromatic nucleophilic substitution of **2** with a DFO gave DFO rifamycin **19** (84% yield), which could be converted quantitatively to the gallium complex **20** under mild conditions. The 1,6-diaminohexane-modified rifamycin **22** could be attached by mixed anhydride coupling to DOTAM siderophore **7** and afforded rifamycin DOTAM conjugate **23** in 79% yield. For the synthesis of cleavable RNAP-I conjugates, the azido linker was incorporated first at the TML, as the natural products otherwise decomposed or isomerized under the strongly acidic reaction conditions required for protecting group cleavage (Figure 9.4B). Ester hydrolysis followed by mixed anhydride activation allowed the attachment of the native or 1,6-diaminohexyl-modified payloads to the TML fragment. According to previous studies, the replacement of sorangicin A's acid moiety with amide derivatives mostly retained their antibiotic activity in *S. aureus* or *E. coli* (Table S9.2).⁴⁷ This encouraged us to conjugate sorangicin A by amide chemistry. Along those lines, SPAAC with a BCN-modified DFO (**47**) or DOTAM (**45**) siderophore yielded the rifamycin (**24-26**, **29/30**), sorangicin A (**33/34**) and corallopyronin A (**36/37**) conjugates. Similarly, also the semi-synthetically modified natural products (**22**, **28**, **32** - Figure 3B bottom) were obtained.

All conjugates, reference natural products (**1**, **27**, **31**, **35**) and modified payloads were subjected to antimicrobial efficiency testing under iron-depleted conditions against MDR pathogens from the ESKAPE panel and against two siderophore-deficient strains (Table 9.2, Figures S9.22-S9.29, Tables S5-S8). While the control antibiotics exhibited activities in the expected ranges, neither the DOTAM siderophore **7**, nor the tested empty TML linker **53** or the linker payload intermediates without the siderophore carrier **65**, **67**, **69** and **70** were active (structures see the SI, MIC in Tables S9.5-S9.8). Interestingly, the covalent conjugate **19** and also its gallium-69 complex **20** exhibited retained activity against MDR *S. aureus*. This underlines the general ability of DFO conjugates to host a radioactive metal cation for PET imaging and upon conjugation to an antimicrobial payload still exert an antibiotic affect. Together with recent data from other studies on the *in vivo* imaging and treatment of microbes with DFO based probes this indicates the potential of DFO conjugates to serve as theranostics in antimicrobial chemotherapy.^{48, 49} In contrast to other studies, no activity increase was seen upon gallium-(III) incorporation.⁵⁰ Solely the uncomplexed compound **19** showed a potent, three fold lower MIC compared to free **1** in MDR *E. coli*. Possibly the direct attachment of DFO to the rifamycin and the steric bulk of the complex negatively affected target binding in the bacteria. Thus analogues with varying distance between DFO unit and the antibiotic should be explored.

Table 9.2. MIC values^a for **18** to **37** in MDR *E. coli*, *S. aureus*, *P. aeruginosa* strains.

Compound	<i>S. aureus</i>	<i>E. coli</i>	<i>P. aeruginosa</i>
1, rifS	≤0.5	25	32
2	4	>32	32
7	-	>32	>32
18	32	13	>32
19	1	8	>32
20	1	>32	>32
21	>32	4	>32 ^{GE}
22	4	>32	32
23	1	>32	>32
24	32	1	>32 ^{GE}
25	1	>32	>32
26	2	>32	>32
27, CHO-rifSV	≤0.5	16	8
28	>32	>32	>32
29	>32	1	>32 ^{GE}
30	>32	2	>32 ^{GE}
31, sorA	2	>32	≥32
32	>32	>32	>32
33	32	16	>32 ^{GE}
34	22	>32	>32
35, corA	>32	>32	>32
35*, corA	2	>32	>32
36	20	2	>32 ^{GE}
37	8	10	32
cefiderocol	>0.64	0.178	0.64
ciprofloxacin	-	0.54	-
amikacin	-	-	20-42
linezolid	3.71	-	-

a values are given in [μM], control compounds in grey, n = 2, DFO = desferrioxamine, rifS = rifamycin S, CHO-rifSV = 3-formyl rifamycin SV, sorA = sorangicin A, corA = corallopyronin A, GE = growth enhancing, 35* = fresh corallopyronin A.

Covalent and cleavable conjugates with a more bulky DOTAM carrier, namely **23**, **25** and **26**, were completely inactive in *E. coli* and *P. aeruginosa*. Their retained activity in *S. aureus* points towards a perturbed bacterial uptake and in turn, as indicated for the ciprofloxacin conjugates, towards a slower, inefficient enzymatic payload release. Expectedly, the free natural products and their derivatives displayed better activities in Gram-positive pathogens than the high molecular weight conjugates, due to a more rapid uptake of smaller compounds over their single layered cell envelope. Notably, the cleavable DFO rifamycin conjugates **24**, **29** and **30** exhibited MIC values around 1-2 μM in MDR *E. coli*, corresponding to a 25-32 fold improvement compared to rifamycins **1** or **2**. On the contrary, natural product based **27** based conjugates **21**, **29** and **30** lead to an increased growth in comparison to the solvent control, upon incubation with *A. baumannii* and *P. aeruginosa* (Figure S9.25-S9.28). This observation indicates that those conjugates shuttled iron into the bacteria, but exerted no antibiotic effect. With regard to the sorangicin conjugates, a basal activity could be detected for sorangicin A (**31**) in *S. aureus* and in siderophore deficient mutants of *E. coli*, but not for the amide modified payload **32**. Conjugates **33** and **34** showed a weak retained activity in *S. aureus* (22-32 μM) and an MIC of 16 μM for **33** in MDR wildtype *E. coli*. Corallopyronin A **35** was known to be sensitive towards basic or acidic conditions as the double bond was then prone to isomerize and form the biologically inactive isomer.²⁷ As the synthesis required minute amounts of base, we re-isolated the unreacted **35** from the reaction and compared its retained antibiotic activity to a novel aliquot of the natural product (**35***) which had not been exposed to basic conditions. The reisolated **35** was inactive in all tested strains, even in *S. aureus*, while fresh **35*** exhibited a 2 μM MIC in MDR *S. aureus* and a 32 μM MIC in MDR *E. faecium*. Due to the general inactivity of **35**, no activity was expected for the conjugates **36** and **37**. Surprisingly both conjugates, despite their synthesis in the presence of base, exhibited potent to moderate activity against MDR *E. coli* and *P. aeruginosa* in the range of 2-32 μM . Overall these results illustrate the potential of siderophore Trojan Horses to enhance the bacterial accumulation and consequently restore the activity of complex natural product antibiotics with cytosolic targets by harnessing TBDT.

9.3 Conclusion

The double layered Gram-negative membrane is a biological barrier that tightly restricts the accumulation of bioactive molecules in bacteria in a by and large unpredictable manner. In this study, we successfully restored the antibiotic activity of complex RNAP inhibitors, namely rifamycin SV, sorangicin A and coralopyronin A, by conjugation to siderophores and TBDT transport into Gram-negative bacteria. Several mono-, di- and triscatecholate as well as hydroxamate units were coupled to rifamycin antibiotics. However just a serendipitous improvement in antibiotic activity was observed for single compounds. This was in agreement with various literature studies that concomitantly observed a greatly reduced activity for most covalent siderophore conjugates attached to payloads with cytoplasmic targets. A systematic exploration of two cleavable linker systems with the payload ciprofloxacin yielded the quinone TML as the superior candidate with the highest retained activity. Finally, the covalent or cleavable attachment of DOTAM or DFO carriers to our natural product effectors yielded a structurally diverse compound collection. Consistently, siderophore conjugation was required to restore antimicrobial potency in Gram-negative pathogens, while the unconjugated linker fragments remained inactive. In sum, we expanded the application of natural and synthetic siderophores as a versatile carriers to enhance the accumulation and restore the potency of complex RNAP inhibitors through enzymatic release in Gram-negative bacteria.¹⁷

Acknowledgements

We thank Dr. Kirsten Harmrolfs, Dr. Linn Müggenburg, Christel Kakoschke and Monika Rettstadt for the measurement of NMR samples and Ulrike Beutling for the mass spectrometric measurements. We are thankful to Marc Stadler and the microbial drug unit at the Helmholtz Centre for Infection Research for providing us with sorangicin A and coralopyronin A.

Funding information

We acknowledge funding by the Joint Program Initiative on Antimicrobial Resistance (JPI AMR, grant number: 01KI1825). C. P. thanks the “Fonds der chemischen Industrie” for a scholarship.

References

1. Theuretzbacher, U.; Gottwalt, S.; Beyer, P.; Butler, M.; Czaplewski, L.; Lienhardt, C.; Moja, L.; Paul, M.; Paulin, S.; Rex, J. H.; Silver, L. L.; Spigelman, M.; Thwaites, G. E.; Paccaud, J. P.; Harbarth, S., Analysis of the clinical antibacterial and antituberculosis pipeline. *Lancet Infect. Dis.* **2019**, *19* (2), e40-e50.
2. Murray, C. J. L.; Ikuta, K. S.; Sharara, F.; Swetschinski, L.; Robles Aguilar, G.; Gray, A.; (...); Naghavi, M., Global burden of bacterial antimicrobial resistance in 2019: a systematic analysis. *The Lancet* **2022**.
3. Prasad, N. K.; Seiple, I. B.; Cirz, R. T.; Rosenberg, O. S., Leaks in the pipeline: a failure analysis of Gram-negative antibiotic development from 2010 to 2020. *Antimicrob. Agents Chemother.* **2022**, *66* (5), e00054-22.
4. De Oliveira, D. M.; Forde, B. M.; Kidd, T. J.; Harris, P. N.; Schembri, M. A.; Beatson, S. A.; Paterson, D. L.; Walker, M. J., Antimicrobial resistance in ESKAPE pathogens. *Clin. Microbiol. Rev.* **2020**, *33* (3), e00181-19.
5. Nikaido, H., Molecular basis of bacterial outer membrane permeability revisited. *Microbiol. Mol. Biol. Rev.* **2003**, *67* (4), 593-656.
6. Zgurskaya, H. I.; López, C. A.; Gnanakaran, S., Permeability barrier of Gram-negative cell envelopes and approaches to bypass it. *ACS Infect. Dis.* **2015**, *1* (11), 512-522.
7. Silver, L. L., A Gestalt approach to Gram-negative entry. *Bioorg. Med. Chem.* **2016**, *24* (24), 6379-6389.
8. Zhao, S.; Adamiak, J. W.; Bonifay, V.; Mehla, J.; Zgurskaya, H. I.; Tan, D. S., Defining new chemical space for drug penetration into Gram-negative bacteria. *Nat. Chem. Biol.* **2020**, *16* (12), 1293-1302.
9. Richter, M. F.; Drown, B. S.; Riley, A. P.; Garcia, A.; Shirai, T.; Svec, R. L.; Hergenrother, P. J., Predictive compound accumulation rules yield a broad-spectrum antibiotic. *Nature* **2017**, *545* (7654), 299-304.
10. Miethke, M.; Marahiel, M. A., Siderophore-based iron acquisition and pathogen control. *Microbiol. Mol. Biol. Rev.* **2007**, *71* (3), 413 – 451.
11. Kramer, J.; Özkaya, Ö.; Kümmerli, R., Bacterial siderophores in community and host interactions. *Nat. Rev. Microbiol.* **2020**, *18* (3), 152-163.
12. Gorska, A.; Sloderbach, A.; Marszall, M. P., Siderophore-drug complexes: potential medicinal applications of the 'Trojan horse' strategy. *Trends Pharmacol. Sci.* **2014**, *35* (9), 442 – 449.

13. Kong, H.; Cheng, W.; Wei, H.; Yuan, Y.; Yang, Z.; Zhang, X., An overview of recent progress in siderophore-antibiotic conjugates. *Eur. J. Med. Chem.* **2019**, *182*, 111615.
14. Wu, J. Y.; Srinivas, P.; Pogue, J. M., Cefiderocol: A novel agent for the management of multidrug-resistant Gram-negative organisms. *Infect. Dis. Ther.* **2020**, *9*(1), 17 – 40.
15. Portsmouth, S.; van Veenhuizen, D.; Echols, R.; Machida, M.; Ferreira, J. C. A.; Ariyasu, M.; Tenke, P.; Nagata, T. D., Cefiderocol versus imipenem-cilastatin for the treatment of complicated urinary tract infections caused by Gram-negative uropathogens: a phase 2, randomised, double-blind, non-inferiority trial. *Lancet Infect. Dis.* **2018**, *18* (12), 1319-1328.
16. Peukert, C.; Langer, L. N. B.; Wegener, S. M.; Tutov, A.; Bankstahl, J. P.; Karge, B.; Bengel, F. M.; Ross, T. L.; Brönstrup, M., Optimization of artificial siderophores as ⁶⁸Ga-complexed PET tracers for *in vivo* imaging of bacterial infections. *J. Med. Chem.* **2021**.
17. Ferreira, K.; Hu, H.-Y.; Fetz, V.; Prochnow, H.; Rais, B.; Müller, P. P.; Brönstrup, M., Multivalent siderophore–DOTAM conjugates as theranostics for imaging and treatment of bacterial infections. *Angew. Chem. Int. Ed.* **2017**, *56* (28), 8272-8276.
18. Pinkert, L.; Lai, Y.-H.; Peukert, C.; Hotop, S.-K.; Karge, B.; Schulze, L. M.; Grunenberg, J.; Brönstrup, M., Antibiotic conjugates with an artificial MECAM-Based siderophore are potent agents against Gram-positive and Gram-negative bacterial pathogens. *J. Med. Chem.* **2021**, *64* (20), 15440-15460.
19. Peukert, C.; Popat Gholap, S.; Green, O.; Pinkert, L.; van den Heuvel, J.; van Ham, M.; Shabat, D.; Brönstrup, M., Enzyme-activated, chemiluminescent siderophore-dioxetane probes enable the selective and highly sensitive detection of bacterial pathogens. *Angew. Chem. Int. Ed.* **2022**, *61*, e202201423.
20. Fritsch, S.; Gasser, V.; Peukert, C.; Pinkert, L.; Kuhn, L.; Perraud, Q.; Normant, V.; Brönstrup, M.; Schalk, I. J., Uptake mechanisms and regulatory responses to MECAM- and DOTAM-based artificial siderophores and their antibiotic conjugates in *Pseudomonas aeruginosa*. *ACS Infect. Dis.* **2022**, *8* (6), 1134–1146.
21. Darst, S. A., New inhibitors targeting bacterial RNA polymerase. *Trends Biochem. Sci.* **2004**, *29* (4), 159-162.
22. Am, G., Rifamycin. I. Isolation and properties of rifamycin B and rifamycin complex. *Antibiot. Ann.* **1959**, *7*, 262-270.

23. Jansen, R.; Wray, V.; Irschik, H.; Reichenbach, H.; Höfle, G., Isolation and spectroscopic structure elucidation of sorangicin a, a new type of macrolide-polyether antibiotic from gliding bacteria-XXX. *Tett. Lett.* **1985**, *26* (49), 6031-6034.
24. Irschik, H.; Jansen, R.; Gerth, K.; Hofle, G.; Reichenbach, H., The sorangicins, novel and powerful inhibitors of eubacterial RNA polymerase isolated from myxobacteria. *J. Antibiot.* **1987**, *40* (1), 7-13.
25. Campbell, E. A.; Pavlova, O.; Zenkin, N.; Leon, F.; Irschik, H.; Jansen, R.; Severinov, K.; Darst, S. A., Structural, functional, and genetic analysis of sorangicin inhibition of bacterial RNA polymerase. *EMBO J.* **2005**, *24* (4), 674-682.
26. Lilic, M.; Chen, J.; Boyaci, H.; Braffman, N.; Hubin, E. A.; Herrmann, J.; Müller, R.; Mooney, R.; Landick, R.; Darst, S. A.; Campbell, E. A., The antibiotic sorangicin A inhibits promoter DNA unwinding in a *Mycobacterium tuberculosis* rifampicin-resistant RNA polymerase. *Proc. Natl. Acad. Sci.* **2020**, *117* (48), 30423-30432.
27. Schäberle, T. F.; Schiefer, A.; Schmitz, A.; König, G. M.; Hoerauf, A.; Pfarr, K., Corallopyronin A – A promising antibiotic for treatment of filariasis. *Int. J. Med. Microbiol.* **2014**, *304* (1), 72-78.
28. O'Neill, A.; Oliva, B.; Storey, C.; Hoyle, A.; Fishwick, C.; Chopra, I., RNA polymerase inhibitors with activity against rifampin-resistant mutants of *Staphylococcus aureus*. *Antimicrob. Agents Chemother.* **2000**, *44* (11), 3163-3166.
29. Schiefer, A.; Hübner, M. P.; Krome, A.; Lämmer, C.; Ehrens, A.; Aden, T.; Koschel, M.; Neufeld, H.; Chaverra-Muñoz, L.; Jansen, R.; Kehraus, S.; König, G. M.; Pogorevc, D.; Müller, R.; Stadler, M.; Hüttel, S.; Hestekamp, T.; Wagner, K.; Pfarr, K.; Hoerauf, A., Corallopyronin A for short-course anti-wolbachial, macrofilaricidal treatment of filarial infections. *PLoS Negl. Trop. Dis.* **2020**, *14* (12), e0008930.
30. Schiefer, A.; Schmitz, A.; Schäberle, T. F.; Specht, S.; Lämmer, C.; Johnston, K. L.; Vassilyev, D. G.; König, G. M.; Hoerauf, A.; Pfarr, K., Corallopyronin A specifically targets and depletes essential obligate *Wolbachia* endobacteria from filarial nematodes *in vivo*. *J. Infect. Dis.* **2012**, *206* (2), 249-257.
31. Bujnowski, K.; Synoradzki, L.; Darlak, R. C.; Zevaco, T. A.; Dinjus, E., Semi-synthetic zwitterionic rifamycins: a promising class of antibiotics; survey of their chemistry and biological activities. *RSC Adv.* **2016**, *6* (115), 114758-114772.
32. John H. van Duzer, A. F. M., William B. Geiss, Douglas G., Joseph Raker, Rifamycin analogues and uses thereof, WO2005020894A2, 2004.

33. Lehar, S. M.; Pillow, T.; Xu, M.; Staben, L.; Kajihara, K. K.; Vandlen, R.; DePalatis, L.; Raab, H.; Hazenbos, W. L.; Hiroshi Morisaki, J.; Kim, J.; Park, S.; Darwish, M.; Lee, B.-C.; Hernandez, H.; Loyet, K. M.; Lupardus, P.; Fong, R.; Yan, D.; Chalouni, C.; Luis, E.; Khalfin, Y.; Plise, E.; Cheong, J.; Lyssikatos, J. P.; Strandh, M.; Koefoed, K.; Andersen, P. S.; Flygare, J. A.; Wah Tan, M.; Brown, E. J.; Mariathasan, S., Novel antibody–antibiotic conjugate eliminates intracellular *S. aureus*. *Nature* **2015**, *527* (7578), 323-328.
34. Bachmann, S. F., Serena Maria; Jansen, Michael; Koenig, Stefan; Linghu, Xin; Ri-Eth, Sebastian; Segraves, Nathaniel L.; Zogg, Andreas. Process for the preparation of an antibody-rifamycin conjugate. WO 2017/152083 A1, 2017.
35. Trebosc, V.; Schellhorn, B.; Schill, J.; Lucchini, V.; Bühler, J.; Bourotte, M.; Butcher, J. J.; Gitzinger, M.; Lociuro, S.; Kemmer, C.; Dale, G. E., *In vitro* activity of rifabutin against 293 contemporary carbapenem-resistant *Acinetobacter baumannii* clinical isolates and characterization of rifabutin mode of action and resistance mechanisms. *J. Antimicrob. Chemother.* **2020**, *75* (12), 3552-3562.
36. Klahn, P.; Bronstrup, M., Bifunctional antimicrobial conjugates and hybrid antimicrobials. *Nat. Prod. Rep.* **2017**, *34* (7), 832-885.
37. Ji, C.; Miller, M. J., Siderophore–fluoroquinolone conjugates containing potential reduction-triggered linkers for drug release: synthesis and antibacterial activity. *BioMetals* **2015**, *28* (3), 541-551.
38. Ji, C.; Miller, P. A.; Miller, M. J., Syntheses and antibacterial activity of *N*-acylated ciprofloxacin derivatives based on the trimethyl lock. *ACS Med. Chem. Lett.* **2015**, *6* (6), 707-710.
39. Ohi, N.; Aoki, B.; Kuroki, T.; Matsumoto, M.; Kojima, K.; Nehashi, T., Semisynthetic beta-lactam antibiotics. III. Effect on antibacterial activity and comt-susceptibility of chlorine-introduction into the catechol nucleus of 6-[(R)-2-[3-(3,4-dihydroxybenzoyl)-3-(3-hydroxypropyl)-1-ureido]-2- phenylacetamido]penicillanic acid. *J. Antibiot.* **1987**, *40* (1), 22-28.
40. Benz, R., Porin from bacterial and mitochondrial outer membrane. *Crit. Rev. Biochem. Mol.* **1985**, *19* (2), 145-190.
41. Prajapati, J. D.; Kleinekathöfer, U.; Winterhalter, M., How to enter a bacterium: bacterial porins and the permeation of antibiotics. *Chem. Rev.* **2021**, *121* (9), 5158-5192.

42. Adams, R. A.; Leon, G.; Miller, N. M.; Reyes, S. P.; Thantrong, C. H.; Thokkadam, A. M.; Lemma, A. S.; Sivaloganathan, D. M.; Wan, X.; Brynildsen, M. P., Rifamycin antibiotics and the mechanisms of their failure. *J. Antibiot.* **2021**, *74* (11), 786-798.
43. Mori, N.; Ishii, Y.; Tateda, K.; Kimura, S.; Kouyama, Y.; Inoko, H.; Mitsunaga, S.; Yamaguchi, K.; Yoshihara, E., A peptide based on homologous sequences of the β -barrel assembly machinery component BamD potentiates antibiotic susceptibility of *Pseudomonas aeruginosa*. *J. Antimicrob. Chemother.* **2012**, *67* (9), 2173-2181.
44. Lee, B.; Yan, J.; Ulhaq, A.; Miller, S.; Seo, W.; Lu, P.; She, R.; Spellberg, B.; Luna, B.; Bradford, P. A., *In vitro* activity of rifabutin and rifampin against antibiotic-resistant *Acinetobacter baumannii*, *Escherichia coli*, *Staphylococcus aureus*, *Pseudomonas aeruginosa*, and *Klebsiella pneumoniae*. *mSphere* **2021**, *6* (6), e00920-21.
45. Rothstein, D. M.; Shalish, C.; Murphy, C. K.; Sternlicht, A.; Campbell, L. A., Development potential of rifalazil and other benzoxazinorifamycins. *Expert Opin. Investig. Drugs* **2006**, *15* (6), 603-623.
46. Ho, M. X.; Hudson, B. P.; Das, K.; Arnold, E.; Ebright, R. H., Structures of RNA polymerase–antibiotic complexes. *Curr. Opin. Struct. Biol.* **2009**, *19* (6), 715-723.
47. Jansen, R.; Schummer, D.; Irschik, H.; Höfle, G., ChemInform Abstract: Antibiotics from gliding bacteria. Part 42. Chemical modification of sorangicin A and structure-activity relationship. Part 1. Carboxyl and hydroxyl group derivatives. *ChemInform* **2010**, *22*.
48. Pandey, A.; Cao, M.; Boros, E., Tracking uptake and metabolism of xenometallomycins using a multi-isotope tagging strategy. *ACS Infect. Dis.* **2022**, *8* (4), 878-888.
49. Petrik, M.; Umlaufova, E.; Raclavsky, V.; Palyzova, A.; Havlicek, V.; Pfister, J.; Mair, C.; Novy, Z.; Popper, M.; Hajdich, M.; Decristoforo, C., ⁶⁸Ga-labelled desferrioxamine-B for bacterial infection imaging. *Eur. J. Nucl. Med. Mol. Imaging* **2021**, *48*, 372.
50. Li, F.; Liu, F.; Huang, K.; Yang, S., Advancement of gallium and gallium-based compounds as antimicrobial agents. *Front. Bioeng. Biotechnol.* **2022**, *10*.

Supporting information

General chemical methods

All reactions that required anhydrous conditions were performed under an argon atmosphere and with dry, commercial solvents. All reactions were carried out at room temperature (23-25 °C) unless stated otherwise. All general reagents, including salts and solvents, were purchased from Sigma-Aldrich, Acros Organics and employed without purification in the respective synthetic procedures. Chemicals and solvents were either p. A. grade or purified by standard techniques. For work up procedures and purifications, solvents with purity grade HPLC grade or p. A. were employed. Glassware was dried at 120 °C in an oven for minimum 24 h prior to being used for synthesis. Indicated yields are calculated based on substance purity $\geq 95\%$ analyzed by NMR spectroscopy and liquid chromatography mass spectrometry (LCMS).

Thin-layer chromatography (TLC)

Reaction progress was controlled by thin layer chromatography (TLC) or Liquid Chromatography-coupled Mass Spectrometry (LCMS). TLC silica gel plates were Merck® 60 F254 and compounds were visualized by irradiation with UV light.

Column chromatography

Preparative normal phase purifications were performed with silica gel Merck® 60 (particle size 0.040-0.063 mm), eluent given in parentheses.

Reverse-phase HPLC (RP-HPLC)

RP-HPLC was performed on a Dionex Ultimate system from Thermo Fisher Scientific® with the HPLC columns indicated below. The eluent is specified in parentheses for the respective synthetic procedure. Two columns (both C18, 250x4.6mm) were used.

- Luna C18, 5 μm , 100 Å, 00G-4252-PO-AX
- Gemini C18, 10 μm , 110 Å, 00G-4436-PO

Characterization of synthetic compounds

All final compounds were characterized by ^1H -, ^{13}C -NMR spectra and mass spectrometry and the spectra are added in the appendix.

NMR spectroscopy

An Bruker Avance III 500 system with a PABBO BB/19F-1H/D Z-GRD probe head (500 MHz for ^1H , 125 MHz for ^{13}C spectra) and an Avance III HD 700 system (BRUKER) equipped with a cryo platform and a CPTCI 1H-13C/15N/D Z-GRD probe head (700 MHz for ^1H , 176 MHz for ^{13}C spectra) was used for NMR measurements. Substances were dissolved in deuterated solvents prior to the measurements and chemical shifts δ are given in parts per million (ppm). Multiplicities are stated as follows: s (singlet), d (doublet), t (triplet), q (quartet), p (quintet) and combinations of the latter. Further included are bs (broad singlet) and m (multiplet). All spectra are interpreted as first-order spectra and coupling constants J are given in Hertz (Hz), which refer to ^1H - ^1H -couplings.

Mass spectrometry

Mass spectra (MS) were measured on Waters Xevo TQD. High-resolution mass spectrometry (HRMS) was performed via a Dionex Ultimate 3000 HPLC system (Thermo Fisher Scientific, Dreieich, Germany) equipped with a DAD detector and a QTOF mass detector with electrospray ionization (ESI) (Bruker maxis HD, Bremen, Germany). Samples were directly injected via an Ultimate 3000RS autosampler (Thermo Fisher Scientific, Dreieich, Germany). The mass-to-charge ratio m/z is indicated.

Chemistry figures and tables

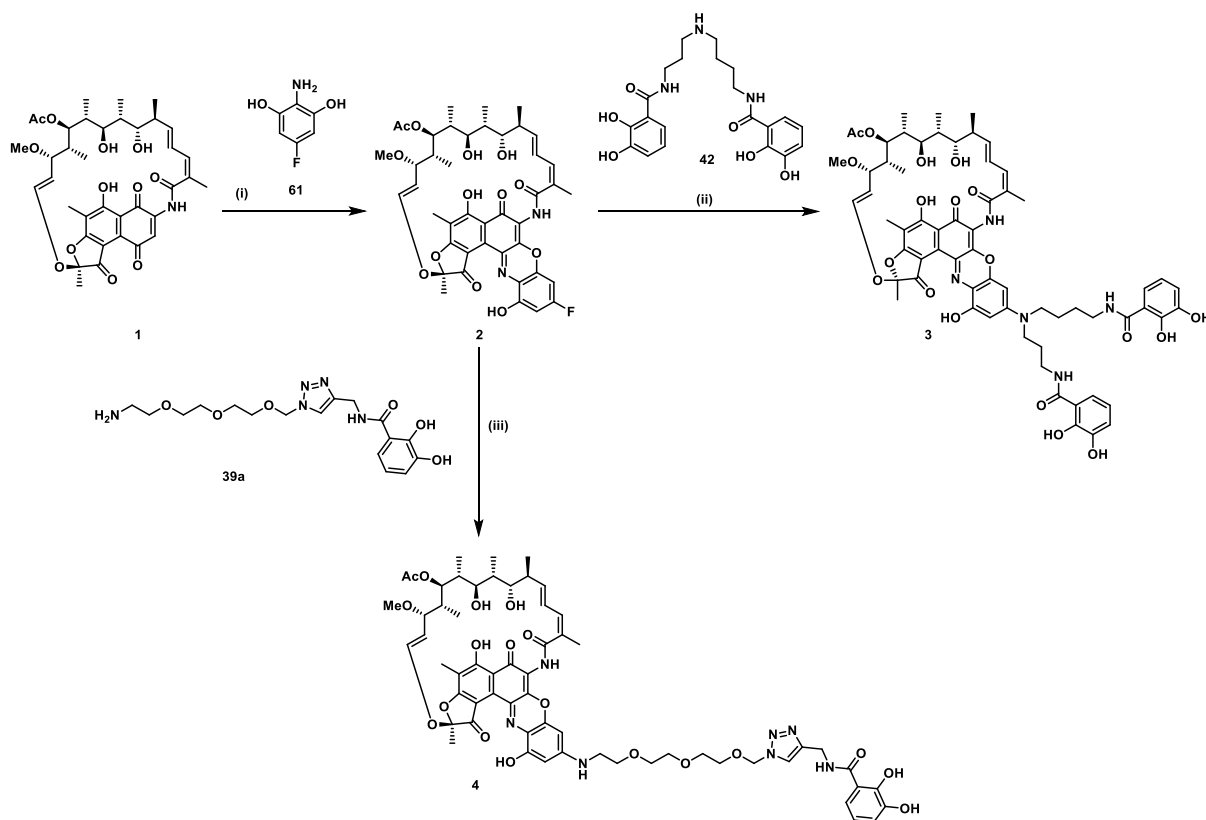


Figure S9.1. Synthesis of mono and dicatechol rifamycin derivatives **2-4**. (i) **61**, benzoquinone or TEMPO, oxygen gas, iPrOAc, 23 °C, 48 h, yield for benzoquinone/O₂: 21% and TEMPO/O₂: 50%, (ii) **42**, THF, DMSO, pyridine, DIPEA, 25-60 °C, 55%. (iii) **39a**, DIPEA, DMSO, THF, 25-45 °C, 30% over two steps,

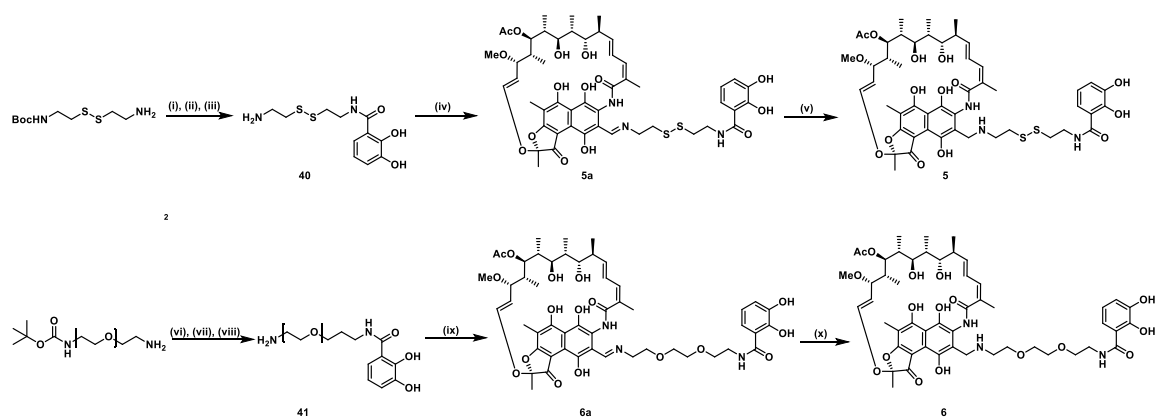


Figure S9.2. Synthesis of 3-formyl monocatechol derivatives **5-6**. (i) **38**, *iso*-butylchloroformate, NMM, THF, 0-23 °C, (ii) TFA, AcOH, DCM, 0-23 °C, (iii) 20% DIPEA in anhydrous MeOH, 87% over three steps, (iv) 3-formyl rifamycin SV **27**, TEA, THF, 0-23 °C, 1 h, 90% crude, (v) NaBH(OAc)₃, 1h, 0-23 °C, 57% (vi) **38**, *iso*-butylchloroformate, NMM, THF, 0-23 °C, (vii) TFA, AcOH, DCM, 0-23 °C, (viii) 20% DIPEA in anhydrous MeOH, 93% over three steps, (ix) 3-formyl rifamycin SV **27**, TEA, THF, 0-23 °C, 1 h, 98% crude, (x) NaBH(OAc)₃, 1h, 0-23 °C, 79%.

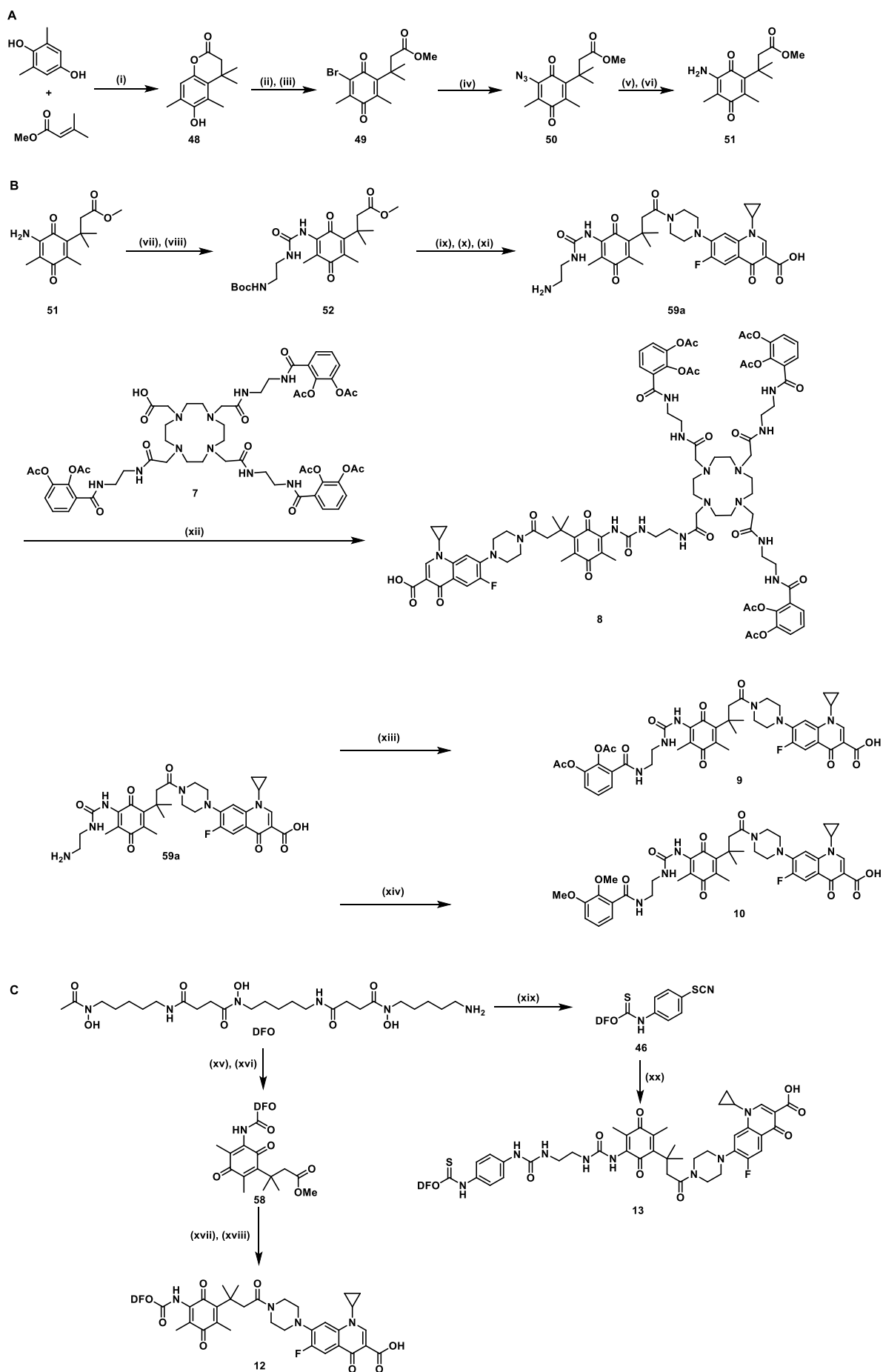


Figure S9.3. Synthesis of ciprofloxacin quinone trimethyllock siderophore conjugates **8-12**. (A) Trimethyllock synthesis: (i) MeSO_3H , 70°C , 2 h, 91%, (ii) Br_2 , AcOH , 23°C , 56%, (iii) SOCl_2 , MeOH , reflux, 50%, (iv) NaN_3 , MeOH , H_2O , 25°C , quant., (v) PPh_3 , DCM , 23°C , (vi) AcOH , THF , H_2O , 32% over two steps. (B) Catechol and DOTAM conjugates: (vii) triphosgene, anhydrous toluene, $23 - 80^\circ\text{C}$, 4h, (viii) then *N*-*boc* ethylene diamine, TEA , DCM , $0 - 23^\circ\text{C}$, 59% over two steps, (ix) 1N NaOH , $\text{MeOH}/\text{H}_2\text{O}$, (x) ciprofloxacin, $\text{EDCI}\cdot\text{HCl}$, HOBt , DIPEA , DCM , DMF , $0 - 23^\circ\text{C}$, overnight, (xi) 25% TFA in anhydrous DCM , $0 - 23^\circ\text{C}$, 2 h, 51% over three steps, (xii) *iso*-butylchloroformate, NMM , THF , $0-23^\circ\text{C}$, 79%, (xiii) **38**, *iso*-butylchloroformate, NMM , THF , $0-23^\circ\text{C}$, 83%, (xiv) 2,3-dimethoxybenzoic acid, *iso*-butylchloroformate, NMM , THF , $0-23^\circ\text{C}$, 89%, (C) DFO conjugates: (xv) triphosgene, anhydrous toluene, 80°C , overnight, (xvi) DMF , TEA , 1 h 0°C , then 1 h at 25°C , 18% over two steps, (xvii) 1N KOH in H_2O , MeOH , 25°C , 3h, (xviii) ciprofloxacin, $\text{EDCI}\cdot\text{HCl}$, HOBt , DIPEA , DCM , DMF , $0 - 23^\circ\text{C}$, overnight, 35% over two steps, (xix) 1,4-dithiocyanatobenzene, 2-propanol/milliQ H_2O (10:1), chloroform , TEA , $0 - 24^\circ\text{C}$, DCM wash, 77%, (xx) **46**, DMF , TEA , 24°C , 73%.

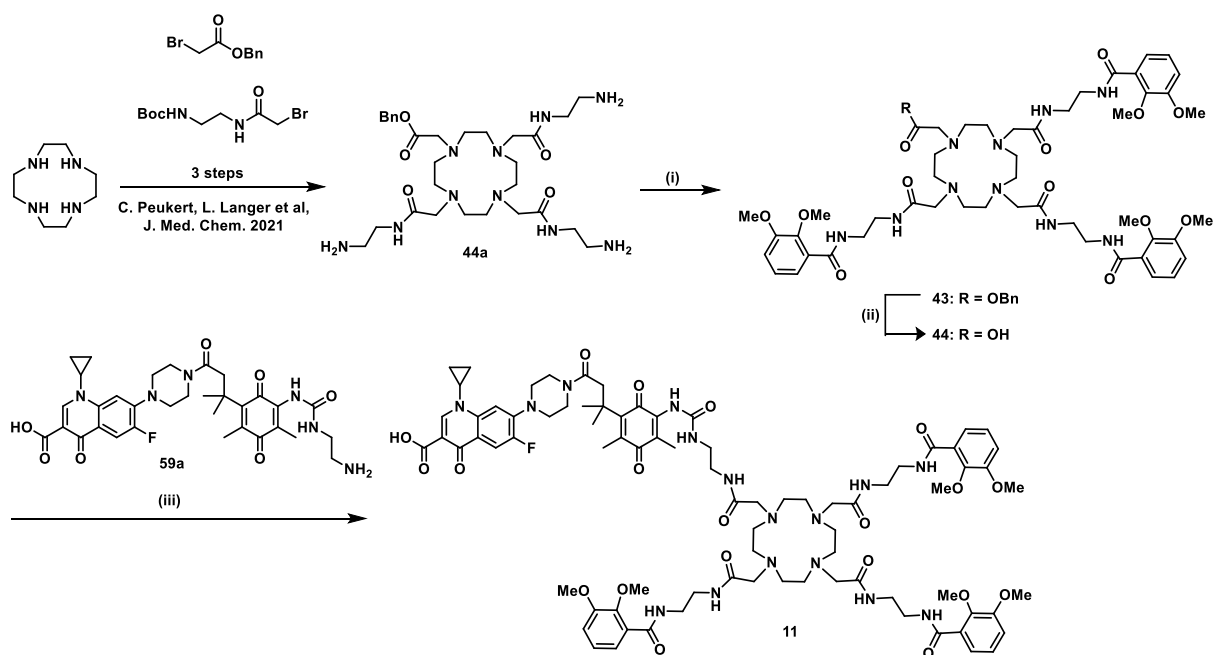


Figure S9.4. Synthesis of ciprofloxacin trimethyllock DOTAM conjugate **11** with methylated catechols. bromides synthesized as described in C. Peukert, L. Langer et al,¹ (i) 2,3-dimethoxybenzoic acid, HATU , DIPEA , DCM , DMF , 25°C , overnight, 73% over three steps, (ii) H_2 , Pd/C , MeOH , 25°C , quant., (iii) *iso*-butylchloroformate, NMM , THF , $0-23^\circ\text{C}$, 71%.

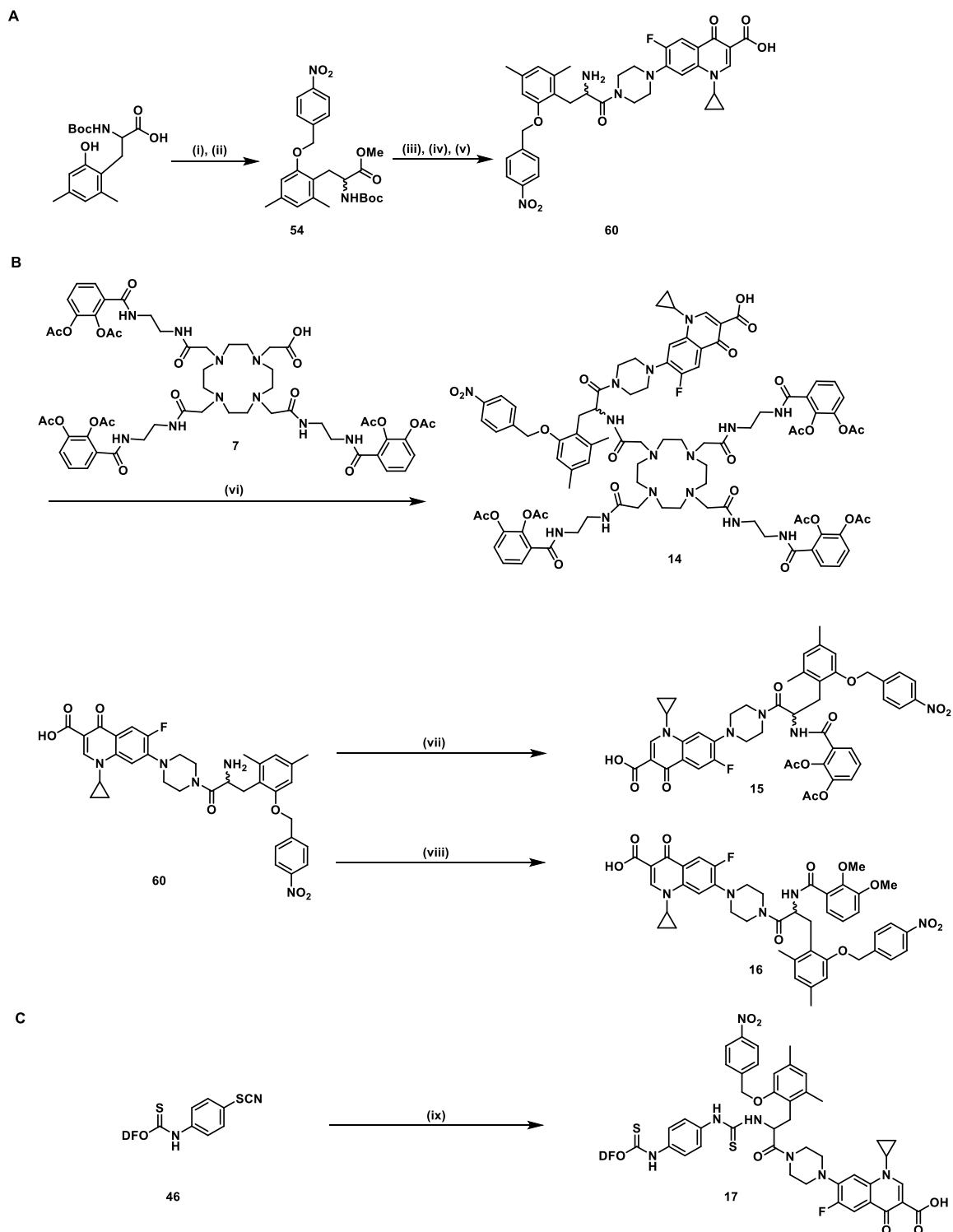


Figure S9.5. Synthesis of ciprofloxacin trimethyllock analogue siderophore conjugates **13-16**. (A) Linker synthesis: (i) dimethoxypropane, MeOH, 20% HCl, 23 °C, 2 h, (ii) *para*-nitrobenzyl bromide, potassium carbonate, ACN, 23 °C, 83% over two steps, (iii) 1N NaOH in H₂O, MeOH, overnight, (iv) ciprofloxacin, EDCI·HCl, HOBT, DIPEA, DCM, DMF, 0 - 23 °C, (v) 25% TFA in anhydrous DCM, 0-22 °C, 2 h, 65% over three steps. (B) Catechol and DOTAM conjugates: (vi) *iso*-butylchloroformate, NMM, THF, 0 - 23 °C, 87%, (vii) **38**, *iso*-butylchloroformate, NMM, THF, 0-23 °C, 69%, (viii) 2,3-dimethoxybenzoic acid, *iso*-butylchloroformate, NMM, THF, 0-23 °C, 81%, (C) DFO conjugates: (ix) **46**, TEA, DMF, 73%.

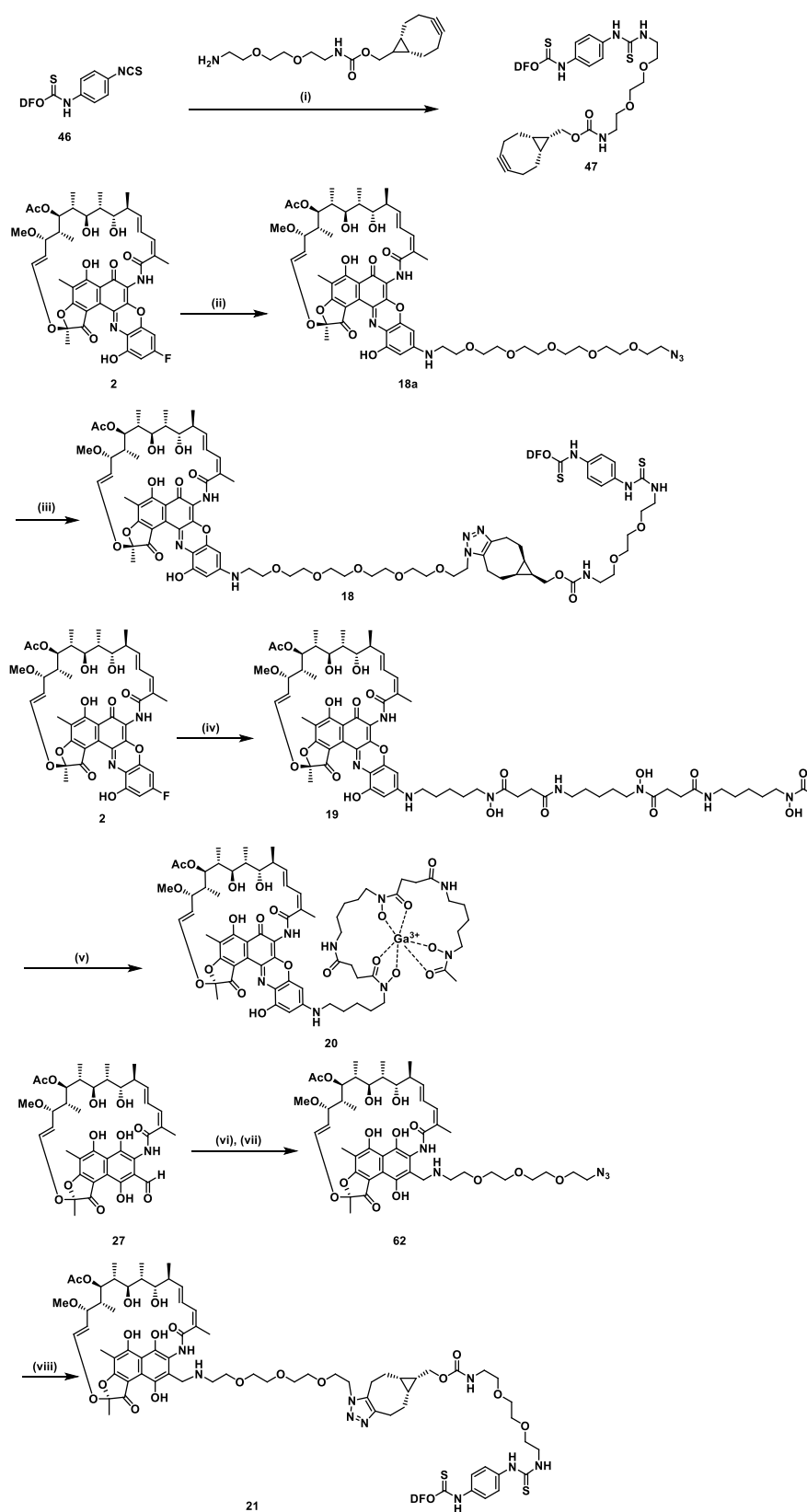


Figure S9.6. Synthesis of covalent DFO rifamycin conjugates **18-21**. (i) DMSO, TEA, 24 °C, 18 h, 51%, (ii) 17-azido-3,6,9,12,15-pentaoxaheptadecan-1-amine, TEA, THF, 24 °C, 48 h, (iii) **47**, ACN, H₂O (1:1), 24 °C, overnight, 88% over two steps, (iv) TEA, DMF, THF, 45 °C, overnight, 84%, (v) GaCl₃, NaOAc pH 4.5, overnight, 23 °C, quant., (vi) 2-(2-(2-(2-azidoethoxy)ethoxy)ethoxy)ethan-1-amine, TEA, THF, 1 h, 23 °C, (vii) NaBH(OAc)₃, THF, 0 - 23 °C, 98%, (viii) **47**, ACN, H₂O (1:1), 24 °C, overnight, 57%.

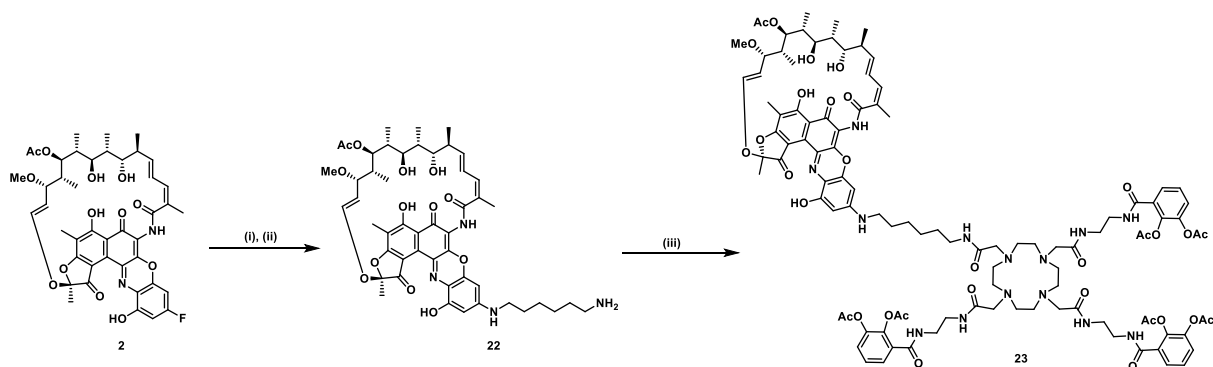


Figure S9.7. Synthesis of covalent rifamycin DOTAM conjugate **23**. (i) N-fmoc 1,6-diaminohexane, TEA, THF, overnight, 23 °C, 92%, (ii) diethylamine, ACN, 23 °C, 2 h, 92%, (iii) **7**, *iso*-butylchloroformate, NMM, THF, 0-23 °C, 79%.

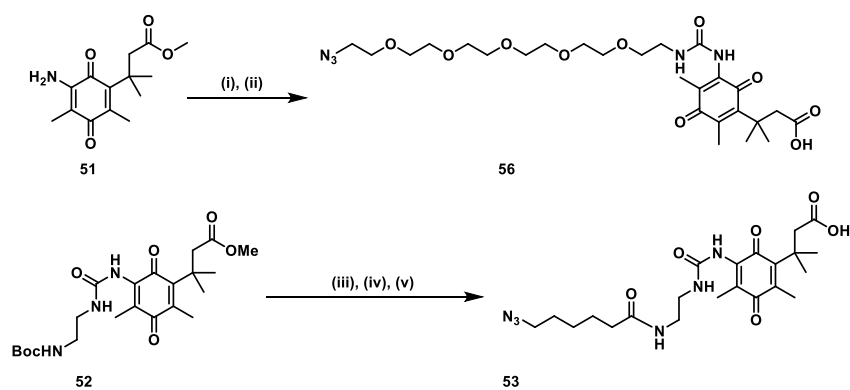


Figure S9.8. Synthesis of azido TML linkers **53** and **53**. (i) triphosgene, toluene, 80 °C, overnight, then reduced pressure, 17-azido-3,6,9,12,15-pentaoxaheptadecan-1-amine, TEA, DCM, 0-24 °C, quant. crude, (ii) 1 M LiOH, MeOH, 23 °C, 2 h, 95%, (iii) 25% TFA, anhydrous DCM, 0-24 °C, 2 h, (iv) 6-azido hexanoic acid, HATU, DIPEA, 24 °C, 2 h, (v) 1 M LiOH in H₂O, MeOH, 3 h, 24 °C, 74% over three steps.

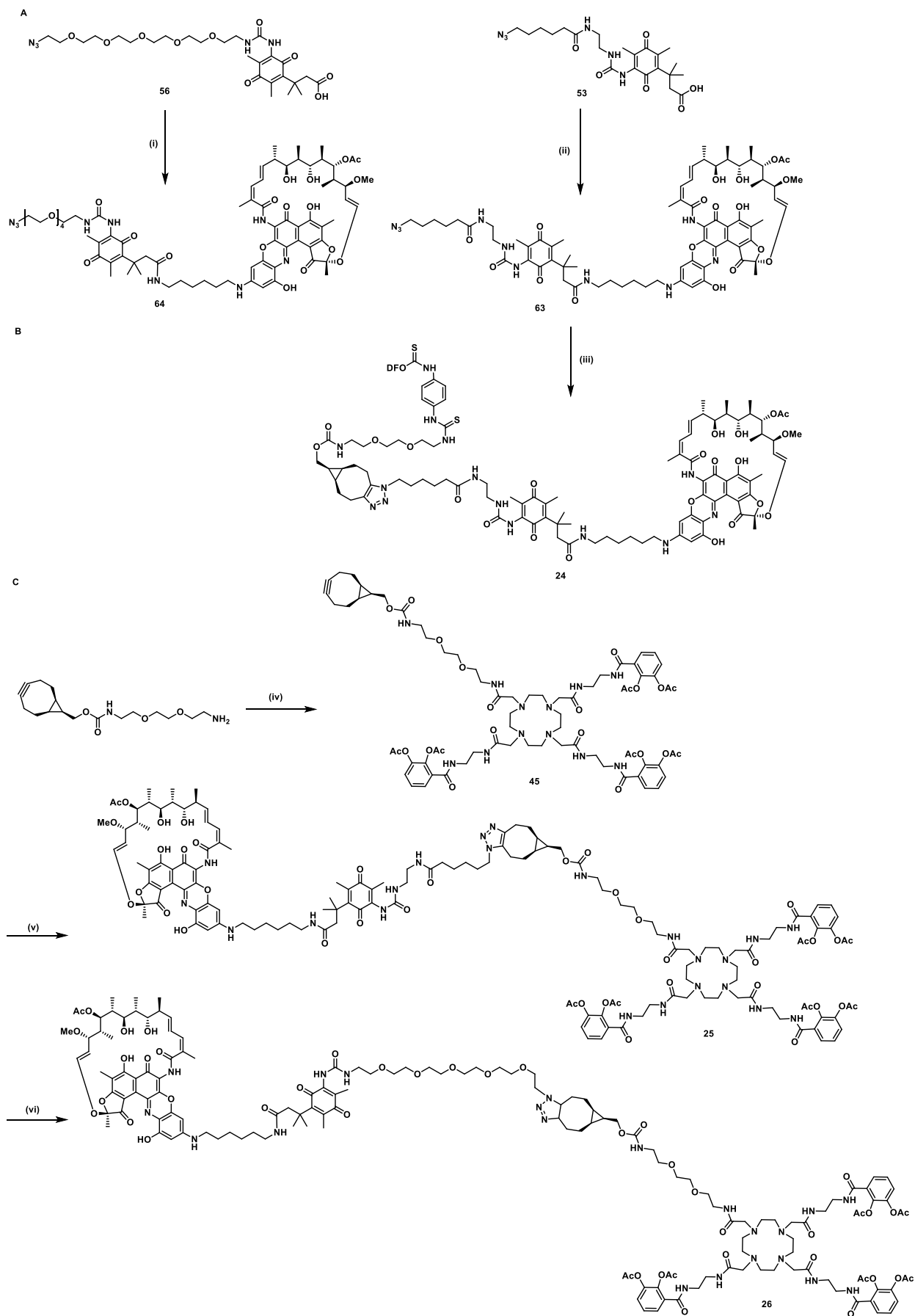


Figure S9.9. Synthesis of cleavable rifamycin DFO and DOTAM conjugates **24-26**. (A) Rifamycin linker fragments: (i) **22**, *iso*-butylchloroformate, NMM, THF, 0-23 °C, 45%, (ii) *iso*-butylchloroformate, NMM, THF, 0-23 °C, 39%, (B) DFO conjugate: (iii) MeOH, 24 °C, overnight, 81%, (C) DOTAM conjugates: (iv) **7**, *iso*-butylchloroformate, NMM, THF, 0-24 °C, 79% crude, (v) **45**, ACN, H₂O, 24 °C, overnight, 79%, (vi) **45**, ACN, H₂O, 24 °C, overnight, 82%.

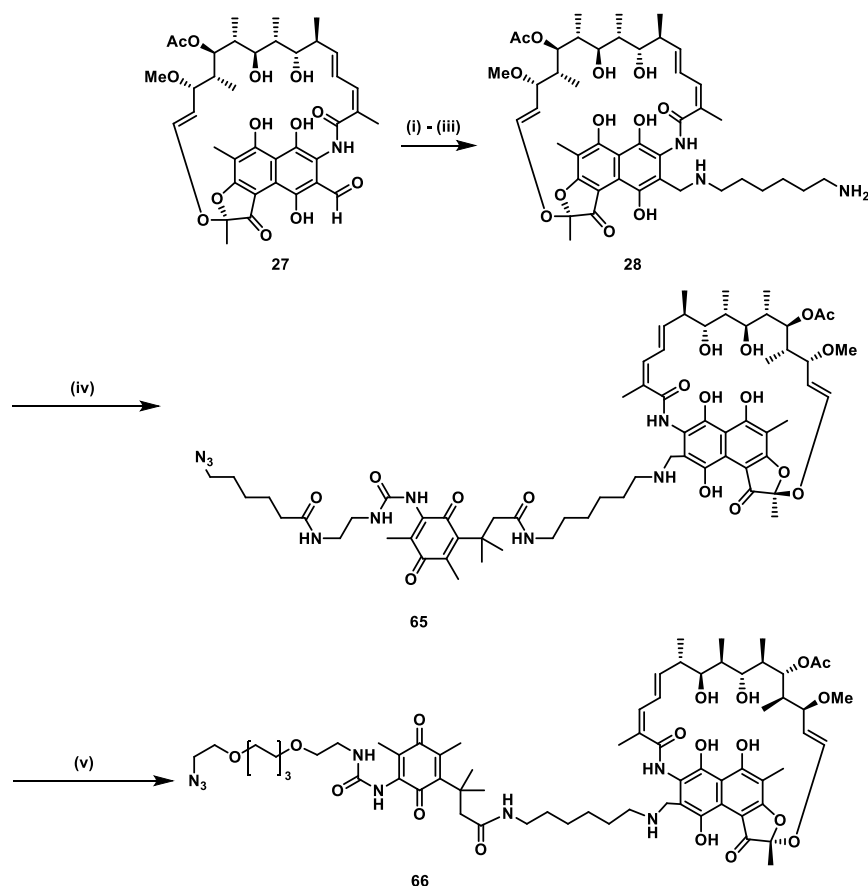


Figure S9.10. Synthesis of rifamycin trimethyllock linker fragments **65** and **66**. (i) N-fmoc 1,6-diaminohexane, TEA, THF, 1 h, (ii) NaBH(OAc)₃, THF, 0 - 23 °C, overnight, (iii) 20% diethylamine, ACN, 23 °C, 45 min, 67% over three steps, (iv) **53**, *iso*-butylchloroformate, NMM, THF, 0-23 °C, overnight, 73%, (v) **56**, *iso*-butylchloroformate, NMM, THF, 0-23 °C, overnight, 76% (38% yield f. EDCI based coupling, not shown).

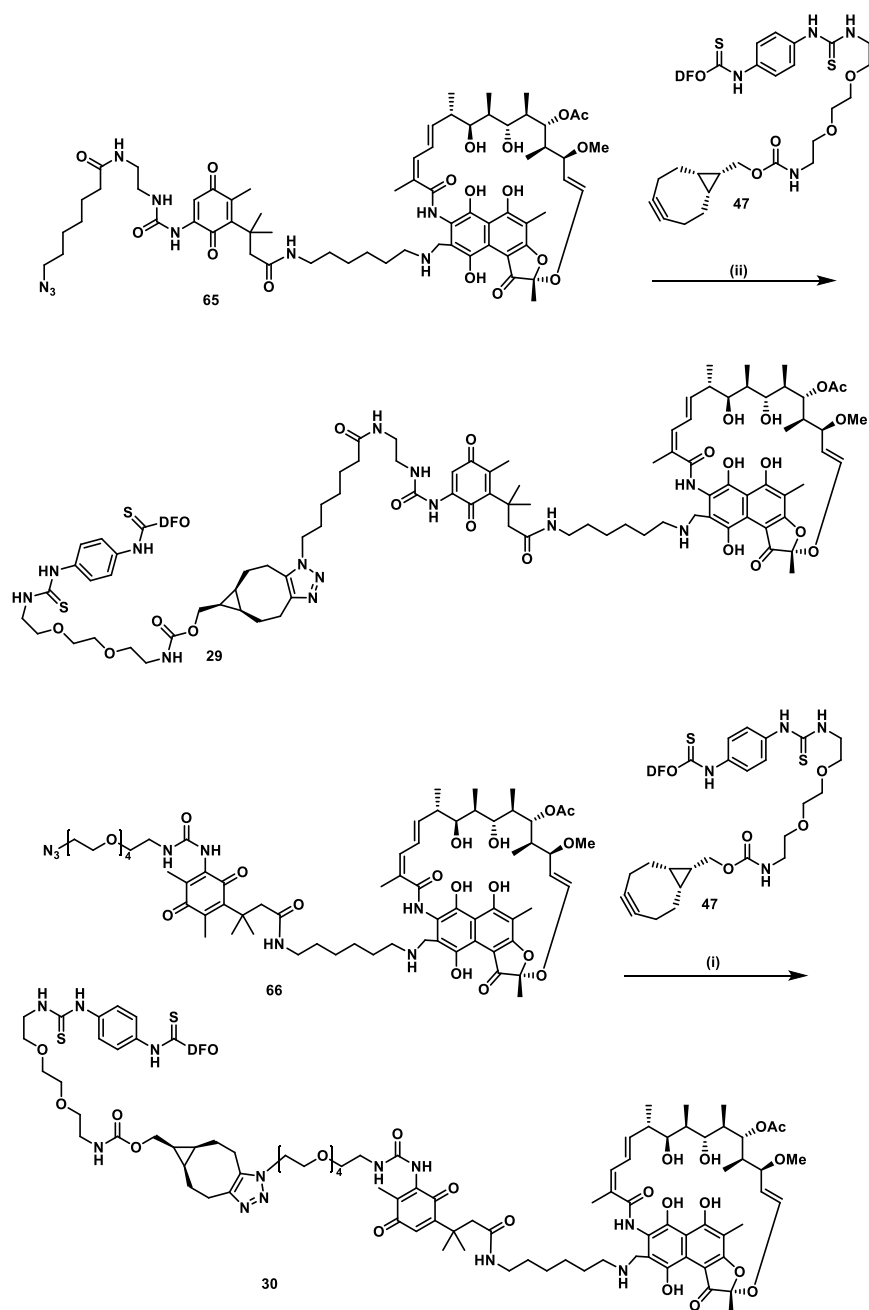


Figure S9.11. Synthesis of cleavable rifamycin trimethyllock DFO conjugates **29** and **30**. (i) ACN, H₂O, (1:1), 24 °C, 30 h, 64%, (ii) ACN, H₂O, (1:1), 24 °C, 30 h, 88%.

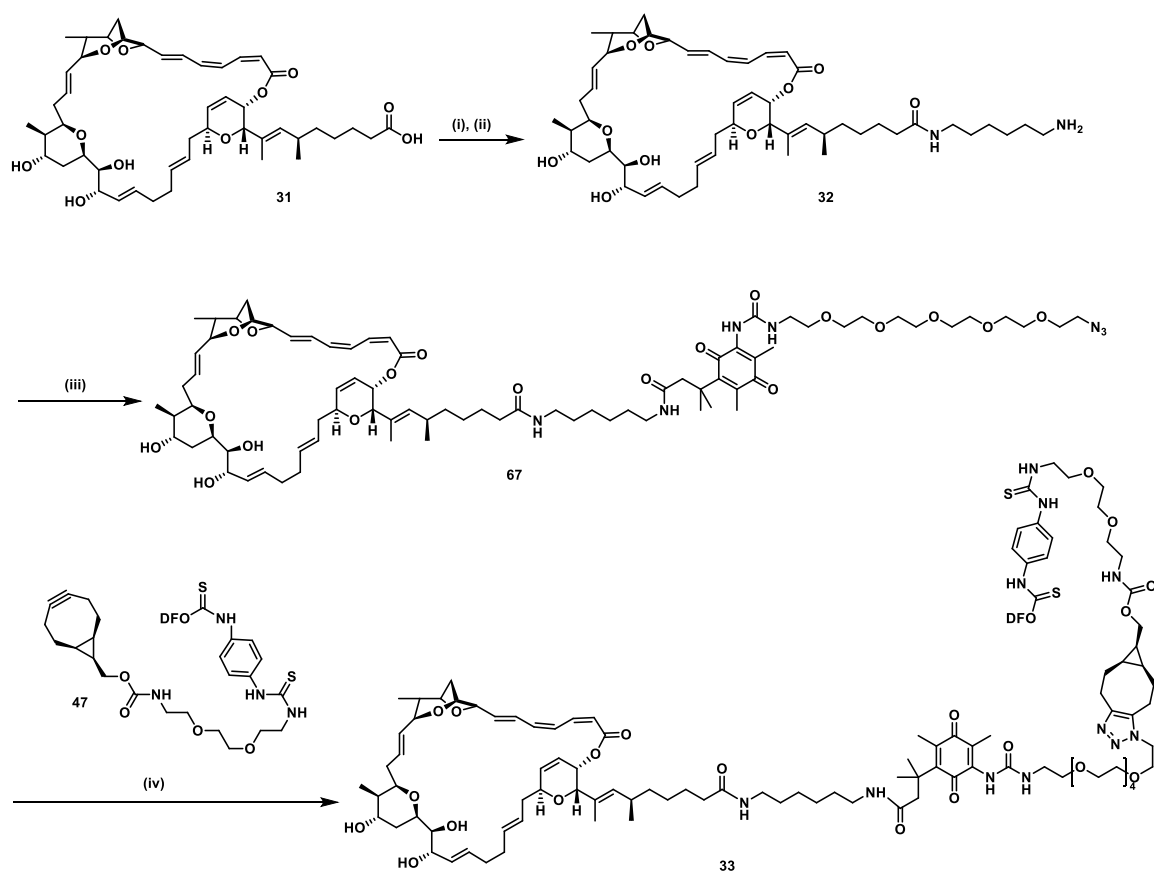


Figure S9.12. Synthesis of cleavable sorangicin trimethyllock DFO conjugate **33**. (i) N-fmoc 1,6-diaminohexane, DIPEA, DCM, DMF, 23 °C, 2 h, (ii) 20% diethylamine, ACN, 1 h, 56% over two steps, (iii) **56**, *iso*-butylchloroformate, NMM, THF, 0-23 °C, overnight, 84%, (iv) ACN, H₂O, (1:1), 24 °C, 30 h, 71%.

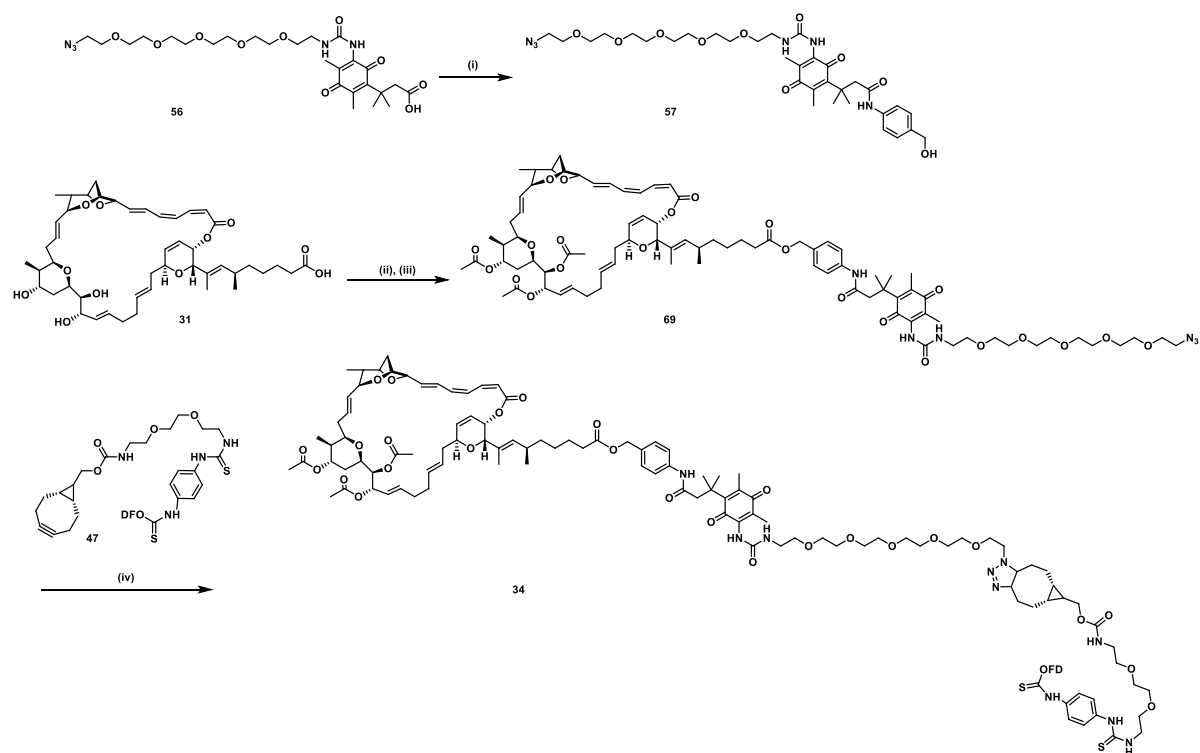


Figure S9.13. Synthesis of cleavable sorangicin trimethyllock DFO conjugate **34**. (i) para-amino benzyl alcohol, *iso*-butylchloroformate, NMM, THF, 0-23 °C, overnight, 77%, (ii) acetic anhydride, THF, pyridine, 24 °C, quant. crude, (iii) *iso*-butylchloroformate, NMM, THF, 10 min 0 °C, 45 min 24 °C, then **57**, NMM, THF, 0 – 24 °C, overnight, 63% over two steps, (iv) ACN, H₂O (1:1), 23 °C, 36 h, 95%.

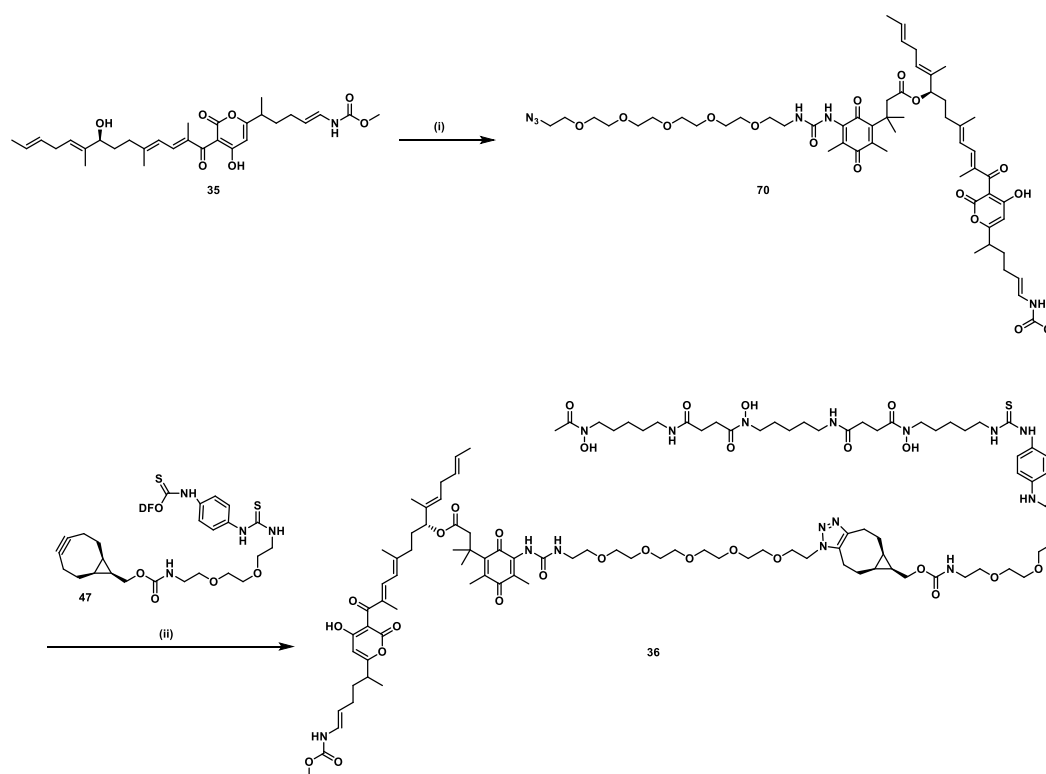


Figure S9.14. Synthesis of cleavable corallopyronin A conjugate **36**. (i) **56**, *iso*-butylchloroformate, NMM, THF, 0 - 24 °C, overnight, 71%, (ii) ACN, H₂O (1:1), 24 °C, 30 h, 79%.

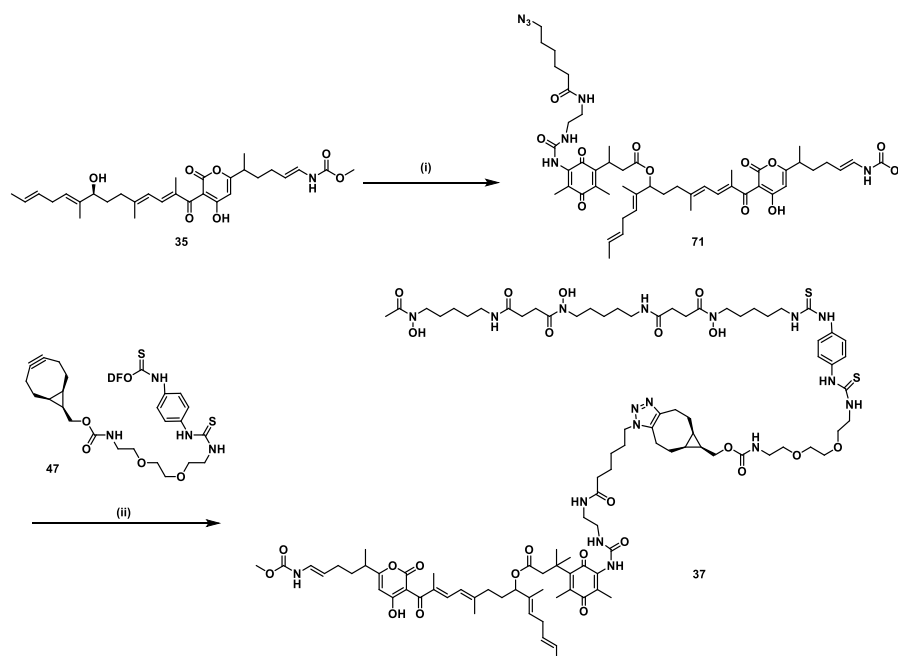
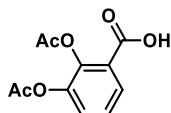


Figure S9.15. Synthesis of cleavable corallopyronin A conjugate **37**. (i) **53**, *iso*-butylchloroformate, pyridine, THF, 0 - 24 °C, 48 h, 75%, (ii) ACN, H₂O (1:1), 24 °C, 30 h, 49%.

Synthesis procedures

Siderophore synthesis

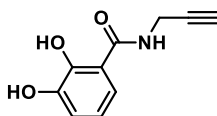
Compound 38



Chemical Formula: C₁₁H₁₀O₆
 Exact Mass: 238,0477
 Molecular Weight: 238,1950

Compound **38** was synthesized as published in C. Peukert, L. Langer et al.¹

Compound 39



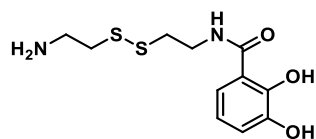
Chemical Formula: C₁₀H₉NO₃
 Exact Mass: 191,0582
 Molecular Weight: 191,1860

Acid **38** (100 mg, 0.42 mmol, 1.0 eq) and HATU (175.6, 0.46 mmol, 1.1 eq) were dissolved in a mixture of DCM/DMF (100 μ L each, 1:1). Then DIPEA (298.7 μ L, 1.68 mmol, 4.0 eq) was added, followed by propargylamine (23.1 mg, 0.42 mmol, 1.0 eq) addition, dropwise diluted in DCM/DMF (1:1, 100 μ L) over 10 minutes at 0 °C. Deacetylation was driven to completion by addition of MeOH (200 μ L) and DIPEA (50 μ L). The reaction mixture was concentrated in vacuo and purified by silica gel chromatography (0-100% PE/EtOAc, 15 mL/min), product containing fractions were identified by LCMS, combined and concentrated in vacuo to yield **39** as a colorless oil (63.5 mg, 0.332 mmol, 79%) that became crystalline at 0 °C.

¹H-NMR (500 MHz, CDCl₃): δ = 7.07-7.05 (ddd, J = 1.61, 7.72 Hz, 1H), 6.93-6.91 (ddd, J = 1.69, 8.35 Hz, 1H), 6.78 (t, J = 7.72 Hz, 1H), 6.52 (bs, 1H), 4.25 (dd, J = 2.5, 5.23 Hz, 2H), 2.32 (t, J = 2.43 Hz, 1H).

¹³C-NMR (126 MHz, CDCl₃): δ = 146.09, 119.01, 118.61, 116.23, 77.16, 72.55, 60.55, 39.74, 29.61, 14.35.

HRMS (ESI) calculated for ([M+H]⁺): m/z = 192.0654; experimental = 192.0655

Compound **40**Chemical Formula: C₁₁H₁₆N₂O₃S₂

Exact Mass: 288,0602

Molecular Weight: 288,3800

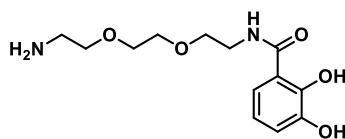
Catechol **38** (94.38 mg, 0.396 mmol, 1.0 eq) was dissolved in anhydrous THF (15 mL), NMM (60 μ L) was added under argon atmosphere at 0 °C, followed by the addition of *iso*-butyl chloroformate (38.4 μ L, 0.396 mmol, 1.0 eq). The reaction turned turbid instantly and stirred at 0 °C for 10 minutes and for 50 minutes at 23 °C. After cooling again to 0 °C N-boc cystamine (100 mg, 0.396 mmol, 1.05 eq), suspended in THF (5 ml) was added together with NMM (60 μ L) dropwise over 5 minutes. The reaction stirred for 10 minutes 0 °C and for 50 minutes at ambient temperature. Then AcOH (1 mL) was added and the reaction was evaporated to dryness. The residue was dried overnight under reduced pressure then dissolved in DCM (10 mL) and cooled to 0 °C where a mixture of TFA/AcOH (1:1, 10 mL) was added at 0 °C. The reaction stirred for two hours at 0 °C before the solvent was evaporated and the residue dried under reduced pressure. Then 20% DIPEA in MeOH (10 mL) was added and the reaction continued stirring for four hours at ambient temperature. The solvent was removed by rotary evaporation and the residue purified by RP-HPLC (10-85% ACN/H₂O, 0.1% HCOOH, 220 nm). The product containing fractions were lyophilized to yield amine **40** a beige oil (99.85 mg, 0.346 mmol, 87%).

¹H-NMR (500 MHz, ACN-d₃): δ = 7.87 (s, 1H), 7.16 (dd, J = 1.45, 8.1), 6.98 (dd, J = 1.74, 8.1 Hz, 1H), 6.75 (t, J = 8.1 Hz, 1H), 3.68 (q, J = 6.46, 12.82 Hz, 2H), 3.30 (t, J = 6.46 Hz, 2H), 3.03 (t, J = 6.65 Hz, 2H), 2.97 (t, J = 6.46 Hz, 2H), 2.30 (bs, 2H).

¹³C-NMR (126 MHz, ACN-d₃): δ = 171.58, 161.57, 161.30, 150.57, 146.97, 120.37, 120.13, 119.55, 119.53, 117.84, 115.55, 39.65, 39.44, 37.99, 35.38.

HRMS (ESI) calculated for ([M+H]⁺): m/z = 289.0675; experimental = 289.0683

Compound 41



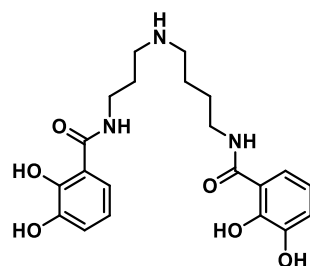
Chemical Formula: C₁₃H₂₀N₂O₅
 Exact Mass: 284,1372
 Molecular Weight: 284,3120

Catechol **38** (95,92 mg, 0.403 mmol, 1.0 eq) was dissolved in anhydrous THF (15 mL), NMM (60 μ L) was added under argon atmosphere at 0 °C, followed by addition of iso-butyl chloroformate (38.4 μ L, 0.403 mmol, 1.0 eq). The reaction turned turbid instantly and stirred at 0 °C for 10 minutes and for 50 minutes at 23 °C. After cooling to 0 °C, mono-boc-cystamin (100 mg, 0.403 mmol, 1.05 eq), suspended in THF (5 ml), was added as a suspension, together with NMM (60 μ L), dropwise over 5 minutes. The reaction stirred for 10 minutes 0 °C and then for 50 minutes at ambient temperature. Then AcOH (1 mL) was added and the reaction was evaporated to dryness. The residue was dried overnight under reduced pressure, then dissolved in DCM (10 mL) and cooled to 0 °C where a mixture of TFA/AcOH (1:1, 10 mL) was added at 0 °C. The reaction stirred for two hours at 0 °C before the solvent was evaporated and the residue dried under reduced pressure. Then 20% DIPEA in MeOH (10 mL) was added and the reaction continued stirring for four hours at ambient temperature. The solvent was removed by rotary evaporation and the residue purified by RP-HPLC (C18, 10-85% ACN/H₂O, 0.1% HCOOH, 220 nm). The product containing fractions were lyophilized to yield amine **41** a beige oil (104,8 mg, 0.369 mmol, 93%).

¹H-NMR (500 MHz, ACN-d₃): δ = 7.92 (m, 1H), 7.19 (dd, J = 1.26, 8.00 Hz, 1H), 6.98 (dd, J = 1.71, 7.66 Hz, 1H), 6.72 (t, J = 7.89 Hz, 1H), 3.65 (m, 4H), 3.59 (s, 4H), 3.53 (q, J = 5.6, 11.20 Hz, 2H), 3.08 (t, J = 5.26 Hz, 2H), 2.60 (bs, 2H).

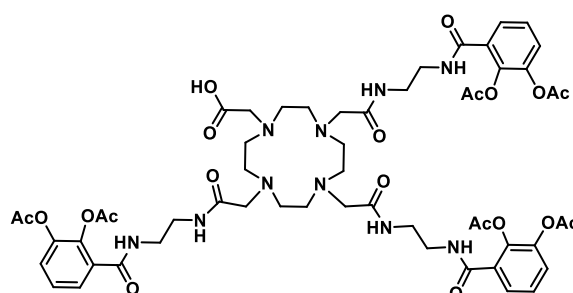
¹³C-NMR (126 MHz, ACN-d₃): δ = 172.02, 162.48, 162.21, 151.02, 147.54, 120.14, 120.08, 119.84, 118.90, 117.50, 116.42, 71.50, 71.39, 70.68, 67.85, 41.06, 40.71.

HRMS (ESI) calculated for ([M+H]⁺): m/z = 285.1445; experimental = 285.1439

Compound **42**

Chemical Formula: $C_{21}H_{27}N_3O_6$
 Exact Mass: 417,1900
 Molecular Weight: 417,4620

This compound was previously synthesized by Miller et al.² Catechol **38** (98.4 mg, 0.41 mmol, 1.2 eq) was dissolved in dry DCM (14 mL) and carbonyldiimidazole (66.98 mg, 0.41 mmol, 1.2 eq) was added in 3 portions at 0 °C. The mildly orange solution stirred 1 hour at 0 °C under argon atmosphere and one more 1 hour at 25 °C. Then spermidine (50 mg, 0.34 mmol, 1.0 eq) was added in anhydrous DCM (1 mL) at 0 °C and a precipitate formed instantly upon addition. The reaction continued stirring at 25 °C overnight and the organic phase was washed subsequently with brine/water (1:1, 2x50 mL), dried over Na_2SO_4 and the solvent was removed *in vacuo*. The residue was dissolved in MeOH (8 mL) and DIPEA (2 mL) was added. The deacetylation reached full conversion after 4 hours and the solvent was removed by rotary evaporation yielding a beige oil that was dried *in vacuo* to yield crude dicatechol **42** (104.5 mg, 0.25 mmol, 73%) which was used without purification directly in the next step.

Compound **7**

Chemical Formula: $C_{55}H_{70}N_{10}O_{20}$
 Exact Mass: 1190,4768
 Molecular Weight: 1191,2150

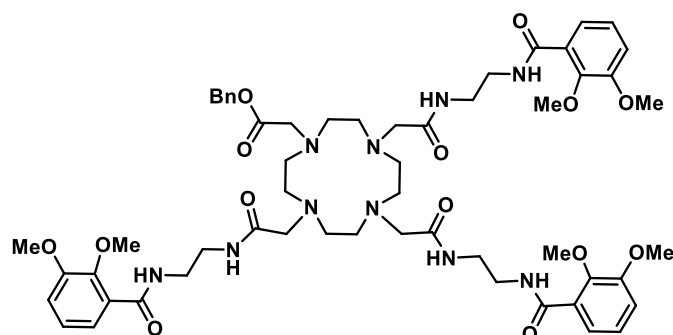
Compound **7** was synthesized as previously described by C. Peukert and L. N. B. Langer et al.¹

¹H-NMR (700 MHz, DMSO-d₆+AcOH-d₄): δ = 8.60 (m, 1H), 8.10 (m, 2H), 7.53 (m, 3H), 7.34 (m, 8H), 7.22 (m, 1H), 3.53 (m, 2H), 3.40 (m, 4H), 3.25 (m, 6H), 3.13 (m, 10H), 3.02 (m, 2H), 2.96 (s, 2H), 2.87 (m, 4H), 2.78 (m, 2H), 2.59 (m, 8H), 2.27 (s, 9H), 2.21 (s, 9H).

¹³C-NMR (176 MHz, DMSO-d₆+AcOH-d₄): δ = 172.03, 171.99, 170.61, 170.52, 170.25, 170.17, 168.57, 168.32, 168.26, 168.13, 167.85, 167.81, 167.67, 166.71, 165.65, 164.62, 164.58, 164.54, 164.49, 142.83, 142.58, 140.21, 140.18, 139.17, 138.55, 131.73, 130.71, 130.66, 130.61, 130.56, 126.72, 126.25, 126.17, 126.10, 125.42, 125.33, 124.89, 124.29, 57.71, 57.12, 53.11, 51.65, 50.29, 47.80, 39.52, 38.93, 38.81, 38.34, 38.16, 38.08, 34.23, 21.05, 20.69, 20.58, 20.47, 20.43, 20.38, 20.34, 20.25, 20.13, 19.99, 1.15.

HRMS (ESI) calculated for ([M+H]⁺): m/z = 1191.4841; experimental = 1191.4846

Compound 43



Chemical Formula: C₅₆H₇₆N₁₀O₁₄
Exact Mass: 1112,5542
Molecular Weight: 1113,2800

Cyclen (20 mg, 0.116 mmol, 1.0 eq) was dissolved in ACN (75 mL) and NaOAc (31.4 mg, 0.371 mmol, 3.2 eq) was added. Then tert-butyl (2-(2-bromoacetamido)ethyl)carbamate (67.3 mg, 0.371 mmol, 3.2 eq), synthesized according to Peukert and Langer et al, was added, dissolved in ACN (25 mL) dropwise at 24 °C over 60 minutes.³ The reaction continued stirring overnight at 24 °C and was filtered. The filter was washed and the flowthrough was concentrated to dryness. The transparent oil was dissolved in ACN (75 mL), K₂CO₃ (32.1 mg, 0.23 mmol, 2.0 eq) was added, followed by the benzyl bromoacetate (31.9 mg, 0.232 mmol, 2.0 eq) in ACN (25 mL) over 10 minutes at 24 °C. The reaction stirred for two hours at ambient temperature and was then filtered. The filtrate was evaporated to dryness. The residue was taken up in DCM (100 mL) and washed with HCl (2x100 mL), NaHCO₃ (2x100 mL), water (2x200 mL) and dried over Na₂SO₄. The solvent was removed in vacuo and the beige solid

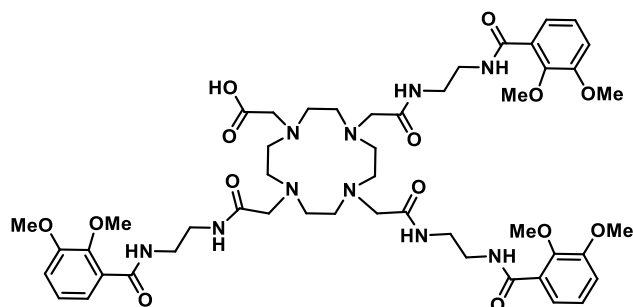
was dissolved in anhydrous DCM (25 mL). Then the reaction was cooled to 0 °C and TFA (25 mL) was added. The reaction continued stirring for 2 hours and was The next day 2,3-dimethoxybenzoic acid (84.6 mg, 0.464 mmol, 4.0 eq) was dissolved under argon atmosphere in dry DCM:DMF (50:2 mL). Then HATU (264.9 mg, 0.697 mmol, 6.0 eq) was added, followed by DIPEA (250 µL). The slight yellow solution was stirred 5 minutes at 24 °C before the crude amine **43a** in anhydrous DCM:DMF (50:3 mL) with DIPEA (250 µL) was added dropwise. Upon addition, the color changed to yellow and the reaction stirred overnight at ambient temperature. Then the solvent was removed *in vacuo*. The residue was taken up in DCM (100 mL) and washed with HCl (2x100 mL), NaHCO₃ (2x100 mL), water (2x200 mL) and dried over Na₂SO₄. The residue was purified by RP-HPLC (10-70% ACN/H₂O, 0.1 % HCOOH, 220 nm) and product containing fractions were jointly lyophilized to yield ester **43** (94.46 mg, 0.085 mmol, 73% over three steps) as a white powder.

¹H-NMR (500 MHz, DMSO-d₆): δ = 8.66 (m, 1H), 8.30 (m, 4H), 8.12 (m, 1H), 7.75 (m, 3H), 7.35 (m, 8H), 7.15 (m, 11H), 5.10 (s, 2H), 3.96 (m, 6H), 3.82 (s, 9H), 3.74 (s, 9H), 3.49 (m, 4H), 3.39 (m, 15H), 3.14 (m, 18H).

¹³C-NMR (176 MHz, DMSO-d₆): δ = 165.85, 165.69, 152.52, 152.49, 146.36, 146.31, 135.59, 129.56, 129.46, 128.43, 128.38, 128.31, 128.22, 128.13, 128.05, 123.97, 120.75, 120.66, 114.87, 114.78, 66.50, 65.85, 60.95, 60.91, 55.95, 55.93, 54.68, 52.33, 50.86, 48.19, 47.73, 38.54, 38.47, 38.05.

HRMS (ESI) calculated for ([M+H]⁺): m/z = 1113.5615; experimental = 1113.5618

Compound 44



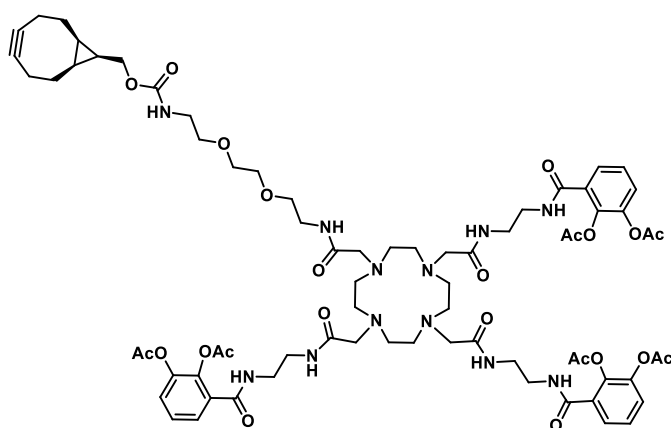
Chemical Formula: $C_{49}H_{70}N_{10}O_{14}$
 Exact Mass: 1022,5073
 Molecular Weight: 1023,1550

Benzyl ester **43** (253 mg, 0.227 mmol, 1.0 eq) was dissolved under argon atmosphere in MeOH (30 mL) and the Pd/C (25 mg, 0.1eq) was added. The atmosphere was changed to hydrogen and the reaction continued stirring overnight at 25 °C. Then the catalyst was removed by filtration over a syringe filter and the reaction was evaporated to dryness to yield crude pure acid **44** (232.4 mg, 0.227 mmol quant.) as a crude, white solid, which was used directly in the next step.

¹H-NMR (500 MHz, DMSO-d₆): δ = 8.32 (m, 6H), 8.09 (m, 9H), 7.22 (s, 9H), 7.07 (s, 9H), 3.83 (m, 8H), 3.75-2.57 (m, 28H).

HRMS (ESI) calculated for ([M+H]⁺): m/z = 1023.5146; experimental = 1023.5159

Compound 45



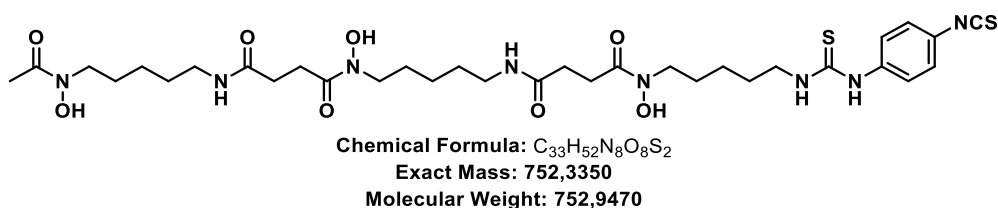
Chemical Formula: $C_{72}H_{96}N_{12}O_{23}$
 Exact Mass: 1496,6711
 Molecular Weight: 1497,6210

The acid **7** (81 mg, 0.068 mmol, 1.0 eq) was dissolved in anhydrous THF (1 mL), NMM (100 μL) was added under argon atmosphere and the reaction was cooled to 0 °C, before iso-

butylchloroformate (6.59 μL , 0.068 mmol, 1.0 eq) was added and the reaction went turbid instantly. The reaction stirred 15 minutes at 0 $^{\circ}\text{C}$ and then 1 h at 24 $^{\circ}\text{C}$. Then BCN amine (25.37 mg, 0.078 mmol, 1.15 eq) was added dropwise at 0 $^{\circ}\text{C}$, dissolved in anhydrous THF (1 mL) and basified with NMM (100 μL) before addition. The reaction continued stirring at 0 $^{\circ}\text{C}$ for 15 minutes and then for 1 hour at 24 $^{\circ}\text{C}$. Then the reaction was quenched with AcOH (200 μL) and the THF was removed *in vacuo* at 30 $^{\circ}\text{C}$. Before the residual solution was diluted 50 times and lyophilized to dryness to yield **45** as a crude white powder (19.06 mg, 0.01 mmol, 79%).

HRMS (ESI) calculated for $([\text{M}+\text{H}]^+)$: $m/z = 1497.6784$; experimental = 1497.6761, calculated for $([\text{M}+2\text{H}]^{2+})$: $m/z = 749.3428$; experimental = 749.3412.

Compound **46**



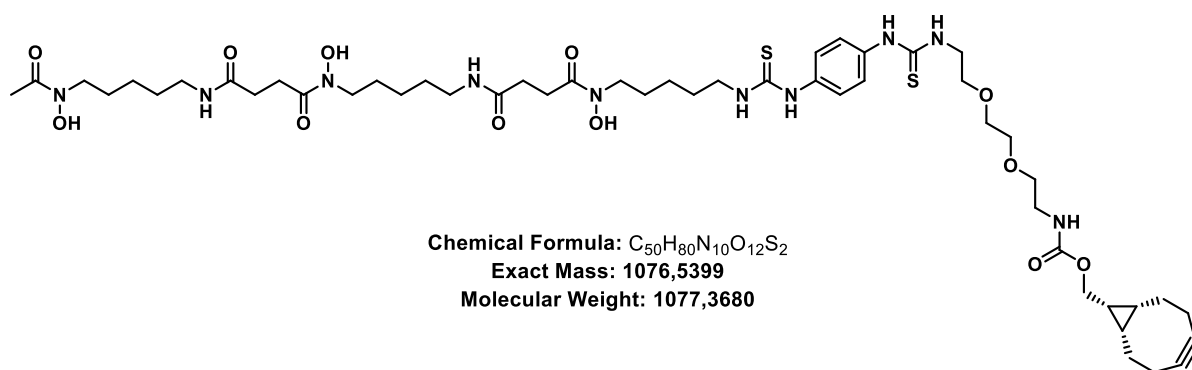
46 was synthesized crude according to a patent by P. S. Donnelly et al.⁴ In particular, desferrioxamine (DFO, 1000 mg, 1,783 mmol, 1.0 eq) was stirred in *i*PrOH/ H_2O (64:6 mL), and a solution of 1,4-dithiocyanatobenzene (1542,11 mg, 8.02 mmol, 4.5 eq) in CHCl_3 (20 mL) was added. Triethylamine (500 μL) was added, and the reaction mixture was stirred for 1.5 h at 25 $^{\circ}\text{C}$. HCl (0.1 M, 100 mL) was added and the organic layer was separated. The solvent was evaporated to give a beige solid which was triturated with CHCl_3 . The remaining solid was filtered off and dried to give modified DFO **46** as a white powder (1033.3 mg, 1.372 mmol, 89%).

$^1\text{H-NMR}$ (500 MHz, DMSO-d_6): $\delta = 8.96$ (m, 1H), 8.45 (m, 1H), 8.00 (m, 7H), 7.74 (m, 1H), 7.38 (s, 4H), 5.11 (s, 2H), 4.00 (m, 2H), 3.71 (m, 2H), 3.50 (m, 5H), 3.37 (m, 6H), 3.29 (m, 2H), 3.12 (m, 4H), 3.01 (m, 2H), 2.92 (m, 6H), 2.08 (s, 2H), 1.91 (s, 1H).

$^{13}\text{C-NMR}$ (126 MHz, DMSO-d_6): $\delta = 171.89$, 171.36, 170.08, 139.91, 125.99, 122.01, 47.05, 46.75, 43.34, 38.40, 30.02, 28.78, 28.00, 27.72, 26.02, 23.59, 23.52, 20.43.

HRMS (ESI) calculated for $([M+H]^+)$: $m/z = 753.3423$; experimental = 753.3525.

Compound **47**



46 (209 mg, 0.278 mmol, 1.0 eq) was suspended in DMSO (5 mL) and continued stirring until complete dissolution (5 min) was observed. Then *N*-[(1*R*,8*S*,9*s*)-Bicyclo[6.1.0]non-4-in-9-ylmethoxycarbonyl]-1,8-diamino-3,6-dioxaoctan (sigma, 100.86 mg, 0.311 mmol, 1.12 eq) was dissolved in DMSO (5 mL) and added dropwise, followed by TEA (300 μ L). The slightly turbid solution cleared after 10 minutes and continued stirring for 18 h at ambient temperature. The next morning the reaction was filtered and purified by RP-HPLC (5-75% H_2O/ACN , 0.1% $HCOOH$, 220 nm). The product containing fractions were identified by LCMS and lyophilized to dryness to yield strained alkyne **47** as a white powder (153.1 mg, 0.142 mmol, 51%).

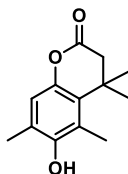
1H -NMR (500 MHz, $DMSO-d_6$): $\delta = 9.60$ (m, 3H), 9.41 (m, 1H), 7.77 (m, 2H), 7.64 (m, 1H), 7.34 (s, 4H), 4.02 (d, $J = 8.34$ Hz, 2H), 3.63 (m, 2H), 3.53 (m, 6H), 3.45-3.40 (m, 8H), 3.33 (m, 1H), 3.11 (q, $J = 5.64, 5.89$, 2H), 3.00 (m, $J = 7.11, 13.49$ Hz, 4H), 2.58-2.54 (m, 4H), 2.54 (, 2.26, 2.20 (m, 4H), 2.15 (m, 2H), 1.96 (s, 3H), 1.52 (m, 8H), 1.38 (q, $J = 7.11, 14.96$ Hz, 4H), 1.24 (m, 6H), 0.85 (t, $J = 9.12$ Hz, 1H).

^{13}C -NMR (126 MHz, $DMSO-d_6$): $\delta = 180.50, 180.28, 171.97, 171.31, 170.13, 156.46, 123.33, 99.00, 69.54, 69.17, 68.59, 61.38, 47.08, 46.78, 43.76, 43.58, 40.43, 39.52, 38.43, 29.90, 28.82, 28.59, 28.22, 27.57, 26.13, 26.03, 23.60, 23.50, 20.86, 20.36, 19.55, 17.66$.

HRMS (ESI) calculated for $([M+H]^+)$: $m/z = 1077,5472$; experimental = 1077.5473

Cleavable linker synthesis

Compound 48



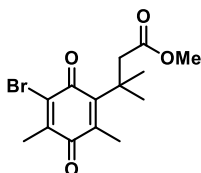
Chemical Formula: C₁₃H₁₆O₃
 Exact Mass: 220,1099
 Molecular Weight: 220,2680

Methanesulfonic acid (100 mL) was filled in a round bottom flask and heated to 70 °C, then 2,6-dimethylbenzene-1,4-diol (5.0 g, 36.21 mmol, 1.0 eq) and methyl 3-methylbut-2-enoate (4.7 g, 41.07 mmol, 1.1 eq) were added carefully each in one portion yielding a brown solution. The reaction was stirred at 70 °C for 2 hours. Then the reaction was diluted with water (100 mL), extracted with EtOAc (3 x 100 mL) and the combined organic extracts were washed with water (1x75mL), sat. NaHCO₃ (2x 75 mL), brine (75 mL) and dried over Na₂SO₄. The solvent was removed *in vacuo* yielding lactone **48** as a crude, beige solid (7.2 g, 32.91 mmol, 91%), which was directly used in the next step without further purification.

¹H-NMR (500 MHz, CDCl₃): δ = 6.71 (s, 1H), 2.56 (s, 2H), 2.37 (s, 3H), 2.22 (s, 3H), 1.45 (s, 6H).

¹³C-NMR (126 MHz, CDCl₃): δ = 168.67, 149.15, 144.77, 128.56, 122.50, 121.96, 116.78, 45.97, 35.35, 27.71, 15.87, 14.39.

Compound 49



Chemical Formula: C₁₄H₁₇BrO₄
 Exact Mass: 328,0310
 Molecular Weight: 329,1900

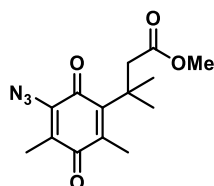
Lactone **48** (7.2 g, 32.91 mmol, 1.0 eq) was dissolved in AcOH (120 mL)/H₂O (30mL) and bromine (1.5 g, 96.92 mmol, 4.0 eq) was added over a dropping funnel over 15 minutes diluted in AcOH (30mL). The brown-orange solution continued stirring overnight, protected from light.

The solvent was evaporated by rotary evaporation in a fume hood (HBr/Br₂ fumes were quenched with sat. Na₂S₂O₃ in the collecting flask) and the residue was partitioned between water and DCM (each 200 mL). The aqueous phase was extracted with DCM (3x150 mL) and the combined extracts were extracted with sat. NaHCO₃ solution (8x250 mL). The NaHCO₃ extracts were acidified to pH < 3 with conc. HCl and extracted with DCM (3x 200 mL). The combined organic extracts were dried over Na₂SO₄ and the solvent was evaporated *in vacuo* yielding crude bromo acid **49a** (4254.4, 13.5 mmol, 56%) as a neon-yellow oil. The acid **49a** (4.3 g, 13.5 mmol, 1.0 eq) was dissolved directly in anhydrous MeOH (100 mL) and cooled to 0 °C. Then SOCl₂ (1.3 mL, 17.6 mmol, 1.3 eq) was added dropwise. The reaction was heated to reflux for two hours and then all volatiles were removed *in vacuo*. The residue was taken up in EtOAc and washed with sat. NaHCO₃ (2x 20 mL), brine (1 x20 mL) and dried over Na₂SO₄. The solvent was removed under reduced pressure to yield ester **49** (2.5 g, 7.5 mmol, 50%) as a crude brown-yellow oil.

¹H-NMR (500 MHz, CDCl₃): δ = 3.59 (s, 3H), 2.99 (s, 2H), 2.18 (s, 3H), 2.14 (s, 3H), 1.44 (s, 6H).

¹³C-NMR (126 MHz, MeOH-d₄): δ = 186.32, 183.68, 174.63, 153.86, 142.19, 141.70, 141.19, 52.05, 48.41, 40.04, 29.28, 14.92, 13.65.

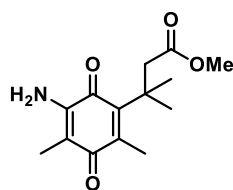
Compound 50



Chemical Formula: C₁₄H₁₇N₃O₄
 Exact Mass: 291,1219
 Molecular Weight: 291,3070

Bromide **49** (2.5 g, 7.5 mmol, 1.0 eq) was dissolved in MeOH (20 mL) and sodium azide (1.5 g, 22.5 mmol, 3.0 eq) was added in one portion. Then H₂O (20 mL) was added and the mixture continued stirring overnight at 25 °C. The organic solvent was removed *in vacuo* and the residual phase was extracted with EtOAc (3 x 100 mL) and the combined organic extracts were washed with brine (1x 200 mL) and dried over Na₂SO₄. The solvent was removed *in vacuo* and yielded the azide **50** (2.2 g, 7.5 mmol, quant.) as an orange-brown oil.

¹H-NMR (500 MHz, CDCl₃): δ = 3.61 (s, 3H), 2.99 (s, 2H), 2.15 (s, 3H), 1.89 (s, 3H), 1.43 (s, 6H).

Compound **XX**

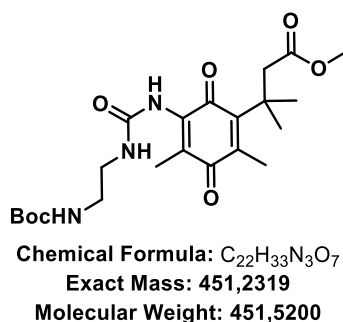
Chemical Formula: C₁₄H₁₉NO₄
 Exact Mass: 265,1314
 Molecular Weight: 265,3090

The azide **50** (2.2 g, 7.63 mmol, 1.0 eq) was dissolved in dry, degassed DCM (100 mL) and PPh₃ (3.6 g, 13.74 mmol, 1.8 eq) was added in three portions. The color of the solution became purple and was stirred at 24 °C for 1 hour. Then the solvent was evaporated by rotary evaporation at 40 °C and shortly dried under reduced pressure. The residue was dissolved in a mixture of AcOH/THF/H₂O (1:1:3, 600 mL) and heated to reflux (ca 100 °C) for 1 hour. The solvent is removed by rotary evaporation and EtOAc and H₂O (each 100 mL) were added. The organic phase is then again washed with sat. NaHCO₃ (3 x 70 mL). The solution was concentrated and purified by silica gel chromatography (DCM/MeOH 4:1 to 2:1) yield amino TML **51** (642.4 mg, 2.42 mmol, 32%) as a blood-red oil. Purification by prepTLC (SiO₂, DCM, max. 5% MeOH) was used additionally to remove traces of triphenylphosphine oxide, which hampered the next reaction step.

¹H-NMR (500 MHz, CDCl₃): δ = 7.80 (s, 1H), 3.10 (s, 2H), 2.91 (s, 3H), 2.76 (s, 3H), 2.13 (bs, 2H), 1.99 (s, 6H).

¹³C-NMR (126 MHz, CDCl₃): δ = 168.75, 149.28, 144.99, 128.79, 122.58, 122.07, 116.98, 77.16, 46.16, 35.55, 27.90, 16.02, 14.55.

HRMS (ESI) calculated for ([M+H]⁺): m/z = 266.1387; experimental = 266.1391.

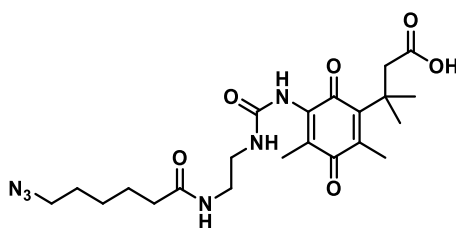
Compound **52**

Amino TML **51** (200 mg, 0.754 mmol, 1.0 eq) was dissolved in anhydrous toluene (30 mL) and triphosgene (894.74 mg, 3.02 mmol, 4.0 eq) was added in one portion under argon atmosphere. The reaction was heated from 23 °C to 80 °C and continued stirring at that temperature overnight. A prominent color change from red to orange was observed after 2 hours. The next day the solvent was removed by rotary evaporation at 40 °C and the residue was dried under reduced pressure for one hour. The carbamate was dissolved in anhydrous DCM (20 mL) and cooled to 0 °C under argon atmosphere. N-boc ethylene-1,6-diamine (101 mg, 0.63 mmol, 6.0 eq) was added dropwise over 5 minutes, diluted in anhydrous DCM (20 mL), followed by addition of TEA (800 μ L, 6.03 μ mol, 8.0 eq) at the same temperature. The reaction continued stirring at 0 °C for 1 hours and for 1 hour at 23 °C and the color changed from orange to canary yellow. The reaction was diluted with DCM (100 mL) and washed with water (2x50 mL), 1 M HCl (2x 75 mL) and brine (2x 75 mL). The organic phase was dried over Na_2SO_4 and concentrated to dryness. The yellow oil was purified by multiple RP-HPLCs (10-60% ACN/ H_2O , 0.1% HCOOH, 220 nm). Yellow fractions were verified to be pure product by LCMS, combined and lyophilized to yield **52** as a canary yellow oil (200.6 mg, 0.44 mmol, 59%).

1H -NMR (500 MHz, DMSO- d_6): δ = 8.11 (s, 1H), 6.74 (t, J = 5.36 Hz, 1H), 6.61 (t, J = 5.21 Hz, 1H), 3.49 (s, 3H), 3.01 (q, J = 6.92, 12.5 Hz, 2H), 2.89 (q, J = 6.92 Hz, 2H), 2.08 (s, 3H), 1.76 (s, 3H), 1.38 (s, 6H), 1.36 (s, 9H).

^{13}C -NMR (126 MHz, DMSO- d_6): δ = 186.76, 186.56, 171.81, 155.59, 153.43, 149.93, 141.18, 139.20, 124.52, 77.31, 51.14, 46.33, 42.02, 37.97, 29.49, 29.46, 28.68, 28.28, 26.00, 13.95, 11.93.

HRMS (ESI) calculated for ($[M+H]^+$): m/z = 452.2392; experimental = 452.2379.

Compound **53**

Chemical Formula: C₂₂H₃₂N₆O₆
 Exact Mass: 476,2383
 Molecular Weight: 476,5340

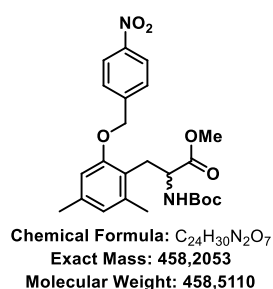
N-boc protected amine **52** (100 mg, 0.221 mmol, 1.0 eq) was dissolved in anhydrous DCM (750 μ L) and TFA (250 μ L) was added at 0 °C. The reaction continued stirring at 24 °C for 2 hours before the reaction was concentrated to dryness and dried overnight under reduced pressure. Then 6-azido hexanoic acid (69.92 mg, 0.443 mmol, 2.0 eq) was dissolved in DCMDMF (10:1, 18 + 2 mL) and HATU (336.86 mg, 0.886 mmol, 4.0 eq) was added. The suspension stirred for 5 minutes until the crude amine and DIPEA (50 μ L) were added together. The reaction stirred for 2 hours at 24 °C and was then diluted with DCM (100 mL) and washed with LiCl (5% w/v, 1x 100 mL), 1 M HCl (2x100 mL) and brine (1x100 mL) before the organic phase was dried over Na₂SO₄. The solvent was removed by rotary evaporation and the residue was again dissolved in MeOH (9 mL) and 1 M LiOH (1 mL) was added. The reaction stirred for 3 hours at 24 °C and was then acidified by dropwise conc. HCl addition. The MeOH was removed by rotary evaporation and the residual aqueous phase (+ 10 mL water) was extracted with DCM (3x20 mL). The combined organic extracts were concentrated *in vacuo* and the residue was purified by RP-HPLC (10-60% ACN/H₂O, 0.1% HCOOH, 220 nm). The product containing fractions were lyophilized to yield a yellow powder as **53** (78.3 mg, 0.164 mmol, 74% over three steps).

¹H-NMR (500 MHz, DMSO-d₆): δ = 12.01 (s, 1H), 8.76 (dd, J = 1.34, 4.32 Hz, 1H), 8.54 (dd, J = 1.46, 8.5 Hz, 1H), 7.52 (q, J = 3.84, 8.16 Hz, 1H), 3.50 (s, 1H), 3.31 (t, J = 7.28 Hz, 4H), 3.10 (m, 1H), 2.69 (s, 3H), 2.21 (t, J = 7.44 Hz, 3H), 2.08 (m, 2H), 1.77 (s, 1H), 1.51 (m, 9H), 1.38 (s, 2H), 1.32 (m, 4H).

¹³C-NMR (126 MHz, DMSO-d₆): δ = 187.21, 186.92, 174.83, 174.58, 172.66, 172.23, 165.06, 162.77, 154.16, 151.62, 150.53, 141.63, 140.08, 139.56, 135.11, 129.35, 125.21, 121.21, 51.62, 50.98, 46.75, 46.23, 38.71, 38.43, 36.25, 35.73, 35.39, 33.97, 31.23, 29.14, 28.48, 28.46, 26.32, 26.27, 26.19, 25.20, 25.08, 24.49, 14.38, 12.31, 9.11.

HRMS (ESI) calculated for ([M+H]⁺): m/z = 477.2456; experimental = 477.2439.

Compound 54



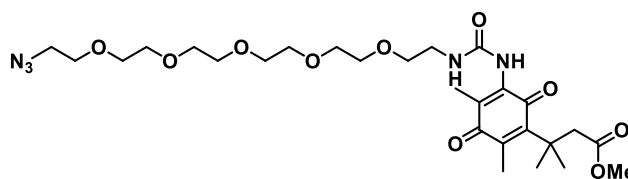
methyl 2-((*t*-butoxycarbonyl)amino)-3-(2,4-dimethyl-6-((4-nitrobenzyl)oxy)phenyl) propanoate (chemspace ID: CSC010216371, 500 mg, 1.62 mmol, 1.0 eq) was dissolved in MeOH (10 mL) and dimethoxy propane (396 μ L, 3.232 mmol, 2.0 eq) was added, followed by 20% HCl (10 μ L). The reaction continued stirring at 23 °C for 2 hours and the solvent was removed *in vacuo*. The residue was dried for two hours under reduced pressure before ACN (10 mL), *para*-nitro benzyl bromide (523.7 mg, 2.42 mmol, 1.5 eq) and K₂CO₃ (446.9 mg, 3.23 mmol, 2.0 eq) were added. The suspension stirred overnight at 23 °C. Then the reaction was filtered and the filter was washed with DCM (100 mL). The solvent was removed *in vacuo* and the residue was washed with ice-cold petrolether. The residue was purified by flash chromatography (C18, 10-100% ACN/H₂O, 220 nm) and product containing fractions were identified by LCMS. The combined fractions were lyophilized to dryness to yield ether **54** (614.71 mg, 1.34 mmol, 83% over two steps) as a yellow oil.

¹H-NMR (500 MHz, DMSO-*d*₆): δ = 8.24 (d, *J* = 8.8 Hz, 2H), 7.76 (d, *J* = 1.53 Hz, 1H), 7.24 (d, *J* = 7.84 Hz, 1H), 6.66 (d, 2H), 5.25 (s, 2H), 4.22 (q, *J* = 7.84, 15.49, 1H), 3.48 (s, 3H), 2.98 (m, 2H), 2.22 (s, 3H), 2.19 (s, 3H), 1.33 (s, 9).

¹³C-NMR (126 MHz, DMSO-*d*₆): δ = 172.80, 156.15, 155.21, 146.86, 145.38, 137.62, 136.43, 127.73, 123.61, 123.46, 121.07, 110.30, 78.22, 68.17, 53.28, 51.57, 39.52, 28.26, 28.09, 27.65, 21.03, 19.19.

DEPT (126 MHz, DMSO-*d*₆): δ = 127.47, 123.35, 123.20, 110.04, 67.92, 53.03, 51.31, 39.52, 28.00, 27.83, 27.39, 20.77, 18.93.

HRMS (ESI) calculated for ([M+H]⁺): *m/z* = 459.2126; experimental = 459.2132.

Compound **55**Chemical Formula: C₂₇H₄₃N₅O₁₀

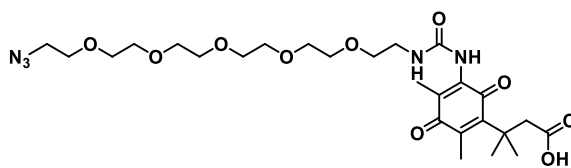
Exact Mass: 597,3010

Molecular Weight: 597,6660

51 (50 mg, 0.188 mmol, 1.0 eq) was dissolved in anhydrous toluene (50 mL) and triphosgene (111.85 mg, 0.377 mmol, 2.0 eq) was added at 23 °C. The reaction was heated to 80 °C for 18 h and then the solvent was removed by rotary evaporation. The residue was dried under reduced pressure for 2 hours. Anhydrous DCM (15 mL) was added under argon atmosphere and the solution was cooled to 0 °C. Then N₃-PEG-NH₂ (230.94 mg, 0.754 mmol, 4.0 eq) dissolved in anhydrous DCM (10 mL) and TEA (500 μL) were added dropwise together at 0 °C. The reaction was equilibrated to 23 °C and continued stirring at this temperature for two hours. The reaction progress was monitored by LCMS and after complete conversion the solvent was removed by rotary evaporation and dissolved in ACN (4 mL), filtered and purified by RP-HPLC (C18, 5-75% ACN/H₂O, 0.1% HCOOH, 220 nm,). The product containing fractions were lyophilized to dryness to yield **55** (285.4 mg, 0.477 mmol, 92%) as an orange oil.

¹H-NMR (500 MHz, MeOH-d₄): δ = 3.66 (m, 18H), 3.57 (m, 5H), 3.37 (q, J = 5.08, 9.87 Hz, 4H), 2.94 (s, 2H), 2.17 (s, 3H), 1.88 (s, 3H), 1.46 (s, 6H).

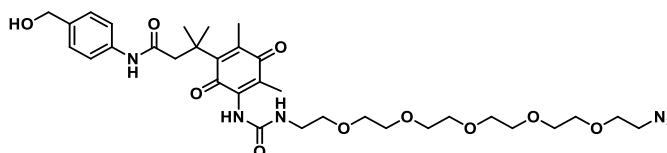
¹³C-NMR (126 MHz, MeOH-d₄): δ = 187.36, 186.38, 172.86, 149.99, 140.15, 139.91, 127.48, 70.23, 70.22, 70.17, 70.16, 70.12, 69.92, 69.74, 50.50, 50.37, 46.69, 38.31, 28.19, 13.23, 11.12.

Compound **56**

Chemical Formula: C₂₆H₄₁N₅O₁₀
 Exact Mass: 583,2853
 Molecular Weight: 583,6390

The ester **55** (29 mg, 0.048 mmol, 1.0) was dissolved in MeOH (900 μ L) and 1M KOH (100 μ L) was added. The reaction continued stirring at 24 °C. Upon completion, the pH was adjusted to two (color change purple to yellow) by the dropwise addition of concentrated HCl on ice. The MeOH fraction was removed by rotary evaporation at 30 °C, then water (10 mL) and brine (10 mL) were added. The aqueous phase was extracted with DCM (3x20 mL) and the combined organic extracts were dried over Na₂SO₄. The solvent was removed *in vacuo* to yield acid **56** (28.04mg, 0.048 mmol, quant.) as a crude oil that was directly used in the next step.

HRMS (ESI) calculated for ([M+H]⁺): m/z = 584.2926; experimental = 584.2937.

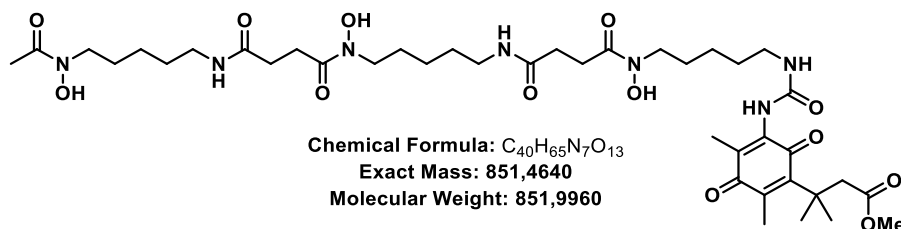
Compound **57**

Chemical Formula: C₃₃H₄₈N₆O₁₀
 Exact Mass: 688,3432
 Molecular Weight: 688,7790

The acid **56** (30 mg, 0.051 mmol, 1.0 eq) was dissolved in anhydrous THF (2.5 mL), NMM (200 μ L) was added under argon atmosphere and the reaction was cooled to 0 °C, before *iso*-butyl chloroformate (4.98 μ L, 0.051 mmol, 1.0 eq) was added and the reaction went turbid instantly. The reaction stirred 15 minutes at 0 °C and then one hour at 24 °C. Then *para*-amino benzyl alcohol (7.6 mg, 0.062 mmol, 1.2 eq) was added at 0 °C, dissolved in anhydrous THF (1 mL), basified with NMM (200 μ L) before addition. The reaction continued stirring at 0 °C for 15 minutes and then for 1 hour at 24 °C. The reaction was diluted with DCM (100 mL) and washed with 1M HCl (3x100 mL), dried over Na₂SO₄ and evaporated to dryness to yield crude **57** as a yellow oil (27.4 mg, 0.04 mmol, 77%).

HRMS (ESI) calculated for ([M+H]⁺): m/z = 689.3505; experimental = 689.3508.

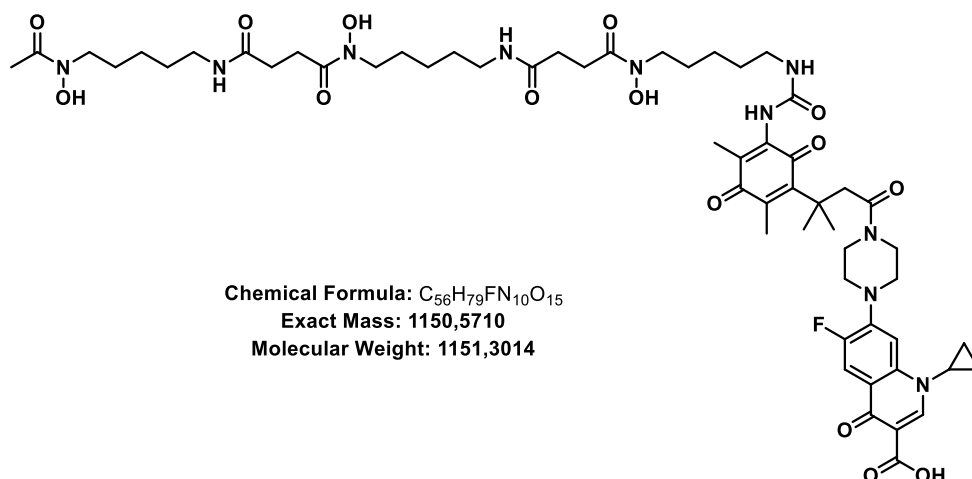
Gyrase inhibitor constructs

Compound **58**

This compound was synthesized according to a modified procedure by Miller et al.² Amino TML **51** (160.5 mg, 0.61 mmol, 1.0 eq) was dissolved in dry toluene (12.5 mL) and triphosgene (538.5 mg, 1.82 mmol, 3.0 eq) was added at 25 °C in one portion under argon atmosphere. Then the reaction was heated to reflux overnight, was then cooled to 25 °C and filtered. The solvent was removed *in vacuo*, the residue was dried under reduced pressure for 30 minutes and then dissolved in anhydrous DMF (1 mL). DFO (339.2 mg, 0.61 mmol, 1 eq) was added in DMF (4.5 mL, solubilize w. heat gun) with TEA (335 μL, 4.84 mmol, 4.0 eq) dropwise at 0 °C over five minutes. The reaction was stirred at 0 °C for one hour and continued stirring at 25 °C for two hours. The base and solvent were removed under reduced pressure and the residue was dissolved in MeOH/ACN/H₂O and purified by RP-HPLC (10-50% ACN, 0.1% HCOOH, 220 nm) to yield **58** as a yellow solid (87.4 mg, 0.102 mmol, 18%).

¹H-NMR (500 MHz, DMSO-d₆): δ = 9.62 (m, 2H), 8.12 (s, 1H), 7.77 (t, J = 5.09 Hz, 2H), 6.62 (t, J = 5.46 Hz, 1H), 3.49 (s, 3H), 3.45 (m, 8H), 3.00 (m, 6H), 2.85 (s, 2H), 2.57 (t, J = 6.31 Hz, 3H), 2.27 (m, 5H), 2.11 (s, 1H), 2.08 (s, 3H), 1.96 (s, 1H), 1.77 (s, 3H), 1.54 (s, 2H), 1.49 (m, 6H), 1.38 (m, 12H), 1.21 (m, 6H).

¹³C-NMR (126 MHz, DMSO-d₆): δ = 186.76, 186.55, 171.98, 171.81, 171.48, 171.34, 170.16, 154.57, 153.44, 149.94, 149.86, 141.18, 139.19, 135.23, 127.78, 126.07, 124.53, 117.66, 106.25, 51.14, 50.89, 47.10, 46.80, 46.44, 46.33, 38.43, 38.05, 37.97, 30.24, 29.92, 29.20, 28.81, 28.68, 27.57, 26.03, 23.49, 23.41, 20.34, 15.24, 13.94, 11.91, 10.99.

Compound **12**

This compound was previously synthesized by Miller et al.² Ester **58** (11.34 mg, 0.013 mmol, 1.0 eq) was dissolved in MeOH. A 5 N KOH solution was added (100 μ L) at 25 °C. The color changed from yellow to a dark red and the reaction stirred 3 h at ambient temperature. After completion, the pH was reversed to 2 with 3 M HCl and the solution was loaded on a milliQ water equilibrated C18-SiO₂ pad. The salts were removed with milliQ water (5 mL) while the compound retained and was then eluted with 70% ACN/H₂O. The yellow solution was frozen in liquid N₂ and lyophilized to yield crude acid **58a**. Acid **58a** was dissolved in DMF (5 mL), cooled to 0 °C before EDCI·HCl (14.5 mg, 0.076 mmol, 5.7 eq) and HOBT (10.25 mg, 0.076 mmol, 5.7 eq) were added. The yellowish solution was stirred at 0 °C for 5 minutes, before ciprofloxacin (6.16 mg, 0.016 mmol, 1.2 eq) and TEA (7.87 μ L, 0.106 mmol, 8.0 eq), followed by DMAP (0.33 mg, 0.003 mmol, 0.2 eq), were added. The mixture was warmed to 25 °C and stirred for 16 h. The next morning, the solvent was removed under reduced pressure and the residue was taken up in 40% ACN in milliQ H₂O, filtered and injected into the HPLC (10-70% ACN/H₂O, 0.1% HCOOH, 220 nm). The product containing fractions were identified by LCMS and lyophilized to yield **12** as a yellow powder overnight (5.4 mg, 0.005 mmol, 35%).

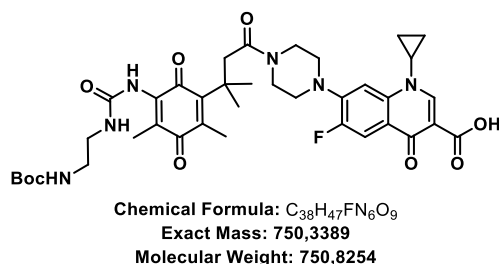
¹H-NMR (700 MHz, DMSO-d₆): δ = 15.19 (s, 1H), 9.61 (m, 3H), 8.67 (s, 3H), 7.99 (s, 1H), 7.93 (d, J = 14.55 Hz, 1H), 7.76 (m, 2H), 7.54 (d, J = 10.91 Hz, 1H), 6.62 (m, 1H), 3.80 (m, 1H), 3.70 (m, 2H), 3.60 (m, 2H), 3.45 (m, 4H), 3.39-3.36 (m, 5H), 3.30 (m, 2H), 2.99 (m, 9H), 2.57 (m, 4H), 2.26 (q, J = 8.13, 15.58 Hz, 4H), 2.07 (s, 3H), 1.96 (s, 3H), 1.76 8s, 3H), 1.49 (m, 8H), 1.41 (s, 6H), 1.34 (m, 12H), 1.20 (m, 12H).

¹³C-NMR (176 MHz, DMSO-d₆): δ = 186.94, 186.62, 176.36, 171.93, 171.27, 169.74, 165.91, 153.37, 152.21, 148.09, 141.09, 139.15, 136.65, 106.75, 50.49, 47.05, 46.75, 45.05, 44.73, 40.56, 40.00, 38.39, 38.09, 35.86, 33.48, 29.86, 29.19, 28.79, 28.70, 27.97, 27.53, 26.00, 25.69, 24.00, 23.47, 23.33, 20.32, 13.85, 11.98, 7.57.

DEPT (176 MHz, DMSO-d₆): δ = 147.85, 110.88, 110.75, 106.13, 50.25, 49.22, 48.78, 46.80, 46.51, 44.81, 44.49, 40.32, 39.52, 39.13, 38.16, 35.63, 33.24, 29.62, 28.95, 28.55, 28.46, 27.73, 27.29, 25.76, 25.45, 23.76, 23.23, 23.09, 20.08, 13.61, 11.74, 7.33, 0.15.

HRMS (ESI) calculated for ([M+H]⁺): m/z = 1151.5783; experimental = 1151.5791.

Compound 59



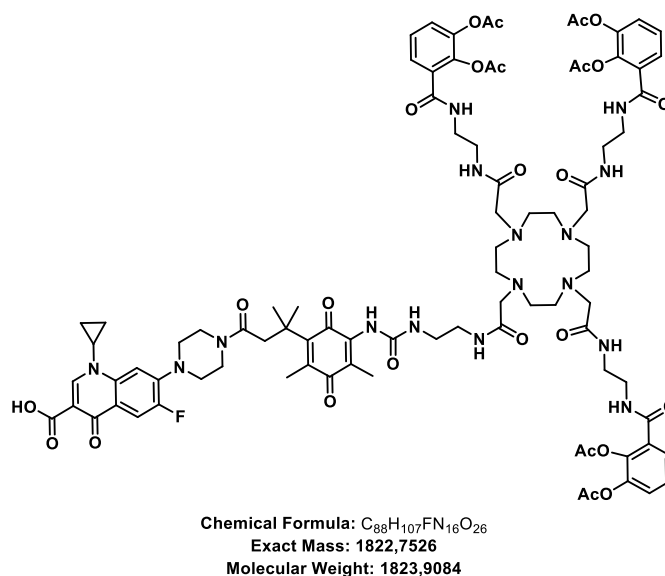
This compound was synthesized with modified conditions from Miller et al.² Ester **52** (20 mg, 0.044 mmol, 1.0 eq) was dissolved in MeOH (1 mL) and 1M NaOH (1 mL) was added at 23 °C. The reaction stirred for two hours, was then acidified with 1M HCl to pH 2 and quickly extracted with DCM (2x25 mL). The combined organic phases were dried over Na₂SO₄ and concentrated to dryness to yield acid **52a** as a crude, yellow oil. This oil was dried under reduced pressure for 1 hour, before DCM / DMF (10 and 1 mL) were added. This was followed by HOBt (13.8 mg, 0.089 mmol, 2.0 eq) and EDCI·HCl (12.1 mg, 0.089 mmol, 2.0 eq) addition at 0 °C under argon atmosphere. The reaction stirred five minutes at 0 °C before ciprofloxacin (22 mg, 0.066 mmol, 1.5 eq in 1 mL DMF) and DIPEA (30 μ L) were added at 0 °C. The ice bath was removed and the reaction continued stirring overnight at 23 °C. The solvent was removed by rotary evaporation and the residue was dissolved in DCM (100 mL) and was washed with 1M HCl/brine (1:1, 3x50 mL), brine (3x50 mL). After drying over Na₂SO₄ the solvent was removed *in vacuo* and the residue was purified by RP-HPLC (C18, 10-70% ACN/H₂O, 0.1 % HCOOH, 220 nm). Product containing fractions were identified by LCMS and lyophilized to yield intermediate **59** (19.6 mg, 0.026 mmol, 59% over two steps) as a yellow oil.

¹H-NMR (700 MHz, DMSO-d₆): δ = 15.20 (s, 1H), 8.67 (s, 1H), 8.09 (s, 1H), 7.93 (d, J = 14.6 Hz, 2H), 7.55 (d, J = 8.73 Hz, 2H), 6.76 (t, J = 5.5 Hz, 1H), 6.67 (t, J = 5.5 Hz, 1H), 4.08 (q, J = 5.22, 10.7 Hz, 1H), 3.81 (m, 1H), 3.70, 3.61 (m, 2H), 3.36 (m, 2H), 3.29 (m, 6H), 3.16 (d, J = 4.95 Hz, 4H), 3.03 (q, J = 6.02, 12.23 Hz, 2H), 2.99 (s, 2H), 2.91 (q, J = 6.02, 11.96 Hz, 2H), 2.07 (s, 3H), 1.91 (s, 1H), 1.77 (s, 3H), 1.41 (s, 6H), 1.34 (s, 9H), 1.31 (m, 2H), 1.19 (m, 2H).

¹³C-NMR (176 MHz, DMSO-d₆): δ = 186.98, 186.54, 176.37, 169.70, 165.90, 153.60, 152.23, 148.09, 144.83, 140.97, 139.15, 136.69, 106.76, 106.40, 77.62, 48.57, 44.99, 44.74, 38.13, 35.86, 35.76, 28.69, 28.17, 21.03, 13.85, 11.96, 7.57.

HRMS (ESI) calculated for ([M+H]⁺): m/z = 751,3461; experimental = 751.3454.

Compound 8



N-boc amine **59** (10 mg, 0.013 mmol, 1.0 eq) was dissolved in anhydrous DCM (0.75 mL) and TFA (0.25 mL) was added at 0 °C. The yellow solution stirred for 2 hours at 24 °C, and was then concentrated to dryness to yield **59a**. The orange residue was dried under reduced pressure for 2 hours. Meanwhile acid **7** (23.8 mg, 0.02 mmol, 1.5 eq) was dissolved in anhydrous THF (500 μL), and NMM (30 μL) was added under argon atmosphere. At 0 °C *iso*-butyl chloroformate (1.4 μL, 0.020 mmol, 1.5 eq) was added and the reaction went turbid instantly. The reaction stirred ten minutes at 0 °C and 1 h at 24 °C. Then amine **59a** was added dropwise at 0 °C, in anhydrous THF (500 μL) and together with NMM (30 μL). The reaction continued stirring at 0 °C for 5 minutes and one hour at 24 °C. Then AcOH (200 μL) was added, the solvent was removed *in vacuo* at 30 °C and the residue was purified by RP-HPLC (C18,

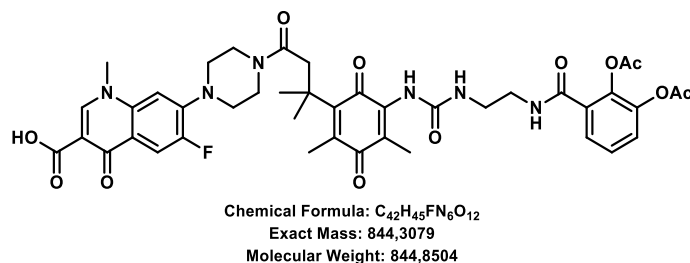
10-70% ACN/H₂O, 1% AcOH, 220 nm). Product containing fractions were combined and lyophilized to yield conjugate **8** as a slightly yellow powder (19.06 mg, 0.01 mmol, 79%).

¹H-NMR (500 MHz, DMSO-d₆+AcOH-d₄): δ = 9.98, 8.67, 8.26, 8.12, 7.95, 7.78, 7.58, 7.44, 6.96, 3.95, 3.82, 3.71, 3.61, 3.47, 3.26, 3.06, 2.89, 2.73, 2.08, 1.79, 1.41, 1.35, 1.31, 1.23, 1.19, 1.10.

¹³C-NMR (176 MHz, DMSO-d₆+AcOH-d₄): δ = 187.02, 186.53, 176.37, 169.75, 169.32, 169.23, 165.84, 153.62, 153.49, 152.20, 148.15, 144.89, 140.92, 140.76, 139.15, 138.49, 136.76, 124.76, 118.82, 116.68, 111.14, 111.01, 106.71, 106.44, 49.87, 49.53, 49.02, 44.99, 44.78, 40.57, 38.80, 38.68, 38.15, 35.87, 34.28, 28.70, 22.58, 22.53, 21.00, 13.89, 12.08, 12.05, 7.59.

HRMS (ESI) calculated for ([M+2H]²⁺): m/z = 953.4101; experimental = 953.4115.

Compound 9



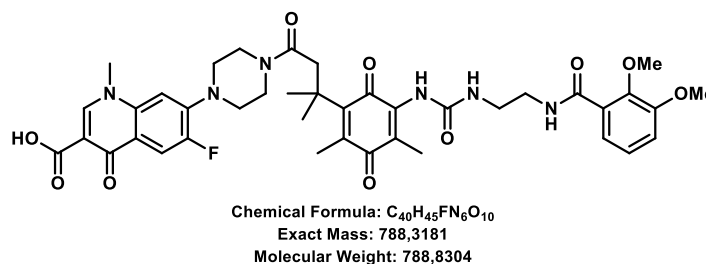
2,3-diacethoxy benzoic acid **38** (2.75 mg, 0.012 mmol, 1.5 eq) was dissolved in anhydrous THF (500 μ L) and anhydrous NMM (10 μ L) was added under argon atmosphere at 0 °C. At this temperature *iso*-butyl chloroformate (1.9 μ L, 0.012 mmol, 1.5 eq) was added and the reaction continued stirring at 0 ° for five minutes. The reaction stirred for 30 minutes at 24 °C. Then the amine **59a** (preparation see above, 5.0 mg, 0.008 mmol, 1.0 eq) was added in THF (500 μ L) with NMM (10 μ L) dropwise at 0 °C. The reaction stirred for 30 minutes at 24 °C and then AcOH (200 μ L) was added. The reaction was concentrated and the residue taken up in ACN, filtered and purified by RP-HPLC (5-80% ACN/H₂O, 1% AcOH, 220 nm). Product containing fractions were lyophilized to yield amide **9** (5.565 mg, 0.006 mmol, 83%) as a yellow powder.

¹H-NMR (500 MHz, DMSO-d₆, 1% AcOH-d₄): δ = 8.67 (m, 1H), 7.92 (m, 1H), 7.54 (m, 1H), 7.44 (m, 1H), 7.34 (m, 1H), 3.81 (m, 2H), 3.69 (m, 3H), 3.61 (m, 3H), 3.34 (m, 6H), 3.27 (m, 3H), 3.18 (m, 3H), 3.05 (t, J = 5.76 Hz, 1H), 2.99 (m, 3H), 2.27 (s, 3H), 2.20 (s, 1H), 2.07 (s, 3H), 1.91 (s, 1H), 1.77 (s, 3H), 1.41 (s, 6H), 1.37 (m, 1H), 1.30 (m, 3H), 1.23 (m, 1H), 1.17 (m, 3H), 1.09 (m, 1H), 0.92 (d, J = 7.16 Hz, 2H), 0.84 (d, J = 6.80 Hz, 3H).

¹³C-NMR (176 MHz, DMSO-d₆+1% AcOH-d₄): δ = 171.94, 168.25, 168.18, 164.98, 164.92, 164.43, 151.74, 143.04, 142.74, 142.04, 139.96, 129.67, 128.62, 128.46, 128.16, 126.65, 126.28, 126.18, 126.04, 125.41, 74.56, 74.53, 74.49, 69.71, 69.55, 69.52, 69.49, 68.65, 38.79, 38.08, 35.84, 28.70, 27.27, 27.14, 18.47, 18.37, 13.85, 7.57.

HRMS (ESI) calculated for ([M+2H]²⁺): m/z = 845.3152; experimental = 845.3158.

Compound 10



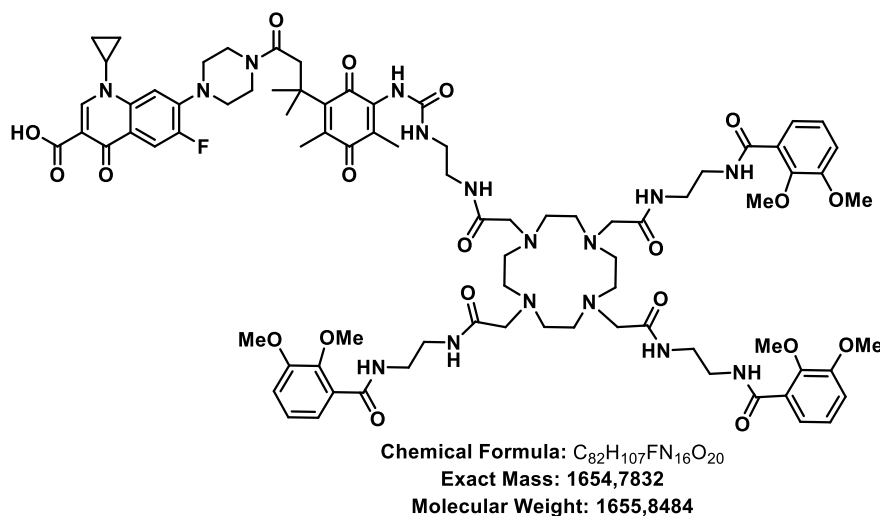
2,3-dimethoxy benzoic acid (2.52 mg, 0.014 mmol, 1.5 eq) was dissolved in anhydrous THF (500 μ L) and anhydrous NMM (10 μ L) was added under argon atmosphere at 0 °C. At this temperature iso-butyl chloroformate (1.7 μ L, 0.014 mmol, 1.5 eq) was added and the reaction continued stirring at 0 ° for five minutes. The reaction stirred for 30 minutes at 24 °C. Then the amine **59a** (6.0 mg, 0.009 mmol, 1.0 eq) was added in THF (500 μ L) with NMM (10 μ L) dropwise at 0 °C. The reaction stirred for 30 minutes at 24 °C and was then concentrated *in vacuo*. The residue was taken up in ACN, filtered and purified by RP-HPLC (5-80% ACN/H₂O, 1% AcOH, 220 nm). Product containing fractions were lyophilized to yield amide **10** (6.703 mg, 0.008 mmol, 89%) as a yellow powder.

¹H-NMR (500 MHz, DMSO-d₆): δ = 15.20 (s, 1H), 8.64 (m, 1H), 8.17 (m, 1H), 7.91 (t, J = 15.78 Hz, 1H), 7.53 (m, 1H), 7.11 (m, 4H), 6.73 (m, 1H), 3.80 (m, 5H), 3.72 (m, 3H), 3.69 (m, 2H), 3.60 (m, 2H), 3.41 (m, 1H), 3.35 (m, 3H), 3.32 (s, 6H), 3.28 (m, 5H), 3.20 (m, 3H), 2.98 (bs, 2H), 2.07 (s, 3H), 1.76 (s, 3H), 1.41 (s, 6H), 1.30 (q, J = 6.58, 13.67 Hz, 3H), 1.23 (m, 1H), 1.17 (m, 2H), 1.09 (m, 1H).

¹³C-NMR (126 MHz, DMSO-d₆): δ = 186.96, 186.53, 169.71, 165.91, 165.43, 153.72, 152.45, 152.36, 148.01, 146.35, 141.01, 139.11, 136.58, 129.25, 123.88, 120.71, 114.77, 110.91, 106.74, 106.34, 60.88, 60.85, 55.89, 45.02, 44.74, 40.54, 38.14, 35.83, 28.68, 13.84, 11.90, 7.56.

HRMS (ESI) calculated for ([M+H]⁺): m/z = 789.3254; experimental = 789.3256.

Compound 11



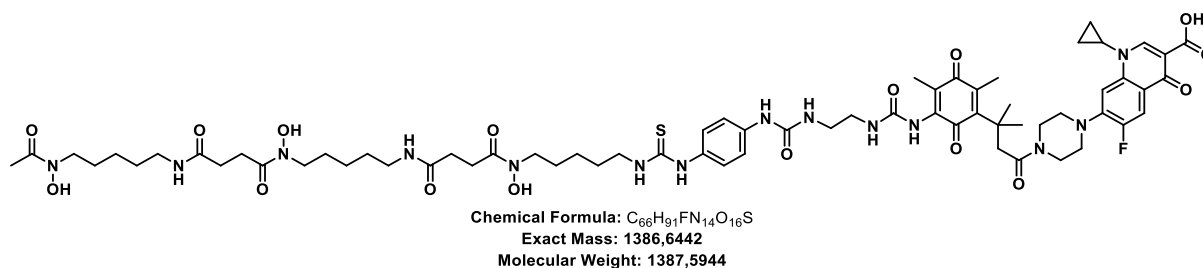
44 was dissolved in DCM/DMF (5/0.25 mL) and HATU (14.87 mg, m.039 mmol, 2.0 eq) was added in one portion. After 5 minutes the amine **59a** (preparation see above, 15.26 mg, 0.023 mmol, 1.2 eq) was added in DCM/DMF (5/0.25 μL) together with DIPEA (100 μL) and the yellow solution stirred overnight at ambient temperature. The solvent was removed by rotary evaporation and the residue was purified by RP-HPLC (C18, 5-85% ACN/H₂O, 0.1% HCOOH, 220 nm) and product containing fractions were lyophilized to yield **11** (21.6 mg, 0.014 mmol, 71%) as a yellow solid.

¹H-NMR (700 MHz, DMSO-d₆): δ = 15.20 (s, 1H), 8.66 (m, 2H), 8.21 (t, J = 5.73 Hz, 1H), 8.12 (m, 1H), 7.91 (d, J = 13.27 Hz, 2H), 7.52 (d, J = 7.21 Hz, 2H), 7.12 (m, 4H), 7.07 (m, 2H), 6.74 (m, 1H), 3.80 (m, 9H), 3.72 (s, 5H), 3.69 (m, 4H), 3.60 (m, 4H), 3.35 (m, 20H), 3.27 (m, 8H), 3.20 (q, J = 5.57, 11.79 Hz, 4H), 2.98 (bs, 4H), 2.07 (s, 6H), 1.91 (s, 2H), 1.76 (s, 6H), 1.41 (s, 12H), 1.30 (q, J = 7.53, 15.23 Hz, 4H), 1.17 (m, 4H).

¹³C-NMR (176 MHz, DMSO-d₆): δ = 186.97, 186.54, 176.35, 169.72, 165.91, 165.44, 153.73, 153.59, 152.46, 152.36, 152.18, 148.03, 146.36, 144.82, 141.02, 139.12, 136.60, 129.26, 124.74, 123.89, 120.72, 114.78, 111.09, 110.96, 106.75, 106.37, 60.85, 55.90, 49.50, 48.99, 45.02, 44.75, 40.54, 40.02, 39.52, 38.14, 35.83, 28.69, 21.03, 13.85, 11.90, 7.56.

HRMS (ESI) calculated for ([M+2H]²⁺): m/z = 823.8988; experimental = 823.9001.

Compound 13



Boc-protected amine **59** (14.4 mg, 0.019 mmol, 1.2 eq) was dissolved in DCM (0.75 mL) and TFA (0.25 mL) was added at 0 °C. The reaction continued stirring two hours at 24 °C and upon full conversion the solution was concentrated to dryness to yield **59a**. After drying for several hours under reduced pressure, the residue was dissolved in anhydrous DMF (500 μL) and isothiocyanate **46** (12.0 mg, 0.016 mmol, 1.0 eq) was added. Then TEA (50 μL) was added and the reaction continued stirring at 24 °C overnight. The base was removed by rotary evaporation, the solution was filtered and purified by RP-HPLC (C18, 10-80% ACN/H₂O, 0.1% HCOOH, 220 nm). The product containing fractions were identified by LCMS and lyophilized to yield pure title compound **13** as a beige solid (19.56 mg, 0.014 mmol, 73% over two steps).

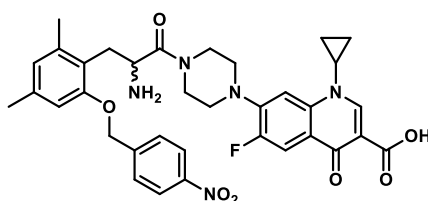
¹H-NMR (700 MHz, DMSO-d₆): δ = 9.62 (m, 3H), 7.90 (m, 1H), 7.77 (m, 2H), 7.54 (d, J = 9.52 Hz, 2H), 7.37 (d, J = 9.18 Hz, 2H), 3.47 (m, 8H), 3.00 (q, J = 6.85, 13.52 Hz, 4H), 2.57 (q, J = 7.68, 13.02 Hz, 4H), 2.27 (q, J = 6.34, 12.52 Hz, 4H), 1.96 (s, 3H), 1.52 (m, 4H), 1.49 (m, 4H), 1.38 (m, 4H), 1.26 (m, 2H), 1.21 (m, 4H).

¹³C-NMR (176 MHz, DMSO-d₆): δ = 187.01, 186.51, 176.35, 169.73, 169.30, 169.22, 165.82, 153.60, 153.48, 152.18, 148.13, 144.87, 140.90, 140.74, 139.13, 138.47, 136.74, 124.74, 118.80, 116.67, 111.12, 110.99, 106.69, 106.42, 49.86, 49.51, 49.01, 44.97, 44.76, 40.55, 38.78, 38.66, 38.14, 35.85, 34.26, 28.68, 22.56, 22.51, 20.98, 13.87, 12.07, 12.03, 7.57.

DEPT (176 MHz, DMSO-d₆): δ = 187.49, 187.00, 176.83, 172.44, 170.21, 169.78, 169.70, 166.30, 165.56, 154.08, 154.02, 153.96, 152.64, 148.61, 145.29, 141.36, 141.22, 139.61, 137.22, 125.13, 119.30, 111.59, 111.40, 107.19, 106.93, 106.89, 49.99, 49.50, 45.45, 45.25, 41.04, 38.62, 36.33, 34.75, 29.16, 23.04, 22.99, 21.47, 14.35, 12.54, 12.51, 8.05.

HRMS (ESI) calculated for ([M+H]⁺): m/z = 1404.6780; experimental = 1404.6788.

Compound 60



Chemical Formula: C₃₅H₃₆FN₅O₇

Exact Mass: 657,2599

Molecular Weight: 657,6994

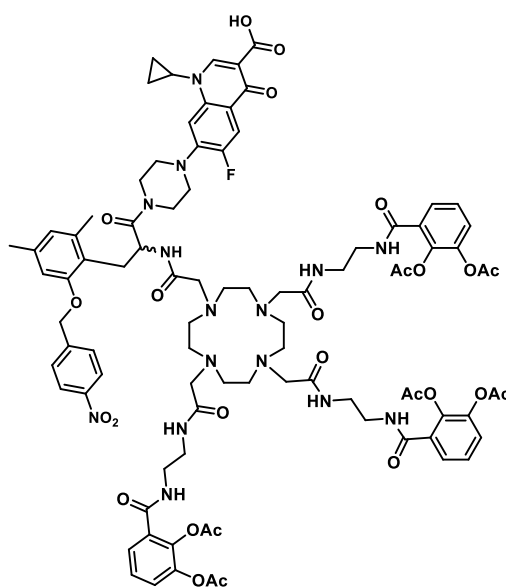
Ester **54** (65 mg, 0.142 mmol, 1.0 eq) was dissolved in MeOH (1 mL) and 1M NaOH (1 mL) was added at 23 °C. The reaction stirred for 2 hours at that temperature, was then acidified with 1M HCl to pH 2 and quickly extracted with DCM (2x25 mL). The combined organic phases were dried over Na₂SO₄ and concentrated to dryness to yield acid **54a** as a yellow, crude oil. This oil was dried for one hour under reduced pressure. Then DCM/DMF (10 and 1 mL) were added, followed by HOBT (38.60 mg, 0.284 mmol, 2.0 eq) and EDCI·HCl (44.01 mg, 0.284 mmol, 2.0 eq) at 0 °C under argon atmosphere. The reaction stirred for five minutes at 0 °C before ciprofloxacin (22 mg, 0.066 mmol, 1.5 eq in 1 mL DMF) and DIPEA (30 μ L) were added. The ice bath was removed and the reaction continued stirring overnight at 23 °C. The solvent was removed by rotary evaporation and the residue was dissolved in DCM (100 mL) and was washed with brine (3x 50 mL). After drying over Na₂SO₄ the solvent was removed *in vacuo* and then TFA/DCM (25%, 0.25:0.75 mL) was added at 0 °C and the reaction continued stirring at 23 °C for two hours. Then the solvent was removed by rotary evaporation and the residue was purified by RP-HPLC (C18, 10-70% ACN/H₂O, 220 nm). Product containing fractions were identified by LCMS and lyophilized to yield amine **60** (60.7 mg, 0.092 mmol, 65% over three steps) as a beige solid.

¹H-NMR (700 MHz, DMSO-d₆): δ = 15.17 (s, 1H), 8.68 (s, 1H), 8.12 (s, 1H), 7.94 (d, J = 11.78 Hz, 1H), 7.61 (d, J = 6.34 Hz, 1H), 3.83 (m, 1H), 3.61 (m, 4H), 3.35 (t, J = 5.25 Hz, 2H), 3.30 (t, J = 5.25 Hz, 1H), 1.32 (m, 2H), 1.19 (m, 2H).

¹³C-NMR (176 MHz, DMSO-d₆): δ = 176.38, 165.87, 161.01, 153.71, 152.30, 148.12, 144.96, 144.90, 139.10, 119.05, 119.00, 111.09, 110.96, 107.04, 106.78, 50.20, 50.18, 49.09, 49.07, 44.39, 35.89, 7.57.

HRMS (ESI) calculated for ([M+H]⁺): m/z = 658.2672; experimental = 658.2673.

Compound 14



Chemical Formula: C₉₀H₁₀₄FN₁₅O₂₆
 Exact Mass: 1829,7261
 Molecular Weight: 1830,8994

Acid **7** (10 mg, 0.008 mmol, 1.0 eq) was dissolved in anhydrous THF (1.0 mL), NMM (30 μL) and *iso*-butyl chloroformate (0.81 μL, 0.008, 1.0 eq) was added at 0 °C. The solution stirred 0 °C for ten minutes and 50 minutes at 24 °C. The amine **60** (6.62 mg, 0.01 mmol, 1.2 eq) was dissolved in anhydrous THF (1.0 mL), NMM (30 μL) was added under argon atmosphere at 0 °C. The reaction stirred ten minutes at 0 °C and then 1 h at 24 °C. The reaction continued stirring at 0 °C for five minutes and then for one hour at 24 °C. Then AcOH (200 μL) was added, the solvent was removed *in vacuo* at 30 °C and the residue was purified by RP-HPLC (C18, 10-70% ACN/H₂O, 1% AcOH, 220 nm). Product containing fractions were combined and lyophilized to yield the conjugate **14** as a slightly yellow powder (13.4 mg, 0.007 mmol, 87%).

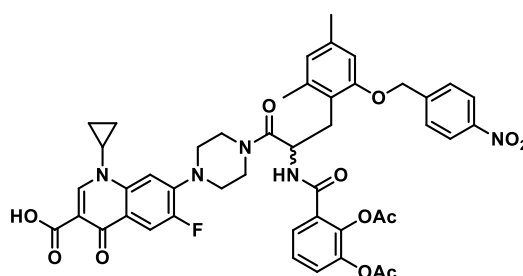
¹H-NMR (700 MHz, DMSO-d₆+AcOH-d₄): δ = 8.67 (s, 3H), 8.10 (d, J = 15.45 Hz, 2H), 7.92 (d, J = 13.18 Hz, 3H), 7.83 (m, 2H), 7.55 (m, 3H), 7.55 (m, 1H), 6.69 (m, 1H), 3.81 (m, 5H), 3.70 (m, 6H), 3.61 (m, 6H), 3.48 (m, 2H), 3.41 (m, 2H), 3.35 (m, 6H), 3.27 (m, 6H), 3.18 (m, 2H), 3.04 (m, 12H), 2.99 (bs, 6H), 2.07 (s, 9H), 1.91 (s, 2H), 1.77 (s, 9H), 1.75 (s, 9H), 1.41 (s, 6H), 1.32 (m, 4H), 1.25 (m, 2H), 1.18 (m, 4H), 1.10 (m, 2H).

¹³C-NMR (176 MHz, DMSO-d₆+AcOH-d₄): δ = 187.02, 186.53, 176.37, 169.75, 169.32, 169.23, 165.84, 153.62, 153.49, 152.20, 148.15, 144.89, 140.92, 140.76, 139.15, 138.49, 136.76, 124.76, 118.82, 116.68, 111.14, 111.01, 106.71, 106.44, 49.87, 49.53, 49.02, 44.99, 44.78, 40.57, 39.52, 38.80, 38.68, 38.15, 35.87, 34.28, 28.70, 22.58, 22.53, 21.00, 13.89, 12.08, 12.05, 7.59.

DEPT (176 MHz, DMSO-d₆): δ = 187.03, 186.53, 176.37, 171.97, 169.75, 169.32, 169.23, 165.83, 165.09, 153.62, 153.55, 153.49, 152.18, 148.15, 144.83, 140.90, 140.76, 139.15, 136.75, 124.67, 118.84, 111.12, 110.94, 106.73, 106.47, 106.42, 49.53, 49.04, 44.99, 44.78, 40.57, 38.15, 35.87, 34.28, 28.70, 22.58, 22.53, 21.00, 13.89, 12.08, 12.05, 7.58.

HRMS (ESI) calculated for ([M+2H]²⁺): m/z = 915.8703; experimental = 915.8707.

Compound 15



Chemical Formula: C₄₆H₄₄FN₅O₁₂
 Exact Mass: 877,2971
 Molecular Weight: 877,8794

Acid **38** (4.2 mg, 0.018 mmol, 2.0 eq) was dissolved in anhydrous THF (500 μL) and anhydrous NMM (30 μL) was added under argon atmosphere at 0 °C. At this temperature *iso*-butyl chloroformate (3 μL, 0.018 mmol, 2.0 eq) was added and the reaction continued stirring at 0 °C for five minutes and for 30 minutes at 24 °C. Then amine **60** (5.8 mg, 0.009 mmol, 1.0 eq) was added in THF (500 μL) with NMM (30 μL) dropwise at 0 °C. The reaction stirred for 30 minutes at 24 °C was then concentrated to dryness. The residue was taken up in ACN and purified by

RP-HPLC (10-80% ACN/H₂O, 1% AcOH, 220 nm) and product containing fractions were lyophilized to yield amide **15** (4.9 mg, 0.006 mmol, 69%) as a beige powder.

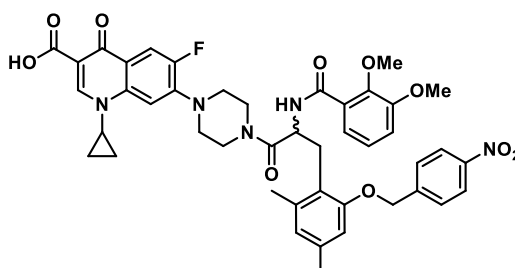
¹H-NMR (500 MHz, ACN-d₃): δ = 15.11 (s, 1H), 8.71 (s, 1H), 8.24 (d, J = 8.69 Hz, 2H), 7.94 (d, J = 13.11 Hz, 1H), 7.81 (d, J = 8-69 Hz, 2H), 7.56 (q, J = 2.69, 6.32 Hz, 1H), 7.51 (d, J = 7.90 Hz, 1H), 7.42 (d, J = 7.27 Hz, 1H), 7.35 (m, 2H), 6.69 (d, J = 21.49 Hz, 2H), 5.43 (q, J = 8.21, 15.48 Hz, 1H), 5.22 (d, J = 2.69 Hz, 2H), 3.66 (m, 3H), 3.49 (m, 1H), 3.18 (m, 6H), 2.57 (m, 1H), 2.31 (s, 3H), 2.27 (d, 6H), 2.20 (s, 3H), 1.39 (s, 2H), 1.33 (m, 2H), 1.27 (m, 1H), 1.13 (m, 1).

¹⁹F-NMR (471 MHz, ACN-d₃): δ = -123.29.

¹³C-NMR (176 MHz, ACN-d₃): δ = 178.29, 171.32, 169.57, 169.42, 167.52, 164.23, 158.06, 155.27, 149.32, 148.64, 146.24, 146.14, 144.29, 141.32, 140.57, 139.85, 138.75, 130.84, 129.31, 127.95, 127.73, 127.25, 126.46, 125.06, 124.63, 121.58, 112.52, 112.39, 111.38, 107.42, 69.88, 50.46, 50.22, 49.26, 46.02, 42.50, 36.74, 35.10, 31.11, 30.70, 21.51, 20.89, 20.82, 20.00, 8.73, 8.69.

HRMS (ESI) calculated for ([M+H]⁺): m/z = 878.3044; experimental = 878.3049.

Compound 16



Chemical Formula: C₄₄H₄₄FN₅O₁₀
 Exact Mass: 821,3072
 Molecular Weight: 821,8594

2,3-dimethoxy benzoic acid (3.3 mg, 0.018 mmol, 2.0 eq) was dissolved in anhydrous THF (500 μ L) and anhydrous NMM (30 μ L) was added under argon atmosphere at 0 °C. At this temperature *iso*-butyl chloroformate (1.8 μ L, 0.018 mmol, 2.0 eq) was added and the reaction continued stirring at 0 ° for five minutes and for 30 minutes at 24 °C. Then amine **60** (6.0 mg,

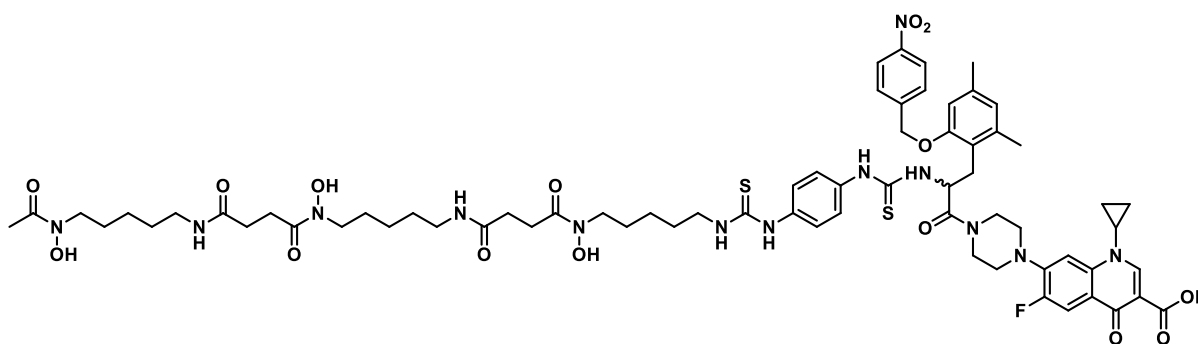
0.009 mmol, 1.0 eq) was added in THF (500 μ L) together with NMM (30 μ L) dropwise at 0 $^{\circ}$ C. The reaction stirred for 30 minutes at 24 $^{\circ}$ C was then concentrated to dryness. The residue was taken up in ACN and purified by RP-HPLC (10-80% ACN/H₂O, 0.1% HCOOH, 220 nm) and product containing fractions were lyophilized to yield amide **16** (6 mg, 0.007 mmol, 81%) as a white powder.

¹H-NMR (700 MHz, ACN-d₃): δ = 15.11 (s, 1H), 8.72 (s, 1H), 8.24 (m, 2H), 7.93 (m, 1H), 7.81 (m, 4H), 7.46 (d, J = 8.63 Hz, 1H), 7.41 (m, 3H), 6.69 (m, 2H), 5.88 (d, J = 8.63 Hz, 1H), 5.26 (m, 5H), 5.00 (m, 1H), 3.78 (s, 1H), 3.71 (m, 4H), 3.63 (m, 2H), 3.24 (m, 3H), 3.05 (m, 5H), 2.35 (s, 3H), 2.29 (s, 3H), 2.19 (s, 5H), 1.35 (m, 2H), 1.34 (m, 2H), 1.27 (m, 2H), 1.14 (m, 1H), 1.13 (m, 1H), 0.88 (m, 6H).

¹³C-NMR (176 MHz, MeOH-d₄): δ = 185.83, 179.59, 175.37, 173.27, 166.09, 161.99, 156.46, 154.67, 148.59, 147.62, 137.85, 137.18, 136.51, 133.61, 132.99, 132.90, 130.73, 125.13, 119.83, 77.90, 70.68, 65.50, 49.00, 45.34, 39.25, 30.50, 28.91, 17.11, 17.06.

HRMS (ESI) calculated for ([M+H]⁺): m/z = 822.3145; experimental = 822.3122.

Compound 17



Chemical Formula: C₆₈H₈₈FN₁₃O₁₅S₂
 Exact Mass: 1409,5948
 Molecular Weight: 1410,6464

Amine **60** (20.96 mg, 0.032 mmol, 1.2 eq) was dissolved in DMF (0.5 mL) and TEA (50 μ L) was added. The isothiocyanate **46** (20.0 mg, 0.027 mmol, 1.0 eq) was added and the reaction continued stirring at 24 $^{\circ}$ C. The base was removed by rotary evaporation, the residual solution was filtered and purified by RP-HPLC (C18, 10-90% ACN/H₂O, 0.1% HCOOH, 220 nm). The product containing fractions were identified by LCMS and lyophilized to yield pure title compound **17** as a beige solid (27.39 mg, 0.019 mmol, 73%).

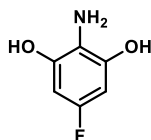
¹H-NMR (700 MHz, DMSO-d₆) δ 9.62 (m, 3H), 9.39 (m, 1H), 7.77 (m, 2H), 7.65 (m, 1H), 7.36 (m, 3H), 7.21 (m, 1H), 3.74 (m, 1H), 3.48 (m, 2H), 3.45 (t, J = 7.51 Hz, 6H), 2.99 (q, J = 7.05, 12.71 Hz, 4H), 2.57 (m, 4H), 2.26 (q, J = 6.59, 12.87 Hz, 4H), 1.96 (s, 3H), 1.54 (m, 4H), 1.49 (m, 4H), 1.38 (m, 4H), 1.26 (m, 2H), 1.21 (m, 5H), 1.01 (m, 6H).

¹³C-NMR (176 MHz, DMSO-d₆): δ = 186.47, 182.02, 181.84, 179.49, 176.37, 171.94, 171.27, 170.09, 168.77, 166.94, 165.92, 163.17, 162.07, 142.75, 142.73, 142.28, 131.95, 126.67, 123.91, 106.76, 82.16, 78.86, 47.11, 47.05, 46.75, 45.69, 43.72, 38.40, 38.38, 29.86, 28.79, 28.66, 28.19, 27.96, 27.54, 26.86, 26.10, 26.00, 23.57, 23.47, 21.64, 21.04, 20.33, 19.76, 12.70, 12.60, 11.03, 10.93, 7.59.

HRMS (ESI) calculated for ([M+H]⁺): m/z = 1410.6021; experimental = 1410.6022

RNAP inhibitor (RNAP-I) constructs

Rifamycin intermediates

Compound **61**Chemical Formula: C₆H₆FNO₂

Exact Mass: 143,0383

Molecular Weight: 143,1174

The title compound **61** was synthesized according to a patent by Bachmann et al.⁵ 1,3,5-trifluoro-2-nitrobenzene (from TCI, 5000 mg, 28.24 mmol, 1.0 eq) was dissolved in iPrOAc (150 mL). Then benzyl alcohol (3.23 ml, 31.06 mmol, 1.1 eq) was added in portions, dropwise over 30 minutes over dropping funnel as a yellow solution, after being mixed with KOtBu (4752.51 mg, 42.35 mmol, 1.5 eq) for 5 minutes in dry iPrOAc (20 mL). The reaction continued stirring at 0 °C for 2 hours. The solvent was removed *in vacuo* and the residue was washed with cold petrolether (bp 60-80°C, 5x 200 mL) over a glass frit to yield crude **61a** which was dried for one hour. The residue was dissolved in anhydrous MeOH/Toluene under argon atmosphere, Pd/C (50 mg, 0.2 eq) was added and the atmosphere was changed to hydrogen. The solution stirred overnight at 35 °C with three balloons. Removal of the solvent by rotary evaporation yielded resorcinol crude **61** as a beige solid, which was washed with ice-cold diethyl ether, petrolether and DCM (each 100 ml) before being dried under reduced pressure (1.9 g, 13.42 mmol, 48% over 2 steps).

61a:

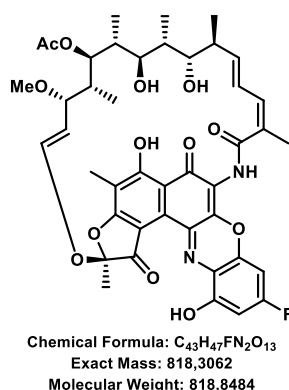
¹H-NMR (500 MHz, CDCl₃): δ = 7.37 (m, 10H), 6.39-6.37 (d, J = 10.42 Hz, 2H), 5.12 (s, 2H).

61:

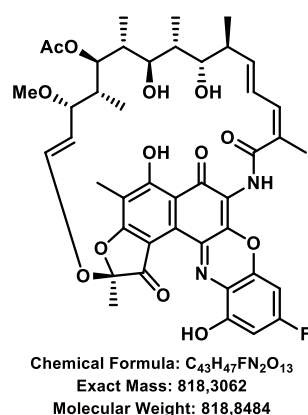
¹H-NMR (500 MHz, CDCl₃): δ = 6.08-6.06 (d, J = 9.73 Hz), 3.46 (bs, 2H).

¹³C-NMR (126 MHz, CDCl₃): δ = 158.08, 156.21, 147.05, 146.95, 117.33, 94.76, 94.56, 49.74, 49.57, 49.40, 49.23, 49.06, 48.89, 48.72.

HRMS (ESI) calculated for ([M+H]⁺): m/z = 144.0456; experimental = 144.0459.

Compound **2** with benzoquinone (BQ)/oxygen as oxidant

The title compound **2** was synthesized according to a patent by Bachmann et al.⁵ **61** (1.0 g, 1.44 mmol, 4.0 eq – 1 eq per cycle, 4 cycles total) and rifamycin S **1** (from TCI, 822.81 mg, 5.75 mmol, 4 eq) were weighed in a glass reactor and dissolved in 25 mL iPrOAc (25 mL) under Argon conditions. The brown-reddish solution continued stirring at ambient temperature for 2 hours and developed a blood red color. Then the solution was cooled to 0 °C and the oxidant benzoquinone (621.45 mg, 5.75 mmol, 4 eq – 1 eq per cycle, 4 cycles in total) was added in iPrOAc (2 mL) over 10 minutes. Then the reaction continued stirring at 25 °C for 1 hour. The addition procedure was repeated till all fluoride **61** and benzoquinone had been added and the reaction continued stirring overnight at 25 °C for 48 h. The reaction was washed with 10% sodium ascorbate (w/v, 200 mL), and water (2x200 mL). The organic phase was dried over Na₂SO₄ and the solvent was removed by rotary evaporation. The residue was purified by SGC (PE - PE/EA 20%, UV-Vis, 24 g silica column) and product containing fractions were identified by TLC (DCM)/LCMS and combined. Then the solvent was removed by rotary evaporation to yield fluoro rifamycin S **2** (252.0 mg, 0.31 mmol, 21%) as a blood red solid.

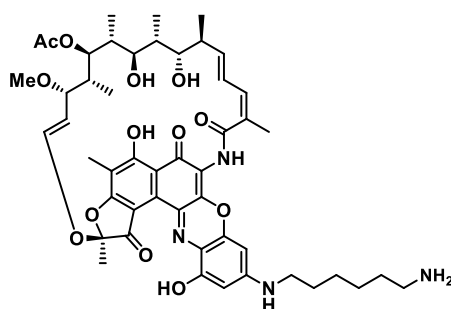
Compound **2** with TEMPO/oxygen as oxidant

The title compound **2** was synthesized according to a patent by Bachmann et al.⁵ **61** (1.0 g, 1.44 mmol, 4.0 eq – 1 eq per cycle, 4 cycles total) and rifamycin S **1** (TCI, 822.81 mg, 5.75 mmol, 4 eq) were weighed in a glass reactor and dissolved in 25 mL iPrOAc (25 mL) under Argon conditions. The brown-reddish solution continued stirring at ambient temperature for 2 hours and developed a blood red color. Then the solution was cooled to 0 °C and the oxidant TEMPO (1122.87 mg, 7.19 mmol, 5 eq – 1.25 eq per cycle, 4 cycles in total) was added in iPrOAc (2 mL) over 10 minutes while the atmosphere was changed to oxygen. Then the reaction continued stirring at 25 °C for 1 hour. Then the flask was charged with argon and the addition procedure was repeated till all fluoride **61** and TEMPO had been added. The reaction continued stirring overnight at 25 °C for 48 h. The reaction was washed with 10% sodium ascorbate (w/v, 200 mL), and water (2x200 mL). The organic phase was dried over Na₂SO₄ and the solvent was removed by rotary evaporation. The residue was purified by SGC (PE - PE/EA 20%, UV-Vis, 24 g silica column) and product containing fractions were identified by TLC (DCM)/LCMS and combined. Then the solvent was removed by rotary evaporation to yield pure **2** (589.5 mg, 0.72 mmol, 50%) as a blood red solid.

¹H-NMR (700 MHz, CD₂Cl₂): δ = 14.35 (s, 1H), 10.23 (s, 1H), 7.47 (bs, 1H), 6.76 (dd, J = 3.22, 10.40 Hz), 6.66 (dd, J = 2.23, 9.29 Hz, 1H), 6.11 (m, 1H), 5.98 (m, 1H), 5.04 (m, 1H), 4.99 (q, J = 8.30, 12.14 Hz, 1H), 3.07 (s, 4H), 2.99 (m, 1H), 2.32 (s, 3H), 2.10 (s, 4H), 2.02 (s, 3H), 1.78 (s, 3H), 1.69 (q, J = 8.13, 13.97 Hz, 1H), 1.55 (bs, 22H), 1.41 (m, 2H), 1.36 (m, 1H), 1.30 (m, 1H), 0.91 (bs, 3H), 0.76 (bs, 3H), 0.53 (bs, 3H).

¹³C-NMR (176 MHz, CD₂Cl₂): δ = 194.38, 184.63, 174.60, 172.52, 169.12, 168.58, 167.12, 158.14, 158.05, 145.25, 143.43, 142.26, 142.10, 140.93, 131.74, 126.63, 120.47, 113.75, 107.89, 100.13, 99.98, 95.46, 95.29, 73.96, 41.63, 37.30, 32.97, 22.61, 21.27, 21.00, 18.81, 17.69, 11.08, 8.09.

HRMS (ESI) calculated for ([M+H]⁺): m/z = 819.3135; experimental = 819.3135.

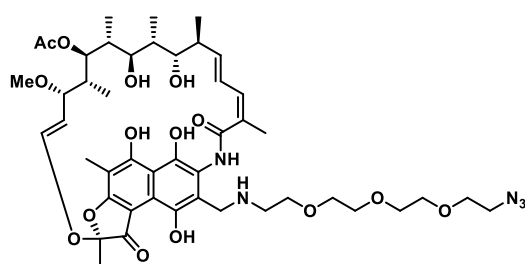
Compound **22**

Chemical Formula: C₄₉H₆₂N₄O₁₃
 Exact Mass: 914,4313
 Molecular Weight: 915,0500

Fluoride **2** (50 mg, 0.061 mmol, 1.0 eq) was dissolved in anhydrous THF (1 mL) under argon conditions. Then N-fmoc 1,6-diaminohexan (22.7 mg, 0.067 mmol, 1.1 eq) and TEA (100 μ L) were added. The reaction continued stirring overnight and a color change from red to blue, as well as a partial cleavage of the fmoc group was observed. The reaction was concentrated to dryness and then ACN (800 μ L) and diethylamine (200 μ L) were added. The reaction continued stirring for one hour at ambient temperature before the solvent was removed and the residue was washed with diethyl ether (3x50 mL, ice-cold, 4000 g, 5 min, 0 $^{\circ}$ C) and dried overnight under reduced pressure to yield **22** as crude, blue solid (51,42 mg, 0.056 mmol, 92%).

¹H-NMR (700 MHz, MeOH-d₄): δ = 6.84 (m, 1H), 6.40 (m, 2H), 6.23 (m, 3H), 5.02 (m, 2H), 3.69 (d, J = 8.61 Hz, 1H), 3.59 (m, 3H), 3.19 (m, 3H), 3.11 (m, 1H), 2.99 (m, 5H), 2.29 (m, 4H), 2.10 (m, 4H), 1.97 (m, 4H), 1.78 (m, 4H), 1.61 (m, 1H), 1.29 (m, 3H), 0.93 (m, 10H), 0.78 (m, 2H), 0.69 (m, 1H), 0.04 (d, J = 7.13 Hz, 3H), -0.30 (d, J = 7.87 Hz, 3H).

HRMS (ESI) calculated for ([M+H]⁺): m/z = 915.4386; experimental = 915.4392.

Compound **62**

Chemical Formula: C₄₆H₆₅N₅O₁₅
 Exact Mass: 927,4477
 Molecular Weight: 928,0460

3-formyl rifamycin SV **27** (abcam: ab143401, 50.0 mg, 0.069 mmol, 1.0 eq) was dissolved in anhydrous THF (15 mL) under argon atmosphere. Then the N₃-PEG-NH₂ (16.5 mg, 0.076 mmol, 1.1 eq) in THF (5 mL) and TEA (50 μL) was added. The solvent was removed *in vacuo* and the residue was taken up in DCM (100 mL). The organic phase was washed with 1 M HCl (2x100 mL), water (1x100 mL), brine (1x50 mL) and dried over Na₂SO₄. The solvent was removed by rotary evaporation and dried under reduced pressure. The residue was dissolved in anhydrous THF (20 mL) under argon atmosphere, cooled to 0 °C before NaBH(OAc)₃ (21.9 mg, 0.103 mmol, 2.0 eq) was added. The reaction continued stirring overnight at 23 °C, was then concentrated to dryness and taken up in DCM (100 mL). The organic phase was washed water (1x100 mL), brine (1x50 mL) and dried over Na₂SO₄. The solvent was removed by rotary evaporation and dried under reduced pressure to yield the amine **62** (62.4 mg, 0.067 mmol, 98% crude).

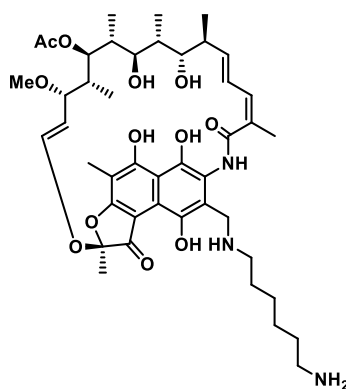
27 (3-formyl rifamycin SV)

¹H-NMR (700 MHz, CD₂Cl₂): δ = 13.11 (s, 1H), 12.64 (s, 1H), 12.26 (s, 1H), 10.61 (s, 1H), 6.48 (m, 2H), 6.23 (d, J = 12.80 Hz, 1H), 6.03 (m, 1H), 5.11 (q, J = 6.77, 12.80 Hz, 1H), 4.91 (d, J = 10.59 Hz, 1H), 3.75 (d, J = 9.85 Hz, 1H), 3.51 (d, J = 6.91 Hz, 1H), 3.02 (m, 4H), 2.37 (m, 1H), 2.25 (s, 3H), 2.08 (s, 3H), 2.05 (m, 4H), 1.81 (s, 3H), 1.77 (m, 1H), 1.51 (m, 1H), 1.35 (m, 1H), 1.00 (d, J = 7.21 Hz, 3H), 0.88 (d, J = 6.77 Hz, 3H), 0.66 (d, J = 6.77 Hz, 3H), -0.33 (d, J = 7.21 Hz, 3H).

62

¹H-NMR (700 MHz, CD₂Cl₂): δ = 8.75 (s, 1H), 6.61 (q, J = 11.16 Hz, 1H), 6.33 (d, J = 10.80 Hz, 1H), 6.15 (d, J = 12.57 Hz, 1H), 6.02 (dd, J = 5.16, 15.96 Hz, 1H), 5.13 (dd, J = 6.13, 12.09 Hz, 1H), 4.98 (d, J = 10.64 Hz, 1H), 3.86 (m, 1H), 3.75 (m, 4H), 3.63 (m, 8H), 3.61 (m, 4H), 3.59 (m, 4H), 3.50 (m, 1H), 3.41 (t, J = 5.07 Hz, 2H), 3.35 (t, J = 4.98 Hz, 2H), 3.05 (s, 3H), 3.02 (m, 2H), 2.33 (m, 1H), 2.14 (s, 3H), 2.11 (s, 3H), 2.03 (s, 3H), 2.01 (m, 1H), 1.77 (s, 3H), 1.74 (m, 1H), 1.56 (m, 1H), 1.49 (m, 1H), 1.00 (d, J = 7.12 Hz, 3H), 0.84 (d, J = 7.12 Hz, 3H), 0.62 (d, J = 6.94 Hz, 3H), -0.14 (d, J = 7.03 Hz, 3H).

Compound 28



Chemical Formula: C₄₄H₆₃N₃O₁₂
 Exact Mass: 825,4412
 Molecular Weight: 825,9970

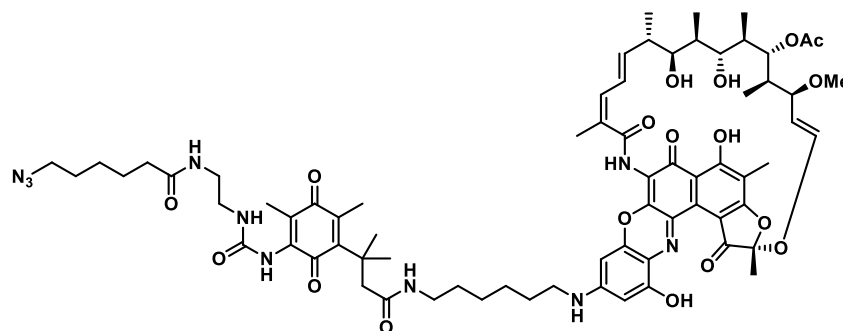
3-formyl rifamycin SV **27** (abcam: ab143401, 100 mg, 0.138 mmol, 1.0 eq) was dissolved in anhydrous THF (15 mL) under argon atmosphere. Then the N-fmoc-1,6-diaminohexane (93.3 mg, 0.276 mmol, 2.0 eq) in THF (5 mL) and TEA (50 μL) was added. The solvent was removed *in vacuo* and the residue was taken up in DCM (100 mL). The organic phase was washed with 1 M HCl (2x100 mL), water (1x100 mL), brine (1x50 mL) and dried over Na₂SO₄. The solvent was removed by rotary evaporation and dried under reduced pressure. The residue was dissolved in anhydrous THF (20 mL) under argon atmosphere, cooled to 0 °C before NaBH(OAc)₃ (58.4 mg, 0.276 mmol, 2.0 eq) was added. The reaction continued stirring overnight at 23 °C, was then concentrated to dryness and taken up in DCM (100 mL). The organic phase was washed water (1x100 mL), brine (1x50 mL) and dried over Na₂SO₄. The solvent was removed by rotary evaporation and dried under reduced pressure to yield **28a**. The residue was dissolved in ACN (16 mL) and diethylamine (4 mL) were added. The solution continued stirring at 23 °C for 45 minutes and was then evaporated by rotary evaporation. The residue was washed with ice-cold petrol ether and diethyl-ether (-20 °C), further drying under reduced pressure gave crude title compound **28** (76.1 mg, 0.092 mmol, 67% over three steps) as a red solid.

¹H-NMR (700 MHz, DMSO-d₆): δ = 7.89 (m, 2H), 7.67 (m, 2H), 7.40 (m, 2H), 7.32 (m, 2H), 4.29 (m, 2H), 4.20 (m, 1H), 3.60 (t, J = 6.14 Hz, 3H), 2.94 (m, 6H), 2.18 (s, 1H), 2.00 (m, 4H), 1.90 (m, 4H), 1.76 (n, 3H), 1.65 (m, 1H), 1.58 (m, 2H), 1.38 (m, 7H), 1.24 (m, 6H), 0.91 (m, 1H), 0.82 (m, 4H).

¹³C-NMR (176 MHz, DMSO-d₆): δ = 172.45, 156.53, 151.93, 144.39, 141.20, 139.65, 128.49, 128.05, 127.48, 125.57, 125.37, 120.58, 67.48, 65.58, 47.25, 40.52, 40.48, 34.85, 30.89, 25.59, 21.53, 21.50.

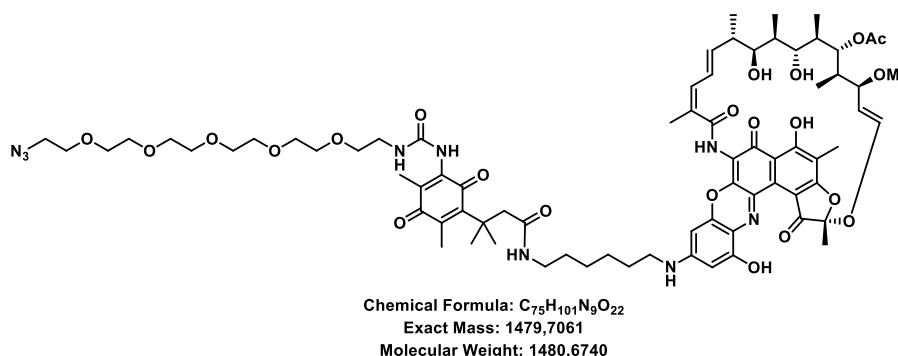
HRMS (ESI) calculated for ([M+H]⁺): m/z = 826.4485; experimental = 826.4433.

Compound **63**

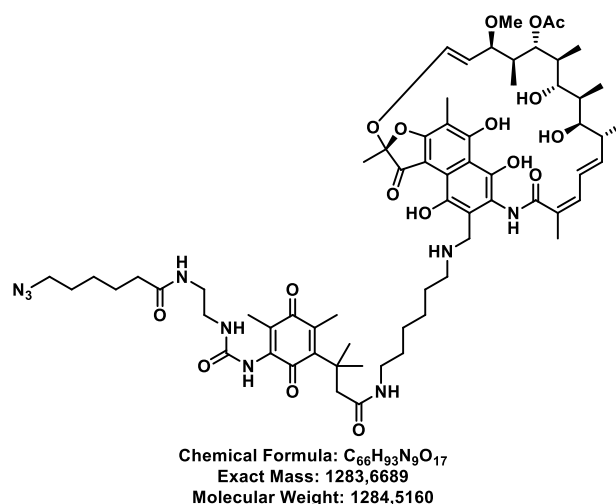


Chemical Formula: C₇₁H₉₂N₁₀O₁₈
 Exact Mass: 1372,6591
 Molecular Weight: 1373,5690

Acid **53** (6 mg, 0.013 mmol, 1.0 eq) was dissolved under argon atmosphere in anhydrous THF (1 mL) and NMM (20 μL) was added. The reaction was cooled to 0 °C and iso-butyl chloroformate (1.22 μL, 0.013 mmol, 1.0 eq) was added. The reaction continued to stir for one hour at 0 °C while the color of the solution changed from yellow to orange. Then the reaction stirred for 15 min at 23 °C, before the amine **22** (11.52 mg, 0.013 mmol, 1.0 eq) diluted in THF (1 mL) and basified with NMM (20 μL) was added at 0 °C. The ice-bath was left to thaw overnight. The solvent was removed by rotary evaporation, the residue diluted with DCM (100 mL) and washed with 1M HCl (3x50 mL), brine (1x50 mL) and dried over Na₂SO₄. The solvent was removed *in vacuo* and residue was dried under reduced pressure to yield crude **63** as a blue solid (6.8 mg, 0.005 mmol, 39%).

Compound **XX64**

Acid **56** (13 mg, 0.029 mmol, 1.0 eq) was dissolved under argon atmosphere in anhydrous THF (1 mL) and NMM (20 μ L) was added. The reaction was cooled to 0 $^{\circ}$ C and iso-butyl chloroformate (2.79 μ L, 0.029 mmol, 1.0 eq) was added. The reaction continued to stir for one hour at 0 $^{\circ}$ C while the color of the solution changed from yellow to orange. Then the reaction stirred for 15 min at 23 $^{\circ}$ C, before the amine **22** (26.3 mg, 0.029 mmol, 1.0 eq) diluted in THF (1 mL) and basified with NMM (20 μ L) was added at 0 $^{\circ}$ C. The ice-bath was left to thaw overnight. The solvent was removed by rotary evaporation, the residue diluted with DCM (100 mL) and washed with 1M HCl (3x50 mL), brine (1x50 mL) and dried over Na_2SO_4 . The solvent was removed *in vacuo* and residue was dried under reduced pressure to yield crude **64** as a blue solid (19.29 mg, 0.013 mmol, 45%).

Compound **65**EDCI/HOBt procedure

Acid **53** (10 mg, 0.021 mmol, 1.0 eq) was dissolved in DCM/DMF (10:1 - 15 mL) and EDCI*HCl (6.52 mg, 0.042 mmol, 2.0 eq), HOBt (5.67 mg, 0.042 mmol, 2.0 eq) and DMAP (1.28 mg, 0.01 mmol, 0.5 eq) were added at 0 $^{\circ}$ C. The mixture stirred 20 minutes at that temperature and

equilibrated to room temperature over 20 minutes. Then the amine **28** (20.81 mg, 0.013 mmol, 1.2 eq) and TEA (30 μ L) were added, dissolved in DCM/DMF (5 mL) at 0 °C, and the ice bath was removed and the reaction continued stirring at ambient temperature for 18 hours. The solvent was removed by rotary evaporation and the residue was purified by RP-HPLC (15%-100% ACN/H₂O, 220 nm, collect all). The product containing fractions were combined and lyophilized to dryness yielding **65** as an orange solid (12.3 mg, 0.01 mmol, 38%).

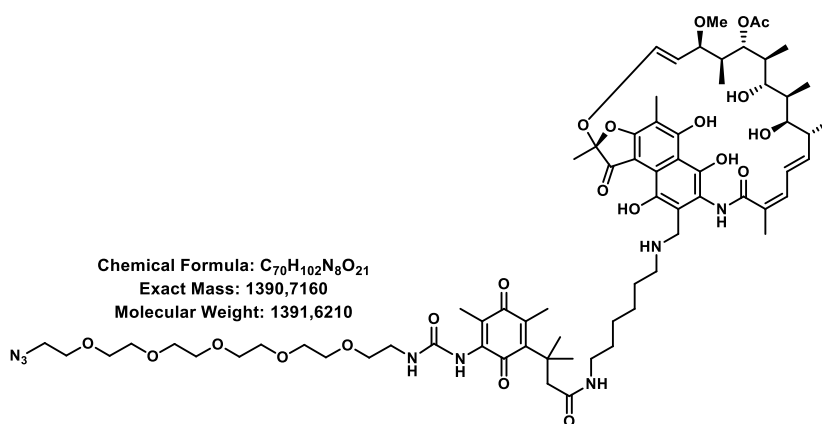
Mixed anhydride procedure

Compound **65** could also be afforded by mixed anhydride coupling, with the same reaction conditions to the procedure of compound **66** below, with nearly the double yield (23.6 mg, 0.02, 73%).

¹H-NMR (700 MHz, DMSO-d₆): δ = 12.77 (s, 1H), 9.30 (bs, 1H), 7.72 (m, 1H), 6.69 (d, 1H), 6.62 (m, 1H), 6.33 (d, J = 10.91 Hz, 1H), 6.24 (d, J = 11.31 Hz, 1H), 6.08 (q, 1H), 5.09 (d, J = 14.66 Hz, 1H), 5.04 (d, J = 3.91 Hz, 1H), 4.90 (q, J = 8.51, 12.89 Hz, 1H), 3.99 (d, J = 8.98 Hz, 1H), 3.68 (m, 2H), 3.29 (m, 5H), 3.24 (d, J = 8.58 Hz, 1H), 3.07 (m, 1H), 2.96 (m, 6H), 2.88 (s, 3H), 2.82 (t, J = 9.81 Hz, 2.29 (m, 1H), 2.03 (m, 6H), 1.97 (m, 7H), 1.91 (s, 3H), 1.77 (s, 1H), 1.69 (m, 2H), 1.64 (s, 3H), 1.50 (m, 8H), 1.34 (m, 5H), 1.27 (m, 8H), 1.22 (m, 6H), 0.99 (m, 2H), 0.92 (d, J = 7.10 Hz, 3H), 0.86 (d, J = 6.95 Hz, 3H), 0.50 (d, J = 6.45 Hz, 3H), -0.33 (d, J = 6.45 Hz, 3H).

DEPT (176 MHz, DMSO-d₆) δ = 142.82, 138.88, 131.31, 128.80, 126.32, 125.66, 117.35, 114.38, 76.05, 75.51, 72.92, 72.63, 55.38, 50.29, 50.26, 39.52, 37.97, 37.84, 37.59, 34.98, 32.40, 31.19, 28.64, 27.75, 25.70, 25.55, 25.31, 24.58, 24.48, 21.81, 20.40, 19.60, 17.95, 10.92, 8.71, 8.53, 7.09.

HRMS (ESI) calculated for ([M+2H]²⁺): m/z = 642.8417 experimental = 642.8423.

Compound **66**

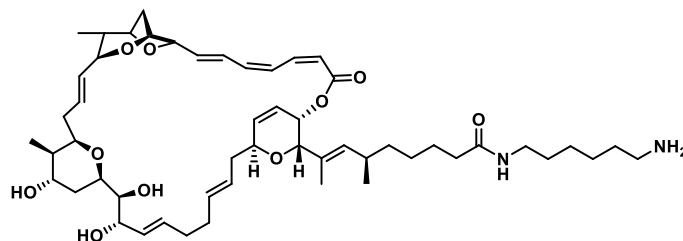
Acid **56** (8 mg, 0.014 mmol, 1.0 eq) was dissolved under argon atmosphere in anhydrous THF (500 μ L) and NMM (15 μ L) was added. The reaction was cooled to 0 $^{\circ}$ C and *iso*-butyl chloroformate (1.87 mg, 0.015 mmol, 1.0 eq) was added. The reaction continued to stir for one hour at 0 $^{\circ}$ C while the color of the solution changed from yellow to orange. Then the reaction stirred for 15 min at 23 $^{\circ}$ C, before amine **28** (22.6 mg, 0.027 mmol, 2.0 eq), diluted in THF (500 μ L) and basified with NMM (15 μ L), was added at 0 $^{\circ}$ C. The ice-bath was left to thaw overnight. The solvent was removed by rotary evaporation and purified by RP-HPLC (10-100% ACN/H₂O, 0.1% HCOOH, 220 nm). The product containing fractions were lyophilized to yield the title compound **66** (13.9 mg, 0.01 mmol, 73%) as a yellow-orange solid.

¹H-NMR (700 MHz, CD₂Cl₂): δ = 8.08 (bs, 1H), 6.54 (q, J = 9.77, 15.52 Hz, 1H), 6.34 (d, J = 10.92 Hz, 1H), 6.23 (dd, J = 7.33, 15.66 Hz, 1H), 6.14 (d, J = 12.79 Hz, 1H), 5.06 (q, J = 6.32, 12.79 Hz, 1H), 4.93 (d, J = 10.06 Hz, 1H), 4.38 (d, J = 13.07 Hz, 1H), 3.62 (m, 18H), 3.44 (m, 2H), 3.38 (m, 4H), 3.28 (bs, 1H), 3.08 (m, 9H), 2.62 (m, 2H), 2.38 (m, 1H), 2.15 (m, 4H), 2.07 (s, 3H), 2.02 (s, 6H), 1.88 (m, 3H), 1.76 (m, 1H), 1.68 (m, 6H), 1.47 (d, J = 11.64 Hz, 8H), 1.42 (s, 6H), 1.29 (m, 10H), 1.19 (m, 2H), 1.01 (d, J = 7.04 Hz, 3H), 0.88 (d, J = 6.03 Hz, 3H), 0.60 (d, J = 7.61 Hz, 3H), -0.19 (d, J = 6.18 Hz, 3H).

¹³C-NMR (176 MHz, CD₂Cl₂): δ = 205.59, 204.73, 204.66, 202.52, 194.46, 193.79, 187.92, 187.72, 187.17, 173.44, 172.69, 172.30, 172.27, 143.42, 138.49, 127.14, 125.42, 125.15, 109.21, 78.58, 77.36, 74.60, 71.07, 70.96, 70.88, 70.79, 70.74, 70.70, 70.60, 70.54, 70.39, 70.38, 57.24, 54.00, 51.80, 51.33, 51.28, 49.75, 47.64, 39.77, 39.16, 38.81, 38.22, 38.00, 34.00, 32.50, 30.59, 30.26, 29.93, 29.60, 29.51, 21.95, 21.19, 20.52, 18.27, 18.21, 14.83, 14.44, 11.22, 9.57, 9.14, 7.37

HRMS (ESI) calculated for ([M+2H]²⁺): m/z = 696.3653; experimental = 696.3651.

Sorangicin A intermediates

Compound **32**

Chemical Formula: $C_{53}H_{80}N_2O_{10}$
 Exact Mass: 904,5813
 Molecular Weight: 905,2270

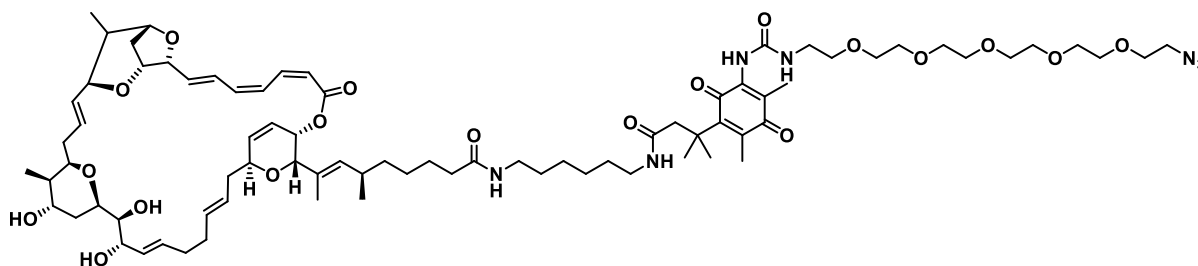
Sorangicin A **31** (50 mg, 0.062 mmol, 1.0 eq) was dissolved in anhydrous DCM/DMF (6 mL 1:10) and HATU (47.12 mg, 0.124 mmol, 2.0 eq) was added. The suspension was stirred at 23 °C for 10 minutes, before the N-fmoc 1,6-diaminohexane (41.84 mg, 0.124 mmol 2.0 eq) and DIPEA (50 μ L) were added. The suspension cleared visibly and the reaction continued stirring 2 hours at 23 °C. Upon completion, the solvent was removed by rotary evaporation. The residue was dissolved in ACN (8 mL) and diethylamine (2 mL) was added. The solution was stirred at 23 °C for 1 hour and then the solvent was removed *in vacuo*. The residue was taken up in ACN (4 mL), purified by RP-HPLC (5-85% ACN/H₂O, 220 nm, collect all) and product containing fractions were lyophilized yielding **32** as a beige solid (38.5 mg, 0.044 mmol, 56%).

¹H-NMR (700 MHz, DMSO-d₆) δ = 7.68 (t, J = 5.12 Hz, 1H), 7.58 (bs, 3H), 7.11 (t, J = 11.88 Hz, 1H), 7.03 (t, J = 11.40 Hz, 1H), 6.92 (t, J = 13.42 Hz, 1H), 6.47 (t, J = 11.40 Hz, 1H), 6.22 (dd, J = 3.67, 15.07 Hz, 1H), 6.14 (dd, J = 3.09, 9.57 Hz, 1H), 5.96 (m, 1H), 5.62 (d, J = 10.91 Hz, 1H), 5.53 (m, 3H), 5.45 (q, J = 4.73, 8.79 Hz, 2H), 5.30 (m, 5H), 5.22 (d, J = 8.31 Hz, 2H), 4.56 (m, 1H), 4.49 (m, 1H), 4.44 (m, 2H), 4.38 (m, 1H), 4.34 (m, 1H), 4.18 (m, 2H), 3.94 (t, J = 5.12 Hz, 1H), 3.73 (t, J = 7.24 Hz, 1H), 3.68 (m, 1H), 3.63 (t, J = 8.31 Hz, 1H), 3.53 (m, 1H), 3.29 (m, 1H), 3.01 (m, 2H), 2.76 (m, 2H), 2.28 (m, 3H), 2.09 (m, 6H), 2.00 (m, 6H), 1.80 (d, J = 10.82 Hz, 1H), 1.54 (s, 3H), 1.50 (m, 4H), 1.43 (m, 3H), 1.36 (m, 4H), 1.27 (m, 6H), 1.13 (m, 4H), 0.78 (d, J = 6.18, 3H), 0.76 (d, J = 7.24 Hz, 3H), 0.71 (d, J = 6.18 Hz, 3H).

$^{13}\text{C-NMR}$ (176 MHz, DMSO- d_6): δ = 172.11, 165.20, 137.63, 136.82, 135.85, 135.00, 132.22, 132.08, 131.87, 130.54, 130.32, 130.20, 129.55, 126.68, 125.39, 124.58, 122.36, 118.38, 80.01, 78.85, 78.44, 76.27, 75.13, 72.97, 72.72, 72.46, 72.14, 71.70, 68.44, 64.73, 40.12, 40.02, 38.81, 38.72, 38.50, 38.22, 36.82, 36.76, 35.66, 35.58, 33.69, 32.57, 32.11, 31.23, 31.09, 29.73, 28.99, 26.94, 26.89, 26.58, 25.86, 25.44, 25.37, 21.62, 20.79, 14.77, 14.17, 13.59, 13.48, 10.26, 10.00.

HRMS (ESI) calculated for $([\text{M}+\text{H}]^+)$: m/z = 905.5886; experimental = 905.5855.

Compound **67**



Chemical Formula: $\text{C}_{79}\text{H}_{119}\text{N}_7\text{O}_{19}$
 Exact Mass: 1469,8561
 Molecular Weight: 1470,8510

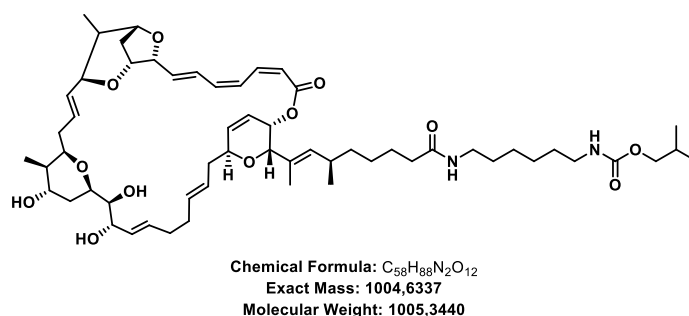
Acid **56** (10 mg, 0.017 mmol, 1.0 eq) was dissolved in dry THF (500 μL) under argon atmosphere, NMM (30 μL) was added and the flask was cooled to 0 $^{\circ}\text{C}$. Then *iso*-butylchloroformate (1.66 μL , 0.017 mmol, 1.0 eq) was added at 0 $^{\circ}\text{C}$ and the reaction continued stirring at that temperature for one hour. The color changed from yellow to orange and the amine **32** (23.3 mg, 0.026 mmol, 1.5 eq) was added in THF (500 μL) with NMM (30 μL) at 0 $^{\circ}\text{C}$. The reaction continued stirring overnight, while the thawing ice bath equilibrated the reaction steadily to ambient temperature. The next morning the solvent was removed and the reaction was purified by RP-HPLC (10-100% ACN/ H_2O , 0.1% HCOOH, 220 nm). Product containing fractions were identified and lyophilized to yield **67** (21.1 mg, 0.14 mmol, 84%) as a slight yellow powder.

¹H-NMR (700 MHz, CD₂Cl₂): δ = 7.13 (t, J = 11.57 Hz, 1H), 7.05 (t, J = 12.82 Hz, 1 H), 6.97 (t, J = 13.45 Hz, 1H), 6.63 (m, 1H), 6.43 (t, J = 10.94 Hz, 1H), 6.24 (m, 1H), 6.06 (m, 3H), 5.73 (m, 1H), 5.57 (m, 2H), 5.53 (m 2H), 5.45 (m, 1H), 5.35 (m, 1H), 4.51 (s, 1H), 4.39 (m, 1H), 4.35 (m, 1H), 4.24 (m, 2H), 4.10 (s, 1H), 3.88 (m, 2H), 3.82 (m, 2H), 3.78 (t, J = 10.01 Hz, 1H), 3.70 (m, 1H), 3.63 (m, 22H), 3.55 (t, J = , 5.63 Hz, 2H), 3.37 (t, J = 5.32 Hz, 4H), 3.10 (m, 4H), 3.04 (m, 1H), 2.60 (dd, J = 12.51, 54.10 Hz, 2H), 2.36 (m, 2H), 2.25 (m, 1H), 2.18 (m, 2H), 2.13 (s, 3H), 2.10 (m, 6H), 1.96 (m, 1H), 1.89 (s, 3H), 1.79 (m, 1H), 1.74 (m, 1H), 1.67 (m, 2H), 1.58 (m, 5H), 1.48 (s, 6H), 1.39 (m, 2H), 1.32 (m, 4H), 1.26 (s, 2H), 1.19 (m, 7H), 0.94 (d, J = 6.74 Hz, 2H), 0.90 (t, J = 6.74, 2H), 0.85 (d, J = 7.41 Hz, 3H), 0.81 (d, J = 6.41 Hz, 3H), 0.77 (d, J = 6.30 Hz, 3H).

¹³C-NMR (176 MHz, CD₂Cl₂): δ = 187.09, 174.46, 166.47, 137.85, 137.13, 136.23, 134.96, 133.90, 132.91, 132.79, 132.22, 131.68, 129.42, 129.17, 127.73, 127.12, 126.08, 123.50, 119.33, 81.00, 80.15, 80.06, 76.65, 76.61, 74.91, 74.54, 74.39, 74.35, 73.83, 73.12, 71.10, 71.07, 71.04, 70.97, 70.92, 70.79, 70.67, 70.59, 70.43, 64.77, 54.00, 51.34, 49.81, 41.35, 40.65, 39.75, 39.53, 39.14, 38.28, 37.52, 37.11, 36.33, 34.66, 33.56, 33.09, 32.56, 31.46, 30.32, 30.28, 29.84, 29.80, 28.39, 27.98, 26.64, 26.56, 26.45, 21.79, 19.36, 19.21, 15.32, 14.79, 14.35, 11.72, 10.89.

HRMS (ESI) calculated for ([M+2H]²⁺): m/z =735.9353; experimental = 735.9352.

Compound 68



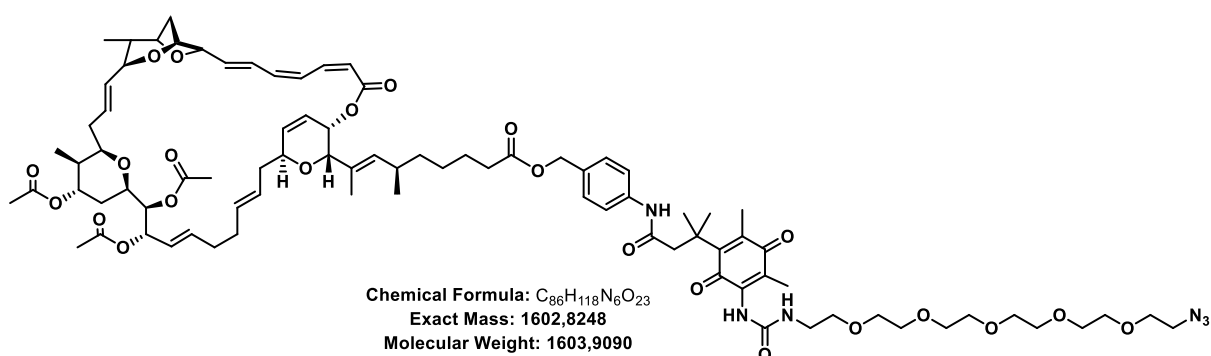
The compound **68** (4.05 mg, 0.004 mmol, 24%) was obtained as a side product during the synthesis of **32**.

¹H-NMR (700 MHz, CD₂Cl₂): δ = 7.13 (t, J = 11.98 Hz, 1H), 7.05 (t, J = 12.11 Hz, 1H), 6.97 (m, 1H), 6.43 (t, J = 10.94 Hz, 1H), 6.22 (dd, J = 4.17, 15.37 Hz, 1H), 6.05 (m, 2H), 5.74 (m, 2H), 5.58 (dt, J = 1.56, 11.59 Hz, 1H), 5.53 (m, 3H), 5.45 (m, 1H), 5.34 (m, 2H), 5.29 (dt, J = 2.21, 9.77, 1H), 4.51 (m, 1H), 4.39 (m, 1H), 4.35 (q, J = 2.21 Hz, 1H), 4.25 (d, J = 5.99 Hz, 1H), 4.19 (q, J = 5.21, 10.61 Hz, 1H), 4.11 (s, 1H), 3.89 (m, 1H), 3.84 (m, 1H), 3.78 (m, 2H), 3.70 (m, 1H), 3.59 (m, 1H), 3.48 (q, J = 5.99, 11.72 Hz, 1H), 3.17 (q, J = 6.77, 12.54 Hz, 2H), 3.12 (q, J = 6.38, 13.15 Hz, 2H), 2.68 (m, 2H), 2.33 (m, 2H), 2.25 (m, 1H), 2.11 (m, 14H), 1.98 (m, 1H), 1.88 (m, 2H), 1.79 (m, 1H), 1.69 (m, 1H), 1.59 (s, 1H), 1.56 (m, 9H), 1.47 (q, J = 7.16, 13.54 Hz, 4H), 1.32 (m, 8H), 1.18 (m, 2H), 0.91 (d, J = 6.77 Hz, 6H), 0.85 (d, J = 6.77 Hz, 3H), 0.81 (d, J = 6.38 Hz, 3H), 0.77. (d, J = 6.38 Hz, 3H).

¹³C-NMR (176 MHz, CD₂Cl₂): δ = 206.95, 174.20, 166.45, 157.37, 137.85, 137.12, 136.20, 134.89, 133.86, 133.04, 132.77, 132.18, 131.78, 129.54, 129.23, 127.76, 127.05, 126.04, 123.48, 119.31, 81.03, 80.14, 80.02, 76.62, 76.46, 74.92, 74.63, 74.39, 73.90, 73.21, 71.30, 70.56, 64.92, 41.36, 41.11, 39.67, 39.54, 38.15, 37.60, 37.16, 36.33, 34.70, 33.46, 33.04, 32.45, 31.30, 31.16, 30.40, 29.89, 28.65, 27.87, 26.68, 26.54, 26.38, 21.67, 19.36, 15.31, 14.70, 10.87.

HRMS (ESI) calculated for ([M+H]⁺): m/z = 1005.6410; experimental = 1005.6415.

Compound 69



Sorangicin A **31** (20 mg, 0.025 mmol, 1.0 eq) was dissolved in anhydrous THF (5 mL) and pyridine (5 mL) and acetic anhydride (25.30 mg, 0.248 mmol, 10.0 eq) were added at 0 °C. Then the reaction continued stirring for 4 hours at 24 °C. The solvent was removed *in vacuo* and the residue dried under reduced pressure for two hours, before anhydrous THF (2.5 mL) and NMM (100 μL) were added under argon atmosphere. The reaction was cooled to 0 °C and then *iso*-butyl chloroformate (2.4 μL, 0.025 mmol, 1.0 eq) was added and the slightly yellow

solution went turbid instantly. The reaction stirred 10 minutes at 0 °C and 45 minutes at 24 °C, before benzyl alcohol **57** (20.48 mg, 0.03 mmol, 1.2 eq) was added in anhydrous THF (2.5 mL) together with anhydrous NMM (100 μ L) at 0 °C. The reaction continued stirring for two hours at 24 °C and was then concentrated to dryness. The residue was purified by RP-HPLC (5-98% ACN/H₂O, 0.1% AcOH, 220 nm, collect all). The product containing fractions were lyophilized to yield **59** (25.2 mg, 0.016 mmol, 63% over two steps) as a beige powder.

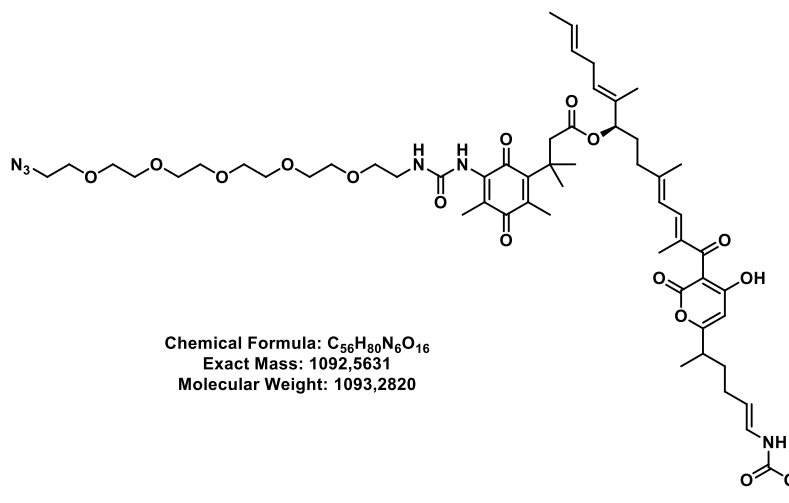
¹H-NMR (600 MHz, DMSO-d₆): δ = 11.92 (s, 1H), 7.08 (m, 2H), 6.92 (m, 1H), 6.45 (t, J = 10.49 Hz, 1H), 6.21 (dd, J = 3.86, 15.28 Hz, 1H), 6.13 (dd, J = 3.15, 10.00 Hz, 1H), 5.95 (m, 1H), 5.62 (m, 2H), 5.43 (m, 3H), 5.34 (m, 1H), 5.24 (m, 3H), 4.82 (d, J = 5.51 Hz, 1H), 4.76 (dd, J = 4.33, 7.25 Hz, 1H), 4.61 (d, J = 2.52 Hz, 1H), 4.49 (m, 1H), 4.36 (m, 2H), 4.19 (m, 2H), 4.07 (m, 1H), 3.75 (m, 1H), 3.65 (m, 3H), 2.30 (m, 2H), 2.10 (m, 9H), 1.98 (s, 3H), 1.94 (m, 3H), 1.78 (d, J = 10.48 Hz, 1H), 1.54 (s, 3H), 1.45 (m, 3H), 1.34 (m, 6H), 1.17 (m, 2H), 1.08 (m, 1H), 0.80 (d, J = 6.62 Hz, 3H), 0.74 (d, J = 7.25 Hz, 3H), 0.70 (d, J = 6.77 Hz, 3H).

¹³C-NMR (151 MHz, DMSO-d₆): δ = 175.00, 170.24, 165.69, 165.64, 138.14, 137.30, 136.35, 135.44, 132.61, 132.57, 132.55, 132.45, 130.33, 130.18, 129.50, 127.33, 125.73, 125.05, 124.85, 122.79, 118.82, 80.47, 80.39, 79.33, 79.02, 78.91, 77.73, 75.58, 73.87, 73.09, 73.03, 72.61, 71.41, 70.53, 70.26, 68.42, 65.28, 38.99, 37.29, 37.03, 35.97, 34.28, 34.11, 32.88, 32.42, 31.64, 29.72, 27.00, 26.91, 26.27, 25.07, 24.96, 21.65, 21.42, 21.28, 21.26, 15.20, 14.02, 13.89, 10.69, 10.62, 6.36.

DEPT (151 MHz, DMSO-d₆): δ = 137.40, 136.56, 135.62, 134.70, 131.87, 131.83, 131.81, 131.71, 129.59, 128.76, 126.73, 126.59, 124.99, 124.31, 122.05, 118.08, 79.65, 78.59, 78.29, 78.17, 77.00, 74.84, 72.35, 72.29, 71.87, 71.76, 70.67, 69.79, 67.96, 67.68, 64.54, 64.44, 38.25, 36.55, 36.29, 35.24, 33.54, 33.37, 32.14, 31.68, 30.91, 28.98, 26.26, 26.17, 24.33, 24.22, 20.91, 20.54, 20.52, 14.46, 13.28, 13.15, 9.88.

HRMS (ESI) calculated for ([M+2H]²⁺): m/z = 802.4197; experimental = 802.4199.

Corallopyronin A intermediates

Compound **70**

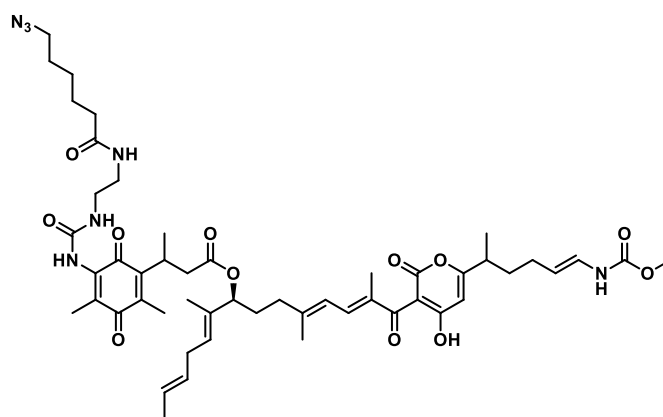
Acid **56** (10 mg, 0.017 mmol, 1.0 eq) was dissolved in dry THF (500 μ L) under argon atmosphere, NMM (15 μ L) was added and the flask was cooled to 0 $^{\circ}$ C. Then *iso*-butylchloroformate (1.66 μ L, 0.017 mmol, 1.0 eq) was added at 0 $^{\circ}$ C and the reaction continued stirring at that temperature for one hour. The color changed from yellow to orange and corallopyronin A **35** (18.08 mg, 0.034 mmol, 2.0 eq) was added in THF (500 μ L) at 0 $^{\circ}$ C. The reaction continued stirring overnight, while the thawing ice bath equilibrated the reaction steadily to ambient temperature. The next morning the solvent was removed and the reaction was purified by RP-HPLC (10-100% ACN/H₂O, 0.1% HCOOH, 220 nm). Product containing fractions were identified and lyophilized to yield **70** (13.35 mg, 0.12 mmol, 71%) as a slight beige powder. The residual, unreacted corallopyronin A **35** was re-isolated and tested for antibiotic activity, as the natural product's double bonds are prone to isomerize under basic conditions.

¹H-NMR (700 MHz, CD₂Cl₂): δ = 7.46 (s, 1H), 7.14 (dd, J = 1.27, 11.67 Hz, 1H), 6.91 (m, 1H), 6.71 (d, J = 10.40 Hz, 1H), 6.43 (m, 3H), 6.28 (dd, J = 1.27, 11.45 Hz, 1H), 6.20 (m, 2H), 5.96 (m, 1H), 5.42 (m, 6H), 5.29 (m, 2H), 4.98 (m, 2H), 4.53 (m, 1H), 3.89 (d, J = 6.62 Hz, 1H), 3.67 (d, J = 5.05 Hz, 4H), 3.63 (m, 18H), 3.61 (s, 4H), 3.56 (t, J = 4.73 Hz, 2H), 3.37 (m, 6H), 3.02 (m, 2H), 2.75 (m, 2H), 2.70 (m, 4H), 2.61 (m, 2H), 2.13 (s, 3H), 1.97 (s, 2H), 1.95 (s, 2H), 1.88 (s, 3H), 1.77 (s, 4H), 1.71 (s, 6H), 1.64 (m, 8H), 1.39 (d, J = 2.00 Hz, 6H), 1.23 (m, 6H), 0.94 (d, J = 6.62 Hz, 3).

¹³C-NMR (176 MHz, CD₂Cl₂): δ = 202.39, 191.88, 187.57, 187.02, 181.42, 176.46, 170.65, 168.91, 161.82, 160.54, 152.98, 152.60, 148.57, 140.92, 140.80, 140.12, 137.75, 137.62, 136.11, 134.31, 132.85, 132.70, 130.42, 130.38, 130.23, 130.19, 127.41, 127.20, 126.49, 126.35, 125.85, 125.81, 125.73, 125.61, 124.92, 123.32, 121.57, 120.90, 114.70, 109.99, 109.63, 101.51, 100.24, 99.60, 74.34, 71.09, 71.03, 70.94, 70.86, 70.76, 70.71, 70.42, 69.71, 69.62, 68.22, 52.82, 51.33, 47.70, 38.77, 38.64, 38.44, 38.38, 37.72, 37.50, 34.89, 33.68, 33.60, 31.75, 31.02, 30.96, 30.76, 29.71, 29.37, 28.38, 27.74, 24.20, 20.01, 19.21, 18.73, 18.30, 18.21, 18.19, 18.16, 18.03, 17.97, 17.91, 17.80, 17.71, 17.65, 14.73, 14.05, 13.87, 13.79, 12.29, 11.13.

HRMS (ESI) calculated for ([M+H+Na]²⁺): m/z = 558.2798 ; experimental = 558.2801.

Compound 71



Chemical Formula: C₅₁H₆₉N₇O₁₂
 Exact Mass: 971,5004
 Molecular Weight: 972,1500

Acid **53** (10 mg, 0.021 mmol, 1.0 eq) was dissolved in dry THF (500 μL) under argon atmosphere, pyridine (5 μL) was added and the flask was cooled to 0 °C. Then *iso*-butylchloroformate (2.03 μL, 0.021 mmol, 1.0 eq) was added at 0 °C and the reaction continued stirring at that temperature for one hour. The color changed from yellow to orange and corallopyronin A **35** (22.14 mg, 0.042 mmol, 2.0 eq) was added in THF (500 μL) at 0 °C. The reaction continued stirring for 48 hours, while the thawing ice bath equilibrated the reaction steadily to ambient temperature. The next morning the solvent was removed and the reaction was purified by RP-HPLC (10-100% ACN/H₂O, 0.1% HCOOH, 220 nm). Product containing fractions were lyophilized to yield **71** (15.358 mg, 0.16 mmol, 75%) as a slight beige powder. The residual, unreacted corallopyronin A **35** was re-isolated and tested for antibiotic activity, as the double bonds are eligible to isomerize under basic conditions.

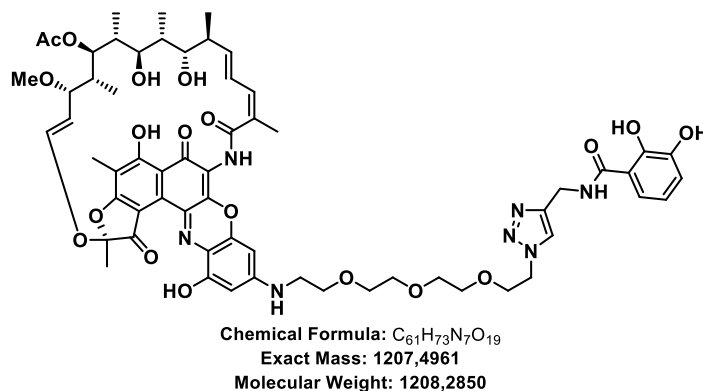
¹H-NMR (700 MHz, CD₂Cl₂): δ = 7.15 (dd, J = 1.89, 11.57 Hz, 1H), 6.45 (m, 2H), 6.33 (m, 1H), 6.28 (m, 1H), 6.15 (s, 1H), 5.96 (m, 1H), 5.87 (m, 1H), 5.40 (m, 5H), 5.28 (t, J = 6.73 Hz, 1H), 5.20 (t, J = 7.16 Hz, 1), 4.97 (m, 2H), 4.73 (m, 1H), 4.52 (t, J = 6.52 Hz, 1), 4.03 (m, 1H), 3.96 (d, J = 6.10 Hz, 2H), 3.67 (m, 6H), 3.26 (m, 1H), 2.75 (m, 2H), 2.68 (m, 4H), 2.59 (m, 1H), 2.42 (t, J = 7.79 Hz, 1H), 2.26 (m, 1H), 2.15 (m, 1H), 1.99 (m, 7H), 1.94 (s, 3H), 1.89 (s, 3H), 1.82 (s, 3H), 1.70 (s, 6H), 1.65 (s, 3H), 1.64 (m, 8H), 1.35 (m, 2H), 1.31 (s, 2H), 1.24 (m, 9H), 0.96 (m, 6H), 0.91 (d, J = 6.73 Hz, 4H).

¹³C-NMR (176 MHz, CD₂Cl₂): δ = 191.36, 190.95, 171.32, 170.03, 168.31, 162.90, 162.77, 161.72, 160.00, 156.64, 154.55, 152.57, 152.42, 151.29, 140.97, 140.13, 140.03, 137.64, 136.74, 135.64, 134.48, 132.69, 131.77, 130.40, 130.32, 130.16, 126.48, 126.46, 126.37, 126.02, 125.85, 125.82, 125.74, 125.64, 124.99, 122.75, 122.64, 121.59, 121.52, 114.54, 114.23, 109.68, 101.23, 100.55, 100.24, 99.60, 98.99, 98.47, 97.87, 97.65, 83.59, 76.81, 76.72, 76.39, 76.10, 76.01, 69.72, 69.68, 69.64, 54.00, 52.80, 51.79, 51.73, 39.07, 38.77, 38.67, 38.57, 38.53, 38.45, 38.32, 38.22, 37.77, 37.51, 35.14, 34.87, 34.69, 34.34, 33.66, 31.13, 31.07, 31.01, 31.00, 30.96, 30.26, 29.88, 28.98, 28.35, 28.20, 27.75, 27.55, 27.17, 26.47, 24.81, 24.56, 19.10, 19.04, 18.95, 18.35, 18.30, 18.20, 18.17, 18.04, 17.94, 17.92, 17.69, 14.28, 12.32, 12.19, 11.16.

HRMS (ESI) calculated for ([M+H+Na]²⁺): m/z = 994.4896; experimental = 994.4899.

Mono and dicatechol rifamycin conjugates

Compound 4



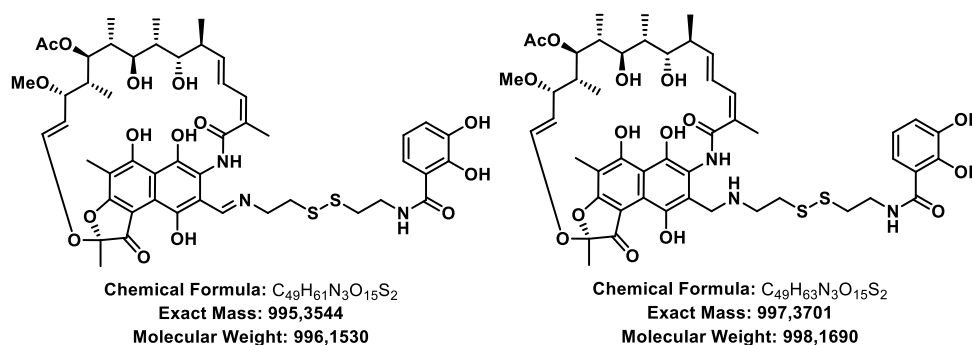
Alkyne **39** (11.9 mg, 0.062 mmol, 3.0 eq) and N_3 -PEG₃-NH₂ (15.9 mg, 0.73 mmol, 3.5 eq) were dissolved in DMSO (200 μ L). Sodium ascorbate (4.11 mg, 0.021 mmol, 1.0 eq), CuSO₄ (3.31 mg, 0.021 mmol, 1.0 eq) and TBTA (2.20 mg, 0.004, 0.2 eq) were premixed in 1xPBS (pH 7.4, 200 μ L) and added to the reaction mixture. The reaction stirred 1 hour at 25 °C. Upon complete consumption of the alkyne, the reaction was diluted with water (10 mL) and freeze-dried overnight. The residue was taken up in dry EA/MeOH and filtered through a syringe filter and concentrated *in vacuo*. The brown solid was taken up in anhydrous DMSO (200 μ L) and added dropwise to fluoro rifamycin **2** (17.0 mg, 0.021 mmol, 1.0 eq) in anhydrous THF under argon conditions at 0 °C. The reaction stirred at 0 °C for 5 minutes and continued stirring at 25 °C for an hours. The addition of anhydrous DIPEA (30 μ L) and warming to maximum 45 °C drove the reaction to completion. The solvent was removed by rotary evaporation and the residual liquid was purified by RP-HPLC (60-90% ACN/H₂O, 1% AcOH, 220 nm,). The product containing fractions were identified by LCMS and lyophilized overnight to yield pure title compound **4** as a blue solid (7.42 mg, 0.006 mmol, 30% over two steps).

¹H-NMR (700 MHz, Tol-d₈, AcOH-d₄, ACN-d₃): δ = 13.24 (s, 1H), 9.52 (s, 1H), 9.22-9.09 (m, 3H), 7.91 (m, 1H), 7.75 (d, J = 11.65 Hz; 1H), 7.58 (d, J = 8.59 Hz, 1H), 7.17 (m, 1H), 6.88 (m, 1H), 6.67 (m, 1H), 6.33 (m, 1H), 6.27 (d, J = 12.06 Hz, 2H), 6.03 (m, 1H), 5.74 (m, 2H), 5.38 (q, J = 7.56, 13.08 Hz, 2H), 5.21 (t, J = 9.81 Hz, 1H), 5.08 (m, 2H), 4.70 (m, 2H), 4.61 (m, 1H), 4.37 (m, 1H), 4.30 (m, 2H), 3.86 (m, 1H), 3.61 (m, 3H), 3.46 (m, 6H), 3.38 (m, 5H), 3.08 (m, 4H), 2.95 (m, 5H), 2.91 (m, 1H), 2.29 (s, 5H), 2.22 (m, 5H), 1.94 (m, 4H), 1.78 (m, 12H), 1.61 (m, 5H), 1.26 (m, 4H), 1.06 (d, J = 7.15 Hz, 4H), 0.99 (d, J = 7.56 Hz, 3H), 0.93 (m, 2H), 0.73 (m, 3H), 0.62 (m, 5H).

$^{13}\text{C-NMR}$ (176 MHz, Toluene- d_8 , AcOH- d_4 , ACN- d_3) δ = 185.23, 181.78, 172.37, 170.72, 170.20, 166.62, 147.22, 144.14, 142.00, 137.32, 137.26, 137.04, 137.00, 132.80, 131.07, 130.56, 128.28, 128.26, 128.23, 127.37, 127.36, 125.10, 124.49, 123.88, 119.19, 118.04, 116.67, 114.91, 107.74, 76.72, 73.03, 72.75, 70.40, 70.29, 70.25, 69.26, 55.85, 49.74, 37.33, 35.13, 32.95, 21.85, 20.72, 16.81, 11.30, 9.40, 7.43.

HRMS (ESI) calculated for ($[\text{M}+\text{H}]^+$): m/z = 1208.5034; experimental = 1208.5025.

Compound **5a** and **5**



3-formyl rifamycin SV **27** (50 mg, 0.069 mmol, 1.0) was dissolved in anhydrous THF (20 mL) under argon atmosphere and the amine **40** (19.9 mg, 0.069 mmol 1.0 eq) was added as a solution in THF (5 mL) with TEA (30 μL) at 0 $^\circ\text{C}$. The ice bath was removed and the color of the solution changed from red to purple over the course of 1 hour at ambient temperature. The reaction was diluted with DCM (100 mL) and washed with 1 M HCl (1x 75 mL), water/brine (1:1, 2x100 mL) and dried over Na_2SO_4 . The solvent was removed in vacuo to yield pure imine **5a** (61.39 mg, 0.062 mmol, 90%) as a red-purple solid. A small fraction of the imine **5a** was directly tested for biological activity in MIC assays and stored under argon in dry DMSO at -20 $^\circ\text{C}$ in the dark. The rest was dissolved in anhydrous THF and $\text{NaBH}(\text{OAc})_3$ (21.91 mg, 0.103 mol, 1.5 eq) was added in one portion at 0 $^\circ\text{C}$ under argon. The reaction stirred 30 minutes at 30 $^\circ\text{C}$ and 30 minutes at ambient temperature. Then the reaction was diluted with DCM (120 mL) and washed with 1 M HCl, water and brine (each 2x100 mL). The organic phase was dried over Na_2SO_4 and the solvent was removed in vacuo to yield crude amine **5** as a red solid (38.99 mg, 0.039 mmol, 57% over 2 steps).

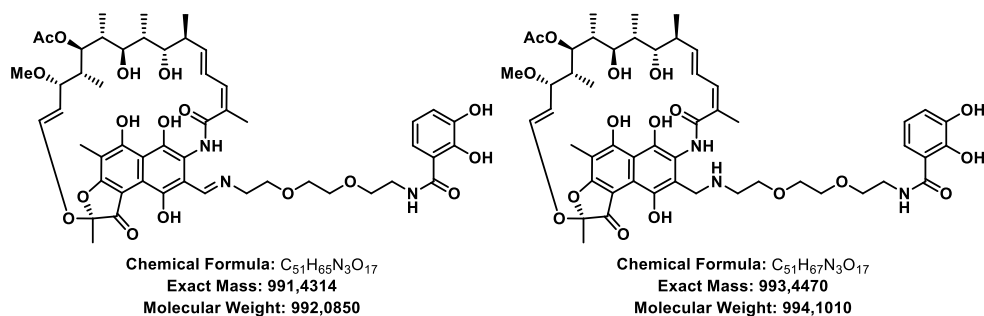
5a:

¹H-NMR (700 MHz, CD₃CN): δ = 12.67 (s, 1H), 12.23 (s, 1H), 10.57 (s, 1H), 6.54 (dd, J = 11.59 Hz, 1H), 6.47 (m, 1H), 6.32 (d, J = 12.35 Hz, 1H), 6.05 (dd, J = 5.04, 15.37 Hz, 1H), 5.10 (m, 1H), 5.01 (d, J = 10.08 Hz, 1H), 3.74 (d, J = 9.58 Hz, 1H), 3.64 (m, 6H), 3.43 (d, J = 8.07 Hz, 1H), 3.10 (m, 1H), 3.02 (m, 2H), 2.97 (s, 3H), 2.33 (m, 1H), 2.22 (s, 3H), 2.06 (s, 3H), 2.00 (s, 3H), 1.80 (m, 9H), 1.39 (s, 3H), 1.26 (m, 1H), 1.15 (m, 1H), 0.95 (d, J = 7.31 Hz, 3H), 0.85 (d, J = 7.31 Hz, 3H), 0.61 (d, J = 6.55 Hz, 3H), -0.39 (d, J = 6.55 Hz, 3H).

5

¹H-NMR (700 MHz, DMSO-d₆): δ = 12.79 (m, 1H), 9.37 (m, 1H), 8.61 (m, 2H), 8.47 (m, 1H), 7.81 (m, 1H), 7.70 (m, 1H), 7.28 (m, 2H), 6.25 (m, 1H), 6.17 (m, 1H), 6.07 (m, 1H), 5.91 (dd, J = 6.52, 16.76 Hz, 1H), 5.08 (m, 1H), 5.00 (m, 2H), 4.90 (m, 1H), 3.28 (m, 2H), 3.15 (m, 1H), 3.09 (m, 1H), 2.89 (m, 4H), 2.73 (s, 1H), 2.02 (m, 3H), 1.97 (m, 5H), 1.91 (m, 3H), 1.89 (m, 2H), 1.64 (s, 1H), 1.35 (s, 1H), 1.23 (bs, 3H), 0.93 (m, 6H), 0.85 (d, J = 7.45 Hz, 3H), 0.81 (d, J = 7.08 Hz, 3H), 0.27 (m, 1H), -0.03 (m, 1H), -0.34 (d, J = 6.89 Hz, 1H).

HRMS (ESI) calculated for ([M+H]⁺): m/z = 998.3774; experimental = 998.3782.

Compound 6a and 6

3-formyl rifamycin SV **27** (50 mg, 0.069 mmol, 1.0) was dissolved in anhydrous THF (20 mL) under argon atmosphere and the amine **41** (19.59 mg, 0.069 mmol 1.0 eq) was added as a solution in THF (5 mL) with TEA (30 μ L) at 0 °C. The ice bath was removed and the color of the solution changed from red to purple over the course of 1 hour at ambient temperature. The reaction was diluted with DCM (100 mL) and washed with 1 M HCl (1x 75 mL), water/brine (1:1, 2x100 mL) and dried over Na₂SO₄. The solvent was removed *in vacuo* to yield pure imine **6a** (61.39 mg, 0.062 mmol, 90%) as a red-purple solid. A small fraction of the imine **6a** was directly tested for biological activity in MIC assays and stored under argon in dry DMSO at -

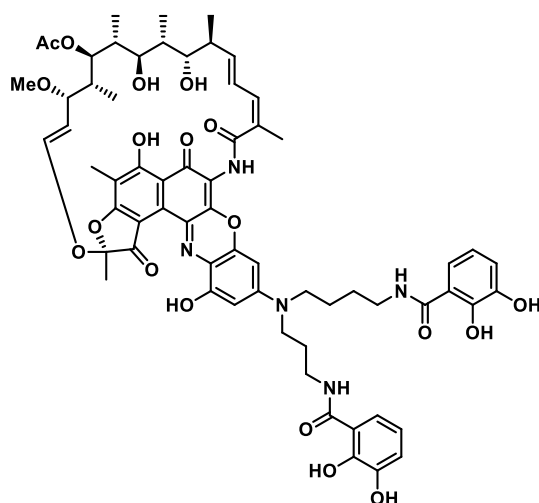
20 °C in the dark. The rest was dissolved in anhydrous THF and NaBH(OAc)₃ (21.91 mg, 0.103 mol, 1.5 eq) was added in one portion at 0 °C under argon. The reaction stirred 30 minutes at 30 °C and 30 minutes at ambient temperature. Then the reaction was diluted with DCM (120 mL) and washed with 1 M HCl, water and brine (each 2x100 mL). The organic phase was dried over Na₂SO₄ and the solvent was removed *in vacuo* to yield crude title compound **6** as a red solid (54.2 mg, 0.055 mmol, 79% over 2 steps).

¹H-NMR (700 MHz, ACN-d₃): δ = 15.11 (s, 1H), 8.72 (s, 2H), 8.25 (m, 2H), 7.94 (m, 1H), 7.81 (m, 2H), 7.47 (d, J = 6.82 Hz, 1H), 7.41 (m, 2H), 6.71 (s, 1H), 6.66 (s, 1H), 5.89 (d, J = 9.97 Hz, 1H), 5.32 (s, 1H), 5.26 (m, 2H), 5.23 (s, 1H), 5.02 (d, J = 7.61 Hz, 1H), 3.78 (s, 1H), 3.72 (m, 2H), 3.63 (m, 2H), 3.24 (m, 2H), 3.05 (m, 4H), 2.98 (m, 1H), 2.51 (m, 1H), 2.34 (m, 5H), 2.32 (m, 2H), 2.29 (m, 4H), 2.19 (m, 2H), 1.79 (m, 1H), 1.34 (d, J = 7.61 Hz, 3), 1.27 (d, J = 5.72 Hz, 3H), 1.13 (d, J = 7.18 Hz, 3H), 0.87 (m, 6H).

¹³C-NMR (176 MHz, ACN-d₃): δ = 189.30, 178.29, 171.84, 167.53, 158.01, 149.32, 148.69, 146.19, 142.56, 140.56, 139.80, 139.55, 138.59, 135.70, 129.64, 129.43, 129.25, 129.12, 128.01, 125.70, 125.05, 124.68, 121.81, 120.81, 120.40, 112.50, 112.37, 111.32, 108.58, 107.41, 71.58, 69.88, 67.35, 50.52, 50.31, 50.22, 45.92, 42.37, 36.73, 31.41, 28.97, 21.48, 21.30, 21.23, 20.08, 19.26, 8.73, 8.69, 1.88.

HRMS (ESI) calculated for ([M+H]⁺): m/z = 994.4543; experimental = 994.4556.

Compound 3



Chemical Formula: C₆₄H₇₃N₅O₁₉
 Exact Mass: 1215,4900
 Molecular Weight: 1216,3040

2 (30 mg, 0.037 mmol, 1.0 eq) was dissolved in dry THF (1 mL) under argon atmosphere and crude dicatechol **42** (30.6 mg, 0.073 mmol, 2.0 eq) was added in THF/DMSO (1:1, 1mL) dropwise at 0 °C over 10 minutes. Then DIPEA (100 µL) and pyridine (100 µL) were added and the reaction was warmed to 45 °C and the color changed from red to blue. The reaction continued stirring overnight and the solvent was removed by rotary evaporation. The residue was dried, filtered over a syringe filter and purified by RP-HPLC (60-100% H₂O/ACN, 0.1% AcOH, 220nm). Product containing fractions were lyophilized overnight to yield dicatechol rifamycin **3** (24.6mg, 0.02 mmol, 55%) as a blue solid.

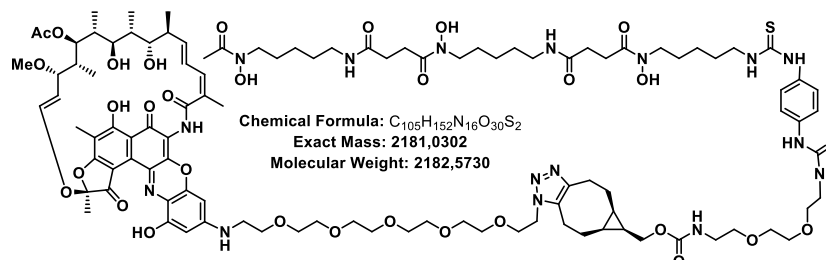
¹H-NMR (700 MHz, CD₂Cl₂): δ = 9.46 (t, J = 2.89 Hz, 1H), 7.45 (d, J = 7.56 Hz, 2H), 7.40 (t, J = 7.65 Hz, 2H), 7.35 (d, J = 7.65 Hz, 1H), 7.01 (dd, J = 7.96, 26.62 Hz, 1H), 6.94 (t, J = 7.65 Hz, 1H), 6.76 (m, 1H), 6.70 (s, 1H), 6.59 (s, 1H), 6.29 (d, 1H), 5.04 (s, 2H), 5.00 (m, 1H), 4.10 (d, J = 7.21 Hz, 1H), 3.57 (m, 9H), 3.07 (m, 2H), 2.91 (d, J = 2.54 Hz, 2H), 2.51 (s, 3H), 2.30 (m, 5H), 2.23 (s, 3H), 2.10 (s, 2H), 2.01 (bs, 3H), 1.97 (s, 3H), 1.75 (m, 4H), 1.60 (m, 3H), 1.56 (s, 8H), 0.89 (m, 9H), 0.83 (m, 6H).

DEPT (176 MHz, DMSO-d₆): δ = 137.65, 136.81, 135.86, 134.95, 132.08, 131.96, 129.01, 128.44, 126.84, 124.56, 122.30, 118.33, 78.84, 78.42, 77.24, 75.09, 72.60, 72.54, 72.11, 70.91, 70.04, 67.92, 64.78, 38.49, 36.54, 35.48, 33.80, 31.93, 31.15, 26.51, 24.58, 20.79, 20.26, 14.71, 13.40, 10.26, 10.13.

HRMS (ESI) calculated for ([M+H]⁺): m/z = 1216.4973; experimental = 1216.4941.

DOTAM and DFO RNAP-I conjugates

Compound 18



Red fluoro rifamycin **2** (7.5 mg, 0.009 mmol, 1.0 eq) and N₃-PEG-NH₂ (5.5 mg, 0.018 mmol, 2.0 eq) were mixed in anhydrous THF (5 mL) and DIPEA (20 μL) was added. The reaction stirred for four hours at ambient temperature. Then the solvent was removed by rotary evaporation and the residue was dissolved in DCM (20 mL). The organic phase was washed with 1 M HCl (2x10 mL) and the organic phase was dried over Na₂SO₄. The solvent was removed *in vacuo* and the residue was dried under reduced pressure to yield crude azide **18a** as a blue solid (quant.). Then azide **18a** (9.6 mg, 0.009 mmol, 1.0 eq) and strained alkyne **47** (14.97 mg, 0.014 mmol, 1.6 eq) were weight in 1.5 mL tubes and then dissolved in degassed mixture of ACN:H₂O (1:1, 300 μL each). The compounds were added together under argon atmosphere and continued stirring for 30 hours at 24 °C. The orange solution was filtered and purified by RP-HPLC (15-98-100% ACN/H₂O, 0.1% HCOOH, 220 nm, collect all.). Product containing fractions were lyophilized to yield **18** (15.55 mg, 0.007 mmol, 82%) as a beige solid. The compound eluted as a diastereomeric mixture in one peak from the HPLC, just one isomer is depicted here.

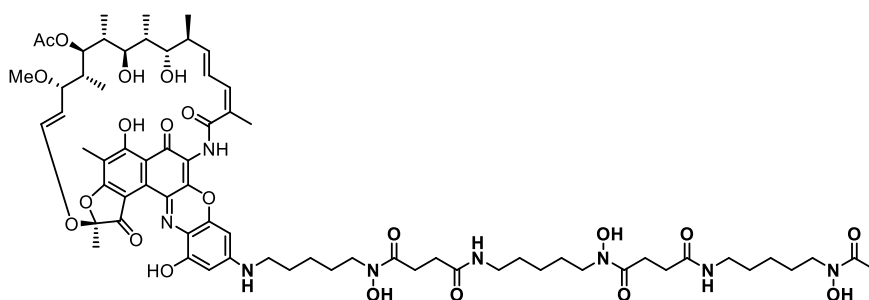
¹H-NMR (600 MHz, DMSO-d₆): δ = 9.62 (m, 4H), 9.16 (m, 1H), 8.41 (m, 1H), 7.78 (m, 4H), 7.65 (m, 2H), 7.34 (m, 4H), 6.47 (m, 2H), 6.37 (m, 2H), 6.21 (m, 1H), 4.63 (m, 1H), 4.57 (m, 1H), 4.48 (m, 1H), 4.37 (m, 1H), 4.09 (m, 4H), 4.01 (m, 2H), 3.63 (t, J = 5.45 Hz, 6H), 3.58 (m, 10H), 3.54 (m, 20H), 3.51 (m, 20H), 3.38 (t, J = 5.45 Hz, 10H), 3.17 (s, 12H), 3.00 (q, J = 5.45, 12.76 Hz, 4H), 2.58 (m, 4H), 2.27 (m, 4H), 2.14 (m, 5H), 2.04 (m, 12H), 2.00 (m, 4H), 1.97 (s, 3H), 1.55 (m, 6H), 1.38 (m, 4H), 1.24 (m, 6H), 0.92 (m, 16H), 0.79 (m, 8H), 0.74 (m, 8H).

¹³C-NMR (151 MHz, DMSO-d₆): δ = 202.07, 195.55, 174.20, 171.77, 170.38, 105.54, 104.53, 86.50, 77.85, 73.59, 70.29, 70.27, 70.24, 70.14, 70.00, 69.70, 69.15, 50.44, 49.06, 47.61, 46.32, 43.55, 38.88, 35.36, 31.76, 31.50, 30.36, 29.48, 29.29, 29.17, 28.04, 26.49, 24.07, 23.96, 23.34, 22.56, 21.18, 20.82, 16.96, 14.43, 12.85, 7.79, 6.84.

DEPT (151 MHz, DMSO-d₆): δ = 86.51, 77.86, 73.60, 70.29, 70.28, 70.25, 70.22, 70.14, 70.12, 69.95, 69.70, 69.69, 69.15, 50.44, 50.41, 49.07, 47.62, 46.33, 43.55, 38.90, 35.36, 31.50, 30.36, 29.48, 29.29, 28.04, 26.49, 23.97, 23.34, 21.18, 20.82, 12.85, 7.79, 6.84.

HRMS (ESI) calculated for ([M+3H]³⁺): m/z = 1091.5223; experimental = 1091.5236.

Compound 19



Chemical Formula: C₆₈H₉₄N₈O₂₁
 Exact Mass: 1358,6534
 Molecular Weight: 1359,5350

2 (50.0 mg, 0.061 mmol, 1.0) was dissolved in anhydrous THF (35 mL) and TEA (0.5 mL) was added under argon atmosphere. DFO (68.47 mg, 0.122 mmol, 2 eq) was added in DMF (20 mL) and dissolved with gentle heating with a heat gun. The clear solution was added quickly to the solution of **2**. The solution was heated to 45 °C overnight and the color changed from blood red to intense blue. Then the solvent was removed by rotary evaporation. The residue was taken up in MeOH/ACN (5 mL) and purified by RP-HPLC (C18, 220 nm, 15-85% ACN/H₂O, collect all). Product containing fractions were lyophilized to dryness to yield **19** (69.5, 0.051 mmol, 84%) as a dark blue solid.

¹H-NMR (600 MHz, DMSO-d₆): δ = 16.61 (s, 1H), 16.41 (s, 1H), 9.63 (m, 4H), 9.14 (m, 1H), 8.61 (m, 1H), 8.34 (m, 1H), 7.77, 6.80 (s, 4H), 6.80 (m, 1H), 6.39 (m, 4H), 6.12 (m, 1H), 6.02 (m, 1H), 5.78 (m, 2H), 5.18 (m, 2H), 4.97 (m, 1H), 4.85 (m, 2H), 4.01 (bs, 1H), 3.59 (m, 1H), 3.47 (m, 10H), 3.19 (m, 3H), 3.02 (m, 10H), 2.86 (bs, 2H), 2.59 (m, 5H), 2.28 (m, 6H), 2.21 (m, 2H), 2.12 (m, 2H), 1.97 (m, 12H), 1.75 (m, 2H), 1.66 (m, 2H), 1.59 (m, 6H), 1.50 (m, 9H), 1.38 (m, 6H), 1.22 (m, 6H), 0.85 (m, 8H), 0.67 (m, 3H), -0.08 (m, 2H), -0.42 (m, 2H).

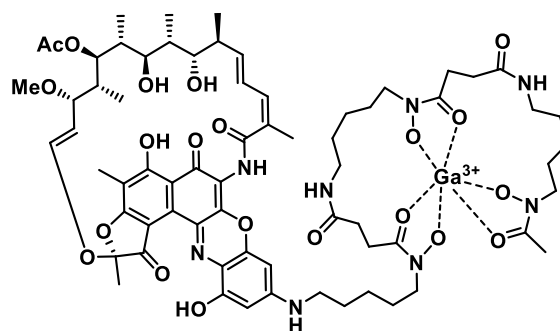
¹³C-NMR (151 MHz, DMSO-d₆): δ = 192.27, 181.12, 180.78, 173.78, 172.00, 171.96, 171.28, 170.47, 170.12, 169.86, 169.25, 168.88, 158.02, 143.82, 143.54, 141.57, 131.72, 130.98,

129.16, 128.11, 125.84, 120.25, 118.81, 113.27, 112.18, 111.05, 109.71, 108.21, 107.35, 106.15, 104.45, 92.67, 77.94, 77.08, 75.67, 75.58, 72.56, 72.18, 55.78, 54.04, 48.58, 47.06, 46.98, 46.77, 43.00, 41.87, 41.44, 39.52, 38.42, 35.49, 32.23, 30.91, 29.84, 28.81, 27.99, 27.55, 26.02, 23.80, 23.77, 23.49, 22.60, 22.30, 20.94, 20.53, 20.34, 19.92, 18.28, 16.35, 12.13, 10.62, 8.98, 7.52, 7.40.

DEPT (151 MHz, DMSO-d₆): δ = 185.17, 185.01, 183.56, 183.56, 182.96, 182.88, 182.82, 178.08, 176.68, 175.41, 144.52, 144.45, 144.38, 139.59, 139.59, 139.59, 138.01, 138.01, 136.74, 135.98, 135.36, 135.35, 135.35, 134.82, 133.21, 130.56, 129.94, 129.94, 129.88, 129.87, 129.87, 129.80, 126.44, 126.39, 126.22, 125.52, 100.00, 76.18, 73.77, 73.69, 73.61, 70.33, 70.20, 70.20, 70.13, 70.06, 70.06, 69.45, 69.43, 69.43, 65.25, 65.18, 64.65, 64.64, 64.64, 63.99, 63.25, 61.98, 61.98, 60.41, 55.55, 55.55, 21.91, 17.13, 16.43.

HRMS (ESI) calculated for ([M+2H]²⁺): m/z = 680.3340; experimental = 680.3349.

Compound **20**



Chemical Formula: C₆₈H₉₁GaN₈O₂₁³⁺

Exact Mass: 1424,5538

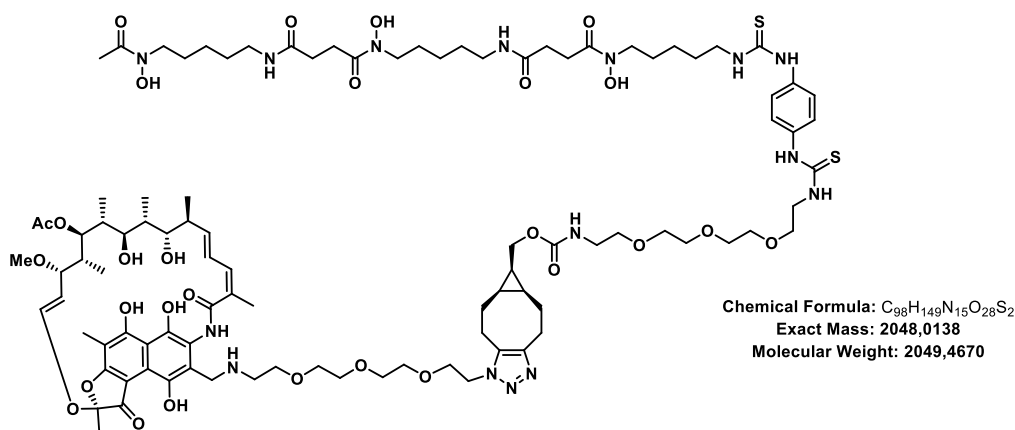
Molecular Weight: 1426,2324

Complex **20** was synthesized according to previously established conditions in Peukert and Langer et al.³ **19** (5 mg, 0.004mmol, 1.0 eq) was dissolved in ddH₂O/ACN mixture (1:1, 200 μ L) and GaCl₃ (0.71 mg, 0.004 mmol, 1.0 eq) was added, dissolved in NaOAc buffer (200 μ L, pH 4.5). The reaction stirred overnight at room temperature, was then acidified with AcOH (200 μ L), immediately diluted with ddH₂O and lyophilized to yield a blue solid as **20** (5.23 mg, 0.004 mmol, quant.).

¹H-NMR (700 MHz, MeOH-d₄): δ = 6.87 (m, 1H), 6.40 (m, 2H), 6.28 (d, J = 11.91 Hz, 1H), 6.22 (m, 2H), 5.01 (m, 2H), 4.58 (s, 5H), 3.90 (m, 2H), 3.71 (d, J = 8.00 Hz, 1H), 3.55 (m, 5H), 3.12 (m, 4H), 2.98 (m, 5H), 2.81 (m, 4H), 2.46 (m, 1H), 2.36 (m, 3H), 2.27 (bs, 3H), 2.16 (bs, 5H), 2.11 (s, 3H), 1.98 (bs, 6H), 1.78 (bs, 5H), 1.72 (m, 7H), 1.62 (m, 6H), 1.50 (m, 11H), 1.32 (m, 10), 0.93 (m, 12H), 0.78 (m, 4H), 0.69 (m, 2H), 0.05 (m, 3H), -0.32 (m, 3H).

HRMS (ESI) calculated for ([M+H]⁺): m/z = 1425.5610; experimental = 1425.5630, calculated for ([M+Na]⁺): m/z = 1447.5430; experimental = 1447.5463, calculated for ([M+2H]²⁺): m/z = 713.2842; experimental = 713.2859.

Compound 21



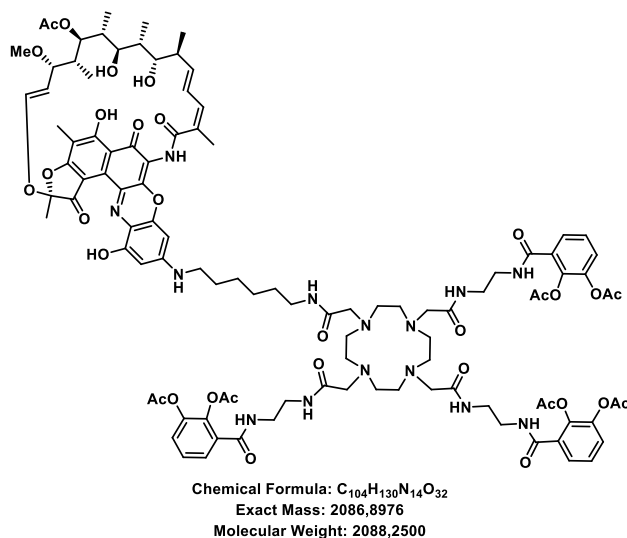
Strained alkyne **47** (20 mg, 0.019 mmol, 1.0 eq) was dissolved in DMSO (1 mL) and the azide **62** (20.67 mg, 0.022 mmol, 1.2 eq) was added dissolved in MeOH (10 mL). The reaction continued stirring for 18 hours at 23 °C. Upon complete consumption of the strained alkyne, DCM was added (30 mL), brine (20 mL) and the organic phases were separated. The organic phase was washed trice with a brine/ddH₂O mixture (1:1), dried over Na₂SO₄ and the solvent was removed by rotary evaporation. The residue was purified by RP-HPLC (15-95% ACN/H₂O 0.1% HCOOH, 220 nm, collect all). The product containing fractions were lyophilized to dryness to yield **21** as a yellow solid (21.3 mg, 0.011 mmol, 57%). The compound eluted as a diastereomeric mixture in one peak from the HPLC, just one isomer is depicted here.

¹H-NMR (700 MHz, DMSO-d₆): δ = 9.62 (m, 4H), 9.39 (m, 1H), 7.77 (m, 2H), 7.63 (m, 1H), 7.33 (q, J = 8.66, 13.66 Hz, 4H), 7.23 (m, 1H), 7.08 (m, 1H), 5.85 (m, 1H), 5.16 (m, 1H), 4.36 (m, 1H), 4.03 (m, 2H), 3.73 (m, 2H), 3.62 (m, 2H), 3.54 (m, 6H), 3.46 (m, 10H), 3.40 (m, 2H), 3.30 (m, 2H), 3.12 (m, 2H), 2.99 (q, J = 6-67, 12.66 Hz, 4H), 2.57 (q, J = 9.66, 14.66 Hz, 4H), 2.27 (q, J = 9.66, 15.33 Hz, 4H), 2.06 (m, 2H), 1.96 (s, 3H), 1.86 (m, 1H), 1.74 (m, 2H), 1.65 (m, 1H), 1.53 (m, 6H), 1.49 (m, 6H), 1.37 (m, 5H), 1.21 (m, 10H), 0.91 (m, 4H), 0.85 (m, 2H), 0.71 (m, 2H).

¹³C-NMR (176 MHz, DMSO-d₆): δ = 201.25, 197.62, 194.57, 193.73, 193.51, 182.45, 180.51, 176.36, 173.86, 171.30, 170.72, 170.55, 170.13, 156.44, 155.22, 155.06, 144.93, 143.14, 133.71, 132.21, 130.46, 126.43, 123.34, 115.52, 75.93, 73.47, 70.77, 69.75, 69.53, 69.16, 68.58, 67.02, 66.67, 66.60, 66.20, 65.76, 61.43, 47.15, 46.78, 43.56, 40.34, 40.02, 39.52, 38.41, 36.57, 33.96, 29.89, 29.19, 28.81, 28.21, 27.56, 26.02, 25.35, 23.49, 22.22, 21.27, 20.86, 20.35, 19.17, 17.31, 16.44, 10.92, 10.17, 9.83, -15.18.

HRMS (ESI) calculated for ([M+3H]³⁺): m/z = 683.6785; experimental = 683.6794.

Compound 23



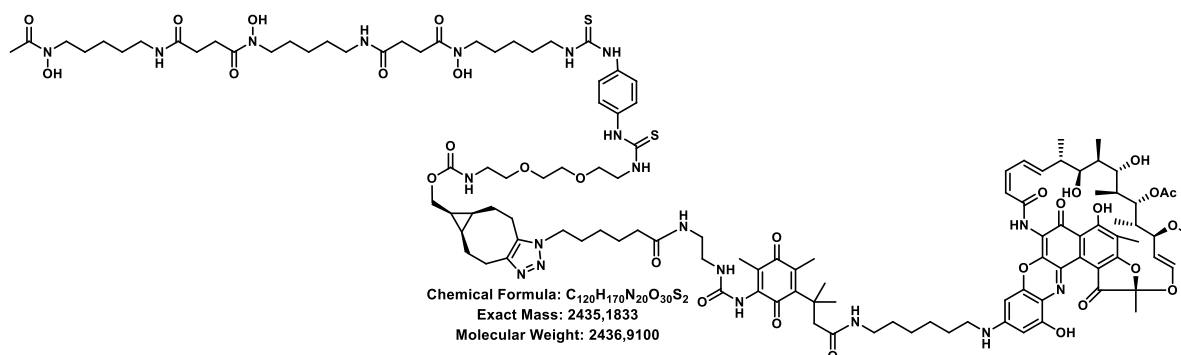
Acid **7** (10 mg, 0.008 mmol, 1.0 eq) was dissolved in anhydrous THF (1 mL), DMF (100 μL), NMM (100 μL) was added under argon atmosphere and the reaction was cooled to 0 °C, before iso-butyl chloroformate (0.81 μL, 0.008 mmol, 1.0 eq) was added and the reaction went turbid instantly. The reaction stirred 5 minutes at 0 °C and then 30 minutes at 24 °C. Then amine **22** (8.45 mg, 0.009 mmol, 1.1 eq) was added dropwise at 0 °C, dissolved in anhydrous THF (1

mL) and basified with NMM (100 μ L) before addition. The reaction continued stirring at 0 $^{\circ}$ C for 5 minutes and then for 30 minutes at 24 $^{\circ}$ C. Then the reaction was quenched with AcOH (200 μ L) and the THF was removed *in vacuo* at 30 $^{\circ}$ C. The residual solution was diluted and purified by RP-HPLC to yield **23** as a blue solid (13.91 mg, 0.007 mmol, 79%).

1 H-NMR (700 MHz, MeOH- d_4): δ = 7.47 (m, 3H), 7.32 (m, 6H), 7.14 (m, 1H), 6.86 (m, 1H), 6.38 (d, J = 10.46 Hz, 1H), 6.32 (m, 1H), 6.26 (d, J = 12.79 Hz, 1H), 6.19 (m, 2H), 3.69 (m, 1H), 3.47 (m, 10H), 3.40 (m, 10H), 3.18 (m, 2H), 3.08 (m, 1H), 2.98 (m, 10H), 2.86 (m, 8H), 2.28 (s, 9H), 2.25 (s, 9H), 2.10 (m, 2H), 1.99 (s, 2H), 1.96 (m, 5H), 1.93 (m, 1H), 1.78 (m, 3H), 1.61 (m, 4H), 1.50 (m, 4H), 1.29 (m, 10H), 1.08 (m, 2H), 0.98 (m, 1H), 0.94 (m, 3H), 0.90 (m, 6H), 0.82 (m, 2H), 0.78 (m, 2H), 0.03 (d, J = 5.81 Hz, 3H), -0.34 (d, J = 5.18 Hz, 3H).

HRMS (ESI) calculated for ($[M+3H]^{3+}$): m/z = 1044.4561; experimental = 1044.4570, calculated for ($[M+4H]^{4+}$): m/z = 696.9756; experimental = 696.9752.

Compound **XX**



The strained alkyne **47** (10 mg, 0.009 mmol, 1.0 eq) was dissolved in anhydrous MeOH (7 mL) and the azide **63** (14.67 mg, 0.011 mmol, 1.0 eq) was added in MeOH (8 mL) under argon atmosphere. The blue solution continued stirring overnight and the reaction progress was monitored by LCMS. The solvent was removed by rotary evaporation and was purified by RP-HPLC (15%-100% ACN/ H_2O 220 nm, collect all). The product containing fractions were lyophilized to dryness to yield **24** (18.24 mg, 0.007 mmol, 81%) as a blue solid. The compound was obtained as a mixture of 1,4 / 1,5 isomer that eluted as one peak from the HPLC. The compound eluted as a diastereomeric mixture in one peak from the HPLC, just one isomer is depicted here.

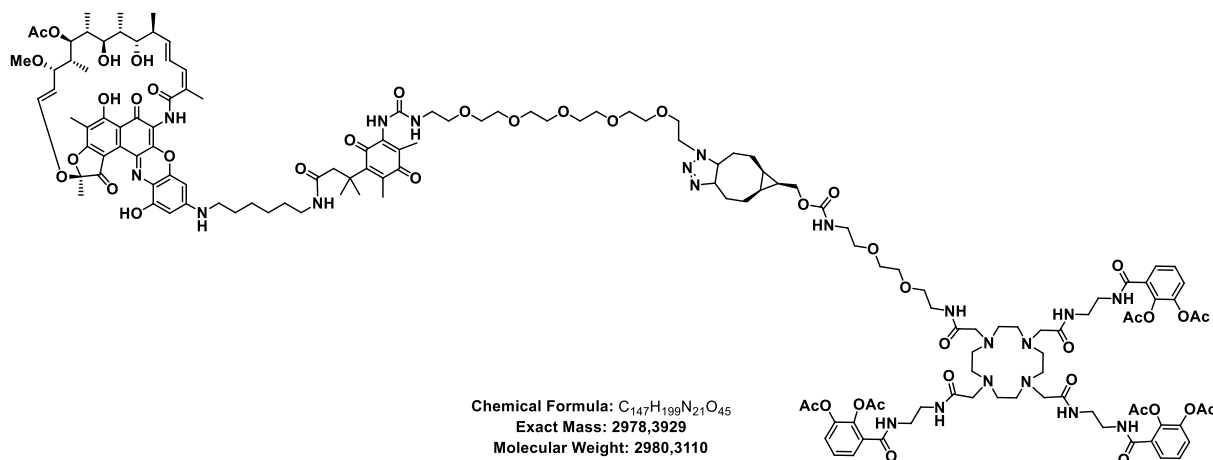
¹H NMR (700 MHz, DMSO-d₆): δ = 9.63 (m, 8H), 9.47 (m, 2H), 7.83 (m, 1H), 7.77 (m, 6H), 7.71 (m, 2H), 7.66 (m, 2H), 7.34 (m, 12H), 7.15 (m, 5H), 4.99 (dd, J = 2.61 Hz, 7.45 Hz, 1H), 4.94 (dd, J = 3.35, 11.36 Hz, 1H), 4.19 (m, 1H), 4.05 (m, 6H), 3.63 (m, 6H), 3.54 (m, 20H), 3.46 (m, 24H), 3.40 (t, J = 6.52 Hz, 10H), 3.11 (q, J = 4.84, 11.73 Hz, 8H), 3.00 (q, J = 6.85, 12.85 Hz, 12H), 2.58 (q, J = 7.08, 12.85 Hz, 12H), 2.27 (q, J = 5.96, 11.36 Hz, 12H), 2.13 (s, 4H), 1.99 (s, 3H), 1.96 (m, 14H), 1.85 (m, 8H), 1.53 (m, 12H), 1.49 (m, 12H), 1.38 (m, 12H), 1.25 (m, 6H), 1.22 (m, 10H), 1.12 (m, 4H), 0.87 (m, 4H), 0.75 (m, 2H).

¹³C-NMR (176 MHz, DMSO-d₆): δ = 212.68, 180.50, 171.96, 171.30, 170.58, 170.12, 156.40, 123.32, 77.65, 76.30, 69.53, 69.15, 68.58, 61.12, 61.02, 47.07, 46.77, 43.73, 43.57, 43.45, 41.33, 40.06, 40.02, 38.42, 32.67, 32.06, 29.89, 28.81, 28.20, 27.99, 27.57, 26.11, 26.02, 23.58, 23.49, 20.63, 20.34, 20.11, 19.19, 18.88, 18.82, 18.72, 18.15, 17.90, 17.83, 17.13.

DEPT (176 MHz, DMSO-d₆): δ = 123.06, 77.39, 76.05, 69.27, 68.89, 68.32, 61.19, 60.86, 60.76, 46.87, 46.81, 46.52, 43.49, 43.31, 43.19, 41.07, 38.16, 32.42, 31.81, 29.64, 28.55, 27.95, 27.73, 27.31, 25.85, 25.76, 23.33, 23.23, 20.37, 20.09, 19.85, 18.62, 18.56, 17.89, 17.65, 17.57, 17.36, 16.87, 16.48.

HRMS (ESI) calculated for ([M+2H]²⁺): m/z = 1181.1117; experimental = 1181.1126.

Compound 25



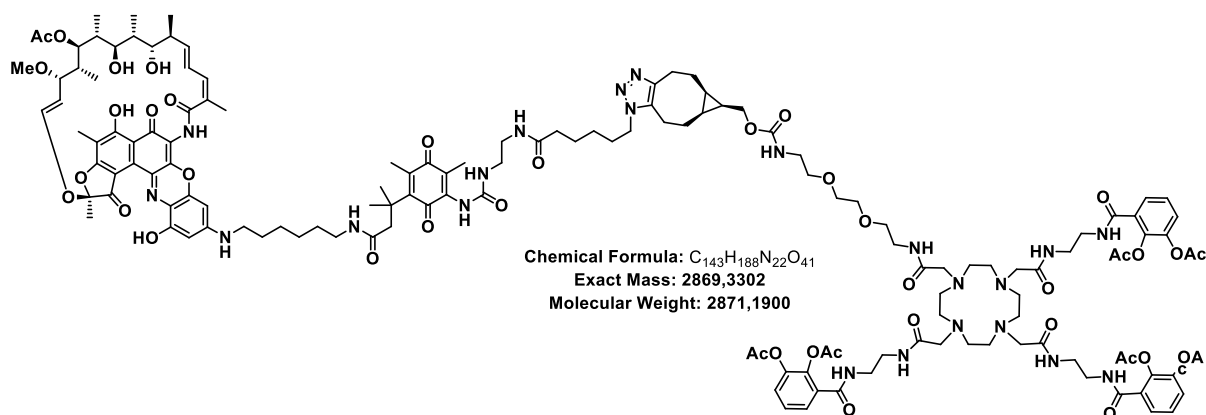
Alkyne **45** (2 mg, 0.001 mmol, 1.0 eq) and azide **64** (1.98 mg, 0.001 mmol, 1.0 eq) were weight in 1.5 mL tubes and then dissolved in degassed mixture of ACN:H₂O (1:1,500 μL each). The compounds were added together, AcOH (10 μL) was added, and the reaction continued stirring

for 30 hours at 24 °C under argon atmosphere. The blue solution was filtered and purified by RP-HPLC (15-98-100% ACN/H₂O, 0.1% HCOOH, 220 nm, collect all.). Product containing fractions were lyophilized to yield **25** (2.995 mg, 0.001 mmol, 82%) as a beige solid. The compound eluted as a diastereomeric mixture in one peak from the HPLC, just one isomer is depicted here.

¹H-NMR (700 MHz, MeOH-d₄): δ = 8.83 (m, 3H), 8.68 (m, 6H), 8.23 (m, 1H), 7.73 (m, 2H), 7.63 (d, J = 12.94 Hz, 1H), 7.56 (m, 1H), 5.59 (t, J = 6.15 Hz, 2H), 5.46 (m, 2H), 5.06 (d, J = 9.97 Hz, 1H), 4.88 (m, 20H), 4.72 (m, 7H), 4.59 (m, 7H), 4.44 (m, 2H), 4.36 (d, J = 11.03 Hz, 4H), 4.26 (m, 9H), 4.15 (m, 1H), 4.07 (m, 2H), 3.63 (s, 9H), 3.60 (s, 9H), 3.52 (t, J = 7.43 Hz, 4H), 3.47 (bs, 3H), 3.43 (bs, 3H), 3.38 (d, J = 9.12 Hz, 1H), 3.34 (m, 2H), 3.20 (bs, 2H), 3.12 (m, 5H), 2.96 (m, 9H), 2.79 (m, 10H), 2.64 (m, 30H), 2.36 (m, 2H), 2.30 (d, J = 7.43 Hz, 3H), 2.26 (m, 6H), 2.14 (m, 2H), 1.41 (d, J = 4.88 Hz, 3H), 1.03 (d, J = 6.79 Hz, 3H).

HRMS (ESI) calculated for ([M+2H]²⁺): m/z = 994.4443; experimental = 994.4454.

Compound **XX**

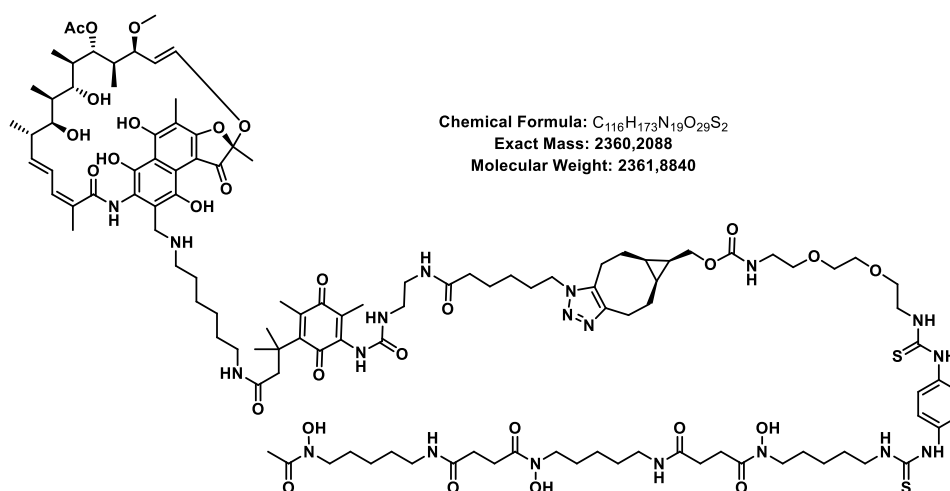


Alkyne **45** (5 mg, 0.003 mmol, 1.0 eq) and azide **63** (4.59 mg, 0.003 mmol, 1.0 eq) were weight in 1.5 mL tubes and then dissolved in degassed mixture of ACN:H₂O (1:1,500 μL each). The compounds were added together, AcOH (10 μL) was added, and the reaction continued stirring for 30 hours at 24 °C under argon atmosphere. The blue solution was filtered and purified by RP-HPLC (15-98-100% ACN/H₂O, 0.1% HCOOH, 220 nm, collect all.). Product containing fractions were lyophilized to yield **26** (7.49 mg, 0.003 mmol, 78%) as a beige solid. The compound eluted as a diastereomeric mixture in one peak from the HPLC, just one isomer is depicted here.

¹H-NMR (700 MHz, MeOH-d₄): δ = 7.48 (m, 3H), 7.34 (m, 6H), 6.88 (m, 1H), 6.38 (m, 1H), 6.28 (m, 1H), 6.21 (m, 1H), 4.26 (m, 1H), 4.11 (m, 1H), 3.71 (d, J = 10.40 Hz, 1H), 3.54 (m, 27H), 3.39 (m, 14H), 3.15 (m, 2H), 2.94 (m, 13H), 2.79 (m, 1H), 2.29 (s, 9H), 2.26 (s, 9H), 2.15 (t, J = 7.24 Hz, 3H), 2.09 (bs, 3H), 1.97 (m, 16H), 1.79 (m, 4H), 1.67 (m, 2H), 1.59 (m, 6H), 1.49 (m, 2H), 1.43 (m, 3H), 1.36 (m, 3H), 1.29 (bs, 10H), 1.01 (m, 2H), 0.95 (m, 3H), 0.91 (m, 5H), 0.05 (d, J = 5.20 Hz, 3H), -0.31 (d, J = 4.52 Hz, 3H).

HRMS (ESI) calculated for ($[M+2H]^{2+}$): m/z = 1435.6724; experimental = 1435.6733, calculated for ($[M+3H]^{3+}$): m/z = 957.4501; experimental = 957.4501.

Compound 29



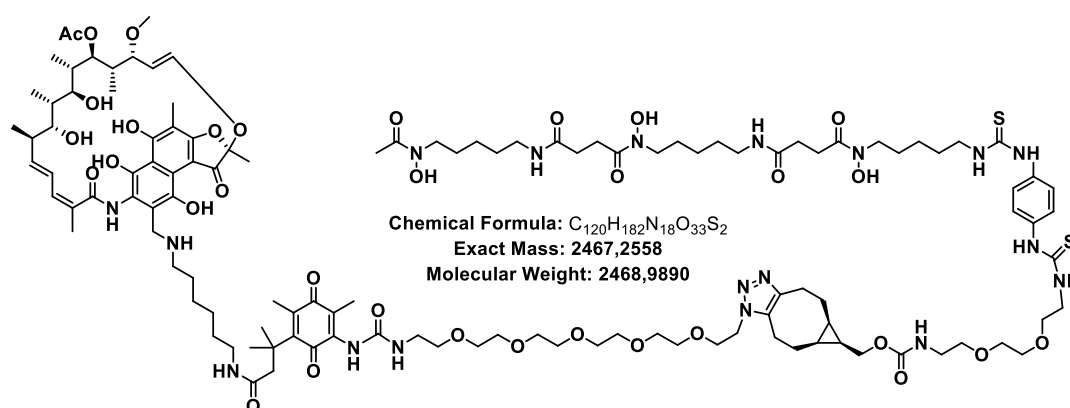
Azide **65** (12.3, 0.0096 mmol, 1.0 eq) and strained alkyne **47** (16.5 mg, 0.0153 mmol, 1.6 eq) were weighed in eppendorf tubes and then dissolved in degassed mixture of ACN:H₂O (1:1, 300 μ L each). The compounds were added together under argon atmosphere and continued stirring for 30 hours at 24 °C. The orange solution was filtered and purified by RP-HPLC (15-98-100% ACN/H₂O, 0.1% HCOOH, 220 nm, collect all.). Product containing fractions were lyophilized to yield **29** (19.85 mg, 0.008 mmol, 88%) as a beige solid. The compound eluted as a diastereomeric mixture in one peak from the HPLC, just one isomer is depicted here.

¹H-NMR (600 MHz, DMSO-d₆): δ = 9.64 (m, 5H), 9.44 (bs, 1H), 8.85 (d, J = 11.28 Hz, 1H), 8.30 (s, 1H), 7.78 (m, 4H), 7.68 (m, 4H), 7.35 (s, 4H), 7.20 (d, J = 5.77 Hz, 2H), 7.12 (m, 2H), 6.32 (d, J = 10.47 Hz, 1H), 6.25 (d, J = 12.75 Hz, 1H), 6.07 (dd, J = 8.19, 15.57 Hz, 1H), 5.07 (m, 2H), 4.90 (q, J = 7.79, 12.48 Hz, 1H), 4.19 (t, J = 6.58 Hz, 2H), 4.04 (m, 5H), 3.69 (m, 2H), 3.64 (m, 7H), 3.55 (m, 15H), 3.46 (m, 13H), 3.41 (m, 7H), 3.12 (q, J = 4.97, 10.87 Hz, 4H), 3.01 (m, 10H), 2.89 (s, 3H), 2.58 (m, 11H), 2.28 (m, 10H), 1.99 (s, 3H), 1.97 (s, 9H), 1.91 (s, 3H), 1.69 (m, 4H), 1.64 (s, 3H), 1.54 (m, 10H), 1.50 (m, 9H), 1.38 (m, 10H), 1.24 (m, 20H), 1.15 (m, 4H), 0.91 (m, 6H), 0.86 (m, 4H), 0.52 (d, J = 6.58 Hz, 3H), -0.33 (d, J = 6.31 Hz, 3H).

¹³C-NMR (151 MHz, DMSO-d₆): δ = 180.98, 180.76, 172.43, 172.23, 172.11, 171.77, 170.60, 169.84, 156.93, 149.46, 143.81, 143.54, 133.17, 126.93, 123.82, 109.19, 99.02, 76.82, 76.27, 73.67, 70.25, 70.00, 69.63, 69.06, 61.92, 56.07, 47.60, 47.55, 47.48, 47.25, 44.22, 44.04, 40.74, 35.66, 33.11, 30.37, 29.79, 29.48, 29.29, 29.01, 28.68, 28.04, 27.36, 26.59, 26.50, 26.28, 26.09, 25.84, 25.24, 24.07, 23.97, 22.60, 22.36, 21.72, 21.12, 20.82, 20.44, 20.26, 20.01, 19.63, 19.35, 19.05, 18.58, 17.77, 14.31, 14.22, 13.11, 12.81, 11.65, 9.44, 9.29, 7.84, 6.36, -12.68.

DEPT (151 MHz, DMSO-d₆): δ = 76.82, 73.67, 70.01, 69.63, 69.06, 61.92, 56.07, 47.60, 47.55, 47.48, 47.25, 44.21, 44.04, 38.90, 38.88, 38.73, 38.52, 38.29, 35.65, 30.37, 29.79, 29.43, 29.29, 28.68, 28.04, 27.36, 26.50, 26.09, 25.84, 25.24, 25.13, 24.06, 23.96, 22.60, 22.35, 21.71, 21.12, 20.86, 20.82, 20.26, 19.62, 19.05, 17.77, 14.31, 11.64, 9.44, 9.29, 7.83.

HRMS (ESI) calculated for ([M+2H]²⁺): m/z = 1181.1117; experimental = 1181.1126.

Compound **30**

Azide **64** (12.3, 0.0096 mmol, 1.0 eq) and strained alkyne **47** (16.5 mg, 0.0153 mmol, 1.6 eq) were weighed in 1.5 mL tubes and then dissolved in degassed mixture of ACN:H₂O (1:1, 300 μ L each). The compounds were added together under argon atmosphere and continued stirring for 30 hours at 24 °C. The orange solution was filtered and purified by RP-HPLC (15-98-100% ACN/H₂O, 0.1% HCOOH, 220 nm, collect all.). Product containing fractions were lyophilized to yield **30** (19.85 mg, 0.008 mmol, 88%) as a beige solid. The compound eluted as a diastereomeric mixture in one peak from the HPLC, just one isomer is depicted here.

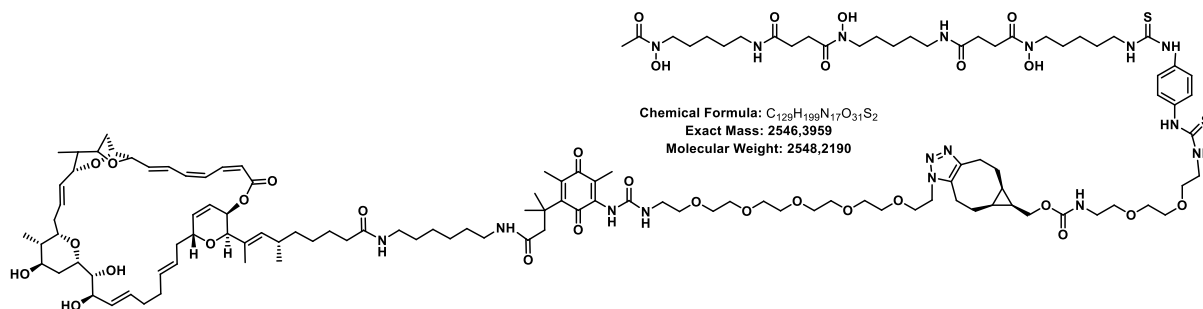
¹H NMR (600 MHz, DMSO-d₆): δ = 9.62 (m, 4H), 7.78 (m, 2H), 7.66 (m, 1H), 7.35 (q, J = 9.65, 12.06 Hz, 4H), 7.11 (m, 1H), 4.39 (t, J = 5.13 Hz, 1H), 4.05 (m, 2H), 3.73 (t, J = 6.03 Hz, 1H), 3.64 (m, 2H), 3.49 (m, 30H), 3.30 (s, 4H), 3.16 (m, 4H), 3.00 (q, J = 6.94, 13.87 Hz, 5H), 2.93 (m, 2H), 2.73 (m, 2H), 2.59 (m, 4H), 2.28 (m, 4H), 2.07 (n, 2H), 1.97 (m, 4H), 1.53 (m, 11H), 1.38 (m, 7H), 1.24 (m, 10H), 1.11 (m, 2H), 0.89 (m, 5H).

¹³C-NMR (151 MHz, DMSO-d₆): δ = 187.71, 180.98, 172.44, 171.77, 170.60, 156.92, 143.64, 134.25, 125.76, 123.84, 70.27, 70.23, 70.14, 70.08, 70.01, 69.83, 69.63, 69.06, 61.93, 47.64, 47.25, 44.24, 44.04, 42.06, 40.53, 40.41, 40.28, 40.14, 40.00, 39.86, 39.72, 39.58, 38.90, 38.88, 38.41, 30.37, 29.48, 29.29, 28.82, 28.69, 28.04, 26.60, 26.50, 25.83, 24.07, 23.97, 22.70, 22.56, 22.44, 21.76, 20.82, 19.66, 19.09, 17.78, 14.75, 14.47, 14.37, 13.48, 13.18, 1.62.

DEPT (151 MHz, DMSO-d₆): δ = 123.84, 70.27, 70.23, 70.14, 70.08, 70.01, 69.83, 69.63, 69.06, 61.93, 47.64, 47.55, 47.25, 45.63, 44.23, 44.04, 42.05, 38.90, 30.36, 29.28, 28.81, 28.68, 28.03, 26.59, 26.50, 25.83, 24.07, 23.96, 22.70, 22.44, 21.76, 20.82, 19.66, 19.09, 17.77, 14.47, 13.48, 13.18, 1.62.

HRMS (ESI) calculated for $([M+2H]^{2+})$: $m/z = 1234.6352$; experimental = 1234.6359.

Compound 33



Azide **67** (18.4 mg, 0.008 mmol, 1.0 eq) and strained alkyne **47** (26.7 mg, 0.011 mmol, 2.0 eq) were weighed in 1.5 mL tubes and then dissolved in degassed mixture of ACN/H₂O (1:1, 300 μ L each). The compounds were added together under argon atmosphere and continued stirring for 30 hours at 24 °C. The orange solution was filtered and purified by RP-HPLC (15-98-100% ACN/H₂O, 0.1% HCOOH, 220 nm, collect all.). Product containing fractions were lyophilized to yield **33** (21.58 mg, 0.009 mmol, 71%) as a yellow solid. The compound eluted as a diastereomeric mixture in one peak from the HPLC, just one isomer is depicted here.

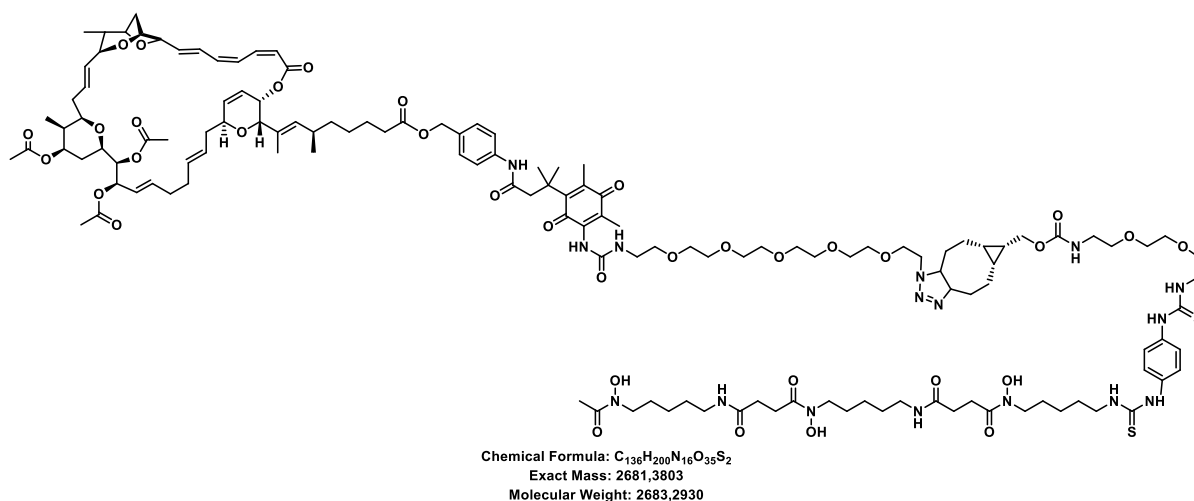
¹H-NMR (600 MHz, DMSO-d₆): $\delta = 9.60$ (m, 3H), 9.39 (bs, 1H), 8.11 (s, 1H), 7.85 (t, $J = 4.51$ Hz, 1H), 7.78 (t, $J = 4.51$ Hz, 1H), 7.65 (t, $J = 5.29$ Hz, 2H), 7.35 (d, $J = 4.51$ Hz, 4H), 7.11 (t, $J = 10.70$ Hz, 2H), 7.04 (t, $J = 11.99$ Hz, 1H), 6.92 (m, 1H), 6.81 (t, $J = 5.93$ Hz, 1H), 6.47 (10.83 Hz, 1H), 6.22 (dd, $J = 4.51, 15.34$ Hz, 1H), 6.14 (dd, $J = 2.97, 10.44$ Hz, 1H), 5.96 (m, 1H), 5.64 (d, $J = 11.86$ Hz, 1H), 5.51 (d, $J = 6.32$ Hz, 1H), 5.45 (m, 1H), 5.30 (m, 1H), 5.23 (m, 2H), 4.56 (d, $J = 2.71$, 1H), 4.50 (m, 1H), 4.43 (t, $J = 5.54$ Hz, 1H), 4.39 (t, $J = 5.29$ Hz, 2H), 4.18 (m, 2H), 4.05 (m, 2H), 3.95 (m, 1H), 3.73 (t, $J = 5.29$ Hz, 2H), 3.64 (m, 2H), 3.53 (m, 17H), 3.46 (m, 15H), 3.42 (q, $J = 5.54, 10.44$ Hz, 5H), 3.19 (q, $J = 5.93, 11.22$), 3.12 (q, $J = 5.29, 11.99$ Hz, 2H), 2.98 (m, 11H), 2.73 (m, 2H), 2.64 (m, 2H), 2.59 (q, $J = 6.70, 12.77$ Hz, 2H), 2.27 (m, 6H), 2.10 (m, 7H), 2.05 (s, 4H), 1.99 (m, 9H), 1.80 (d, $J = 11.60$ Hz, 1H), 1.77 (s, 3H), 1.54 (m, 12H), 1.38 (m, 5H), 1.35 (m, 12H), 1.22 (m, 14H), 1.12 (m, 5H), 0.92 (m, 2H), 0.78 (d, $J = 7.09$ Hz, 3H), 0.76 (d, $J = 7.09$ Hz, 3H), 0.71 (d, $J = 6.70$ Hz, 3H).

¹³C-NMR (151 MHz, DMSO-d₆): δ = 187.49, 186.60, 180.98, 180.77, 172.52, 172.44, 171.77, 171.21, 170.59, 165.66, 156.92, 154.20, 151.82, 143.64, 141.28, 138.09, 138.05, 137.28, 136.31, 135.45, 134.24, 132.70, 132.59, 132.34, 131.01, 130.80, 130.68, 130.01, 127.13, 125.85, 125.72, 125.05, 123.81, 122.84, 118.85, 80.48, 79.32, 78.91, 76.76, 75.60, 73.44, 73.18, 72.92, 72.63, 72.19, 70.27, 70.23, 70.15, 70.08, 70.01, 69.83, 69.64, 69.06, 68.91, 65.22, 61.93, 48.05, 47.64, 47.55, 47.25, 44.24, 44.04, 40.61, 38.99, 38.90, 38.88, 38.79, 38.74, 37.28, 37.23, 36.15, 36.04, 34.18, 33.04, 32.59, 31.56, 30.36, 30.19, 29.60, 29.49, 29.29, 29.05, 28.69, 28.04, 27.15, 27.03, 26.59, 26.50, 25.84, 24.07, 23.97, 22.71, 22.44, 21.76, 21.59, 21.24, 20.82, 19.66, 19.09, 17.78, 15.40, 15.23, 14.37, 14.26, 13.93, 12.78, 10.74, 10.68, 6.36.

DEPT (151 MHz, DMSO-d₆): δ = 138.09, 137.28, 136.31, 135.45, 132.70, 132.59, 132.34, 131.01, 130.80, 130.68, 127.13, 125.85, 125.05, 123.79, 122.84, 118.85, 80.48, 79.32, 78.91, 76.76, 75.60, 73.43, 73.18, 72.92, 72.63, 72.19, 70.27, 70.23, 70.14, 70.08, 70.01, 69.83, 69.63, 69.06, 68.91, 65.22, 61.93, 48.04, 47.64, 47.55, 47.25, 44.23, 44.04, 38.99, 38.90, 38.88, 38.79, 38.73, 37.28, 37.22, 36.15, 36.04, 34.18, 33.04, 32.59, 31.56, 30.36, 30.19, 29.60, 29.49, 29.29, 29.05, 28.68, 28.03, 27.03, 26.59, 26.50, 25.83, 24.07, 23.96, 22.71, 22.44, 21.76, 21.24, 20.82, 19.66, 19.09, 17.77, 15.23, 14.37, 13.93, 12.78, 10.73.

HRMS (ESI) calculated for ([M+3H]³⁺): m/z = 849.8059; experimental = 849.8066.

Compound 34



Azide **69** (14.3 mg, 0.005 mmol, 1.0 eq) and strained alkyne **47** (12.58 mg, 0.010 mmol, 2.0 eq) were weight in 1.5 mL tubes and then dissolved in degassed mixture of ACN:H₂O (1:1, 300 μ L each). The compounds were added together under argon atmosphere and continued

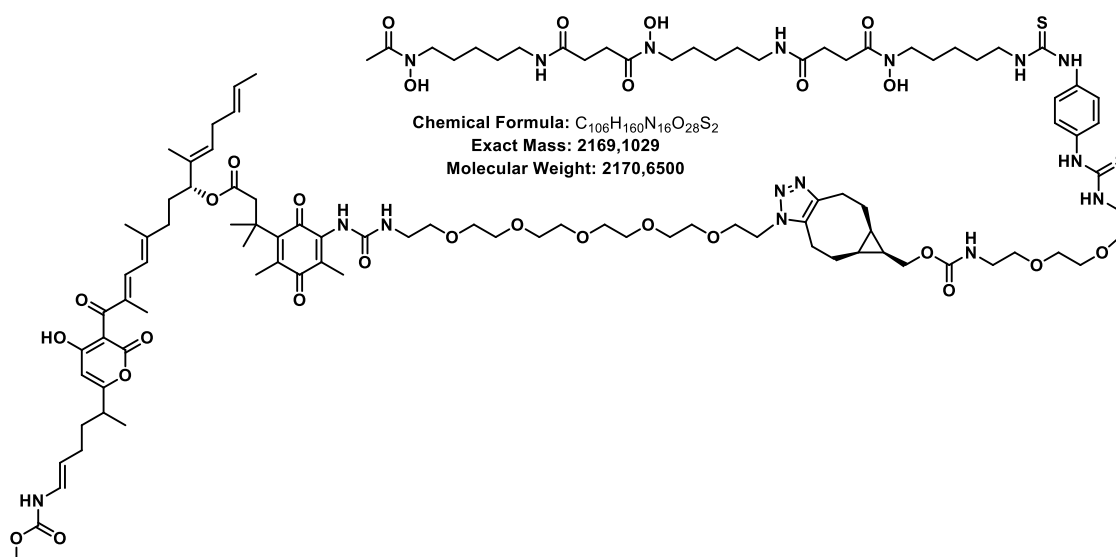
stirring for 30 hours at 24 °C. The orange solution was filtered and purified by RP-HPLC (15-98-100% ACN/H₂O, 0.1% HCOOH, 220 nm, collect all.). Product containing fractions were lyophilized to yield **34** (12.69 mg, 0.005 mmol, 95%) as a beige solid. The compound eluted as a diastereomeric mixture in one peak from the HPLC, just one isomer is depicted here.

¹H-NMR (600 MHz, DMSO-d₆): δ = 7.12 (t, J = 11.06, 1H), 7.03 (m, 1H), 6.92 (m, 1H), 6.48 (t, J = 11.06 Hz, 1H), 6.22 (m, 1H), 6.14 (dd, J = 3.43, 9.34 Hz, 1H), 5.97 (m, 1H), 5.63 (m, 2H), 5.52 (m, 1H), 5.44 (m, 3H), 5.33 (m, 2H), 5.25 (m, 3H), 5.20 (d, J = 9.92 Hz, 1H), 4.50 (m, 1H), 4.35 (m, 3H), 4.19 (m, 3H), 3.67 (m, 9H), 3.17 (s, 3H), 2.55 (s, 3H), 2.30 (m, 4H), 2.13 (m, 15H), 1.96 (10H), 1.80 (m, 2H), 1.55 (m, 8H), 1.41 (m, 10H), 1.27 (m, 4H), 1.17 (m, 5H), 1.07 (m, 2H), 0.78 (d, J = 6.67 Hz, 3H), 0.75 (d, J = 7.06 Hz, 3H), 0.71 (d, J = 7.25 Hz, 3H).

¹³C-NMR (151 MHz, DMSO-d₆): δ = 175.06, 175.00, 170.25, 169.79, 165.69, 165.64, 138.17, 137.23, 136.33, 135.59, 135.44, 135.25, 132.58, 132.45, 132.41, 132.36, 130.21, 130.07, 129.50, 127.47, 127.33, 125.99, 125.16, 125.05, 124.84, 122.94, 122.79, 118.94, 118.82, 80.46, 80.39, 79.41, 79.33, 79.03, 78.91, 77.73, 75.83, 75.76, 75.58, 73.87, 73.37, 73.27, 73.00, 72.60, 72.49, 71.41, 70.53, 68.69, 68.41, 66.82, 65.28, 65.18, 49.06, 40.91, 38.92, 37.36, 37.29, 37.03, 36.82, 35.97, 34.29, 34.04, 33.11, 32.88, 32.45, 31.64, 31.46, 30.98, 27.00, 26.91, 25.07, 24.96, 21.65, 21.42, 21.28, 21.26, 15.23, 15.20, 14.43, 14.02, 13.89, 10.69, 10.62.

DEPT (151 MHz, DMSO-d₆): δ = 137.43, 136.56, 136.50, 135.60, 134.85, 134.71, 134.52, 131.81, 131.71, 131.68, 131.63, 129.59, 129.47, 128.76, 126.73, 126.59, 125.25, 124.99, 124.43, 124.31, 124.10, 122.20, 122.05, 118.23, 118.20, 118.08, 79.74, 79.71, 78.69, 78.60, 78.30, 77.01, 75.10, 75.04, 73.14, 72.65, 72.54, 72.36, 72.30, 72.27, 71.88, 71.77, 71.74, 70.68, 69.80, 67.97, 67.68, 64.55, 64.46, 48.33, 40.17, 38.19, 36.63, 36.55, 36.29, 36.08, 35.23, 33.56, 33.37, 33.31, 32.38, 32.15, 31.71, 30.91, 30.72, 30.25, 28.99, 26.27, 26.18, 24.33, 24.23, 20.92, 20.69, 20.54, 20.52, 14.49, 14.46, 13.29, 13.16, 9.96, 9.88.

HRMS (ESI) calculated for ([M+3H]³⁺): m/z = 894.8007; experimental = 894.8029.

Compound **36**

Azide **70** (10.60 mg, 0.004 mmol, 1.0 eq) and strained alkyne **47** (9.33 mg, 0.008 mmol, 2.0 eq) were weighed in 1.5 mL tubes and then dissolved in degassed mixture of ACN:H₂O (1:1, 300 μ L each). The compounds were added together under argon atmosphere and continued stirring for 30 hours at 24 °C. The orange solution was filtered and purified by RP-HPLC (15-98-100% ACN/H₂O, 0.1% HCOOH, 220 nm, collect all.). Product containing fractions were lyophilized to yield **36** (6.54 mg, 0.003 mmol, 79%) as a beige solid. The compound eluted as a diastereomeric mixture in one peak from the HPLC, just one isomer is depicted here.

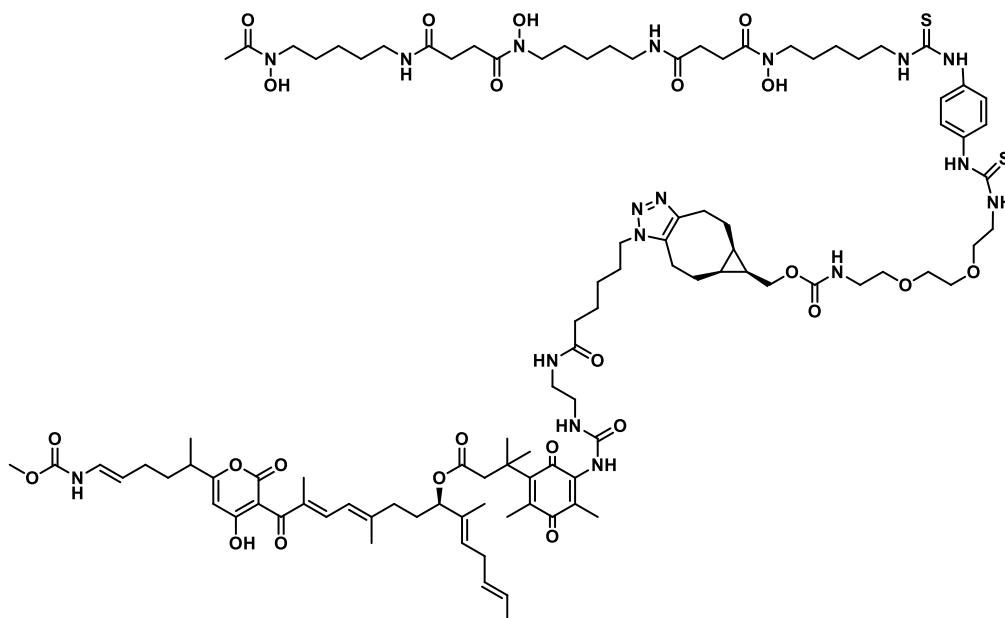
¹H-NMR (600 MHz, DMSO-d₆): δ = 9.62 (m, 5H), 9.39 (m, 1H), 9.21 (d, J = 10.47 Hz, 1H), 7.78 (m, 2H), 7.65 (m, 2H), 7.34 (d, J = 4.79 Hz, 4H), 7.11 (t, J = 5.08 Hz, 1H), 6.73 (m, 1H), 6.34 (m, 1H), 5.35 (m, 2H), 5.12 (t, J = 7.48 Hz, 1H), 5.02 (m, 1H), 4.39 (t, J = 5.08 Hz, 2H), 4.04 (m, 3H), 3.73 (t, J = 5.68 Hz, 2H), 3.64 (m, 3H), 3.56 (m, 21H), 3.46 (m, 25H), 3.22 (m, 3H), 3.13 (q, J = 6.13, 11.22 Hz, 3H), 3.01 (q, J = 6.58, 13.01 Hz, 6H), 2.71 (m, 5H), 2.59 (q, J = 7.33, 12.41 Hz, 4H), 2.27 (q, J = 6.43, 10.77 Hz, 4H), 2.05 (s, 3H), 1.97 (s, 3H), 1.76 (s, 3H), 1.60 (m, 10H), 1.53 (m, 20H), 1.38 (m, 9H), 1.23 (m, 8H), 1.11 (m, 5H), 0.92 (m, 2H).

$^{13}\text{C-NMR}$ (151 MHz, DMSO- d_6): δ = 180.51, 180.28, 171.96, 171.29, 170.12, 168.70, 156.44, 154.17, 143.16, 133.77, 129.94, 129.88, 129.78, 124.86, 124.65, 124.54, 124.31, 123.34, 108.89, 82.69, 75.71, 69.79, 69.75, 69.67, 69.60, 69.53, 69.36, 69.16, 68.58, 67.18, 61.45, 51.63, 47.17, 47.08, 46.77, 43.76, 43.56, 38.42, 38.40, 38.13, 36.80, 36.62, 36.45, 34.21, 30.02, 29.96, 29.89, 28.81, 28.64, 28.57, 28.21, 27.99, 27.56, 26.89, 26.72, 26.64, 26.12, 26.02, 25.35, 24.14, 23.60, 23.49, 23.11, 22.23, 21.97, 21.28, 20.34, 19.18, 18.78, 18.61, 17.90, 17.69, 17.64, 17.30, 13.75, 13.68, 12.28, 5.88.

DEPT (151 MHz, DMSO): δ = 130.42, 130.35, 130.25, 125.34, 125.21, 125.13, 125.02, 123.82, 109.20, 76.19, 70.27, 70.23, 70.14, 70.08, 70.01, 69.83, 69.63, 69.06, 67.65, 61.93, 52.11, 47.64, 47.55, 47.25, 44.24, 44.04, 40.53, 40.39, 40.25, 40.15, 40.11, 40.01, 39.97, 39.87, 39.84, 39.72, 39.70, 39.27, 38.90, 38.88, 38.60, 37.10, 34.68, 33.79, 30.36, 29.29, 29.12, 28.69, 28.03, 27.36, 27.12, 26.60, 26.50, 25.83, 24.61, 24.07, 23.96, 22.70, 22.44, 21.76, 20.82, 19.66, 19.09, 18.38, 18.17, 18.12, 17.77, 14.23, 14.15.

HRMS (ESI) calculated for ($[M+2H]^{2+}$): m/z = 1085.5587; experimental = 1085599.

Compound 37



Chemical Formula: $\text{C}_{102}\text{H}_{151}\text{N}_{17}\text{O}_{24}\text{S}_2$
 Exact Mass: 2062,0559
 Molecular Weight: 2063,5450

Strained alkyne **47** (10 mg, 9 μmol , 1 eq) and azide **71** (9 mg, 9 μmol , 1 eq) were added together and dissolved under Argon atmosphere in a 1:1 mixture of ACN and milliQ water (10

mL in total). The reaction was stirred overnight at 23 °C and the reaction progress was checked by LCMS. The solution obtained a less intense blue color upon full conversion, possibly due to quenching effects of the quinone moiety. The solvent was removed by rotary evaporation and the residue was dissolved in a mixture of ACN:MeOH:DMSO (5 mL) and purified by RP-HPLC (15-85% then 100%, 220 nm, collect all). The product containing fractions be found by LCMS and the product was lyophilized to dryness to yield **37** (5.45 mg, 0.005 mmol, 49%) as a slightly beige solid. The compound eluted as a diastereomeric mixture in one peak from the HPLC, just one isomer is depicted here.

¹H-NMR (700 MHz, DMSO-d₆): δ = 9.59 (m, 4H), 9.35 (m, 1H), 7.84 (m, 1H), 7.77 (m, 2H), 7.67 (m, 2H), 7.34 (q, J = 7.94, 12.15 Hz, 4H), 7.11 (m, 1H), 4.18 (t, J = 6.78 Hz, 2H), 4.04 (m, 2H), 3.63 (m, 3H), 3.54 (m, 8H), 3.45-3.40 (m, 12H), 3.29 (s, 2H), 3.12 (q, J = 6.09, 11.45 Hz, 2H), 3.06 (bs, 2H), 2.99 (q, J = 6.07, 12.15 Hz, 6H), 2.93 (m, 5H), 2.88 (s, 1H), 2.74 (m, 1H), 2.67 (m, 1H), 2.58 (q, J = 8.18, 14.25 Hz, 4H), 2.27 (q, J = 7.24, 12.85 Hz, 4H), 2.01 (m, 7H), 1.96 (s, 4H), 1.76 (s, 1H), 1.68 (m, 3H), 1.64 (bs, 1H), 1.52 (m, 15H), 1.38 (m, 5H), 1.33 (m, 3H), 1.22 (m, 10H), 0.88 (m, 7H).

¹³C-NMR (176 MHz, DMSO-d₆): δ = 180.49, 171.94, 171.28, 170.10, 156.43, 143.32, 132.67, 123.29, 69.51, 69.14, 68.57, 61.42, 55.60, 47.05, 46.97, 46.75, 43.55, 40.00, 38.40, 38.38, 38.24, 35.19, 29.87, 29.30, 28.79, 28.52, 28.19, 27.54, 26.10, 26.00, 25.60, 25.35, 24.74, 24.64, 23.58, 23.47, 22.11, 22.03, 21.85, 21.20, 20.63, 20.33, 19.13, 18.55, 18.17, 17.27, 13.89, 8.94, 8.75, 7.32.

Biology figures and tables

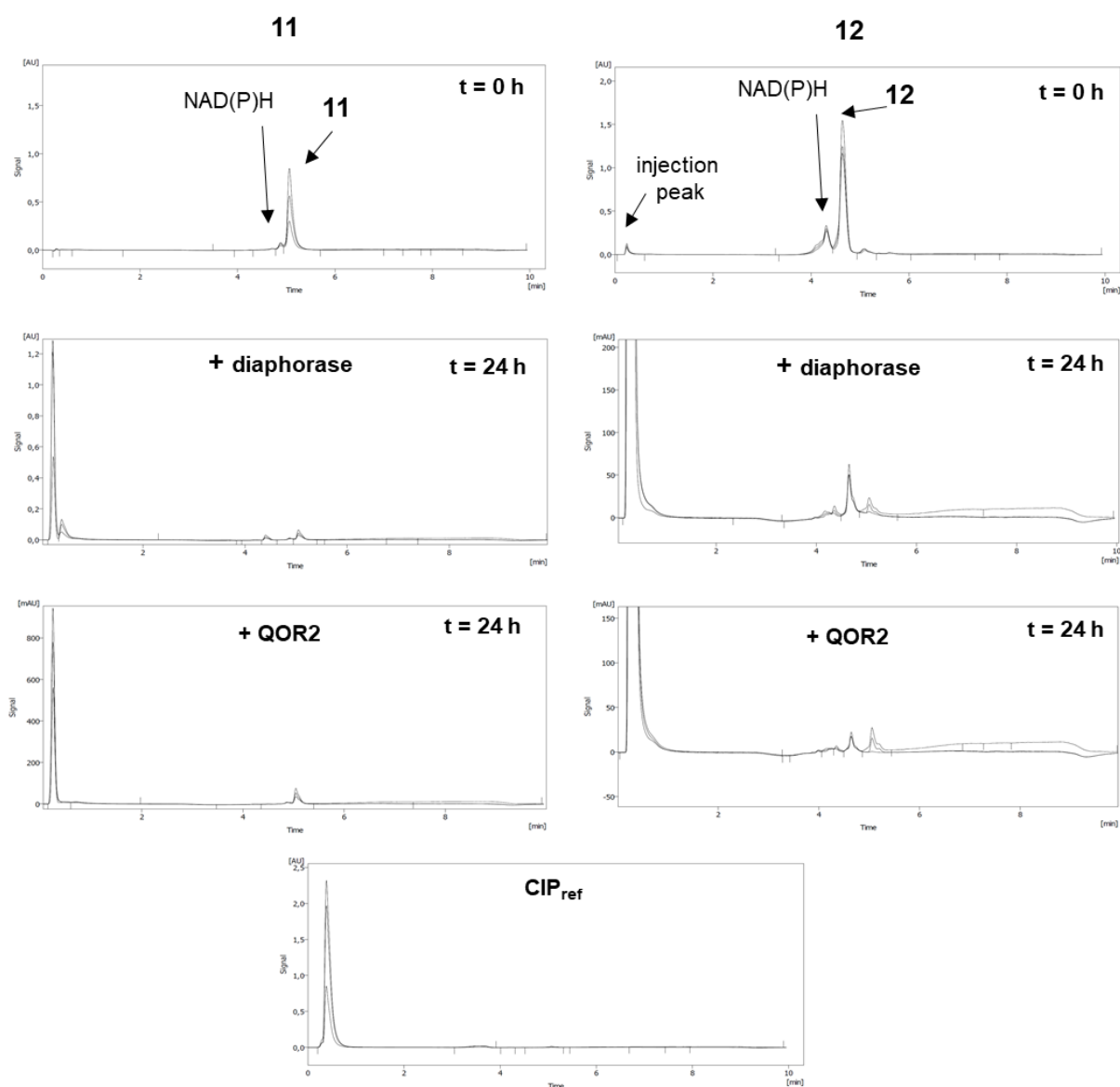
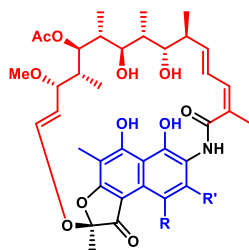


Figure S9.16. Enzymatic cleavage of DFO TML ciprofloxacin conjugate **12** and DOTAM TML ciprofloxacin conjugate **11**. (Left) Analytical HPLC runs from compound **12** at $t = 0$ and 24 h for QOR2 or diaphorase addition. (Right) Analytical HPLC runs from compound **11** at $t = 0$ and 24 h for QOR2 or diaphorase addition. (Bottom) Ciprofloxacin reference injection, all injections in MeOH/ACN/H₂O.

Table S9.1. MIC values of published rifamycin derivatives, with a general structure of the rifamycin macrolide core (red = ansa-bridge, blue = aromatic core) above of the table.^{6, 7, 8, 9}



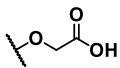
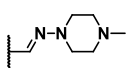
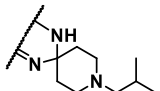
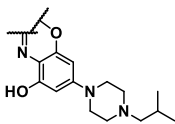
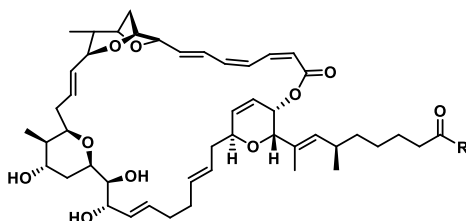
Name	R	R'	MIC <i>S. aureus</i> (µg/mL)	MIC <i>E. coli</i> (µg/mL)
rifamycin SV	OH	H	0.032	8-32
rifamycin B		H	≤0.2-0.08	≥16-32
rifampicin	OH		≤0.01-0.1	4-16
rifabutin			≤0.05	≥25
rifalazil			0.002-0.005	≥8-16

Table S9.2. MIC values of published sorangicin A amide derivatives, adapted from Jansen et al, with a general structure of sorangicin A above the table.¹⁰



Name	R ¹	MIC <i>S aureus</i> (µg/mL)	MIC <i>E. coli</i> (µg/mL)
Sorangicin A	OH	0.016-0.031	6-12
Amide	NH ₂	0.125	-
N-methylamide	NHMe	0.062	-
N-dimethylamide	N(Me) ₂	0.016	25
N-isopropylamide	N(iPr) ₂	0.060	50
N-hexylamide	NH(CH ₂) ₅ CH ₃	1	1000
N-benzylamide	NHBn	0.065-0.125	-
N-methoxyamide	NHOMe	0.008-0.016	25
N-methoxy-N-methylamide	NMe(OMe)	0.000125	>200

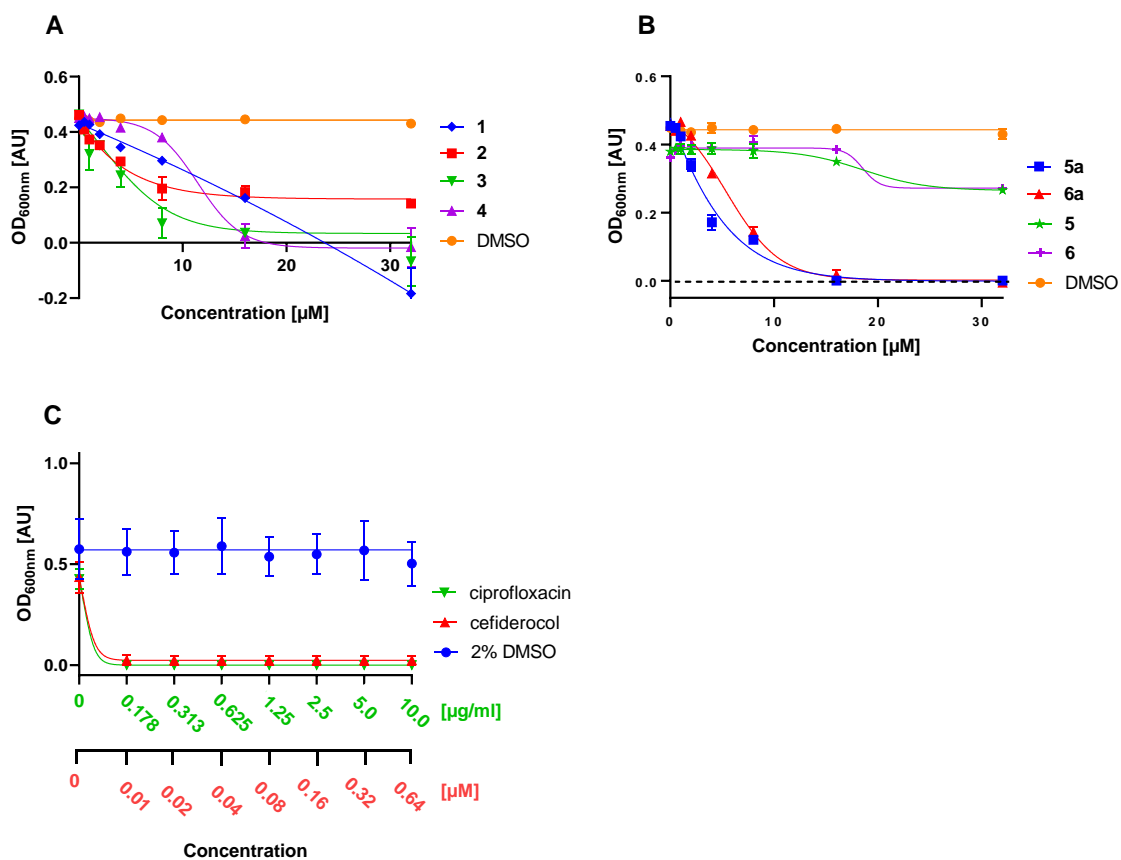


Figure S9.17. Antimicrobial activity of rifamycin conjugates **1** to **6** in MDR *E. coli* in iron-depleted, cation-adjusted medium (IDCAM), over 18 hours at 37 °C, error bars correspond to ± standard error of mean (SEM), n=2.

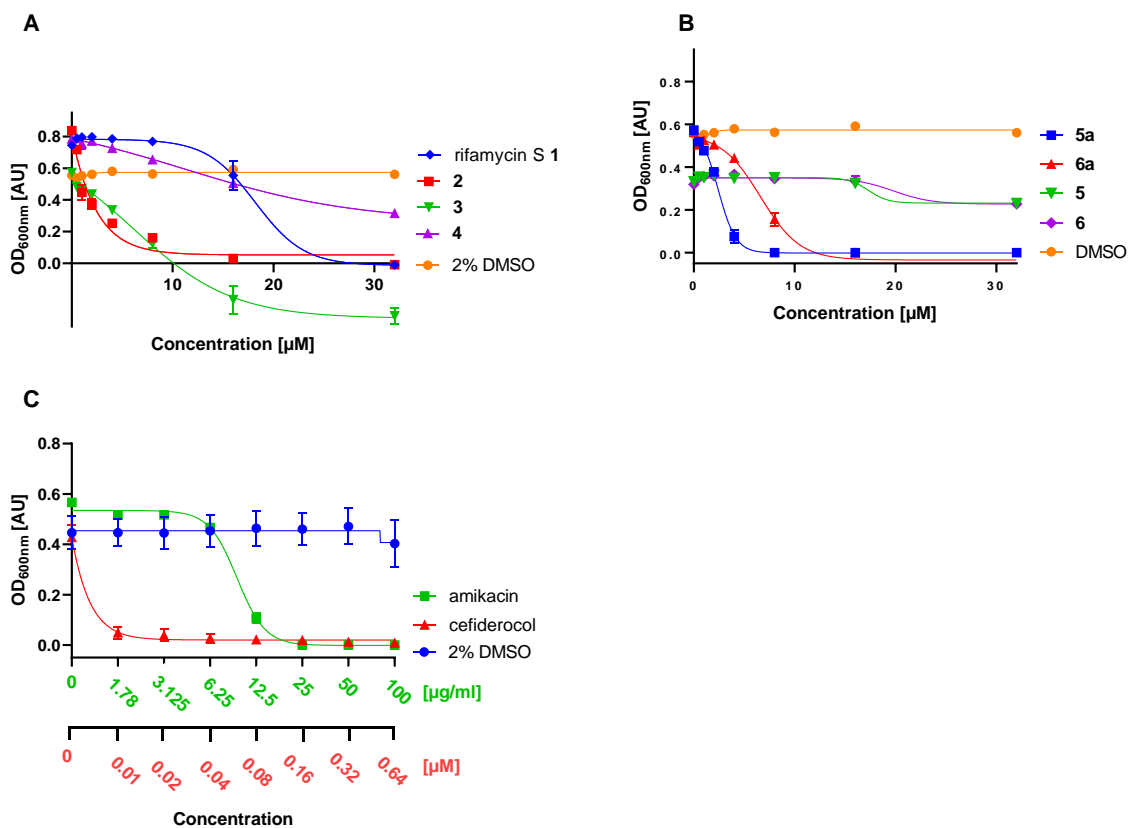


Figure S9.18. Antimicrobial activity of rifamycin conjugates **1** to **6** in MDR *P. aeruginosa* in iron-depleted, cation-adjusted medium (IDCAM), over 18 hours at 37 °C, error bars correspond to \pm standard error of mean (SEM), n = 2.

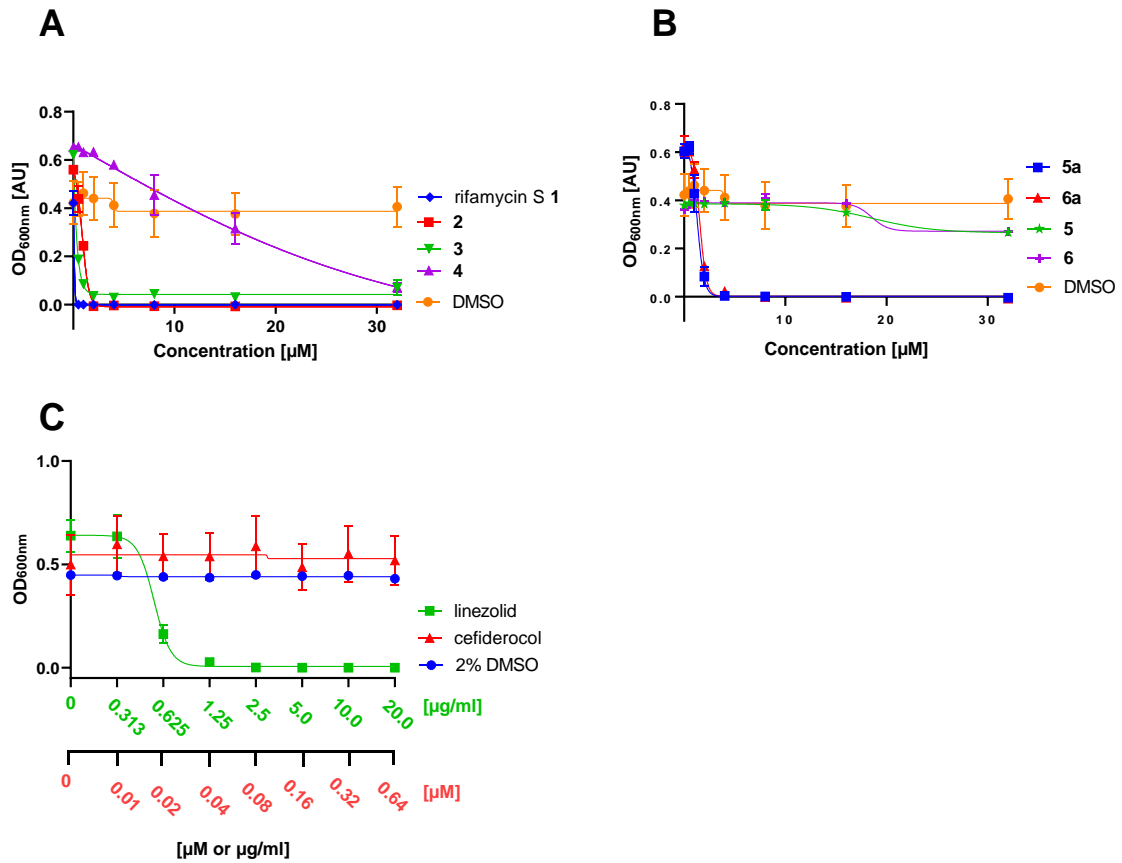


Figure S9.19. Antimicrobial activity of rifamycin conjugates **1** to **6** in MDR *S. aureus* in iron-depleted, cation-adjusted medium (IDCAM), over 18 hours at 37 °C, error bars correspond to \pm standard error of mean (SEM), $n = 2$.

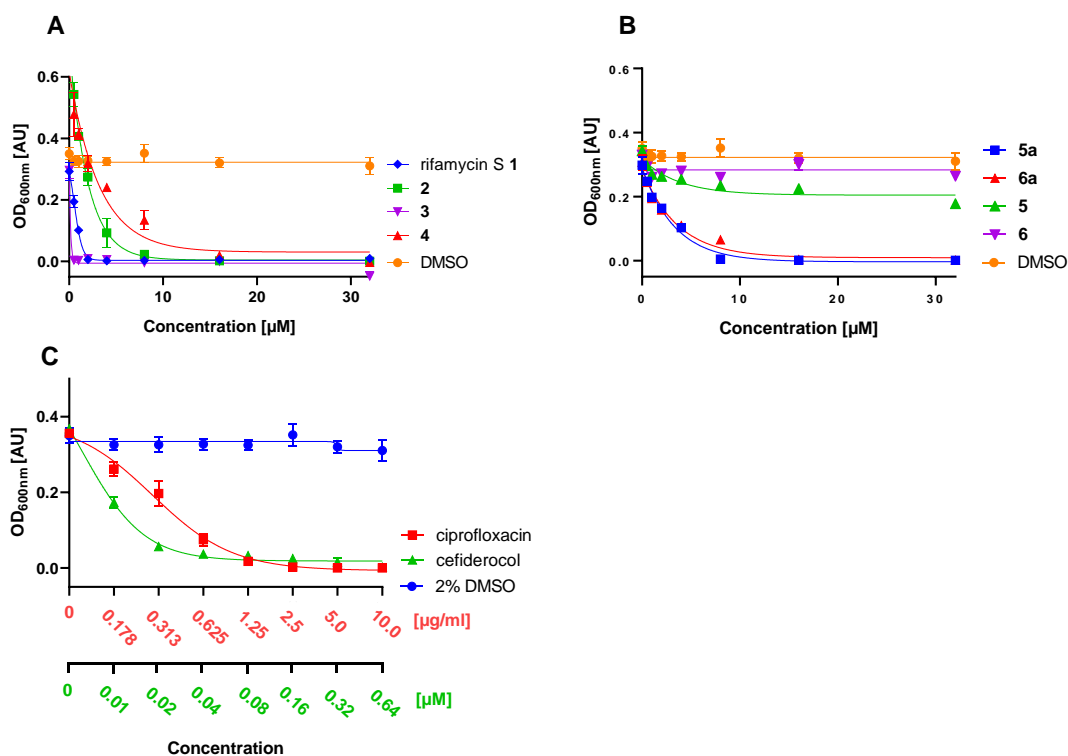


Figure S9.20. Antimicrobial activity of rifamycin conjugates **1** to **6** in MDR *A. baumannii* (DSM30007) in iron-depleted, cation-adjusted medium (IDCAM), over 18 hours at 37 °C, error bars correspond to ± standard error of mean (SEM), n = 2.

Table S9.3. MIC values^a for compounds **1** to **6** in four bacterial strains.

Compound	<i>E. coli</i>	<i>P. aeruginosa</i>	<i>S. aureus</i>	<i>A. baumannii</i>
rifamycin S 1	25	32	≤0.5	2
2	>32	12	2	16
3	16	10	2	0.5
4	20	>32	32	16
formyl rif. SV 27	8	16	≤0.5	-
5a	16	8	4	16
5	>32	>32	>32	>32
6a	16	16	4	16
6	>32	>32	>32	>32
cefiderocol	0.01	0.01	>0.64	0.625
ciprofloxacin	0.538	-	-	3.78
amikacin	-	23.4	-	-
linezolid	-	-	3.71	-

^a values are given in [µM]

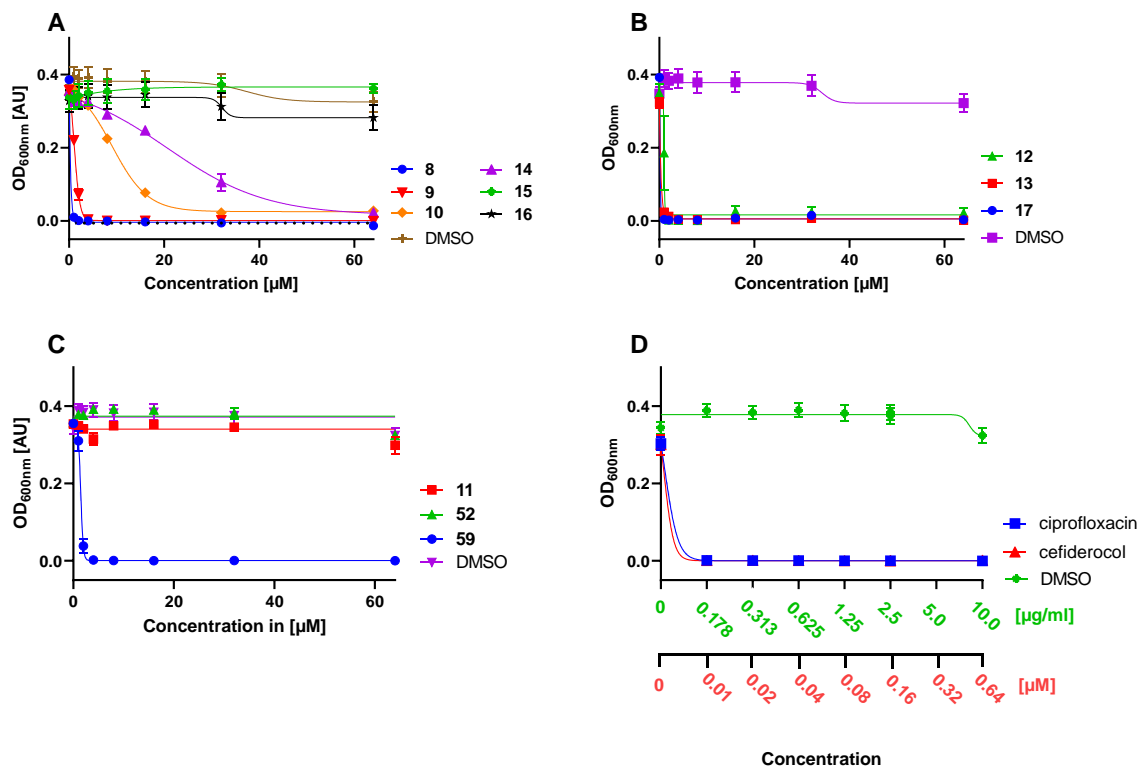


Figure S9.21. Antimicrobial activity of cleavable ciprofloxacin conjugates **8** to **16** in MDR *E. coli*. (A) ciprofloxacin TML / *para*-nitro TA catechol conjugates **8-10**, **13-15**, (B) ciprofloxacin TML / *para*-nitro TA DFO conjugates, (C) ciprofloxacin TML DOTAM with methylated catechols **17**, TML linker **52** and ciprofloxacin TML intermediate **59**, (D) antibiotic controls, in iron-depleted, cation-adjusted medium (IDCAM), over 18 hours at 37 °C, error bars correspond to \pm standard error of mean (SEM), $n = 2-4$.

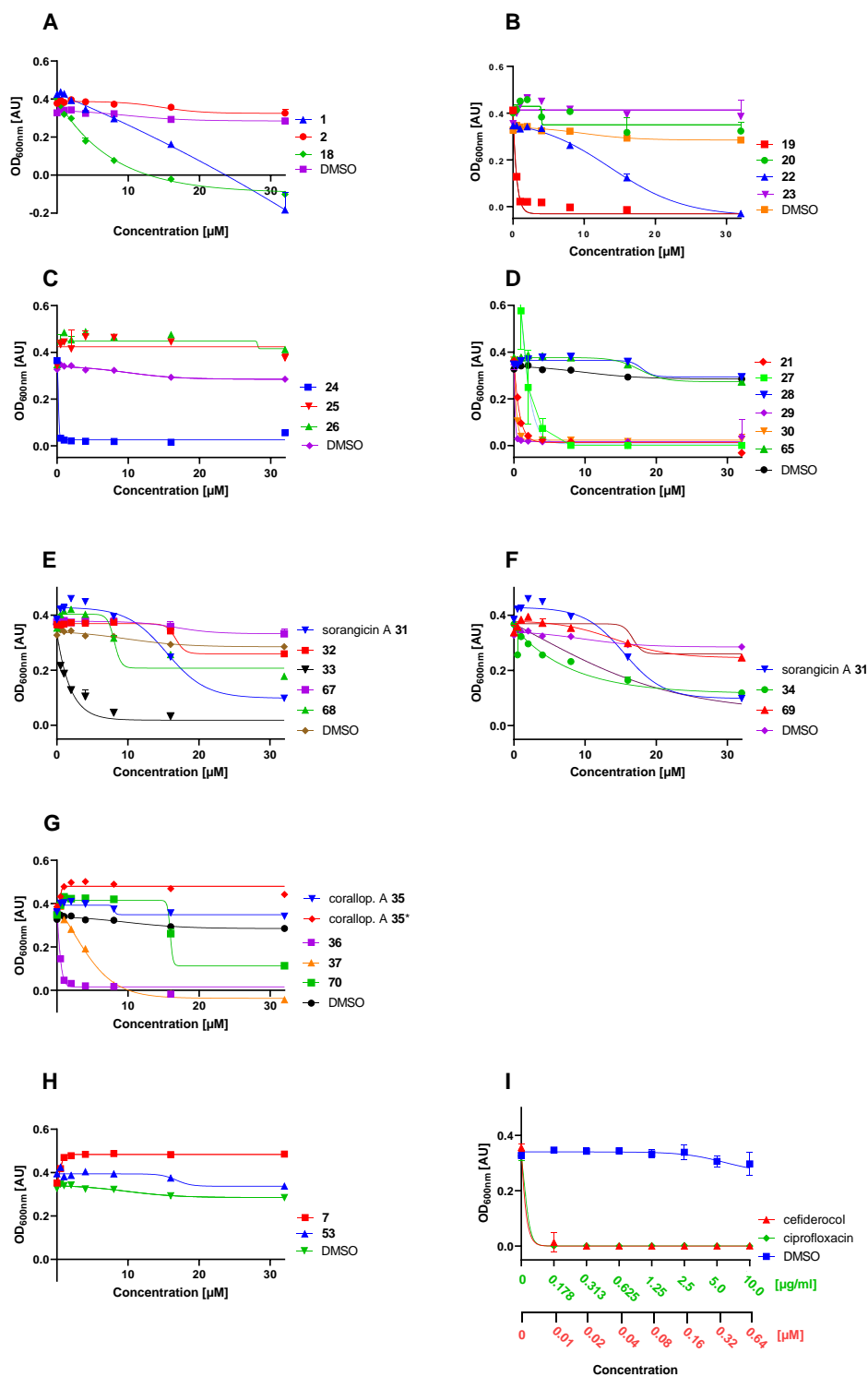


Figure S9.22. Antimicrobial activity of cleavable conjugates and control substances in MDR *E. coli*. (A-C) fluoro rifamycin compounds, (D) formyl rifamycin compounds, (E-F) sorangicin A compounds and (G) corallopyronin A compounds, (H) siderophore **7** and TML linker **53**, (I) control antibiotics cefiderocol and ciprofloxacin, in iron-depleted, cation-adjusted medium (IDCAM) over 18 hours at 37 °C, error bars correspond to \pm standard error of mean (SEM), $n = 2$, corallop. A* = corallopyronin A without exposure to basic conditions, corallop. A = reisolated from basic reaction conditions.

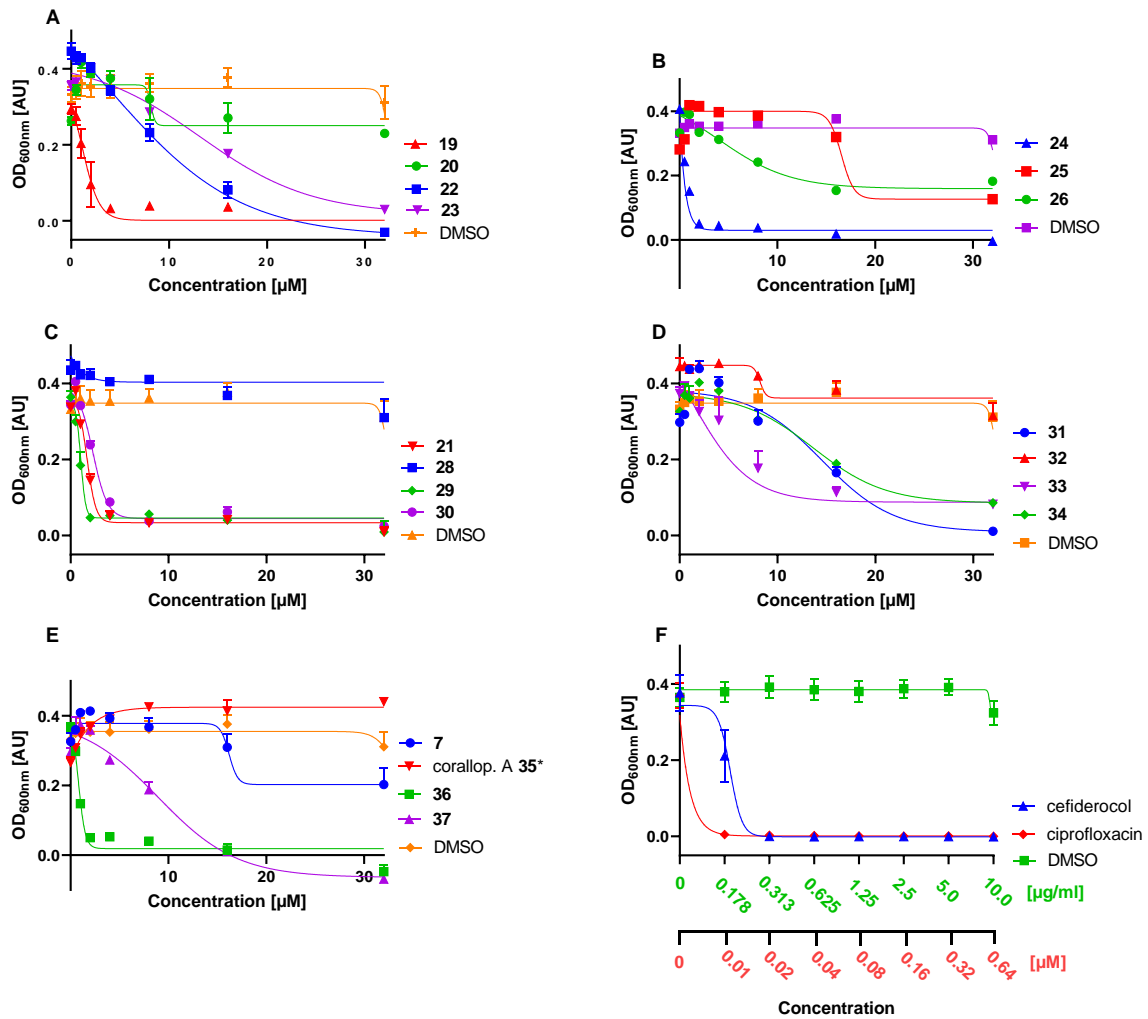


Figure S9.23. Antimicrobial activity of cleavable conjugates and control substances in siderophore-deficient *E. coli* $\Delta entA$ (A-B) fluoro rifamycin S compounds, (C) formyl rifamycin SV compounds, (D) sorangicin A compounds and (E) corallopyronin A compounds and controls, (F) control antibiotics cefiderocol and ciprofloxacin, in iron-depleted, cation-adjusted medium (IDCAM) over 18 hours at 37 °C, error bars correspond to \pm standard error of mean (SEM), n = 2 corallop. A* = corallopyronin A without exposure to basic conditions.

Table S9.4. MIC values^a for 18 to 37 and controls in MDR *E. coli* and *E. coli* Δ entA.

Compound	Chelator	Effector	<i>E. coli</i>	<i>E. coli</i> Δ entA
1	-	RifS	25	-
2	-	RifS	>32	>32
7	DOTAM	-	>32	>32
18	DFO	RifS	13	-
19	DFO	RifS	8	4
20	DFO-Ga	RifS	>32	>32
21	DFO	CHO-RifSV	4	-
22	-	RifS	>32	32
23	DOTAM	RifS	>32	32
24	DFO	RifS	1	4
25	DOTAM	RifS	>32	>32
26	DOTAM	RifS	>32	>32
27	-	RifS	8	-
28	-	CHO-RifSV	>32	>32
29	DFO	CHO-RifSV	1	2
30	DFO	CHO-RifSV	2	8
31	-	SorA	>32	32
32	-	SorA	>32	>32
33	DFO	SorA	16	>32
34	DFO	SorA	>32	>32
35	-	CorA	>32	-
35*	-	CorA	>32	>32
36	DFO	CorA	2	2
37	DFO	CorA	10	16
53	-	-	>32	-
65	-	CHO-RifSV	>32	-
67	-	SorA	>32	-
68	-	SorA	>32	-
69	-	SorA	>32	-
70	-	CorA	>32	-
cefiderocol			0.178	0.313
ciprofloxacin			0.538	0.538
amikacin			-	-
linezolid			-	-

a [μ M] for test compounds and cefiderocol, [μ g/mL] for ciprofloxacin, amikacin, linezolid, DFO = desferrioxamine, RifS=rifamycin S, CHO-RifSV=3-formyl rifamycin SV, SorA=sorangicin A, CorA=corallopyronin A, * = MIC f. CorA w/o base exposition, GE = growth enhancing.

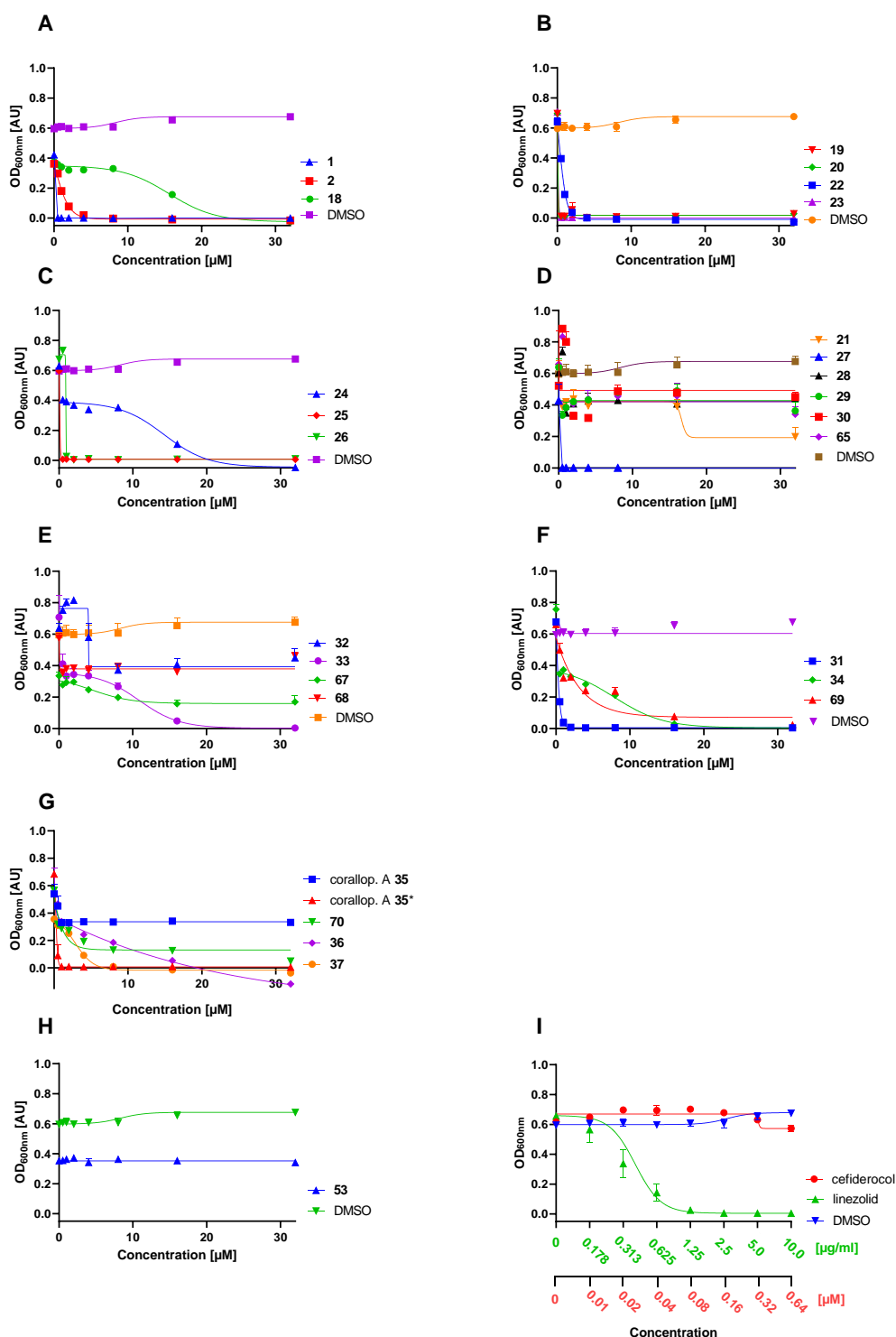


Figure S9.24. Antimicrobial activity of cleavable conjugates and control substances in MDR *S. aureus* (A-C) fluoro rifamycin S compounds, (D) 3-formyl rifamycin SV compounds, (E-F) sorangicin A compounds and (G) corallopyronin A compounds, (H) control linker **53**, (I) control antibiotics cefiderocol and ciprofloxacin, in iron-depleted, cation-adjusted medium (IDCAM) over 18 hours at 37 °C, error bars correspond to \pm standard error of mean (SEM), $n = 2$, corallop. A* = corallopyronin A without exposure to basic conditions, corallop. A = corallopyronin A exposure to basic conditions.

Table S9.5. MIC values^a for 18 to 37 and controls in MDR *S. aureus*.

Compound	Chelator	Effector	<i>S. aureus</i>
1	-	RifS	≤0.5
2	-	RifS	4
7	DOTAM	-	-
18	DFO	RifS	32
19	DFO	RifS	1
20	DFO-Ga	RifS	1
21	DFO	CHO-RifSV	>32
22	-	RifS	4
23	DOTAM	RifS	1
24	DFO	RifS	32
25	DOTAM	RifS	1
26	DOTAM	RifS	2
27	-	CHO-RifSV	≤0.5
28	-	CHO-RifSV	>32
29	DFO	CHO-RifSV	>32
30	DFO	CHO-RifSV	>32
31	-	SorA	2
32	-	SorA	>32
33	DFO	SorA	32
34	DFO	SorA	22
35	-	CorA	>35
35*	-	CorA	2
36	DFO	CorA	20
37	DFO	CorA	8
53	-	-	>32
65	-	CHO-RifSV	>32
67	-	SorA	>32
68	-	SorA	>32
69	-	SorA	≥32
70	-	CorA	>32
cefiderocol			>0.64
ciprofloxacin			-
amikacin			-
linezolid			3.71

^a [μM] for test compounds and cefiderocol, [μg/mL] for ciprofloxacin, amikacin, linezolid, DFO = desferrioxamine, RifS=rifamycin S, CHO-RifSV=3-formyl rifamycin SV, SorA=sorangicin A, CorA=corallopyronin A, * = MIC f. CorA w/o base exposition, GE = growth enhancing.

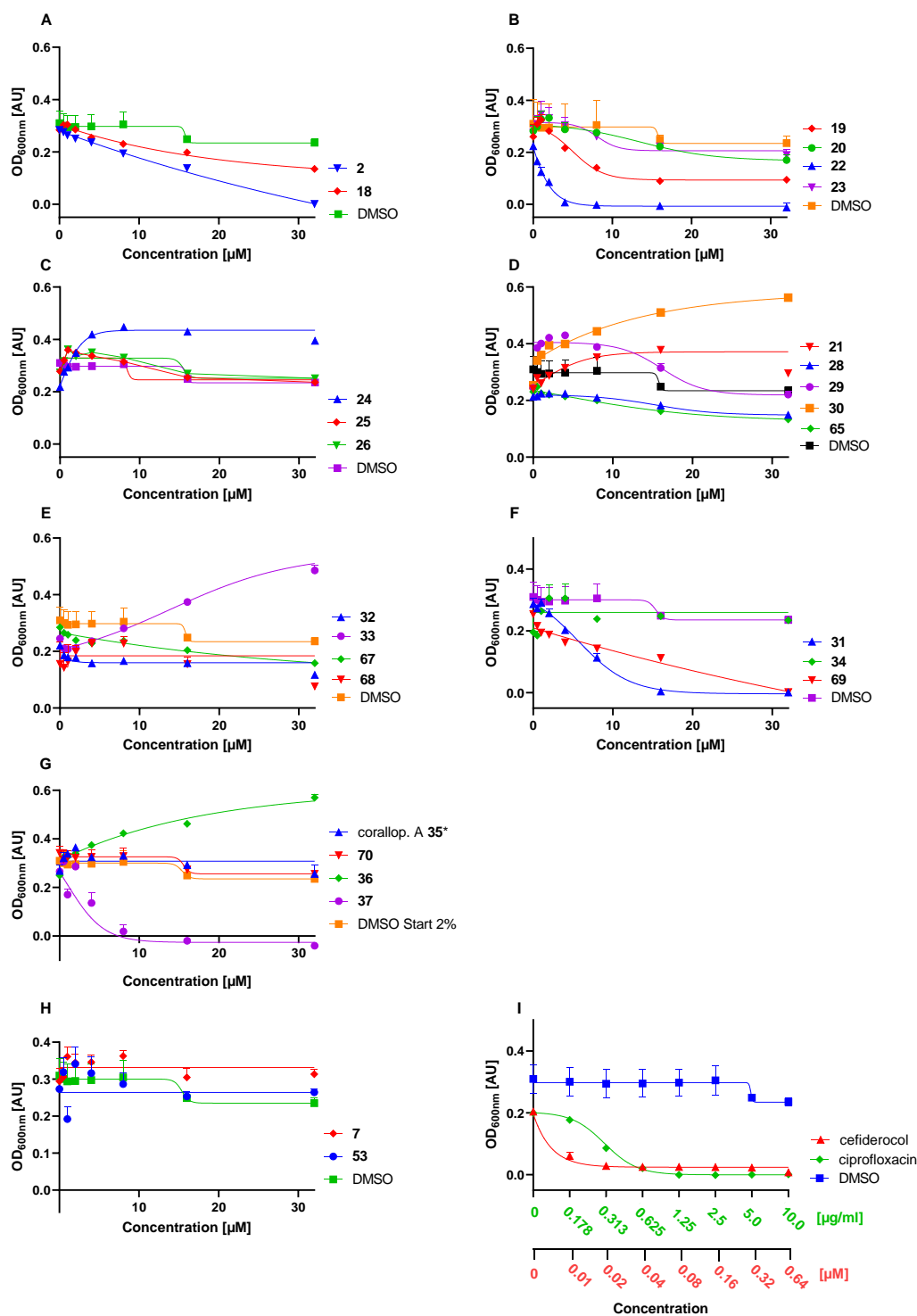


Figure S9.25. Antimicrobial activity of cleavable conjugates and control substances in MDR *A. baumannii* (DSM30007). (A-C) fluoro rifamycin S compounds, (D) formyl rifamycin SV compounds, (E-F) sorangicin A compounds and (G) corallopyronin A compounds, (H) control linker **53** and siderophore **7**, (I) control antibiotics cefiderocol and ciprofloxacin, in iron-depleted, cation-adjusted medium (IDCAM) over 18 hours at 37 °C, error bars correspond to ± standard error of mean (SEM), n = 2, corallop. A* = corallopyronin A without exposure to basic conditions, corallop. A = reisolated from basic reaction conditions.

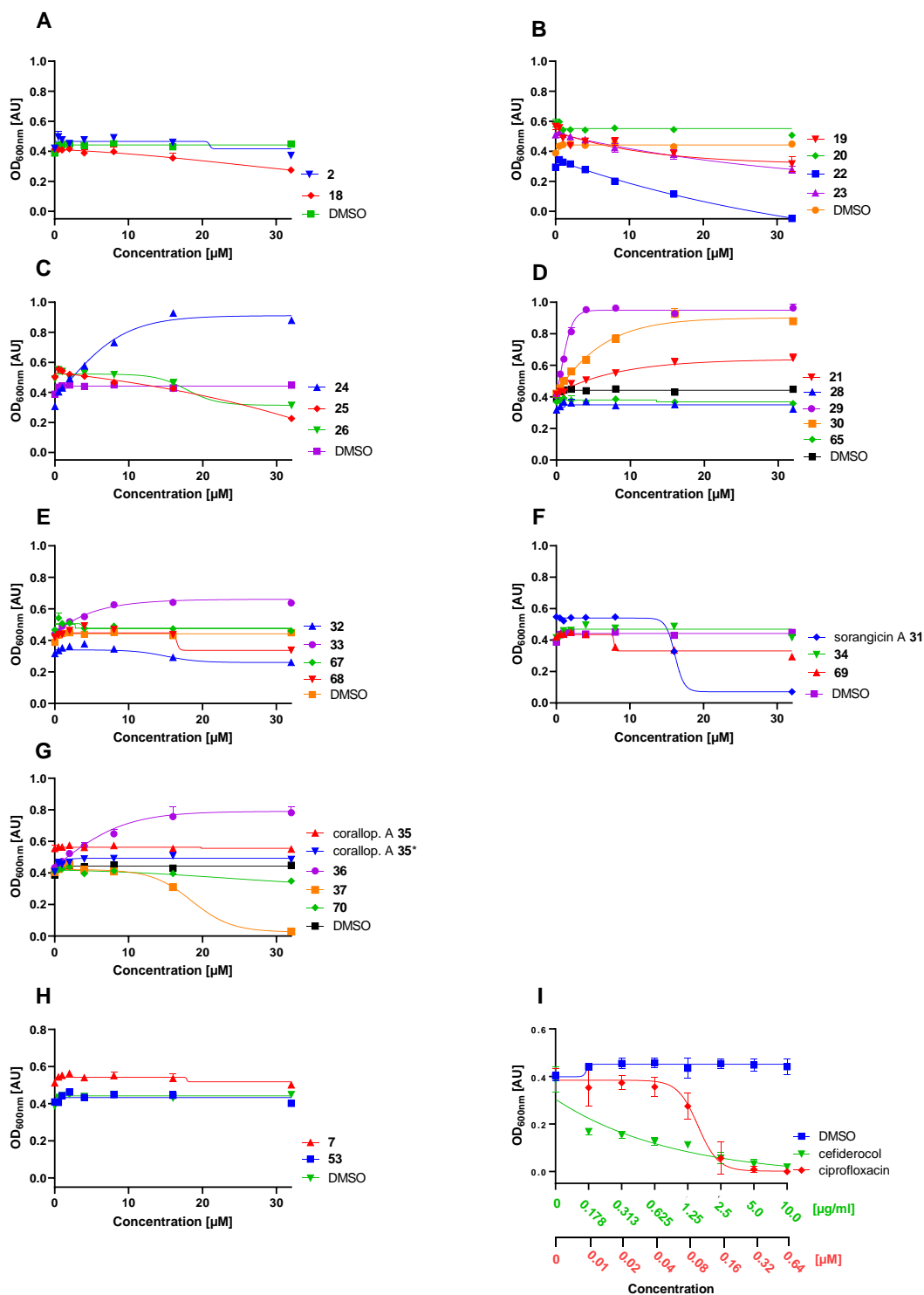


Figure S9.26. Antimicrobial activity of cleavable conjugates and control substances in MDR *A. baumannii* (DSM30008). (A-C) fluoro rifamycin S compounds, (D) formyl rifamycin SV compounds, (E-F) sorangicin A compounds and (G) corallopyronin A compounds, (H) control linker **53** and siderophore **7**, (I) control antibiotics cefiderocol and ciprofloxacin, in iron-depleted, cation-adjusted medium (IDCAM) over 18 hours at 37 °C, error bars correspond to \pm standard error of mean (SEM), $n = 2$, corallop. A* = corallopyronin A without exposure to basic conditions, corallop. A = reisolated from basic reaction conditions.

Table S9.6. MIC values^a for **18** to **37** and controls in MDR *A. baumannii* DSM3007 and DSM30008.

Compound	Chelator	Effector	DSM30007	DSM30008
2	-	RifS	32	>32
7	DOTAM	-	>32	>32
18	DFO	RifS	>32	>32
19	DFO	RifS	>32	>32
20	DFO-Ga	RifS	>32	>32
21	DFO	CHO-RifSV	>32 ^{GE}	>32
22	-	RifS	8	>32
23	DOTAM	RifS	>32	>32
24	DFO	RifS	>32 ^{GE}	>32 ^{GE}
25	DOTAM	RifS	>32	>32
26	DOTAM	RifS	>32	>32
28	-	CHO-RifSV	>32 ^{GE}	>32
29	DFO	CHO-RifSV	>32	>32 ^{GE}
30	DFO	CHO-RifSV	>32 ^{GE}	>32 ^{GE}
31	-	SorA	32	32
32	-	SorA	>32	>32
33	DFO	SorA	>32 ^{GE}	>32 ^{GE}
34	DFO	SorA	>32	>32
35	-	CorA	>32	>32
35*	-	CorA	>32	>32
36	DFO	CorA	>32 ^{GE}	>32 ^{GE}
37	DFO	CorA	8	32
53	-	-	>32	>32
65	-	CHO-RifSV	>32	>32
67	-	SorA	>32	>32
68	-	SorA	>32	>32
69	-	SorA	≥32	>32
70	-	CorA	>32	>32
cefiderocol			0.313	0.64
ciprofloxacin			3.78	7.55
amikacin			-	-
linezolid			-	-

a [μ M] for test compounds and cefiderocol, [μ g/mL] for ciprofloxacin, amikacin, linezolid, DFO = desferrioxamine, RifS=rifamycin S, CHO-RifSV=3-formyl rifamycin SV, SorA=sorangicin A, CorA=coralloypyronin A, * = MIC f. CorA w/o base exposition, GE = growth enhancing.

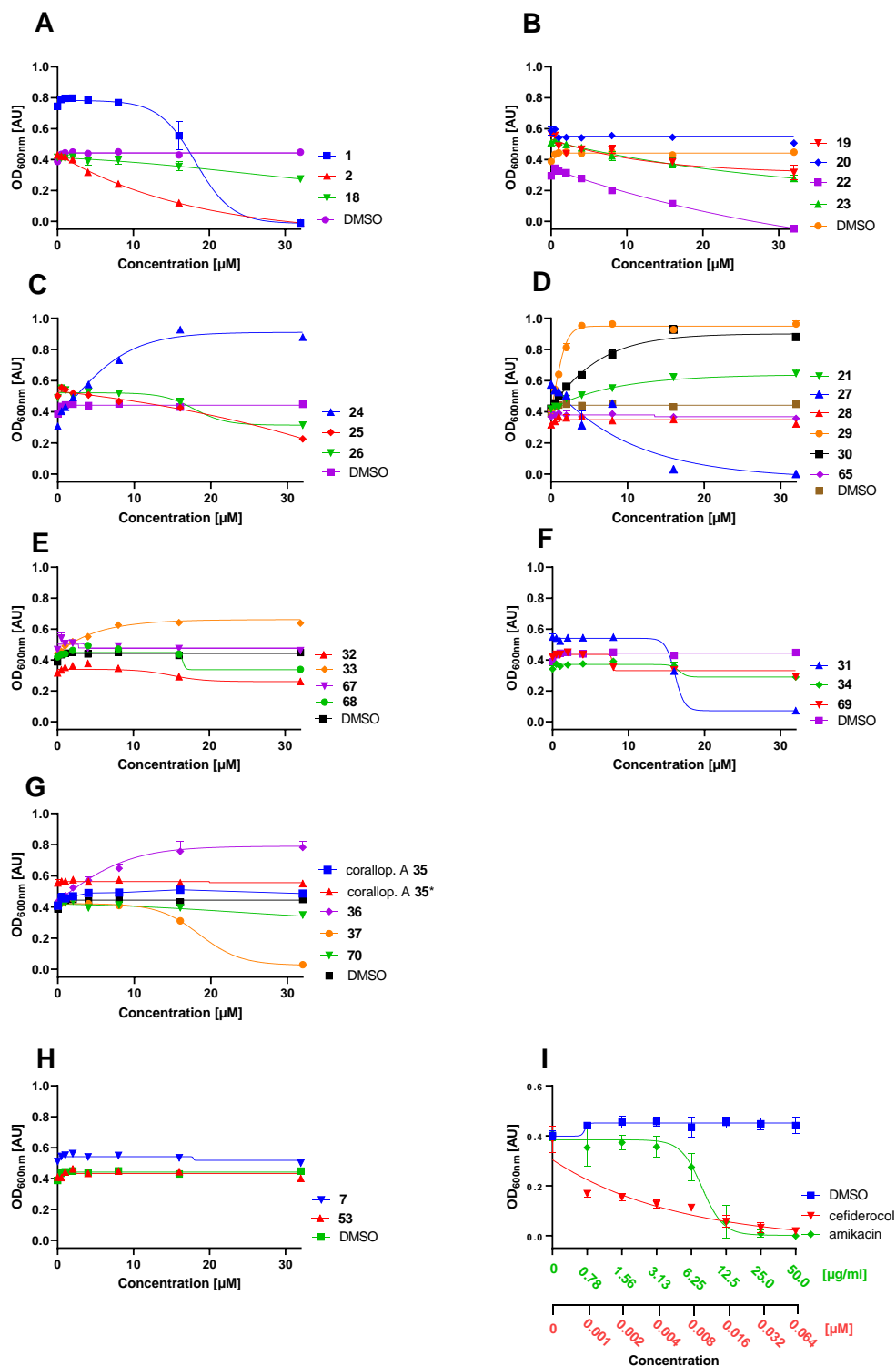


Figure S9.27. Antimicrobial activity of cleavable conjugates and control substances in MDR *P. aeruginosa*. (A-C) fluoro rifamycin S compounds, (D) formyl rifamycin SV compounds, (E-F) sorangicin A compounds and (G) corallopyronin A compounds, (H) control linker **53** and siderophore **7**, (I) control antibiotics cefiderocol and ciprofloxacin, in iron-depleted, cation-adjusted medium (IDCAM) over 18 hours at 37 °C, error bars correspond to \pm standard error of mean (SEM), n = 2, corallop. A* = corallopyronin A without exposure to basic conditions.

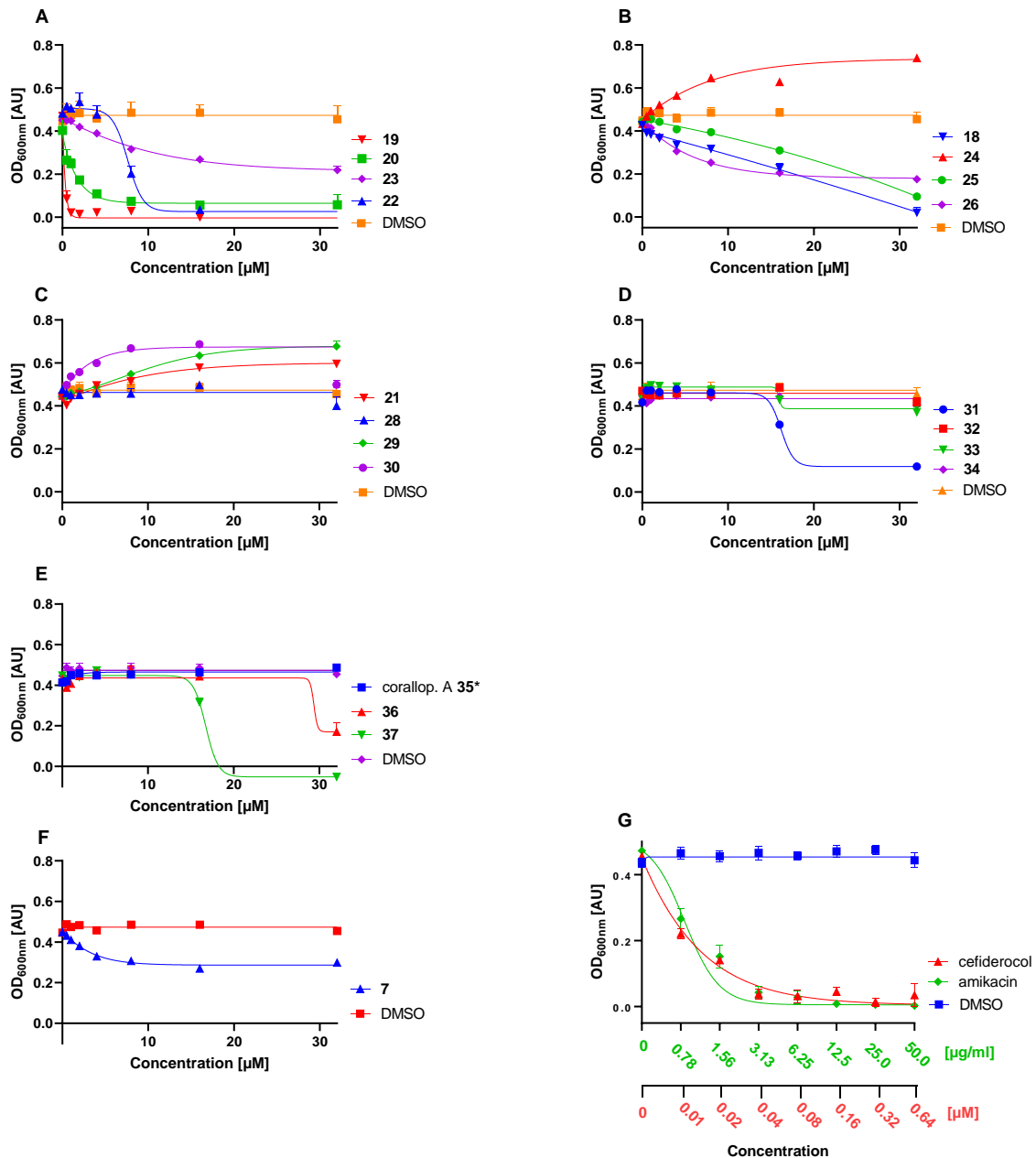


Figure S9.28. Antimicrobial activity of cleavable conjugates and control substances in siderophore-deficient *P. aeruginosa* $\Delta pvdpch$ (A-B) fluoro rifamycin S compounds, (C) formyl rifamycin SV compounds, (D) sorangicin A compounds and (E) corallopyronin A compounds, (F) DOTAM **7** control, (G) control antibiotics cefiderocol and ciprofloxacin, in iron-depleted, cation-adjusted medium (IDCAM) over 18 hours at 37 °C, error bars correspond to \pm standard error of mean (SEM), n = 2 corallop. A* = fresh natural product, corallop. A = reisolated from reaction.

Table S9.7. MIC values^a for 18 to 37 and controls in MDR *P. aeruginosa* and *P. aeruginosa* Δ pvdpch.

Compound	Chelator	Effector	<i>P. aeruginosa</i>	<i>PAO1</i> Δ pvdpch
1	-	RifS	32	-
2	-	RifS	32	-
7	DOTAM	-	>32	>32
18	DFO	RifS	>32	≥32
19	DFO	RifS	>32	4
20	DFO-Ga	RifS	>32	8
21	DFO	CHO-RifSV	>32 ^{GE}	>32 ^{GE}
22	-	RifS	32	16
23	DOTAM	RifS	>32	>32
24	DFO	RifS	>32 ^{GE}	>32 ^{GE}
25	DOTAM	RifS	>32	>32
26	DOTAM	RifS	>32	>32
27	-	CHO-RifSV	32	-
28	-	CHO-RifSV	>32	>32
29	DFO	CHO-RifSV	>32 ^{GE}	>32 ^{GE}
30	DFO	CHO-RifSV	>32 ^{GE}	>32 ^{GE}
31	-	SorA	≥32	>32
32	-	SorA	>32	>32
33	DFO	SorA	>32 ^{GE}	>32
34	DFO	SorA	>32	>32
35	-	CorA	>32	-
35*	-	CorA	>32	>32
36	DFO	CorA	>32 ^{GE}	>32
37	DFO	CorA	≥32	16
53	-	-	>32	-
65	-	CHO-RifSV	>32	-
67	-	SorA	>32	-
68	-	SorA	>32	-
69	-	SorA	>32	-
70	-	CorA	>32	-
cefiderocol			0.64	0.04
ciprofloxacin			-	
amikacin			21.4-5-42	9.46-18.89
linezolid			-	

a [μ M] for test compounds and cefiderocol, [μ g/mL] for ciprofloxacin, amikacin, linezolid, DFO = desferrioxamine, RifS=rifamycin S, CHO-RifS=formyl rifamycin SV, SorA=sorangicin A, CorA=corallopyronin A, GE = growth enhancing.

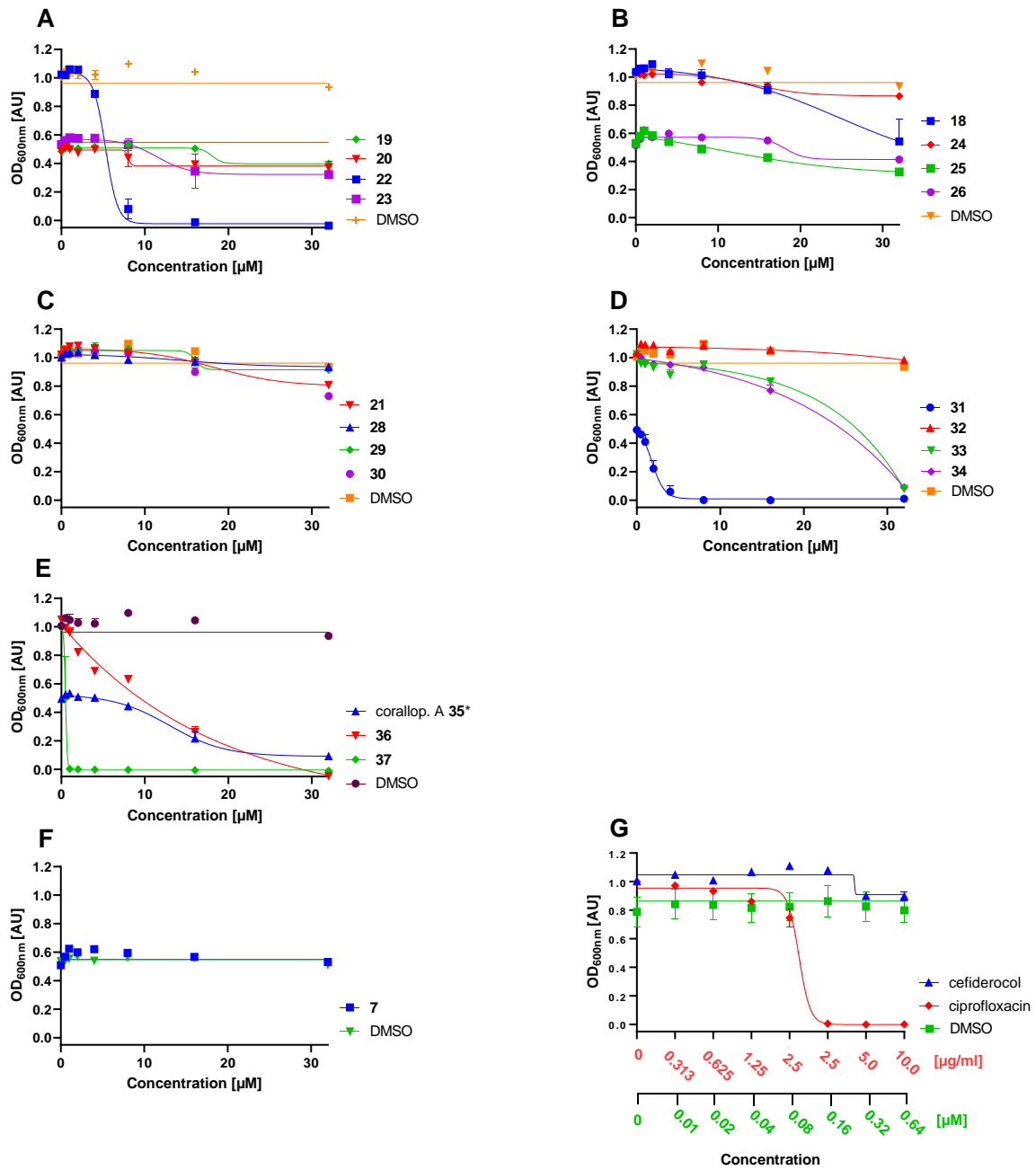


Figure S9.29. Antimicrobial activity of cleavable conjugates and control substances in MDR *E. faecium* (A-B) fluoro rifamycin compounds, (C) formyl rifamycin compounds, (D) sorangicin A compounds and (E) corallopyronin A compounds, (F) DOTAM 7 control, (G) control antibiotics cefiderocol and ciprofloxacin, in iron-depleted, cation-adjusted medium (IDCAM) over 18 hours at 37 °C, error bars correspond to \pm standard error of mean (SEM), n = corallop. A* = corallopyronin A without exposure to basic conditions.

Table S9.8. MIC values^a for 18 to 37 and controls in MDR *E. faecium*.

Compound	Chelator	Effector	<i>E. faecium</i>
2	-	RifS	-
7	DOTAM	-	>32
18	DFO	RifS	>32
19	DFO	RifS	>32
20	DFO-Ga	RifS	>32
21	DFO	CHO-RifSV	>32
22	-	RifS	10
23	DOTAM	RifS	>32
24	DFO	RifS	>32
25	DOTAM	RifS	>32
26	DOTAM	RifS	>32
28	-	CHO-RifSV	>32
29	DFO	CHO-RifSV	>32
30	DFO	CHO-RifSV	>32
31	-	SorA	8
32	-	SorA	>32
33	DFO	SorA	32
34	DFO	SorA	32
35*	-	CorA	32
36	DFO	CorA	32*
37	DFO	CorA	0.5
53	-	-	-
65	-	CHO-RifSV	-
67	-	SorA	-
68	-	SorA	-
69	-	SorA	-
70	-	CorA	-
cefiderocol			>0.64
ciprofloxacin			7.55
amikacin			-
linezolid			-

a [μ M] for test compounds and cefiderocol, [μ g/mL] for ciprofloxacin, amikacin, linezolid, DFO = desferrioxamine, DOTAM = enterobactin mimic, RifS=rifamycin S, CHO-RifSV=3-formyl rifamycin SV, SorA=sorangicin A, CorA=corallopyronin A, * = MIC f. CorA w/o base exposition GE = growth enhancing

Biological methods

Enzymatic quinone TML activation

This procedure was developed based on a publication by Pardeshi et al and our previous work in Peukert et al.^{11, 12}

The NADH stock of NADH (500 mM in MQ water) was diluted 1:100 in 50 mM K₃PO₄ buffer (pH 7.0). The conjugates or control compounds in DMSO were diluted 5 mM NADH in phosphate buffer (final concentration = 150-300 μM) and the enzyme (2.5 μg/mL diaphorase or 1.25 μg/mL QOR2 final conc.) in buffer was added. The mixtures were incubated at 30 °C and 600 rpm. A similarly diluted compound preparation without enzyme was used as t₀ and separated with the sample analytical HPLC program. Samples for analytical HPLC (C18 gemini, 3 μm, NX-C18 110 A, 50 x 2 mm, ACN/H₂O, 0.1% TFA, DAD detector, 0-100% ACN 5 min, 100% ACN 2 min, 100-0% ACN 1 min, 0% ACN 1 min) were quenched with an excess MeOH 1% AcOH. 20 μL / sample were injected and the chromatograms were compared to the reference measurements of the intact conjugates or free payloads at for their overlaid absorption at 220, 254 and 280 nm.

MIC assay

The minimal inhibitory concentration was determined in iron-depleted, cation-adjusted medium (IDCAM), as previously described by L. Pinkert, Y. Lai et al.¹³

Due to their linker and/or their payload nearly all conjugates exhibited a high background signal at 600 nm. Thus the background signal (OD_{600nm} (0h)), after the addition of the bacteria to the compound dilutions, was subtracted from the OD_{600nm} (18h) measurements. This was necessary to allow the minimal inhibitory concentration (MIC) determination in the presence of these strongly colored compounds. However, due to medium evaporation and alteration of the compound and their absorption over 18 h, this caused negative values at high compound concentrations after the subtraction. In that case we used the x axis intersection as to determine the MIC. In accordance with literature we define the MIC as the lowest concentration of an antibiotic that will inhibit the visible growth of a microorganism after overnight incubation.¹⁴

The MDR strains used in the MIC assays are shown in the table below. For the siderophore deficient strains (*E. coli* Δ *entA* and *P. aeruginosa* Δ *pvdpch*) see K. Ferreira et al and Peukert et al.^{1, 15}

Table S1. Bacteria used in the MIC assay.

Strain	DSMZ-#	Antibiotic Resistance	Medium
<i>Escherichia coli</i>	DSM1116	Penicillin G, Oxacillin, Vancomycin, Lincomycin, Bacitracin, Clindamycin, Linezolid, Nystatin, Quinupristin, Teicoplanin, Piperacillin	MHB
<i>Staphylococcus aureus</i>	DSM11822	Colistin, Kanamycin, Aztreonam, Oxacillin, Clindamycin, Nystatin, Lincomycin, Erythromycin, Norfloxacin, Pipedemic acid	TSY
<i>Klebsiella pneumoniae</i>	DSM11678	-	MHB
<i>Acinetobacter baumannii</i>	DSM30007	Penicillin G, Oxacillin, Ampicillin, Cefalotin, Cefazolin, Chloramphenicol, Vancomycin, Lincomycin, Pipedemic acid, Bacitracin, Clindamycin, Linezolid, Nystatin, Quinupristin, Teicoplanin,	MHB
<i>Acinetobacter baumannii</i>	DSM30008	Penicillin G, Oxacillin, Ampicillin, Cefalotin, Cefazolin, Vancomycin, Lincomycin, Linezolid, Nystatin, Quinupristin, Teicoplanin	MHB
<i>Pseudomonas aeruginosa</i>	DSM24068	Penicillin G, Oxacillin, Ampicillin, Mezlocillin, Cefalotin, Cefazolin, Cefotaxime, Chloramphenicol, Vancomycin, Erythromycin, Lincomycin, Ofloxacin, Norfloxacin, Pipedemic acid, Nitrofurantoin, Bacitracin, Kanamycin, Neomycin, Ceftriaxone, Clindamycin, Fosfomicin, Moxifloxacin, Linezolid, Nystatin, Quinupristin, Teicoplanin, Piperacillin	MHB
<i>Enterococcus faecium</i>	DSM20477	Colistin, Polymyxin B, Pipedemic acid, Nystatin, Aztreonam	TSY

Supplementary references

1. Peukert, C.; Langer, L. N. B.; Wegener, S. M.; Tutov, A.; Bankstahl, J. P.; Karge, B.; Bengel, F. M.; Ross, T. L.; Brönstrup, M., Optimization of artificial siderophores as ⁶⁸Ga-complexed PET tracers for *in vivo* imaging of bacterial infections. *J. Med. Chem.* **2021**, *64* (16), 12359-12378.
2. Ji, C.; Miller, M. J., Siderophore–fluoroquinolone conjugates containing potential reduction-triggered linkers for drug release: synthesis and antibacterial activity. *BioMetals* **2015**, *28* (3), 541-551.
3. Paul Stephen Donnelly, S. E. R., Spencer John Williams Novel imaging composition and uses thereof. WO2016058056A1, 2015.
4. Bachmann, S. F., Serena Maria; Jansen, Michael; Koenig, Stefan; Linghu, Xin, Rieth, Sebastian; Segraves, Nathaniel L.; Zogg, Andreas Process for the preparation of an antibody-rifamycin conjugate. PCT/US2017/020711, 2017.
5. Adams, R. A.; Leon, G.; Miller, N. M.; Reyes, S. P.; Thantrong, C. H.; Thokkadam, A. M.; Lemma, A. S.; Sivaloganathan, D. M.; Wan, X.; Brynildsen, M. P., Rifamycin antibiotics and the mechanisms of their failure. *J. Antibiot.* **2021**, *74* (11), 786-798.
6. Mori, N.; Ishii, Y.; Tateda, K.; Kimura, S.; Kouyama, Y.; Inoko, H.; Mitsunaga, S.; Yamaguchi, K.; Yoshihara, E., A peptide based on homologous sequences of the β -barrel assembly machinery component BamD potentiates antibiotic susceptibility of *Pseudomonas aeruginosa*. *J. Antimicrob. Chemother.* **2012**, *67* (9), 2173-2181.
7. Lee, B.; Yan, J.; Ulhaq, A.; Miller, S.; Seo, W.; Lu, P.; She, R.; Spellberg, B.; Luna, B.; Bradford, P. A., *In vitro* activity of rifabutin and rifampin against antibiotic-resistant *Acinetobacter baumannii*, *Escherichia coli*, *Staphylococcus aureus*, *Pseudomonas aeruginosa*, and *Klebsiella pneumoniae*. *mSphere* **2021**, *6* (6), e00920-21.
8. Rothstein, D. M.; Shalish, C.; Murphy, C. K.; Sternlicht, A.; Campbell, L. A., Development potential of rifalazil and other benzoxazinorifamycins. *Expert Opin. Investig. Drugs* **2006**, *15* (6), 603-623.
9. Jansen, R.; Schummer, D.; Irschik, H.; Höfle, G., Antibiotics from gliding bacteria, XLII. Chemical modification of sorangicin A and structure - Activity relationship I: Carboxyl and hydroxyl group derivatives. *Liebigs Ann.* **1990**, *1990* (10), 975-988.
10. Pardeshi, K. A.; Kumar, T. A.; Ravikumar, G.; Shukla, M.; Kaul, G.; Chopra, S.; Chakrapani, H., Targeted antibacterial activity guided by bacteria-specific nitroreductase catalytic activation to produce ciprofloxacin. *Bioconj. Chem.* **2019**, *30* (3), 751-759.
11. Peukert, C.; Popat Gholap, S.; Green, O.; Pinkert, L.; van den Heuvel, J.; van Ham, M.; Shabat, D.; Brönstrup, M., Enzyme-activated, chemiluminescent siderophore-

- dioxetane probes enable the selective and highly sensitive detection of bacterial pathogens. *Angew. Chem. Int. Ed.* **2022**, e202201423.
12. Pinkert, L.; Lai, Y.-H.; Peukert, C.; Hotop, S.-K.; Karge, B.; Schulze, L. M.; Grunenberg, J.; Brönstrup, M., Antibiotic conjugates with an artificial MECAM-based siderophore are potent agents against Gram-positive and Gram-negative bacterial pathogens. *J. Med. Chem.* **2021**, *64* (20), 15440-15460.
 13. Andrews, J. M., Determination of minimum inhibitory concentrations. *J. Antimicrob. Chemother.* **2001**, *48* (suppl_1), 5-16.
 14. Ferreira, K.; Hu, H.-Y.; Fetz, V.; Prochnow, H.; Rais, B.; Müller, P. P.; Brönstrup, M., Multivalent siderophore–DOTAM conjugates as theranostics for imaging and treatment of bacterial infections. *Angew. Chem. Int. Ed.* **2017**, *56* (28), 8272-8276.

10. General Discussion and Outlook

A systematic exploration of siderophores and their conjugates is required to gain a deeper mechanistic understanding of their mode of action, also in the context of resistance development or phenotypic adaptation. The work focused on the derivatization of artificial siderophores for the bacterial targeting in the context of imaging and antibiotic therapy. It produced a number of insights into the molecular mechanisms of bacterial synthetic siderophore transport and generated new knowledge on radioactively and optically labelled sideromycins and their cellular and *in vivo* performance regarding the detection of bacterial infections. This thesis also investigated the efficacy of covalent and cleavable natural product siderophore conjugates which altogether enabled the collection of a large dataset on conjugate-based entry and activity relationships (CER/CAR). The respective subprojects all had different emphasis regarding their aims and methodology, but in sum all parts merged to paint a more detailed picture of synthetic siderophores, combating infectious diseases, as molecular Trojan Horses outlined in the following paragraphs.

10.1 Outlook on synthetic siderophores as bacteria-specific PET tracers

The derivatization efforts of the modular DOTAM siderophore mimics in Publication 1 culminated in the successful development of two structural diverse PET tracers for the imaging of bacterial infections *in vivo*. Both molecules showed a retained iron transport capability, favorable radiochemical properties, sufficient stability in healthy wildtype mice and the ability to rather localize to the site of *E. coli* infection than to the sterile inflammation control. With the incorporation of gallium-68 at the cyclen and not at the site of iron complexation, a microbe-specific tracer with an additional binding site was created and the principal feasibility of the approach was illustrated.

Many pathogen-specific processes have been exploited for imaging purposes. In this context, the target would be ideally highly conserved, thus essential for bacterial survival in a number of bacterial classes and permit uptake of tracers with broad substrate tolerance in both susceptible and drug-resistant organisms at different growth stages.¹³³ Therefore, the widespread occurrence of siderophores, the concurrent uptake machinery and their essential importance for microbial survival makes them an ideal target. To examine to which extent the two frontrunners also accumulate in other relevant ESKAPE pathogens, a set of appropriate “hot” *in vitro* uptake studies and complementary *in vivo* experiments should be conducted. These studies should not be limited to the detection of infection herds but also attempt to monitor antibiotic therapy progress. An optimization of the chemical structure of the two radiotracers, could occur at the iron chelator motif (e.g. the hydroxy pyridines instead of catechol units), at the linker or at the chelator for the radioactive label in order to gain improved

radiochemical and physicochemical properties. With regard to complex stability, the gallium-DOTA complexes were sufficiently stable in human serum and in smaller rodent models. DOTA chelators are very adaptable and can host nearly any radiometal of interest, e.g. $[^{68}\text{Ga}^{3+}]$ (65 pm ion radius, $t_{1/2} = 68$ min) as well as $[^{227}\text{Ac}^{3+}]$ (112 pm, $t_{1/2} = 29$ a). Also $[^{64}\text{Cu}^{2+}]$ (87 pm, $t_{1/2} = 12.7$ hours) and $[^{111}\text{In}^{3+}]$, $t_{1/2} = 2.8$ d] (94 pm) have been reported to form very stable complexes with this sort of chelator.²⁰⁸

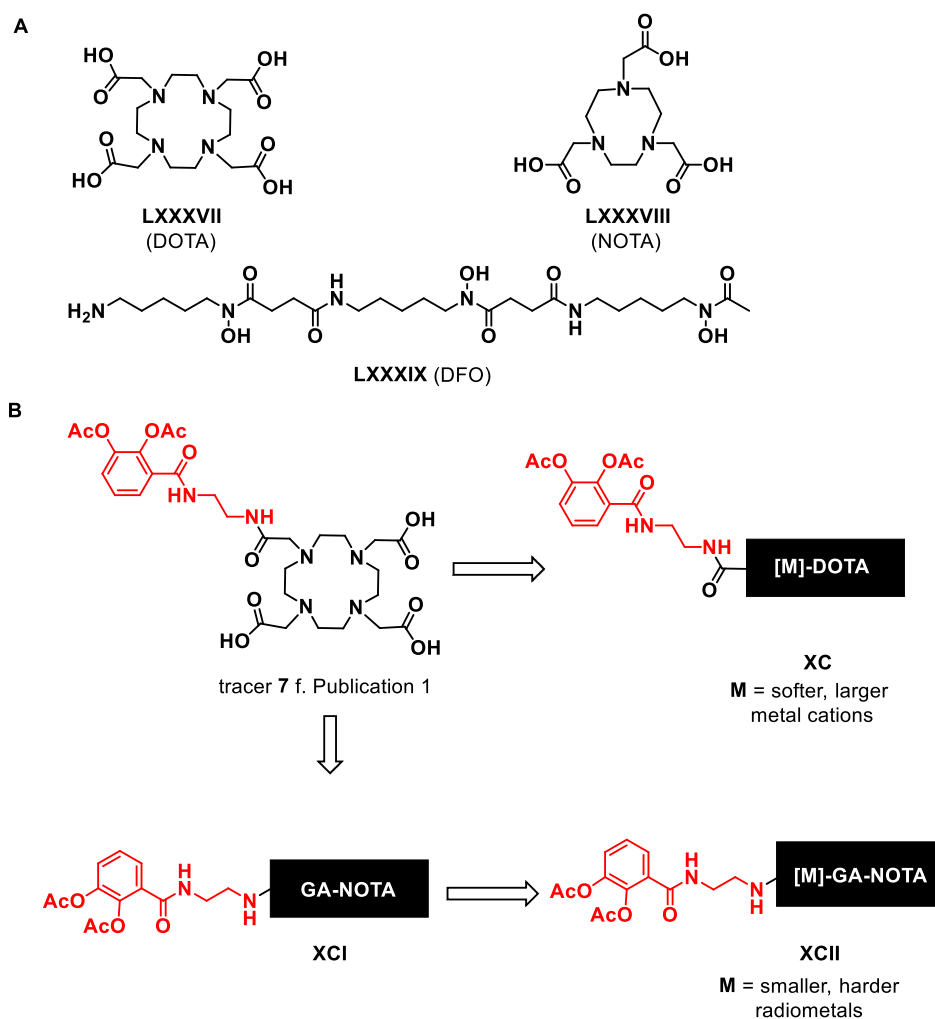


Figure 10.1. Effective radiochelators and future development regarding monocatechol, bacteria-specific PET tracers. (A) Overview of different chelators for chelation of radioactive metal cations, namely DOTA, NOTA and DFO. (B) Outlook for monocatechol, bacteria-specific PET tracers. The overall charge of the complexes is not indicated, as it may vary due to the respective metal cation and the solvation state.

The monocatechol modification directly at the cyclen exhibited a difference in loadability and stability compared to the bimodal triscatechol DOTA construct. Possibly this is the result of steric influences (distortion of the DOTA LXXXVII scaffold) but mainly it is due to the stability of the different solvent complexes.

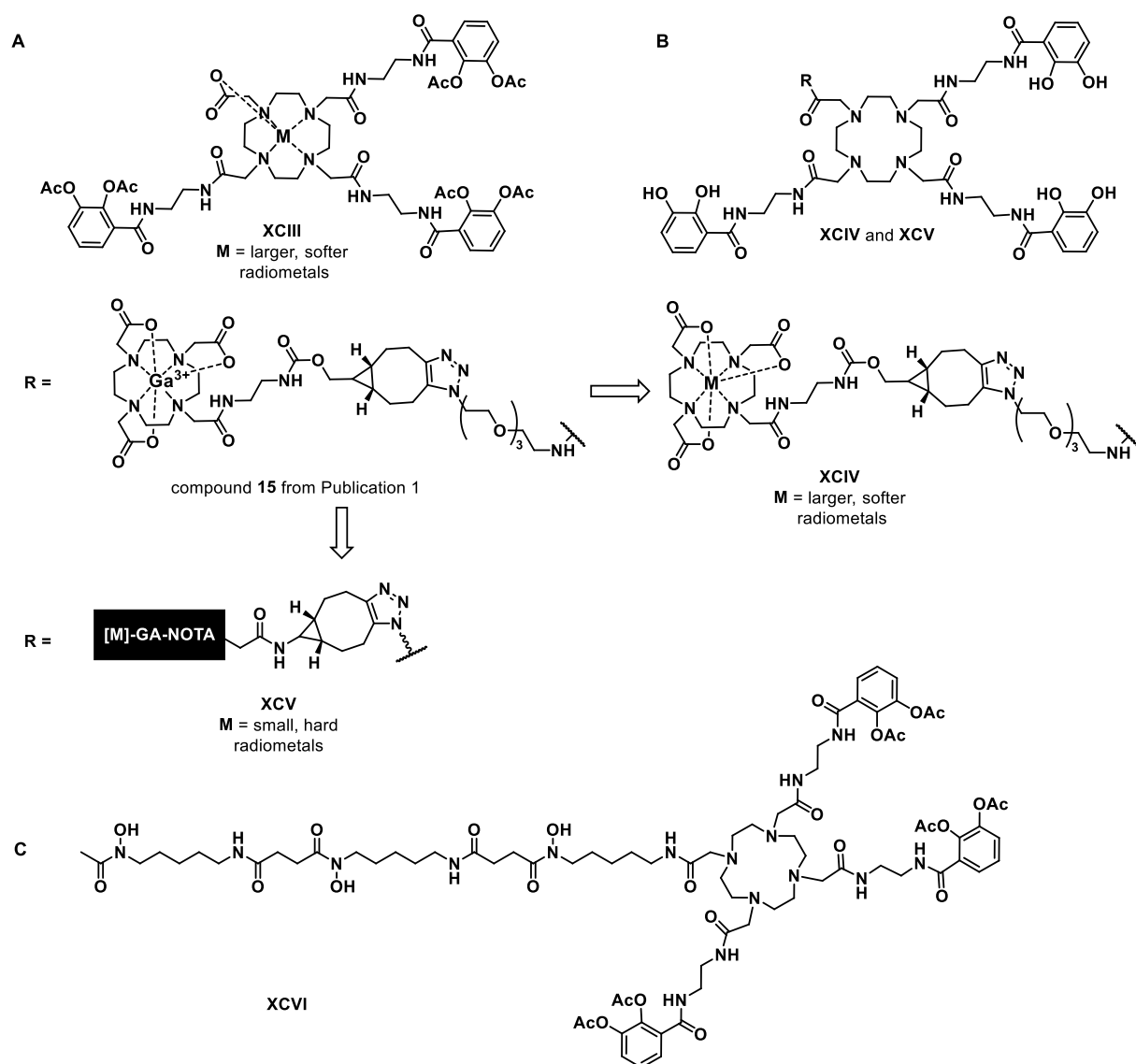


Figure 10.2. Outlook for triscatechol, bacteria-specific PET tracers. (A) Triscatechol DOTAM tracers, complexed with bigger and “softer” radioactive cations as labels. (B) Bimodal triscatechol-DOTA tracers equipped with either a GA-NOTA or complexed with bigger and “softer” radioactive cations as labels. (C) Suggestion of a bimodal DFO-DOTAM tracer which combines hydroxamate and catechol ligands in one molecule. The overall charge of the complexes is not indicated, as it may vary due to the respective metal cation and the solvation state.

Intriguingly, the radiochemistry and *in vivo* data point in the same direction: The more acids were exchanged for amides at the cyclen the less attractive and stable the gallium-68 complexes were. This can be explained at least in part with the HSAB principle, as Ga^{3+} has preference for hard, small anions. Moreover, the cyclen ring is relatively adaptable but in turn also a bit large for gallium-68 isotopes with a larger ionic radius like indium or copper definitely fit better into the cycle.²⁰⁹ The smaller NOTA (2,2',2''-(1,4,7-triazacyclononane-1,4,7-triyl)triacetic acid, **LXXXVII**; Figure 10.1) chelator would be even more suitable for gallium complexation. In contrast, a DOTAM triscatecholate (Figure 10.2B) mainly “offers” amides which would be more attractive for the “softer” copper (PET) or indium (SPECT) isotopes (HSAB principle). This hypothesis is also supported by previous cold complexation data from K. Ferreira et al.^{83, 164} To gain an informed insight, detailed thermodynamic and kinetic data would be required for the different tracer and label combinations.²¹⁰ Also **LXXXIX** was shown to readily form gallium chelates at ambient temperature in high yields and accumulate at infection herds caused by a variety of prokaryotes (Figure 10.1A).^{211, 212} This chelator might also be of interest for theranostic conjugates with heat sensitive natural product payloads that can be employed for imaging but also for antibiotic therapy. Especially since Ga-DFO complexes were shown to exhibit moderate antibiotic efficacy against *P. aeruginosa*, reduce biofilm formation and the severity of keratitis in a rabbit infection model.²¹³ Also a combination of a DFO and DOTAM triscatecholate (**XCVI**) would be interesting for imaging applications, as the tracer potentially could be recognized by hydroxamate as well as catecholate TBDTs (Figure 10.2C).

A detrimental factor for the performance of novel radiotracers is the radiolabel itself, as it was shown to alter the chemical properties and the bacterial uptake. Along those lines, it is important to note that the majority of bacteria-specific PET tracers in development are fluorinated (^{18}F , $t_{1/2} = 107$ min).¹³⁶ A fluorinated version also has the advantage that the label and the carrier molecule are linked via a covalent bond instead of ionic interactions that may be labile dependent on the pH or solvation. Fluorine-18 can be obtained from low energy cyclotrons and is delivered to nearby locations, while gallium-68 can be easily obtained from a benchtop generator, allowing logistically simple and independent radiosynthesis, but with a rather short half-life.²¹⁴ A longer-lasting alternative may be the SPECT isotope gallium-67 which has a half-life of three days, but a lower spatial resolution *in vivo*.

All in all, Publication 1 showcases the proof-of-principle of a novel class of siderophore-based tracers for the radioactive detection and monitoring of microbial infections *in vivo*. A structural optimization based on the initially obtained data, combined with a thorough evaluation of the tracers *in vivo* holds the promise of a clinical application in the near future.

10.2 MECAM-based sideromycins and their resistance mechanisms

The development of a successful conjugation strategy permitted the synthesis of the first antibiotic MECAM sideromycins. One molecule exhibited nanomolar MIC values in Gram-negative bacteria and solely a triple TBDT, TonB or ExbB knockout conferred full resistance. The study peaked in a thorough resistance examination to shed light on potential evasion strategies upon repeated β -lactam MECAM treatment (Publication 2).

The discovered mutations in ExbB and CyoB, had not been described previously and differed from the resistance mechanisms observed for the gold standard cefiderocol (Fetroja®), which also contains a β -lactam warhead.^{215, 216} Resistance to Fetroja was associated with reduced expression of the TBDT PirA and with mutations in the periplasmic binding protein 3 (PBP3) in MDR *A. baumannii*.²¹⁵ Rapid resistance was also found in *Enterobacter spp.* following treatment, due to mutations in the siderophore receptor CirA.²¹⁶ Data from *P. aeruginosa* (Publication 5), following MECAM conjugate treatment, showed an upregulation of the β -lactamase AmpC (proteomics and transcriptomics), which provided reason for the inactivity of the conjugate in this species and nicely illustrated an additional evasion mechanism.

Taken together the results from Publication 2 and 5, qualify the conjugatable MECAM siderophore mimic as a novel 'Trojan Horse' with high potential for bacteria-specific diagnostics and therapeutics. As these antibiotic warheads have also been employed by other studies, this served rather as a proof-of-concept that allowed to compare the efficacy of the MECAM with siderophore Trojan Horses from other groups.³⁹ Future projects could use this efficient carrier with regard to bacteria-specific PET imaging *in vivo*, but also attach periplasm cleavable linker systems together with potent payloads (colistin, murepavadin, antimicrobial peptides or peptide nucleic acids) that would benefit from an enrichment at the infection site or within the bacteria. These approaches should rely on the previously obtained information regarding the TBDTs, the bacterial phenotypic adaptation and the subcompartmental accumulation to build effective molecules for clinical applications.

10.3 Bacteria-specific, optical diagnostics for the point-of-care detection of infections

The conjugation and thorough biological evaluation of siderophore dioxetane conjugates for the sensitive and specific detection of bacterial infections in (i) iron-depleted media, (ii) infected human lung cells and (iii) in human plasma marked an important milestone for the development of broad-spectrum, optical imaging agents. At least two of the probes from Publication 3/4 show the potential as sensitive, broad-spectrum diagnostic agents for the cellular and *in vivo* visualization of MDR bacteria.

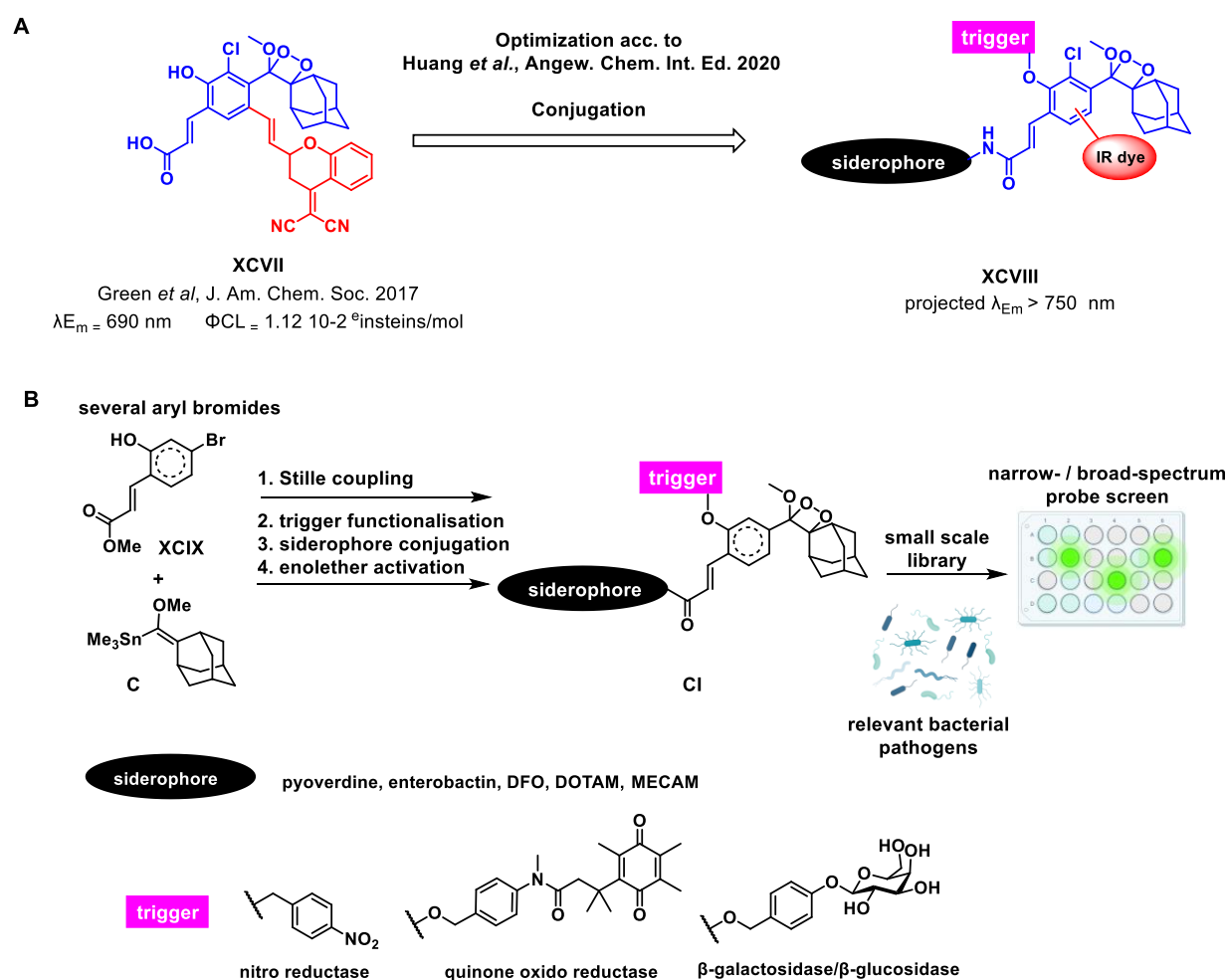


Figure 10.3. Bright outlook for siderophore dioxetane probes. (A) Infrared shifted dioxetanes, by conjugation to a push-pull dicyano-methylchromone (DCMC) chromophore, for the *in vivo* imaging of bacterial infections.^{217, 218} DCMC shown in red, dioxetane in blue, siderophore in black und trigger in pink. (B) Library-based screening for the discovery of narrow- or broad-spectrum probes (dotted benzene ring place holder for diverse set of compatible aromatic cores).

The dioxetane unit of the current frontrunner probes would first require some structural adaptation for the *in vivo* detection of the luminescence signal. Recently, Green *et al* developed a near-infrared (NIR) emissive dioxetane, which is conjugated in *para*-position to a push-pull chromophore (dicyano-methylchromone, DCMC, Figure 10.3A).²¹⁷ Upon conjugation, these DCMC chromophores were shown to yield NIR emissive dyes with high Φ_{CL} and also respectable photostability.²¹⁹ The activation of these NIR dioxetanes proceeds as described in the introduction via an excited-state benzoate but now the extended donor-acceptor pair decays to its ground state with an emission of a NIR photon. The resulting luminophores showed a maximum emission wavelength at 690 nm.^{217, 149} Soon after, a team from Singapore reported NIR dioxetanes with a similar structure but with sulfur or selenium atom instead of the oxygen atom of the DCMC at the benzopyran subunit. As a consequence these molecules displayed an even more NIR-shifted maximum emission wavelength (740-780 nm) and a higher detectable luminescence signal through tissue with increasing thickness, compared to the probe by Green *et al*.²¹⁸ Based on these findings, a suggestion for an NIR siderophore dioxetane conjugate **XCVIII**; is seen as a promising next step for the translation of siderophore conjugates for *in vivo* imaging.

The successful discovery of one broad-spectrum probe was based on the educated selection of an efficiently, widely internalized xenosiderophore (DFO) and trigger moieties that were cleaved by (i) an enzyme class essential to survival and present in most prokaryotes (energy metabolism, oxidoreductases) or (ii) a family of enzymes with a broad substrate tolerance (β -galactosidase, more generally β -glycosidase).^{220, 221, 222} The favorable discovery of a broadly working combination occurred to us, in part, serendipitously but future attempts should invest resources to rationalize this process for cost and efficiency reasons. Very recent advances from the field of dioxetane chemistry could help to realize this challenge and facilitate in particular the synthetic effort. Instead of a minimum five step procedure (depending on the arene functionalization), involving a 'Wittig-Horner cross coupling', a team around P. Baran and D. Shabat employed a key Stille coupling of a functionalized halophenol **XCIX** with an adamantyl-enoether-stannane **C** to afford the corresponding enoether **CI**.¹⁴⁹ This reduced the total number of steps, increased the overall yield with only a photochemical activation with singlet oxygen and methylene blue as the final step to obtain the activated dioxetane (Figure 10.3B).²²³ For a systematic discovery of narrow- or broad-spectrum siderophore-dioxetane probes, this chemistry could be utilized to rapidly generate a number of acrylic ester enoethers. Moreover, the novel synthesis would allow to adapt the central aromatic motif to recent literature developments.²²³ The trigger would be installed at the phenol, followed by hydrolysis of the ester to the acrylate, so that a siderophore carrier could be introduced and finally the photochemical dioxygenation would furnish the active siderophore dioxetane conjugate. Natural chelators like pyoverdine would lead most certainly to a narrow spectrum,

Pseudomonas probe, as demonstrated for a gallium-68 labelled version for PET imaging.¹³⁷ The triggers should leverage the previously explored moieties (TML and β -galactose) but could also explore e.g. *para*-nitro benzyl groups, typically reduced by nitro-reductases and reported to be prevalent in many prokaryotes.²²⁴ The final screening should include MDR ESKAPE pathogens, including clinical isolates and use the summed luminescence and/or fluorescence as a read-out, compared to the probe signal in sterile, iron-deficient medium. Thus, in sum, dioxetane sideromycins hold great potential for additional research to discover novel sensitive and bacteria-specific diagnostics for the facile and rapid detection of *in vivo* infections and of microbial contaminants in pharmaceutical processes and in the food sector.

10.4 From TonB targeting sideromycins towards small molecule drugs

In a proof-of-principle approach, Publication 6 contributed valuable findings to the area of siderophore research and but to the field to antibiotic target identification. It underlined the crucial role of ferric iron for bacterial growth and the central role of the molecular motor TonB in the uptake of ferric siderophore complexes. The study established the TonB-dependent siderophore uptake as a novel target in antimicrobial therapy and translated an overexpression experiment to a panel of tool compounds targeting the periplasmic PPI of the OMR's TonB box with TonB.

However, this can only be the first step, as the MIC values with *Pseudomonas* wildtype strains clearly showed that sideromycins with a molecular weight greater than 3000 Da cannot compete with e.g. pyoverdine (1336 Da). Although all conjugates retained their ability to complex ferric iron according to FeCAS results, a slower complexation kinetic, due to the steric hindrance of the peptide payload, can be imagined.

In this context, the treatment of *E. coli* with a TonB box consensus pentapeptide (ETVIV) significantly reduced the bacteria's virulence, TonB-mediated colicin uptake and killing as well as TonB-mediated ϕ 80 phage bacterial entry. However, the internalization via polypeptide transporters required the addition of concentrations greater than 100 μ M.²²⁵ This underlines the principal feasibility but also the need to transition from bulky sideromycins towards small molecule drugs with more favorable pharmacokinetic properties and sufficient accumulation in the bacterial periplasm. Two approaches that could aid this selection process are a competitive peptide microarray (Figure 10.4A) and/or a phenotypic bacterial screening (Figure 10.4B).

Various studies have employed peptide microarrays to characterize the immune response in the area of cancer, infectious or neurological diseases, e.g. for the screen of epitope-specific antibodies. Such assays use synthetic peptides spotted on glass slides or cellulose support and their performance heavily relies on the spot's diameter and the quality of the peptides.²²⁶

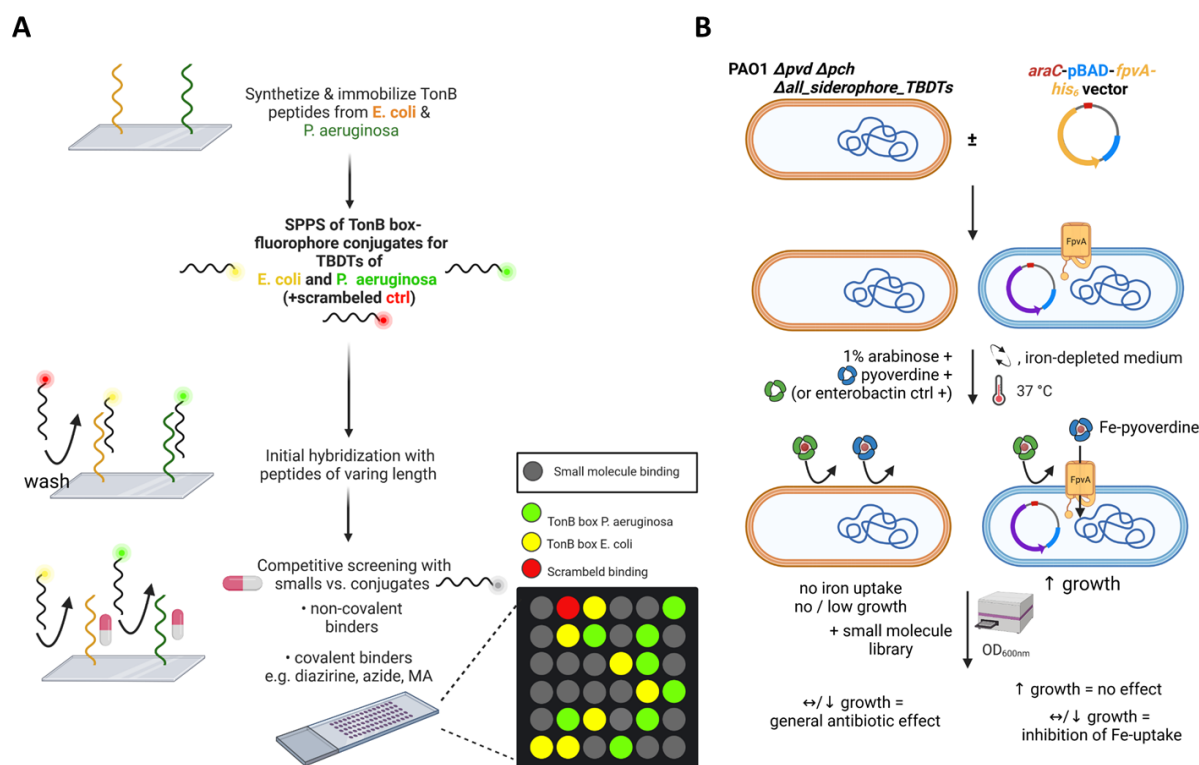


Figure 10.4. Complementary strategies to convert TonB box peptide sideromycins to small molecule drugs. (A) Competitive peptide microarray to screen for small molecules inhibitors that prevent the hybridization of TonB box peptide fluorophore probes (yellow: *E. coli*, green: *P. aeruginosa*) to their complementary, slide-bound TonB peptide sequences, vs. a scrambled control (red). (B) Phenotypic screening in siderophore- and TBBDT-deficient mutant bacteria ± an *araC*-pBAD-TBBDT plasmid containing single TBBDT genes (e.g. *fpvA*). The reconstituted strain would express the TBBDT upon arabinose addition and thus be able to accumulate ferric iron through an exogenously added, receptor compatible siderophore (e.g. pyoverdine). The control strain (no plasmid = no TBBDT) and the transformed strain would be profiled for their growth in iron-depleted medium ± a library of test compounds to identify molecules interfering with siderophore uptake. Figure created with biorender.

To discover small molecules interfering with this PPI, TonB peptides binding to the TBBDT's TonB box, deduced from *in silico* or crystal structure data, would be spotted on a solid support in varying length. Initially, fluorescently labeled TonB box peptides from the same species of varying length would be incubated with these slides to verify their binding in contrast to a scrambled peptide probe. During the screening, small molecules would be added to compete

with the probes for the binding sites at the TonB peptides. Successful test compounds could be identified by 'a loss of signal' and then further examined for their concentration-dependent activity. The compound collection could also extend (initially) to compounds with electrophilic traps (e.g. Michael acceptors, α -ketoamides, epoxyketones or arylfluorosulfates etc.), which could enhance the inhibitor's potency significantly. However, the choice of a specific warhead depends on the nature of the chemical entity to which the bond formation should occur.^{227, 228,}
229

Although target-based strategies have widely dominated drug discovery in general, a significant fraction of first-in-class clinical candidates originate from phenotypic screens.^{230, 231} These rely, rather than on a structurally well-explored active site, on a broader panel of read-outs e.g. on growth, gene expression, cell morphology and more broadly on the manifestation of a beneficial pathogen phenotype upon addition of a small molecule effector. Despite their differences target and phenotypic discovery may go hand in hand, as hits from the above microarray naturally could be evaluated further by the second approach and *vice versa*.²³² In particular, in the screen a *P. aeruginosa* genomic mutant, lacking its endogenous siderophores (e.g. $\Delta pvd \Delta pch$) and TBDTs (e.g. $\Delta pfeA$, $\Delta pirA$, $\Delta fpvA$, $\Delta fptA$, $\Delta hasR$), would serve as the control. This strain cannot accumulate ferric iron, even after the exogenous addition of siderophore ligands (control condition) in iron-depleted medium. To screen for small molecules that interfere with TonB-dependent siderophore uptake, the mutant would be reconstituted with single TBDT genes on an arabinose inducible *araC*-pBAD plasmid (e.g. *fpvA* in Figure 10.4, but also *pfeA* or *pirA*) also carrying a selection marker and his tag. Both strains would be grown in iron-depleted, arabinose-supplemented medium, which should enable TBDT expression, ferric siderophore uptake and growth in the transformed mutant, while the control strain should show diminished or no growth. Finally, the growth of the strains would be profiled in iron-depleted medium to identify molecules interfering with siderophore uptake and bacterial growth. Hits would be compounds that specifically reduce growth in the reconstituted strain, while no effect should be observed in the plasmid lacking control, as this would point towards a general antibiotic activity. Control compounds, known to interfere with the TonB-TonB box PPI could include the peptide siderophore conjugates from Publication 6. As TBDTs also translocate other essential substrates for bacterial growth, i.e. nickel complexes, carbohydrates and vitamin B₁₂, the general disruption of TonB-dependent transport could be a novel, exciting target for the development of broad-spectrum or species-specific antimicrobials.⁹⁰

10.5 A database for effective, streamlined sideromycin development

The collection of covalent and cleavable sideromycins from subprojects Publication 7 and Publication 8 connects a diverse set of siderophores, covalent and self-immolative linker systems of varying length and polarity and many different antibiotic effectors. Especially previously unexplored natural products from the class of RNA polymerase inhibitors (RNAP-I) displayed increased potency vs. MDR Gram-negative bacteria and retained activity vs. Gram-positive ones following chelator conjugation. Due to their ability to also host a radioactive label as gallium-68 instead or aside ferric iron, these molecules hold great potential for the development of potent therapeutics, possibly even theranostics. Together with the structure activity data from Publication 2 and 6, this constitutes to a treasure trove of different sideromycins and biological activity data.

In this context, the number of novel siderophore carriers and sideromycins published over the course of 43 years and the concurrent scientific advancements are continuously increasing and have become overwhelming, even for experts in the field (Figure 10.5).

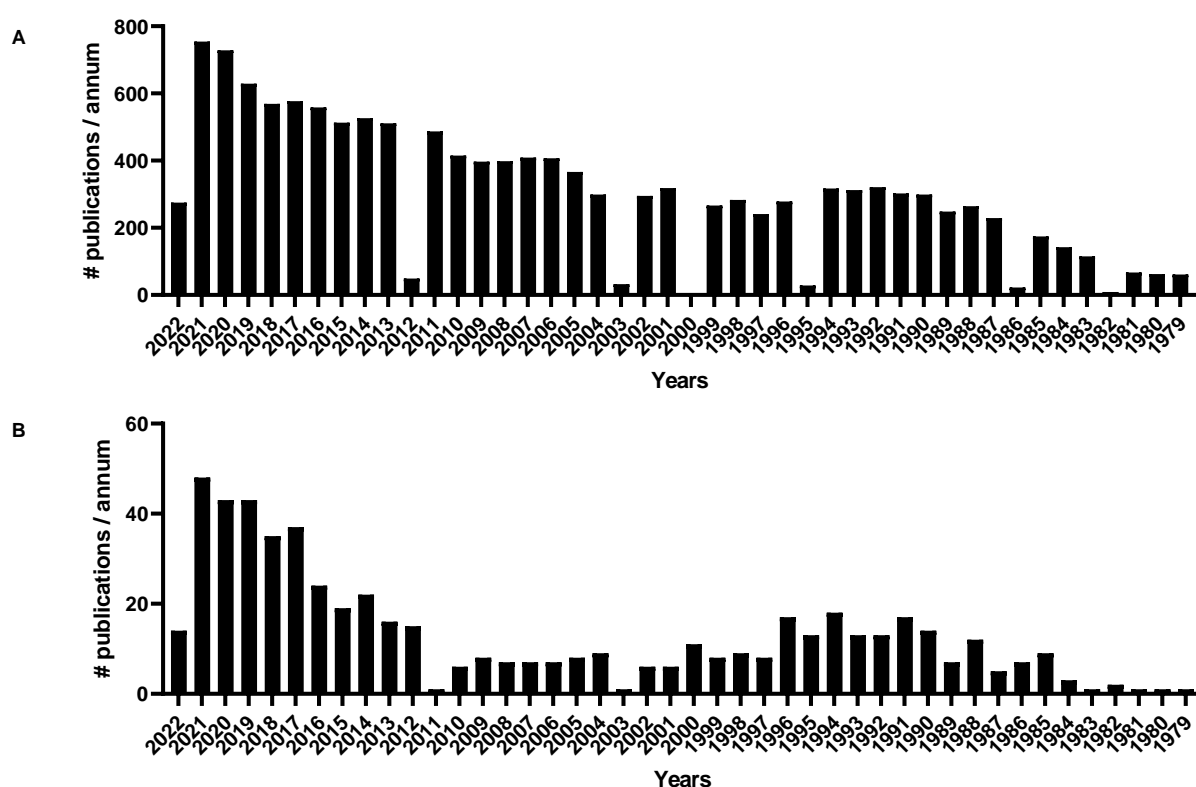


Figure 10.5. Publications on siderophores and siderophore conjugates *per annum*. (A) “Siderophores” and (B) “siderophore conjugates” related publications per annum according to a PubMed search to the interval from 1979 till May 2022.

Scientific advancements certainly build on the exchange of knowledge, the reproducibility of findings and on the continuous adaptation of one's own research in crosstalk with those discoveries.^{233, 234} Numerous improvements have been noted in the area of sideromycins, e.g. with regard to MIC testing, mechanistic or resistance studies, especially since industrial companies have contributed with their own research programs to this area of research.^{93, 81, 106, 39} However, the sheer mass of scientific findings makes it difficult to incorporate these findings, including those from Publications 1-8, into the design of novel sideromycins.

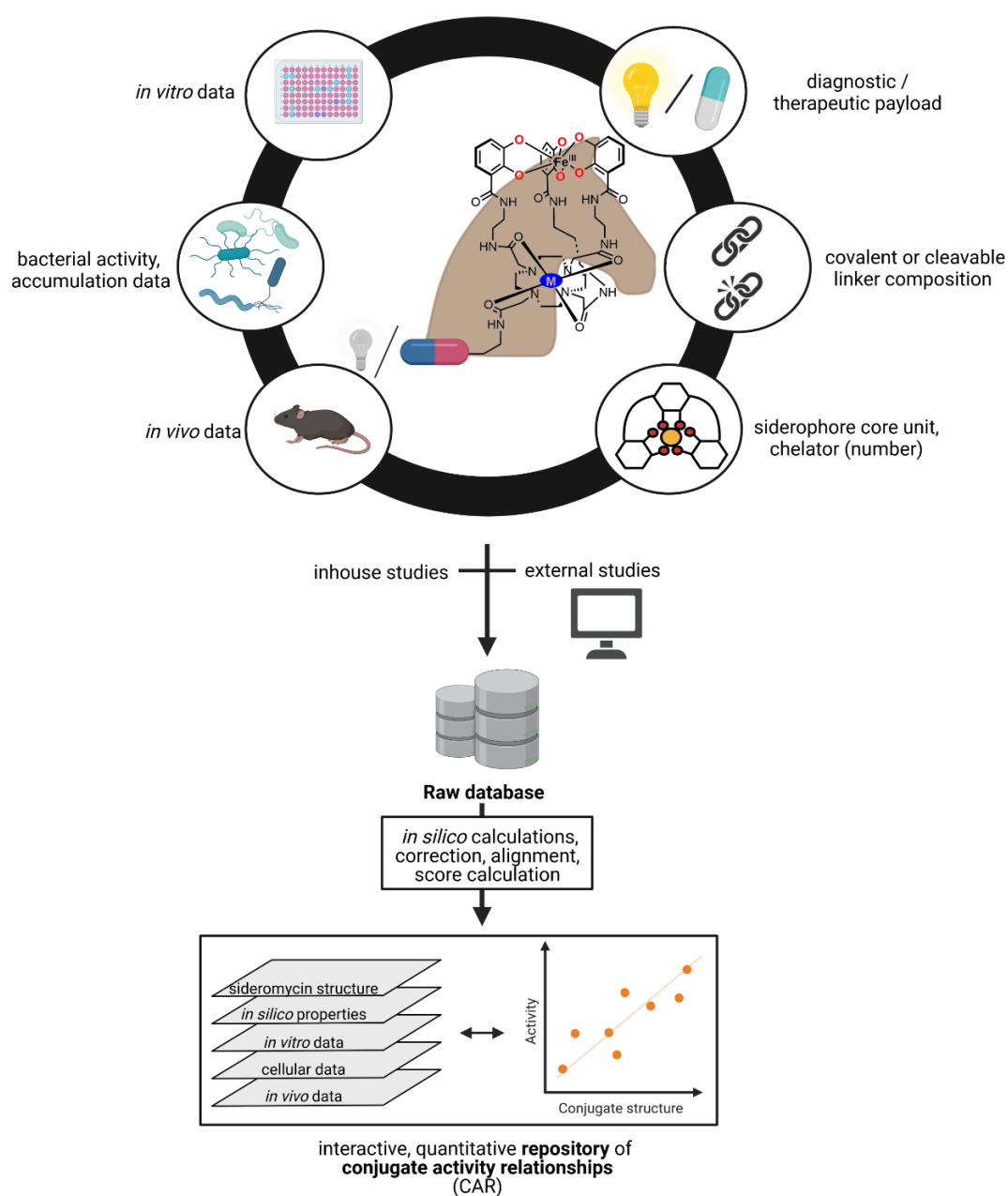


Figure 10.6. Vision for a siderophore repository to build conjugate activity relationships.

Future attempts would massively benefit from a consolidated database, as is available for quite some time for small molecule research programs to generate structure activity relationships.^{235, 236} This tool should ideally collect and compare the chemical diversity (siderophore, linker, payload etc.) of sideromycins from academia and industry with their biological activity data (MIC, test conditions) and with mechanistic insights (TBDTs, subcompartmental accumulation, resistance development, Figure 10.6). Together, these data points would compose a raw dataset that requires data alignment and adjustments based on the measurement parameters from the original experiment. Moreover, the structure of the compound and the biological data could be used to extract *in silico* descriptors for the compound structure (heteroatom, clogP, polar surface area, rotatable bonds etc.) and meaningful scores that hold condensed estimation of the sideromycin's biological efficacy. All in all, the connection and comparison to previous findings could allow the deduction of conjugate-based entry (CER) and activity (CAR) rules for the benefit of the future development of sideromycins. In the long term, such a repository could also aid to identify best practices and general workflows for the successful development of clinically relevant diagnostic and therapeutic siderophore conjugates.

A. Supplementary Data

A.1 Publication 1



Optimization of Artificial Siderophores as ^{68}Ga -Complexed PET Tracers for In Vivo Imaging of Bacterial Infections



Author: Carsten Peukert, Laura N. B. Langer, Sophie M. Wegener, et al

Publication: Journal of Medicinal Chemistry

Publisher: American Chemical Society

Date: Aug 1, 2021

Copyright © 2021, American Chemical Society

PERMISSION/LICENSE IS GRANTED FOR YOUR ORDER AT NO CHARGE

This type of permission/license, instead of the standard Terms and Conditions, is sent to you because no fee is being charged for your order. Please note the following:

- Permission is granted for your request in both print and electronic formats, and translations.
- If figures and/or tables were requested, they may be adapted or used in part.
- Please print this page for your records and send a copy of it to your publisher/graduate school.
- Appropriate credit for the requested material should be given as follows: "Reprinted (adapted) with permission from {COMPLETE REFERENCE CITATION}. Copyright {YEAR} American Chemical Society." Insert appropriate information in place of the capitalized words.
- One-time permission is granted only for the use specified in your RightsLink request. No additional uses are granted (such as derivative works or other editions). For any uses, please submit a new request.

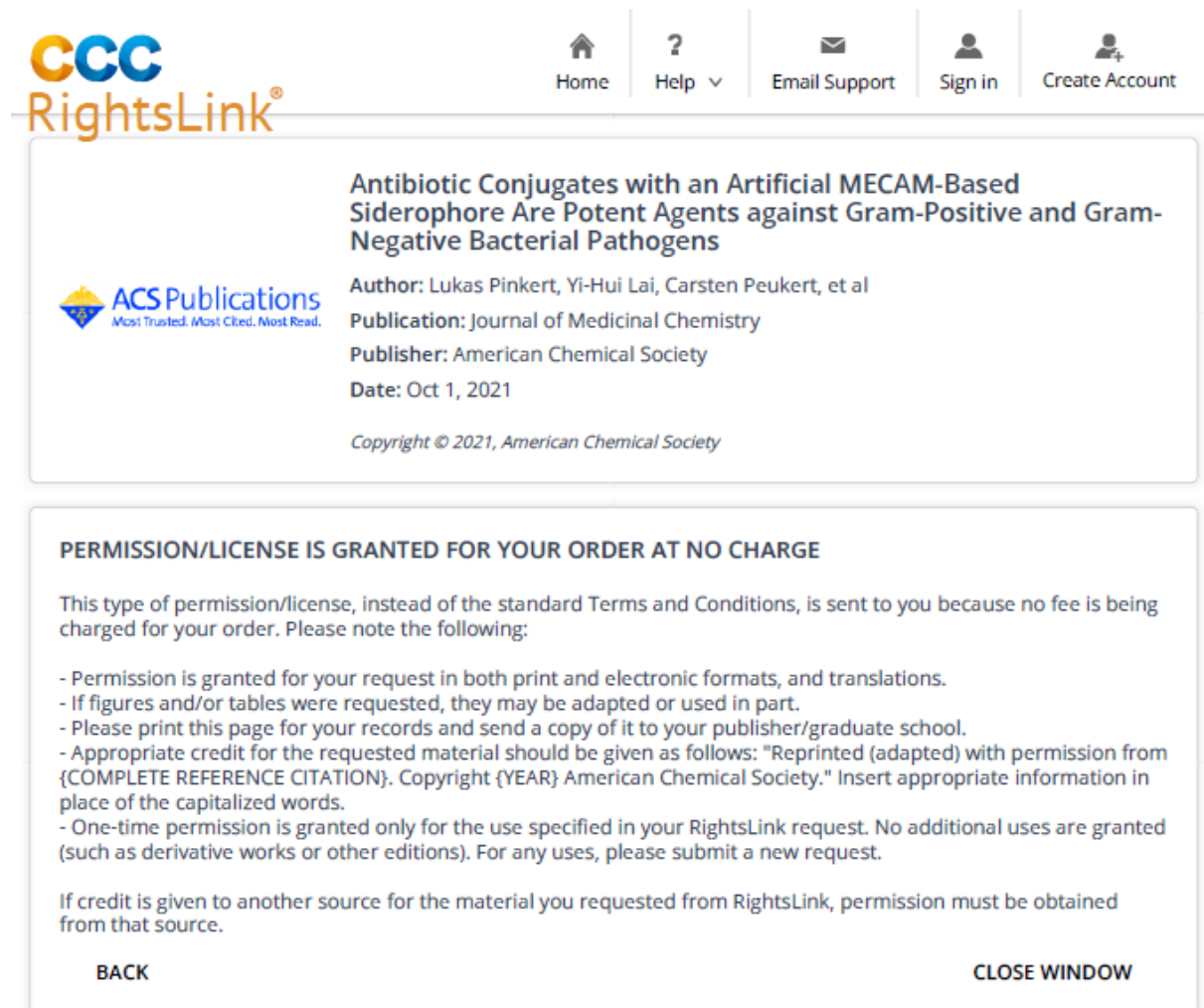
If credit is given to another source for the material you requested from RightsLink, permission must be obtained from that source.

[BACK](#)

[CLOSE WINDOW](#)

Figure A.1. Screenshot of the CCC RightsLink® request for Publication 1.

A.2 Publication 2



CCC RightsLink®

Home | Help ▾ | Email Support | Sign in | Create Account

Antibiotic Conjugates with an Artificial MECAM-Based Siderophore Are Potent Agents against Gram-Positive and Gram-Negative Bacterial Pathogens

ACS Publications
Most Trusted. Most Cited. Most Read.

Author: Lukas Pinkert, Yi-Hui Lai, Carsten Peukert, et al
Publication: Journal of Medicinal Chemistry
Publisher: American Chemical Society
Date: Oct 1, 2021

Copyright © 2021, American Chemical Society

PERMISSION/LICENSE IS GRANTED FOR YOUR ORDER AT NO CHARGE

This type of permission/license, instead of the standard Terms and Conditions, is sent to you because no fee is being charged for your order. Please note the following:

- Permission is granted for your request in both print and electronic formats, and translations.
- If figures and/or tables were requested, they may be adapted or used in part.
- Please print this page for your records and send a copy of it to your publisher/graduate school.
- Appropriate credit for the requested material should be given as follows: "Reprinted (adapted) with permission from {COMPLETE REFERENCE CITATION}. Copyright {YEAR} American Chemical Society." Insert appropriate information in place of the capitalized words.
- One-time permission is granted only for the use specified in your RightsLink request. No additional uses are granted (such as derivative works or other editions). For any uses, please submit a new request.

If credit is given to another source for the material you requested from RightsLink, permission must be obtained from that source.

BACK **CLOSE WINDOW**

Figure A.2. Screenshot of the CCC RightsLink® request for Publication 2.


A.5 Publication 4



CCC RightsLink®

Home Help ▾ Email Support Sign in Create Account

Uptake Mechanisms and Regulatory Responses to MECAM- and DOTAM-Based Artificial Siderophores and Their Antibiotic Conjugates in *Pseudomonas aeruginosa*

 **ACS Publications**
Most Trusted. Most Cited. Most Read.

Author: Sarah Fritsch, Véronique Gasser, Carsten Peukert, et al
Publication: ACS Infectious Diseases
Publisher: American Chemical Society
Date: May 1, 2022

Copyright © 2022, American Chemical Society

PERMISSION/LICENSE IS GRANTED FOR YOUR ORDER AT NO CHARGE

This type of permission/license, instead of the standard Terms and Conditions, is sent to you because no fee is being charged for your order. Please note the following:

- Permission is granted for your request in both print and electronic formats, and translations.
- If figures and/or tables were requested, they may be adapted or used in part.
- Please print this page for your records and send a copy of it to your publisher/graduate school.
- Appropriate credit for the requested material should be given as follows: "Reprinted (adapted) with permission from {COMPLETE REFERENCE CITATION}. Copyright {YEAR} American Chemical Society." Insert appropriate information in place of the capitalized words.
- One-time permission is granted only for the use specified in your RightsLink request. No additional uses are granted (such as derivative works or other editions). For any uses, please submit a new request.

If credit is given to another source for the material you requested from RightsLink, permission must be obtained from that source.

BACK **CLOSE WINDOW**

Figure A.3. Screenshot of the CCC RightsLink® request for publication 5.

Acknowledgements

First and foremost I would like to thank my doctoral supervisor Prof. Dr. Mark Brönstrup, who supported me personally over the years and during countless projects. During these four and a half years he continued to encourage me to cross the boundaries of common knowledge, allowed my creativity to flourish to explore and realize even seemingly enormous, high-risk projects. I am grateful to the “Fonds der chemischen Industrie” for awarding me their two-year “Kekulé Ph.D. fellowship”, which also enabled my visit at the “RSC Medicinal Chemistry Residential School” in the UK. I would also like to thank Prof. Dr. Philipp Klahn and Prof. Dr. Marc Stadler, who supported my research projects with invaluable advice as members of my Thesis Committee. Furthermore, I am deeply grateful to Prof. Dr. Tobias Ross, Prof. Dr. Doron Shabat, Prof. Dr. Isabelle Schalk and their respective research teams for the fruitful collaborations and scientific support, which enabled the numerous, scientific advancements cumulated in this thesis. A special thank you goes to my master's students Anna Tutov and Till Orth for their perpetual diligence, curiosity and endurance in their respective master's projects and the friendly atmosphere in the laboratory and beyond.

Science and especially discoveries strive solely in a collaborative climate and thus I would like to explicitly thank a range of (now) postdocs for their knowledgeable, open ear but also for the memories in- and outside the laboratory: Dr. Charlotte Grandclaudon, Dr. Hazel Fuchs, Dr. Anna Vetter, Dr. Vadim Korotkov and Dr. Lukas Pinkert. Moreover, I would like to express my gratitude to my other colleagues, Julia Friederich, Simon Kalverkamp, Moritz Stappert, Aditya Shekhar, Hannah Wullenkord, Bianka Karge and Bettina Hinkelmann, who supported me in terms of scientific ideas and Ph.D. student life. In addition, I would like to thank Kirsten Harmrolfs, Christel Kakoschke, Linn Müggenburg, Monika Rettstadt and Ulrike Beutling for their kindness and unconditional support, despite submitting countless NMR or HRMS samples which often, required long measurement times due to their high molecular weight. Many thanks also go to Dr. Werner Tegge, Bettina Mehner and Heike Overwin for their warm, helpful nature and their efforts in administrative and organizational matters. Furthermore, I thank also the rest of the chemical biology department for the warm welcome, their support, advice and trust during my stay at the HZI. Finally, I would acknowledge the HZI Graduate School for Infection Research (GS-FIRE) for their support, and the organization of a meaningful Ph.D. program with intriguing scientific and soft skill courses and seminars that shaped my personality and abilities beyond science. Finally, yet importantly my biggest thanks belong to my family and friends, who unanimously supported my bachelor's and master's studies and thus laid the cornerstone for my career. My parents and grandparents, which are an indispensable part of my life, continue to foster and share my passion and fascination for (natural) sciences and are always available for life advice. This work is dedicated to you!

Curriculum vitae and List of Publications

Personal Data

Name **Carsten Peukert**
 Date of Birth **04. August 1992**
 Place of Birth **Konstanz (Baden-Württemberg), Germany**

Education

PhD student, Gottfried-Wilhelm-Leibniz-Universität, Hannover
 Title: **“Using iron to catch a ride – synthetic siderophores as molecular
 ,Trojan Horses’ to visualize and treat MDR bacterial pathogens”**,
 2017-present Supervision: Prof. Dr. Mark Brönstrup, Chemical Biology,
 Helmholtz Centre for Infection Research (HZI), Braunschweig (Germany)
 Master of Science Life Science, University of Konstanz,
 Final grade: A (grade 1.1, with distinction).
 2015-2017 Master thesis: **“Proteomic metabolite profiling”**, Supervision: Prof. Dr. T.
 Böttcher, University of Konstanz, Konstanz
 2012-2015 Bachelor of Science Life Science
 University of Konstanz, Final grade: A- (grade 1.6)
 2012 Abitur (university qualification)
 Maria Ellenrieder Gymnasium, Konstanz, Final grade: A (grade 1.0)

Professional Experience

2017-present **Doctoral Researcher**, Department of Chemical Biology, Helmholtz
 Centre for Infection Research (HZI), Braunschweig (Germany)
 04/2017- **Tutor** in "Organic Chemistry for Biologists", Prof. Dr. T. Böttcher,
 08/2017 University of Konstanz
 Intern at the Department “Oncology & Metastasis”, Prof. Dr. H. Augustin
 01/2017-04/2017 German Cancer Research Centre (DKFZ),
 Intern at the Institute for Diabetes & Obesity, “Metabolism and Cancer”
 10/2016-12/2016 Dr. K. Stemmer, Helmholtz Centre Munich (HMGU)

Awards and Scholarships

- 11/2018-12/2020 Kekulé doctoral researcher stipend from the "Fonds der chemischen Industrie"
- 10/2020 Award for the best talk, at the PhD retreat of the HZI GS-FIRE graduate school

List of Publications

Journal articles

1. "Optimization of Artificial Siderophores as ^{68}Ga -Complexed PET Tracers for *In Vivo* Imaging of Bacterial Infections"
Carsten Peukert and Laura N. B. Langer, Sophie M. Wegener, Anna Tutov, Jens P. Bankstahl, Bianka Karge, Frank M. Bengel, Tobias L. Ross, and Mark Brönstrup, *J. Med. Chem.* **2021**, 64, 16, 12359–12378.
DOI: 10.1021/acs.jmedchem.1c01054
-
2. "Antibiotic Conjugates with an Artificial MECAM-Based Siderophore Are Potent Agents against Gram-Positive and Gram-Negative Bacterial Pathogens"
Lukas Pinkert and Yi-Hui Lai, Carsten Peukert, Sven-Kevin Hotop, Bianka Karge, Lara Marie Schulze, Jörg Grunenberg, and Mark Brönstrup, *J. Med. Chem.* **2021**, 64, 20, 15440–15460.
DOI: 10.1021/acs.jmedchem.1c01482
-
3. "Enzyme-activated, Chemiluminescent Siderophore-Dioxetane Probes Enable the Selective and Highly Sensitive Detection of Bacterial ESKAPE Pathogens"
Carsten Peukert, Sachin Popat Gholap, Ori Green, Lukas Pinkert, Joop van den Heuvel, Marco van Ham, Doron Shabat, Mark Broenstrup, *Angew. Chem. Int. Ed.*, **2022**, e202201423
DOI: 10.1002/anie.202201423
- „Enzymaktivierte, chemilumineszente Siderophor-Dioxetan-Sonden ermöglichen den selektiven und hochempfindlichen Nachweis von bakteriellen Krankheitserregern“
Carsten Peukert, Sachin Popat Gholap, Ori Green, Lukas Pinkert, Joop van den Heuvel, Marco van Ham, Doron Shabat, Mark Broenstrup, *Angew. Chem.*, **2022**, e202201423
DOI: 10.1002/ange.202201423

-
4. "Uptake Mechanisms and Regulatory Responses to MECAM- and DOTAM-based Artificial Siderophores and their Antibiotic Conjugates in *Pseudomonas aeruginosa*"
 Sarah Fritsch, Véronique Gasser, Carsten Peukert, Lukas Pinkert, Lauriane Kuhn, Quentin Perraud, Vincent Normant, Mark Brönstrup and Isabelle J. Schalk, *ACS Infect. Dis.*, **2022**, 8, 6 1134-1146.
 DOI: 10.1021/acsinfectdis.2c00049.
-

Selected conference presentations

- 2nd to 7th Jun.
2019
 Medicinal Chemistry Residential School, RSC, Loughborough, UK
 Courses on phenotypic drug discovery, DMPK, ADME & patents and a poster presentation on "Molecular Trojan Horses to visualize and treat bacterial infections a theranostic approach exploiting bacterial Fe(III) demand"
-
- 3rd to 5th Jul.
2019
 55th International Conference on Medicinal Chemistry Nantes, FR
 Poster on "Synthetic sideromycins - molecular 'Trojan Horses' to visualize and treat bacterial infections",
-
- 29th Aug. to 2nd
Sept. 2021
 26th EFMC International Symposium on Medicinal Chemistry, virtual
 Selected talk on "PET tracers & chemiluminescent probes for bacterial imaging"

General References

1. Fauci, A. S.; Morens, D. M., The perpetual challenge of infectious diseases. *N. Engl. J. Med.* **2012**, 366 (5), 454-461.
2. Morens, D. M.; Folkers, G. K.; Fauci, A. S., Emerging infections: a perpetual challenge. *The Lancet Infect. Dis.* **2008**, 8 (11), 710-719.
3. Krause, R. M., The origin of plagues: Old and new. *Science* **1992**, 257 (5073), 1073-1078.
4. Lloyd, N. C.; Morgan, H. W.; Nicholson, B. K.; Ronimus, R. S., The composition of Ehrlich's Salvarsan: Resolution of a century-old debate. *Angew. Chem. Int. Ed.* **2005**, 44 (6), 941-944.
5. Strebhardt, K.; Ullrich, A., Paul Ehrlich's magic bullet concept: 100 years of progress. *Nat. Rev. Can.* **2008**, 8 (6), 473-480.
6. Fleming, A., The discovery of penicillin. *Br. Med. Bull.* 1944, 2 (1), 4-5.
7. Williams, K., The introduction of 'chemotherapy' using arsphenamine – the first magic bullet. *J. R. Soc. Med.* **2009**, 102 (8), 343-348.
8. Otten, H., Domagk and the development of the sulphonamides. *J. Antimicrob. Chemother.* **1986**, 17 (6), 689-690.
9. Grossman, C. M., The first use of Penicillin in the United States. *Ann. Intern. Med.* **2008**, 149 (2), 135-136.
10. Clatworthy, A. E.; Pierson, E.; Hung, D. T., Targeting virulence: A new paradigm for antimicrobial therapy. *Nat. Chem. Biol.* **2007**, 3 (9), 541-548.
11. Martens, E.; Demain, A. L., The antibiotic resistance crisis, with a focus on the United States. *J. Antibiot.* **2017**, 70 (5), 520-526.
12. Harvey, A. L., Natural products as a screening resource. *Curr. Opin. Chem. Biol.* **2007**, 11 (5), 480-484.
13. Hutchings, M. I.; Truman, A. W.; Wilkinson, B., Antibiotics: past, present and future. *Curr. Opin. Microbiol.* **2019**, 51, 72-80.
14. Darwin M.A., C., On the origin of species by means of natural selection, or the preservation of favored races in the struggle for life. London: John Murray, Albemarle Street: 1859.

15. Larsen, J.; Raisen, C. L.; Ba, X.; Sadgrove, N. J.; Padilla-González, G. F.; Simmonds, M. S. J.; Loncaric, I.; Kerschner, H.; Apfalter, P.; Hartl, R.; Deplano, A.; Vandendriessche, S.; Černá Bolfíková, B.; Hulva, P.; Arendrup, M. C.; Hare, R. K.; Barnadas, C.; Stegger, M.; Sieber, R. N.; Skov, R. L.; Petersen, A.; Angen, Ø.; Rasmussen, S. L.; Espinosa-Gongora, C.; Aarestrup, F. M.; Lindholm, L. J.; Nykäsenoja, S. M.; Laurent, F.; Becker, K.; Walther, B.; Kehrenberg, C.; Cuny, C.; Layer, F.; Werner, G.; Witte, W.; Stamm, I.; Moroni, P.; Jørgensen, H. J.; de Lencastre, H.; Cercenado, E.; García-Garrote, F.; Börjesson, S.; Hæggman, S.; Perreten, V.; Teale, C. J.; Waller, A. S.; Pichon, B.; Curran, M. D.; Ellington, M. J.; Welch, J. J.; Peacock, S. J.; Seilly, D. J.; Morgan, F. J. E.; Parkhill, J.; Hadjirin, N. F.; Lindsay, J. A.; Holden, M. T. G.; Edwards, G. F.; Foster, G.; Paterson, G. K.; Didelot, X.; Holmes, M. A.; Harrison, E. M.; Larsen, A. R., Emergence of methicillin resistance predates the clinical use of antibiotics. *Nature* **2022**, 602, 134-141.
16. D'Costa, V. M.; King, C. E.; Kalan, L.; Morar, M.; Sung, W. W. L.; Schwarz, C.; Froese, D.; Zazula, G.; Calmels, F.; Debruyne, R.; Golding, G. B.; Poinar, H. N.; Wright, G. D., Antibiotic resistance is ancient. *Nature* **2011**, 477 (7365), 457-461.
17. Boolchandani, M.; D'Souza, A. W.; Dantas, G., Sequencing-based methods and resources to study antimicrobial resistance. *Nat. Rev. Gen.* **2019**, 20 (6), 356-370.
18. Breijyeh, Z.; Jubeh, B.; Karaman, R., Resistance of Gram-negative bacteria to current antibacterial agents and approaches to resolve it. *Molecules* **2020**, 25 (6), 1340.
19. Emamalipour, M.; Seidi, K.; Zununi Vahed, S.; Jahanban-Esfahlan, A.; Jaymand, M.; Majdi, H.; Amoozgar, Z.; Chitkushev, L. T.; Javaheri, T.; Jahanban-Esfahlan, R.; Zare, P., Horizontal gene transfer: From evolutionary flexibility to disease progression. *Front. Cell Dev. Biol.* **2020**, 8 (229).
20. Lynch, A. S.; Robertson, G. T., Bacterial and fungal biofilm infections. *Ann. Rev. Med.* 2008, 59 (1), 415-428.
21. Lewis, K., Persister cells, dormancy and infectious disease. *Nat. Rev. Microbiol.* **2007**, 5 (1), 48-56.
22. Azimi, S.; Klementiev, A. D.; Whiteley, M.; Diggle, S. P., Bacterial quorum sensing during infection. *Ann. Rev. Microbiol.* **2020**, 74 (1), 201-219.
23. Rahme, L. G.; Stevens, E. J.; Wolfort, S. F.; Shao, J.; Tompkins, R. G.; Ausubel, F. M., Common virulence factors for bacterial pathogenicity in plants and animals. *Science* **1995**, 268 (5219), 1899-1902.

24. Bottery, M. J.; Pitchford, J. W.; Friman, V.-P., Ecology and evolution of antimicrobial resistance in bacterial communities. *ISME J.* **2021**, 15 (4), 939-948.
25. Cassini, A.; Högberg, L. D.; Plachouras, D.; Quattrocchi, A.; Hoxha, A.; Simonsen, G. S.; Colomb-Cotinat, M.; Kretzschmar, M. E.; Devleeschauwer, B.; Cecchini, M.; Ouakrim, D. A.; Oliveira, T. C.; Struelens, M. J.; Suetens, C.; Monnet, D. L.; Strauss, R.; Mertens, K.; Struyf, T.; Catry, B.; Latour, K.; Ivanov, I. N.; Dobрева, E. G.; Tambic Andrašević, A.; Soprek, S.; Budimir, A.; Paphitou, N.; Žemlicková, H.; Schytte Olsen, S.; Wolff Sönksen, U.; Märtin, P.; Ivanova, M.; Lyytikäinen, O.; Jalava, J.; Coignard, B.; Eckmanns, T.; Abu Sin, M.; Haller, S.; Daikos, G. L.; Gikas, A.; Tsiodras, S.; Kontopidou, F.; Tóth, Á.; Hajdu, Á.; Guólaugsson, Ó.; Kristinsson, K. G.; Murchan, S.; Burns, K.; Pezzotti, P.; Gagliotti, C.; Dumpis, U.; Liuimiene, A.; Perrin, M.; Borg, M. A.; de Greeff, S. C.; Monen, J. C. M.; Koek, M. B. G.; Elstrøm, P.; Zabicka, D.; Deptula, A.; Hryniewicz, W.; Caniça, M.; Nogueira, P. J.; Fernandes, P. A.; Manageiro, V.; Popescu, G. A.; Serban, R. I.; Schréterová, E.; Litvová, S.; Štefkovicová, M.; Kolman, J.; Klavs, I.; Korošec, A.; Aracil, B.; Asensio, A.; Pérez-Vázquez, M.; Billström, H.; Larsson, S.; Reilly, J. S.; Johnson, A.; Hopkins, S., Attributable deaths and disability-adjusted life-years caused by infections with antibiotic-resistant bacteria in the EU and the European Economic Area in 2015: a population-level modelling analysis. *Lancet Infect. Dis.* **2019**, 19 (1), 56-66.
26. Nicolaou, K. C.; Rigol, S., A brief history of antibiotics and select advances in their synthesis. *J. Antibiot.* **2018**, 71 (2), 153-184.
27. Brown, L.; Wolf, J. M.; Prados-Rosales, R.; Casadevall, A., Through the wall: extracellular vesicles in Gram-positive bacteria, mycobacteria and fungi. *Nat. Rev. Microbiol.* **2015**, 13 (10), 620-630.
28. Bartholomew, J. W.; Mittwer, T., The Gram stain. *Bacteriol. Rev.* **1952**, 16 (1), 1-29.
29. Zhang, G.; Meredith, T. C.; Kahne, D., On the essentiality of lipopolysaccharide to Gram-negative bacteria. *Curr. Opin. Microbiol.* **2013**, 16 (6), 779-785.
30. Zhao, S.; Adamiak, J. W.; Bonifay, V.; Mehla, J.; Zgurskaya, H. I.; Tan, D. S., Defining new chemical space for drug penetration into Gram-negative bacteria. *Nat. Chem. Biol.* **2020**, 16 (12), 1293-1302.
31. Yeh, P. J.; Hegreness, M. J.; Aiden, A. P.; Kishony, R., Drug interactions and the evolution of antibiotic resistance. *Nat. Rev. Microbiol.* **2009**, 7 (6), 460-466.
32. Robertson, G. T.; Bonventre, E. J.; Doyle, T. B.; Du, Q.; Duncan, L.; Morris, T. W.; Roche, E. D.; Yan, D.; Lynch, A. S., In vitro evaluation of CBR-2092, a novel rifamycin-

- quinolone hybrid antibiotic: Microbiology profiling studies with *staphylococci* and *streptococci*. *Antimicrob. Agents Chemother.* **2008**, 52 (7), 2324-2334.
33. Karpiuk, I.; Tyski, S., Looking for the new preparations for antibacterial therapy III. New antimicrobial agents from the quinolones group in clinical trials. *Przegl. Epidemiol.* **2013**, 67 (3), 455-60, 557-61.
 34. Galloway, W. R. J. D.; Hodgkinson, J. T.; Bowden, S.; Welch, M.; Spring, D. R., Applications of small molecule activators and inhibitors of quorum sensing in Gram-negative bacteria. *Trends Microbiol.* **2012**, 20 (9), 449-458.
 35. Mitcheltree, M. J.; Pisipati, A.; Syroegin, E. A.; Silvestre, K. J.; Klepacki, D.; Mason, J. D.; Terwilliger, D. W.; Testolin, G.; Pote, A. R.; Wu, K. J. Y.; Ladley, R. P.; Chatman, K.; Mankin, A. S.; Polikanov, Y. S.; Myers, A. G., A synthetic antibiotic class overcoming bacterial multidrug resistance. *Nature* **2021**, 599 (7885), 507-512.
 36. Roberts, K. D.; Zhu, Y.; Azad, M. A. K.; Han, M.-L.; Wang, J.; Wang, L.; Yu, H. H.; Horne, A. S.; Pinson, J.-A.; Rudd, D.; Voelcker, N. H.; Patil, N. A.; Zhao, J.; Jiang, X.; Lu, J.; Chen, K.; Lomovskaya, O.; Hecker, S. J.; Thompson, P. E.; Nation, R. L.; Dudley, M. N.; Griffith, D. C.; Velkov, T.; Li, J., A synthetic lipopeptide targeting top-priority multidrug-resistant Gram-negative pathogens. *Nat. Commun.* **2022**, 13 (1), 1625.
 37. Brem, J.; Panduwawala, T.; Hansen, J. U.; Hewitt, J.; Liepins, E.; Donets, P.; Espina, L.; Farley, A. J. M.; Shubin, K.; Campillos, G. G.; Kiuru, P.; Shishodia, S.; Krahn, D.; Leśniak, R. K.; Schmidt, J.; Calvopiña, K.; Turrientes, M.-C.; Kavanagh, M. E.; Lubriks, D.; Hinchliffe, P.; Langley, G. W.; Aboklaish, A. F.; Eneroth, A.; Backlund, M.; Baran, A. G.; Nielsen, E. I.; Speake, M.; Kuka, J.; Robinson, J.; Grinberga, S.; Robinson, L.; McDonough, M. A.; Rydzik, A. M.; Leissing, T. M.; Jimenez-Castellanos, J. C.; Avison, M. B.; Da Silva Pinto, S.; Pannifer, A. D.; Martjuga, M.; Widlake, E.; Priede, M.; Hopkins Navratilova, I.; Gniadkowski, M.; Belfrage, A. K.; Brandt, P.; Yli-Kauhaluoma, J.; Bacque, E.; Page, M. G. P.; Björkling, F.; Tyrrell, J. M.; Spencer, J.; Lang, P. A.; Baranczewski, P.; Cantón, R.; McElroy, S. P.; Jones, P. S.; Baquero, F.; Suna, E.; Morrison, A.; Walsh, T. R.; Schofield, C. J., Imitation of β -lactam binding enables broad-spectrum metallo- β -lactamase inhibitors. *Nat. Chem.* **2022**, 14 (1), 15-24.
 38. Lomovskaya, O.; Nelson, K.; Rubio-Aparicio, D.; Tsivkovski, R.; Sun, D.; Dudley, M. N., Impact of intrinsic resistance mechanisms on potency of QPX7728, a new ultrabroad-spectrum beta-lactamase inhibitor of serine and metallo-beta-lactamases in

- Enterobacteriaceae*, *Pseudomonas aeruginosa*, and *Acinetobacter baumannii*. *Antimicrob. Agents Chemother.* **2020**, 64 (6), e00552-20.
39. Klahn, P.; Brönstrup, M., Bifunctional antimicrobial conjugates and hybrid antimicrobials. *Nat. Prod. Rep.* **2017**, 34 (7), 832-885.
 40. Brives, C.; Pourraz, J., Phage therapy as a potential solution in the fight against AMR: obstacles and possible futures. *Palgrave Commun.* **2020**, 6 (1), 100.
 41. Tegge, W.; Guerra, G.; Höltke, A.; Schiller, L.; Beutling, U.; Harmrolfs, K.; Gröbe, L.; Wullenkord, H.; Xu, C.; Weich, H.; Brönstrup, M., Selective bacterial targeting and infection-triggered release of antibiotic colistin conjugates. *Angew. Chem. Int. Ed.* **2021**, 60 (33), 17989-17997.
 42. Nikaido, H., Molecular basis of bacterial outer membrane permeability revisited. *Microbiol. Molec. Biol. Rev.* **2003**, 67 (4), 593-656.
 43. Wiener, M. C.; Horanyi, P. S., How hydrophobic molecules traverse the outer membranes of Gram-negative bacteria. *Proc. Natl. Ac. Sci.* **2011**, 108 (27), 10929-10930.
 44. Noinaj, N.; Guillier, M.; Travis J. Barnard; Buchanan, S. K., TonB-dependent transporters: Regulation, structure, and function. *Ann. Rev. Microbiol.* **2010**, 64 (1), 43-60.
 45. Van Gelder, P.; Dumas, F.; Bartoldus, I.; Saint, N.; Prilipov, A.; Winterhalter, M.; Wang, Y.; Philippsen, A.; Rosenbusch, J. P.; Schirmer, T., Sugar transport through maltoporin of *Escherichia coli*: Role of the greasy slide. *J. Bacteriol.* **2002**, 184 (11), 2994-2999.
 46. Tillotson, G. S., Trojan Horse antibiotics - A novel way to circumvent Gram-negative bacterial resistance? *Infect. Dis.* **2016**, 9, 45-52.
 47. Kaplan, J.; Ward, D. M., The essential nature of iron usage and regulation. *Curr. Biol.* **2013**, 23 (15), R642-646.
 48. Burg, A.; Meyerstein, D., Chapter 7 - The chemistry of monovalent copper in aqueous solutions. In *Adv. Inorg. Chem.*, Eldik, R. v.; Ivanović-Burmazović, I., Eds. Academic Press: **2012**; Vol. 64, pp 219-261.
 49. Halliwell, B.; Gutteridge, J. M., Oxygen toxicity, oxygen radicals, transition metals and disease. *Biochem. J.* **1984**, 219 (1), 1-14.

50. Kell, D. B., Iron behaving badly: inappropriate Iron chelation as a major contributor to the etiology of vascular and other progressive inflammatory and degenerative diseases. *BMC Med. Genomics* 2009, 2 (1), 2.
51. Miethke, M.; Marahiel, M. A., Siderophore-based iron acquisition and pathogen control. *Microbiol. Mol. Biol. Rev.* **2007**, 71 (3), 413 – 451.
52. Banin, E.; Vasil, M. L.; Greenberg, E. P., Iron and *Pseudomonas aeruginosa* biofilm formation. *Proc. Natl. Ac. Sci.* **2005**, 102 (31), 11076-11081.
53. Dlouhy, A. C.; Outten, C. E., The iron metallome in eukaryotic organisms. *Met. Ions Life Sci.* **2013**, 12, 241-78.
54. Schalk, I. J.; Mislin, G. L. A., Bacterial iron uptake pathways: Gates for the import of bactericide compounds. *J. Med. Chem.* **2017**, 60 (11), 4573-4576.
55. Wilson, B. R.; Bogdan, A. R.; Miyazawa, M.; Hashimoto, K.; Tsuji, Y., Siderophores in iron metabolism: From mechanism to therapy potential. *Trends Mol. Med.* **2016**, 22 (12), 1077-1090.
56. Allen, G. F.; Toth, R.; James, J.; Ganley, I. G. J. E. r., Loss of iron triggers PINK1/Parkin-independent mitophagy. *EMBO Rep.* **2013**, 14 (12), 1127-1135.
57. Hartmann, H.; Eltzschig, H. K.; Wurz, H.; Hantke, K.; Rakin, A.; Yazdi, A. S.; Matteoli, G.; Bohn, E.; Autenrieth, I. B.; Karhausen, J., Hypoxia-independent activation of HIF-1 by enterobacteriaceae and their siderophores. *J. Gastroenterol.* **2008**, 134 (3), 756-767. e6.
58. Holden, V. I.; Lenio, S.; Kuick, R.; Ramakrishnan, S. K.; Shah, Y. M.; Bachman, M. A., Bacterial siderophores that evade or overwhelm lipocalin 2 induce hypoxia inducible factor 1 α and proinflammatory cytokine secretion in cultured respiratory epithelial cells. *Infect. Immun.* **2014**, 82 (9), 3826-3836.
59. Ji, C.; Juárez-Hernández, R. E.; Miller, M. J., Exploiting bacterial iron acquisition: Siderophore conjugates. *Future Med. Chem.* **2012**, 4 (3), 297-313.
60. Saha, R.; Saha, N.; Donofrio, R. S.; Bestervelt, L. L., Microbial siderophores: A mini review. *J. Basic Microbiol.* **2013**, 53 (4), 303-317.
61. Xiao, G.; van der Helm, D.; Hider, R. C.; Dobbin, P. S., Structure–stability relationships of 3-hydroxypyridin-4-one complexes. *J. Chem. Soc., Dalton Trans.* **1992**, (22), 3265-3271.

General References

62. López-Laguna, H.; Sánchez, J.; Unzueta, U.; Mangués, R.; Vázquez, E.; Villaverde, A., Divalent cations: A molecular glue for protein materials. *Trends Biochem. Sci.* **2020**, 45 (11), 992-1003.
63. Wegner, S. V.; Spatz, J. P., Cobalt(III) as a stable and inert mediator ion between NTA and His6-tagged proteins. *Angew. Chem. Int. Ed.* **2013**, 52 (29), 7593-7596.
64. Shannon, R., Revised effective ionic radii and systematic studies of interatomic distances in halides and chalcogenides. *Acta Crystallogr.* **1976**, 32 (5), 751-767.
65. Hider, R. C.; Kong, X., Chemistry and biology of siderophores. *Nat. Prod. Rep.* **2010**, 27 (5), 637-657.
66. Dhungana, S.; Crumbliss, A. L., Coordination chemistry and redox processes in siderophore-mediated iron transport. *Geomicrobiol. J.* **2005**, 22 (3-4), 87-98.
67. Caudle, M. T.; Stevens, R. D.; Crumbliss, A. L., A monomer-to-dimer shift in a series of 1:1 ferric dihydroxamates probed by electrospray mass spectrometry. *Inorg. Chem.* **1994**, 33 (26), 6111-6115.
68. Hider, R. C.; Hall, A. D., Clinically useful chelators of tripositive elements. Progress in medicinal chemistry. *Prog. Med. Chem.* **1991**, 28, 41-173.
69. Walsh, C. T.; Liu, J.; Rusnak, F.; Sakaitani, M., Molecular studies on enzymes in chorismate metabolism and the enterobactin biosynthetic pathway. *Chem. Rev.* **1990**, 90 (7), 1105-1129.
70. Zhu, W.; Winter, M. G.; Spiga, L.; Hughes, E. R.; Chanin, R.; Mulgaonkar, A.; Pennington, J.; Maas, M.; Behrendt, C. L.; Kim, J.; Sun, X.; Beiting, D. P.; Hooper, L. V.; Winter, S. E., Xenosiderophore utilization promotes bacteroides thetaiotaomicron resilience during colitis. *Cell Host Microbe* **2020**, 27 (3), 376-388.e8.
71. Barry, S. M.; Challis, G. L., Recent advances in siderophore biosynthesis. *Curr. Opin. Chem. Biol.* **2009**, 13 (2), 205-215.
72. Calcott, M. J.; Owen, J. G.; Lamont, I. L.; Ackerley, D. F., Biosynthesis of novel pyoverdines by domain substitution in a nonribosomal peptide synthetase of *Pseudomonas aeruginosa*. *Appl. Environ. Microbiol.* **2014**, 80 (18), 5723-5731.
73. Gehring, A. M.; Bradley, K. A.; Walsh, C. T., Enterobactin biosynthesis in *Escherichia coli*: Isochorismate lyase (EntB) is a bifunctional enzyme that is phosphopantetheinylated by EntD and then acylated by EntE using ATP and 2,3-dihydroxybenzoate. *Biochemistry* **1997**, 36 (28), 8495-8503.

74. Nikaido, H., Molecular basis of bacterial outer membrane permeability revisited. *Microbiol. Mol. Biol. Rev.* **2003**, 67 (4), 593-656.
75. Larsen, R. A.; Thomas, M. G.; Postle, K., Protonmotive force, ExbB and ligand-bound FepA drive conformational changes in TonB. *Mol. Microbiol.* **1999**, 31 (6), 1809-1824.
76. Chu, B. C.; Garcia-Herrero, A.; Johanson, T. H.; Krewulak, K. D.; Lau, C. K.; Peacock, R. S.; Slavinskaya, Z.; Vogel, H. J., Siderophore uptake in bacteria and the battle for iron with the host; a bird's eye view. *Biometals* **2010**, 23 (4), 601-611.
77. Hassan, H.; Troxell, B., Transcriptional regulation by Ferric Uptake Regulator (Fur) in pathogenic bacteria. *Front. Cell. Infect. Microbiol.* **2013**, 3:59.
78. Noinaj, N.; Guillier, M.; Barnard, T. J.; Buchanan, S. K., TonB-Dependent transporters: regulation, structure, and function. *Annu. Rev. Microbiol.* **2010**, 64 (1), 43-60.
79. Adams, H.; Zeder-Lutz, G.; Schalk, I.; Pattus, F.; Celia, H., Interaction of TonB with the outer membrane receptor FpvA of *Pseudomonas aeruginosa*. *J. Bacteriol* 2006, 188 (16), 5752-5761.
80. Josts, I.; Veith, K.; Tidow, H., Ternary structure of the outer membrane transporter FoxA with resolved signaling domain provides insights into TonB-mediated siderophore uptake. *eLife* **2019**, 8, e48528.
81. Kong, H.; Cheng, W.; Wei, H.; Yuan, Y.; Yang, Z.; Zhang, X., An overview of recent progress in siderophore-antibiotic conjugates. *Eur. J. Med. Chem.* **2019**, 182, 111615.
82. Parrow, N. L.; Fleming, R. E.; Minnick, M. F.; Maurelli, A. T., Sequestration and scavenging of iron in infection. *Infect. Immun.* **2013**, 81 (10), 3503-3514.
83. Pearson, R. G., Hard and Soft Acids and Bases. *J. Am. Chem. Soc.* **1963**, 85 (22), 3533-3539.
84. Moynié, L.; Milenkovic, S.; Mislin, G. L. A.; Gasser, V.; Mallocci, G.; Baco, E.; McCaughan, R. P.; Page, M. G. P.; Schalk, I. J.; Ceccarelli, M.; Naismith, J. H., The complex of ferric-enterobactin with its transporter from *Pseudomonas aeruginosa* suggests a two-site model. *Nat. Commun.* **2019**, 10 (1), 3673.
85. Cornelis, P.; Dingemans, J., *Pseudomonas aeruginosa* adapts its iron uptake strategies in function of the type of infections. *Front. Cell. Infect. Microbiol.* **2013**, 3, 75.
86. Josts, I.; Veith, K.; Normant, V.; Schalk, I. J.; Tidow, H., Structural insights into a novel family of integral membrane siderophore reductases. *bioRxiv* preprint 2021.

87. Choi, J.; Ryu, S., Regulation of Iron Uptake by Fine-Tuning the Iron Responsiveness of the Iron Sensor Fur. *Appl Environ. Microbiol.* **2019**, 85 (9), e03026-18.
88. Hassan, H.; Troxell, B., Transcriptional regulation by Ferric Uptake Regulator (Fur) in pathogenic bacteria. *Front. Cell. Infect. Microbiol.* **2013**, 3, 59.
89. Seyoum, Y.; Baye, K.; Humblot, C., Iron homeostasis in host and gut bacteria – a complex interrelationship. *Gut Microbes* **2021**, 13 (1), 1874855.
90. Schauer, K.; Rodionov, D. A.; de Reuse, H., New substrates for TonB-dependent transport: do we only see the ‘tip of the iceberg’? *Trends Biochem. Sci.* **2008**, 33 (7), 330-338.
91. Hickman, S. J.; Cooper, R. E. M.; Bellucci, L.; Paci, E.; Brockwell, D. J., Gating of TonB-dependent transporters by substrate-specific forced remodelling. *Nat. Commun.* **2017**, 8 (1), 14804.
92. Ferguson, A. D.; Ködding, J.; Walker, G.; Bös, C.; Coulton, J. W.; Diederichs, K.; Braun, V.; Welte, W., Active transport of an antibiotic rifamycin derivative by the outer-membrane protein FhuA. *Structure* **2001**, 9 (8), 707-716.
93. Braun, V.; Pramanik, A.; Gwinner, T.; Köberle, M.; Bohn, E., Sideromycins: tools and antibiotics. *BioMetals* **2009**, 22 (1), 3-13.
94. Johnstone, T. C.; Nolan, E. M., Beyond iron: non-classical biological functions of bacterial siderophores. *Dalton Trans.* **2015**, 44 (14), 6320-39.
95. Mathieu, B.; Pierre, C.; Christine, B., Iron Metabolism: A promising target for antibacterial strategies. *Recent Pat. Antiinfect. Drug Discov.* **2009**, 4 (3), 190-205.
96. Rebuffat, S., Microcins in action: amazing defence strategies of *Enterobacteria*. *Biochem. Soc. Trans.* **2012**, 40 (6), 1456-1462.
97. Duquesne, S.; Petit, V.; Peduzzi, J.; Rebuffat, S., Structural and functional diversity of microcins, gene-encoded antibacterial peptides from *Enterobacteria*. *Microb. Physiol.* **2007**, 13 (4), 200-209.
98. Strahsburger, E.; Baeza, M.; Monasterio, O.; Lagos, R., Cooperative uptake of microcin E492 by receptors FepA, Fiu, and Cir and inhibition by the siderophore enterochelin and its dimeric and trimeric hydrolysis products. *Antimicrob. Agents Chemother.* **2005**, 49 (7), 3083-3086.

99. Pages, J. M.; James, C. E.; Winterhalter, M., The porin and the permeating antibiotic: a selective diffusion barrier in Gram-negative bacteria. *Nat. Rev. Microbiol.* **2008**, *6* (12), 893-903.
100. Delcour, A. H., Outer membrane permeability and antibiotic resistance. *Biochim. Biophys. Acta* **2009**, *1794* (5), 808-16.
101. Hancock, R. E., The bacterial outer membrane as a drug barrier. *Trends Microbiol.* **1997**, *5* (1), 37-42.
102. Ji, C.; Miller, P. A.; Miller, M. J., Iron transport-mediated drug delivery: Practical syntheses and *in vitro* antibacterial studies of tris-catecholate siderophore–aminopenicillin conjugates reveals selectively potent antipseudomonal activity. *J. Am. Chem. Soc.* **2012**, *134* (24), 9898-9901.
103. Ghosh, M.; Lin, Y.-M.; Miller, P. A.; Möllmann, U.; Boggess, W. C.; Miller, M. J., Siderophore conjugates of daptomycin are potent inhibitors of carbapenem resistant strains of *Acinetobacter baumannii*. *ACS Infect. Dis.* **2018**, *4* (10), 1529 – 1535.
104. Liu, R.; Miller, P. A.; Vakulenko, S. B.; Stewart, N. K.; Boggess, W. C.; Miller, M. J., A synthetic dual drug sideromycin induces Gram-negative bacteria to commit suicide with a Gram-positive antibiotic. *J. Med. Chem.* **2018**, *61* (9), 3845-3854.
105. Swayambhu, G.; Bruno, M.; Gulick, A. M.; Pfeifer, B. A., Siderophore natural products as pharmaceutical agents. *Curr. Opin. Biotechnol.* **2021**, *69*, 242-251.
106. Negash, K. H.; Norris, J. K. S.; Hodgkinson, J. T., Siderophore-antibiotic conjugate design: New drugs for bad bugs? *Molecules* **2019**, *24* (18), 3314.
107. Ji, C.; Miller, M. J., Siderophore–fluoroquinolone conjugates containing potential reduction-triggered linkers for drug release: synthesis and antibacterial activity. *BioMetals* **2015**, *28* (3), 541-551.
108. Zheng, T.; Bullock, J. L.; Nolan, E. M., Siderophore-mediated cargo delivery to the cytoplasm of *Escherichia coli* and *Pseudomonas aeruginosa*: Syntheses of monofunctionalized enterobactin scaffolds and evaluation of enterobactin–cargo conjugate uptake. *J. Am. Chem. Soc.* **2012**, *134* (44), 18388-18400.
109. Neumann, W.; Sassone-Corsi, M.; Raffatellu, M.; Nolan, E. M., Esterase-catalyzed siderophore hydrolysis activates an enterobactin–ciprofloxacin conjugate and confers targeted antibacterial activity. *J. Am. Chem. Soc.* **2018**, *140* (15), 5193-5201.

110. Zscherp, R.; Coetzee, J.; Vornweg, J.; Grunenberg, J.; Herrmann, J.; Müller, R.; Klahn, P., Biomimetic enterobactin analogue mediates iron-uptake and cargo transport into *E. coli* and *P. aeruginosa*. *Chem. Sci.* **2021**, *12* (30), 10179-10190.
111. Miller, M. J.; Liu, R., Design and syntheses of new antibiotics inspired by nature's quest for iron in an oxidative climate. *Acc. Chem. Res.* **2021**, *54* (7), 1646-1661.
112. Han, S.; Zaniewski, R. P.; Marr, E. S.; Lacey, B. M.; Tomaras, A. P.; Evdokimov, A.; Miller, J. R.; Shanmugasundaram, V., Structural basis for effectiveness of siderophore-conjugated monocarbams against clinically relevant strains of *Pseudomonas aeruginosa*. *Proc. Natl. Ac. Sci.* **2010**, *107* (51), 22002-22007.
113. Tomaras, A. P.; Crandon, J. L.; McPherson, C. J.; Banevicius, M. A.; Finegan, S. M.; Irvine, R. L.; Brown, M. F.; O'Donnell, J. P.; Nicolau, D. P., Adaptation-based resistance to siderophore-conjugated antibacterial agents by *Pseudomonas aeruginosa*. *Antimicrob. Agents Chemother.* **2013**, *57* (9), 4197-4207.
114. Kim, A.; Kutschke, A.; Ehmann, D. E.; Patey, S. A.; Crandon, J. L.; Gorseth, E.; Miller, A. A.; McLaughlin, R. E.; Blinn, C. M.; Chen, A.; Nayar, A. S.; Dangel, B.; Tsai, A. S.; Rooney, M. T.; Murphy-Benenato, K. E.; Eakin, A. E.; Nicolau, D. P. Pharmacodynamic profiling of a siderophore-conjugated monocarbam in *Pseudomonas aeruginosa*: Assessing the risk for resistance and attenuated efficacy. *Antimicrob. Agents Chemother.* **2015**, *59* (12), 7743-7752.
115. Mushtaq, S.; Warner, M.; Livermore, D., Activity of the siderophore monobactam BAL30072 against multiresistant non-fermenters. *J. Antimicrob. Chemother.* **2010**, *65* (2), 266-70.
116. Page, M. G. P.; Dantier, C.; Desarbre, E., *In vitro* properties of BAL30072, a novel siderophore sulfactam with activity against multiresistant Gram-negative bacilli. *Antimicrob. Agents Chemother.* **2010**, *54* (6), 2291-2302.
117. Mima, T.; Kvitko, B. H.; Rholl, D. A.; Page, M. G. P.; Desarbre, E.; Schweizer, H. P., *In vitro* activity of BAL30072 against *Burkholderia pseudomallei*. *Int. J. Antimicrob. Agents* **2011**, *38* (2), 157-159.
118. Sato, T.; Yamawaki, K., Cefiderocol: Discovery, chemistry, and *in vivo* profiles of a novel siderophore cephalosporin. *Clin. Infect. Dis.* **2019**, *69* (Supplement_7), S538-S543.

119. Higgins, P. G.; Stefanik, D.; Page, M. G.; Hackel, M.; Seifert, H., *In vitro* activity of the siderophore monosulfactam BAL30072 against meropenem-non-susceptible *Acinetobacter baumannii*. *J. Antimicrob. Chemother.* **2012**, *67* (5), 1167-9.
120. Provenzani, A.; Hospodar, A. R.; Meyer, A. L.; Leonardi Vinci, D.; Hwang, E. Y.; Butrus, C. M.; Polidori, P., Multidrug-resistant gram-negative organisms: a review of recently approved antibiotics and novel pipeline agents. *Int. J. Clin. Pharm.* **2020**, *42* (4), 1016-1025.
121. Ito, A.; Kohira, N.; Bouchillon, S. K.; West, J.; Rittenhouse, S.; Sader, H. S.; Rhomberg, P. R.; Jones, R. N.; Yoshizawa, H.; Nakamura, R.; Tsuji, M.; Yamano, Y., *In vitro* antimicrobial activity of S-649266, a catechol-substituted siderophore cephalosporin, when tested against non-fermenting Gram-negative bacteria. *J. Antimicrob. Chemother.* **2016**, *71* (3), 670-7.
122. Ito-Horiyama, T.; Ishii, Y.; Ito, A.; Sato, T.; Nakamura, R.; Fukuhara, N.; Tsuji, M.; Yamano, Y.; Yamaguchi, K.; Tateda, K., Stability of novel siderophore cephalosporin S-649266 against clinically relevant carbapenemases. *Antimicrobial Agents and Chemotherapy* **2016**, *60* (7), 4384-4386.
123. Ohi, N.; Aoki, B.; Kuroki, T.; Matsumoto, M.; Kojima, K.; Nehashi, T., Semisynthetic beta-lactam antibiotics. III. Effect on antibacterial activity and comt-susceptibility of chlorine-introduction into the catechol nucleus of 6-[(R)-2-[3-(3,4-dihydroxybenzoyl)-3-(3-hydroxypropyl)-1-ureido]-2- phenylacetamido]penicillanic acid. *J. Antibiot. (Tokyo)* **1987**, *40* (1), 22-8.
124. Zhanel, G. G.; Golden, A. R.; Zelenitsky, S.; Wiebe, K.; Lawrence, C. K.; Adam, H. J.; Idowu, T.; Domalaon, R.; Schweizer, F.; Zhanel, M. A.; Lagacé-Wiens, P. R. S.; Walkty, A. J.; Noreddin, A.; Lynch Iii, J. P.; Karlowsky, J. A., Cefiderocol: A siderophore cephalosporin with activity against carbapenem-resistant and multidrug-resistant Gram-negative bacilli. *Drugs* **2019**, *79* (3), 271-289.
125. Wu, J. Y.; Srinivas, P.; Pogue, J. M., Cefiderocol: A novel agent for the management of multidrug-resistant Gram-negative organisms. *Infect Dis Ther.* **2020**, *9* (1), 17-40.
126. El-Lababidi, R. M.; Rizk, J. G., Cefiderocol: A siderophore cephalosporin. *Ann Pharmacother.* **2020**, *54* (12), 1215-1231.
127. Lee, A. A.; Chen, Y.-C. S.; Ekalestari, E.; Ho, S.-Y.; Hsu, N.-S.; Kuo, T.-F.; Wang, T.-S. A., Facile and versatile chemoenzymatic synthesis of enterobactin analogues and applications in bacterial detection. *Angew. Chem. Int. Ed.* **2016**, *55* (40), 12338-12342.

128. Hughes, L. D.; Rawle, R. J.; Boxer, S. G., Choose your label wisely: Water-soluble fluorophores often interact with lipid bilayers. *PLoS ONE* **2014**, *9* (2), e87649.
129. Jain, S. K., The promise of molecular imaging in the study and treatment of infectious diseases. *Mol. Imaging Biol.* **2017**, *19* (3), 341-347.
130. Caliendo, A. M.; Gilbert, D. N.; Ginocchio, C. C.; Hanson, K. E.; May, L.; Quinn, T. C.; Tenover, F. C.; Alland, D.; Blaschke, A. J.; Bonomo, R. A.; Carroll, K. C.; Ferraro, M. J.; Hirschhorn, L. R.; Joseph, W. P.; Karchmer, T.; MacIntyre, A. T.; Reller, L. B.; Jackson, A. F., Better tests, better care: Improved diagnostics for infectious diseases. *Clin. Infect. Dis.* **2013**, *57* (suppl_3), S139-S170.
131. Ordonez, A. A.; Sellmyer, M. A.; Gowrishankar, G.; Ruiz-Bedoya, C. A.; Tucker, E. W.; Palestro, C. J.; Hammoud, D. A.; Jain, S. K., Molecular imaging of bacterial infections: Overcoming the barriers to clinical translation. *Sci. Transl. Med.* **2019**, *11* (508), eaax8251.
132. Fletcher, J. W.; Djulbegovic, B.; Soares, H. P.; Siegel, B. A.; Lowe, V. J.; Lyman, G. H.; Coleman, R. E.; Wahl, R.; Paschold, J. C.; Avril, N.; Einhorn, L. H.; Suh, W. W.; Samson, D.; Delbeke, D.; Gorman, M.; Shields, A. F., Recommendations on the use of ¹⁸F-FDG PET in oncology. *J. Nucl. Med.* **2008**, *49* (3), 480-508.
133. Mota, F.; Ordonez, A. A.; Firth, G.; Ruiz-Bedoya, C. A.; Ma, M. T.; Jain, S. K., Radiotracer development for bacterial imaging. *J. Med. Chem.* **2020**, *63* (5), 1964-1977.
134. Lucignani, G., The many roads to infection imaging. *Eur. J. Nucl. Med. Mol. Imaging* **2007**, *34* (11), 1873-1877.
135. Ordonez, A. A.; Jain, S. K., Pathogen-specific bacterial imaging in nuclear medicine. *Semin. Nucl. Med.* **2018**, *48* (2), 182-194.
136. Ordonez, A. A.; Weinstein, E. A.; Bambarger, L. E.; Saini, V.; Chang, Y. S.; DeMarco, V. P.; Klunk, M. H.; Urbanowski, M. E.; Moulton, K. L.; Murawski, A. M.; Pokkali, S.; Kalinda, A. S.; Jain, S. K., A systematic approach for developing bacteria-specific imaging tracers. *J. Nucl. Med.* **2017**, *58* (1), 144-150.
137. Petrik, M.; Umlaufova, E.; Raclavsky, V.; Palyzova, A.; Havlicek, V.; Haas, H.; Novy, Z.; Dolezal, D.; Hajduch, M.; Decristoforo, C., Imaging of *Pseudomonas aeruginosa* infection with Ga-68 labelled pyoverdine for positron emission tomography. *Sci. Rep.* **2018**, *8* (1), 15698.

138. Conti, M.; Eriksson, L., Physics of pure and non-pure positron emitters for PET: a review and a discussion. *EJNMMI Physics* **2016**, 3 (1), 8.
139. Palestro, C. J., The current role of gallium imaging in infection. *Semin. Nucl. Med.* **1994**, 24 (2), 128-141.
140. Petrik, M.; Umlaufova, E.; Raclavsky, V.; Palyzova, A.; Havlicek, V.; Pfister, J.; Mair, C.; Novy, Z.; Popper, M.; Hajduch, M.; Decristoforo, C., ⁶⁸Ga-labelled desferrioxamine-B for bacterial infection imaging. *Eur. J. Nucl. Med. Mol. Imaging* **2021**, 48 (2), 372-382.
141. Hong, G.; Antaris, A. L.; Dai, H., Near-infrared fluorophores for biomedical imaging. *Nat. Biomed. Eng.* **2017**, 1 (1), 0010.
142. Alford, R.; Simpson, H. M.; Duberman, J.; Hill, G. C.; Ogawa, M.; Regino, C.; Kobayashi, H.; Choyke, P. L., Toxicity of organic fluorophores used in molecular imaging: literature review. *Mol. Imaging* **2009**, 8 (6), 341-54.
143. Dodeigne, C.; Thunus, L.; Lejeune, R., Chemiluminescence as diagnostic tool. A review. *Talanta* **2000**, 51 (3), 415-439.
144. Saito, K.; Nagai, T., Recent progress in luminescent proteins development. *Curr. Opin. Chem. Biol.* **2015**, 27, 46-51.
145. Kopecky, K. R.; Mumford, C., Luminescence in the thermal decomposition of 3,3,4-trimethyl-1,2-dioxetane. *Can. J. Chem.* **1969**, 47 (4), 709-711.
146. Schaap, A. P.; Handley, R. S.; Giri, B. P., Chemical and enzymatic triggering of 1,2-dioxetanes. 1: Aryl esterase-catalyzed chemiluminescence from a naphthyl acetate-substituted dioxetane. *Tet. Lett.* **1987**, 28 (9), 935-938.
147. Schaap, A. P.; Sandison, M. D.; Handley, R. S., Chemical and enzymatic triggering of 1,2-dioxetanes. 3: alkaline phosphatase-catalyzed chemiluminescence from an aryl phosphate-substituted dioxetane. *Tet. Lett.* **1987**, 28 (11), 1159-1162.
148. Adam, W.; Reinhardt, D.; Saha-Möller, C. R., From the firefly bioluminescence to the dioxetane-based (AMPPD) chemiluminescence immunoassay: a retroanalysis. *Analyst* **1996**, 121 (11), 1527-1531.
149. Green, O.; Eilon, T.; Hananya, N.; Gutkin, S.; Bauer, C. R.; Shabat, D., Opening a gateway for chemiluminescence cell imaging: Distinctive methodology for design of bright chemiluminescent dioxetane probes. *ACS Cent. Sci.* **2017**, 3 (4), 349-358.

150. Roth-Konforti, M. E.; Bauer, C. R.; Shabat, D., Unprecedented Sensitivity in a Probe for monitoring cathepsin B: Chemiluminescence microscopy cell-imaging of a natively expressed enzyme. *Angew. Chem. Int. Ed.* **2017**, *56* (49), 15633-15638.
151. Eilon-Shaffer, T.; Roth-Konforti, M.; Eldar-Boock, A.; Satchi-Fainaro, R.; Shabat, D., ortho-Chlorination of phenoxy 1,2-dioxetane yields superior chemiluminescent probes for in vitro and in vivo imaging. *Org. Biomol. Chem.* **2018**, *16* (10), 1708-1712.
152. Hananya, N.; Green, O.; Blau, R.; Satchi-Fainaro, R.; Shabat, D., A highly efficient chemiluminescence probe for the detection of singlet oxygen in living cells. *Angew. Chem. Int. Ed.* **2017**, *56* (39), 11793-11796.
153. Makishima, A., Chapter Five - Topics of bioluminescence and chemiluminescence. In *Biochem. Mat. Sci.*, Makishima, A., Ed. Elsevier: 2019; pp 77-83.
154. Gnaim, S.; Green, O.; Shabat, D., The emergence of aqueous chemiluminescence: new promising class of phenoxy 1,2-dioxetane luminophores. *Chem. Comm.* **2018**, *54* (17), 2073-2085.
155. Babin, B. M.; Fernandez-Cuervo, G.; Sheng, J.; Green, O.; Ordonez, A. A.; Turner, M. L.; Keller, L. J.; Jain, S. K.; Shabat, D.; Bogoy, M., Chemiluminescent protease probe for rapid, sensitive, and inexpensive detection of live *Mycobacterium tuberculosis*. *ACS Cent. Sci.* **2021**, *7* (5), 803-814.
156. Das, S.; Ihssen, J.; Wick, L.; Spitz, U.; Shabat, D., Chemiluminescent carbapenem-based molecular probe for detection of carbapenemase activity in live bacteria. *Chem. Eur. J.* **2020**, *26* (16), 3647-3652.
157. Gholap, S. P.; Yao, C.; Green, O.; Babjak, M.; Jakubec, P.; Malatinský, T.; Ihssen, J.; Wick, L.; Spitz, U.; Shabat, D., Chemiluminescence detection of hydrogen sulfide release by β -lactamase-catalyzed β -lactam biodegradation: Unprecedented pathway for monitoring β -lactam antibiotic bacterial resistance. *Bioconj. Chem.* **2021**, *32* (5), 991-1000.
158. Roth-Konforti, M.; Green, O.; Hupfeld, M.; Fieseler, L.; Heinrich, N.; Ihssen, J.; Vorberg, R.; Wick, L.; Spitz, U.; Shabat, D., Ultrasensitive detection of *Salmonella* and *Listeria monocytogenes* by small-molecule chemiluminescence probes. *Angew. Chem. Int. Ed.* **2019**, *58* (30), 10361-10367.
159. Neumann, W.; Sassone-Corsi, M.; Raffatellu, M.; Nolan, E. M., Esterase-catalyzed siderophore hydrolysis activates an enterobactin-ciprofloxacin conjugate and confers targeted antibacterial activity. *J. Am. Chem. Soc.* **2018**, *140* (15), 5193 – 5201.

160. Raines, D. J.; Moroz, O. V.; Blagova, E. V.; Turkenburg, J. P.; Wilson, K. S.; Duhme-Klair, A. K., Bacteria in an intense competition for iron: Key component of the *Campylobacter jejuni* iron uptake system scavenges enterobactin hydrolysis product. *Proc. Natl. Acad. Sci.* **2016**, *113* (21), 5850-5855.
161. Mashiach, R.; Meijler, M. M., Total synthesis of pyoverdinin D. *Org. Lett.* **2013**, *15* (7), 1702-1705.
162. Perraud, Q.; Cantero, P.; Roche, B.; Gasser, V.; Normant, V. P.; Kuhn, L.; Hammann, P.; Mislin, G. L. A.; Ehret-Sabatier, L.; Schalk, I. J., Phenotypic Adaptation of *Pseudomonas aeruginosa* by hacking siderophores produced by other microorganisms* *Mol. Cell. Proteomics* **2020**, *19* (4), 589-607.
163. Harris, W. R.; Carrano, C. J.; Cooper, S. R.; Sofen, S. R.; Avdeef, A. E.; McArdle, J. V.; Raymond, K. N., Coordination chemistry of microbial iron transport compounds. 19. Stability constants and electrochemical behavior of ferric enterobactin and model complexes. *J. Am. Chem. Soc.* **1979**, *101* (20), 6097-6104.
164. Ferreira, K.; Hu, H.-Y.; Fetz, V.; Prochnow, H.; Rais, B.; Müller, P. P.; Brönstrup, M., Multivalent siderophore–DOTAM conjugates as theranostics for imaging and treatment of bacterial infections. *Angew. Chem. Int. Ed.* **2017**, *56* (28), 8272-8276.
165. Venuti, M. C.; Rastetter, W. H.; Neilands, J. B., 1,3,5-Tris(N,N',N''-2,3-dihydroxybenzoyl)aminomethylbenzene, a synthetic iron chelator related to enterobactin. *J. Med. Chem.* **1979**, *22* (2), 123-124.
166. Ferreira, K. Synthesis of siderophore-based conjugates to detect and treat bacterial infections. Gottfried Wilhelm Leibniz Universität Hannover, Dissertation, 2018.
167. Ferreira, K.; Hu, H.-Y.; Fetz, V.; Prochnow, H.; Rais, B.; Müller, P. P.; Brönstrup, M., Multivalent siderophore–DOTAM conjugates as theranostics for imaging and treatment of bacterial infections. *Angew. Chem. Int. Ed.* **2017**, *56* (28), 8272-8276.
168. Carrano, C. J.; Raymond, K. N., Ferric ion sequestering agents. 2. Kinetics and mechanism of iron removal from transferrin by enterobactin and synthetic tricatechols. *J. Am. Chem. Soc.* **1979**, *101* (18), 5401-5404.
169. Sletten, E. M.; Bertozzi, C. R., From mechanism to mouse: a tale of two bioorthogonal reactions. *Acc. Chem. Res.* **2011**, *44* (9), 666-676.
170. Tornøe, C.; Christensen, C.; Meldal, M.; Rostovtsev, V.; Green, L.; Fokin, V.; Sharpless, K., A stepwise Huisgen cycloaddition process: Copper (I)-catalyzed

- regioselective "ligation" of azides and terminal alkynes. *J. Org. Chem.* **2002**, *67*, 3057-3064.
171. Bird, R. E.; Lemmel, S. A.; Yu, X.; Zhou, Q. A., Bioorthogonal chemistry and its applications. *Bioconj. Chem.* **2021**, *32* (12), 2457-2479.
172. Huisgen, R., Proceedings of the Chemical Society. October 1961. *Proc. Chem. Soc.* **1961**, 357-396.
173. Tornøe, C. W.; Christensen, C.; Meldal, M., Peptidotriazoles on Solid Phase: [1,2,3]-Triazoles by Regiospecific Copper(I)-catalyzed 1,3-dipolar cycloadditions of terminal alkynes to azides. *J. Org. Chem.* **2002**, *67* (9), 3057-3064.
174. Himo, F.; Lovell, T.; Hilgraf, R.; Rostovtsev, V. V.; Noodleman, L.; Sharpless, K. B.; Fokin, V. V., Copper(I)-catalyzed synthesis of azoles. DFT study predicts unprecedented reactivity and intermediates. *J. Am. Chem. Soc.* **2005**, *127* (1), 210-216.
175. Agard, N. J.; Prescher, J. A.; Bertozzi, C. R., A strain-promoted [3 + 2] azide-alkyne cycloaddition for covalent modification of biomolecules in living systems. *J. Am. Chem. Soc.* **2004**, *126* (46), 15046-15047.
176. Dommerholt, J.; Rutjes, F. P. J. T.; van Delft, F. L., Strain-promoted 1,3-dipolar cycloaddition of cycloalkynes and organic azides. *Top. Curr. Chem.* **2016**, *374* (2), 16.
177. Turner, R. B.; Jarrett, A.; Goebel, P.; Mallon, B., Heats of hydrogenation. IX. Cyclic acetylenes and some miscellaneous olefins. *J. Am. Chem. Soc.* **1973**, *95* (3), 790-792.
178. Bach, R. D., Ring strain energy in the cyclooctyl system. The effect of strain energy on [3+ 2] cycloaddition reactions with azides. *J. Am. Chem. Soc.* **2009**, *131* (14), 5233-5243.
179. Ess, D. H.; Jones, G. O.; Houk, K., Transition states of strain-promoted metal-free click chemistry: 1, 3-dipolar cycloadditions of phenyl azide and cyclooctynes. *Org. Lett.* **2008**, *10* (8), 1633-1636.
180. Saxon, E.; Bertozzi, C. R., Cell surface engineering by a modified Staudinger reaction. *Science* **2000**, *287* (5460), 2007-2010.
181. Ning, X.; Guo, J.; Wolfert, M. A.; Boons, G. J., Visualizing metabolically labeled glycoconjugates of living cells by copper-free and fast Huisgen cycloadditions. *Angew. Chem. Int. Ed.* **2008**, *120* (12), 2285-2287.

182. Ning, X.; Lee, S.; Wang, Z.; Kim, D.; Stubblefield, B.; Gilbert, E.; Murthy, N., Maltodextrin-based imaging probes detect bacteria *in vivo* with high sensitivity and specificity. *Nat. Mater.* **2011**, *10* (8), 602-607.
183. Lehar, S. M.; Pillow, T.; Xu, M.; Staben, L.; Kajihara, K. K.; Vandlen, R.; DePalatis, L.; Raab, H.; Hazenbos, W. L.; Hiroshi Morisaki, J.; Kim, J.; Park, S.; Darwish, M.; Lee, B.-C.; Hernandez, H.; Loyet, K. M.; Lupardus, P.; Fong, R.; Yan, D.; Chalouni, C.; Luis, E.; Khalfin, Y.; Plise, E.; Cheong, J.; Lyssikatos, J. P.; Strandh, M.; Koefoed, K.; Andersen, P. S.; Flygare, J. A.; Wah Tan, M.; Brown, E. J.; Mariathasan, S., Novel antibody–antibiotic conjugate eliminates intracellular *S. aureus*. *Nature* **2015**, *527* (7578), 323-328.
184. Alouane, A.; Labruère, R.; Le Saux, T.; Schmidt, F.; Jullien, L., Self-immolative spacers: Kinetic aspects, structure–property relationships, and applications. *Angew. Chem. Int. Ed.* **2015**, *54* (26), 7492-7509.
185. Wong, P. T.; Choi, S. K., Mechanisms of drug release in nanotherapeutic delivery systems. *Chem. Rev.* **2015**, *115* (9), 3388-3432.
186. Ghosh, M.; Miller, P. A.; Möllmann, U.; Claypool, W. D.; Schroeder, V. A.; Wolter, W. R.; Suckow, M.; Yu, H.; Li, S.; Huang, W.; Zajicek, J.; Miller, M. J., Targeted antibiotic delivery: Selective siderophore conjugation with daptomycin confers potent activity against multidrug resistant *Acinetobacter baumannii* both *in vitro* and *in vivo*. *J. Med. Chem.* **2017**, *60* (11), 4577-4583.
187. Walther, R.; Rautio, J.; Zelikin, A. N., Prodrugs in medicinal chemistry and enzyme prodrug therapies. *Adv. Drug Deliv. Rev.* **2017**, *118*, 65-77.
188. Gilbert, H. F., Thiol/disulfide exchange equilibria and disulfide bond stability. In *Methods in Enzymology*, Academic Press: 1995; Vol. 251, pp 8-28.
189. Yiamsawas, D.; Wagner, M.; Baier, G.; Landfester, K.; Wurm, F. R., Competing and simultaneous click reactions at the interface and in solution. *RSC Adv.* **2016**, *6* (56), 51327-51331.
190. Song, Q.; Yang, J.; Hall, S. C. L.; Gurnani, P.; Perrier, S., Pyridyl disulfide reaction chemistry: An efficient strategy toward redox-responsive cyclic peptide–polymer conjugates. *ACS Macro Letters* **2019**, *8* (10), 1347-1352.
191. Zhang, D.; Fourie-O'Donohue, A.; Dragovich, P. S.; Pillow, T. H.; Sadowsky, J. D.; Kozak, K. R.; Cass, R. T.; Liu, L.; Deng, Y.; Liu, Y.; Hop, C. E. C. A.; Khojasteh, S. C., Catalytic cleavage of disulfide bonds in small molecules and linkers of antibody–drug conjugates. *Drug Metab. Dispos.* **2019**, *47* (10), 1156-1163.

192. Levine, M. N.; Raines, R. T., Trimethyl lock: a trigger for molecular release in chemistry, biology, and pharmacology. *Chem. Sci.* **2012**, 3 (8), 2412-2420.
193. Okoh, O. A.; Klahn, P., Trimethyl lock: A multifunctional molecular tool for drug delivery, cellular imaging, and stimuli-responsive materials. *ChemBioChem* **2018**, 19 (16), 1668-1694.
194. Milstien, S.; Cohen, L. A., Stereopopulation control. I. Rate enhancement in the lactonizations of o-hydroxyhydrocinnamic acids. *J. Am. Chem. Soc.* **1972**, 94 (26), 9158-9165.
195. King, M. M.; Cohen, L. A., Stereopopulation control. VII. Rate enhancement in the lactonization of 3-(o-hydroxyphenyl) propionic acids: dependence on the size of aromatic ring substituents. *J. Am. Chem. Soc.* **1983**, 105 (9), 2752-2760.
196. Jung, M. E.; Piizzi, G., gem-Disubstituent effect: theoretical basis and synthetic applications. *Chem. Rev.* **2005**, 105 (5), 1735-1766.
197. Wang, B.; Nicolaou, M. G.; Liu, S.; Borchardt, R. T., Structural analysis of a facile lactonization system facilitated by a "trimethyl lock". *Bioorg. Chem.* **1996**, 24 (1), 39-49.
198. Winans, R. E.; Wilcox Jr, C. F., Comparison of stereopopulation control with conventional steric effects in lactonization of hydrocoumarinic acids. *J. Am. Chem. Soc.* **1976**, 98 (14), 4281-4285.
199. Karaman, R., Accelerations in the lactonization of trimethyl lock systems are due to proximity orientation and not to strain effects. *Res. Lett. Org. Chem.* **2009**, 2009, 240253.
200. Amsberry, K. L.; Gerstenberger, A. E.; Borchardt, R. T., Amine prodrugs which utilize hydroxy amide lactonization. II. A potential esterase-sensitive amide prodrug. *Pharm. Res.* **1991**, 8 (4), 455-461.
201. Carpino, L. A.; Triolo, S. A.; Berglund, R. A., Reductive lactonization of strategically methylated quinone propionic acid esters and amides. *J. Org. Chem.* **1989**, 54 (14), 3303-3310.
202. Ji, C.; Miller, M. J., Chemical syntheses and *in vitro* antibacterial activity of two desferrioxamine B-ciprofloxacin conjugates with potential esterase and phosphatase triggered drug release linkers. *Bioorg. Med. Chem.* **2012**, 20 (12), 3828-3836.
203. Shigenaga, A.; Ogura, K.; Hirakawa, H.; Yamamoto, J.; Ebisuno, K.; Miyamoto, L.; Ishizawa, K.; Tsuchiya, K.; Otaka, A., Development of a reduction-responsive amino

- acid that induces peptide bond cleavage in hypoxic cells. *ChemBioChem* **2012**, *13* (7), 968-971.
204. Shigenaga, A.; Yamamoto, J.; Hirakawa, H.; Ogura, K.; Maeda, N.; Morishita, K.; Otaka, A., Development of thiol-responsive amide bond cleavage device and its application for peptide nucleic acid-based DNA releasing system. *Tet. Lett.* **2010**, *51* (18), 2525-2528.
205. Shigenaga, A.; Yamamoto, J.; Kohiki, T.; Inokuma, T.; Otaka, A., Invention of stimulus-responsive peptide-bond-cleaving residue (Spr) and its application to chemical biology tools. *J. Pept. Sci.* **2017**, *23* (7-8), 505-513.
206. Ji, C.; Miller, P. A.; Miller, M. J., Syntheses and antibacterial activity of *N*-acylated ciprofloxacin derivatives based on the trimethyl lock. *ACS Med. Chem. Lett.* **2015**, *6* (6), 707-710.
207. Peukert, C.; Langer, L. N. B.; Wegener, S. M.; Tutov, A.; Bankstahl, J. P.; Karge, B.; Bengel, F. M.; Ross, T. L.; Brönstrup, M., Optimization of artificial siderophores as ⁶⁸Ga-complexed PET tracers for *in vivo* imaging of bacterial infections. *J. Med. Chem.* **2021**, *64* (16), 12359-12378.
208. Tsionou, M. I.; Knapp, C. E.; Foley, C. A.; Munteanu, C. R.; Cakebread, A.; Imberti, C.; Eykyn, T. R.; Young, J. D.; Paterson, B. M.; Blower, P. J.; Ma, M. T., Comparison of macrocyclic and acyclic chelators for gallium-68 radiolabeling. *RSC Adv.* **2017**, *7* (78), 49586-49599.
209. Kubíček, V.; Havlíčková, J.; Kotek, J.; Tircsó, G.; Hermann, P.; Tóth, É.; Lukeš, I., Gallium(III) complexes of DOTA and DOTA-monoamide: Kinetic and thermodynamic studies. *Inorg. Chem.* **2010**, *49* (23), 10960-10969.
210. Notni, J.; Pohle, K.; Wester, H.-J., Comparative gallium-68 labeling of TRAP-, NOTA-, and DOTA-peptides: practical consequences for the future of gallium-68-PET. *EJNMMI Res.* **2012**, *2* (1), 28.
211. Petrik, M.; Umlaufova, E.; Raclavsky, V.; Palyzova, A.; Havlicek, V.; Pfister, J.; Mair, C.; Novy, Z.; Popper, M.; Hajduch, M.; Decristoforo, C., ⁶⁸Ga-labelled desferrioxamine-B for bacterial infection imaging. *Eur. J. Nucl. Med. Mol. Imaging* **2021**, *48* (2), 372-382.
212. Caraco, C.; Aloj, L.; Eckelman, W. C., The gallium–deferoxamine complex: stability with different deferoxamine concentrations and incubation conditions. *Appl. Radiat. Isot.* **1998**, *49* (12), 1477-1479.

213. Banin, E.; Lozinski, A.; Brady, K. M.; Berenshtein, E.; Butterfield, P. W.; Moshe, M.; Chevion, M.; Greenberg, E. P.; Banin, E., The potential of desferrioxamine-gallium as an anti-*Pseudomonas* therapeutic agent. *Proc. Natl. Acad. Sci. U.S.A.* **2008**, *105* (43), 16761-16766.
214. Sanchez-Crespo, A., Comparison of Gallium-68 and Fluorine-18 imaging characteristics in positron emission tomography. *Appl. Radiat. Isot.* **2012**, *76*.
215. Malik, S.; Kaminski, M.; Landman, D.; Quale, J., Cefiderocol resistance in *Acinetobacter baumannii*: Roles of β -lactamases, siderophore receptors, and penicillin binding protein 3. *Antimicrob. Agents Chemother.* **2020**, *64* (11), e01221-20.
216. Klein, S.; Boutin, S.; Kocer, K.; Fiedler, M. O.; Störzinger, D.; Weigand, M. A.; Tan, B.; Richter, D.; Rupp, C.; Mieth, M.; Mehrabi, A.; Hackert, T.; Zimmermann, S.; Heeg, K.; Nurjadi, D., Rapid development of cefiderocol resistance in carbapenem-resistant enterobacter cloacae during therapy is associated with heterogeneous mutations in the catecholate siderophore receptor CirA. *Clin. Infect. Dis.* **2021**, *74* (5), 905-908.
217. Green, O.; Gnaim, S.; Blau, R.; Eldar-Boock, A.; Satchi-Fainaro, R.; Shabat, D., A near-infrared dioxetane luminophores with direct chemiluminescence emission mode. *J. Am. Chem. Soc.* **2017**, *139* (37), 13243-13248.
218. Huang, J.; Jiang, Y.; Li, J.; Huang, J.; Pu, K., Molecular chemiluminescent probes with a very long near-infrared emission wavelength for in vivo imaging. *Angew. Chem. Int. Ed.* **2021**, *60* (8), 3999-4003.
219. Fan, J.; Sun, W.; Wang, Z.; Peng, X.; Li, Y.; Cao, J., A fluorescent probe for site I binding and sensitive discrimination of HSA from BSA. *Chem. Comm.* **2014**, *50* (67), 9573-9576.
220. Hansen, W.; Yourassowsky, E., Detection of beta-glucuronidase in lactose-fermenting members of the family Enterobacteriaceae and its presence in bacterial urine cultures. *J Clin Microbiol* **1984**, *20* (6), 1177-1179.
221. Gadelle, D.; Raibaud, P.; Sacquet, E., beta-Glucuronidase activities of intestinal bacteria determined both *in vitro* and *in vivo* in gnotobiotic rats. *Appl. Environ. Microbiol* **1985**, *49* (3), 682-685.
222. Yagi, T., Bacterial NADH-quinone oxidoreductases. *J. Bioenerg. Biomembr.* **1991**, *23* (2), 211-225.

223. Gnaim, S.; Gholap, S. P.; Ge, L.; Das, S.; Gutkin, S.; Green, O.; Shelef, O.; Hananya, N.; Baran, P. S.; Shabat, D., Modular access to diverse chemiluminescent dioxetane-luminophores through convergent synthesis. *Angew. Chem. Int. Ed.* **2022**, *61* (22), e202202187.
224. Roldán, M. D.; Pérez-Reinado, E.; Castillo, F.; Moreno-Vivián, C., Reduction of polynitroaromatic compounds: the bacterial nitroreductases. *FEMS Microbiol. Rev.* **2008**, *32* (3), 474-500.
225. Tuckman, M.; Osburne, M. S., *In vivo* inhibition of TonB-dependent processes by a TonB box consensus pentapeptide. *J. Bacteriol.* **1992**, *174* (1), 320-323.
226. Legutki, J. B.; Zhao, Z.-G.; Greving, M.; Woodbury, N.; Johnston, S. A.; Stafford, P., Scalable high-density peptide arrays for comprehensive health monitoring. *Nat. Commun.* **2014**, *5* (1), 4785.
227. Ghosh, A. K.; Samanta, I.; Mondal, A.; Liu, W. R., Covalent inhibition in drug discovery. *ChemMedChem* **2019**, *14* (9), 889-906.
228. Martin-Gago, P.; Olsen, C. A., Arylfluorosulfate-based electrophiles for covalent protein labeling: A new addition to the arsenal. *Angew Chem Int Ed Engl* **2019**, *58* (4), 957-966.
229. Zhou, S.; Chan, E.; Duan, W.; Huang, M.; Chen, Y. Z., Drug bioactivation, covalent binding to target proteins and toxicity relevance. *Drug Metab Rev* **2005**, *37* (1), 41-213.
230. Swinney, D. C.; Anthony, J., How were new medicines discovered? *Nat. Rev. Drug Discov.* **2011**, *10* (7), 507-519.
231. Silver, L. L., Rational approaches to antibacterial discovery: Pre-genomic directed and phenotypic screening. In *Antibiotic Discovery and Development*, Dougherty, T. J.; Pucci, M. J., Eds. Springer US: Boston, MA, 2012; pp 33-75.
232. Clatworthy, A. E.; Romano, K. P.; Hung, D. T., Whole-organism phenotypic screening for anti-infectives promoting host health. *Nat. Chem. Biol.* **2018**, *14* (4), 331-341.
233. Ribeiro, L. C.; Rapini, M. S.; Silva, L. A.; Albuquerque, E. M., Growth patterns of the network of international collaboration in science. *Scientometrics* **2018**, *114* (1), 159-179.
234. Bettencourt, L. M. A.; Kaiser, D. I.; Kaur, J., Scientific discovery and topological transitions in collaboration networks. *J. Informetr.* **2009**, *3* (3), 210-221.

235. Wawer, M.; Lounkine, E.; Wassermann, A. M.; Bajorath, J., Data structures and computational tools for the extraction of SAR information from large compound sets. *Drug Discov.* **2010**, *15* (15), 630-639.
236. Agrafiotis, D. K.; Shemanarev, M.; Connolly, P. J.; Farnum, M.; Lobanov, V. S., SAR Maps: A new SAR visualization technique for medicinal chemists. *J. Med. Chem.* **2007**, *50* (24), 5926-5937.